Gold mobility in the crust:
From source to ore deposit formation

Zur Erlangung des akademischen Grades eines

DOKTORS DER NATURWISSENSCHAFTEN

(Dr. rer. nat.)

von der KIT - Fakultät für

Bauingenieur-, Geo- und Umweltwissenschaften des

Karlsruher Instituts für Technologie (KIT)

genehmigte

DISSERTATION

Von

M.Sc. Simon Hector

Tag der mündlichen Prüfung: 29. November 2023

Hauptreferent: Prof. Dr. rer. nat. Jochen Kolb

Korreferent: Prof. Dr. Anne-Sylvie André-Mayer

Abstract

Gold is a precious metal with a low concentration in the Earth's crust (~1.2 $ng \cdot g^{-1}$) while Au ore is generally economically exploitable today when it contains more than 1 $\mu g \cdot g^{-1}$ of Au. To form primary Au ore, a three orders of magnitude enrichment is necessary and Au must be efficiently mobilised from a source, transported by a fluid and concentrated in the crust by precipitating mechanisms. This thesis aims to better understand the source-to-sink processes controlling formation of Au deposits and their metal association in orogenic and continental volcanic arc settings. The former is represented by orogenic Au deposits in the Central Lapland Greenstone Belt and the Pohjanmaa Belt (Finland) and the latter by the Nea Kameni volcano and the hybrid epithermal-SMS Au mineralisation of the Kolumbo submarine volcano (Greece). To understand source-to-sink processes, the following research directions are developed: 1) improving Au analysis by laser ablation-inductively coupled plasma-mass spectrometry (LA-ICP-MS) on pressed-powder pellet (PPP); 2) characterisation of the metal sources involved in Au-rich deposit formation; 3) study of Au and other metal mobilisation and transport mechanisms; 4) understanding mineralising processes leading to Au deposit formation.

To better identify Au mobilisation in the crust, a method by PPP-LA-ICP-MS has been developed for whole rock analysis; reaching limit of detection as low as 0.10-0.05 $ng \cdot g^{-1}$ Au and enabling Au analysis of Au-depleted rocks.

The study of Finnish orogenic Au deposits and associated basement rocks shows how the metal association and endowment of deposits are conditioned by local mineralisation conditions, timing of formation during multi-stage mineralising events and source lithology, which control the content of Au, base metals and ligands in metamorphic fluids.

Furthermore, this study stresses the role of magmatic degassing in the formation of Au deposits in volcanic arcs settings. Investigation of magmatic differentiation at Kolumbo reveals that Au and other chalcophile elements are mobilised upon degassing, despite early sulfide saturation. We identify a strong correlation between formation of sulfide-volatile compound drops in the magma and the Kolumbo mineralisation, indicating that metal-rich magmatic fluids are likely involved in porphyry and epithermal deposits formation.

Investigating atypical deposits such as orogenic Au deposits with atypical metal association and hybrid SMS-epithermal deposits provides a deeper understanding of Au mobility in the crust by revealing metal mobilising processes that may be not observed in typical deposits.

Zusammenfassung

Gold ist ein Edelmetall mit einer geringen Konzentration in der Erdkruste (~1.2 $ng \cdot g^{-1}$), während Au-Erz heute ab einem Au-Gehalt von mehr als 1 $\mu g \cdot g^{-1}$ profitabel ist. Um eine Anreicherung um drei Größenordnungen zu erreichen, muss Au aus einer Quelle mobilisiert, durch ein Fluid transportiert und in der Kruste durch effiziente Fällungsmechanismen konzentriert werden. Diese Arbeit zielt darauf ab, die Quelle-Senke-Prozesse besser zu verstehen, die die Bildung von Au-Lagerstätten und ihre Metallassoziation in orogenen und kontinentalen Vulkanbögen kontrollieren. Orogene Au-Lagerstätten im Central Lapland Greenstone Belt und im Pohjanmaa Belt (Finnland) stehen für erstere, letztere für den Vulkan Nea Kameni und die hybride Epithermal-SMS-Au-Mineralisierung von Kolumbo (Griechenland). Auf der Basis dieser Untersuchungsobjekte werden folgende Forschungsschwerpunkte entwickelt: 1) Verbesserung der Au-Analyse durch Laserablation und induktiv gekoppelte Plasma-Massenspektrometrie (LA-ICP-MS) auf Presspulver-Pellets (PPP) zur Untersuchung von Au-Muttergestein und Mobilisierungsprozessen; 2) Charakterisierung der Metallquellen, die bei der Bildung von Au-reichen Lagerstätten eine Rolle spielen; 3) Untersuchung der Mobilisierungs- und Transportmechanismen von Au und anderen Metallen; 4) Untersuchung der Mineralisierungsprozesse, die zur Bildung von Au-Lagerstätten führen, und der Parameter, die die Metallassoziation steuern. Um die Prozesse, die zur Mobilisierung von Au in der Kruste führen, besser einzugrenzen, wurde eine Methode für die PPP-LA-ICP-MS-Analyse entwickelt, die eine Nachweisgrenze für Au von nur 0,10-0,05 $ng \cdot g^{-1}$ erreicht und die Analyse der Au-Verteilung in Au-armen Gesteinen ermöglicht.

Die Untersuchung der finnischen orogenen Au-Lagerstätten und des zugehörigen Grundgebirges zeigt, wie die Metallassoziation und der Gehalt der Lagerstätten von den lokalen Mineralisierungsbedingungen, dem Zeitpunkt der Bildung während der mehrstufigen Mineralisierungsereignisse und der Muttergesteinslithologie abhängen, die den Gehalt an Au, unedlen Metallen und Liganden in den metamorphen Fluiden steuern.

Zusätzlich unterstreicht diese Studie die Rolle der magmatischen Entgasung bei der Bildung von Au-Lagerstätten in Vulkanbögen. Die Untersuchung der magmatischen Differentiation in Kolumbo zeigt, dass Au und andere chalkophile Elemente bei der Entgasung mobilisiert werden, trotz früher Schwefelsättigung. Wir stellen eine starke Korrelation zwischen der Bildung von Sulfid-Gas-Tropfen im Magma und der Mineralisierung von Kolumbo fest, was darauf hindeutet, dass metallreiche, magmatische Fluide wahrscheinlich an der Bildung von Porphyr- und epithermalen Lagerstätten teilhaben.

Die Untersuchung atypischer Lagerstätten wie orogener Au-Lagerstätten mit atypischer Metallvergesellschaftung und hybrider SMS-epithermaler Lagerstätten ermöglicht ein tieferes Verständnis der Au-Mobilität in der Kruste, da sie Metallmobilisierungsprozesse aufzeigen, die in typischen Lagerstätten nicht beobachtet werden können.

Résumé

L'or est un métal précieux peu concentré dans la croûte terrestre (~1.2 $ng \cdot g^{-1}$), tandis qu'un gisement d'or est économiquement exploitable à partir d'une teneur de 1 $\mu g \cdot g^{-1}$ Au. Pour atteindre un tel enrichissement, l'or doit être mobilisé à partir d'une source, transporté par un fluide et concentré dans la croûte par des mécanismes de précipitation efficaces. Cette thèse vise à mieux comprendre les processus qui contrôlent la formation des gisements d'or et leurs assemblages de métaux dans les orogènes et les arcs volcaniques continentaux, de la source à la minéralisation. Les orogènes sont représentés par les gisements d'or orogéniques de la Central Lapland Greenstone Belt et de la Pohjanmaa Belt (Finlande) et les arcs volcaniques continentaux par Nea Kameni et la minéralisation hybride SMS-épithermale de Kolumbo (Grèce). Les axes de recherche suivants sont suivis : 1) Amélioration de l'analyse de l'or par spectrométrie de masse à plasma induit par couplage inductif par ablation au laser (LA-ICP-MS) sur des pastilles de poudre pressée (PPP) pour étudier les roches sources et les processus de mobilisation de l'or; 2) Caractérisation des sources de métaux impliquées dans la formation de gisements riches en or; 3) Étude des mécanismes de mobilisation et de transport de l'or et autres métaux; 4) Compréhension des processus minéralisateurs conduisant à la formation de gisements d'or et des paramètres contrôlant les association métalliques.

Pour mieux contraindre les processus mobilisant l'or dans la croûte, la méthode PPP-LA-ICP-MS a été améliorée pour atteindre une limite de détection de l'or de 0,10-0,05 $ng \cdot g^{-1}$, ce qui est suffisamment bas pour analyser la distribution de l'or dans des roches appauvries.

L'étude des gisements d'or orogéniques de Finlande et des roches du socle qui leur sont associées montre comment l'association et teneur en métaux des gisements sont conditionnées par les conditions locales de minéralisation, la chronologie de formation au cours des évènements minéralisateurs successifs et la lithologie de la source, qui contrôle la teneur en or, métaux de base et ligands dans les fluides métamorphiques.

En outre, cette étude souligne le rôle du dégazage magmatique dans la formation des gisements d'or d'arcs volcaniques. L'étude de la différenciation magmatique à Kolumbo révèle que l'or et d'autres éléments chalcophiles sont mobilisés lors du dégazage, malgré une saturation précoce en soufre du magma. Nous identifions une forte corrélation entre la formation de complexes sulfures-gaz dans le magma et la minéralisation de Kolumbo, indiquant que des fluides magmatiques riches en métaux sont probablement impliqués dans la formation des gisements porphyriques et épithermaux.

L'étude de gisements atypiques tels que les gisements d'or orogéniques à association de métaux atypique et les gisements hybrides SMS-épithermaux permet de mieux comprendre la mobilité de l'or dans la croûte en révélant des processus de mobilisation des métaux qui peuvent ne pas être observés dans les gisements typiques.

Table of contents

1 Introduction

For thousands of years, mankind has been fascinated by Au and it remains to this day a symbol of stability and power. Gold is mostly used in jewellery and as a storage of value as ingots, but still finds industrial uses, mostly for electronic and medical applications. The main reason for this long-lasting enthusiasm and trust in Au as a safe investment are its inalterability and rarity. The rarity of Au reflects a geological reality. As a chalcophile and siderophile element, most of Earth' s Au migrated to the core during planetary differentiation, leaving very little Au in the mantle and the crust, ~1.2 $ng \cdot g^{-1}$ (Saunders et al. 2018) and ~1.3 $ng \cdot g^{-1}$ (Rudnick and Gao 2003), respectively. Gold ore becomes today economically viable when grades of 1 $\mu g \cdot g^{-1}$ (i.e. 1 $g.t^{-1}$) are reached. This means that formation of an Au deposit requires geological processes concentrating Au a thousand times its average crustal abundance. Gold deposits are divided into two categories: primary and secondary Au deposits. The later are sedimentary deposits forming by accumulation of gravity separated Au grains in fluvial or shore environment. This work investigates the processes leading to Au enrichment in the crust and thus considers only primary Au deposits.

Primary Au deposits form in a broad range of pressure and temperature, with various metal associations depending on the nature of the mineralising fluids and geodynamic context. The main recognised types of primary Au deposits are: orogenic Au, Cu-Au porphyry, epithermal, Au-rich volcanogenic massive sulfide (VMS), Au-rich skarn and iron oxide-copper-gold (IOCG) deposits (Fig.1) (Groves et al. 1998; Phillips and Powell 2015). Genetic models of Au deposits represent ideal "end-members" on a continuum of combining mineralising processes. Several mineralising processes may compete or be involved simultaneously in the formation of a single Au deposit (e.g. hydrothermal leaching of the basement rocks and input of metal rich magmatic fluids in submarine volcanic setting) (Sillitoe et al. 1996).

Depending on the geological setting, similar mineralising processes form deposits with different habits, which may be complex to classify. For instance, an Au-Ag epithermal deposit forming in a submarine environment would be referred to as an Au-rich SMS deposit with a strong magmatic component or as hybrid epithermal-SMS deposit (Keith et al. 2018).

To understand the formation of a mineral deposit it is fundamental to consider the whole system: 1) the sources of metals, ligands and fluids, 2) the transport mechanisms and path for the mineralising fluids from the source to the deposit and, 3) the sink, where metals precipitate from the mineralising fluid, forming the deposit. This holistic method requires a multi-scale approach at the regional (geodynamic processes, fluid and metal sources), district (transport paths, faults), deposit and microscopic scales (ore mineralogy and geochemistry, ore precipitation mechanisms). This work proposes to explore the source-to-sink journey of Au in two different settings: orogenic Au deposits in collisional orogens and hybrid epithermal-SMS Au deposit in volcanic arcs.

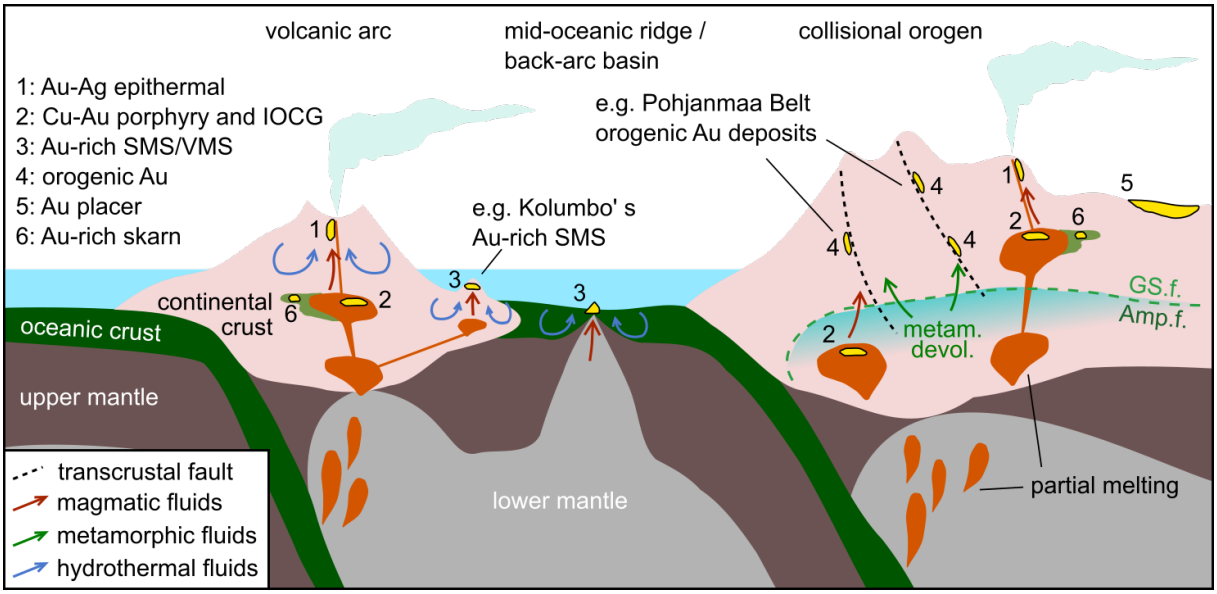

Fig.1: Main types of Au deposits in various geodynamic environments, with associated Au source and transport mechanism. Abbreviations: metam. devol. = metamorphic devolatilisation; GS.f. = greenschist facies; Amp.f. = amphibolite facies (modified from Goldfarb and Groves 2015).

2 Analytical challenges for tracking Au mobility in the crust

For economic reasons, study of Au deposit mainly focuses on the ore. They are extensively investigated by both mining companies and academics, as the main objectives are to understand and predict where the Au is concentrated. Consequently, there are numerous studies exploring the favourable geological settings for Au mineralisation, the morphology of a deposit and the related geochemical, structural and mineralogical footprints. But the sources of Au, mobilisation processes and pathways to the deposits are more difficult to study, particularly because of the very low abundance of Au in the crust ($ng \cdot g^{-1}$ to sub-$ng \cdot g^{-1}$ range; e.g. Pitcairn 2011), raising analytical challenges. Analysis of Au requires careful sample preparation and analytical tools with very low limits of detection (LOD). Commonly used methods for low-concentration Au analysis are solution-based inductively coupled plasma-mass spectrometry (ICP-MS) or solution-based graphite furnace-atomic absorption spectrometry (GF-AAS; e.g. Liu et al. 2019; Pitcairn et al. 2006a; Pitcairn 2011). Both methods require multiple acid digestion of a relatively large quantity of sample material (up to 3 g) prior to analysis, which involve delicate laboratory work, followed by Au pre-concentration techniques (e.g. extraction chromatography, ion exchange resin, precipitation, polyurethane foam and solvent extraction). Recent improvement in the analytical field led to the development of new methods for low-concentration Au analysis by laser-ablation-ICP-MS on pressed-powder-pellets (PPP-LA-ICP-MS) (e.g. Garbe-Schönberg and Müller 2014; Peters and Pettke 2017). This method is safer, faster and cheaper than the previous ones, but also sensitive to Ta and Hf oxide interferences. These oxides may form during ICP-MS analysis and have a very similar mass to Au, artificially increasing the signal of Au. However, fine-tuning allows to limit oxide production and to reach sub-$ng \cdot g^{-1}$ LOD for Au after oxide interference correction (~0.4 $ng \cdot g^{-1}$; Belgrano et al. 2022).

While this LOD is sufficient for most of the crustal samples, source rocks of Au deposits are particularly depleted in Au (e.g. highly metasomatised basaltic rock: 0.17 $ng \cdot g^{-1}$; Patten et al. 2017; amphibolite facies schist: 0.17 $ng \cdot g^{-1}$; Pitcairn et al. 2006b). Improving the LOD for this fast and low-risk method would allow to extend the range of analysis to strongly Au-depleted rocks, which is fundamental to understand large-scale geological processes related to Au deposit formation, especially regarding source of Au (e.g. Patten et al. 2020a; Pitcairn et al. 2006b).

3 Orogenic Au deposits

Orogenic Au deposits refers to epigenetic, Au-only, hydrothermal lode deposits in metamorphic belts, which formed during an orogeny (Goldfarb et al. 2005; Hagemann and Cassidy 2000; Kolb et al. 2015; McCuaig and Kerrich 1998). This category of Au deposits gathers deposits located in very different geological units, formed during most of the Earth's history and within a broad pressure-temperature field. They share, however, enough fundamental similarities to consider them as a single deposit type (Groves et al. 1998).

The formation of orogenic Au deposits usually occurs late in orogenies, during a post-peak metamorphic timing in an active margin/accretion/collision setting (Gebre-Mariam et al. 1995; Goldfarb et al. 2001; Goldfarb et al. 2005; Groves et al. 1998). Orogenic Au deposits are found along a crustal continuum from prehnite-pumpelleyite facies to granulite facies rocks, but mostly form between 1-3 kbar and 250-475°C in greenschist to lower amphibolite facies rocks (Fig.2) (Gebre-Mariam et al. 1995; Kolb et al. 2015).

3.1 Source of metals and fluids

Geochemical data from orogenic Au deposits are often equivocal and usually cannot discriminate clearly a single source for the auriferous fluids (Goldfarb and Groves 2015; Ridley and Diamond 2000). Depending on the genetic model considered responsible for the formation of the deposits, the following fluid and metal sources are involved: magmatic-hydrothermal fluids from upper-to-middle crust intrusions, metamorphic crustal fluids and sub-crustal fluids from metamorphic and magmatic origin (Fig.2) (Bierlein and Pisarevsky 2008; Goldfarb and Groves 2015; Goldfarb and Pitcairn 2023; Groves et al. 2020). The different genetic models listed above are based on the study of different orogenic Au deposits across the world and sometime show limitation to explain the general geochemical and geodynamic consistency within the orogenic Au deposits.

1) The magmatic-hydrothermal model considers that cooling magmatic intrusions within the orogen release fluids and metals and induce convective hydrothermal circulation within the upper-to-middle crust, leading to formation of Au-rich lodes in the vicinity of granites (Sillitoe 1990; Thébaud et al. 2018). This genetic model, however, is not applicable to all the orogenic Au deposits as their formation is not systematically correlated with magmatic activity through geological time, many of them post-dating intrusion emplacement (Goldfarb and Groves 2015; Goldfarb and Pitcairn 2023).
2) The metamorphic devolatilisation model considers that auriferous metamorphic fluids are responsible for the formation of orogenic Au deposits when channelised by fault systems (Gaboury 2019; Phillips and Powell 2010). Metamorphic fluids are produced by devolatilisation of volcano-sedimentary units during prograde metamorphism at the greenschist-amphibolite facies transition (Phillips and Powell 2010; Tomkins 2010). Calculations show that mafic rocks as well as sedimentary rocks may generate as much

as 5 vol.% fluids during metamorphism (Elmer et al. 2006; Fyfe et al. 1978). Considering the volume of fluids involved and the efficiency of Au mobilisation by metamorphic fluids, each cubic kilometer of a source rock is estimated to be able to release 3 to 15 tons of Au even with an initial Au content as low as 2 $ng \cdot g^{-1}$ (Phillips and Powell 2010; Pitcairn et al. 2006b). Thus, virtually any metamorphosed volcano-sedimentary unit can generate auriferous fluids. Orogenic Au deposits located in devolatilised high-grade metamorphic host-rocks do not fit the classic metamorphic crustal model. As these highly metamorphosed rocks are dehydrated, they cannot produce any metamorphic fluids to generate orogenic Au deposits. One explanation is that they formed normally at greenschist-amphibolite metamorphic facies conditions and were further metamorphosed later in their history (Phillips and Powell 2009). Another hypothesis involves complex tectonics where retrograde high-grade metamorphic rocks are thrust on top of prograde rocks at greenschist-amphibolite metamorphic facies conditions, the latter generate auriferous metamorphic fluids that can form orogenic Au deposits in the "dry" hanging wall unit (Kolb et al. 2000; Kolb et al. 2004b; Kolb et al. 2004a; Kolb et al. 2015).

3) The sub-crustal fluid and metal source model aim to account especially for orogenic Au deposits in high-grade metamorphic host-rocks (Goldfarb and Groves 2015; Groves et al. 2020). Several origins are proposed for the fluids, one suggests that the source of fluids and metals is similar to the metamorphic crustal model, but instead of being generated within continental crust, they are released from the metamorphosed subducting oceanic crust (Goldfarb and Groves 2015; Kerrick and Connolly 2001). Other proposed origins involve the participation of mafic mantle-derived magmas

melting the lower crust to produce pseudo-metamorphic fluids (Boorder 2012) or a hybrid mantle plume/devolatilisation process, where Au-enriched oceanic plateaus are produced before being subducted and devolatilised, generating Au-rich fluids (Bierlein and Pisarevsky 2008). Hronsky et al. (2012) suggest that the auriferous fluids are released from Au-rich magmas produced by a fertile subcontinental lithosphere. The sub-crustal model is particularly adapted to the giant Jiadong Au province in China, which is not fitting the other genetic models (Groves et al. 2020). However, this model is controversial and cannot be considered as an "universal" model for orogenic Au deposits formation (Goldfarb and Groves 2015).

3.2 Mineralising fluids and pathway through the crust

The auriferous fluids forming orogenic Au deposits show consistent geochemistry through geological times with near neutral aqueous-carbonic fluids (pH ≈ 5,5) and low-to-moderate salinity usually comprised between 3 and 7 wt.% NaCl eq. (Garofalo et al. 2014; Ridley and Diamond 2000). The fluids can leach metals (Ag, As, Au, Cu, Mo, Sb, Se, Sn, Te) from surrounding rocks and transport them as chloride or hydrosulfide complex (Liu et al. 2014; Pitcairn et al. 2014; Seward 1973; Seward et al. 2014; Tomkins 2010). They travel through the crust from their source following transcrustal faults at boundaries between domains of contrasting competence (e.g. Cadillac fault in Canada; Boulder-Lefroy shear zone in Western Australia; Kiistala shear zone in Finland) (Kolb et al. 2004a; Robert and Poulsen 2001). These deep-rooted structures favour formation of mineral deposits as they cross-cut various lithologies and create pathways for eventual fluids (Gaboury 2019; Kolb et al. 2004a; Sibson et al. 1988).

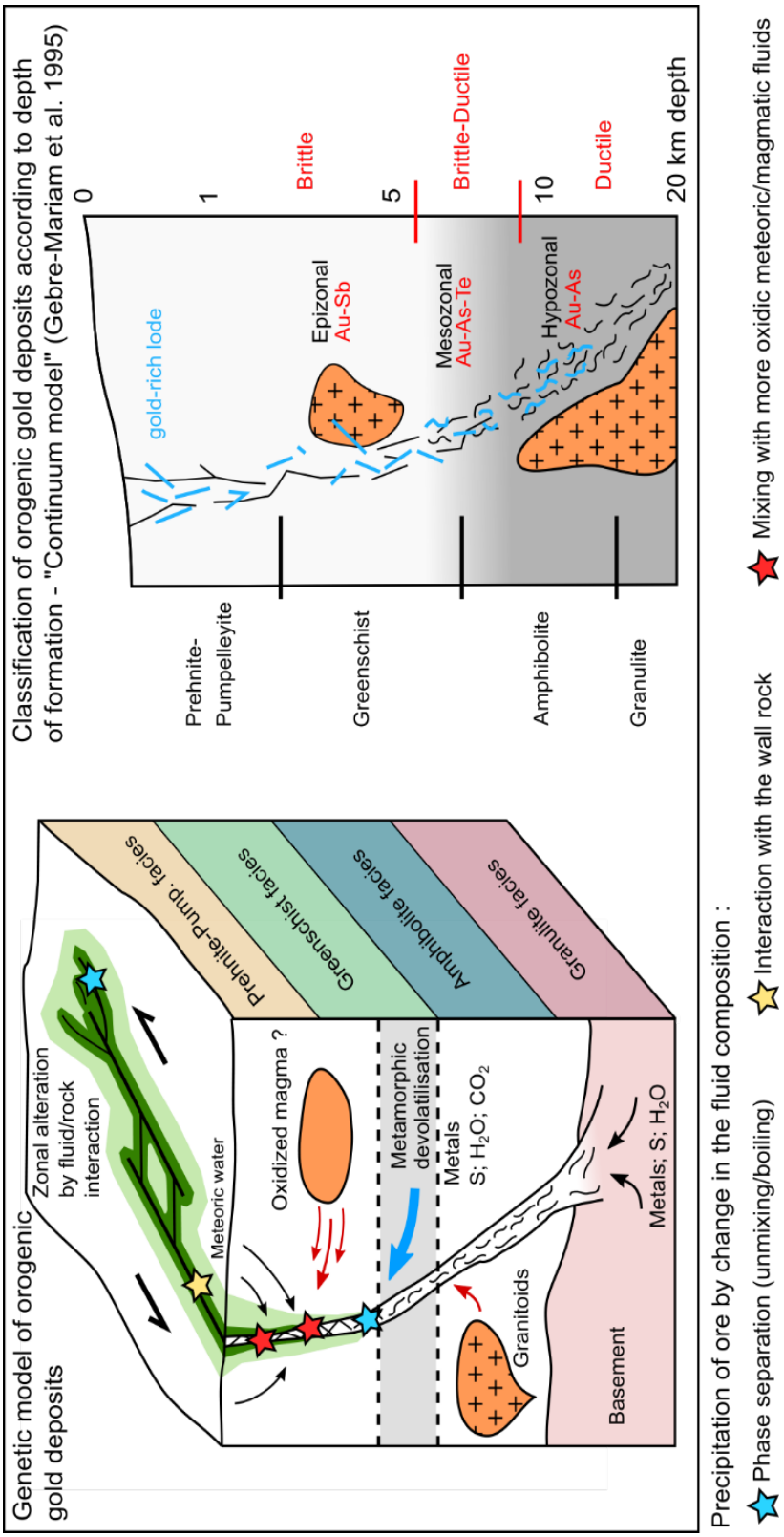

Fig.2: Genetic model for the orogenic Au deposits showing the source of fluids and metals. Modified after Gebre-Mariam et al. (1995); Groves et al. (1998) and Goldfarb and Groves (2015).

3.3 Formation of orogenic Au deposit

Greenstone belts and orogens generally show a complex and long-lived tectonic history with intense shortening, forming transcrustal faults (Robert and Poulsen 2001). Orogenic Au deposits occur in secondary structures (i.e. faults, shear zones and folds) along first order structures (i.e. transcrustal faults) in loci of structural complexity such as fault bends, intersections or duplexes (Eisenlohr et al. 1989; Kolb 2008; Robert and Poulsen 2001). The texture of the Au-rich lodes indicates multistage mineralisation through repeated opening and sealing (Goldfarb et al. 2001; Kolb et al. 2004b). Sibson et al. (1988) introduced the fault-valve model to explain the formation of the veins by repetitive reactivation of faults under fluid pressure. When the fluid pressure exceeds the lithostatic pressure, the rock is fractured and the fluids are flowing suddenly. The resulting pressure drop triggers mineral deposition in the newly opened fractures, eventually sealing the vein and allowing fluid pressure to build up again. The precipitation of Au from auriferous fluids is triggered either by chemical reaction between the fluid and the host-rock (fluid reduction, fluid oxidation, wall-rock sulfidation) or by mixing with other fluids, unmixing or boiling (Fig.2) (Phillips and Powell 2010). This cycle can repeat thousands to millions of times over a few million years, leading to the formation of an Au deposit (Kolb et al. 2004b; Sibson et al. 1988; Weatherley and Henley 2013).

Orogenic Au deposits are usually Au-only, in a way that only Au is economically enriched. The ore occurs as quartz-carbonate veins with 1 to 5 vol.% sulfides, mainly pyrite ± arsenopyrite in greenschist facies rocks and pyrrhotite ± löllingite and arsenopyrite in amphibolite facies rocks (Eilu and Pankka 2009). Chalcopyrite, galena and sphalerite can occur as a minor component in deposits located in higher-grade metamorphic rocks (Eilu and Pankka 2009). Gold occurs in lodes either as “free” Au grains, precipitated among gangue and eventual ore minerals, or trapped in minerals, it is then known as refractory Au. Refractory Au is either present in minerals, usually arsenopyrite and sulfides, as micrometre-scale Au inclusions or

trapped in the structural lattice of arsenide as “invisible Au” (Chryssoulis and McMullen 2005; Kojonen and Johanson 1999; Molnár et al. 2018).

Some orogenic Au deposits show anomalous metal enrichment in Ag, Cu, Co, Ni or Sb in regard of the classic orogenic Au metal association. These deposits are classified as “orogenic Au deposits with atypical metal association” (Eilu 2015) and may include a significant amount of chalcopyrite, cobaltite, pentlandite, gersdorffite and/or stibnite in addition of the classic pyrite, pyrrhotite and/or arsenopyrite assemblage (Eilu et al. 2007; Groves et al. 2003; Nurmi et al. 1991; Vanhanen 2001). These deposits occur in several orogenic Au districts worldwide such as in northern Finland (e.g. Central Lapland Greenstone Belt, Kuusamo Belt, Peräpohja Belt; Eilu 2015), northern Australia (Pine Creek), South Africa (Pilgrim’s Rest) and in Mali (Loulo district) (Goldfarb and Groves 2015; Lawrence et al. 2013). This sub-type of orogenic Au deposits, although scarce, locally show high base metal content (i.e. >1% Cu and >0.2% Co), increasing their economic potential. However, the processes leading to enrichment in base metals in addition to Au in these deposits remain poorly understood.

4 Hybrid SMS-epithermal Au deposit

Depending on the geological setting, mineralising processes can overlap and/or combine, leading to formation of hybrid deposits sharing characteristics with several types of deposits. Hybrid SMS-epithermal Au deposits belong to this category as they are forming from magmatic-hydrothermal fluids in submarine volcanic setting, combining the epithermal and SMS deposit genetic models (Alfieris et al. 2013; Keith et al. 2018; Stoffers et al. 1999).

4.1 Epithermal deposit

Epithermal deposits form in subaerial volcanic settings and represent the uppermost part of a magmatic-hydrothermal system, forming a continuum with porphyry deposits (Hedenquist et al. 1998). At depth, a cooling magmatic intrusion releases metal-rich fluid which eventually evolves in a two-phase, hyper-saline brine with vapor able to form various Au deposits in the surrounding host-rocks and the intrusion itself (i.e. Cu-Au porphyry, Au-rich skarn, IOCG) (Heinrich 2005; Sillitoe 2010). After separation from the brine, the vapor phase gradually condensates into a low to intermediate salinity fluid, able to transport metals as chloride or bisulfide complexes (Heinrich 2005; Pudack et al. 2009). The high geothermal gradient generated by the intrusion may initiate a hydrothermal system, where magmatic fluids travelling upwards, following fractures, eventually mix with groundwater and form epithermal deposits along with various manifestations at the surface (i.e. hot spring, sinter, acid pools, geyser, fumaroles) (Hedenquist et al. 1998; Rowland and Simmons 2012; Simmons et al. 2005). Depending on the proportion of mixing between magmatic fluids and meteoric water, epithermal deposits will have varying metal and mineral association (Sillitoe and Hedenquist 2003), but are usually enriched in Ag, As, Au, Hg, Sb, Tl, a group of elements generally referred to as the "epithermal suite" (Henley 1985).

4.2 Seafloor massive sulfides

Seafloor massive sulfide (SMS) occurrences are known since the 1970's after the discovery of the famous "black smokers" and are considered analogues to ancient VMS deposits (Halbach et al. 1989; Hannington and Scott 1989). They form in submarine volcanic settings where hydrothermal activity is developed, usually along mid-oceanic ridges and volcanic arcs (Hannington et al. 2005). Due to permeability of the crust, availability of heat and open pathways, seawater can circulate within the seafloor (Becker 1989; Brett-Adams et al.

2023; Fisher 1998). As it travels downward, the cold, oxidised seawater progressively warms up and its composition is modified upon fluid-rock interaction, ultimately becoming a hot, reduced hydrothermal fluid able to leach metals (As, Au, Cu, Se, Sb, Pb, Zn) from the surrounding rocks and to transport them as chloride and sulfide complexes (Alt 1995; Nesbitt et al. 1987; Patten et al. 2016). When the hydrothermal fluid is hot enough, it travels up toward the seafloor, cools down and precipitates sulfates and sulfides as it mixes with cold seawater, forming hydrothermal vents (Hannington et al. 2005). Depending on the geological setting, especially the nature of volcanism and lithologies of the sub-seafloor, VMS deposits can show variable metal associations: Cu-Zn (Co-Ni-Au-Ag) in ultramafic setting, Cu-Zn (Au) in mafic-dominated setting, Cu-Zn (Ag-Au) in bimodal-mafic setting, Cu-Zn-Pb in mafic-silliciclastic setting, Cu-Pb-Zn-Ag (Au) in bimodal-felsic setting and Pb-Zn (Cu-Ag-Au) in siliciclastic-felsic setting (Barrie and Hannington 1997; Patten et al. 2022). Base metals are the main economic commodities in VMS and Au is usually accessory (< 2 g.t^{-1}), however, some deposits contain more than 31 metric tons with Au grades > 3.46 g.t^{-1}, and are classified as Au-rich VMS deposits (Mercier-Langevin et al. 2011). The mechanisms leading to Au enrichment in these deposits are still disputed, the following processes have been proposed: 1) subseafloor boiling in a shallow water environment causing enrichment of Au in a vapour-rich fluid (Alfieris et al. 2013; Hannington et al. 1997), 2) high Au content in the mineralising fluid due to elevated Au content in the source rocks or extensive leaching (Patten et al. 2016; Pitcairn 2011), 3) overprint of a VMS deposit by auriferous fluids during regional metamorphism (Dubé et al. 2007) and 4) input of Au from sub-seafloor magmatic intrusions releasing fluids (Patten et al. 2020b; Sillitoe et al. 1996; Yang and Scott 2002). Gold-rich VMS deposits are frequently enriched in the epithermal suite of metals, indicating a link with epithermal mineralisation (Dubé et al. 2007).

4.3 Hybrid SMS-epithermal Au deposit

Arc-related hydrothermal systems differ from those located along mid-oceanic ridges and mature back-arc spreading centres by being hosted in volcano-sedimentary shallow submarine environments and by the important magmatic contribution of fluids and metals to the hydrothermal system (e.g. de Ronde et al. 2005; Hannington et al. 2005; Patten et al. 2020b). While the deposits are very similar to SMS, with formation of sulfide-sulfate chimneys, the magmatic contribution to the hydrothermal system is attested by the amount of magmatic volatiles expelled from the vents (mostly CO_2) and by the enrichment in the "epithermal suite" of metals in the mineralisation in regard to classic SMS, suggesting that these systems are comparable to on-land porphyry-epithermal deposits (Keith et al. 2018). The nature of hybrid SMS-epithermal Au deposits can either be understood as the seafloor manifestation of a submarine epithermal system, where magmatic fluids are mixing in a seawater-derived hydrothermal system instead of meteoric water, or as a submarine hydrothermal venting system dominated by magmatic fluids.

5 Thesis aims

The objective of this thesis is to better understand the source-to-sink processes controlling the formation of Au deposits and their metal association in the continental crust, with a focus on orogenic and continental volcanic arc settings. The orogenic Au deposits in the Central Lapland Greenstone Belt and Pohjanmaa Belt in Finland as well as the Nea Kameni volcano and the hybrid epithermal-SMS Au mineralisation of the Kolumbo submarine volcano in Greece are favourable study areas to develop the following research directions:

1) Improvement of analytical capabilities for investigating samples with low to ultra-low Au (sub-ng·g^{-1}) concentration in whole rock. Analysis of a wide range of rock types, including highly Au-depleted rocks, is necessary for investigating Au source rock and mobilisation processes.
2) Characterisation of the various metal sources involved in Au-rich deposit formation in the continental crust.
3) Study of Au and other metal mobilisation and transport mechanisms in the continental crust.
4) Understanding mineralising processes leading to Au deposit formation and the diversity in metal association in the continental crust.

The broad scope of this work, investigating various Au deposits with different source-to-sink mechanisms offers a better understanding of the mobility of Au through the continental crust and how deposits form.

6 Study areas

6.1 Metamorphosed volcano-sedimentary belts of Finland

The Central Lapland Greenstone Belt and the Pohjanmaa Belt are located in Northern and Western Finland, respectively. They are metamorphosed volcano-sedimentary belts formed during the Svecofennian Orogeny (1920-1770 Ma), and host numerous orogenic Au deposits which formed along major regional shear zones (Fig.3).

The Central Lapland Greenstone Belt contains various types of deposits such as banded iron formation, VMS and orogenic Au deposits, the latter are hosted in volcano-sedimentary sequences along shear zones (Peltonen 2005). They belong to the Kittilä Au-Cu metallogenic area which covers most of the Central Lapland Greenstone Belt and hosts an estimated Au content of 7.83 Moz (Eilu et al. 2012). About half of the orogenic Au occurrences of the Central Lapland Greenstone Belt are considered as orogenic Au deposits with atypical metal association, showing various enrichment in Co, Cu and/or Ni (Molnár et al. 2018; Molnár et al. 2019; Patison 2007; Peltonen 2005). The Central Lapland Greenstone Belt is also characterised by a complex tectonic evolution defined by different deformation and metamorphic events (Hanski and Huhma 2005; Nironen 2017; Sayab et al. 2020). This specific evolution led volcanic and sedimentary rocks to reach greenschist up to upper-amphibolite facies peak conditions (Hölttä et al. 2007; Hölttä and Heilimo 2017). This particular geological setting is ideal for testing systematic metal mobility from both metavolcanic and metasedimentary rocks during prograde metamorphism (thesis aims 2 and 3). This approach allows to test to which extent each lithological unit of the greenstone belt may contribute to the generation of metal-rich metamorphic fluids and to refine the metamorphic devolatilisation model for orogenic Au deposits.

While the Central Lapland Greenstone Belt has been extensively studied during the last decades (Hanski and Huhma 2005; Mänttäri 1995; Molnár et al. 2018; Ward et al. 1989), there is little literature about orogenic Au deposits in the Pohjanmaa Belt. Comparing orogenic Au mineralising processes in both volcano-sedimentary belts will allow to better understand the protracted formation of orogenic Au deposits in the Fennoscandia shield during the Paleoproterozoic (~1.91-1.75 Ga).

The northern part of the Pohjanmaa Belt hosts orogenic Au, porphyry Cu-Au and porphyry Mo, as well as magmatic Ni-Cu-Co sulfide deposits (Eilu et al. 2012). They belong to the Laivakangas Au-Cu metallogenic area, which hosts an estimated Au content of 1.69 Moz (Eilu et al. 2012), including the second largest gold mine of Finland (Laivakangas mine, 0.67 Moz of measured Au resource; Geological Survey of Finland 2019). The orogenic Au deposits show variable metal associations, ranging from Au-only to Au-(Cu-Co-Ni) despite presenting very similar geological setting and spatial proximity (Fig.3-B). The deposits are close to first order shear-zones and show close spatial relationship with plutons (Gaál and Sundblad 1990; Nironen 2005). This distinctive geological setting led some orogenic Au deposits in the area to be classified as overprinted porphyric-hydrothermal Au deposit (Eilu and Pankka 2009). The diversity in metal associations between similar deposits at regional scale raises questions regarding the source of the metals, nature of the fluids and processes leading to the formation of the different ore types (thesis aims 2, 3 and 4).

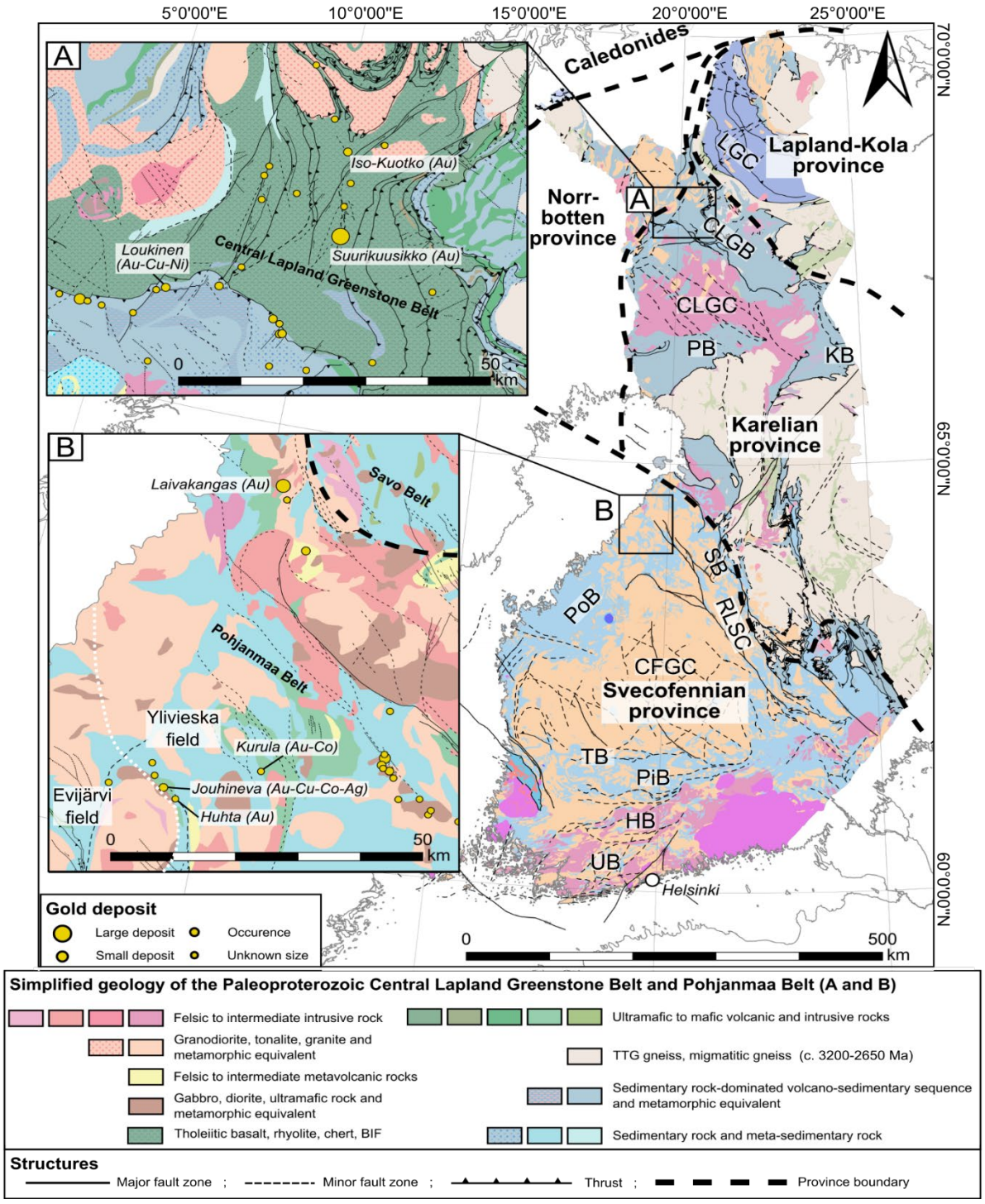

Fig.3: Simplified geological map of Finland (modified from Kähkönen 2005; Koistinen et al. 2001). LGC: Lapland Granulite Complex; CLGB: Central Lapland Greenstone Belt; CLGC: Central Lapland Granitoid Complex; PB: Peräpohja Belt; KB: Kuusamo Belt; RLSC: Raahe-Ladoga Shear Complex; SB: Savo Belt; PoB: Pohjanmaa Belt; CFGC: Central Finland Granitoid Complex; TB: Tampere Belt; PiB: Pirkanmaa Belt; HB: Häme Belt; Uusimaa Belt; (A) Simplified geological map of the Central Lapland Greenstone Belt and its Au deposits; (B) Simplified geological map of the Pohjanmaa Belt and its Au deposits.

6.2 Subaerial and submarine volcanoes in Greece

The Nea Kameni and Kolumbo volcanoes are part of the Christiana-Santorini-Kolumbo volcanic field which belongs to the Hellenic Volcanic Arc, constituting the southern margin of the Aegean Sea (Fig.4-A). Kolumbo is an active submarine volcano hosting a hydrothermal field in the northern part of its crater (Fig.4-B). Boiling CO_2-rich fluids are venting, leading to formation of polymetallic Zn-Pb-(As, Ag, Au, Hg, Sb, Tl)-rich sulfate-sulfide diffusers (Fig.4-B') (Carey et al. 2013; Kilias et al. 2013; Nomikou et al. 2022; Rizzo et al. 2016; Rizzo et al. 2019; Sigurdsson et al. 2006). The volcanic setting of the SMS, it's high content in the epithermal suite of metals and venting style (low temperature ~150-265°C, CO_2-rich fluids) led to a classification as hybrid, Au-rich, SMS-epithermal deposit. This hybrid type of mineralisation is poorly investigated and very little is known about the source-to-sink mechanisms of Au and other metals enriched in the mineralisation, and specifically the role of magmatic degassing. Investigation of fresh volcanic rocks from both Kolumbo and Nea Kameni (Fig.4-C and C') volcanoes allows in-depth understanding of metal behaviour during the complex magmatic evolution of the Christiana-Santorini-Kolumbo volcanic field. Comparison with the Kolumbo hydrothermal field enables to genetically link magmatic processes in the source with metal endowment in hybrid Au-rich SMS epithermal deposit in a continental crust setting (thesis aims 2, 3 and 4).

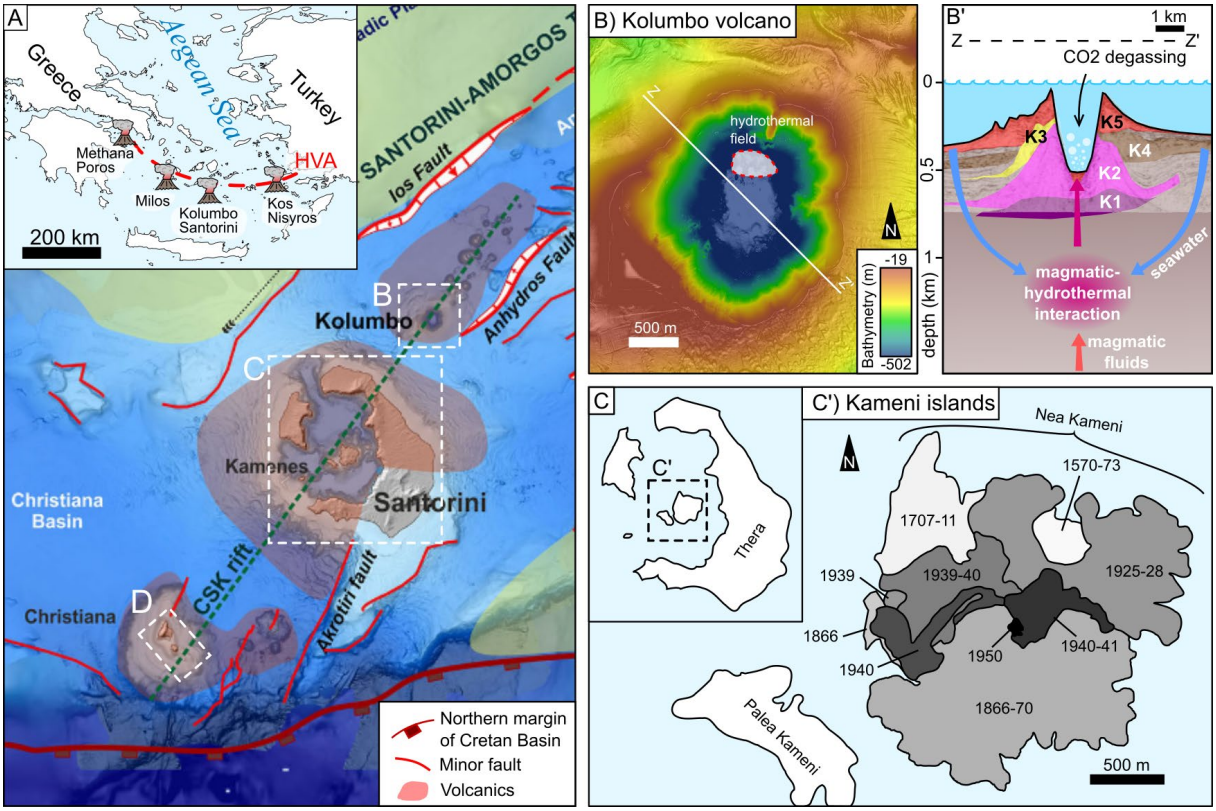

Fig.4: Geological setting of the studied volcanoes : A) Bathymetric map of the Christiana-Santorini-Kolumbo volcanic system and associated tectonic structures (modified after Nomikou et al. 2022); inset : regional map of the Aegean Sea showing the active volcanic systems in the South Aegean volcanic arc; CSVA: Hellenic Volcanic Arc. B) Bathymetric map of the Kolumbo volcano from Nomikou et al. 2022; B') Model of Kolumbo volcano's magmatic-hydrothermal system, volcanic units K1 to K5 are interpreted from seismic reflection imaging (modified after Hübscher et al. 2015). C) Map of the Santorini archipelago. C') Geological map of Nea Kameni showing the successive dacite flows forming the island (modified after Martin et al. 2006).

7 Contribution

Paper I: Improved whole rock low detection limit gold analysis by LA-ICP-MS utilizing pressed-powder-pellets. Patten CGC, Beranoaguirre A, **Hector S**, Gudelius D, Kolb J, Eiche E (2023) International Journal of Mass Spectrometry:117039

For this study, I adapted the protocol for pressed-powder-pellets (PPP) preparation from Peters and Pettke (2017) and Belgrano et al. (2022) and organised its application in our laboratory. I ordered the necessary tools and components (i.e. binding agents, pellets die, adapted laboratory glassware, grinding bowls for the nano-mill, etc.) and tested different milling settings, adjusting milling time and rotation speed, to obtain appropriate rock powder for PPP preparation. I experimented PPP pressing with microcrystalline cellulose and vanillic acid as binding agents. The "sample preparation" section of the paper details the protocol I developed to obtain the most homogenous signal and best measurement precision and accuracy for Au and other trace elements, based on PPP-LA-ICP-MS analysis of standard material certified for Au. I prepared the PPP used for this method (i.e. reference material, blank, Hf- and Ta-spiked pellets) and assisted C. Patten and A. Beranoaguirre in the tuning of the instrumental setup. I assisted C. Patten, A. Beranoaguirre and D. Gudelius for the correction of the Hf and Ta oxide interreferences with Au. Finally, I wrote the "Sample preparation" section of the "Material and methods", participated in the discussion, proof-reading and editing of the manuscript.

Paper II: Multi-source and multi-stage metal mobilization during the tectonic evolution of the Central Lapland Greenstone Belt, Finland: implications for the formation of orogenic Au deposits. Patten CGC, Molnár F, Pitcairn IK, Kolb J, Mertanen S, **Hector S** (2022) Mineralium Deposita

For this study, I draw the regional and metamorphic map of the Central Lapland Greenstone Belt, combining the geological units and metamorphic peak facies with main structural features, the Au deposits and the location of the drill core samples based on careful regional geology literature review. I contributed to the conceptualisation, discussion, proof-reading and editing of the manuscript.

Paper III: Orogenic Au deposits with atypical metal association (Cu, Co, Ni): insights from the Pohjanmaa Belt, western Finland. **Hector S**, Patten CGC, Kolb J, Araujo de Silva A, Walter BF, Molnár F (2023) Ore Geology Reviews:105326

For my first paper as senior author, I selected the study area and organised the cooperation with the company Otsogold and the Geological Survey of Finland (GTK) for the sampling. The field work and drill core sampling took place in October and November 2019, respectively, during which I co-supervised two master students, along with C. Patten. I prepared the samples for petrography (i.e. cutting and thin section preparation). I did the petrographic study (i.e. transmitted/reflected light microscopy and SEM), the microprobe analysis and prepared the samples for S isotope analysis. The conceptualisation, analysis of the results and manuscript writing and editing are the result of my own work and benefitted from discussion and advice by C. Patten, J. Kolb, F. Molnar, B. Walter, A. Araujo de Silva, reviewers and editor.

Paper IV: Magmatic evolution in the Kolumbo volcano and its implication to seafloor massive sulphide formation. **Hector S**, Patten CGC, Beranoaguirre A, Lanari P, Kilias S, Nomikou P, Peillod A, Eiche E, Kolb J (submitted) Mineralium Deposita

For my second paper as senior author, I co-organised, along with C. Patten, the cooperation with our colleagues in Greece. I planned and organised a 3-weeks field campaign on the islands of Thera, Nea Kameni, Ios and Anafi and the shipping of samples from the University of Athens. I processed the samples for petrographic (i.e. cutting and drying) and geochemical analysis (i.e. milling for LOI, CSA and Hg-content, PPP preparation for trace element analysis, glass beads for major element analysis). I did the petrography (transmitted and reflected light microscopy), the CSA and LOI analysis, and the microprobe analysis on magnetite, with the support of P. Lanari. I assisted A. Beranoaguirre with the LA-ICP-MS analysis on PPP and magnetite. The conceptualisation, interpretation of the results and manuscript writing are the result of my own work and benefitted from discussion and advice by C. Patten, J. Kolb, S. Kilias, P. Nomikou, A. Peillod and P. Lanari.

Paper V: Transfer of sulfur and chalcophile metals via sulfide-volatile compound drops in the Christiana-Santorini-Kolumbo volcanic field. Patten CGC, **Hector S**, Kilias S, Ulrich M, Peillod A, Beranoaguirre A, Nomikou, P, Eiche E, Kolb J. (in review) Nature Communications

For this study, I planned the sampling campaign in Nea Kameni with C. Patten and A. Peillod, with the support of P. Nomikou. The sampling took place in October 2020 and was performed by A. Peillod, C. Patten and myself. I processed the samples for petrographic and in-situ geochemical analysis (i.e. cutting and drying). I assisted C. Patten with the petrography (transmitted and reflected light microscopy and SEM) and did the microprobe analysis on magnetite and sulfides, with the support of P. Lanari. I assisted A. Beranoaguirre and C. Patten with the LA-ICP-MS analysis of magnetite and sulfides. I contributed to the conceptualisation, analysis of the results and discussion. I wrote the “Geological setting” section and contributed to proof-reading and editing of the manuscript.

Paper I

-

Improved whole rock low detection limit gold analysis by LA-ICP-MS utilizing pressed-powder-pellets.

Patten CGC, Beranoaguirre A, **Hector S**, Gudelius D, Kolb J, Eiche E (2023) International Journal of Mass Spectrometry:117039

International Journal of Mass Spectrometry 488 (2023) 117039

Contents lists available at ScienceDirect

International Journal of Mass Spectrometry

journal homepage: www.elsevier.com/locate/ijms

Improved whole rock low detection limit gold analysis by LA-ICP-MS utilizing pressed-powder-pellets

C.G.C. Patten [a,*], A. Beranoaguirre [a], S. Hector [a], D. Gudelius [a], J. Kolb [a], E. Eiche [a,b]

[a] Chair of Geochemistry and Economic Geology, Institute of Applied Geosciences, KIT, Germany
[b] Laboratory for Environmental and Raw Materials Analysis, Institute of Applied Geosciences, KIT, Germany

ARTICLE INFO

Article history:
Received 8 December 2022
Received in revised form
7 March 2023
Accepted 9 March 2023
Available online 16 March 2023

ABSTRACT

Analysis of Au in geological materials has been proven useful for understanding geological processes related to the formation of various Au-rich ore deposits. However, the Au concentration in the related source rocks is extremely low (~<1 ng g^{-1}) and the methodologies allowing analysis at sub-ng g^{-1} levels are time-consuming, costly and generally involve the handling of hazardous chemicals. Here we present an improved method for low Au concentration analysis by laser-ablation inductively-coupled-plasma mass-spectrometry (LA-ICP-MS) of pressed-powder-pellets (PPP). Fine instrumental tuning for key parameters such as ICP-MS sample gas flow, torch position, RF power, laser frequency, ablation style and laser gas flow allows increasing the Au sensitivity while keeping oxide production low. The latter is critical when analyzing low Au concentrations as the ICP-MS analysis can be impaired by $^{181}Ta^{16}O$ and $^{180}Hf^{16}O^{1}H$ interferences. Reducing oxide production and quantifying interferences by analyses of matrix-matched Ta- and Hf-doped pellets, allow for efficient corrections. The method improves the method limit of detection with values as low as 0.10–0.05 ng g^{-1} Au and routine analysis of reference materials shows that Au analysis by PPP-LA-ICP-MS is reliable. This contribution highlights that the PPP-LA-ICP-MS method is suitable for investigating Au distribution and behavior in Au-depleted rocks.

1. Introduction

Exploration and understanding of Au-rich ore deposits require efficient methods for analyzing Au in a large variety of geological materials ranging from high-grade Au ore samples to Au-depleted source rocks (e.g. Refs. [1,2]. Gold content in the Earth's crust is low (average continental and oceanic crusts contain 1.3 ng g^{-1} and 1.4 ng g^{-1} Au, respectively [2,3]; and analysis of Au in unmineralized rock samples generally requires dedicated low detection limit methods [4]. Commonly used approaches for low-concentration Au analysis involve multiple acid digestion of a relatively large quantity of sample material (up to 3 g) followed by Au pre-concentration techniques (e.g. extraction chromatography, ion exchange resin, precipitation, polyurethane foam and solvent extraction) before analysis by inductively coupled plasma-mass spectrometry (ICP-MS) or graphite furnace-atomic absorption spectrometry (GF-AAS; e.g. Refs. [2,5,6]. Gold analysis by ICP-MS allows for high sensitivity but is also challenging due to the monoisotopic nature of Au (^{197}Au), its well-known "stickiness" leading to a strong memory effect in the analytical setup as well as strong Ta and Hf oxide interferences [7,8]. Hence, pre-concentration techniques often allow for matrix separation and removal of elements leading to oxide interferences (e.g. Ref. [4]. Development of pressed powder pellets (PPP) for trace element analysis by laser ablation-ICP-MS (LA-ICP-MS; e.g. Refs. [9,10], however, leads to reduced oxide production rates during analysis relative to wet plasma related to solution mode ICP-MS methods and appears as a promising method for low detection limit Au analysis. Recently, Belgrano et al. [8] developed a method for combined analysis of PPP and glass for Au, Ag, Pt, As and Re by LA-ICP-MS validating the use of PPP-LA-ICP-MS analysis for routine analysis of Au in unmineralized rock samples. Oxide interference correction is achieved through zircon and tantalite analysis [8]. The method limit of detection (MLOD) of Au analysis by PPP-LA-ICP-MS is in the sub-ng g^{-1} range (~0.4 ng g^{-1} [8]; and allows for Au analysis of most common geological materials. Analysis of strongly Au-depleted rocks, which is paramount for understanding large-scale geological processes related to Au-rich ore deposit formation (e.g. Refs. [1,11,12,29]), is however limited using this method [8]. In this

* Corresponding author.
E-mail address: clifford.patten@kit.edu (C.G.C. Patten).

https://doi.org/10.1016/j.ijms.2023.117039
1387-3806/

study we improve Au analysis by PPP-LA-ICP-MS by working exclusively on PPP for calibration, oxide interference correction and MLOD characterization allowing for better Au sensitivity.

2. Materials and methods

2.1. Sample preparation

Pressed-powder-pellets are produced following a procedure adapted from Peters and Pettke (2016) and Belgrano et al. [8]. The steps for PPP production include milling, nanomilling and pelletizing. Before starting, careful sampling is paramount for representative results. A representative rock sample (ca. 40 g), free of surface alteration, veins or local heterogeneities is cut, cleaned from any sawing marks, dried and crushed in small pieces avoiding metal contamination as much as possible [4]. After standard planetary agate ring milling, rock powders are nano-milled using a Pulverisette 7 planetary mill (Fritsch GmbH, Idar-Oberstein, Germany). The nanopowders are produced by milling 2.25 g of fine particle powder and 5.6 g of Milli-Q ultrapure water (Merck KGaA, Darmstadt, Germany) with 35 g of 10 mm agate balls in a 45 mL agate milling bowl for 21 min at 800 rpm (7 times 3 min cycles with 1 min cooling between each). Between each sample, the milling bowls are cleaned by milling 2.25 g of pure quartz for 15 min. Milling with agate can possibly lead to SiO_2 sample contamination, but this contamination is considered minimal due to the relative high SiO_2 concentration in most commonly analyzed rocks (>10 wt% SiO_2) and to a relative even contamination between samples and standards, canceling the effect. After milling, the obtained sludge is dried completely at 80 °C and then homogenized using an agate mortar and pestle. The PPP are made of 120 mg nanopowder and 30 mg micro-crystalline cellulose as binding agent (#310697, Sigma-Aldrich, Saint-Louis, USA) homogenized using an agate mortar and pestle and pressed in 10 mm pellets using a stainless-steel pellet die (Maassen GmbH, Reutlingen, Germany) at 1000 MPa for 10 min.

2.2. Instrumental setup

Analyses by LA-ICP-MS were carried out at the Laboratory for Environmental and Raw Materials Analysis (LERA) at the Institute of Applied Geosciences (AGW) of the Karlsruhe Institute of Technology (KIT), using a Teledyne 193 nm Excimer Laser coupled to a Thermo Scientific Element XR High-Resolution ICP-MS (Table 1). Low-concentration Au analysis by ICP-MS requires an extremely clean setup with dedicated tubes, ICP torch, Ni jet sampler and Ni X skimmer cones [7]. The cones as well as the ICP torch are routinely cleaned while tubes are changed when deemed necessary.

2.2.1. ICP-MS setup

Five isotopes are measured with ^{29}Si and ^{44}Ca used for internal calibration, ^{180}Hf and ^{181}Ta for interference quantification and correction, and ^{197}Au. Dwell time on all isotopes is 60 ms except for ^{197}Au which is 240 ms (Table 1). The detector modes used for analysis are counting for ^{197}Au, triple mode for ^{44}Ca, ^{180}Hf and ^{181}Ta, and Faraday cup for ^{29}Si. Nebuliser Ar flow (so-called sample gas flow in Thermo Scientific instruments), plasma-sampling depth (i.e. Z position of the torch) and RF power have been proven to be critical parameters for optimizing Au sensitivity while keeping a low oxide production rate [8,13]. In order to find the best compromise between the three parameters in our laboratory setup, multiple combinations are tested. Thus, the plasma-sampling depth is tested between −6 mm and −3 mm with 0.5 mm steps, the RF power from 1050 W (cold plasma) to 1300 W (hot plasma) in 50 W changes and the Argon flow is shifted between 0.6 l min^{-1} to 0.9 l min^{-1}. These tests are carried out on the relatively low-Au reference material NISTSRM 614 (0.45 μg g^{-1} Au [14]; using laser settings of 20 Hz, 8 mL min^{-1} N_2, 5 J cm^{-2} and a 110 μm round spot.

During routine analysis, the ICP-MS is tuned for Au sensitivity, oxide production rate (ThO/Th) and mass fractionation (U/Th) which is achieved first on the NISTSRM 614 and then double-checked on a reference material pellet (TDB-1). Single analysis consist of pre-ablation linescan, 15 s blank, 25 s analysis and 30 s pause. Pellet ablation with a laser beam of 150 μm and a high frequency of 100 Hz leads to relatively large quantity of material brought to the ICP-MS. After few days of analysis some fine particles can accumulate in the injector of the torch while fine concretions can form on the cones. If not cleaned these can lead to ablation-remobilized contamination [7,8] and an overall decrease in Au sensitivity as well as noisy signal during acquisition. The cones and the injector are routinely cleaned every two-three days for 10–15 min in a Mucasol cleaning solution in ultrasonic bath for maintaining good analytical conditions.

Table 1
Instrument setup and main tuning.

Teledyne 193 nm Excimer Laser			
Cones			Ni jet sampler and Ni X skimmer
Beam style			raster (10 μm.s-1)
Beam diameter			150 μm
Frequency			100 Hz
Energy			5 J.cm-2
He cell			0.3 l.min-1
He cup			0.2 l.min-1
N2			8 mL.min-1
Blank duration			15 s
Analysis duration			25 s
Element XR High-Resolution			
RF Power	1050 W		
Torch depth	−3 mm		
Ar gas	Sample gas		Plasma gas
	0.7 l.min-1		15 l.min-1
Analytes	Si29	Ca44, Hf180, Ta181	Au197
Resolution	Low		
Dwell time	60 ms	60 ms	280 ms
Detector mode	Farraday	Triple	Counting

2.2.2. Laser setup

Two ablation parameters, frequency and ablation style, are tested to achieve the highest Au sensitivity without affecting the oxide production or signal stability. Frequency has a strong control on Au sensitivity as it partly controls the bulk of ablated material brought to the ICP-MS (Pettke et al., 2012). High frequencies of 50, 100 and 200 Hz are examined. Regarding the type of ablation, the high ablation rates used are deemed too high for single spot analysis, which could have led to strong downhole fractionation and therefore, the PPP are ablated using a line scan. Due to the expected low Au signal, the largest available spot size, 150 μm, is used and scan speeds of 10 μm s^{-1} and 20 μm s^{-1} are tried. Variation of He gas flow in the laser cell and the cup cell has no significant impact on the Au sensitivity and it is set at 0.3 l min^{-1} and 0.2 l min^{-1}, respectively. The introduction of N_2, leads to a strong increase of the Au sensitivity (e.g. Ref. [13] and an optimal input of ca. 8 mL min^{-1} N_2 is determined, although this value is tuned every day.

2.3. Oxide interference correction

One of the main issues regarding the Au analysis is the oxide-related polyatomic interferences on ^{197}Au. Major oxide interferences that must be controlled are $^{181}Ta^{16}O$ and $^{180}Hf^{16}O^{1}H$. Although the analysis by PPP-LA-ICP-MS allows for low oxide production rates [8], those must be precisely quantified as they are subsequently used for correcting reference materials, background and samples. At LERA, two approaches are used for quantifying and correcting the oxide production interference, using both the high- and low-resolution modes of the Element XR. High-resolution mode, with a mass resolution of R = 10,000, allows discrimination between the masses of ^{197}Au (196.966 amu) and $^{181}Ta^{16}O$ (196.947 amu) and $^{180}Hf^{16}O^{1}H$ (196.949 amu) interferences. The polyatomic interferences can be measured simultaneously on the same mass window (196.934–196.953 amu) while ^{197}Au is measured on a distinctive mass window (196.957–196.976 amu). The loss in sensitivity during high-resolution mode (~99%), however, only allows analysis of high-concentration samples such as the NISTSRM 610 (23 μg g^{-1} Au; [14].

An alternative method is used in low-resolution mode. Whereas Gilbert et al. [15] claim that analyte-free synthetic basaltic glasses would be best to make matrix-matched interference corrections, Belgrano et al. [8] point out that such glasses can not be easily obtained. In contrast, they proceed with tantalite and zircon for correcting $^{181}Ta^{16}O$ and $^{180}Hf^{16}O^{1}$ H, respectively, assuming both contain negligible amounts of ^{197}Au. Our approach is based on the analysis of three pellets: a natural Au-poor, a Ta-doped and a Hf-doped pellet. The pellets are made from an Au-poor epidosite from the Troodos ophiolite (Au-poor pellet; TSD-041; 0.17 ng g^{-1} Au, 0.06 μg g^{-1} Ta and 1.1 μg g^{-1} Hf; [10]. The doped epidosite pellets are made by adding 25 μl of 1000 μg g^{-1} Ta and 1000 μg g^{-1} Hf standard solutions (Alfa Aesar), respectively, to the 0.24 g of nano-milled epidosite samples. Additional 5 mL of MilliQ water are added and then the samples are dried, homogenized and pelletized following the standard procedure. Moreover, this alternative may prevent the possibility of matrix-related differences in oxide production rates. The $^{181}Ta^{16}O$ interference is quantified as follows:

$$^{181}Ta^{16}O_{Inter} = \frac{Au_{Ta\ doped} - Au_{undoped}}{Ta_{Ta\ doped} - Ta_{undoped}}$$

with $Au_{Ta\ doped}$ the Au cps of the Ta-doped pellet, $Au_{undoped}$ the Au cps of the Au-poor undoped pellet, $Ta_{Ta\ doped}$ the Ta cps of the Ta-doped pellet and $Ta_{undoped}$ the Ta cps of the Au-poor undoped pellet. Similarly, the $Hf^{180}O^{16}H^{1}$ interference is quantified as follows:

$$^{180}Hf^{16}O^{1}H_{Inter} = \frac{Au_{Hf\ doped} - Au_{undoped}}{Hf_{Hf\ doped} - Hf_{undoped}}$$

with $Au_{Hf\ doped}$ the Au cps of the Hf-doped pellet, $Au_{undoped}$ the Au cps of the Au-poor undoped pellet, $Hf_{Hf\ doped}$ the Hf cps of the Hf-doped pellet and $Hf_{undoped}$ the Hf cps of the Au-poor undoped pellet.

2.4. Analytical sequence and data reduction

An analytical sequence consists of 30 samples, 6 reference materials, 3 pellets for interference corrections and one blank pellet. The standards are analyzed four times as blocks within a run and the blocks are evenly distributed between the samples. Within each block, all the standards are analyzed three times. The blank and interference correction pellets are analyzed five times each at the beginning and the end of the sequence. Data reduction is carried out using the software Iolite (Paton et al., 2011). Oxide production rate is calculated by standard bracketing from data of Au-poor undoped, Ta-doped and Hf-doped pellets at the beginning and at the end of each analytical run. Removal of oxide interferences from the sample, standard and background raw counts are achieved before data reduction using the Iolite calculator tool and an ad-hoc python script. The 3DRS plugin is used for data reduction with ^{29}Si as the internal standard and the USGS reference materials BHVO-2, BCR-2 and BIR-1 as well as CCRMP reference materials TDB-1, MRG-1 and UM-2 as external standards. Block calibration is done with the auto-smooth spline model and the calibration is not forced through zero. Calibration using ^{44}Ca as internal standard yields similar results [8] except when analyzing samples with low Ca content (<1%) which yields incoherent Au concentrations. Hence, ^{29}Si is used as the internal standard for routine analysis.

3. Results and discussion

3.1. Optimal measuring conditions

Previous studies [7,8,13] show that a fine-tuning of the instrumentation plays a vital role in Au analysis, as usually only a small amount of analyte is measured. The differences in laser and spectrometer types among the different laboratories require specific and tailored tuning for each apparatus. The effect of nebulizer Ar flow on both the Au sensitivity and oxide production rate (ThO/Th) is tested on NIST SRM 614 by linescan from 0.6 l min^{-1} to 0.9 l min^{-1} (Fig. 1). High Au sensitivity is obtained (60,000–100,000 cps Au) with higher gas flow (0.8–0.9 l min^{-1}), while significantly decreasing (<50,000 cps Au) when reducing the flow (0.6–0.75 l min^{-1}; Fig. 1a). Likewise, a high oxide production rate (>0.15 ThO/Th) is observed with high sample gas flow (0.9 l min^{-1}; Fig. 1b). Oxide production rate drops linearly (down to ~ 0.025) with decreasing gas flow down to 0.6 l min^{-1} (Fig. 1b).

Tuning of the plasma-sampling depth (Z), from −6 mm to −3 mm, appears to have limited effect on the Au sensitivity but significantly affects the oxide production rate (Fig. 1b). The oxide production rate decreases with increasing plasma-sampling depth, especially at high sample gas flow (0.8–0.9 l min^{-1}; Fig. 1b). For instance, the ThO/Th ratio decreases from 0.5% to ~0.2% when moving the torch from −6 mm to −3 mm at a constant nebulizer Ar flow of 0.9 l min^{-1} (Fig. 1b). Combining plasma-sampling depth with sample gas flow allows defining an optimized tuning at ~0.8 l min^{-1} Ar flow and torch depth at ca. −3 to −4 mm for our setup, where a relative high Au sensitivity but low oxide production rate is reached (Fig. 1).

The effect of the RF power on the Au sensitivity and oxide production is tested from 1050 W (cold plasma) to 1300 W (hot

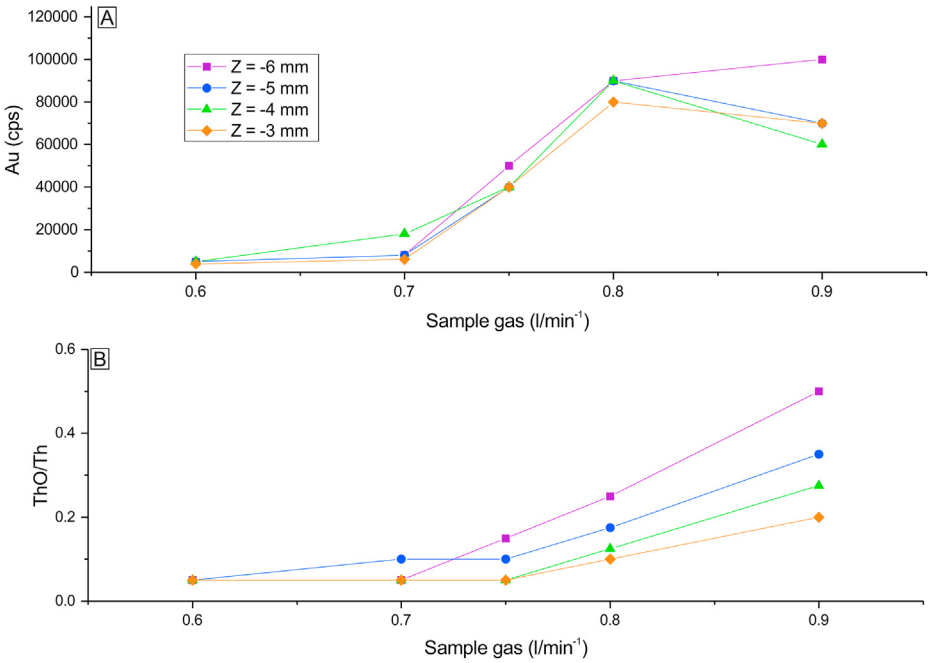

Fig. 1. Variation of A) Au intensity and B) oxide production rate depending on sample gas flow and torch position. Ablation on NIST SRM 614 with laser settings of 20 Hz, 7 mL min^{-1} N_2, 5 J cm^{-2} and 110 μm beam.

plasma) while changing sample gas flow (from 0.65 to 0.9 l min^{-1}) and plasma sampling depth (Z = −3 mm and −4 mm; Fig. 2). Increasing the RF power decreases the Au sensitivity as well as the oxide production rate significantly. For example, at a sample gas flow of 0.65 l min^{-1} and plasma sampling depth of −4 mm, the Au sensitivity decreases from 70,000–80,000 cps Au at an RF power of 1050–1150 W to 10,000–20,000 cps Au at an RF power of 1250–1300 W. Simultaneously the oxide production rate decreases from ~0.20% to <0.01 (Fig. 2). By adjusting the sample gas flow, plasma-sampling depth and the RF power, the following conditions were found to be optimal: 0.7 l min^{-1} and 1050 W or 0.85 l min^{-1} and 1300 W, in both cases with the torch at −3 mm position (Table 2). These optimal conditions, however, vary slightly over time and from the day-to-day analysis.

Regarding the laser system, different frequencies and scan speeds are examined. It is obvious that the higher the frequency, the higher will be the signal, as more material is being ablated. However, several problems may arise, such as plasma overloading and heterogeneous ionization or some non-well-understood effects on the ablation plume [15]. Increasing the laser frequency from 50 Hz to 200 Hz roughly doubles the Au sensitivity (e.g. BHVO-2 from 591 to 1215 cps Au; Fig. 3). At 200 Hz the signal is, however, noisy with frequent transient Au peaks possibly indicating a non-homogenous ablation of the pellet (possibly pieces breaking off the traverse walls). Belgrano et al. [8] show that plasma loading occurs during Au analysis by PPP-LA-ICP-MS but with limited impact. In our study, however, the larger beam size and higher frequency most likely results in higher plasma loading [16]. The effect of plasma loading can be assessed by checking Au/Si variation under different analytical conditions (Fig. 3). Despite a slight increase in Au/Si in the standard BHVO2 with increasing frequency and an over all moderate Au/Si variation (from $0.4*10^6$ to $2.0*10^6$), Au/Si variations are not systematic (Fig. 3). Plasma loading appears problematic for elements with low temperature melting point and for analysis of non matrix-match materials [16,17], which is not the case in our study. Hence, plasma loading appears to have limited impact on Au analysis by PPP-LA-ICP-MS. The best compromise between signal sensitivity and stability is defined at 100 Hz which allows for good Au sensitivity with limited transient Au peaks in the signal. The effects of laser speed on the Au sensitivity appear to have limited consequence (Fig. 3) and is routinely set at 10 μm s^{-1}.

3.2. Polyatomic oxide interference contribution

Characterization of the oxide interference by high-resolution mode has been quantified from ablation of the NIST SRM 610 glass standard which has 23 μg g^{-1} Au, 452 μg g^{-1} Ta and 432 μg g^{-1} Hf (Fig. 4; [14]. Integrated counts per second in high resolution mode for ^{181}Ta, ^{180}Hf and ^{197}Au are $4.99 \cdot 10^6$, $2.04 \cdot 10^6$ and $1.31 \cdot 10^6$ cps, respectively. Combined $^{181}Ta^{16}O$ and $^{180}Hf^{16}O^{1}H$ interference on ^{197}Au is of 347 cps, leading to an oxide production rate of 0.0049%.

Quantification of oxide production during routine analysis on low-resolution is achieved through the analysis of undoped, Ta-doped and Hf-doped pellets. Oxide production rates over ten runs of routine analysis yield 0.0042 ± 0.0007% for $^{181}Ta^{16}O$ and 0.0003 ± 0.0001% for $^{180}Hf^{16}O^{1}H$ (Table 3). The combined oxide production rate determined from high-resolution analysis (0.0049%) is similar to that of the low-resolution mode (0.0045%), validating the approach for accurate characterization of oxide production rates. The routine oxide production rates determined in the low-resolution mode for $^{181}Ta^{16}O$ and $^{180}Hf^{16}O^{1}H$ (0.0042% and 0.00033%, respectively) are slightly lower than those determined by Belgrano et al. [8] by analysis of tantalite and zircon (0.008–0.013% and 0.004–0.009%, respectively).

3.3. Blanks and limit of detection

The interference corrected Au gas blank ranges between ~20 and 80 cps Au depending on daily operating conditions (Fig. 5). Blank improvement occurs during analytical runs with an overall decrease of ~10–20 cps Au within the first 10–15 analyses. Analytical runs spanning over several days also show an overall

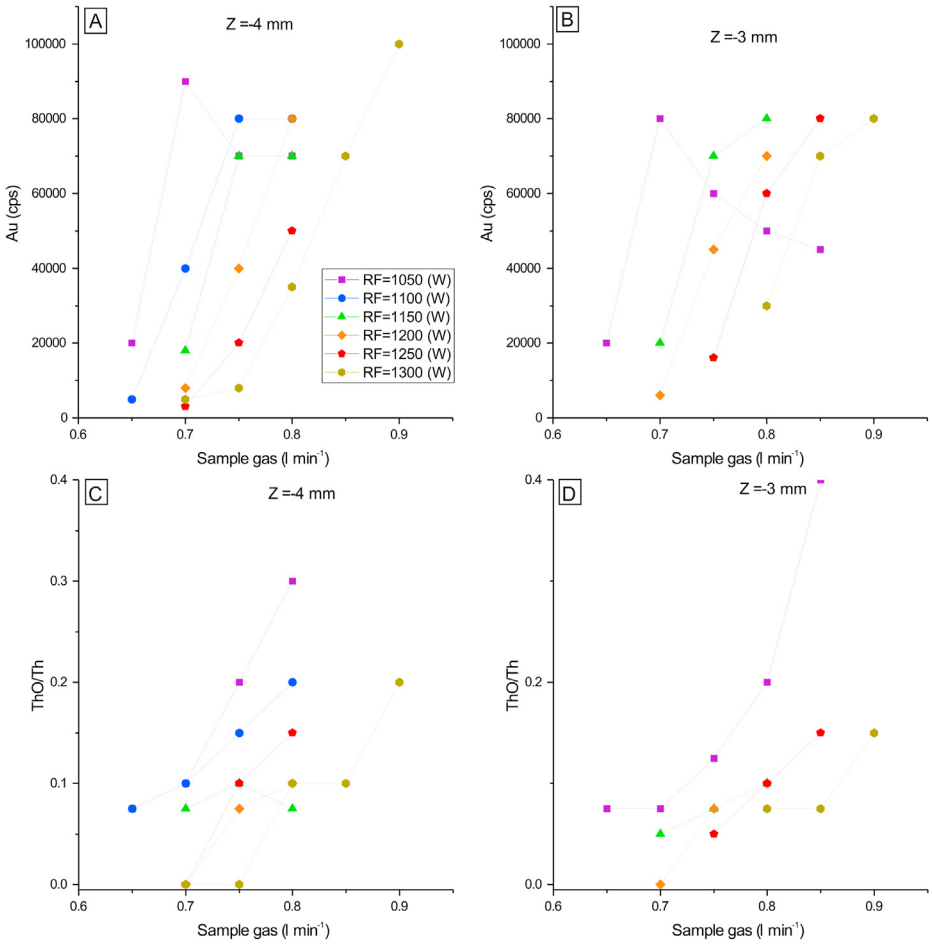

Fig. 2. Effect of the RF power and sample gas flow on Au sensitivity with the torch position at A) −3 mm and B) −4 mm as well as on oxide production with the torch position at A) −3 mm and B) −4 mm. Ablation on NIST SRM 614 with laser settings of 20 Hz, 7 mL min^{-1} N_2, 5 J cm^{-2} and 110 μm beam.

Table 2
Element XR best tunning conditions for key parameters.

RF power	Sample gas	Z position	Au	ThO/Th
(W)	(L/min)	(mm)	(cps)	
1050	**0.7**	**−3**	**70000**	**0.07**
1050	0.7	−4	70000	0.1
1100	0.75	−3	80000	0.1
1150	0.75	−3	60000	0.08
1150	0.75	−4	70000	0.08
1200	0.8	−4	80000	0.15
1300	**0.85**	**−3**	**80000**	**0.07**

Constant parameters: laser frequency 20 Hz, 110 micro spot, 5 J/cm2, N2 15 mL, 0.3 L min^{-1} Ar cell, 0.3 L min^{-1} Ar cup.

decrease in Au background indicating continuous cleansing of the system. Rare transient Au peaks are nevertheless observed in both the gas blanks and in the pellet spectra (Fig. 5). These peaks are due to ablation-remobilized contamination from the removal of Au accumulated in the system (cones, torch and tubes [7,8]; and are removed during data treatment.

The instrumental limit of detection (ILOD) is calculated from the Au corrected gas blank during data reduction in Iolite and using the method of Pettke et al. (2012) which assumes Poisson distribution rather than the normal distribution for very low count rates. Values for the ILOD range from 0.050 to 0.004 ng g^{-1} depending on the analytical runs and have a long-term median ILOD of 0.022 ng g^{-1} (Table 4). The method limit of detection (MLOD), however, should not be calculated from the corrected Au gas blank but rather from the ablation spectra of Au-free material [8]. Confidently Au-free and matrix-match materials, however, are difficult to find [8] but a Au blank pellet has been made from a Au-poor serpentinite from the Troodos ophiolite and is used as a procedural blank. This serpentinite yields a Au concentration below the detection limit (LOD = 0.057 ng g-1) when analyzed by solution ICP-MS using the Pitcairn et al. [4] method and shows low-Au spectra when analyzed by LA-ICP-MS (Fig. 5). Following Belgrano et al. [8], the method limit of detection (MLOD) is defined as the mean + 2σ (99% confidence level) of the repeated analysis of the Au-blank pellet (Table 4). The MLOD varies between runs depending on the instrument operating conditions and ranges between 0.32 and 0.05 ng g^{-1} with a long-term median MLOD of 0.11 ng g^{-1} (Table 4). The Au blank pellet is analyzed at the beginning and the end of each run, showing little variation and implying that despite the high laser yield for Au analysis, the ablation-remobilized contamination is low and constant over time.

The range of the MLOD is below that achieved by Belgrano et al. [8]; 0.38 ng g^{-1}) but still higher than the one from Pitcairn et al. [4]; <0.01 ng g^{-1}) achieved by solution mode analysis. Although improvement of the MLOD as low as 0.05 ng g^{-1} for Au analysis by PPP-LA-ICP-MS might appear as marginal it has nevertheless implications in the method's applications. Gold concentration in rocks generally varies from ~0.5 ng g^{-1} to ~10 ng g^{-1} but Au-depleted rocks generally have Au concentration <1 ng g^{-1} (e.g. Ref. [2].

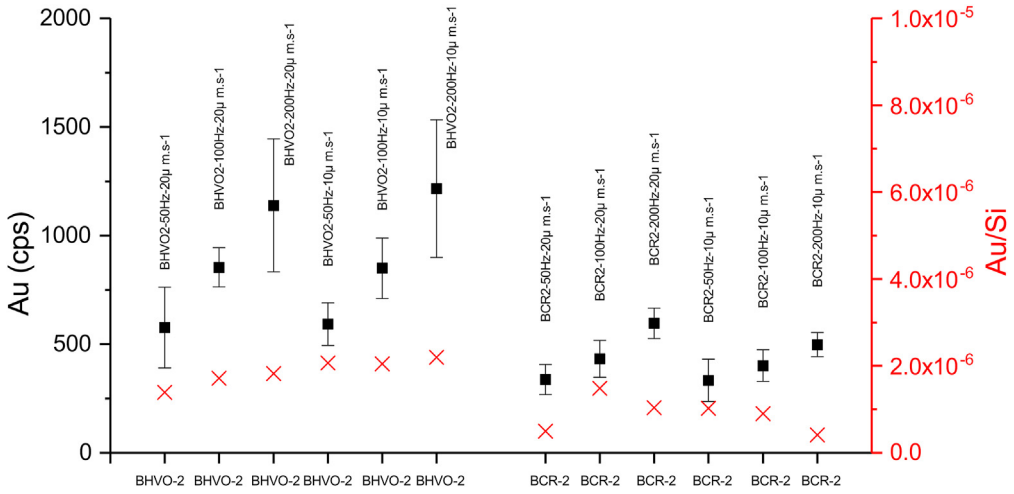

Fig. 3. Effect of laser frequency and raster speed on Au sensitivity and Au/Si from the two pellets made from the reference materials BHVO-2 and BCR-2. The change of laser frequency has a strong effect on Au sensitivity and signal quality while raster speed does not. The Au/Si does not show systematic variations.

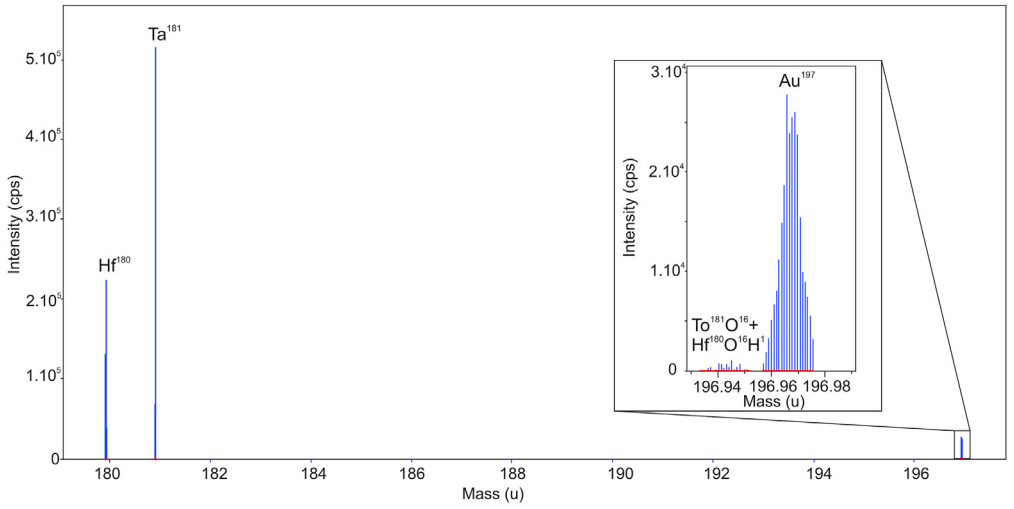

Fig. 4. Signal intensity of ^{181}Ta, ^{180}Hf, ^{197}Au and combined ^{181}Ta^{16}O and ^{180}Hf^{16}O^{1}H during high resolution analysis of NIST SRM 610.

Table 3
Oxide production rate during routine analysis.

		Au	Ta	Hf	Ta	Hf
	n = 50	cps	Cps	cps	µm g-1	µm g-1
TSD-41	Average	102	7.66E+04	5.59E+05	0.08	1.33
	Stdev	23	1.80E+04	1.31E+05	0.01	0.20
TSD-41-Ta	Average	4532	1.05E+08	5.42E+05	104.1	1.35
	Stdev	1656	3.08E+07	1.52E+05	8.6	0.16
TSD-41-Hf	Average	246	7.32E+04	4.71E+07	0.08	114.2
	Stdev	53	2.12E+04	1.36E+07	0.01	8.2
Calculated interference	Average		4.2E-05	3.3E-06		
	Stdev		7.0E-06	1.4E-06		
	Average (%)		4.2E-03	3.3E-04		
	Stdev (%)		7.0E-04	1.4E-04		

Routine operating conditions: RF = 1050W, Sample gas 0.7 L min^{-1}, Z -3mm, laser 100 Hz, 150 µm diameter raster, 5 J/cm-2, N2 8 mL.min-1.

Overview of Au data generated by the method of Pitcairn et al. [4], however, shows that only a few Au-depleted rocks have Au concentration below 0.1 ng g^{-1} (e.g. 6 samples from Refs. [1,12]; none from Refs. [11,18,19]. The quantity of sample used (2.25 g nano-milled) and the MLOD (0.05–0.32 ng g^{-1}) of Au analysis by PPP-LA-ICP-MS is within the range of other methods for low detection limit Au analysis (0.2–15 g and 0.002–0.484 ng g^{-1}, respectively [5]; and references therein). Although analysis of Au-depleted rocks by PPP-LA-ICP-MS is bound to have samples with concentrations below the detection limit, the bulk of the data generated will allow to

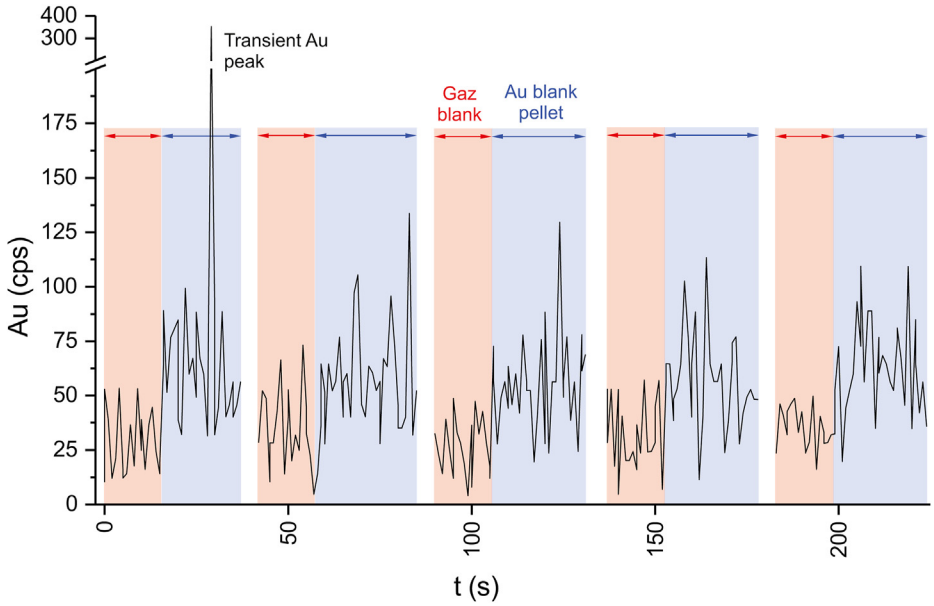

Fig. 5. Gold signal during repeated analysis of the blank pellet showing the gas blank (red) and the pellet blank (blue). The ILOD is calculated from the gas blank while the MLOD is calculated from the pellet blank.

Table 4
Limit of detection.

		Average Au blank Pellet	σ	Method LOD	Instrumental LOD (Pettke et al., 2012)
		(ng g-1)	(ng g-1)	(ng g-1)	(ng g-1)
Run 1	n = 5	0.18	0.070	**0.32**	0.022
Run 2	n = 5	0.08	0.078	**0.24**	0.011
Run 3	n = 5	0.05	0.008	**0.06**	inf*
Run 4	n = 5	0.08	0.017	**0.11**	0.004
Run 5	n = 5	0.04	0.023	**0.08**	inf*
Run 6	n = 5	0.02	0.017	**0.05**	inf*
Run 7	n = 5	0.17	0.048	**0.27**	0.050
Run 8	n = 5	0.17	0.057	**0.28**	0.031
Run 9	n = 4	0.05	0.022	**0.09**	0.012
Run 10	n = 5	0.08	0.038	**0.15**	0.029
Run 11	n = 5	0.07	0.021	**0.11**	inf*

*inf value is returned in Iolite during data reduction when the ILOD tends towards zero as the calibration is not forced through zero.

confidently understand the geological processes related to the Au-depleted rocks.

3.4. Reference materials and method validity

The validity of the method is assessed by checking the reference materials TDB-1, BCR-2, BHVO-2, BIR-1, MRG-1 and UM-2 which have low Au concentrations (Table 5). Well characterized standards for low Au concentration analysis, however, are scarce and show a wide range in Au concentration (Table 5; [8]. This wide range can be due to either the necessity to analyze large material quantity to avoid Au nugget effect [27], standard batch inhomogeneity [8], poor characterization of the standard Au content (e.g. single publication for UM-2 [20], or the analytical method [5]. The TDB-1 standard is, however, a reliable reference material for Au analysis, giving overall consistent results independently from the quantity and method used (Table 5; [6,12,18,20,21,23,25,28]. The average Au concentration for TDB-1 by PPP-LA-ICP-MS (6.19 ± 0.64 ng g^{-1}) is well within the range of published values (5.94–6.76 ppm, Table 5) and has good accuracy and precision (−1.7% and 10.3%, respectively) relative to the CANMET certified value (6.3 ± 1 ng g^{-1}). The average Au concentrations for BCR-2 (0.84 ± 0.15 ng g^{-1}), BHVO-2 (2.39 ± 0.29 ng g^{-1}) and MRG-1 (5.97 ± 0.63 ng g^{-1}) are also within the range of published values (0.82–1.32 ng g^{-1}; 1.2–2.62 ng g^{-1}; 5.4–9 ng g^{-1}, respectively; Table 5; [6,8,20,22,24,26,28], although these standards show a wider Au concentration range. The average Au concentration in BIR-1 (4.29 ± 1.06 ng g^{-1}) is higher than the range of published values (1.6–2.53 ng g^{-1}; Table 5 [8,12,20,22,26]; likely due to batch homogeneity. Finally UM-2 (11.9 ± 1.63 ng g^{-1}) is lower than the single published value by Constantin et al. [20] of 19.2 ± 4.6 ppm (Table 5). Clear evaluation of the method precision and accuracy is difficult due to the lack of well suited reference materials for low Au content. Nevertheless, the consistent Au concentrations for TDB-1, BCR-2, BHVO-2 and MRG-1 relative to published values implies that PPP-LA-ICP-MS Au analysis is reliable, as previously demonstrated by Belgrano et al. [8].

The suitability of the method is further checked by analyzing natural Au-poor samples using both the PPP-LA-ICP-MS method and the multiple acid digest-ICP-MS method from Pitcairn et al. [4]. The analyzed samples are variably serpentinized ultramafic rocks from the Troodos ophiolite (n = 8) as well as the TDB-1 and MRG-1 standards (Fig. 6, Appendix 1). The good correlation (R^2 = 0.92) and equation line close to unity confirm that PPP-LA-ICP-MS is

Table 5
Au concentration of reference materials.

		TDB-1	BCR-2	BHVO-2	MRG-1	BIR-1	UM-2
		(ng g-1)	(ng g-1)	(ng g-1)	(ng g-1)	(ng g-1)	(ng g-1)
This study	Average	**6.19**	**0.84**	**2.39**	**5.97**	**4.29**	**11.9**
	2σ	1.27	0.31	0.57	1.26	1.06	3.26
	n	72	111	110	109	99	45
Belgrano et al. [8]			1.17	1.56		1.99	
PPP-LA-ICP-MS	*2σ*		*0.53*	*0.22*		*0.94*	
Liu et al. (2022)		6.29	0.82	1.2			
GF-AAS	*2σ*	*0.54*	*0.26*	*0.24*			
Cheng et al. [20]		6.1	0.84	1.29			
ICP-MS	*2σ*	*0.7*	*0.05*	*0.24*			
Hughes et al. [21]		6.76					
ICP-MS	*2σ*	*1.9*					
Jochum et al. [22]			1.3	2.6		2.5	
Compilation			-	-		-	
Patten et al. [12]		6.37				2.21	
ICP-MS	*2σ*	*1.02*				*0.74*	
Pitcairn et al. [18]		*6.3*					
ICP-MS	*2σ*	*1.7*					
Goderis et al. [23]		*6.34*					
ICP-MS		-					
Goderis et al. [23]		*5.94*					
ICP-MS		-					
Constantin et al. [20]			1.32	2.62	9	2.53	19.2
INAA	*2σ*		*0.38*	*1.26*	*2.8*	*0.42*	*9.2*
Qi et al. (2003)		6.7					
ICP-MS	*2σ*	*1.4*					
Terashima et al. [24]					7.1		
GF-AAS	*2σ*				*1.6*		
Garuti et al. [25]		6.42					
INAA	*2σ*	*0.1*					
Govindaraju et al. [26]					5.4	1.6	
Compilation					-	-	
CANMET certified value		6.3					
	2σ	*2*					
Range of published values		**5.94–6.76**	**0.82–1.32**	**1.2–2.62**	**5.4–9**	**1.6–2.53**	**-**

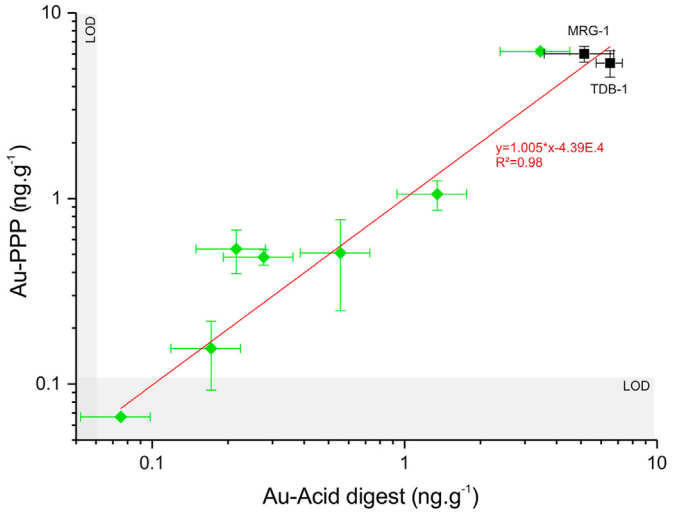

Fig. 6. Method validation by comparing Au concentrations of natural samples from the Troodos ophiolite (green) and reference materials (black) analyzed by both PPP-LA-ICP-MS and by multi-acid digest ultra-low detection limit Au method from Pitcairn et al. [4].

appropriate for Au analysis even in the sub-ng g^{-1} range.

4. Conclusion

The use of matrix-matched PPP for calibration, interference correction (by using Ta- and Hf-doped pellets) and calculation of detection limits allows to push further the use of Au analysis by PPP-LA-ICP-MS. This can be achieved with specific laser and ICP-MS tuning for pellet ablation (e.g. high laser frequency, large beam, raster profiles). Improving the sensitivity and the method limit of detection, even marginally, allows the method to be applied to most geological materials, including Au-depleted rocks.

Author statement

C.G.C. Patten: conceptualization, formal analysis, methodology, funding acquisition, manuscript writing, **A. Beranoaguirre:** conceptualization, formal analysis, methodology, manuscript writing, **S. Hector:** conceptualization, formal analysis, methodology, manuscript editing, **D. Gudelius:** conceptualization, methodology, manuscript editing, **J. Kolb:** Funding acquisition, manuscript editing, **E. Eiche:** Laboratory administration, manuscript editing.

Declaration of competing interest

The authors declare that they have no known competing financial interests or personal relationships that could have appeared to influence the work reported in this paper.

Data availability

Data will be made available on request.

Acknowledgments

The authors would like to thank Thomas Belgrano and an anonymous reviewer for thorough reviews as well as Julia Laskin for editorial handling. This project was funded by the DFG grant INST 121384/213-1 FUGG.

Appendix A. Supplementary data

Supplementary data to this article can be found online at https://doi.org/10.1016/j.ijms.2023.117039.

References

[1] I.K. Pitcairn, D.A.H. Teagle, D. Craw, G.R. Olivo, R. Kerrich, T.S. Brewer, Sources of metals and fluids in orogenic gold deposits: insights from the Otago and Alpone schists, New Zealand, Econ. Geol. 101 (2006a) 1525–1546.
[2] I.K. Pitcairn, Background concentrations of gold in different rock types, B. Appl. Earth Sci. 120 (2011) 31–38.
[3] F.E. Jenner, H.S.C. O'Neill, Analysis of 60 elements in 616 ocean floor basaltic glasses, G-cubed 13 (2012).
[4] I.K. Pitcairn, P.E. Warwick, J.A. Milton, D.A.H. Teagle, Method for ultra-low-level analysis of gold in rocks, Anal. Chem. 78 (2006b) 1290–1295.
[5] Y. Liu, B. Wan, D. Xue, Sample digestion and combined preconcentration methods for the determination of ultra-low gold levels in rocks, Molecules 24 (2019) 1778.
[6] Y. Liu, Z. Wang, D. Xue, Y. Yang, W. Li, H. Cheng, C. Patten, B. Wana, An Improved Analytical Protocol for the Determination of Sub-nanogram Gold in 1–2 G Rock Samples Using GFAAS after Polyurethane Foam Pretreatment, 2020.
[7] K. Schlöglova, M. Wälle, C.A. Heinrich, LA-ICP-MS analysis of fluid inclusions: contamination effects challenging micro-analysis of elements close to their detection limit, J. Anal. At. Spectrom. 32 (2017) 1052–1063.
[8] T.M. Belgrano, J.A. Milton, D.A.H. Teagle, Determination of Ultra-Trace Au, Ag, as, Pt and Re Mass Fractions in Volcanic Glasses and Rock Powders by LA-ICP-MS, Geostandards and Geoanalytical Research, 2022.
[9] D. Garbe-Schönberg, S. Müller, Nano-particulate pressed powder tablets for LA-ICP-MS, J. Anal. At. Spectrom. 29 (2014) 990–1000.
[10] D. Peters, T. Pettke, Evaluation of major to ultra trace element bulk rock chemical analysis of nanoparticulate pressed powder pellets by LA-ICP-MS, Geostand. Geoanal. Res. 41 (2017) 5–28.
[11] I.K. Pitcairn, N. Leventis, G. Beaudoin, S. Faure, C. Guilmette, B. Dubé, A Metasedimentary Source of Gold in Archean Orogenic Gold Deposits, 2021 (Geology).
[12] C.G.C. Patten, I.K. Pitcairn, D.A. Teagle, M. Harris, Mobility of Au and related elements during the hydrothermal alteration of the oceanic crust: implications for the sources of metals in VMS deposits, Miner. Deposita 51 (2015) 1–22.
[13] Z. Hu, Y. Liu, M. Li, S. Gao, L. Zhao, Results for rarely determined elements in MPI-DING, USGS and NIST SRM glasses using laser ablation ICP-MS, Geostand. Geoanal. Res. 33 (2009) 319–335.
[14] K.P. Jochum, U. Nohl, Reference materials in geochemistry and environmental research and the GeoReM database, Chem. Geol. 253 (2008) 50–53.
[15] S. Gilbert, P. Olin, J. Thompson, E. Lounejeva, L. Danyushevsky, Matrix dependency for oxide production rates by LA-ICP-MS, J. Anal. At. Spectrom. 32 (2017) 638–646.
[16] I. Kroslakova, D. Günther, Elemental fractionation in laser ablation-inductively coupled plasma-mass spectrometry: evidence for mass load induced matrix effects in the ICP during ablation of a silicate glass, J. Anal. At. Spectrom. 22 (2007) 51–62.
[17] J. Fietzke, M. Frische, Experimental evaluation of elemental behavior during LA-ICP-MS: influences of plasma conditions and limits of plasma robustness, J. Anal. At. Spectrom. 31 (2016) 234–244.
[18] I.K. Pitcairn, D. Craw, D.A.H. Teagle, Metabasalts as sources of metals in orogenic gold deposits, Miner. Deposita 50 (2015) 373–390.
[19] C.G.C. Patten, I.K. Pitcairn, J.C. Alt, T. Zack, Y. Lahaye, D.A.H. Teagle, K. Markdahl, Metal fluxes during magmatic degassing in the oceanic crust: sulfide mineralisation at ODP site 786B, Izu-Bonin forearc, Miner. Deposita 55 (2020a).
[20] M. Constantin, Trace element data for gold, iridium and silver in seventy geochemical reference materials, Geostand. Geoanal. Res. 33 (2009) 115–132.
[21] H.S.R. Hughes, I. McDonald, J.W. Faithfull, B.G.J. Upton, M. Loocke, Cobalt and precious metals in sulphides of peridotite xenoliths and inferences concerning their distribution according to geodynamic environment: a case study from the Scottish lithospheric mantle, Lithos 240 (2016) 202–227.
[22] K.P. Jochum, U. Weis, B. Schwager, B. Stoll, S.A. Wilson, G.H. Haug, M.O. Andreae, J. Enzweiler, Reference values following ISO guidelines for frequently requested rock reference materials, Geostand. Geoanal. Res. 40 (2016) 333–350.
[23] S. Goderis, B.M. Simonson, I. McDonald, S.W. Hassler, A. Izmer, J. Belza, H. Terryn, F. Vanhaecke, P. Claeys, Ni-rich spinels and platinum group element nuggets condensed from a Late Archaean impact vapour cloud, Earth Planet Sci. Lett. 376 (2013) 87–98.
[24] S. Terashima, M. Taniguchi, Fractional determination of gold in twenty six geological reference materials by sequential extraction with graphite furnace atomic absorption spectrometry, Geostand. Newsl. 24 (2000) 7–17.
[25] G. Garuti, S. Meloni, M. Oddone, NAA of Platinum group elements and gold in reference materials: a comparison of two methods, J. Radioanal. Nucl. Chem. 245 (2000) 17–23.
[26] K. Govindaraju, P.J. Potts, P.C. Webb, J.S. Watson, 1994 report on Whin Sill dolerite WS-E from England and Pitscurrie microgabbro PM-S from Scotland: assessment by one hundred and four international laboratories, Geostand. Newsl. 18 (1994) 211–300.
[27] R.M.S. Louis, Gold in BHVO-1, BIR-1, DNC-1 and BCR-1 by fire-assay preconcentration neutron activation analysis: sample size vs. accuracy, Geostand. Newsl. 11 (1987) 151–157.
[28] H. Cheng, Z. Wang, K. Chen, K. Zong, Z. Zou, T. He, Z. Hu, M. Fischer-Gödde, Y. Liu, High-precision determination of gold mass fractions in geological reference materials by internal standardisation, Geostand. Geoanal. Res. 43 (2019) 663–680.
[29] C.G.C. Patten, I.K. Pitcairn, F. Molnár, J. Kolb, G. Beaudoin, C. Guilmette, A. Peillod, Gold mobilization during metamorphic devolatilization of Archean and Paleoproterozoic metavolcanic rocks, Geology 48 (2020b) 1110–1114.

Supplementary data

Appendix 1. Gold data for serpentinite samples from the Troodos ophiolite shown in figure 6				
Method	Multiple acid digest (Pitcairn 2006b)		PPP-LA-ICP-MS (this study)	
	Au (ng-g-1)	std.dev.	Au (ng-g-1)	std.dev.
TR.19.1.01	3,45	1,06	6,20	0,20
TR.19.1.02	1,35	0,41	1,05	0,19
TR.19.1.03	0,28	0,09	0,48	0,05
TR.19.1.05	0,17	0,05	0,16	0,06
TR.19.1.06	0,08	0,02	0,07	
TR.19.1.07	0,56	0,17	0,51	0,26
TR.19.1.12	0,22	0,07	0,53	0,14
MRG-1	5,15	1,58	6,01	0,59
TDB-1	6,51	0,77	5,37	0,87

Paper II

-

Multi-source and multi-stage metal mobilization during the tectonic evolution of the Central Lapland Greenstone Belt, Finland: implications for the formation of orogenic Au deposits.

Patten CGC, Molnár F, Pitcairn IK, Kolb J, Mertanen S, **Hector S** (2022) Mineralium Deposita

Mineralium Deposita (2023) 58:461–488
https://doi.org/10.1007/s00126-022-01133-z

ARTICLE

Multi-source and multi-stage metal mobilization during the tectonic evolution of the Central Lapland Greenstone Belt, Finland: implications for the formation of orogenic Au deposits

C. G. C. Patten[1] · F. Molnár[2,3] · I. K. Pitcairn[4] · J. Kolb[1] · S. Mertanen[2] · S. Hector[1]

Received: 7 August 2021 / Accepted: 26 July 2022 / Published online: 11 September 2022

Abstract

Precambrian greenstone belts are prospective terrains for orogenic Au deposits worldwide, but the sources of Au, base metals, metalloids, and ligands enriched within the deposits are still debated. Metamorphic devolatilization is a key mechanism for generating Au-rich hydrothermal fluids, but the respective role of the metavolcanic and metasedimentary rocks present within these belts in releasing ore-forming elements is still not fully understood. The Central Lapland Greenstone Belt (CLGB), Finland, one of the largest Paleoproterozoic greenstone belts, hosts numerous orogenic Au deposits and is composed of variably metamorphosed volcanic and sedimentary rocks. Characterization of element behavior during prograde metamorphism highlights that (1) metavolcanic rocks release significant Au, As, Sn, Te, and possibly S; (2) metasedimentary rocks release significant S, C, Cu, As, Se, Mo, Sn, Sb, Te, and U, but limited Au; and (3) metakomatiite releases C and possibly Au. Throughout the CLGB metamorphic evolution, two main stages are identified for metal mobilization: (1) prograde metamorphism at ~ 1.92–1.86 Ga, promoting the formation of typical orogenic Au deposits and (2) late orogenic evolution between ~ 1.83 and 1.76 Ga, promoting the formation of both typical and atypical orogenic Au deposits. The complex lithologic diversity, tectonic evolution, and metamorphic history of the CLGB highlight that metal mobilization can occur at different stages of an orogenic cycle and from different sources, stressing the necessity to consider the complete dynamic and long-lasting evolution of orogenic belts when investigating the source of Au, ligands, metals, and metalloids in orogenic Au deposits.

Keywords Orogenic Au deposits · Metamorphic devolatilization · Metal mobilization · Metavolcanic rocks · Metasedimentary rocks

Introduction

Orogenic Au deposits are structurally controlled hydrothermal ore deposits that form in orogenic belts and account for a significant portion of the present and past global Au production (~ 30%; Frimmel 2018). These deposits are the product of complex large-scale processes, which include the production of metal-rich fluids, the transport of these fluids through the Earth's crust, and the precipitation of metals in structurally controlled locations at various degrees of metamorphism (Groves 1993, 1998; Pitcairn et al. 2006a; Large et al. 2011; Goldfarb and Groves 2015; Kolb et al. 2015). Production of metal-rich fluids is of paramount importance in the formation of any hydrothermal ore deposit (e.g., Fyfe 1987). Recognition of geological formations as sources of metals, ligands, and ore forming fluids is an important step for the investigation of metal-rich hydrothermal

Editorial handling: H. E. Frimmel

✉ C. G. C. Patten
clifford.patten@kit.edu

[1] Institute of Applied Geosciences, Chair of Geochemistry and Economic Geology, Karlsruhe Institute of Technology, 76131 Karlsruhe, Germany

[2] Geological Survey of Finland, P.O. Box 96, FI-02151 Espoo, Finland

[3] Institute of Geography and Earth Sciences, Budapest University, 1117 Budapest, Hungary

[4] Department of Geological Sciences, Stockholm University, SE-106 91 Stockholm, Sweden

fluid genesis and ultimately for hydrothermal ore deposit formation. Although the mechanisms responsible for Au precipitation from hydrothermal fluids and the formation of orogenic Au deposits are fairly well constrained (Groves 1993; Groves et al. 1998; McCuaig and Kerrich 1998; Goldfarb and Groves 2015; Gaboury 2019), the sources of the metals, ligands, and fluids as well as the mineral reactions leading to the formation of Au-rich hydrothermal fluids are still debated (Goldfarb and Groves 2015; Groves et al. 2019). Three main sources have been proposed to generate metal-rich fluids in orogenic gold systems: (1) metamorphic devolatilization of supracrustal rocks (Fyfe 1987; Groves and Phillips 1987; Wyman and Kerrich 1988; Phillips and Powell 2010; Tomkins 2010), (2) subcontinental lithospheric mantle (Groves et al. 2019), and (3) magmatic sources (Burrows et al. 1986; Thébaud et al. 2018; Masurel et al. 2019).

In Precambrian greenstone belts hosting orogenic Au deposits, the source of metals and ligands is particularly cryptic (Goldfarb and Groves 2015; Groves et al. 2019), although metamorphic devolatilization appears to be a key process (Beaudoin and Chiaradia 2016; Patten et al. 2020; Pitcairn et al. 2021). Greenstone belts are dominated by metavolcanic rocks (basalt to rhyolite) with varying proportions of metasedimentary rocks and metakomatiite (de Wit and Ashwal 1995). The respective role of each lithology during metamorphic devolatilization in supplying metals, ligands, and/or hydrothermal fluids during dynamic and long-lasting orogenic evolution still remains poorly constrained. Metamorphic devolatilization of metasedimentary rocks is an efficient mechanism for generating metamorphic fluids enriched in S, As, and Au, the most common elements found in orogenic Au deposits (e.g., Boyle 1966; Pitcairn et al. 2006a, 2021; Tomkins 2010; Large et al. 2011; Goldfarb and Groves 2015). The scarcity of metasedimentary rocks relative to metavolcanic rocks in greenstone belts, however, implies that they cannot solely account for the formation of orogenic Au deposits (Goldfarb and Groves 2015). Metavolcanic rocks in greenstone belts, conversely, have long been suggested as potential source for metals (Phillips et al. 1987; Hronsky et al. 2012; Goldfarb and Groves 2015; Augustin and Gaboury 2017), and although they can release enough Au to account for orogenic gold endowment (Pitcairn et al. 2015; Patten et al. 2020), their capacity in releasing S, As, and other metals remains controversial (Goldfarb and Groves 2015; Pitcairn et al. 2015; Groves et al. 2019).

The Central Lapland Greenstone Belt (CLGB) in northern Finland is one of the largest known Paleoproterozoic greenstone belts (Hanski and Huhma 2005) and is an excellent target to study the source of metals in Precambrian orogenic Au deposits. The CLGB consists of a Paleoproterozoic sequence of oceanic crustal rocks and marine sedimentary rocks. The northern part of the CLGB is dominated by two main volcano-sedimentary sequences: the Kittilä and the Savukoski groups (Fig. 1). The Kittilä Group is dominated by tholeiitic metavolcanic rocks interbedded with various metasedimentary units (Hanski and Huhma 2005). The Savukoski Group is characterized by komatiitic and picritic metavolcanic rocks, which overlay pelitic metasedimentary rocks (Hanski and Huhma 2005). The CLGB displays a complex metamorphic pattern defined by zonation where the central area of the belt is metamorphosed at greenschist facies, whereas the margins are metamorphosed at amphibolite or granulite facies (Hölttä et al. 2007; Hölttä and Heilimo 2017).

The CLGB hosts numerous orogenic Au deposits, such as the 302 t Au Suurikuusikko deposit, but is relatively unexplored compared to other Paleoproterozoic greenstone belts (Mineral Deposit Database of Finland 2022; Niiranen et al. 2015). The orogenic Au deposits are preferentially located along the Kiistala shear zone (KiSZ) and the Sirkka shear zone (SiSZ), and are characterized by typical (Au-only) and atypical (Au-Cu-Co–Ni) metal associations (Eilu et al. 2007; Eilu 2015). Apart of a few occurrences in the marginal zones of the CLGB, most of the Au deposits occur in comparable lithological and structural settings characterized by greenschist facies metamorphism and have formed under similar physico-chemical conditions (Eilu et al. 2007; Eilu 2015). This suggests that the differences in the composition of the various deposits are, to some extent, controlled by the geochemical peculiarities of the source rocks.

In this study, we investigate the extent to which lithological units present in a greenstone belt contribute to the generation of metal-rich metamorphic fluids during metamorphic devolatilization. The outcomes show that combined metamorphic devolatilization of metavolcanic and metasedimentary rocks release sufficient metals and ligands to account for most of the Au and other metal endowments in orogenic Au deposits.

Tectonic setting

The Central Lapland Greenstone Belt

The CLGB is located in northern Finland and is exposed over an area of ≈ 20,000 km^2 (Fig. 1). It rests on the Archean (3.1–2.6 Ga) Karelian Craton. The volcano-sedimentary sequence records a complex geological evolution spanning from 2.45 to 1.76 Ga, including the 1.92–1.80 Ga Svecofennian orogeny (Hanski et al. 2001a; Hanski and Huhma 2005; Nironen 2017; Sayab et al. 2019). The CLGB is bound in the northeast by the Lapland Granulite Complex and to the south by the

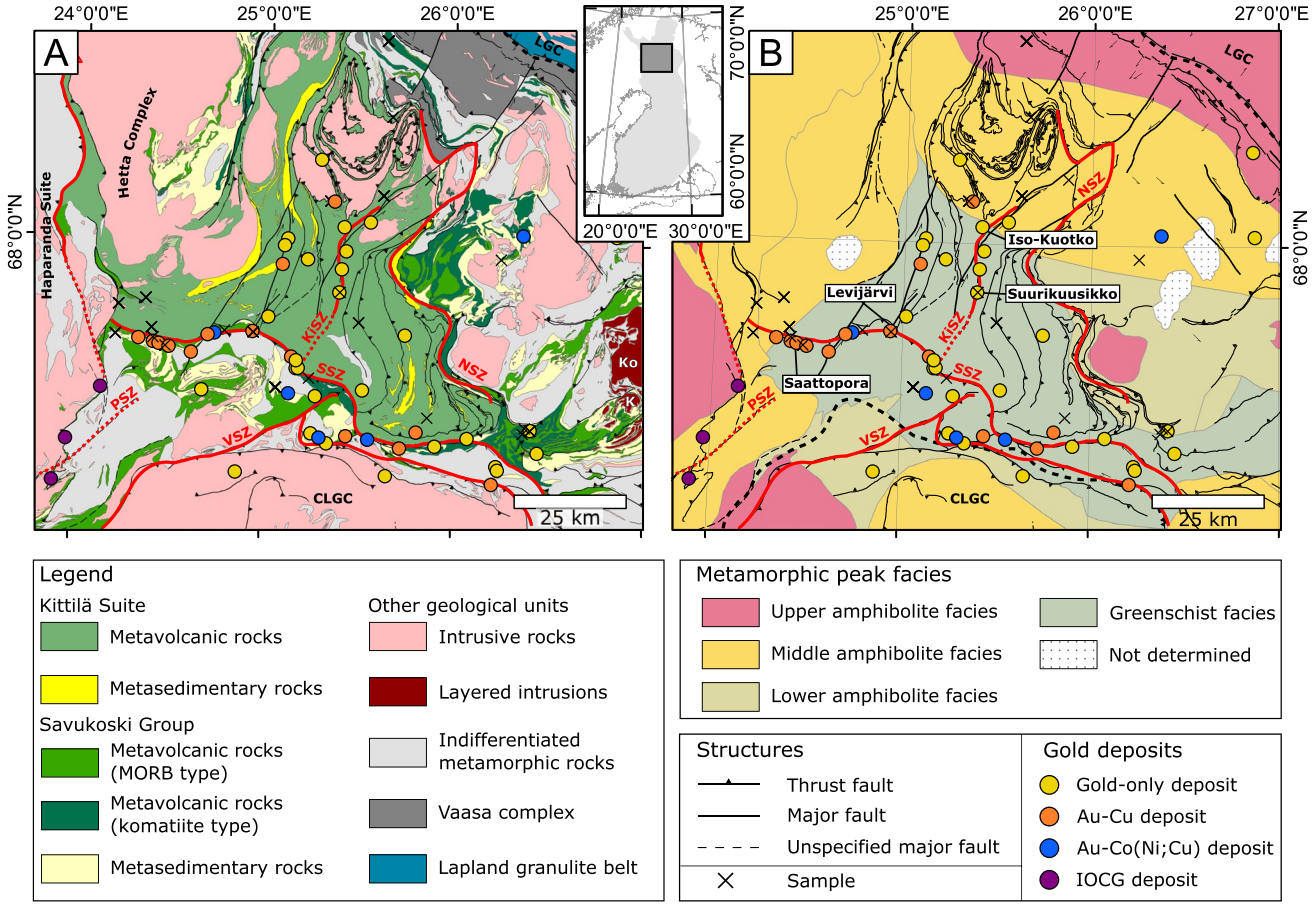

Fig. 1 Regional geological (**A**) and metamorphic map of the CLGB (**B**) showing major lithological units and orogenic Au deposits and showing major fault zones (KiSZ = Kiistala Shear Zone, SiSZ = Sirkka Shear Zone, PSZ: Pajala Shear Zone; VSZ: Venejoki Shear Zone, ESZ: Enontekiö Shear Zone; NSZ = Nolppio Shear Zone) complexes (CLGC = Central Lapland Granitoid Complex, LGC = Lapland Granulite Complex), intrusions (Ko: Koitelainen layered intrusion, K: Kevitsa layered intrusion), and sampled drillcore locations (black crosses). Simplified from the digital database of the Geological Survey of Finland

Central Lapland Granitoid Complex (Fig. 1). The Pajala Shear Zone separates the CLGB from the Norrbotten structural domain in the west. To the east and southeast, the CLG is bound by the Nolppio Thrust and Nolppio Shear Zone.

The CLGB is divided into six main lithostratigraphic units from the base to the top of the lithostratigraphy: the Salla, Onkamo (or Kuusamo), Sodankylä, Savukoski, Kittilä, Laino, and Kumpu groups. The Salla and Onkamo groups are dominated by intermediate to felsic metavolcanic rocks and metakomatiite, respectively. They formed during rifting of the Archean basement at ca. 2.45–2.2 Ga (Hanski and Huhma 2005; Hanski et al. 2001a). At ca. 2.45 Ga, several layered igneous complexes (e.g., Koitelainen layered intrusion) were emplaced in the Salla Group but not the Onkamo Group. The Sodankylä Group is characterized by continental metasedimentary rocks, such as quartzite and mica schist. They correspond to a long depositional period before 2.2 Ga, the age of mafic dikes cutting this unit (Hanski et al. 2001a; Hanski and Huhma 2005). The Sodankylä Group metasedimentary rocks grade transgressively into the deeper-water pelitic sedimentary rocks of the Savukoski Group (Hanski and Huhma 2005). The Savukoski Group metasedimentary rocks are overlain by komatiitic and picritic-dominated metavolcanic rocks with 2.05 Ga minimum age corresponding to the age of the Kevitsa-layered intrusion (Hanski and Huhma 2005; Hanski et al. 2001a). Some of the volcanic rocks in the Kittilä Group are probably parautochthonous, and some consist of 2.01 Ga allochthonous tholeiitic metavolcanic rocks representative of an ancient oceanic lithosphere (Hanski and Huhma 2005). It is subdivided into four formations: (1) the Kautileskä Formation, dominated by metavolcanic rocks with within plate basalt (WPB) affinity and minor metasedimentary rocks such as phyllite, black schist, metagraywacke, and metacarbonate rocks; (2) the Porkonen Formation, dominated

by banded iron formation; (3) the Vesmajärvi Formation, dominated by metavolcanic rocks with mid-oceanic ridge basalt (MORB) affinity; and (4) the Pyhäjärvi Formation, dominated by micaschist and metagreywacke (Lehtonen et al. 1998; Hanski and Huhma 2005). At 1.92 Ga, the Kittilä Group has been thrust onto the Savukoski Group (Hanski and Huhma 2005). Finally, the Laino and Kumpu groups cap unconformably the previous groups and are characterized by molasse-type sediments of ca. 1.88 Ga maximum age (Hanski and Huhma 2005; Hanski et al. 2001a; Hölttä et al. 2007).

Deformation and metamorphism of the CLGB

The CLGB is characterized by a complex tectonic evolution defined by different deformation and metamorphic events in space and time. Following Archean basement extension, deformation occurred at ca. 1.93–1.91 Ga with east–west bulk shortening (D1) as the result of the collision between the Norrbotten and Karelia blocks and development of a foreland fold-and-thrust-belt (Hanski and Huhma 2005; Nironen 2017; Sayab et al. 2019). Tectonic juxtaposition of the Kittilä Group onto the Savukoski Group led to formation of moderately dipping thrust zones within and at the base of the Kittilä Group, such as the KiSZ (Hanski and Huhma 2005; Nironen 2017; Sayab et al. 2019). Shortly after D1, the collision between the Karelia and Lapland-Kola blocks at ca. 1.90–1.89 Ga led to north–south shortening (D2) and thrusting of the Lapland Granulite Belt onto the CLGB from the northeast. To the south, D2 led to a new east–west orientated thrust system with the development of the SiSZ and leading to the thrusting of the Savukoski Group onto the Kittilä Group. The KiSZ, truncated by the SiSZ in the south, acted as transfer fault (Hanski and Huhma 2005; Nironen 2017; Sayab et al. 2019). Progressive clockwise rotation into northeast-vergent compression occurred at ca. 1.88–1.87 Ga (D3), switching the deformation regime from compressional to transpressional and leading to dextral strike-slip in the KiSZ (Hanski and Huhma 2005; Nironen 2017; Sayab et al. 2019). A nearly 90° switch in the regional stress field occurred at ca. 1.84–1.81 Ga leading to a northwest-southeast compressional regime (D4). The D4 led to flipping of the kinematics in the KiSZ from dextral to sinistral strike-slip and to reactivation of the SiSZ (Nironen 2017; Sayab et al. 2019). Orogenic collapse occurred during 1.80–1.77 Ga with NE-SW extension and granite emplacement (Hanski and Huhma 2005; Nironen 2017). At ca. 1.77–1.76 Ga, east–west shortening (D5) led to localized fault reactivation (Nironen 2017; Sayab et al. 2019).

In the CLGB, the Paleoproterozoic volcanic-sedimentary sequence was affected by several metamorphic events, the intensity and timing of which did not occur homogeneously throughout the belt, leading to a complex metamorphic pattern. In the central part of the CLGB, peak metamorphism is inferred at ca. ~ 1.88–1.86 Ga during D2–D3 and reached greenschist-facies conditions at 250–400 °C, the lowest metamorphic grade of the belt (Fig. 1; Hölttä et al. 2007; Hölttä and Heilimo 2017; Nironen 2017; Molnár et al. 2018). Metavolcanic and metasedimentary rocks generally preserved their primary magmatic and sedimentary textures (Hölttä et al. 2007). Age of metamorphism in the external part of the belt is less well constrained. Progressive thrusting of the Lapland Granulite Belt during D2–D3 onto the CLGB from the northeast led to inverted metamorphic gradients in the northeastern part of the latter (Hölttä et al. 2007; Hölttä and Heilimo 2017). Granulite-facies metamorphism (770–890 °C) was initiated at ca. 1.89 Ga at the margin of the Lapland Granulite Belt and propagated towards the southwest into the CLGB until ~ 1.82 Ga, leading to amphibolite-facies metamorphism (Fig. 1; Hölttä and Heilimo 2017; Nironen 2017). In the western part of the CLGB, thrusting towards the east of the Haparanda Suite along the Enontekiö Shear Zone, at ca. 1.86–1.85 Ga, led as well to inverted metamorphic gradient up to mid-amphibolite facies (Bergman et al. 2006; Nironen 2017). Additionally, thrusting during D3–D4 from the south resulted in emplacement of amphibolite-facies metamorphic rocks from the Central Lapland Granitoid Complex onto the Savukoski Group in the southern part of the CLGB along the Venejoki Shear Zone (Fig. 1; Bergman et al. 2006; Hölttä et al. 2007; Hölttä and Heilimo 2017; Nironen 2017; Lahtinen et al. 2018). The resulting effect from thrusting of the Lapland Granulite Belt from the north-northeast, the Haparanda Suite from the west, and the Central Lapland Complex from the south explains the specific concentric metamorphic pattern of the CLGB with greenschist facies in the center and increasing metamorphic grade outwards (Fig. 1). These complex and long-lasting thrusting events on the margins of the CLGB most likely led to different ages of peak metamorphism for the lithological units of the CLGB. These are most likely related to D2–D3, but a more detailed constraint on these ages is not currently available (Hölttä et al. 2007; Hölttä and Heilimo 2017; Nironen 2017; Sayab et al. 2019). A late metamorphic event throughout the belt at around ~ 1.80–1.78 Ga and related to D4–D5 is outlined by U–Pb ages of metamorphic titanites and monazite, possibly related to orogenic collapse (Rastas et al. 2001; Hölttä et al. 2020). Finally, concomitantly to metamorphism, several crustal melting events produced orogenic granitoids at ~ 1.88–1.87 Ga and ~ 1.81–1.77 Ga throughout the CLGB (Fig. 1; Ahtonen et al. 2007; Lahtinen et al. 2018).

Table 1 Main typical and atypical orogenic Au deposits of the CLGB

Deposit	Deposit type	Structural control	Ore assemblage	Age	Deformation stage	Gold occurrence	References
Suurikuusikko	Typical Au-only	KiSZ	Py, Apy	1.92 Ga	D1	Refractory	Patison (2007), Wyche et al. (2015), Molnár et al. (2018), Sayab et al. (2019)
Iso-Kuotko	Typical Au-only	KiSZ	Apy, Py, Po, Cpy, Gn	1.87–1.86 Ga; main event at 1.77–1.76 Ga	D5	Native and refractory	Molnár et al. (2018), Sayab et al. (2019)
Levijärvi-Loukinen	Atypical Au-Cu-Ni-Co	SiSZ	Po, Cpy, Py, Ger, Aspy	1.90–1.76 Ga; main event at 1.8–1.76 Ga	D2–D5	Native and inclusions	Molnár et al. (2017), Kurhila et al. (2017), Holma and Keinanen (2007), Patison (2007), Nironen (2017), Sayab et al. (2019)
Saattopora	Atypical Au-Cu	SiSZ	Po, Cpy, Pn, Ger, Cob, Aspy	1.87–1.79 Ga; main event at 1.82–1.79 Ga	D4	Native and inclusions	Molnár et al. (2019), Patison (2007); Nironen (2017), Sayab et al. (2019)

Py pyrite, *Apy* arsenopyrite, *Po* pyrrhotite, *Cpy* chalcopyrite, *Gn* galena, *Pn* pentlandite, *Cob* cobaltite, *Ger* gesdorffite

Gold endowment in the CLGB

Orogenic Au deposits in the CLGB are spatially controlled by the KiSZ and SiSZ (Fig. 1; Patison 2007). The typical orogenic Au deposits are best represented by the Suurikuusikko deposit (Kittilä mine), the largest Au mine in Europe with ~ 302 t Au reserves, and the Iso-Kuotko deposit, 12 km north of the Suurikuusikko deposit along the KiSZ (Fig. 1; Table 1; Mineral Deposit Database of Finland 2022). The atypical orogenic Au deposits, on the other hand, are best represented by the Au-Cu Saattopora and the Au-Cu-Ni-Co Levijärvi-Loukinen deposits, located in the western and central part of the SiSZ, respectively (Fig. 1; Table 1; Holma and Keinanen 2007; Kurhila et al. 2017; Molnár et al. 2017).

The typical and atypical orogenic Au deposits in the CLGB share many characteristics. They show strong structural control, and the orebodies generally occur as swarms of elongated lodes (Eilu et al. 2007; Eilu 2015). Differences in rheological properties of rock types present, such as ultramafic and metasedimentary rocks, have important control on the mineralization, especially when competency is enhanced by early albite alteration promoting brittle behavior (Eilu et al. 2007; Patison 2007; Eilu 2015). Most of the deposits formed under similar temperature and pressure conditions, at 250–450 °C and 1–3 kbar, respectively, and the ores typically contain 1–5% sulfide with gold being either free, as inclusions or refractory (Eilu et al. 2007; Eilu 2015; Sayab et al. 2016). Despite the similarities, the typical and atypical orogenic Au deposits also show important differences. The typical orogenic Au deposits are generally dominated by pyrite, pyrrhotite, and arsenopyrite whereas the atypical ones show greater mineralogical diversity with pyrite, pyrrhotite, arsenopyrite, chalcopyrite, cobaltite, pentlandite, and gersdorffite, reflecting differences in metal endowment (Table 1; Eilu 2015). The typical orogenic Au deposits are preferentially located along the KiSZ whereas the atypical ones are located along the SiSZ (Fig. 1). Geochronological studies indicate that orogenic Au mineralization in the CLGB occurred during the D1–D3 events, at ~ 1.92–1.86 Ga, and later during the D4–D5 events at ~ 1.81–1.76 Ga (Wyche et al. 2015; Molnár et al. 2018; Sayab et al. 2019). The first Au mineralization stage in the CLGB, occurring as early as 1.92 Ga and apparently pre-dating peak metamorphism at the Suurikuusikko deposit (Wyche et al. 2015; Molnár et al. 2018), appears to be best recorded along the KiSZ whereas the second Au mineralization stage is recorded along both the KiSZ and SiSZ (e.g., Iso-Kuotko, Saattopora and Levijärvi-Loukinen; Table 1).

Sampling and analytical method

A suite of 105 drill core samples from the Kittilä Group and Savukoski Group, distal from the hydrothermally altered zones surrounding gold deposits, were selected. They are representative of the variation in lithology and metamorphic facies within the CLGB (Fig. 1). They include 36 metavolcanic rocks and 17 metasedimentary rocks from the Kittilä Group and 25 metavolcanic and 27 metasedimentary rocks from the Savukoski Group (ESM 1). The metamorphic grade ranges from greenschist to upper amphibolite facies with greenschist-facies samples generally preserving their primary features such as pillow rims and vesicles in metavolcanic rocks, whereas upper amphibolite-facies samples are variably foliated, sheared, and deformed. Of the selected samples, 43 are metamorphosed to greenschist facies (300–400 °C), 35 to lower amphibolite facies (450–550 °C), and 29 to upper amphibolite facies (> 550 °C; Hölttä and Heilimo 2017).

Major and trace elements were analyzed for in two batches by ALS Minerals and Labtium. From the samples sent to ALS Mineral, major elements were analyzed for by XRF; Ba, Ce, Cr, Cs, Dy, Er, Eu, Ga, Cd, Ge, Hf, Ho, La, Lu, Nb, Nd, Pr, Rb, Sm, Sn, Sr, Ta, Tb, Th, Tm, U, V, W, Y, Yb, and Zr by ICP-MS from lithium borate fusion disks after acid digest; Ag, Cd, Co, Cu, Li, Mo, Ni, Pb, Sc, and Zn by ICP-AES after four acid digest (HNO_3, HF, $HClO_4$, HCl); As, Bi, Hg, In, Re, Sb, Sc, Se, Te, and Tl by ICP-MS after aqua regia acid digest; and S and C by LECO furnace. A suite of standards (GIOP-102 for XRF analysis; AMIS0304, GBM908-10, GBM908-5, and GEOMS-03 for ICP-MS analysis; GEOMS-03 for ICP-AES analysis; GGC-09, GS303-9, GS310-10, and GS910-4 for LECO furnace analysis), duplicated samples, and blanks were analyzed to check for accuracy, precision, and limits of detection (ESM 2). For the samples sent to Labtium, major elements were analyzed for by XRF on pressed pellets; Ce, Dy, Er, Eu, Gd, Hf, Ho, La, Lu, Nb, Nd, Pr, Rb, Sm, Ta, Tb, Th, Tm, U, Y, Yb, Ag, As, Be, Bi, Cd, Ce, Dy, Er, Eu, Gd, Hf, Ho, La, Lu, Mo, Nb, Nd, Pr, Rb, Sm, Ta, Tb, Lu, Nb, Nd, Pb, Pr, Rb, Sb, Se, Sm, Sn, Ta, Tb, Te, Th, Tm, U, W, Y, and Yb by ICP-MS after HF-$HClO_4$ and aqua regia digestion; Co, S, Sc, V, and Zr by ICP-AES after HF-$HClO_4$ digest; and C by C-analyzer. A suite of standards was analyzed to check for accuracy, precision, and limit of detections (ESM 2). Gold whole rock analyses were carried out at Stockholm University following the ultra-low detection limit technique developed by Pitcairn et al. (2006b). To minimize possible nugget effects, 3 g of sample powder was digested by HNO_3-HF-aqua regia into liquid solution. The solutions were analyzed using a Thermo Fisher XSeries 2 ICP-MS. The 3σ method detection limit calculated from blank digests is 0.027 ppb. Analytical accuracy and precision were controlled through analyses of CANMET reference material TDB-1 and USGS reference materials WMS-1 and CH-4, which have reproducibility of 104%, 91%, and 87%, respectively (Patten et al. 2020).

Rock classification

Metavolcanic rocks

The Kittilä and Savukoski groups contain several genetically unrelated metavolcanic rocks (Lehtonen et al. 1998; Hanski and Huhma 2005), and thus, metavolcanic rocks show significant variations in major and trace element concentrations (Table 2).

Kittilä Group

Samples from the Kittilä Group are MORB ($n = 13$), WPB ($n = 17$), and boninite-like dikes ($n = 6$; Fig. 2; Hanski and Huhma 2005). The MORB-like samples, which are part of the Vesmajärvi Formation (Lehtonen et al. 1998; Hanski and Huhma 2005), are dominantly basalt (45.2–53.0 wt% SiO_2) with tholeiitic to transitional affinity (Zr/Y < 3.75 and Th/Yb < 0.69; Fig. 2). Relatively flat REE profiles ($La/Yb_{pm} = 1.70 \pm 0.72$; Fig. 2) suggest an E-MORB affinity. The WPB-like samples, which are part of the Kautoleskä Formation (Lehtonen et al. 1998; Hanski and Huhma 2005), are also dominantly basaltic (46.0–51.6 wt% SiO_2), but have slightly higher $Na_2O + K_2O$ content than the MORB-like samples (3.93 ± 1.1 wt%), and three samples classify as trachy-basalt (Fig. 2). The WPB-like samples have a transitional to calc-alkaline affinity (Zr/Y > 4.61 and Th/Yb > 0.42; Fig. 2). The REE profiles show LREE enrichment relative to HREE ($La/Yb_{pm} = 5.91 \pm 2.75$; Fig. 2) and significant negative Ta and Nb anomalies relative to Th ($Ta/Th_{pm} = 0.69 \pm 0.36$ and $Nb/Th_{pm} = 0.76 \pm 0.45$). The boninite-like dikes are characterized by higher MgO (8.79 ± 0.28 wt%) and lower TiO_2 (0.51 ± 0.04 wt%; Table 1) than MORB and WPB and have a transitional affinity (1.7–3.09 Zr/Y and 0.41–0.52 Th/Yb; Fig. 2). Their REE profiles show slight LREE enrichment relative to HREE ($La/Yb_{pm} = 2.1 \pm 0.2$; Fig. 2) and slight negative Ta and Nb anomalies relative to Th ($Ta/Th_{pm} = 0.32 \pm 0.03$ and $Nb/Th_{pm} = 0.44 \pm 0.05$; Fig. 2).

Table 2 Whole rock composition of the different lithologies present in the Kiitilä and Savukoski groups

		SiO_2 wt%	Al_2O_3 wt%	Fe_2O_3 wt%	MgO wt%	CaO wt%	Na_2O wt%	K_2O wt%	TiO_2 wt%	P_2O_5 wt%	MnO wt%	Total wt%	LOI wt%	S wt%	C wt%	Co ppm	Cu ppm	As ppm	Se ppm	Mo ppm	Sn ppm	Sb ppm	Te ppm	Au ppb	U ppm
Metavolcanic rocks from Kittilä Group and Savukoski Suite																									
MORB ($n=19$)	Mean	49.0	14.1	13.6	6.9	10.0	2.5	0.4	1.30	0.18	0.21	98.2	2.1	0.16	0.32	48.70	83.94	11.56	0.62	0.87	1.36	0.16	0.02	1.27	0.03
	σ	2.0	1.0	2.2	1.7	2.2	0.9	0.4	0.40	0.16	0.03	1.1	2.0	0.17	0.40	9.80	51.27	22.30	0.35	0.53	0.84	0.09	0.02	1.91	0.03
	Median	**48.8**	**14.2**	**13.2**	**7.2**	**10.3**	**2.5**	**0.3**	**1.24**	**0.11**	**0.21**	**98.4**	**1.4**	**0.14**	**0.16**	**48.86**	**90.30**	**1.25**	**0.51**	**1.01**	**1.04**	**0.13**	**0.02**	**0.65**	**0.02**
WPB ($n=21$)	Mean	49.2	13.7	13.7	6.3	9.1	3.2	0.8	1.82	0.27	0.22	98.3	2.0	0.13	0.38	47.68	85.22	11.31	0.61	0.89	4.08	0.20	0.02	1.78	0.04
	σ	2.6	1.6	2.2	1.7	2.2	0.9	0.6	0.54	0.11	0.05	1.2	1.7	0.15	0.34	12.71	58.87	19.12	0.27	0.58	9.53	0.21	0.01	2.83	0.04
	Median	**48.7**	**13.7**	**14.2**	**6.1**	**9.1**	**3.1**	**0.8**	**1.84**	**0.24**	**0.22**	**98.7**	**1.7**	**0.09**	**0.22**	**45.51**	**71.38**	**2.11**	**0.59**	**0.69**	**0.66**	**0.12**	**0.02**	**0.69**	**0.02**
Komatiite ($n=16$)	Mean	46.5	7.4	12.3	23.9	8.4	0.6	0.1	0.53	0.04	0.17	100.0	7.9	0.06	1.38	89.11	26.83	1.26	0.18	0.38	0.14	0.15	0.87	0.66	0.02
	σ	3.1	1.9	1.6	5.3	1.9	0.8	0.1	0.24	0.02	0.03	5.0	5.5	0.09	1.55	18.18	31.49	0.98	0.12	1.12	0.07	0.05	3.33	0.57	0.01
	Median	**47.1**	**7.1**	**12.2**	**24.8**	**8.3**	**0.4**	**0.1**	**0.48**	**0.04**	**0.17**	**101.0**	**7.1**	**0.01**	**0.47**	**93.47**	**12.14**	**0.90**	**0.14**	**0.09**	**0.11**	**0.13**	**0.01**	**0.43**	**0.01**
Boninite ($n=6$)	Mean	50.5	14.6	9.2	8.8	10.8	2.5	0.7	0.51	0.04	0.19	97.7	0.9	0.16	0.06	37.54	68.31	1.56	0.31	13.13	1.01	0.08	2.60	0.79	0.03
	σ	1.6	0.7	0.5	0.3	1.0	0.7	0.4	0.04	0.00	0.01	2.8	0.3	0.18	0.07	4.10	51.30	2.85	0.10	0.00	0.00	0.04	6.32	0.47	0.02
	Median	**51.1**	**14.9**	**9.2**	**8.8**	**10.5**	**2.8**	**0.8**	**0.51**	**0.04**	**0.19**	**98.8**	**1.0**	**0.07**	**0.04**	**36.82**	**73.68**	**0.40**	**0.30**	**13.13**	**1.01**	**0.08**	**0.03**	**0.72**	**0.03**
Metasedimentary rocks from Kittilä Group and Savukoski Suite																									
Volcano-clastic rocks ($n=13$)	Mean	53.2	15.0	15.5	4.6	3.1	2.5	1.9	1.7	0.17	0.20	97.9	1.74	0.14	0.30	49.0	60.0	24.2	0.58	0.72	1.40	0.24	0.02	1.39	1.13
	σ	4.9	2.0	2.7	1.9	2.6	1.2	1.2	0.6	0.13	0.09	1.60	1.09	0.13	0.26	9.4	66.3	27.2	0.25	0.89	0.36	0.01	0.31	1.58	0.93
	Median	**52.8**	**14.9**	**15.5**	**3.6**	**2.1**	**2.8**	**1.7**	**1.7**	**0.12**	**0.21**	**98.9**	**1.83**	**0.13**	**0.28**	**45.8**	**39.9**	**9.0**	**0.57**	**0.41**	**0.10**	**0.02**	**0.02**	**0.57**	**1.30**
S- and C-rich metasedi-mentary rocks ($n=31$)	Mean	50.2	13.0	17.1	4.8	5.7	1.7	2.6	1.4	0.31	0.20	96.98	7.17	4.46	2.90	81.1	345	82.4	6.85	16.90	5.12	0.21	0.08	1.86	7.80
	σ	8.0	3.9	8.1	2.8	4.3	1.7	1.5	0.7	0.39	0.20	2.03	3.76	5.26	2.60	122.2	421	169	10.59	23.16	14.99	0.31	0.01	5.38	9.62
	Median	**48.7**	**13.2**	**15.2**	**4.7**	**5.2**	**1.1**	**2.9**	**1.3**	**0.20**	**0.14**	**97.3**	**6.10**	**2.69**	**2.20**	**50.3**	**200**	**13.1**	**1.91**	**9.50**	**0.53**	**0.08**	**0.08**	**0.39**	**4.84**

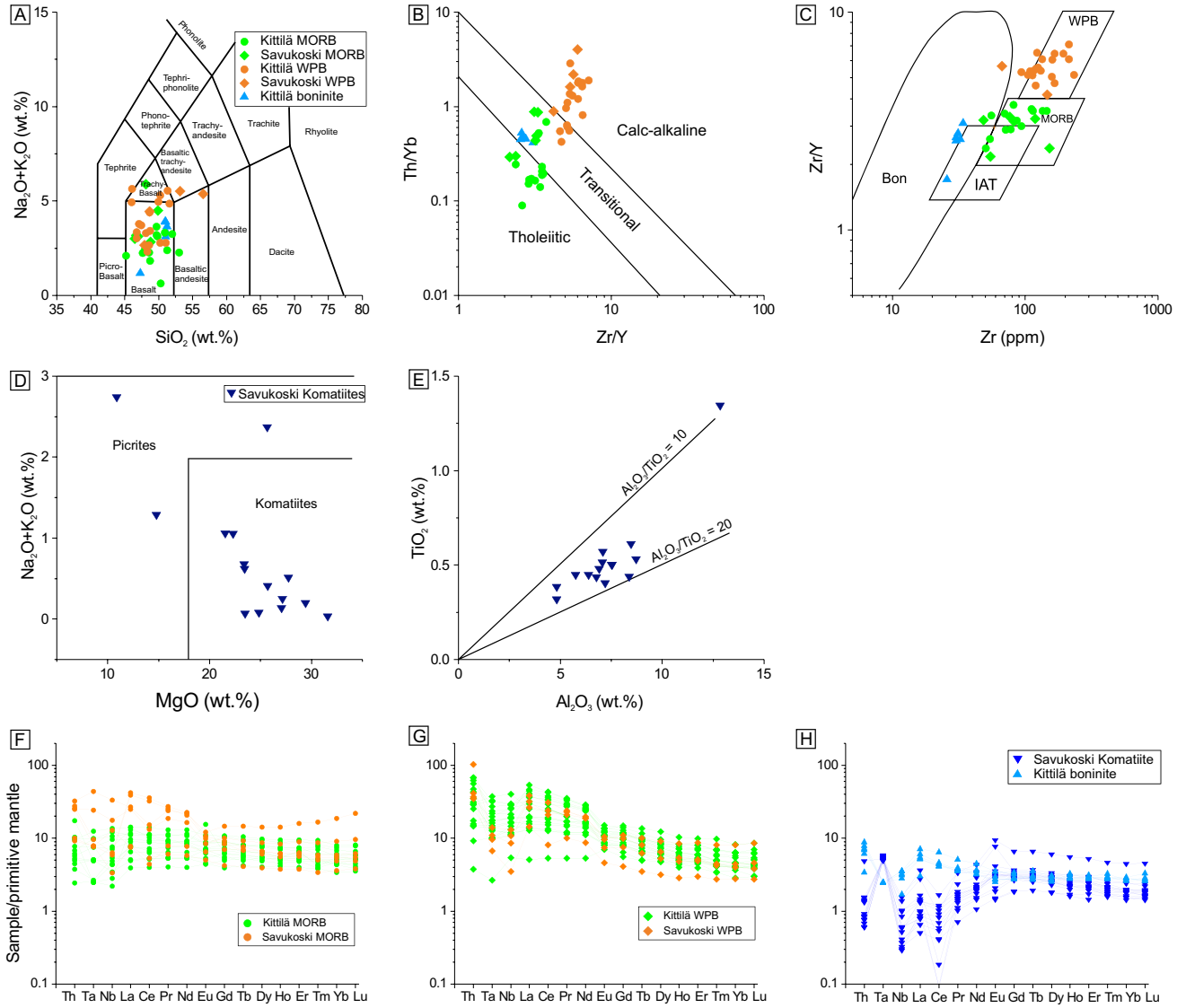

Fig. 2 Geochemical classification of the metavolcanic rocks (MORB, WPB, boninite-like dike and komatiite) from the Kittilä and Savukoski groups. **A** from Le Bas et al. (1986), **B** from Ross and Bédard (2009), **C** from Pearce and Norry (1979), **D** from Le Bas (2000), **E** from Barnes and Often (1990), and **F–H** primitive mantle values from McDonough and Sun (1995)

Savukoski Group

Samples from the Savukoski Group are mostly metakomatiite ($n = 15$) with minor MORB ($n = 6$) and WPB ($n = 4$) type metabasalt. Metakomatiite is characterized by 46.5 ± 3.1 wt% SiO_2 and 23.9 ± 5.3 wt% MgO (Table 2) and is Al-undepleted ($TiO_2/Al_2O_3 = 14.7 \pm 1.89$; Fig. 2; Barnes and Often 1990). Two samples have $Na_2O + K_2O > 2$ wt%, and two have MgO < 18 wt%, but these samples are classified nevertheless as metakomatiite based on their REE profiles (Fig. 2). The REE profiles are characterized by HREE enrichment relative to LREE ($La/Yb_{pm} = 0.66 \pm 0.31$; Fig. 2). The MORB-like samples are basaltic (47.8 ± 1.3 wt% SiO_2) with tholeiitic to transitional affinity (Zr/Y < 2.9 and Th/Yb < 0.55; Fig. 2). They show slightly enriched REE profiles ($La/Yb_{pm} = 3.9 \pm 3.1$; Fig. 2) suggesting an E-MORB affinity similarly to the Kittilä Group. Two samples have transitional Zr/Y and Th/Yb values and REE patterns similar to WPB. The WPB-like samples are basaltic to andesitic (51.6 ± 4.0 wt% SiO_2) with transitional to calc-alkaline affinity (Zr/Y > 4.2 and Th/Yb > 0.89; Fig. 2). The REE profiles are similar to the Kittilä Group with LREE enrichment relative to HREE ($La/Yb_{pm} = 6.2 \pm 2.1$; Fig. 2) and strong negative Ta and Nb anomalies relative to Th ($Ta/Th_{pm} = 0.22 \pm 0.10$ and $Nb/Th_{pm} = 0.20 \pm 0.12$).

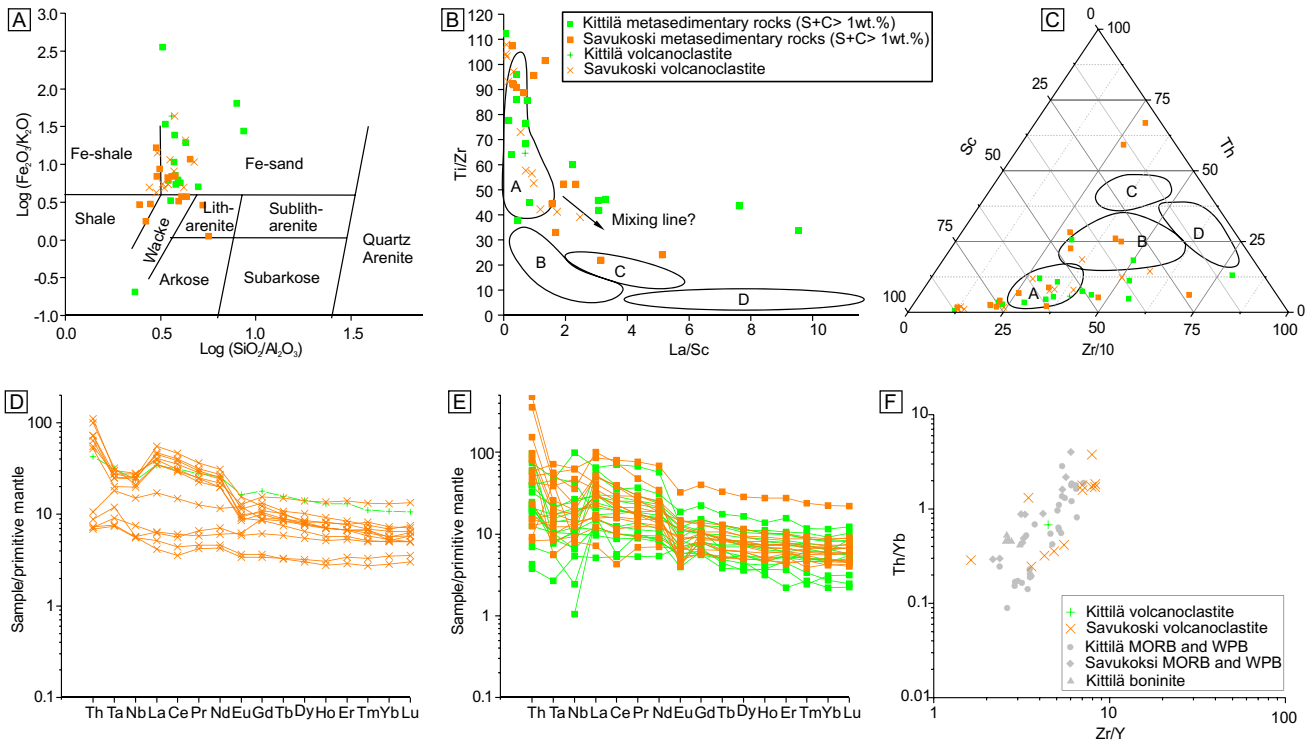

Fig. 3 Geochemical classification of the metasedimentary rocks from the Kittilä and the Savukoski groups. **A** From Herron (1988), **B**, **C** from Bhatia and Crook (1986), A = oceanic island arc, B = continental island arc, C = active continental arc, and D = passive margin, **D**, **E** primitive mantle values from McDonough and Sun (1995), and **F** from Ross and Bédard (2009)

Metasedimentary rocks

Kittilä Group

Metasedimentary rocks occur as intercalated units within the metavolcanic rocks. They comprise mainly metagraywacke, phyllite and black schist with variable sulfide and carbonaceous material contents (Hanski and Huhma 2005). Selected samples classify as wacke and Fe sand (Fig. 3) and show wide range in major and trace element concentrations (Table 2). Immobile trace element concentrations suggest an oceanic-arc dominated source (Fig. 3). These samples have a wide range of S and C contents ranging between 0.02–20.5 wt% S and 0.66–12.4 wt% C but with total S + C > 1 wt%. Samples with the highest S and C contents are black schists with sulfidic seams. One competent and poorly foliated sample with S + C < 1wt% has a composition similar to that of WPB-like samples (Fig. 3) suggesting that it represents a metamorphosed volcanoclastic rock.

Savukoski Group

Metasedimentary rocks are common and constitute the base of the group on top of which the metavolcanic rocks were conformably emplaced (Hanski and Huhma 2005). They mostly consist of phyllite, black schist, and mafic metatuffites (Hanski and Huhma 2005). Selected samples classify as Fe-shale, shale, wacke, and litharenite as protoliths (Fig. 3). Similar to rocks from the Kittilä Group, they show a wide range in major and trace element concentrations (Table 2). The immobile element concentration suggests either an active continental margin or an oceanic island arc source (Fig. 3). The S and C concentrations range between 0.01 and 11.04 wt% and 0.02 and 8.14 wt%, respectively, with black schists being the most S- and C-rich samples. Poorly foliated and competent samples with S + C < 1wt% are common ($n = 12$) and have similar composition to that of MORB and WPB samples, suggesting that they represent metamorphosed volcanoclastic rocks (Fig. 3).

Element distribution related to metamorphism

Metavolcanic and metavolcanoclastic rocks with MORB and WPB signatures

Due to similar geochemistry, metavolcanic and metavolcanoclastic rocks are grouped together when compared to

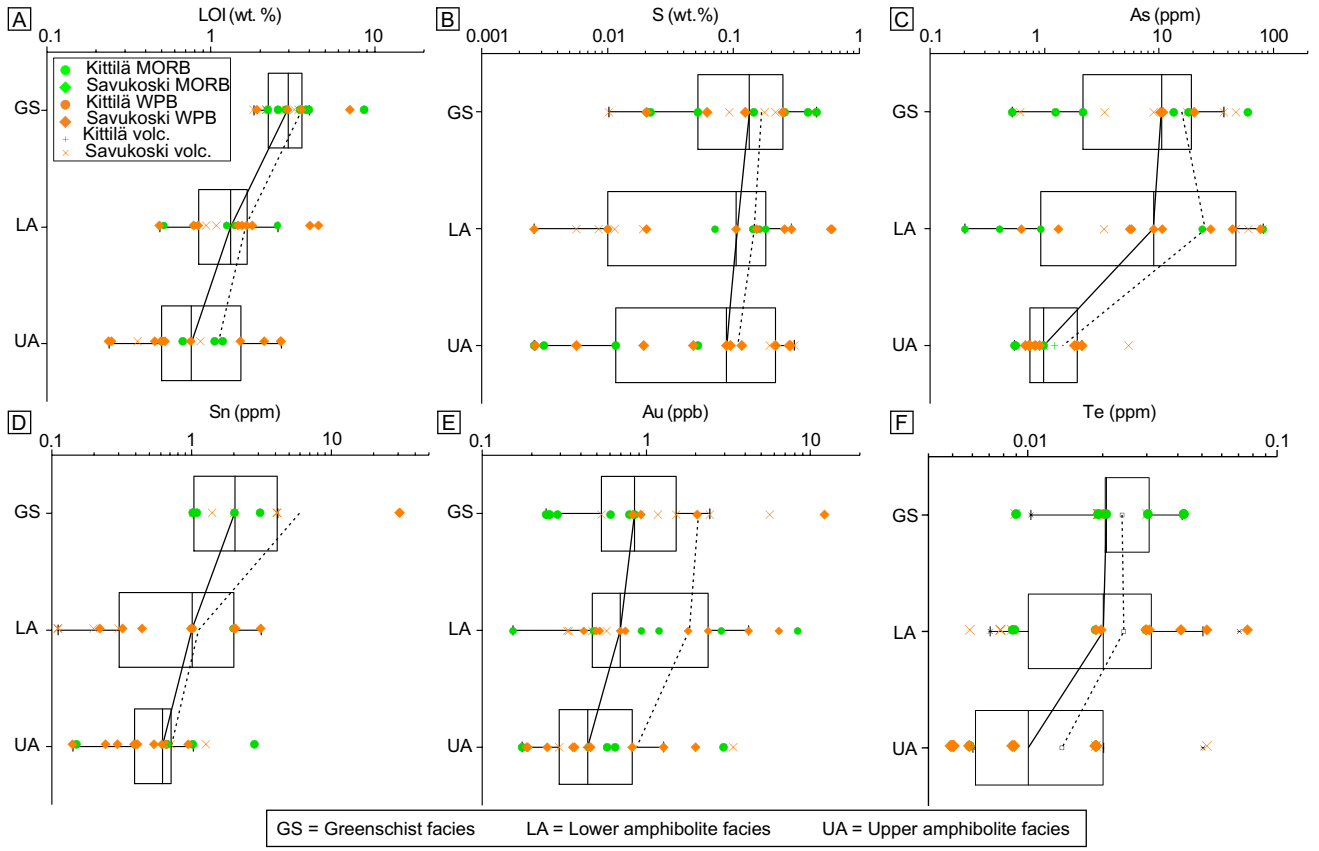

Fig. 4 **A** LOI, **B** S, **C** As, **D** Sn, **E** Au, and **F** Te content in metavolcanic and metavolcanoclastic rocks from Kittilä Group and Savukoksi Group according to their metamorphic facies. Only elements showing systematic variation in composition with metamorphic grade are shown. Solid curve connects median values of each group, whereas dashed curve connects average values. The box ranges are defined by the 25th and 75th percentiles, and the whiskers by the lower and inner fence

metamorphic grade. Boninites, however, are not grouped with MORB and WPB as they are volumetrically minor, not well genetically characterized and geochemically different (Table 2). Differences in trace element distribution in MORB, WPB, and related metavolcanoclastic rocks are observed relative to metamorphism (Fig. 4). To describe variations in element concentration relative to metamorphism, median and box plots are used rather than the average and standard deviation because of the bias induced by outliers in the dataset (Fig. 4). The MORB and WPB-like samples show systematic decrease in LOI from greenschist (median = 2.97 wt%) to lower amphibolite (median = 1.26 wt%) and upper amphibolite facies (median = 0.76 wt%; Fig. 4). Sulfur concentration decreases systematically from greenschist (0.13 wt%) to lower amphibolite (0.10 wt%) and upper amphibolite facies (0.09 wt%), whereas C stays constant (Table 3). Similarly, As, Sn, Sb, Te, and Au concentrations decrease from greenschist (10.5 ppm, 2.05 ppm, 0.14 ppm, 0.021 ppm, and 0.84 ppb, respectively) to lower amphibolite (9.0 ppm, 1.01 ppm, 0.11 ppm, 0.020 ppm, and 0.69 ppb, respectively) and upper amphibolite facies (0.98 ppm, 0.62 ppm, 0.10 ppm, 0.010 ppm, and 0.44 ppb, respectively; Fig. 1; Table 2). Other trace elements do not show systematic variation in concentration with metamorphic grade.

Metakomatiite

Metakomatiite samples show decreasing LOI content from greenschist (12.2 wt%) to lower amphibolite (8.46 wt%) and upper amphibolite facies (3.02 wt%; Fig. 5). Carbon content in upper amphibolite-facies samples (median = 0.15 wt%) is considerably lower than in greenschist and amphibolite-facies samples (median = 1.32 and 1.72 wt%, respectively; Fig. 5; Table 3). Sulfur content does not show systematic changes with metamorphism. Cobalt and Ni concentrations decrease slightly from greenschist (93.7 ppm and 656 ppm, respectively) to lower amphibolite (93.5 ppm and 627 ppm, respectively) and upper amphibolite facies (89.6 ppm and 482 ppm, respectively; Fig. 5; Table 3). Gold does not show systematic changes in concentration with metamorphism although upper amphibolite-facies samples have lower

Table 3 Whole rock composition of the metavolcanic rocks, metasedimentary rocks, and metakomatiites at different metamorphic grades

		LOI wt%	S wt%	C wt%	Co ppm	Cu ppm	As ppm	Se ppm	Mo ppm	Sn ppm	Sb ppm	Te ppm	Au ppb	U ppm
Metavolcanic and metavolcanoclastic rocks (MORB and WPB composition)														
Greenschist	Mean	3.49	0.17	0.38	51.81	96.90	15.9	0.69	1.53	5.88	0.26	0.024	1.85	0.82
	σ	1.81	0.14	0.45	7.17	57.01	17.7	0.25	0.87	10.26	0.33	0.010	2.97	0.74
	Median	**2.97**	**0.13**	**0.28**	**49.95**	**92.24**	**10.5**	**0.72**	**1.04**	**2.05**	**0.14**	**0.021**	**0.84**	**0.44**
Lower amphibolite	Mean	1.43	0.15	0.37	46.55	57.48	25.4	0.55	0.62	1.11	0.20	0.024	1.76	0.63
	σ	1.19	0.18	0.32	13.19	47.70	30.3	0.35	0.64	0.88	0.21	0.017	2.27	0.60
	Median	**1.26**	**0.10**	**0.35**	**44.71**	**55.58**	**9.0**	**0.41**	**0.56**	**1.01**	**0.11**	**0.020**	**0.69**	**0.42**
Upper amphibolite	Mean	1.09	0.11	0.27	47.89	83.85	1.44	0.61	0.84	0.71	0.15	0.014	0.87	0.93
	σ	0.83	0.11	0.26	9.39	65.04	1.18	0.24	0.55	0.63	0.14	0.011	0.98	0.82
	Median	**0.76**	**0.09**	**0.14**	**46.02**	**92.08**	**0.98**	**0.66**	**0.74**	**0.62**	**0.10**	**0.010**	**0.44**	**0.51**
Komatiites														
Greenschist	Mean	11.78	0.096	2.02	95.8	10.7	1.20	0.18	0.06	0.16	0.19	1.85	0.60	0.04
	σ	5.25	0.094	1.94	13.4	12.0	0.96	0.09	0.05	0.10	0.06	4.87	0.36	0.02
	Median	**12.20**	**0.085**	**1.32**	**93.7**	**4.2**	**0.85**	**0.15**	**0.05**	**0.12**	**0.19**	**0.007**	**0.43**	**0.03**
Lower amphibolite	Mean	9.21	0.029	1.86	92.8	31.0	1.85	0.18	1.44	0.11	0.11	0.008	1.07	0.03
	σ	2.13	0.045	0.44	5.3	38.7	1.56	0.08	2.43	0.00	0.00	0.002	1.03	0.00
	Median	**8.48**	**0.003**	**1.72**	**93.5**	**9.6**	**1.82**	**0.17**	**0.07**	**0.11**	**0.11**	**0.007**	**0.65**	**0.03**
Upper amphibolite	Mean	2.50	0.089	0.20	77.5	46.8	0.97	0.18	0.12	0.14	0.13	0.006	0.48	0.45
	σ	0.94	0.130	0.13	24.8	39.2	0.65	0.18	0.09	0.05	0.02	0.000	0.50	0.91
	Median	**3.02**	**0.022**	**0.15**	**89.6**	**41.8**	**0.91**	**0.12**	**0.10**	**0.10**	**0.12**	**0.006**	**0.28**	**0.03**
Metasedimentary rocks (S + C > 1 wt%)														
Greenschist	Mean	7.89	5.60	2.86	101	487	127	5.5	13.4	1.91	8.16	0.30	2.88	7.25
	σ	4.06	6.13	1.89	162	512	219	7.1	16.2	1.28	18.81	0.39	7.17	7.71
	Median	**6.61**	**3.02**	**2.36**	**50**	**373**	**56**	**2.3**	**11.3**	**1.45**	**1.51**	**0.08**	**0.57**	**4.84**
Lower amphibolite	Mean	7.37	4.77	4.41	52	238	51.8	13.4	34.6	2.28	0.91	0.14	0.44	14.02
	σ	3.54	3.85	4.30	38	213	75.5	17.4	35.2	1.50	0.41	0.12	0.44	14.16
	Median	**5.01**	**4.79**	**2.22**	**40**	**200**	**7.8**	**6.9**	**16.8**	**2.10**	**1.09**	**0.09**	**0.29**	**5.65**
Upper amphibolite	Mean	4.67	1.58	1.49	62	123	4.1	4.0	9.07	0.54	0.12	0.05	0.91	3.38
	σ	2.65	3.11	1.09	32	65	4.0	8.0	20.8	0.15	0.04	0.09	0.84	5.83
	Median	**3.73**	**0.21**	**1.07**	**55**	**109**	**2.3**	**0.8**	**0.61**	**0.54**	**0.10**	**0.01**	**0.63**	**1.20**

Au concentrations (median = 0.28 ppb) than greenschist and lower amphibolite-facies samples (0.43 and 0.65 ppb, respectively).

Sulfur and C-rich metasedimentary rocks

The various metasedimentary rocks of the Kittilä Group and the Savukoski Group are referred as to S and C-rich metasedimentary rocks (S + C > 1 wt%) and have decreasing LOI content from greenschist (6.61 wt%) to lower amphibolite (5.01 wt%) and upper amphibolite facies (3.73 wt%; Fig. 6; Table 3). Carbon content shows systematic decrease from greenschist (2.36 wt%) to lower amphibolite (2.22 wt%) and upper amphibolite facies (1.07 wt%) whereas S shows considerably lower concentration in upper amphibolite-facies samples (median = 0.21 wt%) than in greenschist (3.02 wt%) and lower amphibolite-facies samples (4.79 wt%; Table 3). Copper, As, and Sb show systematic decrease in concentration from greenschist (373 ppm, 56 ppm, and 1.51 ppm, respectively) to lower amphibolite (200 ppm, 7.8 ppm, and 1.09, respectively) and upper amphibolite facies (109 ppm, 2.3 ppm, and 0.10 ppm, respectively; Fig. 6; Table 3). Selenium, Mo, Sn, Te, and U have considerably lower concentrations in upper amphibolite-facies samples (0.77 ppm, 0.61 ppm, 0.54 ppm, 0.01 ppm, and 1.20 ppm, respectively) than in greenschist (2.33 ppm, 11.3 ppm, 1.45 ppm, 0.08 ppm, and 4.84 ppm, respectively) and lower amphibolite-facies

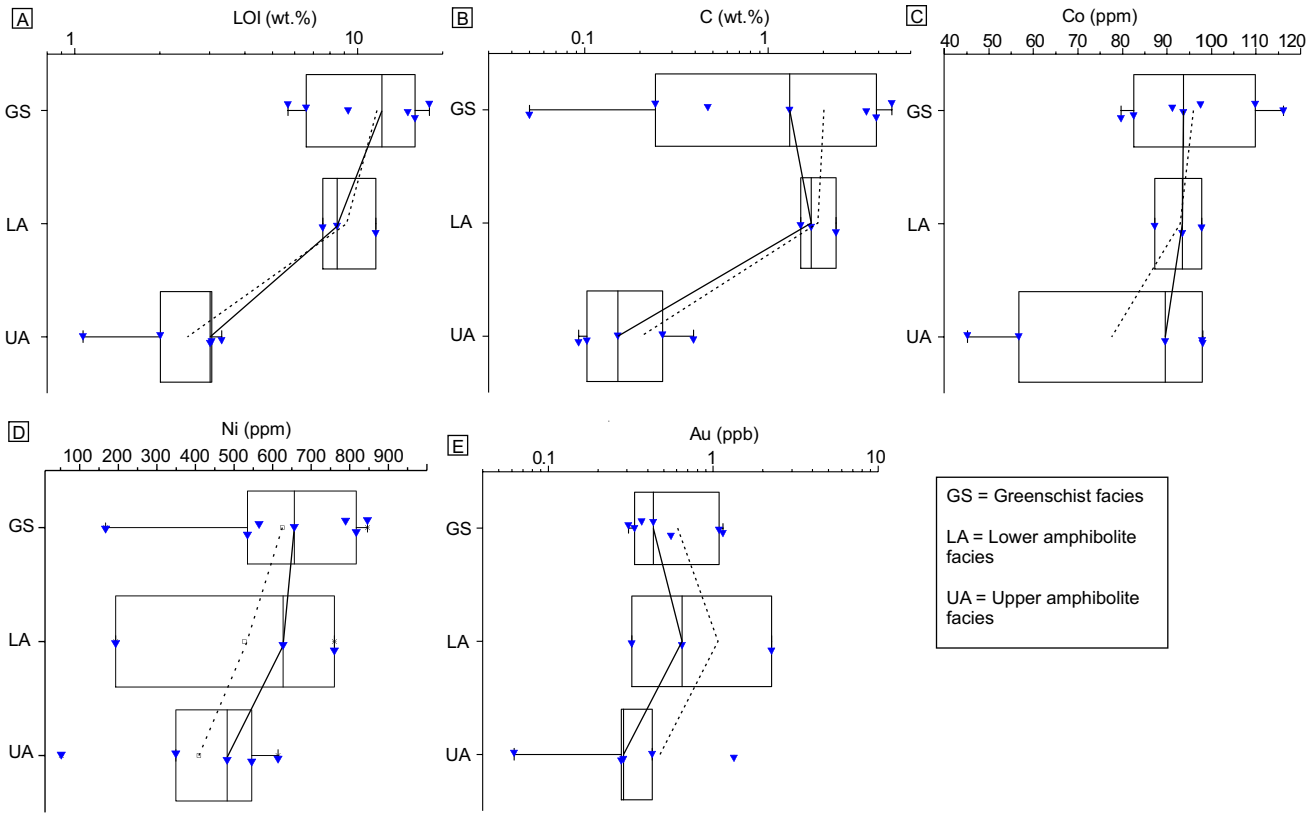

Fig. 5 **A** LOI, **B** C, **C** Co, **D** Ni and **E** Au content in metakomatiites from the Savukoksi Group according to their metamorphic facies. Only elements showing systematic variation in composition with metamorphic grade are shown. Box range and lines as in Fig. 4

samples (6.94 ppm, 16.8 ppm, 2.10 ppm, 0.09 ppm, and 5.65 ppm, respectively; Table 3). Gold and Co do not show systematic decrease relative to metamorphic grade (Fig. 6).

Protolith composition

There are three critical parameters for determining the potential of lithological units as metal source: (1) the primary content of the elements of interest at the onset of metamorphism (defined as the metamorphic protolith composition), (2) the degree of depletion, and (3) the volume of the unit. The metamorphic protolith composition and the volume of the unit buffer the quantity of element availability for hydrothermal mobilization and can be referred to as the metal fertility. The degree of depletion is dependent on the efficiency of hydrothermal fluids in mobilizing the elements out of the source rock. This efficiency is related to the degree of disequilibrium between the fluids and the rocks, which is dependent on the physicochemical characteristics of both the hydrothermal fluids and the rocks. The degree of depletion is inferred through mass variation calculations between protolith and altered rocks (Pitcairn et al. 2006a; Jowitt et al. 2012; Patten et al. 2016). A lithological unit has a high potential as a source if it has both a high metal fertility and is highly depleted.

Metavolcanic rocks with MORB and WPB signature

To determine the mass variations related to metamorphic devolatilization, the different protolith primary composition before the onset of metamorphism must be characterized. Metamorphic protolith composition, however, is notoriously difficult to determine due to the numerous processes that affected trace element concentration before onset of metamorphism. Trace element contents in MORB and WPB-like samples are controlled by differences in mantle source, magmatic processes, and seafloor alteration preceding metamorphism (Tatsumi et al. 1999; Jenner and O'Neill 2012; Webber et al. 2013; Patten et al. 2016). Comparison with modern-day fresh glass MORB and WPB can provide insights into protolith composition, especially for elements which are poorly affected by low-temperature seafloor alteration such as Au (Nesbitt et al. 1987; Pitcairn et al. 2015; Patten et al. 2016). Their use as proxies for metamorphic protolith composition, however, is limited as the differences in mantle source and magmatic differentiation between

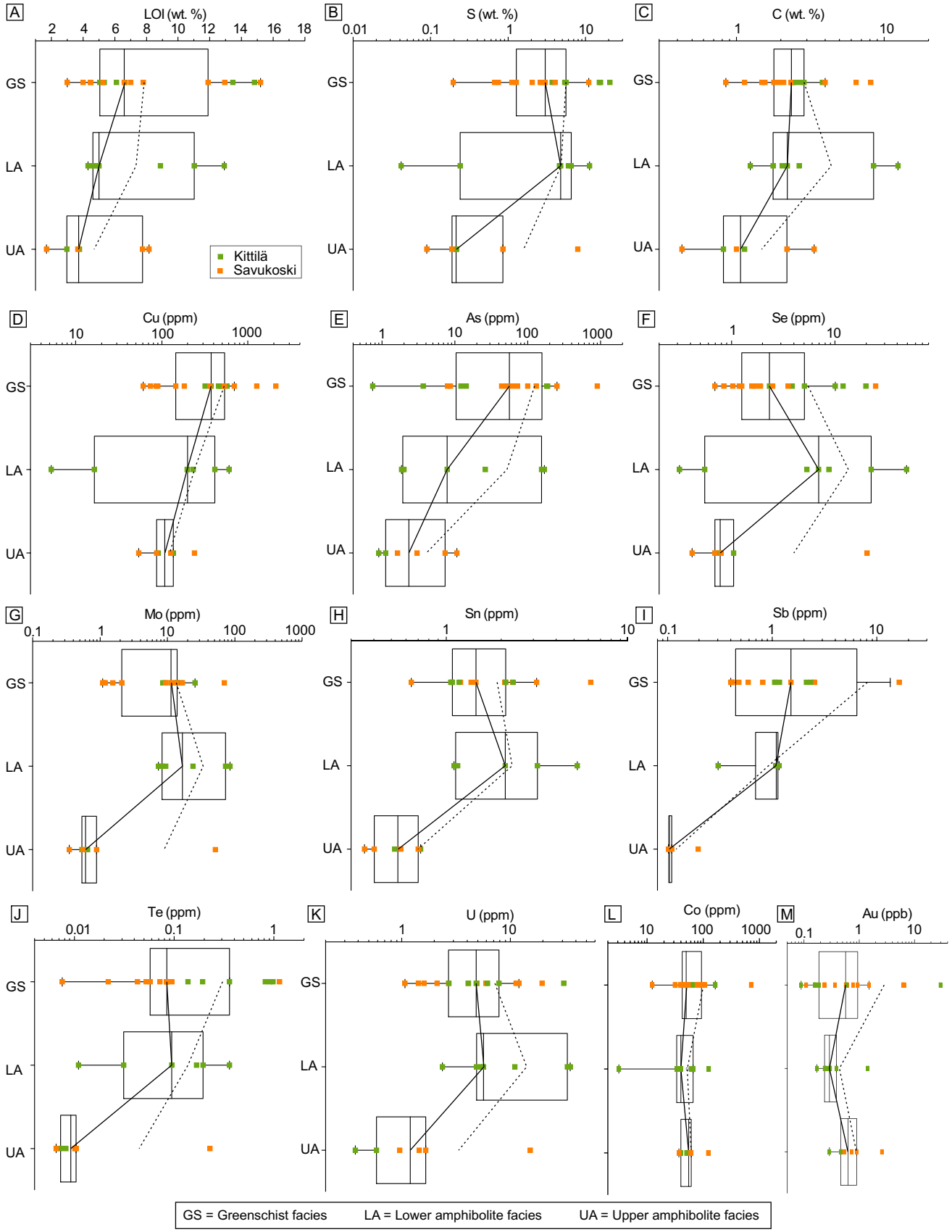

Fig. 6 **A** LOI, **B** S, **C** C, **D** Cu, **E** As, **F** Se, **G** Mo, **H** Sn, **I** Sb, **J** Te, **K** U, **L** Co, and **M** Au content in metasedimentary rocks (S + C > 1 wt%) from the Kittilä and Savukoksi groups according to their metamorphic facies. Box range and lines as in Fig. 4

Precambrian and modern-day MORB and WPB, and related effect on trace element concentration, are not well constrained (Patten et al. 2020). For instance, MORB and WPB from the CLGB show evidence of contamination from the Archean basement via the assimilation-fractionation-crystallization mechanism (Hanski and Huhma 2005; Patten et al. 2020), but the impact on trace element concentration is difficult to estimate. Thus, MORB- and WPB-like samples metamorphosed at greenschist facies are considered better proxies for the metamorphic protolith composition. They have sustained the same magmatic-hydrothermal history as their higher metamorphic grade counterparts, enabling direct comparison, and trace element mobility during sub-greenschist-facies metamorphism can be considered limited (Pitcairn et al. 2006a, 2015). Patten et al. (2020) highlighted that magmatic differentiation trends for Au in MORB and WPB are preserved in greenschist-facies samples from the CLGB, enabling improved characterization of the protolith composition. The Zr/Y ratio, which is not affected by seafloor alteration and sub-greenschist facies metamorphism, is used to differentiate between MORB and WPB magmatic trends. This approach, however, does not work for other elements, which also show systematic decrease with increasing metamorphic grade, such as S, As, Sn, and Sb, as no magmatic differentiation trends are preserved in greenschist-facies samples. These elements have relatively high mobility during low-temperature seafloor alteration (Alt 1995; Jochum and Verma 1996; Patten et al. 2016) preventing preservation of magmatic trends. Hence, the median values of the greenschist facies samples are used as proxies for the metamorphic protolith composition (S = 0.13 wt%, As = 10.5 ppm, Sn = 2.05 ppm, and Sb = 0.14 ppm; Table 3).

Sulfur and C-rich metasedimentary rocks

Trace element content in S and C-rich metasedimentary rocks is highly variable, depending on sediment source and diagenetic processes (Crocket 1993; Ketris and Yudovich 2009; Large et al. 2011; Pitcairn 2011). Sulfide content in metasedimentary rocks of the CLGB has a strong control on Cu, Se, Mo, Sb, Te, and U but limited control on Co, As, Sn, and Au (Figs. 6 and 7). Trace element content in the metamorphic protolith is thus strongly controlled by the primary sulfide content for some elements, and their distribution in variably metamorphosed samples might reflect differences in protolith sulfide content rather than mobilization due to metamorphism. To circumvent this problem, the Co/Mo ratio can be used (Fig. 8). Cobalt and Mo are both hosted by sulfides in metasedimentary rocks (Pitcairn et al. 2006a; Large et al. 2011, 2014; Hu et al. 2016), but during metamorphism, Co is redistributed between sulfide phases, from pyrite to cobaltite and pyrrhotite (Pitcairn et al. 2006a; Large et al. 2014), and

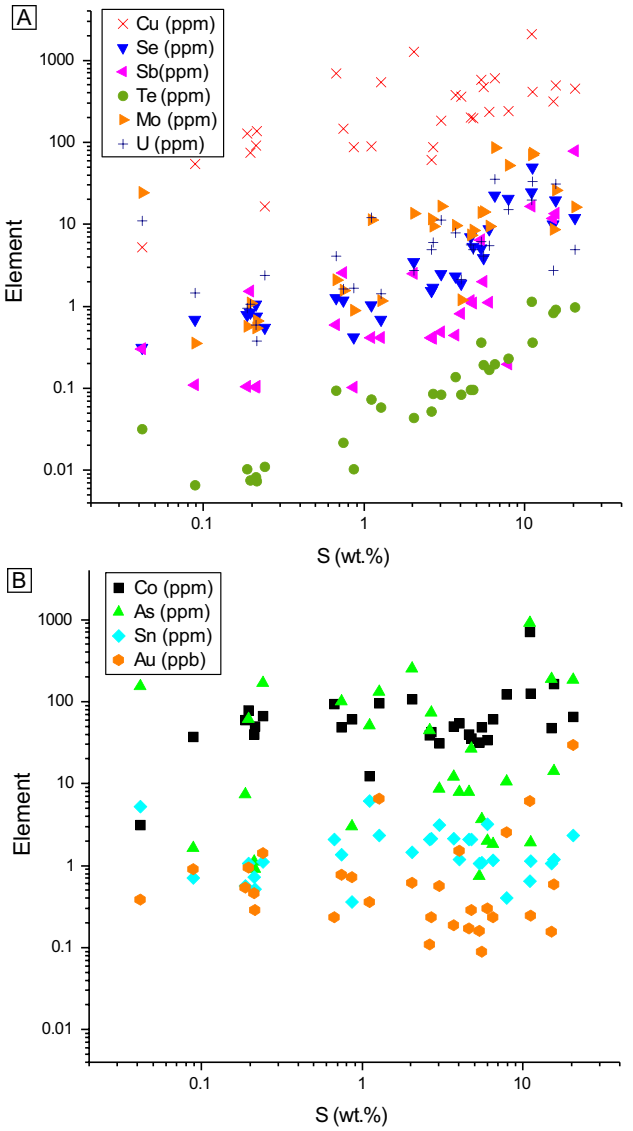

Fig. 7 Trace element content versus S in the metasedimentary rocks from the Kittilä and Savukoski groups. **A** Cu, Mo, Se, Sb, Te, and U show strong correlation with sulfide content whereas **B** Co, As, Sn, and Au do not

can be considered as an immobile element if the metamorphic fluids have relatively low salinity (Fig. 6; Qiu et al. 2021), whereas Mo is efficiently mobilized, showing a similar behavior to S (Large et al. 2011, 2014; Fig. 6). Increasing devolatilization thus leads to increase in the Co/Mo ratio independently of the primary sulfide content (Fig. 8). Correlation of Se, Cu, Sb, Te, and U with the Co/Mo ratio implies that trace element variation is related to metamorphic grade rather than to primary sulfide content. Although some trace element mobility in metasedimentary rocks can occur early before greenschist-facies

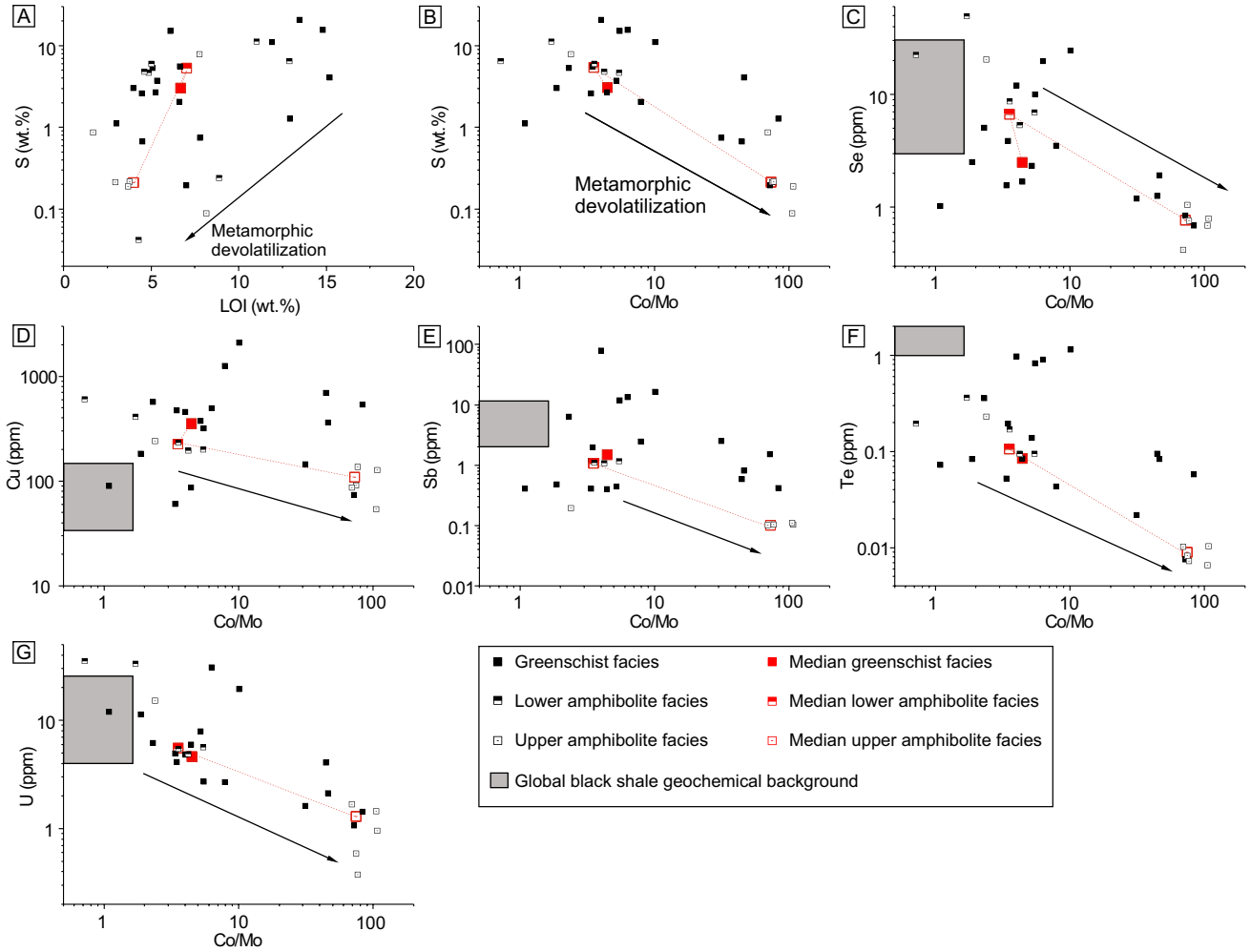

Fig. 8 **A** S vs LOI and **B** S, **C** Se, **D** Cu, **E** Sb, **F** Te, and **G** U vs Co/Mo in metasedimentary rock samples from the Kittilä and Savukoski groups. Increase in Co/Mo ratio indicates metamorphic devolatilization. Geochemical background of global black shales defined by Ketris and Yudovich (2009)

metamorphism (Large et al. 2011; Pitcairn et al. 2006a), the median of greenschist-facies samples is used as proxy for protolith composition (Table 3). Greenschist-facies median values of Co, Cu, As, Se, Mo, Sn, Sb, Te, and U (50 ppm, 373 ppm, 56 ppm, 2.3 ppm, 11.3 ppm, 1.45 ppm, 1.51 ppm, 0.08 ppm, and 4.84 ppm, respectively; Table 3) are comparable to the global median values in black shale as determined by Ketris and Yudovich (2009; 19 ppm, 70 ppm, 30 ppm, 8.7 ppm, 20 ppm, 3.9 ppm, 5.0 ppm, 2.0 ppm, and 8.5 ppm, respectively; Fig. 8). The Cu concentration (373 ppm), however, is considerably higher than the global black shale median (70 ppm), whereas Te (0.08 ppm) and Au (0.57 ppb) concentrations are considerably lower (2.0 ppm and 7 ppb, respectively; Ketris and Yudovich 2009). The discrepancy for Au can possibly be attributed to unfavorable conditions for Au incorporation during sedimentation and diagenesis such as low Au content in seawater at 2.0–1.6 Ga (Large et al. 2015).

Metakomatiite

The trace element content in metakomatiite protolith is controlled by complex processes such as mantle source, degree of mantle melting, melt contamination by supra-crustal rocks, possible sulfide segregation, and seafloor alteration (Barnes and Often 1990; Hanski et al. 2001b; Schandl and Gorton 2012; Heggie et al. 2013). The limited number of metakomatiite samples metamorphosed at greenschist facies ($n = 7$) makes the characterization of trace element distribution in the protolith difficult. The dataset is completed by whole rock data from the Karasjok greenstone belt (Barnes and Often 1990), the northern prolongation of the CLGB in Norway, and from the Peuramaa and Jeesiörova localities along the SiSZ (Hanski et al. 2001b). These rocks, although showing some differences in major element concentration (e.g., the Karasjok komatiites are more TiO_2–rich), share

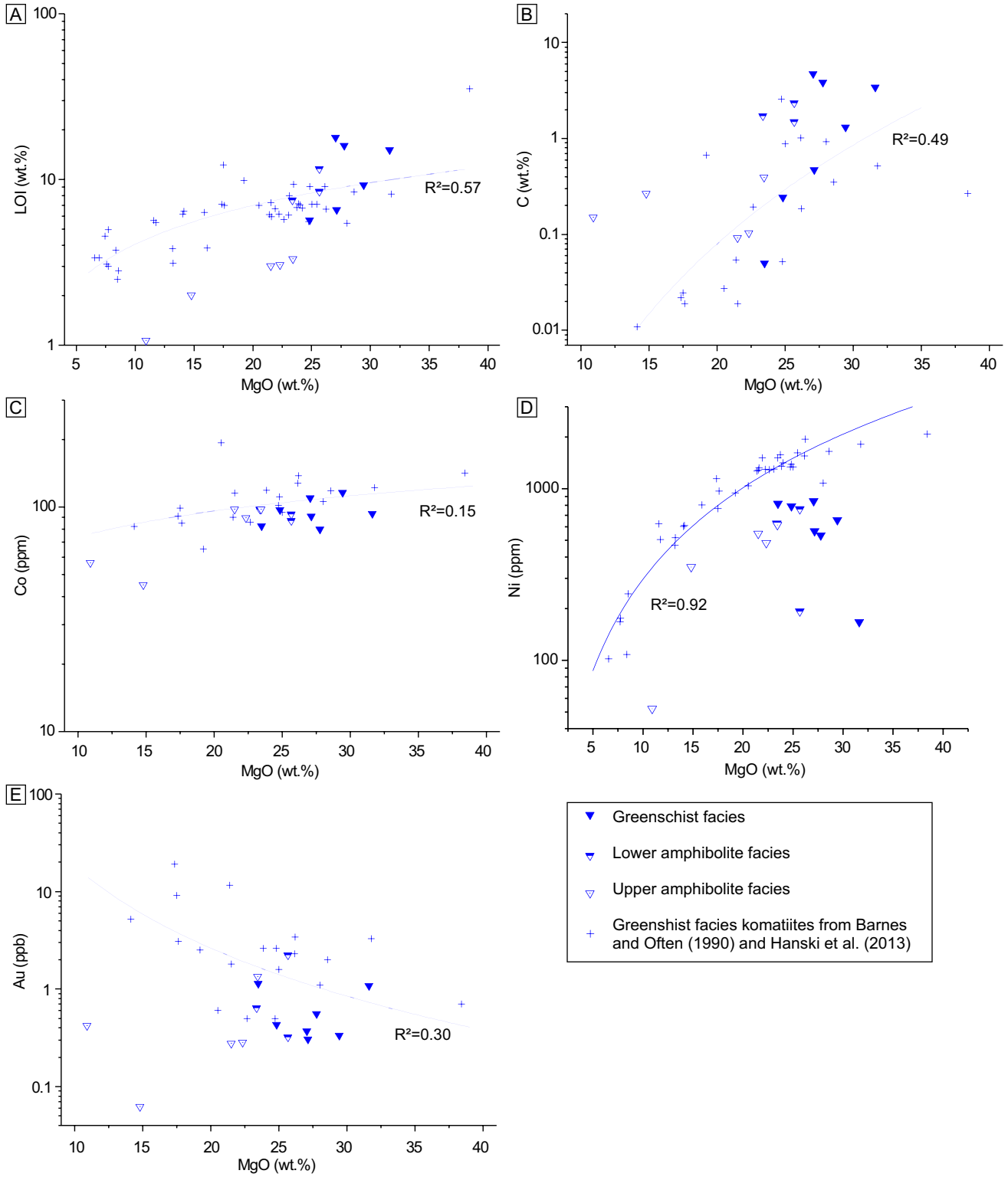

Fig. 9 LOI, C, Co, Ni, and Au content relative to MgO in the metakomatiites from the Savukoski Group. The trend lines are the calculated protolith composition using greenschist facies samples from this study and from Barnes and Often (1990) and Hanski et al. (2013; blue crosses) except for Ni (see text). GS = greenschist, LA = lower amphibolite, UA = upper amphibolite

the same genetic processes to the rocks from this study (Lehtonen et al. 1998; Hanski et al. 2001b), and they were metamorphosed only up to greenschist facies (Barnes and Often 1990). Using these data, magmatic differentiation curves were calculated for Co and Au using MgO (Fig. 9). Nickel concentrations in metakomatiite from this study are lower than those from Barnes and Often (1990), and Hanski et al. (2001b) and do not show clear magmatic differentiation trends. However, the low Ni concentration of upper amphibolite-facies samples relative to greenschist and lower amphibolite facies samples (Fig. 5) is nevertheless partly due to magmatic differentiation as they are characterized by low MgO content (Fig. 9). Nickel distribution in metakomatiite thus cannot be attributed to either magmatic or metamorphic processes, and mass variation related to metamorphism cannot be calculated. The metakomatiite samples are characterized by relatively high LOI and C (Table 1), most likely due to serpentinization and carbonation during seafloor alteration (Barnes and Often 1990; Schandl and Gorton 2012), but LOI and C show nevertheless correlation with MgO (Fig. 9). The calculated trends for the LOI, C, Co, and Au are used as proxies for the metamorphic protolith composition (Fig. 9), whereas the median values of greenschist-facies samples are used as the metamorphic protolith composition for the other elements of interest (Table 3).

Table 4 Mass variation calculations for selected elements at greenschist, lower amphibolites, and upper amphibolite-facies conditions relative to protolith composition

		LOI wt%	S wt%	C wt%	Co ppm	Cu ppm	As ppm	Se ppm	Mo ppm	Sn ppm	Sb ppm	Te ppm	Au* ppb	U ppm
Metavolcanic and metavolcanoclastic rocks (MORB and WPB composition)														
Greenschist	Mean	17.3	22.9	54.1	4.6	3.7	49.3	−2.8	47.3	187.7	81.2	5355	94.1	78.4
	σ	60.9	112.6	186.0	15.4	58.7	167.9	43.6	83.5	501.5	234.9	19,978	393.6	172.9
	Median	**0**	**0**	**0**	**0**	**0**	**0**	**0**	**0**	**0**	**0**	**0**	**−14.8**	**0**
Lower amphibolite	Mean	−51.8	13.9	55.6	−4.5	−39.3	146.0	−17.0	−40.6	−45.7	40.8	17.4	153.9	46.1
	σ	40.2	141.6	136.6	27.1	50.4	293.6	52.2	61.5	42.8	147.5	83.2	312.0	138.7
	Median	**−57.6**	**−18.5**	**46.4**	**−8.3**	**−41.3**	**−12.2**	**−38.8**	**−46.1**	**−50.4**	**−21.5**	**−2.9**	**14.0**	**−1.7**
Upper amphibolite	Mean	−65.4	−16.6	1.7	−1.0	−10.2	−85.9	−11.7	−18.4	−65.3	9.7	−31.8	−21.2	121.9
	σ	27.5	86.2	104.6	19.6	70.7	11.8	34.9	54.3	31.7	97.5	55.3	96.4	194.5
	Median	**−75.8**	**−45.6**	**−44.7**	**−2.7**	**−1.6**	**−90.9**	**−6.7**	**−33.8**	**−71.5**	**−28.5**	**−51.3**	**−58.7**	**30.7**
Komatiites														
Greenschist	Mean	29.3	185.3	243.0	−11.8	−71.8	41.0	19.7	15.1	39.0	−1.6	6.7	−43.2	17.3
	σ	56.7	277.5	374.4	11.6	31.5	111.9	60.4	102.6	86.9	29.9	20.8	43.0	49.9
	Median	**25.2**	**151.6**	**72.2**	**−15.8**	**−88.8**	**0.0**	**0.0**	**0.0**	**0.0**	**0.0**	**0.0**	**−62.6**	**0.0**
Lower amphibolite	Mean	11.0	−14.8	560.2	−11.3	−18.4	116.3	17.2	2790.7	−7.2	−43.0	10.8	−21.8	−5.9
	σ	22.7	133.4	213.8	6.7	102.0	182.5	49.9	4875.0	1.9	1.2	33.5	81.5	1.9
	Median	**0.1**	**−91.0**	**582.4**	**−11.9**	**−74.8**	**112.5**	**10.4**	**30.7**	**−8.2**	**−43.6**	**−7.0**	**−61.9**	**−6.8**
Upper amphibolite	Mean	−63.1	164.0	1661.1	−17.8	23.3	13.7	17.7	137.9	13.9	−35.2	−12.5	−77.8	1175.0
	σ	7.2	385.1	2786.5	19.0	103.2	76.3	118.0	181.3	38.5	11.9	6.6	32.5	2590.4
	Median	**−59.7**	**−34.1**	**95.2**	**−10.8**	**10.0**	**6.4**	**−19.2**	**106.9**	**−12.7**	**−37.2**	**−14.8**	**−87.0**	**−11.5**
Metasedimentary rocks (S + C > 1 wt%)														
Greenschist	Mean	19.6	19.4	85.4	21.2	30.3	30.4	127.3	137.2	18.3	31.5	440.2	257.8	404.6
	σ	26.2	61.5	202.6	80.0	92.8	137.2	394.1	303.8	142.9	88.3	1244.6	461.6	1257.9
	Median	**5.5**	**0.0**	**0.0**	**0.0**	**0.0**	**0.0**	**0.0**	**0.0**	**0.0**	**0.0**	**0.0**	**0.0**	**0.0**
Lower amphibolite	Mean	3.1	11.5	57.9	87.0	198.0	−36.2	−6.9	473.9	204.9	57.1	−39.5	61.6	−23.5
	σ	1.9	53.6	127.4	182.6	246.7	56.9	135.7	749.6	310.6	103.4	27.1	140.8	77.4
	Median	**3.6**	**−24.2**	**58.4**	**−6.0**	**93.9**	**−46.5**	**−86.0**	**198.2**	**47.7**	**44.6**	**−27.6**	**12.1**	**−49.1**
Upper amphibolite	Mean	72.5	−29.3	−47.8	−36.8	112.4	−67.2	−92.6	73.0	−20.0	−62.5	−92.1	−46.5	59.9
	σ	37.9	40.1	102.8	46.3	381.8	17.4	7.1	345.7	183.0	10.3	2.5	106.3	146.5
	Median	**75.6**	**−43.6**	**−92.9**	**−54.8**	**−31.3**	**−70.9**	**−95.8**	**−66.7**	**−94.6**	**−62.7**	**−93.1**	**−89.1**	**10.4**

*Au mass variation calculations in MORB and WPB are from Patten et al. (2020)

Table 5 Mann–Whitney statistical test. Mass variations are significant when the null hypothesis is rejected

		LOI wt%	S wt%	C wt%	Co ppm	Cu ppm	As ppm	Se ppm	Mo ppm	Sn ppm	Sb ppm	Te ppm	Au ppb	U ppm
Metavolcanic and metavolcanoclastic rocks (MORB and WPB composition)														
Greenschist	**Median**	**0.00**	**0.00**	**0.00**	**0.00**	**0.00**	**0.00**	**0.00**	**0.00**	**0.00**	**0.00**	**0.00**	**−14.8**	**0.00**
	p value	1	1	1	1	1	1	1	1	1	1	1	0.53	1
	Null hypothesis	Not rejected	Not rejected	Not rejected	Not rejected	Not rejected	Not rejected	Not rejected	Not rejected	Not rejected	Not rejected	Not rejected	Not rejected	Not rejected
Lower amphibolite	**Median**	**−57.6**	**−18.5**	**46.4**	**−8.3**	**−41.3**	**−12.2**	**−38.8**	**−46.1**	**−50.4**	**−21.5**	**−2.9**	**14.0**	**−1.7**
	p value	**6.50E−05**	0.35	0.62	0.22	**0.02**	0.87	0.16	0.03	**7.67E−04**	0.55	0.20	0.18	0.73
	Null hypothesis	**Rejected**	Not rejected	Not rejected	Not rejected	**Rejected**	Not rejected	Not rejected	Not rejected	**Rejected**	Not rejected	Not rejected	Not rejected	Not rejected
Upper amphibolite	**Median**	**−75.8**	**−45.6**	**−44.7**	**−2.7**	**−1.6**	**−90.9**	**−6.7**	**−33.8**	**−71.5**	**−28.5**	**−51.3**	**−58.7**	**30.7**
	p value	**1.20E−05**	0.20	0.79	0.41	0.62	**5.10E−04**	0.66	0.28	**3.60E−05**	0.21	**2.30E−04**	**0.041**	0.34
	Null hypothesis	**Rejected**	Not rejected	Not rejected	Not rejected	Not rejected	**Rejected**	Not rejected	Not rejected	**Rejected**	Not rejected	**Rejected**	**Rejected**	Not rejected
Komatiites														
Greenschist	**Median**	**25.2**	**151.61**	**72.16**	**−15.8**	**−88.8**	**0.0**	**0.0**	**0.0**	**0.0**	**0.0**	**0.0**	**−62.6**	**0.0**
	p value	0.44	0.97	0.28	0.085	**0.018**	1	1	1	1	1	1	0.064	1
	Null hypothesis	Not rejected	Not rejected	Not rejected	Not rejected	**Rejected**	Not rejected	Not rejected	Not rejected	Not rejected	Not rejected	Not rejected	Not rejected	Not rejected
Lower amphibolite	**Median**	**0.1**	**−91.0**	**582**	**−11.9**	**−75**	**113**	**10.4**	**30.7**	**−8.2**	**−43.6**	**−7.0**	**−61.9**	**−6.8**
	p value	0.43	0.077	0.05	0.19	0.41	0.34	0.63	0.90	0.24	**0.028**	0.70	0.37	0.52
	Null hypothesis	Not rejected	Not rejected	Not rejected	Not rejected	Not rejected	Not rejected	Not rejected	Not rejected	Not rejected	**Rejected**	Not rejected	Not rejected	Not rejected
Upper amphibolite	**Median**	**−59.7**	**−34.1**	**95.2**	**−10.8**	**10**	**6.4**	**−19.2**	**106.9**	**−12.7**	**−37.2**	**−14.8**	**−87.0**	**−11.5**
	p value	**2.63E−04**	1.0	0.11	0.072	0.470	1.00	0.33	0.24	0.32	0.06	0.036	**3.40E−03**	0.52
	Null hypothesis	**Rejected**	Not rejected	Not rejected	Not rejected	Not rejected	Not rejected	Not rejected	Not rejected	Not rejected	Not rejected	Not rejected	**Rejected**	Not rejected
Metasedimentary rocks (S + C > 1 wt%)														
Greenschist	**Median**	**0.0**	**0.0**	**0.0**	**0.0**	**0.0**	**0.0**	**0.0**	**0.0**	**0.0**	**0.0**	**0.0**	**0.0**	**0.0**
	p value	1	1	1	1	1	1	1	1	1	1	1	1	1
	Null hypothesis	Not rejected	Not rejected	Not rejected	Not rejected	Not rejected	Not rejected	Not rejected	Not rejected	Not rejected	Not rejected	Not rejected	Not rejected	Not rejected
Lower amphibolite	**Median**	**−24.2**	**58.4**	**−6.0**	**−19.6**	**−46.5**	**−86.0**	**198.2**	**47.7**	**44.6**	**−27.6**	**12.1**	**−49.1**	**16.6**
	p value	0.6	0.9	0.8	0.4	0.3	0.2	0.5	0.3	0.6	0.4	1.0	0.7	0.2
	Null hypothesis	Not rejected	Not rejected	Not rejected	Not rejected	Not rejected	Not rejected	Not rejected	Not rejected	Not rejected	Not rejected	Not rejected	Not rejected	Not rejected
Upper amphibolite	**Median**	**−43.6**	**−92.9**	**−54.8**	**11.0**	**−70.9**	**−95.8**	**−66.7**	**−94.6**	**−62.7**	**−93.1**	**−89.1**	**10.4**	**−75.2**
	p value	**0.074**	**0.022**	**0.046**	1	**0.039**	**0.0057**	**0.039**	**0.016**	**6.80E−04**	**4.10E−04**	**0.013**	0.55	**0.032**
	Null hypothesis	**Rejected**	**Rejected**	**Rejected**	Not rejected	**Rejected**	**Rejected**	**Rejected**	**Rejected**	**Rejected**	**Rejected**	**Rejected**	Not rejected	**Rejected**

Element depletion during metamorphism

Element depletion of a source is determined using mass variation calculation. Mass variation in trace elements due to prograde metamorphism is defined as the difference between the metamorphic protolith composition and metamorphosed sample:

$$\Delta E = E_p - E_s$$

where ΔE is the element's mass variation, E_p the protolith composition, and E_s the element concentration in the sample of interest. The metamorphic protolith composition is either the median of the greenschist-facies sample or the value determined from differentiation trends when possible (i.e., metakomatiite; Fig. 9). Mass variations for trace elements in greenschist, lower amphibolites, and upper amphibolite facies are compiled in Table 4 for each lithological group. To determine the significance of the calculated mass variations, a Mann–Whitney test for non-normal distribution is used. The null hypothesis specifies no statistical differences relative to the protolith at 0.05 confidence level (Table 5).

Metavolcanic rocks with MORB and WPB signature

Significant mass variation between the lower amphibolite facies and the protolith occurs for the LOI (−57.6%), Cu (−60.3%), and Sn (−50.4%). At the upper amphibolite facies, significant mass variation occurs for the LOI (−75.8%), As (−90.9%), Sn (−71.5%), and Au (−58.7%; Table 5). Systematic and increasing depletion of LOI relative to the protolith, from greenschist to upper amphibolite facies, highlights the devolatilization during prograde metamorphism. Sulfur and C do not show significant mass variations although S mass variation in upper amphibolite-facies samples (median = −45.6%) is significant with a 80% degree of confidence (p value = 0.2; Table 5). A larger dataset would allow to better understand S mobility during metamorphism of MORB and WPB. Arsenic and Au mass variations are significant in the upper amphibolite facies (median = −90.9% and −58.7%, respectively), whereas Sn mass variations are significant in both the lower amphibolite and upper amphibolite facies (median = −50.4% and −71.5%, respectively), implying efficient mobilization of As, Sn, and Au during upper amphibolite-facies metamorphism. Efficient mobilization of As from the metavolcanic rocks is inconsistent with the findings of Pitcairn et al. (2015), which show no As mobilization from metavolcanic rocks of the thick Otago Schist metasedimentary sequence but rather As enrichment. A possible explanation for this discrepancy is that the metavolcanic rocks of the Otago schists interacted with the As-rich metamorphic fluids sourced from the surrounding and voluminous metasedimentary rocks (~95% vol. of the sequence; Pitcairn et al. 2015). In the CLGB, mass variation of Cu is significant in the lower amphibolite facies but not in the upper amphibolite facies, implying that Cu distribution is possibly not solely controlled by prograde metamorphic devolatilization but by cryptic magmatic processes and, therefore, is not considered further here.

Metasedimentary rocks

Significant mass variation in S- and C-rich metasedimentary rocks relative to the metamorphic protolith composition occurs for the LOI (−43.6%), S (−92.9%), C (−54.8%), Cu (−70.9%), As (−95.8%), Se (−66.7%), Mo (−94.6%), Sn (−62.7%), Sb (−93.1%), Te (−89.1%), and U (−75.2%) at the upper amphibolite facies (Table 5). Gold does not show any significant mass variation. The lack of Au mass variation is partly explained by the low Au content of the metamorphic protolith.

Metakomatiite

Relative to the protolith composition, significant mass variation in metakomatiite occurs for Cu in the greenschist facies (−88.8%), for Sb at the lower amphibolite facies (−43.6%), and for the LOI and Au at the upper amphibolite facies (−59.7% and −87%, respectively). Cobalt does not show significant mass variation (Fig. 9; Table 5). The Cu mass variation in the greenschist facies is related to the lower Cu content of the metakomatiites of this study (median = 4.2 ppm) relative to those of Barnes and Often (1990; median = 74.5 ppm) rather than to metamorphism. The reasons for such low values are not understood. The mass variation of LOI and Au, although statistically significant, should be interpreted carefully as the metakomatiite sample population is relatively small (n = 15).

Control of the source on metal endowment in orogenic Au deposits

Mass balance calculation

The 3D shape of the Kittilä Group rock package has been modeled using aeromagnetic and gravity maps as well as seismic profiles, revealing a hull shape with a maximum thickness of 9.5 km in the center and thinning out towards the margins (Fig. 10; Niiranen et al. 2015). The substantial thickening occurred via thrust stacking during D1–D2 (e.g., along the KiSZ; Sayab et al. 2019). From the total of 9500 km^3 calculated for the Kittilä Group, ~1500 km^3 of rocks are inferred to be metamorphosed at the upper amphibolite facies (> 500–550 °C), representing a possible major

source volume for the orogenic Au deposits hosted in the CLGB (Niiranen et al. 2015). The Kittilä Group not only is dominated by metavolcanic rocks but also hosts minor metasedimentary rocks that should be included in mass balance calculations. Assuming a similar relative proportion of metavolcanic rocks to metasedimentary rocks in the Kittilä Group at depth to that at the surface, a proportion of 99.6% to 0.4%, respectively, is determined from GTK DigiKP 1:200,000 digital geological map (Fig. 1). It is estimated that ~ 1494 km^3 of metavolcanic rocks and ~ 6 km^3 of metasedimentary rocks were metamorphosed at upper amphibolite facies. The volume of the Savukoski Group, however, is not constrained but is likely significant (Niiranen, personal communication, 2019). During the tectonic evolution, the Kittilä Group was thrust from the west onto the Savukoski Group, while to the south, the Savukoski Group was thrust onto the Kittilä Group along the SiSZ. It can be inferred, thus, that the Kittilä Group hull structure is surrounded by the Savukoski Group at depth and to the south of the SiSZ (Fig. 10) as implied from the geological map (Fig. 1). Unlike the Kittilä Group, the Savukoski rock package most likely did not sustain extensive thickening at depth due to thrust stacking making it considerably less voluminous in the source zone. We use a conservative volume of half that of the Kittilä rock package (~ 750 km^3). The relative proportion of metavolcanic rocks to metasedimentary rocks and metakomatiites in the Savukoski Group from the GTK DigiKP 1:200,000 digital geological map is 29.7%, 29.4%, and 40.9%, respectively. Assuming a similar ratio at depth, a volume of ~ 223 km^3 of metavolcanic rocks, ~ 220 km^3 of metasedimentary rocks, and ~ 307 km^3 of metakomatiites is estimated to have been metamorphosed at the upper amphibolite facies in the Savukoski Group.

Mass balance calculations were carried out for the Kittilä Group and Savukoski Group rocks using the metamorphic protolith compositions (Table 3), the calculated element mass variations (Table 4), the estimated rock volumes in the source areas, and the densities of 3003 kg/m^3 for metavolcanic rocks, 2962 kg/m^3 for metasedimentary rocks, and 2971 kg/m^3 for metakomatiite (ESM 1). The calculated mass balances are semi-quantitative as uncertainties cannot be propagated (the highest uncertainty being related to the volume of the source zones and the lithological unit proportions). They nevertheless provide insight into the order of magnitude of the element flux from the different source volumes with staggering quantities of S, C, Cu, and As (> 100 Mt), Se, Mo, Sn, and U (> 1 Mt), and Sb, Te, and Au (> 1000 t; Table 6) being mobilized. The total Au mobilized from both the Kittilä and Savukoski groups (~ 2500 t) is one order of magnitude higher than the reported Au resources in the CLGB orogenic Au deposit (~ 440 t; Mineral Deposit Database of Finland 2022). The calculated quantity of mobilized Au is lower than the 4425–7080 t Au estimated by Niiranen et al. (2015) but of the same order of magnitude, the difference being caused by the overestimated protolith Au composition (2 ppb) used by Niiranen et al. (2015). Bulk Cu endowment in the CLGB orogenic Au deposits is not well constrained, but a minimum estimate of 0.13 Mt Cu (compilation from Saattopora, Levijärvi, Tepsa, Riikoski and Sirkka deposits) implies that the total Cu mobilized from both the Kittilä Group and the Savukoski Group (~ 180 Mt Cu) is significantly higher than the bulk Cu endowment in the deposits. The endowments of other metals in the CLGB are even less well constrained, but it can be assumed that, similarly to Au and Cu, the metal quantities mobilized from the sources are significantly higher than the ones trapped in the deposits.

Different sources for typical and atypical orogenic Au deposits?

The different lithological proportions of metavolcanic rocks, metasedimentary rocks, and metakomatiite between the Kittilä and Savukoski groups have important control on the element quantity mobilized during metamorphic devolatilization. The metavolcanic rocks released significant Au, As, Sn, Te, and possibly S, whereas the metasedimentary rocks released significant S, C, Cu, As, Se, Mo, Sn, Sb, Te, and U and the metakomatiites released C and possibly Au. Nickel and Co do not show systematic mobilization and a clear source for Ni and Co cannot be determined. The presence of evaporites in metamorphic belts appears as important for Co mobilization either by acting as a Co source (Qiu et al. 2021) and/or by providing Cl for forming Co–Cl complexes (Brugger et al. 2016; Qiu et al. 2021). Although some metaevaporites remnants are locally present within the CLGB, they appear to be limited and restricted to the southern part of the belt (Frietsch et al. 1997), and possibly had little impact on regional scale metal mobilization. They could have, nevertheless, locally and transiently favored Co mobilization, possibly promoting some atypical mineralization (Frietsch et al. 1997). Noteworthy, the atypical orogenic Au deposits of the CLGB are rather Cu-rich than Co-rich in comparison with the Kuusamo Belt, for instance, which hosts several Au and Au–Co orogenic deposits showing evidence of mineralizing fluids with an evaporitic component (Vasilopoulos et al. 2021).

In the Kittilä Group, which is dominated by metavolcanic rocks (~ 99.6 vol%), the metamorphic fluids generated by devolatilization would have been preferentially enriched in Au, As, Sn, Te, and possibly S. The metasedimentary rocks, although minor (~ 0.4 vol%), would still have provided large quantities of S and As to the metamorphic fluids (~ 490 Mt S and ~ 0.9 Mt As; Table 6). In the Savukoksi Group, however, metasedimentary rocks represent a large volume fraction

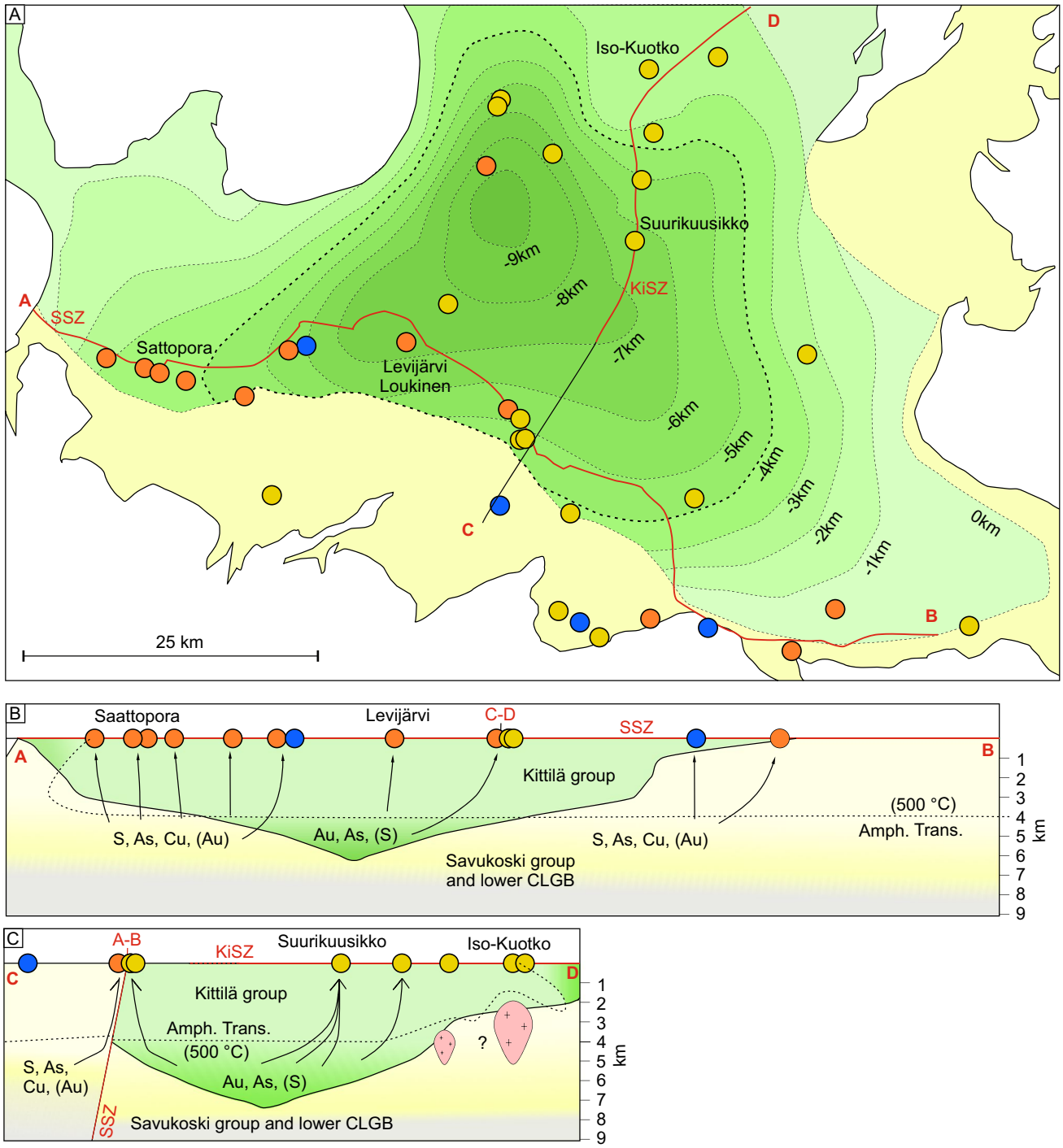

Fig. 10 Block model of the CLGB where metals are mobilized from the source at depth. **a** Projection of the Kittilä Group thickness from Niiranen et al. (2015) onto the surface. The greenschist to amphibolite facies transition occurs at > 4-km depth (thick dashed line). The typical deposits are located preferentially above the source dominated by the Kittilä Group whereas the atypical deposits are located preferentially above the Savukoski Group. **b** Schematic representation of the Sirkka shear zone (SiSZ) footwall with thickness of the Kittilä Group and potential metal source volumes. **c** Schematic representation of the Kiistala shear zone (KiSZ) prolonged to the SE with thickness of the Kittilä Group and potential metal source volumes. Ore deposit color legend as in Fig. 1

(29.7 vol%) implying that the metamorphic fluids would have been enriched in a larger suite of elements such as S, C, Cu, As, Se, Mo, Sn, Sb, Te, Au, and U (Table 6).

The lithological variability in the source is interpreted to have significant control on the style of mineralization and metal endowment in the orogenic Au deposits of the

Table 6 Mass balance calculations for metal mobilization from the source areas of the Kittilä and Savukoski groups

	S	C	Co	Cu	As	Se	Mo	Sn	Sb	Te	Au	U
	wt%	wt%	ppm	ppm	ppm	ppm	ppm	ppm	ppm	ppm	ppb	ppm
Protolith composition												
Kittilä Metavolcanic rocks	0.13	0.28	49.95	92.24	10.54	0.72	1.04	2.05	0.14	0.02	0.84	0.44
Kittilä Metasedimentary rocks	3.0	2.4	49.7	373.5	55.7	2.3	11.3	1.5	1.5	0.08	0.6	4.8
Savukoski Metavolcanic rocks	0.13	0.28	49.95	92.24	10.54	0.72	1.04	2.05	0.14	0.02	0.84	0.44
Savukoski Komatiites	0.08	1.32	93.70	4.24	0.85	0.15	0.05	0.12	0.19	0.01	0.43	0.03
Savukoski Metasedimentary rocks	3.0	2.4	49.7	373.5	55.7	2.3	11.3	1.5	1.5	0.1	0.6	4.8
Mass in source area (t)												
Kittilä Metavolcanic rocks	6.0E+09	1.3E+10	2.2E+08	4.1E+08	4.7E+07	3.2E+06	4.7E+06	9.2E+06	6.4E+05	9.3E+04	3.8E+03	2.0E+06
Kittilä Metasedimentary rocks	5.3E+08	4.1E+08	8.7E+05	6.6E+06	9.8E+05	4.1E+04	2.0E+05	2.6E+04	2.7E+04	1.5E+03	1.0E+01	8.5E+04
Savukoski Metavolcanic rocks	8.9E+08	1.9E+09	3.3E+07	6.2E+07	7.1E+06	4.8E+05	7.0E+05	1.4E+06	9.5E+04	1.4E+04	5.7E+02	3.0E+05
Savukoski Komatiites	7.7E+08	1.2E+10	8.5E+07	3.9E+06	7.8E+05	1.4E+05	4.5E+04	1.1E+05	1.8E+05	6.6E+03	4.0E+02	3.2E+04
Savukoski Metasedimentary rocks	2.0E+10	1.5E+10	3.2E+07	2.4E+08	3.6E+07	1.5E+06	7.4E+06	9.5E+05	9.9E+05	5.5E+04	3.7E+02	3.2E+06
Depletion (%)												
Kittilä Metavolcanic rocks	*−45.6*				−90.9			−71.5		−51.3	−58.7	
Kittilä Metasedimentary rocks	−92.9	−54.8		−70.9	−95.8	−66.7	−94.6	−62.7	−93.1	−89.1		−75.2
Savukoski Metavolcanic rocks	*−45.6*				−90.9			−71.5		−51.3	−58.7	
Savukoski Komatiites											*−87.0*	
Savukoski Metasedimentary rocks	−92.9	−54.8		−70.9	−95.8	−66.7	−94.6	−62.7	−93.1	−89.1		−75.2
Mass balance (t)												
Kittilä Metavolcanic rocks	*2.7E+09*				4.3E+07			6.6E+06		4.8E+04	2.2E+03	
Kittilä Metasedimentary rocks	4.9E+08	2.3E+08		4.7E+06	9.4E+05	2.7E+04	1.9E+05	1.6E+04	2.5E+04	1.3E+03		6.4E+04
Savukoski Metavolcanic rocks	*4.1E+08*				6.4E+06			9.8E+05		7.1E+03	3.3E+02	
Savukoski Komatiites											*3.4E+02*	
Savukoski Metasedimentary rocks	1.8E+10	8.4E+09		1.7E+08	3.5E+07	1.0E+06	7.0E+06	5.9E+05	9.2E+05	4.9E+04		2.4E+06
Total Kittilä	**4.9E+08**	**2.3E+08**		**4.7E+06**	**4.4E+07**	**2.7E+04**	**1.9E+05**	**6.6E+06**	**2.5E+04**	**4.9E+04**	**2.2E+03**	**6.4E+04**
Total Savukoski	**1.8E+10**	**8.4E+09**		**1.7E+08**	**4.1E+07**	**1.0E+06**	**7.0E+06**	**1.6E+06**	**9.2E+05**	**5.6E+04**	**6.8E+02**	**2.4E+06**
Total Kittilä and Savukoski	**1.9E+10**	**8.6E+09**		**1.8E+08**	**8.5E+07**	**1.0E+06**	**7.2E+06**	**8.2E+06**	**9.4E+05**	**1.1E+05**	**2.9E+03**	**2.4E+06**

Numbers in italic (S in metavolcanic rocks and Au in metakomatiites) have high uncertainties and are not included in the final mass balance calculations

CLGB. The spatial distribution of the typical orogenic Au deposits along the KiSZ and SiSZ and the atypical along the SiSZ supports this argument. By projecting the thickness of the Kittilä Group onto the geological map, the dominant rock types present at depth in the source can be inferred (Fig. 10). Following the approach of Niiranen et al. (2015), the potential source is defined as the rock volume that has been metamorphosed at upper amphibolite-facies conditions (> 500–550 °C). In the Kittilä Group, the transition to amphibolite-facies conditions is inferred to be recorded at 4.05–5.35 km below the erosion surface level, based on greenschist-facies conditions recorded at the surface (~ 350 °C, Hölttä et al. 2007) and a temperature gradient of 37 °C/km during metamorphism (Niiranen et al. 2015). The transition to amphibolite facies becomes shallower in the CLGB to the north due to an inverted metamorphic gradient caused by thrusting of the Lapland Granulite Belt and to the west by thrusting of the Haparanda Suite (Fig. 10).

Although the block model in Fig. 10 only represents the end product of the Svecofennian orogeny, it still allows determination of the rock types potentially present in the source at the time of metamorphic evolution. The Kittilä Group is considered to prevail in the source volume where it is thicker than 4–5 km at depth, corresponding to the core of the CLGB, whereas the Savukoski Group prevails in the source volume where the Kittilä Group is thinner than 4–5 km and to the south of the SiSZ where the Kittilä Group is absent (Fig. 10). Along the KiSZ, the Kittilä Group is thick, especially in the southern section (> 7 km; Fig. 10), and thus, metamorphic fluids produced during metamorphic devolatilization of this rock volume would have been Au, As, and S-rich, accounting for the formation of typical orogenic Au deposit such as the Suurikuusikko deposit. The $\delta^{34}S$ signature of disseminated and vein-hosted auriferous pyrite in metavolcanic rocks at Suurikuusikko ranges between 0 and + 5‰ with few negative values for low Au bearing disseminated pyrite in metasedimentary rocks (to − 5‰; Molnár et al. 2017). The most common pyrite signature of 0 to + 5‰ can be attributed to a homogenized source, most likely buffered by the Kittilä Group metavolcanic rocks ($\delta^{34}S$ of altered oceanic crust of ~ + 1‰; Alt 1995; Molnár et al. 2017), whereas the few negative $\delta^{34}S$ values could be inherited from primary sedimentary-related pyrite or from fluids buffered by the Kittilä Group black schist (− 3 to + 4‰; Hanski and Huhma 2005).

The Kittilä Group present on the northern side of the SiSZ exceeds 4 km in thickness only over a limited area in the central part of the shear zone (Fig. 10). The Savukoski Group and possibly the other lower CLGB units and Archean basement are thus likely to be the dominant metal and ligand sources at depth along the SiSZ. Metamorphic fluid produced during metamorphic devolatilization would have been thus preferentially enriched in S, C, Cu, As, Se, Mo, Sn, Sb, Te, and U with lesser Au, promoting the formation of atypical orogenic Au along the SiSZ. The $\delta^{34}S$ signature of sulfides (pyrite, pyrrhotite, and chalcopyrite) from the Sattopora deposit ranges between 1 and + 4‰ in the northern orebody, in contact with the Kittilä Group and between − 1 and + 18‰ in the southern orebody, in contact with the Savukoski Group (Molnár et al. 2019). Within the wide range of the S isotope ratios in the southern orebody, two peaks are observed, one at ~ + 2‰ (range ~ − 1 to + 4‰), similarly to the northern orebody, and a second at ~ + 7–+ 8‰ (range ~ + 5 to + 9‰; Molnár et al. 2019). The $\delta^{34}S$ range of sulfides form the northern and southern orebody between ~ − 1 and + 4‰ can be attributed to a source strongly buffered by metavolcanic rocks, similarly to the Suurikuusikko deposit (Molnár et al. 2019). Instead, the $\delta^{34}S$ range of sulfides from the southern orebody between ~ + 5 to + 9 ‰ is explained by buffering of the mineralizing fluids by the Savukoski Group black schists, which have high $\delta^{34}S$ values (up to + 27‰; Hanski and Huhma 2005; Molnár et al. 2019). The presence of light hydrocarbons in fluid inclusions from the Sattopora deposit may imply C-rich metasedimentary rocks in the source, such as Savukoski Group black schists (Molnár et al. 2019).

Metal mobilization and orogenic Au mineralization in an evolving orogen

Orogenic Au deposits in the CLGB show multiple hydrothermal events with distinct stages of ore accumulation (Wyche et al. 2015; Molnár et al. 2018; Sayab et al. 2019). Two main stages of orogenic Au mineralization are currently recognized within the CLGB defined by an early-stage associated with peak metamorphism and a stage associated with late orogenic evolution (e.g., Molnár et al. 2018). The relationship between metal source zones and ore deposits is, however, difficult to establish as the ages of the causative metamorphic events for metal mobilization from the different units of the CLGB, mainly the Kittilä and Savukoski groups, are poorly constrained.

1. Au mineralization related to peak metamorphism

The earliest known mineralizing stage occurred within the Kittilä Group along the KiSZ and is defined by the main Au stage of the Suurikuusikko deposit, which is dated at 1.916 Ga and interpreted to be related to D1 (Wyche et al. 2015; Sayab et al. 2019). Prograde metamorphic devolatilization of rocks belonging to the Kittilä Group (Fig. 10) is interpreted to have occurred close to peak metamorphism at ~ 1.88–1.86 Ga, related to D2–D3 and generating Au-, As-, and S-rich metamorphic fluids. A conundrum arises

as the Re-Os isochron age of the Suurikuusikko deposit (1.916 ± 0.016 Ga) pre-dates peak metamorphism and associated metal mobilization. This discrepancy is difficult to account for, but further dating of both the Surrikuusiko deposit and peak metamorphism of the Kittilä and Savukoski groups could provide new insight. For instance, the northern part of the CLGB, in addition to inverted metamorphism, has been intruded by various magmatic bodies such as the Taatsi granodiorite (1.92–1.91 Ga), the Ruoppapalo granodiorite (1.91–1.90 Ga; Nironen 2017), and numerous porphyry dikes within the Kittilä Group dated at ca. 1.92 Ga (Rastas et al. 2001; Molnár et al. 2018). The effect of numerous magmas intruding or underplating the Kittilä Group could have led to substantial heating at its base, especially in its north-north-eastern part. The combined effect of inverted metamorphic gradient, due to thrusting of the Lapland Granulite Belt, and the excessive external heat from magmatic bodies possibly led to earlier peak metamorphism and metamorphic devolatilization at the base of Kittilä Group than in its shallower part, resembling to a "deep-earlier" metamorphic scenario (Stüwe et al. 1993; Stüwe 1998). Apart from the Suurikuusikko age conundrum, the Iso-Kuotko minimum age of mineralization at 1.87–1.86 Ga and associated with D1–D3 (Molnár et al. 2018; Sayab et al. 2019) fits with metal mobilization from the Kittilä Group source zone during prograde metamorphic devolatilization. Noteworthy, stress regime switch from compression (D2, ~ 1.90–1.89 Ga) to transpression (D3, ~ 1.88–1.87 Ga) would have increased crustal permeability, favoring large-scale fluid migration along major shear zone (e.g., KiSZ) and ore formation (Goldfarb et al. 1991, 2005; Bierlein et al. 2004; Sayab et al. 2019).

2. Au mineralization during late orogenic evolution

The second major epigenetic-hydrothermal typical and atypical stage that occurred in the CLGB during the latest stages of the Svecofennian orogeny corresponds to the main mineralization stages in the Iso-Kuotko, Saattopora and Levijärvi deposits (Patison 2007; Molnár et al. 2018, 2019; Sayab et al. 2019). These stages, occurring within a time window from ca. 1.83 to 1.76 Ga, are associated with D4–D5 deformation (Patison 2007; Molnár et al. 2018; Sayab et al. 2019) and appear apparently incompatible with metal mobilization during prograde metamorphic devolatilization during D2–D3. During the late Svecofennian orogeny evolution, however, a widespread thermal event, granitoid magmatism and high-grade metamorphism occurred (Hölttä et al. 2020), such as in the eastern Pajala Shear Zone (ca. 1.82–1.78 Ga; Bergman et al. 2006), the Hetta Complex (ca. 1.77 Ga; Ahtonen et al. 2007), and in parts of the Central Lapland Granitoid Complex (1.90–1.76 Ga; Corfu and Evins 2002; Nironen 2017; Lahtinen et al. 2018). The causes of this magmatism and metamorphism, such as lithospheric delamination, crustal erosion and asthenospheric upwelling, crustal melting following orogenic thickening or the far field effect of the amalgamation of Amazonia, Sarmatia, and Svecofennia (Corfu and Evins 2002; Lahtinen et al. 2005; Kukkonen et al. 2008), remain cryptic but most likely resulted in regional-scale lithospheric heating of the crust (Hölttä et al. 2020). Such event could have led to late-stage metamorphic fluid flow (Gonçalves et al. 2019), likely during D4–D5 (~ 1.84–1.76 Ga), associated with the SiSZ reactivation (Patison 2007) and possibly with late-stage metal mobilization from rocks that might have sustained only limited metal loss during earlier metamorphic devolatilization events. Again, a better understanding of the metamorphic evolution of the group units throughout the CLGB, especially of the Savukoski Group south of the SiSZ, would allow to build more robust genetic links between metal mobilization from source zones and ore deposits. Alternatively to metamorphic devolatilization, deep crustal or subcontinental lithospheric mantle fluid could have been generated during the latest stages of orogenic evolution accounting for the late-stage mineralizing events in the CLGB (Goldfarb and Groves 2015). A deep crustal source of mineralizing fluids is suggested by the Pb isotopic signature of galena from the Iso-Kuotko deposit, which shows an Archean basement component (Molnár et al. 2018). However, the different metal endowment of deposits along the KiSZ and SiSZ still suggests partial control of a shallower crustal source possibly explained by mixing of deep and mid-crustal fluids (LaFlamme et al. 2018).

Conclusions

Characterization of metal mobilization during prograde metamorphism of metavolcanic rocks, metasedimentary rocks, and metakomatiite from the CLGB enables us to test the metamorphic devolatilization model applied to the Paleoproterozoic greenstone belt. The main outcomes of the study are:

- The different investigated rock types show different metal mobilization during prograde metamorphism. Metavolcanic rocks show strong Au, As, and Sn and also possibly S depletion. Sulfur- and C-rich (S + C > 1 wt%) metasedimentary rocks show significant depletion of S, C, Cu, As, Se, Mo, Sn, Sb, Te, and U. Limited data from metakomatiite suggest that Au could be mobilized during prograde metamorphism. No clear mobilization of Ni and Co has been related to metamorphic devolatilization.
- When investigating metamorphic devolatilization from a source, all the rock types present should be considered and not only the dominant one. The metamorphic fluids produced from the devolatilization of the Kittilä Group were preferentially enriched in Au, As, Sn, Te, and S with the metavolcanic rocks (> 95% vol.) providing the bulk of these elements. The minor metasedimen-

tary rocks (< 5% vol.) most likely acted as an additional source, enhancing the metamorphic fluid metal content. On the contrary, metamorphic devolatilization from the Savukoski Group led to metamorphic fluids preferentially enriched in S, C, Cu, As, Se, Mo, Sn, Sb, Te, and U due to the large volume of metasedimentary rocks (> 40% vol.). These metamorphic fluids possibly had limited Au enrichment, relative to the Kittilä Group, due to the lower volume of metavolcanic rocks (~ 34% vol.) and the lack of Au depletion from the metasedimentary rocks.

- The style of mineralization and the bulk metal endowment of the deposits are strongly controlled by the nature of the source rocks at depth. Block reconstruction of the central CLGB highlights that the source of typical orogenic Au deposits along the KiSZ is dominated at depth by the Kittilä Group whereas the source of atypical Au deposits along the SiSZ is dominated at depth by the Savukoksi Group.
- A two stage model for Au mineralization in the CLGB is proposed:

    1. The primary stage associated with metamorphic devolatilization related to early stage of prograde metamorphism reaching peak metamorphism at ~ 1.88–1.86 Ga related to D2–D3. Devolatilization occurred preferentially from the Kititilä Group promoting the formation of typical orogenic Au deposits. Better dating of the metamorphic evolution of the CLGB unit groups, especially in the northern part of the belt, could reveal if this process can account for the formation of the Suurikuusikko deposit which predates peak metamorphism according to the presently available geochronological data. This stage occurred mainly within the Kittilä Group and along the KiSZ.
    2. The second stage associated with late orogenic evolution between ~ 1.83 and 1.76 Ga. In addition to the typical orogenic gold deposits, gold ores with atypical metal associations were also formed. Widespread granitoid magmatism, indicating that the mid-crust was at least locally hot at this stage of tectonic evolution, and high-grade metamorphism present throughout the Svecofennian orogeny, likely promoted late metamorphic fluid flow and possibly late metal mobilization. Additionally, deep crustal fluids from the lower crust or even the sub-continental lithospheric mantle could have been involved. This stage is mainly recorded along the SiSZ.

Within the frame of the debate regarding the source of metals in orogenic Au deposit, this study highlights that in the CLGB, and most likely in other Precambrian greenstone belts, combined metamorphic devolatilization of both metavolcanic and metasedimentary rocks can account for the formation of orogenic Au deposits. Further insight, however, could be gained by better linking the causative metamorphic events responsible for metal mobilization from the source zones with the ore deposits throughout the complex tectono-metamorphic evolution of an orogeny. Finally, mobilization of metals by metamorphic devolatilization does not preclude the implication of other deep-seated or magmatic sources which might also contribute also to orogenic Au endowment of Precambrian greenstone belts.

Supplementary Information The online version contains supplementary material available at https://doi.org/10.1007/s00126-022-01133-z.

Acknowledgements The authors would like to thank R. Goldfarb and an anonymous reviewer for thorough reviews as well as H. Frimmel and G. Beaudoin for editorial handling.

Funding Open Access funding enabled and organized by Projekt DEAL. This research was financially supported the Academy of Finland supported MinSysPro – Mineral Systems and Mineral Prospectivity in Finnish Lapland (grant No.281670) and the Academy of Finland and DAAD supported OroTecT (Orogenic gold deposits and post-orogenic tectonothermal evolution on Precambrian terranes: sources of ore-forming components and preservation of ore deposist – grant no. 315188) projects. Partial financial support was provided by Stockholm University, Sweden.

Declarations

Conflict of interest The authors declare no competing interests.

References

Ahtonen N, Holtta P, Huhma H (2007) Intracratonic Palaeoproterozoic granitoids in northern Finland: prolonged and episodic crustal melting events revealed by Nd isotopes and U-Pb ages on zircon. Bull Geol Soc Finl 79:143

Alt JC (1995) Sulfur isotopic profile through the oceanic crust: sulfur mobility and seawater-crustal sulfur exchange during hydrothermal alteration. Geology 23:585–588

Augustin J, Gaboury D (2017) Plume-related basaltic rocks in the Mana gold district in western Burkina Faso, West Africa : implications for exploration and the source of gold in orogenic deposits. J Afr Earth Sci Paleoproterozoic 129:17–30

Barnes S-J, Often M (1990) Ti-rich komatiites from northern Norway. Contrib to Mineral Petrol 105:42–54

Beaudoin G, Chiaradia M (2016) Fluid mixing in orogenic gold deposits: evidence from the HO-Sr isotope composition of the Val-d'Or vein field (Abitibi, Canada). Chem Geol 437:7–18
Bergman S, Billström K, Persson P-O et al (2006) U-Pb age evidence for repeated Palaeoproterozoic metamorphism and deformation near the Pajala shear zone in the northern Fennoscandian shield. GFF 128:7–20
Bhatia MR, Crook KAW (1986) Trace element characteristics of greywackes and tectonic setting discrimination of sedimentary basins. Contrib Mineral Petrol 92:181–193
Bierlein FP, Christie AB, Smith PK (2004) A comparison of orogenic gold mineralisation in central Victoria (AUS), western South Island (NZ) and Nova Scotia (CAN): implications for variations in the endowment of Palaeozoic metamorphic terrains. Ore Geol Rev 25:125–168
Boyle RW (1966) Origin of the gold and silver in the gold deposits of the Meguma Series. Nova Scotia Can Mineral 8:662
Brugger J, Liu W, Etschmann B et al (2016) A review of the coordination chemistry of hydrothermal systems, or do coordination changes make ore deposits? Chem Geol 447:219–253
Burrows DR, Wood PC, Spooner ETC (1986) Carbon isotope evidence for a magmatic origin for Archaean gold-quartz vein ore deposits. Nature 321:851
Corfu F, Evins PM (2002) Late Palaeoproterozoic monazite and titanite U-Pb ages in the Archaean Suomujärvi Complex, N-Finland. Precambrian Res 116:171–181
Crocket JH (1993) Distribution of gold in the Earth' s crust. In: Foster RP (eds) Gold Metallogeny and Exploration 1:36
de Wit MJ, Ashwal LD (1995) Greenstone belts: what are they? South African J Geol 98:505–520
Eilu P, Pankka H, Keinänen V et al (2007) Characteristics of gold mineralisation in the greenstone belts of northern Finland. Geol Surv Finland Spec Pap 44:57–106
Eilu P (2015) Overview on gold deposits in Finland. In: Maier WD, Lahtinen R, O'Brien H (eds) Mineral deposits of Finland. Elsevier, Amsterdam, pp 377–410
Frietsch R, Tuisku P, Martinsson O, Perdahl J-A (1997) Early proterozoic Cu-(Au) and Fe ore deposits associated with regional Na-Cl metasomatism in northern Fennoscandia. Ore Geol Rev 12:1–34
Frimmel HE (2018) Episodic concentration of gold to ore grade through Earth's history. Earth-Sci Rev 180:148–158
Fyfe WS (1987) Tectonics, fluids and ore deposits: mobilization and remobilization. Ore Geol Rev 2:21–36
Gaboury D (2019) Parameters for the formation of orogenic gold deposits. Appl Earth Sci 128:124–133
Goldfarb RJ, Groves DI (2015) Orogenic gold: common or evolving fluid and metal sources through time. Lithos 233:2–26
Goldfarb RJ, Snee LW, Miller LD, Newberry RJ (1991) Rapid dewatering of the crust deduced from ages of mesothermal gold deposits. Nature 354:296–298
Goldfarb R, Baker T, Dube B et al (2005) Distribution, character and genesis of gold deposits in metamorphic terranes. Econ Geol 100th Anniv Vol 407–450
Gonçalves GO, Lana C, Buick IS et al (2019) Twenty million years of post-orogenic fluid production and hydrothermal mineralization across the external Araçuaí orogen and adjacent São Francisco craton, SE Brazil. Lithos 342:557–572
Groves DI (1993) The crustal continuum model for late-Archaean lode-gold deposits of the Yilgarn Block, Western Australia. Miner Depos 28:366–374
Groves DI, Phillips GN (1987) The genesis and tectonic control on Archaean gold deposits of the western Australian shield—a metamorphic replacement model. Ore Geol Rev 2:287–322
Groves DI, Goldfarb RJ, Gebre-Mariam M et al (1998) Orogenic gold deposits: a proposed classification in the context of their crustal distribution and relationship to other gold deposit types. Ore Geol Rev 13:7–27
Groves DI, Santosh M, Deng J et al (2019) A holistic model for the origin of orogenic gold deposits and its implications for exploration. Miner Depos 55:1–18
Groves DI (1998) Orogenic gold deposits: a proposed classification in the context of their crustal distribution and relationship to other gold deposit types
Hanski E, Huhma H, Rastas P, Kamenetsky VS (2001a) The Palaeoproterozoic komatiite–picrite association of Finnish Lapland. J Petrol 42:855–876
Hanski E, Huhma H, Vaasjoki M (2001b) Geochronology of northern Finland : a summary and discussion. Geol Surv Finl Spec Pap 33:255–279
Hanski E, Huhma H (2005) Central Lapland greenstone belt. In: Lehtinen M, Nurmi PA, Rämö OT (eds) Precambrian Geology of Finland - Key to the Evolution of the Fennoscandian Shield. Elesvier B. V., pp 139–194
Heggie GJ, Barnes SJ, Fiorentini ML (2013) Application of lithogeochemistry in the assessment of nickel-sulphide potential in komatiite belts from northern Finland and Norway. Bull Geol Soc Finl 85:107–126
Herron MM (1988) Geochemical classification of terrigenous sands and shales from core or log data. J Sediment Res 58:820–829
Holma MJ, Keinanen VJ (2007) The Levijärvi–Loukinen gold occurrence: an example of orogenic gold mineralization with atypical metal association. In: Ojala VJ (eds) Goldin the Central Lapland Greenstone Belt, Finland. Geol Surv Finl Spec Pap, pp 165–184
Hölttä P, Heilimo E (2017) Metamorphic map of Finland. Geol Surv Finland Spec Pap 60:77–128
Hölttä P, Väisänen M, Väänänen J, Manninen T (2007) Paleoproterozoic metamorphism and deformation in Central Lapland, Finland. Gold Cent Lapl Greenstone Belt Geol Surv Finl Spec Pap 44:9–58
Hölttä P, Huhma H, Lahaye Y et al (2020) Paleoproterozoic metamorphism in the northern Fennoscandian Shield: age constraints revealed by monazite. Int Geol Rev 62:360–387
Hronsky JMA, Groves DI, Loucks RR, Begg GC (2012) A unified model for gold mineralisation in accretionary orogens and implications for regional-scale exploration targeting methods. Miner Depos 47:339–358
Hu S-Y, Evans K, Fisher L et al (2016) Associations between sulfides, carbonaceous material, gold and other trace elements in polyframboids: implications for the source of orogenic gold deposits, Otago Schist, New Zealand. Geochim Cosmochim Acta 180:197–213
Jenner FE, O'Neill HSC (2012) Major and trace analysis of basaltic glasses by laser-ablation ICP-MS. Geochem Geophys Geosystems 13:1–17
Jochum KP, Verma SP (1996) Extreme enrichment of Sb, Tl and other trace elements in altered MORB. Chem Geol 130:289–299. https://doi.org/10.1016/0009-2541(96)00014-9
Jowitt SM, Jenkin GRT, Coogan LA, Naden J (2012) Quantifying the release of base metals from source rocks for volcanogenic massive sulfide deposits: effects of protolith composition and alteration mineralogy. J Geochem Explor 118:47–59
Ketris MP, Yudovich YE (2009) Estimations of Clarkes for Carbonaceous biolithes: world averages for trace element contents in black shales and coals. Int J Coal Geol 78:135–148
Kolb J, Dziggel A, Bagas L (2015) Hypozonal lode gold deposits : a genetic concept based on a review of the New Consort, Renco, Hutti, Hira Buddini, Navachab, Nevoria and The Granites deposits. Precambrian Res 262:20–44
Kukkonen IT, Kuusisto M, Lehtonen M, Peltonen P (2008) Delamination of eclogitized lower crust: control on the

crust–mantle boundary in the central Fennoscandian shield. Tectonophysics 457:111–127
Kurhila M, Molnár F, O'Brien H et al (2017) U-Pb dating of hydrothermal monazite and xenotime from the Levijärvi-Loukinen gold deposit, Central Lapland Greenstone Belt, Northern Finland. In: 3rd Finnish National Colloquium of Geosciences Espoo, 15–16 March 2017. p 56
LaFlamme C, Jamieson JW, Fiorentini ML et al (2018) Investigating sulfur pathways through the lithosphere by tracing mass independent fractionation of sulfur to the Lady Bountiful orogenic gold deposit, Yilgarn Craton. Gondwana Res 58:27–38
Lahtinen R, Huhma H, Sayab M et al (2018) Age and structural constraints on the tectonic evolution of the Paleoproterozoic Central Lapland Granitoid Complex in the Fennoscandian Shield. Tectonophysics 745:305–325
Lahtinen R, Korja A, Nironen M (2005) Paleoproterozoic tectonic evolution. In: Developments in Precambrian Geology. Elsevier, pp 481–531
Large RR, Bull SW, Maslennikov VV (2011) A carbonaceous sedimentary source-rock model for Carlin-type and orogenic gold deposits. Econ Geol 106:331–358
Large RR, Halpin JA, Danyushevsky LV et al (2014) Trace element content of sedimentary pyrite as a new proxy for deep-time ocean–atmosphere evolution. Earth Planet Sci Lett 389:209–220
Large RR, Gregory DD, Steadman JA et al (2015) Gold in the oceans through time. Earth Planet Sci Lett 428:139–150
Le Bas MJ (2000) IUGS Reclassification of the high-Mg and picritic volcanic rocks. J Petrol 41:1467–1470
Le Bas MJ, Le Maitre RW, Streckeisen A et al (1986) A chemical classification of volcanic rocks based on the total alkali-silica diagram. J Petrol 27:745–750
Lehtonen M, Airo ML, Eilu P et al (1998) The stratigraphy, petrology and geochemistry of the Kittilä greenstone area, northern Finland. A Report of the Lapland Volcanite Project. Geol Surv Finland, Rep Investig 140:1–144
Masurel Q, Thébaud N, Allibone A et al (2019) Intrusion-related affinity and orogenic gold overprint at the Paleoproterozoic Bonikro Au–(Mo) deposit (Côte d'Ivoire, West African Craton). Miner Depos 57:557–580
McCuaig TC, Kerrich R (1998) P—T—t—deformation—fluid characteristics of lode gold deposits: evidence from alteration systematics. Ore Geol Rev 12:381–453
McDonough WF, Sun Ss (1995) The composition of the Earth. Chem Geol 120:223–253
Mineral Deposit Database of Finland (2022) Digital map database [Electronic resource]. Geological Survey of Finland [referred 21.01.2022]. Available at: http://gtkdata.gtk.fi/MDaE/index.html
Molnár F, Middleton A, Stein H et al (2018) Repeated syn-and post-orogenic gold mineralization events between 1.92 and 1.76 Ga along the Kiistala Shear Zone in the Central Lapland Greenstone Belt, northern Finland. Ore Geol Rev 101:936–959
Molnár F, Lahaye Y, Hugh Ob et al (2019) The Saattopora orogenic Au-Cu deposit, Central Lapland Greenstone belt, Finland: fluid sources and timing of hydrothermal processes. In: 15th Biennal SGA Meeting. pp 723–726
Molnár F, OBrien H, Lahaye Y et al (2017) Multi-stage hydrothermal processes and diverse metal associations in orogenic gold deposits of the Central Lapland Greenstone Belt, Finland. In: Mineral Resources to Discover–14th SGA Biennial Meeting. pp 63–66
Nesbitt BE, St. Louis RM, Muehlenbachs K (1987) Distribution of gold in altered basalts of DSDP hole 504B. Can J Earth Sci 24:201–209
Niiranen T, Lahti I, Nykänen V (2015) The orogenic gold potential of the Central Lapland Greenstone Belt, Northern Fennoscandian Shield. In: Mineral Deposits of Finland. Elsevier, pp 733–752
Nironen M (2017) Structural interpretation of the Peräpohja and Kuusamo belts and Central Lapland, and a tectonic model for northern Finland. Geol Surv Finland Rep Investig 234:53
Patison NL (2007) Structural controls on gold mineralisation in the Central Lapland Greenstone Belt. In: Gold in the Central Lapland Greenstone Belt, Finland, pp 107–122
Patten CGC, Pitcairn IK, Teagle DAH, Harris M (2016) Mobility of Au and related elements during the hydrothermal alteration of the oceanic crust: implications for the sources of metals in VMS deposits. Miner Depos 51:179–200
Patten CGC, Pitcairn IK, Molnár F et al (2020) Gold mobilization during metamorphic devolatilization of Archean and Paleoproterozoic metavolcanic rocks. Geology 48:1110–1114
Pearce JA, Norry MJ (1979) Petrogenetic implications of Ti, Zr, Y, and Nb variations in volcanic rocks. Contrib Mineral Petrol 69:33–47
Phillips GN, Powell R (2010) Formation of gold deposits: a metamorphic devolatilization model. J Metamorph Geol 28:689–718
Phillips GN, Groves DI, Brown IJ (1987) Source requirements for the Golden Mile, Kalgoorlie: significance to the metamorphic replacement model for Archean gold deposits. Can J Earth Sci 24:1643–1651
Pitcairn IK (2011) Background concentrations of gold in different rock types. Appl Earth Sci 120:31–38
Pitcairn IK, Teagle DAH, Craw D et al (2006a) Sources of metals and fluids in orogenic gold deposits: insights from the Otago and Alpone schists, New Zealand. Econ Geol 101:1525–1546
Pitcairn IK, Warwick PE, Milton JA, Teagle DAH (2006b) Method for ultra-low-level analysis of gold in rocks. Anal Chem 78:1290–1295
Pitcairn IK, Craw D, Teagle DAH (2015) Metabasalts as sources of metals in orogenic gold deposits. Miner Depos 50:373–390
Pitcairn IK, Leventis N, Beaudoin G et al (2021) A metasedimentary source of gold in Archean orogenic gold deposits. Geology 49:862–866
Qiu Z-J, Fan H-R, Goldfarb R et al (2021) Cobalt concentration in a sulfidic sea and mobilization during orogenesis: implications for targeting epigenetic sediment-hosted Cu-Co deposits. Geochim Cosmochim Acta 305:1–18
Rastas P, Huhma H, Hanski E et al (2001) U-Pb isotopic studies on the Kittila greenstone area, central Lapland, Finland. Geol Surv Finland Spec Pap 33:95–142
Ross P-S, Bédard JH (2009) Magmatic affinity of modern and ancient subalkaline volcanic rocks determined from trace-element discriminant diagrams. Can J Earth Sci 46:823–839
Sayab M, Suuronen J-P, Molnár F et al (2016) Three-dimensional textural and quantitative analyses of orogenic gold at the nanoscale. Geology 44:739–742
Sayab M, Molnár F, Aerden D et al (2019) A succession of near-orthogonal horizontal tectonic shortenings in the Paleoproterozoic Central Lapland Greenstone Belt of Fennoscandia: constraints from the world-class Suurikuusikko gold deposit. Miner Depos 55:1605–1624
Schandl ES, Gorton MP (2012) Hydrothermal alteration and CO2 metasomatism (natural carbon sequestration) of komatiites in the south-western Abitibi greenstone belt. Can Mineral 50:129–146
Stüwe K (1998) Tectonic constraints on the timing relationships of metamorphism, fluid production and gold-bearing quartz vein emplacement. Ore Geol Rev 13:219–228
Stüwe K, Will TM, Zhou S (1993) On the timing relationship between fluid production and metamorphism in metamorphic piles: some implications for the origin of post-metamorphic gold mineralisation. Earth Planet Sci Lett 114:417–430

Tatsumi Y, Oguri K, Shimoda G (1999) The behaviour of platinum-group elements during magmatic differentiation in Hawaiian tholeiites. Geochem J 33:237–247

Thébaud N, Sugiono D, LaFlamme C et al (2018) Protracted and polyphased gold mineralisation in the Agnew district (Yilgarn Craton, Western Australia). Precambrian Res 310:291–304

Tomkins AG (2010) Windows of metamorphic sulfur liberation in the crust : implications for gold deposit genesis. Geochim Cosmochim Acta 74:3246–3259

Vasilopoulos M, Molnár F, O'Brien H et al (2021) Geochemical signatures of mineralizing events in the Juomasuo Au–Co deposit, Kuusamo belt, northeastern Finland. Miner Depos 56:1195–1222

Webber AP, Roberts S, Taylor RN, Pitcairn IK (2013) Golden plumes: substantial gold enrichment of oceanic crust during ridge-plume interaction. Geology 41:87–90

Wyche NL, Eilu P, Koppström K et al (2015) The Suurikuusikko gold deposit (Kittilä mine), northern Finland. In: Mineral deposits of Finland. Elsevier, pp 411–433

Wyman D, Kerrich R (1988) Alkaline magmatism, major structures, and gold deposits; implications for greenstone belt gold metallogeny. Econ Geol 83:454–461

Supplementary data

Sample	Locality (depth)	Easting	Norhting	Metamorphic fascies	Group	Rock type	Density	SiO2	Al2O3	Fe2O3	MgO	CaO	Na2O	K2O	TiO2	P2O5	MnO	Total	LOI	S	C	C carb
							kg/m³	%	%	%	%	%	%	%	%	%	%	%	%	%	%	%
92009593-1	92009593	451987	7504714	Greenschist	Kittilä	Boninite	n.d.	47,30	13,40	8,48	8,40	12,60	1,09	0,08	0,46	0,04	0,17	92,01		0,01	0,19	n.d.
FEMO-2016-4.01	M52/2741-88/313 121.3-121.5	3383286	7533752	Lower amphibolite	Kittila	Boninite	2961	51,07	14,97	8,84	9,05	11,00	2,71	0,39	0,47	0,04	0,20	98,76	0,47	0,03	0,04	n.d.
FEMO-2016-4.02	M52/2741-88/313 124.1-124.25	3383286	7533752	Lower amphibolite	Kittila	Boninite	2942	51,25	14,86	9,07	9,07	10,28	2,81	0,84	0,50	0,04	0,18	98,91	0,76	0,08	0,01	n.d.
FEMO-2016-4.03	M52/2741-88/313 131.9-132.1	3383286	7533752	Lower amphibolite	Kittila	Boninite	2959	50,98	15,15	9,29	8,63	9,85	2,92	0,99	0,53	0,04	0,20	98,57	0,98	0,37	0,03	n.d.
FEMO-2016-4.04	M52/2741-88/313 135.3-135.45	3383286	7533752	Lower amphibolite	Kittila	Boninite	2956	51,27	14,27	9,76	8,99	10,66	2,59	0,69	0,55	0,04	0,19	99,01	1,03	0,40	0,02	n.d.
FEMO-2016-4.05	M52/2741-88/313 137.6-137.85	3383286	7533752	Lower amphibolite	Kittila	Boninite	n.d.	51,04	15,06	9,46	8,61	10,34	2,94	0,93	0,57	0,05	0,19	99,20	1,39	0,05	0,05	n.d.
FEMO 2017 13.1	M274100R514 53.15-53.60	413326	7524137	Greenschist	Savukoski	Komatiite	2880	47,70	7,07	13,29	27,77	8,47	0,04	0,48	0,52	0,03	0,20	105,57	16,00	0,01	3,88	3,85
FEMO 2017 13.2	M274100R514 90.35-90.70	413326	7524137	Greenschist	Savukoski	Komatiite	2838	47,45	8,73	14,16	27,06	4,59	0,04	0,10	0,53	0,04	0,13	102,83	18,00	0,00	4,72	4,68
FEMO 2017 12.2	M371489R540 77.00-77.50	3475224	7504904	Greenschist	Savukoski	Komatiite	2852	51,61	4,82	11,69	31,62	8,45	0,03	0,00	0,32	0,02	0,24	108,81	15,10	0,00	3,44	3,43
FEMO 2017 12.3	M371489R540 96.85-97.30	3475224	7504904	Greenschist	Savukoski	Komatiite	2926	49,28	7,54	9,89	27,16	7,92	0,20	0,05	0,50	0,04	0,17	102,76	6,58	0,00	0,47	0,46
FEMO 2017 12.4	M371489R540 121.00-121.40	3475224	7504904	Greenschist	Savukoski	Komatiite	2925	48,14	7,52	12,22	29,43	7,98	0,11	0,09	0,50	0,04	0,16	106,20	9,29	0,14	1,32	1,29
FEMO 2017 14.1	S371487R3303 24.50-25.10	3474000	7505500	Greenschist	Savukoski	Komatiite	2592	47,13	7,09	13,23	24,84	7,86	0,06	0,02	0,57	0,04	0,14	100,99	5,68	0,21	0,24	0,21
	92009708	468690	7540120	Greenschist	Savukoski	Komatiite	n.d.	43,30	4,82	8,91	23,50	9,90	0,05	0,02	0,39	0,02	0,16	91,07		0,03	0,05	
FEMO 2017 12.1	M371489R540 63.80-64.30	3475224	7504904	Greenschist	Savukoski	Komatiite	2936	49,86	5,75	11,55	25,69	8,87	0,39	0,02	0,45	0,03	0,18	102,80	8,48	0,00	1,50	1,49
FEMO 2017 15.1	S371487R3283 9.25-9.50	3473475	7504220	Greenschist	Savukoski	Komatiite	2973	48,99	7,22	12,34	25,67	5,39	2,22	0,15	0,41	0,01	0,14	102,54	11,60	0,00	2,35	2,31
FEMO 2017 4.01	3811-NR-001-78 15.00-15.30	3443590	7592435	Lower amphibolite	Savukoski	Komatiite	3096	41,28	6,91	11,87	23,39	9,66	0,57	0,11	0,48	0,04	0,19	94,50	7,54	0,08	1,72	1,72
FEMO 2017 6.01	3558-NR-002-78 39.10-39.40	3443910	7592770	Upper amphibolite	Savukoski	Komatiite	3204	40,92	12,85	15,63	10,91	10,85	2,37	0,38	1,35	0,05	0,19	95,49	1,07	0,01	0,15	0,13
FEMO 2017 5.03	3811-NR-003-78 129.90-130.20	3444240	7592990	Upper amphibolite	Savukoski	Komatiite	3034	46,67	6,77	13,48	14,81	12,11	1,09	0,20	0,44	0,09	0,12	95,79	2,01	0,32	0,27	0,26
FEMO 2017 6.02	3558-NR-002-78 41.90-42.20	3443910	7592770	Upper amphibolite	Savukoski	Komatiite	3113	45,15	8,37	11,73	22,33	7,61	0,98	0,08	0,44	0,03	0,15	96,87	3,06	0,02	0,10	0,08
FEMO 2017 6.03	3558-NR-002-78 72.90-73.20	3443910	7592770	Upper amphibolite	Savukoski	Komatiite	3158	45,76	6,40	11,80	23,43	8,27	0,56	0,06	0,45	0,03	0,18	96,95	3,32	0,01	0,39	0,38
FEMO 2017 5.04	3811-NR-003-78 146.00-146.40	3444240	7592990	Upper amphibolite	Savukoski	Komatiite	3070	44,11	8,46	13,21	21,52	7,71	0,98	0,08	0,61	0,06	0,17	96,93	3,02	0,08	0,09	0,07
FEMO-2016-2.01	KTÄ/SP-60 9.40-9.60	3390780	7526189	Greenschist	Kittila	MORB	n.d.	48,71	15,06	15,71	8,31	7,82	1,79	0,04	1,31	0,09	0,22	99,06	8,66	0,02	1,69	n.d.
FEMO-2016-2.02	KTÄ/SP-60 11.46-11.61	3390780	7526189	Greenschist	Kittila	MORB	n.d.	48,57	15,36	15,34	7,16	7,52	2,20	0,08	1,56	0,11	0,19	98,09	3,83	0,46	0,62	n.d.
FEMO-2016-6.02	KAR.1 58.6-58.95	3425967	7552430	Greenschist	Kittila	MORB	2945	49,84	13,63	18,11	4,22	7,37	2,89	0,25	1,94	0,20	0,24	98,68	2,58	0,39	0,38	n.d.
FEMO-2016-6.05	KAR.1 115.7-116.1	3425967	7552430	Greenschist	Kittila	MORB	3012	49,71	14,24	17,11	4,69	7,14	3,48	0,15	1,97	0,13	0,21	98,84	2,24	0,26	0,17	n.d.
FEMO-2016-9.01	274305-C2 30.85-31.1	3435989	7529642	Greenschist	Kittila	MORB	2996	50,28	14,36	14,86	6,18	10,14	0,60	0,03	1,31	0,10	0,23	98,09	3,54	0,15	0,28	n.d.
FEMO-2016-9.03	274305-C2 48.7-49.1	3435989	7529642	Greenschist	Kittila	MORB	2933	53,01	13,23	13,19	7,86	7,30	2,22	0,06	1,21	0,09	0,20	98,36	2,89	0,02	0,07	n.d.
FEMO-2016-9.04	274305-C2 57.7-57.95	3435989	7529642	Greenschist	Kittila	MORB	2987	50,88	14,23	12,40	7,67	10,33	3,23	0,08	0,95	0,06	0,21	100,04	4,00	0,05	0,56	n.d.
FEMO-2016-7.01	372280R304 23.10-23.35	3442605	7557737	Lower amphibolite	Kittila	MORB	2974	51,27	14,45	10,13	7,88	11,16	2,14	0,26	0,76	0,07	0,16	98,29	1,42	0,07	0,47	n.d.
FEMO-2016-8.01	SUK-22 23.9-24.2	3430642	7556533	Lower amphibolite	Kittila	MORB	3199	45,21	14,12	14,81	4,50	16,05	1,61	0,50	1,82	0,19	0,28	99,09	0,00	0,01	0,08	n.d.
FEMO-2016-7.03	372280R304 69.2-69-45	3442605	7557737	Lower amphibolite	Kittila	MORB	3053	47,97	14,07	13,65	5,63	12,73	2,25	0,20	1,64	0,11	0,23	98,47	2,56	0,14	0,81	n.d.
FEMO-2016-7.07	372280R304 94.05-94.25	3442605	7557737	Lower amphibolite	Kittila	MORB	3049	47,63	13,15	15,75	6,68	11,09	2,08	0,18	1,80	0,14	0,22	98,72	1,26	0,14	0,35	n.d.
FEMO-2016-3.01	KTÄ/HOV-11 3.70-3.80	3390459	7528447	Lower amphibolite	Kittila	MORB	n.d.	52,00	14,16	11,79	7,04	10,20	3,00	0,25	1,07	0,10	0,16	99,77	0,52	0,16	0,02	n.d.
FEMO-2016-3.02	KTÄ/HOV-11 32.75-32.90	3390459	7528447	Lower amphibolite	Kittila	MORB	n.d.	49,67	14,55	10,30	9,15	11,29	2,58	0,63	0,87	0,08	0,14	99,26	0,80	0,18	0,06	n.d.
FEMO 2017 1.01	M274184R305 77.85-78.20	382216	7523933	Lower amphibolite	Savukoski	MORB	2995	46,70	14,61	12,85	7,36	10,65	2,53	0,64	1,13	0,61	0,25	97,32	1,48	0,59	0,16	0,15
FEMO 2017 1.02	M274184R305 83.80-84.10	382216	7523933	Lower amphibolite	Savukoski	MORB	3025	46,99	15,01	12,11	7,26	10,47	2,65	0,48	1,15	0,58	0,22	96,92	0,79	0,29	0,05	0,05
FEMO 2017 4.12	3811-NR-001-78 224.50-224.80	3443590	7592435	Upper amphibolite	Savukoski	MORB	3020	46,51	10,69	12,94	10,91	10,90	1,94	1,06	0,84	0,08	0,21	96,09	1,06	0,00	0,09	0,08
FEMO 2017 4.13	3811-NR-001-78 237.50-237.90	3443590	7592435	Upper amphibolite	Savukoski	MORB	3011	49,87	13,18	12,81	5,71	9,26	3,37	1,13	1,24	0,25	0,18	97,00	0,51	0,05	0,05	0,05
FEMO 2017 4.14	3811-NR-001-78 245.60-245.90	3443590	7592435	Upper amphibolite	Savukoski	MORB	2993	48,15	13,75	13,35	4,67	8,82	4,73	1,16	1,40	0,30	0,21	96,55	0,68	0,00	0,14	0,12
FEMO 2017 4.1	3811-NR-001-78 201.10-201.45	3443590	7592435	Upper amphibolite	Savukoski	MORB	3096	48,83	15,15	11,03	7,53	10,37	2,46	0,37	0,67	0,09	0,16	96,66	1,19	0,01	0,10	0,09
FEMO-2015-113.4	Suurikuusikko, Etela pit surface	432311	7532546	Greenschist	Kittila	WPB	2958	51,56	14,10	12,54	6,12	7,82	4,70	0,16	1,84	0,18	0,19	99,21	1,92	0,02	n.d.	n.d.
FEMO-2015-113.5	Suurikuusikko, Etela pit surface	432355	7532528	Greenschist	Kittila	WPB	2907	50,23	15,44	15,25	6,73	6,15	2,45	0,34	2,55	0,22	0,22	99,59	3,61	0,12	n.d.	n.d.
FEMO-2015-113.6	Suurikuusikko, Etela pit surface	432348	7532472	Greenschist	Kittila	WPB	3052	48,34	14,79	12,99	8,22	11,20	1,89	0,43	1,81	0,16	0,27	100,11	2,97	0,06	n.d.	n.d.
FEMO-2015-113.2	Suurikuusikko, Etela pit surface	432330	7532510	Greenschist	Kittila	WPB	2733	48,74	14,38	16,16	6,29	7,40	2,86	0,56	2,49	0,19	0,20	99,27	7,14	0,25	n.d.	n.d.
FEMO-2016-7.08	372280R304 116.4-116.7	3442605	7557737	Lower amphibolite	Kittila	WPB	3064	51,06	12,88	14,21	5,50	9,37	2,04	0,75	1,94	0,17	0,22	98,14	4,07	0,61	1,06	n.d.
FEMO-2016-1.05	KTÄ/SP-057 128.30-128.50	3389203	7534967	Lower amphibolite	Kittila	WPB	n.d.	48,56	15,33	13,15	7,43	9,54	2,58	0,09	1,57	0,12	0,17	98,55	4,57	0,10	0,93	n.d.
FEMO-2016-7.04	372280R304 81.3-81.63	3442605	7557737	Lower amphibolite	Kittila	WPB	3051	46,74	13,38	16,67	5,55	10,58	2,50	0,52	2,56	0,24	0,25	99,00	1,67	0,25	0,57	n.d.
FEMO-2016-8.02	SUK-22 43.35-43.6	3430642	7556533	Lower amphibolite	Kittila	WPB	3019	48,10	17,48	9,82	3,85	14,42	2,84	0,46	1,53	0,33	0,19	99,02	0,49	0,01	0,10	n.d.
FEMO-2016-8.03	SUK-22 57.4-57.75	3430642	7556533	Lower amphibolite	Kittila	WPB	3044	46,02	12,83	11,97	9,83	11,53	2,91	2,03	1,32	0,38	0,23	99,06	1,56	0,02	0,26	n.d.
FEMO-2016-8.04	SUK-22 67.20-67.45	3430642	7556533	Lower amphibolite	Kittila	WPB	2992	46,07	14,43	12,61	7,39	10,59	3,92	1,73	1,49	0,46	0,23	98,93	1,80	0,15	0,35	n.d.
FEMO 2017 2.04	M274184R310 66.35-66.75	382503	7523737	Lower amphibolite	Savukoski	WPB	3095	47,93	9,73	15,01	9,34	10,41	1,87	0,79	1,76	0,22	0,32	97,38	0,84	0,00	0,05	0,05
FEMO 2017 10.2	K372298R19 22.10-22.50	453029	7558055	Upper amphibolite	Kittilä	WPB	2973	47,12	14,04	11,77	5,88	11,43	3,30	0,48	1,87	0,21	0,14	96,25	2,69	0,28	0,79	0,78
FEMO 2017 10.4	K372298R19 30.00-30.40	453029	7558055	Upper amphibolite	Kittilä	WPB	3104	46,73	13,34	14,53	5,50	11,30	3,15	0,20	2,07	0,24	0,20	97,25	2,13	0,22	0,69	0,67

Sample	C non carb	Cl *	Li	Be	Sc	V	Cr	Co	Ni	Cu	Zn	Ga	As	Se	Rb	Sr	Y	Zr	Nb	Mo	Pd	Ag	Cd	Sn	Sb	Te	Ba	La
	%	%	ppm	ppm	ppm	ppm	ppm	ppm	ppm	ppm	ppm	ppm	ppm	ppm	ppm	ppm	ppm	ppm	ppm	ppm	ppb	ppm	ppm	ppm	ppm	ppm	ppm	ppm
92009593-1	n.d.	n.d.	7,19		22,40	213,00	365,00	40,50	112,00	120,00	76,30	19,00	7,37	0,14	0,87	90,80	15,20	25,80	1,21							15,50	31,80	2,08
FEMO-2016-4.01	n.d.	n.d.	10,05		3,42	212,01	653,11	36,17	111,53	9,04	279,33	12,16	0,50	0,30	8,14	285,36	11,05	34,16	2,21					1,00	0,05	0,01	334,59	3,62
FEMO-2016-4.02	n.d.	n.d.	20,15		4,43	222,71	564,34	37,29	108,84	45,35	288,21	12,80	0,81	0,40	44,74	282,17	11,39	30,23	2,32					1,01		0,01	576,43	4,13
FEMO-2016-4.03	n.d.	n.d.	20,20		5,56	235,34	212,11	36,36	87,87	102,01	465,63	14,95	0,30	0,40	37,98	222,21	11,31	31,31	2,53	13,13			0,81	1,01		0,03	578,75	3,74
FEMO-2016-4.04	n.d.	n.d.	10,11		4,75	222,31	242,52	43,45	94,99	118,23	153,60	11,52	0,10	0,30	23,85	216,25	11,82	30,32	2,02					1,01	0,11	0,04	225,34	3,54
FEMO-2016-4.05	n.d.	n.d.	20,28		5,88	235,30	202,84	31,44	86,21	15,21	180,53	14,20	0,30	0,30	36,71	281,95	12,47	32,45	2,54					1,01		0,02	328,60	4,87
FEMO 2017 13.1	0,06	0,02	10,84	0,54	23,45	172,08	1520,43	79,68	535,10	12,14	24,75		0,90	0,15	23,45	64,24	9,11	28,29	0,44	0,11	12,96	0,01	0,02	0,17	0,25	0,01	23,57	0,90
FEMO 2017 13.2	0,06	0,02	18,43	0,16	25,70	215,77	2254,69	109,83	846,12	3,15	66,67		2,86	0,16	5,18	48,85	10,84	36,37	0,73	0,01	13,82	0,01	0,05	0,12	0,13	0,01	9,70	0,93
FEMO 2017 12.2	0,06	0,01	2,90	0,06	20,55	153,27	1811,37	93,70	167,20	2,55	12,77		0,81	0,09	0,23	76,29	6,92	25,54	0,23	0,01	7,08	0,01	0,01	0,12	0,13	0,01	17,42	0,35
FEMO 2017 12.3	0,05	0,01	7,80	0,05	22,97	168,81	1549,20	91,24	565,19	1,50	42,74		0,43	0,14	1,58	20,51	10,42	29,92	0,27	0,01	8,01	0,01	0,01	0,11	0,25	0,01	10,68	0,59
FEMO 2017 12.4	0,05	0,01	8,22	0,05	23,34	190,68	2476,65	116,16	656,42	34,52	39,45		1,81	0,34	3,25	70,57	8,77	32,88	0,43	0,09	11,51	0,03	0,02	0,11	0,15	0,01	15,34	0,67
FEMO 2017 14.1	0,05	0,01	1,59	0,05	26,07	198,14	2045,02	97,48	789,40	4,24	28,61		0,42	0,29	0,21	3,07	8,11	36,03	0,60	0,12	5,09	0,01	0,01	0,37	0,23	0,01	5,30	0,94
			3,50		18,90	181,00	2460,00	82,50	817,00	17,00	84,90	11,00		0,12	0,60	12,30	6,96	18,00	0,42							12,90	23,90	0,55
FEMO 2017 12.1	0,05	0,03	3,49	0,05	24,85	190,73	1133,50	87,19	192,91	7,74	9,81		0,31	0,11	0,35	56,02	11,33	33,79	0,44	0,01	11,66	0,01	0,01	0,11	0,11	0,01	23,98	0,54
FEMO 2017 15.1	0,06	0,01	36,53	0,06	24,02	173,64	1758,99	93,47	759,97	9,58	50,74		1,82	0,17	6,12	53,33	10,10	31,57	0,29	4,25	14,09	0,01	0,03	0,11	0,11	0,01	18,04	0,45
FEMO 2017 4.01	0,05	0,03	2,17	0,05	24,34	181,48	337,97	97,80	627,03	75,74	9,78		3,42	0,26	2,12	83,79	9,24	27,17	0,71	0,07	4,46	0,07	0,05	0,11	0,11	0,01	14,13	1,14
FEMO 2017 6.01	0,05	0,19	23,87	0,07	39,14	422,74	35,90	56,74	52,18	6,57	32,36		0,93	0,09	2,46	31,86	20,73	60,68	0,99	0,12	28,42	0,08	0,20	0,20	0,12	0,01	52,59	1,91
FEMO 2017 5.03	0,05	0,14	15,12	0,11	19,61	165,47	228,80	45,15	349,33	96,42	26,56		0,91	0,50	2,53	45,15	14,10	21,45	1,10	0,27	7,97	0,35	0,17	0,16	0,15	0,01	33,71	2,51
FEMO 2017 6.02	0,05	0,03	3,72	0,05	27,67	193,10	429,57	89,63	482,23	12,80	30,98		2,07	0,06	0,71	8,57	9,81	24,78	0,21	0,08	11,05	0,01	0,03	0,10	0,14	0,01	7,23	0,59
FEMO 2017 6.03	0,05	0,02	5,38	0,05	22,47	168,78	265,08	97,95	614,03	76,62	11,39		0,41	0,12	0,66	24,64	8,50	23,82	0,22	0,02	2,28	0,09	0,05	0,10	0,10	0,01	9,32	0,69
FEMO 2017 5.04	0,05	0,05	6,92	0,05	28,69	223,98	313,78	98,06	546,01	41,80	39,22		0,54	0,12	1,30	11,25	11,87	29,93	0,37	0,10	12,18	0,05	0,08	0,10	0,10	0,01	14,45	1,01
FEMO-2016-2.01	n.d.	n.d.	21,92		51,17	337,51	273,95	55,89	79,99	10,96	122,73	22,24	59,94	0,77	1,31	81,09	20,49	70,13	3,84					1,10	0,14	0,02	7,12	3,51
FEMO-2016-2.02	n.d.	n.d.	10,41		11,24	428,74	135,28	49,95	73,88	138,40	156,09	24,35	0,52	0,73	0,73	98,65	31,22	93,66	5,10					3,12	0,24	0,04	6,87	6,14
FEMO-2016-6.02	n.d.	n.d.	10,27		6,26	463,11	10,27	45,18	14,38	129,38	150,95	25,57	18,18	1,03	3,18	166,35	41,38	145,81	9,65					2,05	0,41	0,02	48,16	9,76
FEMO-2016-6.05	n.d.	n.d.	10,23		6,34	652,79		63,44	24,56	66,51	118,69	22,41	13,51	1,13	2,56	168,83	31,10	111,53	6,86	1,02			0,51	2,05	0,24	0,02	28,14	6,65
FEMO-2016-9.01	n.d.	n.d.	20,75		5,81	354,80	72,62	53,95	71,58	97,52	104,78	22,20	2,18	0,21	0,93	234,46	26,87	77,81	3,11					1,04	0,24	0,01	11,31	4,46
FEMO-2016-9.03	n.d.	n.d.	20,61		4,43	326,60	72,12	47,39	72,12	72,12	100,97	15,56	2,16		1,44	131,36	24,62	71,09	2,47					1,03	0,13	0,03	22,15	3,40
FEMO-2016-9.04	n.d.	n.d.	10,42		4,27	303,12	72,92	57,29	82,29	161,46	90,62	14,06	1,25		1,87	107,29	20,73	54,17	1,56	1,04			0,52	1,04	0,19	0,04	37,50	2,71
FEMO-2016-7.01	n.d.	n.d.	10,15		6,09	266,86	598,65	39,57	113,64	90,30	78,13	15,83	23,84	0,51	3,35	177,57	16,64	55,81	3,15					1,01	0,08	0,01	85,33	5,38
FEMO-2016-8.01	n.d.	n.d.	10,00		8,10	412,00	110,00	36,00	65,00	2,00	78,00	23,20	82,10	0,50	2,30	173,00	38,40	135,00	7,60				0,70	2,00	0,29	0,02	53,90	8,00
FEMO-2016-7.03	n.d.	n.d.	10,27		9,86	387,06	123,20	62,63	90,35	120,12	118,07	18,58	0,92	0,31	1,44	201,74	27,21	86,24	3,49					1,03	0,10	0,01	17,97	5,13
FEMO-2016-7.07	n.d.	n.d.	10,13		9,72	404,16	101,29	52,67	65,84	81,03	109,40	21,27	0,41	0,41	0,51	253,23	32,52	114,46	8,61	1,01			0,71	2,03	0,05	0,03	18,44	7,60
FEMO-2016-3.01	n.d.	n.d.	10,05		3,72	327,71	160,84	35,18	78,41	51,27	78,41	19,60	0,20	0,40	5,73	162,35	21,71	81,42	5,43					1,01		0,01	36,59	8,95
FEMO-2016-3.02	n.d.	n.d.	20,16		5,65	249,01	544,39	48,39	184,49	68,55	70,57	15,22	0,20	0,71	15,63	230,86	21,27	50,41	2,02					2,02		0,01	114,42	9,58
FEMO 2017 1.01	0,05	0,19	33,10	0,14	32,90	250,81	90,88	32,19	122,87	153,33	32,49		5,53	1,32	22,34	49,76	26,20	82,25	4,52	0,59	1,93	0,09	0,03	0,32	0,18	0,03	146,22	29,04
FEMO 2017 1.02	0,05	0,17	24,20	0,08	33,57	241,97	68,46	34,99	77,43	141,15	37,30		5,74	1,14	13,11	46,88	23,19	76,62	4,21	0,53	1,51	0,09	0,11	0,22	0,10	0,07	85,70	26,92
FEMO 2017 4.12	0,05	0,09	27,50	0,25	36,20	252,79	144,60	63,80	70,68	6,07	31,35		0,55	0,20	55,51	5,36	25,18	54,60	9,12	0,23	6,17	0,01	0,03	0,68	0,10	0,01	58,65	5,14
FEMO 2017 4.13	0,05	0,06	10,45	0,44	34,08	261,37	34,08	48,86	26,94	92,08	41,22		0,82	0,40	52,88	17,09	36,59	118,62	12,67	1,66	4,83	0,06	0,09	1,03	0,10	0,02	34,18	17,19
FEMO 2017 4.14	0,05	0,04	19,13	0,96	33,54	235,66	24,98	46,02	23,06	5,34	65,46		0,99	0,56	38,17	8,76	64,05	152,07	23,77	1,54	4,33	0,02	0,13	2,83	0,10	0,01	38,27	18,53
FEMO 2017 4.1	0,05	0,03	13,57	0,08	30,78	189,33	43,03	51,84	46,78	107,32	25,31		0,56	0,25	19,03	27,03	15,19	48,60	2,38	0,18	12,45	0,03	0,03	0,15	0,10	0,01	24,30	5,35
FEMO-2015-113.4	n.d.	n.d.				346,71			101,97	71,38	91,78		20,39		2,04	0,00	20,39	105,03	7,95									9,48
FEMO-2015-113.5	n.d.	n.d.				449,29			51,88	62,26	124,51				4,67	0,00	31,44	158,75	13,49					31,13				13,70
FEMO-2015-113.6	n.d.	n.d.				349,37			92,75	82,45	144,28	30,92	10,31		6,08	0,00	20,41	109,24	8,55					30,92				8,86
FEMO-2015-113.2	n.d.	n.d.				399,75			86,20	150,85	129,30		10,77		9,59	0,00	21,98	133,61	8,19									13,36
FEMO-2016-7.08	n.d.	n.d.	20,87		9,39	320,28	146,06	42,77	94,94	41,73	129,36	21,49	0,63	1,36	15,13	217,00	45,28	233,69	21,18	2,09				2,09		0,03	134,58	21,91
FEMO-2016-1.05	n.d.	n.d.	10,49		5,87	339,76	209,73	73,40	125,84	55,58	141,56	20,24	76,97	0,63	1,68	168,83	17,62	93,33	10,49					3,15	0,24	0,02	26,11	9,54
FEMO-2016-7.04	n.d.	n.d.	10,17		10,68	419,07	91,54	45,77	60,01	66,12	108,84	23,60	1,32	0,41	13,32	186,65	35,30	166,81	13,32				0,51	2,03	0,05	0,03	155,63	13,12
FEMO-2016-8.02	n.d.	n.d.			4,12	291,44	10,05	19,09	16,08	2,01	65,32	22,41	9,04	0,30	7,74	700,47	24,32	130,65	15,18	1,00				1,00	0,17	0,02	232,15	36,68
FEMO-2016-8.03	n.d.	n.d.	30,48		6,50	199,14	528,32	43,69	200,15	57,91	124,97	17,88	10,67	0,41	48,16	535,43	18,90	122,94	18,49					1,02	0,46	0,04	637,03	20,52
FEMO-2016-8.04	n.d.	n.d.	30,56		9,27	210,84	275,00	39,72	83,52	98,80	124,26	22,92	43,80	0,41	42,27	591,77	22,51	125,28	28,52				0,71	1,02	0,89	0,04	743,53	17,32
FEMO 2017 2.04	0,05	0,13	41,05	0,23	35,61	278,40	72,93	61,13	60,22	3,93	33,29		28,34	0,59	43,58	11,20	21,69	117,01	7,66	0,69	9,78	0,03	0,04	0,44	0,12	0,05	267,31	18,26
FEMO 2017 10.2	0,05	0,06	7,00	0,10	33,74	361,09	21,30	69,03	87,55	130,65	28,81		0,91	0,70	10,49	25,31	22,12	113,16	11,83	0,50	1,13	0,02	0,11	0,30	0,10	0,01	119,34	10,80
FEMO 2017 10.4	0,05	0,03	1,33	0,09	34,35	419,18	10,22	52,24	30,98	144,16	22,49		0,83	0,74	1,02	23,21	25,97	119,62	11,55	0,61	1,43	0,01	0,05	0,25	0,10	0,01	12,27	11,66

Sample	Ce	Pr	Nd	Eu	Gd	Tb	Dy	Ho	Er	Tm	Yb	Lu	Hf	Ta	W	Au	Pb	Bi	Th	U
	ppm	ppm	ppm	ppm	ppm	ppm	ppm	ppm	ppm	ppm	ppm	ppm	ppm	ppm	ppm	ppb	ppm	ppm	ppm	ppm
92009593-1				0,47	1,64		2,27	0,53	1,50				0,93			0,85	0,00	0,04	0,29	0,00
FEMO-2016-4.01	7,33	0,99	4,42	0,42	1,73	0,29	1,88	0,46	1,37	0,22	1,27	0,20	1,00			0,16	4,02	0,01	0,52	0,25
FEMO-2016-4.02	8,16	1,02	4,74	0,50	1,65	0,32	2,01	0,48	1,41	0,21	1,41	0,19	1,01	0,10		0,52		0,02	0,67	0,29
FEMO-2016-4.03	7,88	0,98	4,34	0,45	1,69	0,33	2,19	0,45	1,33	0,20	1,36	0,20	1,11	0,10	1,01	1,15	9,09	0,04	0,62	0,38
FEMO-2016-4.04	7,28	1,09	4,95	0,59	1,92	0,30	2,00	0,52	1,43	0,24	1,30	0,21	1,01	0,10		1,47		0,05	0,59	0,25
FEMO-2016-4.05	11,36	1,40	6,09	0,59	2,02	0,39	2,22	0,47	1,34	0,21	1,43	0,24	0,91	0,10	1,01	0,58	2,03	0,02	0,75	0,55
FEMO 2017 13.1	1,82	0,47	2,96	0,55	1,77	0,29	1,86	0,37	1,03	0,13	0,80	0,12	2,13	0,24	0,59	0,56	0,35	0,04	0,07	0,04
FEMO 2017 13.2	2,12	0,51	3,14	0,50	1,94	0,35	2,19	0,44	1,22	0,16	0,92	0,12	1,96	0,24	8,29	0,37	0,79	0,04	0,07	0,04
FEMO 2017 12.2	0,72	0,20	1,45	0,26	1,13	0,21	1,32	0,28	0,82	0,12	0,71	0,12	1,42	0,23	7,20	1,09	0,96	0,02	0,06	0,03
FEMO 2017 12.3	1,23	0,38	2,66	0,53	1,87	0,33	2,10	0,43	1,20	0,16	0,96	0,14	1,55	0,21	0,54	0,31	0,18	0,01	0,42	0,03
FEMO 2017 12.4	1,47	0,42	2,79	0,53	1,81	0,31	1,86	0,35	0,99	0,12	0,77	0,11	2,61	0,22	2,64	0,33	1,48	0,04	0,12	0,08
FEMO 2017 14.1	2,02	0,66	3,94	0,55	1,74	0,28	1,68	0,33	0,92	0,13	0,75	0,11	1,56	0,21	17,70	0,43	0,08	0,01	0,12	0,03
				0,24	1,10		1,35	0,26	0,70	0,00	0,00	0,00	0,44	0,00	0,00	1,15	0,00	0,04	0,13	0,00
FEMO 2017 12.1	1,05	0,36	2,38	0,60	1,87	0,34	2,16	0,45	1,26	0,17	0,98	0,14	1,43	0,22	2,84	0,32	0,27	0,01	0,07	0,03
FEMO 2017 15.1	0,96	0,28	1,96	0,32	1,65	0,30	1,97	0,41	1,16	0,15	0,90	0,14	1,57	0,23	1,31	2,25	0,59	0,01	0,08	0,03
FEMO 2017 4.01	0,74	0,48	2,72	0,52	1,70	0,30	1,88	0,38	1,06	0,14	0,90	0,13	1,55	0,22	3,14	0,65	1,67	0,03	0,07	0,03
FEMO 2017 6.01	1,61	0,97	5,87	1,60	3,92	0,72	4,47	0,91	2,52	0,34	2,20	0,33	2,33	0,20	7,13	0,43	4,75	0,01	0,13	0,07
FEMO 2017 5.03	2,97	0,93	4,64	1,31	2,05	0,37	2,32	0,48	1,42	0,19	1,20	0,16	1,36	0,20	5,72	0,06	5,40	0,01	0,11	2,07
FEMO 2017 6.02	0,17	0,31	2,07	0,35	1,76	0,32	2,10	0,42	1,17	0,15	0,97	0,14	1,54	0,21	4,76	0,28	0,87	0,01	0,05	0,03
FEMO 2017 6.03	0,17	0,40	2,58	0,48	1,58	0,28	1,79	0,36	1,00	0,13	0,87	0,12	1,46	0,21	6,48	1,34	2,71	0,01	0,05	0,03
FEMO 2017 5.04	0,33	0,44	2,91	0,70	2,17	0,40	2,48	0,51	1,42	0,19	1,19	0,18	1,66	0,21	4,53	0,28	3,74	0,01	0,05	0,03
FEMO-2016-2.01	9,42	1,47	7,23	1,17	3,32	0,54	4,00	0,84	2,52	0,37	2,25	0,37	2,30	0,11		0,26	2,19	0,01	0,32	0,16
FEMO-2016-2.02	15,61	2,32	12,49	1,49	5,28	0,87	5,55	1,14	3,28	0,52	2,83	0,44	2,71	0,31	1,04	0,29		0,02	0,49	0,46
FEMO-2016-6.02	24,95	3,61	17,56	1,84	6,43	1,14	7,20	1,55	4,58	0,69	3,95	0,60	3,80	0,51	1,03	0,61	2,05	0,02	0,81	0,35
FEMO-2016-6.05	16,58	2,54	12,38	1,22	4,87	0,85	5,71	1,24	3,51	0,56	3,37	0,49	2,97	0,31	1,02	0,79	4,09	0,01	0,65	0,21
FEMO-2016-9.01	11,31	1,76	8,71	1,18	4,33	0,73	4,56	0,90	3,09	0,32	2,65	0,39	1,97	0,21		0,26	7,26		0,45	0,10
FEMO-2016-9.03	9,17	1,51	7,42	0,90	3,68	0,62	4,08	0,90	2,78	0,38	2,49	0,38	1,96	0,21		0,25	4,12	0,01	0,38	0,11
FEMO-2016-9.04	7,08	1,11	5,42	0,74	2,95	0,56	3,61	0,74	2,31	0,29	2,33	0,30	1,56	0,10	3,12	0,84	4,17		0,21	
FEMO-2016-7.01	11,87	1,47	7,20	0,76	2,35	0,46	2,98	0,68	1,91	0,28	1,68	0,26	1,52	0,10	3,04	8,39	4,06	0,01	0,88	0,27
FEMO-2016-8.01	19,90	2,96	15,60	1,45	6,29	1,02	6,96	1,43	4,39	0,60	3,66	0,58	4,20	0,40	1,00	2,85	4,00	0,01	0,84	0,52
FEMO-2016-7.03	12,83	2,04	10,57	1,15	4,03	0,69	4,85	0,90	3,19	0,31	2,56	0,39	2,26	0,21	1,03	0,93	3,08	0,01	0,42	0,42
FEMO-2016-7.07	19,65	3,10	14,69	1,40	5,37	0,87	5,94	1,20	3,58	0,45	3,05	0,44	3,55	0,41		1,20	3,04	0,02	0,58	0,34
FEMO-2016-3.01	19,40	2,57	11,56	1,05	3,13	0,60	3,77	0,87	2,50	0,37	2,16	0,33	2,41	0,20	1,01	0,47	2,01	0,02	1,49	0,69
FEMO-2016-3.02	18,15	2,48	11,49	2,60	3,72	0,65	4,01	0,82	2,38	0,35	2,14	0,28	1,71	0,10		0,15		0,02	0,52	2,11
FEMO 2017 1.01	63,47	7,48	30,46	1,79	5,44	0,82	4,89	1,01	2,92	0,41	2,67	0,41	3,44	0,40	10,36	0,75	2,47	0,06	2,36	0,39
FEMO 2017 1.02	57,67	6,98	28,13	1,65	4,99	0,74	4,47	0,92	2,69	0,37	2,42	0,36	2,75	0,32	11,39	1,79	2,64	0,12	2,12	0,45
FEMO 2017 4.12	7,86	2,17	10,52	1,09	4,19	0,76	4,84	1,01	3,02	0,43	2,90	0,46	2,03	0,31	13,65	0,17	2,98	0,02	0,85	1,48
FEMO 2017 4.13	23,62	5,13	22,22	1,42	5,95	1,00	6,37	1,37	4,29	0,64	4,48	0,71	3,22	1,00	23,42	0,65	11,06	0,06	2,19	1,59
FEMO 2017 4.14	27,19	6,56	29,61	2,02	8,76	1,58	10,47	2,32	7,68	1,24	9,18	1,61	3,88	1,80	15,91	0,58	5,82	0,05	2,74	2,79
FEMO 2017 4.1	9,43	1,67	7,81	0,84	2,50	0,45	2,88	0,62	1,81	0,25	1,77	0,28	2,23	0,32	25,41	2,95	1,90	0,02	0,78	0,15
FEMO-2015-113.4	23,76	3,37	16,11	1,43	4,69	0,71	4,38	0,82	2,24	0,31	1,94	0,31	3,26	0,41		12,21			2,14	0,61
FEMO-2015-113.5	34,14	4,67	22,83	1,87	6,64	1,04	6,43	1,25	3,53	0,52	3,11	0,52	5,08	0,73		0,92			3,01	0,42
FEMO-2015-113.6	22,57	3,30	16,08	1,34	4,74	0,72	4,53	0,82	2,27	0,31	1,96	0,31	4,74	0,52		0,83			2,68	0,31
FEMO-2015-113.2	33,73	4,74	21,87	1,83	5,71	0,86	4,96	0,97	2,59	0,32	2,05	0,32	3,12	0,54		2,04			2,48	0,43
FEMO-2016-7.08	52,27	7,49	32,03	2,24	8,89	1,47	9,09	1,69	4,78	0,72	4,06	0,64	6,57	1,36		0,42	4,17	0,04	2,45	1,05
FEMO-2016-1.05	22,65	3,15	15,10	1,45	3,83	0,55	3,50	0,76	1,90	0,25	1,42	0,22	2,52	0,42		0,49	3,15	0,02	0,79	0,35
FEMO-2016-7.04	32,45	4,66	20,75	1,83	6,89	1,06	6,23	1,34	3,81	0,52	3,15	0,47	4,58	0,71		0,69	7,12	0,02	1,33	1,12
FEMO-2016-8.02	76,88	9,70	36,28	1,80	6,10	0,86	4,55	0,85	2,39	0,33	2,01	0,28	3,52	0,90	3,01	0,52	6,03	0,01	5,74	1,98
FEMO-2016-8.03	45,11	5,55	21,54	1,36	4,75	0,66	3,62	0,65	2,13	0,25	1,81	0,22	2,84	0,81	1,02	2,38	8,13	0,01	1,47	0,47
FEMO-2016-8.04	41,86	5,49	22,41	1,49	4,96	0,70	3,93	0,71	2,37	0,31	1,97	0,30	2,65	1,53	2,04	4,19	10,19	0,02	2,58	1,11
FEMO 2017 2.04	42,16	5,80	25,52	1,77	5,87	0,88	4,77	0,89	2,44	0,31	1,96	0,28	2,94	0,39	12,81	6,40	2,53	0,20	3,15	0,42
FEMO 2017 10.2	26,95	4,01	18,83	1,60	5,20	0,79	4,63	0,91	2,48	0,32	2,01	0,29	2,92	0,61	6,45	0,36	0,45	0,01	1,28	0,33
FEMO 2017 10.4	28,93	4,23	19,63	1,75	5,74	0,90	5,29	1,03	2,87	0,37	2,28	0,33	2,92	0,56	6,36	0,36	0,59	0,01	1,25	0,72

Sample	Locality (depth)	Easting	Norhting	Metamorphic fascies	Group	Rock type	Density	SiO2	Al2O3	Fe2O3	MgO	CaO	Na2O	K2O	TiO2	P2O5	MnO	Total	LOI	S	C	C carb
							kg/m³	%	%	%	%	%	%	%	%	%	%	%	%	%	%	%
FEMO 2017 9.01	M274188R312 23.85-24.20	382933	7530617	Upper amphibolite	Kittilä	WPB	3056	47,46	10,32	15,66	6,88	8,76	2,01	1,71	1,71	0,29	0,26	95,06	2,69	0,00	0,69	0,67
FEMO 2017 9.02	M274188R312 39.30-39.60	382933	7530617	Upper amphibolite	Kittilä	WPB	2982	48,66	12,55	15,33	6,38	8,69	3,51	0,90	2,12	0,33	0,22	98,67	0,76	0,09	0,22	0,15
FEMO 2017 9.03	M274188R312 47.10-47.40	382933	7530617	Upper amphibolite	Kittilä	WPB	2994	51,30	13,50	14,21	4,94	6,38	4,71	0,83	2,22	0,44	0,20	98,73	0,25	0,28	0,09	0,05
FEMO 2017 9.04	M274188R312 61.35-61.60	382933	7530617	Upper amphibolite	Kittilä	WPB	3053	49,96	13,65	15,61	4,55	6,98	3,98	0,98	2,33	0,47	0,23	98,76	0,46	0,09	0,17	0,15
FEMO 2017 9.05	M274188R312 135.50-135.80	382933	7530617	Upper amphibolite	Kittilä	WPB	2976	50,21	13,80	15,76	4,56	6,18	4,49	0,82	2,36	0,43	0,32	98,93	0,53	0,02	0,17	0,16
FEMO 2017 4.08	3811-NR-001-78 155.20-155.50	3443590	7592435	Upper amphibolite	Savukoski	WPB	2877	53,18	14,46	9,18	8,35	6,75	4,72	0,80	0,50	0,11	0,14	98,19	1,53	0,05	0,09	0,09
FEMO 2017 4.11	3811-NR-001-78 212.60.212.95	3443590	7592435	Upper amphibolite	Savukoski	WPB	3064	48,66	13,18	14,35	4,94	9,09	3,36	1,09	1,43	0,28	0,19	96,58	0,24	0,12	0,05	0,05
FEMO 2017 4.09	3811-NR-001-78 185.40.186.00	3443590	7592435	Upper amphibolite	Savukoski	WPB	2832	56,56	13,61	9,99	3,72	6,60	3,67	1,70	0,80	0,23	0,14	97,03	0,50	0,01	0,10	0,09
FEMO-2015-15.1	R-511 12021594 8.60-8.75	413126	7524147	Greenschist	Savukovski	Metasediment	n.d.	56,38	13,02	14,27	6,51	1,68	0,08	3,83	2,08	0,98	0,13	98,97	4,50	0,67	0,85	
FEMO-2016-2.01	KTÄ/SP-60 9.40-9.60	3390780	7526189	Greenschist	Kittila	Metasediment	n.d.	48,71	15,06	15,71	8,31	7,82	1,79	0,04	1,31	0,09	0,22	99,06	8,66	0,02	1,69	
FEMO 2017 3.03	M274184R301 56.50-56.80	393365	7521182	Greenschist	Savukoski	Metasediment	2894	45,88	12,14	21,05	5,99	3,98	0,55	2,97	2,07	0,20	0,56	95,39	7,02	0,20	1,57	1,50
FEMO-2016-5.01	M52/2734-74/520 48.1-48.4	3418157	7514888	Greenschist	Savukovski	Metasediment	2740	74,31	13,16	4,24	1,63	0,46	1,11	3,76	0,42	0,02	0,03	99,15	3,01	1,11	1,13	
FEMO 2017 3.05	M274184R301 73.10-73.40	393365	7521182	Greenschist	Savukoski	Metasediment	3025	38,21	12,65	25,81	5,03	5,22	0,07	3,73	1,60	0,17	0,87	93,34	7,80	0,75	2,35	1,77
FEMO 2017 3.01	M274184R301 15.90-16.20	393365	7521182	Greenschist	Savukoski	Metasediment	3020	42,78	12,39	24,86	5,13	2,82	0,39	3,69	1,58	0,20	0,45	94,28	6,61	2,05	1,94	1,00
FEMO-2016-5.03	M52/2734-74/520 59.75-60.1	3418157	7514888	Greenschist	Savukovski	Metasediment	2805	61,32	15,04	11,89	4,14	0,53	1,55	3,18	1,14	0,07	0,07	98,94	4,46	2,62	1,50	
FEMO-2016-5.04	M52/2734-74/520 69.75-70.1	3418157	7514888	Greenschist	Savukovski	Metasediment	2791	61,27	15,52	11,87	4,08	0,51	1,12	3,65	1,07	0,07	0,10	99,25	5,26	2,69	2,09	
FEMO-2016-5.02	M52/2734-74/520 53.8-54.15	3418157	7514888	Greenschist	Savukovski	Metasediment	2771	66,33	12,61	10,05	2,93	0,68	1,56	3,51	0,55	0,03	0,04	98,30	4,00	3,02	1,79	
FEMO-2015-15.2	R-511 12021595 11.90-12.00	413126	7524147	Greenschist	Savukovski	Metasediment	n.d.	44,27	15,84	14,11	8,19	8,31	0,14	4,71	1,73	0,17	0,25	97,72	12,93	1,28	3,99	
FEMO-2016-2.03	KTÄ/SP-60 19.05-19.20	3390780	7526189	Greenschist	Kittila	Metasediment	n.d.	51,77	13,69	15,23	2,68	6,51	3,04	2,12	2,05	0,30	0,15	97,52	5,35	3,70	2,54	
FEMO-2014-12.1	R-409 12021476 9.95-92.00	3432620	7535832	Greenschist	Kittila	Metasediment	n.d.	53,60	10,78	14,65	2,87	8,14	0,05	2,87	1,12	0,08	0,07	94,25	5,07	5,36	2,36	
FEMO-2014-11.1	R-476 29101420 45.90-46.30	432514	7532960	Greenschist	Kittila	Metasediment	n.d.	49,72	12,68	16,34	4,10	7,24	0,13	2,60	1,75	0,09	0,10	94,74	6,65	5,56	2,41	
FEMO-2015-14.1	R-521 12021587 66.25-66.45	413074	7524099	Greenschist	Savukovski	Metasediment	n.d.	35,12	14,30	15,76	7,46	12,95	0,08	5,32	1,98	0,21	0,32	93,53	15,19	4,05	6,45	
FEMO-2016-9.02	274305-C2 43.4-43.6	3435989	7529642	Greenschist	Kittila	Metasediment	3220	47,96	1,20	33,17	2,19	8,33	0,04	0,11	0,10	0,42	0,16	93,68	6,10	15,08	2,87	
FEMO 2017 3.04	M274184R301 62.05-62.40	393365	7521182	Greenschist	Savukoski	Metasediment	3224	47,90	10,58	28,36	1,76	1,23	1,58	2,41	0,70	0,32	0,12	94,97	11,90	11,04	8,14	0,11
FEMO-2014-12.2	R-409 12021473 35.60-35.65	3432620	7535832	Greenschist	Kittila	Metasediment	n.d.	47,52	5,96	34,59	1,80	4,88	0,06	0,54	0,52	2,12	0,78	98,76	14,81	15,53	3,82	
FEMO-2014-11.2	R-476 29101427 116.15-116.40	432514	7532960	Greenschist	Kittila	Metasediment	n.d.	47,50	5,48	32,01	1,90	7,50	0,09	1,16	0,44	0,65	0,09	96,84	13,46	20,56	2,76	
FEMO-2016-7.02	372280R304 35.22-35-47	3442605	7557737	Lower amphibolite	Kittila	Metasediment	2843	42,70	11,96	11,11	15,22	12,69	0,55	3,35	0,67	0,19	0,16	98,61	8,89	0,24	2,06	
FEMO-2016-1.03	KTÄ/SP-057 98.03-98.30	3389203	7534967	Lower amphibolite	Kittila	Metasediment	n.d.	57,76	24,86	0,87	0,96	0,91	6,50	4,22	2,59	0,41	0,01	99,09	4,30	0,04	2,67	
FEMO-2016-1.02	KTÄ/SP-057 47.75-47.90	3389203	7534967	Lower amphibolite	Kittila	Metasediment	n.d.	52,13	14,01	18,11	6,90	2,06	1,96	1,68	1,61	0,20	0,11	98,77	4,87	4,63	1,24	
FEMO-2016-1.04	KTÄ/SP-057 101.25-101.5	3389203	7534967	Lower amphibolite	Kittila	Metasediment	n.d.	50,77	13,33	14,49	5,28	6,03	2,76	2,66	1,29	0,18	0,14	96,93	4,61	4,79	2,22	
FEMO-2016-1.01	KTÄ/SP-057 13.15-13-35	3389203	7534967	Lower amphibolite	Kittila	Metasediment	n.d.	50,23	14,43	18,01	5,98	3,53	2,50	2,95	1,52	0,25	0,08	99,47	5,01	5,99	1,77	
FEMO-2016-3.04	KTÄ/HOV-11 107.8.108	3390459	7528447	Lower amphibolite	Kittila	Metasediment	n.d.	55,76	13,92	15,54	3,51	2,32	3,91	2,74	0,90	0,22	0,07	98,88	12,91	6,51	12,42	
FEMO-2016-3.03	KTÄ/HOV-11 104.85-105	3390459	7528447	Lower amphibolite	Kittila	Metasediment	n.d.	49,55	11,62	25,18	3,40	3,21	3,53	1,29	0,73	0,20	0,08	98,79	11,02	11,22	8,48	
FEMO 2017 11.1	K372298R18 28.00-28.30	452921	7558118	Upper amphibolite	Kittilä	Metasediment	3045	47,43	12,65	15,17	4,67	9,79	3,28	0,62	2,24	0,36	0,20	96,42	2,97	0,21	0,82	0,80
FEMO 2017 4.05	3811-NR-001-78 107.55-107.85	3443590	7592435	Upper amphibolite	Savukoski	Metasediment	2931	45,80	15,31	10,38	5,18	11,78	4,37	0,63	2,09	0,32	0,17	96,01	3,68	0,19	1,00	0,87
FEMO 2017 4.06	3811-NR-001-78 116.40-116.80	3443590	7592435	Upper amphibolite	Savukoski	Metasediment	2909	51,17	16,34	10,05	5,20	7,81	3,99	1,15	1,33	0,11	0,15	97,30	1,70	0,86	0,43	0,34
FEMO 2017 10.3	K372298R19 25.40-25.70	453029	7558055	Upper amphibolite	Kittilä	Metasediment	3001	46,12	13,75	14,71	5,09	10,93	3,39	0,43	2,12	0,25	0,20	97,01	3,77	0,22	1,13	1,03
FEMO 2017 5.01	3811-NR-003-78 86.20-86.50	3444240	7592990	Upper amphibolite	Savukoski	Metasediment	2935	41,94	15,82	9,01	2,46	15,84	0,91	5,08	2,58	0,40	0,17	94,22	8,16	0,09	2,20	2,17
FEMO 2017 4.03	3811-NR-001-78 74.95-75.25	3443590	7592435	Upper amphibolite	Savukoski	Metasediment	3256	44,97	12,42	24,48	6,70	1,86	1,01	3,54	0,72	0,33	0,13	96,18	7,75	7,90	3,36	0,05
FEMO-2016-5.06	M52/2734-74/520 141.4-141.6	3418157	7514888	Greenschist	Savukovski	Volcanoclastite	2872	53,29	19,28	15,47	3,28	1,15	1,85	3,13	1,70	0,12	0,12	99,40	2,89	0,01	0,02	
FEMO-2016-5.07	M52/2734-74/520 146.7-147	3418157	7514888	Greenschist	Savukovski	Volcanoclastite	2826	52,78	17,29	16,58	3,24	1,11	4,46	1,17	2,07	0,16	0,11	98,97	2,19	0,13	0,05	
FEMO-2016-5.08	M52/2734-74/520 150.1-150.45	3418157	7514888	Greenschist	Savukovski	Volcanoclastite	n.d.	59,13	12,43	18,15	3,33	0,92	1,02	1,70	2,19	0,16	0,17	99,21	2,21	0,21	0,02	
FEMO-2016-5.09	M52/2734-74/520 156.25-156.55	3418157	7514888	Greenschist	Savukovski	Volcanoclastite	2863	57,57	17,38	15,15	3,43	0,41	0,85	3,10	1,57	0,12	0,11	99,71	3,28	0,41	0,02	
FEMO 2017 3.02	M274184R301 49.60-50.00	393365	7521182	Greenschist	Savukoski	Volcanoclastite	2930	46,94	15,68	18,58	2,80	1,35	2,15	4,39	1,97	0,16	0,24	94,27	1,83	0,09	0,46	0,12
FEMO-2016-5.05	M52/2734-74/520 93.0-93.3	3418157	7514888	Greenschist	Savukovski	Volcanoclastite	2824	58,47	13,62	14,60	4,05	2,08	3,23	0,70	1,82	0,12	0,13	98,85	3,47	0,18	0,56	
FEMO 2017 1.04	M274184R305 87.35-87.70	382216	7523933	Lower amphibolite	Savukoski	Volcanoclastite	2896	50,33	15,48	13,63	6,93	3,80	2,82	2,49	1,09	0,07	0,23	96,88	1,09	0,01	0,40	0,08
FEMO 2017 1.03	M274184R305 85.40-85.75	382216	7523933	Lower amphibolite	Savukoski	Volcanoclastite	2913	51,50	14,87	12,94	7,55	3,51	2,85	2,40	1,06	0,08	0,23	96,99	1,32	0,02	0,57	0,05
FEMO 2017 2.01	M274184R310 12.60-12.95	382503	7523737	Lower amphibolite	Savukoski	Volcanoclastite	2829	49,30	13,18	20,95	7,30	5,98	0,44	0,48	0,73	0,07	0,43	98,87	0,01	0,01	0,06	0,05
FEMO 2017 2.02	M274184R310 33.80-34.25	382503	7523737	Lower amphibolite	Savukoski	Volcanoclastite	2928	50,01	14,07	15,95	7,06	3,32	3,09	1,38	1,29	0,09	0,24	96,49	0,94	0,01	0,63	0,09
FEMO 2017 4.04	3811-NR-001-78 83.75-84.05	3443590	7592435	Upper amphibolite	Savukoski	Volcanoclastite	2906	53,24	14,34	13,15	3,59	5,53	3,36	1,62	2,36	0,39	0,21	97,79	0,36	0,30	0,12	0,09
FEMO 2017 4.07	3811-NR-001-78 124.80-125.20	3443590	7592435	Upper amphibolite	Savukoski	Volcanoclastite	2838	62,38	14,91	10,57	2,35	1,99	3,41	2,12	1,28	0,12	0,13	99,26	0,87	0,19	0,28	0,06
FEMO 2017 10.1	K372298R19 15.80-16.10	453029	7558055	Upper amphibolite	Kittilä	Volcanoclastite	3045	46,25	12,75	16,21	4,58	9,75	3,28	0,37	2,64	0,51	0,23	96,58	2,10	0,23	0,66	0,65

Sample	C non carb	Cl *	Li	Be	Sc	V	Cr	Co	Ni	Cu	Zn	Ga	As	Se	Rb	Sr	Y	Zr	Nb	Mo	Pd	Ag	Cd	Sn	Sb	Te	Ba	La
	%	%	ppm	ppm	ppm	ppm	ppm	ppm	ppm	ppm	ppm	ppm	ppm	ppm	ppm	ppm	ppm	ppm	ppm	ppm	ppb	ppm	ppm	ppm	ppm	ppm	ppm	ppm
FEMO 2017 9.01	0,05	0,27	45,18	0,19	31,08	264,48	82,33	53,41	76,98	6,90	118,35		2,11	0,58	73,89	35,40	26,55	160,54	9,37	1,28	3,50	0,02	0,05	0,40	0,10	0,01	1965,62	25,01
FEMO 2017 9.02	0,07	0,13	27,92	0,15	22,67	313,41	52,00	50,09	69,33	196,51	112,87		2,12	0,76	25,29	20,66	25,80	166,28	14,01	1,44	3,22	0,46	0,26	0,41	0,22	0,02	691,32	25,60
FEMO 2017 9.03	0,05	0,14	28,07	0,22	18,85	241,61	15,04	41,51	26,07	154,39	90,23		1,83	0,87	27,97	13,94	30,08	193,49	18,15	1,47	1,30	0,11	0,09	0,62	0,17	0,02	610,55	30,68
FEMO 2017 9.04	0,05	0,20	31,35	0,26	19,59	262,22	11,75	38,18	15,07	55,36	98,46		1,93	0,80	30,14	19,79	35,16	214,00	20,50	1,20	1,31	0,05	0,08	0,66	0,12	0,01	833,88	31,95
FEMO 2017 9.05	0,05	0,30	34,59	0,28	20,21	290,56	11,06	41,82	8,65	11,16	98,53		2,11	0,66	28,85	19,50	30,06	213,14	20,21	0,53	1,01	0,07	0,14	0,96	0,22	0,01	446,39	28,05
FEMO 2017 4.08	0,05	0,05	19,81	0,09	28,65	159,49	184,88	45,51	50,59	115,80	32,51		0,73	0,18	20,11	7,72	11,89	67,04	2,48	0,08	6,20	0,04	0,03	0,14	0,10	0,01	98,54	9,98
FEMO 2017 4.11	0,05	0,04	16,04	0,19	33,28	255,64	19,35	54,74	32,48	187,47	42,10		0,74	0,55	43,81	8,42	34,99	146,36	9,25	0,51	10,53	0,05	0,07	0,39	0,10	0,02	91,23	21,95
FEMO 2017 4.09	0,05	0,02	10,25	0,38	24,33	182,94	21,01	38,40	23,62	94,29	39,20		0,68	0,46	56,49	23,02	20,00	120,62	6,13	0,16	7,64	0,03	0,04	0,54	0,10	0,01	129,67	26,44
FEMO-2015-15.1			20,95		18,54	54,48		93,24	146,67	694,58	17,81	27,13		1,26	89,05	12,57	125,19	569,91	44,73	2,10				2,10	0,59	0,09	110,53	58,35
FEMO-2016-2.01			21,92		51,17	337,51	273,95	55,89	79,99	10,96	122,73	22,24	59,94	0,77	1,31	81,09	20,49	70,13	3,84					1,10	0,14	0,02	7,12	3,51
FEMO 2017 3.03	0,06	0,44	22,78	1,06	39,29	383,20	186,74	78,37	74,70	73,94	44,26		60,88	0,84	67,57	7,99	27,31	115,50	10,01	1,09	1,08	0,02	0,04	1,07	1,51	0,01	96,07	10,79
FEMO-2016-5.01			20,63		2,48	110,35	30,94	12,38	38,16	89,72	9,28	19,39	50,43	1,03	141,80	18,67	40,63	176,35	25,37	11,34				6,19	0,41	0,07	327,96	69,10
FEMO 2017 3.05	0,58	0,61	24,88	0,67	39,50	387,37	100,28	48,88	60,45	145,13	51,29		100,28	1,19	88,49	8,18	29,90	103,66	8,78	1,56	1,42	0,02	0,07	1,36	2,53	0,02	178,95	11,68
FEMO 2017 3.01	0,94	0,67	20,76	0,56	34,63	373,16	118,29	107,54	134,42	1258,21	34,41		250,57	3,53	90,66	4,62	27,96	103,24	9,95	13,55	6,67	0,20	0,04	1,45	2,48	0,04	106,46	10,97
FEMO-2016-5.03			20,94		10,26	260,75	157,08	38,75	101,58	60,74	23,04	23,35	43,98	1,57	128,81	19,69	19,48	130,90	12,04	11,52				2,09	0,41	0,05	215,72	19,90
FEMO-2016-5.04			21,12		8,87	309,40	147,83	42,24	103,48	86,59	13,73	23,34	72,44	1,69	130,41	18,58	19,64	122,49	10,14	9,50				2,11	0,40	0,08	249,21	20,70
FEMO-2016-5.02			20,85		6,98	188,68	62,55	31,27	131,34	183,47	15,64	17,72	8,65	2,50	163,14	25,23	30,75	137,60	16,37	16,68				3,13	0,48	0,08	205,88	35,86
FEMO-2015-15.2			11,52		20,17	407,98	195,92	95,66	154,43	537,06	13,83	25,93	130,81	0,69	97,27	31,23	22,93	114,10	6,68	1,15				2,30	0,41	0,06	164,81	8,30
FEMO-2016-2.03			10,58		40,42	418,99	158,71	49,73	105,80	373,49	93,11	20,42	12,06	2,33	48,56	118,50	35,97	128,02	13,33	9,52				2,12	0,44	0,14	454,96	16,61
FEMO-2014-12.1			10,57		11,84	354,05	116,25	31,71	114,14	571,76	720,77	17,23	0,74	5,07	61,40	29,06	16,38	98,29	4,65	13,74			4,97	1,06	6,40	0,36	624,60	8,45
FEMO-2014-11.1			21,51		8,71	412,99	204,34	48,40	187,14	474,29	457,08	19,14	3,66	3,87	48,50	55,39	19,04	122,61	7,21	13,98			2,80	1,08	1,98	0,19	593,67	6,56
FEMO-2015-14.1			11,94		11,70	325,93	119,39	54,92	216,10	360,56	28,65	25,91	7,88	1,91	90,98	43,34	21,85	117,00	13,61	1,19			0,60	1,19	0,81	0,08	312,80	15,64
FEMO-2016-9.02			10,70		1,18	109,10	21,39	47,06	372,24	317,69	873,90	2,25	187,19	10,05	2,67	28,67	28,24	17,11	0,75	8,56		1,18	5,35	1,07	11,82	0,82	27,49	11,23
FEMO 2017 3.04	8,03	0,22	8,35	1,70	13,83	500,75	112,04	713,39	537,33	2103,59	9,15		897,46	24,58	52,48	4,46	43,10	94,89	6,35	70,42	38,87	0,26	0,07	0,64	16,35	1,14	68,60	21,61
FEMO-2014-12.2			11,76		10,94	382,33	117,64	163,52	259,99	496,45	181,17	9,88	14,23	19,76	13,41	59,53	72,00	67,06	4,82	25,88		2,00	1,18	1,18	13,35	0,91	147,05	36,12
FEMO-2014-11.2			11,61		4,76	233,45	255,51	65,04	239,25	455,28	228,80	9,41	182,93	11,96	26,13	45,30	27,29	44,13	1,74	16,26		0,81	1,51	2,32	78,40	0,98	344,94	10,57
FEMO-2016-7.02			32,97		5,83	140,68	450,63	65,95	301,15	16,49	117,60	12,64	168,71	0,55	56,71	113,76	12,86	92,32	70,23					1,10		0,01	585,81	44,40
FEMO-2016-1.03			20,91		3,87	752,66	303,16	3,14		5,23	24,04	40,04	154,19	0,31	71,29	80,39	16,20	371,10	30,52	24,04				5,23	0,30	0,03	1688,26	11,92
FEMO-2016-1.02			31,56		46,60	448,09	178,82	39,97	157,78	199,85	200,91	24,09	7,78	6,94	35,76	88,99	31,87	124,12	8,63	7,36				2,10	1,17	0,09	295,57	7,78
FEMO-2016-1.04			21,00		41,05	403,18	188,99	35,70	161,69	196,34	140,69	20,47	26,25	5,35	54,18	110,77	28,98	120,74	7,77	8,40				2,10	1,08	0,09	460,92	10,29
FEMO-2016-1.01			42,12		43,49	404,37	200,08	33,70	220,09	232,72	206,40	25,69	2,00	8,74	67,39	129,52	47,49	240,09	19,17	9,48		0,63	0,74	3,16	1,11	0,17	520,20	19,90
FEMO-2016-3.04			34,51		24,96	877,58	253,04	60,96	556,68	603,84	121,92	23,58	1,84	22,43	77,64	65,10	35,66	119,62	10,93	85,11				1,15		0,20	554,38	20,82
FEMO-2016-3.03			22,51		13,96	850,92	281,39	124,94	1006,25	413,08	141,82	18,80	1,91	49,19	45,58	63,82	41,42	95,67	7,32	73,16				1,13		0,36	228,49	42,66
FEMO 2017 11.1	0,05	0,09	12,48	0,33	29,30	385,89	5,16	40,03	19,19	90,80	54,68		1,11	1,05	15,48	27,96	43,13	175,40	17,44	0,54	1,03	0,02	0,07	0,72	0,10	0,01	92,86	20,95
FEMO 2017 4.05	0,12	0,02	17,57	0,28	36,91	304,68	203,81	60,10	139,34	126,86	44,71		7,31	0,79	15,29	25,48	24,12	141,42	33,80	0,56	2,08	0,11	0,12	0,56	0,10	0,01	207,97	24,23
FEMO 2017 4.06	0,08	0,04	33,08	0,49	39,18	293,12	186,25	61,17	148,60	87,12	48,85		3,01	0,42	55,88	10,79	23,82	54,96	5,78	0,89	5,29	0,06	0,06	0,36	0,10	0,01	135,37	4,91
FEMO 2017 10.3	0,10	0,05	6,66	0,25	34,85	379,76	43,59	50,25	45,26	136,30	43,70		0,91	0,76	11,65	33,19	26,22	147,74	14,77	0,66	1,04	0,02	0,14	0,52	0,10	0,01	107,16	14,36
FEMO 2017 5.01	0,05	0,13	41,17	1,16	29,01	310,93	23,43	36,79	33,39	54,19	111,67		1,63	0,69	90,98	71,27	33,72	162,03	43,90	0,35	1,09	0,05	0,10	0,70	0,11	0,01	203,64	28,36
FEMO 2017 4.03	3,31	0,07	56,23	0,55	20,01	488,35	472,04	122,90	1326,92	240,37	87,01		10,59	20,45	112,03	28,93	31,76	131,60	14,03	51,45	21,75	1,00	0,18	0,40	0,20	0,23	230,58	33,72
FEMO-2016-5.06			20,60		18,64	257,49	123,59	42,23	80,34	5,15	50,47	31,10	8,96	0,51	84,66	37,39	35,33	247,19	17,20					4,12	0,07	0,01	1246,23	32,24
FEMO-2016-5.07			20,45		39,06	322,13	132,94	59,31	79,77	140,10	60,34	27,51	3,37	0,72	45,81	60,54	28,43	235,20	18,41					2,05	0,10	0,02	463,25	38,04
FEMO-2016-5.08			20,46		30,79	323,20	132,96	43,98	85,91	97,16	50,12	21,89	0,61	0,61	56,15	18,41	28,02	232,17	19,64					2,05	0,07	0,03	391,73	28,02
FEMO-2016-5.09			20,68		12,51	252,30	124,08	47,56	63,07	229,55	39,29	30,61	17,79	0,83	71,55	14,27	30,50	240,93	17,79					4,14	0,08	0,02	1004,03	30,92
FEMO 2017 3.02	0,34	0,75	18,46	0,92	36,92	410,98	145,83	61,70	40,38	39,87	40,79		47,22	0,57	93,92	3,26	28,45	121,36	10,71	2,54	1,02	0,02	0,05	1,42	1,33	0,02	210,08	11,73
FEMO-2016-5.05			10,36		33,68	308,84	217,64	45,60	103,64	92,24	18,65	23,21	37,00	0,52	26,95	17,00	27,05	189,66	14,09					1,04	0,11	0,02	72,96	24,04
FEMO 2017 1.04	0,31	0,17	117,32	0,12	42,07	215,42	188,12	60,48	85,16	2,63	63,72		81,01	0,21	89,81	14,26	11,02	60,68	3,93	0,09	1,01	0,01	0,01	0,11	0,10	0,01	576,49	3,57
FEMO 2017 1.03	0,53	0,14	107,46	0,09	41,67	213,91	184,51	44,71	87,19	9,23	59,81		46,84	0,24	85,26	16,42	12,57	60,83	4,01	0,09	1,42	0,01	0,01	0,11	0,10	0,01	643,76	2,84
FEMO 2017 2.01	0,05	0,10	25,60	0,50	31,10	147,01	37,70	50,21	15,90	10,90	12,00		3,32	0,39	16,50	38,10	28,90	47,00	4,06	0,01	4,10	0,07	0,06	0,20	0,17	0,01	41,00	4,43
FEMO 2017 2.02	0,54	0,13	129,26	0,08	44,74	250,44	123,20	61,90	56,25	35,45	46,45		60,89	0,26	34,84	3,94	20,80	74,73	5,35	0,08	1,51	0,04	0,01	0,30	0,10	0,01	498,86	4,30
FEMO 2017 4.04	0,05	0,04	28,20	0,17	44,26	289,06	35,63	45,77	28,00	10,44	249,92		5,41	0,91	43,26	8,83	56,01	193,71	14,96	1,43	1,00	0,06	0,54	0,71	0,65	0,02	543,00	24,29
FEMO 2017 4.07	0,22	0,12	38,03	0,15	22,50	159,40	133,17	31,07	65,88	42,07	73,65		0,98	0,76	72,74	9,18	23,00	182,60	19,87	0,77	3,83	0,04	0,07	1,28	0,10	0,05	375,29	26,73
FEMO 2017 10.1	0,05	0,13	7,26	0,38	33,94	393,56	12,98	41,91	17,07	65,52	35,78		1,23	0,96	7,24	26,99	54,89	245,33	17,07	0,74	1,02	0,01	0,06	0,68	0,10	0,01	104,27	23,51

Sample	Ce	Pr	Nd	Eu	Gd	Tb	Dy	Ho	Er	Tm	Yb	Lu	Hf	Ta	W	Au	Pb	Bi	Th	U
	ppm	ppm	ppm	ppm	ppm	ppm	ppm	ppm	ppm	ppm	ppm	ppm	ppm	ppm	ppm	ppb	ppm	ppm	ppm	ppm
FEMO 2017 9.01	60,62	7,91	33,86	2,08	7,08	1,00	5,60	1,06	2,88	0,37	2,25	0,32	3,24	0,41	8,83	0,44	3,13	0,02	4,01	0,31
FEMO 2017 9.02	59,56	7,85	33,05	2,02	6,83	0,98	5,39	1,03	2,81	0,36	2,24	0,33	3,65	0,67	6,17	1,28	2,38	0,05	3,67	0,49
FEMO 2017 9.03	67,27	9,03	37,90	2,32	7,61	1,10	6,13	1,16	3,31	0,42	2,66	0,38	4,21	0,97	14,24	0,25	1,93	0,05	4,75	0,48
FEMO 2017 9.04	75,35	9,46	39,28	2,51	8,30	1,25	7,11	1,37	3,90	0,50	3,08	0,45	4,39	1,32	15,57	0,19	2,48	0,04	5,74	0,63
FEMO 2017 9.05	64,75	8,28	34,59	2,13	7,11	1,05	5,98	1,19	3,40	0,44	2,81	0,40	4,43	1,12	16,59	0,19	7,41	0,05	5,30	0,42
FEMO 2017 4.08	14,32	2,77	11,78	0,77	2,45	0,38	2,34	0,47	1,44	0,20	1,36	0,20	2,39	0,27	30,07	0,46	4,67	0,02	2,97	0,29
FEMO 2017 4.11	37,29	6,30	26,67	1,61	6,55	1,08	6,69	1,39	4,18	0,60	3,97	0,63	3,74	0,57	23,76	0,82	1,71	0,02	3,54	0,31
FEMO 2017 4.09	55,28	6,62	25,33	1,25	4,47	0,67	3,89	0,79	2,33	0,33	2,16	0,34	3,20	0,45	28,75	2,00	2,49	0,04	8,70	1,30
FEMO-2015-15.1	143,53	20,95	92,61	5,43	23,68	3,57	21,06	4,49	13,20	1,76	11,05	1,62	14,67	2,93	5,24	0,24	7,33	0,22	4,97	4,09
FEMO-2016-2.01	9,42	1,47	7,23	1,17	3,32	0,54	4,00	0,84	2,52	0,37	2,25	0,37	2,30	0,11		0,26	2,19	0,01	0,32	0,16
FEMO 2017 3.03	28,50	4,19	20,62	1,95	6,15	0,97	5,65	1,10	3,16	0,44	2,80	0,43	3,34	0,59	26,34	0,94	0,89	0,09	1,07	1,07
FEMO-2016-5.01	130,46	13,25	46,72	0,67	6,36	1,14	6,99	1,50	4,16	0,65	4,16	0,67	5,98	2,17	1,03	0,36	6,19	0,46	40,84	11,96
FEMO 2017 3.05	27,61	3,79	17,02	1,44	5,44	0,92	5,84	1,20	3,60	0,49	3,25	0,49	3,09	0,50	10,76	0,78	2,80	0,55	1,30	1,61
FEMO 2017 3.01	20,32	3,42	16,45	1,53	5,37	0,88	5,50	1,12	3,25	0,45	2,90	0,44	3,18	0,41	3,33	0,61	2,06	0,96	1,98	2,70
FEMO-2016-5.03	40,63	4,66	18,43	0,82	3,42	0,58	3,62	0,79	2,15	0,35	2,25	0,34	3,77	0,84		0,11	3,14	0,61	8,25	4,92
FEMO-2016-5.04	40,23	4,86	20,06	0,97	3,41	0,55	3,62	0,79	2,09	0,35	2,06	0,32	3,59	0,74	1,06	0,23		0,92	7,09	5,98
FEMO-2016-5.02	67,76	7,22	24,81	0,69	5,03	0,92	6,00	1,19	3,63	0,56	3,58	0,54	4,69	1,77	2,08	0,57	8,34	0,60	30,23	11,31
FEMO-2015-15.2	17,98	2,51	12,22	1,04	4,61	0,68	4,43	0,84	2,75	0,40	2,36	0,36	3,00	0,35	5,76	6,57	3,46	0,39	0,70	1,43
FEMO-2016-2.03	36,61	4,70	21,37	1,87	6,05	1,06	6,66	1,44	4,00	0,57	3,51	0,49	3,60	0,63	1,06	0,19	3,17	0,39	1,61	7,88
FEMO-2014-12.1	17,65	2,60	11,41	0,89	3,35	0,41	2,72	0,60	1,75	0,18	1,52	0,23	2,75	0,42	1,06	0,16	13,74	0,08	1,72	6,19
FEMO-2014-11.1	15,49	2,46	10,97	0,96	3,73	0,53	3,18	0,68	2,13	0,25	1,34	0,18	3,44	0,43	2,15	0,09	4,30	0,15	1,06	4,11
FEMO-2015-14.1	34,38	4,91	20,42	1,16	4,86	0,69	4,48	0,81	2,55	0,29	2,13	0,30	3,70	0,72	4,78	1,51	5,97	2,45	1,28	2,13
FEMO-2016-9.02	9,95	2,76	11,45	0,66	3,62	0,55	4,06	0,74	2,67	0,36	2,47	0,33	0,43		2,14	0,16	75,95	0,15	0,36	2,73
FEMO 2017 3.04	37,61	5,82	24,69	2,45	8,16	1,38	8,40	1,68	4,85	0,67	4,28	0,65	2,64	0,23	11,41	6,18	48,25	50,07	6,83	19,55
FEMO-2014-12.2	62,82	10,13	41,65	3,12	13,41	1,91	12,18	2,25	7,53	0,87	5,71	0,91	1,88	0,35	2,35	0,59	37,65	0,33	2,11	30,82
FEMO-2014-11.2	21,83	3,82	15,45	0,79	4,75	0,65	3,98	0,79	2,51	0,35	2,22	0,41	1,16	0,23	2,32	29,61	51,10	0,16	0,59	4,84
FEMO-2016-7.02	124,75	18,41	76,83	2,18	6,48	0,70	3,34	0,52	1,07	0,20	1,09	0,16	1,98	1,87		1,42	2,20	0,01	3,42	2,37
FEMO-2016-1.03	31,67	5,15	25,82	1,41	4,01	0,48	2,63	0,61	2,27	0,46	3,00	0,64	10,56	1,99	4,18	0,39	7,32	0,01	6,24	11,03
FEMO-2016-1.02	17,88	2,65	12,73	1,09	4,75	0,79	5,51	1,22	3,47	0,53	3,22	0,42	3,89	0,42	1,05	0,17	9,47	0,27	1,51	5,65
FEMO-2016-1.04	21,94	3,11	14,59	1,17	4,83	0,76	5,14	1,13	2,89	0,49	2,87	0,41	3,78	0,31	1,05	0,29	5,25	0,51	1,92	4,88
FEMO-2016-1.01	44,96	6,34	27,80	2,01	9,02	1,40	8,08	1,82	5,08	0,76	4,52	0,76	6,32	0,84		0,30	7,37	0,19	3,34	5,43
FEMO-2016-3.04	35,08	4,88	19,67	1,21	6,11	0,92	6,03	1,31	3,66	0,54	3,13	0,51	3,57	0,58	9,20	0,24	6,90	0,84	5,08	35,43
FEMO-2016-3.03	68,21	8,17	33,20	1,51	7,57	1,33	7,71	1,65	4,68	0,64	3,96	0,63	3,15	0,34	6,75	0,24	13,51	1,38	8,15	33,32
FEMO 2017 11.1	50,97	6,97	31,37	2,35	8,81	1,39	8,42	1,69	4,84	0,65	4,10	0,60	3,84	0,90	6,11	0,46	1,30	0,01	2,75	0,59
FEMO 2017 4.05	44,82	6,87	28,80	2,09	6,25	0,93	5,19	1,00	2,78	0,37	2,33	0,35	6,31	1,58	5,86	0,53	1,28	0,01	3,68	0,96
FEMO 2017 4.06	7,63	1,88	9,50	1,12	3,85	0,68	4,48	0,96	2,93	0,42	2,74	0,43	2,76	1,71	10,10	0,72	1,53	0,05	0,77	1,67
FEMO 2017 10.3	34,13	5,04	22,89	1,88	6,09	0,93	5,39	1,05	2,92	0,37	2,36	0,33	3,32	0,71	7,44	0,29	2,82	0,01	1,78	0,37
FEMO 2017 5.01	51,89	8,04	34,27	2,44	7,76	1,20	6,84	1,35	3,80	0,53	3,33	0,49	4,01	2,29	6,44	0,90	3,36	0,01	4,34	1,45
FEMO 2017 4.03	69,28	8,09	31,54	1,38	6,15	0,94	5,68	1,17	3,55	0,51	3,43	0,55	3,43	1,07	26,86	2,56	20,88	0,77	13,05	15,23
FEMO-2016-5.06	71,17	8,70	37,08	1,92	7,88	1,17	7,48	1,51	4,08	0,57	3,42	0,56	6,59	1,03	1,03	1,52		0,04	6,09	1,46
FEMO-2016-5.07	82,53	10,01	41,93	2,59	7,29	1,07	6,35	1,33	3,73	0,51	3,20	0,48	6,24	1,02	1,02	2,43	3,07	0,05	5,46	1,46
FEMO-2016-5.08	62,80	7,90	32,83	1,67	6,21	0,97	5,76	1,17	3,22	0,50	2,55	0,43	5,93	1,13		1,18	2,05	0,07	4,68	1,09
FEMO-2016-5.09	68,35	8,18	34,54	1,57	6,48	1,10	6,09	1,35	3,69	0,61	3,62	0,53	6,62	1,14	3,10	0,91	5,17	0,08	6,22	2,49
FEMO 2017 3.02	26,41	3,52	15,60	2,05	5,29	0,91	5,66	1,14	3,27	0,46	2,84	0,43	3,43	0,74	5,98	5,63	1,00	0,11	0,91	2,05
FEMO-2016-5.05	52,23	6,26	26,63	1,44	5,99	0,92	5,81	1,17	3,21	0,50	2,80	0,47	4,77	0,83		0,53		0,03	4,44	1,34
FEMO 2017 1.04	7,84	1,27	6,20	0,62	2,16	0,35	2,23	0,46	1,39	0,20	1,41	0,22	2,43	0,30	5,59	0,33	0,68	0,01	0,59	0,08
FEMO 2017 1.03	6,32	1,17	5,83	0,57	2,02	0,35	2,36	0,51	1,62	0,24	1,73	0,26	2,49	0,31	4,60	0,34	0,78	0,03	0,62	0,04
FEMO 2017 2.01	10,80	1,61	8,16	1,05	5,37	0,97	6,05	1,16	3,21	0,43	2,61	0,37	2,08	0,49	14,40	0,57	3,91	0,04	0,75	0,07
FEMO 2017 2.02	10,07	1,83	9,59	0,99	3,67	0,64	4,06	0,85	2,55	0,37	2,50	0,37	2,63	0,37	9,07	0,47	0,66	0,03	0,62	0,07
FEMO 2017 4.04	52,69	6,89	29,61	2,17	9,28	1,64	10,34	2,23	6,74	0,97	6,43	0,99	4,71	1,31	57,31	3,38	6,97	0,03	8,47	2,71
FEMO 2017 4.07	55,28	6,77	26,63	1,53	5,14	0,82	4,82	0,94	2,73	0,38	2,48	0,37	4,40	1,24	28,05	0,30	3,14	0,10	9,38	1,30
FEMO 2017 10.1	54,69	7,71	34,65	2,75	10,63	1,71	10,53	2,15	6,22	0,83	5,31	0,79	4,60	1,30	16,05	0,43	0,65	0,01	3,60	0,51

ALS Finland Oy Test report

Karjalankatu 1
Outokumpu FIN-83500

QC CERTIFICATE	20-déc-16
OT16203914	

SAMPLE PREPARATION		ANALYTICAL PROCEDURES		
DESCRIPTION		ALS CODE	DESCRIPTION	INSTRUMENT
WEI-21	Received Sample Weight	ME-MS42	Up to 34 elements by ICP-MS	ICP-MS
	Sample login - Rcd w/o BarCode	S-IR08	Total Sulphur (Leco)	LECO
CRU-QC	Crushing QC Test	C-IR07	Total Carbon (Leco)	LECO
PUL-QC	Pulverizing QC Test	ME-MS81	Lithium Borate Fusion ICP-MS	ICP-MS
	Fine crushing - 70% <2mm	ME-4ACD81	Base Metals by 4-acid dig.	ICP-AES
SPL-21	Split sample - riffle splitter	ME-XRF26	Whole Rock By Fusion/XRF	XRF
PUL-31	Pulverize split to 85% <75 um	OA-GRA05x	LOI for XRF	WST-SEQ

Method	ME-XRF26	ME-XRF26	ME-XRF26	ME-XRF26	ME-XRF26	ME-XRF26	ME-XRF26	ME-XRF26	ME-XRF26	ME-XRF26	ME-XRF26	ME-XRF26	ME-XRF26	OA-GRA05x	ME-XRF26		ME-MS81	ME-MS81	ME-MS81	ME-MS81	ME-MS81
Analyte	Al2O3	BaO	CaO	Cr2O3	Fe2O3	K2O	MgO	MnO	Na2O	P2O5	SiO2	SrO	TiO2	LOI 1000	Total		Ba	Ce	Cr	Cs	Dy
Units	%	%	%	%	%	%	%	%	%	%	%	%	%	%	%		ppm	ppm	ppm	ppm	ppm
LOR	0,01	0,01	0,01	0,01	0,01	0,01	0,01	0,01	0,01	0,01	0,01	0,01	0,01	0,01	0,01		0,5	0,5	10	0,01	0,05
AMIS0250														33,33							
Target Range - Lower Bound														31,82							
Upper Bound														35,19							
AMIS0304																	2830	8460	100	0,45	143,5
Target Range - Lower Bound																	2340	7280	70	0,35	119,0
Upper Bound																	2860	8900	120	0,45	145,5
AMIS0304														7,21							
AMIS0304														7,11							
AMIS0304														7,05							
Target Range - Lower Bound														7,07							
Upper Bound														7,83							
AMIS0356														20,12							
AMIS0356														20,03							
AMIS0356														20,00							
Target Range - Lower Bound														19,20							
Upper Bound														21,24							
AMIS0362														10,44							
Target Range - Lower Bound														9,80							
Upper Bound														10,86							
GBM908-10																					
Target Range - Lower Bound																					
Upper Bound																					
GBM908-5																					
Target Range - Lower Bound																					
Upper Bound																					
GEOMS-03																					
Target Range - Lower Bound																					
Upper Bound																					
GEOMS-03																					
Target Range - Lower Bound																					
Upper Bound																					
GGC-03																					
Target Range - Lower Bound																					
Upper Bound																					
GGC-09																					
Target Range - Lower Bound																					
Upper Bound																					
GGC-09																					
Target Range - Lower Bound																					
Upper Bound																					
GIOP-102	2,08	<0.01	3,79	0,01	36,30	0,04	3,69	0,43	0,09	0,17	53,05	<0.01	0,08		103,00						
Target Range - Lower Bound	1,93	<0.01	3,57	<0.01	35,66	0,03	3,49	0,38	0,06	0,15	52,14	<0.01	0,05		<0.01						
Upper Bound	2,17	0,02	3,93	0,02	37,56	0,07	3,85	0,46	0,12	0,21	54,66	0,02	0,11		0,02						
GRE-3																	7130	4300	50	0,10	85,9
GRE-3																	6630	4000	50	0,09	88,5
Target Range - Lower Bound																	6280	3920	30	0,08	83,0
Upper Bound																	7670	4790	70	0,13	101,5
GS303-8																					
GS303-8																					
Target Range - Lower Bound																					
Upper Bound																					
GS303-8																					
Target Range - Lower Bound																					
Upper Bound																					
GS310-10																					
Target Range - Lower Bound																					
Upper Bound																					
GS910-4																					
Target Range - Lower Bound																					
Upper Bound																					
GS910-4																					
Target Range - Lower Bound																					
Upper Bound																					
ICP-4																					
Target Range - Lower Bound																					
Upper Bound																					
MRGeo08																					
Target Range - Lower Bound																					
Upper Bound																					
MRGeo08																					
Target Range - Lower Bound																					

Method	ME-MS81	ME-MS81	ME-MS81	ME-MS81	ME-MS81	ME-MS81	ME-MS81	ME-MS81	ME-MS81	ME-MS81	ME-MS81	ME-MS81	ME-MS81	ME-MS81	ME-MS81	ME-MS81	ME-MS81	ME-MS81	ME-MS81	ME-MS81	ME-MS81
Analyte	Er	Eu	Ga	Gd	Ge	Hf	Ho	La	Lu	Nb	Nd	Pr	Rb	Sm	Sn	Sr	Ta	Tb	Th	Tm	U
Units	ppm	ppm	ppm	ppm	ppm	ppm	ppm	ppm	ppm	ppm	ppm	ppm	ppm	ppm	ppm	ppm	ppm	ppm	ppm	ppm	ppm
LOR	0,03	0,03	0,1	0,05	5	0,2	0,01	0,5	0,01	0,2	0,1	0,03	0,2	0,03	1	0,1	0,1	0,01	0,05	0,01	0,05
AMIS0250																					
Target Range - Lower Bound																					
Upper Bound																					
AMIS0304	36,5	162,5	48,9	369	7	29,9	19,70	3640	2,03	>2500	4290	>1000	11,5	654	26	3640	13,1	37,2	473	3,68	26,4
Target Range - Lower Bound	30,6	135,0	47,8	309	<5	25,0	16,20	3250	1,83	4670	3610	925	9,3	543	22	3060	11,1	30,8	406	3,14	21,6
Upper Bound	37,4	165,0	58,7	377	18	31,0	19,80	3970	2,26	>2500	4410	>1000	11,8	664	29	3740	13,8	37,7	496	3,86	26,5
AMIS0304																					
AMIS0304																					
AMIS0304																					
Target Range - Lower Bound																					
Upper Bound																					
AMIS0356																					
AMIS0356																					
AMIS0356																					
Target Range - Lower Bound																					
Upper Bound																					
AMIS0362																					
Target Range - Lower Bound																					
Upper Bound																					
GBM908-10																					
Target Range - Lower Bound																					
Upper Bound																					
GBM908-5																					
Target Range - Lower Bound																					
Upper Bound																					
GEOMS-03																					
Target Range - Lower Bound																					
Upper Bound																					
GEOMS-03																					
Target Range - Lower Bound																					
Upper Bound																					
GGC-03																					
Target Range - Lower Bound																					
Upper Bound																					
GGC-09																					
Target Range - Lower Bound																					
Upper Bound																					
GGC-09																					
Target Range - Lower Bound																					
Upper Bound																					
GIOP-102																					
Target Range - Lower Bound																					
Upper Bound																					
GRE-3	28,1	70,1	37,6	179,5	<5	18,3	12,90	2220	1,72	>2500	1770	497	0,9	267	44	2080	164,0	19,70	117,0	2,98	108,0
GRE-3	28,4	74,2	34,9	182,0	5	19,1	12,95	2010	1,67	>2500	1675	464	0,4	257	40	1910	161,0	19,90	109,5	2,86	107,5
Target Range - Lower Bound	25,9	67,7	37,5	172,0	<5	17,6	12,15	2000	1,62	3170	1650	447	<0.2	251	40	1885	145,5	19,50	105,5	2,76	100,5
Upper Bound	31,8	82,8	46,0	210	10	22,0	14,90	2450	2,00	>2500	2020	546	1,1	307	51	2300	178,0	23,8	129,5	3,40	123,0
GS303-8																					
GS303-8																					
Target Range - Lower Bound																					
Upper Bound																					
GS303-8																					
Target Range - Lower Bound																					
Upper Bound																					
GS310-10																					
Target Range - Lower Bound																					
Upper Bound																					
GS910-4																					
Target Range - Lower Bound																					
Upper Bound																					
GS910-4																					
Target Range - Lower Bound																					
Upper Bound																					
ICP-4																					
Target Range - Lower Bound																					
Upper Bound																					
MRGeo08																					
Target Range - Lower Bound																					
Upper Bound																					
MRGeo08																					
Target Range - Lower Bound																					

Method	ME-MS81	ME-MS81	ME-MS81	ME-MS81	ME-MS81	ME-4ACD81	ME-4ACD81	ME-4ACD81	ME-4ACD81	ME-4ACD81	ME-4ACD81	ME-4ACD81	ME-4ACD81	ME-4ACD81	ME-4ACD81	ME-MS42	ME-MS42	ME-MS42	ME-MS42
Analyte	V	W	Y	Yb	Zr	Ag	Cd	Co	Cu	Li	Mo	Ni	Pb	Sc	Zn	As	Bi	Hg	In
Units	ppm	ppm	ppm	ppm	ppm	ppm	ppm	ppm	ppm	ppm	ppm	ppm	ppm	ppm	ppm	ppm	ppm	ppm	ppm
LOR	5	1	0,5	0,03	2	0,5	0,5	1	1	10	1	1	2	1	2	0,1	0,01	0,005	0,005
AMIS0250																			
Target Range - Lower Bound																			
Upper Bound																			
AMIS0304	398	6	419	17,35	1190														
Target Range - Lower Bound	331	3	369	15,25	1005														
Upper Bound	415	7	452	18,75	1230														
AMIS0304																			
AMIS0304																			
AMIS0304																			
Target Range - Lower Bound																			
Upper Bound																			
AMIS0356																			
AMIS0356																			
AMIS0356																			
Target Range - Lower Bound																			
Upper Bound																			
AMIS0362																			
Target Range - Lower Bound																			
Upper Bound																			
GBM908-10																55,0	1,28	0,021	0,025
Target Range - Lower Bound																49,4	1,09	<0.005	0,012
Upper Bound																60,6	1,35	0,028	0,034
GBM908-5																5,0	0,81	0,029	0,010
Target Range - Lower Bound																5,7	0,78	0,017	<0.005
Upper Bound																7,1	0,98	0,043	0,026
GEOMS-03						1,3	0,5	11	141	40	3	55	8	13	47				
Target Range - Lower Bound						<0.5	<0.5	9	124		<1	48	3		40				
Upper Bound						1,8	1,4	15	144		5	60	11		54				
GEOMS-03																>250	0,31	0,627	0,039
Target Range - Lower Bound																553	0,31	0,582	0,030
Upper Bound																>250	0,40	0,799	0,054
GGC-03																			
Target Range - Lower Bound																			
Upper Bound																			
GGC-09																			
Target Range - Lower Bound																			
Upper Bound																			
GGC-09																			
Target Range - Lower Bound																			
Upper Bound																			
GIOP-102																			
Target Range - Lower Bound																			
Upper Bound																			
GRE-3	1160	3	318	14,30	899														
GRE-3	1110	1	310	14,10	960														
Target Range - Lower Bound	1000	<1	288	13,90	870														
Upper Bound	1235	5	353	17,10	1070														
GS303-8																			
GS303-8																			
Target Range - Lower Bound																			
Upper Bound																			
GS303-8																			
Target Range - Lower Bound																			
Upper Bound																			
GS310-10																			
Target Range - Lower Bound																			
Upper Bound																			
GS910-4																			
Target Range - Lower Bound																			
Upper Bound																			
GS910-4																			
Target Range - Lower Bound																			
Upper Bound																			
ICP-4						28,1	16,8	29	1900	300	73	356	1845	23	6110				
Target Range - Lower Bound						24,7	15,7	27	1785	260	71	346	1735	20	5710				
Upper Bound						31,3	20,3	35	2060	350	89	425	2130	26	6990				
MRGeo08						4,5	1,9	19	632	30	14	705	1120	12	801				
Target Range - Lower Bound						3,2	1,1	17	586	<10	12	621	969	10	722				
Upper Bound						5,7	3,4	23	676	50	18	761	1190	15	886				
MRGeo08																35,0	0,74	0,078	0,170
Target Range - Lower Bound																29,6	0,60	0,053	0,137

Method	ME-MS42	ME-MS42	ME-MS42	ME-MS42	ME-MS42	ME-MS42	S-IR08	C-IR07
Analyte	Re	Sb	Sc	Se	Te	Tl	S	C
Units	ppm	ppm	ppm	ppm	ppm	ppm	%	%
LOR	0,001	0,05	0,1	0,2	0,01	0,02	0,01	0,01
AMIS0250								
Target Range - Lower Bound								
Upper Bound								
AMIS0304								
Target Range - Lower Bound								
Upper Bound								
AMIS0304								
AMIS0304								
AMIS0304								
Target Range - Lower Bound								
Upper Bound								
AMIS0356								
AMIS0356								
AMIS0356								
Target Range - Lower Bound								
Upper Bound								
AMIS0362								
Target Range - Lower Bound								
Upper Bound								
GBM908-10	<0.001	1,28	2,0	0,7	0,06	0,22		
Target Range - Lower Bound	<0.001	1,06	1,8	0,5	0,02	0,15		
Upper Bound	0,002	1,55	2,4	1,3	0,07	0,27		
GBM908-5	<0.001	0,14	1,4	0,7	0,04	0,36		
Target Range - Lower Bound	<0.001	<0.05	1,3	0,5	0,03	0,31		
Upper Bound	0,003	0,25	1,9	1,4	0,07	0,47		
GEOMS-03								
Target Range - Lower Bound								
Upper Bound								
GEOMS-03	0,002	12,80	9,5	2,3	0,12	0,88		
Target Range - Lower Bound	<0.001	10,15	8,1	1,9	0,08	0,79		
Upper Bound	0,003	13,85	10,2	2,9	0,13	1,11		
GGC-03								17,45
Target Range - Lower Bound								17,00
Upper Bound								18,25
GGC-09								3,00
Target Range - Lower Bound								2,84
Upper Bound								3,06
GGC-09							4,57	
Target Range - Lower Bound							4,42	
Upper Bound							4,76	
GIOP-102								
Target Range - Lower Bound								
Upper Bound								
GRE-3								
GRE-3								
Target Range - Lower Bound								
Upper Bound								
GS303-8								0,15
GS303-8								0,16
Target Range - Lower Bound								0,14
Upper Bound								0,18
GS303-8							0,16	
Target Range - Lower Bound							0,14	
Upper Bound							0,18	
GS310-10								1,06
Target Range - Lower Bound								1,03
Upper Bound								1,13
GS910-4								2,65
Target Range - Lower Bound								2,55
Upper Bound								2,75
GS910-4							8,29	
Target Range - Lower Bound							7,97	
Upper Bound							8,57	
ICP-4								
Target Range - Lower Bound								
Upper Bound								
MRGeo08								
Target Range - Lower Bound								
Upper Bound								
MRGeo08	0,009	3,76	8,4	1,4	0,04	0,86		
Target Range - Lower Bound	0,006	2,80	6,7	0,6	<0.01	0,64		

Method	ME-XRF26	ME-XRF26	ME-XRF26	ME-XRF26	ME-XRF26	ME-XRF26	ME-XRF26	ME-XRF26	ME-XRF26	ME-XRF26	ME-XRF26	ME-XRF26	ME-XRF26	OA-GRA05x	ME-XRF26		ME-MS81	ME-MS81	ME-MS81	ME-MS81	ME-MS81
Analyte	Al2O3	BaO	CaO	Cr2O3	Fe2O3	K2O	MgO	MnO	Na2O	P2O5	SiO2	SrO	TiO2	LOI 1000	Total		Ba	Ce	Cr	Cs	Dy
Units	%	%	%	%	%	%	%	%	%	%	%	%	%	%	%		ppm	ppm	ppm	ppm	ppm
LOR	0,01	0,01	0,01	0,01	0,01	0,01	0,01	0,01	0,01	0,01	0,01	0,01	0,01	0,01	0,01		0,5	0,5	10	0,01	0,05
Upper Bound																					
NCSDC79001	0,61	0,07	52,4	<0.01	1,04	0,17	0,41	0,02	0,35	37,0	3,34	0,09	0,04		101,30						
Target Range - Lower Bound	0,53	0,04	50,1	<0.01	0,96	0,14	0,39	<0.01	0,29	35,9	3,10	0,05	<0.01		97,99						
Upper Bound	0,63	0,08	52,5	0,02	1,12	0,20	0,47	0,04	0,37	37,8	3,42	0,10	0,06		102,00						
OGGeo08																					
Target Range - Lower Bound																					
Upper Bound																					
OREAS-121																	972	42,4	30	0,69	2,30
Target Range - Lower Bound																	877	40,5	30	0,61	2,16
Upper Bound																	1075	50,7	70	0,77	2,76
SARM-3	13,58	0,06	3,14	<0.01	9,97	5,54	0,26	0,75	8,39	0,04	52,42	0,58	0,48		100,05						
Target Range - Lower Bound	13,19	0,03	3,06	<0.01	9,55	5,27	0,25	0,71	8,05	0,03	51,16	0,48	0,43		97,99						
Upper Bound	14,11	0,07	3,38	0,02	10,27	5,75	0,31	0,83	8,69	0,08	53,64	0,60	0,53		102,00						
SARM-5	4,19	<0.01	2,63	3,59	12,75	0,08	25,5	0,23	0,34	0,01	51,09	<0.01	0,18		100,40						
SARM-5	4,18	0,01	2,65	3,59	12,78	0,09	25,5	0,22	0,35	0,01	51,30	<0.01	0,18		100,65						
Target Range - Lower Bound	3,99	<0.01	2,52	3,41	12,26	0,06	24,6	0,19	0,33	<0.01	49,88	<0.01	0,17		97,99						
Upper Bound	4,37	0,03	2,80	3,75	13,14	0,12	26,1	0,25	0,41	0,04	52,32	0,02	0,23		102,00						
STD 90824																					
Target Range - Lower Bound																					
Upper Bound																					
SY-4																	338	119,0	10	1,46	18,85
Target Range - Lower Bound																	306	109,5	<10	1,34	16,35
Upper Bound																	375	134,5	30	1,66	20,1
SY-4	20,86	0,04	7,95	<0.01	6,24	1,68	0,51	0,11	7,08	0,12	49,99	0,14	0,28	99,68							
SY-4	20,76	0,04	7,94	<0.01	6,16	1,68	0,51	0,11	7,10	0,13	49,89	0,14	0,28	99,43							
Target Range - Lower Bound	20,07	<0.01	7,74	<0.01	5,95	1,56	0,49	0,08	6,81	0,10	48,70	0,11	0,25	97,31							
Upper Bound	21,31	0,06	8,36	0,04	6,47	1,76	0,59	0,13	7,39	0,16	51,10	0,17	0,32	101,30							
ORIGINAL														3,83							
DUP														3,74							
Target Range - Lower Bound														3,68							
Upper Bound														3,89							
ORIGINAL														6,21							
DUP														6,12							
Target Range - Lower Bound														6,00							
Upper Bound														6,33							
ORIGINAL														1,70							
DUP														1,73							
Target Range - Lower Bound														1,66							
Upper Bound														1,77							
FEMO-2016-01																					
DUP																					
Target Range - Lower Bound																					
Upper Bound																					
FEMO-2016-02																					
DUP														4,87							
Target Range - Lower Bound														4,87							
Upper Bound														4,74							
														5,00							
FEMO-2016-05																					
DUP																					
Target Range - Lower Bound																					
Upper Bound																					
FEMO-2016-09																	430	34,6	150	1,09	6,29
DUP																	447	33,0	160	1,15	6,55
Target Range - Lower Bound																	416	31,6	140	1,05	6,05
Upper Bound																	461	36,0	170	1,19	6,79
FEMO-2016-10	14,09	<0.01	10,15	0,02	11,73	0,25	7,00	0,16	2,98	0,10	51,73	0,01	1,06		100,25						
DUP	14,12	0,01	10,15	0,02	11,80	0,25	7,02	0,17	2,97	0,10	51,90	0,02	1,05		100,55						
Target Range - Lower Bound	13,88	<0.01	9,99	<0.01	11,58	0,23	6,89	0,15	2,89	0,09	51,03	<0.01	1,02		99,39						
Upper Bound	14,33	0,02	10,30	0,03	11,95	0,27	7,13	0,18	3,06	0,11	52,60	0,02	1,09		101,40						

Method	ME-MS81	ME-MS81	ME-MS81	ME-MS81	ME-MS81	ME-MS81	ME-MS81	ME-MS81	ME-MS81	ME-MS81	ME-MS81	ME-MS81	ME-MS81	ME-MS81	ME-MS81	ME-MS81	ME-MS81	ME-MS81	ME-MS81	ME-MS81	ME-MS81
Analyte	Er	Eu	Ga	Gd	Ge	Hf	Ho	La	Lu	Nb	Nd	Pr	Rb	Sm	Sn	Sr	Ta	Tb	Th	Tm	U
Units	ppm	ppm	ppm	ppm	ppm	ppm	ppm	ppm	ppm	ppm	ppm	ppm	ppm	ppm	ppm	ppm	ppm	ppm	ppm	ppm	ppm
LOR	0,03	0,03	0,1	0,05	5	0,2	0,01	0,5	0,01	0,2	0,1	0,03	0,2	0,03	1	0,1	0,1	0,01	0,05	0,01	0,05
Upper Bound																					
NCSDC79001																					
Target Range - Lower Bound																					
Upper Bound																					
OGGeo08																					
Target Range - Lower Bound																					
Upper Bound																					
OREAS-121	1,24	1,09	10,9	3,06	<5	6,0	0,46	19,6	0,18	7,9	18,7	4,64	81,9	3,36	1	127,5	0,5	0,48	5,00	0,19	203
Target Range - Lower Bound	1,20	0,90	9,3	2,47		5,4	0,43	18,2	0,18	7,7	17,1	4,23	77,2	3,28	<1	121,5	0,3	0,38	4,96	0,17	193,5
Upper Bound	1,54	1,16	11,5	3,13		7,0	0,55	23,4	0,24	9,8	21,1	5,23	94,8	4,08	3	148,5	0,8	0,48	6,18	0,23	237
SARM-3																					
Target Range - Lower Bound																					
Upper Bound																					
SARM-5																					
SARM-5																					
Target Range - Lower Bound																					
Upper Bound																					
STD 90824																					
Target Range - Lower Bound																					
Upper Bound																					
SY-4	15,10	2,00	36,2	14,20	<5	11,4	4,26	57,1	2,15	13,5	57,3	15,15	55,7	13,30	8	1235	0,8	2,64	1,39	2,26	0,83
Target Range - Lower Bound	12,75	1,77	31,4	12,55	<5	9,8	3,86	51,7	1,88	11,5	51,2	13,45	49,3	11,40	6	1070	0,7	2,33	1,11	2,06	0,66
Upper Bound	15,65	2,23	38,6	15,45	12	12,4	4,74	64,3	2,32	14,5	62,8	16,55	60,7	14,00	10	1310	1,1	2,87	1,47	2,54	0,94
SY-4																					
SY-4																					
Target Range - Lower Bound																					
Upper Bound																					
ORIGINAL																					
DUP																					
Target Range - Lower Bound																					
Upper Bound																					
ORIGINAL																					
DUP																					
Target Range - Lower Bound																					
Upper Bound																					
ORIGINAL																					
DUP																					
Target Range - Lower Bound																					
Upper Bound																					
FEMO-2016-01																					
DUP																					
Target Range - Lower Bound																					
Upper Bound																					
FEMO-2016-02																					
DUP																					
Target Range - Lower Bound																					
Upper Bound																					
FEMO-2016-05																					
DUP																					
Target Range - Lower Bound																					
Upper Bound																					
FEMO-2016-09	3,78	1,77	19,3	5,72	<5	3,4	1,36	15,7	0,46	12,6	20,2	4,44	45,9	5,45	2	112,0	0,6	1,00	1,52	0,54	7,45
DUP	3,96	1,74	20,4	5,95	<5	3,6	1,39	15,6	0,54	13,3	20,0	4,49	50,1	5,62	2	114,5	0,7	0,99	1,63	0,57	7,71
Target Range - Lower Bound	3,65	1,64	18,8	5,49	<5	3,1	1,30	14,4	0,47	12,1	19,0	4,21	45,4	5,23	<1	107,5	0,5	0,94	1,45	0,52	7,15
Upper Bound	4,09	1,87	20,9	6,18	10	3,9	1,45	16,9	0,54	13,8	21,2	4,72	50,6	5,84	3	119,0	0,8	1,05	1,70	0,59	8,01
FEMO-2016-10																					
DUP																					
Target Range - Lower Bound																					
Upper Bound																					

Method	ME-MS81	ME-MS81	ME-MS81	ME-MS81	ME-MS81	ME-4ACD81	ME-4ACD81	ME-4ACD81	ME-4ACD81	ME-4ACD81	ME-4ACD81	ME-4ACD81	ME-4ACD81	ME-4ACD81	ME-4ACD81	ME-MS42	ME-MS42	ME-MS42	ME-MS42
Analyte	V	W	Y	Yb	Zr	Ag	Cd	Co	Cu	Li	Mo	Ni	Pb	Sc	Zn	As	Bi	Hg	In
Units	ppm	ppm	ppm	ppm	ppm	ppm	ppm	ppm	ppm	ppm	ppm	ppm	ppm	ppm	ppm	ppm	ppm	ppm	ppm
LOR	5	1	0,5	0,03	2	0,5	0,5	1	1	10	1	1	2	1	2	0,1	0,01	0,005	0,005
Upper Bound																36,4	0,76	0,087	0,179
NCSDC79001																			
Target Range - Lower Bound																			
Upper Bound																			
OGGeo08						20,1	18,6	96	8320	30	914	8870	7230	9	7180				
Target Range - Lower Bound						17,7	16,2	86	7800	<10	841	8000	6510	8	6500				
Upper Bound						22,7	21,0	108	8980	50	1030	9770	7970	13	7950				
OREAS-121	26	<1	11,9	1,34	255														
Target Range - Lower Bound	12	<1	10,8	1,25	232														
Upper Bound	34	2	14,4	1,59	288														
SARM-3																			
Target Range - Lower Bound																			
Upper Bound																			
SARM-5																			
SARM-5																			
Target Range - Lower Bound																			
Upper Bound																			
STD 90824																			
Target Range - Lower Bound																			
Upper Bound																			
SY-4	10	<1	126,5	14,70	614														
Target Range - Lower Bound	<5	<1	106,5	13,30	523														
Upper Bound	18	3	131,5	16,30	643														
SY-4																			
SY-4																			
Target Range - Lower Bound																			
Upper Bound																			
ORIGINAL																			
DUP																			
Target Range - Lower Bound																			
Upper Bound																			
ORIGINAL																			
DUP																			
Target Range - Lower Bound																			
Upper Bound																			
ORIGINAL																			
DUP																			
Target Range - Lower Bound																			
Upper Bound																			
FEMO-2016-01																			
DUP																			
Target Range - Lower Bound																			
Upper Bound																			
FEMO-2016-02																			
DUP																			
Target Range - Lower Bound																			
Upper Bound																			
FEMO-2016-05						<0.5	<0.5	70	53	10	<1	120	3	44	135				
DUP						<0.5	<0.5	58	55	10	<1	116	<2	42	130				
Target Range - Lower Bound						<0.5	<0.5	60	51	<10	<1	111	<2	40	124				
Upper Bound						1,0	1,0	68	57	20	2	125	4	46	141				
FEMO-2016-09	396	1	34,0	3,32	121														
DUP	425	2	35,2	3,71	128														
Target Range - Lower Bound	385	<1	32,4	3,31	116														
Upper Bound	436	2	36,8	3,72	133														
																0,2	0,02	<0.005	0,007
FEMO-2016-10																0,3	0,02	<0.005	0,007
DUP																<0.1	<0.01	<0.005	<0.005
Target Range - Lower Bound																			
Upper Bound																			

Method	ME-MS42	ME-MS42	ME-MS42	ME-MS42	ME-MS42	ME-MS42	S-IR08	C-IR07
Analyte	Re	Sb	Sc	Se	Te	Tl	S	C
Units	ppm	ppm	ppm	ppm	ppm	ppm	%	%
LOR	0,001	0,05	0,1	0,2	0,01	0,02	0,01	0,01
Upper Bound	0,010	3,90	8,4	1,5	0,04	0,92		
NCSDC79001								
Target Range - Lower Bound								
Upper Bound								
OGGeo08								
Target Range - Lower Bound								
Upper Bound								
OREAS-121								
Target Range - Lower Bound								
Upper Bound								
SARM-3								
Target Range - Lower Bound								
Upper Bound								
SARM-5								
SARM-5								
Target Range - Lower Bound								
Upper Bound								
STD 90824							18,90	
Target Range - Lower Bound							17,80	
Upper Bound							19,15	
SY-4								
Target Range - Lower Bound								
Upper Bound								
SY-4								
SY-4								
Target Range - Lower Bound								
Upper Bound								
ORIGINAL								
DUP								
Target Range - Lower Bound								
Upper Bound								
ORIGINAL								
DUP								
Target Range - Lower Bound								
Upper Bound								
ORIGINAL								
DUP								
Target Range - Lower Bound								
Upper Bound								
FEMO-2016-01							5,69	1,68
DUP							5,90	1,69
Target Range - Lower Bound							5,64	1,63
Upper Bound							5,95	1,74
FEMO-2016-02								
DUP								
Target Range - Lower Bound								
Upper Bound								
FEMO-2016-05								
DUP								
Target Range - Lower Bound								
Upper Bound								
FEMO-2016-09								
DUP								
Target Range - Lower Bound								
Upper Bound								
FEMO-2016-10	0,001	<0.05	3,7	0,4	0,01	0,03		
DUP								
Target Range - Lower Bound								
Upper Bound								

Labtium Oy Test report
Labtium Oy
PL/P.O. Box 1500
FI-70211 Kuopio
Report No.: 025368 27.12.2017
***Printout of printouts can be sent on demand to the authors**

Analytical method description: Multielement analysis by XRF-technique from pressed pellet Analytical method: 175X
Analyzed in laboratory: Sodankyla

Analytical method code	175X*	175X*	175X*	175X*	175X*	175X*	175X*	175X*	175X*	175X *	175X*	175X*	175X*	175X*	175X*	175X*	175X*	175X*	175X*
Parameter	A1203 *	As *	Ba *	Bi *	CaO *	Ce *	CI *	Cr *	Cu *	Fe203 *	Ga *	K20 *	La *	MgO *	MnO *	Mo *	Na20 *	Nb *	Ni *
Unit	%	%	%	%	%	%	%	ok	%	%	%	%	%	%	%	%	%	%	%
Detection Limit	0,01	0,001	0,002	0,003	0,003	0,003	0,01	0,002	0,002	0,01	0,003	0,003	0,003	0,02	0,005	0,001	0,03	0,002	0,002
17030230 / QCGBMS304-6	11,57	0,272	0,054	<0.003	10,390	0,005	0,08	0,039	0,422	9,67	<0.003	1,818	<0.003	3,11	0,092	<0.001	1,64	<0.002	0,216
17030230 (2) / QCGBMS304-6	11,53	0,273	0,051	<0.003	10,380	0,006	0,08	0,039	0,421	9,64	<0.003	1,816	<0.003	3,11	0,089	<0.001	1,63	<0.002	0,217
17030231 / QC1	13,92	<0.001	0,059	<0.003	1,050	0,007	0,01	<0.002	<0.002	1,46	<0.003	5,515	0,005	0,20	0,030	<0.001	3,23	0,002	0,003
17030231 (2) I QC1	13,87	<0.001	0,061	<0.003	1,060	0,007	0,01	<0.002	<0.002	1,46	<0.003	5,537	0,004	0,20	0,028	<0.001	3,24	<0.002	<0.002
17030232 / QC2	1,96	<0.001	<0.002	<0.003	5,680	<0.003	0,04	0,565	0,005	12,26	<0.003	0,048	<0.003	29,06	0,162	<0.001	0,17	<0.002	0,086
17030232 (2) I QC2	1,97	<0.001	<0.002	<0.003	5,640	<0.003	0,04	0,562	0,005	12,11	<0.003	0,047	<0.003	28,93	0,162	<0.001	0,17	<0.002	0,085
17030233 / QCMerck	0,04	<0.001	<0.002	<0.003	<0.003	<0.003	<0.01	<0.002	<0.002	0,01	<0.003	0,004	<0.003	0,02	<0.005	<0.001	<0.03	<0.002	<0.002
17030233 (2) / QCMerck	0,04	<0.001	<0.002	<0.003	<0.003	<0.003	<0.01	<0.002	<0.002	0,01	<0.003	0,004	<0.003	0,02	<0.005	<0.001	0,03	<0.002	<0.002

Analytical method descript Multi-element analysis by ICP-MS Analytical method: 308M
Analyzed in laboratory: Kuopio

	308M	308M	308M	308M	308M	308M	308M	308M	308M	308M	308M	308M	308M	308M	308M	308M	308M	308M	308M
Parameter	Ce	Dy	Er	Eu	Gd	Hf	Ho	La	Lu	Nb	Nd	Pr	Rb	Sm	Ta	Tb	Th	Tm	U
Unit	mg/kg	mg/kg	mg/kg	mg/kg	mg/kg	mg/kg	mg/kg	mg/kg	mg/kg	mg/kg	mg/kg	mg/kg	mg/kg	mg/kg	mg/kg	mg/kg	mg/kg	mg/kg	mg/kg
Detection Limit	0,1	0,1	0,2	0,1	0,2	0,5	0,1	0,1	0,1	0,2	0,2	0,1	0,2	0,2	0,2	0,1	0,5	0,1	0,2
17034617 / QC0153B	12,3	2,60	1,70	0,72	2,39	2,31	0,56	5,46	0,26	2,06	8,15	1,81	21,6	2,18	<0.2	0,41	2,66	0,24	0,30
17034618 / QCGBMS304-6	54,8	4,40	2,69	1,21	4,88	3,03	0,91	30,5	0,37	4,60	25,1	6,59	92,7	4,91	0,32	0,73	11,4	0,37	7,07
17034619 / QCSOKEA	<0.1	<0.1	<0.2	<0.1	<0.2	0,96	<0.1	0,14	<0.1	<0.2	<0.2	<0.1	<0.2	<0.2	<0.2	<0.1	1,49	<0.1	<0.2
17034619 (2) / QCSOKEA	<0.1	<0.1	<0.2	<0.1	<0.2	0,93	<0.1	0,12	<0.1	0,22	<0.2	<0.1	<0.2	<0.2	<0.2	<0.1	1,79	<0.1	<0.2
17034620 / QCSY-4	125	19,4	15,3	2,02	14,9	12,9	4,49	58,0	2,22	14,5	59,1	15,1	50,7	13,2	0,77	2,82	10,2	2,37	1,11
17034620 (2) I QCSY-4	125	19,5	15,4	2,02	15,0	13,3	4,62	59,3	2,14	15,5	59,3	15,3	54,0	13,1	1,22	2,79	8,29	2,34	0,93

Labtium Oy Test report
Labtium Oy
PL/P.O. Box 1500
FI-70211 Kuopio
Report No.: 025368
***Printout of printouts can be ser**

Analytical method code	175X "	175X "	175X*	175X"	175X*	175X "	175X*	175X*	175X*	175X*	175X*	175X*	175X*	175X *	175X *	175X *
Parameter	P205 *	Pb *	Rb *	S*	Sb *	Sc *	Si02 *	Sn *	Sr *	Th *	TiO2 *	U*	V	Y*	Zn *	Zr *
Unit	%	%	%	%	%	%	%	%	%	%	%	%	%	%	%	%
Detection Limit	0,006	0,003	0,001	0,01	0,005	0,002	0,01	0,003	0,001	0,003	0,003	0,001	0,001	0,001	0,002	0,001
17030230 / QCGBMS304-6	0,220	0,039	<0.001	1,58	0,016	<0.002	49,58	<0.003	0,019	0,004	0,498	<0.001	0,015	0,003	0,126	0,018
17030230 (2) / QCGBMS304-6	0,216	0,038	<0.001	1,56	0,017	<0.002	49,51	<0.003	0,019	0,004	0,496	<0.001	0,016	0,003	0,125	0,018
17030231 / QC1	0,044	0,004	<0.001	<0.01	<0.005	<0.002	74,22	<0.003	0,015	0,004	0,127	<0.001	0,002	0,004	0,004	0,013
17030231 (2) I QC1	0,043	0,005	<0.001	<0.01	<0.005	<0.002	74,23	<0.003	0,014	0,004	0,126	<0.001	0,002	0,004	0,004	0,012
17030232 / QC2	0,032	<0.003	<0.001	0,08	<0.005	<0.002	44,41	<0.003	0,004	<0.003	0,155	<0.001	0,014	<0.001	0,009	0,001
17030232 (2) I QC2	0,029	<0.003	<0.001	0,08	<0.005	<0.002	44,14	<0.003	0,003	<0.003	0,155	<0.001	0,013	<0.001	0,009	<0.001
17030233 / QCMerck	<0.006	<0.003	<0.001	<0.01	<0.005	<0.002	97,11	<0.003	<0.001	<0.003	<0.003	<0.001	<0.001	<0.001	<0.002	<0.001
17030233 (2) / QCMerck	<0.006	<0.003	<0.001	<0.01	<0.005	<0.002	97,01	<0.003	<0.001	<0.003	<0.003	<0.001	<0.001	<0.001	<0.002	<0.001

	308M	308M
Parameter	Y	Yb
Unit	mg/kg	mg/kg
Detection Limit	0,2	0,2
17034617 / QC0153B	14,8	1,63
17034618 / QCGBMS304-6	25,3	2,36
17034619 / QCSOKEA	<0.2	<0.2
17034619 (2) / QCSOKEA	<0.2	<0.2
17034620 / QCSY-4	120	15,8
17034620 (2) I QCSY-4	123	15,3

Labtium Oy Test report
Labtium Oy
PL/P.O. Box 1500
FI-70211 Kuopio
Report No.: 025368 27.12.2017
***Printout of printouts can be sent on demand to the authors**

Analytical method description: Multi-element analysi by ICP-OES Analytical method: 308P
Analyzed in laboratory: Kuopio

	308P	308P	308P	308P
Parameter	Co	Sc	V	Zr
Unit	mg/kg	mg/kg	mg/kg	mg/kg
Detection Limit	5	2	5	
17033551 / QCSOKEA	<5	<2	<5	<5
17033551 (2) I QCSOKEA	<5	<2	<5	8
17033552 / QCSY-4	<5	<2	<5	489
17033552 (2) I QCSY-4	<5	<2	6,7	519
17033553 / QCGBMS304-6	118	14,4	159	163
17033554 / QC0153B	14,2	16,5	230	68

Analytical method description: Analysis of C by combustion technique Analytical method: 811L
Analyzed in laboratory: Kuopio

Parameter	C*
Unit	%
Detection Limit	0,05
17031053 / QCSOKEA	<0.05
17031054 / QCGS900-5	0,66
17031054 (2) / QCGS900-5	0,66
17031055 / QCGS310-7	4,12
17031055 (2) / QCGS310-7	4,14

Paper III

-

Orogenic Au deposits with atypical metal association (Cu, Co, Ni): insights from the Pohjanmaa Belt, western Finland.

Hector S, Patten CGC, Kolb J, Araujo de Silva A, Walter BF, Molnár F (2023) Ore Geology Reviews:105326

Ore Geology Reviews 154 (2023) 105326

Contents lists available at ScienceDirect

Ore Geology Reviews

journal homepage: www.elsevier.com/locate/oregeorev

Orogenic Au deposits with atypical metal association (Cu, Co, Ni): Insights from the Pohjanmaa Belt, western Finland

Simon Hector [a,b,*], Clifford G.C. Patten [a,b], Jochen Kolb [a,b], Andressa de Araujo Silva [a,b], Benjamin F. Walter [a,b], Ferenc Molnár [c,d]

[a] Institute of Applied Geosciences, Chair of Geochemistry and Economic Geology, Karlsruhe Institute of Technology, 76131 Karlsruhe, Germany
[b] Laboratory for Environmental and Raw Materials Analysis (LERA), Adenauerring 20b, 76131 Karlsruhe, Germany
[c] Geological Survey of Finland, Vuorimiehentie 5, 02151 Espoo, Finland
[d] Department of Mineralogy, Institute of Geography and Geology, Eötvös Loránd University, 1177 Budapest, Pázmány Péter s. 1/C, Hungary

ARTICLE INFO

Keywords:
Orogenic gold
Pohjanmaa Belt
Cobalt
Atypical metal association
Finland

ABSTRACT

The Laivakangas Au-Cu metallogenic area is characterised by orogenic Au deposits with both Au-only and with atypical (Au ± Cu, Co, Ni) metal associations. Here we study and compare four examples to better constrain the parameters controlling enrichment in base metals in addition to Au. We selected two typical Au-only deposits, the Laivakangas and the Huhta deposits and two orogenic Au deposits with atypical metal association, the Jouhineva Au-Cu-Co-Ag and the Kurula Au-Co deposits. All four deposits record multiple successive mineralisation events with local variations in their respective metal association. Two auriferous mineralisation events are identified, (1) a ubiquitous As-Au-(Co, Ni) event close to peak metamorphism (620–430 °C) where Au occurs either as invisible Au in arsenides or as inclusion in arsenopyrite; (2) a later Cu(-Au)-rich sulfide event on the retrograde path where Au locally occurs as free, native grains along with chalcopyrite. From S isotope studies of the sulfide and sulfarsenide minerals and relations between the deposits and surrounding rocks, we propose that the variation in metal association of the ore fluid is linked to the diversity of lithologies involved in metamorphic fluid production. Multi-event hydrothermal mineralisation and relatively reduced redox conditions appear critical to increase the Au endowment in a deposit and to introduce atypical metals. Results of this study provide a new comprehension of the variability of metal association in orogenic Au deposits of the Laivakangas Au-Cu metallogenic area and elsewhere.

1. Introduction

Precambrian orogenic Au deposits are epigenetic, and commonly hosted in greenstone belts. They usually form at post-peak metamorphic conditions in an active orogenic setting, along transcrustal faults under transpressive or compressive stress, and within a broad PT window (150–700 °C; 0.5-7kbar) (Gebre-Mariam et al., 1995; Goldfarb et al., 2001, 2005; Groves et al., 1998; Kolb et al., 2015). Orogenic Au deposits, also known as Au-only deposits, usually contain only Au as a commodity (Eilu 2015; Goldfarb and Groves 2015; Groves et al., 1998). Some deposits, however, known as orogenic Au deposits with atypical metal association, show economic enrichment in Co, Ni and/or Cu, which can be exploited as by-products (Eilu 2015). These deposits are present in several orogenic Au districts worldwide such as in northern Finland (e.g. Central Lapland Greenstone Belt, Kuusamo Belt, Peräpohja Belt; Eilu 2015), northern Australia (Pine Creek), South Africa (Pilgrim's Rest) and in Mali (Loulo district) (Goldfarb and Groves 2015; Lawrence et al., 2013). This sub-type of orogenic Au deposits, although scarce, shows interesting economic value due to the polymetallic nature of the deposits. However, formation, and more specifically, processes leading to enrichment in base metals in relation to Au remain poorly understood.

The Paleoproterozoic orogenic belts of Finland and their related orogenic Au deposits with typical and atypical metal associations have been extensively studied; e.g. Central Lapland Greenstone Belt, Kuusamo Belt, Peräpohja Belt and to a lesser extent, the Pohjanmaa Belt (Fig. 1-A - Molnár et al., 2018; Pankka and Vanhanen 1992; Vanhanen et al., 2015; Vasilopoulos et al., 2021). These types of orogenic Au deposits share many similar features. They occur together in greenstone and schist belts along the same shear zones, they form over extended periods in multi-event hydrothermal systems during the same

* Corresponding author.
E-mail address: simon.hector@kit.edu (S. Hector).

https://doi.org/10.1016/j.oregeorev.2023.105326
Received 20 October 2022; Received in revised form 13 January 2023; Accepted 27 January 2023
Available online 30 January 2023

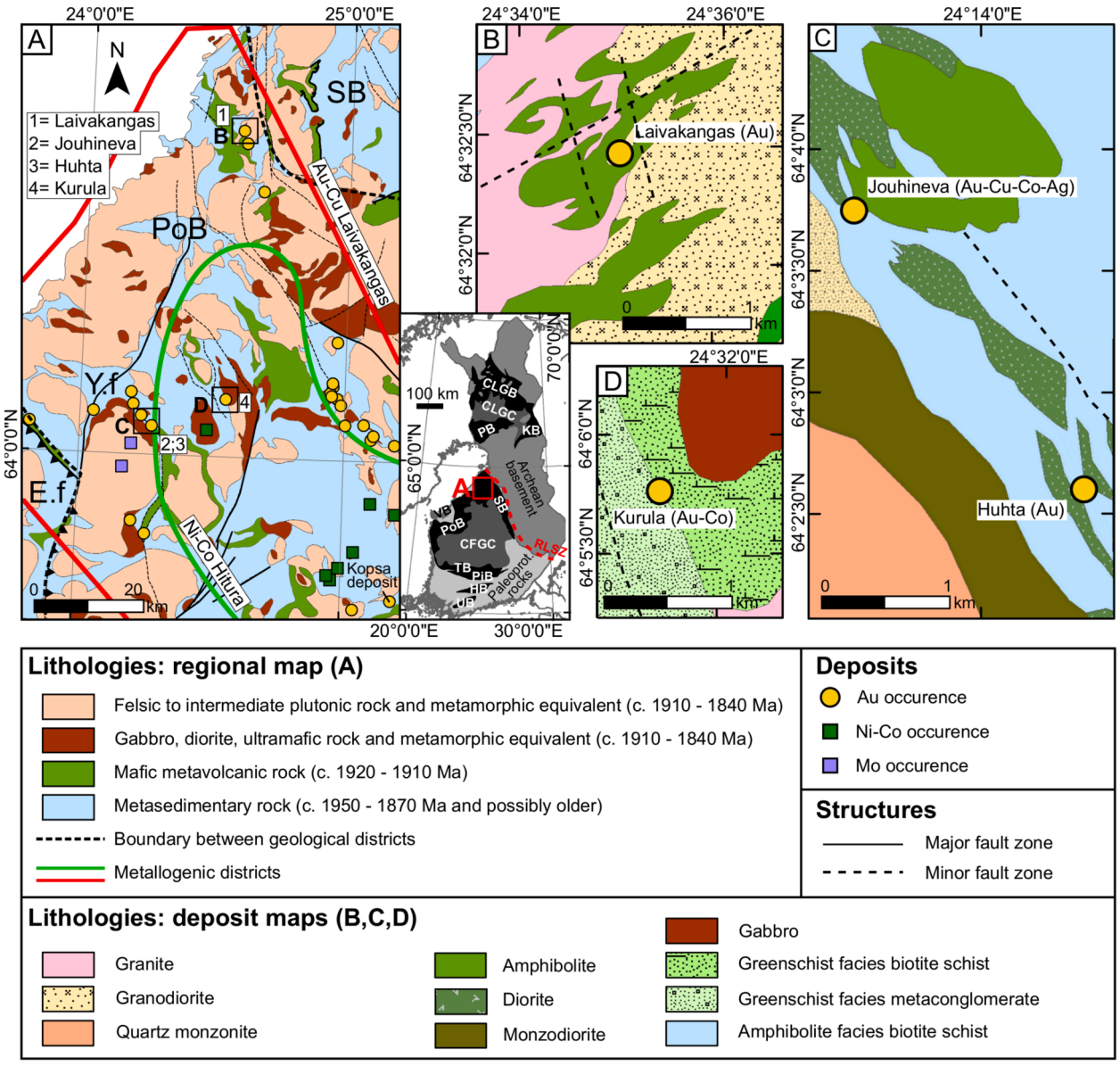

Fig. 1. Geological setting (for location in Finland, see inset in A; CFGC: Central Finland Granitoid Complex; CLGB: Central Lapland Greenstone Belt; CLGC: Central Lapland Granitoid Complex; HB: Häme Belt; KB: Kuusamo Belt; PB: Peräpohja Belt; PiB: Pirkanmaa Belt; PoB: Pohjanmaa Belt; RLSZ: Raahe-Ladoga Shear Zone; SB: Savo Belt; TB: Tampere Belt; UB: Uusimaa Belt; VB: Vaasa Batholith). (A) Geological map of the Pohjanmaa Belt showing the metallogenic areas and major deposits (Y.f = Ylivieska field; E.f = Evijärvi field) (after Eilu et al., 2012); (B) Local geology of the Laivakangas deposit (Au); (C) Local geology of the Jouhineva deposit (Au-Cu-Co-Ag) and the Huhta deposit (Au); (D) Local geology of the Kurula deposit (Au-Co). Maps modified from (Bedrock of Finland – DigiKP).

geodynamic event and display overall similar type of ore (Kurhila et al., 2017; Molnár et al., 2017; Vanhanen 2001; Vasilopoulos et al., 2021, 2022; Witt et al., 2020). Orogenic Au deposits with atypical metal association show distinctive endowments; the ones from the Central Lapland Greenstone and Pohjanmaa belts are enriched in Au-Cu ± (Ag, Co, Ni) and those from the Kuusamo and Peräpohja belts are rich in Au-Co ± (Cu, U, LREE) (Eilu 2015). Coexistence of orogenic Au deposits with typical and atypical metal associations along the same structures raises questions regarding the source of the metals, nature of the fluids and relative timing of formation of the different ore types. Several mechanisms have been proposed to account for the diverse base metal association in atypical orogenic Au deposits. Goldfarb et al. (2001) highlight that orogenic Au deposits with high base metal content tend to occur in deformed Paleoproterozoic intracratonic basins. These basins can contain evaporitic rocks and salt-rich brines which can generate saline metamorphic fluids, promoting base metal mobilisation via chloride-complexes (Haverinen 2020; Qiu et al., 2021; Tapio et al., 2021; Vasilopoulos et al., 2021; Yardley 2005; Yardley and Graham 2002). Alternatively, orogenic Au deposits with atypical metal association can be spatially associated with intrusions; these are sometimes classified as porphyry Cu-Au deposits overprinted by orogenic Au mineralisation, in an attempt to account for their atypical metal association, even if the genetic link with the intrusion is not explicit (e.g. Jouhineva Au-Cu-Co-Ag deposit; Geological Survey of Finland, 2019b; see also the Chibougamau Cu-Au(-Mo) mining district; Pilote et al., 1995). Finally, multi-event mineralisation is a common feature in orogenic Au deposits with atypical metal association, with different metals being enriched at different mineralisation events; highlighting the complexity of these deposits (Molnár et al., 2017; Novoselov et al., 2015; Patten et al., 2022; Vanhanen 2001; Vasilopoulos et al., 2022).

In this study, we investigate typical orogenic Au deposits (Laivakangas and Huhta) and orogenic Au deposits with atypical metal association (Jouhineva and Kurula) from the Pohjanmaa Belt, in western Finland, to better understand the mechanisms leading to different metal

endowment in orogenic Au deposits. We highlight that orogenic Au mineralisation in the Pohjanmaa Belt is related to two main mineralisation events with different metal association. These events are expressed by various intensity in the different deposits and account for the observed metal enrichment in the deposits.

2. Regional geology of the pohjanmaa belt

Finland lies within the Fennoscandian Shield. Its Precambrian geology incorporates the Archean cratons of Norbotten, Kola and Karelia in the north and east and by a Paleoproterozoic part, the Svecofennian domain, in the south and west. The main Archean domain is the Karelian province, where Archean rocks are partially covered by Paleoproterozoic rocks, forming greenstone belts with numerous orogenic Au deposits (Fig. 1-A) (e.g. Central Lapland Greenstone Belt, Peräpohja Belt, Kuusamo Belt - Eilu 2015; Hanski and Huhma 2005; Laajoki, 2005). The contact between the Karelian province and the Svecofennian domain is marked by the Raahe-Ladoga Shear Zone. The Paleoproterozoic geology of Finland is the result of the complex Svecofennian orogeny, leading to the formation of the Fennoscandian shield. Recent models suggest the evolution of the diachronous Svecofennian orogeny comprised five distinct, but temporally overlapping orogenic events, each of which dominated within specific spatially separated belts that were progressively amalgamated. They are: the Lapland-Kola orogeny (ca. 1960 to ca. 1870 Ma), the Lapland-Savo orogeny (ca. 1930 to ca. 1890 Ma), the Fennian orogeny (ca. 1900 to ca. 1850 Ma), the Svecobaltic orogeny (ca. 1840 to ca. 1780 Ma) and the Nordic orogeny (ca. 1820 to ca. 1770 Ma) (Korja et al., 2006; Lahtinen et al., 2005). The formation of the Fennoscandian shield started with the accretion of the Archean cratons of Kola, Karelia and Norbotten during the Lapland-Kola orogeny. In the south, accretion of the Keitele micro-continent and Paleoproterozoic volcano-sedimentary arcs against the Karelian Province during the Lapland-Savo orogeny and later orogenies led to the formation of the Svecofennian province and its volcano-sedimentary belts containing orogenic Au deposits (Savo Belt, Pohjanmaa Belt, Tampere Belt, Pirkanmaa Belt, Häme Belt and Uusimaa Belt). The oldest is the Savo Belt, thrust above the Karelian province during the Lapland-Savo orogeny (Korja et al., 2006; Lahtinen et al., 2005). The following Fennian orogeny led to the formation of the Pohjanmaa Belt. The Skellefte district in Sweden is proposed to be the continuation of the Pohjanmaa Belt (Lahtinen et al., 2014). The general crustal structure of the Svecofennian accretionary orogen is a north-east plunging succession of superposing nappes made of volcano-sedimentary units and granite intrusions of the Central Lapland Granitoid Complex (Mints et al., 2020).

The Pohjanmaa Belt corresponds now to the coast of Finland in the north-western part of the former Western Finland Province. This schist belt is limited to the north by the Raahe-Ladoga Shear Zone (Nironen et al., 2002), to the east by the Savo Belt and the Central Finland Granitoid Complex, and continues to the south-west as the Pirkanmaa and Tampere belts (Lahtinen et al., 2014) (Fig. 1-A). The Pohjanmaa Belt is divided into the Ylivieska and the Evijärvi fields, which are considered to represent a volcanic-arc and accretionary prism, respectively (Fig. 1-A) (Kähkönen 2005). syn-kinematic and post-kinematic granites (e.g. Rautio batholith) belonging to the Central Lapland Granitoid Complex intruded the Pohjanmaa Belt (Haapala and Rämö, 2015; Luukas et al., 2017) (Fig. 1-A). The Ylivieska field is thrust south-westward over the Evijärvi field. The Evijärvi field is composed of various *meta*-sedimentary and mafic *meta*-volcanic rocks with mid-ocean-ridge basalt and within-plate basalt affinities (Fig. 1-A). They are considered part of the lower sedimentary group of the central part of the Svecofennian orogen (Lahtinen et al., 2002). Peak metamorphism in the Pohjanmaa Belt reached low- to medium-amphibolite facies at ca. 1890–1880 Ma in its central part, but increases to the south-west up to lower-granulite facies conditions where crustal melting led to the formation of the Vaasa Batholith (Chopin et al., 2020; Kähkönen 2005; Mäkitie 1999, 2000; Mäkitie et al., 2012; Mäkitie and Lahti 1991; Vaarma 1990; Vaarma and Pipping 1997). The Ylivieska field contains ca. 1900 to 1880 Ma arc-type *meta*-volcanic and *meta*-sedimentary rocks belonging to the upper sedimentary group of Central Svecofennia (Kähkönen 2005) (Fig. 1-A). The *meta*-volcanic rocks are characteristic of a shallow water to sub-aerial environment and range from basalt to K-rhyolite with calc-alkaline, mature island-arc affinity (Kähkönen 2005). The *meta*-sedimentary rocks are typical of fluvial and shallow water environments (Lahtinen et al., 2002). The Ylivieska plutonic suite locally intruded the *meta*-volcano-sedimentary rocks. It consists mainly of *syn*-orogenic, mafic, layered intrusions with minor ultramafic rocks and local magmatic Ni-Cu-Co sulfide occurrences (Kiuttu 2020; Luukas et al., 2017) (Fig. 1-A). It formed at ca. 1880 Ma during the accretion stage of the Fennian Orogen along subvertical shear zones (Peltonen 2005).

2.1. Metallogeny of the Pohjanmaa Belt

The Au deposits of the Pohjanmaa Belt are mostly located in the Laivakangas Au-Cu metallogenic area within the Ylivieska field, where the main mineralisation style is orogenic Au with a few porphyry Cu-Au and porphyry Mo deposits (Fig. 1-A) (Eilu et al., 2012). The orogenic Au deposits locally contain anomalous Cu and/or Co and Ni (Eilu 2015; Isohanni 1984; Sipilä 1988). They are usually located close to shear zones and show spatial association with *syn*-orogenic, ca. 1890–1860 Ma tonalite and granodiorite (Gaál and Sundblad 1990; Nironen 2005). There is no precise age data of the Au deposits. Nevertheless, Sundblad et al. (1993) studied isotopic Pb data in galena from epigenetic Au deposits in the Skellefte District and the Pohjanmaa Belt, and suggest that the Au deposits formed approximately 10 to 20 m.y. after the surrounding host rocks, constraining their age of formation at approximately 1880–1850 Ma. The Laivakangas Au-Cu metallogenic area comprises the Hitura Ni-Co metallogenic area in its central part (Fig. 1-A) (Eilu et al., 2012). It contains mainly small magmatic Ni-Cu-Co sulfide deposits in *syn*-orogenic ultramafic to mafic layered intrusions (1890–1870 Ma; Peltonen 2005). The orogenic Au deposits with typical and atypical metal association share a similar geological setting (Fig. 1-B to D). All the deposits comprise sets of quartz veins and disseminated ore hosted in *meta*-volcanic to *meta*-sedimentary rocks and share similar metamorphic grade. However, the deposits display different metal associations and contents.

3. Orogenic Au deposits of the Pohjanmaa Belt

3.1. The Laivakangas and the Huhta Au deposits

The Laivakangas Au deposit is a mine located in the north of the Pohjanmaa Belt (Fig. 1-A). It is exploited in two open-pits and has 48.58 tonnes of Au reserve (Bektas and Vathavooran 2019). It is classified as a typical orogenic Au deposit, although it has metal zonation fromAu-As to Au-Cu and Au-Mo-W, interpreted to result from interaction with magmatic fluids in the deposit formation (Geological Survey of Finland, 2019d; Mäkelä 1984). The host rocks consist of a mafic *meta*-volcanic unit, intruded by granodiorite prior to regional metamorphism (Fig. 1-B). Mineralized sets of quartz veins cross-cut the host rocks. Younger syeno-granite and dolerite dykes post-date regional peak metamorphism and cross-cut all the previous lithologies and veins. The host rocks reached peak middle amphibolite facies conditions at 575 ± 50 °C and 5 kbar (Mäkelä 1984) at ca. 1890–1860 Ma, according to regional metamorphic peak dating on monazite U-Pb data from migmatite (Hölttä et al., 2019). The ore is hosted in sheeted quartz-sulfide vein arrays in several subparallel shear zones hosted in *meta*-volcanic rocks and *meta*-granodiorite. Individual veins are planar, narrow (2–5 mm, rarely 2–5 cm wide) and display localized pinch and swell structures, although the auriferous structure is continuous over tens of metres (Bektas and Vathavooran 2019).

The Huhta Au deposit comprises a typical orogenic Au mineralisation. It is located in the central western part of the Ylivieska field, within

the Laivakangas Au-Cu metallogenic area, and is in direct proximity to the Hitura Ni-Co metallogenic area (Fig. 1-A) (Geological Survey of Finland, 2019a). There is no estimation of resources available for this deposit. The host rocks reached peak lower amphibolite facies conditions at 545 ± 30 °C at 1810–1800 Ma (Hölttä et al., 2019; Hölttä and Heilimo 2017). The deposit is formed by two main lode zones hosted by intermediate to felsic *meta*-volcanic rocks (Fig. 1-C). The lodes are subvertical and are oriented west-northwest. The ore is located in quartz-sulfide veins and shear bands in the host rocks.

3.2. The Jouhineva Au-Cu-Co-Ag and the Kurula Au-Co deposits

The Jouhineva (also known as Pölla) deposit is located 2.8 km northwest of the Huhta deposit (Fig. 1-C), along the same tectonic structure. It lies within the Laivakangas Au-Cu metallogenic area close to the Hitura Ni-Co metallogenic area (Fig. 1-A). Test mining of 5000 t of mineralisation from an open pit in 1984 produced 40.5 tonnes of Cu, 4.5 kilograms of Au, 40 kilograms of Ag and 9 tonnes of Co (Geological Survey of Finland, 2019b). The host rocks are lower amphibolite facies *meta*-andesite and intermediate *meta*-tuff (Geological Survey of Finland, 2019b). Metamorphic peak conditions reached temperatures of 545 ± 30 °C at 1810–1800 Ma (Hölttä et al., 2019; Hölttä and Heilimo 2017). The mineralisation is hosted by quartz-sulphide veins and shear zones that are up to 6 m wide and 20–200 m long, forming a set of subparallel, near-vertical, north-west-trending lodes.

The Kurula Au-Co deposit lies in both the Laivakangas Au-Cu and Hitura Ni-Co metallogenic areas, located in the central part of the Pohjanmaa Belt (Fig. 1-A; D) and is classified as an atypical orogenic Au deposit (Geological Survey of Finland, 2019c). There is no estimation of resources available for this deposit. The host rocks reached the middle amphibolite facies at 620 ± 40 °C between 1870 and 1800 Ma (Hölttä et al., 2019; Hölttä and Heilimo 2017). The deposit comprises a mineralized quartz-tourmaline-arsenide-sulfide vein network hosted in intermediate to felsic *meta*-volcanic rocks at the contact between *meta*-volcanic and *meta*-sedimentary units of the Ylivieska Group (Geological Survey of Finland, 2019c; Sipilä 1983, 1988).

4. Sampling and analytical methods

Field work was carried out in the northern and southern pits of the Laivakangas mine where 14 representative samples of the different host and mineralized rocks were collected. In addition, 39 representative samples of mineralized veins and host rocks were collected from 10 drill cores at different depth intervals (ESM 1). Drill core sampling was performed at the drill core storage facility of the Geological Survey of Finland in Loppi where 75, 31 and 40 samples of the Jouhineva, Huhta and Kurula deposits have been collected respectively. Representative samples of mineralized veins and different wall and host rocks were collected from the drill cores at different depth intervals according to the petrological features and geochemical data provided by the GTK (ESM 1). The drill cores of the Jouhineva deposit showing the highest Co content are already oversampled and could not be resampled.

After careful investigation, 98 polished thin sections were prepared for petrological study. Petrography of ore and host rock was studied using transmitted and reflected light microscopy and scanning electron microscopy using a TESCAN VEGA 3 scanning electron microscope (SEM). Ore mineral composition was determined by electron microprobe analysis (EPMA) using a JEOL 8900 Superprobe at the Eberhard Karls University of Tübingen. The following elements were measured: Ag, Au, As, Bi, Co, Cu, Fe, Hg, Ni, S, Sb, Zn (ESM 2). Operating conditions were an accelerating voltage of 25 kV at a probe current of 20nA with a focused beam. K-lines were used for As, Co, Fe, Ni, S, Zn; K-lines for Cu; L-lines for Au, Ag, Bi, Hg and Sb. X-ray lines and background positions were selected to minimize interference during analysis. Overlap correction was applied for Au and Zn. PhiRhoZet correction was applied for data reduction. Native metals were used as calibration standards for Ag, Au, Bi, Co, Cu, Ni and Zn, and pyrite for Fe and S, cinnabar for Hg, stibnite for Sb, and GaAs for As.

Sulfur isotope analysis was performed in the Laboratory of Environmental and Raw Materials Analysis (Institute of Applied Geosciences, Karlsruhe Institute of Technology) on monomineralic powders of sulfides (arsenopyrite, chalcopyrite, pyrite and pyrrhotite). The sulfides were carefully sampled with a micro-drill after observation with a binocular microscope to control sample homogeneity. Each sulfide sample was divided into three portions containing 100 µg of S and packed with V_2O_5 as catalyst in tin cups. The samples were heated at 1020 °C and the combustion products were transported in a continuous He flow through a reactor to form SO_2. The resulting products were sorted by an Eurovector elemental analyser, ionized and analysed with an Isoprime isotopic ratio mass spectrometer (IRMS). Reference material data are provided in ESM 3.

5. Results

5.1. Gold-only orogenic deposits

The Laivakangas, Huhta, Jouhineva and Kurula deposits formed in two hydrothermal events: (1) a ubiquitous As-Au (Co, Ni) event, locally subdivided in stages based on the mineralogy; (2) a Cu(-Au) sulfide event locally overprinting the previous event veins. A late barren alteration event affects the mineralized veins in the Laivakangas and Jouhineva deposits (Fig. 2).

5.2. Laivakangas Au deposit

The auriferous quartz veins of the Laivakangas deposit are typically millimetres to several centimetres wide and are generally parallel to the host rock foliation (Fig. 3-A, B). They cross-cut and overprint barren, feldspar-dominated hydrothermal veins (Fig. 3-D), and are mainly composed of quartz and K-feldspar with accessory chlorite, biotite, pumpellyite, titanite, ilmenite, rutile, apatite, scheelite, zircon and rare carbonates. They are mostly deformed showing undulose extinction of quartz. Two main mineralisation events are defined: (1) an As-Au(–Co) event forming auriferous quartz veins containing Ni-Co-Fe arsenide with invisible Au; (2) a sulfide (Cu-Au) event, locally overprinting the previous event, forming auriferous quartz-sulfide veins with free, native Au (Fig. 2-A; Fig. 4-A). Theevents are not ubiquitous, leading to different ore mineral populations and content within veins (Fig. 3-C to E).

During the mineralisation event 1, Ni-Co-Fe arsenides, mainly löllingite and minor clinosafflorite $(Co,Ni,Fe)As_2$), occur in the quartz veins as < 1 mm inclusions in younger arsenopyrite (Fig. 3-F to H). Löllingite is locally enriched in Co, Ni and Ag (Table 1, ESM 2). The vein selvedges show brown to black, centimetre-scale hydrothermal alteration halos with disseminated arsenopyrite and pyrite, and replacement of plagioclase by sericite and biotite by chlorite, in the first millimetres of the alteration halo.

The mineralisation event 2 is characterized by: a) new auriferous quartz veins which locally cross-cut the previous vein generation and contain pyrite (Py1), chalcopyrite, pyrrhotite and minor sphalerite, molybdenite, free grains of native Au and Bi-(Te, Au, Ag, Cu) minerals; and b) overprinting of the event 1 veins with replacement of the Ni-Co-Fe arsenides by arsenopyrite and formation of previously listed sulfides (Fig. 2-A). Arsenopyrite occurs as euhedral to subhedral grains which are locally fractured (Fig. 3-I). It is commonly zoned and/or has event 1 Ni-Co-Fe arsenide, Au and Bi-(Te, Au, Ag, Cu) inclusions (Fig. 3-F to I). It shows overall homogeneous composition with little to no Co and Ni (Table 1). Arsenopyrite grains containing an event 1 clinosafflorite or a Co-rich löllingite core have higher Co– and Ni-contents (up to 2.5 and 1.5 wt%, respectively; Table 1, ESM 2). Arsenopyrite is also locally enriched in Ag, up to 330 ppm (Table 1). Chalcopyrite and pyrrhotite occur in the veins as grains parallel to the foliation or as fracture fills in the gangue minerals, mainly feldspar and quartz (Fig. 3-J and K).

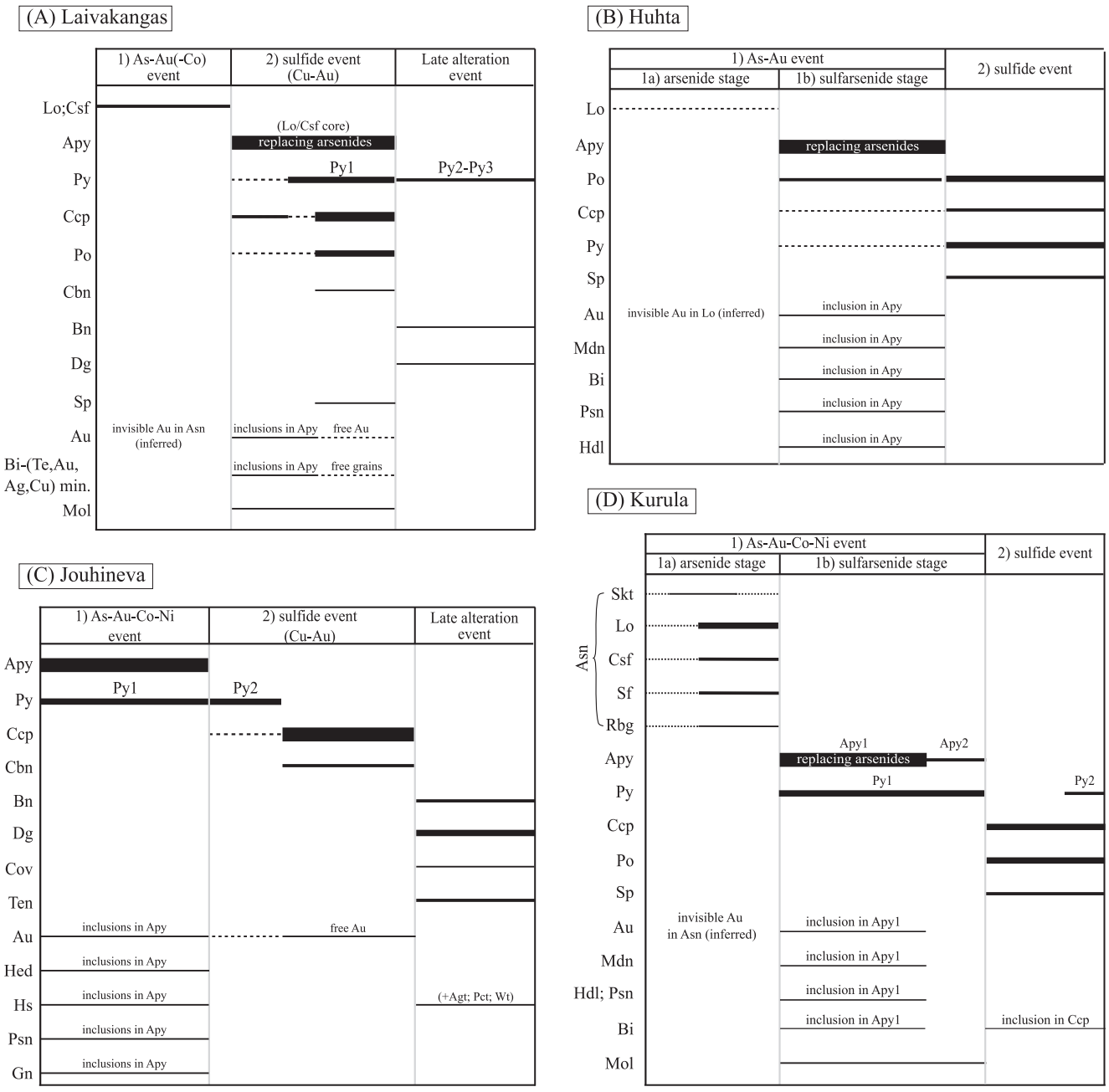

Fig. 2. (A) Paragenetic sequence of the Laivakangas deposit; (B) Paragenetic sequence of the Huhta deposit. Abbreviations as in previous figures; (C) Paragenetic sequence of the Jouhineva deposit; (D) Paragenetic sequence of the Kurula deposit. Abbreviations as in Fig. 3; Bi = native bismuth; Cov = covellite; Csf = clino-safflorite; Dg = digenite; Gn = galena; Hdl = hedleyite; Hs = hessite; Mdn = maldonite; Mol = molybdenite; Psn = pilsenite; Rbg = rammelsbergite; Sf = safflorite; Skt = skutterudite; Sp = sphalerite; Ten = tennantite.

Chalcopyrite locally has cubanite exsolution lamellae (Fig. 3-J), and sphalerite and molybdenite inclusions. Pyrite (Py1) grains are commonly pristine in an assemblage with chalcopyrite and pyrrhotite. Visible Au is identified as native Au inclusions and as free, native Au grains among sulfides and in fractures of vein filling silicates. Gold inclusions represent 80 to 90 vol% of the visible Au, and occur in arsenopyrite and Ni-Co-Fe arsenide and rarely, in pyrrhotite or chalcopyrite (Fig. 3-F to I). They commonly occur together with Bi-(Te, Au, Ag, Cu) minerals at a volumetric ratio of 1:5. Free, native Au grains represent 10 to 20 vol% of the visible Au. They occur as < 50 μm grains in the gangue commonly along with Bi-(Te, Au, Ag, Cu) minerals and chalcopyrite in the auriferous quartz veins (Fig. 3-K). Bi-(Te, Au, Ag, Cu) minerals are found as tellurides and Bi-rich minerals, which tend to occur together in the following proportions: native Bi (30 vol%), hedleyite (23 vol%), pilsenite (16 vol%), wittichenite (13 vol%), bismite (10 vol%), hessite (7 vol%), volynskite (<2 vol%) and maldonite (<2 vol%). Gold grains can contain variable amounts of Ag (5.47–21.90 wt%; Table 1, ESM 2). Pyrite (Py1) is either enriched in Cu (up to 8 wt%) or in As (up to 6 wt%) when altered and spatially related to chalcopyrite and arsenopyrite, respectively (Table 1, ESM 2). Pyrite is locally enriched in Ag, Bi, Co, Ni and Zn (Table 1). Chalcopyrite contains Ag and shows local enrichment in Au and Bi, up to 350 ppm and 4510 ppm, respectively (Table 1). Pyrrhotite contains traces of Cu, Ni and Ag (Table 1). This mineralisation event is associated with millimetre- to centimetre-scale, hydrothermal sericite-chlorite alteration haloes characterized by greenish-white-coloured zones. It shows partial to complete chloritisation of biotite

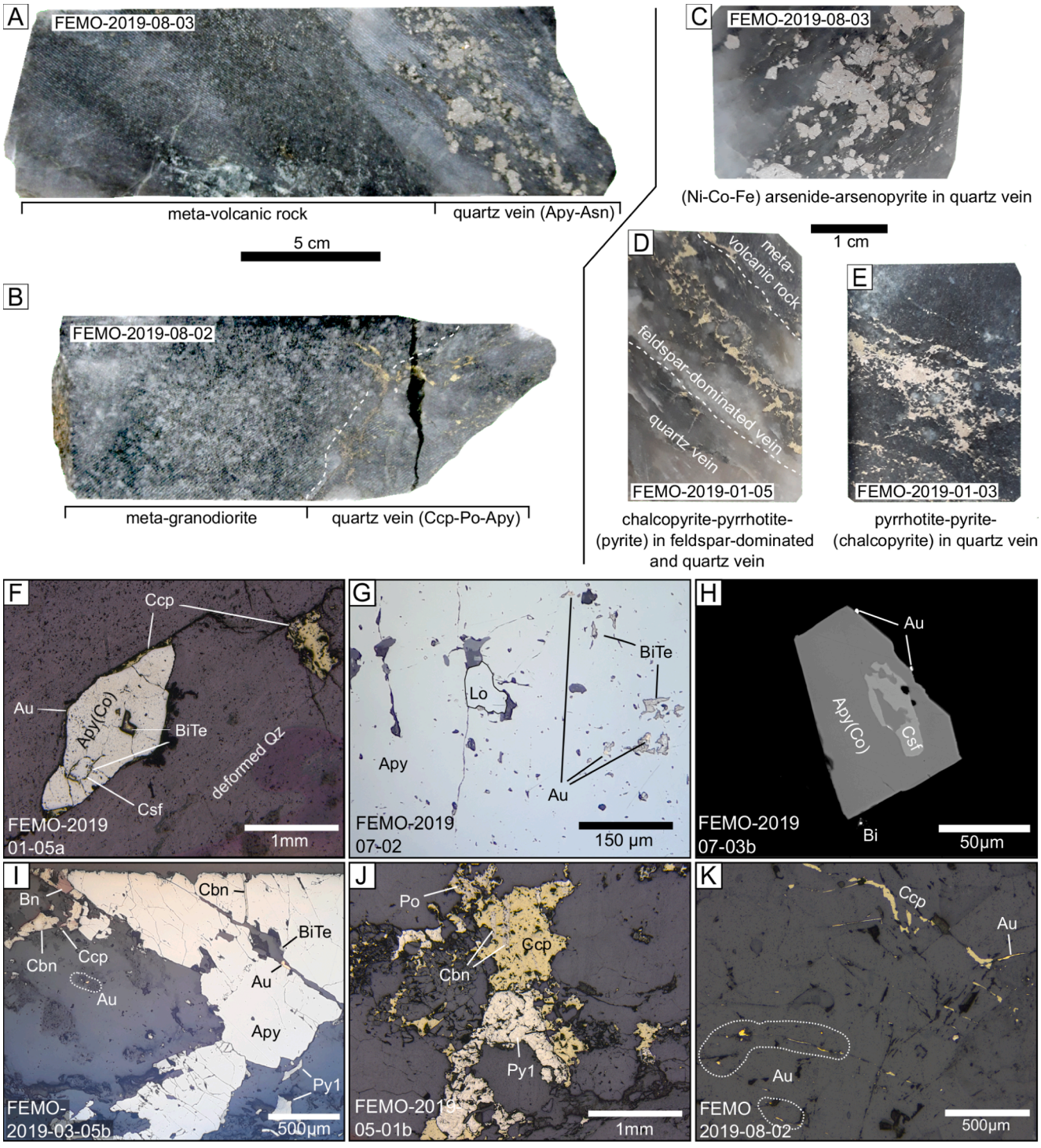

Fig. 3. Representative ore samples from the Laivakangas deposit. (A-E) Auriferous quartz veins with arsenides, sulfarsenides and sulfides; (F) Co-rich arsenopyrite containing a clinosafflorite core, Au and Bi-(Te, Au, Ag, Cu) grains; (G) Detail of arsenopyrite with löllingite core and Au-rich and Bi-(Te, Au, Ag, Cu) grains; (H) Back-scattered electron-image (BSE-image) of Co-rich arsenopyrite with a clinosafflorite core and native Au and Bi grains; (I) Fractured arsenopyrite with cubanite along fractures, surrounded by pyrite (Py1), chalcopyrite and cubanite. Bornite replaces chalcopyrite. Au and Bi-(Te, Au, Ag, Cu) grains in arsenopyrite, along fractures and as free grains in the gangue; (J) Cubanite lamellae in chalcopyrite with pyrrhotite and pyrite (Py1); (K) Trail of Au and chalcopyrite in quartz vein. Abbreviations: Apy = arsenopyrite; Asn = Ni-Co-Fe arsenide; Au = gold; BiTe = Bi-(Te, Au, Ag, Cu) = bismuth, hedleyite, pilsenite, hessite, wittichenite, volynskite, maldonite; Bn = bornite; Ccp = chalcopyrite; Chl = chlorite; Csf = clinosafflorite; Cbn = cubanite; Lo = löllingite; Po = pyrrhotite; Py = pyrite; Qz = quartz.

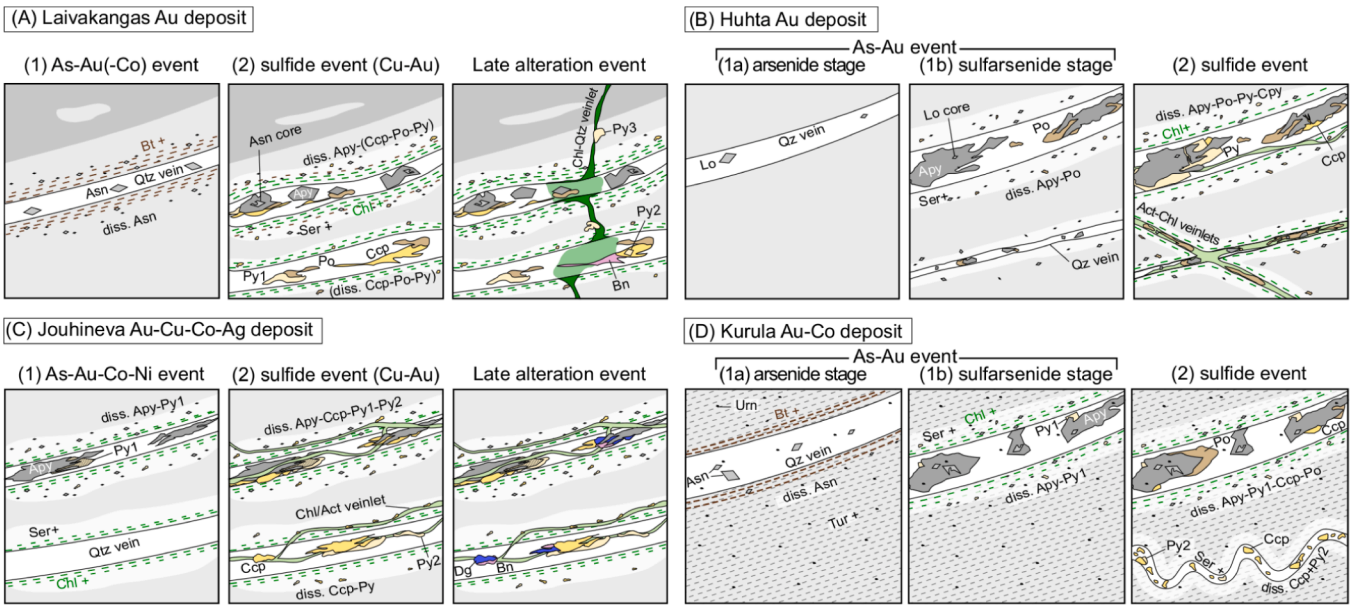

Fig. 4. (A) Summary of the hydrothermal veins and alteration zones in the Laivakangas deposit. (1) Mineralisation event 1, quartz veins with löllingite and other Ni-Co-Fe arsenides with invisible Au. Hydrothermal biotite-(Ni-Co-Fe) arsenide alteration zone along vein selvedges; (2) Mineralisation event 2, arsenide is replaced by arsenopyrite with Au exsolutions in overprinted event 1 veins; chalcopyrite, pyrrhotite, pyrite (Py1), and free, native Au grains in event 2 veins. Hydrothermal sericite-chlorite alteration zone along vein selvedges; Late alteration event forming chlorite-quartz veinlets with pyrite (Py2, Py3) and bornite. Abbreviations as in previous figures. (B) Summary of the hydrothermal veins and alteration zones of the Huhta deposit. (1) Stage 1a of the mineralisation event 1, quartz veins containing little löllingite; (2) Stage 1b of the mineralisation event 1, quartz veins containing pyrrhotite and arsenopyrite with Au inclusions replacing löllingite. Local hydrothermal sericite-arsenopyrite-pyrrhotite alteration zone along vein selvedges; (3) Mineralisation event 2, actinolite-chlorite-rich veinlets with pyrrhotite, pyrite and minor chalcopyrite. Abbreviations as in previous figures. (C) Summary of the hydrothermal veins and alteration zones in the Jouhineva deposit. (1) Mineralisation event 1, quartz veins with arsenopyrite and Au inclusions, and pyrite (Py1); hydrothermal sericite-chlorite-arsenopyrite-pyrite (Py1) alteration zone; (2) Mineralisation event 2, actinolite-chlorite-rich veinlets with chalcopyrite and pyrite (Py2) cross-cut event 1 quartz veins and host rock. Free native Au grains occur with chalcopyrite; Late alteration event replacing chalcopyrite by bornite and digenite. Abbreviations as in previous figures. (D) Summary of the hydrothermal veins and alteration zones in the Kurula deposit. (1) Stage 1a of the mineralisation event 1, quartz veins with Ni-Co-Fe arsenides containing invisible Au. Hydrothermal tourmaline-biotite alteration zone with accessory (Ni-Co-F) arsenides; (2) Stage 1b of the mineralisation event 1, pyrite (Py1) and arsenopyrite (Apy1) with Au inclusions replace the arsenides (stage 1a). Sericite-chlorite alteration along veins selvedges and local disseminated arsenopyrite and pyrite in the hydrothermal alteration zone; (3) Mineralisation event 2, quartz veins with chalcopyrite, pyrrhotite and accessory sphalerite. Pyrite (Py2) locally replaces chalcopyrite. Local disseminated chalcopyrite in the hydrothermal alteration zone. Abbreviations as in previous figures.

Table 1
Electron microprobe data of main ore minerals of the Laivakangas, Jouhineva, Huhta and Kurula deposits (see ESM 2 for detailed data).

Laivakangas (wt.%)	n	Fe	δ	Co	δ	Ni	δ	Cu	δ	Ag	δ	Au	δ	Zn	δ	As	δ	Sb	δ	Bi	δ	S	δ	Hg	δ	Total	δ
Arsenopyrite	111	33,32	0,79	0,32	0,43	0,17	0,30	<LOD	<LOD	<LOD	<LOD	<LOD	<LOD	<LOD	<LOD	48,12	0,72	<LOD	<LOD	<LOD	<LOD	19,11	0,58	<LOD	<LOD	101,12	0,65
Chalcopyrite	59	29,71	0,63	<LOD	<LOD	<LOD	<LOD	33,87	0,69	0,02	0,02	<LOD	<LOD	0,02	0,05	0,08	0,20	<LOD	<LOD	<LOD	<LOD	34,64	0,40	<LOD	<LOD	98,12	1,04
Löllingite	51	26,87	1,06	0,54	0,44	0,52	0,51	<LOD	<LOD	<LOD	<LOD	<LOD	<LOD	<LOD	<LOD	69,82	1,88	<LOD	<LOD	0,38	2,41	2,19	0,43	<LOD	<LOD	100,24	0,61
Pyrite	52	43,43	3,25	0,14	0,34	0,04	0,08	0,86	1,07	0,03	0,03	<LOD	<LOD	0,02	0,04	2,39	3,21	<LOD	<LOD	0,12	0,29	49,80	4,18	<LOD	<LOD	98,41	1,33
Pyrrhotite	20	59,55	0,26	<LOD	<LOD	<LOD	<LOD	0,05	0,03	<LOD	<LOD	<LOD	<LOD	<LOD	<LOD	0,05	0,12	<LOD	<LOD	<LOD	<LOD	38,96	0,53	<LOD	<LOD	98,59	0,42

Jouhineva (wt.%)	n	Fe	δ	Co	δ	Ni	δ	Cu	δ	Ag	δ	Au	δ	Zn	δ	As	δ	Sb	δ	Bi	δ	S	δ	Hg	δ	Total	δ
Arsenopyrite	113	32,53	2,08	1,53	1,75	0,10	0,12	<LOD	<LOD	<LOD	<LOD	<LOD	<LOD	<LOD	<LOD	47,65	1,35	0,03	0,03	0,05	0,04	19,59	1,11	<LOD	<LOD	101,51	0,51
Bornite	5	10,96	0,13	<LOD	<LOD	<LOD	<LOD	61,73	1,40	0,05	0,01	<LOD	<LOD	<LOD	<LOD	0,03	0,02	<LOD	<LOD	0,05	0,04	25,86	0,36	<LOD	<LOD	98,69	1,85
Chalcopyrite	28	29,25	3,12	<LOD	<LOD	0,01	0,02	33,85	0,47	0,03	0,03	<LOD	<LOD	0,16	0,79	0,67	2,63	0,03	0,10	0,04	0,04	34,64	1,12	<LOD	<LOD	98,67	1,56
Cubanite	2	36,06	0,17	<LOD	<LOD	0,19	0,04	17,36	1,22	0,13	0,02	<LOD	<LOD	0,01	0,01	0,70	0,34	<LOD	<LOD	0,07	0,08	42,60	0,11	<LOD	<LOD	97,17	0,42
Digenite	4	0,02	0,01	<LOD	<LOD	<LOD	<LOD	78,04	0,33	0,06	0,02	<LOD	<LOD	<LOD	<LOD	<LOD	<LOD	<LOD	<LOD	0,04	0,03	21,12	0,31	0,04	0,02	99,34	0,24
Pyrite	22	32,53	2,08	1,53	1,75	0,10	0,12	<LOD	<LOD	<LOD	<LOD	<LOD	<LOD	<LOD	<LOD	47,65	1,35	0,03	0,03	0,05	0,04	19,59	1,11	<LOD	<LOD	101,51	0,51
Tennantite	14	10,96	0,13	<LOD	<LOD	<LOD	<LOD	61,73	1,40	0,05	0,01	<LOD	<LOD	<LOD	<LOD	0,03	0,02	<LOD	<LOD	0,05	0,04	25,86	0,36	<LOD	<LOD	98,69	1,85

Huhta (wt.%)	n	Fe	δ	Co	δ	Ni	δ	Cu	δ	Ag	δ	Au	δ	Zn	δ	As	δ	Sb	δ	Bi	δ	S	δ	Hg	δ	Total	δ
Arsenopyrite	50	34,22	0,69	<LOD	<LOD	0,03	0,06	<LOD	<LOD	<LOD	<LOD	<LOD	<LOD	<LOD	<LOD	46,75	1,78	0,04	0,04	<LOD	<LOD	20,17	1,35	<LOD	<LOD	101,34	0,83
Chalcopyrite	24	30,05	0,72	<LOD	<LOD	<LOD	<LOD	32,04	1,72	0,02	0,01	<LOD	<LOD	<LOD	<LOD	1,93	2,14	<LOD	<LOD	<LOD	<LOD	34,80	1,01	<LOD	<LOD	98,89	1,32
Pyrrhotite	17	58,95	2,59	<LOD	<LOD	<LOD	<LOD	<LOD	<LOD	<LOD	<LOD	<LOD	<LOD	<LOD	<LOD	2,32	4,64	<LOD	<LOD	<LOD	<LOD	37,62	2,40	<LOD	<LOD	98,97	0,90
Pyrite	29	45,91	0,84	<LOD	<LOD	<LOD	<LOD	<LOD	<LOD	<LOD	<LOD	<LOD	<LOD	<LOD	<LOD	0,37	0,63	<LOD	<LOD	<LOD	<LOD	51,85	1,27	<LOD	<LOD	98,21	1,92

Kurula (wt.%)	n	Fe	δ	Co	δ	Ni	δ	Cu	δ	Ag	δ	Au	δ	Zn	δ	As	δ	Sb	δ	Bi	δ	S	δ	Hg	δ	Total	δ
Arsenopyrite	78	30,21	1,83	3,23	1,59	0,17	0,16	<LOD	<LOD	<LOD	<LOD	<LOD	<LOD	<LOD	<LOD	49,41	1,72	<LOD	<LOD	0,09	0,39	18,11	1,15	<LOD	<LOD	101,37	0,60
Chalcopyrite	10	29,99	0,18	<LOD	<LOD	<LOD	<LOD	33,61	0,81	0,02	0,01	<LOD	<LOD	0,06	0,09	0,04	0,03	<LOD	<LOD	<LOD	<LOD	34,93	0,29	<LOD	<LOD	98,70	0,64
Löllingite	4	26,51	0,24	0,71	0,08	0,55	0,05	<LOD	<LOD	<LOD	<LOD	<LOD	<LOD	<LOD	<LOD	69,07	0,47	<LOD	<LOD	<LOD	<LOD	2,31	0,45	<LOD	<LOD	99,21	0,48
Pyrrhotite	5	60,17	0,05	<LOD	<LOD	0,01	0,01	<LOD	<LOD	<LOD	<LOD	<LOD	<LOD	<LOD	<LOD	0,04	0,02	<LOD	<LOD	<LOD	<LOD	38,63	0,41	<LOD	<LOD	98,96	0,43
Pyrite	10	46,12	0,35	<LOD	<LOD	0,03	0,03	0,40	0,58	<LOD	<LOD	<LOD	<LOD	<LOD	<LOD	0,53	0,64	<LOD	<LOD	<LOD	<LOD	52,41	0,72	<LOD	<LOD	99,50	0,87
Rammelsbergite	1	7,89	-	0,11	-	25,81	-	<LOD	-	<LOD	-	<LOD	-	<LOD	-	59,91	-	0,05	-	<LOD	-	2,85	-	<LOD	-	96,74	-
Safflorite	21	20,97	2,85	6,11	1,89	0,97	0,55	<LOD	<LOD	<LOD	<LOD	<LOD	<LOD	<LOD	<LOD	71,05	1,17	<LOD	<LOD	0,09	0,09	1,42	0,67	<LOD	<LOD	100,65	0,48
Skutterudite	13	2,76	1,00	16,29	2,01	2,03	0,82	<LOD	<LOD	<LOD	<LOD	<LOD	<LOD	<LOD	<LOD	78,81	0,66	<LOD	<LOD	<LOD	<LOD	0,20	0,08	<LOD	<LOD	100,17	0,77

	Fe	Co	Ni	Cu	Ag	Au	Zn	As	Sb	Bi	S	Hg
Det. limit Laivakangas (ppm)	71	81	70	718	102	202	95	211	249	428	95	337
Det. limit Jouhineva(ppm)	70	80	70	743	102	200	94	213	245	416	94	329
Det. limit Huhta (ppm)	69	81	68	731	99	197	92	204	243	410	96	323
Det. limit Kurula (ppm)	104	101	111	1295	135	329	148	336	363	695	153	543

and amphibole, sericitisation of plagioclase and K-feldspar and disseminated chalcopyrite, pyrrhotite and pyrite (Py1) in the hydrothermal alteration zone. Late chlorite-quartz veinlets locally cross-cut the host rock and earlier veins, forming additional pyrite, bornite and digenite (Fig. 2-A), which locally replace chalcopyrite (Fig. 3-I).

5.3. Huhta Au deposit

In the Huhta deposit, the host rock foliation is cross-cut by auriferous quartz veins and actinolite-chlorite-sulfide veinlets (Fig. 5 A to D). The auriferous quartz-(sulfide) veins are a few millimetres to several centimetres wide and are usually deformed, showing undulose extinction of quartz and elongated, recrystallized quartz grains. Two mineralisation events are defined: (1) an As-Au event, subdivided into two stages; (1a) auriferous quartz-arsenide veins with löllingite containing invisible Au; (1b) auriferous quartz-sulfarsenide-sulfide veins defined by arsenopyrite with Au inclusions as well as pyrrhotite; (2) a sulfide event, locally overprinting the previous event, forming actinolite-chlorite-rich veinlets with chalcopyrite-pyrite-pyrrhotite-sphalerite (Fig. 2-B; Fig. 4-B).

Stage 1a is mostly cryptic and identified through rare löllingite cores preserved in stage 1b arsenopyrite (Fig. 2-B). Stage 1b is a continuation of stage 1a and is characterized by auriferous quartz veins with arsenopyrite and minor pyrrhotite. Arsenopyrite is euhedral to subhedral, locally forming clusters in veins (Fig. 5-C; -E to J). Locally it has pyrite, pyrrhotite, chalcopyrite, Au and gangue mineral inclusions (Fig. 5-G). It has low contents of Co and Ni (<0.57 and < 0.38 wt%, respectively) as

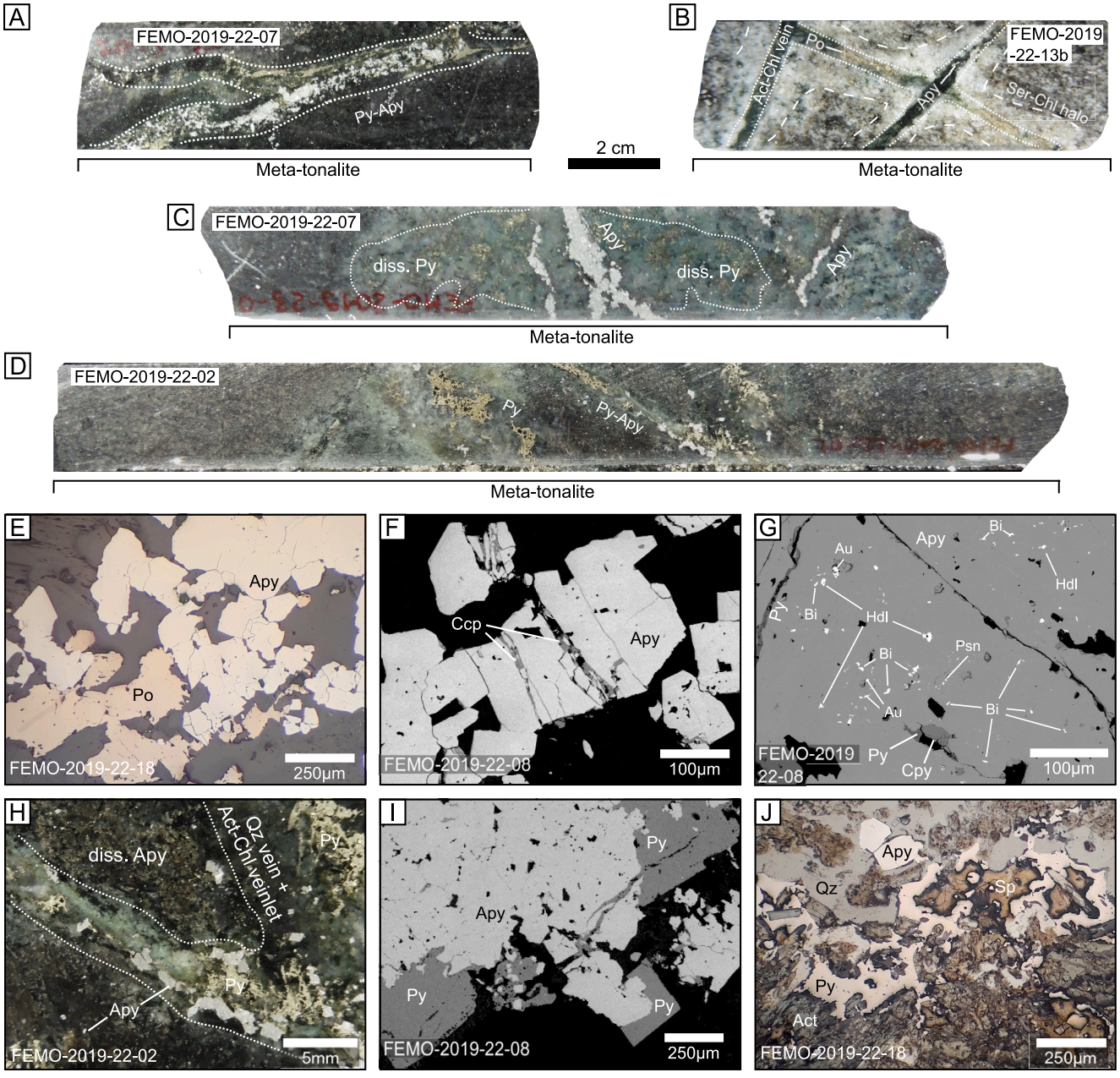

Fig. 5. Representative ore samples of the Huhta deposit. (A-D) Auriferous quartz veins with arsenopyrite, pyrite, pyrrhotite and hydrothermal sericite-chlorite alteration halos; (E) Arsenopyrite and pyrrhotite in quartz vein; (F) BSE-image of arsenopyrite with chalcopyrite fracture-filling; (G) BSE-image of fractured arsenopyrite showing Au, Bi, hedleyite and pilsenite inclusions. Pyrite and chalcopyrite fill fractures and porosity; (H) Quartz vein with arsenopyrite (stage 1b) cross-cut by actinolite-chlorite-rich veinlet with pyrite (event 2). Hydrothermal sericite-chlorite-arsenopyrite alteration zone in *meta*-tonalite along the vein selvedges; (I) BSE-image of fractured arsenopyrite with euhedral pyrite replacing arsenopyrite along the rims and filling the fractures; (J) Actinolite-chlorite-rich veinlet with pyrite and sphalerite in quartz vein with arsenopyrite. Abbreviations as in previous figures; Chl = chlorite; Hdl = hedleyite; Psn = pilsenite; Ser = sericite.

well as trace concentrations of Sb, Bi, Cu, Hg, Ag and Zn (Table 1, ESM 2). Pyrrhotite occurs as patchy grains, generally in association with arsenopyrite and local chalcopyrite inclusions (Fig. 5-E). Gold occurs as disseminated, < 50 μm inclusions in arsenopyrite, commonly together with Bi, hedleyite, pilsenite and maldonite, at a volumetric ratio of 1:10 (Fig. 5-G). Gold grains contain various amounts of Ag (avg. 21.10 wt%), locally occurring as electrum. Invisible Au occurs rarely in chalcopyrite, pyrrhotite and pyrite (ESM 2). The veins have centimetre- to metre-scale hydrothermal alteration haloes characterized by a greenish-white bleached zone in the host rock (Fig. 5-A to D). Compared to unaltered rock, the bleached zone contains disseminated arsenopyrite and pyrite, and is depleted in mafic minerals, while plagioclase is replaced by sericite.

The mineralisation event 2 locally overprints the previous event, it is characterized by actinolite-chlorite-rich veinlets dominated by patchy pyrrhotite and porous pyrite grains with minor chalcopyrite and sphalerite. Pyrite has euhedral to patchy habits (Fig. 5-I and J) and locally fills fractures in arsenopyrite, replacing it along the rims (Fig. 5-I). Chalcopyrite and sphalerite are generally associated with pyrite, locally filling fractures (Fig. 5-F and J). The hydrothermal alteration halo in the host rock around actinolite-chlorite-rich veinlets is a few millimetres wide; it contains disseminated pyrrhotite, pyrite and chalcopyrite; plagioclase is replaced by sericite, biotite by chlorite, hornblende by fine-grained actinolite and ilmenite by titanite (Fig. 5-B-D).

5.4. Orogenic Au deposits with atypical metal associations

5.4.1. Jouhineva Au-Cu-Co-Ag deposit

Mineralisation at the Jouhineva deposit occurred in two events forming two vein sets: (1) an As-Au-Co-Ni event forming auriferous

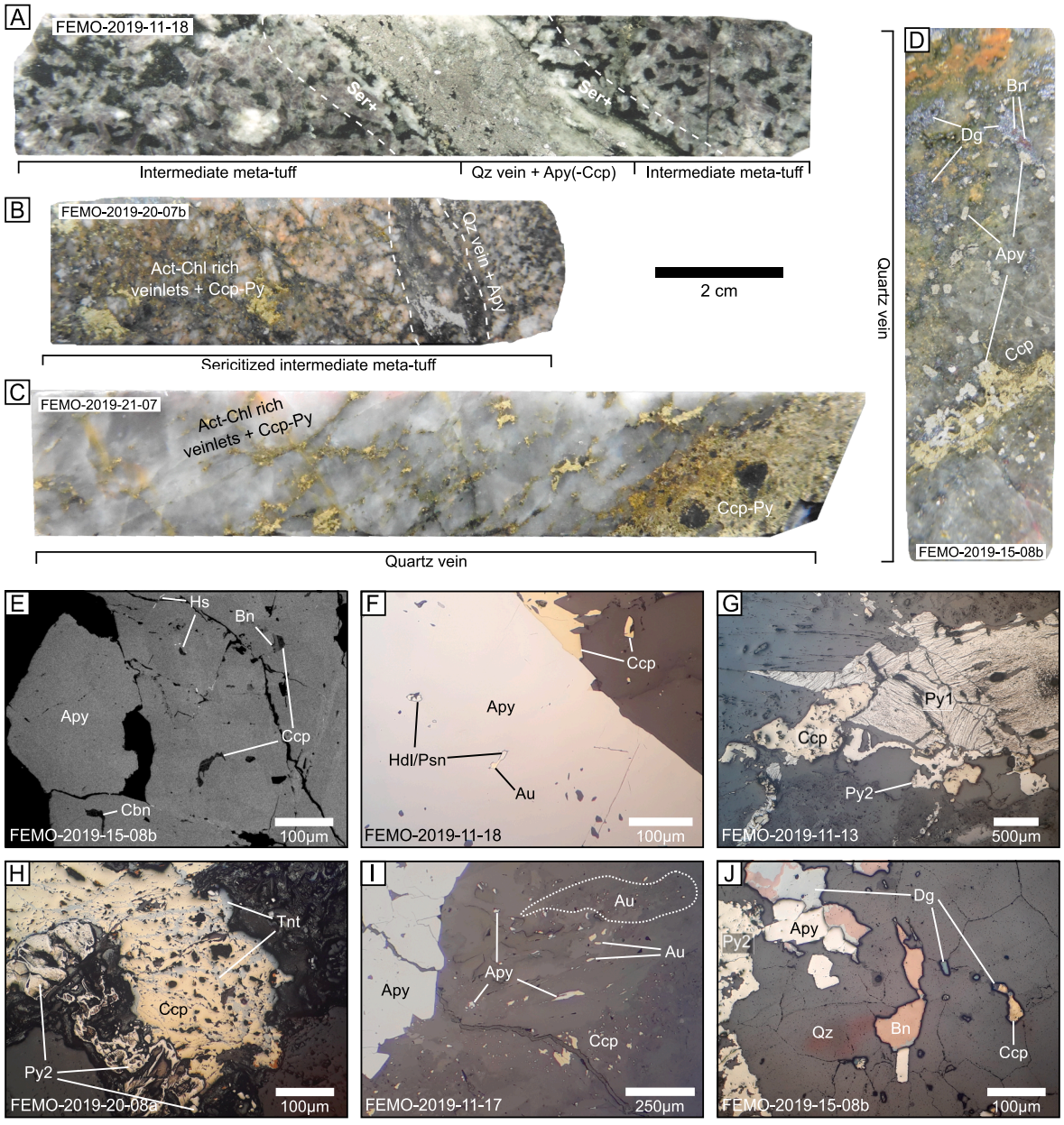

Fig. 6. Representative ore samples of the Jouhineva deposit. (A-D) Mineralized quartz veins with arsenopyrite, chalcopyrite, pyrite, digenite and bornite; (E) BSE-image of arsenopyrite containing Au, hedleyite, hessite, cubanite, chalcopyrite and bornite inclusions. Arsenopyrite shows compositional zoning; (F) Gold and hedleyite inclusions in arsenopyrite; (G) Spongy and fractured pyrite (Py1) with pristine pyrite (Py2) and chalcopyrite; (H) Spongy pyrite with chalcopyrite being replaced by tennantite along fractures and porosity; (I) Disseminated free, native Au and chalcopyrite with arsenopyrite; (J) Quartz vein with pyrite and disseminated arsenopyrite and chalcopyrite. Bornite and digenite replace chalcopyrite. Abbreviations as in previous figures.

quartz-sulfarsenide-sulfide veins defined by arsenopyrite with Au inclusions and slight Ni and Co enrichment; and (2) a sulfide (Cu-Au) event, locally overprinting the previous event, forming auriferous actinolite-chlorite-rich veinlets with pyrite and chalcopyrite, along with free, native Au. A late barren alteration event overprints the mineralized veins, replacing chalcopyrite by bornite, digenite and tennantite (Fig. 2-C; Fig. 4-C).

The mineralisation event 1 is characterized by auriferous quartz-sulfide veins. The veins are a few millimetres to tens of centimetres wide and are usually deformed, showing undulose extinction of quartz, elongated quartz grains (Fig. 6-A to D). They mainly contain quartz with accessory apatite, biotite, K-feldspar, plagioclase, scheelite, titanite and zircon. Arsenopyrite is the main ore mineral with minor pyrite. Arsenopyrite is euhedral to subhedral, locally zoned and commonly forms clusters in veins (Fig. 6-A and D). They locally host Au, hedleyite, pilsenite, hessite and galena inclusions (Fig. 6-E and F). Arsenopyrite contains various amounts of Co and Ni (<6.82 and < 0.54 wt%, respectively) as well as traces of Sb, Bi, Cu, Hg, Ag and Zn (Table 1; ESM 2). Pyrite (Py1) is euhedral to subhedral with a spongy or porous texture (Fig. 6-G). Gold occurs as disseminated < 50 μm inclusions in arsenopyrite. It represents up to 10 vol% of the visible Au (Fig. 6-F) and occurs commonly together with < 50 μm hedleyite, pilsenite, hessite and galena grains at a volumetric ratio of 1:10. The veins have millimetre- to centimetre-scale greenish-white hydrothermal alteration halos characterized by disseminated arsenopyrite and pyrite (Py1) and replacement of plagioclase by sericite and biotite by chlorite.

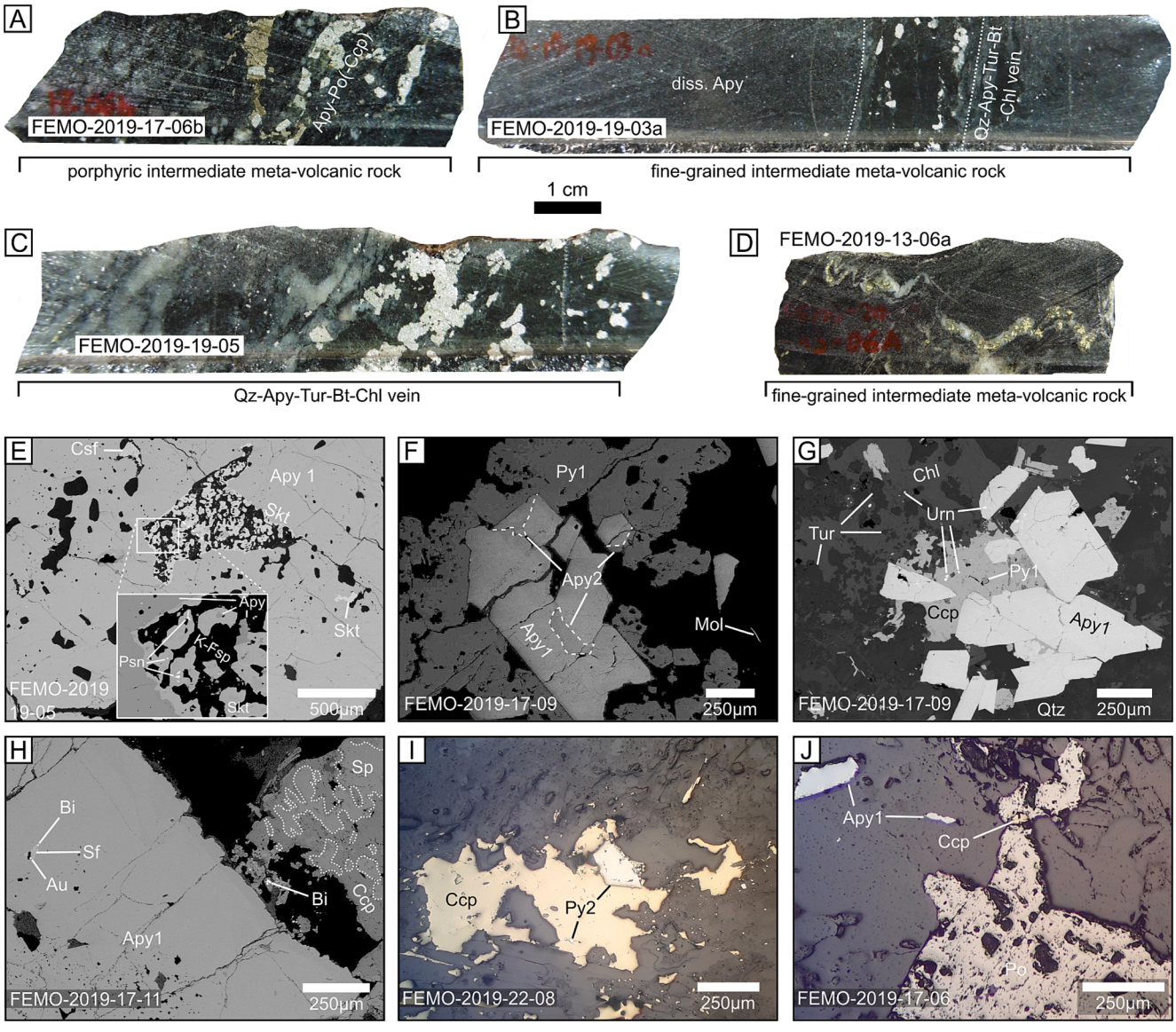

Fig. 7. Representative ore samples of the Kurula deposit. (A-D) Mineralized quartz veins with arsenopyrite, pyrrhotite and chalcopyrite. (E) BSE-image of arsenopyrite (Apy1) containing Ni-Co-Fe arsenide inclusions. Ni-Co-Fe arsenides form a patchy assemblage with arsenopyrite and K-feldspar. Pilsenite is disseminated in arsenopyrite (Apy1) and Ni-Co-Fe arsenides; (F) BSE-image of fractured arsenopyrite (Apy1 and Apy2) and pyrite (Py1) in quartz vein. Arsenopyrite (Apy1) shows a tone contrast linked to variability in Co content; (G) BSE-image of arsenopyrite (Apy1) cluster with chalcopyrite and pyrite (Py1) in quartz vein. Uraninite forms inclusions in sulfides and gangue minerals; (H) BSE-image of fractured arsenopyrite (Apy1) with safflorite inclusion. Gold and Bi occur at the contact between safflorite and arsenopyrite (Apy1). Patchy chalcopyrite-sphalerite assemblage rims arsenopyrite (Apy1), Bi forms inclusions in chalcopyrite; (I) Chalcopyrite and euhedral pyrite (Py2) in deformed quartz vein; (J) Arsenopyrite (Apy1) and spongy pyrrhotite with chalcopyrite inclusion in quartz vein. Abbreviations as in previous figures; Bt = biotite Csf = clinosafflorite; K-Fsp = K-feldspar; Tur = tourmaline.

The mineralisation event 2 is characterized by actinolite-chlorite-sulfide veinlets locally cross-cutting and overprinting the previous auriferous quartz-sulfide veins. Sulfides are dominated by chalcopyrite and patchy pyrite (Py2) stretched along the foliation or filling fractures in quartz (Fig. 2-C; Fig. 6-G and H). Chalcopyrite occurs in significantly higher proportions than in the other deposits (Fig. 2), locally forming massive to semi-massive sulfide veins (Fig. 6-C and D). It contains Ag and shows localized enrichment in Au and Bi whereas pyrite contains traces of As, Cu, Co, Ni and Ag (Table 1; ESM 2). Locally, chalcopyrite and arsenopyrite have cubanite inclusions which have traces of As, Co, Ni and Ag (Table 1; ESM 2). Free native Au occurs as < 50 μm grains along with chalcopyrite in proximity of arsenopyrite in the quartz veins. It represents 90 vol% of the visible Au (Fig. 6-I). The actinolite-chlorite-sulfide veinlets have millimetre- to metre-scale, greenish-white, hydrothermal alteration halos characterized by disseminated chalcopyrite, pyrite (Py2) and rare Au, and replacement of biotite by chlorite and hornblende by fine-grained actinolite.

A late barren alteration event affected chalcopyrite, which is locally replaced by tennantite and Ag-rich minerals (pearceite, hessite, argentite) along newly formed fractures (Fig. 2-C; Fig. 6-E and H). Bornite and digenite locally replace chalcopyrite (Fig. 6-J). Tennantite contains < 4.08 wt% Zn and traces of Co, Ni, Sb and Ag. Bornite contains traces of Ag, Sb, As, Bi, Au and Hg and digenite contains traces of Bi, Fe and Hg (Table 1 and ESM 2).

5.4.2. Kurula Au-Co deposit

In the Kurula deposit, the host rocks are cross-cut by sets of quartz-sulfide veins generally cross-cutting the foliation. The veins are a few millimetres to several centimetres wide and are generally sheared and locally folded (Fig. 7-A to D). They show internal deformation such as elongated, recrystallized quartz and quartz with undulose extinction. The mineralisation is the result of two events forming two sets of veins, locally overprinting each other: (1) an As-Au-Co-Ni event characterized by auriferous quartz-sulfide veins with arsenides and sulfarsenides; and (2) a sulfide event, locally overprinting the previous event, forming quartz-sulfide veins with chalcopyrite, pyrrhotite and sphalerite (Fig. 2-D; Fig. 4-D).

The mineralisation event 1 is subdivided into two stages: (1a) auriferous quartz veins with (Ni-Co-Fe) arsenides and invisible Au; and (1b) pyrite and replacement of arsenides by arsenopyrite (Apy1) with Au inclusions. Stage 1a is characterized by auriferous quartz veins with Ni-Co-Fe arsenides such as löllingite, clinosafflorite, safflorite, skutterudite and rammelsbergite (Fig. 2-D). The arsenides occur as < 1 mm inclusions in stage 1b arsenopyrite (Apy1). The inclusions locally form a patchy assemblage with K-feldspar and arsenopyrite (Apy1) (Fig. 7-E). Löllingite contains little Co and Ni, safflorite has a heterogeneous composition and contains < 11.15 wt% Co, < 2.28 wt% Ni and traces of Sb, Bi, Cu, Hg, Ag and Zn and rammelsbergite contains traces of Sb, Bi, and Co and skutterudite traces of Sb, Bi, Cu, Hg and Ag (Table 1, ESM 2).

Stage 1b is continued prolongation from stage 1a and is characterized by arsenopyrite (Apy1) and pyrite (Py1) with minor Au, maldonite, Bi, hedleyite, pilsenite and molybdenite (Fig. 2-D). Arsenopyrite (Apy1) forms euhedral to subhedral grains, locally fractured and commonly forming clusters (Fig. 7-C and G). Locally, it contains inclusions of Ni-Co-Fe arsenides and gangue minerals as well as Au, Bi, hedleyite, pilsenite and maldonite inclusions (Fig. 7-E and H). It is locally chemically zoned, two types are identified, one with low Ni and high Co content (<5.95 wt %) and another with slightly enriched Ni contents (<0.94 wt%, ESM 2). Arsenopyrite (Apy1) contains traces of Sb, Bi, Cu, Au, Hg, Ag and Zn (Table 1, ESM 2). Gold occurs as < 50 μm inclusions in arsenopyrite (Apy1). The Au inclusions occur commonly together with Bi, hedleyite, pilsenite and maldonite at a volumetric ratio of 1:10. Gold grains contain small amounts of Ag, As, Fe and traces of Bi, Co, Cu, Ni, S (Table 1, ESM2). Where arsenopyrite (Apy1) contains Ni-Co-Fe arsenide cores, the inclusions tend to be concentrated at the contact between both minerals (Fig. 7-E). A second generation of arsenopyrite (Apy2) occurs locally as overgrowth on arsenopyrite (Apy1), generally with pyrite (Py1) (Fig. 7-F). Arsenopyrite (Apy2) is not chemically zoned and Co is below detection limit (Table 1, ESM 2). Pyrite (Py1) occurs as euhedral to subhedral deformed grains. Pyrite (Py1) shows porosity, gangue mineral inclusions and locally a spongy texture (Fig. 7-F). The gangue of the event 1 veins is composed of quartz, tourmaline, plagioclase, biotite, K-feldspar and accessory actinolite, apatite, scheelite, titanite and zircon. The host rock within a few centimetres of the mineralized hydrothermal veins contains hydrothermal tourmaline, sericite, chlorite and disseminated arsenopyrite and pyrite (Py1). Plagioclase is replaced by sericite and biotite by chlorite (Fig. 7-B).

The mineralisation event 2 is characterized by quartz-sulfide veins with chalcopyrite, pyrrhotite, sphalerite and pyrite (Py2), which locally cross-cut and overprint the veins of event 1 (Fig. 2-D). Chalcopyrite occurs as deformed grains and locally forms a patchy texture with sphalerite and pyrite (Py2) (Fig. 7-H and I). It locally contains pyrite (Py2), gangue mineral and rare Bi inclusions (Fig. 7-I). Pyrite (Py2) is pristine, euhedral to subeuhedral and locally replaces chalcopyrite (Fig. 7-I). Pyrrhotite occurs as spongy and porous deformed grains. It locally has pyrite, chalcopyrite and gangue mineral inclusions (Fig. 7-J). Chalcopyrite contains traces of Ag, Sb, Bi, Hg and Zn; pyrite contains traces of Cu, Hg and Zn; and pyrrhotite has traces of As and Au (Table 1, ESM 2). The host rock within a few centimetres of the mineralized hydrothermal veins contains hydrothermal tourmaline, sericite, chlorite and disseminated chalcopyrite, pyrrhotite and pyrite (Py2). Plagioclase and biotite are replaced by sericite and chlorite respectively.

5.5. Arsenopyrite geothermometry

The arsenopyrite geothermometer from Kretschmar and Scott (1976) is applied to the arsenopyrite-bearing assemblages of the four deposits. Arsenopyrite shows a natural compositional heterogeneity compared to the theoretical As content (33.33 at.% As) and can contain significant amounts of Co, Ni, Sb, leading to anomalous temperature estimates (Sharp et al. 1985). All data has been carefully sorted and data with Fe/(As + S) < 0.5 and/or Σ(Co, Ni, Sb) > 1 wt% were removed (Kretschmar and Scott 1976).

5.5.1. Laivakangas Au deposit

Arsenopyrite in equilibrium with pyrrhotite and löllingite has an As content of 34.72 ± 0.48 at.% As (n = 3) and yields an average temperature of 485 ± 25 °C for the mineralisation event 2 (Fig. 8-A). Arsenopyrite only in equilibrium with löllingite has a consistent As content of 34.71 ± 0.50 at.% As (n = 25) and thus yields the same temperature (Fig. 8-A).

5.5.2. Huhta Au deposit

Arsenopyrite is in equilibrium with pyrrhotite. Data from disseminated arsenopyrite in the hydrothermal alteration zone and arsenopyrite in a quartz vein are plotted (Fig. 8-B). Arsenopyrite from the quartz vein shows compositional zoning with the As content varying between 30.19 and 34.90 at.% As (Fig. 8-B'). This variation is either caused by changing conditions during deposition (Sharp et al. 1985) or by diffusion/remobilisation of As. This scattered data yields an average temperature of 475 ± 125 °C (n = 10) for the stage 1b of the mineralisation event 1. Arsenopyrite FEMO-2019–22-13b-22 (see Fig. 8-B and B') does not show evidence of remobilisation and is considered as reference value for the As content in arsenopyrite. The compositional data yields a temperature

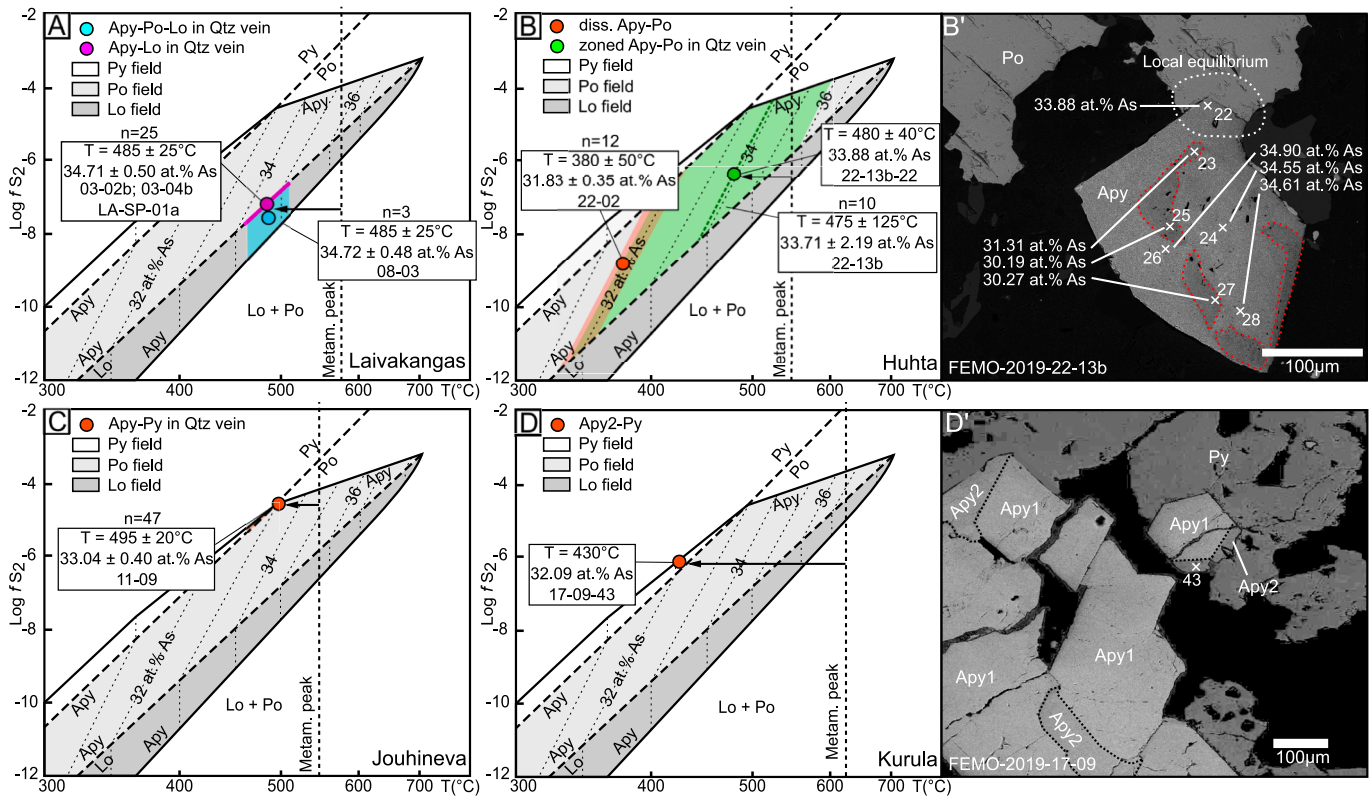

Fig. 8. Arsenopyrite geothermometry. (A) Laivakangas deposit; (B) Huhta deposit, analysis 22-13b-22 is considered representative of the arsenopyrite As content; (B') BSE-image of a zoned arsenopyrite in equilibrium with pyrrhotite. Contrast has been increased. The arsenopyrite grain shows patchy As-poor zones in the centre and at the rim of the grain; (C) Jouhineva deposit; (D) Kurula deposit and (D') arsenopyrite 2 in equilibrium with pyrite.

of 480 ± 40 °C, which is close to the average temperature determined using all the data. Disseminated arsenopyrite, locally in equilibrium with pyrrhotite, yields a lower temperature of 380 ± 50 °C, with a consistent As content (31.83 ± 0.35 at.% As; n = 12).

5.5.3. *Jouhineva Au-Cu-Co-Ag deposit*

Arsenopyrite is in equilibrium with pyrite (Py1). However, arsenopyrite in direct contact with pyrite (Py1) has a Σ(Co, Ni, Sb) > 1 wt% and cannot be used. Geothermometry using valid arsenopyrite data yields an average temperature of 495 ± 20 °C for the mineralisation event 1 (Fig. 8-C; n = 47). This temperature is obtained from arsenopyrite grains not in local equilibrium with pyrite (Py1). However, the As content in arsenopyrite is consistent (33.04 ± 0.40 at.% As) and there is no evidence for several generations of arsenopyrite and neither pyrrhotite nor löllingite are observed in the samples.

5.5.4. *Kurula Au-Co deposit*

Arsenopyrite (Apy1 and Apy2) are in equilibrium with pyrite. Arsenopyrite (Apy1) typically contains several wt.% of Co and Ni, preventing reliable temperature estimation. Due to the rare occurrence of arsenopyrite (Apy2), only one measurement matches all the required criteria with an As content of 32.09 at.% (Fig. 8-D'). The data yields a temperature of 430 °C for the stage 1b of the mineralisation event 1 (Fig. 8-D).

5.6. *Sulfur isotopes*

The $\delta^{34}S$ signature of arsenopyrite, pyrrhotite, pyrite and chalcopyrite from the four deposits show a relatively wide range from + 1.39 ‰ to + 8.21 ‰ (Fig. 9; Table 2). This variation is rather deposit-related as mineralisation event or mineral-related as, within each deposit, arsenopyrite and sulfides forming during different events show a similar

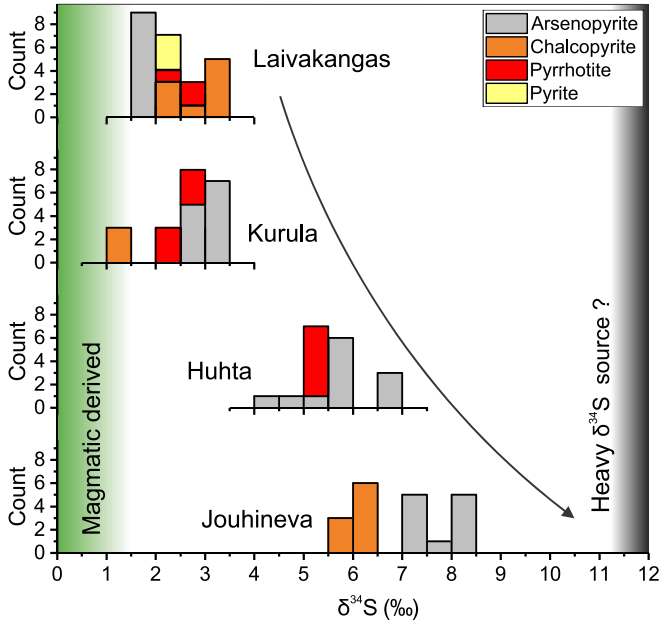

Fig. 9. Range of δ34S in sulfides of the Laivakangas, Jouhineva, Huhta and Kurula ores (see ESM 2 for data).

range in $\delta^{34}S$ (Table 2). A different $\delta^{34}S$ range is observed between the Laivakangas (+1.52-+3.17 ‰ $\delta^{34}S$), Huhta (+4.44-+6.55 ‰ $\delta^{34}S$), Jouhineva (+5.87-+8.21 ‰ $\delta^{34}S$) and Kurula deposits (+1.39-+3.17 ‰ $\delta^{34}S$, Table 2). Noticeably there is a marked difference in $\delta^{34}S$ between the Laivakangas and Kurula deposits, which have lighter $\delta^{34}S$ (+1.39-

Table 2
Summary of S isotope data on sulfides of the Laivakangas, Jouhineva, Huhta and Kurula deposits (see ESM 3 for detailed data).

Deposit	Mineral	n	mean $\delta^{34}S$ (‰)	2σ (‰)	Min. value	Max. value
Laivakangas	Apy	12	+1.95	0.56	+1.52	+2.43
Laivakangas	Po	3	+2.55	0.13	+2.47	+2.63
Laivakangas	Py	3	+2.37	0.04	+2.34	+2.39
Laivakangas	Ccp	9	+2.77	0.99	+2.04	+3.17
Jouhineva	Apy	11	+7.71	0.77	+7.20	+8.21
Jouhineva	Ccp	9	+6.03	0.17	+5.87	+6.17
Huhta	Po	6	+5.12	0.08	+5.04	+5.18
Huhta	Apy	12	+5.67	1.31	+4.44	+6.55
Kurula	Ccp	3	+1.43	0.07	+1.39	+1.47
Kurula	Apy	12	+3.02	0.20	+2.83	+3.17
Kurula	Po	6	+2.48	0.33	+2.19	+2.67

+3.17 ‰), and the Jouhineva and Huhta deposits, which have the heavier S isotopic composition (+4.44-+8.21 ‰).

6. Discussion

6.1. Multi-event orogenic Au deposits

The detailed characterisation of the paragenetic sequences of the Laivakangas, Huhta, Jouhineva and Huhta deposits highlights that orogenic Au mineralisation in the Pohjanmaa Belt is of a complex multi-event, multi-stage origin. Regionally, two main hydrothermal mineralisation events are defined, each with a specific metal association. Their respective intensity in the different deposits accounts for the bulk metal endowment and ultimately to the classification of each deposit as Au-only or orogenic Au with atypical metal association. The two main mineralisation events are: 1) an As-Au (Co, Ni) event in all four deposits, characterized by arsenides and/or sulfarsenides locally enriched in Ni and Co. Gold likely occurs as invisible Au in the arsenides and occurs as Au inclusions in sulfarsenides; 2) a sulfide event with Cu(-Au) mostly expressed at the Laivakangas and Jouhineva deposits. Event 2 is characterized by chalcopyrite and other sulfides and free, native Au in fractures of vein quartz and silicates, and locally as scarce Au inclusions in pyrrhotite and chalcopyrite.

6.1.1. Laivakangas Au deposit

The As-Au(–Co) mineralisation event 1, defined by auriferous quartz-arsenide veins, occurred close to the metamorphic peak at a temperature between 575 ± 50 °C (Mäkelä 1984) and 485 ± 25 °C, i.e. temperature of formation of arsenopyrite during the event 2 (Fig. 3; Fig. 8-A). Invisible Au (below 202 ppm in arsenides; ESM 2) is inferred to occur in Ni-Co-Fe arsenides based on petrological relationships between Ni-Co-Fe arsenides, replacing arsenopyrite (event 2) and Au inclusions (see next paragraph; Fig. 3-F to H). Furthermore, arsenopyrite is locally enriched in Ag which tends to be enriched alongside Au in arsenides and arsenopyrite (Lee et al., 2019). The limited extent of preserved arsenides and the relatively low Ni and Co content in replacing arsenopyrite account for the low bulk enrichment of Ni and Co at Laivakangas. Up to 90 % of the visible Au of the Laivakangas deposit is Au inclusions trapped almost exclusively in arsenopyrite and Ni-Co-Fe arsenide implying the mineralisation event 1 is the main Au stage.

The sulfide (Cu-Au) mineralisation event 2 is defined by new auriferous quartz-sulfide veins and by auriferous quartz-sulfarsenide-sulfide veins where it overprints the previous veins of the event 1 (see section 6.1.1). It is inferred to have occurred at 485 ± 25 °C (arsenopyrite geothermometry; Fig. 8-A), which is supported by the chalcopyrite-pyrrhotite-cubanite assemblage that indicates temperatures of < 500 °C (Yund and Kullerud 1966). The overprinting veins are characterized by the replacement of Ni-Co-Fe arsenide (event 1) by arsenopyrite (Fig. 2-A). Local enrichment in Co and Ni, Ni-Co-Fe arsenide cores and Au and Bi-(Te, Au, Ag, Cu) mineral inclusions in arsenopyrite (Fig. 3-F to H) are interpreted as showing the retrograde reaction of Ni-Co-Fe arsenide and pyrrhotite to arsenopyrite (1) (Neumayr et al. 1993; Tomkins and Mavrogenes 2001):

$$FeAs_2 + FeS + 0.5S_2 \rightarrow 2FeAsS \quad (1)$$

Pyrrhotite is rarely observed in assemblage with Ni-Co-Fe arsenide, although it is a necessary partner for the retrograde reaction. It is possible that pyrrhotite was completely consumed by the reaction. The reaction of Ni-Co-Fe arsenide with the higher fS_2 fluid of event 2 appears a better alternative which would be concomitant with sulfide precipitation (Barton 1969):

$$FeAs_2 + 2H_2S_{(aq)} + Fe^{2+}_{(aq)} \rightarrow 2FeAsS + 4H_{2(aq)} \quad (2)$$

Replacement of Ni-Co-Fe arsenide by arsenopyrite forces invisible Au as solid solution within the arsenides to exsolve as Au inclusion because Au is not well incorporated into arsenopyrite at temperatures above 300 °C (Neumayr et al. 1993, based on Cathelineau et al. 1989; Tomkins and Mavrogenes 2001). The rare Au inclusions in chalcopyrite and pyrrhotite as well as free, native Au grains indicate a new hydrothermal input of Au during the sulfide (Cu-Au) event 2 (Fig. 2-A; Fig. 3-K). The relative scarcity of pyrrhotite and chalcopyrite in the overprinting veins compared to the newly formed veins (see Fig. 4-A) is likely because most of the sulfidation was taken in converting the previous arsenides to arsenopyrites instead of forming new sulfides.

6.1.2. Huhta Au deposit

The As-Au mineralisation event 1 of the Huhta deposit is subdivided into two stages: an As-Au arsenide stage (1a) and an As-S-Au sulfarsenide stage (1b) (Fig. 2-B; Fig. 4-B). Stage 1a consists of quartz veins with a little löllingite possibly containing invisible Au, as indicated by its replacement by arsenopyrite containing Au inclusions. Stage 1b likely occurred on the early retrograde metamorphic path at 480 ± 40 °C (arsenopyrite geothermometry; Fig. 8-B) after peak metamorphism (545 ± 30 °C; Hölttä and Heilimo 2017). It is characterized by arsenopyrite with Au inclusions and rare löllingite cores (stage 1a), minor pyrrhotite and accessory chalcopyrite and pyrite (Fig. 2-B). Rare löllingite cores in arsenopyrite suggest that a portion of the arsenopyrite formed by replacement of the previous löllingite, either by reaction with a higher fS_2 fluid or by retrograde reaction between löllingite and pyrrhotite (Barton 1969; Tomkins and Mavrogenes 2001), as described above for the Laivakangas deposit. Au inclusions in löllingite-free arsenopyrite are explained either by complete replacement of löllingite or by co-precipitation of native Au and arsenopyrite from the stage 1b hydrothermal fluid (Fig. 5-G). The estimated temperature of formation for arsenopyrite of 480 ± 40 °C is close to the estimated temperature of arsenopyrite formation for the Jouhineva deposit (470–495 °C). Which suggest that stage 1b in the Huhta deposit is the equivalent of the mineralisation event 1 in the Jouhineva deposit. As the two deposits are located only 2.8 km apart along the same structure, these similar temperatures indicate that arsenopyrite formed at similar timing on the retrograde metamorphic path. However, the two deposits show different metal enrichments, with no Ni and Co and significantly less Cu in the Huhta deposit than in Jouhineva deposit.

The mineralisation event 2 in the Huhta deposit is defined by pyrrhotite, pyrite, minor chalcopyrite and sphalerite in actinolite-chlorite-rich veinlets. It likely occurred during latest stages of retrograde metamorphism, under greenschist facies conditions, and appears to be Au barren (Fig. 2-B).

6.1.3. Jouhineva Au-Cu-Co-Ag deposit

The As-Au-Co(-Ni) mineralisation event 1 occurred during retrogression after peak metamorphism (545 ± 30 °C; Hölttä and Heilimo 2017) at approx. 470–495 °C (arsenopyrite geothermometry; Fig. 8-C). It is characterized by quartz veins with arsenopyrite, with Au inclusions, and minor pyrite (Py1) (Fig. 2-C). Cobaltite is described in the literature

but has not been observed in this study due to sample bias (Geological Survey of Finland, 2019b). However, as cobaltite and arsenopyrite are both sulfarsenides with overlapping stability fields (Scharrer et al., 2019), both minerals likely formed at similar conditions. Arsenopyrite contains on average 1.53 wt% Co, which reflects the overall Co enrichment of the deposit relative to Laivakangas and Huhta. The Cu-Au mineralisation event 2 is responsible for the main hydrothermal input of Au, it is characterized by actinolite-chlorite-rich veinlets and major chalcopyrite, minor pyrite (Py2), cubanite and free, native Au (Fig. 2-C). Mineralisation occurred during retrograde metamorphism at greenschist facies conditions according to the mineral assemblage. The Jouhineva deposit has been proposed to be a Cu porphyry deposit linked to the formation of the Rautio batholith and later overprinted by orogenic Au. This is unlikely as the Rautio batholith formed at 1890–1880 Ma (Huhma 1986); i.e. before peak metamorphism (ca. 1880–1810 Ma; Hölttä et al., 2019) and the hydrothermal mineralisation events occurred after metamorphic peak during retrograde terrane exhumation.

6.1.4. Kurula Au-Co deposit

The As-Au-Co-Ni mineralisation event 1 of the Kurula deposit is subdivided into two stages: an As-Au-Co-Ni arsenide stage (1a) and an As-S(-Au) sulfarsenide stage (1b) (Fig. 2-D; Fig. 4-D). Stage 1a appears to have occurred after the peak of metamorphism, which implies a temperature of formation between 620 ± 40 °C (peak metamorphism temperature; Hölttä and Heilimo 2017) and 430 °C (stage 1b arsenopyrite geothermometry; Fig. 8-D). Nickel-Co-Fe arsenides in veins and disseminated in the host rock result in significant endowment in Co and Ni relative to the other deposits (Fig. 2-D). Nickel-Co-Fe arsenides are inferred to contain invisible Au, based on Au inclusions in replacing arsenopyrite (Apy1, stage 1b) (Fig. 7-E).

Stage 1b is continuous to stage 1a and is characterized by replacement of Ni-Co-Fe arsenides (stage 1a) by arsenopyrite (Apy1;Fig. 2-D). According to arsenopyrite geothermometry, it occurred during retrograde metamorphism at 430 °C (Fig. 8-D). The absence of pyrrhotite in the assemblage suggests that, like in the Laivakangas deposit, arsenopyrite (Apy1) formed after reaction of Ni-Co-Fe arsenides with a higher fS_2 fluid (Barton 1969). Arsenopyrite is the only sulfarsenide replacing the Ni-Co-Fe arsenides, the absence of cobaltite is likely caused by the relative scarcity of skutterudite (Co-rich arsenide) compared to Fe-rich safflorite and löllingite in the arsenide assemblage. The availability of Fe instead of sufficient Co led to formation of Co-rich arsenopyrite (Apy1) instead of cobaltite. Limited metal input appears to be associated with the stage 1b in the Kurula deposit. The sulfide event 2 shows little evidence of Au enrichment (Fig. 2-D).

6.2. As-Au (Co, Ni) and Au-Cu mineralisation processes

Arsenopyrite of the Jouhineva deposit hosts fewer Au and Bi-(Te, Au, Ag, Cu) mineral inclusions than the arsenopyrite that replaced arsenides at the other deposits during mineralisation event 1. This difference is likely caused by the origin of the arsenopyrite. Indeed, arsenides such as löllingite are commonly enriched in Au and can accommodate Au up to several hundred ppm in their crystal lattice (Neumayr et al. 1993). On the other hand, arsenopyrite cannot incorporate Au efficiently (<10 ppm) in its structure at temperatures above 300 °C (after Neumayr et al. 1993, based on Cathelineau et al. 1989). Thus, during replacement of arsenides by arsenopyrite, Au cannot stay in the crystal lattice and Au and Bi-(Te, Au, Ag, Cu) mineral inclusions will form in arsenopyrite. Conversely, arsenopyrite that precipitates directly from a fluid or directly formed by fluid-rock reaction contains fewer Au and Bi-(Te, Au, Ag, Cu) mineral inclusions as they do not form from an Au-rich precursor (i.e. arsenides).

The stability of arsenides and sulfarsenide, in hydrothermal systems is highly sensitive to fS_2 and fO_2 (e.g. Scharrer et al., 2019). Arsenides usually form by reduction of an oxidized, As-rich and S-poor fluid. Already small amounts of S will directly lead to sulfarsenide formation (Scharrer et al., 2019). The main mechanisms proposed for fluid reduction are: dissolution of graphite or Fe^{2+} -bearing minerals and/or pre-existing sulfides from the metamorphic host rocks as well as influx of hydrocarbons or H_2S (Kissin, 1993; Kreissl et al., 2018; Markl et al., 2016). Metamorphic fluids related to orogenic Au deposits generally contain significant amounts of H_2S (Goldfarb and Groves 2015), which is likely to inhibit arsenide formation (Scharrer et al., 2019). The Jouhineva and the Huhta deposits show no to very scarce arsenide, indicating that conditions were not sufficiently reduced to compensate for the relatively high fS_2 of the fluids. In comparison, the Laivakangas and the Kurula deposits, had lower fS_2 than Jouhineva and Huhta (Fig. 8), favouring arsenide formation. The host rock of the Kurula deposit contains graphite which likely buffers the system to reducing conditions, promoting Fe-Ni-Co arsenide formation. Hence, fS_2 and redox conditions are important for the formation of arsenides over sulfarsenides and entrapment of Au during the regional As-Au(Co-Ni) mineralisation event 1. Cobalt and Ni content is more likely controlled by the original Co and Ni content in the fluid, as they can precipitate in arsenides and sulfarsenides over a broad range of fS_2 and redox conditions (Scharrer et al., 2019). Higher solubility of Co as chloride complex than Ni at a given salinity explains the higher proportion of Co relative to Ni in the studied orogenic Au deposits with atypical metal associations (Brugger et al., 2016).

Copper enrichment in the investigated deposits is related to the Cu (-Au) mineralisation event 2, expressed by sulfide minerals, mostly chalcopyrite. This event occurs systematically later and independently from the As-Au (Co, Ni) regional mineralisation event 1. Chalcopyrite is a minor to trace mineral in many orogenic Au deposits and has been observed in each of the studied deposits. Chalcopyrite, however, generally occurs as a minor mineral (Huhta, Kurula, Laivakangas) except in the Jouhineva deposit where it is present in significantly larger quantities (Fig. 6-C and D). Gold enrichment may occur in the form of free, native grains or as rare inclusions in chalcopyrite and pyrrhotite (Laivakangas, Jouhineva). The threshold for the classification of orogenic Au deposits as atypical Au-Cu deposits is arbitrary and is related to economic, rather than geological considerations.

6.3. Constraints on the source and fluids

The studied Au deposits of the Pohjanmaa Belt formed through two hydrothermal events during the Fennoscandian orogeny, shortly after peak metamorphism at amphibolite facies and during retrograde evolution in greenschist facies. Although the deposits share a similar succession of mineralisation events, they do not show the same metal endowment indicating possibly either different mineralizing conditions, deposit type or different fluid sources.

6.3.1. Are atypical orogenic Au deposits related to porphyry mineralisation?

The relative Cu-enrichment in the orogenic Au deposits of the Laivakangas Au-Cu metallogenic area has been suggested to be partly related to a porphyry style Cu ± Au mineral system, overprinted by orogenic Au mineralisation (Eilu 2015, Geological Survey of Finland, 2019b). Cu-Au porphyry deposits linked to the Svecofennian orogeny have been identified in the Pohjanmaa belt (Kopsa Cu-Au deposit; Gaal and Isohanni, 1979); although, the studied orogenic deposits show very little similarities. The Kopsa deposit is located in the south-east of the study area, within the Hitura metallogenic area (Fig. 1- A). It is hosted in already metamorphosed host rocks, where the mineralisation is occurring as a quartz vein stockwork with major chalcopyrite, arsenopyrite and pyrrhotite. In addition, this stockwork is surrounded by a broad zone of disseminated pyrite-pyrrhotite and has been altered over a width of several hundred metres to a potassic assemblage with a propylitic halo (Gaal and Isohanni, 1979). Such extensive alteration and disseminated mineralisation are not observed in the studied orogenic Au

deposits. The typical features of porphyry-related deposits can however be affected by later metamorphic events, making them harder to identify as such. Examples of porphyry-related deposits metamorphosed to greenschist-lower amphibolite facies (e.g. Chapada Cu-Au deposit in Brazil, de Oliveira et al., 2016; Chibougamau Cu-Au(-Mo) mining district, Pilote et al. 1995, Lac Troilus in Canada, Fraser 1993) still display a recognizable succession of alteration haloes, despite the modified mineralogy. The original argillic and potassic alteration are identified by a metamorphic assemblage rich in kyanite and biotite, respectively, and disseminated sulfides are observed in the host rock (Fraser 1993; de Oliveira et al., 2016). In the case of the Chibougamau mining district, the porphyry-related deposits were metamorphosed at greenschist facies (Jolly 1974) and contain locally late auriferous hydrothermal breccia, interpreted as orogenic Au overprint and/or remobilisation during metamorphism (Guha and Koo 1975; Mathieu et al., 2019). However, the alteration halo is still identifiable by high K values in the whole rock geochemistry as well as mineral assemblage in the veins specific to magmato-hydrothermal systems (e.g. albite and magnetite) (Mathieu 2019; Mathieu et al., 2019).

By contrast, the rather narrow hydrothermal alteration zones and the mineralogy of the host rocks observed in the studied deposits are characteristic of orogenic Au deposits (Eilu and Groves, 2001) and are not consistent with the features observed in porphyry-related deposits, metamorphosed or not. Additionally, the Cu(-Au) mineralisation observed in the studied deposits systematically post-dates the As-Au (Co, Ni) mineralisation event and does not fit with the model of overprinted Cu ± Au porphyry. If the studied deposits are not overprinted Cu ± Au porphyry, we do not rule out that the Cu enrichment observed during the Cu(-Au) event could have a magmatic source. Indeed, during the time span of mineralisation, there is *syn*-orogenic magmatic activity in the Svecofennian orogen that could have led to production of Cu(-Au) rich magmatic fluids (Nironen 2005; Peltonen 2005).

6.3.2. *Potential of metamorphic fluids for atypical metal enrichment in orogenic Au deposits*

Although local variations in redox conditions affects the mineralogy (arsenides vs sulfarsenides) the diversity in metal enrichment between the studied deposits and the mineralisation events most likely imply that the respective ore fluids had differing metal contents during the metallogenic evolution. While it has been shown by Ridley and Diamond (2000) that ore fluids forming orogenic Au deposits usually display very similar geochemistry due to homogenisation by interaction with the different wall rocks between the source area and the depositional site, several recent studies underline how the lithological diversity of the source rocks impacts the metal content of the fluids during metamorphic devolatilisation (Patten et al., 2020, 2022; Zhao et al., 2011). The variability in metal enrichment between the deposits and mineralisation events can be a consequence of the dynamic nature of orogenic processes, during which different lithological units follow different metamorphic paths (e.g. Kolb et al., 2000, 2015), leading to the generation of metamorphic fluids with diverse metal association (e.g. Patten et al., 2022). Cobalt, Cu and Ni can be transported in hydrothermal fluids as chloride complexes at salinities as low as ca. 3 wt% NaCl at 440 °C, which is characteristic of orogenic Au ore fluids (Liu et al., 2011, 2012). The presence of *meta*-evaporite, although not reported in the Pohjanmaa Belt, can lead to higher fluid salinity, enhancing base metal mobilisation from the source zones (Brugger et al., 2016; Qiu et al., 2021; Vasilopoulos et al., 2021). The $\delta^{34}S$ signature of the studied deposits (Fig. 9) is within the range of metamorphic fluids (+0 to + 9 ‰; McCuaig and Kerrich 1998). The Laivakangas and Kurula deposits, however, have a low $\delta^{34}S$ range (+1.39 to + 3.17 ‰; Table 2; Fig. 9), relative to the Jouhineva and Huhta deposits (+4.44 to + 8.21 ‰; Table 2; Fig. 9). Several processes can affect the S isotopic signature during precipitation, such as temperature, S species, pH and fO_2, (e.g. Hutchison et al., 2020; Ohmoto 1986). The overall similar precipitation conditions during the sulfide mineralisation event 2 (greenschist facies metamorphic conditions) at the different deposits, however, suggest that the differences in $\delta^{34}S$ are related to different isotopic fluid signature, buffered at depth by different lithologies and along the transport path, rather than precipitation mechanisms.

The lithological variability in the source can have an important control on base metal endowment in orogenic Au deposits. Although Au, As and S can be readily mobilized from both *meta*-sedimentary and *meta*-volcanic rocks (Large et al., 2011; Patten et al., 2020, 2022; Pitcairn et al., 2006, 2021) the relative proportion of *meta*-sedimentary rocks (including *meta*-evaporite) to *meta*-volcanic rocks in metamorphic fluid production zones likely control the content of base metals available for ore formation (Patten et al., 2022). Local and transient changes in the metal content of the fluid over time can explain the small-scale variation of metal association between deposits belonging to the same structural system (e.g. Jouhineva and Huhta deposits).

7. Conclusion

The investigation of four orogenic Au deposits from the Pohjanmaa Belt with different metal association allows a better understanding of the parameters controlling atypical base metal enrichment in orogenic Au deposits. The Laivakangas, Huhta, Jouhineva and Kurula deposits formed by multiple hydrothermal mineralisation during two main regional-scale auriferous events: (1) a ubiquitous As-Au (Co, Ni) event close to peak metamorphism inamphibolite facies, where Au is likely trapped as invisible Au in arsenides or co-precipitated as inclusions in arsenopyrite, (2) a Cu(-Au) sulfide event on the retrograde metamorphic path in greenschist facies where Au forms free, native grains along with chalcopyrite. Importantly, the different base metals in the atypical orogenic Au deposits of the Pohjanmaa Belt are not introduced simultaneously in the studied deposits. Our data reveal that Ni and Co are enriched during the early hydrothermal stages, while Cu was introduced later in the metallogenic evolution. The relative intensity of each mineralisation event can eventually control the metal endowment resulting in either classic orogenic Au or Au-Cu, Au-Co and Au-Cu-Co deposits. Additionally, redox conditions and S fugacity appear to be an important parameter to enhance Au grades during the mineralisation event 1, as Ni-Co-Fe arsenides can trap more Au than arsenopyrite. Replacement of Ni-Co-Fe arsenides by arsenopyrite leads to formation of Au inclusions, which are easier to recover during ore processing than invisible Au.

Declaration of Competing Interest

The authors declare that they have no known competing financial interests or personal relationships that could have appeared to influence the work reported in this paper.

Data availability

Data will be made available on request.

Acknowledgments

We would like to thank Thomas Wenzel and Sebastian Staude from Eberhard Karls University of Tübingen for assistance with SEM analysis, Otsogold for providing support and access to samples of the Laivakangas mine, the Geological Survey of Finland (GTK) for granting access to the national drill core archive in Loppi and the Federal Institute for Geosciences and the Federal Institute for Geosciences and Natural Resources (BGR) for funding. This project was also supported by the OroTECT project (Academy of Finland grant No. 315188) in accordance with the agreement between the Academy of Finland and DAAD. The authors would like to thank the reviewers and the editor for their helpful and constructive comments.

Appendix A. Supplementary data

Supplementary data to this article can be found online at https://doi.org/10.1016/j.oregeorev.2023.105326.

References

Barton, P.B., 1969. Thermochemical study of the system Fe-As-S. Geochimica et Cosmochimica Acta 33, 841–857.

Bedrock of Finland – DigiKP. Digital map database [Electronic resource]. Espoo: Geological Survey of Finland [referred 16.08.2022]. Version 2.1.

Bektas R, Vathavooran A (2019) Laiva, Finland NI 43-101 Resource Update.

Brugger, J., Liu, W., Etschmann, B., Mei, Y., Sherman, D.M., Testemale, D., 2016. A review of the coordination chemistry of hydrothermal systems, or do coordination changes make ore deposits? Chemical Geology 447, 219–253.

Cathelineau M, Boiron M-C, Holliger P, Marion P, Denis M (1989) Gold in Arsenopyrites: Crystal Chemistry, Location and State, Physical and Chemical Conditions of Deposition. In: Keays RR, Ramsay WRH, Groves DI (eds) The Geology of Gold Deposits. Society of Economic Geologists, pp 328–341.

Chopin, F., Korja, A., Nikkilä, K., Hölttä, P., Korja, T., Abdel Zaher, M., Kurhila, M., Eklund, O., Rämö, O.T., 2020. The Vaasa Migmatitic Complex (Svecofennian Orogen, Finland): Buildup of a LP-HT Dome During Nuna Assembly. Tectonics 39.

de Oliveira, C.G., de Oliveira, F.B., Della Giustina, M.E.S., Marques, G.C., Dantas, E.L., Pimentel, M.M., Buhn, B.M., 2016. The Chapada Cu–Au deposit, Mara Rosa magmatic arc, Central Brazil: Constraints on the metallogenesis of a Neoproterozoic large porphyry-type deposit. Ore Geology Reviews 72, 1–21.

Eilu, P., 2015. Overview on Gold Deposits in Finland. In: Mineral Deposits of Finland. Elsevier 377–410.

Eilu, P., Ahtola, T., Äikäs, O., Halkoaho, T., Heikura, P., Hulkki, H., Iljina, M., Juopperi, H., Karinen, T., Kärkkäinen, N., Konnunaho, J., Kontinen, A., Kontoniemi, O., Korkiakoski, E., Korsakova, M., Kuivasaari, T., Kyläkoski, M., Makkonen, H., Niiranen, T., Nikander, J., Nykänen, V., Perdahl, J.-A., Pohjolainen, E., Räsänen, J., Sorjonen-Ward, P., Tiainen, M., Tontti, M., Torppa, A., Västi, K., 2012. Metallogenic areas in Finland. In: Eilu, P. (Ed.), Mineral Deposits and Metallogeny of Fennoscandia. Geological Survey of Finland, Espoo, pp. 207–342.

Eilu P, Groves DI (2001) Primary alteration and geochemical dispersion haloes of Archaean orogenic gold deposits in the Yilgarn Craton: the pre-weathering scenario. GEEA 1:183–200Eilu P (2015) Overview on Gold Deposits in Finland. In: Mineral Deposits of Finland. Elsevier, pp 377–410.

Fraser, R.J., 1993. The Lac Troilus gold-copper deposit, northwestern Quebec; a possible Archean porphyry system. Economic Geology 88, 1685–1699.

Gaál G, Sundblad K (1990) Metallogeny of gold in the Fennoscandian Shield. Mineralium Deposita 25 (Suppl):S 104 - S 114.

Gaal, G., Isohanni, M., 1979. Characteristics of igneous intrusions and various wall rocks in some Precambrian porphyry copper-molybdenum deposits in Pohjanmaa, Finland. Economic Geology 74, 1198–1210.

Gebre-Mariam, M., Hagemann, S.G., Groves, D.I., 1995. A classification scheme for epigenetic Archaean lode-gold deposits. Mineralium Deposita:408–410.

Geological Survey of Finland (2019b) Jouhineva. Mineral Deposit Report n° 309.

Geological Survey of Finland (2019c) Kurula. Mineral Deposit Report n° 307.

Goldfarb, R.J., Groves, D.I., 2015. Orogenic gold: Common or evolving fluid and metal sources through time. Lithos 233, 2–26.

Goldfarb, R.J., Groves, D.I., Gardoll, S., 2001. Orogenic gold and geologic time: a global synthesis. Ore Geology Reviews 18, 1–75.

Goldfarb, R.J., Baker, T., Dubé, B., Groves, D.I., Hart, C.J.R., Gosselin, P., 2005. Distribution, Character, and Genesis of Gold Deposits in Metamorphic Terranes. In: Hedenquist, J.W. (Ed.), Economic Geology: One Hundredth Anniversary Volume: 1905–2005. Society of Economic Geologists Inc, Littleton, CO, pp. 407–450.

Groves, D.I., Goldfarb, R.J., Gebre-Mariam, M., Hagemann, S.G., Robert, F., 1998. Orogenic gold deposits: A proposed classification in the context of their crustal distribution and relationship to other gold deposit types. Ore Geology Reviews 13, 7–27.

Guha, J., Koo, J., 1975. Role of Fluid State Mobilisation during Metamorphism of the Henderson Ore Bodies, Chibougamau, Quebec. Canada. Can. J. Earth Sci. 12, 1516–1523.

Haapala, I., Rämö, O.T., 2015. Mineral Deposits Related to Granitic Rocks. In: Mineral Deposits of Finland. Elsevier 531–556.

Hanski, E., Huhma, H., 2005. Central Lapland Greenstone Belt. In: Lehtinen, M., Nurmi, P.A., Rämö, O.T. (Eds.), Precambrian Geology of Finland: Key to the Evolution of the Fennoscandian Shield, 1. ed. Elsevier, Amsterdam, pp. 139–194.

Haverinen, J., 2020. Evaporites in the Central Lapland Greenstone Belt. University of Helsinki. M.Sc. thesis,.

Hölttä, P., Heilimo, E., 2017. Metamorphic map of Finland. In: Nironen, M. (Ed.), Bedrock of Finland at the Scale 1:1 000 000: Major Stratigraphic Units, Metamorphism and Tectonic Evolution. Geological Survey of Finland, Espoo, pp. 77–128.

Hölttä, P., Huhma, H., Lahaye, Y., Mänttäri, I., Lukkari, S., O'Brien, H., 2019. Paleoproterozoic metamorphism in the northern Fennoscandian Shield: age constraints revealed by monazite. International Geology Review 30, 1–28.

Huhma, H., 1986. Sm-Nd, U-Pb and Pb-Pb isotopic evidence for the origin of the Early Proterozoic Svecokarelian crust in Finland. Bulletin.

Hutchison, W., Finch, A.A., Boyce, A.J., 2020. The sulfur isotope evolution of magmatic-hydrothermal fluids: insights into ore-forming processes. Geochimica et Cosmochimica Acta 288, 176–198.

Isohanni, M., 1984. Malminetsintätyöt Kalajoen Jouhinevalla vuosina 1978–1983 (in Finnish). Report of Investigation.

Jolly W.T.; Regional metamorphic zonation as an aid in study of Archean terrains; Abitibi region, Ontario. The Canadian Mineralogist 1974;; 12 (7): 499–508.

Kähkönen, Y., 2005. Svecofennian supracrustal rocks. In: Lehtinen, M., Nurmi, P.A., Rämö, O.T. (Eds.), Precambrian Geology of Finland: Key to the Evolution of the Fennoscandian Shield, 1. ed. Elsevier, Amsterdam, pp. 343–406.

Kissin SA (1993) The geochemistry of transport and deposition in the formation of five-element (Ag-Ni-Co-As-Bi) veins. In: Maurice YT (ed) Proceedings of the Eighth Quadrennial IAGOD Symposium: Held in Ottawa, Canada, August 12-18, 1990 / papers presented at the symposium on topics related to general problems on the genesis of ore deposits and on studies of the ore geology of specific districts or deposits. E. Schweizerbart, Stuttgart.

Kiuttu L (2020) Petrology and mineral chemistry of the Ylivieska gabbro-peridotite intrusion: constraints on the petrogenesis and Ni sulfide ore potential. Master's thesis.

Kolb, J., Dziggel, A., Bagas, L., 2015. Hypozonal lode gold deposits: A genetic concept based on a review of the New Consort, Renco, Hutti, Hira Buddini, Navachab, Nevoria and The Granites deposits. Precambrian Research 262, 20–44.

Kolb J, Meyer FM, Kisters AFM (2000) Amphibolite facies gold mineralisation at Renco, Zimbabwe: Conditions of ore formation. In: Rammlmair D (ed) Applied mineralogy in research, economy, technology, ecology and culture: Proceedings of the sixth International Congress on Applied Mineralogy / Göttingen, Germany, 17-19 July 2000 / ICAM 2000. A.A. Balkema, Rotterdam, Brookfield, pp 355–357.

Korja, A., Lahtinen, R., Nironen, M., 2006. The Svecofennian orogen: a collage of microcontinents and island arcs. Geological Society, London, Memoirs 32, 561–578.

Kreissl, S., Gerdes, A., Walter, B.F., Neumann, U., Wenzel, T., Markl, G., 2018. Reconstruction of a >200 Ma multi-stage "five element" Bi-Co-Ni-Fe-As-S system in the Penninic Alps, Switzerland. Ore Geology Reviews 95, 746–788.

Kretschmar, U., Scott, S.D., 1976. Phase relations involving arsenopyrite in the system Fe-As-S and their application. Canadian Mineralogist 14, 364–386.

Kurhila M, Molnár F, O'Brien H, Tiljander M, Johanson B, Middleton A (2017) U-Pb dating of hydrothermal monazite and xenotime from the Levijärvi-Loukinen gold deposit, Central Lapland Greenstone Belt, Northern Finland. In: Hölttä P, Nenonen K, Eerola T (eds) Guide 63: Abstract Book, pp 56–57.

Laajoki, K., 2005. Karelian supracrustals rocks. In: Lehtinen, M., Nurmi, P.A., Rämö, O.T. (Eds.), Precambrian Geology of Finland: Key to the Evolution of the Fennoscandian Shield, 1. ed. Elsevier, Amsterdam, pp. 279–342.

Lahtinen, R., Huhma, H., Kousa, J., 2002. Contrasting source components of the Paleoproterozoic Svecofennian metasediments: Detrital zircon U-Pb, Sm–Nd and geochemical data. Precambrian Research 116, 81–109.

Lahtinen, R., Korja, A., Nironen, M., 2005. Paleoproterozoic tectonic evolution. In: Lehtinen, M., Nurmi, P.A., Rämö, O.T. (Eds.), Precambrian Geology of Finland: Key to the Evolution of the Fennoscandian Shield, 1. ed. Elsevier, Amsterdam, pp. 481–532.

Lahtinen, R., Johnston, S.T., Nironen, M., 2014. The Bothnian coupled oroclines of the Svecofennian Orogen: a Palaeoproterozoic terrane wreck. Terra Nova 26, 330–335.

Large, R.R., Bull, S.W., Maslennikov, V.V., 2011. A Carbonaceous Sedimentary Source-Rock Model for Carlin-Type and Orogenic Gold Deposits. Economic Geology 106, 331–358.

Lawrence, D.M., Treloar, P.J., Rankin, A.H., Harbidge, P., Holliday, J., 2013. The Geology and Mineralogy of the Loulo Mining District, Mali, West Africa: Evidence for Two Distinct Styles of Orogenic Gold Mineralisation. Economic Geology 108, 199–227.

Lee, M., Shin, D., Yoo, B., Im, H., Pak, S., Choi, S., 2019. LA-ICP-MS trace element analysis of arsenopyrite from the Samgwang gold deposit, South Korea, and its genetic implications. Ore Geology Reviews 114, 103147.

Liu, W., Borg, S.J., Testemale, D., Etschmann, B., Hazemann, J.-L., Brugger, J., 2011. Speciation and thermodynamic properties for cobalt chloride complexes in hydrothermal fluids at 35–440°C and 600bar: An in-situ XAS study. Geochimica et Cosmochimica Acta 75, 1227–1248.

Liu, W., Migdisov, A., Williams-Jones, A., 2012. The stability of aqueous nickel(II) chloride complexes in hydrothermal solutions: Results of UV–Visible spectroscopic experiments. Geochimica et Cosmochimica Acta 94, 276–290.

Luukas, J., Kousa, J., Nironen, M., Vuollo, J., 2017. Major stratigraphic units in the bedrock of Finland, and an approach to tectonostratigraphic division. In: Nironen, M. (Ed.), Bedrock of Finland at the Scale 1:1 000 000: Major Stratigraphic Units, Metamorphism and Tectonic Evolution. Geological Survey of Finland, Espoo, pp. 9–40.

Mäkelä, M., 1984. Raahen Laivakankaan kvartsi-arseenikiisu-kultaesiintymä. (in Finnish): The quartz-arsenopyrite-gold mineralisation of Laivakangas. University of Turku, Raahe, Finland. Unpublished M.Sc thesis.

Mäkitie, H., 1999. Structural analysis and metamorphism of Palaeoproterozoic metapelites in the Seinajoki-Ilmajoki area, western Finland. BULLETIN-GEOLOGICAL SOCIETY OF FINLAND 71, 305–328.

Mäkitie, H., 2000. Granitoids (1.89-1.87 Ga), diatexites (1.89-1.88 Ga) and granitic pegmatites (1.80-1.79 Ga), and structural-metamorphic evolution in the Seinäjoki region, western Finland. Ph. D. Thesis.

Mäkitie H, Lahti S (1991) Seinfijoen kartta-alueen kallioperä. Summary: Pre-Quaternary rocks of the Seinäjoki map-sheet area. Geological Map of Finland 1: 1 000 000. Explanation to the maps of Pre-Quaternary rocks, sheet 2222 Seinäjoki, Espoo.

Mäkitie, H., Sipilä, P., Kujala, H., Lindberg, A., Kotilainen, A., 2012. Formation mechanism of the Vaasa Batholith in the Fennoscandian shield: Petrographic and geochemical constraints. Bull Geol Soc Finland 84, 141–166.

Markl, G., Burisch, M., Neumann, U., 2016. Natural fracking and the genesis of five-element veins. Mineral. Deposita 51, 703–712.

Mathieu, L., 2019. Detecting magmatic-derived fluids using pyrite chemistry: Example of the Chibougamau area, Abitibi Subprovince. Québec. Ore Geology Reviews 114, 103127.
Mathieu, L., Racicot, D., 2019. Petrogenetic Study of the Multiphase Chibougamau Pluton: Archaean Magmas Associated with Cu–Au Magmato-Hydrothermal Systems. Minerals 9, 174.
McCuaig, T.C., Kerrich, R., 1998. P—T—t—deformation—fluid characteristics of lode gold deposits: evidence from alteration systematics. Ore Geology Reviews 12, 381–453.
Mints, M.V., Glaznev, V.N., Muravina, O.M., Sokolova, E.Y., 2020. 3D model of Svecofennian Accretionary Orogen and Karelia Craton based on geology, reflection seismics, magnetotellurics and density modelling: Geodynamic speculations. Geoscience Frontiers 11, 999–1023.
Molnár, F., O'Brien, H., Lahaye, Y., Kurhila, M., Middleton, A., Johanson, B., 2017. Multi-stage hydrothermal processes and diverse metal associations in orogenic gold deposits of the Central Lapland greenstone belt, Finland. In: Mercier-Langevin, P. (Ed.), Mineral Resources to Discover. Québec, Canada, pp. 63–66.
Molnár, F., Middleton, A., Stein, H., O'Brien H, Lahaye Y, Huhma H, Pakkanen L, Johanson B,, 2018. Repeated syn- and post-orogenic gold mineralisation events between 1.92 and 1.76 Ga along the Kiistala Shear Zone in the Central Lapland Greenstone Belt, northern Finland. Ore Geology Reviews 101, 936–959.
Neumayr, P., Cabri, L.J., Groves, D.I., Mikucki, E.J., Jackman, J.A., 1993. The mineralogical distribution of gold and relative timing of gold mineralisation in two Archaean settings of high metamorphic grade in Australia. Canadian Mineralogist 31, 711–725.
Nironen, M., 2005. Proterozoic orogenic granitoid rocks. In: Lehtinen, M., Nurmi, P.A., Rämö, O.T. (Eds.), Precambrian Geology of Finland: Key to the Evolution of the Fennoscandian Shield, 1. ed. Elsevier, Amsterdam, pp. 443–480.
Nironen, M., Lahtinen, R., Koistinen, T., 2002. Subdivision of Finnish bedrock: an attempt to harmonize terminology. Geologi 54 (1), 8–14.
Novoselov, K., Belogub, E., Kotlyarov, V., Mikhailov, A., 2015. Ore mineralogy and formation conditions of the Pirunkoukku gold occurrence (Finland). ejm 27, 639–649.
Ohmoto, H., 1986. Stable isotope geochemistry of ore deposits. In: Valley, J.W., Taylor, H.P., O'Neil, J.R. (Eds.), Stable Isotopes in High Temperature Geological Processes, Chapter 14. De Gruyter, Berlin, Boston, pp. 491–560.
Pankka, H.S., Vanhanen, E.J., 1992. Early proterozoic Au-Co-U mineralisation in the Kuusamo district, northeastern Finland. Precambrian Research 58, 387–400.
Patten, C.G.C., Pitcairn, I.K., Molnár, F., Kolb, J., Beaudoin, G., Guilmette, C., Peillod, A., 2020. Gold mobilisation during metamorphic devolatilisation of Archean and Paleoproterozoic metavolcanic rocks. Geology 48, 1110–1114.
Patten, C.G.C., Molnár, F., Pitcairn, I.K., Kolb, J., Mertanen, S., Hector, S., 2022. Multi-source and multi-stage metal mobilisation during the tectonic evolution of the Central Lapland Greenstone Belt, Finland: implications for the formation of orogenic Au deposits. Mineral, Deposita.
Peltonen, P., 2005. Svecofennian mafic-ultramafic intrusions. In: Lehtinen, M., Nurmi, P. A., Rämö, O.T. (Eds.), Precambrian Geology of Finland: Key to the Evolution of the Fennoscandian Shield, 1. ed. Elsevier, Amsterdam, pp. 407–442.
Pilote, P., Robert, F., Sinclair, W.D., Kirkham, R.V., Daigneault, R., 1995. Porphyry-type mineralisation in the Doré Lake complex: Clark Lake and Merrill Island areas, Day 3: Geological Survey of Canada. Open File Report 3143, 65–86.
Pitcairn, I.K., Teagle, D.A.H., Craw, D., Olivo, G.R., Kerrich, R., Brewer, T.S., 2006. Sources of Metals and Fluids in Orogenic Gold Deposits: Insights from the Otago and Alpine Schists, New Zealand. Economic Geology 101, 1525–1546.
Pitcairn, I.K., Leventis, N., Beaudoin, G., Faure, S., Guilmette, C., Dubé, B., 2021. A metasedimentary source of gold in Archean orogenic gold deposits. Geology 49, 862–866.
Qiu, Z.-J., Fan, H.-R., Goldfarb, R., Tomkins, A.G., Yang, K.-F., Li, X.-C., Xie, L.-W., Liu, X., 2021. Cobalt concentration in a sulfidic sea and mobilisation during orogenesis: Implications for targeting epigenetic sediment-hosted Cu-Co deposits. Geochimica et Cosmochimica Acta 305, 1–18.
Ridley JR, Diamond LW (2000) Fluid chemistry of orogenic lode gold deposits and implications for genetic models. In: Hagemann SG, Brown PE (eds) Gold in 2000. Society of Economic Geologists, [Littleton, Colorado], pp 141–162.
Scharrer, M., Kreissl, S., Markl, G., 2019. The mineralogical variability of hydrothermal native element-arsenide (five-element) associations and the role of physicochemical and kinetic factors concerning sulfur and arsenic. Ore Geology Reviews 113, 103025.
Sharp, Z.D., Essene, E.J., Kelly, W.C., 1985. A re-examination of the arsenopyrite geothermometer: pressure considerations and applications to natural assemblages. Canadian Mineralogist 23, 517–534.
Sipilä, E., 1983. Koboltti-kulta-aiheen (M19/2431/-88/1/10) jatkotutkimukset Ylivieskan Kurulassa 1978–83. (in Finnish).
Sipilä, E., 1988. Kurulan kulta-koboltti-turmaliinibreksian lisäselvitys Winkie-kairauksella 1985. (in Finnish).
Sundblad, K., Weihed, P., Billström, K., Markkula, H., Mäkelä, M., 1993. Source of metals and age constraints for epigenetic gold deposits in the Skellefte and Pohjanmaa districts, central part of the Fennoscandian Shield. Mineralium Deposita 28, 181–190.
Geological Survey of Finland (2019a) Huhta. Mineral Deposit Report n° 446.
Geological Survey of Finland (2019d) Laivakangas. Mineral Deposit Report n° 298.
Tapio, J., Ranta, J.-P., Cook, N., Lahaye, Y., O'Brien, H., 2021. Paleoproterozoic Rajapalot Au-Co system associated with evaporites: Chemical composition and boron isotope geochemistry of tourmaline, and sulfur isotopes of sulfates, Peräpohja belt, northern Finland. Precambrian Research 365, 106410.
Tomkins, A.G., Mavrogenes, J.A., 2001. Redistribution of Gold within Arsenopyrite and Lollingite during Pro- and Retrograde Metamorphism: Application to Timing of Mineralisation. Economic Geology 96, 525–534.
Vaarma, M., 1990. Pohjanmaan liuskevyöhykkeen geologia Evijärven alueella. Phil. Lic, Thesis.
Vaarma M, Pipping F (1997) Pre-Quaternary rocks of the Alajärvi and Evijärvi map-sheet areas (in Finnish with English summary). Explanation to the maps of Pre-Quaternary rocks. Sheets 2313 and 2314. Geological map of Finland 1: 100 000. Geol. Surv. Finland.
Vanhanen, E., 2001. Geology, mineralogy and geochemistry of the Fe-Co- Au-(U) deposits in the Paleoproterozoic Kuusamo Schist Belt, northeastern Finland. Bulletin, Espoo, Finland.
Vanhanen, E., Cook, N.D.J., Hudson, M.R., Dahlenborg, L., Ranta, J.-P., Havela, T., Kinnunen, J., Molnár, F., Prave, A.R., Oliver, N.H.S., 2015. The Rompas Prospect, Peräpohja Schist Belt, Northern Finland. In: Mineral Deposits of Finland. Elsevier 467–484.
Vasilopoulos, M., Molnár, F., O'Brien, H., Lahaye, Y., Lefèbvre, M., Richard, A., André-Mayer, A.-S., Ranta, J.-P., Talikka, M., 2021. Geochemical signatures of mineralizing events in the Juomasuo Au–Co deposit, Kuusamo belt, northeastern Finland. Mineral. Deposita 56, 1195–1222.
Vasilopoulos, M., Molnár, F., Ranta, J.-P., O'Brien, H., 2022. Mineralogical, lithogeochemical and sulfide trace element characteristics of the Hirvilavanmaa Au-only and the base metal-rich Naakenavaara orogenic gold deposits in the Central Lapland belt, northern Finland. Journal of Geochemical Exploration:107132.
Witt, W.K., Hagemann, S.G., Roberts, M., Davies, A., 2020. Cobalt enrichment at the Juomasuo and Hangaslampi polymetallic deposits, Kuusamo Schist Belt, Finland: a role for an orogenic gold fluid? In: Miner Deposita 55 (2), 381–388.
Yardley, B.W.D., 2005. 100th Anniversary Special Paper: Metal Concentrations in Crustal Fluids and Their Relationship to Ore Formation. Economic Geology 100, 613–632.
Yardley, B.W.D., Graham, J.T., 2002. The origins of salinity in metamorphic fluids. Geofluids 2, 249–256.
Yund, R.A., Kullerud, G., 1966. Thermal Stability of Assemblages in the Cu-Fe-S System. J. Petrology 7, 454–488.
Zhao, H.-X., Frimmel, H.E., Jiang, S.-Y., Dai, B.-Z., 2011. LA-ICP-MS trace element analysis of pyrite from the Xiaoqinling gold district, China: Implications for ore genesis. Ore Geology Reviews 43, 142–153.

Supplementary data

Deposit	Drill-core ID	Coordinate (ETRS-TM35FIN)		Azimuth	Dip	Sample ID	Depth		Lithology	Mineralisation
		Latitude	Longitude				FROM	TO		
Laivakangas	LAN 11041	7158865.314	383805.942	-	-	FEMO-2019-1-01	397,00	397.1	Metavolcanic rock + quartz vein	Ccp-Apy (<1mm) in quartz vein
Laivakangas	LAN 11041	7158865.314	383805.942	-	-	FEMO-2019-1-02	399.1	399.2	Metavolcanic rock + syeno granite	Ccp (mm scale) with chlorite veinlets
Laivakangas	LAN 11041	7158865.314	383805.942	-	-	FEMO-2019-1-03	402.4	402.6	Metavolcanic rock	Ccp-Po-Py (<1mm) disseminated
Laivakangas	LAN 11041	7158865.314	383805.942	-	-	FEMO-2019-1-04	405.4	405.55	Metavolcanic rock + meta-granodiorite	Apy (mm scale) at contact between lithologies
Laivakangas	LAN 11041	7158865.314	383805.942	-	-	FEMO-2019-1-05	415.8	416,00	Metavolcanic rock + quartz veins	Ccp-Apy in mm-scale vein within quartz vein
Laivakangas	LAN 11041	7158865.314	383805.942	-	-	FEMO-2019-1-06	423.2	423.4	Metavolcanic rock + quartz veins	Ccp (mm scale) in veins
Laivakangas	LAN 11041	7158865.314	383805.942	-	-	FEMO-2019-1-07	432.7	432.8	Metavolcanic rock + syeno granite	-
Laivakangas	LAN-11027	7158903.237	383757.694	-	-	FEMO-2019-2-01	98.8	98.9	Metavolcanic rock + syeno granite	disseminated Apy-Ccp (<1mm)
Laivakangas	LAN-11027	7158903.237	383757.694	-	-	FEMO-2019-2-02	102.2	102.3	Meta-granodiorite + quartz vein + syeno granite	disseminated Apy-Ccp (<1mm) in meta-granodiorite
Laivakangas	LAN-11027	7158903.237	383757.694	-	-	FEMO-2019-2-03	107.2	107.6	Metavolcanic rock + quartz veins	Apy (Ccp) (mm to cm scale) in quartz vein
Laivakangas	LAN-11027	7158903.237	383757.694	-	-	FEMO-2019-2-04	103.5	103.6	Meta-granodioirite	Ccp-Apy (<1mm) disseminated
Laivakangas	LAN-897	7158947.343	383559.362	-	-	FEMO-2019-3-01	28.4	28.5	Metavolcanic rock	Apy-Ccp in veins and dessiminated (<1mm)
Laivakangas	LAN-897	7158947.343	383559.362	-	-	FEMO-2019-3-02	29.3	29.4	Metavolcanic rock	Apy-Ccp in quartz veins 1-5 mm size. Apy-Ccp dessiminated (<1mm)
Laivakangas	LAN-897	7158947.343	383559.362	-	-	FEMO-2019-3-03	51.6	51.7	Metavolcanic rock	-
Laivakangas	LAN-897	7158947.343	383559.362	-	-	FEMO-2019-3-04	57.9	58.05	Metavolcanic rock	Apy-Ccp (mm-scale) in quartz veins and dessiminated (<1mm)
Laivakangas	LAN-897	7158947.343	383559.362	-	-	FEMO-2019-3-05	58.5	58.75	Metavolcanic rock + syeno granite	Apy-Ccp (mm-scale) at contact between lithologies
Laivakangas	LAN11023	7159025.2	383813.499	-	-	FEMO-2019-4-01	170.8	-	Metavolcanic rock	-
Laivakangas	LAN11023	7159025.2	383813.499	-	-	FEMO-2019-4-02	213,00	-	Metavolcanic rock	-
Laivakangas	LAN11023	7159025.2	383813.499	-	-	FEMO-2019-4-03	215,00	-	Metavolcanic rock	-
Laivakangas	LAN11023	7159025.2	383813.499	-	-	FEMO-2019-4-04	218,00	-	Metavolcanic rock	-
Laivakangas	LAN-11017	7159269.889	384150.364	-	-	FEMO-2019-5-01	174,00	174.2	quartz vein + meta-granodiorite	Ccp cm-scale in quartz vein
Laivakangas	LAN-11017	7159269.889	384150.364	-	-	FEMO-2019-5-02	180.5	180.7	Meta-granodiorite + quartz veinlets	few small sulfides in the quartz veins
Laivakangas	LAN-11017	7159269.889	384150.364	-	-	FEMO-2019-5-03	196.4	196.6	Meta-granodiorite + quartz veins	quartz vein rich in Ccp- Py- Po (mm to cm scale)
Laivakangas	LAN-11017	7159269.889	384150.364	-	-	FEMO-2019-5-04	200.5	200.6	Syeno granite	-
Laivakangas	LAN - 0611	7159188.1084	384171.3707	-	-	FEMO-2019-6-01	23.4	23.5	Meta-granodiorite + quartz veins	Ccp (<1mm) in quartz veins and disseminated
Laivakangas	LAN - 0611	7159188.1084	384171.3707	-	-	FEMO-2019-6-02	24,00	25.15	Meta-granodioirite	Ccp (<1mm) disseminated
Laivakangas	LAN - 0611	7159188.1084	384171.3707	-	-	FEMO-2019-6-03	27.45	27.5	quartz vein + meta-granodiorite	Ccp (mm-scale) in quartz vein
Laivakangas	LAN - 866	7158968.005	383609.933	-	-	FEMO-2019-7-01	62.5	62.6	Metavolcanic rock + quartz veins	Ccp (<1mm) along quartz veins and disseminated
Laivakangas	LAN - 866	7158968.005	383609.933	-	-	FEMO-2019-7-02	71.9	80,00	Metavolcanic rock + quartz veins	Apy- Ccp (<1mm) in quartz veins
Laivakangas	LAN - 866	7158968.005	383609.933	-	-	FEMO-2019-7-03	72.2	72.4	Metavolcanic rock + quartz veins	Ccp (Apy) (<1mm) in quartz veins
Laivakangas	LAN - 866	7158968.005	383609.933	-	-	FEMO-2019-7-04	74.35	74.45	Metavolcanic rock	disseminated (<1mm) sulfides
Laivakangas	LAN - 866	7158968.005	383609.933	-	-	FEMO-2019-7-05	76.5	76.6	Metavolcanic rock	disseminated Apy (<1mm)
Laivakangas	LAN - 11012	7158989.568	384086.895	-	-	FEMO-2019-8-01	74,00	74.1	Metavolcanic rock	-
Laivakangas	LAN - 11012	7158989.568	384086.895	-	-	FEMO-2019-8-02	75.5	75.6	quartz vein + meta-granodiorite	Ccp-Po-Apy (mm to cm scale) in quartz vein
Laivakangas	LAN - 11012	7158989.568	384086.895	-	-	FEMO-2019-8-03	75.8	76,00	Metavolcanic rock	Apy-Ccp-Po (mm to cm scale) in quartz vein
Laivakangas	LAN - 11012	7158989.568	384086.895	-	-	FEMO-2019-8-04	76.4	76.6	Meta-granodiorite + metavolcanic rock xenolith	-
Laivakangas	LAN-562	7159901.9474	384521.7232	-	-	FEMO-2019-9-01	54.8	55,00	Meta-granodiorite + quartz veins	disseminated Ccp (<1mm)
Laivakangas	LAN-562	7159901.9474	384521.7232	-	-	FEMO-2019-9-02	57.4	57.6	Meta-granodioirite	veinlets of Ccp (<1mm)
Laivakangas	LAN-869	7159594.666	384236.0564	-	-	FEMO-2019-10-01	215.3	215.5	Metavolcanic rock	disseminated Apy (<1mm)
Laivakangas	Tailings samples	-	-	-	-	LAIVA-SP-01	-	-	Metavolcanic rock + quartz veins	Apy-Ccp-Po (mm to cm scale) in quartz vein
Laivakangas	Tailings samples	-	-	-	-	LAIVA-SP-02	-	-	Metavolcanic rock	Apy-Ccp-Po (mm to cm scale) in quartz vein
Laivakangas	Tailings samples	-	-	-	-	LAIVA-SP-03	-	-	Quartz vein	Apy-Ccp-Po (mm to cm scale) in quartz vein
Laivakangas	Tailings samples	-	-	-	-	LAIVA-SP-04	-	-	Meta-granodioirite + metavolcanic rock + quartz vein	Mol (mm-scale) in quartz vein
Laivakangas	Tailings samples	-	-	-	-	LAIVA-SP-05	-	-	Syeno granite	-
Laivakangas	Tailings samples	-	-	-	-	LAIVA-SP-06	-	-	Metavolcanic rock	-
Laivakangas	South pit sample	7159011	383822	-	-	LAIVA-SP-07	-	-	Metavolcanic rock	Apy-Ccp-Po (mm to cm scale) in quartz vein
Laivakangas	South pit sample	7159011	383822	-	-	LAIVA-SP-08	-	-	Metavolcanic rock	Apy-Ccp-Po (mm to cm scale) in quartz vein
Laivakangas	South pit sample	7159011	383822	-	-	LAIVA-SP-09	-	-	Metavolcanic rock + quartz vein	-
Laivakangas	Tailings samples	-	-	-	-	LAIVA-NP-10	-	-	Quartz vein	-
Laivakangas	Tailings samples	-	-	-	-	LAIVA-NP-11	-	-	Metavolcanic rock	-

Deposit	Drill-core ID	Coordinate (ETRS-TM35FIN)		Azimuth	Dip	Sample ID	Depth		Lithology	Mineralisation
		Latitude	Longitude				FROM	TO		
Laivakangas	Tailings samples	-	-	-	-	LAIVA-NP-12	-	-	Metavolcanic rock	-
Laivakangas	Tailings samples	-	-	-	-	LAIVA-NP-13	-	-	Metavolcanic rock	-
Laivakangas	Tailings samples	-	-	-	-	LAIVA-NP-14	-	-	Metavolcanic rock	-
Jouhineva	KJ/JO-34	7107205.76	365054.57	56	45	FEMO-2019-11-01	9.25	9.35	Metavolcanic rock	-
Jouhineva	KJ/JO-34	7107205.76	365054.57	56	45	FEMO-2019-11-02	13.7	13.85	Metavolcanic rock	-
Jouhineva	KJ/JO-34	7107205.76	365054.57	56	45	FEMO-2019-11-03	35.2	35.3	Metavolcanic rock	Cov?
Jouhineva	KJ/JO-34	7107205.76	365054.57	56	45	FEMO-2019-11-04	44.1	45,00	Metavolcanic rock	Lo and disseminated sulfides
Jouhineva	KJ/JO-34	7107205.76	365054.57	56	45	FEMO-2019-11-05	44.1	45,00	Metavolcanic rock	Lo and disseminated sulfides
Jouhineva	KJ/JO-34	7107205.76	365054.57	56	45	FEMO-2019-11-06	48.05	48.15	Metavolcanic rock	sulfides in chlorite shear zone
Jouhineva	KJ/JO-34	7107205.76	365054.57	56	45	FEMO-2019-11-08	69,00	69.1	Metavolcanic rock	sulfides in chlorite shear zone
Jouhineva	KJ/JO-34	7107205.76	365054.57	56	45	FEMO-2019-11-09	69.2	69.3	Metavolcanic rock	Py in chlorite shear zone
Jouhineva	KJ/JO-34	7107205.76	365054.57	56	45	FEMO-2019-11-10	69.35	69.4	Metavolcanic rock	Py in chlorite shear zone
Jouhineva	KJ/JO-34	7107205.76	365054.57	56	45	FEMO-2019-11-11	69.5	69.6	Metavolcanic rock	Py in chlorite shear zone
Jouhineva	KJ/JO-34	7107205.76	365054.57	56	45	FEMO-2019-11-12	82.8	82.9	Metavolcanic rock	-
Jouhineva	KJ/JO-34	7107205.76	365054.57	56	45	FEMO-2019-11-13	100.3	100.4	Metavolcanic rock	Ccp (<1mm) disseminated
Jouhineva	KJ/JO-34	7107205.76	365054.57	56	45	FEMO-2019-11-14	124.1	124.2	Metavolcanic rock	-
Jouhineva	KJ/JO-34	7107205.76	365054.57	56	45	FEMO-2019-11-15	141.9	142,00	Metavolcanic rock	Ccp-Apy in sheared quartz vein
Jouhineva	KJ/JO-34	7107205.76	365054.57	56	45	FEMO-2019-11-16	144.3	144.4	Metavolcanic rock	Ccp in quartz vein
Jouhineva	KJ/JO-34	7107205.76	365054.57	56	45	FEMO-2019-11-17	159.7	160,00	Metavolcanic rock	Ccp in chlorite shear zone
Jouhineva	KJ/JO-34	7107205.76	365054.57	56	45	FEMO-2019-11-18	160.1	160.2	Metavolcanic rock	Py in quartz vein and Ccp in chlorite shear zone
Jouhineva	KJ/JO-34	7107205.76	365054.57	56	45	FEMO-2019-11-19	160.55	160.7	Metavolcanic rock	Ccp in chlorite shear zone
Jouhineva	KJ/JO-57	7107569.22	364785.76	236	44.6	FEMO-2019-12-01	7.4	7.6	Andesite	-
Jouhineva	KJ/JO-57	7107569.22	364785.76	236	44.6	FEMO-2019-12-02	23.1	23.2	Andesite	sulfide (<1mm) disseminated
Jouhineva	KJ/JO-57	7107569.22	364785.76	236	44.6	FEMO-2019-12-03	26.3	26.4	Andesite	sulfide (<1mm) disseminated
Jouhineva	KJ/JO-57	7107569.22	364785.76	236	44.6	FEMO-2019-12-04	36,00	36.1	Andesite	-
Jouhineva	KJ/JO-57	7107569.22	364785.76	236	44.6	FEMO-2019-12-05	52.7	52.8	Andesite	-
Jouhineva	KJ/JO/-92/R-96	7106768.19	366449.02	-	-	FEMO-2019-14-01	55.6	55.7	Metavolcanic rock	-
Jouhineva	KJ/JO/-92/R-96	7106768.19	366449.02	-	-	FEMO-2019-14-02	72.65	72.75	Metavolcanic rock	-
Jouhineva	KJ/JO/-92/R-96	7106768.19	366449.02	-	-	FEMO-2019-14-03	94.7	94.8	Metavolcanic rock	-
Jouhineva	KJ/JO/-92/R-96	7106768.19	366449.02	-	-	FEMO-2019-14-04	121.2	121.35	Metavolcanic rock	-
Jouhineva	KJ/JO/-92/R-96	7106768.19	366449.02	-	-	FEMO-2019-14-05	197.9	198,00	Metavolcanic rock	Ccp (<1mm) disseminated
Jouhineva	KJ/JO/-92/R-96	7106768.19	366449.02	-	-	FEMO-2019-14-06	198.1	198.2	Metavolcanic rock	Ccp (<1mm) disseminated
Jouhineva	KJ/JO/-92/R-96	7106768.19	366449.02	-	-	FEMO-2019-14-07	204.1	204.2	Metavolcanic rock	Ccp.Apy (<1mm) disseminated
Jouhineva	KJ/JO/-92/R-96	7106768.19	366449.02	-	-	FEMO-2019-14-08	206.05	200.2	Metavolcanic rock	Ccp.Apy (<1mm) disseminated
Jouhineva	KJ/JO/-92/R-96	7106768.19	366449.02	-	-	FEMO-2019-14-09	208.85	209.05	Metavolcanic rock	Ccp.Apy (<1mm) disseminated
Jouhineva	KJ/JO-76	7107162.98	365129.11	56	45	FEMO-2019-15-01	8.1	8.2	Metavolcanic rock	-
Jouhineva	KJ/JO-76	7107162.98	365129.11	56	45	FEMO-2019-15-02	10.4	10.5	Metavolcanic rock	-
Jouhineva	KJ/JO-76	7107162.98	365129.11	56	45	FEMO-2019-15-03	10.6	10.7	Chlorite	-
Jouhineva	KJ/JO-76	7107162.98	365129.11	56	45	FEMO-2019-15-04	10.7	10.8	Quartz vein	Apy(Ccp) (mm to cm scale) in quartz vein
Jouhineva	KJ/JO-76	7107162.98	365129.11	56	45	FEMO-2019-15-05	12.7	12.8	Metavolcanic rock	-
Jouhineva	KJ/JO-76	7107162.98	365129.11	56	45	FEMO-2019-15-06	13.6	13.7	Metavolcanic rock	-
Jouhineva	KJ/JO-76	7107162.98	365129.11	56	45	FEMO-2019-15-07	14.4	14.5	Metavolcanic rock	-
Jouhineva	KJ/JO-76	7107162.98	365129.11	56	45	FEMO-2019-15-08	25.3	25.4	Quartz vein	Py-Apy(Ccp) (mm to cm scale) in quartz vein
Jouhineva	KJ/JO-76	7107162.98	365129.11	56	45	FEMO-2019-15-09	27.7	27.85	Andesite	-
Jouhineva	KJ/JO/-69	7107257.11	365140.36	236	46.3	FEMO-2019-16-01	10.5	10.7	Metavolcanic rock	-
Jouhineva	KJ/JO/-69	7107257.11	365140.36	236	46.3	FEMO-2019-16-02	13.7	13.85	Metavolcanic rock	-
Jouhineva	KJ/JO/-69	7107257.11	365140.36	236	46.3	FEMO-2019-16-03	25.5	25.6	Metavolcanic rock	-
Jouhineva	KJ/JO/-69	7107257.11	365140.36	236	46.3	FEMO-2019-16-04	30.55	30.65	Metavolcanic rock	-
Jouhineva	KJ/JO/-69	7107257.11	365140.36	236	46.3	FEMO-2019-16-05	32.1	32.2	Metavolcanic rock	-
Jouhineva	KJ/JO/-69	7107257.11	365140.36	236	46.3	FEMO-2019-16-06	35.5	35.6	Metavolcanic rock	-
Jouhineva	KJ/JO/-69	7107257.11	365140.36	236	46.3	FEMO-2019-16-07	36.05	36.1	Metavolcanic rock	-
Jouhineva	KJ/JO-23	7107071.03	365170.17	56	42.8	FEMO-2019-20-01	64.6	64.7	Metavolcanic rock	-
Jouhineva	KJ/JO-23	7107071.03	365170.17	56	42.8	FEMO-2019-20-02	90.6	90.7	Metavolcanic rock	rare Apy along quartz-chlorite veinlets
Jouhineva	KJ/JO-23	7107071.03	365170.17	56	42.8	FEMO-2019-20-03	90.9	91,00	Metavolcanic rock	-
Jouhineva	KJ/JO-23	7107071.03	365170.17	56	42.8	FEMO-2019-20-04	93.1	93.2	Metavolcanic rock	Ccp (<1mm) in quartz-chlorite veinlets
Jouhineva	KJ/JO-23	7107071.03	365170.17	56	42.8	FEMO-2019-20-05	93.7	93.8	Metavolcanic rock	Apy (<1mm) in quartz-chlorite veinlets
Jouhineva	KJ/JO-23	7107071.03	365170.17	56	42.8	FEMO-2019-20-06	98.4	98.5	Metavolcanic rock	Apy-Ccp (<1mm) in quartz-chlorite veinlets

Deposit	Drill-core ID	Coordinate (ETRS-TM35FIN)		Azimuth	Dip	Sample ID	Depth		Lithology	Mineralisation
		Latitude	Longitude				FROM	TO		
Jouhineva	KJ/JO-23	7107071.03	365170.17	56	42.8	FEMO-2019-20-07	98.8	98.9	Metavolcanic rock	Py-Apy (mm to cm scale) in quartz-chlorite veins
Jouhineva	KJ/JO-23	7107071.03	365170.17	56	42.8	FEMO-2019-20-08	100.7	100.8	Metavolcanic rock	Ccp (up to 2cm) with quartz-chlorite veinlets
Jouhineva	KJ/JO-23	7107071.03	365170.17	56	42.8	FEMO-2019-20-09	101.2	101.3	Metavolcanic rock	Ccp (mm to cm scale) with quartz-chlorite veinlets
Jouhineva	KJ/JO-23	7107071.03	365170.17	56	42.8	FEMO-2019-20-10	103.9	104,00	Meta-granodiorite	Apy (<1mm) disseminated
Jouhineva	KJ/JO-23	7107071.03	365170.17	56	42.8	FEMO-2019-20-11	105.5	105.7	Meta-granodiorite	Apy (<1mm) disseminated
Jouhineva	KJ/JO-23	7107071.03	365170.17	56	42.8	FEMO-2019-20-12	107.4	107.6	Meta-granodiorite	Apy (<1mm) disseminated
Jouhineva	KJ/JO-23	7107071.03	365170.17	56	42.8	FEMO-2019-20-13	121.9	122,00	Meta-granodiorite	-
Jouhineva	KJ/JO-23	7107071.03	365170.17	56	42.8	FEMO-2019-20-14	124,00	124.4	Meta-granodiorite	Ccp (mm to cm scale) in quartz veins
Jouhineva	KJ/JO-23	7107071.03	365170.17	56	42.8	FEMO-2019-20-15	134.7	134.8	Meta-granodiorite	Po?. Py? traces in quartz veins
Jouhineva	KJ/JO-23	7107071.03	365170.17	56	42.8	FEMO-2019-20-16	100,00	100.1	Metavolcanic rock	Apy (cm scale) in quartz chlorite vein
Jouhineva	KJ/JO/-22	7107159.23	365268.85	236	43	FEMO-2019-21-01	26,00	26.1	Metavolcanic rock	oxides in quartz vein
Jouhineva	KJ/JO/-22	7107159.23	365268.85	236	43	FEMO-2019-21-02	27.05	27.2	Metavolcanic rock	oxides in quartz vein
Jouhineva	KJ/JO/-22	7107159.23	365268.85	236	43	FEMO-2019-21-03	60.8	60.9	Metavolcanic rock	small sulfide near shear zone
Jouhineva	KJ/JO/-22	7107159.23	365268.85	236	43	FEMO-2019-21-04	79.1	79.35	Calcite vein + metavolcnic rock	Ccp (mm-scale) disseminated
Jouhineva	KJ/JO/-22	7107159.23	365268.85	236	43	FEMO-2019-21-05	93.7	94.2	Metavolcanic rock	Ccp-Po along fractures
Jouhineva	KJ/JO/-22	7107159.23	365268.85	236	43	FEMO-2019-21-06	95.4	95.5	Quartz vein	Ccp-Po in veinlets along fractures
Jouhineva	KJ/JO/-22	7107159.23	365268.85	236	43	FEMO-2019-21-07	99.85	99.95	Metavolcanic rock	Ccp in quartz veinlets
Jouhineva	KJ/JO/-22	7107159.23	365268.85	236	43	FEMO-2019-21-08	101.5	101.6	Meta-granodiorite	Po (<1mm) in quartz-chlorite veinlets
Jouhineva	KJ/JO/-22	7107159.23	365268.85	236	43	FEMO-2019-21-09	123.1	123.25	Metavolcanic rock	Ccp (<1mm) in quartz veinlets
Huhta	M-52/KL/2431/2005/R538	7105198.08	366967.62	237	45	FEMO-2019-22-01	18.3	18.6	Meta-tonalite	Apy (<1mm)in quartz veinlet
Huhta	M-52/KL/2431/2005/R538	7105198.08	366967.62	237	45	FEMO-2019-22-02	28.3	28.5	Meta-tonalite	Py (<1mm) in quartz-chlorite veinlets
Huhta	M-52/KL/2431/2005/R538	7105198.08	366967.62	237	45	FEMO-2019-22-02.2	30.8	31,00	Meta-tonalite	Py (<1mm) in quartz-chlorite veinlets
Huhta	M-52/KL/2431/2005/R538	7105198.08	366967.62	237	45	FEMO-2019-22-03	32.9	33.1	Meta-tonalite	-
Huhta	M-52/KL/2431/2005/R538	7105198.08	366967.62	237	45	FEMO-2019-22-04	33.8	33.9	Meta-tonalite	-
Huhta	M-52/KL/2431/2005/R538	7105198.08	366967.62	237	45	FEMO-2019-22-05	34.6	34.8	Meta-tonalite	-
Huhta	M-52/KL/2431/2005/R538	7105198.08	366967.62	237	45	FEMO-2019-22-06	35.2	35.3	Meta-tonalite	-
Huhta	M-52/KL/2431/2005/R538	7105198.08	366967.62	237	45	FEMO-2019-22-07	43.2	43.4	Meta-tonalite	Po. Ccp? (cm scale) with chlorite in veinlets
Huhta	M-52/KL/2431/2005/R538	7105198.08	366967.62	237	45	FEMO-2019-22-08	46.6	46.8	Meta-tonalite	Po (mm scale) in quartz vein
Huhta	M-52/KL/2431/2005/R538	7105198.08	366967.62	237	45	FEMO-2019-22-09	50.3	50.65	Meta-tonalite	Po (mm scale) in quartz vein
Huhta	M-52/KL/2431/2005/R538	7105198.08	366967.62	237	45	FEMO-2019-22-10	60.8	61,00	Meta-tonalite	Py (mm scale) in quartz vein
Huhta	M-52/KL/2431/2005/R538	7105198.08	366967.62	237	45	FEMO-2019-22-11	73.1	73.3	Meta-tonalite	Apy. Py. Po
Huhta	M-52/KL/2431/2005/R538	7105198.08	366967.62	237	45	FEMO-2019-22-12	81,00	81.15	Meta-tonalite	Apy. Py. Po
Huhta	M-52/KL/2431/2005/R538	7105198.08	366967.62	237	45	FEMO-2019-22-13	90,00	90.25	Meta-tonalite	Apy (<1mm) in quartz-chlorite veinlets
Huhta	M-52/KL/2431/2005/R538	7105198.08	366967.62	237	45	FEMO-2019-22-14	92.7	93,00	Meta-tonalite	Apy (<1mm) in quartz-chlorite veinlets
Huhta	M-52/KL/2431/2005/R538	7105198.08	366967.62	237	45	FEMO-2019-22-15	101,00	101.3	Meta-tonalite	Apy (<1mm) in quartz-chlorite veinlets
Huhta	M-52/KL/2431/2005/R538	7105198.08	366967.62	237	45	FEMO-2019-22-16	107.6	108.4	Meta-tonalite	Apy (<1mm) in quartz-chlorite veinlets
Huhta	M-52/KL/2431/2005/R538	7105198.08	366967.62	237	45	FEMO-2019-22-17	111.1	111.3	Meta-tonalite	Apy (<1mm) in quartz-chlorite veinlets
Huhta	M-52/KL/2431/2005/R538	7105198.08	366967.62	237	45	FEMO-2019-22-18	116.3	116.4	Meta-tonalite	Apy (<1mm) in quartz-chlorite veinlets
Huhta	M-52/KL/2431/2005/R538	7105198.08	366967.62	237	45	FEMO-2019-22-19	119.2	119.5	Meta-tonalite	Apy (<1mm) in quartz-chlorite veinlets
Huhta	M-52/KL/2431/2005/R538	7105198.08	366967.62	237	45	FEMO-2019-22-20	120.7	121,00	Meta-tonalite	Apy (<1mm) in quartz-chlorite veinlets
Huhta	M-52/KL/2431/2005/R537	7105164.09	366918.64	237	45	FEMO-2019-23-01	8.25	8.4	Meta-tonalite	Apy-(Py?)(mm scale) in veins and disseminated
Huhta	M-52/KL/2431/2005/R537	7105164.09	366918.64	237	45	FEMO-2019-23-02	8.4	8.6	Meta-tonalite	Apy(mm scale) in veins and disseminated
Huhta	M-52/KL/2431/2005/R537	7105164.09	366918.64	237	45	FEMO-2019-23-03	9.15	9.35	Meta-tonalite	Apy-(Py?)(mm scale) in veins and disseminated
Huhta	M-52/KL/2431/2005/R537	7105164.09	366918.64	237	45	FEMO-2019-23-04	10.05	10.2	Meta-tonalite	-
Huhta	M-52/KL/2431/2005/R537	7105164.09	366918.64	237	45	FEMO-2019-23-05	14.5	14.85	Meta-tonalite	Apy (mm scale) in veins and disseminated
Huhta	M-52/KL/2431/2005/R537	7105164.09	366918.64	237	45	FEMO-2019-23-06	15.05	15.2	Meta-tonalite	Apy (mm scale) in veins and disseminated
Huhta	M-52/KL/2431/2005/R537	7105164.09	366918.64	237	45	FEMO-2019-23-07	15.6	15.8	Meta-tonalite	Apy (mm scale) in veins and disseminated
Huhta	M-52/KL/2431/2005/R537	7105164.09	366918.64	237	45	FEMO-2019-23-08	19.85	20.05	Meta-tonalite	-
Huhta	M-52/KL/2431/2005/R537	7105164.09	366918.64	237	45	FEMO-2019-23-09	23.15	23.25	Meta-tonalite	Apy (mm scale) disseminated
Huhta	M-52/KL/2431/2005/R537	7105164.09	366918.64	237	45	FEMO-2019-23-10	45.95	46.3	Meta-tonalite	Apy (mm scale) disseminated
Kurula	M-52/2431/-75/309	7110035.24	380607.07	183	45	FEMO-2019-13-01	6.6	6.7	Metavolcanic rock	-
Kurula	M-52/2431/-75/309	7110035.24	380607.07	183	45	FEMO-2019-13-02	23,00	23.05	Metavolcanic rock	-
Kurula	M-52/2431/-75/309	7110035.24	380607.07	183	45	FEMO-2019-13-03	29.4	29.6	Metavolcanic rock	Ccp-Apy (mm scale) in veinlets and disseminated

Deposit	Drill-core ID	Coordinate (ETRS-TM35FIN)		Azimuth	Dip	Sample ID	Depth		Lithology	Mineralisation
		Latitude	Longitude				FROM	TO		
Kurula	M-52/2431/-75/309	7110035.24	380607.07	183	45	FEMO-2019-13-04	50.5	50.6	Metavolcanic rock	Ccp (mm scale) disseminated
Kurula	M-52/2431/-75/309	7110035.24	380607.07	183	45	FEMO-2019-13-05	51.5	51.6	Metavolcanic rock	Ccp (mm scale) along deformed quartz veins
Kurula	M-52/2431/-75/309	7110035.24	380607.07	183	45	FEMO-2019-13-06	104.4	104.15	Metavolcanic rock	Ccp(<1mm) disseminated
Kurula	M-52/2431/-75/309	7110035.24	380607.07	183	45	FEMO-2019-13-07	107.05	107.1	Metavolcanic rock	Ccp (<1mm) in veinlets
Kurula	M-52/2431/-75/309	7110035.24	380607.07	183	45	FEMO-2019-13-08	124.1	124.2	Metavolcanic rock	-
Kurula	M-52/2431/-75/308	7109990.25	380605.07	183	45	FEMO-2019-17-01	11.4	11.5	Metavolcanic rock	-
Kurula	M-52/2431/-75/308	7109990.25	380605.07	183	45	FEMO-2019-17-02	23.8	23.9	Metavolcanic rock	Py. Apy (<1mm) in veinlets and disseminated
Kurula	M-52/2431/-75/308	7109990.25	380605.07	183	45	FEMO-2019-17-03	26.2	26.3	Metavolcanic rock	Py. Apy. Ccp? (<1mm) in veinlets and disseminated
Kurula	M-52/2431/-75/308	7109990.25	380605.07	183	45	FEMO-2019-17-04	30.5	30.6	Metavolcanic rock	Py. Apy. Ccp? (<1mm) in veinlets and disseminated
Kurula	M-52/2431/-75/308	7109990.25	380605.07	183	45	FEMO-2019-17-05	36,00	36.1	Metavolcanic rock	Py. Apy (<1mm) in veinlets and disseminated
Kurula	M-52/2431/-75/308	7109990.25	380605.07	183	45	FEMO-2019-17-06	38.1	28.2	Metavolcanic rock	Py. Apy (<1mm) in veinlets and disseminated
Kurula	M-52/2431/-75/308	7109990.25	380605.07	183	45	FEMO-2019-17-07	38.4	38.5	Metavolcanic rock	Py. Apy (<1mm) in veinlets and disseminated
Kurula	M-52/2431/-75/308	7109990.25	380605.07	183	45	FEMO-2019-17-08	42.5	42.6	Metavolcanic rock	Apy (<1mm) disseminated
Kurula	M-52/2431/-75/308	7109990.25	380605.07	183	45	FEMO-2019-17-09	49.4	49.5	Metavolcanic rock	Apy. Py. Ccp (mm to cm scale) in quartz veins and disseminated
Kurula	M-52/2431/-75/308	7109990.25	380605.07	183	45	FEMO-2019-17-10	51.3	51.4	Metavolcanic rock	Apy. Py (<1mm) in veinlets and disseminated
Kurula	M-52/2431/-75/308	7109990.25	380605.07	183	45	FEMO-2019-17-11	52,00	52.1	Metavolcanic rock	Apy. Py (<1mm) in veinlets and disseminated
Kurula	M-52/2431/-75/308	7109990.25	380605.07	183	45	FEMO-2019-17-12	52.2	52.3	Metavolcanic rock	Apy. Py (<1mm) in veinlets and disseminated
Kurula	M-52/2431/-75/308	7109990.25	380605.07	183	45	FEMO-2019-17-13	52.35	52.4	Metavolcanic rock	Apy. Py (<1mm) in veinlets and disseminated
Kurula	M-52/2431/-75/308	7109990.25	380605.07	183	45	FEMO-2019-17-14	53.15	53.35	Metavolcanic rock	Apy. Py (<1mm) in veinlets and disseminated
Kurula	M-52/2431/-75/308	7109990.25	380605.07	183	45	FEMO-2019-17-15	60.8	60.9	Metavolcanic rock	-
Kurula	M-52/2431/-75/308	7109990.25	380605.07	183	45	FEMO-2019-17-16	68.8	68.9	Metavolcanic rock	-
Kurula	R316/-85	7109965.26	380615.06	3	45	FEMO-2019-18-01	3.05	3.15	Metavolcanic rock	-
Kurula	R316/-85	7109965.26	380615.06	3	45	FEMO-2019-18-02	9.9	9.95	Metavolcanic rock	Apy. Ccp (mm scale) in breccia
Kurula	R316/-85	7109965.26	380615.06	3	45	FEMO-2019-18-03	15,00	15.05	Metavolcanic rock	Apy. Ccp (mm scale) in breccia
Kurula	R316/-85	7109965.26	380615.06	3	45	FEMO-2019-18-04			Metavolcanic rock	Apy. Ccp (mm scale) in breccia
Kurula	R316/-85	7109965.26	380615.06	3	45	FEMO-2019-18-05	19.45	19.6	Metavolcanic rock	Apy. Ccp (mm scale) in breccia
Kurula	R316/-85	7109965.26	380615.06	3	45	FEMO-2019-18-06	20.3	20.45	Metavolcanic rock	Apy. Ccp (mm scale) in breccia
Kurula	R316/-85	7109965.26	380615.06	3	45	FEMO-2019-18-07	20.5	20.55	Metavolcanic rock	Apy. Ccp (mm scale) in breccia
Kurula	R317/-85	7109964.26	380625.06	3	45	FEMO-2019-19-01	3.4	3.65	Metavolcanic rock	-
Kurula	R317/-85	7109964.26	380625.06	3	45	FEMO-2019-19-02	10.35	10.45	Metavolcanic rock	-
Kurula	R317/-85	7109964.26	380625.06	3	45	FEMO-2019-19-03A	21.7	21.95	Metavolcanic rock	Apy (mm scale) in breccia
Kurula	R317/-85	7109964.26	380625.06	3	45	FEMO-2019-19-03B	21.7	21.95	Metavolcanic rock	Apy (mm scale) in breccia
Kurula	R317/-85	7109964.26	380625.06	3	45	FEMO-2019-19-04	26,00	26.15	Metavolcanic rock	sulfides (mm scale) in breccia
Kurula	R317/-85	7109964.26	380625.06	3	45	FEMO-2019-19-05	27.55	28,00	Metavolcanic rock	Apy. Ccp? (mm scale) in breccia
Kurula	R317/-85	7109964.26	380625.06	3	45	FEMO-2019-19-06	28.2	28.25	Metavolcanic rock	Apy. Ccp? (mm scale) in breccia
Kurula	R317/-85	7109964.26	380625.06	3	45	FEMO-2019-19-07	28.9	28.95	Metavolcanic rock	Ccp (mm scale) in breccia
Kurula	R317/-85	7109964.26	380625.06	3	45	FEMO-2019-19-08	29.6	29.7	Metavolcanic rock	-

Microprobe data

	Fe	Co	Ni	Cu	Ag	Au	Zn	As	Sb	Bi	S	Hg
Det. limit Laivakangas (ppm)	71	81	70	718	102	202	95	211	249	428	95	337
Det. limit Jouhineva(ppm)	70	80	70	743	102	200	94	213	245	416	94	329
Det. limit Huhta (ppm)	69	81	68	731	99	197	92	204	243	410	96	323
Det. limit Kurula (ppm)	104	101	111	1295	135	329	148	336	363	695	153	543

Deposit	sample	#	Mineral	Fe (wt%)	Co (wt%)	Ni (wt%)	Cu (wt%)	Ag (wt%)	Au (wt%)	Zn (wt%)	As (wt%)	Sb (wt%)	Bi (wt%)	S (wt%)	Hg (wt%)	Total (wt%)
Laivakangas	08-03	172	Löllingite	27,97	0,14	0,05	<LOD	<LOD	<LOD	0,02	70,40	<LOD	<LOD	2,38	<LOD	101,00
Laivakangas	08-03	173	Löllingite	27,82	0,14	0,06	<LOD	<LOD	<LOD	<LOD	70,06	<LOD	0,06	2,41	<LOD	100,56
Laivakangas	08-03	174	Löllingite	27,60	0,16	0,02	<LOD	<LOD	<LOD	<LOD	69,47	0,03	<LOD	2,34	<LOD	99,62
Laivakangas	08-03	175	Löllingite	27,72	0,15	0,02	<LOD	<LOD	<LOD	<LOD	70,12	<LOD	<LOD	2,42	<LOD	100,49
Laivakangas	08-03	176	Löllingite	27,76	0,16	0,01	<LOD	<LOD	<LOD	<LOD	69,87	<LOD	0,05	2,49	<LOD	100,38
Laivakangas	08-03	177	Arsenopyrite	33,48	0,08	<LOD	<LOD	0,03	<LOD	<LOD	48,69	<LOD	0,14	18,67	<LOD	101,09
Laivakangas	08-03	178	Arsenopyrite	32,64	0,06	<LOD	<LOD	<LOD	<LOD	0,01	48,83	<LOD	<LOD	18,78	<LOD	100,33
Laivakangas	08-03	179	Arsenopyrite	33,53	0,10	0,01	<LOD	<LOD	<LOD	<LOD	48,41	<LOD	<LOD	18,86	<LOD	100,91
Laivakangas	08-03	180	Arsenopyrite	33,66	<LOD	<LOD	<LOD	<LOD	<LOD	<LOD	47,80	<LOD	0,05	19,07	<LOD	100,58
Laivakangas	08-03	181	Arsenopyrite	33,78	<LOD	<LOD	<LOD	0,03	<LOD	<LOD	48,04	0,03	<LOD	18,78	<LOD	100,65
Laivakangas	08-03	182	Arsenopyrite	33,72	<LOD	<LOD	<LOD	<LOD	<LOD	<LOD	48,29	<LOD	<LOD	19,15	<LOD	101,16
Laivakangas	08-03	183	Chalcopyrite	29,97	<LOD	<LOD	33,84	0,03	0,03	<LOD	0,16	<LOD	<LOD	34,63	0,042	98,70
Laivakangas	08-03	184	Chalcopyrite	29,60	<LOD	<LOD	33,94	0,01	<LOD	0,01	0,02	<LOD	<LOD	33,79	<LOD	97,40
Laivakangas	08-03	185	Chalcopyrite	29,69	<LOD	<LOD	33,84	0,07	<LOD	<LOD	<LOD	<LOD	0,05	34,89	<LOD	98,56
Laivakangas	08-03	186	Pyrrhotite	59,90	<LOD	<LOD	<LOD	<LOD	<LOD	<LOD	0,11	<LOD	0,11	37,44	<LOD	97,60
Laivakangas	08-03	187	Pyrrhotite	59,91	<LOD	<LOD	<LOD	<LOD	<LOD	0,01	0,11	<LOD	<LOD	38,45	<LOD	98,55
Laivakangas	08-03	188	Pyrrhotite	60,01	<LOD	<LOD	<LOD	<LOD	<LOD	<LOD	0,07	<LOD	<LOD	38,66	<LOD	98,74
Laivakangas	08-03	189	Pyrrhotite	60,13	<LOD	0,01	0,08	<LOD	0,03	<LOD	0,07	<LOD	<LOD	38,65	<LOD	98,97
Laivakangas	08-03	190	Chalcopyrite	29,86	<LOD	<LOD	33,14	0,07	<LOD	<LOD	0,56	0,04	0,05	34,88	<LOD	98,62
Laivakangas	08-03	191	Chalcopyrite	29,96	<LOD	<LOD	33,30	<LOD	0,02	<LOD	0,37	<LOD	<LOD	34,44	<LOD	98,11
Laivakangas	08-03	192	Pyrrhotite	59,57	<LOD	<LOD	<LOD	0,01	<LOD	<LOD	0,55	<LOD	<LOD	38,42	<LOD	98,62
Laivakangas	08-03	193	Chalcopyrite	29,97	<LOD	0,01	31,75	<LOD	<LOD	0,02	<LOD	<LOD	<LOD	34,06	0,104	95,92
Laivakangas	08-03	194	Chalcopyrite	29,74	<LOD	<LOD	33,62	0,03	<LOD	<LOD	0,12	<LOD	<LOD	34,81	0,052	98,41
Laivakangas	08-03	195	Arsenopyrite	33,53	0,04	<LOD	<LOD	<LOD	<LOD	<LOD	47,96	<LOD	<LOD	19,54	<LOD	101,07
Laivakangas	08-03	196	Arsenopyrite	33,88	<LOD	<LOD	<LOD	0,01	<LOD	<LOD	47,92	<LOD	<LOD	19,01	<LOD	100,82
Laivakangas	08-03	197	Arsenopyrite	33,75	<LOD	0,01	<LOD	<LOD	<LOD	<LOD	47,55	<LOD	<LOD	18,97	<LOD	100,28
Laivakangas	08-03	198	Arsenopyrite	33,83	<LOD	<LOD	0,17	<LOD	<LOD	<LOD	47,90	<LOD	<LOD	19,16	<LOD	101,06
Laivakangas	08-03	199	Löllingite	27,92	0,12	0,03	<LOD	<LOD	<LOD	<LOD	69,50	<LOD	<LOD	2,37	<LOD	100,02
Laivakangas	08-03	200	Löllingite	27,94	0,14	0,02	<LOD	<LOD	<LOD	<LOD	69,77	0,04	<LOD	2,52	0,081	100,59
Laivakangas	08-03	201	Löllingite	27,59	0,15	0,03	0,10	<LOD	<LOD	<LOD	69,48	<LOD	<LOD	2,45	<LOD	99,82
Laivakangas	08-03	202	Löllingite	27,89	0,12	0,03	<LOD	<LOD	<LOD	<LOD	70,14	<LOD	0,08	2,39	<LOD	100,67
Laivakangas	08-03	203	Löllingite	27,81	0,16	0,03	<LOD	<LOD	<LOD	<LOD	69,64	<LOD	0,16	2,43	0,06	100,32
Laivakangas	08-03	204	Löllingite	27,98	0,14	0,04	<LOD	0,03	<LOD	<LOD	69,64	0,06	<LOD	2,48	<LOD	100,43
Laivakangas	08-03	205	Löllingite	27,76	0,14	0,03	<LOD	<LOD	<LOD	<LOD	69,74	0,05	<LOD	2,36	<LOD	100,14
Laivakangas	08-03	206	Löllingite	27,79	0,13	0,03	<LOD	<LOD	<LOD	<LOD	69,91	<LOD	0,05	2,39	<LOD	100,31
Laivakangas	08-03	207	Löllingite	27,53	0,12	0,03	<LOD	<LOD	<LOD	<LOD	69,92	<LOD	0,11	2,52	<LOD	100,29
Laivakangas	08-03	208	Löllingite	27,83	0,13	0,02	<LOD	<LOD	<LOD	<LOD	69,51	<LOD	<LOD	2,45	<LOD	99,95
Laivakangas	08-03	209	Arsenopyrite	33,81	0,03	<LOD	<LOD	<LOD	<LOD	0,02	46,72	<LOD	<LOD	19,21	<LOD	99,79
Laivakangas	08-03	210	Arsenopyrite	33,56	0,03	0,01	<LOD	<LOD	<LOD	0,01	48,28	<LOD	<LOD	18,67	<LOD	100,56
Laivakangas	08-03	211	Arsenopyrite	33,11	0,04	<LOD	0,24	<LOD	<LOD	<LOD	47,94	0,05	<LOD	19,19	<LOD	100,56
Laivakangas	03-01b	212	Arsenopyrite	33,73	0,02	0,02	<LOD	0,01	<LOD	<LOD	47,29	<LOD	<LOD	19,64	0,073	100,78
Laivakangas	03-01b	213	Arsenopyrite	33,63	0,06	0,05	<LOD	<LOD	<LOD	0,01	48,67	0,06	0,12	18,82	<LOD	101,42
Laivakangas	03-01b	214	Arsenopyrite	33,85	0,05	0,02	<LOD	0,02	<LOD	<LOD	47,88	0,03	<LOD	19,7	<LOD	101,55
Laivakangas	03-01b	215	Arsenopyrite	33,88	<LOD	0,02	<LOD	<LOD	<LOD	<LOD	47,34	<LOD	<LOD	19,4	<LOD	100,64
Laivakangas	03-01b	216	Arsenopyrite	33,33	<LOD	0,02	<LOD	0,01	<LOD	<LOD	47,87	<LOD	<LOD	19,27	<LOD	100,50
Laivakangas	03-01b	217	Arsenopyrite	33,81	<LOD	<LOD	<LOD	0,01	<LOD	<LOD	47,36	<LOD	<LOD	19,4	0,065	100,65
Laivakangas	03-01b	218	Arsenopyrite	33,85	<LOD	0,02	<LOD	<LOD	<LOD	0,01	47,81	<LOD	<LOD	19,69	<LOD	101,38
Laivakangas	03-01b	219	Arsenopyrite	33,83	<LOD	0,02	<LOD	<LOD	<LOD	<LOD	47,51	0,03	<LOD	19,92	<LOD	101,31
Laivakangas	03-01b	220	Löllingite	27,03	0,28	0,49	<LOD	<LOD	<LOD	<LOD	68,31	<LOD	0,05	2,56	<LOD	98,72
Laivakangas	03-01b	221	Löllingite	27,12	0,27	0,46	<LOD	<LOD	<LOD	<LOD	69,54	<LOD	0,06	2,58	<LOD	100,03
Laivakangas	03-01b	222	Chalcopyrite	29,04	<LOD	<LOD	33,74	0,03	<LOD	0,01	0,07	<LOD	<LOD	35,05	<LOD	97,94
Laivakangas	03-01b	223	Pyrite	43,26	<LOD	<LOD	<LOD	<LOD	<LOD	<LOD	9,28	<LOD	<LOD	48,03	<LOD	100,59
Laivakangas	03-01b	224	Pyrite	44,68	<LOD	<LOD	0,12	0,03	<LOD	<LOD	2,60	<LOD	<LOD	51,27	<LOD	98,71
Laivakangas	03-01b	225	Pyrite	43,06	<LOD	<LOD	<LOD	<LOD	<LOD	<LOD	8,31	<LOD	<LOD	47,09	<LOD	98,53
Laivakangas	03-01b	226	Pyrite	41,90	<LOD	<LOD	<LOD	0,03	<LOD	<LOD	14,44	<LOD	<LOD	42,74	0,046	99,16
Laivakangas	03-01b	227	Arsenopyrite	33,07	0,13	0,10	<LOD	0,02	<LOD	<LOD	47,98	0,05	<LOD	18,45	<LOD	99,80
Laivakangas	03-01b	228	Arsenopyrite	33,27	0,07	0,03	<LOD	<LOD	<LOD	<LOD	47,65	<LOD	<LOD	18,49	0,138	99,64
Laivakangas	03-01b	229	Löllingite	27,09	0,23	0,26	<LOD	<LOD	<LOD	<LOD	70,24	<LOD	0,05	1,05	<LOD	98,95
Laivakangas	03-01b	230	Löllingite	23,50	0,18	0,21	<LOD	<LOD	<LOD	<LOD	57,49	0,06	17,27	0,981	<LOD	99,72
Laivakangas	03-01b	231	Arsenopyrite	33,78	0,08	0,07	<LOD	0,03	<LOD	<LOD	47,56	<LOD	<LOD	19,43	<LOD	100,94
Laivakangas	03-01b	232	Arsenopyrite	33,46	0,07	0,12	<LOD	<LOD	<LOD	0,01	47,94	<LOD	<LOD	18,91	0,043	100,56
Laivakangas	03-01b	233	Chalcopyrite	29,90	<LOD	<LOD	33,52	0,04	<LOD	0,01	0,04	0,04	<LOD	34,44	<LOD	98,00
Laivakangas	03-01b	234	Chalcopyrite	29,55	<LOD	<LOD	33,90	0,03	<LOD	0,03	<LOD	<LOD	<LOD	34,68	<LOD	98,20
Laivakangas	03-01b	235	Chalcopyrite	29,86	<LOD	<LOD	33,36	0,03	<LOD	0,07	<LOD	<LOD	<LOD	34,52	<LOD	97,85
Laivakangas	03-01b	236	Chalcopyrite	29,72	<LOD	<LOD	34,14	0,02	<LOD	0,25	0,03	<LOD	<LOD	34,61	<LOD	98,81
Laivakangas	04-02	237	Arsenopyrite	32,06	0,88	0,66	0,12	0,01	<LOD	<LOD	48,60	<LOD	<LOD	18,63	<LOD	100,96
Laivakangas	04-02	238	Arsenopyrite	32,80	<LOD	0,08	<LOD	<LOD	<LOD	<LOD	45,49	<LOD	0,12	20,7	<LOD	99,19
Laivakangas	04-02	239	Arsenopyrite	32,49	0,64	0,61	0,09	<LOD	<LOD	<LOD	49,49	0,03	<LOD	18,55	0,047	101,94
Laivakangas	04-02	240	Arsenopyrite	31,70	1,45	0,60	<LOD	<LOD	<LOD	<LOD	49,38	<LOD	0,10	18,17	<LOD	101,39
Laivakangas	04-02	241	Arsenopyrite	32,78	0,63	0,42	<LOD	0,01	<LOD	<LOD	49,19	<LOD	0,05	18,7	<LOD	101,78
Laivakangas	04-02	242	Arsenopyrite	31,75	1,41	0,91	<LOD	<LOD	<LOD	<LOD	48,48	<LOD	<LOD	18,73	<LOD	101,28
Laivakangas	04-02	243	Arsenopyrite	32,84	0,77	0,34	<LOD	<LOD	<LOD	<LOD	47,50	<LOD	0,13	19,35	<LOD	100,94
Laivakangas	04-02	244	Arsenopyrite	31,73	1,31	0,77	<LOD	<LOD	<LOD	<LOD	48,32	<LOD	0,05	18,29	0,043	100,52
Laivakangas	04-02	245	Arsenopyrite	32,26	0,86	0,38	0,08	<LOD	<LOD	<LOD	48,90	<LOD	<LOD	18,38	<LOD	100,86
Laivakangas	04-02	246	Arsenopyrite	33,06	0,88	0,11	0,14	0,02	<LOD	<LOD	47,70	0,03	<LOD	19,33	0,04	101,31
Laivakangas	04-02	247	Chalcopyrite	29,93	<LOD	<LOD	34,12	0,02	<LOD	<LOD	0,08	<LOD	<LOD	34,35	<LOD	98,50
Laivakangas	04-02	248	Chalcopyrite	29,54	<LOD	<LOD	33,25	0,03	<LOD	<LOD	<LOD	<LOD	<LOD	35,03	<LOD	97,87
Laivakangas	04-02	249	Chalcopyrite	28,63	<LOD	<LOD	32,46	0,02	<LOD	<LOD	<LOD	<LOD	<LOD	33,57	<LOD	94,76
Laivakangas	04-02	250	Arsenopyrite	33,39	0,39	0,10	0,16	0,02	<LOD	<LOD	47,41	<LOD	<LOD	19,35	<LOD	100,82
Laivakangas	04-02	251	Arsenopyrite	32,16	0,90	0,27	<LOD	0,02	<LOD	<LOD	48,06	<LOD	<LOD	18,13	<LOD	99,54
Laivakangas	04-02	252	Arsenopyrite	32,27	0,77	0,64	0,11	<LOD	<LOD	0,01	48,55	<LOD	<LOD	18,78	<LOD	101,13
Laivakangas	04-02	253	Arsenopyrite	33,23	0,44	0,25	<LOD	<LOD	<LOD	<LOD	47,94	<LOD	0,07	19,14	0,053	101,12
Laivakangas	04-02	254	Arsenopyrite	32,59	0,57	0,51	0,13	<LOD	<LOD	<LOD	47,20	<LOD	<LOD	19,1	<LOD	100,09
Laivakangas	04-02	255	Arsenopyrite	32,66	0,78	0,24	<LOD	<LOD	<LOD	<LOD	48,75	<LOD	<LOD	18,47	<LOD	100,89
Laivakangas	04-02	256	Arsenopyrite	32,16	0,99	0,64	<LOD	<LOD	<LOD	<LOD	48,39	<LOD	0,07	18,75	0,045	101,04
Laivakangas	04-02	257	Arsenopyrite	33,12	0,23	0,71	<LOD	<LOD	<LOD	<LOD	47,67	<LOD	<LOD	19,12	<LOD	100,84
Laivakangas	04-02	258	Arsenopyrite	34,37	<LOD	0,03	<LOD	<LOD	<LOD	<LOD	46,34	0,03	<LOD	20,39	<LOD	101,16
Laivakangas	04-02	259	Arsenopyrite	33,12	0,62	0,19	0,11	<LOD	<LOD	0,02	48,19	<LOD	<LOD	18,67	<LOD	100,92
Laivakangas	04-02	260	Arsenopyrite	32,96	0,58	0,29	<LOD	<LOD	<LOD	<LOD	48,49	0,03	<LOD	18,24	<LOD	100,59
Laivakangas	04-02	261	Arsenopyrite	33,86	<LOD	0,14	<LOD	0,02	<LOD	<LOD	47,93	<LOD	<LOD	19,35	<LOD	101,30
Laivakangas	04-02	262	Arsenopyrite	32,56	0,83	0,38	<LOD	<LOD	<LOD	<LOD	49,30	0,04	<LOD	17,93	<LOD	101,03

Deposit	sample	#	Mineral	Fe (wt%)	Co (wt%)	Ni (wt%)	Cu (wt%)	Ag (wt%)	Au (wt%)	Zn (wt%)	As (wt%)	Sb (wt%)	Bi (wt%)	S (wt%)	Hg (wt%)	Total (wt%)
Laivakangas	04-02	263	Chalcopyrite	29,77	<LOD	<LOD	33,60	0,03	<LOD	<LOD	0,13	0,03	0,09	34,97	0,054	98,68
Laivakangas	04-02	264	Chalcopyrite	29,85	<LOD	<LOD	33,32	0,01	<LOD	<LOD	0,06	<LOD	<LOD	34,6	<LOD	97,89
Laivakangas	04-02	265	Chalcopyrite	28,50	<LOD	<LOD	33,39	0,01	<LOD	0,26	1,45	0,04	0,35	34,26	<LOD	98,29
Laivakangas	03-02b	266	Arsenopyrite	31,96	0,63	1,04	<LOD	<LOD	<LOD	<LOD	47,84	<LOD	0,07	18,89	<LOD	100,44
Laivakangas	03-02b	267	Arsenopyrite	32,39	0,54	0,65	0,14	<LOD	<LOD	<LOD	48,01	<LOD	<LOD	19,08	<LOD	100,80
Laivakangas	03-02b	268	Arsenopyrite	33,52	0,21	0,10	<LOD	<LOD	<LOD	<LOD	48,67	<LOD	0,13	18,51	<LOD	101,14
Laivakangas	03-02b	269	Arsenopyrite	33,94	0,14	0,05	0,19	<LOD	<LOD	<LOD	48,14	<LOD	0,09	19,6	<LOD	102,15
Laivakangas	03-02b	270	Arsenopyrite	33,76	0,17	0,05	0,21	<LOD	<LOD	<LOD	48,07	<LOD	0,09	19,16	<LOD	101,51
Laivakangas	03-02b	271	Chalcopyrite	29,71	<LOD	<LOD	34,42	<LOD	<LOD	0,02	<LOD	<LOD	<LOD	34,79	<LOD	99.012
Laivakangas	03-02b	272	Chalcopyrite	29,97	<LOD	<LOD	33,51	0,03	<LOD	<LOD	0,06	<LOD	<LOD	34,81	0,084	98.466
Laivakangas	03-02b	273	Chalcopyrite	29,90	<LOD	<LOD	33,68	0,01	<LOD	0,01	0,07	<LOD	<LOD	34,81	<LOD	98.484
Laivakangas	03-02b	274	Pyrite	46,34	<LOD	<LOD	0,13	<LOD	<LOD	0,03	<LOD	<LOD	<LOD	52,5	<LOD	99.018
Laivakangas	03-02b	275	Pyrite	46,40	<LOD	<LOD	0,21	<LOD	<LOD	<LOD	<LOD	<LOD	<LOD	53,17	<LOD	99.776
Laivakangas	03-02b	276	Chalcopyrite	29,91	<LOD	<LOD	32,19	0,05	<LOD	<LOD	<LOD	<LOD	<LOD	35	<LOD	97.170
Laivakangas	03-02b	277	Chalcopyrite	29,99	<LOD	<LOD	34,69	0,03	<LOD	0,01	<LOD	<LOD	<LOD	34,47	<LOD	99.255
Laivakangas	03-02b	278	Chalcopyrite	30,08	<LOD	<LOD	34,12	0,03	0,04	<LOD	0,03	<LOD	<LOD	34,96	<LOD	99.270
Laivakangas	03-02b	279	Chalcopyrite	30,06	<LOD	<LOD	33,43	0,03	<LOD	<LOD	<LOD	0,05	<LOD	34,64	0,045	98.268
Laivakangas	03-02b	280	Chalcopyrite	30,10	<LOD	<LOD	34,26	0,01	<LOD	<LOD	<LOD	0,05	<LOD	35,04	<LOD	99.510
Laivakangas	03-02b	281	Arsenopyrite	34,11	0,03	0,02	<LOD	<LOD	<LOD	<LOD	48,24	<LOD	<LOD	19,62	<LOD	102,02
Laivakangas	03-02b	282	Arsenopyrite	33,52	0,15	<LOD	<LOD	<LOD	<LOD	<LOD	48,03	<LOD	<LOD	19,6	<LOD	101,30
Laivakangas	03-02b	283	Arsenopyrite	34,03	0,14	0,01	<LOD	<LOD	<LOD	<LOD	48,18	<LOD	0,05	20	<LOD	102,41
Laivakangas	03-02b	284	Arsenopyrite	33,82	0,22	0,01	<LOD	<LOD	<LOD	<LOD	48,24	0,03	<LOD	19,4	<LOD	101,72
Laivakangas	03-02b	285	Arsenopyrite	33,80	0,22	0,02	0,14	<LOD	<LOD	<LOD	48,29	<LOD	0,08	19,23	<LOD	101,77
Laivakangas	03-02b	286	Löllingite	26,82	0,66	0,32	<LOD	<LOD	<LOD	<LOD	72,62	<LOD	<LOD	0,679	0,061	101.268
Laivakangas	03-02b	287	Löllingite	27,41	0,47	0,25	<LOD	0,02	<LOD	<LOD	70,57	<LOD	0,07	2,28	<LOD	101.148
Laivakangas	03-02b	288	Arsenopyrite	33,70	0,24	<LOD	<LOD	<LOD	<LOD	<LOD	47,30	0,05	0,06	19,72	<LOD	101,07
Laivakangas	03-02b	289	Arsenopyrite	33,69	0,25	<LOD	<LOD	<LOD	<LOD	<LOD	47,97	<LOD	0,05	19,95	<LOD	101,91
Laivakangas	03-02b	290	Löllingite	27,44	0,44	0,25	0,09	<LOD	<LOD	<LOD	70,62	<LOD	0,09	2,39	<LOD	101.322
Laivakangas	03-02b	291	Löllingite	27,55	0,43	0,24	<LOD	<LOD	<LOD	<LOD	70,34	<LOD	<LOD	2,4	<LOD	100.961
Laivakangas	03-02b	292	Arsenopyrite	33,93	0,16	0,01	<LOD	0,03	<LOD	<LOD	47,93	0,03	0,07	19,57	0,063	101,79
Laivakangas	03-02b	293	Arsenopyrite	33,69	0,23	0,03	<LOD	0,02	<LOD	<LOD	48,50	<LOD	<LOD	19,28	<LOD	101,74
Laivakangas	03-02b	294	Arsenopyrite	33,44	0,23	0,04	<LOD	<LOD	<LOD	<LOD	48,63	0,03	<LOD	19,19	<LOD	101,56
Laivakangas	03-02b	295	Arsenopyrite	33,79	0,22	0,04	<LOD	<LOD	<LOD	<LOD	48,42	<LOD	<LOD	18,94	<LOD	101,41
Laivakangas	03-02b	296	Arsenopyrite	33,80	0,09	<LOD	<LOD	<LOD	<LOD	<LOD	47,57	<LOD	<LOD	19,59	<LOD	101,05
Laivakangas	03-02b	297	Arsenopyrite	34,03	0,11	0,01	<LOD	0,02	<LOD	<LOD	47,59	<LOD	<LOD	19,65	0,059	101,47
Laivakangas	03-02b	298	Arsenopyrite	33,48	0,19	0,04	<LOD	<LOD	<LOD	<LOD	48,33	<LOD	0,06	18,95	<LOD	101,05
Laivakangas	03-02b	299	Arsenopyrite	33,69	0,18	0,04	<LOD	0,02	<LOD	<LOD	48,75	<LOD	0,09	19,23	<LOD	102,00
Laivakangas	03-02b	300	Löllingite	27,76	0,43	0,24	<LOD	0,02	<LOD	<LOD	69,99	<LOD	<LOD	2,6	0,062	101.138
Laivakangas	03-02b	301	Löllingite	27,76	0,39	0,25	<LOD	<LOD	<LOD	<LOD	68,86	<LOD	<LOD	2,67	<LOD	99.944
Laivakangas	03-02b	302	Arsenopyrite	33,71	0,18	0,03	<LOD	<LOD	<LOD	<LOD	48,87	<LOD	0,06	19,44	<LOD	102,29
Laivakangas	03-02b	303	Arsenopyrite	34,23	0,08	<LOD	0,13	<LOD	<LOD	0,02	46,98	0,03	<LOD	20,06	0,036	101,56
Laivakangas	03-02b	304	Arsenopyrite	34,26	<LOD	<LOD	<LOD	<LOD	<LOD	<LOD	47,44	<LOD	0,08	19,76	0,064	101,61
Laivakangas	03-02b	305	Arsenopyrite	34,10	<LOD	0,02	<LOD	<LOD	<LOD	<LOD	47,12	0,03	<LOD	19,8	<LOD	101,07
Laivakangas	03-02b	306	Arsenopyrite	34,14	<LOD	0,01	<LOD	<LOD	<LOD	<LOD	48,00	0,04	<LOD	20,12	<LOD	102,31
Laivakangas	03-02b	307	Chalcopyrite	29,93	<LOD	<LOD	34,25	0,01	<LOD	0,01	0,03	<LOD	0,08	35,03	0,046	99.400
Laivakangas	03-02b	308	Chalcopyrite	29,39	<LOD	<LOD	33,78	<LOD	<LOD	<LOD	0,15	<LOD	<LOD	35,02	<LOD	98.365
Laivakangas	03-02b	309	Chalcopyrite	30,12	<LOD	<LOD	34,53	0,01	<LOD	<LOD	0,18	<LOD	<LOD	35,07	0,06	99.979
Laivakangas	03-02b	310	Chalcopyrite	30,13	<LOD	<LOD	33,99	0,02	<LOD	<LOD	0,10	<LOD	<LOD	34,75	<LOD	99.005
Laivakangas	03-02b	311	Pyrite	46,10	<LOD	<LOD	0,17	0,05	<LOD	<LOD	0,13	<LOD	<LOD	51,72	<LOD	98.211
Laivakangas	03-02b	312	Pyrite	45,40	<LOD	<LOD	0,10	0,10	<LOD	<LOD	0,37	<LOD	0,04	51,68	0,038	97.733
Laivakangas	03-02b	313	Pyrite	45,82	<LOD	<LOD	0,09	0,03	<LOD	0,26	0,10	0,04	<LOD	52,17	0,039	98.548
Laivakangas	03-02b	314	Löllingite	26,72	0,56	0,88	<LOD	<LOD	<LOD	<LOD	70,69	0,03	<LOD	2,21	<LOD	101.100
Laivakangas	03-02b	315	Löllingite	26,79	0,48	0,91	<LOD	0,04	<LOD	<LOD	70,55	<LOD	0,05	2,11	<LOD	100.990
Laivakangas	03-02b	316	Löllingite	26,78	0,39	0,71	<LOD	0,01	<LOD	0,01	70,11	<LOD	<LOD	2,51	<LOD	100.673
Laivakangas	03-02b	317	Arsenopyrite	33,70	<LOD	0,11	<LOD	0,02	<LOD	0,02	47,41	<LOD	<LOD	19,38	<LOD	100,63
Laivakangas	03-02b	318	Arsenopyrite	33,86	0,08	0,10	<LOD	0,01	<LOD	<LOD	48,32	<LOD	<LOD	19,31	<LOD	101,69
Laivakangas	03-02b	319	Arsenopyrite	33,41	0,18	0,14	<LOD	0,02	<LOD	<LOD	49,17	<LOD	<LOD	18,63	<LOD	101,54
Laivakangas	03-02b	320	Arsenopyrite	31,88	0,74	1,12	<LOD	<LOD	<LOD	<LOD	48,93	<LOD	<LOD	18,54	<LOD	101,21
Laivakangas	03-02b	321	Arsenopyrite	33,67	0,14	0,08	<LOD	<LOD	<LOD	0,01	48,46	<LOD	0,05	19,25	<LOD	101,66
Laivakangas	03-02b	322	Arsenopyrite	33,53	0,19	0,13	<LOD	<LOD	<LOD	<LOD	48,80	<LOD	<LOD	18,84	<LOD	101,49
Laivakangas	03-02b	323	Löllingite	26,73	0,75	0,83	<LOD	0,02	<LOD	<LOD	69,97	<LOD	0,12	2,24	0,065	100.728
Laivakangas	03-02b	324	Löllingite	26,70	0,47	1,11	0,09	<LOD	<LOD	<LOD	70,17	0,04	<LOD	2,29	<LOD	100.905
Laivakangas	03-02b	325	Arsenopyrite	32,79	0,88	0,17	0,10	<LOD	<LOD	0,02	48,60	<LOD	<LOD	18,69	<LOD	101,24
Laivakangas	03-02b	326	Arsenopyrite	33,13	0,65	0,23	<LOD	<LOD	<LOD	<LOD	48,92	<LOD	0,12	18,66	0,04	101,74
Laivakangas	03-02b	327	Arsenopyrite	34,11	0,05	0,02	<LOD	<LOD	<LOD	<LOD	46,08	<LOD	<LOD	20,09	0,055	100,40
Laivakangas	03-02b	328	Arsenopyrite	34,35	0,05	0,01	<LOD	<LOD	<LOD	<LOD	47,38	<LOD	0,05	20,17	<LOD	102,02
Laivakangas	03-02b	329	Arsenopyrite	34,07	0,08	0,06	<LOD	<LOD	<LOD	0,01	47,77	<LOD	<LOD	19,58	0,04	101,60
Laivakangas	03-02b	330	Chalcopyrite	29,84	<LOD	<LOD	33,22	0,03	<LOD	0,01	0,10	<LOD	0,09	34,8	<LOD	98.093
Laivakangas	03-02b	331	Chalcopyrite	29,97	<LOD	<LOD	34,39	<LOD	<LOD	0,01	<LOD	<LOD	<LOD	35,17	<LOD	99.574
Laivakangas	03-02b	332	Electrum	3,82	<LOD	<LOD	<LOD	17,88	63,76	<LOD	3,01	<LOD	<LOD	0,546	<LOD	89.016
Laivakangas	03-04b	334	Arsenopyrite	34,04	<LOD	0,01	<LOD	<LOD	<LOD	<LOD	47,89	<LOD	0,14	19,42	<LOD	101,50
Laivakangas	03-04b	335	Arsenopyrite	29,58	2,54	1,50	0,09	<LOD	<LOD	<LOD	49,29	<LOD	0,09	17,93	0,056	101,08
Laivakangas	03-04b	336	Arsenopyrite	30,04	1,99	1,48	0,11	<LOD	<LOD	<LOD	49,55	0,04	<LOD	17,16	<LOD	100,37
Laivakangas	03-04b	337	Chalcopyrite	30,05	<LOD	<LOD	33,75	0,02	<LOD	<LOD	0,03	<LOD	<LOD	35,14	0,061	99.079
Laivakangas	03-04b	338	Chalcopyrite	29,76	<LOD	<LOD	34,44	0,03	<LOD	0,01	<LOD	0,03	<LOD	34,45	<LOD	98.724
Laivakangas	03-04b	339	Chalcopyrite	29,72	<LOD	<LOD	34,27	0,02	<LOD	0,01	<LOD	<LOD	<LOD	34,83	<LOD	98.917
Laivakangas	03-04b	340	Chalcopyrite	30,07	<LOD	<LOD	34,10	0,01	<LOD	0,02	0,03	<LOD	<LOD	34,49	<LOD	98.732
Laivakangas	03-04b	341	Chalcopyrite	29,85	<LOD	<LOD	34,56	<LOD	<LOD	<LOD	<LOD	<LOD	<LOD	33,53	0,043	98.008
Laivakangas	03-04b	342	Chalcopyrite	30,07	<LOD	<LOD	33,27	0,02	<LOD	0,03	0,05	0,05	<LOD	34,2	<LOD	97.693
Laivakangas	03-04b	343	Chalcopyrite	29,93	<LOD	<LOD	34,53	0,03	<LOD	<LOD	0,06	<LOD	0,07	33,39	<LOD	98.044
Laivakangas	03-04b	344	Pyrite	42,37	<LOD	0,30	1,35	0,13	<LOD	0,02	5,97	<LOD	<LOD	48,79	<LOD	98.926
Laivakangas	03-04b	345	Pyrite	42,68	<LOD	0,12	1,15	0,08	<LOD	0,01	3,94	<LOD	0,06	48,98	0,039	97.058
Laivakangas	03-04b	346	Pyrite	43,97	<LOD	0,10	0,84	0,07	<LOD	0,01	4,30	<LOD	<LOD	49,88	<LOD	99.176
Laivakangas	03-04b	347	Pyrite	42,76	<LOD	<LOD	0,29	0,04	<LOD	<LOD	6,72	<LOD	<LOD	48,79	<LOD	98.607
Laivakangas	03-04b	348	Pyrite	43,45	<LOD	0,01	0,59	0,04	<LOD	0,03	4,91	<LOD	<LOD	49,99	<LOD	99.028
Laivakangas	03-04b	349	Pyrite	46,20	<LOD	<LOD	0,92	<LOD	<LOD	0,02	0,09	<LOD	0,05	52,15	<LOD	99.433
Laivakangas	03-04b	350	Pyrite	45,60	<LOD	0,02	1,37	0,03	<LOD	0,02	0,03	0,03	<LOD	52,77	<LOD	99.892
Laivakangas	03-04b	351	Pyrite	45,67	<LOD	0,01	1,36	0,03	<LOD	0,08	0,03	<LOD	<LOD	52,08	<LOD	99.271
Laivakangas	03-04b	352	Pyrite	45,08	<LOD	0,02	1,05	0,03	<LOD	0,04	0,04	<LOD	<LOD	53,28	<LOD	99.550
Laivakangas	03-04b	353	Pyrite	44,56	<LOD	<LOD	0,82	<LOD	<LOD	0,01	0,05	0,03	<LOD	55,12	<LOD	100.598
Laivakangas	03-04b	354	Löllingite	25,46	1,43	1,33	<LOD	<LOD	<LOD	<LOD	70,44	<LOD	<LOD	2	0,055	100.715
Laivakangas	03-04b	355	Löllingite	25,61	1,04	1,25	<LOD	<LOD	<LOD	<LOD	70,61	<LOD	<LOD	1,83	<LOD	100.374
Laivakangas	03-04b	356	Löllingite	25,83	0,93	1,16	<LOD	0,03	<LOD	0,01	70,52	<LOD	<LOD	1,68	0,038	100.228
Laivakangas	03-04b	357	Löllingite	25,71	0,96	1,28	<LOD	<LOD	<LOD	<LOD	70,17	<LOD	<LOD	1,43	<LOD	99.567
Laivakangas	03-04b	358	Löllingite	26,18	0,91	1,08	<LOD	0,02	<LOD	0,01	70,78	<LOD	0,10	2	<LOD	101.084
Laivakangas	03-04b	359	Löllingite	26,17	1,11	0,85	<LOD	<LOD	<LOD	<LOD	70,42	<LOD	0,05	2,23	<LOD	100.844
Laivakangas	03-04b	360	Löllingite	25,87	1,07	1,05	<LOD	0,02	<LOD	<LOD	71,10	<LOD	0,06	1,8	<LOD	100.989
Laivakangas	03-04b	361	Löllingite	25,66	1,39	1,14	<LOD	0,03	<LOD	<LOD	70,21	<LOD	<LOD	1,71	<LOD	100.168
Laivakangas	03-04b	362	Löllingite	25,25	1,19	1,01	<LOD	<LOD	<LOD	<LOD	69,92	<LOD	<LOD	2,02	<LOD	99.431

Deposit	sample	#	Mineral	Fe (wt%)	Co (wt%)	Ni (wt%)	Cu (wt%)	Ag (wt%)	Au (wt%)	Zn (wt%)	As (wt%)	Sb (wt%)	Bi (wt%)	S (wt%)	Hg (wt%)	Total (wt%)
Laivakangas	03-04b	363	Löllingite	25,53	1,46	1,17	<LOD	0,012	<LOD	<LOD	69,96	0,034	0,062	1,96	<LOD	100.187
Laivakangas	03-04b	364	Löllingite	26,54	0,966	0,598	<LOD	<LOD	<LOD	<LOD	69,76	<LOD	<LOD	2,14	<LOD	100.010
Laivakangas	03-04b	365	Löllingite	26,52	0,817	0,715	<LOD	<LOD	<LOD	<LOD	71,01	<LOD	<LOD	2,03	<LOD	101.216
Laivakangas	03-04b	366	Löllingite	25,42	1,15	1,56	<LOD	<LOD	<LOD	<LOD	70,12	<LOD	0,18	2,01	<LOD	100.457
Laivakangas	03-04b	367	Löllingite	25,48	0,906	1,48	<LOD	<LOD	<LOD	0,013	69,99	<LOD	0,088	1,96	0,068	100.028
Laivakangas	03-04b	368	Arsenopyrite	33,48	0,097	0,033	<LOD	<LOD	<LOD	<LOD	48,05	<LOD	<LOD	19,39	<LOD	101,05
Laivakangas	03-04b	369	Arsenopyrite	33,7	0,135	0,037	0,147	<LOD	<LOD	0,015	48,23	<LOD	0,057	19,4	<LOD	101,72
Laivakangas	03-04b	370	Arsenopyrite	33,54	0,276	0,061	<LOD	<LOD	<LOD	<LOD	48,37	<LOD	<LOD	19,22	<LOD	101,47
Laivakangas	03-04b	371	Arsenopyrite	33,56	0,326	0,089	<LOD	<LOD	<LOD	<LOD	47,89	<LOD	<LOD	18,57	<LOD	100,44
Laivakangas	03-04b	372	Arsenopyrite	33,77	0,069	0,013	<LOD	<LOD	<LOD	<LOD	48,21	<LOD	0,064	19,07	<LOD	101,20
Laivakangas	03-04b	373	Arsenopyrite	33,61	0,282	0,03	<LOD	<LOD	<LOD	0,015	48,41	<LOD	<LOD	18,7	<LOD	101,05
Laivakangas	03-04b	374	Arsenopyrite	33,93	0,382	<LOD	<LOD	<LOD	<LOD	<LOD	46,93	<LOD	<LOD	20,39	<LOD	101,63
Laivakangas	03-04b	375	Chalcopyrite	29,58	<LOD	<LOD	33,37	0,044	<LOD	<LOD	<LOD	<LOD	<LOD	34,1	<LOD	97.124
Laivakangas	03-04b	376	Chalcopyrite	29,58	<LOD	<LOD	34,13	0,029	<LOD	<LOD	<LOD	0,052	<LOD	34,36	<LOD	98.168
Laivakangas	03-04b	377	Chalcopyrite	29,53	<LOD	<LOD	33,81	0,048	<LOD	<LOD	0,027	<LOD	<LOD	34,78	<LOD	98.232
Laivakangas	03-04b	378	Chalcopyrite	29,9	<LOD	<LOD	34,13	<LOD	<LOD	0,011	0,064	<LOD	<LOD	34,27	<LOD	98.405
Laivakangas	03-04b	379	Löllingite	25,47	1,19	0,678	<LOD	<LOD	<LOD	<LOD	68,41	<LOD	0,048	2,11	<LOD	97.914
Laivakangas	03-04b	380	Löllingite	26,11	1,22	0,716	<LOD	<LOD	<LOD	<LOD	69,67	<LOD	<LOD	2,1	<LOD	99.893
Laivakangas	03-04b	381	Arsenopyrite	32,82	0,633	0,078	<LOD	<LOD	<LOD	<LOD	48,6	<LOD	<LOD	18,77	<LOD	100,90
Laivakangas	03-04b	382	Arsenopyrite	32,68	0,711	0,076	<LOD	<LOD	<LOD	<LOD	45,95	<LOD	0,08	18,84	0,056	98,39
Laivakangas	03-04b	383	Chalcopyrite	29,86	<LOD	<LOD	34,83	<LOD	<LOD	<LOD	<LOD	<LOD	<LOD	34,62	<LOD	99.329
Laivakangas	03-04b	384	Chalcopyrite	29,97	<LOD	<LOD	34,34	0,013	<LOD	<LOD	<LOD	<LOD	<LOD	34,49	<LOD	98.834
Laivakangas	03-04b	385	Chalcopyrite	30,13	<LOD	<LOD	33,75	0,02	<LOD	<LOD	<LOD	0,035	<LOD	34,72	0,037	98.692
Laivakangas	03-04b	386	Chalcopyrite	30,03	<LOD	<LOD	33,86	0,024	<LOD	<LOD	<LOD	<LOD	0,089	34,89	<LOD	98.899
Laivakangas	03-04b	387	Chalcopyrite	30,2	<LOD	<LOD	33,37	0,04	<LOD	0,021	<LOD	<LOD	<LOD	34,91	0,06	98.601
Laivakangas	03-04b	388	Pyrite	45,52	<LOD	<LOD	1,29	0,054	<LOD	0,034	0,024	<LOD	<LOD	52,74	<LOD	99.672
Laivakangas	03-04b	389	Pyrite	45,81	<LOD	<LOD	0,517	0,024	<LOD	0,03	0,034	<LOD	<LOD	52,64	<LOD	99.081
Laivakangas	03-04b	390	Pyrite	36,07	<LOD	0,009	3,73	<LOD	<LOD	0,017	0,078	<LOD	<LOD	44,33	0,039	84.288
Laivakangas	03-04b	391	Pyrite	45,64	<LOD	<LOD	1,28	<LOD	0,029	0,022	0,051	<LOD	<LOD	53,28	<LOD	100.325
Laivakangas	03-04b	392	Pyrite	46,18	<LOD	<LOD	0,551	0,013	0,034	0,016	<LOD	0,025	<LOD	52,12	<LOD	98.982
Laivakangas	03-04b	393	Pyrite	45,44	<LOD	<LOD	1,42	<LOD	<LOD	0,024	0,03	<LOD	<LOD	52,51	<LOD	99.448
Laivakangas	03-04b	394	Pyrite	46,23	<LOD	<LOD	0,574	<LOD	<LOD	<LOD	0,033	<LOD	<LOD	51,48	<LOD	98.317
Laivakangas	03-04b	395	Pyrite	45,94	<LOD	<LOD	0,426	<LOD	<LOD	0,01	0,08	<LOD	<LOD	52,73	<LOD	99.198
Laivakangas	03-04b	396	Pyrite	42,18	<LOD	0,022	0,531	0,046	<LOD	0,033	0,677	<LOD	<LOD	50,89	<LOD	94.391
Laivakangas	03-04b	397	Pyrite	44,33	<LOD	0,02	0,722	0,055	<LOD	0,023	0,459	<LOD	0,051	53,09	<LOD	98.751
Laivakangas	03-04b	398	Pyrite	43,84	<LOD	0,02	0,411	0,055	<LOD	0,035	0,545	0,034	<LOD	51,54	<LOD	96.490
Laivakangas	03-04b	399	Pyrite	36,09	<LOD	0,01	0,37	0,023	<LOD	0,016	5,05	<LOD	<LOD	38,52	<LOD	80.102
Laivakangas	03-04b	400	Pyrite	36,3	<LOD	0,016	0,329	0,026	<LOD	<LOD	5,24	<LOD	<LOD	39,58	<LOD	81.500
Laivakangas	03-04b	401	Pyrite	37,04	<LOD	<LOD	0,145	<LOD	<LOD	0,01	5,74	<LOD	<LOD	40,46	<LOD	83.421
Laivakangas	03-04b	402	Pyrite	37,7	<LOD	0,011	0,245	<LOD	<LOD	0,016	5,93	<LOD	<LOD	40,39	0,04	84.333
Laivakangas	03-04b	403	Pyrite	37,93	<LOD	<LOD	0,161	0,041	<LOD	<LOD	5,8	<LOD	<LOD	40,89	<LOD	84.857
Laivakangas	LA-SP-01A	404	Arsenopyrite	33,72	<LOD	0,009	<LOD	0,032	<LOD	<LOD	48,86	<LOD	<LOD	19,01	0,059	101,69
Laivakangas	LA-SP-01A	405	Arsenopyrite	33,77	<LOD	<LOD	<LOD	<LOD	<LOD	<LOD	48,42	0,038	0,062	19,02	<LOD	101,31
Laivakangas	LA-SP-01A	406	Arsenopyrite	33,84	<LOD	<LOD	<LOD	<LOD	<LOD	<LOD	48,92	0,043	0,058	18,9	<LOD	101,76
Laivakangas	LA-SP-01A	407	Löllingite	28,13	0,096	0,026	<LOD	<LOD	<LOD	<LOD	70,31	<LOD	<LOD	2,49	0,063	101,16
Laivakangas	LA-SP-01A	408	Löllingite	28,18	0,112	0,038	<LOD	<LOD	<LOD	<LOD	70,18	<LOD	<LOD	2,52	<LOD	101,03
Laivakangas	LA-SP-01A	409	Löllingite	27,98	0,107	0,033	<LOD	<LOD	<LOD	<LOD	69,56	<LOD	<LOD	2,58	<LOD	100,27
Laivakangas	LA-SP-01A	410	Löllingite	28,08	0,082	0,033	<LOD	<LOD	<LOD	<LOD	70,32	0,039	0,057	2,64	<LOD	101,26
Laivakangas	LA-SP-01A	411	Arsenopyrite	33,82	<LOD	<LOD	<LOD	<LOD	<LOD	<LOD	48,78	<LOD	<LOD	18,45	<LOD	101,05
Laivakangas	LA-SP-01A	412	Arsenopyrite	33,83	<LOD	<LOD	0,08	<LOD	<LOD	0,011	48,61	<LOD	<LOD	19,26	<LOD	101,79
Laivakangas	LA-SP-01A	413	Arsenopyrite	33,53	<LOD	<LOD	<LOD	<LOD	<LOD	<LOD	48,7	<LOD	<LOD	18,96	<LOD	101,19
Laivakangas	LA-SP-01A	414	Arsenopyrite	33,34	0,319	0,144	0,113	0,024	<LOD	<LOD	48,26	<LOD	<LOD	19,24	<LOD	101,44
Laivakangas	LA-SP-01A	415	Arsenopyrite	32,48	0,529	0,423	0,209	<LOD	<LOD	<LOD	49,16	<LOD	0,056	17,45	<LOD	100,31
Laivakangas	LA-SP-01A	416	Arsenopyrite	33,34	0,368	0,202	<LOD	<LOD	<LOD	<LOD	47,84	<LOD	<LOD	19,31	<LOD	101,06
Laivakangas	LA-SP-01A	417	Arsenopyrite	33,78	0,336	0,119	<LOD	<LOD	<LOD	<LOD	48,03	<LOD	0,133	19,75	<LOD	102,15
Laivakangas	LA-SP-01A	418	Arsenopyrite	33,4	0,367	0,146	<LOD	0,012	<LOD	<LOD	48,44	<LOD	0,093	18,94	0,053	101,45
Laivakangas	LA-SP-01A	419	Chalcopyrite	29,5	<LOD	<LOD	34,17	0,021	<LOD	0,03	0,038	<LOD	<LOD	34,52	<LOD	98,29
Laivakangas	LA-SP-01A	420	Arsenopyrite	33,03	0,38	0,125	<LOD	<LOD	<LOD	<LOD	48,07	0,03	<LOD	19,1	<LOD	100,74
Laivakangas	LA-SP-01A	421	Arsenopyrite	33,33	0,401	0,105	<LOD	<LOD	<LOD	<LOD	48,39	<LOD	<LOD	19,32	<LOD	101,55
Laivakangas	LA-SP-01A	422	Arsenopyrite	32,61	0,724	0,209	<LOD	<LOD	<LOD	<LOD	49,04	<LOD	<LOD	18,53	<LOD	101,11
Laivakangas	LA-SP-01A	423	Löllingite	25,26	0,983	1,6	<LOD	<LOD	<LOD	0,016	69,97	<LOD	<LOD	2,25	<LOD	100,14
Laivakangas	LA-SP-01A	424	Arsenopyrite	33,05	0,556	0,155	<LOD	<LOD	<LOD	<LOD	48,51	<LOD	0,065	19,01	<LOD	101,35
Laivakangas	03-05a	425	Tennantite	3,95	<LOD	<LOD	42,13	0,045	<LOD	4,03	19,84	<LOD	<LOD	29,12	<LOD	99,12
Laivakangas	03-05a	426	Bornite	11,12	<LOD	<LOD	62,11	0,06	0,021	<LOD	0,127	<LOD	<LOD	25,62	<LOD	99,07
Laivakangas	03-05a	429	Pyrite	40,29	0,85	0,123	2,5	0,065	<LOD	<LOD	4,15	<LOD	<LOD	47,14	<LOD	95,13
Laivakangas	03-05a	430	Pyrite	41,12	0,858	0,121	2,35	0,059	<LOD	<LOD	4,26	<LOD	0,1	47,25	0,136	96,25
Laivakangas	03-05a	432	Bornite	13,09	0,212	0,021	53,04	0,04	<LOD	<LOD	0,868	<LOD	0,47	31,51	<LOD	99,25
Laivakangas	03-05a	433	Pyrite	39,96	0,912	0,131	2,9	0,086	<LOD	<LOD	4,8	<LOD	0,947	47,46	<LOD	97,20
Laivakangas	03-05a	434	Pyrite	40,17	0,863	0,131	3,05	0,081	<LOD	<LOD	4,8	<LOD	1,04	47,63	<LOD	97,77
Laivakangas	03-05a	435	Pyrite	39,99	0,998	0,172	2,86	0,079	<LOD	<LOD	4,9	<LOD	0,898	47,33	<LOD	97,24
Laivakangas	03-05a	437	Pyrite	38,57	1,18	0,375	3,65	0,052	<LOD	0,011	5,07	<LOD	1,1	46,92	0,051	96,98
Laivakangas	03-05a	438	Pyrite	38,88	1,16	0,316	3,69	0,082	<LOD	<LOD	5,02	<LOD	1,06	46,84	<LOD	97,06
Laivakangas	03-05a	439	Chalcopyrite	28,45	<LOD	<LOD	33,88	<LOD	<LOD	<LOD	0,049	<LOD	<LOD	34,8	0,05	97,25
Laivakangas	03-05a	440	Chalcopyrite	28,69	<LOD	<LOD	33,52	0,023	<LOD	<LOD	0,073	<LOD	0,043	34,77	<LOD	97,15
Laivakangas	03-05a	441	Chalcopyrite	28,71	<LOD	<LOD	34,48	<LOD	<LOD	<LOD	<LOD	<LOD	0,117	34,83	<LOD	98,18
Laivakangas	03-05a	442	Chalcopyrite	26,28	<LOD	<LOD	36,24	0,043	<LOD	<LOD	0,033	<LOD	0,218	34,16	<LOD	96,98
Laivakangas	03-05a	443	Pyrrhotite	59,38	<LOD	<LOD	<LOD	0,013	<LOD	<LOD	<LOD	<LOD	<LOD	38,72	<LOD	98,11
Laivakangas	03-05a	444	Pyrrhotite	59,39	<LOD	<LOD	<LOD	0,015	<LOD	<LOD	<LOD	<LOD	<LOD	38,97	<LOD	98,38
Laivakangas	01-03	445	Pyrrhotite	59,39	<LOD	<LOD	<LOD	<LOD	<LOD	<LOD	<LOD	<LOD	<LOD	39,11	<LOD	98,50
Laivakangas	01-03	446	Pyrrhotite	59,26	<LOD	<LOD	<LOD	<LOD	<LOD	<LOD	<LOD	<LOD	<LOD	39,45	<LOD	98,71
Laivakangas	01-03	447	Pyrrhotite	59,37	<LOD	<LOD	0,093	<LOD	<LOD	<LOD	<LOD	<LOD	<LOD	39,27	<LOD	98,73
Laivakangas	01-03	448	Pyrrhotite	59,45	<LOD	<LOD	<LOD	<LOD	<LOD	<LOD	<LOD	<LOD	<LOD	39,37	<LOD	98,82
Laivakangas	01-03	449	Pyrite	46	<LOD	<LOD	<LOD	<LOD	<LOD	<LOD	<LOD	<LOD	<LOD	52,67	<LOD	98,67
Laivakangas	01-03	450	Pyrite	46,23	<LOD	<LOD	<LOD	0,015	<LOD	<LOD	<LOD	<LOD	<LOD	53,18	<LOD	99,43
Laivakangas	01-03	451	Pyrite	46,26	<LOD	<LOD	<LOD	<LOD	<LOD	<LOD	<LOD	<LOD	<LOD	52,6	<LOD	98,86
Laivakangas	01-03	452	Pyrite	46,39	<LOD	<LOD	<LOD	<LOD	<LOD	<LOD	<LOD	<LOD	<LOD	52,88	<LOD	99,28
Laivakangas	01-03	453	Pyrite	45,87	<LOD	<LOD	<LOD	<LOD	<LOD	<LOD	<LOD	<LOD	<LOD	53,28	<LOD	99,20
Laivakangas	01-03	454	Pyrite	46,3	<LOD	<LOD	<LOD	<LOD	<LOD	<LOD	<LOD	<LOD	<LOD	52,57	<LOD	98,87
Laivakangas	01-03	455	Chalcopyrite	30,31	<LOD	<LOD	33,43	0,024	<LOD	<LOD	0,044	<LOD	<LOD	34,94	<LOD	98,75
Laivakangas	01-03	456	Chalcopyrite	30,5	<LOD	<LOD	33,09	0,035	<LOD	<LOD	<LOD	<LOD	<LOD	34,65	<LOD	98,28
Laivakangas	01-03	457	Chalcopyrite	30,08	<LOD	<LOD	34,24	0,03	<LOD	<LOD	<LOD	<LOD	<LOD	34,8	<LOD	99,15
Laivakangas	01-03	458	Chalcopyrite	29,76	<LOD	<LOD	34,9	0,032	<LOD	<LOD	<LOD	<LOD	<LOD	35,1	<LOD	99,81
Laivakangas	01-03	459	Chalcopyrite	30,16	<LOD	<LOD	34,67	0,016	<LOD	<LOD	<LOD	<LOD	<LOD	34,96	<LOD	99,82
Laivakangas	01-03	460	Chalcopyrite	30,11	<LOD	<LOD	34,32	0,038	<LOD	<LOD	<LOD	<LOD	<LOD	34,84	<LOD	99,32
Laivakangas	01-03	461	Pyrrhotite	59,48	<LOD	<LOD	0,17	<LOD	<LOD	<LOD	<LOD	<LOD	<LOD	38,75	<LOD	98,40
Laivakangas	01-03	462	Pyrrhotite	59,51	<LOD	<LOD	<LOD	<LOD	<LOD	<LOD	<LOD	<LOD	<LOD	39,3	<LOD	98,81
Laivakangas	01-03	463	Pyrrhotite	59,4	<LOD	<LOD	<LOD	<LOD	<LOD	<LOD	<LOD	<LOD	<LOD	39,34	<LOD	98,80
Laivakangas	01-03	464	Pyrrhotite	59,56	<LOD	<LOD	<LOD	<LOD	<LOD	<LOD	<LOD	<LOD	<LOD	39,41	<LOD	98,98
Laivakangas	01-03	465	Pyrrhotite	59,61	<LOD	<LOD	<LOD	<LOD	<LOD	<LOD	<LOD	<LOD	<LOD	39,18	<LOD	98,79

Deposit	sample	#	Mineral	Fe (wt%)	Co (wt%)	Ni (wt%)	Cu (wt%)	Ag (wt%)	Au (wt%)	Zn (wt%)	As (wt%)	Sb (wt%)	Bi (wt%)	S (wt%)	Hg (wt%)	Total (wt%)
Laivakangas	01-03	466	Pyrrhotite	59,14	<LOD	<LOD	<LOD	0,014	<LOD	<LOD	<LOD	<LOD	<LOD	38,41	<LOD	97,58
Laivakangas	01-03	467	Gold inclusion	7,92	<LOD	<LOD	6,51	9,56	71,82	<LOD	<LOD	<LOD	<LOD	12	<LOD	107,81
Laivakangas	01-03	468	Gold inclusion	16,52	<LOD	<LOD	12,58	5,41	43,18	<LOD	<LOD	<LOD	<LOD	21,59	<LOD	99,28
Laivakangas	01-03	471	Pyrite	46,04	<LOD	0,009	0,082	<LOD	<LOD	<LOD	<LOD	<LOD	<LOD	53,25	<LOD	99,38
Laivakangas	01-03	472	Pyrite	46,02	<LOD	<LOD	<LOD	<LOD	<LOD	<LOD	<LOD	<LOD	<LOD	53,17	<LOD	99,22
Laivakangas	01-03	473	Pyrite	46,43	<LOD	<LOD	<LOD	0,013	0,023	<LOD	0,026	<LOD	<LOD	53,14	<LOD	99,63
Laivakangas	01-03	474	Pyrite	46,34	<LOD	<LOD	<LOD	<LOD	<LOD	<LOD	0,028	<LOD	<LOD	53,13	<LOD	99,50
Laivakangas	01-03	475	Pyrrhotite	59,34	<LOD	<LOD	<LOD	<LOD	<LOD	<LOD	<LOD	<LOD	<LOD	39,77	<LOD	99,11
Laivakangas	01-03	476	Pyrrhotite	59,52	<LOD	<LOD	<LOD	<LOD	<LOD	<LOD	0,025	<LOD	<LOD	39,28	<LOD	98,85
Laivakangas	01-03	477	Pyrrhotite	59,58	<LOD	<LOD	0,082	<LOD	<LOD	<LOD	<LOD	<LOD	<LOD	39,15	<LOD	98,83
Jouhineva	11-09	1	Arsenopyrite	33,93	0,09	<LOD	<LOD	<LOD	<LOD	<LOD	46,89	<LOD	0,177	20,37	<LOD	101,56
Jouhineva	11-09	2	Arsenopyrite	34,21	0,038	<LOD	<LOD	<LOD	<LOD	<LOD	46,18	<LOD	<LOD	20,71	0,054	101,21
Jouhineva	11-09	3	Arsenopyrite	33,94	0,077	<LOD	<LOD	<LOD	<LOD	<LOD	46,21	<LOD	<LOD	19,94	<LOD	100,22
Jouhineva	11-09	4	Arsenopyrite	34,23	0,028	<LOD	<LOD	0,02	<LOD	0,012	46,91	<LOD	0,048	20,53	<LOD	101,82
Jouhineva	11-09	5	Arsenopyrite	34,4	<LOD	<LOD	0,091	<LOD	<LOD	<LOD	46,8	<LOD	<LOD	20,5	<LOD	101,82
Jouhineva	11-09	6	Arsenopyrite	34,39	<LOD	0,01	<LOD	0,026	<LOD	<LOD	46,71	<LOD	<LOD	20,6	<LOD	101,74
Jouhineva	11-09	7	Arsenopyrite	34,18	0,023	<LOD	<LOD	<LOD	<LOD	0,015	45,98	0,029	<LOD	20,44	0,08	100,78
Jouhineva	11-09	8	Pyrite	44,93	<LOD	0,013	0,565	<LOD	<LOD	<LOD	0,517	<LOD	0,069	51,88	0,061	98,04
Jouhineva	11-09	9	Pyrite	45,91	<LOD	<LOD	0,222	<LOD	<LOD	<LOD	0,233	<LOD	0,056	53,49	<LOD	99,93
Jouhineva	11-09	10	Pyrite	44,65	<LOD	0,093	0,873	0,028	<LOD	0,019	2,13	0,028	<LOD	49,33	<LOD	97,16
Jouhineva	11-09	11	Chalcopyrite	27,94	<LOD	<LOD	33,29	0,033	<LOD	<LOD	0,307	<LOD	<LOD	34,8	<LOD	96,39
Jouhineva	11-09	12	Arsenopyrite	34,51	<LOD	<LOD	<LOD	0,02	<LOD	<LOD	46,37	<LOD	<LOD	20,84	<LOD	101,75
Jouhineva	11-09	13	Arsenopyrite	33,88	0,144	0,067	<LOD	<LOD	<LOD	<LOD	47,59	0,037	<LOD	20,03	<LOD	101,75
Jouhineva	11-09	14	Arsenopyrite	34,29	0,081	<LOD	<LOD	<LOD	<LOD	<LOD	46,44	0,029	0,084	20,68	<LOD	101,61
Jouhineva	11-09	15	Arsenopyrite	33,92	0,095	0,021	<LOD	0,019	<LOD	<LOD	46,97	<LOD	0,095	20,16	<LOD	101,29
Jouhineva	11-09	16	Arsenopyrite	33,84	0,061	<LOD	<LOD	<LOD	<LOD	<LOD	46,8	<LOD	0,142	19,72	<LOD	100,57
Jouhineva	11-09	17	Arsenopyrite	34,47	<LOD	<LOD	<LOD	<LOD	<LOD	<LOD	45,49	<LOD	0,072	21,34	<LOD	101,38
Jouhineva	11-09	18	Arsenopyrite	34,06	0,113	0,037	<LOD	<LOD	<LOD	<LOD	47,38	<LOD	<LOD	19,82	<LOD	101,43
Jouhineva	11-09	19	Arsenopyrite	34,33	0,048	0,016	<LOD	<LOD	<LOD	<LOD	47,08	0,03	<LOD	20,28	<LOD	101,82
Jouhineva	11-09	20	Arsenopyrite	34,34	0,029	0,013	<LOD	<LOD	<LOD	0,015	46,93	0,053	0,058	19,66	<LOD	101,10
Jouhineva	11-09	21	Pyrite	45,48	<LOD	0,062	0,112	<LOD	<LOD	<LOD	1,86	<LOD	<LOD	52,25	<LOD	99,77
Jouhineva	11-09	22	Pyrite	45,01	<LOD	0,095	0,398	<LOD	<LOD	<LOD	0,171	0,038	<LOD	51,43	0,077	97,25
Jouhineva	11-09	23	Pyrite	46,01	<LOD	0,075	0,167	<LOD	<LOD	<LOD	0,169	<LOD	0,055	53,02	0,05	99,56
Jouhineva	11-09	24	Pyrite	45,23	<LOD	0,075	1,03	<LOD	<LOD	<LOD	0,253	<LOD	<LOD	51,68	0,068	98,37
Jouhineva	11-09	25	Pyrite	45,52	<LOD	0,104	0,457	<LOD	<LOD	<LOD	0,311	0,044	0,057	52	<LOD	98,50
Jouhineva	11-09	26	Pyrite	45,32	<LOD	<LOD	0,113	<LOD	<LOD	<LOD	3,24	<LOD	<LOD	50,83	<LOD	99,53
Jouhineva	11-09	27	Arsenopyrite	34,66	<LOD	<LOD	<LOD	0,012	<LOD	0,01	45,75	<LOD	<LOD	20,81	<LOD	101,28
Jouhineva	11-09	28	Arsenopyrite	34,64	<LOD	<LOD	<LOD	<LOD	<LOD	<LOD	46,66	<LOD	0,051	20,94	<LOD	102,29
Jouhineva	11-09	29	Arsenopyrite	34,68	<LOD	<LOD	<LOD	0,013	<LOD	<LOD	46,46	<LOD	<LOD	21,09	<LOD	102,27
Jouhineva	11-09	30	Arsenopyrite	34,66	<LOD	<LOD	<LOD	<LOD	<LOD	<LOD	46,41	<LOD	0,09	21,02	<LOD	102,20
Jouhineva	11-09	31	Arsenopyrite	34,39	<LOD	<LOD	<LOD	<LOD	<LOD	0,012	46,73	<LOD	0,117	20,67	<LOD	101,93
Jouhineva	11-09	32	Arsenopyrite	34,46	<LOD	<LOD	<LOD	<LOD	<LOD	<LOD	46,56	<LOD	<LOD	20,81	<LOD	101,86
Jouhineva	11-09	33	Arsenopyrite	34,59	<LOD	<LOD	<LOD	<LOD	<LOD	<LOD	45,91	<LOD	<LOD	21,24	<LOD	101,76
Jouhineva	11-09	34	Arsenopyrite	34,31	<LOD	<LOD	<LOD	0,015	<LOD	<LOD	46,75	0,039	<LOD	20,99	<LOD	102,12
Jouhineva	11-09	35	Arsenopyrite	34,14	<LOD	<LOD	<LOD	<LOD	<LOD	0,016	46,45	<LOD	0,094	20,73	0,036	101,47
Jouhineva	11-09	36	Arsenopyrite	34,64	<LOD	<LOD	<LOD	<LOD	<LOD	<LOD	46,4	<LOD	<LOD	20,54	<LOD	101,60
Jouhineva	11-09	37	Arsenopyrite	34,54	<LOD	<LOD	<LOD	<LOD	<LOD	<LOD	45,91	0,04	0,114	20,64	<LOD	101,26
Jouhineva	11-09	38	Arsenopyrite	34,37	<LOD	<LOD	<LOD	<LOD	<LOD	<LOD	46,95	<LOD	<LOD	20,63	<LOD	102,03
Jouhineva	11-09	39	Arsenopyrite	34,38	<LOD	<LOD	<LOD	<LOD	<LOD	0,012	46,52	<LOD	<LOD	20,53	0,043	101,51
Jouhineva	11-09	40	Arsenopyrite	34,62	<LOD	<LOD	<LOD	<LOD	<LOD	0,013	46,8	<LOD	0,107	20,72	<LOD	102,30
Jouhineva	11-09	41	Arsenopyrite	34,59	<LOD	<LOD	<LOD	<LOD	<LOD	<LOD	45,2	<LOD	<LOD	20,06	<LOD	99,87
Jouhineva	11-09	42	Arsenopyrite	34,36	<LOD	0,009	<LOD	<LOD	<LOD	<LOD	46,6	0,06	<LOD	20,11	<LOD	101,20
Jouhineva	11-09	43	Arsenopyrite	34,52	<LOD	<LOD	<LOD	<LOD	<LOD	<LOD	45,86	0,044	<LOD	20,48	<LOD	100,96
Jouhineva	11-09	44	Arsenopyrite	34,43	<LOD	<LOD	<LOD	<LOD	<LOD	<LOD	46,73	<LOD	<LOD	20,63	<LOD	101,80
Jouhineva	11-09	45	Arsenopyrite	34,38	<LOD	<LOD	<LOD	<LOD	<LOD	<LOD	45,82	<LOD	0,113	21,1	<LOD	101,41
Jouhineva	11-09	46	Arsenopyrite	34,47	<LOD	<LOD	<LOD	<LOD	<LOD	<LOD	46,85	0,045	<LOD	20,5	<LOD	101,98
Jouhineva	11-09	47	Arsenopyrite	34,61	<LOD	<LOD	<LOD	<LOD	<LOD	<LOD	46,07	0,139	0,149	20,85	<LOD	101,86
Jouhineva	11-09	48	Arsenopyrite	34,4	<LOD	<LOD	<LOD	<LOD	<LOD	<LOD	46,65	0,067	0,066	20,15	<LOD	101,35
Jouhineva	11-09	49	Arsenopyrite	34,47	<LOD	<LOD	<LOD	<LOD	<LOD	<LOD	46,87	<LOD	<LOD	20,58	<LOD	101,95
Jouhineva	11-09	50	Arsenopyrite	34,59	<LOD	<LOD	<LOD	<LOD	<LOD	<LOD	46,59	0,025	<LOD	20,66	<LOD	101,90
Jouhineva	11-09	51	Arsenopyrite	34,41	<LOD	<LOD	<LOD	<LOD	<LOD	<LOD	47,31	0,033	0,14	20,23	<LOD	102,14
Jouhineva	11-09	52	Arsenopyrite	34,41	<LOD	<LOD	<LOD	<LOD	<LOD	<LOD	46,39	<LOD	0,048	20,82	<LOD	101,67
Jouhineva	11-09	53	Arsenopyrite	34,64	<LOD	<LOD	<LOD	<LOD	<LOD	0,01	46,56	<LOD	<LOD	20,77	<LOD	101,99
Jouhineva	11-09	54	Arsenopyrite	34,58	<LOD	<LOD	0,078	<LOD	<LOD	<LOD	46,2	0,043	<LOD	20,35	<LOD	101,25
Jouhineva	11-09	55	Arsenopyrite	34,04	<LOD	<LOD	<LOD	<LOD	<LOD	<LOD	46,84	<LOD	0,084	20,6	<LOD	101,56
Jouhineva	11-09	56	Arsenopyrite	34,56	<LOD	<LOD	<LOD	<LOD	<LOD	<LOD	45,75	<LOD	0,098	20,45	0,059	100,95
Jouhineva	11-09	57	Arsenopyrite	34,46	<LOD	<LOD	<LOD	<LOD	<LOD	<LOD	46,95	<LOD	<LOD	20,38	<LOD	101,84
Jouhineva	15-08b	58	Arsenopyrite	30,14	3,44	0,103	0,077	<LOD	<LOD	<LOD	48,86	0,086	<LOD	18,87	0,061	101,64
Jouhineva	15-08b	59	Arsenopyrite	31,05	2,98	0,049	<LOD	<LOD	<LOD	<LOD	48,58	0,031	0,16	18,77	<LOD	101,62
Jouhineva	15-08b	60	Arsenopyrite	32,41	1,86	0,049	<LOD	<LOD	<LOD	<LOD	47,97	<LOD	<LOD	19,76	<LOD	102,10
Jouhineva	15-08b	61	Arsenopyrite	31,79	2,05	0,041	<LOD	<LOD	<LOD	<LOD	47,04	<LOD	<LOD	20,13	<LOD	101,11
Jouhineva	15-08b	62	Arsenopyrite	30,03	3,77	0,149	<LOD	<LOD	<LOD	<LOD	49,44	0,039	0,045	18,4	<LOD	101,87
Jouhineva	15-08b	63	Arsenopyrite	30,34	3,5	0,094	<LOD	<LOD	<LOD	0,014	49	<LOD	0,082	18,58	<LOD	101,68
Jouhineva	15-08b	64	Arsenopyrite	30,29	3,54	0,102	<LOD	0,021	<LOD	<LOD	49,28	0,029	0,061	18,71	<LOD	102,09
Jouhineva	15-08b	65	Bornite	11,05	<LOD	<LOD	61,44	0,041	<LOD	<LOD	0,053	<LOD	<LOD	25,68	<LOD	98,29
Jouhineva	15-08b	66	Bornite	11,04	<LOD	<LOD	62,87	0,052	0,044	<LOD	<LOD	<LOD	0,116	26,21	0,035	100,37
Jouhineva	15-08b	67	Bornite	10,74	<LOD	<LOD	59,44	0,052	<LOD	<LOD	0,052	<LOD	<LOD	25,33	0,039	95,67
Jouhineva	15-08b	68	Bornite	10,95	<LOD	<LOD	62,19	0,037	<LOD	<LOD	<LOD	0,035	0,049	26,1	<LOD	99,36
Jouhineva	15-08b	69	Bornite	11,02	<LOD	<LOD	62,71	0,044	<LOD	<LOD	<LOD	<LOD	<LOD	25,98	<LOD	99,75
Jouhineva	15-08b	70	Digenite	0,042	<LOD	<LOD	77,85	0,062	<LOD	<LOD	<LOD	<LOD	<LOD	20,97	0,042	98,99
Jouhineva	15-08b	71	Digenite	0,023	<LOD	<LOD	78,47	0,055	<LOD	<LOD	<LOD	<LOD	0,055	20,88	0,056	99,56
Jouhineva	15-08b	72	Digenite	0,024	<LOD	<LOD	77,72	0,039	<LOD	<LOD	<LOD	<LOD	<LOD	21,58	<LOD	99,41
Jouhineva	15-08b	73	Digenite	0,007	<LOD	<LOD	78,11	0,086	<LOD	<LOD	<LOD	<LOD	0,08	21,06	0,039	99,38
Jouhineva	15-08b	74	Pyrite	46,29	<LOD	0,073	<LOD	0,018	<LOD	<LOD	<LOD	<LOD	<LOD	52,45	<LOD	98,85
Jouhineva	15-08b	75	Pyrite	46,01	<LOD	0,214	0,206	0,016	<LOD	<LOD	<LOD	<LOD	<LOD	51,3	0,064	97,85
Jouhineva	15-08b	76	Pyrite	46,08	<LOD	0,146	<LOD	<LOD	<LOD	<LOD	<LOD	<LOD	<LOD	52,07	<LOD	98,40
Jouhineva	15-08b	77	Pyrite	46,18	<LOD	0,147	<LOD	<LOD	<LOD	<LOD	<LOD	0,043	0,06	51,71	<LOD	98,15
Jouhineva	15-08b	78	Arsenopyrite	29,6	4,6	0,078	<LOD	<LOD	<LOD	<LOD	47,94	0,061	<LOD	19,67	0,037	101,99
Jouhineva	15-08b	79	Arsenopyrite	30,17	4,1	0,074	<LOD	<LOD	<LOD	<LOD	47,32	0,042	0,044	19,92	<LOD	101,77
Jouhineva	15-08b	80	Arsenopyrite	27,48	5,79	0,163	<LOD	<LOD	<LOD	<LOD	49,91	0,04	0,083	17,43	<LOD	100,93
Jouhineva	15-08b	81	Arsenopyrite	26,38	6,82	0,236	0,084	<LOD	<LOD	<LOD	50,66	<LOD	0,066	17,07	<LOD	101,32
Jouhineva	15-08b	82	Arsenopyrite	27,04	6,39	0,189	<LOD	<LOD	<LOD	0,012	50,43	<LOD	<LOD	17,53	<LOD	101,62
Jouhineva	15-08b	83	Chalcopyrite	29,62	0,025	<LOD	34,17	0,045	0,026	<LOD	0,631	0,037	<LOD	34,05	<LOD	98,60
Jouhineva	15-08b	84	Chalcopyrite	30,04	<LOD	<LOD	33,38	0,028	<LOD	<LOD	0,359	<LOD	0,067	35,3	0,034	99,21
Jouhineva	15-08b	85	Chalcopyrite	29,77	0,056	<LOD	33,19	<LOD	<LOD	<LOD	0,572	<LOD	<LOD	33,83	<LOD	97,48
Jouhineva	15-08b	86	Chalcopyrite	29,28	<LOD	<LOD	33,01	0,022	<LOD	<LOD	0,125	<LOD	<LOD	31,89	<LOD	94,33
Jouhineva	15-08b	87	Chalcopyrite	29,01	<LOD	<LOD	33,74	<LOD	0,029	<LOD	0,2	<LOD	<LOD	30,6	0,082	93,66
Jouhineva	15-08b	88	Arsenopyrite	30,22	3,28	0,09	<LOD	<LOD	<LOD	<LOD	48,6	<LOD	<LOD	18,04	<LOD	100,27
Jouhineva	15-08b	89	Arsenopyrite	30,03	3,94	0,134	<LOD	0,016	<LOD	0,016	49,58	<LOD	<LOD	18,41	<LOD	102,14

Deposit	sample	#	Mineral	Fe (wt%)	Co (wt%)	Ni (wt%)	Cu (wt%)	Ag (wt%)	Au (wt%)	Zn (wt%)	As (wt%)	Sb (wt%)	Bi (wt%)	S (wt%)	Hg (wt%)	Total (wt%)
Jouhineva	15-08b	90	Arsenopyrite	30,57	3,39	0,097	<LOD	0,012	<LOD	0,012	48,97	<LOD	<LOD	18,87	<LOD	102,01
Jouhineva	15-08b	91	Arsenopyrite	28,19	5,07	0,286	<LOD	<LOD	<LOD	<LOD	50,9	0,051	<LOD	17,14	<LOD	101,68
Jouhineva	15-08b	92	Arsenopyrite	30,64	3,45	0,104	<LOD	<LOD	<LOD	<LOD	47,59	0,05	<LOD	18,65	<LOD	100,56
Jouhineva	15-08b	93	Pyrite	46,04	<LOD	0,153	0,355	0,013	<LOD	<LOD	0,051	0,034	<LOD	51,44	<LOD	98,13
Jouhineva	15-08b	94	Pyrite	45,82	<LOD	0,173	0,081	<LOD	<LOD	0,012	0,047	<LOD	0,042	51,08	<LOD	97,29
Jouhineva	15-08b	95	Pyrite	46,38	<LOD	0,087	<LOD	<LOD	<LOD	<LOD	0,023	<LOD	<LOD	52,73	<LOD	99,26
Jouhineva	15-08b	96	Pyrite	44,45	<LOD	0,178	2,39	0,038	<LOD	<LOD	<LOD	0,03	<LOD	50,97	0,041	98,12
Jouhineva	15-08b	97	Pyrite	46,21	<LOD	0,108	<LOD	<LOD	<LOD	<LOD	0,084	<LOD	<LOD	52,72	<LOD	99,12
Jouhineva	15-08b	98	Arsenopyrite	31,76	2,12	0,036	0,232	0,017	<LOD	<LOD	45,25	0,031	<LOD	20,22	<LOD	99,67
Jouhineva	15-08b	99	Arsenopyrite	29,43	3,96	0,165	<LOD	<LOD	<LOD	<LOD	49,86	0,069	0,045	17,57	<LOD	101,12
Jouhineva	15-08b	100	Arsenopyrite	27,98	5,86	0,152	<LOD	<LOD	<LOD	<LOD	48,43	0,086	0,099	18,37	0,045	101,05
Jouhineva	15-08b	101	Arsenopyrite	28,88	4,53	0,135	<LOD	<LOD	<LOD	<LOD	49,11	0,041	<LOD	18,38	0,049	101,14
Jouhineva	15-08b	102	Arsenopyrite	29,98	3,63	0,109	0,142	<LOD	<LOD	<LOD	48,72	<LOD	0,108	18,56	0,046	101,31
Jouhineva	15-08b	103	Arsenopyrite	30,53	3,38	0,092	<LOD	<LOD	<LOD	<LOD	48,86	0,08	<LOD	18,85	<LOD	101,79
Jouhineva	15-08b	104	Arsenopyrite	31,88	2,34	0,042	<LOD	<LOD	<LOD	<LOD	47,26	0,073	0,157	20,26	<LOD	102,08
Jouhineva	15-08b	105	Arsenopyrite	28,41	4,5	0,192	<LOD	<LOD	<LOD	<LOD	49,59	0,102	<LOD	17,74	<LOD	100,55
Jouhineva	15-08b	106	Arsenopyrite	32,52	1,75	0,034	<LOD	<LOD	<LOD	<LOD	46,93	0,063	0,069	20,12	<LOD	101,49
Jouhineva	15-08b	107	Arsenopyrite	31,46	2,36	0,048	0,274	<LOD	<LOD	<LOD	47,65	0,049	0,044	19,6	<LOD	101,50
Jouhineva	15-08b	108	Arsenopyrite	28,8	4,62	0,198	<LOD	<LOD	<LOD	<LOD	49,97	<LOD	<LOD	17,74	<LOD	101,40
Jouhineva	15-08b	109	Arsenopyrite	28,79	4,59	0,214	0,282	0,012	<LOD	<LOD	50,28	<LOD	<LOD	17,71	<LOD	101,88
Jouhineva	15-08b	110	Arsenopyrite	28,93	4,45	0,208	<LOD	<LOD	<LOD	<LOD	49,86	0,066	<LOD	17,81	<LOD	101,37
Jouhineva	15-08b	111	Arsenopyrite	28,81	4,7	0,241	0,088	<LOD	<LOD	<LOD	50,36	0,036	<LOD	17,75	<LOD	101,99
Jouhineva	15-08b	112	Arsenopyrite	31,33	2,77	0,063	0,094	<LOD	<LOD	<LOD	48,08	0,085	<LOD	19,09	<LOD	101,54
Jouhineva	15-08b	113	Arsenopyrite	32,32	1,98	0,019	<LOD	<LOD	<LOD	<LOD	46,92	<LOD	0,063	19,32	0,044	100,71
Jouhineva	15-08b	114	Arsenopyrite	30,99	2,92	0,062	0,124	<LOD	<LOD	<LOD	47,73	0,041	0,122	18,92	<LOD	100,91
Jouhineva	15-08b	115	Arsenopyrite	32,19	1,5	0,166	0,084	<LOD	<LOD	0,011	48,37	<LOD	0,12	18,89	<LOD	101,35
Jouhineva	15-08b	116	Arsenopyrite	31,84	2,21	0,047	<LOD	<LOD	<LOD	<LOD	46,99	<LOD	0,083	19,95	<LOD	101,18
Jouhineva	15-08b	117	Arsenopyrite	31,63	2,2	0,019	<LOD	<LOD	<LOD	<LOD	46,82	<LOD	<LOD	19,38	<LOD	100,06
Jouhineva	20-08a	118	Arsenopyrite	33,05	0,936	0,061	0,092	<LOD	<LOD	0,014	47,4	0,062	<LOD	19,76	<LOD	101,40
Jouhineva	20-08a	119	Arsenopyrite	32,53	1,31	0,185	<LOD	0,012	<LOD	<LOD	47,89	0,037	<LOD	19,36	<LOD	101,36
Jouhineva	20-08a	120	Arsenopyrite	32,68	1,24	0,162	<LOD	<LOD	<LOD	0,013	48,29	<LOD	<LOD	18,95	<LOD	101,34
Jouhineva	20-08a	121	Arsenopyrite	32,73	1,29	0,231	<LOD	<LOD	<LOD	0,014	48,04	<LOD	<LOD	19,73	<LOD	102,04
Jouhineva	20-08a	122	Chalcopyrite	29,97	<LOD	<LOD	34,22	0,033	<LOD	0,014	0,159	<LOD	<LOD	35,06	<LOD	99,48
Jouhineva	20-08a	123	Chalcopyrite	29,96	<LOD	<LOD	33,52	<LOD	<LOD	<LOD	0,149	<LOD	0,062	35,21	<LOD	98,90
Jouhineva	20-08a	124	Chalcopyrite	29,93	<LOD	<LOD	33,34	0,012	<LOD	<LOD	0,031	<LOD	0,152	34,98	<LOD	98,45
Jouhineva	20-08a	125	Chalcopyrite	29,63	<LOD	<LOD	34,29	<LOD	<LOD	<LOD	<LOD	<LOD	<LOD	35,14	<LOD	99,09
Jouhineva	20-08a	126	Chalcopyrite	30,06	<LOD	<LOD	33,97	0,037	<LOD	0,011	<LOD	<LOD	<LOD	34,79	<LOD	98,90
Jouhineva	20-08a	127	Chalcopyrite	29,83	<LOD	<LOD	34,39	<LOD	0,032	<LOD	<LOD	<LOD	0,087	34,2	<LOD	98,58
Jouhineva	20-08a	128	Chalcopyrite	29,87	<LOD	<LOD	33,66	0,015	<LOD	<LOD	0,139	<LOD	<LOD	34,5	<LOD	98,22
Jouhineva	20-08a	129	Tennantite	5,83	<LOD	<LOD	41,53	0,045	<LOD	2,53	20,04	<LOD	<LOD	28,56	0,035	98,61
Jouhineva	20-08a	130	Tennantite	5,53	<LOD	<LOD	41,28	0,03	<LOD	2,71	20,15	0,092	<LOD	28,21	0,034	98,04
Jouhineva	20-08a	131	Tennantite	5,85	<LOD	<LOD	41,9	0,028	<LOD	2,91	19,7	0,185	<LOD	28,92	<LOD	99,50
Jouhineva	20-08a	132	Chalcopyrite	29,32	<LOD	<LOD	33,55	0,041	<LOD	0,059	0,573	<LOD	<LOD	35,03	<LOD	98,60
Jouhineva	20-08a	133	Tennantite	6,19	<LOD	<LOD	41,76	0,035	<LOD	2,92	19,27	<LOD	<LOD	29,23	<LOD	99,43
Jouhineva	20-08a	134	Tennantite	14,19	0,036	0,157	32,1	0,195	<LOD	4,08	13,64	<LOD	0,042	33,75	0,066	98,26
Jouhineva	20-08a	135	Chalcopyrite	13,53	0,038	0,121	33,15	0,154	<LOD	4,18	14,07	0,549	<LOD	33,5	0,079	99,37
Jouhineva	20-08a	136	Tennantite	15,71	0,029	0,211	30,14	0,184	<LOD	3,59	13,81	<LOD	<LOD	36,01	<LOD	99,69
Jouhineva	20-08a	137	Tennantite	14,86	0,051	0,176	30,64	0,151	<LOD	2,87	14,9	0,079	<LOD	34,26	<LOD	98,00
Jouhineva	20-08a	138	Chalcopyrite	30,09	<LOD	<LOD	34,38	0,019	<LOD	<LOD	<LOD	<LOD	<LOD	35,48	<LOD	100,02
Jouhineva	20-08a	139	Chalcopyrite	30,14	<LOD	<LOD	34,01	0,015	<LOD	<LOD	0,06	<LOD	<LOD	35,44	<LOD	99,69
Jouhineva	20-08a	140	Chalcopyrite	30,12	<LOD	<LOD	34,77	0,019	<LOD	<LOD	<LOD	<LOD	0,12	35,29	0,043	100,36
Jouhineva	20-08a	141	Chalcopyrite	30,19	<LOD	<LOD	33,19	0,014	<LOD	<LOD	0,027	<LOD	<LOD	35,4	<LOD	98,83
Jouhineva	20-08a	142	Chalcopyrite	30,17	<LOD	<LOD	34,14	<LOD	0,031	<LOD	<LOD	<LOD	0,061	35,14	<LOD	99,56
Jouhineva	20-08a	143	Arsenopyrite	32,73	1,3	0,195	<LOD	0,025	<LOD	<LOD	48,06	0,03	0,054	18,5	<LOD	100,89
Jouhineva	20-08a	144	Arsenopyrite	32,73	1,22	0,181	<LOD	0,017	<LOD	<LOD	47,89	<LOD	0,112	19,25	0,084	101,56
Jouhineva	20-08a	145	Arsenopyrite	32,9	1,21	0,182	<LOD	<LOD	<LOD	<LOD	47,96	0,026	0,067	19,25	0,088	101,73
Jouhineva	20-08a	146	Arsenopyrite	34,25	0,494	0,024	<LOD	<LOD	<LOD	<LOD	45,52	0,086	<LOD	21,58	<LOD	101,96
Jouhineva	20-08a	147	Arsenopyrite	33,85	0,678	0,058	<LOD	<LOD	<LOD	<LOD	47,04	0,033	<LOD	20,28	<LOD	101,95
Jouhineva	20-08a	148	Tennantite	23,87	0,035	0,187	26,12	0,14	<LOD	1,09	8,3	<LOD	<LOD	37,09	<LOD	96,85
Jouhineva	20-08a	149	Tennantite	23,09	0,024	0,207	26,84	0,132	<LOD	1,18	8,95	0,058	<LOD	36,98	0,045	97,51
Jouhineva	20-08a	150	Cubanite	35,94	0,024	0,162	18,22	0,138	<LOD	<LOD	0,457	<LOD	<LOD	42,52	<LOD	97,46
Jouhineva	20-08a	151	Pyrite	37,63	0,068	0,249	14,41	0,16	<LOD	<LOD	0,697	<LOD	<LOD	44,31	<LOD	97,54
Jouhineva	20-08a	152	Pyrite	41,38	0,038	0,224	8,11	0,096	<LOD	<LOD	0,514	<LOD	<LOD	47,72	0,048	98,13
Jouhineva	20-08a	153	Cubanite	36,18	0,035	0,224	16,5	0,113	<LOD	0,017	0,943	0,032	0,128	42,67	<LOD	96,87
Jouhineva	20-08a	154	Chalcopyrite	29,99	<LOD	<LOD	33,72	0,014	<LOD	<LOD	0,053	<LOD	<LOD	34,98	0,047	98,80
Jouhineva	20-08a	155	Chalcopyrite	30,08	<LOD	<LOD	34,1	0,02	<LOD	<LOD	0,034	<LOD	<LOD	35,46	0,06	99,77
Jouhineva	20-08a	156	Chalcopyrite	30,02	<LOD	<LOD	34,08	0,014	0,021	<LOD	0,163	<LOD	0,07	35,27	0,038	99,68
Jouhineva	20-08a	157	Chalcopyrite	30,04	<LOD	<LOD	34,71	<LOD	<LOD	<LOD	0,056	<LOD	<LOD	35,19	<LOD	100,00
Jouhineva	20-08a	158	Chalcopyrite	29,86	<LOD	<LOD	33,97	0,026	<LOD	<LOD	0,025	<LOD	0,182	34,9	<LOD	98,96
Jouhineva	20-08a	159	Tennantite	6	<LOD	<LOD	41,42	0,018	<LOD	2,36	20,04	0,041	<LOD	29,87	<LOD	99,77
Jouhineva	20-08a	160	Tennantite	5,27	<LOD	<LOD	41,12	<LOD	<LOD	2,9	20,42	<LOD	<LOD	28,58	<LOD	98,29
Jouhineva	20-08a	161	Tennantite	5,37	<LOD	<LOD	42,51	0,034	<LOD	2,82	20,08	0,037	<LOD	28,89	0,038	99,82
Jouhineva	20-08a	162	Tennantite	5,6	<LOD	<LOD	41,85	0,051	<LOD	2,44	19,95	<LOD	<LOD	29,85	0,037	99,79
Jouhineva	20-08a	163	Tennantite	5,05	<LOD	<LOD	41,46	0,073	<LOD	3,07	20,12	<LOD	<LOD	29,06	<LOD	98,87
Jouhineva	20-16	164	Arsenopyrite	32,54	1,23	0,143	<LOD	0,012	<LOD	0,011	48,4	0,036	0,079	19,56	<LOD	102,04
Jouhineva	20-16	165	Arsenopyrite	33,42	0,949	0,045	<LOD	<LOD	<LOD	<LOD	47,21	0,056	0,053	20,24	<LOD	101,97
Jouhineva	20-16	166	Arsenopyrite	32,56	1,19	0,148	<LOD	<LOD	<LOD	<LOD	48,46	0,028	<LOD	19,37	0,076	101,83
Jouhineva	20-16	167	Arsenopyrite	31,35	1,94	0,494	<LOD	<LOD	<LOD	<LOD	49,08	0,028	<LOD	18,12	0,039	101,08
Jouhineva	20-16	168	Arsenopyrite	31,26	2	0,539	<LOD	0,015	<LOD	<LOD	49,67	0,053	0,06	17,79	<LOD	101,43
Jouhineva	20-16	169	Arsenopyrite	32,34	1,36	0,213	<LOD	<LOD	<LOD	<LOD	48,63	<LOD	<LOD	19,15	<LOD	101,73
Jouhineva	20-16	170	Arsenopyrite	32,17	1,49	0,225	<LOD	0,038	<LOD	<LOD	48,55	0,06	0,111	19,03	<LOD	101,75
Jouhineva	20-16	171	Chalcopyrite	30,13	<LOD	<LOD	33,9	0,031	<LOD	<LOD	0,361	<LOD	<LOD	35,41	<LOD	99,87
Jouhineva	20-16	172	Chalcopyrite	30,13	<LOD	<LOD	34,02	0,045	<LOD	<LOD	0,243	<LOD	<LOD	33,71	<LOD	98,18
Jouhineva	20-16	173	Chalcopyrite	30,19	<LOD	<LOD	33,85	0,049	<LOD	<LOD	0,291	0,051	<LOD	35,24	0,045	99,73
Jouhineva	20-16	174	Arsenopyrite	32,95	1,06	0,119	<LOD	<LOD	<LOD	<LOD	48,31	0,051	<LOD	19,61	<LOD	102,11
Jouhineva	20-16	175	Arsenopyrite	31,3	1,93	0,544	<LOD	<LOD	<LOD	<LOD	50,09	0,037	<LOD	17,48	<LOD	101,38
Jouhineva	20-16	176	Arsenopyrite	32,69	1,28	0,185	<LOD	<LOD	<LOD	<LOD	47,6	0,041	0,077	18,95	0,047	100,93
Jouhineva	20-16	177	Arsenopyrite	32,36	1,35	0,211	<LOD	<LOD	<LOD	<LOD	48,52	<LOD	0,052	18,73	<LOD	101,26
Jouhineva	20-16	178	Arsenopyrite	32,32	1,42	0,245	0,077	<LOD	<LOD	<LOD	48,79	0,034	<LOD	18,64	<LOD	101,53
Jouhineva	20-16	179	Arsenopyrite	32,44	1,26	0,203	<LOD	<LOD	<LOD	<LOD	48,52	0,061	0,099	18,91	<LOD	101,50
Jouhineva	20-16	180	Arsenopyrite	33,29	0,812	0,088	<LOD	<LOD	<LOD	0,011	47,74	<LOD	<LOD	19,79	<LOD	101,75
Jouhineva	20-16	181	Arsenopyrite	33,47	0,845	0,048	<LOD	<LOD	<LOD	<LOD	47,28	0,065	0,131	19,97	<LOD	101,81
Jouhineva	20-16	182	Arsenopyrite	33,76	0,632	0,049	0,163	<LOD	<LOD	0,011	46,85	<LOD	<LOD	20,16	<LOD	101,66
Jouhineva	20-16	183	Arsenopyrite	31,32	1,97	0,432	<LOD	<LOD	<LOD	<LOD	49,73	0,065	0,046	17,6	<LOD	101,20
Jouhineva	20-16	184	Arsenopyrite	31,55	1,97	0,369	<LOD	<LOD	<LOD	<LOD	49,54	0,028	<LOD	18,18	<LOD	101,64
Jouhineva	20-16	185	Arsenopyrite	31,75	1,94	0,356	<LOD	<LOD	<LOD	<LOD	48,97	<LOD	<LOD	18,54	<LOD	101,60
Jouhineva	20-16	186	Arsenopyrite	32,58	1,38	0,193	<LOD	<LOD	<LOD	<LOD	48,65	<LOD	0,102	18,93	0,048	101,96
Jouhineva	20-16	187	Pyrite	46,53	<LOD	<LOD	<LOD	<LOD	<LOD	<LOD	0,211	0,026	0,094	53,21	<LOD	100,09
Jouhineva	20-16	188	Pyrite	46,39	<LOD	<LOD	0,191	<LOD	<LOD	0,021	0,182	<LOD	<LOD	53,38	<LOD	100,20

Deposit	sample	#	Mineral	Fe (wt%)	Co (wt%)	Ni (wt%)	Cu (wt%)	Ag (wt%)	Au (wt%)	Zn (wt%)	As (wt%)	Sb (wt%)	Bi (wt%)	S (wt%)	Hg (wt%)	Total (wt%)
Huhta	22-02	1	Arsenopyrite	34,27	<LOD	<LOD	<LOD	0,021	<LOD	0,021	43,99	0,08	<LOD	21,52	<LOD	99,90
Huhta	22-02	2	Arsenopyrite	33,76	0,015	<LOD	<LOD	<LOD	<LOD	<LOD	43,56	0,06	<LOD	20,95	<LOD	98,35
Huhta	22-02	3	Arsenopyrite	34,56	<LOD	<LOD	<LOD	<LOD	<LOD	<LOD	44,72	0,055	0,071	20,92	<LOD	100,34
Huhta	22-02	4	Arsenopyrite	34,83	<LOD	<LOD	<LOD	<LOD	<LOD	<LOD	45,03	0,097	<LOD	21,77	<LOD	101,75
Huhta	22-02	5	Arsenopyrite	34,72	<LOD	<LOD	<LOD	<LOD	<LOD	<LOD	44,67	0,052	0,051	21,95	<LOD	101,45
Huhta	22-02	6	Arsenopyrite	34,76	<LOD	<LOD	<LOD	<LOD	<LOD	<LOD	44,98	0,068	<LOD	21,4	<LOD	101,23
Huhta	22-02	7	Arsenopyrite	34,44	<LOD	<LOD	<LOD	0,011	<LOD	<LOD	45,16	0,049	<LOD	21,62	<LOD	101,38
Huhta	22-02	8	Arsenopyrite	34,27	<LOD	0,011	<LOD	<LOD	<LOD	<LOD	45,14	0,174	<LOD	20,86	<LOD	100,46
Huhta	22-02	9	Arsenopyrite	34,78	<LOD	<LOD	0,166	0,037	<LOD	<LOD	45,72	0,177	0,071	21,13	<LOD	102,10
Huhta	22-02	10	Arsenopyrite	34,9	<LOD	<LOD	<LOD	<LOD	<LOD	<LOD	45,37	<LOD	<LOD	21,55	<LOD	101,84
Huhta	22-02	11	Arsenopyrite	34,62	0,024	<LOD	<LOD	0,024	<LOD	<LOD	46,1	0,027	<LOD	21	<LOD	101,86
Huhta	22-02	12	Arsenopyrite	34,66	<LOD	<LOD	<LOD	<LOD	<LOD	<LOD	44,92	0,106	<LOD	20,83	<LOD	100,55
Huhta	22-02	13	Arsenopyrite	34,8	<LOD	<LOD	0,097	0,021	<LOD	<LOD	45,33	<LOD	<LOD	21,15	<LOD	101,41
Huhta	22-02	14	Arsenopyrite	34,44	<LOD	<LOD	<LOD	<LOD	<LOD	<LOD	46,76	<LOD	<LOD	20,33	<LOD	101,59
Huhta	22-02	15	Arsenopyrite	33,8	0,204	0,065	<LOD	<LOD	<LOD	<LOD	48,44	<LOD	<LOD	19,16	0,047	101,72
Huhta	22-02	16	Arsenopyrite	34,12	<LOD	<LOD	<LOD	<LOD	<LOD	<LOD	46,34	<LOD	0,075	20,53	<LOD	101,17
Huhta	22-02	17	Arsenopyrite	34,33	0,016	<LOD	<LOD	<LOD	<LOD	0,016	46,41	<LOD	<LOD	20,49	<LOD	101,30
Huhta	22-02	18	Arsenopyrite	33,58	0,205	0,108	<LOD	0,024	<LOD	<LOD	48,97	<LOD	<LOD	18,61	<LOD	101,54
Huhta	22-02	19	Arsenopyrite	33,75	0,162	0,048	<LOD	<LOD	<LOD	<LOD	48,4	<LOD	<LOD	19,12	<LOD	101,50
Huhta	22-02	20	Arsenopyrite	33,82	0,208	0,055	<LOD	<LOD	<LOD	<LOD	48,5	0,033	0,064	19,12	0,049	101,85
Huhta	22-02	21	Arsenopyrite	34,64	0,01	<LOD	<LOD	<LOD	<LOD	<LOD	46,99	0,045	0,072	20,66	<LOD	102,44
Huhta	22-02	22	Arsenopyrite	34,57	0,016	0,014	<LOD	0,019	<LOD	<LOD	46,62	0,057	0,064	20,4	<LOD	101,78
Huhta	22-02	23	Pyrite	46,42	<LOD	<LOD	<LOD	<LOD	<LOD	<LOD	0,048	<LOD	<LOD	52,01	<LOD	98,49
Huhta	22-02	24	Pyrite	46,47	<LOD	<LOD	<LOD	<LOD	<LOD	<LOD	0,034	<LOD	<LOD	52,94	<LOD	99,44
Huhta	22-02	25	Pyrite	46,53	<LOD	<LOD	0,118	<LOD	<LOD	0,01	<LOD	<LOD	0,057	52,2	<LOD	98,94
Huhta	22-02	26	Pyrite	46,21	<LOD	<LOD	<LOD	<LOD	<LOD	0,015	<LOD	<LOD	<LOD	51,69	0,047	97,96
Huhta	22-02	27	Pyrite	46,09	<LOD	<LOD	<LOD	<LOD	<LOD	0,017	<LOD	<LOD	0,079	51,33	<LOD	97,52
Huhta	22-02	28	Pyrite	45,91	<LOD	<LOD	<LOD	<LOD	<LOD	0,022	<LOD	<LOD	<LOD	51,97	0,055	97,96
Huhta	22-02	29	Pyrite	46,3	<LOD	<LOD	<LOD	0,025	<LOD	0,013	<LOD	<LOD	<LOD	52,15	<LOD	98,50
Huhta	22-07	30	Electrum	1,49	<LOD	<LOD	<LOD	35,13	61,02	<LOD	2,9	<LOD	<LOD	0,09	<LOD	100,63
Huhta	22-07	31	Chalcopyrite	30,09	<LOD	<LOD	32,64	0,029	0,027	<LOD	1,78	<LOD	<LOD	34,86	<LOD	99,43
Huhta	22-07	32	Chalcopyrite	30,25	<LOD	<LOD	32,6	<LOD	<LOD	<LOD	1,83	<LOD	<LOD	34,68	<LOD	99,38
Huhta	22-07	33	Chalcopyrite	30,27	<LOD	<LOD	33,43	<LOD	<LOD	<LOD	0,184	<LOD	<LOD	35,43	<LOD	99,33
Huhta	22-07	34	Arsenopyrite	33,83	<LOD	0,035	<LOD	<LOD	<LOD	0,018	48,61	<LOD	<LOD	19,24	<LOD	101,83
Huhta	22-07	35	Arsenopyrite	33,55	0,138	0,075	<LOD	<LOD	<LOD	<LOD	48,63	<LOD	0,055	18,41	<LOD	100,87
Huhta	22-07	36	Pyrite	46,33	<LOD	<LOD	<LOD	0,017	<LOD	<LOD	0,023	<LOD	<LOD	51,34	<LOD	97,72
Huhta	22-07	37	Pyrite	46,37	<LOD	<LOD	<LOD	<LOD	<LOD	<LOD	0,519	<LOD	<LOD	52	<LOD	98,92
Huhta	22-07	38	Chalcopyrite	30,3	<LOD	<LOD	33,65	0,031	<LOD	<LOD	0,173	<LOD	<LOD	35,45	<LOD	99,64
Huhta	22-07	39	Chalcopyrite	30,41	<LOD	<LOD	33,15	0,017	<LOD	<LOD	0,126	<LOD	0,067	35,67	<LOD	99,49
Huhta	22-07	40	Pyrite	46,23	<LOD	<LOD	<LOD	<LOD	0,02	<LOD	0,238	<LOD	<LOD	52,12	<LOD	98,61
Huhta	22-07	41	Pyrite	46,58	<LOD	<LOD	<LOD	<LOD	<LOD	<LOD	0,155	<LOD	0,101	52,16	<LOD	99,08
Huhta	22-07	42	Pyrite	46,26	<LOD	<LOD	<LOD	<LOD	<LOD	<LOD	0,662	<LOD	0,126	52,31	<LOD	99,37
Huhta	22-07	43	Arsenopyrite	34,24	<LOD	<LOD	<LOD	<LOD	<LOD	<LOD	46,73	<LOD	0,067	20,56	0,078	101,67
Huhta	22-07	44	Arsenopyrite	34,48	<LOD	<LOD	<LOD	<LOD	<LOD	<LOD	46,1	0,043	0,055	20,4	<LOD	101,13
Huhta	22-07	45	Pyrite	45,77	<LOD	0,013	<LOD	<LOD	<LOD	0,011	<LOD	<LOD	0,06	50,24	<LOD	96,10
Huhta	22-07	46	Pyrite	46,52	Löl	0,008	<LOD	0,011	<LOD	0,015	<LOD	<LOD	<LOD	52,17	<LOD	98,76
Huhta	22-07	47	Pyrite	46,19	<LOD	<LOD	<LOD	<LOD	<LOD	<LOD	0,031	0,036	<LOD	52,24	<LOD	98,51
Huhta	22-07	48	Pyrite	45,83	<LOD	<LOD	<LOD	<LOD	<LOD	<LOD	<LOD	<LOD	<LOD	52,57	0,057	98,47
Huhta	22-07	49	Pyrite	43,89	<LOD	<LOD	0,093	<LOD	<LOD	0,022	0,021	<LOD	<LOD	48,09	<LOD	92,12
Huhta	22-07	51	Arsenopyrite	34,38	<LOD	<LOD	<LOD	<LOD	<LOD	<LOD	47,1	<LOD	<LOD	19,68	<LOD	101,16
Huhta	22-07	52	Pyrrhotite	60,14	<LOD	<LOD	<LOD	0,021	<LOD	0,014	1,41	<LOD	<LOD	38,74	<LOD	100,32
Huhta	22-07	53	Pyrrhotite	59,95	<LOD	<LOD	<LOD	0,012	<LOD	<LOD	1,56	<LOD	<LOD	38,58	<LOD	100,14
Huhta	22-07	55	Chalcopyrite	30,1	<LOD	<LOD	32,58	0,018	<LOD	<LOD	1,94	0,042	<LOD	35,25	<LOD	99,94
Huhta	22-07	56	Chalcopyrite	30,7	<LOD	<LOD	30,42	0,01	<LOD	<LOD	5,7	<LOD	0,049	34,45	0,075	101,41
Huhta	22-07	57	Chalcopyrite	30,53	<LOD	<LOD	29,33	<LOD	<LOD	<LOD	6,48	<LOD	0,043	33,68	0,034	100,10
Huhta	22-07	58	Chalcopyrite	30,44	<LOD	<LOD	32,76	<LOD	<LOD	<LOD	1,98	<LOD	0,064	34,91	<LOD	100,16
Huhta	22-07	59	Chalcopyrite	30,53	<LOD	<LOD	31,9	0,031	<LOD	0,02	1,37	<LOD	<LOD	35,88	0,067	99,80
Huhta	22-07	60	Chalcopyrite	30,06	<LOD	<LOD	32,8	0,016	<LOD	<LOD	2,02	<LOD	0,115	34,38	<LOD	99,41
Huhta	22-07	61	Arsenopyrite	33,88	0,127	0,047	<LOD	0,014	<LOD	<LOD	48,83	0,083	0,071	19,07	<LOD	102,16
Huhta	22-07	62	Arsenopyrite	33,98	0,059	0,026	0,104	0,015	<LOD	<LOD	48,2	<LOD	<LOD	19,28	<LOD	101,71
Huhta	22-08	63	Arsenopyrite	34,91	<LOD	<LOD	<LOD	<LOD	<LOD	<LOD	44,93	0,088	<LOD	21,44	<LOD	101,42
Huhta	22-08	64	Arsenopyrite	33,75	<LOD	0,013	<LOD	<LOD	<LOD	<LOD	49,06	0,07	<LOD	18,46	<LOD	101,38
Huhta	22-08	65	Arsenopyrite	33,71	<LOD	<LOD	<LOD	0,043	<LOD	<LOD	48,91	<LOD	0,087	19,04	<LOD	101,81
Huhta	22-08	66	Arsenopyrite	33,84	<LOD	<LOD	<LOD	<LOD	<LOD	<LOD	48,96	<LOD	0,062	18,99	<LOD	101,86
Huhta	22-08	67	Chalcopyrite	30,11	<LOD	<LOD	33,1	0,017	<LOD	<LOD	1,72	<LOD	<LOD	34,67	<LOD	99,64
Huhta	22-08	68	Chalcopyrite	29,84	<LOD	<LOD	33,19	0,034	<LOD	<LOD	1,96	<LOD	<LOD	33,56	<LOD	98,63
Huhta	22-08	69	Chalcopyrite	29,75	<LOD	<LOD	32,41	0,029	<LOD	<LOD	1,84	<LOD	<LOD	33,17	<LOD	97,23
Huhta	22-08	70	Chalcopyrite	29,19	<LOD	<LOD	32,84	<LOD	<LOD	<LOD	1,39	<LOD	<LOD	34,94	<LOD	98,43
Huhta	22-08	71	Pyrite	45,83	<LOD	<LOD	<LOD	<LOD	<LOD	<LOD	0,609	<LOD	<LOD	49,92	<LOD	96,37
Huhta	22-08	72	Pyrite	43,81	<LOD	<LOD	<LOD	0,015	<LOD	<LOD	2,33	<LOD	<LOD	49,41	<LOD	95,63
Huhta	22-08	73	Pyrite	45,42	<LOD	<LOD	0,138	0,023	<LOD	0,011	2,02	0,026	<LOD	52,74	0,056	100,44
Huhta	22-08	74	Pyrite	45,24	<LOD	<LOD	<LOD	<LOD	<LOD	<LOD	1,65	<LOD	<LOD	51,8	<LOD	98,70
Huhta	22-08	77	Electrum	4,24	<LOD	<LOD	<LOD	14,54	73,79	<LOD	7,64	0,064	<LOD	2,27	<LOD	102,54
Huhta	22-08	78	Electrum	21,55	<LOD	<LOD	<LOD	8,85	40,17	<LOD	19,82	<LOD	<LOD	12,79	<LOD	103,18
Huhta	22-08	80	Electrum	2,45	<LOD	<LOD	<LOD	17,63	76,6	<LOD	4,31	<LOD	<LOD	0,401	<LOD	101,41
Huhta	22-08	81	Electrum	2,36	<LOD	<LOD	<LOD	17,12	75,65	<LOD	4,61	<LOD	<LOD	0,231	<LOD	99,97
Huhta	22-08	82	Pyrite	46,43	<LOD	<LOD	<LOD	<LOD	<LOD	0,011	0,157	<LOD	0,071	53,27	0,035	99,98
Huhta	22-08	83	Pyrite	46,4	<LOD	<LOD	<LOD	0,018	<LOD	0,01	0,374	<LOD	0,049	52,81	<LOD	99,68
Huhta	22-08	84	Pyrite	46,27	<LOD	<LOD	<LOD	<LOD	<LOD	<LOD	0,25	<LOD	0,09	51,68	<LOD	98,30
Huhta	22-08	85	Pyrite	46,12	<LOD	<LOD	<LOD	<LOD	<LOD	<LOD	1,21	0,038	0,115	53,3	<LOD	100,81
Huhta	22-08	86	Pyrite	46,36	<LOD	<LOD	0,089	<LOD	<LOD	<LOD	0,205	<LOD	<LOD	52,58	<LOD	99,24
Huhta	22-08	87	Arsenopyrite	34,7	<LOD	<LOD	<LOD	<LOD	<LOD	<LOD	45,8	<LOD	0,1	21,02	<LOD	101,63
Huhta	22-08	88	Arsenopyrite	34,08	<LOD	<LOD	<LOD	0,011	<LOD	<LOD	47,73	<LOD	0,048	19,52	<LOD	101,43
Huhta	22-08	89	Arsenopyrite	34,13	<LOD	<LOD	<LOD	<LOD	<LOD	<LOD	48,21	0,057	<LOD	19,06	<LOD	101,47
Huhta	22-08	90	Pyrrhotite	57,14	<LOD	<LOD	<LOD	<LOD	<LOD	<LOD	5,79	<LOD	<LOD	33,85	<LOD	96,86
Huhta	22-08	91	Pyrrhotite	50,45	<LOD	<LOD	<LOD	<LOD	<LOD	<LOD	16,82	<LOD	0,082	31,07	<LOD	98,43
Huhta	22-08	92	Arsenopyrite	36,74	0,037	<LOD	<LOD	<LOD	<LOD	<LOD	43,78	<LOD	0,101	23,27	<LOD	103,98
Huhta	22-08	93	Pyrrhotite	58,6	<LOD	<LOD	<LOD	<LOD	<LOD	0,015	3,16	<LOD	0,099	38,37	<LOD	100,24
Huhta	22-08	94	Pyrrhotite	55,4	<LOD	<LOD	<LOD	<LOD	<LOD	0,016	10,25	<LOD	<LOD	33,37	<LOD	99,07
Huhta	22-08	95	Arsenopyrite	33,97	0,048	0,02	<LOD	<LOD	<LOD	0,01	47,61	<LOD	<LOD	19,08	<LOD	100,81
Huhta	22-08	96	Arsenopyrite	33,66	0,102	0,06	<LOD	<LOD	<LOD	<LOD	48,57	<LOD	0,133	18,37	<LOD	100,90
Huhta	22-08	97	Arsenopyrite	33,77	0,072	0,024	<LOD	<LOD	<LOD	<LOD	48,51	<LOD	<LOD	19,11	0,051	101,55
Huhta	22-13b	98	Pyrite	43,32	<LOD	<LOD	0,205	<LOD	<LOD	<LOD	<LOD	<LOD	<LOD	49,88	<LOD	93,43
Huhta	22-13b	99	Pyrite	46,22	<LOD	0,033	<LOD	<LOD	<LOD	<LOD	<LOD	<LOD	<LOD	52,78	<LOD	99,05
Huhta	22-13b	100	Pyrite	46	<LOD	<LOD	<LOD	<LOD	<LOD	<LOD	0,048	<LOD	<LOD	54	<LOD	100,07
Huhta	22-13b	101	Pyrrhotite	59,23	<LOD	<LOD	0,165	<LOD	<LOD	0,014	<LOD	<LOD	<LOD	38,39	0,06	97,86
Huhta	22-13b	102	Pyrrhotite	58,84	<LOD	<LOD	<LOD	<LOD	<LOD	<LOD	<LOD	<LOD	<LOD	39,47	<LOD	98,33
Huhta	22-13b	104	Pyrrhotite	60,07	<LOD	<LOD	<LOD	<LOD	<LOD	<LOD	<LOD	<LOD	0,071	37,92	<LOD	98,07
Huhta	22-13b	105	Pyrrhotite	60,02	<LOD	<LOD	<LOD	<LOD	<LOD	<LOD	<LOD	<LOD	<LOD	38,83	<LOD	98,88

Deposit	sample	#	Mineral	Fe (wt%)	Co (wt%)	Ni (wt%)	Cu (wt%)	Ag (wt%)	Au (wt%)	Zn (wt%)	As (wt%)	Sb (wt%)	Bi (wt%)	S (wt%)	Hg (wt%)	Total (wt%)
Huhta	22-13b	106	Pyrrhotite	60,2	<LOD	<LOD	<LOD	<LOD	<LOD	0,027	0,048	<LOD	<LOD	38,99	<LOD	99,27
Huhta	22-13b	107	Chalcopyrite	29,56	<LOD	<LOD	33,29	0,014	<LOD	<LOD	<LOD	<LOD	<LOD	35,34	<LOD	98,23
Huhta	22-13b	108	Chalcopyrite	29,94	<LOD	<LOD	32,22	0,024	<LOD	<LOD	<LOD	<LOD	0,047	35,38	0,033	97,66
Huhta	22-13b	110	Chalcopyrite	32,35	<LOD	<LOD	30,41	0,028	<LOD	<LOD	<LOD	<LOD	<LOD	35,84	<LOD	98,63
Huhta	22-13b	111	Chalcopyrite	29,8	<LOD	<LOD	33,88	0,012	<LOD	0,013	<LOD	<LOD	<LOD	35,55	<LOD	99,30
Huhta	22-13b	112	Chalcopyrite	30,46	<LOD	<LOD	33,33	0,015	<LOD	<LOD	<LOD	<LOD	<LOD	35,33	<LOD	99,17
Huhta	22-13b	113	Arsenopyrite	32,29	0,572	0,375	0,11	0,011	<LOD	<LOD	49,43	<LOD	<LOD	17,33	<LOD	100,12
Huhta	22-13b	114	Arsenopyrite	33,09	0,365	0,225	<LOD	<LOD	<LOD	0,01	49,2	<LOD	<LOD	18,31	<LOD	101,22
Huhta	22-13b	115	Arsenopyrite	32,77	0,207	0,075	<LOD	<LOD	<LOD	<LOD	47,18	<LOD	<LOD	18,82	<LOD	99,13
Huhta	22-13b	116	Pyrrhotite	59,57	<LOD	<LOD	<LOD	<LOD	<LOD	<LOD	0,135	<LOD	0,083	38,79	<LOD	98,65
Huhta	22-13b	117	Pyrrhotite	60,4	<LOD	<LOD	<LOD	<LOD	<LOD	<LOD	<LOD	<LOD	<LOD	39,04	0,035	99,51
Huhta	22-13b	118	Pyrrhotite	60,43	<LOD	<LOD	<LOD	<LOD	0,026	<LOD	0,065	<LOD	0,115	38,42	<LOD	99,06
Huhta	22-13b	119	Arsenopyrite	34,34	0,032	0,03	<LOD	<LOD	<LOD	0,011	47,29	<LOD	<LOD	19,71	0,047	101,50
Huhta	22-13b	120	Arsenopyrite	34,68	<LOD	<LOD	<LOD	<LOD	<LOD	<LOD	44,56	0,038	<LOD	21,89	<LOD	101,21
Huhta	22-13b	121	Arsenopyrite	33,83	0,036	0,026	<LOD	<LOD	<LOD	<LOD	47,88	<LOD	<LOD	19,32	<LOD	101,11
Huhta	22-13b	122	Arsenopyrite	35,27	<LOD	<LOD	0,091	<LOD	<LOD	0,014	43,76	<LOD	0,058	22,98	<LOD	102,19
Huhta	22-13b	123	Arsenopyrite	33,62	0,031	0,017	0,109	0,048	<LOD	0,023	48,24	<LOD	<LOD	19,09	<LOD	101,18
Huhta	22-13b	124	Arsenopyrite	35,18	<LOD	<LOD	<LOD	<LOD	<LOD	<LOD	43,57	<LOD	<LOD	22,72	<LOD	101,50
Huhta	22-13b	125	Arsenopyrite	34,06	0,026	0,014	<LOD	<LOD	<LOD	<LOD	47,98	<LOD	<LOD	19,18	<LOD	101,31
Huhta	22-13b	126	Chalcopyrite	28,67	<LOD	<LOD	31,59	0,024	<LOD	<LOD	1,64	<LOD	<LOD	34,78	<LOD	96,70
Huhta	22-13b	127	Chalcopyrite	29,43	<LOD	<LOD	31,07	0,038	<LOD	0,01	2,3	<LOD	<LOD	36,11	<LOD	98,96
Huhta	22-13b	128	Chalcopyrite	28,91	<LOD	<LOD	26,36	0,029	<LOD	<LOD	8,12	<LOD	<LOD	31,63	<LOD	95,10
Huhta	22-13b	129	Chalcopyrite	29,44	<LOD	<LOD	30,04	0,024	<LOD	0,054	3,74	<LOD	0,074	34,28	<LOD	97,65
Huhta	22-13b	130	Pyrrhotite	60,47	<LOD	<LOD	<LOD	0,032	<LOD	<LOD	0,144	<LOD	<LOD	38,67	<LOD	99,36
Huhta	22-13b	131	Pyrrhotite	60,62	<LOD	<LOD	<LOD	<LOD	<LOD	<LOD	0,043	<LOD	<LOD	38,72	<LOD	99,47
Huhta	22-13b	132	Pyrrhotite	60,53	<LOD	<LOD	<LOD	0,011	<LOD	<LOD	<LOD	0,037	<LOD	38,36	0,038	99,05
Kurula	17-07	1	Arsenopyrite	33,27	0,225	0,394	<LOD	<LOD	<LOD	<LOD	48,62	<LOD	<LOD	19,13	<LOD	101,69
Kurula	17-07	2	Arsenopyrite	33,29	0,637	0,151	0,163	<LOD	<LOD	<LOD	48,01	<LOD	<LOD	19,68	<LOD	101,97
Kurula	17-07	3	Arsenopyrite	32,83	0,608	0,26	<LOD	<LOD	<LOD	<LOD	48,24	<LOD	<LOD	19,6	<LOD	101,56
Kurula	17-07	4	Chalcopyrite	29,78	<LOD	<LOD	33,73	0,017	<LOD	<LOD	0,07	<LOD	0,105	34,48	<LOD	98,20
Kurula	17-07	5	Chalcopyrite	30,16	<LOD	<LOD	33,67	0,024	<LOD	<LOD	<LOD	<LOD	<LOD	34,79	<LOD	98,73
Kurula	17-07	6	Chalcopyrite	30	<LOD	<LOD	34,01	<LOD	<LOD	<LOD	<LOD	<LOD	<LOD	34,94	<LOD	98,98
Kurula	17-07	7	Pyrrhotite	60,13	<LOD	0,019	<LOD	<LOD	<LOD	<LOD	<LOD	<LOD	<LOD	38,86	<LOD	99,07
Kurula	17-07	8	Pyrrhotite	60,16	<LOD	<LOD	<LOD	<LOD	0,052	<LOD	0,054	<LOD	<LOD	38,49	<LOD	98,81
Kurula	17-07	9	Pyrrhotite	60,2	<LOD	0,015	<LOD	<LOD	<LOD	<LOD	0,043	<LOD	<LOD	38,69	<LOD	99,08
Kurula	17-07	10	Rammelsbergite	7,89	0,108	25,81	<LOD	<LOD	<LOD	<LOD	59,91	0,053	<LOD	2,85	<LOD	96,74
Kurula	17-07	11	Arsenopyrite	31,98	1,11	0,608	<LOD	<LOD	<LOD	<LOD	49,01	<LOD	<LOD	18,56	<LOD	101,27
Kurula	17-07	12	Arsenopyrite	30,96	1,2	0,73	<LOD	<LOD	<LOD	<LOD	49,14	<LOD	0,083	17,96	<LOD	100,09
Kurula	17-07	13	Arsenopyrite	31,07	1,31	0,936	<LOD	<LOD	<LOD	<LOD	49,62	<LOD	<LOD	17,53	<LOD	100,49
Kurula	17-07	14	Löllingite	26,36	0,746	0,58	<LOD	0,014	<LOD	<LOD	69,59	<LOD	<LOD	2,02	<LOD	99,34
Kurula	17-07	15	Löllingite	26,66	0,599	0,508	<LOD	<LOD	<LOD	<LOD	68,44	0,055	<LOD	2,64	<LOD	98,94
Kurula	17-07	16	Löllingite	26,75	0,698	0,507	<LOD	0,016	<LOD	<LOD	69,07	<LOD	<LOD	2,74	<LOD	99,83
Kurula	17-07	17	Löllingite	26,25	0,775	0,59	<LOD	<LOD	<LOD	<LOD	69,16	<LOD	0,084	1,83	<LOD	98,74
Kurula	17-06	18	Pyrite	46,61	<LOD	0,027	<LOD	<LOD	<LOD	<LOD	<LOD	<LOD	<LOD	50,71	<LOD	97,36
Kurula	17-06	19	Pyrite	46,65	<LOD	0,019	<LOD	<LOD	<LOD	<LOD	<LOD	<LOD	<LOD	52,8	<LOD	99,51
Kurula	17-06	20	Arsenopyrite	33,81	0,269	0,02	<LOD	<LOD	<LOD	<LOD	47,22	<LOD	<LOD	19,96	<LOD	101,28
Kurula	17-06	21	Arsenopyrite	33,11	0,522	0,184	<LOD	<LOD	<LOD	<LOD	48,33	<LOD	0,095	18,65	<LOD	100,89
Kurula	17-06	22	Arsenopyrite	33,94	0,192	0,018	<LOD	<LOD	<LOD	<LOD	46,74	<LOD	<LOD	20,38	<LOD	101,27
Kurula	17-06	23	Chalcopyrite	30,19	<LOD	<LOD	33,67	0,019	<LOD	<LOD	0,092	<LOD	<LOD	34,77	<LOD	98,79
Kurula	17-06	24	Chalcopyrite	30,05	<LOD	<LOD	33,78	0,038	<LOD	0,047	<LOD	0,059	0,083	34,83	<LOD	98,93
Kurula	17-06	25	Pyrrhotite	60,24	<LOD	<LOD	<LOD	<LOD	<LOD	<LOD	<LOD	<LOD	<LOD	39,1	<LOD	99,50
Kurula	17-06	26	Pyrrhotite	60,12	<LOD	<LOD	<LOD	<LOD	<LOD	<LOD	0,064	<LOD	<LOD	38,03	<LOD	98,33
Kurula	17-06	27	Arsenopyrite	34,19	0,387	0,048	<LOD	<LOD	<LOD	<LOD	45,34	<LOD	<LOD	19,81	<LOD	99,87
Kurula	19-05	28	Skutterudite	2,12	17,77	1,43	<LOD	<LOD	<LOD	<LOD	78,75	<LOD	0,124	0,252	<LOD	100,46
Kurula	19-05	29	Skutterudite	2,08	17,79	1,36	<LOD	<LOD	<LOD	<LOD	79,4	<LOD	<LOD	0,201	<LOD	100,90
Kurula	19-05	30	Arsenopyrite	27,72	5,59	0,14	<LOD	<LOD	<LOD	<LOD	51,61	<LOD	<LOD	16,94	<LOD	102,02
Kurula	19-05	31	Arsenopyrite	27,87	5,56	0,14	<LOD	0,018	<LOD	<LOD	50,98	0,043	<LOD	16,9	<LOD	101,57
Kurula	19-05	32	Safflorite	17,06	9,04	2,09	0,145	<LOD	<LOD	<LOD	72,19	<LOD	0,177	0,48	<LOD	101,23
Kurula	19-05	33	Safflorite	16,74	9,4	2,16	<LOD	<LOD	<LOD	<LOD	71,78	<LOD	<LOD	0,695	<LOD	100,85
Kurula	19-05	34	Arsenopyrite	28,14	5,3	0,125	<LOD	<LOD	<LOD	0,015	50,55	<LOD	<LOD	17,37	<LOD	101,60
Kurula	19-05	35	Arsenopyrite	28,28	5,18	0,114	<LOD	<LOD	<LOD	<LOD	50,65	<LOD	<LOD	17,29	<LOD	101,55
Kurula	19-05	36	Arsenopyrite	27,94	5,49	0,164	<LOD	0,014	<LOD	<LOD	51,16	<LOD	<LOD	17,35	<LOD	102,16
Kurula	19-05	37	Arsenopyrite	28,06	5,42	0,131	<LOD	<LOD	<LOD	<LOD	51,24	<LOD	<LOD	17,34	<LOD	102,33
Kurula	19-05	38	Arsenopyrite	27,6	5,43	0,141	<LOD	<LOD	<LOD	<LOD	50,91	<LOD	<LOD	16,74	<LOD	100,87
Kurula	19-05	39	Arsenopyrite	27,54	5,49	0,122	<LOD	<LOD	<LOD	<LOD	51,42	<LOD	0,118	16,66	<LOD	101,35
Kurula	19-05	40	Skutterudite	1,3	19,12	0,838	<LOD	0,019	<LOD	<LOD	79,24	0,048	<LOD	0,111	<LOD	100,68
Kurula	19-05	41	Skutterudite	1,22	19,26	0,82	<LOD	<LOD	<LOD	<LOD	79,03	<LOD	<LOD	0,116	<LOD	100,50
Kurula	19-05	42	Skutterudite	1,29	19,11	1,05	<LOD	<LOD	<LOD	<LOD	79,59	<LOD	<LOD	0,074	<LOD	101,17
Kurula	19-05	43	Safflorite	18,21	8,73	1,53	<LOD	<LOD	<LOD	<LOD	70,3	<LOD	<LOD	1,67	<LOD	100,45
Kurula	19-05	44	Skutterudite	3,67	14,25	3,01	<LOD	<LOD	<LOD	<LOD	79,16	<LOD	0,135	0,137	<LOD	100,40
Kurula	19-05	45	Skutterudite	3,53	14,86	2,53	<LOD	<LOD	<LOD	<LOD	77,7	<LOD	0,093	0,166	<LOD	98,92
Kurula	19-05	46	Skutterudite	3,39	14,92	2,4	<LOD	<LOD	<LOD	<LOD	78,89	<LOD	<LOD	0,279	<LOD	99,91
Kurula	19-05	47	Skutterudite	3,34	14,62	2,81	<LOD	<LOD	<LOD	<LOD	79,2	<LOD	<LOD	0,239	<LOD	100,21
Kurula	19-05	48	Skutterudite	3,77	14,89	2,46	<LOD	<LOD	<LOD	<LOD	79,1	<LOD	0,078	0,292	<LOD	100,74
Kurula	19-05	49	Skutterudite	3,11	16,03	1,98	<LOD	<LOD	<LOD	<LOD	78,51	<LOD	0,09	0,276	<LOD	100,01
Kurula	19-05	50	Skutterudite	3,36	14,72	2,74	<LOD	<LOD	<LOD	<LOD	78,75	<LOD	<LOD	0,299	<LOD	99,88
Kurula	19-05	51	Safflorite	11,76	11,15	2,28	<LOD	<LOD	<LOD	0,016	74,09	<LOD	0,149	1,04	<LOD	100,53
Kurula	19-05	52	Skutterudite	3,63	14,38	2,9	<LOD	<LOD	<LOD	<LOD	77,26	<LOD	<LOD	0,189	<LOD	98,45
Kurula	17-09	53	Arsenopyrite	29,96	3,56	0,129	0,277	0,025	<LOD	<LOD	49,65	<LOD	0,123	18,54	<LOD	102,26
Kurula	17-09	54	Arsenopyrite	29,65	3,81	0,177	<LOD	0,038	<LOD	<LOD	50,12	<LOD	<LOD	17,91	<LOD	101,74
Kurula	17-09	55	Arsenopyrite	30,74	3,02	0,108	0,226	<LOD	<LOD	<LOD	48,63	<LOD	<LOD	18,25	<LOD	100,99
Kurula	17-09	56	Arsenopyrite	29,57	3,88	0,182	0,164	<LOD	<LOD	<LOD	50,03	<LOD	<LOD	17,93	<LOD	101,79
Kurula	17-09	57	Arsenopyrite	29,56	4,09	0,186	<LOD	<LOD	<LOD	0,017	50,02	0,049	<LOD	17,96	<LOD	102,04
Kurula	17-09	58	Arsenopyrite	29,78	3,76	0,14	<LOD	0,023	<LOD	0,024	48,57	<LOD	0,071	17,77	0,085	100,24
Kurula	17-09	59	Pyrite	45,8	<LOD	<LOD	1,45	<LOD	<LOD	<LOD	0,063	<LOD	<LOD	53,16	0,067	100,57
Kurula	17-09	60	Pyrite	45,97	<LOD	0,017	0,819	<LOD	<LOD	0,026	0,061	<LOD	<LOD	52,15	<LOD	99,07
Kurula	17-09	61	Pyrite	45,53	<LOD	0,064	1,33	<LOD	<LOD	<LOD	0,068	<LOD	<LOD	53,09	<LOD	100,09
Kurula	17-09	62	Chalcopyrite	30,21	<LOD	<LOD	31,4	0,019	<LOD	<LOD	0,07	<LOD	<LOD	35,33	<LOD	97,10
Kurula	17-09	63	Chalcopyrite	29,86	<LOD	<LOD	33,47	0,025	<LOD	<LOD	0,046	<LOD	<LOD	35,49	<LOD	98,93
Kurula	17-09	64	Pyrite	46,13	<LOD	<LOD	<LOD	<LOD	<LOD	<LOD	1,41	<LOD	<LOD	52,02	<LOD	99,62
Kurula	17-09	65	Pyrite	46,2	<LOD	<LOD	<LOD	<LOD	<LOD	<LOD	1,01	<LOD	<LOD	52,74	<LOD	99,97
Kurula	17-09	66	Pyrite	46,19	<LOD	<LOD	<LOD	<LOD	<LOD	<LOD	0,505	<LOD	<LOD	52,37	0,067	99,21
Kurula	17-09	67	Pyrite	45,84	<LOD	0,071	<LOD	<LOD	<LOD	<LOD	1,74	<LOD	<LOD	52,25	<LOD	99,96
Kurula	17-09	68	Pyrite	46,28	<LOD	0,044	<LOD	<LOD	<LOD	<LOD	0,428	<LOD	<LOD	52,84	<LOD	99,61
Kurula	17-09	69	Arsenopyrite	29,24	4,45	0,128	<LOD	<LOD	<LOD	<LOD	49,84	<LOD	<LOD	17,49	<LOD	101,25
Kurula	17-09	70	Arsenopyrite	27,13	5,67	0,236	<LOD	<LOD	<LOD	<LOD	50,34	<LOD	<LOD	16,69	<LOD	100,15
Kurula	17-09	71	Arsenopyrite	28,59	4,68	0,209	<LOD	<LOD	<LOD	<LOD	50,93	<LOD	<LOD	17,34	<LOD	101,79
Kurula	17-09	72	Arsenopyrite	28,04	4,9	0,356	<LOD	<LOD	<LOD	<LOD	49,54	0,086	<LOD	16,6	<LOD	99,54
Kurula	17-09	73	Arsenopyrite	29,2	4,25	0,268	<LOD	0,014	<LOD	<LOD	50,68	<LOD	<LOD	17,49	0,095	102,14

Deposit	sample	#	Mineral	Fe (wt%)	Co (wt%)	Ni (wt%)	Cu (wt%)	Ag (wt%)	Au (wt%)	Zn (wt%)	As (wt%)	Sb (wt%)	Bi (wt%)	S (wt%)	Hg (wt%)	Total (wt%)
Kurula	17-09	74	Arsenopyrite	28,96	4,41	0,273	<LOD	<LOD	<LOD	<LOD	50,86	<LOD	<LOD	17	<LOD	101,57
Kurula	17-09	75	Arsenopyrite	30,02	3,63	0,192	<LOD	<LOD	<LOD	<LOD	49,74	<LOD	<LOD	18,1	<LOD	101,68
Kurula	17-09	76	Arsenopyrite	29,9	3,78	0,175	<LOD	<LOD	<LOD	0,021	49,51	<LOD	<LOD	18,06	<LOD	101,53
Kurula	17-09	77	Arsenopyrite	29,22	4,14	0,165	<LOD	<LOD	<LOD	<LOD	49,83	0,067	0,13	17,84	<LOD	101,47
Kurula	17-09	78	Arsenopyrite	29,6	3,85	0,174	<LOD	<LOD	<LOD	<LOD	50,28	0,07	<LOD	17,81	<LOD	101,86
Kurula	17-09	79	Arsenopyrite	29,35	3,97	0,14	<LOD	<LOD	<LOD	<LOD	49,8	0,047	<LOD	17,54	<LOD	100,91
Kurula	17-09	80	Arsenopyrite	29,39	4,13	0,14	<LOD	<LOD	<LOD	<LOD	49,95	0,07	<LOD	17,78	<LOD	101,46
Kurula	17-09	81	Arsenopyrite	29,6	3,45	0,204	<LOD	<LOD	<LOD	<LOD	49,37	<LOD	<LOD	18,17	<LOD	100,86
Kurula	17-09	82	Arsenopyrite	27,21	5,95	0,236	<LOD	0,019	<LOD	<LOD	51,44	<LOD	<LOD	16,62	<LOD	101,55
Kurula	17-09	83	Arsenopyrite	27,73	5,44	0,275	<LOD	<LOD	<LOD	<LOD	51,03	0,047	<LOD	16,73	0,1	101,40
Kurula	17-09	84	Arsenopyrite	29,52	4,18	0,171	<LOD	<LOD	<LOD	<LOD	50,13	0,039	<LOD	17,83	<LOD	101,89
Kurula	17-09	85	Arsenopyrite	30,74	3,15	0,078	<LOD	0,03	<LOD	<LOD	48,95	0,044	<LOD	18,82	<LOD	101,87
Kurula	17-09	86	Arsenopyrite	27,97	5,16	0,336	<LOD	0,014	<LOD	<LOD	51,51	0,075	0,133	16,65	<LOD	101,86
Kurula	17-09	87	Arsenopyrite	28,16	5,05	0,235	<LOD	<LOD	<LOD	<LOD	51,28	0,045	<LOD	16,72	<LOD	101,53
Kurula	17-09	88	Arsenopyrite	33,92	0,403	0,342	<LOD	<LOD	<LOD	<LOD	45,13	<LOD	<LOD	20,94	<LOD	100,74
Kurula	17-09	89	Arsenopyrite	33,34	0,658	0,545	<LOD	<LOD	<LOD	<LOD	44,7	<LOD	<LOD	20,97	<LOD	100,31
Kurula	17-09	90	Arsenopyrite	29,3	3,83	0,147	<LOD	0,024	<LOD	<LOD	50	<LOD	<LOD	17,85	<LOD	101,15
Kurula	17-09	91	Arsenopyrite	29,11	4,03	0,171	<LOD	<LOD	<LOD	<LOD	50,09	<LOD	<LOD	18	<LOD	101,43
Kurula	17-09	92	Arsenopyrite	28,41	4,9	0,192	<LOD	<LOD	<LOD	<LOD	50,78	<LOD	<LOD	17,14	<LOD	101,45
Kurula	17-09	93	Arsenopyrite	28,23	4,84	0,359	<LOD	0,032	<LOD	<LOD	51,47	0,051	<LOD	16,7	0,075	101,81
Kurula	17-09	94	Arsenopyrite	31,08	2,99	0,068	<LOD	0,027	<LOD	<LOD	48,19	<LOD	<LOD	19,02	<LOD	101,38
Kurula	17-09	95	Arsenopyrite	31,15	2,9	0,092	<LOD	<LOD	<LOD	<LOD	48,21	<LOD	<LOD	18,8	0,07	101,27
Kurula	17-11	96	Arsenopyrite	30,74	2,84	0,065	<LOD	<LOD	0,037	<LOD	49,4	<LOD	0,105	18,02	<LOD	101,28
Kurula	17-11	97	Arsenopyrite	30,98	2,71	0,063	<LOD	<LOD	<LOD	<LOD	49,52	<LOD	<LOD	18,21	<LOD	101,55
Kurula	17-11	98	Arsenopyrite	30,84	2,84	0,072	<LOD	<LOD	<LOD	0,017	49,39	<LOD	<LOD	17,86	<LOD	101,08
Kurula	17-11	99	Bismuth inclusion	1,17	0,169	<LOD	<LOD	<LOD	0,766	<LOD	5,38	<LOD	93,23	0,588	<LOD	101,33
Kurula	17-11	100	Chalcopyrite	29,97	<LOD	<LOD	34,14	0,034	<LOD	0,308	<LOD	<LOD	<LOD	34,91	<LOD	99,40
Kurula	17-11	101	Chalcopyrite	30,03	<LOD	<LOD	34,12	<LOD	<LOD	0,102	<LOD	<LOD	<LOD	34,85	<LOD	99,10
Kurula	17-11	102	Chalcopyrite	29,67	<LOD	<LOD	34,15	0,029	<LOD	0,082	<LOD	<LOD	<LOD	34,88	<LOD	98,84
Kurula	17-11	103	Sphalerite	4,35	<LOD	<LOD	<LOD	<LOD	<LOD	61,99	<LOD	0,043	<LOD	34,45	<LOD	100,88
Kurula	17-11	104	Sphalerite	3,74	<LOD	<LOD	<LOD	<LOD	<LOD	62,76	<LOD	<LOD	<LOD	33,7	<LOD	100,26
Kurula	17-11	105	Sphalerite	3,46	<LOD	<LOD	<LOD	<LOD	<LOD	63,06	<LOD	<LOD	<LOD	32,66	<LOD	99,20
Kurula	17-11	106	Safflorite	21,84	5,46	0,931	<LOD	<LOD	<LOD	<LOD	71,11	<LOD	0,094	1,44	<LOD	101,01
Kurula	17-11	107	Safflorite	21,95	5,31	0,939	<LOD	<LOD	<LOD	<LOD	70,97	<LOD	<LOD	1,5	<LOD	100,70
Kurula	17-11	108	Safflorite	21,99	5,46	0,807	<LOD	<LOD	<LOD	<LOD	70,86	<LOD	<LOD	1,35	<LOD	100,50
Kurula	17-11	109	Safflorite	22	5,22	0,79	<LOD	<LOD	<LOD	<LOD	70,02	<LOD	0,396	1,39	0,056	99,91
Kurula	17-11	110	Arsenopyrite	31,03	2,73	0,055	<LOD	<LOD	<LOD	<LOD	49,4	<LOD	0,159	18,18	<LOD	101,57
Kurula	17-11	111	Arsenopyrite	29,93	3,43	0,09	<LOD	<LOD	<LOD	<LOD	50,71	<LOD	<LOD	17,14	<LOD	101,30
Kurula	17-11	112	Arsenopyrite	30,8	2,82	0,068	<LOD	<LOD	<LOD	<LOD	49,67	<LOD	<LOD	18,2	<LOD	101,65
Kurula	17-11	113	Arsenopyrite	31,18	2,38	0,039	0,177	<LOD	<LOD	<LOD	49,26	<LOD	<LOD	18,61	<LOD	101,66
Kurula	17-11	114	Bismuth inclusion	6,62	0,677	0,025	<LOD	0,102	28,53	<LOD	12,28	0,386	52,7	3,79	<LOD	105,11
Kurula	17-11	115	Arsenopyrite	27,79	2,52	0,044	<LOD	<LOD	5,84	<LOD	45,29	<LOD	3,51	16,89	<LOD	101,88
Kurula	17-11	116	Maldonite	1,47	0,202	<LOD	<LOD	0,602	53,03	<LOD	6,32	0,049	37,8	1,5	<LOD	100,97
Kurula	17-11	117	Arsenopyrite	30,55	2,91	0,057	<LOD	0,034	<LOD	<LOD	49,89	<LOD	<LOD	17,79	<LOD	101,31
Kurula	17-11	118	Arsenopyrite	30,56	3	0,064	<LOD	<LOD	<LOD	<LOD	49,95	<LOD	<LOD	17,96	<LOD	101,55
Kurula	17-11	119	Arsenopyrite	30,43	2,94	0,071	<LOD	<LOD	<LOD	<LOD	50,11	0,057	<LOD	17,27	<LOD	101,03
Kurula	17-11	120	Arsenopyrite	30,3	2,92	0,068	<LOD	<LOD	<LOD	<LOD	50,02	<LOD	<LOD	17,96	<LOD	101,30
Kurula	17-11	121	Arsenopyrite	30,41	2,83	0,104	<LOD	<LOD	<LOD	<LOD	50,41	0,045	<LOD	17,52	0,073	101,49
Kurula	17-11	122	Arsenopyrite	31	2,62	0,074	<LOD	<LOD	<LOD	<LOD	49,81	0,062	<LOD	18,13	<LOD	101,80
Kurula	17-11	123	Arsenopyrite	30,82	2,44	0,041	<LOD	<LOD	<LOD	<LOD	49,27	<LOD	<LOD	18,59	0,064	101,27
Kurula	17-11	124	Arsenopyrite	31,51	2,33	0,03	<LOD	<LOD	<LOD	<LOD	49,1	<LOD	0,088	18,56	<LOD	101,68
Kurula	17-11	125	Safflorite	23,42	4,57	0,619	<LOD	<LOD	<LOD	<LOD	69,8	<LOD	<LOD	2,51	<LOD	101,00
Kurula	17-11	126	Safflorite	23,42	4,58	0,64	<LOD	<LOD	<LOD	<LOD	69,62	<LOD	<LOD	2,55	<LOD	100,85
Kurula	17-11	127	Safflorite	23,02	4,55	0,623	<LOD	<LOD	<LOD	0,019	70,09	<LOD	<LOD	2,19	<LOD	100,51
Kurula	17-11	128	Safflorite	23,54	4,44	0,628	<LOD	<LOD	<LOD	<LOD	69,83	<LOD	0,075	2,47	<LOD	100,99
Kurula	17-11	129	Safflorite	23,52	4,38	0,611	<LOD	<LOD	<LOD	<LOD	70,21	<LOD	0,074	2,34	<LOD	101,18
Kurula	17-11	130	Safflorite	22,13	5,14	0,738	<LOD	<LOD	<LOD	<LOD	71,87	<LOD	0,087	0,837	<LOD	100,86
Kurula	17-11	131	Safflorite	21,84	5,46	0,808	<LOD	<LOD	<LOD	<LOD	71,85	<LOD	<LOD	1,17	<LOD	101,18
Kurula	17-11	135	Arsenopyrite	30,92	2,72	0,045	<LOD	<LOD	<LOD	<LOD	49,46	<LOD	<LOD	18,13	0,071	101,35
Kurula	17-11	136	Arsenopyrite	30,81	2,79	0,058	<LOD	<LOD	<LOD	<LOD	49,74	<LOD	0,089	18,14	<LOD	101,70
Kurula	17-11	137	Arsenopyrite	30,49	2,95	0,084	<LOD	<LOD	<LOD	<LOD	49,88	<LOD	<LOD	18,45	<LOD	101,93
Kurula	17-11	138	Arsenopyrite	30,63	2,96	0,1	<LOD	0,014	<LOD	<LOD	49,77	<LOD	0,133	18,58	0,129	102,33
Kurula	17-11	139	Arsenopyrite	30,25	3,37	0,126	<LOD	0,034	<LOD	<LOD	49,19	<LOD	<LOD	18,32	<LOD	101,43
Kurula	17-11	140	Arsenopyrite	30,5	3,17	0,079	<LOD	<LOD	<LOD	<LOD	49,7	<LOD	<LOD	18,67	<LOD	102,20
Kurula	17-11	141	Arsenopyrite	29,68	3,4	0,142	<LOD	<LOD	<LOD	0,015	50,45	<LOD	<LOD	18,24	<LOD	101,95
Kurula	17-11	142	Safflorite	21,76	5,17	0,776	<LOD	<LOD	<LOD	<LOD	72,31	<LOD	<LOD	0,643	<LOD	100,67
Kurula	17-11	143	Safflorite	21,55	5,6	0,794	<LOD	0,021	<LOD	<LOD	72,24	<LOD	0,09	0,737	0,061	101,13
Kurula	17-11	144	Safflorite	21,9	5,14	0,799	<LOD	<LOD	<LOD	<LOD	72,06	<LOD	0,148	0,479	<LOD	100,60
Kurula	17-11	145	Gold inclusion	1,37	0,46	0,061	<LOD	0,31	94,04	<LOD	5,79	<LOD	0,675	<LOD	<LOD	102,71
Kurula	17-11	146	Arsenopyrite	34,26	<LOD	<LOD	<LOD	0,025	<LOD	<LOD	44,38	<LOD	<LOD	21,85	<LOD	100,68
Kurula	17-11	147	Arsenopyrite	34,42	<LOD	<LOD	<LOD	<LOD	<LOD	<LOD	42,73	0,069	<LOD	22,41	<LOD	99,76
Kurula	17-11	148	Arsenopyrite	30,45	2,88	0,065	<LOD	<LOD	<LOD	<LOD	49,12	0,038	<LOD	18,01	<LOD	100,60
Kurula	17-11	149	Arsenopyrite	30,32	2,87	0,048	<LOD	0,021	<LOD	<LOD	49,26	<LOD	<LOD	18,14	<LOD	100,66
Kurula	17-11	150	Safflorite	20,64	6,99	0,588	<LOD	<LOD	<LOD	<LOD	70,24	<LOD	<LOD	1,45	<LOD	99,98
Kurula	17-11	151	Safflorite	21,12	6,26	0,56	<LOD	<LOD	<LOD	<LOD	69,75	<LOD	0,181	1,52	<LOD	99,44
Kurula	17-11	152	Safflorite	20,9	6,29	0,63	<LOD	<LOD	<LOD	<LOD	70,77	<LOD	<LOD	1,35	<LOD	99,99
Kurula	17-11	153	Gold inclusion	2,13	0,341	0,013	0,482	1,71	91,82	<LOD	4,21	<LOD	<LOD	0,839	<LOD	101,55
Kurula	17-11	154	Bismuth inclusion	1,95	0,385	<LOD	<LOD	<LOD	<LOD	0,024	7,13	<LOD	91,98	0,112	<LOD	101,62

S isotopes data

Deposit	Sample	Mineral	d34S (‰)
Jouhineva	FEMO-2019-20-16	Apy	7.48
Jouhineva	FEMO-2019-20-16	Apy	7.37
Jouhineva	FEMO-2019-20-16	Apy	7.21
Jouhineva	FEMO-2019-20-16	Apy	7.26
Jouhineva	FEMO-2019-20-16	Apy	7.20
Jouhineva	FEMO-2019-11-18	Apy	8.21
Jouhineva	FEMO-2019-11-18	Apy	8.07
Jouhineva	FEMO-2019-11-18	Apy	8.04
Jouhineva	FEMO-2019-11-18	Apy	7.94
Jouhineva	FEMO-2019-11-18	Apy	8.03
Jouhineva	FEMO-2019-11-18	Apy	8.03
Jouhineva	FEMO-2019-20-08	Ccp	6.04
Jouhineva	FEMO-2019-20-08	Ccp	6.01
Jouhineva	FEMO-2019-20-08	Ccp	5.96
Jouhineva	FEMO-2019-20-16	Ccp	6.10
Jouhineva	FEMO-2019-20-16	Ccp	6.09
Jouhineva	FEMO-2019-20-16	Ccp	6.17
Jouhineva	FEMO-2019-20-08	Ccp	6.02
Jouhineva	FEMO-2019-20-08	Ccp	5.97
Jouhineva	FEMO-2019-20-08	Ccp	5.87
Kurula	FEMO-2019-13-06	Ccp	1.42
Kurula	FEMO-2019-13-06	Ccp	1.47
Kurula	FEMO-2019-13-06	Ccp	1.39
Kurula	FEMO-2019-17-11	Apy	3.12
Kurula	FEMO-2019-17-11	Apy	3.09
Kurula	FEMO-2019-17-11	Apy	3.02
Kurula	FEMO-2019-17-11	Apy	2.92
Kurula	FEMO-2019-17-11	Apy	2.83
Kurula	FEMO-2019-17-11	Apy	2.95
Kurula	FEMO-2019-19-05	Apy	3.16
Kurula	FEMO-2019-19-05	Apy	3.17
Kurula	FEMO-2019-19-05	Apy	3.04
Kurula	FEMO-2019-19-05	Apy	3.04
Kurula	FEMO-2019-19-05	Apy	2.94
Kurula	FEMO-2019-19-05	Apy	2.95
Kurula	FEMO-2019-17-07	Po	2.19
Kurula	FEMO-2019-17-07	Po	2.37
Kurula	FEMO-2019-17-07	Po	2.46
Kurula	FEMO-2019-17-06	Po	2.67
Kurula	FEMO-2019-17-06	Po	2.58
Kurula	FEMO-2019-17-06	Po	2.63
Laivakangas	FEMO-2019-03-01	Apy	1.94
Laivakangas	FEMO-2019-03-01	Apy	1.90
Laivakangas	FEMO-2019-03-01	Apy	1.91
Laivakangas	FEMO-2019-03-01	Apy	1.84
Laivakangas	FEMO-2019-03-01	Apy	1.97
Laivakangas	FEMO-2019-03-01	Apy	1.84
Laivakangas	FEMO-2019-08-03	Apy	2.30
Laivakangas	FEMO-2019-08-03	Apy	2.40
Laivakangas	FEMO-2019-08-03	Apy	2.43
Laivakangas	FEMO-2019-08-03	Apy	1.67
Laivakangas	FEMO-2019-08-03	Apy	1.52

Deposit	Sample	Mineral	d34S (‰)
Laivakangas	FEMO-2019-08-03	Apy	1.67
Laivakangas	FEMO-2019-01-03	Po	2.47
Laivakangas	FEMO-2019-01-03	Po	2.63
Laivakangas	FEMO-2019-01-03	Po	2.55
Laivakangas	FEMO-2019-01-03	Py	2.34
Laivakangas	FEMO-2019-01-03	Py	2.37
Laivakangas	FEMO-2019-01-03	Py	2.39
Laivakangas	FEMO-2019-01-05	Ccp	2.04
Laivakangas	FEMO-2019-01-05	Ccp	2.08
Laivakangas	FEMO-2019-01-05	Ccp	2.10
Laivakangas	FEMO-2019-05-01	Ccp	2.97
Laivakangas	FEMO-2019-05-01	Ccp	3.14
Laivakangas	FEMO-2019-05-01	Ccp	3.11
Laivakangas	FEMO-2019-05-01	Ccp	3.17
Laivakangas	FEMO-2019-05-01	Ccp	3.14
Laivakangas	FEMO-2019-05-01	Ccp	3.17
Huhta	FEMO-2019-22-07	Po	5.12
Huhta	FEMO-2019-22-07	Po	5.11
Huhta	FEMO-2019-22-07	Po	5.18
Huhta	FEMO-2019-22-07	Po	5.13
Huhta	FEMO-2019-22-07	Po	5.04
Huhta	FEMO-2019-22-07	Po	5.12
Huhta	FEMO-2019-22-03	Apy	5.80
Huhta	FEMO-2019-22-03	Apy	5.73
Huhta	FEMO-2019-22-03	Apy	5.83
Huhta	FEMO-2019-22-07	Apy	6.51
Huhta	FEMO-2019-22-07	Apy	6.55
Huhta	FEMO-2019-22-07	Apy	6.51
Huhta	FEMO-2019-22-18	Apy	5.55
Huhta	FEMO-2019-22-18	Apy	5.53
Huhta	FEMO-2019-22-18	Apy	5.63
Huhta	FEMO-2019-22-02	Apy	4.44
Huhta	FEMO-2019-22-02	Apy	4.52
Huhta	FEMO-2019-22-02	Apy	5.40

Deposit	Mineral	n	mean $\delta^{34}S$ (‰)	2σ (‰)	Min. value	Max. value
Laivakangas	Apy	12	+1.95	0.56	+1.52	+2.43
Laivakangas	Po	3	+2.55	0.13	+2.47	+2.63
Laivakangas	Py	3	+2.37	0.04	+2.34	+2.39
Laivakangas	Ccp	9	+2.77	0.99	+2.04	+3.17
Jouhineva	Apy	11	+7.71	0.77	+7.20	+8.21
Jouhineva	Ccp	9	+6.03	0.17	+5.87	+6.17
Huhta	Po	6	+5.12	0.08	+5.04	+5.18
Huhta	Apy	12	+5.67	1.31	+4.44	+6.55
Kurula	Ccp	3	+1.43	0.07	+1.39	+1.47
Kurula	Apy	12	+3.02	0.20	+2.83	+3.17
Kurula	Po	6	+2.48	0.33	+2.19	+2.67

Reference sample	Material	recommended δ-value	Uncertainty 1σ-level	d34S/d32S	Uncertainty 1σ-level	n
IAEA S-1	Ag2S	-0.3	-	-0.33	0.03	3
IAEA S-3	Ag2S	-32.28	0.22	-32.3	0.2	3
NBS-127	BaSO4	21.17	0.12	21.19	0.13	3
CDS (in-house std)	CdS			11.09	0.1	28

Paper IV

-

Magmatic evolution in the Kolumbo volcano and its implication to seafloor massive sulphide formation.

Hector S, Patten CGC, Beranoaguirre A, Lanari P, Kilias S, Nomikou P, Peillod A, Eiche E, Kolb J (submitted) Mineralium Deposita

Magmatic evolution in the Kolumbo volcano and its implication to seafloor massive sulphide formation

Simon Hector[1, 2], Clifford Patten[1, 2], Aratz Beranoaguirre[1, 2], Pierre Lanari[3], Stephanos Kilias[4], Paraskevi Nomikou[4], Alexandre Peillod[1, 2], Elisabeth Eiche[1, 2], Jochen Kolb[1, 2]

[1] *Institute of Applied Geosciences, Chair of Geochemistry and Economic Geology, KIT, Karlsruhe, Germany*

[2]*Laboratory for Environmental and Raw Materials Analysis (LERA), Adenauerring 20b, 76131 Karlsruhe, Germany*

[3] *Institute of Geological Sciences, University of Bern, 3012 Bern, Switzerland*

[4] *Department of Geology and Geoenvironment, National and Kapodistrian University of Athens, Zografou Campus, 15784 Athens, Greece*

Keywords : Seafloor massive sulphide, trace metal geochemistry, magnetite, Kolumbo volcano

Corresponding author: Simon Hector

simon.hector@kit.edu

1 Abstract

Seafloor massive sulphides (SMS) form in various marine hydrothermal settings, particularly within volcanic arcs, where magmatic fluids may contribute to the metal budget of the hydrothermal system. Here we study the Kolumbo volcano, a submarine volcano in the central Hellenic Volcanic Arc (HVA), hosting an active hydrothermal system. Sulfate-sulphide diffusers forming a Zn-Pb SMS show elevated As, Ag, Au, Hg, Sb and Tl contents. These elements have similar volatile behaviour during magmatic degassing and are common in arc-related hydrothermal systems. Trace-element data of igneous magnetite, combined with whole rock geochemistry and numerical modelling, highlight the behaviour of chalcophile elements during magmatic differentiation. We report that, despite early magmatic sulphide saturation, chalcophile element concentrations in the magma do not decrease until water saturation and degassing. The conservation of chalcophile elements in the magma during magmatic

differentiation indicates that most of the magmatic sulphides do not fractionate. Upon degassing, As, Ag, Au, Cu, Hg, Sb, Sn, Pb and Zn get depleted in the magma as they partition in the volatiles, either from the melt or during formation of sulphide-volatile compounds and subsequent oxidation of sulphide. After degassing, the residual chalcophile elements in the melt are incorporated into magnetite. Trace-element data of magnetite enables to identify sulphide saturation during magmatic differentiation and discriminate between pre- and post-degassing magnetite. Our data highlights how magmatic degassing contributes to the metal budget in magmatic-hydrothermal systems forming SMS and demonstrates that igneous magnetite geochemistry is a powerful tool to track metal-mobilizing processes during magmatic differentiation.

2 Introduction

The study of modern ore forming systems is crucial to better understand the formation of mineral deposits in the past and provides useful models to the exploration industry. In this perspective, actively forming seafloor massive sulphide (SMS) are considered analogues to ancient polymetallic volcanogenic massive sulphide (VMS) and provide important insight into understanding their formation (Halbach et al. 1989; Hannington and Scott 1989). Seafloor massive sulphide form on the seafloor where hydrothermal activity is developed (i.e. mid-oceanic ridge, arc volcanism, rift, hot spot; Hannington et al. 2005). Arc-related hydrothermal systems differ in many aspects from those located along the mid-oceanic ridge and mature back-arc spreading centres, mostly by the important magmatic contribution of fluids and metals to the hydrothermal system (e.g. de Ronde et al. 2005; Hannington et al. 2005; Patten et al. 2020).

Magmatic volatiles contribution to arc-related, submarine, hydrothermal systems (e.g. Kolumbo volcano, Carey et al. 2013; Kilias et al. 2013; Rizzo et al. 2016; Rizzo et al. 2019; Sigurdsson et al. 2006 – Brothers volcano in the Kermadec arc, Berkenbosch et al. 2012; de Ronde et al. 2005; Gruen et al. 2014; Keith et al. 2018 – SuSu Knolls in the Manus back-arc

basin, Craddock et al. 2010; Craddock and Bach 2010; Thal et al. 2016; Yeats et al. 2014) suggest that these systems are comparable to on-land porphyry-epithermal deposits (Keith et al. 2018). In porphyry-epithermal deposits, metals are considered to be mostly carried by magmatic fluids exsolved from hydrous magmas in the mid- to upper crust (Richards 2011). Thus, metal fractionation by magmatic processes such as sulphide saturation and degassing appear to be key parameters to control the formation of metal-rich magmatic fluids in arc-related hydrothermal systems. Sulphide saturation in the magma will extract most of the chalcophile and siderophile elements of a silicate magma (including As, Ag, Au, Hg, Sb and Tl) and concentrate them into an immiscible sulphide phase (Fontboté et al. 2017; Jenner et al. 2010; Park et al. 2015; Sun et al. 2004). Similarly, magmatic degassing leads to formation of a ligand-rich volatile phase (e.g. S, Cl, F, CO_2) able to form complexes with metals and remove them from the magma if it is still fertile (i.e. before sulphide saturation) (Fontboté et al. 2017). If the magma reaches sulphide saturation before volatile saturation, most of the chalcophile and siderophile metals are removed from the magma as sulfide phases fractionate, leaving too little metals available in the melt for the aqueous fluids and volatiles to generate metal-rich magmatic-hydrothermal fluids. However, volatile bubbles may nucleate on sulphide liquid droplets to form low buoyancy sulphide-volatile compounds, transporting sulfides — and their metals — toward the shallow part of the magmatic system (Blanks et al. 2020; Mungall et al. 2015). Additionally, oxidation of the sulphides by the volatiles within the sulphide-volatile compound may lead to metal transfer to the volatile phase and eventually to the magmatic-hydrothermal system (Patten et al. under review). Therefore, investigating the timing between sulphide and volatile saturation and degassing in the melt is crucial to understand how these processes affect the metal fertility of the magma. To do so, petrogenetic indicator minerals, such as magnetite, prove to be useful to constrain geochemical conditions of a system.

Magnetite is a common mineral forming in various magmatic systems, which trace-element composition is frequently used to identify it’s origin (i.e. hydrothermal, igneous, ore-deposit

related) (Dare et al. 2014; Nadoll et al. 2014). Additionally, trace-element composition in igneous magnetite gives insight into the melt composition at the time of magnetite crystallization and enables to identify simultaneous formation of other mineral phases, such as sulphides (Dare et al. 2014; Huang et al. 2019). Indeed, chalcophile elements are slightly incompatible to compatible in magnetite, and compositional variation of the melt can be recorded in the trace element content of magnetite (Dare et al. 2012).

In this study, we investigate the submarine Kolumbo volcano and it's SMS in order to understand how magmatic processes contribute to the metal budget of SMS forming from volcanic arc magmatic-hydrothermal system. Trace-element composition of igneous magnetite and whole rock geochemistry along magmatic differentiation is combined with petrology and numerical modelling in order to investigate the timing between sulphide saturation, volatile saturation and degassing, and to highlight how these processes affect the metal content of the magma. This enables to estimate the metal fertility of the magma during magmatic differentiation, the magmatic input of metals into the magmatic-hydrothermal system and ultimately the magmatic contribution to the formation of SMS.

3 Geological setting

3.1 The Kolumbo volcano

The submarine Kolumbo volcano is located in the Anhydros basin and belongs to the Christiana-Santorini-Kolumbo volcanic field, in the centre of the Hellenic Volcanic Arc (HVA) in the southern Aegean Sea (Fig. 1a-inset). Volcanic activity along the HVA is linked to subduction of the African Plate underneath the Aegean Microplate (Papanikolaou 2013), which can be traced back at least to the Pliocene (Fytikas et al. 1984; Preine et al. 2022). The 450 kilometres long arc stretches from W to E from the Methana peninsula (Saronic Gulf) through the islands of Milos, Antimilos and Santorini (Cyclades) and Kos and Nisyros (Dodecanese) together with submarine volcanoes (Nomikou et al. 2013). Regional NW-SE extension leads to

crustal thinning and opening of extensional basins (Agostini et al. 2010), including the Anhydros basin NE of Santorini, between the Ios and Anafi islands (Fig. 1a) (Nomikou et al. 2016). It hosts the Kolumbo volcano as well as 25 other volcanic cones developing along the Christiana-Santorini-Kolumbo rift, forming the Kolumbo Volcanic Chain (Fig. 1a) (Hooft et al. 2017; Nomikou et al. 2012; Nomikou et al. 2019).

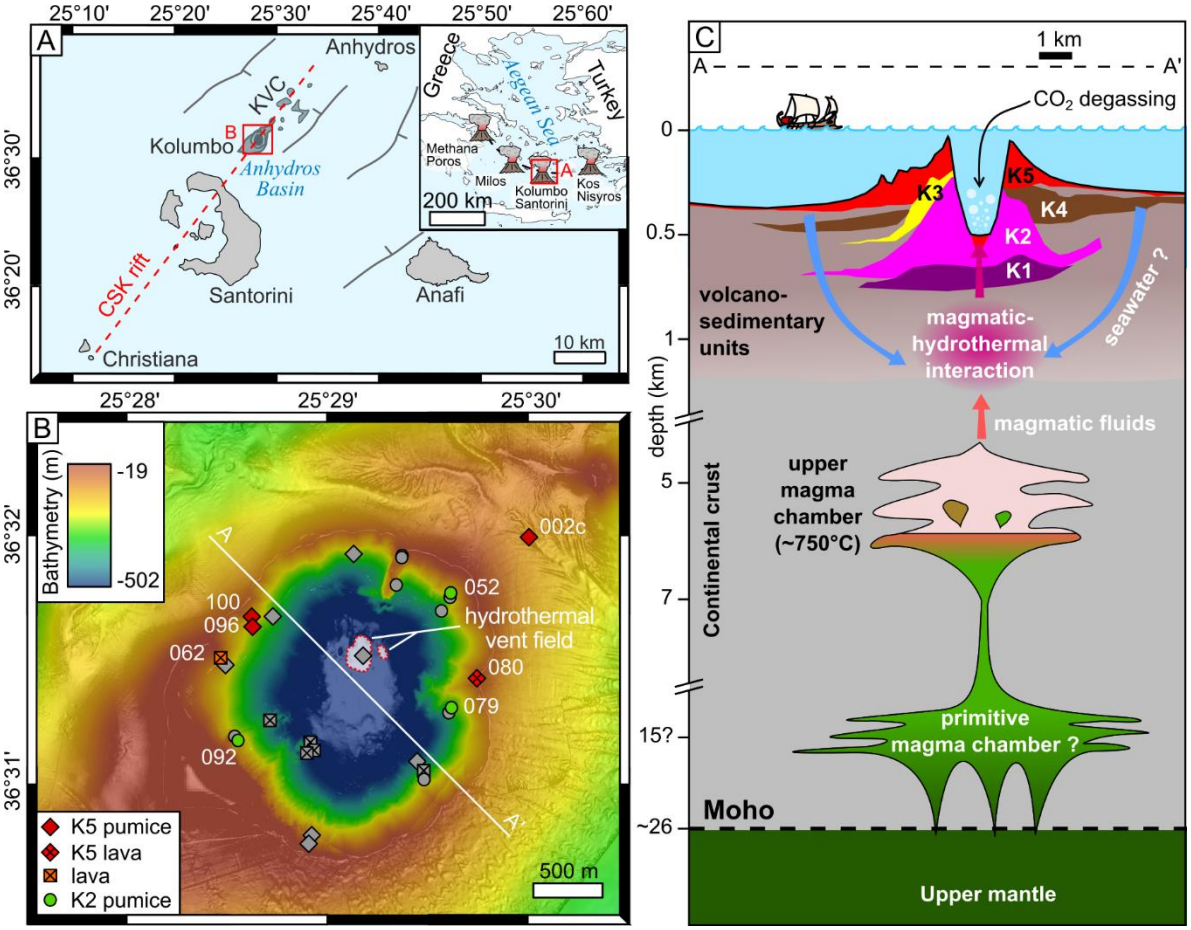

Fig. 1: Geological setting of the Kolumbo volcano. (A) Location of the Kolumbo volcano in the Anhydros basin – KVC: Kolumbo Volcanic Chain; inset: location of Kolumbo within the Hellenic Volcanic Arc. (B) Bathymetric map of the Kolumbo volcano (modified after Nomikou et al. 2022) showing the sampling location (samples from Klaver et al. 2016 in grey). (C) Schematic cross-section of Kolumbo' s magmatic-hydrothermal system (see B for location). Moho depth inferred from Schmid et al. (2022).

The Kolumbo volcano showed important seismic activity in the last decades (e.g. earthquake swarms of 2006-2007) and is considered the most active volcanic system in the

region at present time (Dimitriadis et al. 2010; Hübscher et al. 2015; Rizzo et al. 2019; Schmid et al. 2022). Its volcanic cone has an elongated shape following a NE trend with a 3 kilometres basal diameter, it rises from 500 metres below sea level and reaches 19 metres below sea level at its highest point (Fig. 1b) (Nomikou et al. 2012; Nomikou et al. 2022). The last eruption of 1650 CE formed a 1.7 kilometres wide crater in the centre of the volcanic cone (Fouqué 1879; Sigurdsson et al. 2006). The crater slopes are steep and the crater bottom is at 502 metres below sea level (Nomikou et al. 2012; Nomikou et al. 2022). The northern part of the crater hosts a hydrothermal field where boiling CO_2-rich fluids with temperature as high as 265°C are venting, leading to formation of polymetallic Zn-Pb-(As, Ag, Au, Hg, Sb, Tl)-rich sulphate-sulphide diffusers (Fig. 1b) (Carey et al. 2013; Kilias et al. 2013; Nomikou et al. 2022; Rizzo et al. 2016; Rizzo et al. 2019; Sigurdsson et al. 2006). Interaction of magmatic gases with the hydrothermal system of Kolumbo is estimated to occur at ca. 270°C and at ca. 1 kilometre below sea level (i.e. ca. 500 metre below the seafloor) (Fig. 1c) (Rizzo et al. 2019).

Five distinct cycles of mostly submarine volcanism are identified by seismic imaging (Hübscher et al. 2015; Preine et al. 2022). They form a superposition of five circular, cone-shaped stratigraphic units labelled K1 to K5 interbedded with volcano-sedimentary rocks labelled SK1 to SK4 (Fig. 1c) (Hübscher et al. 2015). The timing of volcanic activity is poorly constrained, but is estimated to start with the second volcanic phase of the Christiana-Santorini-Kolumbo volcanic field between ca. 1.6 and 0.7 Ma (Preine et al. 2022). Only the K5 unit is linked with certainty to the 1650 CE eruption, based on witness testify (Fouqué 1879; Hübscher et al. 2015).

Kolumbo has been sampled in 2010 by the remotely operated vehicle (ROV) Hercules during the cruise NA007 of the exploration vessel *Nautilus* and during winter 2022-2023 by drilling during the expedition n°398 of the International Ocean Discovery Program. At the time of this work, only samples collected with the ROV belonging to the outcropping units K2 and K5 are available. They consist of basaltic to andesitic lava flows and rhyolitic pumice (Klaver

et al. 2016). Pumice contains centimetre-sized mafic enclaves usually showing chilled margin, indicating injection of mafic magma into a cooler, more evolved host magma (Cantner et al. 2014; Klaver et al. 2016). Klaver et al. (2016) propose that Kolumbo' s magma is derived from high-Al, hydrous, mafic arc magmas differentiating at the base of the arc crust. Rhyolitic magma is produced by prolonged differentiation in addition to mixing with lower crustal melt before rising adiabatically until degassing and formation of an upper magma chamber as a partly solidified mush. Injection of less evolved, hydrous, mafic magma at the base of the upper chamber likely acted as eruption trigger (Fig. 1c) (Cantner et al. 2014; Klaver et al. 2016; Konstantinou 2020).

Seismic tomography and analysis of seismic activity during the last twenty years recognize a shallow magmatic chamber, but its exact location is still disputed (Chrapkiewicz et al. 2022; Dimitriadis et al. 2009; Dimitriadis et al. 2010; Schmid et al. 2022). Seismic tomography using data from earthquakes between 2002 and 2005 maps a low velocity zone interpreted as a magma chamber at 6-7 kilometres below Kolumbo' s seafloor (Dimitriadis et al. 2010). More recently, high resolution seismic tomography using airgun-generated waves locates a magma chamber at 2-4 kilometres depth below the seafloor (Chrapkiewicz et al. (2022), whereas McVey et al. (2020) do not recognize any melt between 3-5 kilometres by seismic tomography using ocean bottom seismometers. Seismic activity below the Kolumbo volcano in 2003 is interpreted to indicate magma storage at 6-9 kilometres depth (Dimitriadis et al. 2009). Conversely, Schmid et al. (2022) suggest that the strong seismic activity at 6-9 kilometres depth reflects a rheologically strong layer obstructing melt ascending toward a 2-4 kilometres deep magma chamber. Petrology- and geochemistry-based pre-eruption magma storage modelling indicates that a rhyolitic magma at a temperature of 750°C was stored at a depth of 5-6 kilometres prior to the 1650 CE eruption (Fig. 1c; Cantner et al. 2014).

4 Sampling and methods

4.1 Sample localities

The samples from the Kolumbo volcano were collected by a remote-operated vehicle of the exploration vessel *Nautilus* (cruise NA007) in 2010. Limitation of the robot arm only allowed sampling of loose rocks of ~10 centimetres in size, however, it was possible to sample pumice and lava from the K2 and K5 units (Fig. 1b).

4.2 Methods

Chemical analysis were performed at the Laboratory for Environmental and Raw Materials Analysis at the Institute of Applied Geosciences in Karlsruhe, Germany, with the exception of electron probe micro-analysis (EPMA), which was performed at the Institute of Geological Sciences of the University of Bern, Switzerland and Hg content measurement by atomic absorption spectroscopy at the Oceanic and Continental Environment and Paleoenvironment mixed research unit (UMR EPOC) in Bordeaux, France. Petrography was studied using transmitted and reflected light microscopy.

4.2.1 Whole rock geochemistry

The major element composition was measured by X-ray fluorescence (XRF) (S4 Explorer, Bruker AXS) on glass beads with BHVO-1, MRG-1, RGM-1 and SY-2 as reference material to control analytical precision and accuracy (ESM1). Carbon and sulphur content were measured on rock powder by solid state infrared absorption using a Carbon-Sulphur Analyzer (CS-2000, Eltra) with steel (92400-3050), ductile iron (92400-3100) and barium sulphate (90821) standards from Eltra as reference material to control analytical precision and accuracy (ESM1). Trace element content was measured by laser-ablation inductively-coupled-plasma mass-spectrometry on pressed powder pellets (PPP-LA-ICP-MS) using a Teledyne 193 nm Excimer Laser coupled to an ICP-MS (Element XR ThermoFisher) with spot size of 85 µm,

laser frequency of 10 Hz, fluence of 5 J.cm^{-2}, He, Ar and N flow of 0.3 L.min^{-1}, 0.85 L.min^{-1} and 10 mL.min^{-1}, respectively. Pressed powder pellets (PPP) are prepared following the method described in Patten et al. (2023). The SiO_2 content from XRF analyses was used for internal standard calibration. The following isotopes were measured: ^{7}Li, ^{29}Si, ^{31}P, ^{32}S, ^{35}Cl, ^{44}Ca, ^{45}Sc, ^{49}Ti, ^{51}V, ^{53}Cr, ^{55}Mn, ^{57}Fe, ^{59}Co, ^{60}Ni, ^{63}Cu, ^{66}Zn, ^{75}As, ^{78}Se, ^{85}Rb, ^{88}Sr, ^{89}Y, ^{90}Zr, ^{93}Nb, ^{95}Mo, ^{107}Ag, ^{118}Sn, ^{121}Sb, ^{125}Te, ^{137}Ba, ^{139}La, ^{140}Ce, ^{141}Pr, ^{146}Nd, ^{147}Sm, ^{151}Eu, ^{157}Gd, ^{159}Tb, ^{161}Dy, ^{165}Ho, ^{167}Er, ^{169}Tm, ^{172}Yb, ^{175}Lu, ^{178}Hf, ^{181}Ta, ^{197}Au, ^{202}Hg, ^{205}Tl, ^{208}Pb, ^{209}Bi, ^{232}Th and ^{238}U. Calibration and data quality checking was done using PPP of standards BHVO-1, BHVO-2, BCR-2 and BIR-1 from the USGS. In order to improve data quality, the Au content was measured a second time, on the same apparatus, following the method of ultra-low detection of Au on PPP-LA-ICP-MS developed by Patten et al. (2023). The following isotopes were measured: ^{29}Si, ^{44}Ca, ^{180}Hf, ^{181}Ta and ^{197}Au. The SiO_2 content from XRF analyses was used for internal standard calibration. Calibration and data quality checking was done using PPP of standards BHVO-2, BCR-2, BIR-1 from the USGS, MRG-1 and TDB-1 from NRCan and TSD-41, an in-house epidosite standard. Data reduction of both PPP-LA-ICP-MS analysis was done using the Iolite software 3DRS plugin v.4.8.3 (Paton et al. 2011). Accuracy and precision for reference materials (<15% for most elements) as well as limits of detections are detailed in Supplementary data (ESM1). The Hg content in the samples was measured by spectrophotometry with a direct Hg analyser DMA-80 (Milestone) using standards BCR-277R and TCEGir (in-house) for calibration (ESM1).

4.2.2 Magnetite composition

Major element composition of magnetite was measured by EPMA (JEOL JXA-8200 Superprobe) using the following synthetic and natural standard reference materials: anorthite (Al_2O_3, CaO), orthoclase (SiO_2), magnetite (FeO), forsterite (MgO), rutile (TiO_2), metal nickel (NiO), spinel (Cr_2O_3), sphalerite (ZnO) and pyrolusite (MnO). Spot analyses for Al, Si, Ca, Fe,

Mg, Ti, Ni, Cr, Zn and Mn were performed using 15 keV accelerating voltage, 20 nA specimen current, and 40 s dwell time (10 s for each background after 20 s on peak) (ESM2). Trace element composition of magnetite was measured by in-situ LA-ICP-MS analysis, on the same apparatus as for PPP-LA-ICP-MS analysis, with spot size of 35 µm, laser frequency of 10 Hz, fluence of 5 $J.cm^{-2}$, He and N flow of 0.3 $L.min^{-1}$ and 10 $mL.min^{-1}$, respectively. The Fe data from EMPA analysis was used for internal standard calibration of LA-ICP-MS data. The following isotopes were measured: ^{29}Si, ^{32}S, ^{49}Ti, ^{51}V, ^{55}Mn, ^{57}Fe, ^{59}Co, ^{60}Ni, ^{63}Cu, ^{66}Zn, ^{75}As, ^{95}Mo, ^{107}Ag, ^{111}Cd, ^{115}In, ^{118}Sn, ^{121}Sb, ^{125}Te, ^{182}W, ^{197}Au, ^{205}Tl, ^{208}Pb, ^{209}Bi, ^{232}Th, ^{238}U. Calibration and data quality was checked using basaltic glasses BHVO-2, BCR-2 and BIR-1 from the USGS. Although non-matrix matching, calibration of magnetite using Fe-rich basaltic standards is adequate (Dare et al. 2012). Data reduction was done using the Iolite software 3DRS plugin. Accuracy and precision for reference materials (<15% for most elements) as well as limits of detections are detailed in Supplementary data (ESM2).

5 Results

5.1 Petrography of Kolumbo volcano rocks

The samples of the Kolumbo volcano belong to the K2 and K5 volcanic units. Two types of samples were collected, intermediate to felsic pumice (K2 and K5 units) and mafic to felsic lava (K5 unit only) (Fig. 2a-d). As the samples are mostly composed of a glass to microcrystalline matrix, their igneous classification can not be determined petrographically. Further distinctions (e.g. rhyolite pumice and trachyte pumice) is based on geochemical data described in the corresponding section.

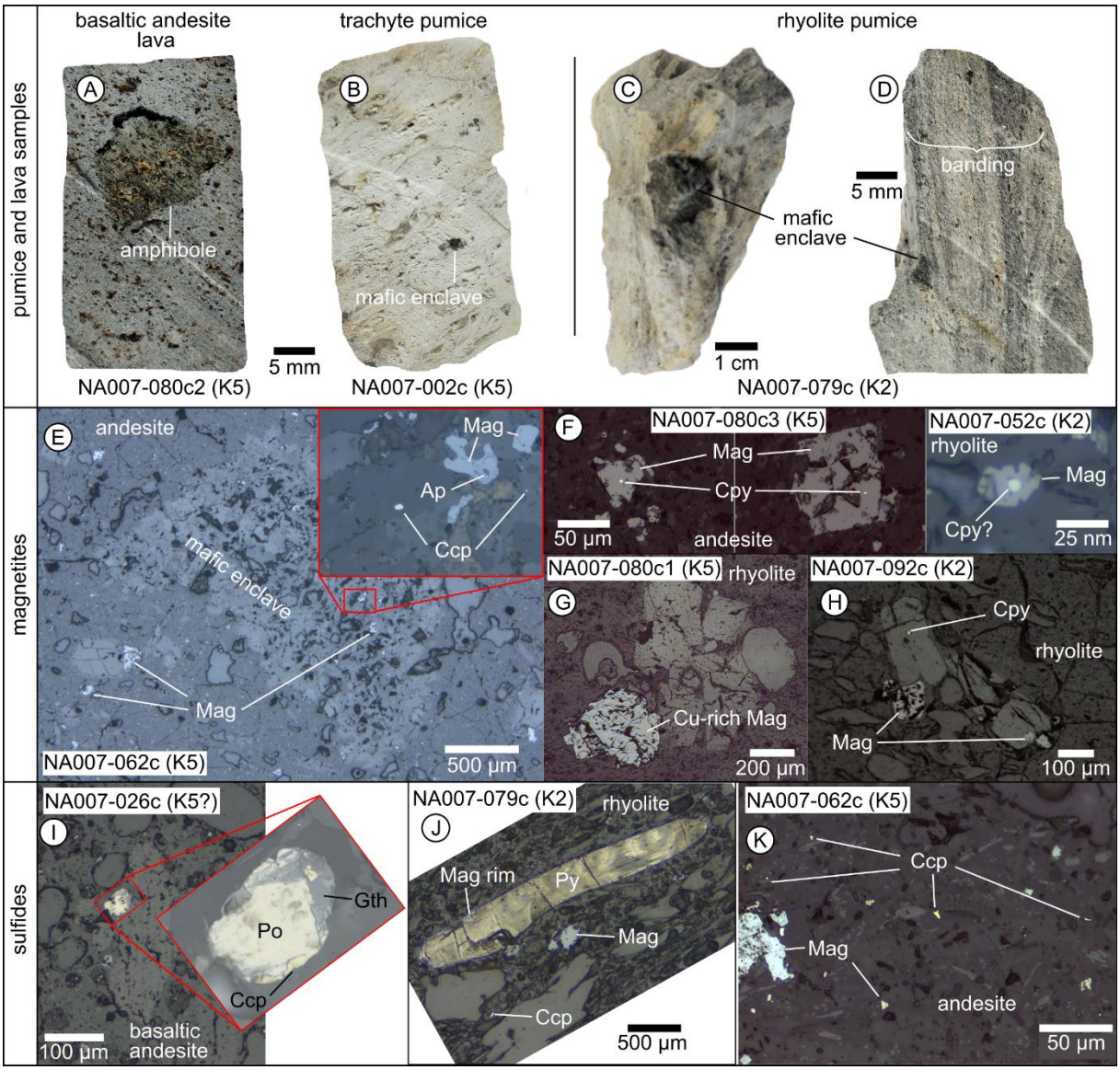

Fig. 2 : Petrography of Kolumbo' s volcanic rocks. (A) Basaltic andesite lava sample with an amphibole xenocryst. (B) Trachyte pumice with mafic enclave. (C and D) Rhyolite pumice with banded texture and mafic enclaves with quenched margin. (E) Mafic enclave with disseminated magnetite and sulphides in andesite matrix with disseminated magnetite. (F) Idiomorphic magnetite with sulphide inclusions. (G and H) Phenocryst clusters with plagioclase, amphibole and magnetite, locally containing sulphide inclusions. (I) Sulphide bleb of pyrrhotite and chalcopyrite with oxidized goethite rim in basaltic andesite pumice. (J) Pyrite with magnetite rim in rhyolite pumice with chalcopyrite and magnetite. (K) Disseminated chalcopyrite and magnetite in andesite matrix.

5.1.1 K2 unit

The K2 unit consists of a tens of metres thick volcanoclastic sequence normally overlaid by later volcano-sedimentary units but locally outcropping in Kolumbo' s crater since the 1650 CE eruption (Hübscher et al. 2015). The samples are light grey pumices with ~40 vol.% vesicles (<1 mm), locally showing dark grey bands (Fig. 2d). The glass matrix contains 1 to 3 vol.% phenocrysts, mostly plagioclase, biotite and magnetite (<1 vol.%) as well as rare orthopyroxene, amphibole and quartz. Mafic microcrystalline enclaves are ubiquitous (~1 vol.%) and range from <1mm to 2 cm in size (Fig. 2c, d). They are composed of 30 to 50 vol.% microcrystalline matrix with acicular plagioclase, amphibole and magnetite (<1 vol.%) containing larger phenocrysts of amphibole, clinopyroxene and plagioclase (<500 μm). The enclaves have a quenched margin texture and the contact with the matrix is sharp, indicating rapid crystallisation. The contact usually has increased vesicularity compared to the rest of the rock.

5.1.2 K5 unit

The K5 unit consists of a tens of metres thick volcanoclastic sequence with lava flows shaping Kolumbo' s volcanic cone since the 1650 CE eruption (Hübscher et al. 2015; Klaver et al. 2016). The K5 pumice is white to grey with 40 to 70 vol.% vesicles and contain 1 to 3 vol.% phenocrysts, mostly plagioclase, biotite and magnetite (<1 vol.%) as well as rare apatite, orthopyroxene, amphibole and quartz (Fig. 2b). The K5 lava usually contains <5 vol.% vesicles, 60 vol.% microcrystalline matrix and 35 vol.% phenocrysts (Fig. 2a). The phenocrysts are clinopyroxene, plagioclase, amphibole and magnetite (<1 vol.%). In both pumice and lava, phenocrysts occur locally as single plagioclase or amphibole grains (<2 cm) showing evidence of resorption, or as clusters (<2 mm) containing plagioclase ± amphibole ± clinopyroxene ±

magnetite and <50 vol.% vesicles (Fig. 2a, b, g, h). Mafic microcrystalline enclaves ubiquitous in the samples(~1 vol.%). They are similar to those in K2. They range from <1 mm to 2 cm in size and have a quenched margin, indicating rapid crystallisation. They are composed of 30 to 50 vol.% microcrystalline matrix with acicular plagioclase, amphibole and magnetite (<1 vol.%) containing larger phenocrysts of amphibole, clinopyroxene and plagioclase (<500 µm).The contact with the host rock is sharp and shows increased vesicularity (Fig. 2e).

5.1.3 Magnetite

Magnetite is ubiquitous in the volcanic samples of Kolumbo and shows three main habits: (1) small (<50 µm), idiomorphic magnetite in enclaves, where it is disseminated in the matrix, forms inclusions in silicates or is locally associated with sulphides (Fig. 2e); (2) sub-idiomorphic to idiomorphic magnetite (<100 µm) in the matrix, where it is usually fractured or fragmented and locally contains sulphide inclusions (Fig. 2f); (3) sub-idiomorphic magnetite (<200 µm) in clusters, where it is usually fractured and rounded, locally has sulphide inclusions and may show compositional zoning (Fig. 2g, h).

5.1.4 Sulphides

Sulphides, although relatively scarce, are present in most of the volcanic samples of Kolumbo. The most common mineral is pyrrhotite along with less abundant chalcopyrite and pyrite (Fig. 2e, f, i, j, k). They form xenomorphic grains which are usually <100 µm, but exceptionally at mm-scale (Fig. 2j, k). The grains are usually monomineralic (pyrrhotite or chalcopyrite) but may form a pyrrhotite-chalcopyrite-pyrite assemblage, locally replaced by magnetite and goethite (Fig. 2i). Additionally, sulphides locally occur as inclusions (<10 µm) in all types of magnetite and in the phenocrysts (Fig. 2f, h).

5.2 Geochemistry

5.2.1 Whole rock geochemistry of lava and enclaves

Major element composition from our samples and data from previous studies (Cantner et al. 2014; Klaver et al. 2016) show that the K2 and K5 units record similar differentiation processes, from basaltic andesite to rhyolite and are considered to be representative of the magmatic system evolution. The trace element content in the whole rock is varying during magmatic differentiation following trends. As the rock composition becomes more felsic (MgO > 0.9 wt.%), Ag, As, Hg, Pb, Sb, Sn and Tl contents increase, while Au, Co, Cu, Fe, Ni, Ti, V and Zn contents remain relatively constant. With further magmatic differentiation, (MgO <0.9 wt.%) Ag, As, Au, Co, Cu, Hg, Pb, Sb, Sn and Zn contents decrease (Fig. 3a-k), while Bi and Tl content is increasing (Fig. 3l, m).

5.2.2 Magnetite geochemistry

Magnetite shows limited major element variation in all samples: Fe 58.1-68.1 wt.%; Ti 1.14-8.06 wt.%, Si 0.02-2.49 wt.%; Al 0.54-2.45 wt.%; Mg 0.10-2.14 wt.%; Cr <0.01-2.14 wt.%; Mn <0.01-1.67 wt.%; Ca <0.01-0.65 wt.%. The Al, Co, Cr, Cu, Ga, Mg, Ni, Sc and V contents are higher in mafic rocks, while Ag, As, Bi, Ge, Hf, Mn, Mo, Nb, P, Pb, Sb, Sn, Ta, Ti, W, Y, Zn and Zr contents are enriched in felsic rocks (Fig. 3a-m).

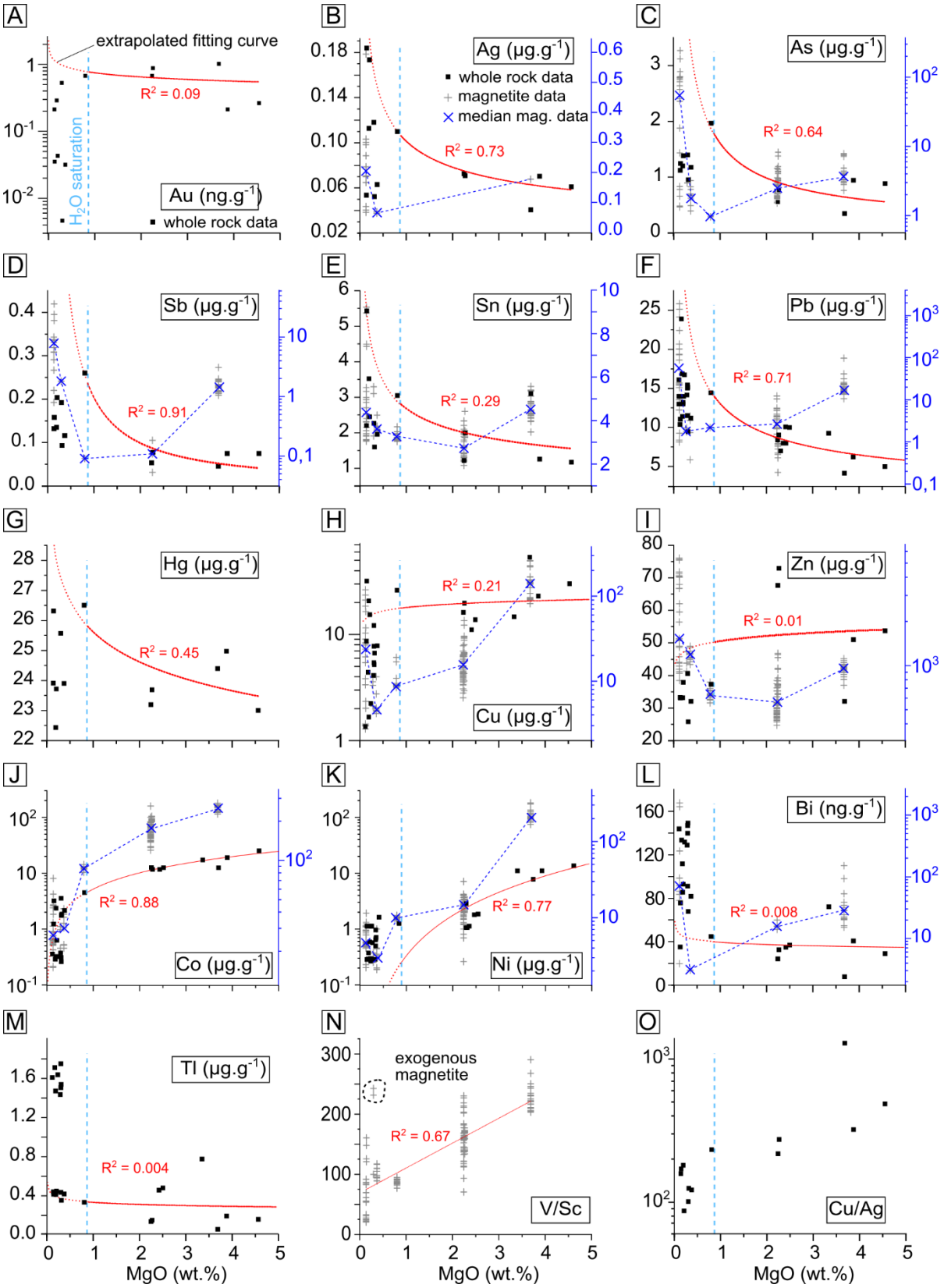

Fig. 3: Chalcophile element content in the whole rock and magnetite during differentiation as shown by whole rock MgO-data (Note: scale of whole rock and magnetite data are different). (A to M) Fitting curves (in red) are calculated based on data >0.9 wt.% MgO (i.e. before water saturation) and indicate the evolution of metal concentration in the whole rock during magmatic

differentiation. The dotted section of the fitting curves is extrapolated toward MgO=0 wt.% to simulate the evolution of metal concentration in the whole rock during magmatic differentiation in absence of water saturation, degassing and associated metal removal. Blue dotted lines connect medians of magnetite data. (N) V/Sc ratio in magnetite at various MgO-contents. (O) Cu/Ag ratio in whole rock at various MgO-contents.

5.3 Melt evolution modelling with COMAGMAT 3.75

The evolution of the melt was modelled using COMAGMAT 3.75 (Ariskin and Barmina 2004) to decipher the processes leading to metal mobilization from the melt. This model is based on a combination of empirical and thermodynamic calculations of mineral-melt equilibrium and can simulate magma fractionation. An average whole rock composition of the three most mafic sample compositions is used as a proxy for starting composition of the melt. The pressure constrain is set to decrease from 200 to 90 MPa to reflect the ascending melt in an upper reservoir located between 6 and 3 kilometres depth. The accuracy of the model is controlled by samples data, because of the limited number of available samples, it is not very well constrained between 0.8-2.0 and 2.5-3.0 wt.% MgO. Multiple model runs using the redox (fO_2 FMQ + 0.5 to 1.5) and the H_2O content (1 to 3 wt.%) as varying parameters show that the starting conditions producing a model fitting best the evolution of the major element composition are fO_2 FMQ + 1 and 2.0 wt.% H_2O. According to the model, using these best fit parameters, magnetite crystallisation starts as the melt reaches 2.5 wt.% MgO. The water content increases during magmatic differentiation from 2.0 wt.% to 4.3 wt.% H_2O at 0.9 wt.% MgO, then water saturation is reached and water content decreases to 2.9 wt.% in the most evolved melt.

6 Discussion

6.1 Magmatic differentiation at Kolumbo

6.1.1 Petrology and geochemistry

The petrological and geochemical diversity of the samples illustrates a complex magmatic history at Kolumbo. Mafic enclaves with chilled margin in intermediate to felsic rocks indicate injection of mafic magma into an evolved magma chamber (Fig. 2b-d), while samples with trachytic composition (e.g. NA007-002c) indicate magmatic differentiation of the mafic magma or its mixing with the evolved magma. The basaltic andesite or andesite composition of the mafic enclaves indicate that their parent melt is not a direct product of mantle melting but already started to differentiate in a deeper magma chamber before reaching the shallow evolved magma chamber. Whole rock trace element data supports this by the compatible element-depleted nature of the most mafic rocks, likely a result of fractionated magmatic differentiation (Fig. 4). Slightly lower Ti and V relative to MORB may be the result of early magnetite crystallization, while lower Cu content likely reflects early sulphide formation. The high As, Ag, Sb, Tl and Pb contents in basaltic andesite relative to MORB can be either related to early differentiation, as these elements are mostly incompatible (Fig. 4), or to mantle enrichment due to supra-subduction zone contamination by slab dehydration, particularly in As, Sb and Pb (Hattori et al. 2005; Patten et al. 2017).

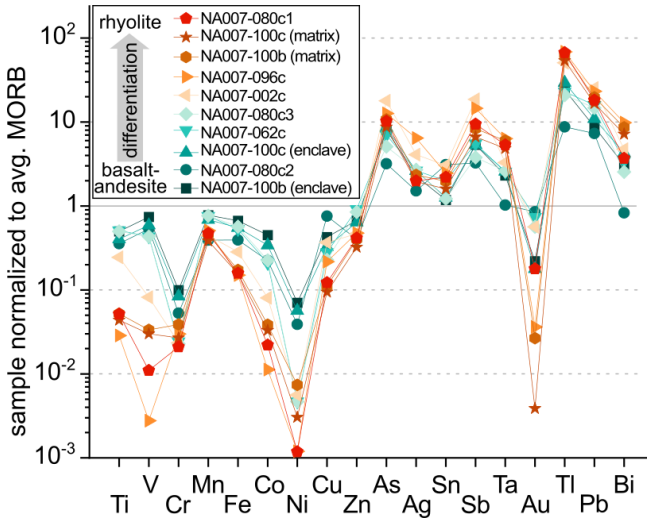

Fig. 4: Whole rock trace element data normalized to average mid-oceanic ridge basalt, based on Arevalo and McDonough (2010).

6.1.2 Melt evolution modelling

The best fitting parameters of fO_2 FMQ + 1 and 2 wt.% H_2O are within the range of other arc volcanic systems where the mantle-source is oxidized (Bucholz and Kelemen 2019; Richards 2015). The modelled evolution of the Si, Ti, Al, Ca and K contents with decreasing MgO or increasing differentiation fit well with sample composition (Annex 1). The modelled Fe content is slightly higher as measured in the samples during the early differentiation stages (>2 wt.% MgO), possibly due to model limitations preventing early formation of magnetite (Annex 1). Increased magnetite crystallization below 2.5 wt.% MgO is, however, successfully reproduced in the model. The modelled P content increases with progressive differentiation while it decreases in the geochemical data (Annex 1). This discrepancy is caused by apatite crystallization which is not supported by the modelling. Apatite crystallization is contemporaneous with magnetite formation (Fig. 2e), leading to a decreasing P_2O_5 content in the melt as magnetite crystallization increases (c.f. Jenner et al. 2010). The Na content in the modelled melt reproduces the sample composition during differentiation until 0.5 wt.% MgO, then it decreases as albite forms. Conversely, Na-contents remain constant in the samples with MgO <0.5 wt.%, indicating that plagioclase did not fractionate during late differentiation. Except for the minor limitations discussed here, the model well describes sample geochemistry. Key information that is drawn from the model is increased magnetite formation below 2.5 wt.% MgO and water saturation at ~0.9 wt.% MgO.

6.2 Controlling magmatic processes

6.2.1 Continuous magnetite crystallization or magnetite crisis?

The magnetite crisis, as defined by Jenner et al. (2010), refers to chemical changes in the melt related to sudden magnetite crystallization during melt differentiation at ~2.5 wt.%

MgO and is a critical mechanism to mobilize chalcophile elements during arc magma evolution. Formation of magnetite drives the redox in the melt toward reduced conditions by incorporating Fe^{3+} in its crystal lattice. This favours sulphide saturation and chalcophile element partitioning from the silicate melt into sulphide phases (Jenner et al. 2010). Magnetite crisis is generally expressed in the melt chemistry by a sharp drop in Fe and Ti. Additionally, the drop of the V/Sc ratio is a good proxy for magnetite formation as V is more compatible in magnetite than Sc (Dare et al. 2014; Jenner et al. 2010). In Kolumbo, the Fe and Ti contents, and V/Sc ratios decrease with magmatic differentiation until 2.5 wt.% MgO while the model indicates increased values (Fig. 5a, b). This discrepancy is explained by the lack of modelled magnetite crystallisation at MgO > 2.5 wt.% while igneous magnetite is observed in all rocks at Kolumbo (Fig. 2e, 5d). Below 2.5 wt.% MgO, the amount of magnetite forming and fractionating increases, as supported by the matching model and data (Fig. 5a, b). Magnetite fractionation is supported by the evolution of the V/Sc ratio in igneous magnetite (Fig. 3n). As V is highly compatible in magnetite, magnetite forming early during magmatic differentiation will have a higher V/Sc ratio than magnetite forming at a later stage of magmatic differentiation. The constantly decreasing V/Sc ratio in magnetite as the host-rock is more and more differentiated indicates that magnetite is autochthonous and that earlier magnetite is removed from the magma. Among magnetite hosted in rhyolite, a few grains show higher V/Sc ratio, indicating that these are likely allochthonous and formed from a more mafic melt (Fig. 3n).

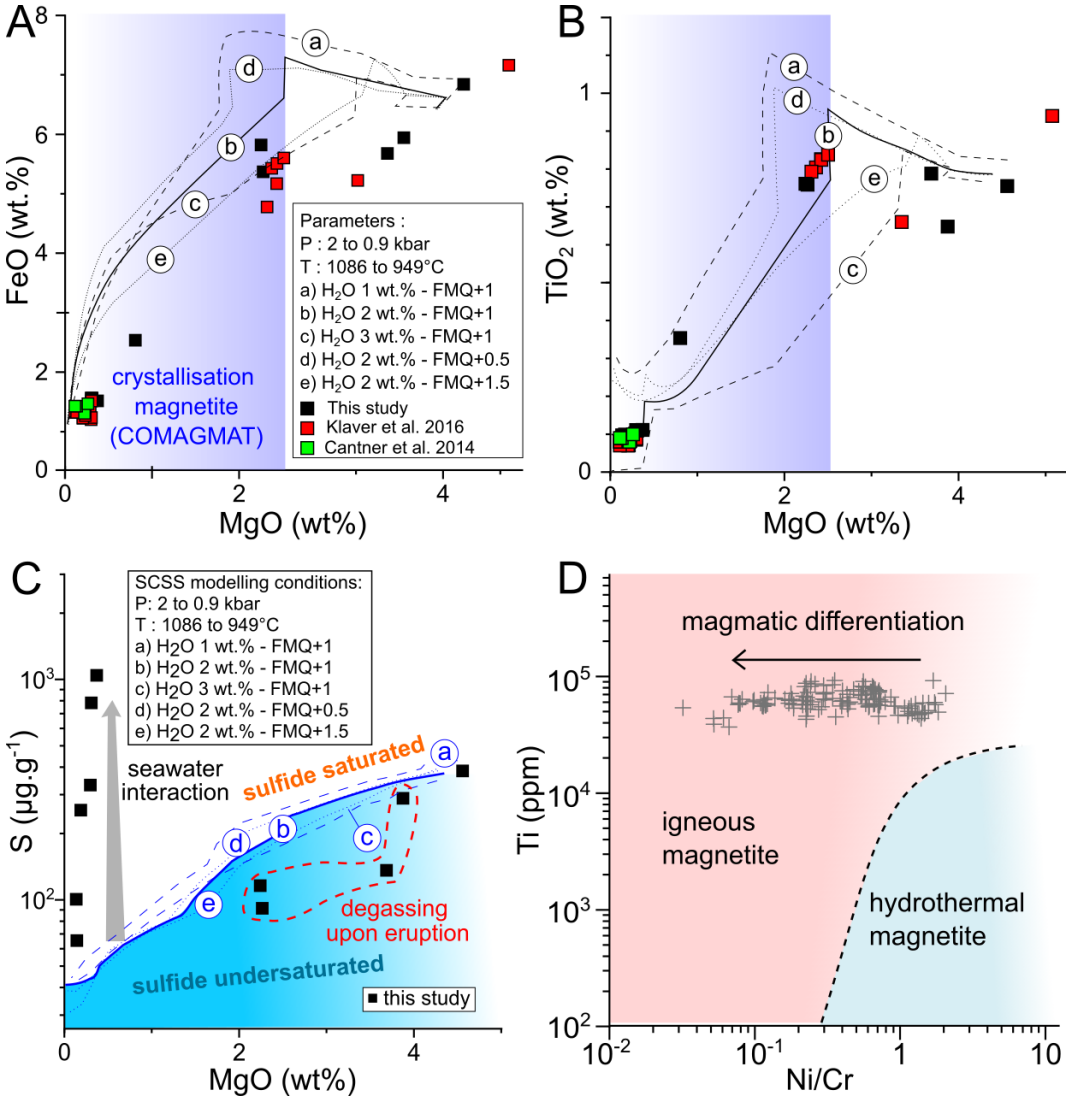

Fig. 5 : Model of the geochemical evolution of melt compared to whole rock data. (A and B) Measured vs. modelled FeO and TiO_2 contents in the melt during magmatic differentiation. Modelling was performed using COMAGMAT 3.75 (after Ariskin and Barmina 2004). (C) Measured vs. modelled S-content of the evolution of the SCSS versus MgO content in the melt during magmatic differentiation (after Smythe et al. 2017, using modelled melt composition) (D) Magnetite classification into magmatic and hydrothermal magnetite based on Dare et al. (2014).

6.2.2 Sulphide saturation

Sulphur concentration at sulphide saturation (SCSS) evolution during magmatic differentiation is modelled using the method developed by Smythe et al. (2017) with a melt composition calculated by COMAGMAT 3.75. In comparison to SCSS values modelled for MORB (c.f. Jugo 2009; SCSS = 2000 µg.g^{-1} S), the SCSS in Kolumbo' s most primitive melts

is relatively low (~300 µg.g^{-1} S) and indicates that the melt is sulphide-saturated during the whole magmatic differentiation (Fig. 5c). This is supported by the observation of sulphides in all samples and their shape indicates crystallization from sulphide liquid (Fig. 2e-k, 5c) (Patten et al. 2013). Sulphur values below the SCSS indicating that intermediate samples are S undersaturated (between 2.0 and 3.7 wt.% MgO), despite presence of sulphide droplets in the matrix and inclusions in phenocrysts, is likely the result of loss of S by degassing upon eruption. Outlying high S (>500 µg.g^{-1}) in felsic samples can be explained by seawater/rock interaction upon eruption. The mechanisms triggering early sulphide saturation are unclear, but may be related to magnetite or amphibole crystallization. Magnetite crystallization, changes the redox of the melt toward more reduced conditions, favouring S saturation (Jenner et al. 2010; Richards 2015). Similarly, amphibole replacing clinopyroxene modifies the redox of the melt and can trigger sulphide saturation as the primitive basaltic melt evolves to andesite in the lower crustal reservoir (Georgatou et al. 2021; Georgatou et al. 2022).

6.2.3 Degassing

Understanding the degassing processes in Kolumbo is critical to address metal transfer in the system as degassing volatiles carry ligands and metals (Hedenquist and Lowenstern 1994). However, initial volatile content of the samples has been altered by eruption degassing and interaction with seawater (Fig. 5c). Thus, the best proxy for assessing degassing is to use water saturation given by the modelling of the melt evolution during magmatic differentiation. The modelled evolution of the volatile content during magmatic differentiation fits well to the data, supporting water saturation at 0.9 wt.% MgO (Annex 1). However, initial volatile content in the model (2 wt.% H_2O) is lower than the average loss on ignition (LOI) measured on the most mafic samples (3.23 wt.% LOI). This is likely caused by seawater/rock interaction after eruption increasing the volatile content (Cl, S, H_2O, CO_2) in the samples in regard to their pre-eruption values (Coogan and Gillis 2018; Haraguchi et al. 2014). Loss on ignition on rhyolite

samples gives a post-water saturation volatile content of 2.84 wt.% in lava, well reproduced by the model, but increasing up to 7.07 wt.% in pumices. However, as pumice form during the eruption as a mixture of degassing volatiles and magma, they might not be representative of the initial volatile content. Degassing of magmatic volatile species is controlled by the confining pressure, temperature, oxidation state and volatile content in the magma. Usually, magmatic volatiles are released in the following order: CO_2 <SO_2-H_2S <H_2O (and halogens), due to increasing solubility in the melt (Mavrogenes and O'Neill 1999; Rouwet et al. 2019). As CO_2 is saturated early in magmatic arc systems, it starts to separate from the silicate melt in the lower crust (Lowenstern 2001). In the case of Kolumbo CO_2 effervescence likely occurs in the lower crust where differentiation from basalt to basaltic andesite occurs. Our model predicts water saturation at 0.9 wt.% MgO (i.e. during trachyte formation) in the upper magma chamber (between 7 and 2 km depth). This indicates that SO_2 degassing could have taken place somewhere between 15 and 2 km depth, during magma ascend or in the upper magma chamber. However, early sulphide saturation might have prevented SO_2 degassing by sequestrating S in a solid or liquid sulphide phase. As the magma degasses, volatile bubbles can nucleate on sulphide phases, leading to formation of sulphide-volatile compounds (Barnes et al. 2019; Mungall et al. 2015).

6.3 Metal flux during melt evolution

6.3.1 Pre-water saturation magmatic differentiation

Before water saturation is reached during magmatic differentiation V, Ni, Co, Cu, Ti, Au and Zn are progressively depleted, whereas Sn, Ag, As, Sb, Pb and Tl are enriched (Fig. 3a-n). Depletion in V, Ni, Co and to some extent Fe and Ti is related to crystallization and settling of magnetite (c.f. Dare et al. 2014). Despite early sulphide saturation, there is no notable chalcophile element depletion in the magma before rhyolite formation and water saturation,

implying more complex processes during the magmatic evolution than simple sulphide phases formation and settling (Fig. 3a-m).

6.3.2 Insight from magnetite before water saturation

Magnetite in Kolumbo' s volcanic rocks is of magmatic origin and almost exclusively autochthonous (Fig. 3n, 5d). Thus, magnetite trace element composition reflects the metal content in the melt while the whole rock composition is considered representative of the magma (i.e. melt plus mineral phases) composition. The contrasting metal content between magnetite and its host rock gives insights into metal mobilizing processes during magmatic differentiation. From basaltic andesite to trachyte differentiation stages, the Cu content in the magma show a slightly decreasing trend but remains almost constant (avg. 28 $\mu g.g^{-1}$) while it decreases from avg. 141 $\mu g.g^{-1}$ to 10 $\mu g.g^{-1}$ in the corresponding magnetite (Fig. 3h). While Cu remain in the magma, there is less and less Cu available in the melt for magnetite during magmatic differentiation, indicating that most of the Cu is trapped in a mineral phase mostly remaining in the magma, most likely sulphides. Strongly magnetite-compatible chalcophile elements, such as Ni (Dare et al. 2014), show a different behaviour. Nickel is depleted simultaneously in magnetite and in the magma during magmatic differentiation (Fig. 3k). This indicates that, unlike sulphide phases, magnetite fractionates from the magma after crystallizing (Fig. 3k, 8a stage 1). Cobalt is slightly less depleted than Ni in the magma as magnetite fractionates (Fig. 3j). As Co is less compatible than Ni in magnetite, more is incorporated in sulphides and remain in the magma.

6.3.3 Metal budget at sulphide saturation

In Kolumbo, the melt is sulphide saturated at least since the basaltic andesite differentiation stage, as observed petrographically and supported by modelling (Fig. 2e-k, 5c).

Consistent drop in the Cu/Ag ratio along differentiation is typical of chalcopyrite crystallization (Fig. 3o) (Jenner et al. 2010; Jenner et al. 2015), however sulphide liquid is also forming, as observed petrographically (Fig. 2i). The slight depletion in Cu during magmatic differentiation indicates that some chalcopyrite fractionates (Fig. 3h). Despite early sulphide crystallization, chalcophile and siderophile elements in the samples are not significantly depleted during magmatic differentiation and even get enriched for Ag, As, Au, Bi, Hg, Pb, Sb and Sn prior water saturation, indicating that sulphides phases mostly remain floating in the melt during differentiation (Fig. 3a-j, 8a stage 1). This is likely linked to the limited size of the sulphides phases and the increasing viscosity of the melt as it differentiates, reducing their settling potential (Fig. 2k), (Holzheid 2010). Settling of sulphides phases can also be prevented by formation of sulphide-volatile compound as the magma degasses (Mungall et al. 2015; Yao and Mungall 2020). As a volatile bubble grow on a sulphide liquid droplet, the average buoyancy of the compound can eventually lead it to float in the melt or rise (Yao and Mungall 2020).

6.3.4 Metal mobility upon degassing

Degassing is recognized as an important process to mobilize metals from a magmatic melt, as the volatiles are rich in ligands such as Cl or S that can transport metals as sulphide or chloride complexes (Gammons and Williams-Jones 1997; Nadeau et al. 2021). In Kolumbo, according to modelling, water saturation is reached at 0.9 wt.% MgO during the trachyte differentiation stage. Previous degassing that could happen before water saturation (i.e. SO_2, H_2S, CO_2) did not have a significant impact on the metal content of the samples. To have a first order insight of metal mobility after water saturation, the metal content in the samples after water saturation is compared to a metal content of "undegassed magma" modelled by extrapolating a curve fitting pre-water saturation data (i.e. >0.9 wt.% MgO). It appears that the most chalcophile elements (i.e. Ag, Au, Cu, Hg), with the notable exception of Bi and Tl, as

well as less chalcophile elements (i.e. As, Sb, Sn, Pb, Zn) are depleted in the samples after water saturation in comparison to the "undegassed magma" (Fig. 3a-m, 8a stage 2, 8b). This indicates partitioning of metals into the volatile phase, as shown by frequent oxidation of sulphide phases (Fig. 2i, j). Volatile phase/sulphide interaction in sulphide-volatile compounds leads to metal transfer into the volatile phase as the sulphide gets oxidized to magnetite (Patten et al. under review). The sudden drop of the Cu/Ag ratio after water saturation is likely related to the higher partition coefficient of Cu (K_{DCu} = 198-660) in the volatile phase than Ag ($K_{D\ Ag}$ = 116-244) as volatiles oxidize sulphides (Fig. 3o) (Patten et al. under review).

6.3.5 Magnetite as metal flux tracer

The competing compatibility of chalcophile elements in sulphides, volatile phase and magnetite allows to use igneous magnetite as a tracer for metal fluxes in the melt during magmatic differentiation and, by extension, to track metal mobilizing magmatic processes. Given that igneous magnetite is autochthonous, the V/Sc ratio in magnetite enables to track the degree of magmatic differentiation and can be calibrated by referring to the whole rock composition of the host rock (Fig. 6). Decreasing Cu content in magnetite during magmatic differentiation before water saturation reflects sulphide saturation (Fig. 6). High Cu content at low V/Sc ratio indicates post-water degassing magnetite formation (Fig. 6). After degassing, chalcophile elements are locally enriched in magnetite (Fig. 3a-m). This behaviour is the result of the competing partitioning of chalcophile elements between sulphides and magnetite. In absence of S in the melt after degassing, the residual chalcophile elements that did not partition in volatiles are incorporated in the magnetite (Fig. 8a stage 3, 8b).

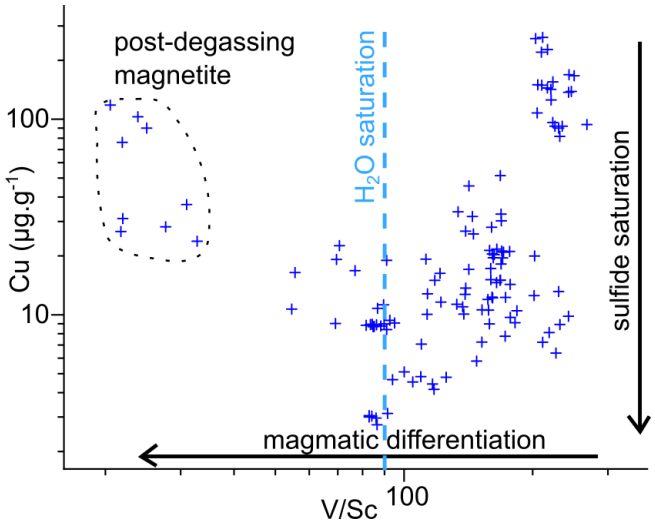

Fig. 6: Cu content in igneous magnetite compared to its V/Sc ratio. Water saturation is given by COMAGMAT 3.75 modelling and placed on the V/Sc axis after calibration with the magnetite host rock composition.

6.4 Comparison with other arc volcanoes

Sulphide saturation, formation of sulphide phases and fractionation are among the main processes controlling chalcophile element contents in melt during magmatic differentiation. The Cu/Ag ratio in the whole rock compared to the MgO content helps to understand how chalcophile elements were mobilized as it highlights if sulphide liquid or crystalline sulphide phases formed at sulphide saturation (Li and Audétat 2012; Patten et al. 2013). While formation of a sulphide liquid is not changing the Cu/Ag ratio, as both elements have similar compatibility in sulphide liquid, formation of crystalline sulphide phases leads to a decrease of the Cu/Ag ratio as Cu is more compatible than Ag in these phases (Jenner et al. 2015; Li and Audétat 2012). The Cu/Ag ratio in a basalt is usually close to the mantle ratio (~3000±500) and remains unchanged during magmatic differentiation as long as only sulphide liquid forms (e.g. Niuatahi volcano) (Fig. 7) (Brandl et al. 2022; Park et al. 2015; Wang et al. 2019). Formation and fractionation of crystalline sulphide phases leads to a progressively decreasing Cu/Ag ratio from the mantle value in the whole rock during magmatic differentiation, as observed in samples from the Manaus and Lau basin, Valu Fa Ridge and Brothers volcano (Fig. 7) (Brandl et al. 2022; Jenner et al. 2010; Jenner et al. 2012; Jenner et al. 2015). In Kolumbo, the Cu/Ag ratio

develops in a similar way during differentiation as in the Nisyros volcano during early differentiation stages (Georgatou et al. 2022). Then, Cu/Ag ratio in Kolumbo decreases continuously between ~4.5 and ~0.9 wt.% MgO and extrapolation of the Cu/Ag ratio for more mafic composition yields a mantel-like Cu/Ag ratio at basaltic composition (Fig. 7). This indicates uninterrupted formation and partial fractionation of crystalline sulphide phases in Kolumbo' s melt since early lower crustal differentiation of basaltic melt until the trachyte/rhyolite stage in the upper magma chamber. Degassing after water saturation at ~0.9 wt.% MgO in Kolumbo leads to a stronger decrease in the Cu/Ag ratio as Cu is more compatible than Ag in a volatile phase exsolving from the melt or in volatiles during sulphide-volatile compound formation (Fig. 7) (Patten et al. under review).

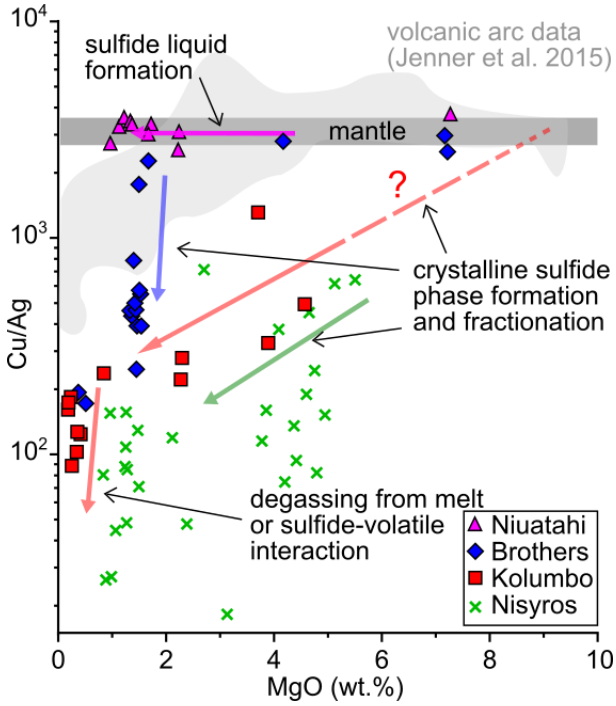

Fig. 7- Evolution of the Cu/Ag ratio compared to MgO content in volcanic rock samples of different arc volcanos. Niuatahi data are from Park et al. (2015) and Wang et al. (2019), Brothers volcano data are from Brandl et al. (2022) and Nisyros data are from Georgatou et al. (2022).

6.5 Hydrothermal mineralization

6.5.1 Metal sources

The sulphide-sulphates diffusers are Zn-Pb rich and show high As, Ag, Au, Hg, Sb and Tl content, while being relatively Cu poor (Ahmad 2018; Kilias et al. 2013). As the mineralizing fluids expelled by the diffusers have a magmatic component (Carey et al. 2013) and As, Ag, Au, Hg, Sb, Sn, Pb and Zn are removed from the magma during degassing (Fig. 9), these metals enriched in the diffusers are most likely issued from the magma. Conversely, Tl is enriched in the diffusers but do not seem to be lost during degassing, which indicates that other metal sources than the magma are involved in Kolumbo' s magmatic-hydrothermal system (Fig. 3m, 8c). In the case of recent VMS deposits in mid-oceanic ridge setting, the wall rocks represent the source of Zn and Cu that are mobilized by hydrothermal leaching (Brauhart et al. 2001; Patten et al. 2016; Skirrow and Franklin 1994). Similarly, in volcanic arc environments, especially in continental crust, felsic rocks are enriched in Ag, As, Pb, Sb, Sn and Tl compared to MORB. Such elements are leached by hydrothermal fluids and enriched in sulphide deposits (Shikazono 2003; Shu et al. 2022; Stanton 1994). Thus, the metal association of Kolumbo 's mineralization is likely resulting from a combination of magma degassing and hydrothermal wall rock leaching (Fig. 8c, 9). Knowing the nature of basement/surrounding rocks is fundamental for SMS exploration (and by extension for VMS exploration too) as it will have an impact on the metal association in the mineralization.

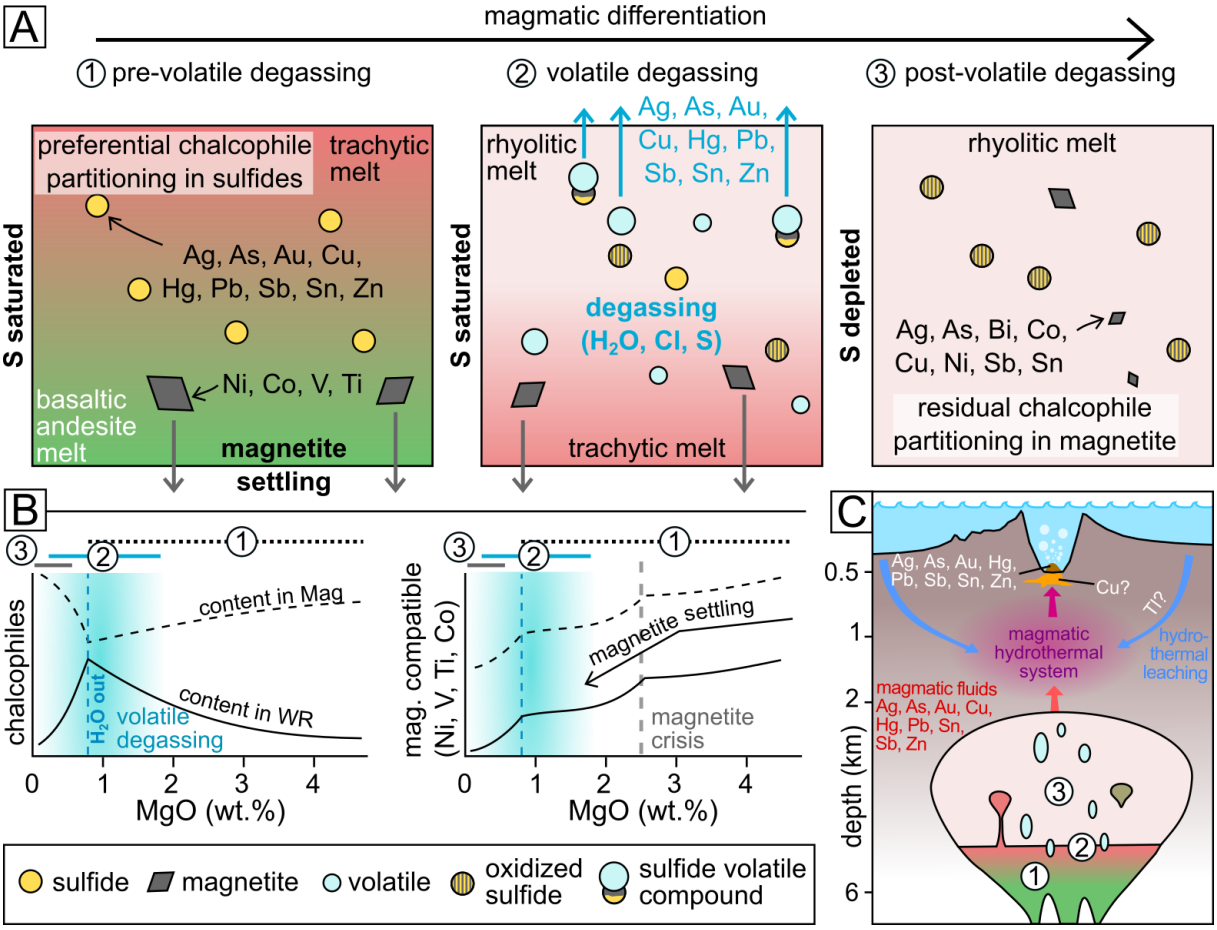

Fig. 8: Conceptual model of metal mobility during magmatic differentiation and related hydrothermal processes. (A) 1) Before degassing, the melt is S-saturated, chalcophile elements (Ag, As, Au, Cu, Hg, Sn, Sb, Pb and Zn) fractionate preferably in sulphide phases while Ni, Co, V, Ti are partitioned preferably in magnetite. The sulphide phases are floating in the magma while magnetite settles. 2) At degassing, sulphide phases are oxidized by formation of sulphide-volatile compounds or interaction with volatiles. Chalcophile elements are removed from the sulphides and likely transported as S- or Cl-complexes. 3) After degassing, the system is S-depleted, the residual chalcophile elements in the melt partition into magnetite, locally forming chalcophile element-rich magnetite. (B) Chalcophile and magnetite-compatible elements in whole rock and magnetite during differentiation. (C) Model of metal transfer within Kolumbo's magmatic-hydrothermal system.

6.5.2 Temperature control on metal enrichment at deposit scale

Despite Cu being mobilized during degassing, Cu is not strongly enriched in the hydrothermal diffusers of Kolumbo, suggesting that Cu is trapped somewhere else in the system (Fig. 9). Metal zoning is frequent in VMS deposits and is controlled by temperature-dependent

sulphide solubility (Large 1992). In Kolumbo, the venting hydrothermal fluids temperature reach 265°C and sub-seafloor boiling occurs below the diffusers (Nomikou et al. 2022). Thus, the Cu lost during degassing is most likely trapped in the deeper/hotter parts of the hydrothermal system, while the Zn-Pb(-Au) rich diffusers only represent the cooler part of the system (Hannington et al. 2005). The metal association observed in the diffusers correspond to low temperature VMS deposits (<300°C) which usually show enrichment in Zn, Pb, Ag, Au, Cd, Sn, Sb, As, Hg, ±Tl, ±W (Hannington 2014). Additionally, the high concentration of As, Sb, Hg, and Tl in the diffusers supports boiling and zone refining processes, as these elements are easily mobilized in the vapour phase and tend to be highly enriched in VMS deposits that formed from boiling hydrothermal fluids (Hannington 2014).

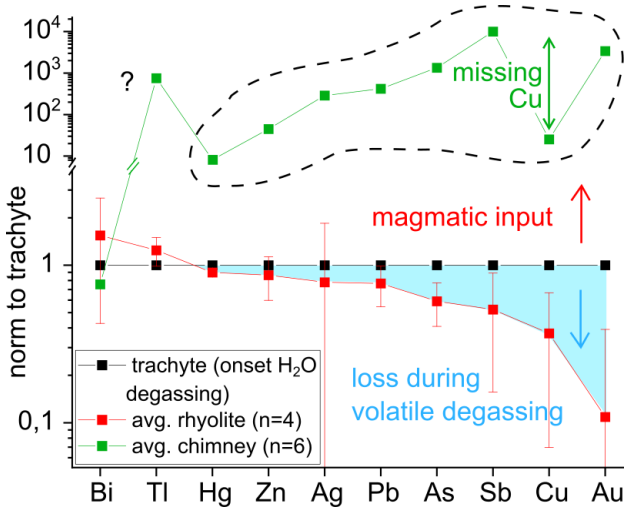

Fig. 9: Average metal content in Kolumbo' s sulphide-sulphate diffusers and volcanic samples normalized to trachyte. Trachyte composition corresponds to onset of water saturation and degassing.

7 Conclusions

The study of the Kolumbo volcano and its mineralization gives insight on how magmatic processes lead to metal transfer to the magmatic-hydrothermal system in arc-volcanic setting. Combining in-situ magnetite trace element with whole rock data and modelling enables to track metal behaviour in the magma during differentiation. Early and long lasted sulphide saturation

in the melt leads to fractionation of chalcophile elements in sulphide phases. Most of the sulphides, however, remain in the magma, either because of the small size of the sulphides and viscosity of the magma or because of formation of sulphide-volatile compounds. Upon degassing, As, Ag, Au, Cu, Hg, Sb, Sn, Pb and Zn are depleted in the magma. These metals are partitioned in the volatiles, either from the melt or during sulphide oxidation by volatiles. After degassing, the remaining chalcophile elements in the melt are incorporated into magnetite as the melt became sulphur undersaturated. The metals lost during magmatic degassing are enriched in the SMS, indicating their magmatic source. However, the mineralization is also enriched in Tl, which is not depleted in the magma during degassing. This indicates that other metal sources and processes, likely hydrothermal leaching of wall rocks, also contribute to the metal budget of the mineralization. Trace-element content in igneous magnetite is a powerful tool to track metal behaviour during magmatic differentiation. It enables to identify sulphide saturation, to estimate chalcophile element content changes in the melt and to discriminate between pre- and post-degassing magnetite.

8 Acknowledgments

This work is funded by the German Research Foundation (DFG - SPP Program DOME grant PA 3523/2-1 and INST 121384/213-1 FUGG). This work was supported by Institute for Exploration (IFE-USA) and the collaborative project “New Frontiers in the Ocean Exploration 2010” between the Graduate School of Oceanography at the University of Rhode Island (URI-USA) and the Faculty of Geology & Geoenvironment, (NKUA). Bell K.L.C., and Carey S. are greatly acknowledged for operational support and their participation in data collection. The officers and the crew of the E/V NAUTILUS are gratefully acknowledged for their important and effective contribution to the field work and sampling. PN acknowledges support by SANTORY program which is funded by the Hellenic Foundation for Research and Innovation (HFRI) (Grant Number 1850).

9 Statements and Declarations

Competing interest : The authors declare no competing interests.

10 References

Agostini S, Doglioni C, Innocenti F, Manetti P, Tonarini S (2010) On the geodynamics of the Aegean rift. Tectonophysics 488:7–21

Ahmad Q (2018) The source of metals in the recent polymetallic seafloor massive sulfide mineralization at the Kolumbo arc-volcano, Greece. M.Sc. thesis, Karlsruhe Institute of Technology

Arevalo R, McDonough WF (2010) Chemical variations and regional diversity observed in MORB. Chemical Geology 271:70–85

Ariskin AA, Barmina GS (2004) COMAGMAT: Development of a magma crystallization model and its petrological applications. Geochemistry International 42:1–157

Barnes SJ, Le Vaillant M, Godel B, Lesher CM (2019) Droplets and Bubbles: Solidification of Sulphide-rich Vapour-saturated Orthocumulates in the Norilsk-Talnakh Ni–Cu–PGE Ore-bearing Intrusions. Journal of Petrology 60:269–300

Berkenbosch HA, de Ronde CEJ, Gemmell JB, McNeill AW, Goemann K (2012) Mineralogy and Formation of Black Smoker Chimneys from Brothers Submarine Volcano, Kermadec Arc. Economic Geology 107:1613–1633

Blanks DE, Holwell DA, Fiorentini ML, Moroni M, Giuliani A, Tassara S, González-Jiménez JM, Boyce AJ, Ferrari E (2020) Fluxing of mantle carbon as a physical agent for metallogenic fertilization of the crust. Nat Commun 11:4342

Brandl PA, Portnyagin M, Zeppenfeld H, Tepley FJ, Ronde CE de, Timm C, Hauff F, Garbe-Schönberg D, Bousquet R (2022) The Origin of Magmas and Metals at the Submarine Brothers Volcano, Kermadec Arc, New Zealand. Economic Geology

Brauhart CW, Huston DL, Groves DI, Mikucki EJ, Gardoll SJ (2001) Geochemical Mass-Transfer Patterns as Indicators of the Architecture of a Complete Volcanic-Hosted Massive Sulfide Hydrothermal Alteration System, Panorama District, Pilbara, Western Australia. Economic Geology 96:1263–1278

Bucholz CE, Kelemen PB (2019) Oxygen fugacity at the base of the Talkeetna arc, Alaska. Contrib Mineral Petrol 174

Cantner K, Carey S, Nomikou P (2014) Integrated volcanologic and petrologic analysis of the 1650AD eruption of Kolumbo submarine volcano, Greece. Journal of Volcanology and Geothermal Research 269:28–43

Carey S, Nomikou P, Bell KC, Lilley M, Lupton JE, Roman C, Stathopoulou E, Bejelou K, Ballard R (2013) CO2 degassing from hydrothermal vents at Kolumbo submarine volcano, Greece, and the accumulation of acidic crater water. Geology 41:1035–1038

Chrapkiewicz K, Paulatto M, Heath BA, Hooft EEE, Nomikou P, Papazachos CB, Schmid F, Toomey DR, Warner MR, Morgan JV (2022) Magma Chamber Detected Beneath an Arc Volcano With Full-Waveform Inversion of Active-Source Seismic Data. Geochem Geophys Geosyst 23

Coogan LA, Gillis KM (2018) Low-Temperature Alteration of the Seafloor: Impacts on Ocean Chemistry. Annu. Rev. Earth Planet. Sci. 46:21–45

Craddock PR, Bach W (2010) Insights to magmatic–hydrothermal processes in the Manus back-arc basin as recorded by anhydrite. Geochimica et Cosmochimica Acta 74:5514–5536

Craddock PR, Bach W, Seewald JS, Rouxel OJ, Reeves E, Tivey MK (2010) Rare earth element abundances in hydrothermal fluids from the Manus Basin, Papua New Guinea: Indicators of sub-seafloor hydrothermal processes in back-arc basins. Geochimica et Cosmochimica Acta 74:5494–5513

Dare SAS, Barnes S-J, Beaudoin G, Méric J, Boutroy E, Potvin-Doucet C (2014) Trace elements in magnetite as petrogenetic indicators. Miner Deposita 49:785–796

Dare SA, Barnes S-J, Beaudoin G (2012) Variation in trace element content of magnetite crystallized from a fractionating sulfide liquid, Sudbury, Canada: Implications for provenance discrimination. Geochimica et Cosmochimica Acta 88:27–50

de Ronde CEJ, Hannington M, Stoffers P, Wright IC, Ditchburn RG, Reyes AG, Baker ET, Massoth GJ, Lupton JE, Walker SL, Greene RR, Soong CWR, Ishibashi J, Lebon GT, Bray CJ, Resing JA (2005) Evolution of a Submarine Magmatic-Hydrothermal System: Brothers Volcano, Southern Kermadec Arc, New Zealand. Economic Geology 100:1097–1133

Dimitriadis I, Karagianni E, Panagiotopoulos D, Papazachos C, Hatzidimitriou P, Bohnhoff M, Rische M, Meier T (2009) Seismicity and active tectonics at Coloumbo Reef (Aegean Sea, Greece): Monitoring an active volcano at Santorini Volcanic Center using a temporary seismic network. Tectonophysics 465:136–149

Dimitriadis I, Papazachos C, Panagiotopoulos D, Hatzidimitriou P, Bohnhoff M, Rische M, Meier T (2010) P and S velocity structures of the Santorini–Coloumbo volcanic system (Aegean Sea, Greece) obtained by non-linear inversion of travel times and its tectonic implications. Journal of Volcanology and Geothermal Research 195:13–30

Fontboté L, Kouzmanov K, Chiaradia M, Pokrovski GS (2017) Sulfide Minerals in Hydrothermal Deposits. ELEMENTS 13:97–103

Fouqué F (1879) Santorin et ses éruptions. G. Masson, Paris

Fytikas M, Innocenti F, Manetti P, Peccerillo A, Mazzuoli R, Villari L (1984) Tertiary to Quaternary evolution of volcanism in the Aegean region. Geological Society, London, Special Publications 17:687–699

Gammons CH, Williams-Jones AE (1997) Chemical mobility of gold in the porphyry-epithermal environment. Economic Geology 92:45–59

Georgatou A, Chiaradia M, Kouzmanov K (2021) T-P-fO2 conditions of sulfide saturation in magmatic enclaves and their host lavas. Lithos 398-399:106313

Georgatou A, Chiaradia M, Klaver M (2022) Deep to Shallow Sulfide Saturation at Nisyros Active Volcano. Geochem Geophys Geosyst 23

Gruen G, Weis P, Driesner T, Heinrich CA, de Ronde CEJ (2014) Hydrodynamic modeling of magmatic–hydrothermal activity at submarine arc volcanoes, with implications for ore formation. Earth and Planetary Science Letters 404:307–318

Halbach P, Nakamura K, Wahsner M, Lange J, Sakai H, Käselitz L, Hansen R-D, Yamano M, Post J, Prause B, Seifert R, Michaelis W, Teichmann F, Kinoshita M, Märten A, Ishibashi J, Czerwinski S, Blum N (1989) Probable modern analogue of Kuroko-type massive sulphide deposits in the Okinawa Trough back-arc basin. Nature 338:496–499

Hannington M (2014) Volcanogenic Massive Sulfide Deposits. In: Treatise on Geochemistry. Elsevier, pp 463–488

Hannington M, Scott SD (1989) Gold Mineralization in Volcanogenic Massive Sulfides : Implications of Data from Active Hydrothermal Vents on the Modern Sea Floor. In: Keays RR, Ramsay WRH, Groves DI (eds) The Geology of Gold Deposits : The Perspectives in 1988. Society of Economic Geologists, pp 491–507

Hannington M, de Ronde CEJ, Petersen S (2005) Sea-Floor Tectonics and Submarine Hydrothermal Systems. In: Hedenquist J, Thompson JFH, Goldfarb RJ, Richards JP (eds) One Hundredth Anniversary Volume. Society of Economic Geologists

Haraguchi S, Ishizuka H, Ishii T, Fujioka K, Yuasa M, Shibasaki H (2014) Low- and high-temperature alterations of volcanic rocks in the northwestern Philippine Sea, and association with volcanic settings. Island Arc 23:324–343

Hattori K, Takahashi Y, Guillot S, Johanson B (2005) Occurrence of arsenic (V) in forearc mantle serpentinites based on X-ray absorption spectroscopy study. Geochimica et Cosmochimica Acta 69:5585–5596

Hedenquist JW, Lowenstern JB (1994) The role of magmas in the formation of hydrothermal ore deposits. Nature 370:519–527

Holzheid A (2010) Separation of sulfide melt droplets in sulfur saturated silicate liquids. Chemical Geology 274:127–135

Hooft EE, Nomikou P, Toomey DR, Lampridou D, Getz C, Christopoulou M-E, O'Hara D, Arnoux GM, Bodmer M, Gray M, Heath BA, VanderBeek BP (2017) Backarc tectonism, volcanism, and mass wasting shape seafloor morphology in the Santorini-Christiana-Amorgos region of the Hellenic Volcanic Arc. Tectonophysics 712-713:396–414

Huang X-W, Sappin A-A, Boutroy É, Beaudoin G, Makvandi S (2019) Trace Element Composition of Igneous and Hydrothermal Magnetite from Porphyry Deposits: Relationship to Deposit Subtypes and Magmatic Affinity. Economic Geology 114:917–952

Hübscher C, Ruhnau M, Nomikou P (2015) Volcano-tectonic evolution of the polygenetic Kolumbo submarine volcano/Santorini (Aegean Sea). Journal of Volcanology and Geothermal Research 291:101–111

Jenner FE, St. O'Neill HC, Arculus RJ, Mavrogenes JA (2010) The Magnetite Crisis in the Evolution of Arc-related Magmas and the Initial Concentration of Au, Ag and Cu. Journal of Petrology 51:2445–2464

Jenner FE, Arculus RJ, Mavrogenes JA, Dyriw NJ, Nebel O, Hauri EH (2012) Chalcophile element systematics in volcanic glasses from the northwestern Lau Basin. Geochem Geophys Geosyst 13:n/a-n/a

Jenner FE, Hauri EH, Bullock ES, König S, Arculus RJ, Mavrogenes JA, Mikkelson N, Goddard C (2015) The competing effects of sulfide saturation versus degassing on the behavior of the chalcophile elements during the differentiation of hydrous melts. Geochem Geophys Geosyst 16:1490–1507

Jugo PJ (2009) Sulfur content at sulfide saturation in oxidized magmas. Geology 37:415–418

Keith M, Haase KM, Klemd R, Smith DJ, Schwarz-Schampera U, Bach W (2018) Constraints on the source of Cu in a submarine magmatic-hydrothermal system, Brothers volcano, Kermadec island arc. Contrib Mineral Petrol 173

Kilias SP, Nomikou P, Papanikolaou D, Polymenakou PN, Godelitsas A, Argyraki A, Carey S, Gamaletsos P, Mertzimekis TJ, Stathopoulou E, Goettlicher J, Steininger R, Betzelou K, Livanos I, Christakis C, Bell KC, Scoullos M (2013) New insights into hydrothermal vent processes in the unique shallow-submarine arc-volcano, Kolumbo (Santorini), Greece. Sci Rep 3:2421

Klaver M, Carey S, Nomikou P, Smet I, Godelitsas A, Vroon P (2016) A distinct source and differentiation history for Kolumbo submarine volcano, Santorini volcanic field, Aegean arc. Geochem Geophys Geosyst 17:3254–3273

Konstantinou KI (2020) Magma chamber evolution during the 1650 AD Kolumbo eruption provides clues about past and future volcanic activity. Sci Rep 10:15423

Large RR (1992) Australian volcanic-hosted massive sulfide deposits; features, styles, and genetic models. Economic Geology 87:471–510

Li Y, Audétat A (2012) Partitioning of V, Mn, Co, Ni, Cu, Zn, As, Mo, Ag, Sn, Sb, W, Au, Pb, and Bi between sulfide phases and hydrous basanite melt at upper mantle conditions. Earth and Planetary Science Letters 355-356:327–340

Lowenstern J (2001) Carbon dioxide in magmas and implications for hydrothermal systems. Miner Deposita 36:490–502

Mavrogenes JA, O'Neill HS (1999) The relative effects of pressure, temperature and oxygen fugacity on the solubility of sulfide in mafic magmas. Geochimica et Cosmochimica Acta 63:1173–1180

McVey BG, Hooft E, Heath BA, Toomey DR, Paulatto M, Morgan JV, Nomikou P, Papazachos CB (2020) Magma accumulation beneath Santorini volcano, Greece, from P-wave tomography. Geology 48:231–235

Mungall JE, Brenan JM, Godel B, Barnes SJ, Gaillard F (2015) Transport of metals and sulphur in magmas by flotation of sulphide melt on vapour bubbles. Nature Geosci 8:216–219

Nadeau O, Mick E, Robidoux P, Grassa F, Brusca L, Voinot A, Leybourne MI (2021) Lithium isotopes and Cu-Au concentrations in hydrothermal alterations from Solfatara Volcano, Campi Flegrei caldera complex, and La Fossa volcano, Vulcano Island, Italy: Insights into epithermal ore forming environments. Ore Geology Reviews 130:103934

Nadoll P, Angerer T, Mauk JL, French D, Walshe J (2014) The chemistry of hydrothermal magnetite: A review. Ore Geology Reviews 61:1–32

Nomikou P, Carey S, Papanikolaou D, Croff Bell K, Sakellariou D, Alexandri M, Bejelou K (2012) Submarine volcanoes of the Kolumbo volcanic zone NE of Santorini Caldera, Greece. Global and Planetary Change 90-91:135–151

Nomikou P, Carey S, Croff Bell KL, Papanikolaou D, Bejelou K, Alexandri M, Cantner K, Martin JF (2013) Morphological analysis and related volcanic features of the Kolumbo submarine volcanic chain (NE of Santorini Island, Aegean Volcanic Arc). zfg_suppl 57:29–47

Nomikou P, Druitt TH, Hübscher C, Mather TA, Paulatto M, Kalnins LM, Kelfoun K, Papanikolaou D, Bejelou K, Lampridou D, Pyle DM, Carey S, Watts AB, Weiß B, Parks MM (2016) Post-eruptive flooding of Santorini caldera and implications for tsunami generation. Nat Commun 7:13332

Nomikou P, Hübscher C, Carey S (2019) The Christiana–Santorini–Kolumbo Volcanic Field. ELEMENTS 15:171–176

Nomikou P, Polymenakou PN, Rizzo AL, Petersen S, Hannington M, Kilias SP, Papanikolaou D, Escartin J, Karantzalos K, Mertzimekis TJ, Antoniou V, Krokos M, Grammatikopoulos L, Italiano F, Caruso CG, Lazzaro G, Longo M, Sciré Scappuzzo S,

D'Alessandro W, Grassa F, Bejelou K, Lampridou D, Katsigera A, Dura A (2022) SANTORY: SANTORini's Seafloor Volcanic ObservatorY. Front. Mar. Sci. 9

Papanikolaou D (2013) Tectonostratigraphic models of the Alpine terranes and subduction history of the Hellenides. Tectonophysics 595-596:1–24

Park J-W, Campbell IH, Kim J, Moon J-W (2015) The Role of Late Sulfide Saturation in the Formation of a Cu- and Au-rich Magma: Insights from the Platinum Group Element Geochemistry of Niuatahi-Motutahi Lavas, Tonga Rear Arc. Journal of Petrology 56:59–81

Paton C, Hellstrom J, Paul B, Woodhead J, Hergt J (2011) Iolite: Freeware for the visualisation and processing of mass spectrometric data. J. Anal. At. Spectrom. 26:2508

Patten C, Barnes S-J, Mathez EA, Jenner FE (2013) Partition coefficients of chalcophile elements between sulfide and silicate melts and the early crystallization history of sulfide liquid: LA-ICP-MS analysis of MORB sulfide droplets. Chemical Geology 358:170–188

Patten C, Pitcairn IK, Teagle D (2017) Hydrothermal mobilisation of Au and other metals in supra-subduction oceanic crust: Insights from the Troodos ophiolite. Ore Geology Reviews 86:487–508

Patten C, Beranoaguirre A, Hector S, Gudelius D, Kolb J, Eiche E (2023) Improved whole rock low detection limit gold analysis by LA-ICP-MS utilizing pressed-powder-pellets. International Journal of Mass Spectrometry:117039

Patten CGC, Hector S, Kilias SP, Ulrich M, Peillod A, Beranoaguirre A, Nomikou P, Eiche E, Kolb J (under review) Transfer of sulfur and chalcophile metals via sulfide-volatile compound drops in the Christiana-Santorini-Kolumbo volcanic field. Nat Commun

Patten CGC, Pitcairn IK, Teagle DAH, Harris M (2016) Mobility of Au and related elements during the hydrothermal alteration of the oceanic crust: implications for the sources of metals in VMS deposits. Miner Deposita 51:179–200

Patten CGC, Pitcairn IK, Alt JC, Zack T, Lahaye Y, Teagle DAH, Markdahl K (2020) Metal fluxes during magmatic degassing in the oceanic crust: sulfide mineralisation at ODP site 786B, Izu-Bonin forearc. Miner Deposita 55:469–489

Preine J, Karstens J, Hübscher C, Nomikou P, Schmid F, Crutchley GJ, Druitt TH, Papanikolaou D (2022) Spatio-temporal evolution of the Christiana-Santorini-Kolumbo volcanic field, Aegean Sea. Geology 50:96–100

Richards JP (2011) Magmatic to hydrothermal metal fluxes in convergent and collided margins. Ore Geology Reviews 40:1–26

Richards JP (2015) The oxidation state, and sulfur and Cu contents of arc magmas: implications for metallogeny. Lithos 233:27–45

Rizzo AL, Caracausi A, Chavagnac V, Nomikou P, Polymenakou PN, Mandalakis M, Kotoulas G, Magoulas A, Castillo A, Lampridou D (2016) Kolumbo submarine volcano (Greece): An active window into the Aegean subduction system. Sci Rep 6:28013

Rizzo AL, Caracausi A, Chavagnac V, Nomikou P, Polymenakou PN, Mandalakis M, Kotoulas G, Magoulas A, Castillo A, Lampridou D, Marusczak N, Sonke JE (2019) Geochemistry of CO2-Rich Gases Venting From Submarine Volcanism: The Case of Kolumbo (Hellenic Volcanic Arc, Greece). Front. Earth Sci. 7

Rouwet D, Hidalgo S, Joseph EP, González-Ilama G (2019) Fluid Geochemistry and Volcanic Unrest: Dissolving the Haze in Time and Space. In: Gottsmann J, Neuberg J, Scheu B (eds) Volcanic Unrest. Springer International Publishing, Cham, pp 221–239

Schmid F, Petersen G, Hooft E, Paulatto M, Chrapkiewicz K, Hensch M, Dahm T (2022) Heralds of Future Volcanism: Swarms of Microseismicity Beneath the Submarine Kolumbo Volcano Indicate Opening of Near-Vertical Fractures Exploited by Ascending Melts. Geochem Geophys Geosyst 23

Shikazono N (2003) Geochemical and tectonic evolution of arc-backarc hydrothermal systems: Implication for origin of Kuroko and epithermal vein-type mineralizations and

the global geochemical cycle, 1st ed. Developments in geochemistry, vol 8. Elsevier, Amsterdam, Boston

Shu Y, Nielsen SG, Le Roux V, Wörner G, Blusztajn J, Auro M (2022) Sources of dehydration fluids underneath the Kamchatka arc. Nat Commun 13:4467

Sigurdsson H, Carey S, Alexandri M, Vougioukalakis G, Croff K, Roman C, Sakellariou D, Anagnostou C (2006) Marine investigations of Greece's Santorini volcanic field. Eos, Trans. Am. Geophys. Union 87:337–342

Skirrow RG, Franklin JM (1994) Silicification and metal leaching in semiconformable alteration beneath the Chisel Lake massive sulfide deposit, Snow Lake, Manitoba. Economic Geology 89:31–50

Smythe DJ, Wood BJ, Kiseeva ES (2017) The S content of silicate melts at sulfide saturation: New experiments and a model incorporating the effects of sulfide composition. American Mineralogist 102:795–803

Stanton RL (1994) Ore elements in arc lavas. Oxford science publications. Clarendon Press; Oxford University Press, Oxford, New York

Sun W, Arculus RJ, Kamenetsky VS, Binns RA (2004) Release of gold-bearing fluids in convergent margin magmas prompted by magnetite crystallization. Nature 431:975–978

Thal J, Tivey M, Yoerger DR, Bach W (2016) Subaqueous cryptodome eruption, hydrothermal activity and related seafloor morphologies on the andesitic North Su volcano. Journal of Volcanology and Geothermal Research 323:80–96

Wang Z, Park J-W, Wang X, Zou Z, Kim J, Zhang P, Li M (2019) Evolution of copper isotopes in arc systems: Insights from lavas and molten sulfur in Niuatahi volcano, Tonga rear arc. Geochimica et Cosmochimica Acta 250:18–33

Yao Z, Mungall JE (2020) Flotation mechanism of sulphide melt on vapour bubbles in partially molten magmatic systems. Earth and Planetary Science Letters 542:116298

Yeats CJ, Parr JM, Binns RA, Gemmell JB, Scott SD (2014) The SuSu Knolls Hydrothermal Field, Eastern Manus Basin, Papua New Guinea: An Active Submarine High-Sulfidation Copper-Gold System. Economic Geology 109:2207–2226

Annex

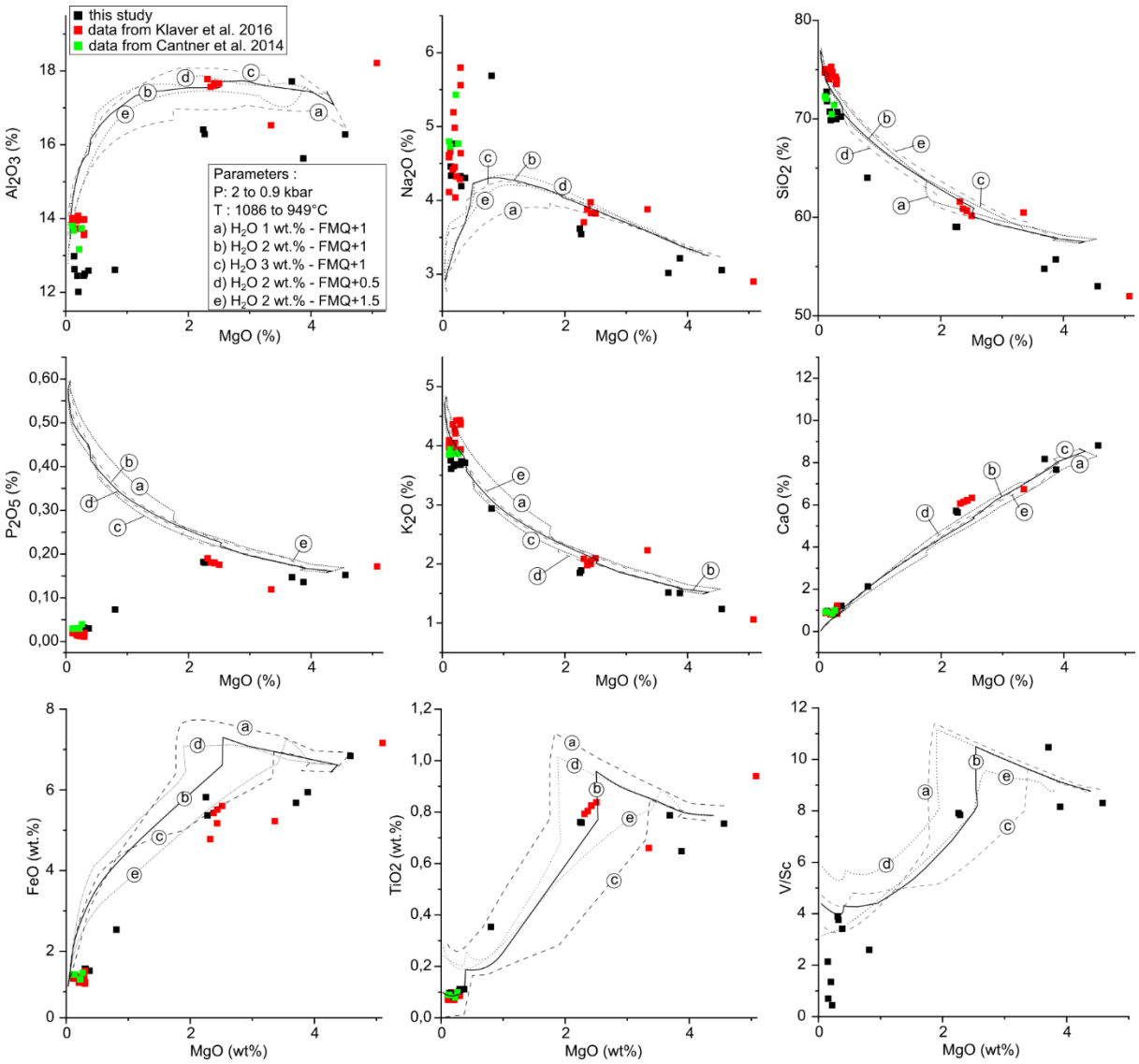

Annex 1: Model of the geochemical evolution of melt using COMAGMAT 3.75 (Ariskin and Barmina 2004) for several H_2O content and fO_2 parameters compared to whole rock data.

Supplementary data

Whole rock geochemistry

					XRF on glass beads											
Sample	Details	Northing	Easting	Lithology	**Na2O (wt%)**	**MgO (wt%)**	**Al2O3 (wt%)**	**SiO2 (wt%)**	**P2O5 (wt%)**	**K2O (wt%)**	**CaO (wt%)**	**TiO2 (wt%)**	**MnO (wt%)**	**Fe2O3tot (wt%)**	**LOI (wt%)**	**SUM**
NA007-002c	Pumices (1650CE)	36,32570	25,30896	Trachyte	5,69	0,80	12,61	64,03	0,07	2,94	2,13	0,35	0,07	2,83	7,07	98,62
NA007-052c	Pumice (K2)	36,31814	25,29636	Rhyolite	4,45	0,19	12,45	70,74	0,03	3,66	0,90	0,09	0,09	1,49	5,02	99,11
NA007-062c	lava (1650CE)	36,31577	25,28511	Andesite	3,54	2,27	16,29	59,03	0,18	1,89	5,64	0,76	0,13	5,98	3,45	99,15
NA007-079c	Pumice (K2)	36,31357	25,29626	Rhyolite	4,33	0,30	12,46	70,00	0,03	3,68	1,12	0,11	0,08	1,75	5,99	99,85
NA007-080c1	lava (1650CE)	36,31493	25,29760	Rhyolite	4,46	0,14	12,98	72,77	0,03	3,76	0,97	0,10	0,09	1,59	2,84	99,70
NA007-080c2	lava (1650CE)	36,31493	25,29760	Basaltic Andesite	3,02	3,69	17,72	54,78	0,15	1,52	8,17	0,79	0,10	6,32	2,60	98,85
NA007-080c3	lava (1650CE)	36,31493	25,29760	Andesite	3,62	2,24	16,41	59,04	0,18	1,85	5,72	0,76	0,14	6,48	2,67	99,10
NA007-092c	Pumice (K2)	36,31264	25,28578	Rhyolite	4,34	0,14	12,63	71,80	0,03	3,61	0,90	0,09	0,09	1,54	4,32	99,50
NA007-096c	Pumices (1650CE)	36,31701	25,28677	Rhyolite	4,77	0,21	12,02	69,87	0,02	3,69	0,80	0,08	0,09	1,38	5,88	98,80
NA007-100b (enclave)	Pumices (1650CE)	36,31742	25,28602	Basaltic Andesite	3,06	4,56	16,28	53,01	0,15	1,24	8,82	0,75	0,14	7,61	2,97	98,57
NA007-100b (matrix)	Pumices (1650CE)	36,31742	25,28602	Rhyolite	4,31	0,37	12,59	70,24	0,03	3,71	1,22	0,11	0,08	1,70	4,83	99,19
NA007-100c (enclave)	Pumices (1650CE)	36,31742	25,28602	Basaltic Andesite	3,22	3,87	15,63	55,73	0,14	1,51	7,68	0,65	0,13	6,61	4,14	99,30
NA007-100c (matrix)	Pumices (1650CE)	36,31742	25,28602	Rhyolite	4,19	0,31	12,51	70,71	0,03	3,74	1,17	0,11	0,08	1,75	4,51	99,12

	CSA		Fe titration			PPP-LA-ICP-MS								
Sample	**C (wt%)**	**S (wt%)**	FeO wt%	Fe2O3 wt%	Fe++/FeO	Li7_ppm	2SD	LOD	Si29_ppm	2SD	LOD	P31_ppm	2SD	LOD
NA007-002c	3,0E-02	2,2E-01	1,66	1,17	0,51	1,9E+01	4,1E-01	3,5E-02	2,7E+05	1,2E+03	7,3E+01	3,2E+02	7,7E+01	4,5E+00
NA007-052c	2,0E-02	2,6E-02	0,98	0,51	0,57	1,8E+01	4,3E-01	3,4E-02	2,7E+05	3,8E+03	7,0E+01	8,9E+01	2,2E+01	2,6E+00
NA007-062c	3,6E-02	9,2E-03	3,54	2,44	0,51	9,9E+00	1,9E-01	3,5E-02	2,4E+05	3,5E+03	6,5E+01	7,4E+02	2,6E+01	5,1E+00
NA007-079c	2,6E-02	3,3E-02	1,06	0,69	0,52	1,9E+01	4,9E-01	3,4E-02	2,8E+05	1,6E+03	6,8E+01	9,6E+01	4,9E+01	2,5E+00
NA007-080c1	2,2E-02	1,0E-02	0,64	0,94	0,35	1,6E+01	5,5E-01	3,4E-02	2,4E+05	2,6E+03	6,5E+01	7,1E+01	1,4E+01	2,2E+00
NA007-080c2	2,4E-02	1,4E-02	2,38	3,94	0,33	5,3E+00	5,0E-01	3,8E-02	1,6E+05	3,2E+03	8,6E+01	4,2E+02	6,7E+01	5,3E+00
NA007-080c3	7,7E-02	1,2E-02	3,90	2,58	0,52	7,7E+00	1,7E-01	3,4E-02	2,4E+05	2,5E+03	6,9E+01	7,2E+02	5,6E+01	5,3E+00
NA007-092c	2,7E-02	6,5E-03	0,93	0,61	0,52	1,8E+01	3,3E-01	3,6E-02	2,6E+05	2,2E+03	7,1E+01	8,3E+01	3,5E+01	2,6E+00
NA007-096c	not enough material	enough mate	0,83	0,55	0,52	2,3E+01	1,8E+00	3,5E-02	2,8E+05	3,9E+03	6,9E+01	6,4E+01	2,9E+01	2,2E+00
NA007-100b (enclave)	1,7E-02	3,8E-02	3,46	4,15	0,39	1,9E+01	3,5E-01	3,7E-02	2,6E+05	3,0E+03	7,5E+01	8,3E+01	3,0E+01	2,6E+00
NA007-100b (matrix)	5,9E-02	1,0E-01	0,82	0,88	0,41	1,2E+01	2,7E-01	3,7E-02	2,3E+05	3,1E+03	6,6E+01	6,3E+02	7,5E+01	4,6E+00
NA007-100c (enclave)	2,1E-02	2,9E-02	2,48	4,14	0,32	1,5E+01	2,0E-01	3,5E-02	2,2E+05	4,2E+03	6,7E+01	7,5E+01	2,4E+01	2,4E+00
NA007-100c (matrix)	2,4E-01	7,8E-02	0,76	0,99	0,37	1,2E+01	5,0E-01	3,7E-02	2,1E+05	3,0E+03	7,3E+01	5,2E+02	7,2E+01	5,0E+00

	PPP-LA-ICP-MS													
Sample	S32_ppm	2SD	LOD	Cl35_ppm	2SD	LOD	Ca44_ppm	2SD	LOD	Sc45_ppm	2SD	LOD	Ti49_ppm	2SD	LOD
NA007-002c	6,7E+02	4,8E+02	2,5E+00	9,4E+04	1,0E+04	2,2E+02	9,3E+03	8,8E+02	2,4E+00	7,9E+00	2,7E-01	3,9E-02	2,1E+03	1,5E+02	1,3E-01
NA007-052c	6,9E+01	1,3E+01	8,8E-01	3,6E+04	5,3E+03	2,1E+02	n.d.	n.d.	n.d.	1,4E+00	6,8E-02	3,7E-02	3,6E+02	2,4E+01	9,8E-02
NA007-062c	4,9E+01	8,9E+00	6,8E-01	1,3E+04	7,8E+02	1,9E+02	3,7E+04	6,3E+02	3,4E+00	1,4E+01	3,8E-01	3,9E-02	4,3E+03	2,2E+02	1,1E-01
NA007-079c	1,1E+02	2,6E+01	1,2E+00	4,2E+04	7,9E+03	2,1E+02	1,3E+03	3,2E+02	6,0E-01	2,7E+00	1,2E+00	2,9E-02	5,7E+02	3,3E+01	1,1E-01
NA007-080c1	3,5E+01	6,9E+00	5,3E-01	1,5E+04	3,2E+03	1,9E+02	n.d.	n.d.	n.d.	1,3E+00	5,6E-02	2,8E-02	4,4E+02	4,0E+01	1,0E-01
NA007-080c2	3,7E+01	9,8E+00	6,1E-01	7,2E+03	3,3E+03	1,8E+02	3,6E+04	2,1E+03	3,7E+00	1,3E+01	1,2E+00	3,9E-02	3,0E+03	3,2E+02	1,2E-01
NA007-080c3	4,1E+01	1,2E+01	6,0E-01	1,1E+04	1,7E+03	1,8E+02	3,6E+04	1,0E+03	3,4E+00	1,4E+01	6,5E-01	3,7E-02	4,2E+03	1,1E+02	1,2E-01
NA007-092c	2,8E+01	4,2E+01	3,7E-01	1,1E+04	2,8E+03	1,8E+02	n.d.	n.d.	n.d.	1,5E+00	4,0E-02	4,5E-02	2,9E+02	5,6E+01	8,8E-02
NA007-096c	1,2E+02	1,1E+02	1,1E+00	2,9E+05	5,5E+05	2,0E+02	n.d.	n.d.	n.d.	1,6E+00	3,0E-02	4,5E-02	2,4E+02	1,1E+01	8,1E-02
NA007-100b (enclave)	6,9E+01	2,9E+01	8,8E-01	2,3E+04	5,8E+03	1,9E+02	1,2E+03	6,9E+02	6,4E-01	2,4E+00	1,8E-01	4,8E-02	4,4E+02	1,6E+02	9,5E-02
NA007-100b (matrix)	4,6E+02	6,7E+01	2,3E+00	1,2E+04	1,4E+03	1,8E+02	5,9E+04	2,1E+03	3,8E+00	2,2E+01	8,0E-01	4,4E-02	4,2E+03	1,1E+02	1,4E-01
NA007-100c (enclave)	2,6E+01	1,9E+01	3,9E-01	1,6E+04	2,6E+03	1,9E+02	n.d.	n.d.	n.d.	2,0E+00	1,0E-01	4,2E-02	3,7E+02	3,6E+01	1,1E-01
NA007-100c (matrix)	3,0E+02	3,1E+01	2,1E+00	7,4E+03	6,7E+02	1,8E+02	4,6E+04	2,7E+03	3,8E+00	1,8E+01	1,2E+00	4,4E-02	3,4E+03	2,5E+02	1,3E-01

	PPP-LA-ICP-MS													
Sample	V51_ppm	2SD	LOD	Cr53_ppm	2SD	LOD	Mn55_ppm	2SD	LOD	Fe57_ppm	2SD	LOD	Co59_ppm	2SD	LOD
NA007-002c	2,0E+01	7,9E-01	2,7E-02	7,6E+00	1,0E+00	8,9E-01	5,9E+02	1,1E+01	5,5E-01	2,1E+04	7,8E+02	4,3E+00	4,5E+00	9,6E-02	3,2E-02
NA007-052c	1,9E+00	1,0E-01	5,4E-02	6,6E+00	4,9E-01	1,2E+00	6,4E+02	2,2E+01	5,5E-01	1,1E+04	4,3E+02	4,6E+00	2,4E+00	8,1E-02	3,0E-02
NA007-062c	1,1E+02	8,6E+00	2,5E-02	7,9E+00	5,0E-01	8,7E-01	1,0E+03	3,9E+01	5,4E-01	3,9E+04	1,7E+03	3,9E+00	1,2E+01	4,2E-01	3,0E-02
NA007-079c	1,1E+01	8,1E-01	3,0E-02	5,9E+00	5,9E-01	7,5E-01	6,4E+02	3,4E+01	5,4E-01	1,3E+04	5,9E+02	5,3E+00	3,6E+00	3,4E-01	3,6E-02
NA007-080c1	2,8E+00	1,4E-01	7,0E-02	6,8E+00	8,1E-01	7,4E-01	6,2E+02	1,8E+01	5,3E-01	1,2E+04	5,3E+02	5,2E+00	1,2E+00	9,7E-02	3,3E-02
NA007-080c2	1,3E+02	1,1E+01	2,7E-02	1,7E+01	1,8E+00	6,1E-01	5,2E+02	4,8E+01	5,9E-01	2,9E+04	2,1E+03	4,9E+00	1,3E+01	1,1E+00	3,6E-02
NA007-080c3	1,1E+02	5,4E+00	2,4E-02	7,4E+00	8,9E-01	8,0E-01	1,0E+03	5,2E+01	5,4E-01	4,1E+04	1,5E+03	4,3E+00	1,3E+01	5,3E-01	3,2E-02
NA007-092c	1,0E+00	4,5E-01	2,6E-02	8,7E+00	5,7E-01	1,7E+00	6,1E+02	1,3E+01	5,7E-01	1,1E+04	6,7E+02	4,2E+00	3,2E+00	7,7E-01	2,9E-02
NA007-096c	6,9E-01	1,2E-01	2,2E-02	9,8E+00	8,1E-01	1,4E+00	6,7E+02	2,1E+01	5,6E-01	1,1E+04	1,8E+02	3,8E+00	6,3E-01	4,7E-02	2,7E-02
NA007-100b (enclave)	8,4E+00	1,2E+00	2,6E-02	1,3E+01	2,9E+00	1,1E+00	6,1E+02	4,0E+01	5,9E-01	1,3E+04	1,4E+03	3,8E+00	2,2E+00	2,7E-01	2,7E-02
NA007-100b (matrix)	1,9E+02	3,8E+00	2,6E-02	3,2E+01	7,4E-01	5,5E-01	1,0E+03	3,0E+01	5,7E-01	4,8E+04	1,1E+03	3,6E+00	2,5E+01	5,1E-01	3,1E-02
NA007-100c (enclave)	7,5E+00	7,0E-01	2,7E-02	8,7E+00	5,7E-01	1,2E+00	5,1E+02	1,9E+01	5,6E-01	1,1E+04	1,1E+03	4,3E+00	1,8E+00	1,2E-01	3,1E-02
NA007-100c (matrix)	1,5E+02	1,2E+01	2,6E-02	2,7E+01	1,3E+00	5,6E-01	9,1E+02	5,5E+01	5,8E-01	4,0E+04	2,8E+03	3,9E+00	1,9E+01	9,5E-01	3,1E-02

	PPP-LA-ICP-MS													
Sample	Ni60_ppm	2SD	LOD	Cu63_ppm	2SD	LOD	Zn66_ppm	2SD	LOD	As75_ppm	2SD	LOD	Se78_ppm	2SD	LOD
NA007-002c	1,1E+00	2,8E-01	4,9E-02	2,6E+01	1,2E+00	3,5E-02	3,7E+01	2,1E+00	1,5E-01	2,0E+00	5,1E-02	2,1E-02	n.d.	n.d.	n.d.
NA007-052c	2,2E-01	2,9E-02	4,7E-02	2,1E+01	7,4E-01	3,4E-02	3,3E+01	1,9E+00	1,4E-01	1,2E+00	2,5E-02	2,1E-02	9,7E-02	1,1E-01	4,6E-03
NA007-062c	9,4E-01	9,9E-02	4,7E-02	2,0E+01	4,8E-01	3,5E-02	7,3E+01	6,2E+00	1,6E-01	7,7E-01	2,8E-02	2,0E-02	1,8E-01	1,3E-01	8,4E-03
NA007-079c	5,5E-01	8,5E-02	5,1E-02	1,2E+01	1,6E+00	3,7E-02	4,1E+01	2,3E+00	1,5E-01	1,4E+00	4,7E-02	2,4E-02	3,4E-01	4,8E-01	1,9E-02
NA007-080c1	2,4E-01	6,9E-02	4,8E-02	8,5E+00	6,9E-01	3,5E-02	3,3E+01	3,8E+00	1,5E-01	1,1E+00	2,6E-02	2,3E-02	1,1E+00	n.d.	6,5E-02
NA007-080c2	7,8E+00	8,5E-01	5,3E-02	5,3E+01	4,4E+00	3,9E-02	3,2E+01	5,6E+00	1,6E-01	3,5E-01	1,6E-02	2,6E-02	n.d.	n.d.	n.d.
NA007-080c3	9,4E-01	1,2E-01	4,7E-02	1,6E+01	9,0E-01	3,5E-02	6,8E+01	3,7E+00	1,6E-01	5,6E-01	2,8E-02	2,0E-02	4,6E-01	n.d.	2,4E-02
NA007-092c	3,1E-01	1,5E-01	4,6E-02	3,2E+01	6,4E+00	3,5E-02	3,3E+01	2,2E+00	1,3E-01	1,2E+00	1,3E-01	2,0E-02	2,5E-01	1,7E-01	1,3E-02
NA007-096c	2,4E-01	7,7E-02	4,6E-02	1,5E+01	9,1E+00	3,5E-02	3,8E+01	2,0E+00	1,3E-01	1,4E+00	1,9E-01	1,9E-02	2,6E-01	2,4E-01	1,4E-02
NA007-100b (enclave)	1,5E+00	9,4E-01	4,8E-02	7,7E+00	4,6E-01	3,6E-02	3,2E+01	3,3E+00	1,3E-01	1,2E+00	3,1E-02	2,2E-02	1,3E-01	1,3E-01	6,4E-03
NA007-100b (matrix)	1,4E+01	1,1E+00	4,9E-02	3,0E+01	2,6E+00	3,7E-02	5,4E+01	3,5E+00	1,5E-01	8,9E-01	2,5E-02	2,0E-02	8,9E-03	n.d.	3,8E-04
NA007-100c (enclave)	6,1E-01	7,0E-02	4,8E-02	6,6E+00	2,6E-01	3,7E-02	2,6E+01	2,5E+00	1,3E-01	9,6E-01	2,4E-02	2,0E-02	3,0E-01	2,0E-01	1,5E-02
NA007-100c (matrix)	1,1E+01	6,3E-01	5,2E-02	2,3E+01	2,1E+00	3,7E-02	5,1E+01	6,1E+00	1,6E-01	9,5E-01	4,7E-02	2,2E-02	n.d.	n.d.	n.d.

	PPP-LA-ICP-MS													
Sample	Rb85_ppm	2SD	LOD	Sr88_ppm	2SD	LOD	Y89_ppm	2SD	LOD	Zr90_ppm	2SD	LOD	Nb93_ppm	2SD	LOD
NA007-002c	8,8E+01	7,4E-01	8,0E-03	9,8E+01	1,1E+01	6,5E-03	3,6E+01	7,2E-01	1,7E-03	2,6E+02	4,2E+00	4,0E-03	9,7E+00	3,5E-01	1,2E-03
NA007-052c	9,3E+01	2,7E+00	8,3E-03	6,0E+01	2,1E+00	6,4E-03	1,9E+01	3,6E-01	1,7E-03	1,1E+02	2,4E+00	4,5E-03	1,7E+01	3,7E-01	8,2E-04
NA007-062c	3,4E+01	1,0E+00	7,9E-03	4,9E+02	1,0E+01	6,5E-03	2,1E+01	5,4E-01	1,7E-03	1,4E+02	3,3E+00	4,8E-03	9,3E+00	2,3E-01	8,5E-04
NA007-079c	9,5E+01	3,1E+00	6,8E-03	6,2E+01	4,1E+00	5,8E-03	2,2E+01	3,1E+00	1,6E-03	5,5E+02	9,8E+02	4,1E-03	1,8E+01	7,0E-01	7,9E-04
NA007-080c1	8,7E+01	2,0E+00	7,2E-03	5,0E+01	1,1E+00	5,8E-03	2,0E+01	2,0E+00	1,9E-03	9,7E+01	4,7E+00	4,2E-03	1,6E+01	1,5E+00	1,0E-03
NA007-080c2	1,4E+01	7,5E-01	8,1E-03	5,0E+02	8,8E+00	6,5E-03	1,0E+01	5,8E-01	1,4E-03	5,3E+01	1,0E+01	6,0E-03	3,7E+00	5,4E-01	9,7E-04
NA007-080c3	3,3E+01	1,1E+00	7,2E-03	4,8E+02	1,1E+01	6,3E-03	2,1E+01	8,3E-01	1,5E-03	1,4E+02	3,5E+00	4,1E-03	9,1E+00	2,8E-01	1,2E-03
NA007-092c	9,0E+01	2,0E+00	8,9E-03	5,9E+01	2,9E+00	7,0E-03	1,9E+01	2,7E-01	1,9E-03	1,0E+02	3,5E+00	4,5E-03	1,6E+01	2,6E-01	9,2E-04
NA007-096c	9,9E+01	2,4E+00	8,7E-03	5,0E+01	1,9E+00	6,7E-03	2,1E+01	5,5E-01	2,2E-03	1,0E+02	4,1E+00	4,6E-03	1,8E+01	2,2E-01	9,4E-04
NA007-100b (enclave)	9,5E+01	2,6E+00	9,1E-03	5,8E+01	3,3E+00	6,8E-03	1,9E+01	5,8E-01	2,3E-03	1,1E+02	3,6E+01	4,4E-03	1,7E+01	9,3E-01	1,3E-03
NA007-100b (matrix)	3,0E+01	4,8E-01	8,9E-03	4,1E+02	1,3E+01	7,2E-03	1,8E+01	7,1E-01	2,2E-03	7,6E+01	1,4E+00	5,4E-03	7,6E+00	6,7E-02	9,6E-04
NA007-100c (enclave)	7,8E+01	1,3E+00	8,6E-03	4,8E+01	1,5E+00	7,4E-03	1,6E+01	4,0E-01	1,7E-03	8,0E+01	7,7E+00	4,9E-03	1,4E+01	1,8E-01	1,6E-03
NA007-100c (matrix)	3,4E+01	1,3E+00	8,4E-03	3,3E+02	1,2E+01	7,3E-03	1,7E+01	1,1E+00	1,7E-03	7,2E+01	3,4E+00	4,6E-03	8,2E+00	4,6E-01	1,5E-03

	PPP-LA-ICP-MS													
Sample	Mo95_ppm	2SD	LOD	Ag107_ppm	2SD	LOD	Sn118_ppm	2SD	LOD	Sb121_ppm	2SD	LOD	Te125_ppm	2SD	LOD
NA007-002c	3,5E+00	1,7E-01	2,6E-02	1,1E-01	4,1E-03	6,2E-03	3,1E+00	5,4E-02	1,3E-02	2,6E-01	1,9E-02	7,4E-03	2,4E-02	3,6E-03	5,7E-03
NA007-052c	3,7E+00	5,2E-02	2,6E-02	1,1E-01	1,2E-02	6,3E-03	3,5E+00	1,7E-01	1,4E-02	1,4E-01	4,0E-03	6,8E-03	2,4E-02	6,5E-03	2,3E-03
NA007-062c	2,4E+00	1,2E-01	2,3E-02	7,1E-02	4,9E-03	6,9E-03	2,0E+00	9,8E-02	1,3E-02	7,7E-02	3,7E-03	5,9E-03	1,1E-02	1,5E-03	5,4E-03
NA007-079c	4,1E+00	2,2E-01	2,4E-02	1,2E-01	1,5E-01	6,3E-03	2,3E+00	1,1E-01	1,5E-02	1,9E-01	9,1E-03	7,2E-03	2,3E-02	8,0E-03	7,0E-03
NA007-080c1	3,5E+00	2,6E-01	2,3E-02	5,4E-02	5,7E-03	6,6E-03	2,2E+00	1,1E-01	1,4E-02	1,3E-01	1,2E-02	6,7E-03	n.d.	n.d.	n.d.
NA007-080c2	3,9E-01	2,7E-01	1,0E-02	4,1E-02	5,3E-03	9,1E-03	3,1E+00	5,9E-01	1,5E-02	4,5E-02	2,8E-03	7,2E-03	n.d.	n.d.	n.d.
NA007-080c3	2,0E+00	1,7E-01	2,1E-02	7,3E-02	4,7E-03	5,6E-03	1,2E+00	2,1E-01	1,2E-02	5,3E-02	6,5E-03	5,6E-03	8,6E-03	6,6E-03	3,7E-03
NA007-092c	3,6E+00	2,5E-01	3,1E-02	1,8E-01	2,1E-02	5,9E-03	5,4E+00	1,0E+00	1,5E-02	1,6E-01	3,3E-02	6,3E-03	1,7E-02	6,9E-03	5,1E-03
NA007-096c	4,2E+00	3,9E-01	2,5E-02	1,7E-01	1,9E-01	6,5E-03	2,5E+00	1,4E-01	1,3E-02	2,0E-01	4,0E-02	7,7E-03	2,2E-02	6,3E-03	6,4E-03
NA007-100b (enclave)	4,0E+00	1,4E-01	3,2E-02	6,3E-02	6,9E-03	8,0E-03	2,0E+00	4,1E-02	1,5E-02	1,2E-01	5,6E-03	7,3E-03	2,8E-02	7,2E-03	7,3E-03
NA007-100b (matrix)	1,4E+00	1,2E-01	2,1E-02	6,1E-02	4,5E-03	8,0E-03	1,2E+00	5,3E-02	1,3E-02	7,5E-02	1,0E-02	5,9E-03	4,7E-03	4,6E-03	3,1E-03
NA007-100c (enclave)	3,0E+00	1,1E-01	2,5E-02	5,3E-02	7,2E-03	8,2E-03	1,6E+00	7,0E-02	1,1E-02	9,3E-02	4,8E-03	7,2E-03	1,4E-02	8,9E-03	4,7E-03
NA007-100c (matrix)	1,5E+00	1,5E-01	2,1E-02	7,1E-02	1,0E-02	7,3E-03	1,3E+00	6,5E-02	1,4E-02	7,5E-02	4,1E-03	6,8E-03	8,0E-03	2,6E-03	5,4E-03

	PPP-LA-ICP-MS													
Sample	Ba137_ppm	2SD	LOD	La139_ppm	2SD	LOD	Ce140_ppm	2SD	LOD	Pr141_ppm	2SD	LOD	Nd146_ppm	2SD	LOD
NA007-002c	4,5E+02	1,5E+01	1,7E-02	2,4E+01	8,6E-01	1,2E-03	4,9E+01	1,3E+00	6,6E-04	5,5E+00	1,5E-01	3,2E-04	2,0E+01	5,3E-01	1,0E-03
NA007-052c	4,0E+02	1,1E+01	1,6E-02	2,4E+01	4,4E-01	8,3E-04	4,4E+01	1,3E+00	4,1E-04	4,6E+00	9,4E-02	2,5E-04	1,5E+01	2,6E-01	2,9E-03
NA007-062c	3,6E+02	1,1E+01	9,7E-03	1,6E+01	3,3E-01	8,9E-04	3,1E+01	7,7E-01	5,7E-04	4,0E+00	1,1E-01	3,9E-04	1,6E+01	4,1E-01	9,0E-04
NA007-079c	3,8E+02	1,9E+01	1,9E-02	2,5E+01	1,2E+00	9,4E-04	4,6E+01	2,3E+00	5,3E-04	4,8E+00	2,5E-01	5,6E-04	1,6E+01	9,3E-01	1,6E-03
NA007-080c1	3,4E+02	4,9E+00	1,5E-02	2,3E+01	2,1E+00	1,2E-03	4,4E+01	5,7E+00	6,6E-04	4,8E+00	6,9E-01	6,9E-04	1,6E+01	2,6E+00	2,1E-03
NA007-080c2	1,9E+02	8,6E+00	1,2E-02	8,5E+00	4,8E-01	1,0E-03	1,8E+01	1,9E+00	1,3E-03	2,3E+00	1,9E-01	7,6E-04	9,3E+00	6,9E-01	2,6E-03
NA007-080c3	3,4E+02	6,1E+00	1,8E-02	1,6E+01	6,6E-01	1,1E-03	3,1E+01	1,3E+00	5,7E-04	3,9E+00	1,5E-01	3,4E-04	1,6E+01	6,6E-01	2,0E-03
NA007-092c	4,0E+02	7,4E+00	2,0E-02	2,3E+01	4,7E-01	6,4E-04	4,3E+01	4,6E-01	5,9E-04	4,5E+00	8,1E-02	3,0E-04	1,5E+01	3,0E-01	1,6E-03
NA007-096c	4,2E+02	1,2E+01	1,8E-02	2,6E+01	8,7E-01	1,5E-03	4,8E+01	1,3E+00	6,1E-04	5,0E+00	1,4E-01	6,4E-04	1,7E+01	4,7E-01	2,4E-03
NA007-100b (enclave)	3,8E+02	2,8E+01	1,5E-02	2,3E+01	5,3E-01	1,2E-03	4,3E+01	4,5E-01	8,2E-04	4,5E+00	5,2E-02	4,4E-04	1,5E+01	2,3E-01	1,8E-03
NA007-100b (matrix)	2,1E+02	5,9E+00	2,1E-02	1,7E+01	8,2E-01	1,2E-03	3,4E+01	1,6E+00	5,5E-04	4,2E+00	2,1E-01	1,8E-04	1,7E+01	8,7E-01	3,5E-03
NA007-100c (enclave)	3,2E+02	1,6E+01	1,5E-02	1,9E+01	5,4E-01	1,0E-03	3,5E+01	1,3E+00	9,6E-04	3,8E+00	1,3E-01	3,8E-04	1,3E+01	4,8E-01	2,5E-03
NA007-100c (matrix)	2,1E+02	1,1E+01	1,7E-02	1,7E+01	1,8E+00	9,4E-04	3,3E+01	3,9E+00	9,3E-04	4,0E+00	4,1E-01	2,1E-04	1,5E+01	1,5E+00	1,3E-03

	PPP-LA-ICP-MS														
Sample	Sm147_ppm	2SD	LOD	Eu151_ppm	2SD	LOD	Gd157_ppm	2SD	LOD	Tb159_ppm	2SD	LOD	Dy161_ppm	2SD	LOD
NA007-002c	4,4E+00	2,1E-01	2,9E-03	8,4E-01	1,3E-02	1,2E-03	4,7E+00	1,3E-01	7,5E-03	8,7E-01	3,4E-02	6,8E-04	5,4E+00	9,8E-02	2,9E-03
NA007-052c	2,7E+00	9,2E-02	1,1E-03	4,0E-01	1,3E-02	8,4E-04	2,4E+00	1,0E-01	7,9E-03	4,3E-01	1,5E-02	7,3E-04	2,8E+00	7,3E-02	2,6E-03
NA007-062c	3,5E+00	8,8E-02	3,3E-03	1,1E+00	3,3E-02	7,7E-04	3,5E+00	5,4E-02	6,6E-03	5,9E-01	1,3E-02	3,0E-04	3,6E+00	1,4E-01	1,0E-03
NA007-079c	2,9E+00	1,6E-01	1,6E-03	4,0E-01	2,4E-02	7,9E-04	2,6E+00	8,3E-02	4,7E-03	4,4E-01	2,4E-02	5,6E-04	3,0E+00	2,0E-01	9,6E-04
NA007-080c1	2,9E+00	4,8E-01	1,6E-03	3,6E-01	1,4E-02	1,1E-03	2,6E+00	4,1E-01	5,6E-03	4,4E-01	7,3E-02	4,7E-04	2,9E+00	3,6E-01	2,0E-03
NA007-080c2	2,0E+00	1,8E-01	2,5E-03	6,4E-01	4,6E-02	9,8E-04	1,8E+00	1,2E-01	9,8E-03	2,7E-01	2,3E-02	5,4E-04	1,7E+00	1,4E-01	3,3E-03
NA007-080c3	3,4E+00	1,6E-01	1,8E-03	1,0E+00	4,4E-02	1,2E-03	3,5E+00	1,5E-01	8,2E-03	5,7E-01	3,4E-02	4,1E-04	3,5E+00	1,5E-01	2,9E-03
NA007-092c	2,8E+00	6,1E-02	2,6E-03	4,1E-01	8,5E-03	1,5E-03	2,4E+00	7,5E-02	5,7E-03	4,1E-01	1,1E-02	4,3E-04	2,7E+00	4,2E-02	2,1E-03
NA007-096c	3,0E+00	9,1E-02	1,2E-03	4,0E-01	8,9E-03	8,8E-04	2,6E+00	1,4E-01	6,0E-03	4,7E-01	1,4E-02	5,6E-04	3,1E+00	7,5E-02	1,7E-03
NA007-100b (enclave)	2,7E+00	7,0E-02	3,0E-03	3,7E-01	1,3E-02	5,1E-04	2,5E+00	7,4E-02	8,3E-03	4,1E-01	1,0E-02	5,0E-04	2,8E+00	7,3E-02	1,5E-03
NA007-100b (matrix)	3,3E+00	1,4E-01	3,1E-03	9,2E-01	2,4E-02	1,1E-03	3,1E+00	1,7E-01	8,9E-03	5,1E-01	3,1E-02	6,0E-04	3,1E+00	1,8E-01	1,3E-03
NA007-100c (enclave)	2,3E+00	7,6E-02	2,3E-03	3,2E-01	1,3E-02	1,4E-03	2,0E+00	9,7E-02	7,3E-03	3,5E-01	2,7E-02	6,8E-04	2,3E+00	9,9E-02	3,7E-03
NA007-100c (matrix)	3,0E+00	2,3E-01	3,3E-03	7,9E-01	5,6E-02	6,7E-04	2,8E+00	2,1E-01	1,1E-02	4,7E-01	4,1E-02	6,0E-04	2,9E+00	2,4E-01	3,9E-03

	PPP-LA-ICP-MS														
Sample	Ho165_ppm	2SD	LOD	Er167_ppm	2SD	LOD	Tm169_ppm	2SD	LOD	Yb172_ppm	2SD	LOD	Lu175_ppm	2SD	LOD
NA007-002c	1,2E+00	4,8E-02	2,3E-04	3,7E+00	8,0E-02	1,5E-03	5,9E-01	2,6E-02	7,8E-04	4,1E+00	1,3E-01	3,4E-03	6,8E-01	2,7E-02	6,9E-04
NA007-052c	6,1E-01	1,5E-02	3,4E-04	2,0E+00	8,3E-02	3,6E-03	3,5E-01	8,3E-03	6,0E-04	2,4E+00	6,1E-02	4,2E-03	4,0E-01	9,9E-03	4,6E-04
NA007-062c	7,6E-01	2,2E-02	3,1E-04	2,2E+00	4,4E-02	1,6E-03	3,5E-01	8,0E-03	5,6E-04	2,2E+00	7,2E-02	1,8E-03	3,5E-01	1,6E-02	2,5E-04
NA007-079c	6,8E-01	7,4E-02	2,9E-04	2,3E+00	4,2E-01	2,2E-03	4,0E-01	1,1E-01	4,6E-04	3,0E+00	1,1E+00	4,4E-03	5,1E-01	2,5E-01	2,4E-04
NA007-080c1	6,2E-01	8,2E-02	2,0E-04	2,0E+00	2,3E-01	2,6E-03	3,3E-01	2,0E-02	6,9E-04	2,3E+00	1,4E-01	2,5E-03	3,7E-01	1,7E-02	2,4E-04
NA007-080c2	3,4E-01	2,0E-02	5,7E-04	9,5E-01	6,8E-02	2,7E-03	1,5E-01	1,0E-02	7,2E-04	9,1E-01	3,3E-02	4,1E-03	1,4E-01	9,6E-03	3,9E-04
NA007-080c3	7,4E-01	2,8E-02	4,3E-04	2,2E+00	1,0E-01	1,4E-03	3,3E-01	1,6E-02	5,1E-04	2,2E+00	1,2E-01	1,5E-03	3,5E-01	1,4E-02	6,5E-04
NA007-092c	6,1E-01	1,4E-02	3,5E-04	1,9E+00	4,9E-02	1,5E-03	3,3E-01	1,6E-02	8,4E-04	2,3E+00	7,5E-02	4,4E-03	3,8E-01	1,4E-02	2,9E-04
NA007-096c	6,8E-01	2,7E-02	4,1E-04	2,2E+00	7,8E-02	1,5E-03	3,7E-01	1,5E-02	7,1E-04	2,7E+00	3,1E-02	6,3E-03	4,2E-01	1,7E-02	2,8E-04
NA007-100b (enclave)	6,2E-01	1,7E-02	4,1E-04	2,0E+00	7,0E-02	2,9E-03	3,3E-01	9,3E-03	1,1E-03	2,4E+00	5,5E-02	4,1E-03	3,7E-01	2,1E-02	5,5E-04
NA007-100b (matrix)	6,4E-01	4,1E-02	3,8E-04	1,9E+00	8,5E-02	2,1E-03	2,9E-01	1,4E-02	1,2E-03	1,9E+00	8,3E-02	3,7E-03	2,8E-01	1,7E-02	3,1E-04
NA007-100c (enclave)	5,2E-01	2,2E-02	3,3E-04	1,7E+00	5,8E-02	3,4E-03	2,8E-01	1,8E-02	1,0E-03	1,9E+00	1,1E-01	1,2E-03	3,2E-01	1,4E-02	8,7E-04
NA007-100c (matrix)	6,0E-01	6,2E-02	8,7E-04	1,8E+00	1,6E-01	1,9E-03	2,8E-01	2,7E-02	7,2E-04	1,8E+00	1,7E-01	2,2E-03	2,8E-01	2,2E-02	5,9E-04

	PPP-LA-ICP-MS														
Sample	Hf178_ppm	2SD	LOD	Ta181_ppm	2SD	LOD	Au197_ppm*	2SD	LOD	Hg202_ppm**	2SD	LOD	Tl205_ppm	2SD	LOD
NA007-002c	6,7E+00	2,2E-01	1,7E-03	7,4E-01	5,4E-02	1,8E-03	3,7E-03	6,5E-04	7,4E-03	9,2E-02	7,8E-02	1,9E-02	3,4E-01	6,7E-03	2,4E-03
NA007-052c	3,2E+00	8,0E-02	1,5E-03	1,3E+00	5,8E-02	1,6E-03	3,8E-03	1,8E-03	7,7E-03	8,1E-02	n.d.	2,0E-02	4,1E-01	1,8E-02	2,7E-03
NA007-062c	3,5E+00	9,6E-02	9,6E-04	5,7E-01	2,0E-02	1,7E-03	2,7E-03	3,6E-04	5,5E-03	1,5E-02	n.d.	5,1E-03	1,5E-01	1,1E-02	2,3E-03
NA007-079c	9,1E+00	1,3E+01	1,4E-03	1,4E+00	7,9E-02	1,6E-03	5,3E-03	1,6E-03	8,9E-03	7,4E-02	5,0E-02	1,7E-02	4,4E-01	1,9E-02	2,2E-03
NA007-080c1	2,8E+00	1,4E-01	2,7E-03	1,2E+00	5,8E-02	1,3E-03	3,9E-03	1,0E-03	6,2E-03	n.d.	n.d.	n.d.	4,4E-01	2,3E-02	2,7E-03
NA007-080c2	1,5E+00	1,6E-01	2,6E-03	2,3E-01	2,9E-02	1,4E-03	4,1E-03	1,3E-03	6,2E-03	3,5E-02	1,9E-02	1,0E-02	5,8E-02	6,5E-03	2,6E-03
NA007-080c3	3,4E+00	9,2E-02	2,1E-03	5,8E-01	2,6E-02	1,5E-03	6,9E-03	5,1E-03	1,3E-02	n.d.	n.d.	n.d.	1,4E-01	5,1E-03	2,8E-03
NA007-092c	3,1E+00	1,4E-01	2,7E-03	1,3E+00	2,7E-02	1,5E-03	4,1E-03	9,9E-04	5,0E-03	2,9E-02	3,4E-02	9,0E-03	4,2E-01	1,8E-02	2,9E-03
NA007-096c	3,3E+00	1,4E-01	1,1E-03	1,4E+00	4,0E-02	1,1E-03	8,8E-03	6,6E-03	1,8E-02	9,0E-02	n.d.	2,4E-02	4,5E-01	3,1E-02	2,7E-03
NA007-100b (enclave)	3,5E+00	7,9E-01	2,2E-03	1,3E+00	4,1E-02	2,2E-03	8,5E-03	8,2E-03	1,6E-02	6,6E-02	n.d.	2,2E-02	4,2E-01	1,6E-02	2,3E-03
NA007-100b (matrix)	2,1E+00	1,3E-01	2,0E-03	5,2E-01	1,3E-02	1,6E-03	3,5E-03	4,1E-04	7,0E-03	1,2E-02	n.d.	4,9E-03	1,6E-01	2,1E-02	2,5E-03
NA007-100c (enclave)	2,4E+00	1,3E-01	1,6E-03	1,1E+00	3,0E-02	1,6E-03	5,4E-03	3,1E-03	9,9E-03	1,9E-02	2,2E-03	7,0E-03	3,6E-01	1,3E-02	3,2E-03
NA007-100c (matrix)	2,0E+00	1,4E-01	2,3E-03	5,8E-01	4,0E-02	1,9E-03	4,4E-03	2,2E-03	8,9E-03	n.d.	n.d.	n.d.	1,9E-01	1,4E-02	3,0E-03

*Please use Au values measured by ultra-low Au PPP-LA-ICP-MS

	PPP-LA-ICP-MS															DMA
Sample	Pb208_ppm	2SD	LOD	Bi209_ppm	2SD	LOD	Th232_ppm	2SD	LOD	U238_ppm	2SD	LOD	Au (ppm)	2SD (ppm)	LOD (ppm)	Hg (ppm)
NA007-002c	1,4E+01	1,7E-01	3,1E-03	4,5E-02	3,2E-03	1,7E-03	1,6E+01	2,5E-01	3,2E-04	5,3E+00	8,5E-01	4,7E-04	6,7E-04	2,1E-04	5,312E-05	26,51
NA007-052c	1,1E+01	2,6E-01	3,4E-03	8,6E-02	8,8E-03	1,5E-03	1,2E+01	2,3E-01	3,1E-04	2,8E+00	7,6E-02	6,5E-04	2,9E-04	7,7E-05	5,312E-05	22,44
NA007-062c	9,1E+00	3,6E-01	2,8E-03	3,3E-02	3,1E-03	1,2E-03	4,6E+00	7,7E-02	3,0E-04	1,4E+00	4,8E-02	2,8E-04	8,8E-04	8,2E-05	5,312E-05	23,70
NA007-079c	1,2E+01	7,9E-01	3,1E-03	9,1E-02	8,6E-03	1,9E-03	1,1E+01	5,5E-01	4,5E-04	2,8E+00	6,0E-01	3,9E-04	5,3E-04	1,7E-04	5,312E-05	25,58
NA007-080c1	1,0E+01	5,7E-01	3,0E-03	3,5E-02	1,5E-03	1,7E-03	1,1E+01	5,5E-01	4,1E-04	2,5E+00	2,6E-01	2,5E-04	2,1E-04	1,6E-04	5,312E-05	23,92
NA007-080c2	4,2E+00	2,7E-01	3,2E-03	7,9E-03	1,7E-03	1,6E-03	1,9E+00	2,2E-01	8,6E-04	5,1E-01	6,6E-02	4,1E-04	1,0E-03	3,3E-04	5,312E-05	24,41
NA007-080c3	8,4E+00	2,3E-01	2,4E-03	2,4E-02	8,1E-04	1,3E-03	4,5E+00	9,7E-02	4,3E-04	1,3E+00	3,1E-02	2,6E-04	6,8E-04	1,6E-04	5,312E-05	23,21
NA007-092c	1,1E+01	3,8E-01	3,0E-03	7,6E-02	6,3E-03	1,8E-03	1,2E+01	3,0E-01	3,5E-04	2,7E+00	8,7E-02	3,3E-04	3,5E-05	4,7E-05	5,312E-05	26,32
NA007-096c	1,3E+01	1,9E+00	2,3E-03	9,3E-02	4,4E-03	1,3E-03	1,3E+01	4,1E-01	6,9E-04	3,0E+00	3,2E-02	5,4E-04	4,3E-05	1,4E-04	5,312E-05	23,73
NA007-100b (enclave)	1,1E+01	2,0E-01	4,4E-03	8,2E-02	6,5E-03	1,4E-03	1,1E+01	4,6E-01	8,0E-04	2,6E+00	1,4E-01	5,6E-04	2,6E-04	1,0E-04	5,312E-05	23,01
NA007-100b (matrix)	5,0E+00	1,5E-01	3,4E-03	2,9E-02	4,3E-03	1,3E-03	6,8E+00	1,6E-01	7,8E-04	1,5E+00	7,7E-02	5,3E-04	3,2E-05	5,4E-04	5,312E-05	23,91
NA007-100c (enclave)	9,5E+00	4,3E-01	3,8E-03	6,8E-02	3,4E-03	1,5E-03	1,0E+01	4,5E-01	6,0E-04	2,3E+00	1,2E-01	5,0E-04	2,1E-04	2,1E-04	5,312E-05	n.d.
NA007-100c (matrix)	6,2E+00	4,8E-01	4,3E-03	4,1E-02	4,8E-03	1,7E-03	7,2E+00	2,8E-01	6,3E-04	1,6E+00	9,1E-02	4,0E-04	4,7E-06	2,6E-04	5,312E-05	24,98

Standard PPP-LA-ICP-MS

AVERAGE	Li7_ppm_mean	Si29_ppm_mean	P31_ppm_mean	S32_ppm_mean	Cl35_ppm_mean	Ca44_ppm_mean	Sc45_ppm_mean	Ti49_ppm_mean	V51_ppm_mean	Cr53_ppm_mean	Mn55_ppm_mean	Fe57_ppm_mean	Co59_ppm_mean
BCR-2	9,30E+00	2,67E+05	1,56E+03	3,52E+02	3,77E+02	5,18E+04	3,30E+01	1,35E+04	4,17E+02	2,19E+01	1,56E+03	9,35E+04	3,79E+01
BHVO-1	5,10E+00	2,30E+05	1,26E+03	1,26E+02	3,57E+02	8,55E+04	3,19E+01	1,69E+04	3,25E+02	2,95E+02	1,36E+03	8,65E+04	4,54E+01
BHVO-2	4,48E+00	2,54E+05	1,13E+03	2,42E+02	4,13E+02	8,02E+04	3,04E+01	1,60E+04	3,11E+02	2,87E+02	1,27E+03	8,25E+04	4,31E+01
BIR-1	3,40E+00	1,98E+05	8,90E+01	7,55E+01	1,16E+02	8,88E+04	4,02E+01	5,31E+03	2,98E+02	3,71E+02	1,25E+03	7,29E+04	4,88E+01

2SD													
BCR-2	4,42E-01	1,84E+04	1,52E+02	5,59E+01	2,27E+02	2,89E+03	2,05E+00	8,49E+02	2,35E+01	9,27E+00	1,22E+02	5,30E+03	2,74E+00
BHVO-1	4,47E-01	6,14E+03	8,88E+01	3,61E+01	1,75E+02	4,02E+03	1,55E+00	9,95E+02	1,52E+01	1,88E+01	9,77E+01	4,24E+03	2,85E+00
BHVO-2	2,45E-01	1,81E+04	8,14E+01	5,10E+01	2,20E+02	4,81E+03	1,85E+00	9,17E+02	1,70E+01	1,46E+01	7,30E+01	4,93E+03	2,18E+00
BIR-1	7,79E-01	2,74E+04	5,48E+01	3,52E+01	8,68E+01	1,08E+04	5,26E+00	7,18E+02	3,82E+01	5,41E+01	1,26E+02	7,89E+03	4,75E+00

Precision	Li	Si	P	S	Cl	Ca	Sc	Ti	V	Cr	Mn	Fe	Co
BCR-2	0,95	0,93	0,90	0,84	0,40	0,94	0,94	0,94	0,94	0,58	0,92	0,94	0,93
BHVO-1	0,91	0,97	0,93	0,71	0,51	0,95	0,95	0,94	0,95	0,94	0,93	0,95	0,94
BHVO-2	0,95	0,93	0,93	0,79	0,47	0,94	0,94	0,94	0,95	0,95	0,94	0,94	0,95
BIR-1	0,77	0,86	0,38	0,53	0,25	0,88	0,87	0,86	0,87	0,85	0,90	0,89	0,90

ACCURACY	Li	Si	P	S	Cl	Ca	Sc	Ti	V	Cr	Mn	Fe	Co
BCR-2	1,02	1,06	0,99	1,11	3,93	1,02	0,98	0,99	1,00	1,38	1,03	0,97	1,01
BHVO-1	1,09	0,99	1,04	1,66	3,84	1,05	1,02	1,03	1,03	1,02	1,04	1,00	1,01
BHVO-2	1,00	1,10	0,97	1,47	3,86	0,98	0,95	0,98	0,98	1,00	0,97	0,95	0,96
BIR-1	1,06	0,89	0,68	1,08	2,64	0,94	0,93	0,92	0,93	0,94	0,93	0,91	0,93

STD VALUES	Li	Si	P	S	Cl	Ca	Sc	Ti	V	Cr	Mn	Fe	Co
BCR-2*	9,13	252396	1567,9852	318	96	50843,758	33,53	13576,41	417,6	15,85	1522,667	96311,9241	37,33
BHVO-1*	4,68	232718,46	1210,1372	76	93	81690,21	31,42	16435,548	313,8	287,6	1308,1305	86170,1456	44,9
BHVO-2*	4,5	231830,4	1171,734	164	107	81475,8	31,83	16369,614	318,2	287,2	1308,905	86659,7487	44,89
BIR-1*	3,203	223370,46	130,92	70	44	94983,63	43,21	5746,4478	320,6	392,9	1340,6595	79735,362	52,22

*Prefered values : Jochum K.P., Weis U., Schwager B., Stoll B., Wilson S.A., Haug G.H., Andreae M.O, Enzweiler J.; | Geostandards and Geoanalytical Research 40 (3) | [2016] 333-350 Title: Reference values following ISO guidelines for frequently requested rock reference materials doi: 10.1111/j.1751-908X.2015.00392.x

Standard PPP-LA

AVERAGE	Ni60_ppm_mean	Cu63_ppm_mean	Zn66_ppm_mean	As75_ppm_mean	Se78_ppm_mean	Rb85_ppm_mean	Sr88_ppm_mean	Y89_ppm_mean	Zr90_ppm_mean	Nb93_ppm_mean	Mo95_ppm_mean	Ag107_ppm_mean	Sn118_ppm_mean
BCR-2	1,39E+01	1,85E+01	1,25E+02	8,83E-01	3,05E-01	4,61E+01	3,44E+02	3,58E+01	1,90E+02	1,27E+01	2,11E+02	7,77E-02	2,30E+00
BHVO-1	1,17E+02	1,38E+02	1,01E+02	6,70E-01	3,12E-01	9,56E+00	4,03E+02	2,71E+01	1,78E+02	1,96E+01	1,90E+00	9,63E-02	2,11E+00
BHVO-2	1,11E+02	1,20E+02	1,10E+02	8,62E-01	2,11E-01	8,73E+00	3,79E+02	2,54E+01	1,67E+02	1,81E+01	4,65E+00	8,98E-02	1,83E+00
BIR-1	1,53E+02	1,14E+02	6,12E+01	1,25E-01	3,10E-01	5,24E-01	1,03E+02	1,50E+01	1,41E+01	3,93E-01	6,61E-02	3,63E-02	7,23E-01

2SD

BCR-2	5,57E+00	6,10E+00	1,78E+01	6,89E-02	3,88E-01	2,07E+00	1,90E+01	2,15E+00	9,87E+00	8,41E-01	5,62E+01	1,60E-02	1,61E-01
BHVO-1	6,17E+00	2,00E+01	1,72E+01	8,52E-02	4,59E-01	5,65E-01	1,90E+01	1,27E+00	8,03E+00	1,39E+00	5,49E-01	1,61E-02	2,23E-01
BHVO-2	6,11E+00	1,41E+01	1,46E+01	5,52E-02	3,03E-01	4,35E-01	1,59E+01	1,28E+00	9,27E+00	1,26E+00	1,69E+00	1,21E-02	1,23E-01
BIR-1	1,71E+01	1,95E+01	1,56E+01	2,50E-02	4,60E-01	2,14E-01	1,15E+01	2,47E+00	2,94E+00	2,10E-01	4,47E-02	1,43E-02	1,40E-01

Precision	Ni	Cu	Zn	As	Se	Rb	Sr	Y	Zr	Nb	Mo	Ag	Sn
BCR-2	0,60	0,67	0,86	0,92	-0,27	0,96	0,94	0,94	0,95	0,93	0,73	0,79	0,93
BHVO-1	0,95	0,86	0,83	0,87	-0,47	0,94	0,95	0,95	0,95	0,93	0,71	0,83	0,89
BHVO-2	0,94	0,88	0,87	0,94	-0,44	0,95	0,96	0,95	0,94	0,93	0,64	0,86	0,93
BIR-1	0,89	0,83	0,74	0,80	-0,48	0,59	0,89	0,84	0,79	0,47	0,32	0,61	0,81

ACCURACY	Ni	Cu	Zn	As	Se	Rb	Sr	Y	Zr	Nb	Mo	Ag	Sn
BCR-2	1,10	0,94	0,96	1,03	3,71	1,00	1,02	0,99	1,02	1,02	0,84	0,86	1,01
BHVO-1	0,97	1,01	0,96	1,19	3,47	1,00	1,01	1,03	1,02	1,06	1,79	1,36	1,01
BHVO-2	0,92	0,93	1,06	1,23	1,17	0,94	0,96	0,98	0,97	1,00	1,14	1,01	1,03
BIR-1	0,91	0,94	0,87	0,73	16,33	2,49	0,95	0,96	0,96	0,71	0,97	0,88	1,03

STD VALUES	Ni	Cu	Zn	As	Se	Rb	Sr	Y	Zr	Nb	Mo	Ag	Sn
BCR-2*	12,57	19,66	129,5	0,86	0,082	46,02	337,4	36,07	186,5	12,44	250,6	0,09	2,28
BHVO-1*	120	137,2	105,1	0,565	0,09	9,52	399,2	26,23	174,6	18,53	1,061	0,071	2,09
BHVO-2*	119,8	129,3	103,9	0,7	0,18	9,261	394,1	25,91	171,2	18,1	4,07	0,089	1,776
BIR-1*	168,9	120,7	70,4	0,17	0,019	0,21	108,6	15,6	14,8	0,553	0,068	0,041	0,701

Standard PPP-LA

AVERAGE	Sb121_ppm_ mean	Te125_ppm_ mean	Ba137_ppm_ mean	La139_ppm_ mean	Ce140_ppm_ mean	Pr141_ppm_ mean	Nd146_ppm_ mean	Sm147_ppm _mean	Eu151_ppm_ mean	Gd157_ppm_ mean	Tb159_ppm_ mean	Dy161_ppm_ mean	Ho165_ppm_ mean
BCR-2	2,98E-01	2,10E-02	6,81E+02	2,51E+01	5,47E+01	6,81E+00	2,84E+01	6,50E+00	1,95E+00	6,70E+00	1,05E+00	6,34E+00	1,30E+00
BHVO-1	1,37E-01	9,02E-03	1,39E+02	1,61E+01	3,91E+01	5,60E+00	2,55E+01	6,32E+00	2,13E+00	6,51E+00	9,77E-01	5,51E+00	1,02E+00
BHVO-2	1,32E-01	1,39E-02	1,34E+02	1,48E+01	3,56E+01	5,13E+00	2,34E+01	5,84E+00	1,97E+00	6,03E+00	9,06E-01	5,13E+00	9,56E-01
BIR-1	4,55E-01	1,66E-02	7,62E+00	6,73E-01	2,32E+00	3,52E-01	2,34E+00	1,05E+00	5,00E-01	1,74E+00	3,30E-01	2,43E+00	5,35E-01

2SD

BCR-2	8,02E-02	1,02E-02	3,36E+01	1,51E+00	4,18E+00	4,30E-01	1,87E+00	4,19E-01	1,10E-01	4,92E-01	7,15E-02	4,53E-01	9,27E-02
BHVO-1	4,74E-02	6,04E-03	8,21E+00	9,11E-01	2,38E+00	3,06E-01	1,36E+00	3,08E-01	1,04E-01	3,31E-01	5,25E-02	2,88E-01	6,54E-02
BHVO-2	2,54E-02	7,07E-03	7,45E+00	8,79E-01	2,25E+00	2,77E-01	1,24E+00	2,86E-01	9,35E-02	3,12E-01	5,07E-02	2,61E-01	5,11E-02
BIR-1	8,61E-02	6,62E-02	2,28E+00	1,84E-01	4,79E-01	8,87E-02	5,01E-01	1,95E-01	6,22E-02	3,24E-01	6,39E-02	4,21E-01	9,14E-02

Precision	Sb	Te	Ba	La	Ce	Pr	Nd	Sm	Eu	Gd	Tb	Dy	Ho
BCR-2	0,73	0,51	0,95	0,94	0,92	0,94	0,93	0,94	0,94	0,93	0,93	0,93	0,93
BHVO-1	0,65	0,33	0,94	0,94	0,94	0,95	0,95	0,95	0,95	0,95	0,95	0,95	0,94
BHVO-2	0,81	0,49	0,94	0,94	0,94	0,95	0,95	0,95	0,95	0,95	0,94	0,95	0,95
BIR-1	0,81	-2,99	0,70	0,73	0,79	0,75	0,79	0,81	0,88	0,81	0,81	0,83	0,83

ACCURACY	Sb	Te	Ba	La	Ce	Pr	Nd	Sm	Eu	Gd	Tb	Dy	Ho
BCR-2	0,99	5,25	1,00	1,00	1,03	1,00	1,00	0,99	0,98	0,98	0,97	0,99	0,99
BHVO-1	0,88	1,24	1,03	1,04	1,03	1,03	1,03	1,02	1,04	1,04	1,03	1,04	1,04
BHVO-2	1,28	0,99	1,02	0,97	0,95	0,96	0,96	0,97	0,97	0,97	0,97	0,97	0,97
BIR-1	0,99	2,91	1,13	1,07	1,21	0,95	0,98	0,94	0,96	0,96	0,91	0,95	0,94

STD VALUES	Sb	Te	Ba	La	Ce	Pr	Nd	Sm	Eu	Gd	Tb	Dy	Ho
BCR-2*	0,302	0,004	683,9	25,08	53,12	6,827	28,26	6,547	1,989	6,811	1,077	6,424	1,313
BHVO-1*	0,155	0,0073	134,4	15,44	38,08	5,419	24,78	6,165	2,053	6,285	0,9455	5,272	0,9839
BHVO-2*	0,1034	0,014	130,9	15,2	37,53	5,339	24,27	6,023	2,043	6,207	0,9392	5,28	0,9887
BIR-1*	0,462	0,0057	6,75	0,627	1,92	0,3723	2,397	1,113	0,5201	1,809	0,3623	2,544	0,5718

Standard PPP-LA

AVERAGE	Er167_ppm_mean	Tm169_ppm_mean	Yb172_ppm_mean	Lu175_ppm_mean	Hf178_ppm_mean	Ta181_ppm_mean	Au197_ppm_mean	Hg202_ppm_mean	Tl205_ppm_mean	Pb208_ppm_mean	Bi209_ppm_mean	Th232_ppm_mean	U238_ppm_mean
BCR-2	3,64E+00	5,21E-01	3,39E+00	5,03E-01	5,03E+00	8,01E-01	2,75E-03	1,10E-02	2,79E-01	1,12E+01	5,06E-02	5,84E+00	1,69E+00
BHVO-1	2,60E+00	3,41E-01	2,04E+00	2,85E-01	4,56E+00	1,21E+00	3,92E-03	2,23E-01	3,74E-02	1,92E+00	1,14E-02	1,28E+00	4,31E-01
BHVO-2	2,45E+00	3,23E-01	1,93E+00	2,70E-01	4,32E+00	1,13E+00	3,17E-03	4,21E-02	8,27E-02	1,33E+01	1,38E-02	1,19E+00	4,19E-01
BIR-1	1,60E+00	2,41E-01	1,58E+00	2,40E-01	5,32E-01	5,22E-02	4,06E-03	3,45E-02	7,05E-03	3,63E+00	6,06E-03	1,18E-01	3,37E-02
2SD													
BCR-2	2,62E-01	4,26E-02	2,34E-01	3,91E-02	3,00E-01	5,66E-02	1,40E-03	1,72E-02	2,19E-02	1,89E+00	7,10E-03	3,44E-01	1,22E-01
BHVO-1	1,55E-01	2,55E-02	1,38E-01	1,80E-02	2,79E-01	7,19E-02	1,67E-03	1,50E-01	1,16E-02	2,33E-01	3,16E-03	1,07E-01	3,45E-02
BHVO-2	1,37E-01	1,99E-02	1,11E-01	1,71E-02	2,61E-01	6,49E-02	1,42E-03	6,29E-02	9,83E-03	4,04E+00	2,47E-03	1,02E-01	3,21E-02
BIR-1	2,81E-01	4,00E-02	2,68E-01	3,93E-02	8,84E-02	4,19E-02	4,48E-03	3,97E-02	3,87E-03	5,71E-01	2,86E-03	1,70E-01	1,66E-02

Precision	Er	Tm	Yb	Lu	Hf	Ta	Au	Hg	Tl	Pb	Bi	Th	U
BCR-2	0,93	0,92	0,93	0,92	0,94	0,93	0,49	-0,57	0,92	0,83	0,86	0,94	0,93
BHVO-1	0,94	0,93	0,93	0,94	0,94	0,94	0,57	0,33	0,69	0,88	0,72	0,92	0,92
BHVO-2	0,94	0,94	0,94	0,94	0,94	0,94	0,55	-0,49	0,88	0,70	0,82	0,91	0,92
BIR-1	0,82	0,83	0,83	0,84	0,83	0,20	-0,10	-0,15	0,45	0,84	0,53	-0,44	0,51

ACCURACY	Er	Tm	Yb	Lu	Hf	Ta	Au	Hg	Tl	Pb	Bi	Th	U
BCR-2	0,99	0,98	1,00	1,00	1,01	1,02	2,11	9,16	1,04	1,06	1,01	1,00	1,00
BHVO-1	1,04	1,04	1,03	1,03	1,03	1,03	1,78	22,30	0,81	0,94	0,95	1,04	1,03
BHVO-2	0,98	0,96	0,97	0,98	0,97	0,98	1,22	21,03	3,69	8,02	0,93	0,97	1,02
BIR-1	0,95	0,94	0,97	0,97	0,91	1,26	0,00	4,73	3,36	1,19	1,19	3,60	3,20

STD VALUES	Er	Tm	Yb	Lu	Hf	Ta	Au	Hg	Tl	Pb	Bi	Th	U
BCR-2*	3,67	0,5341	3,392	0,5049	4,972	0,785	0,0013	0,0012	0,267	10,59	0,05	5,828	1,683
BHVO-1*	2,501	0,3289	1,987	0,2775	4,44	1,174	0,0022	0,01	0,0461	2,037	0,0121	1,225	0,4182
BHVO-2*	2,511	0,3349	1,994	0,2754	4,47	1,154	0,0026	0,002	0,0224	1,653	0,0148	1,224	0,412
BIR-1*	1,68	0,2558	1,631	0,2484	0,5822	0,0414	2,5	0,0073	0,0021	3,037	0,0051	0,0328	0,01051

Standard PPP-LA-ICP-MS - setting for Au analysis

													Raw Au			Au corrected for Hf and Ta oxides interferences		
	Si29_mean	Si29_2SD	Si29_LOD	Ca44_mean	Ca44_2SD	Ca44_LOD	Hf180_mean	Hf180_2SD	Hf180_LOD	Ta181_mean	Ta181_2SD	Ta181_LOD	Au197_mean	Au197_2SD	Au197_LOD	Au2_mean	Au2_2SD	Au2_LOD
	(ppm)	(ppm)	(ppm)	(ppm)	(ppm)	(ppm)	(ppm)	(ppm)	(ppm)	(ppm)	(ppm)	(ppm)	(ppm)	(ppm)	(ppm)	(ppm)	(ppm)	(ppm)
BCR-2																		
BCR2-1	2,51E+05	3,48E+04	6,58E-01	5,40E+04	7,41E+03	3,85E-01	4,62E+00	6,70E-01	6,22E-05	7,00E-01	1,05E-01	2,84E-05	1,09E-03	5,07E-04	2,65E-05	9,64E-04	5,73E-04	2,65E-05
BCR2-2	2,36E+05	5,58E+04	5,75E-01	5,13E+04	9,46E+03	3,84E-01	4,44E+00	6,96E-01	5,14E-05	6,77E-01	1,09E-01	2,03E-05	1,11E-03	6,28E-04	2,89E-05	9,96E-04	7,37E-04	2,89E-05
BCR2-3	2,49E+05	5,15E+04	6,45E-01	5,42E+04	8,29E+03	4,18E-01	4,62E+00	7,25E-01	1,19E-04	7,05E-01	1,18E-01	7,92E-05	1,29E-03	6,68E-04	3,05E-05	1,19E-03	7,88E-04	3,05E-05
BCR2-4	2,56E+05	5,19E+04	8,15E-01	4,93E+04	1,15E+04	4,35E-01	4,82E+00	7,01E-01	8,21E-05	7,37E-01	1,26E-01	5,48E-05	1,11E-03	4,58E-04	5,68E-05	9,28E-04	5,30E-04	5,68E-05
BCR2-5	2,57E+05	2,82E+04	8,20E-01	5,01E+04	8,01E+03	4,33E-01	4,80E+00	4,94E-01	1,05E-04	7,48E-01	8,66E-02	4,82E-05	1,15E-03	8,25E-04	6,23E-05	9,73E-04	9,76E-04	6,23E-05
BCR2-6	2,36E+05	2,41E+04	1,00E+00	4,73E+04	5,11E+03	5,31E-01	4,66E+00	4,40E-01	3,79E-05	7,30E-01	4,44E-02	4,73E-05	9,65E-04	3,82E-04	7,87E-05	7,66E-04	4,42E-04	7,87E-05
BCR2-7	2,55E+05	5,43E+04	1,09E+00	4,53E+04	1,12E+04	5,34E-01	4,78E+00	8,04E-01	1,93E-05	7,37E-01	1,24E-01	5,16E-05	8,68E-04	6,97E-04	6,42E-05	6,56E-04	8,06E-04	6,42E-05
BCR2-8	2,52E+05	4,68E+04	9,74E-01	4,55E+04	9,67E+03	5,21E-01	4,81E+00	6,98E-01	1,94E-05	7,41E-01	1,19E-01	4,05E-05	8,85E-04	8,78E-04	6,37E-05	6,73E-04	1,00E-03	6,37E-05
BCR2-9	2,43E+05	5,64E+04	9,65E-01	4,33E+04	1,45E+04	4,73E-01	4,76E+00	8,69E-01	1,90E-04	7,30E-01	1,12E-01	4,27E-05	1,00E-03	1,07E-03	6,07E-05	8,22E-04	1,24E-03	6,07E-05
BCR2-10	2,46E+05	2,97E+04	1,50E+00	4,34E+04	1,44E+04	7,14E-01	5,14E+00	9,77E-01	2,79E-05	8,02E-01	1,20E-01	4,12E-05	8,97E-04	8,51E-04	7,35E-05	6,13E-04	9,58E-04	7,35E-05
BCR2-11	2,40E+05	1,99E+04	1,52E+00	4,04E+04	8,29E+03	6,93E-01	4,97E+00	6,14E-01	1,18E-04	7,99E-01	1,10E-01	4,19E-05	6,82E-04	8,11E-04	7,48E-05	3,82E-04	8,89E-04	7,48E-05
BCR2-12	2,42E+05	2,41E+04	1,50E+00	4,16E+04	8,07E+03	6,79E-01	5,04E+00	7,64E-01	2,79E-05	7,88E-01	9,81E-02	3,73E-05	7,76E-04	1,23E-03	7,15E-05	4,87E-04	1,40E-03	7,15E-05
Reference Values	*2,53E+05*	*0,00E+00*		*5,13E+04*	*0,00E+00*		*4,80E+00*	*0,00E+00*		*7,50E-01*	*0,00E+00*		*8,40E-04*	*0,00E+00*		*8,40E-04*	*0,00E+00*	
Average	*2,47E+05*	*3,98E+04*	*1,00E+00*	*4,72E+04*	*9,65E+03*	*5,17E-01*	*4,79E+00*	*7,04E-01*	*7,17E-05*	*7,41E-01*	*1,06E-01*	*4,45E-05*	*9,86E-04*	*7,51E-04*	*5,77E-05*	*7,88E-04*	*8,62E-04*	*5,77E-05*
Precision (+-15%)	*0,98*			*0,92*			*1,00*			*0,99*			*1,17*			*0,94*		
Accuracy	*0,16*			*0,20*			*0,15*			*0,14*			*0,76*			*1,09*		
BHVO-2																		
BHVO-2-1	2,32E+05	3,23E-11	4,66E-01	6,30E+04	4,84E+03	3,57E-01	3,76E+00	4,56E-01	2,78E-05	9,45E-01	1,03E-01	3,37E-05	2,31E-03	1,15E-03	2,60E-05	2,29E-03	1,34E-03	2,60E-05
BHVO-2-2	2,32E+05	2,83E-11	4,48E-01	6,48E+04	7,29E+03	2,83E-01	3,76E+00	5,62E-01	3,41E-05	9,44E-01	1,49E-01	4,30E-05	2,10E-03	7,88E-04	2,76E-05	2,04E-03	9,04E-04	2,76E-05
BHVO-2-3	2,32E+05	3,62E-11	4,58E-01	6,53E+04	7,29E+03	2,92E-01	3,81E+00	7,00E-01	7,76E-06	9,58E-01	1,71E-01	1,08E-05	2,26E-03	9,59E-04	2,43E-05	2,23E-03	1,11E-03	2,43E-05
BHVO-2-4	2,32E+05	2,11E-11	6,10E-01	6,04E+04	7,36E+03	3,45E-01	3,85E+00	4,17E-01	9,83E-06	9,87E-01	9,64E-02	3,06E-05	2,20E-03	8,09E-04	4,02E-05	2,10E-03	9,26E-04	4,02E-05
BHVO-2-5	2,32E+05	2,95E-11	7,53E-01	7,09E+04	2,27E+04	3,95E-01	3,92E+00	7,12E-01	5,74E-05	1,02E+00	1,83E-01	6,19E-05	2,37E-03	9,72E-04	5,05E-05	2,29E-03	1,09E-03	5,05E-05
BHVO-2-6	2,32E+05	1,34E-11	5,86E-01	7,02E+04	2,25E+04	3,92E-01	3,87E+00	5,69E-01	6,68E-05	1,01E+00	1,38E-01	2,63E-05	2,35E-03	7,41E-04	4,45E-05	2,26E-03	8,39E-04	4,45E-05
BHVO-2-7	2,32E+05	0,00E+00	8,89E-01	7,84E+04	1,34E+04	4,67E-01	3,94E+00	1,08E+00	6,42E-05	1,02E+00	2,73E-01	3,75E-05	2,49E-03	1,62E-03	5,37E-05	2,42E-03	1,83E-03	5,37E-05
BHVO-2-8	2,32E+05	1,50E-11	8,17E-01	8,02E+04	1,96E+04	4,86E-01	4,14E+00	9,96E-01	5,69E-05	1,08E+00	2,66E-01	2,66E-05	2,54E-03	1,06E-03	6,18E-05	2,43E-03	1,14E-03	6,18E-05
BHVO-2-9	2,32E+05	2,88E-11	7,48E-01	7,93E+04	9,35E+03	4,50E-01	4,06E+00	4,99E-01	6,55E-05	1,05E+00	1,40E-01	4,52E-05	2,46E-03	1,18E-03	5,63E-05	2,36E-03	1,35E-03	5,63E-05
BHVO-2-10	2,32E+05	0,00E+00	1,29E+00	8,39E+04	7,59E+03	7,52E-01	4,48E+00	4,35E-01	8,04E-05	1,17E+00	1,35E-01	3,73E-05	2,77E-03	1,85E-03	8,79E-05	2,55E-03	2,07E-03	8,79E-05
BHVO-2-11	2,32E+05	2,95E-11	1,20E+00	8,29E+04	6,97E+03	7,26E-01	4,42E+00	3,61E-01	2,12E-05	1,16E+00	9,72E-02	6,49E-05	2,80E-03	1,18E-03	8,85E-05	2,58E-03	1,31E-03	8,85E-05
BHVO-2-12	2,32E+05	0,00E+00	1,26E+00	8,65E+04	7,68E+03	7,28E-01	4,53E+00	3,67E-01	1,23E-04	1,19E+00	1,03E-01	5,29E-05	3,16E-03	1,96E-03	9,49E-05	2,97E-03	2,22E-03	9,49E-05
Reference Values	*2,32E+05*	*6,54E+02*		*8,15E+04*	*4,29E+02*		*4,47E+00*	*2,50E-02*		*1,15E+00*	*1,90E-02*		*2,60E-03*	*0,00E+00*		*2,60E-03*	*0,00E+00*	
Average	*2,32E+05*	*1,95E-11*	*7,94E-01*	*7,38E+04*	*1,14E+04*	*4,73E-01*	*4,04E+00*	*5,96E-01*	*5,12E-05*	*1,04E+00*	*1,55E-01*	*3,92E-05*	*2,48E-03*	*1,19E-03*	*5,47E-05*	*2,38E-03*	*1,34E-03*	*5,47E-05*
Precision (+-15%)	*1,00*			*0,91*			*0,90*			*0,90*			*0,96*			*0,91*		
Accuracy	*0,00*			*0,15*			*0,15*			*0,15*			*0,48*			*0,57*		
BIR-1																		
BIR-1-1	2,24E+05	3,51E-11	5,56E-01	9,98E+04	1,23E+04	4,29E-01	6,74E-01	2,97E-01	4,35E-05	5,46E-02	2,23E-02	5,22E-05	3,42E-03	3,02E-03	3,17E-05	3,99E-03	3,51E-03	3,17E-05
BIR-1-2	2,24E+05	3,45E-11	5,95E-01	1,01E+05	1,14E+04	4,42E-01	6,87E-01	2,58E-01	1,14E-05	5,50E-02	1,40E-02	2,75E-05	3,51E-03	2,47E-03	3,65E-05	4,10E-03	2,88E-03	3,65E-05
BIR-1-3	2,24E+05	3,58E-11	5,44E-01	1,01E+05	1,10E+04	4,66E-01	6,83E-01	2,04E-01	1,17E-05	5,66E-02	1,84E-02	6,30E-06	3,63E-03	1,97E-03	3,71E-05	4,24E-03	2,29E-03	3,71E-05
BIR-1-4	2,24E+05	3,96E-11	7,95E-01	9,17E+04	5,86E+03	5,41E-01	5,71E-01	2,07E-01	1,83E-05	3,79E-02	8,69E-03	3,57E-05	3,10E-03	8,58E-04	6,86E-05	3,63E-03	9,95E-04	6,86E-05
BIR-1-5	2,24E+05	3,22E-11	7,52E-01	9,33E+04	5,73E+03	5,12E-01	5,82E-01	1,96E-01	4,91E-05	4,00E-02	1,19E-02	6,43E-05	3,40E-03	1,50E-03	5,87E-05	3,98E-03	1,74E-03	5,87E-05
BIR-1-6	2,24E+05	3,87E-11	7,64E-01	9,30E+04	8,13E+03	5,10E-01	5,92E-01	2,70E-01	1,27E-05	4,29E-02	2,10E-02	3,92E-05	3,86E-03	4,19E-03	5,61E-05	4,52E-03	4,87E-03	5,61E-05
BIR-1-7	2,24E+05	3,91E-11	1,18E+00	1,09E+05	2,59E+04	7,24E-01	5,97E-01	2,01E-01	1,09E-04	4,17E-02	1,45E-02	6,91E-05	3,47E-03	1,32E-03	8,81E-05	4,03E-03	1,52E-03	8,81E-05
BIR-1-8	2,24E+05	3,31E-11	9,93E-01	1,06E+05	3,33E+04	6,20E-01	6,28E-01	3,02E-01	7,01E-05	4,45E-02	2,17E-02	7,59E-05	3,38E-03	1,64E-03	6,81E-05	3,93E-03	1,90E-03	6,81E-05
BIR-1-9	2,24E+05	3,26E-11	1,06E+00	1,07E+05	2,58E+04	6,02E-01	5,68E-01	1,69E-01	1,57E-05	4,13E-02	1,64E-02	3,70E-05	3,19E-03	1,33E-03	6,50E-05	3,71E-03	1,53E-03	6,50E-05
BIR-1-10	2,24E+05	3,80E-11	1,52E+00	1,06E+05	8,27E+03	8,94E-01	6,27E-01	2,22E-01	1,36E-04	5,16E-02	1,20E-02	1,47E-04	4,46E-03	4,31E-03	1,24E-04	5,13E-03	4,86E-03	1,24E-04
BIR-1-11	2,24E+05	3,11E-11	1,52E+00	1,09E+05	1,00E+04	9,15E-01	6,49E-01	1,86E-01	1,06E-04	5,39E-02	1,33E-02	1,42E-04	3,46E-03	2,00E-03	1,10E-04	4,00E-03	2,26E-03	1,10E-04
BIR-1-12	2,24E+05	3,71E-11	1,52E+00	1,08E+05	1,07E+04	9,10E-01	6,37E-01	2,18E-01	1,07E-04	5,15E-02	1,34E-02	1,44E-04	3,74E-03	2,88E-03	1,10E-04	4,32E-03	3,24E-03	1,10E-04
Reference Values	*2,24E+05*	*8,88E+02*		*9,50E+04*	*4,29E+02*		*5,82E-01*	*8,80E-03*		*4,14E-02*	*2,00E-03*		*2,50E-03*	*4,20E-07*		*2,50E-03*	*4,20E-07*	
Average	*2,24E+05*	*3,56E-11*	*9,84E-01*	*1,02E+05*	*1,40E+04*	*6,30E-01*	*6,25E-01*	*2,28E-01*	*5,76E-05*	*4,76E-02*	*1,56E-02*	*7,00E-05*	*3,55E-03*	*2,29E-03*	*7,12E-05*	*4,13E-03*	*2,63E-03*	*7,12E-05*
Precision (+-15%)	*1,00*			*1,07*			*1,07*			*1,15*			*1,42*			*1,65*		
Accuracy	*0,00*			*0,14*			*0,36*			*0,33*			*0,65*			*0,64*		

Standard PPP-LA-ICP-MS - setting for Au analysis

													Raw Au			Au corrected for Hf and Ta oxides interferences		
	Si29_mean	Si29_2SD	Si29_LOD	Ca44_mean	Ca44_2SD	Ca44_LOD	Hf180_mean	Hf180_2SD	Hf180_LOD	Ta181_mean	Ta181_2SD	Ta181_LOD	Au197_mean	Au197_2SD	Au197_LOD	Au2_mean	Au2_2SD	Au2_LOD
	(ppm)	(ppm)	(ppm)	(ppm)	(ppm)	(ppm)	(ppm)	(ppm)	(ppm)	(ppm)	(ppm)	(ppm)	(ppm)	(ppm)	(ppm)	(ppm)	(ppm)	(ppm)
MRG-1																		
MRG-1-2	1,83E+05	2,81E-11	7,13E-01	1,16E+05	7,36E+03	5,20E-01	4,56E+00	4,69E-01	3,10E-05	9,32E-01	3,34E-01	5,61E-05	5,28E-03	1,58E-03	4,48E-05	5,74E-03	1,78E-03	4,48E-05
MRG-1-3	1,83E+05	3,30E-11	7,21E-01	1,16E+05	1,50E+04	5,00E-01	4,46E+00	6,50E-01	3,04E-05	8,88E-01	2,35E-01	3,10E-05	4,87E-03	1,54E-03	4,16E-05	5,29E-03	1,79E-03	4,16E-05
MRG-1-4	1,83E+05	2,28E-11	7,15E-01	1,16E+05	4,80E+03	5,84E-01	4,34E+00	2,72E-01	6,52E-05	9,18E-01	3,69E-01	5,72E-05	5,38E-03	2,41E-03	6,13E-05	5,83E-03	2,82E-03	6,13E-05
MRG-1-5	1,83E+05	2,73E-11	7,91E-01	1,15E+05	7,54E+03	5,85E-01	4,49E+00	8,44E-01	2,41E-05	8,49E-01	1,66E-01	9,73E-06	5,37E-03	1,56E-03	6,37E-05	5,84E-03	1,81E-03	6,37E-05
MRG-1-6	1,83E+05	2,71E-11	6,96E-01	1,14E+05	8,29E+03	4,88E-01	4,33E+00	6,96E-01	1,21E-05	8,51E-01	2,20E-01	5,44E-05	5,39E-03	2,22E-03	5,76E-05	5,84E-03	2,53E-03	5,76E-05
MRG-1-7	1,83E+05	2,71E-11	8,94E-01	9,82E+04	7,18E+03	5,74E-01	4,24E+00	6,99E-01	1,51E-05	8,69E-01	4,00E-01	6,06E-05	5,01E-03	2,66E-03	5,93E-05	5,38E-03	3,02E-03	5,93E-05
MRG-1-8	1,83E+05	2,82E-11	8,59E-01	9,86E+04	1,13E+04	5,92E-01	4,22E+00	6,26E-01	6,28E-05	8,61E-01	3,34E-01	4,11E-05	5,84E-03	4,60E-03	7,46E-05	6,35E-03	5,30E-03	7,46E-05
MRG-1-9	1,83E+05	1,56E-11	1,25E+00	9,58E+04	1,09E+04	7,68E-01	4,22E+00	7,48E-01	1,58E-04	9,55E-01	4,90E-01	8,30E-05	5,89E-03	2,36E-03	8,54E-05	6,38E-03	2,65E-03	8,54E-05
MRG-1-10	1,83E+05	3,58E-11	1,79E+00	9,60E+04	1,65E+04	8,85E-01	3,42E+00	5,85E-01	1,33E-04	6,42E-01	9,78E-02	1,01E-04	5,85E-03	2,40E-03	1,30E-04	6,32E-03	2,75E-03	1,30E-04
MRG-1-11	1,83E+05	4,04E-11	1,53E+00	1,01E+05	2,70E+04	8,56E-01	3,57E+00	8,72E-01	2,41E-05	7,09E-01	2,54E-01	6,32E-05	5,19E-03	2,81E-03	1,18E-04	5,53E-03	3,13E-03	1,18E-04
MRG-1-12	1,83E+05	4,04E-11	1,68E+00	9,94E+04	2,39E+04	8,96E-01	3,53E+00	9,42E-01	1,17E-04	6,96E-01	2,14E-01	1,07E-04	5,53E-03	3,54E-03	1,20E-04	5,92E-03	4,00E-03	1,20E-04
Reference Values	*1,83E+05*	*0,00E+00*		*1,05E+05*	*0,00E+00*		*3,76E+00*	*0,00E+00*		*8,00E-01*	*0,00E+00*		*5,40E-03*	*0,00E+00*		*5,40E-03*	*0,00E+00*	
Average	*1,83E+05*	*2,96E-11*	*1,06E+00*	*1,06E+05*	*1,27E+04*	*6,59E-01*	*4,12E+00*	*6,73E-01*	*6,12E-05*	*8,34E-01*	*2,83E-01*	*6,04E-05*	*5,42E-03*	*2,52E-03*	*7,79E-05*	*5,86E-03*	*2,87E-03*	*7,79E-05*
Precision	*1,00*			*1,01*			*1,10*			*1,04*			*1,00*			*1,08*		
Accuracy	*0,00*			*0,12*			*0,16*			*0,34*			*0,46*			*0,49*		
TDB-1																		
TDB-1-top-1	2,34E+05	3,76E-11	5,90E-01	5,20E+04	4,86E+03	3,59E-01	3,52E+00	1,08E+00	6,87E-05	5,70E-01	8,99E-02	2,72E-05	3,92E-03	2,09E-03	3,14E-05	4,31E-03	2,40E-03	3,14E-05
TDB-1-top-2	2,34E+05	3,01E-11	5,56E-01	5,15E+04	4,19E+03	3,26E-01	3,80E+00	1,73E+00	4,52E-05	5,82E-01	8,70E-02	2,54E-05	4,47E-03	4,58E-03	3,22E-05	4,94E-03	5,33E-03	3,22E-05
TDB-1-top-3	2,34E+05	3,25E-11	6,08E-01	6,62E+04	9,61E+03	3,54E-01	3,80E+00	9,36E-01	3,43E-05	6,07E-01	8,15E-02	2,85E-05	4,86E-03	3,27E-03	4,23E-05	5,36E-03	3,78E-03	4,23E-05
TDB-1-top-4	2,34E+05	2,93E-11	6,32E-01	6,38E+04	1,61E+04	3,60E-01	3,65E+00	8,65E-01	9,60E-06	6,12E-01	7,47E-02	3,90E-05	4,55E-03	1,73E-03	4,17E-05	5,00E-03	2,01E-03	4,17E-05
TDB-1-top-5	2,34E+05	2,97E-11	8,62E-01	6,33E+04	1,99E+04	4,93E-01	4,36E+00	1,80E+00	1,76E-05	6,72E-01	2,20E-01	2,25E-05	6,64E-03	5,53E-03	6,09E-05	7,35E-03	6,37E-03	6,09E-05
TDB-1-top-6	2,34E+05	3,13E-11	7,67E-01	6,17E+04	1,13E+04	4,66E-01	3,86E+00	1,31E+00	8,28E-05	6,34E-01	1,51E-01	2,56E-05	6,33E-03	1,57E-02	5,78E-05	7,00E-03	1,82E-02	5,78E-05
TDB-1-top-8	2,34E+05	2,26E-11	1,35E+00	6,87E+04	7,45E+03	7,18E-01	4,48E+00	1,02E+00	8,72E-05	7,36E-01	8,81E-02	8,97E-05	6,03E-03	2,49E-03	1,07E-04	6,44E-03	2,79E-03	1,07E-04
TDB-1-top-7	2,34E+05	3,41E-11	1,18E+00	7,22E+04	9,60E+03	6,66E-01	4,50E+00	1,29E+00	1,94E-05	7,56E-01	8,29E-02	5,46E-05	5,43E-03	3,06E-03	7,66E-05	5,75E-03	3,46E-03	7,66E-05
Reference Values	*2,34E+05*	*0,00E+00*		*5,55E+04*	*0,00E+00*		*4,50E+00*	*0,00E+00*		*7,20E-01*	*0,00E+00*		*6,30E-03*	*1,00E-07*		*6,30E-03*	*1,00E-07*	
Average	*2,34E+05*	*3,09E-11*	*8,18E-01*	*6,24E+04*	*1,04E+04*	*4,68E-01*	*4,00E+00*	*1,25E+00*	*4,56E-05*	*6,46E-01*	*1,09E-01*	*3,91E-05*	*5,28E-03*	*4,80E-03*	*5,63E-05*	*5,77E-03*	*5,54E-03*	*5,63E-05*
Precision (+-15%)	*1,00*			*1,13*			*0,89*			*0,90*			*0,84*			*0,92*		
Accuracy	*0,00*			*0,17*			*0,31*			*0,17*			*0,91*			*0,96*		
TSD-41																		
TSD-41-1	2,60E+05	4,03E-11	6,12E-01	1,05E+05	1,09E+04	4,76E-01	1,29E+00	2,51E-01	3,75E-05	8,26E-02	1,98E-02	1,68E-05	2,67E-04	4,20E-04	1,49E-05	3,05E-04	4,83E-04	1,49E-05
TSD-41-2	2,60E+05	3,30E-11	5,88E-01	1,04E+05	1,05E+04	4,81E-01	1,27E+00	3,15E-01	1,03E-05	8,53E-02	3,55E-02	2,41E-05	2,29E-04	4,06E-04	1,24E-05	2,66E-04	4,74E-04	1,24E-05
TSD-41-3	2,60E+05	3,98E-11	5,49E-01	1,03E+05	1,11E+04	3,75E-01	1,26E+00	2,69E-01	3,72E-05	7,72E-02	1,96E-02	2,28E-05	2,43E-04	4,22E-04	1,45E-05	2,75E-04	4,81E-04	1,45E-05
TSD-41-4	2,60E+05	3,42E-11	8,32E-01	1,04E+05	6,87E+03	4,97E-01	1,28E+00	2,53E-01	5,02E-05	7,16E-02	1,47E-02	5,42E-05	1,69E-04	2,41E-04	3,02E-05	1,96E-04	2,81E-04	3,02E-05
TSD-41-5	2,60E+05	3,55E-11	7,28E-01	1,02E+05	7,65E+03	4,69E-01	1,26E+00	2,42E-01	4,55E-05	7,37E-02	1,88E-02	5,13E-05	1,70E-04	4,04E-04	2,85E-05	1,96E-04	4,62E-04	2,85E-05
TSD-41-6	2,60E+05	4,40E-11	7,38E-01	1,02E+05	8,77E+03	4,71E-01	1,32E+00	3,81E-01	1,24E-05	7,19E-02	2,32E-02	3,04E-05	2,28E-04	3,71E-04	3,09E-05	2,66E-04	4,28E-04	3,09E-05
TSD-41-7	2,60E+05	3,30E-11	9,57E-01	9,47E+04	1,27E+04	5,68E-01	1,30E+00	4,08E-01	1,58E-05	7,83E-02	2,92E-02	3,20E-05	2,47E-04	4,34E-04	3,79E-05	2,84E-04	4,99E-04	3,79E-05
TSD-41-8	2,60E+05	3,91E-11	1,03E+00	9,92E+04	3,50E+04	5,93E-01	1,34E+00	5,28E-01	6,83E-05	8,03E-02	4,17E-02	5,97E-05	2,51E-04	6,44E-04	4,09E-05	2,91E-04	7,45E-04	4,09E-05
TSD-41-9	2,60E+05	3,87E-11	9,38E-01	9,31E+04	1,29E+04	5,60E-01	1,35E+00	4,52E-01	1,53E-05	8,07E-02	4,19E-02	4,68E-05	3,23E-04	4,74E-04	4,10E-05	3,64E-04	5,51E-04	4,10E-05
TSD-41-10	2,60E+05	3,88E-11	1,38E+00	1,38E+05	1,08E+04	8,46E-01	1,47E+00	5,35E-01	1,29E-04	8,42E-02	1,75E-02	1,03E-04	2,73E-04	6,70E-04	4,06E-05	3,65E-04	7,60E-04	4,06E-05
TSD-41-11	2,60E+05	4,18E-11	1,37E+00	1,38E+05	1,09E+04	8,65E-01	1,42E+00	1,77E-01	1,02E-04	9,29E-02	2,58E-02	8,34E-05	4,51E-04	6,75E-04	5,11E-05	5,64E-04	7,70E-04	5,11E-05
TSD-41-12	2,60E+05	4,32E-11	1,31E+00	1,38E+05	1,40E+04	8,62E-01	1,48E+00	2,78E-01	2,38E-05	9,90E-02	4,32E-02	9,35E-05	5,68E-04	8,17E-04	6,60E-05	6,93E-04	9,28E-04	6,60E-05
Reference Values	*2,60E+05*	*0,00E+00*		*1,15E+05*	*0,00E+00*		*1,10E+00*	*0,00E+00*		*5,50E-02*	*0,00E+00*		*1,70E-04*	*0,00E+00*		*1,70E-04*	*0,00E+00*	
Average	*2,60E+05*	*3,85E-11*	*9,20E-01*	*1,10E+05*	*1,27E+04*	*5,89E-01*	*1,34E+00*	*3,41E-01*	*4,55E-05*	*8,15E-02*	*2,76E-02*	*5,15E-05*	*2,85E-04*	*4,98E-04*	*3,41E-05*	*3,39E-04*	*5,72E-04*	*3,41E-05*
Precision (+-15%)	*1,00*			*0,96*			*1,21*			*1,48*			*1,68*			*1,99*		
Accuracy	*0,00*			*0,12*			*0,25*			*0,34*			*1,75*			*1,69*		

Standard Hg for atomic absorption spectroscopy

certification	Hg(ppm)	Standard deviation	min	max
TCEGir (in-house)	140	8,6	131,4	148,6
BCR277R	128	17	111	145

TCEGir measured (n=8)	183,1	2,2
yield	131%	
BCR277R measured (n=4)	157,0	1,7
yield	123%	
average correction	127%	

sample	Hg(ppm)*	Hg(ppm)**
NA007-002c	31,2	26,5
NA007-052c	26,4	22,4
NA007-062c	27,9	23,7
NA007-079	30,1	25,6
NA007-80c1	28,1	23,9
NA007-80c2	28,7	24,4
NA007-80c3	27,3	23,2
NA007-92c	31,0	26,3
NA007-96c	27,9	23,7
NA007-100b2	27,1	23,0
NA007-100b1	28,1	23,9
NA007-100c1	29,4	25,0

*raw data

**corrected data (-15%)

Standards XRF on glass beads

Standard	Na2O (wt%)	MgO (wt%)	Al2O3 (wt%)	SiO2 (wt%)	P2O5 (wt%)	K2O (wt%)	CaO (wt%)	TiO2 (wt%)	MnO (wt%)	Fe2O3 (wt%)	SUM (wt%)
BHVO-1	2,225	7,167	13,551	49,345	0,268	0,531	11,267	2,728	0,171	12,034	99,287
BHVO-1	2,239	7,127	13,502	49,3	0,273	0,53	11,258	2,727	0,17	12,042	99,168
BHVO-1	2,239	7,135	13,503	49,199	0,271	0,531	11,235	2,729	0,171	12,051	99,064
MRG-1	0,78	13,236	8,381	38,41	0,069	0,196	14,634	3,739	0,174	18,088	97,707
MRG-1	0,783	13,218	8,366	38,253	0,071	0,196	14,613	3,748	0,174	18,104	97,526
MRG-1	0,784	13,208	8,376	38,351	0,068	0,196	14,573	3,753	0,174	18,119	97,602
RGM-1	4,005	0,302	13,547	72,486	0,047	4,275	1,22	0,27	0,036	1,905	98,093
RGM-1	3,992	0,305	13,536	72,327	0,044	4,276	1,224	0,269	0,036	1,904	97,913
RGM-1	3,968	0,302	13,475	72,242	0,046	4,255	1,208	0,269	0,036	1,908	97,709
SY-2	4,266	2,67	12,074	60,074	0,436	4,499	8,021	0,145	0,317	6,519	99,021
SY-2	4,255	2,673	12,068	60,241	0,435	4,502	8,019	0,146	0,316	6,511	99,166
SY-2	4,245	2,657	12,068	59,923	0,436	4,492	7,969	0,145	0,317	6,527	98,779

Mean value (n=3)	Na2O (wt%)	MgO (wt%)	Al2O3 (wt%)	SiO2 (wt%)	P2O5 (wt%)	K2O (wt%)	CaO (wt%)	TiO2 (wt%)	MnO (wt%)	Fe2O3 (wt%)	LOI (wt%)	SUM (wt%)	factor
BHVO-1	2,23	7,14	13,52	49,28	0,27	0,53	11,25	2,73	0,17	12,04	0,304	99,17	0,99696
MRG-1	0,78	13,22	8,37	38,34	0,07	0,20	14,61	3,75	0,17	18,10	1,56	97,61	0,9844
RGM-1	3,99	0,30	13,52	72,35	0,05	4,27	1,22	0,27	0,04	1,91	0,8	97,91	0,992
SY-2	4,26	2,67	12,07	60,08	0,44	4,50	8,00	0,15	0,32	6,52	1,08	98,99	0,9892

Mean value corrected for LOI	Na2O (wt%)	MgO (wt%)	Al2O3 (wt%)	SiO2 (wt%)	P2O5 (wt%)	K2O (wt%)	CaO (wt%)	TiO2 (wt%)	MnO (wt%)	Fe2O3 (wt%)	LOI (wt%)	SUM (wt%)
BHVO-1	2,23	7,12	13,48	49,13	0,27	0,53	11,22	2,72	0,17	12,01	0,304	99,18
MRG-1	0,77	13,01	8,24	37,74	0,07	0,19	14,38	3,69	0,17	17,82	1,56	97,65
RGM-1	3,96	0,30	13,41	71,77	0,05	4,23	1,21	0,27	0,04	1,89	0,8	97,92
SY-2	4,21	2,64	11,94	59,43	0,43	4,45	7,92	0,14	0,31	6,45	1,08	99,00

Certified value	Na2O (wt%)	MgO (wt%)	Al2O3 (wt%)	SiO2 (wt%)	P2O5 (wt%)	K2O (wt%)	CaO (wt%)	TiO2 (wt%)	MnO (wt%)	Fe2O3 (wt%)	LOI (wt%)	SUM (wt%)
BHVO-1*	2,313	7,213	13,69	49,79	0,2773	0,5256	11,43	2,742	0,1689	12,32	0,304	100,7738
MRG-1**	0,74	13,55	8,47	39,12	0,08	0,18	14,7	3,77	0,17	17,94	1,56	100,28
RGM-1*	4,086	0,284	13,83	73,12	0,0491	4,293	1,178	0,2654	0,0387	1,871	0,8	99,8152
SY-2**	4,31	2,69	12,04	60,11	0,43	4,45	7,96	0,15	0,32	6,31	1,08	99,85

*Prefered values : Jochum K.P., Weis U., Schwager B., Stoll B., Wilson S.A., Haug G.H., Andreae M.O, Enzweiler J.;
| Geostandards and Geoanalytical Research 40 (3) | [2016] 333-350 Title: Reference values following ISO guidelines for frequently requested rock reference materials doi: 10.1111/j.1751-908X.2015.00392.x
**Govindaraju K.; | Geostandards Newsletter 18 | [1994] 1-158 Title: 1994 compilation of working values and sample description for 383 geostandards doi: 10.1046/j.1365-2494.1998.53202081.x-i1

Test value (+-5wt%)	Na2O (wt%)	MgO (wt%)	Al2O3 (wt%)	SiO2 (wt%)	P2O5 (wt%)	K2O (wt%)	CaO (wt%)	TiO2 (wt%)	MnO (wt%)	Fe2O3 (wt%)
BHVO-1	0,96	0,99	0,98	0,99	0,97	1,01	0,98	0,99	1,01	0,97
MRG-1	1,04	0,96	0,97	0,96	0,85	1,07	0,98	0,98	1,01	0,99
RGM-1	0,97	1,06	0,97	0,98	0,92	0,99	1,03	1,01	0,92	1,01
SY-2	0,98	0,98	0,99	0,99	1,00	1,00	0,99	0,96	0,98	1,02

magnetite microprobe data

Sample	analysis	No,	Al2O3	SiO2	CaO	FeO	MgO	TiO2	NiO	Cr2O3	ZnO	MnO	Total
NA007-079c	079cA-1	1	1,46	0,10	0,04	79,71	0,41	13,21	< Det. Lim	0,01	0,24	1,38	96,55
NA007-079c	079cA-2	2	1,39	0,10	0,05	79,12	0,45	13,05	< Det. Lim	0,02	0,21	1,46	95,85
NA007-079c	079cA-3	3	1,41	0,15	0,02	79,73	0,49	12,65	0,01	0,02	0,19	1,47	96,13
NA007-079c	079cA-4	4	2,66	0,51	0,10	83,83	0,63	3,92	< Det. Lim	0,03	0,12	0,86	92,65
NA007-079c	079cA-5	5	1,67	0,32	0,04	87,50	0,52	1,91	< Det. Lim	0,01	0,11	0,82	92,90
NA007-079c	079cA-6	6	1,44	0,11	0,02	79,35	0,27	12,91	0,00	0,01	0,16	1,37	95,64
NA007-079c	079cA-7	7	1,42	0,14	0,01	79,78	0,37	13,05	0,01	0,04	0,22	1,51	96,55
NA007-100c (matrix)	100cA-matrix-1	8	1,32	0,14	0,04	83,55	0,77	7,28	0,01	0,01	0,23	1,69	95,04
NA007-100c (matrix)	100cA-matrix-2	9	1,44	0,13	0,02	83,60	0,72	7,10	< Det. Lim	0,01	0,15	1,71	94,89
NA007-100c (matrix)	100cA-matrix-3	10	1,42	0,13	0,05	84,73	0,68	5,87	< Det. Lim	0,00	0,19	1,58	94,65
NA007-100c (matrix)	100cA-matrix-4	11	1,59	0,66	0,14	86,01	0,71	3,10	< Det. Lim	0,02	0,11	1,31	93,65
NA007-100c (matrix)	100cA-matrix-5	12	2,51	5,33	0,11	82,34	0,51	1,95	< Det. Lim	< Det. Lim	0,08	1,12	93,95
NA007-100c (matrix)	100cA-matrix-6	13	1,58	0,24	0,05	86,82	0,74	2,28	< Det. Lim	0,00	0,12	1,40	93,24
NA007-100c (matrix)	100cA-matrix-7	14	1,41	0,20	0,06	83,11	0,75	5,42	< Det. Lim	0,02	0,14	1,66	92,76
NA007-100c (matrix)	100cA-matrix-8	15	1,28	0,15	0,04	82,72	0,89	7,06	0,03	< Det. Lim	0,24	2,16	94,56
NA007-100c (matrix)	100cA-matrix-9	16	1,17	0,14	0,02	83,62	0,85	6,35	< Det. Lim	< Det. Lim	0,22	2,10	94,48
NA007-100c (matrix)	100cA-matrix-10	17	1,43	0,23	0,04	87,15	0,65	2,86	< Det. Lim	< Det. Lim	0,15	1,29	93,79
NA007-100c (enclave)	100cA-enclave-1	18	9,89	76,78	0,58	0,90	0,05	0,15	< Det. Lim	< Det. Lim	0,03	0,07	88,45
NA007-100c (enclave)	100cA-enclave-2	19	2,38	3,42	0,91	80,03	1,68	5,13	< Det. Lim	0,03	0,09	1,03	94,69
NA007-100c (enclave)	100cA-enclave-3	20	4,04	5,08	0,65	76,92	0,94	5,97	< Det. Lim	0,03	0,11	1,09	94,83
NA007-100c (enclave)	100cA-enclave-4	21	1,92	4,31	0,18	78,73	1,01	6,63	0,04	0,03	0,15	1,46	94,46
NA007-100c (enclave)	100cA-enclave-5	22	1,47	0,76	0,22	82,39	1,01	6,06	0,01	0,04	0,11	1,28	93,35
NA007-100c (enclave)	100cA-enclave-6	23	1,31	0,48	0,19	82,06	1,04	6,47	< Det. Lim	0,04	0,10	1,32	93,01
NA007-100c (enclave)	100cA-enclave-7	24	1,45	0,16	0,08	81,70	1,09	8,23	< Det. Lim	0,04	0,09	1,06	93,89
NA007-100c (enclave)	100cA-enclave-8	25	1,24	0,31	0,15	81,61	1,08	8,28	< Det. Lim	0,01	0,11	1,15	93,94
NA007-100c (enclave)	100cA-enclave-9	26	1,44	0,13	0,10	79,91	1,12	9,43	< Det. Lim	0,02	0,18	1,65	93,99
NA007-100c (enclave)	100cA-enclave-10	27	1,46	0,18	0,10	84,03	0,83	5,93	0,01	0,02	0,13	1,66	94,35
NA007-100c (enclave)	100cA-enclave-11	28	1,30	0,19	0,08	82,51	1,01	7,84	0,01	0,03	0,16	1,41	94,52
NA007-100c (enclave)	100cA-enclave-12	29	1,01	0,17	0,14	83,09	0,82	6,53	0,00	0,04	0,20	1,51	93,52
NA007-100c (enclave)	100cA-enclave-13	30	1,60	0,20	0,21	82,87	0,94	6,82	0,01	0,02	0,11	1,23	94,01
NA007-100c (enclave)	100cA-enclave-14	31	1,29	0,19	0,14	82,47	0,95	7,20	0,02	0,00	0,18	1,33	93,78
NA007-002c	002cA-1	32	1,91	0,07	0,06	79,19	1,43	12,54	< Det. Lim	0,05	0,10	0,68	96,02
NA007-002c	002cA-2	33	1,94	0,08	0,07	79,27	1,39	12,37	< Det. Lim	0,06	0,08	0,65	95,91
NA007-002c	002cA-3	34	1,96	0,05	0,04	79,01	1,37	12,78	< Det. Lim	0,04	0,11	0,67	96,03
NA007-002c	002cA-4	35	1,91	0,07	0,04	79,19	1,46	12,47	0,02	0,02	0,12	0,66	95,94
NA007-002c	002cA-5	36	1,88	0,10	0,09	78,72	1,44	12,56	< Det. Lim	0,05	0,05	0,68	95,57
NA007-002c	002cA-6	37	1,90	0,09	0,12	79,08	1,45	12,85	< Det. Lim	0,02	0,13	0,65	96,29
NA007-002c	002cA-7	38	1,93	0,08	0,03	78,59	1,38	12,80	0,01	0,04	0,11	0,67	95,65
NA007-002c	002cA-8	39	1,91	0,06	0,02	79,05	1,30	12,97	< Det. Lim	0,04	0,08	0,64	96,06
NA007-002c	002cA-9	40	1,91	0,07	0,00	77,87	1,43	12,91	0,01	0,02	0,10	0,65	94,98
NA007-002c	002cA-10	41	1,82	0,09	0,07	77,71	1,50	12,63	< Det. Lim	0,05	0,03	0,67	94,60
NA007-002c	002cA-11	42	1,81	0,09	0,09	77,42	1,43	12,54	< Det. Lim	0,03	0,10	0,65	94,17

Sample	analysis	No,	Al2O3	SiO2	CaO	FeO	MgO	TiO2	NiO	Cr2O3	ZnO	MnO	Total
NA007-002c	002cA-12	43	1,88	0,06	0,04	78,84	1,44	12,67	0,03	0,04	0,10	0,66	95,76
NA007-002c	002cA-13	44	1,82	0,08	0,03	78,74	1,46	12,82	< Det. Lim	0,02	0,13	0,65	95,75
NA007-002c	002cA-14	45	2,04	0,10	0,09	78,50	1,41	12,39	0,00	0,02	0,03	0,64	95,22
NA007-080c2	080c2b-1	46	4,39	0,09	0,02	77,20	3,49	9,72	0,11	1,23	0,01	0,40	96,66
NA007-080c2	080c2b-2	47	4,63	0,07	0,00	75,46	3,56	9,14	0,08	3,13	0,05	0,42	96,54
NA007-080c2	080c2b-3	48	4,37	0,07	0,02	76,80	3,51	9,61	0,06	1,29	0,11	0,41	96,26
NA007-080c2	080c2b-4	49	3,85	0,08	0,04	77,35	3,06	10,78	0,07	0,13	0,08	0,43	95,87
NA007-080c2	080c2b-5	50	1,11	0,13	0,10	76,99	0,16	13,45	0,03	0,12	0,17	0,28	92,53
NA007-080c2	080c2b-6	51	1,72	0,15	0,15	74,75	0,89	13,16	< Det. Lim	0,11	0,17	0,43	91,53
NA007-080c2	080c2b-7	52	4,31	0,07	0,31	77,37	3,26	9,54	< Det. Lim	0,09	0,10	0,46	95,51
NA007-080c2	080c2b-8	53	4,04	0,07	0,06	77,69	3,08	10,00	0,05	0,13	0,02	0,41	95,56
NA007-080c2	080c2b-9	54	4,14	0,08	0,02	78,32	3,12	9,98	0,02	0,10	0,08	0,41	96,27
NA007-080c2	080c2b-10	55	3,96	0,09	0,02	78,32	3,04	10,09	0,02	0,11	0,07	0,44	96,15
NA007-062c	062cA-1	56	1,56	0,11	0,07	79,90	0,40	12,06	< Det. Lim	0,01	0,20	1,36	95,65
NA007-062c	062cA-2	57	1,53	0,10	0,07	79,94	0,34	12,21	0,01	< Det. Lim	0,14	1,48	95,82
NA007-062c	062cA-3	58	1,48	0,14	0,04	80,02	0,39	11,44	0,02	0,03	0,13	1,43	95,11
NA007-062c	062cA-4	59	1,52	0,15	0,03	80,24	0,42	11,33	< Det. Lim	< Det. Lim	0,18	1,46	95,33
NA007-062c	062cA-5	60	1,56	0,14	0,03	79,50	0,39	11,66	0,01	0,01	0,21	1,52	95,03
NA007-062c	062cA-6	61	1,55	0,49	0,06	78,22	0,41	12,67	0,01	0,02	0,21	1,41	95,03
NA007-062c	062cA-7	62	0,00	36,85	0,01	1,27	0,01	0,08	0,04	0,01	0,06	0,03	38,35
NA007-062c	062cA-8	63	1,47	0,10	0,06	79,88	0,38	12,14	< Det. Lim	0,00	0,11	1,38	95,51
NA007-062c	062cA-9	64	1,41	0,14	0,05	80,11	0,48	12,05	< Det. Lim	0,02	0,18	1,45	95,88
NA007-062c	062cA-10	65	1,47	0,14	0,03	80,24	0,39	12,63	< Det. Lim	< Det. Lim	0,23	1,32	96,44
NA007-062c	062cA-11	66	1,48	0,09	0,04	79,96	0,35	12,54	< Det. Lim	< Det. Lim	0,21	1,34	96,01
NA007-062c	062cA-12	67	1,52	0,10	0,03	80,11	0,38	12,50	< Det. Lim	0,00	0,13	1,33	96,09
NA007-092c	092cA-1	68	3,86	0,10	0,03	80,11	2,09	10,23	< Det. Lim	0,05	0,10	0,57	97,14
NA007-092c	092cA-2	69	3,88	0,13	0,04	80,04	2,07	10,07	< Det. Lim	0,04	0,05	0,57	96,89
NA007-092c	092cA-3	70	2,28	16,02	3,69	56,87	9,30	11,07	< Det. Lim	0,03	0,11	0,73	100,11
NA007-092c	092cA-4	71	4,59	0,10	0,02	78,84	3,02	8,89	< Det. Lim	0,06	0,07	0,47	96,06
NA007-092c	092cA-5	72	4,34	0,10	0,03	78,97	2,91	8,95	0,02	0,04	0,10	0,47	95,93
NA007-092c	092cA-6	73	4,35	0,11	0,07	78,09	2,69	10,22	< Det. Lim	0,05	0,02	0,50	96,10
NA007-092c	092cA-7	74	4,35	0,10	0,06	78,42	2,64	10,12	< Det. Lim	0,04	0,04	0,49	96,25
NA007-092c	092cA-8	75	4,49	0,08	0,03	78,45	2,51	9,64	< Det. Lim	0,07	0,00	0,51	95,78
NA007-092c	092cA-9	76	4,33	0,10	0,04	78,99	2,23	10,01	0,02	0,06	0,10	0,50	96,39
NA007-092c	092cA-10	77	3,02	0,33	0,09	74,76	2,00	12,94	0,01	0,05	0,18	0,58	93,95

Standard data			
Element	Standard	name	Mass(%)
Al2O3	anorthosite	H081_anor81	36,46
SiO2	orthose	H053_orth53	64,20
CaO	anorthosite	H081_anor81	19,57
FeO	magnetite	B46_magt46	93,09
MgO	forsterite	H15_fors15	57,30
TiO2	rutile	B11_ruti11	99,99
NiO	nickel	A16_ni16	127,25
Cr2O3	spinel	B29_spin29	42,98
ZnO	sphalerite	C19_zns19	83,51
MnO	pyrolusite	B07_pyro7	76,96

	Det. Lim.
Al (ppm)	79
Si (ppm)	104
Ca (ppm)	85
Fe (ppm)	193
Mg (ppm)	71
Ti (ppm)	120
Ni (ppm)	191
Cr (ppm)	119
Zn (ppm)	326
Mn (ppm)	125

LA-ICP-MS on magnetite

< Det. Lim = inferior to detection limit; n.d. = not determined

Sample	Analysis	Li7_mean	Li7_2SD	Li7_LOD	Be9_mean	Be9_2SD	Be9_LOD	Na23_mean	Na23_2SD	Na23_LOD	Mg25_mean	Mg25_2SD	Mg25_LOD	Al27_mean
		(ppm)	(ppm)	(ppm)	(ppm)	(ppm)	(ppm)	(ppm)	(ppm)	(ppm)	(ppm)	(ppm)	(ppm)	(ppm)
NA007-002c	002c_A_1	1,67E+00	9,32E-01	1,30E-01	6,92E-02	8,97E-02	1,45E-01	n.d.	n.d.	n.d.	8,68E+03	3,40E+03	5,39E+00	1,36E+04
NA007-002c	002c_A_10	1,27E+00	4,17E-01	1,03E-01	5,13E-02	8,03E-02	1,23E-01	n.d.	n.d.	n.d.	7,83E+03	1,61E+03	4,33E+00	1,11E+04
NA007-002c	002c_A_11	1,62E+00	8,17E-01	1,05E-01	6,28E-02	8,74E-02	3,42E-02	n.d.	n.d.	n.d.	8,61E+03	2,80E+03	4,26E+00	1,10E+04
NA007-002c	002c_A_12	1,34E+00	2,04E-01	1,14E-01	7,01E-02	1,55E-01	9,57E-02	n.d.	n.d.	n.d.	8,29E+03	1,01E+03	4,84E+00	1,15E+04
NA007-002c	002c_A_13	1,19E+00	5,64E-01	1,11E-01	3,18E-02	4,32E-02	2,47E-01	n.d.	n.d.	n.d.	8,05E+03	2,36E+03	4,40E+00	1,10E+04
NA007-002c	002c_A_14	1,36E+00	7,05E-01	1,20E-01	2,93E-02	2,76E-02	8,21E-02	n.d.	n.d.	n.d.	8,09E+03	2,68E+03	4,79E+00	1,06E+04
NA007-002c	002c_A_2	1,27E+00	4,54E-01	1,01E-01	3,69E-02	5,51E-02	2,71E-01	n.d.	n.d.	n.d.	7,91E+03	1,45E+03	3,81E+00	1,15E+04
NA007-002c	002c_A_3	1,40E+00	9,14E-01	1,18E-01	4,25E-02	5,53E-02	6,33E-02	n.d.	n.d.	n.d.	7,83E+03	1,72E+03	4,20E+00	1,11E+04
NA007-002c	002c_A_4	1,40E+00	1,79E-01	1,06E-01	3,86E-02	4,91E-02	2,81E-01	n.d.	n.d.	n.d.	7,83E+03	1,39E+03	4,31E+00	1,12E+04
NA007-002c	002c_A_5	1,21E+00	5,24E-01	1,13E-01	6,21E-02	1,64E-01	3,64E-02	n.d.	n.d.	n.d.	8,02E+03	1,35E+03	4,36E+00	1,13E+04
NA007-002c	002c_A_6	1,28E+00	4,77E-01	9,17E-02	4,40E-02	7,00E-02	1,07E-01	n.d.	n.d.	n.d.	7,87E+03	1,84E+03	3,88E+00	1,11E+04
NA007-002c	002c_A_7	1,20E+00	4,79E-01	9,32E-02	5,83E-02	8,45E-02	7,26E-02	n.d.	n.d.	n.d.	7,93E+03	1,06E+03	3,71E+00	1,12E+04
NA007-002c	002c_A_8	1,30E+00	5,62E-01	9,79E-02	3,47E-02	5,29E-02	2,09E-01	n.d.	n.d.	n.d.	7,89E+03	1,37E+03	3,89E+00	1,13E+04
NA007-002c	002c_A_9	1,16E+00	6,87E-01	9,90E-02	3,93E-02	6,66E-02	4,30E-02	n.d.	n.d.	n.d.	7,85E+03	1,77E+03	4,03E+00	1,09E+04
NA007-062c	062C_A_1	1,19E+00	8,33E-01	1,51E-01	8,06E-02	1,42E-01	3,53E-02	5,83E+02	6,79E+02	1,85E+00	1,96E+04	3,62E+03	3,64E+00	3,18E+04
NA007-062c	062C_A_10	1,71E+00	6,02E-01	1,23E-01	9,28E-02	1,18E-01	2,97E-02	4,25E+02	2,61E+03	1,62E+00	1,48E+04	1,95E+03	3,22E+00	2,42E+04
NA007-062c	062C_A_11	1,62E+00	4,14E-01	1,61E-01	1,14E-01	1,06E-01	5,32E-02	9,04E+02	1,54E+03	2,37E+00	1,85E+04	3,15E+03	4,16E+00	2,85E+04
NA007-062c	062C_A_12	1,49E+00	5,73E-01	1,20E-01	1,33E-01	1,21E-01	8,50E-02	3,14E+02	6,40E+02	1,58E+00	1,78E+04	4,34E+03	3,53E+00	2,72E+04
NA007-062c	062C_A_13	2,64E+00	1,88E+00	1,38E-01	5,05E-01	6,03E-01	5,77E-02	2,42E+03	2,68E+03	2,11E+00	2,04E+04	3,51E+03	3,25E+00	3,27E+04
NA007-062c	062C_A_14	1,03E+00	5,43E-01	1,13E-01	6,00E-02	6,26E-02	3,72E-02	1,19E+02	1,17E+03	9,05E-01	1,94E+04	2,13E+03	2,90E+00	2,66E+04
NA007-062c	062C_A_15	6,91E-01	3,48E-01	8,99E-02	7,75E-02	9,54E-02	2,58E-02	n.d.	n.d.	n.d.	1,92E+04	2,52E+03	2,70E+00	2,67E+04
NA007-062c	062C_A_16	1,30E+00	6,40E-01	1,03E-01	7,80E-02	1,31E-01	3,07E-02	6,21E+02	2,48E+03	1,68E+00	1,84E+04	2,32E+03	3,00E+00	2,70E+04
NA007-062c	062C_A_17	1,67E+00	5,47E-01	1,18E-01	7,83E-02	6,37E-02	3,86E-02	3,85E+02	3,48E+02	1,57E+00	1,63E+04	4,07E+03	3,02E+00	2,46E+04
NA007-062c	062C_A_18	1,10E+00	3,46E-01	1,10E-01	9,65E-02	1,19E-01	8,77E-02	3,96E+02	3,54E+02	1,56E+00	2,20E+04	3,28E+03	3,01E+00	2,88E+04
NA007-062c	062C_A_2	2,30E+00	8,63E-01	1,56E-01	1,41E-01	1,94E-01	2,92E-02	1,36E+03	1,79E+03	2,17E+00	1,71E+04	3,20E+03	3,38E+00	2,68E+04
NA007-062c	062C_A_3	3,21E+01	1,71E+02	1,61E-01	7,98E-02	1,11E-01	9,43E-02	n.d.	n.d.	n.d.	1,65E+04	2,96E+03	3,34E+00	2,45E+04
NA007-062c	062C_A_4	1,12E+00	5,05E-01	1,06E-01	5,53E-02	8,09E-02	3,49E-02	n.d.	n.d.	n.d.	1,64E+04	2,32E+03	3,10E+00	2,65E+04
NA007-062c	062C_A_5	5,59E+00	1,27E+00	1,72E-01	9,41E-02	1,32E-01	6,08E-02	1,78E+03	2,29E+03	2,45E+00	1,49E+04	2,55E+03	3,76E+00	2,37E+04
NA007-062c	062C_A_6	3,22E+00	6,52E-01	1,32E-01	7,13E-02	1,03E-01	3,83E-02	6,78E+02	1,33E+02	1,78E+00	1,39E+04	2,20E+03	3,17E+00	2,39E+04
NA007-062c	062C_A_7	2,55E+00	6,32E-01	1,47E-01	1,22E-01	6,48E-02	3,28E-02	4,14E+02	3,86E+02	1,65E+00	1,73E+04	4,02E+03	3,34E+00	2,40E+04
NA007-062c	062C_A_8	1,02E+00	4,95E-01	1,39E-01	9,20E-02	1,18E-01	1,18E-01	n.d.	n.d.	n.d.	1,85E+04	2,21E+03	3,68E+00	2,73E+04
NA007-062c	062C_A_9	1,48E+00	1,29E+00	1,77E-01	8,61E-02	1,48E-01	4,51E-02	8,23E+01	2,05E+02	7,31E-01	1,74E+04	2,91E+03	3,98E+00	2,68E+04
NA007-079c	079c_A_1	3,04E+00	6,38E-01	1,21E-01	1,34E-01	1,21E-01	5,37E-02	n.d.	n.d.	n.d.	3,69E+03	5,43E+02	6,36E+00	1,01E+04
NA007-079c	079c_A_3	2,61E+00	1,03E+00	2,20E-01	1,13E-01	1,79E-01	1,49E-01	n.d.	n.d.	n.d.	5,40E+03	1,03E+03	2,50E+01	1,36E+04
NA007-079c	079c_A_4	2,57E+00	1,42E+00	2,27E-01	8,40E-02	1,90E-01	2,54E-01	n.d.	n.d.	n.d.	5,73E+03	8,82E+02	2,40E+01	1,28E+04
NA007-080c1	080c1_A_1	4,91E+00	6,17E-01	1,11E-01	5,94E-02	7,82E-02	1,14E-01	n.d.	n.d.	n.d.	2,60E+03	3,23E+02	3,73E+00	5,90E+03
NA007-080c1	080c1_A_10	9,16E+00	1,21E+00	8,04E-02	2,32E+00	8,45E-01	1,12E-02	1,42E+03	1,96E+03	6,90E-01	4,23E+03	9,35E+02	2,11E+00	9,13E+03
NA007-080c1	080c1_A_11	6,04E+00	1,31E+00	9,27E-02	2,26E-01	2,48E-01	1,06E-02	n.d.	n.d.	n.d.	2,99E+03	6,56E+02	2,99E+00	7,59E+03
NA007-080c1	080c1_A_12	6,90E+00	1,90E+00	8,28E-02	4,28E-01	2,79E-01	3,39E-02	1,94E+01	1,76E+03	2,52E-02	2,91E+03	4,65E+02	2,57E+00	7,44E+03
NA007-080c1	080c1_A_13	5,73E+00	1,79E+00	1,03E-01	9,05E-02	1,01E-01	1,49E-02	n.d.	n.d.	n.d.	3,05E+03	4,91E+02	3,94E+00	8,22E+03
NA007-080c1	080c1_A_14	4,56E+00	2,10E+00	9,70E-02	7,63E-02	1,10E-01	1,39E-02	n.d.	n.d.	n.d.	2,93E+03	4,73E+02	3,86E+00	7,88E+03
NA007-080c1	080c1_A_15	5,02E+00	7,42E-01	8,88E-02	1,68E-01	1,84E-01	3,42E-02	n.d.	n.d.	n.d.	2,93E+03	3,86E+02	3,48E+00	8,30E+03
NA007-080c1	080c1_A_16	1,01E+01	1,82E+00	8,42E-02	2,63E+00	8,08E-01	3,88E-02	1,30E+03	3,21E+02	7,91E-01	4,09E+03	2,85E+02	2,32E+00	8,89E+03
NA007-080c1	080c1_A_17	6,66E+00	8,25E-01	8,25E-02	2,45E+00	3,11E-01	1,23E-02	1,20E+03	3,55E+02	7,48E-01	4,16E+03	4,84E+02	2,12E+00	8,91E+03
NA007-080c1	080c1_A_18	8,35E+00	4,89E+00	1,14E-01	2,01E+00	1,15E+00	1,77E-02	2,09E+03	3,01E+03	1,33E+00	4,80E+03	8,18E+02	3,83E+00	1,39E+04
NA007-080c1	080c1_A_19	6,98E+00	9,55E-01	6,85E-02	2,44E+00	4,62E-01	1,06E-02	8,24E+02	3,71E+02	6,42E-01	4,46E+03	6,18E+02	2,22E+00	8,73E+03
NA007-080c1	080c1_A_2	4,77E+00	1,18E+00	1,07E-01	4,44E-02	7,44E-02	1,49E-01	n.d.	n.d.	n.d.	2,60E+03	4,74E+02	3,52E+00	6,09E+03
NA007-080c1	080c1_A_21	2,14E+00	7,19E-01	1,51E-01	5,16E-02	1,20E-01	7,10E-02	n.d.	n.d.	n.d.	3,43E+03	9,37E+02	6,42E+00	9,14E+03
NA007-080c1	080c1_A_22	3,73E+00	1,54E+00	1,37E-01	7,73E-02	1,60E-01	6,34E-02	n.d.	n.d.	n.d.	3,48E+03	3,98E+02	6,17E+00	9,25E+03
NA007-080c1	080c1_A_3	4,96E+00	1,54E+00	8,45E-02	4,98E-02	7,55E-02	6,43E-02	n.d.	n.d.	n.d.	2,69E+03	4,53E+02	3,09E+00	6,10E+03
NA007-080c1	080c1_A_4	1,03E+01	1,96E+00	9,44E-02	2,11E+00	4,40E-01	3,95E-02	2,39E+03	1,05E+03	9,25E-01	3,52E+03	1,11E+03	2,63E+00	1,08E+04
NA007-080c1	080c1_A_5	1,08E+01	4,73E+00	9,79E-02	1,00E+00	1,32E-01	1,88E-02	2,65E+02	2,19E+02	3,26E-01	2,62E+03	2,42E+02	3,01E+00	6,51E+03
NA007-080c1	080c1_A_6	8,78E+00	8,57E+00	1,50E-01	5,13E-01	5,75E-01	6,30E-02	8,05E+02	5,96E+03	7,57E-01	2,96E+03	1,14E+03	5,64E+00	9,54E+03
NA007-080c1	080c1_A_7	5,54E+00	2,40E+00	1,05E-01	2,14E-01	3,38E-01	4,64E-02	n.d.	n.d.	n.d.	2,91E+03	7,74E+02	3,55E+00	7,11E+03
NA007-080c1	080c1_A_8	8,07E+00	2,59E+00	9,86E-02	1,87E+00	3,47E-01	3,58E-02	8,43E+02	7,87E+02	6,25E-01	3,77E+03	8,37E+02	2,54E+00	8,75E+03
NA007-080c1	080c1_A_9	9,46E+00	1,40E+00	1,19E-01	2,11E+00	6,81E-01	5,20E-02	1,45E+03	6,19E+02	1,03E+00	3,88E+03	4,04E+02	3,21E+00	8,70E+03
NA007-080c2	080c2_B_1	6,53E+00	2,12E+00	1,27E-01	5,19E-01	6,94E-01	2,96E-02	1,46E+03	4,16E+02	2,20E+00	1,85E+04	3,60E+03	3,32E+00	1,97E+04
NA007-080c2	080c2_B_10	5,73E+00	5,78E-01	1,36E-01	5,05E-01	3,25E-01	2,67E-02	1,57E+03	3,49E+02	2,29E+00	2,15E+04	3,25E+03	2,91E+00	2,43E+04
NA007-080c2	080c2_B_11	5,49E+00	2,34E+00	9,27E-02	3,61E-01	2,65E-01	4,68E-02	9,78E+02	3,89E+02	1,65E+00	1,44E+04	4,63E+03	2,18E+00	1,85E+04
NA007-080c2	080c2_B_12	8,00E+00	1,37E+00	1,31E-01	6,36E-01	2,45E-01	2,38E-02	1,89E+03	3,45E+02	2,07E+00	1,66E+04	7,72E+02	2,66E+00	2,27E+04
NA007-080c2	080c2_B_13	9,72E+00	3,53E+00	1,42E-01	3,74E-01	3,46E-01	3,50E-02	2,07E+03	2,02E+03	2,49E+00	1,86E+04	3,33E+03	3,13E+00	2,35E+04
NA007-080c2	080c2_B_14	7,59E+00	1,20E+00	1,46E-01	3,71E-01	2,67E-01	3,21E-02	9,50E+02	3,41E+02	2,30E+00	1,59E+04	1,05E+03	3,00E+00	2,06E+04
NA007-080c2	080c2_B_15	7,03E+00	2,10E+00	1,21E-01	5,14E-01	2,02E-01	5,24E-02	3,21E+03	3,28E+03	2,01E+00	2,23E+04	8,25E+03	2,44E+00	2,15E+04
NA007-080c2	080c2_B_16	6,53E+00	1,12E+00	1,33E-01	6,03E-01	4,71E-01	7,11E-02	3,03E+03	4,68E+03	2,29E+00	1,71E+04	2,22E+03	2,79E+00	2,62E+04
NA007-080c2	080c2_B_17	6,29E+00	2,13E+00	1,34E-01	2,40E-01	2,85E-01	1,08E-01	1,50E+03	1,48E+02	2,46E+00	1,81E+04	3,00E+03	3,03E+00	2,35E+04
NA007-080c2	080c2_B_18	6,50E+00	9,18E-01	2,12E-01	7,73E-01	2,92E-01	1,62E-01	1,47E+03	2,07E+02	3,34E+00	1,81E+04	2,62E+03	4,19E+00	2,76E+04
NA007-080c2	080c2_B_19	8,24E+00	2,12E+00	1,43E-01	3,69E-01	1,25E-01	4,09E-02	2,21E+03	3,12E+02	2,54E+00	1,76E+04	5,17E+02	3,05E+00	2,45E+04
NA007-080c2	080c2_B_2	1,48E+01	6,25E+00	1,45E-01	7,41E-01	2,63E-01	3,80E-02	2,80E+03	4,30E+02	2,71E+00	1,79E+04	6,04E+03	3,87E+00	2,24E+04
NA007-080c2	080c2_B_20	5,73E+00	6,53E-01	1,30E-01	1,94E-01	1,16E-01	4,26E-02	1,09E+03	5,65E+01	2,39E+00	1,80E+04	2,01E+03	2,90E+00	2,26E+04
NA007-080c2	080c2_B_21	6,85E+00	3,43E+00	1,37E-01	2,33E-01	2,25E-01	3,13E-02	1,74E+03	1,25E+03	2,23E+00	1,66E+04	5,65E+03	2,65E+00	2,06E+04
NA007-080c2	080c2_B_22	6,95E+00	7,83E-01	1,34E-01	1,69E-01	1,03E-01	4,38E-02	1,14E+03	2,27E+02	2,34E+00	1,59E+04	2,69E+03	2,80E+00	2,07E+04
NA007-080c2	080c2_B_23	6,80E+00	1,26E+00	1,35E-01	1,52E-01	4,79E-02	3,29E-02	1,14E+03	3,36E+02	2,27E+00	1,63E+04	2,39E+03	2,68E+00	2,15E+04
NA007-080c2	080c2_B_24	5,74E+00	7,26E-01	1,37E-01	2,74E-01	1,71E-01	3,38E-02	1,94E+03	1,42E+03	2,48E+00	1,94E+04	4,27E+02	2,87E+00	2,61E+04
NA007-080c2	080c2_B_25	4,26E+00	6,35E-01	1,34E-01	1,38E-01	1,57E-01	7,93E-02	9,91E+02	7,18E+02	2,07E+00	1,87E+04	9,50E+02	2,45E+00	2,36E+04
NA007-080c2	080c2_B_4	6,57E+00	2,67E+00	1,42E-01	2,64E-01	2,33E-01	3,16E-02	1,57E+03	4,88E+02	2,38E+00	2,23E+04	1,15E+04	3,33E+00	2,39E+04

Analysis	Al27_2SD	Al27_LOD	Si29_mean	Si29_2SD	Si29_LOD	P31_mean	P31_2SD	P31_LOD	K39_mean	K39_2SD	K39_LOD	Ca43_mean	Ca43_2SD	Ca43_LOD
	(ppm)	(ppm)	(ppm)	(ppm)	(ppm)	(ppm)	(ppm)	(ppm)	(ppm)	(ppm)	(ppm)	(ppm)	(ppm)	(ppm)
002c_A_1	7,28E+03	1,12E+00	n.d.	n.d.	n.d.	6,96E+03	1,38E+04	2,54E+01	4,64E+01	3,83E+01	7,43E-01	1,10E+04	2,48E+04	8,84E+01
002c_A_10	2,12E+03	8,22E-01	n.d.	n.d.	n.d.	< Det. Lim	1,47E+02	7,46E+01	n.d.	n.d.	n.d.	n.d.	n.d.	n.d.
002c_A_11	2,96E+03	1,60E+00	n.d.	n.d.	n.d.	< Det. Lim	1,88E+02	7,30E+01	9,32E+01	4,12E+02	7,78E-01	n.d.	n.d.	n.d.
002c_A_12	1,25E+03	9,01E-01	n.d.	n.d.	n.d.	< Det. Lim	2,17E+02	1,12E+03	n.d.	n.d.	n.d.	n.d.	n.d.	n.d.
002c_A_13	2,18E+03	8,12E-01	n.d.	n.d.	n.d.	n.d.	n.d.	n.d.	n.d.	n.d.	n.d.	n.d.	n.d.	n.d.
002c_A_14	1,93E+03	8,96E-01	n.d.	n.d.	n.d.	n.d.	n.d.	n.d.	n.d.	n.d.	n.d.	n.d.	n.d.	n.d.
002c_A_2	2,69E+03	7,70E-01	n.d.	n.d.	n.d.	4,45E+03	3,81E+03	2,31E+01	3,78E+01	3,40E+01	5,59E-01	6,12E+03	7,76E+03	7,57E+01
002c_A_3	2,44E+03	8,50E-01	n.d.	n.d.	n.d.	2,54E+03	3,85E+03	2,61E+01	n.d.	n.d.	n.d.	3,43E+03	7,49E+03	7,71E+01
002c_A_4	1,95E+03	8,42E-01	n.d.	n.d.	n.d.	< Det. Lim	1,89E+02	4,77E+01	2,06E+00	3,62E+01	8,52E-02	n.d.	n.d.	n.d.
002c_A_5	1,82E+03	8,43E-01	n.d.	n.d.	n.d.	< Det. Lim	2,13E+02	6,09E+03	1,22E+01	1,07E+02	3,73E-01	n.d.	n.d.	n.d.
002c_A_6	2,83E+03	7,61E-01	n.d.	n.d.	n.d.	6,06E+00	3,47E+02	2,17E+00	n.d.	n.d.	n.d.	n.d.	n.d.	n.d.
002c_A_7	1,56E+03	7,16E-01	n.d.	n.d.	n.d.	< Det. Lim	1,81E+02	7,02E+01	n.d.	n.d.	n.d.	n.d.	n.d.	n.d.
002c_A_8	1,88E+03	7,36E-01	n.d.	n.d.	n.d.	< Det. Lim	1,53E+02	6,67E+01	n.d.	n.d.	n.d.	n.d.	n.d.	n.d.
002c_A_9	2,25E+03	7,85E-01	n.d.	n.d.	n.d.	< Det. Lim	1,45E+02	6,52E+01	n.d.	n.d.	n.d.	n.d.	n.d.	n.d.
062C_A_1	7,73E+03	8,54E-01	n.d.	n.d.	n.d.	n.d.	n.d.	n.d.	3,47E+02	2,32E+02	1,34E+00	n.d.	n.d.	n.d.
062C_A_10	4,17E+03	7,76E-01	n.d.	n.d.	n.d.	n.d.	n.d.	n.d.	4,71E+02	4,20E+02	1,12E+00	n.d.	n.d.	n.d.
062C_A_11	6,10E+03	1,02E+00	n.d.	n.d.	n.d.	9,33E+00	7,56E+01	1,44E+00	3,35E+02	1,96E+02	1,54E+00	n.d.	n.d.	n.d.
062C_A_12	7,21E+03	8,58E-01	n.d.	n.d.	n.d.	7,15E+01	7,49E+01	6,83E+00	2,73E+02	1,02E+02	1,30E+00	n.d.	n.d.	n.d.
062C_A_13	6,30E+03	8,02E-01	n.d.	n.d.	n.d.	4,76E+01	1,50E+02	5,05E+00	1,44E+03	1,34E+03	1,13E+00	n.d.	n.d.	n.d.
062C_A_14	3,29E+03	7,25E-01	n.d.	n.d.	n.d.	n.d.	n.d.	n.d.	1,08E+02	1,51E+02	1,32E+00	n.d.	n.d.	n.d.
062C_A_15	3,20E+03	6,82E-01	n.d.	n.d.	n.d.	n.d.	n.d.	n.d.	3,42E+01	1,48E+01	2,73E+00	n.d.	n.d.	n.d.
062C_A_16	4,02E+03	7,53E-01	n.d.	n.d.	n.d.	n.d.	n.d.	n.d.	1,68E+02	9,87E+01	1,16E+00	n.d.	n.d.	n.d.
062C_A_17	3,50E+03	7,71E-01	n.d.	n.d.	n.d.	n.d.	n.d.	n.d.	4,59E+02	1,04E+02	1,09E+00	n.d.	n.d.	n.d.
062C_A_18	3,14E+03	7,54E-01	n.d.	n.d.	n.d.	n.d.	n.d.	n.d.	3,20E+02	2,47E+02	1,10E+00	n.d.	n.d.	n.d.
062C_A_2	3,66E+03	7,89E-01	n.d.	n.d.	n.d.	n.d.	n.d.	n.d.	8,56E+02	6,45E+02	1,19E+00	n.d.	n.d.	n.d.
062C_A_3	3,90E+03	7,84E-01	n.d.	n.d.	n.d.	n.d.	n.d.	n.d.	5,25E+02	2,18E+02	1,15E+00	n.d.	n.d.	n.d.
062C_A_4	2,99E+03	7,34E-01	n.d.	n.d.	n.d.	< Det. Lim	1,73E+02	1,94E+02	3,14E+01	6,80E+00	4,57E+00	n.d.	n.d.	n.d.
062C_A_5	8,01E+03	8,75E-01	n.d.	n.d.	n.d.	< Det. Lim	4,55E+01	7,20E+02	1,22E+03	2,43E+03	1,30E+00	7,33E+02	3,44E+03	3,00E+01
062C_A_6	2,76E+03	7,53E-01	n.d.	n.d.	n.d.	1,86E+02	3,36E+02	1,13E+01	7,27E+02	2,05E+02	1,09E+00	n.d.	n.d.	n.d.
062C_A_7	3,17E+03	8,00E-01	n.d.	n.d.	n.d.	n.d.	n.d.	n.d.	7,03E+02	3,21E+02	1,17E+00	n.d.	n.d.	n.d.
062C_A_8	3,20E+03	8,87E-01	n.d.	n.d.	n.d.	n.d.	n.d.	n.d.	2,25E+02	1,13E+02	1,39E+00	n.d.	n.d.	n.d.
062C_A_9	4,64E+03	9,67E-01	n.d.	n.d.	n.d.	n.d.	n.d.	n.d.	4,07E+02	3,96E+02	1,43E+00	n.d.	n.d.	n.d.
079c_A_1	1,39E+03	7,27E-01	n.d.	n.d.	n.d.	7,38E+03	1,17E+04	2,38E+01	9,06E+02	2,62E+02	9,02E-01	8,28E+03	1,88E+04	7,05E+01
079c_A_3	2,98E+03	2,18E+00	n.d.	n.d.	n.d.	< Det. Lim	3,82E+02	1,51E+02	6,12E+02	2,80E+02	1,89E+00	n.d.	n.d.	n.d.
079c_A_4	2,60E+03	2,42E+00	n.d.	n.d.	n.d.	< Det. Lim	4,71E+02	6,81E+02	5,23E+01	1,25E+02	1,22E+00	n.d.	n.d.	n.d.
080c1_A_1	7,59E+02	4,40E-01	n.d.	n.d.	n.d.	n.d.	n.d.	n.d.	n.d.	n.d.	n.d.	n.d.	n.d.	n.d.
080c1_A_10	5,62E+02	3,25E-01	n.d.	n.d.	n.d.	3,53E+02	4,43E+02	8,74E+00	1,21E+03	1,82E+02	4,85E-01	n.d.	n.d.	n.d.
080c1_A_11	1,59E+03	4,12E-01	n.d.	n.d.	n.d.	5,65E+02	8,12E+02	1,09E+01	1,47E+02	1,92E+02	5,06E-01	n.d.	n.d.	n.d.
080c1_A_12	1,29E+03	3,66E-01	n.d.	n.d.	n.d.	1,16E+02	3,33E+02	6,89E+00	3,58E+02	3,21E+02	4,78E-01	n.d.	n.d.	n.d.
080c1_A_13	1,41E+03	5,18E-01	n.d.	n.d.	n.d.	< Det. Lim	2,09E+02	7,91E+01	n.d.	n.d.	n.d.	n.d.	n.d.	n.d.
080c1_A_14	1,25E+03	5,19E-01	n.d.	n.d.	n.d.	< Det. Lim	1,32E+02	2,47E+02	2,12E+01	1,28E+01	3,24E-01	n.d.	n.d.	n.d.
080c1_A_15	1,31E+03	4,68E-01	n.d.	n.d.	n.d.	n.d.	n.d.	n.d.	8,06E+01	1,65E+01	4,82E-01	n.d.	n.d.	n.d.
080c1_A_16	8,37E+02	3,76E-01	n.d.	n.d.	n.d.	1,30E+02	1,17E+02	7,85E+00	1,72E+03	1,61E+02	5,27E-01	n.d.	n.d.	n.d.
080c1_A_17	1,18E+03	3,46E-01	n.d.	n.d.	n.d.	3,66E+02	3,28E+02	9,20E+00	1,30E+03	5,18E+02	4,94E-01	n.d.	n.d.	n.d.
080c1_A_18	9,93E+03	6,21E-01	n.d.	n.d.	n.d.	2,24E+02	3,54E+02	1,24E+01	3,35E+03	4,40E+03	9,05E-01	n.d.	n.d.	n.d.
080c1_A_19	8,48E+02	3,84E-01	n.d.	n.d.	n.d.	9,59E+01	9,93E+01	6,55E+00	8,58E+02	1,05E+02	5,15E-01	n.d.	n.d.	n.d.
080c1_A_2	1,27E+03	4,19E-01	n.d.	n.d.	n.d.	n.d.	n.d.	n.d.	n.d.	n.d.	n.d.	n.d.	n.d.	n.d.
080c1_A_21	2,59E+03	8,92E-01	< Det. Lim	1,50E+04	1,30E+04	6,47E+02	7,67E+02	1,68E+01	1,03E+02	1,49E+02	7,64E-01	n.d.	n.d.	n.d.
080c1_A_22	6,77E+02	8,90E-01	n.d.	n.d.	n.d.	4,05E+02	1,41E+03	1,57E+01	1,89E+02	2,76E+02	8,41E-01	n.d.	n.d.	n.d.
080c1_A_3	1,05E+03	3,77E-01	n.d.	n.d.	n.d.	n.d.	n.d.	n.d.	n.d.	n.d.	n.d.	n.d.	n.d.	n.d.
080c1_A_4	2,90E+03	3,89E-01	n.d.	n.d.	n.d.	3,36E+03	4,33E+03	1,36E+01	1,50E+03	2,94E+02	5,65E-01	4,82E+03	6,06E+03	5,25E+01
080c1_A_5	4,59E+02	4,06E-01	n.d.	n.d.	n.d.	3,35E+01	7,68E+01	4,70E+00	8,21E+02	1,29E+02	5,83E-01	n.d.	n.d.	n.d.
080c1_A_6	9,52E+03	6,26E-01	n.d.	n.d.	n.d.	< Det. Lim	1,84E+02	7,90E+01	8,27E+02	7,96E+02	9,30E-01	n.d.	n.d.	n.d.
080c1_A_7	2,45E+03	4,50E-01	n.d.	n.d.	n.d.	7,12E+02	1,18E+03	1,31E+01	9,69E+01	2,02E+02	5,18E-01	n.d.	n.d.	n.d.
080c1_A_8	2,32E+03	3,80E-01	n.d.	n.d.	n.d.	2,76E+04	4,27E+04	1,31E+01	1,11E+03	3,90E+02	5,55E-01	4,84E+04	7,53E+04	7,29E+01
080c1_A_9	6,39E+02	4,77E-01	n.d.	n.d.	n.d.	2,17E+04	5,16E+03	1,56E+01	1,28E+03	2,85E+02	6,81E-01	3,61E+04	2,70E+03	8,62E+01
080c2_B_1	2,47E+03	8,78E-01	n.d.	n.d.	n.d.	1,54E+02	1,03E+02	1,12E+01	4,40E+02	1,75E+02	1,20E+00	n.d.	n.d.	n.d.
080c2_B_10	2,61E+03	7,53E-01	n.d.	n.d.	n.d.	3,56E+02	1,46E+02	1,37E+01	5,08E+02	2,85E+02	1,12E+00	n.d.	n.d.	n.d.
080c2_B_11	5,92E+03	5,69E-01	n.d.	n.d.	n.d.	1,64E+02	1,36E+02	9,07E+00	2,27E+02	6,85E+01	8,50E-01	n.d.	n.d.	n.d.
080c2_B_12	2,48E+03	6,94E-01	n.d.	n.d.	n.d.	4,95E+02	2,56E+02	1,37E+01	4,88E+02	7,01E+01	1,01E+00	n.d.	n.d.	n.d.
080c2_B_13	4,25E+03	8,28E-01	n.d.	n.d.	n.d.	7,91E+02	8,04E+02	1,73E+01	5,43E+02	4,92E+02	1,20E+00	5,56E+02	3,01E+03	3,62E+01
080c2_B_14	1,62E+03	7,97E-01	n.d.	n.d.	n.d.	2,40E+02	1,40E+02	1,32E+01	2,89E+02	9,10E+01	1,17E+00	n.d.	n.d.	n.d.
080c2_B_15	1,45E+03	6,72E-01	n.d.	n.d.	n.d.	1,12E+02	1,49E+02	8,68E+00	4,37E+02	1,72E+02	9,64E-01	n.d.	n.d.	n.d.
080c2_B_16	7,72E+03	7,03E-01	n.d.	n.d.	n.d.	2,18E+02	2,32E+02	1,23E+01	6,24E+02	9,88E+02	1,08E+00	4,11E+02	4,35E+03	3,13E+01
080c2_B_17	4,74E+03	7,94E-01	n.d.	n.d.	n.d.	3,05E+02	5,92E+01	1,46E+01	4,59E+02	7,74E+01	1,16E+00	n.d.	n.d.	n.d.
080c2_B_18	2,12E+03	1,09E+00	n.d.	n.d.	n.d.	4,35E+02	1,24E+01	2,06E+01	5,07E+02	9,38E+01	1,60E+00	n.d.	n.d.	n.d.
080c2_B_19	3,64E+03	7,97E-01	n.d.	n.d.	n.d.	6,52E+02	3,74E+02	1,65E+01	8,56E+02	2,68E+01	1,15E+00	3,91E+02	1,35E+03	3,45E+01
080c2_B_2	3,12E+03	9,92E-01	n.d.	n.d.	n.d.	2,86E+02	1,48E+02	1,61E+01	1,08E+03	3,87E+02	1,35E+00	n.d.	n.d.	n.d.
080c2_B_20	1,99E+03	7,55E-01	n.d.	n.d.	n.d.	4,97E+01	6,65E+01	6,91E+00	2,87E+02	2,11E+01	1,15E+00	n.d.	n.d.	n.d.
080c2_B_21	4,83E+03	7,02E-01	n.d.	n.d.	n.d.	2,68E+02	2,17E+02	1,25E+01	6,76E+02	2,30E+02	1,01E+00	n.d.	n.d.	n.d.
080c2_B_22	1,03E+03	7,47E-01	n.d.	n.d.	n.d.	2,00E+02	4,10E+01	1,25E+01	3,57E+02	1,20E+00	1,10E+00	n.d.	n.d.	n.d.
080c2_B_23	3,23E+03	7,38E-01	n.d.	n.d.	n.d.	4,78E+01	1,26E+02	5,91E+00	3,91E+02	8,51E+01	1,05E+00	n.d.	n.d.	n.d.
080c2_B_24	2,48E+03	7,61E-01	n.d.	n.d.	n.d.	2,18E+02	2,79E+02	1,32E+01	4,54E+02	2,50E+02	1,16E+00	1,69E+02	9,93E+02	2,06E+01
080c2_B_25	2,11E+03	6,53E-01	n.d.	n.d.	n.d.	1,40E+02	1,42E+02	9,76E+00	2,48E+02	6,79E+01	1,00E+00	n.d.	n.d.	n.d.
080c2_B_4	6,17E+03	8,51E-01	n.d.	n.d.	n.d.	3,32E+02	2,19E+02	1,48E+01	3,94E+02	1,90E+02	1,24E+00	n.d.	n.d.	n.d.

Analysis	Ca44_mean	Ca44_2SD	Ca44_LOD	Sc45_mean	Sc45_2SD	Sc45_LOD	Ti47_mean	Ti47_2SD	Ti47_LOD	V51_mean	V51_2SD	V51_LOD	Cr53_mean	Cr53_2SD
	(ppm)	(ppm)	(ppm)	(ppm)	(ppm)	(ppm)	(ppm)	(ppm)	(ppm)	(ppm)	(ppm)	(ppm)	(ppm)	(ppm)
002c_A_1	1,36E+04	3,22E+04	1,01E+01	2,68E+01	4,31E+00	9,52E-02	5,58E+04	7,08E+03	8,04E-01	2,06E+03	3,29E+02	8,62E-02	2,54E+01	1,23E+01
002c_A_10	n.d.	n.d.	n.d.	2,54E+01	6,73E+00	6,77E-02	5,65E+04	1,07E+04	7,39E-01	2,19E+03	3,92E+02	7,13E-02	1,60E+01	6,71E+00
002c_A_11	n.d.	n.d.	n.d.	2,71E+01	8,93E+00	6,96E-02	6,09E+04	1,97E+04	7,91E-01	2,21E+03	5,69E+02	7,56E-02	1,32E+01	4,03E+00
002c_A_12	n.d.	n.d.	n.d.	2,46E+01	9,16E+00	7,91E-02	5,82E+04	6,67E+03	8,42E-01	2,13E+03	2,22E+02	8,35E-02	1,72E+01	2,81E+00
002c_A_13	n.d.	n.d.	n.d.	2,38E+01	4,89E+00	7,05E-02	5,64E+04	1,12E+04	7,61E-01	2,26E+03	4,83E+02	7,76E-02	1,45E+01	6,07E+00
002c_A_14	n.d.	n.d.	n.d.	2,49E+01	4,80E+00	7,06E-02	5,57E+04	5,42E+03	8,34E-01	2,23E+03	6,52E+02	8,26E-02	1,50E+01	3,47E+00
002c_A_2	6,15E+03	9,51E+03	7,63E+00	2,56E+01	5,50E+00	7,23E-02	5,78E+04	1,32E+04	6,22E-01	2,14E+03	4,47E+02	6,87E-02	2,18E+01	6,27E+00
002c_A_3	2,69E+03	7,31E+03	6,60E+00	2,26E+01	5,67E+00	7,93E-02	5,26E+04	9,37E+03	7,17E-01	1,99E+03	4,46E+02	7,45E-02	2,16E+01	5,28E+00
002c_A_4	n.d.	n.d.	n.d.	2,36E+01	5,93E+00	7,86E-02	5,62E+04	1,47E+04	7,28E-01	2,15E+03	6,37E+02	7,73E-02	1,30E+01	1,49E+01
002c_A_5	n.d.	n.d.	n.d.	2,33E+01	3,60E+00	7,77E-02	5,38E+04	1,43E+04	7,35E-01	2,16E+03	3,72E+02	7,77E-02	9,19E+00	2,02E+00
002c_A_6	n.d.	n.d.	n.d.	2,42E+01	7,21E+00	6,81E-02	5,54E+04	1,84E+04	6,88E-01	2,21E+03	6,65E+02	6,92E-02	1,60E+01	4,92E+00
002c_A_7	n.d.	n.d.	n.d.	2,55E+01	4,04E+00	6,53E-02	5,69E+04	8,72E+03	6,42E-01	2,15E+03	3,31E+02	6,44E-02	1,52E+01	5,03E+00
002c_A_8	n.d.	n.d.	n.d.	2,59E+01	5,00E+00	6,65E-02	5,67E+04	1,41E+04	6,58E-01	2,19E+03	4,53E+02	6,76E-02	1,34E+01	4,00E+00
002c_A_9	n.d.	n.d.	n.d.	2,42E+01	4,83E+00	6,95E-02	5,46E+04	9,82E+03	6,54E-01	2,06E+03	3,71E+02	7,04E-02	1,56E+01	5,98E+00
062C_A_1	n.d.	n.d.	n.d.	2,35E+01	2,69E+00	8,25E-02	5,57E+04	5,67E+03	9,40E-01	3,76E+03	5,34E+02	1,02E-01	1,70E+01	2,80E+00
062C_A_10	n.d.	n.d.	n.d.	2,50E+01	2,75E+00	6,58E-02	6,19E+04	9,76E+03	8,59E-01	4,22E+03	8,13E+02	9,21E-02	3,70E+01	5,91E+00
062C_A_11	n.d.	n.d.	n.d.	2,32E+01	2,24E+00	8,97E-02	5,87E+04	3,48E+03	1,16E+00	3,93E+03	2,13E+02	1,19E-01	1,48E+02	1,51E+01
062C_A_12	n.d.	n.d.	n.d.	2,18E+01	4,93E+00	7,66E-02	5,66E+04	1,27E+04	9,40E-01	3,71E+03	8,15E+02	9,76E-02	1,49E+02	3,07E+01
062C_A_13	n.d.	n.d.	n.d.	2,29E+01	2,14E+00	7,30E-02	5,91E+04	4,58E+03	9,09E-01	3,63E+03	6,26E+02	9,48E-02	1,46E+02	2,18E+01
062C_A_14	n.d.	n.d.	n.d.	2,22E+01	3,71E+00	6,14E-02	5,66E+04	8,97E+03	7,90E-01	3,85E+03	6,02E+02	8,28E-02	1,44E+02	3,36E+01
062C_A_15	n.d.	n.d.	n.d.	2,20E+01	2,50E+00	5,78E-02	5,54E+04	7,53E+03	7,36E-01	3,80E+03	7,90E+02	7,88E-02	1,36E+02	2,34E+01
062C_A_16	n.d.	n.d.	n.d.	2,21E+01	3,18E+00	6,33E-02	5,59E+04	6,32E+03	8,41E-01	3,78E+03	2,49E+02	8,50E-02	1,42E+02	2,63E+01
062C_A_17	n.d.	n.d.	n.d.	2,34E+01	2,70E+00	6,04E-02	6,06E+04	5,86E+03	8,28E-01	3,96E+03	3,65E+02	8,35E-02	7,54E+01	9,05E+00
062C_A_18	n.d.	n.d.	n.d.	2,21E+01	3,82E+00	6,49E-02	6,33E+04	9,52E+03	8,40E-01	3,90E+03	7,34E+02	8,53E-02	1,53E+02	2,05E+01
062C_A_2	n.d.	n.d.	n.d.	3,00E+01	3,75E+00	7,16E-02	6,61E+04	5,43E+03	8,85E-01	4,19E+03	5,39E+02	9,41E-02	2,61E+01	2,93E+00
062C_A_3	n.d.	n.d.	n.d.	3,07E+01	4,11E+00	7,29E-02	6,33E+04	9,04E+03	8,98E-01	4,11E+03	6,24E+02	9,00E-02	2,18E+01	8,84E+00
062C_A_4	n.d.	n.d.	n.d.	3,02E+01	4,88E+00	6,31E-02	6,45E+04	8,60E+03	8,17E-01	4,16E+03	6,27E+02	8,48E-02	2,02E+01	4,22E+00
062C_A_5	8,46E+02	4,06E+03	2,18E+00	3,20E+01	4,50E+00	7,76E-02	8,47E+04	5,89E+03	1,02E+00	5,38E+03	4,11E+02	1,04E-01	3,59E+01	7,13E+00
062C_A_6	n.d.	n.d.	n.d.	3,09E+01	2,07E+00	6,49E-02	7,03E+04	1,21E+04	8,51E-01	4,39E+03	8,04E+02	8,69E-02	2,80E+01	3,71E+00
062C_A_7	n.d.	n.d.	n.d.	2,97E+01	3,72E+00	7,03E-02	7,00E+04	1,54E+04	2,14E+00	4,29E+03	7,37E+02	9,38E-02	2,36E+01	8,85E+00
062C_A_8	n.d.	n.d.	n.d.	2,39E+01	2,07E+00	8,35E-02	5,57E+04	5,20E+03	1,07E+00	3,95E+03	3,54E+02	1,02E-01	1,91E+01	1,29E+01
062C_A_9	n.d.	n.d.	n.d.	2,48E+01	5,03E+00	9,00E-02	6,04E+04	1,65E+04	1,08E+00	4,04E+03	9,48E+02	1,11E-01	4,12E+01	1,11E+01
079c_A_1	8,35E+03	2,04E+04	5,82E+00	4,83E+00	8,05E-01	5,71E-02	5,88E+04	8,45E+03	1,07E+00	4,83E+02	9,77E+01	6,91E-02	3,28E+01	6,99E+00
079c_A_3	n.d.	n.d.	n.d.	3,82E+00	1,35E+00	9,75E-02	6,08E+04	1,23E+04	2,12E+00	8,85E+02	3,47E+02	1,40E-01	3,55E+01	7,59E+00
079c_A_4	n.d.	n.d.	n.d.	3,69E+00	8,80E-01	9,40E-02	6,36E+04	1,36E+04	2,10E+00	8,96E+02	2,21E+02	1,46E-01	4,17E+01	1,26E+01
080c1_A_1	n.d.	n.d.	n.d.	5,83E+00	6,46E-01	5,77E-02	5,71E+04	6,29E+03	5,79E-01	4,83E+02	6,52E+01	5,67E-02	1,72E+01	3,72E+00
080c1_A_10	1,86E+02	1,69E+03	4,59E-01	3,24E+01	6,46E+00	3,11E-02	9,07E+04	6,68E+03	4,28E-01	6,65E+02	7,81E+01	4,26E-02	2,77E+01	7,11E+00
080c1_A_11	n.d.	n.d.	n.d.	7,75E+00	2,90E+00	4,29E-02	6,37E+04	1,26E+04	9,36E-01	5,36E+02	1,03E+02	4,97E-02	2,54E+01	4,25E+00
080c1_A_12	n.d.	n.d.	n.d.	9,45E+00	2,64E+00	3,38E-02	6,23E+04	8,77E+03	4,62E-01	5,25E+02	9,74E+01	4,51E-02	2,71E+01	5,17E+00
080c1_A_13	n.d.	n.d.	n.d.	6,54E+00	1,46E+00	5,12E-02	6,37E+04	1,12E+04	6,46E-01	5,62E+02	1,03E+02	5,91E-02	8,27E+00	2,12E+00
080c1_A_14	n.d.	n.d.	n.d.	6,13E+00	9,84E-01	5,21E-02	6,05E+04	1,23E+04	6,12E-01	5,30E+02	1,38E+02	6,00E-02	5,58E+00	1,19E+00
080c1_A_15	n.d.	n.d.	n.d.	6,49E+00	1,24E+00	4,51E-02	6,28E+04	9,33E+03	5,83E-01	5,38E+02	8,05E+01	5,26E-02	6,62E+00	2,80E+00
080c1_A_16	n.d.	n.d.	n.d.	3,09E+01	2,22E+00	3,35E-02	8,34E+04	7,61E+03	4,69E-01	6,79E+02	1,10E+02	4,77E-02	2,65E+01	6,15E+00
080c1_A_17	n.d.	n.d.	n.d.	3,06E+01	7,91E+00	2,92E-02	8,19E+04	1,12E+04	4,46E-01	6,66E+02	9,57E+01	4,26E-02	3,44E+01	3,27E+00
080c1_A_18	n.d.	n.d.	n.d.	1,87E+01	5,44E+00	5,06E-02	7,13E+04	1,10E+04	7,26E-01	5,79E+02	1,48E+02	6,97E-02	3,57E+01	5,00E+00
080c1_A_19	n.d.	n.d.	n.d.	2,45E+01	5,87E+00	3,18E-02	8,23E+04	1,20E+04	4,74E-01	6,78E+02	1,33E+02	4,82E-02	3,21E+01	4,18E+00
080c1_A_2	n.d.	n.d.	n.d.	6,12E+00	1,02E+00	5,26E-02	5,68E+04	9,35E+03	5,50E-01	5,14E+02	8,80E+01	5,39E-02	1,87E+01	2,90E+00
080c1_A_21	n.d.	n.d.	n.d.	6,81E+00	1,34E+00	7,75E-02	4,30E+04	8,26E+03	8,58E-01	3,72E+02	6,69E+01	7,70E-02	9,81E+00	3,61E+00
080c1_A_22	n.d.	n.d.	n.d.	6,71E+00	5,96E-01	7,87E-02	4,58E+04	6,31E+03	8,64E-01	3,59E+02	5,60E+01	7,93E-02	1,07E+01	4,20E+00
080c1_A_3	n.d.	n.d.	n.d.	5,72E+00	8,37E-01	4,50E-02	5,78E+04	4,90E+03	5,17E-01	5,24E+02	1,13E+02	4,99E-02	1,88E+01	2,86E+00
080c1_A_4	5,53E+03	7,05E+03	4,70E+00	2,78E+01	6,97E+00	3,91E-02	7,27E+04	9,09E+03	5,07E-01	6,09E+02	1,35E+02	5,15E-02	4,81E+01	4,68E+01
080c1_A_5	n.d.	n.d.	n.d.	1,69E+01	3,33E+00	4,29E-02	6,53E+04	8,17E+03	5,43E-01	5,56E+02	1,20E+02	5,45E-02	3,53E+01	1,33E+01
080c1_A_6	n.d.	n.d.	n.d.	7,18E+00	2,21E+00	7,98E-02	5,49E+04	1,19E+04	8,59E-01	4,99E+02	1,21E+02	8,30E-02	1,51E+01	1,03E+01
080c1_A_7	n.d.	n.d.	n.d.	8,51E+00	4,66E+00	4,83E-02	6,26E+04	2,21E+04	5,72E-01	5,25E+02	1,19E+02	5,55E-02	1,95E+01	6,64E+00
080c1_A_8	5,26E+04	8,53E+04	5,68E+00	2,73E+01	6,24E+00	3,81E-02	8,63E+04	7,45E+03	4,98E-01	6,83E+02	1,20E+02	5,03E-02	2,65E+01	2,68E+00
080c1_A_9	3,74E+04	4,72E+03	6,82E+00	2,81E+01	6,27E+00	4,70E-02	8,76E+04	7,90E+03	6,26E-01	6,70E+02	8,71E+01	6,21E-02	2,94E+01	2,68E+00
080c2_B_1	n.d.	n.d.	n.d.	2,89E+01	4,82E+00	6,38E-02	7,72E+04	8,95E+03	9,04E-01	6,06E+03	2,84E+02	9,72E-02	3,33E+02	2,04E+01
080c2_B_10	n.d.	n.d.	n.d.	2,75E+01	5,13E+00	5,87E-02	7,91E+04	1,61E+04	1,14E+00	5,95E+03	1,24E+03	8,76E-02	3,24E+02	5,44E+01
080c2_B_11	n.d.	n.d.	n.d.	2,50E+01	5,02E+00	4,38E-02	7,14E+04	1,57E+04	2,16E+00	5,28E+03	1,16E+03	6,62E-02	8,67E+01	1,92E+01
080c2_B_12	n.d.	n.d.	n.d.	3,04E+01	5,07E+00	5,58E-02	9,20E+04	1,27E+04	7,59E-01	6,17E+03	7,94E+02	7,93E-02	1,15E+02	1,78E+01
080c2_B_13	2,04E+02	3,43E+03	8,24E-01	2,54E+01	4,33E+00	6,72E-02	7,56E+04	7,12E+03	9,24E-01	5,73E+03	8,49E+02	9,46E-02	2,80E+02	2,41E+01
080c2_B_14	n.d.	n.d.	n.d.	2,86E+01	1,11E+00	6,11E-02	7,73E+04	5,73E+03	8,50E-01	5,86E+03	3,64E+02	9,12E-02	3,51E+02	1,32E+01
080c2_B_15	n.d.	n.d.	n.d.	2,86E+01	2,71E+00	5,44E-02	7,98E+04	1,29E+04	7,49E-01	5,88E+03	9,29E+02	7,87E-02	3,06E+02	5,26E+01
080c2_B_16	7,74E+01	5,40E+03	3,60E-01	2,38E+01	1,61E+00	6,20E-02	6,89E+04	5,87E+03	1,17E+00	5,95E+03	3,62E+02	8,29E-02	4,36E+02	5,02E+01
080c2_B_17	n.d.	n.d.	n.d.	2,43E+01	5,10E+00	6,44E-02	8,15E+04	5,92E+03	8,68E-01	5,91E+03	1,24E+03	9,35E-02	3,91E+02	2,84E+01
080c2_B_18	n.d.	n.d.	n.d.	2,56E+01	2,81E+00	9,39E-02	7,47E+04	9,37E+02	1,17E+00	5,72E+03	1,82E+02	1,27E-01	5,01E+02	5,25E+01
080c2_B_19	n.d.	n.d.	n.d.	2,72E+01	1,29E+00	6,67E-02	9,06E+04	4,02E+03	9,29E-01	6,01E+03	4,70E+02	9,07E-02	3,78E+02	1,67E+01
080c2_B_2	n.d.	n.d.	n.d.	2,81E+01	3,13E+00	7,77E-02	8,13E+04	6,32E+03	1,08E+00	6,09E+03	1,04E+03	1,09E-01	3,64E+02	3,10E+01
080c2_B_20	n.d.	n.d.	n.d.	2,38E+01	3,38E+00	6,16E-02	7,39E+04	1,10E+04	8,46E-01	5,47E+03	6,31E+02	8,72E-02	3,12E+02	3,11E+01
080c2_B_21	n.d.	n.d.	n.d.	2,54E+01	5,61E+00	5,57E-02	7,64E+04	1,98E+04	7,53E-01	5,61E+03	3,74E+02	8,04E-02	2,87E+02	2,29E+01
080c2_B_22	n.d.	n.d.	n.d.	2,45E+01	2,33E+00	6,07E-02	7,37E+04	2,31E+03	8,36E-01	6,04E+03	6,56E+02	8,57E-02	2,85E+02	2,32E+01
080c2_B_23	n.d.	n.d.	n.d.	2,40E+01	1,52E+00	5,92E-02	7,32E+04	1,09E+04	7,97E-01	5,84E+03	7,80E+02	8,15E-02	2,99E+02	5,04E+01
080c2_B_24	n.d.	n.d.	n.d.	2,26E+01	8,76E-01	6,67E-02	7,10E+04	4,47E+03	8,24E-01	6,06E+03	7,41E+02	8,92E-02	4,87E+02	4,90E+01
080c2_B_25	n.d.	n.d.	n.d.	2,06E+01	1,60E+00	5,71E-02	6,66E+04	9,69E+03	7,32E-01	5,99E+03	3,17E+02	7,66E-02	3,60E+02	2,07E+01
080c2_B_4	n.d.	n.d.	n.d.	2,91E+01	5,19E+00	6,50E-02	8,23E+04	5,39E+03	9,36E-01	6,12E+03	1,00E+03	9,62E-02	3,52E+02	7,77E+01

Analysis	Cr53_LOD	Mn55_mean	Mn55_2SD	Mn55_LOD	Fe57_mean	Fe57_2SD	Fe57_LOD	Co59_mean	Co59_2SD	Co59_LOD	Ni60_mean	Ni60_2SD	Ni60_LOD	Cu63_mean
	(ppm)	(ppm)	(ppm)	(ppm)	(ppm)	(ppm)	(ppm)	(ppm)	(ppm)	(ppm)	(ppm)	(ppm)	(ppm)	(ppm)
002c_A_1	1,46E+00	4,49E+03	9,35E+02	2,20E+00	6,15E+05	0,00E+00	1,04E+01	8,87E+01	1,08E+01	5,73E-02	1,01E+01	1,25E+00	1,42E-01	1,68E+01
002c_A_10	1,28E+00	4,30E+03	7,58E+02	1,77E+00	6,10E+05	0,00E+00	7,50E+00	8,97E+01	1,48E+01	4,54E-02	9,80E+00	1,83E+00	1,13E-01	8,89E+00
002c_A_11	1,42E+00	4,98E+03	1,00E+03	1,85E+00	6,10E+05	0,00E+00	7,65E+00	9,26E+01	3,01E+01	4,60E-02	9,71E+00	1,93E+00	1,10E-01	8,84E+00
002c_A_12	1,38E+00	4,52E+03	1,19E+03	2,03E+00	6,10E+05	0,00E+00	8,52E+00	8,95E+01	1,02E+01	5,33E-02	1,00E+01	1,46E+00	1,25E-01	1,08E+01
002c_A_13	1,35E+00	4,71E+03	1,68E+03	1,85E+00	6,10E+05	0,00E+00	7,31E+00	8,90E+01	1,85E+01	4,61E-02	1,04E+01	3,79E+00	1,12E-01	9,07E+00
002c_A_14	1,39E+00	4,49E+03	8,48E+02	1,99E+00	6,10E+05	0,00E+00	7,60E+00	8,96E+01	2,19E+01	5,28E-02	9,09E+00	2,09E+00	1,20E-01	8,99E+00
002c_A_2	1,06E+00	4,59E+03	1,17E+03	1,72E+00	6,15E+05	0,00E+00	7,97E+00	8,64E+01	1,52E+01	4,38E-02	9,44E+00	2,01E+00	1,10E-01	8,91E+00
002c_A_3	1,15E+00	4,42E+03	1,36E+03	1,89E+00	6,15E+05	0,00E+00	8,51E+00	8,10E+01	1,49E+01	4,81E-02	9,45E+00	1,61E+00	1,18E-01	8,76E+00
002c_A_4	1,48E+00	4,38E+03	7,46E+02	1,90E+00	6,08E+05	0,00E+00	8,48E+00	8,63E+01	1,05E+01	4,99E-02	9,70E+00	1,65E+00	1,22E-01	1,90E+01
002c_A_5	2,00E+00	4,48E+03	6,04E+02	1,89E+00	6,08E+05	0,00E+00	8,44E+00	8,66E+01	1,70E+01	4,83E-02	9,89E+00	2,45E+00	1,10E-01	9,37E+00
002c_A_6	1,16E+00	4,14E+03	8,08E+02	1,69E+00	6,10E+05	0,00E+00	7,34E+00	8,57E+01	1,71E+01	4,35E-02	9,80E+00	3,26E+00	1,11E-01	8,39E+00
002c_A_7	1,18E+00	4,53E+03	7,67E+02	1,62E+00	6,10E+05	0,00E+00	6,98E+00	8,77E+01	1,31E+01	4,32E-02	1,07E+01	4,89E+00	1,00E-01	8,94E+00
002c_A_8	1,24E+00	4,45E+03	1,02E+03	1,67E+00	6,10E+05	0,00E+00	7,02E+00	8,54E+01	1,68E+01	4,30E-02	9,67E+00	2,18E+00	9,62E-02	8,69E+00
002c_A_9	1,24E+00	4,18E+03	6,07E+02	1,69E+00	6,10E+05	0,00E+00	7,09E+00	8,68E+01	1,53E+01	4,47E-02	9,48E+00	1,43E+00	9,51E-02	8,72E+00
062C_A_1	1,66E+00	3,66E+03	5,84E+02	2,28E+00	6,13E+05	0,00E+00	4,95E+00	2,15E+02	3,19E+01	7,89E-02	1,55E+01	3,70E+00	1,25E-01	1,72E+01
062C_A_10	1,14E+00	4,18E+03	7,19E+02	1,93E+00	6,14E+05	0,00E+00	4,44E+00	1,98E+02	2,68E+01	6,56E-02	1,49E+01	1,76E+00	9,78E-02	3,27E+01
062C_A_11	1,39E+00	3,83E+03	6,80E+02	2,54E+00	6,14E+05	0,00E+00	5,99E+00	2,16E+02	1,22E+01	8,74E-02	1,70E+01	3,49E+00	1,31E-01	2,12E+01
062C_A_12	1,13E+00	3,62E+03	8,26E+02	2,11E+00	6,14E+05	0,00E+00	4,85E+00	2,17E+02	4,94E+01	7,34E-02	1,75E+01	3,58E+00	1,03E-01	1,95E+01
062C_A_13	1,08E+00	3,57E+03	5,29E+02	2,00E+00	6,14E+05	0,00E+00	4,73E+00	2,18E+02	1,76E+01	6,81E-02	1,61E+01	2,55E+00	9,94E-02	2,13E+01
062C_A_14	9,71E-01	3,63E+03	4,90E+02	1,78E+00	6,14E+05	0,00E+00	4,16E+00	2,09E+02	2,75E+01	5,88E-02	1,71E+01	1,29E+01	9,48E-02	1,23E+01
062C_A_15	9,01E-01	3,46E+03	2,98E+02	1,68E+00	6,14E+05	0,00E+00	3,89E+00	2,08E+02	2,49E+01	5,71E-02	1,56E+01	2,55E+00	8,63E-02	7,77E+00
062C_A_16	9,64E-01	3,68E+03	4,87E+02	1,80E+00	6,14E+05	0,00E+00	4,36E+00	2,07E+02	2,78E+01	6,21E-02	1,60E+01	4,68E+00	8,72E-02	2,09E+01
062C_A_17	1,04E+00	3,78E+03	5,57E+02	1,84E+00	6,14E+05	0,00E+00	4,35E+00	2,08E+02	5,48E+01	6,24E-02	1,88E+01	3,35E+00	9,82E-02	3,02E+01
062C_A_18	9,95E-01	3,50E+03	3,78E+02	1,81E+00	6,22E+05	0,00E+00	4,32E+00	2,07E+02	3,73E+01	6,26E-02	1,77E+01	4,05E+00	1,01E-01	2,11E+01
062C_A_2	1,36E+00	4,60E+03	2,62E+02	2,06E+00	6,13E+05	0,00E+00	4,58E+00	2,05E+02	1,74E+01	7,28E-02	1,18E+01	2,14E+00	1,08E-01	2,68E+01
062C_A_3	1,36E+00	4,21E+03	1,17E+03	2,02E+00	6,08E+05	0,00E+00	4,50E+00	2,00E+02	3,74E+01	7,28E-02	1,29E+01	2,69E+00	1,05E-01	3,36E+01
062C_A_4	1,31E+00	4,06E+03	5,19E+02	1,89E+00	6,12E+05	0,00E+00	4,29E+00	2,04E+02	2,45E+01	6,63E-02	1,38E+01	2,36E+00	9,65E-02	1,01E+01
062C_A_5	1,35E+00	5,02E+03	7,15E+02	2,22E+00	5,81E+05	0,00E+00	5,16E+00	1,99E+02	2,78E+01	8,34E-02	1,24E+01	5,17E-01	1,26E-01	5,15E+01
062C_A_6	1,20E+00	4,65E+03	6,40E+02	1,90E+00	5,81E+05	0,00E+00	4,41E+00	1,87E+02	1,67E+01	6,76E-02	1,21E+01	2,30E+00	1,05E-01	4,56E+01
062C_A_7	1,39E+00	4,81E+03	8,41E+02	2,03E+00	6,22E+05	0,00E+00	4,66E+00	2,08E+02	2,34E+01	7,16E-02	1,29E+01	2,41E+00	1,08E-01	3,18E+01
062C_A_8	1,66E+00	3,65E+03	5,02E+02	2,22E+00	6,14E+05	0,00E+00	8,59E+00	2,05E+02	2,20E+01	7,59E-02	1,77E+01	3,78E+00	1,10E-01	2,17E+01
062C_A_9	1,46E+00	3,85E+03	5,87E+02	2,38E+00	6,14E+05	0,00E+00	5,48E+00	2,17E+02	8,00E+01	8,47E-02	1,86E+01	8,75E+00	1,29E-01	2,03E+01
079c_A_1	9,98E-01	9,47E+03	1,58E+03	1,76E+00	6,18E+05	0,00E+00	6,70E+00	2,11E+01	3,42E+00	5,56E-02	2,60E+00	5,10E-01	1,23E-01	5,11E+00
079c_A_3	2,50E+00	1,01E+04	3,59E+03	3,62E+00	6,19E+05	0,00E+00	1,32E+01	2,94E+01	7,57E+00	1,53E-01	3,45E+00	9,61E-01	3,47E-01	8,92E+00
079c_A_4	2,41E+00	1,05E+04	2,41E+03	3,71E+00	6,19E+05	0,00E+00	1,35E+01	3,11E+01	6,22E+00	1,54E-01	5,03E+00	5,00E+00	3,03E-01	9,82E+00
080c1_A_1	9,10E-01	9,31E+03	1,86E+03	1,57E+00	5,60E+05	0,00E+00	4,14E+00	2,26E+01	2,20E+00	6,01E-02	4,15E+00	6,47E-01	9,03E-02	3,05E+00
080c1_A_10	5,59E-01	9,92E+03	7,01E+02	1,11E+00	6,22E+05	0,00E+00	3,00E+00	2,48E+01	3,68E+00	3,86E-02	6,77E+00	1,35E+00	6,20E-02	1,18E+02
080c1_A_11	6,89E-01	9,75E+03	9,96E+02	1,28E+00	6,22E+05	0,00E+00	3,46E+00	2,34E+01	2,41E+00	4,79E-02	4,61E+00	5,84E-01	7,16E-02	9,03E+00
080c1_A_12	5,95E-01	9,22E+03	1,89E+03	1,17E+00	5,97E+05	0,00E+00	3,21E+00	2,28E+01	3,76E+00	4,32E-02	4,67E+00	8,93E-01	7,07E-02	1,65E+01
080c1_A_13	1,56E+00	1,12E+04	1,39E+03	1,56E+00	6,24E+05	0,00E+00	4,27E+00	2,51E+01	1,25E+00	5,90E-02	4,76E+00	8,97E-01	8,70E-02	2,97E+00
080c1_A_14	2,74E+00	9,75E+03	1,65E+03	1,50E+00	6,24E+05	0,00E+00	4,07E+00	2,51E+01	7,99E+00	5,45E-02	4,41E+00	1,32E+00	8,55E-02	2,74E+00
080c1_A_15	1,66E+00	1,10E+04	1,47E+03	1,37E+00	6,24E+05	0,00E+00	3,69E+00	2,43E+01	2,79E+00	4,94E-02	4,84E+00	1,09E+00	8,36E-02	3,00E+00
080c1_A_16	6,19E-01	1,00E+04	1,79E+03	1,18E+00	6,22E+05	0,00E+00	3,35E+00	2,84E+01	2,74E+00	4,10E-02	7,87E+00	1,09E+00	6,78E-02	3,10E+01
080c1_A_17	5,53E-01	1,10E+04	2,04E+03	1,08E+00	6,23E+05	0,00E+00	2,98E+00	4,31E+01	4,26E+00	3,65E-02	7,57E+00	5,14E-01	6,24E-02	2,67E+01
080c1_A_18	9,21E-01	1,29E+04	1,79E+03	1,78E+00	6,22E+05	0,00E+00	4,84E+00	3,33E+01	1,14E+01	6,05E-02	6,35E+00	2,54E+00	9,08E-02	3,66E+01
080c1_A_19	5,96E-01	1,03E+04	1,82E+03	1,16E+00	6,22E+05	0,00E+00	3,19E+00	3,13E+01	3,99E+00	3,99E-02	7,76E+00	3,28E+00	6,63E-02	2,82E+01
080c1_A_2	8,25E-01	9,42E+03	1,41E+03	1,49E+00	5,60E+05	0,00E+00	4,00E+00	2,26E+01	4,15E+00	5,70E-02	3,99E+00	8,71E-01	8,83E-02	3,03E+00
080c1_A_21	2,60E+00	8,83E+03	1,56E+03	2,07E+00	6,22E+05	0,00E+00	5,81E+00	1,54E+01	2,01E+00	1,01E-01	2,21E+00	5,57E-01	1,49E-01	1,07E+01
080c1_A_22	2,08E+00	8,92E+03	2,01E+03	2,07E+00	6,22E+05	0,00E+00	5,64E+00	1,50E+01	2,66E+00	9,57E-02	2,44E+00	1,74E+00	1,37E-01	1,40E+01
080c1_A_3	7,43E-01	9,29E+03	2,00E+03	1,33E+00	5,54E+05	0,00E+00	3,45E+00	2,22E+01	3,26E+00	4,95E-02	4,22E+00	8,92E-01	7,42E-02	3,13E+00
080c1_A_4	6,57E-01	1,01E+04	3,16E+03	1,33E+00	5,60E+05	0,00E+00	3,53E+00	2,44E+01	4,28E+00	4,90E-02	5,93E+00	1,39E+00	7,76E-02	7,62E+01
080c1_A_5	7,01E-01	9,27E+03	9,34E+02	1,38E+00	5,60E+05	0,00E+00	3,70E+00	2,06E+01	1,29E+00	5,15E-02	4,86E+00	6,28E-01	8,76E-02	2,38E+01
080c1_A_6	1,48E+00	1,07E+04	3,14E+03	2,18E+00	5,60E+05	0,00E+00	5,89E+00	2,26E+01	3,62E+00	8,65E-02	4,35E+00	6,18E-01	1,39E-01	1,92E+01
080c1_A_7	8,48E-01	9,43E+03	2,59E+03	1,50E+00	6,22E+05	0,00E+00	4,11E+00	2,34E+01	4,60E+00	5,71E-02	4,44E+00	1,01E+00	8,43E-02	1,10E+01
080c1_A_8	6,64E-01	1,02E+04	2,21E+03	1,29E+00	6,22E+05	0,00E+00	3,53E+00	2,48E+01	1,64E+00	4,71E-02	6,89E+00	1,33E+00	8,04E-02	9,01E+01
080c1_A_9	8,19E-01	1,03E+04	7,36E+02	1,59E+00	6,22E+05	0,00E+00	4,43E+00	2,41E+01	2,24E+00	5,83E-02	6,64E+00	8,94E-01	9,73E-02	1,03E+02
080c2_B_1	1,08E+00	4,03E+03	5,19E+02	2,03E+00	5,99E+05	0,00E+00	4,88E+00	2,65E+02	3,67E+01	6,71E-02	2,25E+02	4,67E+01	1,14E-01	2,20E+02
080c2_B_10	1,01E+00	3,43E+03	5,38E+02	1,87E+00	5,99E+05	0,00E+00	4,36E+00	2,46E+02	1,73E+01	6,14E-02	2,14E+02	2,39E+01	1,01E-01	1,44E+02
080c2_B_11	7,77E-01	3,51E+03	5,25E+02	1,40E+00	5,99E+05	0,00E+00	3,28E+00	2,35E+02	4,21E+01	4,50E-02	1,79E+02	3,34E+01	7,49E-02	2,62E+02
080c2_B_12	9,57E-01	3,89E+03	4,28E+02	1,71E+00	5,99E+05	0,00E+00	4,01E+00	2,45E+02	1,30E+01	5,69E-02	1,95E+02	1,34E+01	9,94E-02	2,59E+02
080c2_B_13	1,11E+00	3,74E+03	1,91E+02	2,02E+00	5,99E+05	0,00E+00	4,88E+00	2,47E+02	3,45E+01	6,55E-02	2,00E+02	1,21E+01	1,19E-01	9,21E+01
080c2_B_14	1,04E+00	4,18E+03	3,35E+02	1,90E+00	5,99E+05	0,00E+00	4,55E+00	2,60E+02	1,71E+01	6,16E-02	1,68E+02	1,40E+01	1,09E-01	1,08E+02
080c2_B_15	8,77E-01	4,04E+03	6,17E+02	1,62E+00	5,99E+05	0,00E+00	3,86E+00	2,60E+02	3,03E+01	5,22E-02	2,01E+02	2,44E+01	9,22E-02	1,50E+02
080c2_B_16	9,53E-01	3,73E+03	4,67E+02	1,78E+00	5,99E+05	0,00E+00	4,36E+00	2,66E+02	3,11E+01	5,82E-02	2,35E+02	2,99E+01	1,03E-01	1,67E+02
080c2_B_17	1,14E+00	3,72E+03	2,65E+02	1,95E+00	5,99E+05	0,00E+00	4,65E+00	2,62E+02	4,45E+01	6,25E-02	2,26E+02	3,40E+01	1,12E-01	1,37E+02
080c2_B_18	1,70E+00	3,41E+03	6,98E+00	2,70E+00	5,99E+05	0,00E+00	6,64E+00	2,39E+02	1,21E+01	8,38E-02	2,60E+02	1,39E+01	1,51E-01	1,55E+02
080c2_B_19	1,21E+00	4,11E+03	4,43E+02	1,99E+00	5,99E+05	0,00E+00	4,88E+00	2,45E+02	2,89E+01	6,31E-02	2,11E+02	1,47E+01	1,10E-01	1,25E+02
080c2_B_2	1,31E+00	4,46E+03	6,96E+02	2,35E+00	5,99E+05	0,00E+00	1,38E+01	2,45E+02	3,42E+01	8,09E-02	2,05E+02	4,76E+01	1,32E-01	2,27E+02
080c2_B_20	1,10E+00	3,71E+03	2,22E+02	1,88E+00	5,99E+05	0,00E+00	4,52E+00	2,47E+02	2,43E+01	6,04E-02	1,95E+02	9,74E+00	1,05E-01	9,00E+01
080c2_B_21	9,44E-01	3,67E+03	5,71E+02	1,70E+00	5,99E+05	0,00E+00	4,23E+00	2,27E+02	3,01E+01	5,42E-02	1,86E+02	1,42E+01	9,79E-02	1,42E+02
080c2_B_22	1,01E+00	3,51E+03	1,98E+01	1,83E+00	5,99E+05	0,00E+00	4,42E+00	2,28E+02	1,25E+01	5,74E-02	2,03E+02	3,48E+01	1,08E-01	1,39E+02
080c2_B_23	9,70E-01	3,79E+03	4,48E+02	1,75E+00	5,99E+05	0,00E+00	4,30E+00	2,34E+02	2,44E+01	5,43E-02	2,12E+02	3,43E+01	9,42E-02	1,69E+02
080c2_B_24	1,05E+00	3,30E+03	2,32E+02	1,91E+00	5,99E+05	0,00E+00	4,72E+00	2,59E+02	2,93E+01	5,92E-02	3,21E+02	5,15E+01	1,05E-01	9,40E+01
080c2_B_25	8,73E-01	3,23E+03	3,32E+02	1,62E+00	5,99E+05	0,00E+00	3,95E+00	2,54E+02	1,44E+01	4,83E-02	3,12E+02	4,08E+01	9,15E-02	1,05E+02
080c2_B_4	1,11E+00	4,19E+03	8,56E+02	2,08E+00	5,99E+05	0,00E+00	2,59E+01	2,75E+02	4,74E+01	7,05E-02	2,27E+02	9,44E+01	1,14E-01	1,49E+02

Analysis	Cu63_2SD	Cu63_LOD	Zn66_mean	Zn66_2SD	Zn66_LOD	Ga69_mean	Ga69_2SD	Ga69_LOD	Ge72_mean	Ge72_2SD	Ge72_LOD	Ge73_mean	Ge73_2SD
	(ppm)	(ppm)	(ppm)	(ppm)	(ppm)	(ppm)	(ppm)	(ppm)	(ppm)	(ppm)	(ppm)	(ppm)	(ppm)
002c_A_1	1,22E+01	8,86E-02	6,77E+02	2,15E+02	4,42E-01	1,71E+01	1,10E+01	1,43E-01	2,05E+00	1,12E+00	2,40E-01	2,11E+00	1,55E+00
002c_A_10	1,39E+00	8,12E-02	6,12E+02	9,83E+01	3,42E-01	1,39E+01	2,78E+00	1,03E-01	1,26E+00	4,01E-01	2,65E-01	1,02E+00	1,92E-01
002c_A_11	2,50E+00	8,12E-02	5,80E+02	1,64E+02	3,64E-01	1,30E+01	2,90E+00	1,02E-01	1,03E+00	1,51E-01	3,07E-01	9,51E-01	2,36E-01
002c_A_12	2,33E+00	9,25E-02	7,69E+02	6,78E+01	3,85E-01	1,42E+01	1,31E+00	1,09E-01	1,15E+00	1,73E-01	3,34E-01	1,02E+00	9,29E-02
002c_A_13	2,11E+00	8,70E-02	6,25E+02	1,26E+02	3,66E-01	1,37E+01	2,99E+00	1,05E-01	1,20E+00	5,43E-01	2,79E-01	1,02E+00	2,49E-01
002c_A_14	1,60E+00	8,97E-02	6,08E+02	1,19E+02	3,80E-01	1,35E+01	2,10E+00	1,09E-01	1,21E+00	3,90E-01	3,02E-01	9,97E-01	1,72E-01
002c_A_2	2,62E+00	7,17E-02	6,09E+02	2,14E+02	3,45E-01	1,33E+01	3,28E+00	9,41E-02	1,65E+00	6,06E-01	2,00E-01	1,50E+00	5,86E-01
002c_A_3	2,61E+00	8,32E-02	5,88E+02	1,38E+02	3,63E-01	1,31E+01	2,92E+00	1,01E-01	1,35E+00	7,52E-01	2,44E-01	1,30E+00	5,50E-01
002c_A_4	1,45E+01	6,46E-02	6,98E+02	2,38E+02	3,75E-01	1,31E+01	2,32E+00	1,04E-01	1,14E+00	3,89E-01	2,83E-01	9,82E-01	1,46E-01
002c_A_5	2,79E+00	8,56E-02	6,70E+02	1,99E+02	3,81E-01	1,30E+01	1,25E+00	1,06E-01	1,22E+00	1,89E-01	2,64E-01	9,69E-01	1,15E-01
002c_A_6	1,37E+00	8,01E-02	5,56E+02	1,42E+02	3,37E-01	1,32E+01	3,22E+00	9,77E-02	1,11E+00	3,69E-01	2,66E-01	9,88E-01	2,82E-01
002c_A_7	1,44E+00	7,46E-02	6,42E+02	1,07E+02	3,15E-01	1,34E+01	2,66E+00	9,34E-02	1,18E+00	4,62E-01	2,41E-01	1,01E+00	1,96E-01
002c_A_8	2,31E+00	7,08E-02	6,34E+02	1,56E+02	3,12E-01	1,32E+01	2,24E+00	9,38E-02	1,14E+00	2,76E-01	2,50E-01	9,94E-01	1,48E-01
002c_A_9	1,72E+00	7,93E-02	6,14E+02	1,58E+02	3,30E-01	1,36E+01	3,69E+00	9,93E-02	1,25E+00	4,29E-01	2,43E-01	9,99E-01	2,44E-01
062C_A_1	6,94E+00	8,88E-02	7,44E+02	3,60E+02	3,94E-01	1,93E+01	2,39E+00	1,19E-01	1,25E+00	5,13E-01	4,67E-01	1,32E+00	1,65E-01
062C_A_10	3,02E+01	7,06E-02	7,24E+02	1,10E+02	3,28E-01	1,72E+01	1,63E+00	9,50E-02	1,24E+00	3,03E-01	3,59E-01	1,21E+00	9,43E-02
062C_A_11	7,22E+00	9,40E-02	7,86E+02	7,96E+01	4,45E-01	1,97E+01	1,86E+00	1,23E-01	1,53E+00	4,70E-01	4,36E-01	1,40E+00	1,36E-01
062C_A_12	5,00E+00	7,86E-02	6,74E+02	2,82E+02	4,04E-01	1,88E+01	3,18E+00	1,05E-01	1,38E+00	4,36E-01	3,95E-01	1,32E+00	2,25E-01
062C_A_13	7,67E+00	7,61E-02	6,72E+02	1,74E+02	3,64E-01	1,83E+01	1,43E+00	8,33E-02	1,28E+00	4,54E-01	3,77E-01	1,29E+00	1,51E-01
062C_A_14	5,12E+00	7,48E-02	5,85E+02	9,43E+01	3,25E-01	1,66E+01	2,21E+00	9,19E-02	1,08E+00	3,56E-01	3,74E-01	1,13E+00	1,92E-01
062C_A_15	1,25E+00	7,81E-02	5,46E+02	1,26E+02	3,15E-01	1,58E+01	1,39E+00	8,66E-02	9,83E-01	3,84E-01	3,79E-01	1,04E+00	1,37E-01
062C_A_16	1,23E+01	6,81E-02	7,10E+02	1,15E+02	3,26E-01	1,68E+01	1,45E+00	8,11E-02	1,29E+00	2,83E-01	3,12E-01	1,18E+00	9,33E-02
062C_A_17	7,80E+00	6,56E-02	8,20E+02	1,12E+02	3,38E-01	1,56E+01	1,96E+00	7,83E-02	1,31E+00	3,91E-01	2,94E-01	1,09E+00	1,23E-01
062C_A_18	1,44E+01	7,40E-02	6,44E+02	9,07E+01	3,26E-01	1,59E+01	1,55E+00	7,96E-02	1,29E+00	2,95E-01	3,10E-01	1,12E+00	1,16E-01
062C_A_2	4,72E+00	7,59E-02	9,39E+02	1,70E+02	3,73E-01	1,82E+01	2,66E+00	9,05E-02	1,32E+00	4,90E-01	3,81E-01	1,33E+00	2,25E-01
062C_A_3	9,70E+00	7,33E-02	9,57E+02	3,66E+02	3,57E-01	1,81E+01	2,21E+00	9,61E-02	1,49E+00	4,82E-01	3,30E-01	1,31E+00	1,58E-01
062C_A_4	1,73E+00	7,93E-02	6,33E+02	1,36E+02	3,26E-01	1,76E+01	2,38E+00	9,84E-02	1,01E+00	4,66E-01	4,54E-01	1,18E+00	1,78E-01
062C_A_5	1,52E+01	8,60E-02	1,13E+03	1,40E+02	3,99E-01	1,58E+01	2,09E+00	7,44E-02	1,73E+00	6,50E-01	3,10E-01	1,32E+00	2,59E-01
062C_A_6	1,16E+01	7,17E-02	1,21E+03	1,71E+02	3,34E-01	1,68E+01	1,40E+00	6,66E-02	1,90E+00	5,92E-01	2,54E-01	1,34E+00	9,59E-02
062C_A_7	9,40E+00	7,25E-02	1,19E+03	3,28E+02	3,54E-01	1,74E+01	2,29E+00	8,20E-02	1,64E+00	5,33E-01	3,05E-01	1,36E+00	2,43E-01
062C_A_8	1,30E+01	8,62E-02	7,37E+02	2,64E+02	3,90E-01	1,89E+01	2,88E+00	1,15E-01	1,31E+00	3,50E-01	4,26E-01	1,31E+00	1,98E-01
062C_A_9	8,11E+00	9,38E-02	7,47E+02	2,74E+02	4,25E-01	2,06E+01	4,27E+00	1,17E-01	1,93E+00	2,10E+00	3,68E-01	1,43E+00	2,63E-01
079c_A_1	9,14E-01	1,71E-01	9,16E+02	1,69E+02	3,83E-01	1,38E+01	2,72E+00	7,67E-02	2,60E+00	1,66E+00	1,71E-01	2,44E+00	2,13E+00
079c_A_3	2,62E+00	4,03E-01	1,04E+03	4,14E+02	7,86E-01	2,69E+01	4,73E+00	2,92E-01	2,45E+00	7,39E-01	5,59E-01	2,06E+00	3,62E-01
079c_A_4	4,54E+00	3,69E-01	1,24E+03	6,64E+02	7,59E-01	2,80E+01	3,17E+00	3,00E-01	2,50E+00	8,72E-01	5,87E-01	2,21E+00	3,18E-01
080c1_A_1	5,47E-01	1,73E-01	9,44E+02	1,59E+02	2,59E-01	1,21E+01	1,35E+00	6,44E-02	1,50E+00	2,61E-01	2,00E-01	9,59E-01	9,00E-02
080c1_A_10	2,11E+01	3,57E-02	5,23E+03	8,49E+02	1,84E-01	1,13E+01	3,16E+00	1,67E-02	1,11E+01	1,92E+00	1,12E-01	4,25E+00	5,33E-01
080c1_A_11	7,19E+00	4,74E-02	1,52E+03	4,97E+02	2,18E-01	1,10E+01	2,02E+00	4,04E-02	2,59E+00	1,61E+00	1,50E-01	1,31E+00	5,91E-01
080c1_A_12	1,42E+01	3,65E-02	1,98E+03	7,33E+02	1,89E-01	1,02E+01	2,19E+00	3,41E-02	3,13E+00	1,31E+00	1,24E-01	1,51E+00	3,71E-01
080c1_A_13	9,30E-01	1,69E-01	1,36E+03	4,30E+02	2,68E-01	1,26E+01	2,04E+00	6,41E-02	1,45E+00	5,37E-01	2,14E-01	1,03E+00	2,11E-01
080c1_A_14	6,24E-01	1,70E-01	1,04E+03	1,93E+02	2,54E-01	1,21E+01	2,17E+00	5,38E-02	1,41E+00	6,19E-01	2,00E-01	9,57E-01	1,37E-01
080c1_A_15	8,22E-01	1,01E-01	1,33E+03	2,47E+02	2,33E-01	1,16E+01	2,42E+00	5,04E-02	1,34E+00	3,58E-01	1,83E-01	9,52E-01	2,25E-01
080c1_A_16	3,87E+00	3,78E-02	5,40E+03	3,26E+02	2,05E-01	1,10E+01	6,79E-01	1,86E-02	1,18E+01	2,01E+00	1,26E-01	4,70E+00	5,26E-01
080c1_A_17	2,58E+00	3,49E-02	4,04E+03	9,54E+02	1,74E-01	1,01E+01	1,41E+00	1,65E-02	1,18E+01	2,18E+00	1,16E-01	4,60E+00	7,26E-01
080c1_A_18	1,31E+01	5,03E-02	3,36E+03	4,39E+02	3,05E-01	1,49E+01	5,45E+00	4,40E-02	7,03E+00	2,21E+00	1,88E-01	3,22E+00	7,18E-01
080c1_A_19	4,74E+00	3,58E-02	4,09E+03	9,82E+02	1,97E-01	1,08E+01	1,04E+00	2,16E-02	1,10E+01	2,62E+00	1,21E-01	4,34E+00	6,25E-01
080c1_A_2	8,69E-01	1,54E-01	1,05E+03	2,33E+02	2,45E-01	1,19E+01	2,08E+00	5,72E-02	1,43E+00	3,63E-01	1,96E-01	9,77E-01	1,81E-01
080c1_A_21	9,47E+00	8,18E-02	1,15E+03	2,99E+02	3,62E-01	1,53E+01	2,95E+00	1,04E-01	1,45E+00	7,91E-01	3,16E-01	1,22E+00	2,52E-01
080c1_A_22	2,12E+01	7,54E-02	1,48E+03	2,66E+02	3,58E-01	1,48E+01	1,78E+00	9,44E-02	1,51E+00	3,67E-01	3,04E-01	1,15E+00	1,46E-01
080c1_A_3	1,48E+00	1,14E-01	9,91E+02	2,30E+02	2,22E-01	1,15E+01	1,67E+00	5,15E-02	1,54E+00	6,54E-01	1,67E-01	9,56E-01	1,78E-01
080c1_A_4	4,71E+01	4,40E-02	4,34E+03	8,20E+02	2,21E-01	1,09E+01	2,44E+00	2,32E-02	9,76E+00	2,40E+00	1,37E-01	4,56E+00	1,74E+00
080c1_A_5	7,54E+00	4,61E-02	3,35E+03	1,05E+03	2,32E-01	1,04E+01	8,84E-01	2,93E-02	5,52E+00	3,78E-01	1,44E-01	2,40E+00	2,40E-01
080c1_A_6	1,34E+01	7,80E-02	1,53E+03	3,38E+02	3,80E-01	1,54E+01	4,42E+00	8,23E-02	2,29E+00	1,77E+00	2,76E-01	1,38E+00	2,93E-01
080c1_A_7	1,39E+01	5,42E-02	1,48E+03	1,03E+03	2,48E-01	1,25E+01	1,66E+00	5,35E-02	2,67E+00	2,02E+00	1,72E-01	1,42E+00	6,92E-01
080c1_A_8	2,47E+01	3,94E-02	4,23E+03	8,06E+02	2,07E-01	1,14E+01	2,33E+00	2,26E-02	1,32E+01	7,35E+00	1,34E-01	7,51E+00	5,98E+00
080c1_A_9	2,76E+01	4,70E-02	5,29E+03	1,84E+02	2,69E-01	1,20E+01	1,87E+00	2,70E-02	1,33E+01	2,98E+00	1,63E-01	6,47E+00	2,07E+00
080c2_B_1	4,22E+01	7,36E-02	1,02E+03	3,83E+02	3,65E-01	1,70E+01	3,48E+00	6,88E-02	1,73E+00	5,59E-01	2,92E-01	1,39E+00	2,48E-01
080c2_B_10	2,82E+01	5,98E-02	9,64E+02	1,67E+02	3,33E-01	1,62E+01	1,96E+00	5,45E-02	1,86E+00	3,02E-01	2,45E-01	1,30E+00	2,24E-01
080c2_B_11	7,33E+01	4,83E-02	8,03E+02	2,52E+02	2,51E-01	1,31E+01	3,65E+00	4,09E-02	1,74E+00	1,38E+00	1,80E-01	1,08E+00	3,12E-01
080c2_B_12	2,96E+01	6,16E-02	9,51E+02	1,53E+02	3,03E-01	1,53E+01	5,77E-01	4,70E-02	1,86E+00	3,38E-01	2,22E-01	1,30E+00	1,58E-01
080c2_B_13	1,18E+01	6,98E-02	9,99E+02	1,74E+02	3,74E-01	1,64E+01	2,17E+00	5,94E-02	1,81E+00	6,66E-01	2,81E-01	1,36E+00	2,41E-01
080c2_B_14	9,74E+00	6,26E-02	9,79E+02	1,17E+02	3,71E-01	1,54E+01	8,94E-01	5,42E-02	1,79E+00	2,49E-01	2,54E-01	1,22E+00	8,74E-02
080c2_B_15	5,61E+01	5,34E-02	9,23E+02	1,84E+02	2,93E-01	1,49E+01	1,59E+00	4,83E-02	1,81E+00	4,14E-01	2,12E-01	1,27E+00	1,87E-01
080c2_B_16	1,78E+01	5,89E-02	9,40E+02	8,25E+01	3,25E-01	1,55E+01	1,61E+00	4,30E-02	1,77E+00	1,29E-01	2,37E-01	1,28E+00	1,44E-01
080c2_B_17	1,48E+01	7,06E-02	8,99E+02	1,70E+02	3,70E-01	1,45E+01	1,01E+00	5,34E-02	1,74E+00	1,04E-01	2,55E-01	1,19E+00	1,03E-01
080c2_B_18	1,08E+00	9,12E-02	1,05E+03	1,05E+02	5,11E-01	1,67E+01	5,27E-01	8,26E-02	1,88E+00	1,38E-02	3,69E-01	1,35E+00	4,22E-02
080c2_B_19	4,61E+00	7,01E-02	1,02E+03	3,59E+01	3,66E-01	1,49E+01	6,76E-01	5,56E-02	1,65E+00	4,52E-01	2,75E-01	1,25E+00	6,21E-02
080c2_B_2	6,08E+01	8,35E-02	1,12E+03	2,16E+02	4,24E-01	1,85E+01	2,11E+00	7,71E-02	2,14E+00	2,85E-01	3,21E-01	1,47E+00	2,54E-01
080c2_B_20	1,91E+01	6,62E-02	8,37E+02	8,70E+01	3,45E-01	1,38E+01	1,30E+00	5,73E-02	1,45E+00	6,36E-01	2,72E-01	1,04E+00	1,13E-01
080c2_B_21	1,26E+01	5,80E-02	9,51E+02	7,26E+01	3,21E-01	1,42E+01	1,51E+00	4,80E-02	1,73E+00	7,98E-01	2,29E-01	1,16E+00	1,29E-01
080c2_B_22	9,78E+00	6,43E-02	8,71E+02	3,88E+01	3,42E-01	1,38E+01	5,58E-01	5,06E-02	1,71E+00	3,34E-01	2,43E-01	1,11E+00	9,01E-02
080c2_B_23	4,02E+01	5,95E-02	9,95E+02	2,64E+02	3,32E-01	1,56E+01	2,49E+00	5,13E-02	1,71E+00	3,92E-01	2,40E-01	1,23E+00	2,03E-01
080c2_B_24	9,94E+00	6,75E-02	9,18E+02	6,62E+01	3,53E-01	1,55E+01	2,19E+00	5,30E-02	1,49E+00	4,21E-01	2,78E-01	1,14E+00	1,33E-01
080c2_B_25	1,34E+02	5,49E-02	7,33E+02	1,38E+02	3,19E-01	1,33E+01	1,32E+00	4,96E-02	1,34E+00	2,53E-01	2,41E-01	9,86E-01	1,15E-01
080c2_B_4	2,32E+01	7,40E-02	1,08E+03	2,32E+02	3,87E-01	1,74E+01	3,48E+00	6,62E-02	1,92E+00	4,28E-01	2,85E-01	1,36E+00	3,45E-01

Analysis	Ge73_LOD	Ge74_mean	Ge74_2SD	Ge74_LOD	As75_mean	As75_2SD	As75_LOD	Rb85_mean	Rb85_2SD	Rb85_LOD	Sr88_mean	Sr88_2SD	Sr88_LOD	Y89_mean
	(ppm)	(ppm)	(ppm)	(ppm)	(ppm)	(ppm)	(ppm)	(ppm)	(ppm)	(ppm)	(ppm)	(ppm)	(ppm)	(ppm)
002c_A_1	4,11E-02	5,92E-01	3,97E+00	6,55E-02	5,90E+00	6,07E+00	3,36E-01	3,57E-01	5,40E-01	2,43E-02	9,40E+00	1,75E+01	9,70E-03	5,60E+01
002c_A_10	1,29E-01	5,92E-01	7,74E-01	6,98E-02	4,26E-01	6,37E-01	6,11E-02	8,13E-02	5,39E-02	4,48E-02	1,17E+00	8,34E-01	2,98E-03	4,84E-01
002c_A_11	1,29E-01	3,78E-01	4,30E-01	5,32E-02	7,02E-01	7,00E-01	9,94E-02	5,67E-01	1,75E+00	1,75E-02	2,25E+00	2,15E+00	6,14E-03	7,75E-01
002c_A_12	1,58E-01	7,60E-01	5,86E-01	9,58E-02	8,87E-01	7,32E-01	1,26E-01	1,29E-01	5,93E-02	3,09E-02	1,72E+00	8,97E-01	5,70E-03	5,09E-01
002c_A_13	1,22E-01	5,14E-01	1,01E+00	6,69E-02	2,21E-02	8,91E-01	4,04E-03	8,03E-02	2,49E-02	4,05E-02	1,23E+00	1,05E+00	3,50E-03	7,04E-01
002c_A_14	1,27E-01	3,81E-01	3,90E-01	5,80E-02	1,56E-01	1,03E+00	3,00E-02	8,25E-02	4,12E-02	4,84E-02	1,35E+00	7,96E-01	3,98E-03	4,69E-01
002c_A_2	4,13E-02	1,15E+00	9,47E-01	1,09E-01	1,01E+00	1,82E+00	1,14E-01	2,98E-01	1,74E-01	1,71E-02	6,44E+00	5,44E+00	6,61E-03	3,55E+01
002c_A_3	5,92E-02	8,46E-01	1,27E+00	1,01E-01	1,08E+00	1,01E+00	1,37E-01	8,44E-02	2,57E-02	3,41E-02	3,63E+00	5,48E+00	6,24E-03	2,31E+01
002c_A_4	1,07E-01	5,51E-01	8,36E-01	7,46E-02	1,01E+00	1,96E+00	1,30E-01	1,20E-01	1,01E-01	2,81E-02	1,52E+00	1,43E+00	4,92E-03	4,45E-01
002c_A_5	1,12E-01	6,62E-01	5,73E-01	8,30E-02	5,03E-01	1,16E+00	7,53E-02	1,97E-01	4,96E-01	2,21E-02	1,10E+00	6,96E-01	3,85E-03	4,24E-01
002c_A_6	1,01E-01	5,94E-01	7,44E-01	6,84E-02	6,56E-01	8,99E-01	8,41E-02	7,58E-02	3,93E-02	4,57E-02	1,16E+00	6,35E-01	2,85E-03	1,51E+00
002c_A_7	9,13E-02	5,70E-01	3,02E-01	6,14E-02	4,49E-01	1,01E+00	5,81E-02	8,36E-02	5,56E-02	3,43E-02	1,21E+00	7,13E-01	3,40E-03	4,90E-01
002c_A_8	1,03E-01	4,11E-01	1,12E+00	4,96E-02	4,30E-01	1,43E+00	5,98E-02	7,50E-02	4,99E-02	4,73E-02	1,17E+00	8,23E-01	3,36E-03	4,60E-01
002c_A_9	1,23E-01	6,16E-01	7,79E-01	6,87E-02	4,38E-01	1,06E+00	6,06E-02	7,43E-02	4,94E-02	5,36E-02	9,91E-01	9,67E-01	2,33E-03	4,61E-01
062C_A_1	1,72E-01	4,45E-01	1,58E+00	5,74E-02	2,50E+00	8,29E-01	3,73E-01	8,90E-01	5,70E-01	3,07E-02	3,55E+01	2,80E+01	1,96E-02	4,16E-01
062C_A_10	1,28E-01	1,45E+00	1,19E+00	1,23E-01	3,09E+00	9,27E-01	3,25E-01	1,17E+00	5,40E-01	2,55E-02	6,02E+00	1,19E+00	1,27E-02	3,91E-01
062C_A_11	1,59E-01	1,45E+00	9,43E-01	1,53E-01	4,83E+00	3,13E+00	4,22E-01	4,63E-01	1,42E-01	5,28E-02	2,26E+01	2,85E+01	1,89E-02	1,05E+00
062C_A_12	1,39E-01	1,29E+00	8,60E-01	1,17E-01	3,09E+00	9,24E-01	3,56E-01	5,36E-01	1,65E-01	3,41E-02	9,89E+00	5,86E+00	1,70E-02	5,18E-01
062C_A_13	1,22E-01	1,40E+00	8,33E-01	1,24E-01	4,08E+00	1,52E+00	3,32E-01	2,88E+00	2,57E+00	2,25E-02	4,78E+01	4,90E+01	1,57E-02	2,67E+00
062C_A_14	1,54E-01	8,71E-04	5,32E-01	1,17E-04	2,50E+00	1,41E+00	2,99E-01	2,97E-01	2,15E-01	6,59E-02	4,46E+00	1,72E+00	1,43E-02	2,61E-01
062C_A_15	1,63E-01	n.d.	n.d.	n.d.	1,84E+00	1,66E+00	2,81E-01	2,36E-01	8,58E-02	1,05E-01	3,55E+00	7,02E-01	9,91E-03	1,69E-01
062C_A_16	1,16E-01	1,09E+00	1,07E+00	9,92E-02	4,16E+00	2,45E+00	3,00E-01	4,17E-01	2,24E-01	3,80E-02	5,75E+00	1,92E+00	9,68E-03	4,17E-01
062C_A_17	1,17E-01	1,59E+00	1,03E+00	1,35E-01	4,03E+00	9,92E-01	3,10E-01	1,03E+00	2,87E-01	2,14E-02	7,89E+00	6,43E+00	1,29E-02	7,87E-01
062C_A_18	1,21E-01	1,02E+00	1,06E+00	9,80E-02	3,81E+00	2,48E+00	3,03E-01	5,20E-01	2,30E-01	2,90E-02	6,36E+00	2,06E+00	9,42E-03	5,00E-01
062C_A_2	1,04E-01	2,02E+00	1,24E+00	1,56E-01	3,23E+00	7,59E-01	3,41E-01	2,01E+00	1,02E+00	2,50E-02	2,89E+01	1,85E+01	1,53E-02	1,50E+00
062C_A_3	1,19E-01	1,97E+00	2,01E+00	1,53E-01	3,27E+00	1,87E+00	3,35E-01	1,34E+00	6,80E-01	2,22E-02	8,58E+00	1,64E+00	1,57E-02	5,65E-01
062C_A_4	1,73E-01	7,63E-02	9,85E-01	9,80E-03	1,96E+00	4,91E-01	3,10E-01	2,37E-01	8,35E-02	1,84E-01	5,18E+00	6,71E-01	1,27E-02	2,67E-01
062C_A_5	7,74E-02	6,75E+00	1,14E+00	2,78E-01	7,79E+00	1,22E+00	3,62E-01	2,34E+00	4,44E+00	2,57E-02	6,17E+01	5,39E+01	1,63E-02	2,08E+00
062C_A_6	7,68E-02	6,58E+00	1,86E+00	2,34E-01	6,85E+00	1,69E+00	3,23E-01	1,80E+00	6,29E-01	2,04E-02	1,41E+01	4,68E+00	1,75E-02	9,57E-01
062C_A_7	8,82E-02	4,45E+00	2,24E+00	2,17E-01	4,39E+00	4,54E-01	3,44E-01	1,30E+00	6,71E-01	2,46E-02	1,53E+01	4,60E+00	1,57E-02	1,71E+00
062C_A_8	1,73E-01	7,13E-01	6,41E-01	8,07E-02	3,02E+00	8,26E-01	3,59E-01	6,79E-01	3,98E-01	3,28E-02	5,44E+00	1,37E+00	1,46E-02	3,44E-01
062C_A_9	1,71E-01	1,06E+00	1,65E+00	1,06E-01	2,96E+00	7,45E-01	3,98E-01	7,39E-01	3,50E-01	3,42E-02	6,45E+00	2,05E+00	1,40E-02	3,92E-01
079c_A_1	3,49E-02	5,26E+00	1,48E+00	1,95E-01	2,77E+00	1,96E+00	2,17E-01	3,11E+00	1,80E+00	1,44E-02	9,61E+00	1,14E+01	8,58E-03	5,70E+01
079c_A_3	2,50E-01	3,36E+00	1,46E+00	2,76E-01	1,29E+00	2,24E+00	1,91E-01	2,21E+00	1,41E+00	3,36E-02	n.d.	n.d.	n.d.	1,94E+00
079c_A_4	2,31E-01	3,65E+00	1,46E+00	2,73E-01	2,97E+00	4,02E+00	3,37E-01	3,86E-01	5,14E-01	4,81E-02	n.d.	n.d.	n.d.	9,80E-01
080c1_A_1	5,78E-02	3,55E+00	4,23E-01	1,46E-01	1,24E+00	2,96E-01	2,34E-01	9,86E-02	4,53E-02	2,98E-02	3,97E+00	5,13E-01	8,52E-03	4,27E-01
080c1_A_10	1,27E-02	5,06E+01	1,25E+01	1,25E-01	9,40E+01	2,17E+01	1,63E-01	1,95E+00	4,01E-01	8,44E-03	5,71E+01	1,61E+01	7,03E-03	1,10E+02
080c1_A_11	2,69E-02	7,83E+00	5,95E+00	1,40E-01	8,05E+00	8,68E+00	1,97E-01	3,92E-01	3,77E-01	1,33E-02	8,82E+00	6,68E+00	8,83E-03	1,17E+01
080c1_A_12	1,76E-02	1,34E+01	6,27E+00	1,22E-01	1,74E+01	1,33E+01	1,70E-01	6,06E-01	3,93E-01	1,00E-02	1,16E+01	1,07E+01	6,43E-03	1,73E+01
080c1_A_13	5,65E-02	3,28E+00	1,23E+00	1,39E-01	1,51E+00	1,83E+00	2,40E-01	1,92E-01	4,16E-01	2,36E-02	2,92E+00	1,04E+00	5,60E-03	1,30E-01
080c1_A_14	4,71E-02	3,31E+00	7,01E-01	1,36E-01	1,26E+00	4,99E-01	2,30E-01	1,39E-01	3,54E-02	3,14E-02	3,58E+00	7,67E-01	6,60E-03	3,21E-01
080c1_A_15	4,66E-02	3,85E+00	1,17E+00	1,28E-01	1,78E+00	1,37E+00	2,11E-01	2,38E-01	1,86E-01	1,80E-02	3,95E+00	1,39E+00	6,20E-03	4,19E-01
080c1_A_16	1,46E-02	5,38E+01	1,37E+01	1,37E-01	8,25E+01	2,06E+01	1,84E-01	4,23E+00	1,11E+00	1,01E-02	5,33E+01	9,83E+00	7,37E-03	1,15E+02
080c1_A_17	1,21E-02	5,01E+01	6,19E+00	1,23E-01	9,68E+01	1,52E+01	1,68E-01	3,05E+00	3,78E+00	9,95E-03	3,55E+01	6,98E+00	7,48E-03	1,31E+02
080c1_A_18	2,55E-02	2,96E+01	1,15E+01	1,92E-01	4,71E+01	1,79E+01	2,66E-01	1,38E+01	2,21E+01	1,68E-02	2,22E+01	6,33E+00	1,03E-02	6,76E+01
080c1_A_19	1,39E-02	4,48E+01	1,10E+01	1,33E-01	7,20E+01	1,58E+01	1,82E-01	1,15E+00	2,21E-01	1,01E-02	3,29E+01	7,99E+00	7,13E-03	9,90E+01
080c1_A_2	4,90E-02	3,61E+00	9,27E-01	1,41E-01	1,28E+00	4,27E-01	2,25E-01	9,11E-02	6,46E-02	3,66E-02	3,92E+00	8,34E-01	9,47E-03	3,51E-01
080c1_A_21	8,03E-02	2,68E+00	1,71E+00	1,66E-01	2,48E+00	1,84E+00	3,22E-01	2,42E-01	1,37E-01	3,91E-02	4,99E-01	1,27E+00	1,44E-03	2,06E+00
080c1_A_22	8,90E-02	2,65E+00	6,99E-01	1,69E-01	2,24E+00	8,74E-01	3,20E-01	3,69E-01	7,48E-01	2,49E-02	n.d.	n.d.	n.d.	2,13E-01
080c1_A_3	4,30E-02	3,45E+00	7,22E-01	1,23E-01	1,24E+00	8,40E-01	2,05E-01	7,87E-02	2,99E-02	4,00E-02	3,68E+00	5,81E-01	6,95E-03	2,95E-01
080c1_A_4	1,61E-02	4,17E+01	1,32E+01	1,55E-01	8,23E+01	1,47E+01	2,01E-01	2,14E+00	2,86E-01	1,09E-02	6,07E+01	1,11E+01	9,41E-03	1,30E+02
080c1_A_5	1,88E-02	2,47E+01	2,92E+00	1,57E-01	4,30E+01	1,00E+01	2,11E-01	1,27E+00	1,43E-01	1,17E-02	2,98E+01	4,08E+00	1,14E-02	5,62E+01
080c1_A_6	6,15E-02	6,13E+00	2,15E+00	2,18E-01	7,62E+00	2,86E+00	3,37E-01	3,43E+00	5,88E+00	2,00E-02	1,83E+01	2,77E+01	1,56E-02	9,58E+00
080c1_A_7	3,24E-02	8,00E+00	9,04E+00	1,62E-01	9,25E+00	1,40E+01	2,34E-01	2,77E-01	2,96E-01	1,42E-02	9,71E+00	9,31E+00	7,25E-03	1,40E+01
080c1_A_8	1,56E-02	4,10E+01	6,77E+00	1,47E-01	6,39E+01	1,94E+01	1,90E-01	2,00E+00	7,70E-01	1,14E-02	9,36E+01	7,43E+01	9,28E-03	3,00E+02
080c1_A_9	1,91E-02	5,01E+01	1,68E+01	1,83E-01	8,94E+01	6,84E+01	2,39E-01	2,42E+00	5,95E-01	1,26E-02	8,05E+01	4,08E+01	1,07E-02	2,17E+02
080c2_B_1	7,56E-02	5,50E+00	9,95E-01	2,41E-01	3,75E+00	2,47E+00	3,48E-01	6,20E-01	3,18E-01	3,05E-02	2,42E+01	9,24E+00	1,44E-02	3,13E+00
080c2_B_10	6,52E-02	6,65E+00	8,86E-01	2,40E-01	3,75E+00	2,12E+00	3,20E-01	8,34E-01	5,39E-01	2,64E-02	2,86E+01	1,45E+01	1,39E-02	3,01E+00
080c2_B_11	4,69E-02	5,13E+00	1,25E+00	1,78E-01	2,81E+00	9,70E-01	2,40E-01	3,84E-01	1,29E-01	2,36E-02	1,48E+01	4,43E+00	9,72E-03	2,06E+00
080c2_B_12	5,13E-02	7,47E+00	1,50E+00	2,34E-01	3,62E+00	1,10E+00	2,99E-01	6,27E-01	9,96E-02	2,49E-02	2,61E+01	6,17E+00	1,00E-02	3,04E+00
080c2_B_13	6,46E-02	5,90E+00	2,29E+00	2,51E-01	3,77E+00	1,44E+00	3,42E-01	1,03E+00	1,41E-01	2,66E-02	4,62E+01	6,05E+01	1,18E-02	6,43E+00
080c2_B_14	6,02E-02	6,60E+00	8,84E-01	2,54E-01	3,08E+00	1,88E+00	3,30E-01	4,92E-01	1,19E-01	3,23E-02	1,60E+01	3,79E+00	1,31E-02	1,44E+00
080c2_B_15	5,23E-02	6,60E+00	1,35E+00	2,14E-01	5,88E+00	7,36E+00	2,78E-01	5,87E-01	1,50E-01	2,27E-02	1,66E+01	9,44E+00	9,67E-03	2,43E+00
080c2_B_16	5,41E-02	7,51E+00	1,93E+00	2,47E-01	4,54E+00	3,87E+00	3,12E-01	1,00E+00	1,84E+00	2,18E-02	5,67E+01	1,52E+02	1,25E-02	2,70E+00
080c2_B_17	5,82E-02	6,88E+00	7,56E-01	2,70E-01	3,05E+00	3,79E-01	3,38E-01	5,65E-01	1,38E-01	2,76E-02	2,00E+01	1,39E+00	1,34E-02	1,85E+00
080c2_B_18	9,30E-02	5,82E+00	3,41E-02	3,39E-01	3,95E+00	2,42E+00	4,67E-01	7,41E-01	1,20E-02	4,39E-02	1,88E+01	1,79E+00	1,77E-02	2,35E+00
080c2_B_19	6,05E-02	6,31E+00	7,73E-01	2,64E-01	4,16E+00	2,15E+00	3,44E-01	9,20E-01	1,72E-01	2,32E-02	3,56E+01	8,31E+00	1,51E-02	3,89E+00
080c2_B_2	8,58E-02	5,52E+00	2,73E+00	2,82E-01	6,36E+00	8,83E+00	3,90E-01	2,44E+00	1,44E+00	2,71E-02	4,94E+01	2,77E+01	1,65E-02	4,64E+00
080c2_B_20	6,95E-02	4,12E+00	1,23E-01	2,37E-01	2,62E+00	6,58E-01	3,23E-01	4,16E-01	4,13E-02	3,38E-02	1,35E+01	9,69E-01	1,21E-02	1,29E+00
080c2_B_21	5,65E-02	6,65E+00	1,59E+00	2,30E-01	7,42E+00	2,83E+00	2,97E-01	1,03E+00	2,02E-01	2,07E-02	2,44E+01	7,29E+00	1,18E-02	1,80E+00
080c2_B_22	5,75E-02	5,55E+00	1,03E+00	2,43E-01	3,13E+00	2,89E-01	3,17E-01	5,24E-01	1,15E-01	3,14E-02	2,07E+01	4,83E+00	1,24E-02	1,40E+00
080c2_B_23	5,74E-02	5,93E+00	1,33E+00	2,36E-01	7,29E+00	5,45E+00	3,04E-01	6,01E-01	1,52E-01	2,94E-02	1,96E+01	5,45E+00	1,21E-02	1,16E+00
080c2_B_24	7,01E-02	5,20E+00	8,56E-01	2,43E-01	2,91E+00	1,07E+00	3,28E-01	5,20E-01	1,44E-01	3,26E-02	3,00E+01	2,36E+01	1,20E-02	1,16E+00
080c2_B_25	6,90E-02	3,42E+00	4,32E-01	1,92E-01	2,16E+00	1,07E+00	2,82E-01	4,22E-01	2,51E-02	2,85E-02	9,96E+00	4,01E+00	8,78E-03	9,72E-01
080c2_B_4	6,78E-02	6,76E+00	1,71E+00	2,60E-01	4,15E+00	3,68E+00	3,69E-01	6,17E-01	1,99E-01	3,23E-02	1,97E+01	5,58E+00	1,52E-02	1,82E+00

Analysis	Y89_2SD	Y89_LOD	Zr90_mean	Zr90_2SD	Zr90_LOD	Nb93_mean	Nb93_2SD	Nb93_LOD	Mo95_mean	Mo95_2SD	Mo95_LOD	Ag107_mean	Ag107_2SD	Ag107_LOD
	(ppm)	(ppm)	(ppm)	(ppm)	(ppm)	(ppm)	(ppm)	(ppm)	(ppm)	(ppm)	(ppm)	(ppm)	(ppm)	(ppm)
002c_A_1	1,13E+02	4,74E-03	4,56E+01	1,27E+01	1,12E-02	1,31E+01	3,33E+00	5,72E-03	3,58E+00	1,72E+00	5,21E-02	8,59E-03	6,25E-02	4,24E-03
002c_A_10	1,24E-01	1,26E-03	4,28E+01	1,15E+01	6,05E-03	1,23E+01	2,92E+00	4,47E-03	4,02E+00	8,49E-01	4,43E-02	n.d.	n.d.	n.d.
002c_A_11	8,26E-01	4,77E-03	5,52E+01	3,01E+01	1,17E-02	2,69E+01	2,04E+01	5,63E-03	4,35E+00	1,28E+00	4,25E-02	1,07E-02	4,04E-02	5,96E-03
002c_A_12	1,83E-01	5,47E-03	4,29E+01	1,20E+01	7,88E-03	1,25E+01	1,29E+00	5,97E-03	4,26E+00	1,33E+00	5,37E-02	1,29E-03	4,84E-02	8,93E-04
002c_A_13	7,20E-01	5,85E-03	4,24E+01	1,39E+01	1,26E-02	1,20E+01	3,59E+00	5,73E-03	4,59E+00	1,03E+00	5,69E-02	1,05E-03	2,93E-02	5,93E-04
002c_A_14	9,48E-02	1,63E-03	4,10E+01	5,76E+00	1,56E-02	1,19E+01	2,54E+00	5,49E-03	4,31E+00	1,22E+00	3,52E-02	7,42E-03	6,03E-02	4,61E-03
002c_A_2	4,56E+01	3,43E-03	4,37E+01	1,16E+01	6,54E-03	1,24E+01	4,24E+00	4,15E-03	4,00E+00	1,89E+00	4,32E-02	n.d.	n.d.	n.d.
002c_A_3	3,96E+01	3,97E-03	3,79E+01	1,05E+01	1,33E-02	1,19E+01	3,41E+00	1,60E-03	4,06E+00	1,07E+00	2,78E-02	n.d.	n.d.	n.d.
002c_A_4	8,06E-02	1,79E-03	4,05E+01	1,14E+01	1,02E-02	1,23E+01	2,63E+00	6,83E-03	4,18E+00	6,81E-01	3,06E-02	6,17E-02	2,64E-01	1,39E-02
002c_A_5	1,72E-01	6,34E-03	4,16E+01	8,14E+00	1,28E-02	1,24E+01	2,95E+00	4,03E-03	4,20E+00	1,44E+00	5,27E-02	n.d.	n.d.	n.d.
002c_A_6	3,04E+00	4,94E-03	4,11E+01	1,27E+01	7,43E-03	1,22E+01	3,74E+00	6,20E-03	4,00E+00	1,82E+00	4,21E-02	n.d.	n.d.	n.d.
002c_A_7	1,01E-01	5,38E-03	4,26E+01	8,24E+00	8,97E-03	1,23E+01	1,95E+00	8,89E-04	4,06E+00	1,25E+00	3,74E-02	n.d.	n.d.	n.d.
002c_A_8	1,26E-01	1,05E-03	4,20E+01	9,33E+00	7,51E-03	1,27E+01	3,18E+00	3,34E-03	4,21E+00	1,72E+00	4,31E-02	n.d.	n.d.	n.d.
002c_A_9	8,76E-02	5,45E-03	4,09E+01	8,02E+00	9,56E-03	1,20E+01	1,83E+00	8,96E-04	4,17E+00	1,49E+00	2,70E-02	n.d.	n.d.	n.d.
062C_A_1	2,99E-01	2,75E-03	3,42E+01	4,54E+00	2,00E-02	3,64E+00	6,27E-01	7,51E-03	1,16E+00	5,83E-01	6,18E-02	7,17E-03	2,79E-02	1,10E-02
062C_A_10	1,51E-01	3,18E-03	5,48E+01	3,53E+00	1,22E-02	8,45E+00	9,52E-01	4,09E-03	1,56E+00	5,99E-01	5,56E-02	4,88E-03	3,79E-02	5,39E-03
062C_A_11	6,70E-01	1,97E-03	4,40E+01	2,65E+00	2,45E-02	5,62E+00	8,53E-01	9,18E-03	1,54E+00	5,14E-01	7,23E-02	1,27E-02	3,33E-02	1,28E-02
062C_A_12	1,93E-01	9,29E-04	3,91E+01	8,47E+00	1,71E-02	4,57E+00	1,17E+00	7,41E-03	1,29E+00	8,96E-01	4,91E-02	3,25E-02	3,90E-02	1,31E-02
062C_A_13	2,90E+00	4,56E-03	4,02E+01	1,37E+01	1,72E-02	3,99E+00	1,03E+00	5,88E-03	1,64E+00	9,61E-01	6,00E-02	3,21E-03	3,40E-02	3,17E-03
062C_A_14	1,72E-01	2,10E-03	2,98E+01	4,10E+00	1,13E-02	4,26E+00	7,29E-01	4,18E-03	1,27E+00	6,94E-01	3,97E-02	2,62E-04	2,76E-02	4,27E-04
062C_A_15	1,13E-01	3,66E-04	2,85E+01	4,17E+00	1,28E-02	3,49E+00	7,46E-01	6,90E-03	9,92E-01	4,85E-01	4,55E-02	5,33E-03	3,45E-02	6,13E-03
062C_A_16	3,06E-01	6,86E-04	3,63E+01	4,99E+00	1,04E-02	4,78E+00	1,00E+00	5,21E-03	1,48E+00	9,87E-01	4,99E-02	5,46E-03	3,38E-02	5,15E-03
062C_A_17	5,82E-01	4,34E-03	5,13E+01	4,09E+00	1,81E-02	8,23E+00	7,41E-01	1,79E-03	2,12E+00	6,36E-01	6,01E-02	1,58E-02	3,46E-02	1,18E-02
062C_A_18	1,60E-01	4,10E-03	3,46E+01	9,05E+00	9,86E-03	3,91E+00	1,11E+00	4,37E-03	1,77E+00	9,77E-01	5,89E-02	1,43E-02	5,09E-02	5,02E-03
062C_A_2	8,35E-01	1,46E-03	6,31E+01	5,08E+00	1,15E-02	1,09E+01	1,04E+00	2,28E-02	1,96E+00	5,62E-01	6,30E-02	2,99E-02	5,37E-02	1,33E-02
062C_A_3	2,00E-01	2,76E-03	6,80E+01	1,00E+01	1,50E-02	1,19E+01	2,59E+00	1,97E-02	1,58E+00	6,87E-01	5,28E-02	1,07E-02	1,72E-02	1,08E-02
062C_A_4	9,50E-02	5,45E-04	6,59E+01	8,37E+00	1,74E-02	1,01E+01	1,66E+00	4,12E-03	1,32E+00	6,78E-01	4,60E-02	1,48E-02	3,86E-02	1,06E-02
062C_A_5	2,38E+00	6,97E-03	1,17E+02	1,62E+01	1,15E-02	2,47E+01	8,24E-01	8,52E-03	4,55E+00	7,72E-01	9,17E-02	4,40E-02	4,93E-02	2,05E-02
062C_A_6	1,98E-01	3,40E-03	7,95E+01	1,22E+01	1,08E-02	1,41E+01	2,26E+00	7,28E-03	2,48E+00	6,80E-01	6,15E-02	1,97E-02	4,77E-02	1,01E-02
062C_A_7	2,41E+00	5,70E-03	6,36E+01	1,79E+00	2,11E-02	1,06E+01	1,66E+00	7,72E-03	2,49E+00	6,85E-01	7,19E-02	2,22E-02	3,26E-02	1,36E-02
062C_A_8	8,80E-02	2,38E-03	3,82E+01	4,76E+00	1,62E-02	4,76E+00	7,63E-01	1,05E-02	1,16E+00	5,56E-01	6,63E-02	9,26E-03	3,52E-02	1,19E-02
062C_A_9	2,52E-01	2,94E-03	4,53E+01	8,16E+00	2,18E-02	5,38E+00	1,26E+00	6,60E-03	1,28E+00	9,97E-01	6,13E-02	2,45E-03	3,42E-02	4,74E-03
079c_A_1	1,00E+02	6,12E-03	2,05E+01	4,18E+00	8,67E-03	1,19E+02	2,55E+01	3,63E-03	5,19E+01	1,09E+01	4,07E-02	4,41E-02	5,64E-02	1,21E-02
079c_A_3	2,97E+00	8,64E-03	2,29E+01	5,66E+00	1,93E-02	1,11E+02	3,41E+01	9,38E-03	5,68E+01	2,71E+01	1,08E-01	n.d.	n.d.	n.d.
079c_A_4	3,06E-01	3,49E-03	1,98E+01	4,58E+00	2,82E-02	1,13E+02	3,57E+01	9,81E-03	5,52E+01	2,21E+01	1,16E-01	6,51E-02	9,26E-02	2,25E-02
080c1_A_1	4,92E-02	2,90E-03	2,32E+01	2,87E+00	9,02E-03	8,68E+01	1,23E+01	5,80E-03	3,45E+01	4,59E+00	3,02E-02	2,83E-02	2,62E-02	8,80E-03
080c1_A_10	3,13E+01	3,57E-03	3,53E+02	1,24E+02	6,56E-03	2,75E+02	7,24E+01	3,74E-03	4,75E+01	1,05E+01	3,31E-02	2,93E-01	1,29E-01	9,26E-03
080c1_A_11	1,35E+01	7,77E-04	5,82E+01	4,07E+01	6,93E-03	1,12E+02	2,37E+01	2,33E-03	3,78E+01	6,79E+00	4,43E-02	6,14E-02	5,61E-02	7,41E-03
080c1_A_12	2,09E+01	6,72E-04	7,64E+01	6,00E+01	5,10E-03	1,18E+02	3,09E+01	2,79E-03	3,73E+01	8,15E+00	4,17E-02	8,77E-02	6,00E-02	8,00E-03
080c1_A_13	1,27E-01	2,58E-04	3,14E+01	1,00E+01	1,03E-02	1,09E+02	4,19E+01	3,11E-03	3,36E+01	1,44E+01	5,67E-02	6,92E-02	5,92E-02	8,67E-03
080c1_A_14	1,70E-01	4,28E-04	2,43E+01	2,48E+00	8,89E-03	9,51E+01	2,41E+01	3,62E-03	3,35E+01	1,00E+01	4,38E-02	5,01E-02	5,93E-02	8,27E-03
080c1_A_15	2,07E-01	1,49E-03	2,96E+01	6,79E+00	8,27E-03	9,49E+01	2,20E+01	2,40E-03	3,46E+01	6,29E+00	4,86E-02	6,56E-02	1,17E-01	8,51E-03
080c1_A_16	1,37E+01	3,35E-03	5,79E+02	1,19E+02	7,99E-03	3,26E+02	5,60E+01	1,14E-03	5,18E+01	1,38E+01	4,13E-02	3,01E-01	5,88E-02	1,09E-02
080c1_A_17	2,42E+01	2,41E-03	5,20E+03	3,56E+03	7,41E-03	2,87E+02	5,45E+01	2,37E-03	4,78E+01	3,58E+00	3,48E-02	5,94E-01	3,46E-01	7,71E-03
080c1_A_18	4,45E+01	5,61E-03	3,84E+02	2,07E+02	1,07E-02	2,30E+02	8,49E+01	3,80E-03	4,35E+01	1,08E+01	7,27E-02	1,87E-01	5,60E-02	1,39E-02
080c1_A_19	2,19E+01	7,35E-03	4,93E+02	1,79E+02	8,03E-03	2,61E+02	5,13E+01	3,47E-03	4,33E+01	1,12E+01	4,33E-02	2,57E-01	8,78E-02	8,19E-03
080c1_A_2	1,11E-01	2,46E-03	2,83E+01	4,64E+00	8,32E-03	8,97E+01	2,17E+01	3,08E-03	3,53E+01	1,19E+01	3,28E-02	4,88E-02	4,52E-02	9,39E-03
080c1_A_21	2,67E+00	3,86E-03	2,34E+01	7,15E+00	1,43E-02	5,81E+01	1,23E+01	4,03E-03	2,62E+01	7,57E+00	6,31E-02	1,05E-02	4,25E-02	3,73E-03
080c1_A_22	1,48E+00	1,02E-03	1,85E+01	5,55E+00	1,05E-02	5,60E+01	1,41E+01	7,54E-03	2,61E+01	7,17E+00	7,48E-02	1,46E-02	4,77E-02	5,76E-03
080c1_A_3	1,36E-01	2,17E-03	2,19E+01	1,85E+00	4,22E-03	8,99E+01	1,27E+01	3,13E-03	3,48E+01	9,61E+00	3,27E-02	3,21E-02	3,62E-02	6,99E-03
080c1_A_4	8,85E+01	4,57E-03	5,08E+02	3,14E+01	5,80E-03	2,80E+02	3,00E+01	4,28E-03	4,46E+01	1,19E+01	3,99E-02	3,12E-01	1,35E-01	8,43E-03
080c1_A_5	1,59E+01	3,08E-03	2,11E+02	4,49E+01	6,84E-03	1,76E+02	2,25E+01	4,35E-03	4,12E+01	7,71E+00	4,16E-02	1,68E-01	6,52E-02	1,33E-02
080c1_A_6	5,02E+00	2,02E-03	8,46E+01	3,09E+01	1,26E-02	1,39E+02	4,33E+01	5,75E-03	4,48E+01	3,20E+01	7,36E-02	1,01E-01	1,67E-01	1,64E-02
080c1_A_7	1,56E+01	3,46E-03	5,74E+01	5,26E+01	1,10E-02	1,08E+02	6,21E+01	4,02E-03	3,64E+01	1,42E+01	4,08E-02	7,59E-02	5,73E-02	8,01E-03
080c1_A_8	2,98E+02	3,45E-03	2,62E+02	7,30E+01	1,17E-02	2,44E+02	7,81E+01	3,61E-03	4,82E+01	7,12E+00	3,95E-02	1,90E-01	4,86E-02	1,05E-02
080c1_A_9	1,10E+02	5,31E-03	3,09E+02	1,23E+02	1,02E-02	2,45E+02	9,56E+01	5,09E-03	4,67E+01	1,41E+01	5,64E-02	2,20E-01	1,49E-01	1,29E-02
080c2_B_1	1,26E+00	4,98E-03	6,02E+01	1,22E+01	1,50E-02	9,88E+00	2,24E+00	7,65E-03	4,53E+00	2,51E+00	8,65E-02	6,25E-02	4,95E-02	1,51E-02
080c2_B_10	7,21E-01	5,47E-03	4,80E+01	1,83E+01	1,39E-02	6,43E+00	2,06E+00	8,22E-03	3,94E+00	1,84E+00	7,60E-02	3,20E-02	5,35E-02	9,96E-03
080c2_B_11	7,58E-01	1,17E-03	5,37E+01	1,28E+01	6,81E-03	8,46E+00	1,27E+00	4,85E-03	3,46E+00	8,82E-01	6,10E-02	2,55E-02	5,16E-02	7,68E-03
080c2_B_12	7,56E-01	1,69E-03	7,70E+01	2,26E+01	1,30E-02	1,06E+01	1,11E+00	7,16E-03	5,33E+00	1,98E+00	6,35E-02	3,79E-02	9,31E-02	1,15E-02
080c2_B_13	8,05E+00	5,70E-03	5,28E+01	6,04E+00	4,75E-03	8,15E+00	7,50E-01	7,53E-03	3,39E+00	8,70E-01	9,77E-02	5,48E-02	7,96E-02	1,65E-02
080c2_B_14	4,23E-01	1,92E-03	6,98E+01	4,73E+00	1,85E-02	1,14E+01	1,89E+00	9,07E-03	3,39E+00	6,51E-01	8,08E-02	1,98E-02	5,59E-02	8,15E-03
080c2_B_15	7,09E-01	4,74E-03	6,65E+01	1,08E+01	1,11E-02	1,01E+01	1,32E+00	3,83E-03	4,30E+00	1,63E+00	5,63E-02	2,50E-01	3,92E-01	1,60E-02
080c2_B_16	2,20E+00	5,17E-03	4,97E+01	1,10E+01	1,34E-02	7,70E+00	1,73E+00	6,05E-03	3,59E+00	2,75E-01	6,41E-02	1,78E-01	7,71E-02	1,94E-02
080c2_B_17	3,46E-01	4,87E-03	5,33E+01	1,05E+01	5,48E-03	7,45E+00	1,06E+00	7,73E-03	3,03E+00	3,28E-01	8,64E-02	1,79E-02	1,83E-02	8,33E-03
080c2_B_18	5,21E-01	7,56E-03	5,46E+01	4,46E+00	2,51E-02	7,59E+00	4,63E-01	1,39E-02	3,06E+00	3,22E-01	1,21E-01	5,22E-02	1,14E-01	1,81E-02
080c2_B_19	1,60E+00	6,23E-03	6,51E+01	9,30E+00	1,58E-02	8,71E+00	1,55E+00	3,17E-03	4,20E+00	9,54E-01	8,83E-02	6,97E-02	1,57E-01	1,68E-02
080c2_B_2	6,93E-01	5,79E-03	6,27E+01	9,10E+00	1,99E-02	9,67E+00	1,08E+00	1,10E-02	5,42E+00	2,59E+00	1,03E-01	8,57E-02	1,42E-01	1,46E-02
080c2_B_20	3,21E-01	4,81E-03	4,85E+01	5,25E+00	1,63E-02	8,03E+00	1,32E+00	9,30E-03	2,70E+00	1,01E+00	7,25E-02	4,19E-03	2,95E-02	3,39E-03
080c2_B_21	4,59E-01	4,75E-03	5,81E+01	8,63E+00	1,60E-02	8,75E+00	1,31E+00	7,53E-03	3,01E+00	5,71E-01	6,86E-02	7,66E-02	1,57E-01	1,41E-02
080c2_B_22	1,95E-01	4,25E-03	5,17E+01	4,29E+00	1,62E-02	8,11E+00	2,38E-01	5,83E-03	3,13E+00	5,68E-01	7,67E-02	1,74E-02	3,55E-02	9,09E-03
080c2_B_23	3,62E-01	4,38E-03	5,40E+01	8,96E+00	2,91E-02	8,71E+00	1,60E+00	7,40E-03	2,90E+00	1,00E+00	7,58E-02	4,60E-02	7,89E-02	1,06E-02
080c2_B_24	2,25E-01	1,80E-03	4,69E+01	5,94E+00	1,75E-02	6,52E+00	9,10E-01	6,97E-03	2,68E+00	1,38E+00	5,73E-02	3,15E-02	3,34E-02	1,31E-02
080c2_B_25	3,84E-01	3,86E-03	4,35E+01	7,30E+00	1,70E-02	6,15E+00	1,37E+00	8,46E-03	2,20E+00	1,04E+00	6,12E-02	3,97E-02	1,19E-01	9,87E-03
080c2_B_4	3,76E-01	7,92E-03	5,84E+01	5,61E+00	9,40E-03	9,01E+00	6,32E-01	9,86E-03	3,78E+00	4,26E-01	8,72E-02	2,50E-02	7,54E-02	1,09E-02

Analysis	Cd111_mean	Cd111_2SD	Cd111_LOD	In113_mean	In113_2SD	In113_LOD	In115_mean	In115_2SD	In115_LOD	Sn118_mean	Sn118_2SD	Sn118_LOD	Sb121_mean
	(ppm)	(ppm)	(ppm)	(ppm)	(ppm)	(ppm)	(ppm)	(ppm)	(ppm)	(ppm)	(ppm)	(ppm)	(ppm)
002c_A_1	1,20E-01	1,81E-01	3,64E-02	1,13E-01	6,78E-02	3,36E-02	2,48E-01	8,18E-02	4,31E-03	3,72E+00	1,91E+00	3,64E-02	3,86E-01
002c_A_10	9,70E-02	1,14E-01	3,05E-02	9,54E-02	3,41E-02	1,46E-02	2,23E-01	7,05E-02	1,82E-03	3,20E+00	5,89E-01	1,84E-02	4,14E-02
002c_A_11	7,75E-02	1,10E-01	3,03E-02	9,90E-02	4,67E-02	1,36E-02	2,30E-01	9,32E-02	1,96E-03	3,35E+00	5,55E-01	2,27E-02	7,08E-02
002c_A_12	5,89E-02	6,18E-02	4,00E-02	9,61E-02	4,09E-02	3,03E-02	2,39E-01	5,77E-02	2,44E-03	3,49E+00	2,41E-01	2,14E-02	9,07E-02
002c_A_13	4,30E-02	3,40E-02	4,26E-02	1,09E-01	7,22E-02	2,31E-02	2,20E-01	7,91E-02	1,96E-03	3,24E+00	8,18E-01	2,12E-02	7,11E-03
002c_A_14	4,59E-02	6,24E-02	5,74E-02	8,40E-02	4,56E-02	1,85E-02	2,35E-01	5,97E-02	6,32E-04	3,09E+00	4,47E-01	2,13E-02	1,01E-03
002c_A_2	4,81E-02	5,91E-02	1,21E-02	9,32E-02	7,00E-02	2,51E-02	2,16E-01	6,77E-02	2,99E-03	3,17E+00	7,24E-01	2,49E-02	5,44E-02
002c_A_3	6,48E-02	2,84E-02	4,82E-02	7,73E-02	2,25E-02	3,19E-02	2,27E-01	6,05E-02	8,30E-04	3,40E+00	1,18E+00	2,04E-02	9,68E-02
002c_A_4	8,62E-02	1,35E-01	1,27E-02	8,34E-02	6,20E-02	3,03E-02	2,57E-01	5,86E-02	3,94E-03	3,15E+00	6,77E-01	2,64E-02	1,59E-01
002c_A_5	5,87E-02	7,58E-02	1,45E-02	7,59E-02	2,59E-02	4,45E-02	2,24E-01	3,03E-02	4,96E-03	3,09E+00	3,76E-01	2,41E-02	1,38E-01
002c_A_6	9,01E-02	8,33E-02	3,62E-02	9,98E-02	6,30E-02	2,95E-02	2,12E-01	4,94E-02	2,69E-03	3,07E+00	6,55E-01	1,56E-02	5,65E-02
002c_A_7	7,78E-02	7,84E-02	4,77E-02	8,19E-02	4,07E-02	2,33E-02	2,16E-01	5,11E-02	2,27E-03	3,15E+00	5,26E-01	2,31E-02	6,17E-02
002c_A_8	5,58E-02	7,90E-02	2,87E-02	9,05E-02	4,00E-02	3,83E-02	2,19E-01	7,68E-02	2,75E-03	3,13E+00	6,20E-01	2,01E-02	1,07E-02
002c_A_9	6,83E-02	7,38E-02	7,78E-03	8,99E-02	4,84E-02	2,98E-02	2,08E-01	6,09E-02	1,81E-03	3,04E+00	5,35E-01	2,31E-02	4,73E-02
062C_A_1	1,19E-01	7,88E-02	1,54E-02	1,05E-01	4,55E-02	2,88E-02	2,38E-01	1,65E-01	4,12E-03	7,56E+00	2,46E+01	6,44E-02	4,84E-02
062C_A_10	1,32E-01	1,18E-01	1,11E-02	1,23E-01	6,29E-02	1,76E-02	4,39E-01	7,02E-01	4,59E-03	2,65E+01	1,06E+02	3,28E-02	5,70E-02
062C_A_11	1,56E-01	7,68E-02	4,41E-02	1,46E-01	1,02E-01	3,84E-02	2,93E-01	6,94E-02	6,82E-03	3,42E+00	2,54E-01	1,20E-01	7,82E-02
062C_A_12	9,41E-02	9,47E-02	5,23E-02	1,12E-01	5,56E-02	2,67E-02	3,59E-01	5,47E-01	4,07E-03	1,88E+01	8,83E+01	3,68E-02	1,00E-01
062C_A_13	9,48E-02	7,21E-02	1,02E-01	1,03E-01	5,49E-02	4,07E-02	2,45E-01	1,49E-01	2,96E-03	7,40E+00	2,29E+01	4,34E-02	6,92E-02
062C_A_14	9,48E-02	8,80E-02	1,17E-02	8,36E-02	5,62E-02	1,85E-02	2,38E-01	2,92E-01	2,78E-03	1,07E+01	3,76E+01	3,36E-02	2,50E-02
062C_A_15	8,91E-02	4,67E-02	4,89E-02	9,76E-02	3,87E-02	2,10E-02	1,60E-01	2,16E-02	3,04E-03	3,42E+00	1,41E+00	5,74E-02	2,88E-02
062C_A_16	1,08E-01	6,09E-02	3,09E-02	1,18E-01	5,95E-02	1,61E-02	3,69E-01	5,75E-01	3,99E-03	2,44E+01	9,64E+01	2,62E-02	5,27E-02
062C_A_17	1,21E-01	6,00E-02	3,09E-02	1,21E-01	3,78E-02	6,31E-03	2,90E-01	4,82E-02	2,75E-03	3,42E+00	8,92E-01	5,66E-02	1,09E-01
062C_A_18	8,07E-02	6,42E-02	1,45E-02	1,02E-01	4,70E-02	2,60E-02	2,79E-01	3,35E-01	3,91E-03	1,51E+01	5,40E+01	2,58E-02	7,87E-02
062C_A_2	1,44E-01	1,01E-01	3,22E-02	1,60E-01	8,87E-02	1,50E-02	3,11E-01	5,50E-02	4,53E-03	3,22E+00	3,93E-01	1,70E-01	8,27E-02
062C_A_3	1,76E-01	1,26E-01	2,70E-02	1,44E-01	6,45E-02	1,51E-02	3,30E-01	1,11E-01	4,79E-03	4,43E+00	2,52E+00	6,68E-02	1,09E-01
062C_A_4	1,27E-01	5,68E-02	4,90E-02	1,22E-01	5,62E-02	2,45E-02	2,80E-01	6,23E-02	3,02E-03	3,93E+00	5,20E+00	6,42E-02	1,29E-02
062C_A_5	1,71E-01	3,13E-02	4,51E-02	2,01E-01	1,45E-01	1,86E-02	4,32E-01	4,09E-02	4,54E-03	3,26E+00	5,20E-01	8,87E-02	1,84E-01
062C_A_6	2,00E-01	4,52E-02	3,84E-02	2,01E-01	1,02E-01	1,69E-02	4,58E-01	7,52E-02	2,84E-03	3,54E+00	3,71E-01	6,61E-02	2,40E-01
062C_A_7	1,49E-01	1,20E-01	1,29E-02	1,49E-01	9,16E-02	1,61E-02	3,62E-01	1,07E-01	3,15E-03	3,35E+00	3,14E-01	7,77E-02	7,44E-02
062C_A_8	1,03E-01	6,84E-02	7,57E-02	9,97E-02	4,82E-02	3,31E-02	3,20E-01	4,54E-01	3,83E-03	1,84E+01	8,03E+01	4,03E-02	8,91E-02
062C_A_9	1,26E-01	4,21E-02	5,92E-02	1,36E-01	7,56E-02	2,71E-02	3,30E-01	3,24E-01	5,10E-03	1,14E+01	4,45E+01	4,29E-02	8,29E-02
079c_A_1	5,77E-02	6,06E-02	5,67E-02	9,34E-02	6,06E-02	1,41E-02	1,75E-01	3,78E-02	1,87E-03	3,30E+00	7,81E-01	2,19E-02	1,80E+00
079c_A_3	5,64E-02	8,78E-02	2,62E-01	1,33E-01	8,40E-02	7,14E-02	2,32E-01	7,12E-02	4,43E-03	5,23E+00	1,05E+00	7,03E-02	3,24E-01
079c_A_4	6,23E-02	1,03E-01	1,79E-01	1,19E-01	3,35E-02	9,79E-02	2,57E-01	5,24E-02	6,61E-03	5,56E+00	7,03E-01	6,55E-02	4,56E-01
080c1_A_1	4,45E-02	9,33E-02	2,80E-02	7,86E-02	5,08E-02	2,27E-02	1,55E-01	2,55E-02	2,70E-03	3,14E+00	3,44E-01	1,92E-02	3,73E-03
080c1_A_10	9,01E-02	1,70E-01	2,90E-02	1,42E-01	3,34E-02	1,04E-02	3,90E-01	1,29E-01	1,80E-03	5,34E+00	3,47E+00	1,67E-02	5,61E+00
080c1_A_11	5,63E-02	9,03E-02	2,29E-02	9,16E-02	5,92E-02	1,49E-02	2,36E-01	8,58E-02	1,14E-03	4,32E+00	1,66E+00	2,33E-02	7,21E-01
080c1_A_12	6,17E-02	7,60E-02	1,90E-02	9,16E-02	3,55E-02	1,28E-02	2,58E-01	1,38E-01	2,16E-03	9,02E+00	2,37E+01	1,86E-02	1,27E+00
080c1_A_13	4,88E-02	8,65E-02	3,34E-02	7,38E-02	4,60E-02	2,95E-02	1,89E-01	7,14E-02	2,03E-03	3,31E+00	7,60E-01	3,25E-02	n.d.
080c1_A_14	3,81E-02	1,00E-01	4,41E-03	5,64E-02	2,98E-02	2,21E-02	1,65E-01	4,91E-02	2,72E-03	3,28E+00	5,82E-01	2,62E-02	n.d.
080c1_A_15	7,89E-02	1,29E-01	1,76E-02	7,05E-02	2,39E-02	1,69E-02	1,70E-01	2,83E-02	1,79E-03	3,40E+00	1,18E+00	2,36E-02	6,40E-02
080c1_A_16	7,93E-02	6,69E-02	2,72E-02	2,01E-01	1,13E-01	1,02E-02	7,97E-01	1,19E-01	1,15E-03	4,96E+00	3,04E-01	1,58E-02	9,07E+00
080c1_A_17	9,66E-02	1,14E-01	1,89E-02	3,00E-01	5,06E-02	1,08E-02	9,92E-01	1,82E-01	1,52E-03	5,51E+00	6,18E-01	1,85E-02	9,99E+00
080c1_A_18	9,38E-02	9,95E-02	2,31E-02	2,27E-01	8,30E-02	1,82E-02	8,41E-01	1,82E-01	2,63E-03	1,01E+01	1,13E+01	3,33E-02	6,68E+00
080c1_A_19	3,43E-02	7,91E-02	1,72E-02	1,96E-01	9,46E-02	8,28E-03	6,42E-01	2,31E-01	1,21E-03	4,31E+00	7,62E-01	1,70E-02	8,07E+00
080c1_A_2	5,81E-02	8,57E-02	2,25E-02	7,03E-02	2,73E-02	1,94E-02	1,52E-01	2,29E-02	4,93E-03	3,10E+00	7,31E-01	1,97E-02	n.d.
080c1_A_21	n.d.	n.d.	n.d.	1,02E-01	6,82E-02	2,51E-02	2,27E-01	5,58E-02	3,80E-03	4,59E+00	1,66E+00	5,17E-02	2,68E-02
080c1_A_22	2,55E-02	1,40E-01	2,24E-02	1,49E-01	9,29E-02	2,24E-02	2,72E-01	7,50E-02	3,31E-03	8,95E+00	8,18E+00	3,79E-02	7,76E-02
080c1_A_3	2,26E-02	5,26E-02	2,23E-02	7,97E-02	6,56E-02	8,80E-03	1,53E-01	5,33E-02	1,81E-03	3,05E+00	6,10E-01	1,70E-02	< Det. Lim
080c1_A_4	1,48E-01	8,07E-02	2,98E-02	2,84E-01	6,33E-02	9,70E-03	7,96E-01	1,70E-01	1,65E-03	5,06E+00	1,25E+00	1,72E-02	8,75E+00
080c1_A_5	7,40E-02	6,76E-02	9,60E-03	1,26E-01	4,80E-02	1,73E-02	3,69E-01	5,91E-02	2,64E-03	3,93E+00	3,02E-01	2,68E-02	2,78E+00
080c1_A_6	1,02E-01	7,95E-02	4,84E-02	1,58E-01	1,35E-01	1,93E-02	2,99E-01	9,84E-02	2,45E-03	4,84E+00	1,38E+00	5,08E-02	7,96E-01
080c1_A_7	3,31E-02	6,20E-02	4,74E-03	8,43E-02	3,76E-02	3,48E-03	1,95E-01	9,76E-02	2,08E-03	3,53E+00	1,50E+00	3,45E-02	6,68E-01
080c1_A_8	1,29E-01	8,45E-02	1,89E-02	1,12E-01	8,10E-02	1,37E-02	2,89E-01	2,98E-02	2,30E-03	3,96E+00	2,83E-01	2,03E-02	4,18E+00
080c1_A_9	2,25E-01	1,52E-01	3,82E-02	1,67E-01	8,98E-02	2,04E-02	5,30E-01	5,19E-01	3,04E-03	3,42E+01	1,04E+02	2,33E-02	5,57E+00
080c2_B_1	2,11E-01	1,07E-01	4,55E-02	2,07E-01	9,98E-02	6,89E-03	3,79E-01	1,13E-01	4,50E-03	4,84E+00	1,21E+00	5,88E-02	1,26E+00
080c2_B_10	1,79E-01	1,13E-01	4,12E-02	1,42E-01	5,59E-02	2,26E-02	2,99E-01	5,25E-02	4,23E-03	4,23E+00	3,13E-01	6,18E-02	1,59E+00
080c2_B_11	1,40E-01	1,23E-01	2,84E-02	1,73E-01	6,31E-02	4,40E-03	3,64E-01	6,60E-02	3,37E-03	4,41E+00	1,34E+00	3,74E-02	1,12E+00
080c2_B_12	1,84E-01	7,96E-02	1,20E-02	2,32E-01	3,65E-02	1,97E-02	4,12E-01	3,69E-02	4,16E-03	5,35E+00	1,77E+00	4,32E-02	1,77E+00
080c2_B_13	1,50E-01	8,62E-02	4,59E-02	1,62E-01	1,06E-01	2,70E-02	3,95E-01	2,48E-02	6,30E-03	4,68E+00	6,39E-01	6,82E-02	1,39E+00
080c2_B_14	1,40E-01	1,75E-01	4,07E-02	1,95E-01	7,58E-02	2,60E-02	4,25E-01	4,94E-02	1,22E-03	5,56E+00	9,37E-01	5,25E-02	1,59E+00
080c2_B_15	1,40E-01	8,89E-02	3,93E-02	1,77E-01	5,95E-02	2,17E-02	4,19E-01	1,43E-01	3,99E-03	4,79E+00	1,03E+00	4,44E-02	1,59E+00
080c2_B_16	1,14E-01	7,82E-02	5,01E-02	1,86E-01	1,05E-01	7,66E-03	4,24E-01	8,71E-02	4,69E-03	4,89E+00	7,78E-01	5,44E-02	1,44E+00
080c2_B_17	9,84E-02	1,87E-02	6,13E-02	1,93E-01	1,28E-01	2,20E-02	3,80E-01	4,99E-02	5,57E-03	3,98E+00	1,98E-01	6,68E-02	1,42E+00
080c2_B_18	1,88E-01	3,90E-02	3,55E-02	1,58E-01	4,08E-02	3,87E-02	3,84E-01	6,42E-03	7,34E-03	4,76E+00	2,35E-01	2,27E-01	1,58E+00
080c2_B_19	1,21E-01	1,47E-01	5,61E-02	1,54E-01	7,77E-02	2,11E-02	4,02E-01	9,30E-02	5,80E-03	4,32E+00	6,03E-01	6,59E-02	1,83E+00
080c2_B_2	1,90E-01	1,37E-01	4,66E-02	2,37E-01	1,37E-01	2,37E-02	3,77E-01	1,37E-01	5,13E-03	5,12E+00	1,54E+00	6,82E-02	1,97E+00
080c2_B_20	8,78E-02	2,95E-02	4,44E-02	1,42E-01	8,96E-02	2,94E-02	3,53E-01	2,30E-02	3,02E-03	3,96E+00	2,71E-01	6,31E-02	1,05E+00
080c2_B_21	1,57E-01	2,12E-02	3,02E-02	1,61E-01	9,53E-02	2,40E-02	3,41E-01	4,24E-02	5,37E-03	4,11E+00	4,01E-01	5,97E-02	1,90E+00
080c2_B_22	1,63E-01	1,05E-02	4,23E-02	1,31E-01	4,19E-02	1,04E-02	3,36E-01	4,50E-02	5,37E-03	4,27E+00	3,68E-01	5,76E-02	1,51E+00
080c2_B_23	1,67E-01	1,79E-01	1,39E-02	1,81E-01	1,46E-01	1,89E-02	3,66E-01	4,57E-02	5,21E-03	4,49E+00	6,40E-01	5,51E-02	1,48E+00
080c2_B_24	1,11E-01	4,59E-02	1,79E-02	1,32E-01	8,92E-02	2,18E-02	3,30E-01	4,83E-02	3,80E-03	4,13E+00	1,18E-01	5,73E-02	3,08E+00
080c2_B_25	8,50E-02	4,35E-02	4,54E-02	9,25E-02	7,17E-02	1,94E-02	2,51E-01	4,96E-02	3,64E-03	3,48E+00	1,58E-01	4,89E-02	1,51E+00
080c2_B_4	2,16E-01	2,01E-01	1,31E-02	2,09E-01	8,50E-02	2,02E-02	4,31E-01	2,74E-02	6,07E-03	5,41E+00	6,49E-01	6,47E-02	8,15E+00

Analysis	Sb121_2SD	Sb121_LOD	Cs133_mean	Cs133_2SD	Cs133_LOD	Ba137_mean	Ba137_2SD	Ba137_LOD	La139_mean	La139_2SD	La139_LOD	Ce140_mean	Ce140_2SD
	(ppm)	(ppm)	(ppm)	(ppm)	(ppm)	(ppm)	(ppm)	(ppm)	(ppm)	(ppm)	(ppm)	(ppm)	(ppm)
002c_A_1	4,70E-01	3,09E-02	1,93E-02	1,95E-02	6,85E-03	1,05E+01	2,82E+01	8,04E-02	3,17E+01	6,41E+01	1,32E-03	7,74E+01	1,72E+02
002c_A_10	1,31E-01	1,78E-02	5,50E-03	4,10E-02	5,53E-03	2,48E+00	8,21E-01	2,60E-01	1,12E-01	3,22E-02	4,20E-02	1,21E-01	4,60E-02
002c_A_11	1,70E-01	1,45E-02	1,40E-02	4,16E-02	6,12E-03	4,87E+00	8,44E+00	6,11E-02	2,76E-01	5,14E-01	9,34E-03	4,36E-01	9,81E-01
002c_A_12	6,00E-02	1,81E-02	n.d.	n.d.	n.d.	2,99E+00	8,83E-01	1,61E-01	1,21E-01	2,53E-02	5,53E-02	1,34E-01	6,71E-02
002c_A_13	5,98E-02	5,80E-03	n.d.	n.d.	n.d.	2,25E+00	4,61E-01	7,72E-01	1,93E-01	2,87E-01	1,08E-02	3,99E-01	8,95E-01
002c_A_14	4,88E-02	9,45E-04	< Det. Lim	7,20E-03	8,44E-02	2,24E+00	3,95E-01	6,82E-01	1,05E-01	2,03E-02	2,93E-02	1,12E-01	2,18E-02
002c_A_2	6,82E-02	2,07E-02	3,97E-03	1,51E-02	3,71E-03	3,19E+00	1,21E+00	9,65E-02	2,05E+01	2,57E+01	3,79E-03	5,18E+01	6,24E+01
002c_A_3	1,33E-01	2,56E-02	1,59E-03	1,02E-02	3,17E-03	2,58E+00	8,30E-01	1,55E-01	1,42E+01	2,31E+01	4,14E-03	3,90E+01	6,38E+01
002c_A_4	2,95E-01	1,91E-02	6,99E-03	1,67E-02	4,62E-03	2,79E+00	9,15E-01	4,52E-02	1,56E-01	8,19E-02	1,28E-02	4,69E-01	4,89E-01
002c_A_5	2,20E-01	2,33E-02	8,41E-03	1,20E-02	3,55E-03	3,13E+00	2,78E+00	1,37E-01	1,36E-01	1,46E-01	4,91E-03	1,87E-01	3,47E-01
002c_A_6	9,35E-02	1,78E-02	1,68E-03	1,02E-02	2,08E-03	2,42E+00	7,31E-01	4,68E-02	7,69E-01	1,99E+00	8,03E-03	1,74E+00	4,53E+00
002c_A_7	1,34E-01	2,98E-02	2,64E-03	1,15E-02	3,59E-03	2,64E+00	1,73E+00	3,43E-02	1,23E-01	4,22E-02	2,20E-02	1,37E-01	2,90E-02
002c_A_8	6,76E-02	7,01E-03	3,32E-03	8,70E-03	3,18E-03	2,18E+00	5,20E-01	5,09E-01	1,13E-01	2,04E-02	2,63E-02	1,22E-01	3,34E-02
002c_A_9	9,20E-02	1,62E-02	3,83E-03	9,55E-03	3,16E-03	2,41E+00	1,03E+00	3,84E-01	1,30E-01	5,82E-02	1,96E-02	1,61E-01	8,80E-02
062C_A_1	7,91E-02	3,51E-02	4,60E-02	4,92E-02	8,65E-03	7,97E+00	4,44E+00	1,18E-01	3,35E-01	1,64E-01	2,76E-03	8,57E-01	4,27E-01
062C_A_10	8,39E-02	2,02E-02	6,59E-02	5,85E-02	6,70E-03	5,24E+00	3,51E+00	2,33E-01	2,59E-01	1,27E-01	7,93E-03	6,09E-01	2,10E-01
062C_A_11	9,21E-02	2,86E-02	3,36E-02	1,21E-02	1,19E-02	1,60E+01	1,38E+01	3,31E-02	5,89E-01	1,97E-01	1,15E-02	1,30E+00	3,92E-01
062C_A_12	1,07E-01	2,63E-02	4,92E-02	3,11E-02	9,25E-03	7,62E+00	3,95E+00	1,55E-01	4,64E-01	1,65E-01	7,66E-03	9,85E-01	2,76E-01
062C_A_13	1,18E-01	1,89E-02	8,00E-02	9,08E-02	7,83E-03	3,14E+01	3,28E+01	4,32E-02	1,71E+00	1,77E+00	4,73E-03	3,43E+00	3,11E+00
062C_A_14	1,06E-01	1,43E-02	1,03E-02	2,22E-02	5,79E-03	4,72E+00	2,21E+00	2,23E-01	2,22E-01	1,30E-01	2,67E-03	5,32E-01	2,94E-01
062C_A_15	1,61E-01	1,20E-02	4,37E-03	1,11E-02	8,09E-03	3,81E+00	8,27E-01	8,62E-01	1,39E-01	5,57E-02	4,75E-02	3,71E-01	1,21E-01
062C_A_16	3,32E-02	1,60E-02	3,15E-02	2,67E-02	8,13E-03	6,13E+00	3,57E+00	8,77E-02	3,81E-01	2,25E-01	1,27E-02	8,11E-01	3,57E-01
062C_A_17	7,78E-02	1,90E-02	5,92E-02	4,05E-02	8,59E-03	6,58E+00	4,35E+00	1,07E-01	4,83E-01	1,69E-01	1,07E-02	1,08E+00	2,57E-01
062C_A_18	1,35E-01	1,62E-02	2,68E-02	2,50E-02	6,03E-03	6,87E+00	2,80E+00	2,52E-02	3,53E-01	1,97E-01	8,69E-03	8,44E-01	4,11E-01
062C_A_2	8,14E-02	2,31E-02	1,28E-01	7,95E-02	7,90E-03	2,00E+01	1,24E+01	8,51E-02	7,91E-01	4,75E-01	9,50E-03	1,96E+00	1,16E+00
062C_A_3	1,16E-01	3,08E-02	1,04E-01	5,90E-02	1,15E-02	6,52E+00	3,30E+00	2,09E-01	3,58E-01	1,00E-01	2,35E-03	8,73E-01	1,13E-01
062C_A_4	4,15E-02	1,91E-02	3,13E-03	7,63E-03	7,72E-03	4,13E+00	1,01E+00	6,90E-01	1,42E-01	2,22E-02	1,09E-02	4,06E-01	5,95E-02
062C_A_5	1,16E-01	2,95E-02	2,06E-01	1,10E-01	9,61E-03	3,11E+01	4,57E+01	1,09E-01	1,95E+00	2,55E+00	1,10E-02	4,03E+00	4,73E+00
062C_A_6	2,57E-01	2,21E-02	2,44E-01	9,31E-02	6,17E-03	9,63E+00	3,27E+00	8,95E-02	7,82E-01	1,62E-01	6,89E-03	1,68E+00	2,33E-01
062C_A_7	1,03E-01	1,87E-02	1,03E-01	5,40E-02	9,03E-03	8,82E+00	3,70E+00	2,91E-02	6,40E-01	3,01E-01	6,03E-03	1,61E+00	7,53E-01
062C_A_8	1,12E-01	2,60E-02	4,11E-02	4,13E-02	9,63E-03	6,15E+00	4,32E+00	1,94E-01	3,16E-01	2,44E-01	1,06E-02	7,15E-01	3,74E-01
062C_A_9	1,33E-01	2,00E-02	6,48E-02	7,76E-02	9,10E-03	6,62E+00	1,91E+00	1,53E-01	3,68E-01	1,44E-01	8,45E-03	9,65E-01	3,32E-01
079c_A_1	1,42E+00	2,38E-02	8,89E-02	4,69E-02	7,28E-03	1,21E+01	7,75E+00	4,34E-02	5,94E+01	1,07E+02	3,69E-03	1,39E+02	2,52E+02
079c_A_3	3,70E-01	3,69E-02	5,93E-02	5,67E-02	1,23E-02	1,17E+01	4,22E+00	1,59E-01	1,70E+00	2,58E+00	1,33E-02	3,54E+00	7,78E+00
079c_A_4	6,73E-01	5,26E-02	1,25E-02	1,84E-02	8,91E-03	5,91E+00	1,51E+00	9,62E-02	6,26E-01	2,80E-01	1,46E-02	1,05E+00	5,38E-01
080c1_A_1	6,87E-02	4,18E-03	2,80E-03	9,37E-03	3,04E-03	2,99E+00	3,11E-01	2,95E-01	2,06E-01	3,12E-02	1,43E-02	3,08E-01	8,53E-02
080c1_A_10	1,54E+00	1,52E-02	1,55E+00	5,16E-01	3,22E-03	7,70E+01	1,21E+01	2,95E-02	4,12E+01	1,92E+01	2,52E-03	7,97E+01	2,95E+01
080c1_A_11	8,93E-01	1,89E-02	1,61E-01	1,66E-01	2,82E-03	8,94E+00	8,66E+00	9,00E-03	7,41E+00	7,92E+00	5,24E-03	1,69E+01	1,79E+01
080c1_A_12	1,09E+00	1,56E-02	3,47E-01	2,32E-01	4,04E-03	1,39E+01	1,39E+01	3,23E-02	6,83E+00	9,15E+00	3,33E-03	1,82E+01	2,57E+01
080c1_A_13	n.d.	n.d.	8,28E-03	1,45E-02	4,64E-03	2,91E+00	1,01E+00	1,75E-01	1,14E-01	2,91E-02	3,20E-02	2,80E-01	3,63E-01
080c1_A_14	n.d.	n.d.	6,23E-03	8,31E-03	4,12E-03	4,51E+00	5,20E-01	4,72E-02	3,13E-01	7,80E-02	6,26E-03	4,89E-01	1,42E-01
080c1_A_15	2,80E-01	1,06E-02	1,17E-02	9,45E-03	3,99E-03	6,05E+00	1,28E+00	4,46E-02	2,82E-01	1,26E-01	3,23E-03	1,34E+00	1,06E+00
080c1_A_16	8,29E-01	1,67E-02	1,80E+00	3,80E-01	3,18E-03	6,90E+01	3,07E+00	3,27E-02	7,39E+01	1,29E+01	1,09E-03	1,44E+02	2,01E+01
080c1_A_17	9,55E-01	1,79E-02	1,80E+00	3,24E-01	5,08E-03	6,53E+01	9,93E+00	3,22E-02	7,88E+01	2,02E+01	3,42E-03	1,47E+02	3,79E+01
080c1_A_18	2,56E+00	2,47E-02	9,91E-01	2,15E-01	4,42E-03	6,44E+01	3,33E+01	5,28E-02	4,98E+01	4,00E+01	1,37E-03	1,55E+02	9,62E+01
080c1_A_19	1,48E+00	1,60E-02	1,47E+00	4,31E-01	4,39E-03	5,40E+01	1,31E+01	7,95E-03	6,23E+01	2,07E+01	3,72E-03	1,20E+02	4,22E+01
080c1_A_2	n.d.	n.d.	6,34E-03	1,66E-02	3,88E-03	2,69E+00	5,15E-01	6,27E-01	1,60E-01	2,89E-02	4,75E-02	2,24E-01	4,16E-02
080c1_A_21	1,26E-01	9,10E-03	9,73E-03	3,54E-02	6,04E-03	3,22E+00	1,36E+00	1,84E-01	3,67E+00	4,07E+00	4,07E-03	8,29E+00	8,88E+00
080c1_A_22	1,66E-01	1,77E-02	3,16E-03	1,23E-02	5,21E-03	3,32E+00	2,75E+00	4,65E-02	2,38E-01	2,33E-01	8,30E-03	8,41E-01	7,97E-01
080c1_A_3	4,16E-02	1,01E+00	5,28E-03	9,34E-03	3,33E-03	2,48E+00	4,47E-01	1,04E+00	1,51E-01	3,33E-02	1,00E-02	2,06E-01	5,29E-02
080c1_A_4	2,86E+00	2,08E-02	1,19E+00	3,66E-01	6,39E-03	5,87E+01	9,87E+00	4,26E-02	1,04E+02	9,56E+01	4,96E-03	2,23E+02	2,39E+02
080c1_A_5	1,92E-01	2,05E-02	7,63E-01	1,10E-01	6,58E-03	4,01E+01	1,05E+01	2,95E-02	2,09E+01	4,25E+00	3,80E-03	4,22E+01	1,25E+01
080c1_A_6	3,59E-01	3,41E-02	2,64E-01	4,89E-01	8,90E-03	2,73E+01	2,08E+01	6,50E-02	6,45E+00	2,71E+00	2,07E-03	2,93E+01	1,25E+01
080c1_A_7	1,18E+00	1,88E-02	1,83E-01	2,54E-01	5,63E-03	9,81E+00	1,10E+01	4,85E-02	8,10E+00	7,94E+00	3,61E-03	1,91E+01	2,04E+01
080c1_A_8	6,78E-01	1,98E-02	1,23E+00	1,60E-01	5,66E-03	6,45E+01	2,53E+01	4,17E-02	2,52E+02	2,91E+02	4,52E-03	5,86E+02	7,34E+02
080c1_A_9	1,01E+00	2,43E-02	1,49E+00	4,53E-01	5,65E-03	6,80E+01	3,42E+01	4,31E-02	1,65E+02	7,61E+01	5,36E-03	3,48E+02	2,18E+02
080c2_B_1	3,33E-01	2,71E-02	1,57E-01	7,01E-02	8,09E-03	1,16E+01	3,91E+00	6,83E-02	1,73E+00	7,24E-01	2,28E-03	4,13E+00	2,00E+00
080c2_B_10	4,57E-01	2,54E-02	2,60E-01	8,23E-02	6,44E-03	2,08E+01	3,62E+01	9,14E-02	2,12E+00	7,50E-01	5,05E-03	4,65E+00	1,85E+00
080c2_B_11	3,41E-01	2,17E-02	1,69E-01	9,41E-02	6,88E-03	8,40E+00	3,00E+00	1,80E-02	1,25E+00	5,90E-01	4,55E-03	2,99E+00	1,28E+00
080c2_B_12	3,02E-01	3,02E-02	2,28E-01	6,86E-02	6,53E-03	1,29E+01	2,83E+00	7,05E-02	2,04E+00	6,59E-01	5,23E-03	4,65E+00	1,34E+00
080c2_B_13	3,84E-01	2,79E-02	2,05E-01	6,88E-02	6,55E-03	2,52E+01	3,19E+01	7,53E-02	4,53E+00	1,19E+00	7,42E-03	8,94E+00	8,72E+00
080c2_B_14	4,07E-01	3,53E-02	2,35E-01	5,94E-02	8,10E-03	7,68E+00	2,14E+00	1,73E-01	1,01E+00	8,82E-02	7,26E-03	2,43E+00	3,19E-01
080c2_B_15	6,48E-01	1,72E-02	1,95E-01	8,56E-02	7,16E-03	9,51E+00	2,22E+00	8,77E-02	1,41E+00	3,43E-01	6,51E-03	3,35E+00	1,18E+00
080c2_B_16	2,58E-01	1,87E-02	2,72E-01	6,17E-02	9,25E-03	3,18E+01	8,29E+01	2,36E-02	2,44E+00	4,23E+00	2,39E-03	5,66E+00	7,83E+00
080c2_B_17	2,88E-01	2,57E-02	1,76E-01	3,81E-02	8,68E-03	1,02E+01	1,58E+00	8,31E-02	2,45E+00	2,40E+00	5,80E-03	4,08E+00	1,74E+00
080c2_B_18	6,95E-01	5,25E-02	2,79E-01	1,32E-01	1,24E-02	1,30E+01	4,98E-01	1,22E-01	2,05E+00	1,37E+00	1,10E-02	9,47E+00	1,07E+01
080c2_B_19	1,59E-01	3,53E-02	1,90E-01	5,18E-02	6,68E-03	1,40E+01	3,03E+00	9,15E-02	4,55E+00	4,13E+00	6,74E-03	8,50E+00	4,56E+00
080c2_B_2	5,66E-01	2,88E-02	2,54E-01	1,56E-01	9,15E-03	1,89E+01	5,56E+00	1,20E-01	6,28E+00	3,17E+00	1,01E-02	1,03E+01	5,46E+00
080c2_B_20	1,66E-01	2,54E-02	1,75E-01	6,87E-02	8,98E-03	7,50E+00	1,07E+00	1,31E-01	7,82E-01	1,23E-01	7,89E-03	2,05E+00	4,26E-02
080c2_B_21	4,88E-01	2,46E-02	2,20E-01	5,66E-02	6,40E-03	1,13E+01	6,41E+00	6,75E-02	1,48E+00	4,83E-01	4,70E-03	3,23E+00	7,60E-01
080c2_B_22	1,03E-01	2,68E-02	1,50E-01	6,14E-02	8,56E-03	9,44E+00	1,54E+00	3,72E-02	1,30E+00	4,72E-01	3,00E-03	2,73E+00	4,46E-01
080c2_B_23	5,82E-01	2,33E-02	1,77E-01	7,35E-02	9,18E-03	1,07E+01	3,07E+00	7,86E-02	1,17E+00	5,89E-01	6,94E-03	2,55E+00	7,42E-01
080c2_B_24	1,59E-01	3,87E-02	2,01E-01	8,36E-02	8,08E-03	1,78E+01	1,62E+01	2,72E-02	1,05E+00	3,07E-01	7,00E-03	2,15E+00	3,07E-01
080c2_B_25	4,77E-01	2,97E-02	1,36E-01	7,62E-02	7,64E-03	5,72E+00	1,14E+00	1,26E-01	7,79E-01	2,48E-01	2,35E-03	2,05E+00	9,77E-01
080c2_B_4	3,06E+01	3,86E-02	2,27E-01	5,60E-02	7,46E-03	1,02E+01	7,95E+00	1,06E-01	1,23E+00	9,05E-02	7,91E-03	2,63E+00	4,33E-01

Analysis	Ce140_LOD	Pr141_mean	Pr141_2SD	Pr141_LOD	Nd146_mean	Nd146_2SD	Nd146_LOD	Sm147_mean	Sm147_2SD	Sm147_LOD	Eu151_mean	Eu151_2SD	Eu151_LOD
	(ppm)	(ppm)	(ppm)	(ppm)	(ppm)	(ppm)	(ppm)	(ppm)	(ppm)	(ppm)	(ppm)	(ppm)	(ppm)
002c_A_1	4,82E-03	1,13E+01	2,70E+01	8,03E-04	4,91E+01	1,02E+02	1,34E-02	1,12E+01	2,42E+01	5,99E-03	1,12E+00	2,25E+00	1,87E-03
002c_A_10	1,48E-02	1,75E-02	1,10E-02	1,99E-03	3,60E-02	4,73E-02	3,94E-03	n.d.	n.d.	n.d.	n.d.	n.d.	n.d.
002c_A_11	5,46E-03	5,01E-02	1,22E-01	4,11E-03	1,63E-01	4,13E-01	1,46E-02	3,40E-03	1,03E-01	6,32E-04	n.d.	n.d.	n.d.
002c_A_12	2,06E-02	1,77E-02	1,08E-02	1,02E-02	2,27E-02	4,07E-02	6,55E-03	n.d.	n.d.	n.d.	< Det. Lim	9,97E-04	7,26E+00
002c_A_13	5,70E-03	6,22E-02	1,81E-01	8,68E-04	1,84E-01	5,16E-01	4,25E-03	1,97E-03	1,35E-01	2,86E-04	n.d.	n.d.	n.d.
002c_A_14	4,91E-02	1,49E-02	1,04E-02	3,29E-03	2,41E-02	2,75E-02	4,72E-03	n.d.	n.d.	n.d.	n.d.	n.d.	n.d.
002c_A_2	2,89E-03	6,42E+00	7,42E+00	6,77E-04	3,07E+01	3,87E+01	2,18E-02	7,16E+00	8,87E+00	5,00E-03	7,06E-01	8,84E-01	1,53E-03
002c_A_3	3,25E-03	5,03E+00	8,60E+00	2,32E-03	2,31E+01	3,82E+01	5,64E-03	4,82E+00	7,89E+00	6,80E-03	4,84E-01	7,93E-01	2,10E-03
002c_A_4	5,45E-03	3,01E-02	3,30E-02	1,48E-03	8,02E-02	8,80E-02	5,84E-03	n.d.	n.d.	n.d.	n.d.	n.d.	n.d.
002c_A_5	9,01E-03	2,24E-02	2,62E-02	7,82E-03	6,23E-02	1,84E-01	6,11E-03	n.d.	n.d.	n.d.	n.d.	n.d.	n.d.
002c_A_6	3,74E-03	2,35E-01	6,23E-01	6,68E-04	1,10E+00	2,98E+00	3,86E-03	2,15E-01	6,76E-01	3,98E-03	1,37E-02	7,35E-02	7,86E-04
002c_A_7	8,12E-03	1,95E-02	1,26E-02	4,39E-03	4,09E-02	3,60E-02	3,35E-03	n.d.	n.d.	n.d.	n.d.	n.d.	n.d.
002c_A_8	8,65E-03	1,70E-02	7,24E-03	7,17E-03	3,86E-02	6,94E-02	1,14E-02	n.d.	n.d.	n.d.	n.d.	n.d.	n.d.
002c_A_9	8,88E-03	2,08E-02	1,01E-02	1,24E-03	7,06E-02	1,17E-01	3,54E-03	n.d.	n.d.	n.d.	n.d.	n.d.	n.d.
062C_A_1	1,26E-02	8,62E-02	5,71E-02	1,58E-03	3,29E-01	1,82E-01	1,05E-02	1,46E-01	6,26E-02	1,41E-02	6,93E-02	2,02E-02	2,33E-02
062C_A_10	2,38E-03	6,98E-02	4,05E-02	5,91E-03	2,42E-01	1,86E-01	8,62E-03	8,83E-02	8,62E-02	1,58E-02	3,57E-02	1,07E-02	4,54E-02
062C_A_11	8,39E-03	1,56E-01	5,89E-02	2,06E-03	5,92E-01	2,43E-01	1,20E-02	2,06E-01	1,70E-01	1,62E-02	8,57E-02	6,08E-02	1,39E-02
062C_A_12	7,76E-03	1,04E-01	1,97E-02	5,13E-03	4,22E-01	2,14E-01	7,63E-03	1,65E-01	1,60E-01	1,07E-02	5,09E-02	2,19E-02	5,60E-03
062C_A_13	5,63E-03	4,36E-01	4,46E-01	9,73E-04	1,61E+00	1,77E+00	5,89E-03	4,39E-01	3,67E-01	7,55E-03	1,09E-01	7,27E-02	9,93E-03
062C_A_14	1,16E-02	5,18E-02	2,84E-02	5,63E-03	1,62E-01	1,18E-01	7,86E-03	6,93E-02	7,05E-02	1,47E-02	2,82E-02	1,82E-02	1,95E-02
062C_A_15	4,49E-02	2,88E-02	7,43E-03	3,08E-02	9,06E-02	4,52E-02	1,42E-02	5,51E-02	3,27E-02	1,96E-02	3,02E-02	2,26E-02	6,96E-03
062C_A_16	1,39E-02	8,76E-02	5,24E-02	1,09E-03	3,53E-01	2,73E-01	5,75E-03	8,10E-02	7,71E-02	1,13E-02	3,22E-02	1,42E-02	6,55E-03
062C_A_17	6,12E-03	1,22E-01	4,55E-02	1,32E-03	4,27E-01	2,70E-01	7,57E-03	1,50E-01	1,03E-01	2,85E-02	4,31E-02	2,22E-02	1,38E-02
062C_A_18	6,71E-03	8,71E-02	5,14E-02	1,14E-03	3,45E-01	2,45E-01	6,00E-03	1,27E-01	9,26E-02	8,47E-03	3,72E-02	2,06E-02	4,17E-03
062C_A_2	4,84E-03	2,21E-01	1,10E-01	1,23E-03	8,46E-01	5,15E-01	2,12E-02	2,46E-01	1,89E-01	1,04E-02	1,18E-01	6,59E-02	3,56E-03
062C_A_3	9,03E-03	1,34E-01	1,88E-01	3,77E-03	3,92E-01	2,27E-01	8,23E-03	1,26E-01	5,46E-02	1,35E-02	5,23E-02	2,59E-02	7,43E-03
062C_A_4	2,88E-02	3,77E-02	1,54E-02	1,04E-02	1,42E-01	6,99E-02	6,91E-02	8,06E-02	4,94E-02	2,26E-02	4,15E-02	1,18E-02	1,22E-02
062C_A_5	4,72E-03	4,76E-01	6,45E-01	4,04E-03	1,93E+00	2,37E+00	1,33E-02	3,74E-01	4,77E-01	1,72E-02	1,72E-01	1,98E-01	1,66E-02
062C_A_6	6,73E-03	2,03E-01	5,95E-02	2,93E-03	8,14E-01	2,82E-01	7,50E-03	2,49E-01	2,11E-01	9,88E-03	6,58E-02	1,57E-02	4,52E-03
062C_A_7	4,07E-03	2,04E-01	1,56E-01	1,35E-03	9,98E-01	1,05E+00	7,99E-03	2,68E-01	4,44E-01	1,09E-02	9,55E-02	9,42E-02	3,97E-03
062C_A_8	9,43E-03	6,65E-02	4,46E-02	2,13E-03	3,36E-01	1,13E-01	2,57E-02	1,13E-01	7,08E-02	1,76E-02	4,10E-02	1,51E-02	1,67E-02
062C_A_9	9,14E-03	1,04E-01	4,17E-02	5,59E-03	3,67E-01	2,02E-01	9,28E-03	1,09E-01	5,71E-02	1,87E-02	5,19E-02	3,52E-02	8,68E-03
079c_A_1	3,27E-03	1,95E+01	3,61E+01	5,80E-04	8,30E+01	1,56E+02	1,55E-02	1,51E+01	2,77E+01	4,29E-03	8,03E-01	1,57E+00	1,32E-03
079c_A_3	4,98E-03	4,26E-01	8,42E-01	5,05E-03	1,57E+00	3,54E+00	8,04E-03	2,47E-01	8,29E-01	8,20E-03	n.d.	n.d.	n.d.
079c_A_4	5,92E-03	1,23E-01	8,90E-02	1,54E-03	4,21E-01	4,33E-01	3,52E-02	5,69E-02	1,68E-01	4,72E-03	n.d.	n.d.	n.d.
080c1_A_1	8,18E-03	2,22E-02	1,71E-02	1,15E-03	4,62E-02	6,59E-02	4,35E-03	1,64E-02	2,99E-02	3,11E-02	n.d.	n.d.	n.d.
080c1_A_10	2,80E-03	1,30E+01	7,98E+00	5,25E-04	4,95E+01	2,79E+01	3,24E-03	1,26E+01	6,78E+00	3,82E-03	3,05E-01	1,45E-01	1,22E-03
080c1_A_11	5,43E-04	2,38E+00	2,44E+00	4,86E-04	9,40E+00	9,63E+00	2,98E-03	2,10E+00	2,23E+00	3,53E-03	7,72E-02	6,45E-02	3,48E-03
080c1_A_12	1,87E-03	2,21E+00	2,98E+00	4,09E-04	9,08E+00	1,19E+01	2,52E-03	2,24E+00	2,73E+00	2,99E-03	4,87E-02	7,32E-02	8,61E-04
080c1_A_13	8,56E-03	7,28E-03	1,20E-02	1,55E-03	2,60E-02	2,13E-01	1,57E-03	2,60E-02	4,97E-02	7,28E-03	n.d.	n.d.	n.d.
080c1_A_14	8,38E-04	4,57E-02	2,73E-02	2,08E-03	1,26E-01	1,10E-01	2,60E-03	4,86E-02	4,32E-02	4,90E-03	1,88E-03	1,43E-02	2,89E-04
080c1_A_15	2,86E-03	6,26E-02	4,05E-02	1,76E-03	1,88E-01	1,53E-01	2,44E-03	5,36E-02	6,11E-02	4,30E-03	n.d.	n.d.	n.d.
080c1_A_16	7,54E-04	2,27E+01	3,52E+00	6,78E-04	7,93E+01	1,15E+01	4,17E-03	1,72E+01	2,20E+00	1,32E-02	3,65E-01	6,44E-02	1,55E-03
080c1_A_17	6,70E-04	2,59E+01	1,08E+01	6,00E-04	9,05E+01	2,83E+01	3,70E-03	1,94E+01	5,97E+00	4,34E-03	4,16E-01	1,71E-01	1,38E-03
080c1_A_18	3,71E-03	1,58E+01	1,26E+01	2,33E-03	5,37E+01	4,07E+01	1,35E-02	1,14E+01	8,24E+00	1,50E-02	2,36E-01	2,35E-01	4,87E-03
080c1_A_19	2,18E-03	1,96E+01	6,64E+00	1,67E-03	6,80E+01	1,89E+01	3,23E-03	1,51E+01	4,74E+00	3,76E-03	3,13E-01	1,33E-01	1,19E-03
080c1_A_2	3,92E-02	1,08E-02	4,66E-03	1,96E-03	1,41E-02	3,74E-02	2,99E-03	2,02E-02	2,80E-02	7,56E-03	n.d.	n.d.	n.d.
080c1_A_21	5,26E-03	9,87E-01	1,28E+00	3,07E-03	4,14E+00	4,97E+00	5,66E-03	8,54E-01	1,14E+00	6,73E-03	4,41E-02	6,39E-02	1,95E-03
080c1_A_22	6,99E-03	6,28E-02	1,09E-01	9,02E-04	1,67E-01	2,68E-01	1,18E-02	8,25E-02	7,81E-02	9,20E-03	2,02E-04	1,08E-02	1,01E-04
080c1_A_3	3,68E-02	9,34E-03	5,17E-03	1,45E-03	8,88E-03	2,78E-02	1,56E-03	1,09E-02	1,45E-02	1,09E-02	< Det. Lim	3,83E-03	1,40E+00
080c1_A_4	2,62E-03	3,49E+01	3,88E+01	9,16E-04	1,32E+02	1,62E+02	5,67E-03	2,53E+01	2,65E+01	6,65E-03	1,18E+00	2,04E+00	2,18E-03
080c1_A_5	4,50E-03	6,67E+00	1,21E+00	2,61E-03	2,53E+01	4,60E+00	1,46E-02	6,07E+00	6,83E-01	6,67E-03	1,68E-01	8,10E-02	2,06E-03
080c1_A_6	5,92E-03	1,96E+00	9,26E-01	1,26E-03	6,73E+00	3,33E+00	1,85E-02	1,46E+00	6,07E-01	9,18E-03	6,99E-02	9,98E-02	6,69E-03
080c1_A_7	2,54E-03	2,58E+00	2,50E+00	1,86E-03	1,08E+01	1,16E+01	3,42E-03	2,44E+00	2,47E+00	4,06E-03	9,69E-02	1,46E-01	4,28E-03
080c1_A_8	4,04E-03	8,15E+01	9,61E+01	2,08E-03	3,49E+02	4,14E+02	4,54E-03	7,03E+01	8,06E+01	5,33E-03	3,85E+00	4,65E+00	1,70E-03
080c1_A_9	4,96E-03	5,28E+01	3,13E+01	2,39E-03	2,33E+02	1,76E+02	2,28E-02	4,42E+01	2,71E+01	9,00E-03	2,30E+00	1,46E+00	2,86E-03
080c2_B_1	5,40E-03	3,90E-01	1,81E-01	1,40E-03	1,42E+00	7,53E-01	2,13E-02	2,81E-01	1,57E-01	1,11E-02	4,93E-02	1,02E-02	1,19E-02
080c2_B_10	5,94E-03	5,33E-01	2,20E-01	1,29E-03	1,76E+00	6,27E-01	7,71E-03	4,16E-01	2,81E-01	9,63E-03	6,38E-02	1,77E-02	3,39E-03
080c2_B_11	2,65E-03	3,35E-01	1,62E-01	8,45E-04	1,16E+00	6,11E-01	5,02E-03	2,58E-01	2,74E-01	6,18E-03	2,89E-02	2,87E-02	2,66E-03
080c2_B_12	4,87E-03	5,13E-01	1,95E-01	1,18E-03	1,73E+00	8,35E-01	1,70E-02	4,11E-01	1,73E-01	8,74E-03	4,99E-02	3,32E-02	3,22E-03
080c2_B_13	5,67E-03	1,21E+00	1,89E+00	3,95E-03	4,13E+00	6,07E+00	9,74E-03	9,37E-01	1,50E+00	1,18E-02	1,53E-01	2,22E-01	3,84E-03
080c2_B_14	6,10E-03	2,99E-01	8,26E-02	3,78E-03	8,34E-01	4,38E-01	9,02E-03	2,56E-01	2,47E-01	1,14E-02	4,18E-02	3,60E-02	4,15E-03
080c2_B_15	5,53E-03	4,22E-01	1,72E-01	9,94E-04	1,29E+00	6,74E-01	5,87E-03	2,72E-01	1,68E-01	2,18E-02	4,27E-02	2,45E-02	2,61E-03
080c2_B_16	3,79E-03	6,48E-01	9,89E-01	1,45E-03	2,50E+00	4,66E+00	8,80E-03	4,92E-01	1,20E+00	1,09E-02	1,25E-01	2,82E-01	3,45E-03
080c2_B_17	5,40E-03	3,70E-01	1,03E-01	4,94E-03	9,80E-01	4,26E-01	1,10E-02	1,68E-01	7,41E-02	1,42E-02	4,13E-02	2,12E-02	4,79E-03
080c2_B_18	1,00E-02	5,86E-01	6,28E-01	7,54E-03	1,66E+00	1,59E+00	3,85E-02	4,15E-01	3,05E-01	2,44E-02	8,48E-02	1,51E-02	7,88E-03
080c2_B_19	5,27E-03	8,99E-01	5,22E-01	4,18E-03	3,64E+00	2,10E+00	2,85E-02	7,23E-01	5,20E-01	1,39E-02	5,82E-02	2,85E-02	4,59E-03
080c2_B_2	5,30E-03	1,01E+00	4,49E-01	1,84E-03	4,12E+00	2,70E+00	1,13E-02	7,30E-01	4,70E-01	1,38E-02	8,25E-02	7,32E-02	1,37E-02
080c2_B_20	5,41E-03	2,26E-01	4,43E-03	4,25E-03	7,44E-01	3,94E-01	1,08E-02	2,42E-01	6,97E-02	1,34E-02	1,99E-02	1,07E-02	4,97E-03
080c2_B_21	4,55E-03	4,15E-01	5,86E-02	1,39E-03	1,21E+00	4,78E-01	8,19E-03	2,84E-01	2,25E-01	1,02E-02	3,12E-02	3,25E-02	3,40E-03
080c2_B_22	6,15E-03	3,19E-01	4,78E-02	4,53E-03	9,80E-01	1,60E-01	1,05E-02	2,69E-01	2,19E-01	1,30E-02	2,24E-02	1,38E-02	4,38E-03
080c2_B_23	4,79E-03	2,69E-01	4,43E-02	1,27E-03	8,45E-01	3,56E-01	7,22E-03	2,17E-01	9,35E-02	8,98E-03	2,78E-02	4,63E-03	2,91E-03
080c2_B_24	4,12E-03	2,75E-01	6,63E-02	1,57E-03	9,14E-01	5,90E-01	8,72E-03	1,66E-01	8,71E-02	1,12E-02	4,87E-02	4,40E-02	3,50E-03
080c2_B_25	5,54E-03	2,28E-01	7,66E-02	2,81E-03	7,38E-01	3,38E-01	7,65E-03	1,48E-01	1,62E-01	9,71E-03	1,86E-02	3,18E-02	2,96E-03
080c2_B_4	6,49E-03	3,00E-01	1,07E-01	1,44E-03	9,82E-01	4,96E-01	8,58E-03	2,96E-01	1,75E-01	1,08E-02	5,06E-02	2,91E-02	4,58E-03

Analysis	Gd157_mean	Gd157_2SD	Gd157_LOD	Gd158_mean	Gd158_2SD	Gd158_LOD	Tb159_mean	Tb159_2SD	Tb159_LOD	Dy161_mean	Dy161_2SD	Dy161_LOD	Ho165_mean
	(ppm)	(ppm)	(ppm)	(ppm)	(ppm)	(ppm)	(ppm)	(ppm)	(ppm)	(ppm)	(ppm)	(ppm)	(ppm)
002c_A_1	1,10E+01	2,21E+01	2,29E-02	1,08E+01	2,21E+01	1,63E-02	1,58E+00	3,18E+00	1,06E-03	8,44E+00	1,74E+01	5,61E-03	1,66E+00
002c_A_10	8,56E-02	2,87E-02	2,10E-01	3,95E-02	3,24E-02	2,01E-01	5,75E-03	7,63E-03	8,77E-03	6,02E-03	4,09E-02	1,37E-03	2,59E-02
002c_A_11	1,41E-01	8,69E-02	6,29E-02	9,32E-02	1,23E-01	1,90E-02	1,13E-02	1,53E-02	5,30E-03	8,61E-02	1,68E-01	5,69E-03	3,66E-02
002c_A_12	9,37E-02	5,76E-02	1,59E-01	4,38E-02	2,06E-02	8,48E-02	7,96E-03	8,26E-03	2,54E-03	1,97E-02	4,51E-02	5,11E-03	2,23E-02
002c_A_13	1,32E-01	1,63E-01	7,63E-02	6,26E-02	9,75E-02	7,08E-03	1,10E-02	1,36E-02	1,41E-03	4,52E-02	9,99E-02	1,41E-02	2,71E-02
002c_A_14	8,20E-02	2,55E-02	4,84E-02	3,57E-02	2,14E-02	1,29E-01	7,52E-03	1,02E-02	1,29E-02	2,44E-02	4,85E-02	4,68E-03	2,11E-02
002c_A_2	7,71E+00	9,75E+00	2,85E-02	6,95E+00	8,18E+00	1,24E-02	1,01E+00	1,24E+00	8,76E-04	6,14E+00	7,76E+00	4,69E-03	1,10E+00
002c_A_3	5,53E+00	9,01E+00	2,83E-02	5,54E+00	9,43E+00	1,55E-02	8,04E-01	1,40E+00	4,12E-03	4,27E+00	7,55E+00	6,34E-03	8,41E-01
002c_A_4	1,18E-01	6,85E-02	8,75E-02	7,67E-02	3,28E-02	1,07E-02	7,51E-03	1,04E-02	4,84E-03	3,10E-03	3,95E-02	6,93E-04	2,33E-02
002c_A_5	8,87E-02	3,39E-02	2,21E-01	5,18E-02	2,90E-02	8,23E-02	5,29E-03	7,23E-03	2,12E-03	1,60E-02	6,27E-02	2,65E-03	2,36E-02
002c_A_6	3,44E-01	7,65E-01	3,71E-02	3,46E-01	8,48E-01	1,97E-02	4,05E-02	9,29E-02	3,06E-03	1,77E-01	4,65E-01	3,82E-03	6,39E-02
002c_A_7	1,11E-01	4,74E-02	4,69E-02	5,38E-02	3,68E-02	1,01E-02	4,78E-03	7,60E-03	1,65E-03	1,18E-02	2,63E-02	7,80E-03	2,32E-02
002c_A_8	9,97E-02	5,85E-02	9,74E-02	5,80E-02	4,51E-02	3,99E-02	7,67E-03	1,09E-02	4,15E-03	1,76E-02	5,09E-02	1,81E-03	2,15E-02
002c_A_9	1,00E-01	6,18E-02	6,91E-02	4,42E-02	2,88E-02	8,83E-02	7,01E-03	8,12E-03	1,37E-03	1,37E-02	4,31E-02	1,76E-03	2,18E-02
062C_A_1	1,51E-01	6,40E-02	1,90E-01	9,01E-02	8,41E-02	6,36E-03	1,09E-02	1,65E-02	4,72E-03	n.d.	n.d.	n.d.	n.d.
062C_A_10	9,69E-02	5,89E-02	1,07E-01	7,27E-02	4,50E-02	2,10E-02	1,09E-02	1,35E-02	1,12E-03	n.d.	n.d.	n.d.	n.d.
062C_A_11	2,15E-01	2,35E-01	1,93E-02	1,53E-01	1,42E-01	3,07E-02	2,38E-02	1,74E-02	5,11E-03	2,14E-02	1,29E-01	3,04E-03	2,11E-02
062C_A_12	1,47E-01	1,57E-01	3,42E-02	1,32E-01	1,10E-01	1,54E-02	1,31E-02	2,16E-02	1,29E-03	n.d.	n.d.	n.d.	n.d.
062C_A_13	3,79E-01	3,01E-01	4,28E-02	3,79E-01	4,45E-01	2,15E-02	7,22E-02	7,49E-02	5,39E-03	2,23E-01	5,28E-01	3,68E-03	7,21E-02
062C_A_14	8,31E-02	6,12E-02	1,01E-02	4,83E-02	8,64E-02	1,44E-02	1,05E-02	9,74E-03	3,16E-03	n.d.	n.d.	n.d.	n.d.
062C_A_15	4,87E-02	4,94E-02	7,43E-02	2,54E-02	2,91E-02	2,35E-02	3,95E-03	8,21E-03	3,12E-03	n.d.	n.d.	n.d.	n.d.
062C_A_16	7,96E-02	1,01E-01	3,90E-02	9,38E-02	8,08E-02	2,14E-02	1,05E-02	1,28E-02	1,05E-03	n.d.	n.d.	n.d.	n.d.
062C_A_17	1,69E-01	1,51E-01	3,93E-02	1,31E-01	1,48E-01	1,74E-02	2,94E-02	3,45E-02	1,43E-03	7,30E-02	1,47E-01	2,43E-03	1,42E-03
062C_A_18	1,09E-01	6,61E-02	7,50E-03	8,29E-02	8,33E-02	2,21E-02	1,53E-02	1,32E-02	4,89E-03	n.d.	n.d.	n.d.	n.d.
062C_A_2	3,68E-01	2,37E-01	4,76E-02	2,82E-01	1,43E-01	1,77E-02	4,49E-02	2,95E-02	4,01E-03	1,13E-01	1,73E-01	3,32E-03	3,04E-02
062C_A_3	1,93E-01	9,40E-02	6,10E-02	1,00E-01	1,06E-01	2,27E-02	1,47E-02	1,44E-02	1,12E-03	n.d.	n.d.	n.d.	n.d.
062C_A_4	1,59E-01	8,73E-02	9,03E-02	3,69E-02	3,55E-02	3,09E-02	5,87E-03	1,29E-02	2,57E-03	n.d.	n.d.	n.d.	n.d.
062C_A_5	5,65E-01	1,02E+00	3,73E-02	4,95E-01	7,61E-01	3,03E-02	8,18E-02	1,35E-01	6,50E-03	3,51E-01	5,17E-01	1,08E-02	7,06E-02
062C_A_6	2,85E-01	2,12E-01	4,43E-02	2,67E-01	4,12E-01	6,08E-03	2,95E-02	2,37E-02	3,78E-03	3,66E-02	1,44E-01	4,38E-03	1,83E-02
062C_A_7	3,83E-01	5,02E-01	4,72E-02	3,22E-01	5,47E-01	2,06E-02	5,66E-02	6,74E-02	5,75E-03	2,41E-01	5,34E-01	1,30E-02	5,20E-02
062C_A_8	1,65E-01	1,36E-01	1,02E-01	6,83E-02	4,11E-02	3,25E-02	1,07E-02	1,20E-02	1,44E-03	n.d.	n.d.	n.d.	n.d.
062C_A_9	1,81E-01	5,34E-02	1,62E-02	1,07E-01	6,91E-02	6,13E-03	1,83E-02	2,15E-02	5,40E-03	n.d.	n.d.	n.d.	n.d.
079c_A_1	1,30E+01	2,43E+01	1,73E-02	1,31E+01	2,40E+01	9,86E-03	1,81E+00	3,33E+00	2,94E-03	1,01E+01	1,90E+01	4,06E-03	2,01E+00
079c_A_3	3,97E-01	5,13E-01	1,04E-01	2,67E-01	4,90E-01	7,99E-03	5,97E-02	8,91E-02	1,23E-02	3,25E-01	1,07E+00	1,01E-02	8,92E-02
079c_A_4	2,43E-01	1,61E-01	8,47E-02	1,12E-01	6,25E-02	4,72E-02	2,40E-02	1,72E-02	3,28E-03	1,34E-01	1,67E-01	1,32E-02	5,59E-02
080c1_A_1	1,60E-01	4,48E-02	1,11E-01	6,95E-02	2,22E-02	6,82E-02	n.d.	n.d.	n.d.	4,31E-02	3,92E-02	8,09E-03	5,34E-03
080c1_A_10	1,38E+01	6,85E+00	2,45E-02	1,41E+01	8,34E+00	9,08E-03	2,96E+00	1,68E+00	1,77E-03	2,28E+01	1,19E+01	3,66E-03	4,97E+00
080c1_A_11	1,97E+00	1,91E+00	1,54E-02	2,04E+00	2,16E+00	9,47E-03	3,40E-01	4,25E-01	2,68E-03	2,28E+00	2,75E+00	3,35E-03	5,47E-01
080c1_A_12	2,48E+00	3,11E+00	1,84E-02	2,37E+00	2,85E+00	1,06E-02	5,53E-01	6,80E-01	2,23E-03	3,99E+00	5,16E+00	9,49E-03	8,12E-01
080c1_A_13	9,24E-02	4,42E-02	1,04E-01	4,49E-02	3,09E-02	2,60E-02	n.d.	n.d.	n.d.	n.d.	n.d.	n.d.	7,64E-03
080c1_A_14	1,22E-01	9,64E-02	3,76E-02	7,01E-02	6,96E-02	1,30E-02	2,69E-03	1,12E-02	1,43E-03	4,00E-02	7,73E-02	7,56E-03	1,32E-02
080c1_A_15	1,14E-01	9,68E-02	3,46E-02	5,89E-02	5,57E-02	2,01E-02	2,34E-03	1,21E-02	1,11E-03	3,49E-02	7,83E-02	1,61E-03	1,83E-02
080c1_A_16	1,72E+01	2,17E+00	2,56E-02	1,84E+01	2,02E+00	1,23E-02	3,86E+00	7,30E-01	3,59E-03	2,76E+01	5,11E+00	4,70E-03	5,59E+00
080c1_A_17	1,80E+01	4,94E+00	1,42E-02	1,79E+01	6,03E+00	9,19E-03	3,79E+00	1,12E+00	2,34E-03	2,83E+01	8,91E+00	4,17E-03	5,89E+00
080c1_A_18	1,05E+01	9,05E+00	2,50E-02	1,10E+01	8,25E+00	1,56E-02	2,24E+00	1,77E+00	1,09E-03	1,60E+01	1,15E+01	5,91E-03	3,26E+00
080c1_A_19	1,49E+01	4,95E+00	1,52E-02	1,48E+01	5,50E+00	1,14E-02	3,19E+00	1,31E+00	6,77E-04	2,30E+01	9,21E+00	1,08E-02	4,84E+00
080c1_A_2	1,29E-01	3,85E-02	4,25E-01	6,74E-02	3,53E-02	6,50E-02	n.d.	n.d.	n.d.	3,66E-02	3,96E-02	6,63E-03	5,99E-03
080c1_A_21	1,12E+00	2,54E+00	3,23E-02	7,52E-01	8,80E-01	1,33E-02	1,09E-01	1,38E-01	1,16E-03	6,13E-01	6,71E-01	5,76E-03	1,26E-01
080c1_A_22	1,17E-01	1,54E-01	6,37E-02	5,52E-02	6,90E-02	1,32E-02	8,27E-03	2,37E-02	2,66E-03	7,03E-03	1,11E-01	5,96E-04	1,85E-02
080c1_A_3	1,18E-01	3,82E-02	6,72E-01	5,65E-02	4,44E-02	6,90E-02	n.d.	n.d.	n.d.	3,57E-02	3,95E-02	3,94E-03	2,79E-03
080c1_A_4	2,53E+01	3,01E+01	2,31E-02	2,65E+01	2,96E+01	1,69E-02	4,67E+00	3,69E+00	1,17E-03	3,01E+01	2,05E+01	1,43E-02	6,26E+00
080c1_A_5	7,00E+00	1,06E+00	2,13E-02	7,12E+00	1,45E+00	4,91E-03	1,56E+00	5,45E-01	1,19E-03	1,12E+01	3,04E+00	6,32E-03	2,71E+00
080c1_A_6	1,71E+00	5,48E-01	3,57E-02	1,68E+00	6,52E-01	1,74E-02	3,69E-01	2,83E-01	1,63E-03	2,32E+00	9,96E-01	2,65E-02	4,98E-01
080c1_A_7	2,60E+00	2,42E+00	2,57E-02	2,55E+00	2,55E+00	8,98E-03	4,57E-01	4,78E-01	3,01E-03	3,18E+00	2,96E+00	3,85E-03	6,87E-01
080c1_A_8	6,76E+01	7,68E+01	1,89E-02	6,90E+01	7,92E+01	1,27E-02	1,03E+01	1,12E+01	9,48E-04	6,31E+01	6,39E+01	5,05E-03	1,27E+01
080c1_A_9	4,20E+01	2,36E+01	1,96E-02	4,50E+01	2,90E+01	1,27E-02	7,06E+00	4,16E+00	1,61E-03	4,38E+01	2,63E+01	2,33E-02	8,81E+00
080c2_B_1	2,83E-01	1,45E-01	4,34E-02	2,95E-01	7,71E-02	7,10E-03	6,46E-02	3,87E-02	5,18E-03	2,53E-01	2,84E-01	1,45E-02	8,93E-02
080c2_B_10	2,56E-01	1,64E-01	3,32E-02	4,03E-01	7,32E-02	2,19E-02	5,84E-02	2,95E-02	1,65E-03	3,34E-01	3,14E-01	5,88E-03	7,89E-02
080c2_B_11	1,96E-01	1,33E-01	2,10E-02	2,40E-01	1,77E-01	1,03E-02	5,63E-02	3,78E-02	2,83E-03	1,90E-01	1,73E-01	8,79E-03	5,85E-02
080c2_B_12	3,92E-01	2,13E-01	2,67E-02	3,60E-01	1,95E-01	1,53E-02	5,59E-02	3,92E-02	4,15E-03	3,57E-01	1,84E-01	5,65E-03	8,07E-02
080c2_B_13	7,97E-01	1,27E+00	2,61E-02	8,82E-01	1,40E+00	1,95E-02	1,16E-01	1,45E-01	2,06E-03	6,13E-01	7,68E-01	2,17E-02	1,29E-01
080c2_B_14	1,07E-01	1,51E-01	7,63E-03	1,80E-01	3,61E-02	7,53E-03	4,55E-02	2,05E-02	5,32E-03	1,44E-01	1,44E-01	4,79E-03	2,51E-02
080c2_B_15	2,08E-01	2,04E-01	2,27E-02	3,06E-01	1,97E-01	1,75E-02	4,82E-02	1,37E-02	3,30E-03	2,84E-01	2,37E-01	4,33E-03	6,15E-02
080c2_B_16	3,94E-01	7,64E-01	3,53E-02	4,18E-01	5,11E-01	2,61E-02	8,46E-02	8,36E-02	5,53E-03	3,87E-01	7,86E-01	7,18E-03	8,56E-02
080c2_B_17	1,20E-01	5,40E-02	1,82E-02	1,90E-01	1,77E-01	2,75E-02	5,22E-02	1,52E-02	2,41E-03	2,07E-01	1,97E-01	7,31E-03	2,74E-02
080c2_B_18	2,99E-01	3,37E-01	4,48E-02	3,64E-01	3,72E-01	3,11E-02	8,96E-02	4,03E-02	1,00E-02	3,52E-01	4,96E-01	1,49E-02	7,17E-02
080c2_B_19	6,29E-01	6,77E-01	1,38E-02	7,10E-01	6,16E-01	2,39E-02	1,12E-01	3,34E-02	4,71E-03	5,58E-01	6,73E-01	1,03E-02	1,01E-01
080c2_B_2	6,30E-01	5,62E-01	5,01E-02	6,52E-01	5,34E-01	2,77E-02	1,09E-01	9,11E-02	6,09E-03	5,61E-01	4,93E-01	9,83E-03	1,23E-01
080c2_B_20	1,43E-01	1,11E-01	1,74E-02	2,03E-01	1,63E-01	3,25E-02	3,39E-02	3,73E-02	2,47E-03	8,14E-02	3,87E-02	4,22E-03	2,30E-02
080c2_B_21	1,41E-01	2,99E-01	2,25E-02	2,33E-01	1,04E-01	1,40E-02	4,50E-02	2,58E-02	3,80E-03	7,07E-02	9,64E-02	6,65E-03	4,21E-02
080c2_B_22	1,11E-01	9,12E-02	1,99E-02	2,00E-01	1,26E-01	1,64E-02	4,40E-02	1,87E-02	2,35E-03	1,53E-01	6,64E-02	6,03E-03	2,65E-02
080c2_B_23	3,98E-02	5,54E-02	2,57E-03	1,38E-01	1,26E-01	1,95E-02	2,72E-02	1,35E-02	4,07E-03	4,98E-02	1,02E-01	1,76E-03	1,00E-02
080c2_B_24	7,95E-02	1,35E-01	1,21E-02	1,51E-01	6,11E-02	1,58E-02	3,76E-02	1,55E-02	4,66E-03	2,70E-02	9,61E-02	1,30E-03	2,19E-02
080c2_B_25	8,52E-02	7,33E-02	1,36E-02	1,41E-01	9,18E-02	1,73E-02	2,61E-02	1,25E-02	1,84E-03	n.d.	n.d.	n.d.	1,51E-02
080c2_B_4	1,84E-01	1,47E-01	4,53E-02	2,46E-01	1,48E-01	1,73E-02	3,85E-02	2,56E-02	6,78E-03	1,05E-01	8,23E-02	3,54E-03	3,30E-02

Analysis	Ho165_2SD	Ho165_LOD	Er167_mean	Er167_2SD	Er167_LOD	Tm169_mean	Tm169_2SD	Tm169_LOD	Yb172_mean	Yb172_2SD	Yb172_LOD	Lu175_mean	Lu175_2SD
	(ppm)	(ppm)	(ppm)	(ppm)	(ppm)	(ppm)	(ppm)	(ppm)	(ppm)	(ppm)	(ppm)	(ppm)	(ppm)
002c_A_1	3,43E+00	1,09E-03	4,09E+00	7,34E+00	5,13E-03	5,21E-01	1,04E+00	1,13E-03	n.d.	n.d.	n.d.	3,75E-01	8,83E-01
002c_A_10	2,23E-02	8,42E-03	4,73E-02	4,65E-02	7,38E-03	2,08E-02	1,06E-02	3,08E-03	n.d.	n.d.	n.d.	n.d.	n.d.
002c_A_11	2,73E-02	2,26E-03	1,00E-01	1,10E-01	7,47E-03	2,62E-02	2,23E-02	2,68E-03	n.d.	n.d.	n.d.	2,82E-02	5,61E-02
002c_A_12	7,85E-03	7,12E-03	5,52E-02	7,02E-02	1,15E-02	2,41E-02	2,04E-02	1,16E-02	n.d.	n.d.	n.d.	6,01E-03	1,84E-02
002c_A_13	2,11E-02	2,68E-03	5,93E-02	3,96E-02	7,78E-03	2,10E-02	1,44E-02	3,03E-03	n.d.	n.d.	n.d.	n.d.	n.d.
002c_A_14	7,03E-03	6,42E-03	3,68E-02	3,15E-02	1,40E-02	2,48E-02	1,37E-02	8,31E-03	n.d.	n.d.	n.d.	n.d.	n.d.
002c_A_2	1,32E+00	9,16E-04	2,84E+00	3,35E+00	4,16E-03	3,39E-01	3,88E-01	9,46E-04	n.d.	n.d.	n.d.	2,66E-01	3,18E-01
002c_A_3	1,41E+00	1,25E-03	2,05E+00	3,18E+00	5,68E-03	2,66E-01	4,41E-01	1,30E-03	n.d.	n.d.	n.d.	1,87E-01	3,27E-01
002c_A_4	1,25E-02	8,42E-03	5,85E-02	4,05E-02	9,47E-03	2,24E-02	9,28E-03	4,45E-03	n.d.	n.d.	n.d.	n.d.	n.d.
002c_A_5	8,40E-03	3,25E-03	4,40E-02	5,66E-02	1,19E-02	2,09E-02	1,12E-02	5,31E-03	n.d.	n.d.	n.d.	n.d.	n.d.
002c_A_6	1,17E-01	1,08E-03	1,74E-01	3,46E-01	4,33E-03	3,47E-02	4,00E-02	1,49E-03	n.d.	n.d.	n.d.	9,97E-03	3,05E-02
002c_A_7	1,41E-02	2,16E-03	5,19E-02	3,37E-02	5,93E-03	2,09E-02	1,19E-02	2,76E-03	n.d.	n.d.	n.d.	n.d.	n.d.
002c_A_8	7,23E-03	2,52E-03	4,73E-02	4,05E-02	6,19E-03	1,86E-02	5,93E-03	3,66E-03	n.d.	n.d.	n.d.	n.d.	n.d.
002c_A_9	1,16E-02	3,02E-03	6,38E-02	5,66E-02	4,98E-03	2,38E-02	2,02E-02	2,05E-02	n.d.	n.d.	n.d.	1,24E-03	1,53E-02
062C_A_1	n.d.	n.d.	n.d.	n.d.	n.d.	1,99E-02	1,84E-02	6,41E-03	9,84E-03	7,96E-02	8,68E-04	2,42E-02	2,53E-02
062C_A_10	n.d.	n.d.	n.d.	n.d.	n.d.	1,40E-02	1,25E-02	1,26E-03	6,92E-02	2,41E-01	9,53E-03	2,92E-02	2,68E-02
062C_A_11	1,55E-02	8,78E-04	6,69E-02	1,59E-01	4,13E-03	3,57E-02	2,65E-02	2,31E-03	1,42E-01	2,13E-01	7,77E-03	4,00E-02	2,62E-02
062C_A_12	n.d.	n.d.	n.d.	n.d.	n.d.	1,82E-02	2,39E-02	1,30E-03	3,26E-02	6,54E-02	2,28E-03	3,02E-02	1,75E-02
062C_A_13	1,19E-01	8,95E-04	2,47E-01	3,83E-01	4,37E-03	5,70E-02	4,97E-02	1,30E-03	3,87E-01	5,33E-01	1,76E-02	7,40E-02	7,11E-02
062C_A_14	n.d.	n.d.	n.d.	n.d.	n.d.	1,19E-02	2,51E-02	8,67E-04	5,25E-02	9,06E-02	2,26E-03	2,10E-02	2,05E-02
062C_A_15	n.d.	n.d.	n.d.	n.d.	n.d.	6,79E-03	7,67E-03	6,95E-04	1,91E-02	1,07E-01	1,17E-03	1,88E-02	1,92E-02
062C_A_16	n.d.	n.d.	3,16E-02	1,29E-01	1,44E-03	1,10E-02	1,79E-02	8,56E-04	5,57E-02	1,08E-01	2,58E-03	1,92E-02	1,42E-02
062C_A_17	1,71E-02	7,01E-05	5,55E-02	5,91E-02	9,32E-03	1,99E-02	1,69E-02	1,34E-03	1,54E-01	8,04E-02	5,53E-03	2,93E-02	1,49E-02
062C_A_18	n.d.	n.d.	3,81E-02	1,11E-01	1,83E-03	1,20E-02	2,45E-02	9,05E-04	6,41E-02	1,44E-01	3,09E-03	2,43E-02	1,86E-02
062C_A_2	4,65E-02	8,02E-04	9,25E-02	1,27E-01	3,14E-03	3,69E-02	3,10E-02	1,71E-03	1,85E-01	1,87E-01	5,61E-03	6,06E-02	5,85E-02
062C_A_3	n.d.	n.d.	n.d.	n.d.	n.d.	1,85E-02	1,23E-02	1,63E-03	4,73E-02	8,22E-02	2,79E-03	3,07E-02	1,68E-02
062C_A_4	n.d.	n.d.	n.d.	n.d.	n.d.	1,79E-02	1,26E-02	1,23E-03	5,75E-02	9,42E-02	2,49E-03	1,88E-02	1,86E-02
062C_A_5	1,16E-01	2,19E-03	2,08E-01	4,48E-01	9,57E-03	5,12E-02	8,12E-02	5,91E-03	1,94E-01	3,80E-01	1,16E-02	4,17E-02	2,07E-02
062C_A_6	3,11E-02	6,32E-04	5,48E-02	1,54E-01	2,60E-03	2,58E-02	1,47E-02	1,66E-03	1,12E-01	1,40E-01	5,10E-03	3,21E-02	3,03E-02
062C_A_7	1,01E-01	1,09E-03	1,55E-01	2,46E-01	4,74E-03	4,24E-02	6,11E-02	1,75E-03	1,92E-01	1,72E-01	6,32E-03	4,12E-02	4,52E-02
062C_A_8	n.d.	n.d.	n.d.	n.d.	n.d.	1,42E-02	1,86E-02	1,72E-03	5,08E-02	1,35E-01	3,42E-03	2,64E-02	3,05E-02
062C_A_9	n.d.	n.d.	n.d.	n.d.	n.d.	1,72E-02	1,77E-02	1,50E-03	8,71E-02	1,54E-01	4,12E-03	2,87E-02	3,66E-02
079c_A_1	3,84E+00	7,86E-04	5,09E+00	9,54E+00	3,62E-03	6,07E-01	1,14E+00	8,15E-04	n.d.	n.d.	n.d.	4,27E-01	8,18E-01
079c_A_3	1,34E-01	3,35E-03	1,91E-01	3,26E-01	1,13E-02	4,23E-02	3,92E-02	3,90E-03	n.d.	n.d.	n.d.	1,52E-02	3,69E-02
079c_A_4	2,40E-02	8,73E-03	9,88E-02	3,85E-02	1,78E-02	2,89E-02	1,64E-02	9,02E-03	n.d.	n.d.	n.d.	4,07E-03	2,52E-02
080c1_A_1	1,11E-02	5,79E-04	n.d.	n.d.	n.d.	1,13E-02	5,70E-03	2,06E-03	1,53E-02	8,60E-02	1,24E-03	n.d.	n.d.
080c1_A_10	2,87E+00	7,17E-04	1,75E+01	9,95E+00	3,32E-03	3,07E+00	1,60E+00	7,38E-04	2,65E+01	1,50E+01	3,75E-03	4,36E+00	2,82E+00
080c1_A_11	5,69E-01	6,57E-04	1,74E+00	2,18E+00	3,00E-03	2,93E-01	3,58E-01	6,86E-04	2,38E+00	2,97E+00	3,42E-03	3,89E-01	5,21E-01
080c1_A_12	1,03E+00	5,56E-04	2,85E+00	3,50E+00	8,55E-03	5,27E-01	6,07E-01	5,79E-04	4,51E+00	5,22E+00	9,78E-03	6,86E-01	9,44E-01
080c1_A_13	7,96E-03	6,80E-04	n.d.	n.d.	n.d.	1,41E-02	7,95E-03	3,02E-03	4,30E-02	9,29E-02	6,81E-03	n.d.	n.d.
080c1_A_14	1,47E-02	7,02E-04	2,16E-02	4,55E-02	1,18E-03	1,14E-02	1,44E-02	8,77E-04	5,76E-02	6,84E-02	2,21E-03	8,98E-03	7,74E-03
080c1_A_15	1,93E-02	6,11E-04	3,85E-02	6,81E-02	1,45E-03	1,57E-02	1,24E-02	7,11E-04	1,02E-01	5,23E-02	2,39E-03	8,49E-03	2,17E-02
080c1_A_16	8,42E-01	9,14E-04	1,98E+01	3,40E+00	4,22E-03	3,55E+00	4,69E-01	9,52E-04	2,90E+01	5,20E+00	4,79E-03	4,70E+00	1,07E+00
080c1_A_17	1,78E+00	8,11E-04	2,06E+01	5,24E+00	3,76E-03	3,73E+00	9,92E-01	8,48E-04	3,32E+01	7,35E+00	4,27E-03	5,42E+00	1,35E+00
080c1_A_18	2,66E+00	1,14E-03	1,13E+01	7,82E+00	5,30E-03	1,97E+00	1,65E+00	1,19E-03	1,69E+01	1,31E+01	5,99E-03	2,60E+00	1,73E+00
080c1_A_19	2,07E+00	7,06E-04	1,62E+01	5,52E+00	3,25E-03	2,95E+00	1,27E+00	7,41E-04	2,49E+01	9,68E+00	3,70E-03	3,60E+00	1,60E+00
080c1_A_2	1,19E-02	5,43E-04	n.d.	n.d.	n.d.	1,26E-02	9,52E-03	1,51E-03	3,38E-02	6,22E-02	1,86E-03	n.d.	n.d.
080c1_A_21	1,26E-01	1,27E-03	3,30E-01	4,12E-01	4,99E-03	4,96E-02	4,43E-02	1,30E-03	3,44E-01	4,40E-01	5,70E-03	2,40E-02	3,88E-02
080c1_A_22	3,77E-02	1,47E-03	n.d.	n.d.	n.d.	5,75E-03	6,01E-03	1,12E-03	4,83E-02	1,27E-01	1,01E-02	3,19E-04	2,25E-02
080c1_A_3	1,03E-02	2,83E-04	n.d.	n.d.	n.d.	9,68E-03	6,93E-03	1,24E-03	7,62E-03	5,36E-02	1,74E-03	n.d.	n.d.
080c1_A_4	3,25E+00	1,22E-03	2,05E+01	8,94E+00	1,31E-02	3,18E+00	7,34E-01	1,22E-03	2,80E+01	4,96E+00	1,46E-02	4,25E+00	9,18E-01
080c1_A_5	7,51E-01	1,26E-03	9,34E+00	2,98E+00	1,34E-02	1,55E+00	3,22E-01	1,27E-03	1,41E+01	2,16E+00	6,54E-03	2,28E+00	5,23E-01
080c1_A_6	3,30E-01	1,70E-03	1,88E+00	7,81E-01	7,75E-03	2,80E-01	1,43E-01	1,77E-03	2,68E+00	1,41E+00	2,03E-02	4,31E-01	1,68E-01
080c1_A_7	7,92E-01	7,59E-04	2,19E+00	2,51E+00	3,47E-03	3,90E-01	3,97E-01	7,88E-04	3,01E+00	3,60E+00	1,43E-02	4,57E-01	5,35E-01
080c1_A_8	1,17E+01	9,93E-04	3,79E+01	3,25E+01	4,57E-03	5,41E+00	3,92E+00	1,01E-03	4,05E+01	2,58E+01	1,40E-02	6,14E+00	3,79E+00
080c1_A_9	5,54E+00	1,68E-03	2,78E+01	1,79E+01	7,77E-03	4,28E+00	2,59E+00	1,72E-03	3,45E+01	1,99E+01	8,84E-03	5,37E+00	2,96E+00
080c2_B_1	4,59E-02	1,39E-03	2,38E-01	2,23E-01	6,54E-03	8,43E-02	7,44E-02	1,87E-03	3,87E-01	3,38E-01	8,16E-03	6,72E-02	5,24E-02
080c2_B_10	3,26E-02	1,26E-03	3,85E-01	7,24E-01	7,20E-03	4,75E-02	4,12E-02	1,55E-03	4,49E-01	3,42E-01	7,94E-03	7,86E-02	6,22E-02
080c2_B_11	5,62E-02	7,96E-04	1,97E-01	1,95E-01	4,33E-03	4,27E-02	3,31E-02	3,55E-03	3,28E-01	1,95E-01	5,21E-03	6,06E-02	4,82E-02
080c2_B_12	6,29E-02	1,18E-03	4,16E-01	1,47E-01	6,64E-03	5,64E-02	4,51E-02	3,38E-03	4,42E-01	1,73E-01	1,84E-02	8,92E-02	6,92E-02
080c2_B_13	1,05E-01	1,77E-03	4,69E-01	3,79E-01	9,13E-03	8,65E-02	3,66E-02	2,09E-03	6,42E-01	3,04E-01	1,02E-02	1,01E-01	2,79E-02
080c2_B_14	2,29E-02	9,12E-04	1,95E-01	2,48E-01	7,61E-03	2,79E-02	1,73E-02	1,61E-03	2,45E-01	1,72E-01	8,51E-03	4,92E-02	3,49E-02
080c2_B_15	3,82E-02	8,93E-04	2,90E-01	7,32E-02	5,39E-03	4,56E-02	4,16E-02	1,16E-03	4,53E-01	1,59E-01	6,06E-03	8,52E-02	3,20E-02
080c2_B_16	1,17E-01	1,48E-03	3,07E-01	3,31E-01	8,07E-03	6,52E-02	9,35E-02	1,84E-03	5,10E-01	7,93E-01	9,19E-03	9,18E-02	1,14E-01
080c2_B_17	1,54E-02	1,21E-03	1,51E-01	7,54E-02	9,43E-03	4,25E-02	1,24E-02	2,18E-03	3,21E-01	1,61E-01	1,12E-02	6,28E-02	1,58E-02
080c2_B_18	3,15E-02	3,04E-03	4,11E-01	4,44E-01	1,88E-02	5,80E-02	5,16E-02	3,99E-03	4,76E-01	5,87E-01	2,04E-02	9,64E-02	5,79E-02
080c2_B_19	8,63E-02	2,03E-03	4,37E-01	2,62E-01	1,11E-02	7,02E-02	2,10E-02	5,38E-03	5,72E-01	2,36E-01	1,22E-02	9,48E-02	1,65E-02
080c2_B_2	1,33E-01	5,68E-03	4,94E-01	4,65E-01	1,03E-02	7,96E-02	5,51E-02	5,73E-03	7,28E-01	4,70E-01	2,50E-02	1,50E-01	1,15E-01
080c2_B_20	4,07E-02	1,08E-03	1,74E-01	1,36E-01	9,78E-03	1,77E-02	3,76E-02	1,62E-03	2,06E-01	5,14E-02	2,15E-02	4,34E-02	2,18E-02
080c2_B_21	2,32E-02	1,10E-03	1,67E-01	7,61E-02	7,30E-03	3,10E-02	9,77E-03	1,47E-03	1,73E-01	9,76E-02	7,45E-03	4,64E-02	3,42E-02
080c2_B_22	1,49E-02	1,14E-03	1,55E-01	9,85E-02	9,44E-03	4,06E-02	6,50E-03	2,02E-03	1,65E-01	2,28E-01	9,52E-03	4,45E-02	7,80E-03
080c2_B_23	1,17E-02	3,70E-04	9,98E-02	9,34E-02	5,94E-03	2,13E-02	2,35E-02	1,07E-03	1,95E-01	2,24E-01	6,75E-03	3,68E-02	3,32E-02
080c2_B_24	1,75E-02	8,00E-04	1,21E-01	1,02E-01	7,59E-03	1,22E-02	1,14E-02	1,03E-03	1,71E-01	2,16E-01	7,86E-03	3,27E-02	3,54E-02
080c2_B_25	3,77E-02	5,97E-04	1,10E-01	1,10E-01	6,81E-03	1,41E-02	1,73E-02	1,03E-03	7,31E-02	5,43E-02	1,31E-02	2,90E-02	1,14E-02
080c2_B_4	4,06E-02	9,53E-04	1,54E-01	2,05E-01	6,01E-03	3,58E-02	2,06E-02	1,64E-03	2,85E-01	2,63E-01	7,76E-03	6,98E-02	3,24E-02

Analysis	Lu175_LOD	Hf177_mean	Hf177_2SD	Hf177_LOD	Ta181_mean	Ta181_2SD	Ta181_LOD	W183_mean	W183_2SD	W183_LOD	Au197_mean	Au197_2SD	Au197_LOD
	(ppm)	(ppm)	(ppm)	(ppm)	(ppm)	(ppm)	(ppm)	(ppm)	(ppm)	(ppm)	(ppm)	(ppm)	(ppm)
002c_A_1	1,34E-03	n.d.	n.d.	n.d.	6,51E-01	2,12E-01	6,97E-03	3,68E+02	1,94E+03	3,02E-02	2,08E-02	3,40E-02	1,93E-02
002c_A_10	n.d.	n.d.	n.d.	n.d.	6,56E-01	1,97E-01	1,21E-03	3,69E-02	6,50E-02	3,16E-02	n.d.	n.d.	n.d.
002c_A_11	1,14E-03	n.d.	n.d.	n.d.	1,62E+00	1,06E+00	5,91E-03	7,41E-02	1,04E-01	4,42E-02	n.d.	n.d.	n.d.
002c_A_12	6,02E-04	n.d.	n.d.	n.d.	6,70E-01	9,94E-02	2,04E-03	3,29E-02	3,02E-02	3,87E-02	7,59E-03	1,19E-02	4,32E-02
002c_A_13	n.d.	n.d.	n.d.	n.d.	6,29E-01	2,24E-01	1,48E-03	2,59E-02	5,65E-02	2,24E-02	9,54E-03	1,73E-02	2,08E-02
002c_A_14	n.d.	n.d.	n.d.	n.d.	6,43E-01	1,76E-01	1,46E-03	2,80E-02	1,35E-01	2,88E-02	7,41E-03	8,95E-03	3,91E-02
002c_A_2	1,09E-03	n.d.	n.d.	n.d.	6,71E-01	2,23E-01	1,45E-03	3,74E-02	4,67E-02	3,24E-02	6,48E-03	1,18E-02	3,99E-01
002c_A_3	1,47E-03	n.d.	n.d.	n.d.	6,02E-01	1,58E-01	4,97E-03	2,47E-02	6,42E-02	3,05E-02	9,86E-03	1,67E-02	2,79E-02
002c_A_4	n.d.	n.d.	n.d.	n.d.	6,87E-01	2,56E-01	1,91E-03	6,31E-02	9,37E-02	4,66E-02	n.d.	n.d.	n.d.
002c_A_5	n.d.	n.d.	n.d.	n.d.	6,13E-01	1,89E-01	1,90E-03	1,28E-02	5,88E-02	2,48E-02	n.d.	n.d.	n.d.
002c_A_6	4,45E-04	n.d.	n.d.	n.d.	5,93E-01	1,71E-01	4,44E-03	1,26E-02	8,49E-02	2,60E-02	n.d.	n.d.	n.d.
002c_A_7	n.d.	n.d.	n.d.	n.d.	6,64E-01	2,62E-01	1,07E-03	1,29E-02	6,41E-02	1,94E-02	n.d.	n.d.	n.d.
002c_A_8	n.d.	n.d.	n.d.	n.d.	6,98E-01	1,17E-01	3,76E-03	4,74E-02	7,46E-02	1,47E-02	n.d.	n.d.	n.d.
002c_A_9	8,45E-05	n.d.	n.d.	n.d.	6,59E-01	2,23E-01	4,99E-03	1,35E-02	7,66E-02	2,05E-02	n.d.	n.d.	n.d.
062C_A_1	2,01E-03	6,18E-01	2,64E-01	8,63E-03	2,04E-01	7,18E-02	6,47E-03	< Det. Lim	3,85E-02	3,48E-01	< Det. Lim	1,52E-02	1,36E-01
062C_A_10	4,79E-03	1,49E+00	3,26E-01	8,02E-03	3,65E-01	9,85E-02	1,87E-03	3,18E-02	5,35E-02	2,08E-02	1,11E-03	6,75E-03	3,80E-03
062C_A_11	3,04E-03	9,23E-01	5,70E-01	3,65E-02	2,86E-01	1,35E-01	3,42E-03	5,33E-02	2,11E-01	4,43E-02	< Det. Lim	1,07E-02	2,75E-02
062C_A_12	1,83E-03	8,46E-01	3,69E-01	8,50E-03	1,97E-01	8,73E-02	5,76E-03	2,93E-03	6,38E-02	4,82E-03	< Det. Lim	1,32E-02	2,64E-02
062C_A_13	1,60E-03	8,84E-01	4,42E-01	8,11E-03	2,15E-01	9,15E-02	1,93E-03	1,60E-02	1,02E-01	1,99E-02	< Det. Lim	1,11E-02	1,29E-02
062C_A_14	1,36E-03	6,80E-01	2,82E-01	6,06E-03	2,35E-01	7,37E-02	1,46E-03	n.d.	n.d.	n.d.	< Det. Lim	1,76E-02	4,25E-02
062C_A_15	1,28E-03	6,06E-01	3,91E-01	5,68E-03	1,76E-01	7,56E-02	5,60E-03	n.d.	n.d.	n.d.	< Det. Lim	1,32E-02	1,31E-02
062C_A_16	1,48E-03	8,19E-01	2,90E-01	6,74E-03	2,63E-01	6,60E-02	1,60E-03	n.d.	n.d.	n.d.	< Det. Lim	9,93E-03	2,55E-02
062C_A_17	1,95E-03	1,41E+00	4,76E-01	9,54E-03	4,13E-01	1,13E-01	2,22E-03	8,00E-03	5,29E-02	1,16E-02	n.d.	n.d.	n.d.
062C_A_18	1,52E-03	8,77E-01	2,77E-01	7,22E-03	2,42E-01	1,15E-01	5,78E-03	1,22E-02	7,25E-02	8,83E-03	< Det. Lim	1,38E-02	1,54E-02
062C_A_2	1,94E-03	1,63E+00	3,56E-01	2,50E-02	4,17E-01	6,49E-02	2,21E-03	2,35E-02	9,65E-02	2,72E-02	< Det. Lim	1,95E-02	3,57E-02
062C_A_3	1,76E-03	1,70E+00	6,42E-01	8,42E-03	3,93E-01	1,13E-01	1,96E-03	4,60E-03	7,85E-02	7,25E-03	< Det. Lim	9,19E-03	1,95E-02
062C_A_4	1,48E-03	1,55E+00	4,83E-01	6,60E-03	3,27E-01	1,22E-01	1,54E-03	7,29E-03	7,20E-02	1,16E-02	< Det. Lim	1,24E-02	4,28E-02
062C_A_5	7,70E-03	3,40E+00	5,81E-01	1,85E-02	1,24E+00	1,66E-01	8,83E-03	4,89E-02	7,48E-02	3,17E-02	5,83E-03	2,69E-02	1,07E-02
062C_A_6	2,01E-03	1,74E+00	6,08E-01	9,76E-03	4,41E-01	1,42E-01	2,27E-03	n.d.	n.d.	n.d.	2,03E-04	1,14E-02	1,12E-03
062C_A_7	2,15E-03	1,75E+00	6,61E-01	1,04E-02	4,68E-01	1,13E-01	2,42E-03	9,33E-03	6,28E-02	2,26E-02	< Det. Lim	1,16E-02	2,20E-02
062C_A_8	2,20E-03	9,70E-01	3,11E-01	9,96E-03	2,27E-01	7,38E-02	6,32E-03	4,06E-03	9,01E-02	1,16E-02	n.d.	n.d.	n.d.
062C_A_9	2,07E-03	9,04E-01	6,55E-01	9,37E-03	1,91E-01	5,41E-02	6,79E-03	n.d.	n.d.	n.d.	2,01E-03	1,55E-02	6,13E-03
079c_A_1	9,78E-04	n.d.	n.d.	n.d.	4,07E+00	7,76E-01	1,28E-03	1,33E-01	8,75E-02	2,80E-02	6,01E-03	1,08E-02	3,69E-02
079c_A_3	1,34E-02	n.d.	n.d.	n.d.	3,99E+00	1,01E+00	2,69E-03	1,89E-01	2,19E-01	7,77E-02	1,50E-02	4,90E-02	5,03E-02
079c_A_4	1,96E-03	n.d.	n.d.	n.d.	3,95E+00	9,46E-01	2,50E-03	1,35E-01	2,67E-01	5,37E-02	1,78E-02	2,71E-02	2,71E-02
080c1_A_1	n.d.	7,64E-01	1,44E-01	6,51E-03	3,09E+00	4,32E-01	1,49E-03	9,93E-02	6,65E-02	3,75E-02	n.d.	n.d.	n.d.
080c1_A_10	9,42E-04	3,71E+00	2,20E+00	4,70E-03	4,12E+00	2,11E+00	2,70E-03	6,82E+00	4,56E+00	1,50E-02	6,46E-03	6,43E-03	3,92E-03
080c1_A_11	8,35E-04	1,28E+00	6,96E-01	4,38E-03	3,44E+00	7,45E-01	4,06E-03	6,69E-01	9,69E-01	1,49E-02	4,26E-04	4,56E-03	1,43E-03
080c1_A_12	7,16E-04	1,15E+00	7,62E-01	3,83E-03	3,30E+00	7,36E-01	3,01E-03	1,06E+00	1,08E+00	1,54E-02	n.d.	n.d.	n.d.
080c1_A_13	n.d.	9,09E-01	4,90E-01	5,32E-03	3,04E+00	1,67E+00	3,58E-03	1,16E-01	9,95E-02	3,54E-02	< Det. Lim	1,07E-02	2,31E-02
080c1_A_14	3,11E-04	8,35E-01	3,23E-01	4,97E-03	3,37E+00	1,17E+00	1,13E-03	1,04E-01	6,79E-02	2,72E-02	n.d.	n.d.	n.d.
080c1_A_15	2,68E-04	8,22E-01	3,13E-01	4,25E-03	2,97E+00	1,19E+00	3,70E-03	1,28E-01	8,50E-02	2,48E-02	7,10E-03	2,74E-02	5,50E-03
080c1_A_16	1,19E-03	8,99E+00	2,62E+00	1,53E-02	4,67E+00	8,04E-01	3,18E-03	8,13E+00	1,52E+00	1,91E-02	4,33E-03	6,84E-03	6,38E-03
080c1_A_17	1,06E-03	9,93E+01	3,58E+01	5,44E-03	4,62E+00	9,17E-01	1,23E-03	1,08E+01	3,09E+00	1,16E-02	3,31E-03	9,17E-03	4,61E-03
080c1_A_18	1,51E-03	7,86E+00	5,34E+00	7,61E-03	4,47E+00	1,83E+00	1,78E-03	5,63E+00	3,27E+00	1,94E-02	1,44E-02	4,65E-02	1,09E-02
080c1_A_19	9,14E-04	6,91E+00	2,79E+00	4,66E-03	4,28E+00	1,81E+00	3,16E-03	6,80E+00	2,77E+00	2,01E-02	2,32E-03	8,09E-03	5,98E-03
080c1_A_2	n.d.	7,86E-01	2,32E-01	5,57E-03	3,06E+00	5,72E-01	4,32E-03	1,06E-01	4,42E-02	4,05E-02	n.d.	n.d.	n.d.
080c1_A_21	8,94E-04	7,65E-01	3,14E-01	8,73E-03	2,20E+00	4,94E-01	5,66E-03	1,72E-01	2,36E-01	3,17E-02	2,16E-03	1,41E-02	1,14E-02
080c1_A_22	7,83E-05	6,37E-01	3,07E-01	9,83E-03	2,05E+00	3,16E-01	2,14E-03	1,38E-01	1,23E-01	5,72E-02	5,82E-03	1,37E-02	9,16E-03
080c1_A_3	n.d.	7,71E-01	2,68E-01	3,87E-03	3,06E+00	4,38E-01	8,87E-04	9,90E-02	7,17E-02	3,18E-02	< Det. Lim	1,28E-02	1,15E-01
080c1_A_4	1,60E-03	8,33E+00	8,62E-01	7,82E-03	3,88E+00	7,92E-01	1,80E-03	1,17E+01	4,27E+00	2,52E-02	5,07E-03	4,41E-03	5,34E-03
080c1_A_5	1,66E-03	2,87E+00	3,59E-01	8,20E-03	3,61E+00	4,85E-01	5,39E-03	4,06E+00	3,24E-01	2,02E-02	n.d.	n.d.	n.d.
080c1_A_6	2,12E-03	2,10E+00	5,81E-01	1,11E-02	3,66E+00	8,78E-01	2,57E-03	1,30E+00	7,47E-01	3,18E-02	1,11E-03	5,97E-03	4,17E-03
080c1_A_7	9,65E-04	1,14E+00	6,60E-01	5,08E-03	3,46E+00	6,34E-01	1,16E-03	9,31E-01	1,50E+00	1,54E-02	< Det. Lim	1,14E-02	1,60E-02
080c1_A_8	1,30E-03	2,62E+00	9,64E-01	1,62E-02	4,54E+00	1,19E+00	3,77E-03	3,39E+00	1,93E+00	1,93E-02	2,16E-03	9,28E-03	5,06E-03
080c1_A_9	2,22E-03	3,52E+00	1,06E+00	1,12E-02	4,15E+00	1,06E+00	5,42E-03	5,56E+00	4,38E+00	3,59E-02	1,22E-03	1,27E-02	3,04E-03
080c2_B_1	2,32E-03	1,88E+00	1,08E+00	1,20E-02	4,85E-01	2,41E-01	2,73E-03	9,32E-02	8,56E-02	9,74E-03	7,56E-04	2,41E-02	6,54E-03
080c2_B_10	2,15E-03	1,50E+00	1,25E+00	2,57E-02	3,56E-01	1,09E-01	2,56E-03	2,97E-01	2,50E-01	4,26E-02	1,22E-03	8,74E-03	1,34E-02
080c2_B_11	1,36E-03	1,46E+00	5,75E-01	7,40E-03	4,11E-01	1,83E-01	1,69E-03	6,83E-02	1,20E-01	2,64E-02	< Det. Lim	1,08E-02	2,05E-03
080c2_B_12	1,93E-03	2,16E+00	5,88E-01	1,03E-02	4,77E-01	2,07E-01	2,36E-03	7,66E-02	9,07E-02	2,54E-02	< Det. Lim	3,28E-03	7,62E-03
080c2_B_13	2,64E-03	1,64E+00	8,05E-01	1,40E-02	4,56E-01	2,08E-01	6,80E-03	3,49E-01	6,95E-01	3,03E-02	8,92E-03	1,80E-02	8,29E-03
080c2_B_14	2,50E-03	1,88E+00	5,21E-01	1,31E-02	4,66E-01	1,16E-01	2,99E-03	6,05E-02	6,93E-02	2,60E-02	5,51E-03	1,14E-02	1,23E-02
080c2_B_15	1,60E-03	1,65E+00	3,47E-01	8,55E-03	4,38E-01	1,70E-01	1,96E-03	3,20E-01	1,31E+00	3,53E-02	2,08E-03	1,19E-02	1,45E-02
080c2_B_16	2,39E-03	1,36E+00	6,29E-01	1,24E-02	3,15E-01	1,13E-01	7,02E-03	6,22E-02	9,53E-02	3,59E-02	< Det. Lim	7,27E-03	8,48E-03
080c2_B_17	3,06E-03	1,54E+00	6,36E-01	1,62E-02	3,04E-01	9,49E-02	3,72E-03	7,63E-02	1,60E-01	3,74E-02	4,89E-03	2,21E-02	1,68E-02
080c2_B_18	5,43E-03	1,56E+00	1,04E-01	2,89E-02	3,25E-01	9,53E-02	1,23E-02	1,42E+00	3,95E+00	7,41E-02	9,71E-04	1,01E-02	1,89E-01
080c2_B_19	3,15E-03	1,68E+00	8,41E-01	1,70E-02	3,95E-01	2,14E-01	3,88E-03	4,34E-01	3,37E-01	5,00E-02	6,83E-03	1,60E-02	1,49E-02
080c2_B_2	3,08E-03	1,90E+00	9,83E-01	1,62E-02	3,91E-01	6,45E-02	3,73E-03	4,96E-01	6,51E-01	6,03E-02	< Det. Lim	1,63E-02	1,92E-02
080c2_B_20	3,01E-03	1,20E+00	2,79E-01	1,58E-02	2,93E-01	1,23E-01	7,00E-03	1,27E-01	2,30E-01	2,90E-02	< Det. Lim	7,31E-03	9,18E-03
080c2_B_21	2,28E-03	1,74E+00	4,67E-01	1,21E-02	4,40E-01	1,06E-01	6,39E-03	2,36E-01	1,60E-01	3,91E-02	2,08E-03	1,82E-02	2,62E-02
080c2_B_22	2,94E-03	1,46E+00	6,16E-01	1,55E-02	4,03E-01	3,46E-02	3,56E-03	2,73E-01	1,77E-01	3,41E-02	< Det. Lim	7,54E-03	9,44E-03
080c2_B_23	2,06E-03	1,50E+00	4,79E-01	1,07E-02	3,44E-01	1,16E-01	2,45E-03	7,33E-02	1,98E-01	2,84E-02	< Det. Lim	1,49E-02	6,43E-03
080c2_B_24	2,47E-03	1,20E+00	2,79E-01	1,30E-02	3,21E-01	8,98E-02	6,62E-03	7,93E-02	1,45E-01	9,59E-03	6,07E-03	1,31E-02	1,31E-02
080c2_B_25	2,22E-03	1,29E+00	2,83E-01	1,15E-02	2,59E-01	1,19E-01	5,56E-03	9,86E-02	2,21E-01	1,97E-02	5,40E-03	1,26E-02	9,76E-03
080c2_B_4	2,31E-03	1,54E+00	3,47E-01	1,18E-02	4,57E-01	9,24E-02	2,77E-03	7,74E-02	8,38E-02	2,32E-02	1,23E-03	1,72E-02	1,16E-02

Analysis	Pb208_mean	Pb208_2SD	Pb208_LOD	Bi209_mean	Bi209_2SD	Bi209_LOD	Th232_mean	Th232_2SD	Th232_LOD	U238_mean	U238_2SD	U238_LOD
	(ppm)	(ppm)	(ppm)	(ppm)	(ppm)	(ppm)	(ppm)	(ppm)	(ppm)	(ppm)	(ppm)	(ppm)
002c_A_1	2,19E+00	2,08E+00	1,28E-02	1,24E-02	1,55E-02	6,10E-03	1,29E+00	3,29E+00	1,38E-03	4,39E-01	1,06E+00	8,48E-04
002c_A_10	1,45E-01	4,25E-01	1,12E-03	6,51E-03	1,04E-02	1,11E-02	8,28E-03	1,02E-02	2,46E-03	1,66E-02	1,95E-02	3,89E-04
002c_A_11	2,41E-01	2,89E-01	5,77E-03	5,27E-03	4,27E-03	1,87E-02	1,75E-01	4,58E-01	1,57E-03	9,14E-02	2,04E-01	8,73E-04
002c_A_12	9,05E-01	1,01E+00	2,56E-03	8,93E-03	9,15E-03	1,95E-03	1,08E-02	1,48E-02	3,12E-03	2,14E-02	1,48E-02	7,05E-04
002c_A_13	9,03E-02	3,83E-01	1,08E-03	6,10E-03	3,74E-03	1,24E-02	7,85E-03	1,31E-02	3,10E-03	1,81E-02	2,36E-02	4,89E-04
002c_A_14	6,09E-02	1,89E-01	3,54E-03	5,60E-03	4,37E-03	1,00E-02	n.d.	n.d.	n.d.	2,10E-02	1,71E-02	5,06E-04
002c_A_2	7,14E-01	2,12E+00	5,14E-03	8,23E-03	5,86E-03	6,39E-03	7,11E-01	8,69E-01	1,15E-03	2,46E-01	2,54E-01	6,98E-04
002c_A_3	6,70E-01	1,32E+00	2,30E-03	6,23E-03	3,83E-03	1,31E-02	7,05E-01	1,30E+00	1,55E-03	1,97E-01	3,37E-01	9,36E-04
002c_A_4	1,56E+00	3,86E+00	2,44E-03	1,07E-02	4,79E-03	6,37E-03	6,14E-02	8,02E-02	1,68E-03	3,93E-02	7,87E-02	7,93E-04
002c_A_5	4,88E-01	1,06E+00	6,60E-03	7,44E-03	8,24E-03	8,66E-03	7,95E-02	2,93E-01	1,73E-03	2,37E-01	1,02E+00	1,00E-03
002c_A_6	1,73E-01	4,01E-01	1,13E-03	6,92E-03	1,13E-02	1,24E-02	4,61E-02	1,02E-01	1,15E-03	3,58E-02	4,87E-02	4,88E-04
002c_A_7	6,81E-01	1,27E+00	1,35E-03	5,23E-03	7,55E-03	1,21E-02	1,11E-02	1,27E-02	1,51E-03	2,16E-02	1,82E-02	3,81E-04
002c_A_8	1,22E-01	3,32E-01	8,93E-04	5,48E-03	5,67E-03	1,60E-02	1,74E-02	6,13E-02	1,22E-03	1,92E-02	2,35E-02	3,54E-04
002c_A_9	3,36E-01	1,16E+00	1,35E-03	7,41E-03	9,98E-03	9,63E-03	1,35E-02	2,43E-02	1,47E-03	1,62E-02	1,76E-02	3,42E-04
062C_A_1	4,17E-01	2,97E-01	1,27E-02	7,64E-03	9,49E-03	6,89E-03	4,47E-02	7,88E-02	1,50E-03	1,25E-01	6,60E-02	1,03E-03
062C_A_10	6,63E-01	1,55E+00	7,99E-03	7,20E-03	8,69E-03	1,02E-02	3,49E-02	5,70E-02	1,28E-03	1,22E-01	1,05E-01	9,10E-04
062C_A_11	7,92E-01	5,74E-01	1,68E-02	6,16E-03	5,85E-03	2,89E-02	6,15E-02	8,40E-02	2,52E-03	4,78E-01	3,52E-01	1,76E-03
062C_A_12	9,24E-01	6,89E-01	8,58E-03	1,02E-02	9,45E-03	6,01E-03	8,39E-02	7,27E-02	1,56E-03	4,40E-01	2,49E-01	1,04E-03
062C_A_13	1,30E+00	4,71E-01	2,72E-03	1,07E-02	8,81E-03	5,62E-03	4,49E-01	4,49E-01	1,57E-03	5,91E-01	4,47E-01	9,87E-04
062C_A_14	5,39E-01	1,73E+00	7,25E-03	4,94E-03	7,81E-03	2,38E-02	2,22E-02	5,78E-02	9,36E-04	2,33E-01	2,19E-01	7,50E-04
062C_A_15	2,18E-01	6,31E-01	8,27E-03	5,31E-03	8,39E-03	2,10E-02	n.d.	n.d.	n.d.	2,12E-02	1,71E-02	5,49E-04
062C_A_16	4,23E-01	2,71E-01	7,40E-03	3,98E-03	6,10E-03	5,14E-01	5,56E-02	8,66E-02	1,18E-03	3,66E-01	2,86E-01	8,14E-04
062C_A_17	5,39E-01	2,13E-01	1,13E-02	6,08E-03	6,96E-03	1,30E-02	2,32E-01	1,20E-01	1,80E-03	6,96E-01	2,27E-01	1,14E-03
062C_A_18	8,72E-01	7,34E-01	8,89E-03	6,69E-03	8,32E-03	9,53E-03	8,86E-02	9,09E-02	1,32E-03	4,57E-01	6,88E-01	8,78E-04
062C_A_2	6,84E-01	5,53E-01	3,65E-03	6,23E-03	8,12E-03	1,25E-02	2,11E-01	1,95E-01	1,83E-03	2,34E-01	9,29E-02	1,12E-03
062C_A_3	5,66E-01	8,54E-01	3,37E-03	4,71E-03	8,19E-03	2,56E-02	2,24E-02	2,37E-02	1,19E-03	2,47E-01	1,25E-01	9,78E-04
062C_A_4	1,89E-01	1,60E-01	2,47E-02	5,01E-03	9,21E-03	1,76E-02	n.d.	n.d.	n.d.	3,05E-02	3,20E-02	4,29E-03
062C_A_5	1,45E+00	2,17E+00	6,12E-03	1,15E-02	2,53E-02	1,08E-02	6,94E-01	1,44E+00	3,63E-03	7,99E-01	4,08E-01	2,21E-03
062C_A_6	1,98E+00	5,61E+00	1,41E-02	5,44E-03	9,58E-03	1,58E-02	6,68E-02	1,82E-02	1,71E-03	4,19E-01	2,57E-01	1,16E-03
062C_A_7	4,17E-01	1,86E-01	1,15E-02	1,14E-02	1,06E-02	5,49E-03	8,09E-02	3,95E-02	1,86E-03	2,87E-01	9,38E-02	1,23E-03
062C_A_8	4,02E-01	4,45E-01	4,26E-03	4,87E-03	3,83E-03	2,30E-02	2,89E-02	6,64E-02	1,55E-03	1,08E-01	5,93E-02	1,15E-03
062C_A_9	5,05E-01	4,19E-01	3,62E-03	9,00E-03	9,26E-03	7,16E-03	4,05E-02	5,51E-02	1,49E-03	1,75E-01	9,49E-02	1,11E-03
079c_A_1	2,13E+00	1,19E+00	1,69E-03	1,15E-02	7,37E-03	4,18E-03	2,34E+00	3,99E+00	1,00E-03	6,42E-01	1,08E+00	6,26E-04
079c_A_3	1,72E+00	9,04E-01	1,37E-02	3,34E-02	9,83E-02	1,68E-03	6,06E-01	2,47E-01	2,26E-03	1,40E-01	3,95E-02	1,21E-03
079c_A_4	1,96E+00	1,91E+00	1,07E-02	1,74E-02	2,02E-02	1,42E-02	2,90E-01	2,27E-01	2,20E-03	1,08E-01	2,54E-02	1,08E-03
080c1_A_1	3,51E-01	1,97E+00	5,10E-03	9,85E-03	1,21E-02	1,66E-03	6,58E-03	1,94E-02	6,96E-04	2,45E-02	1,49E-02	6,38E-04
080c1_A_10	2,51E+01	1,47E+01	4,64E-03	8,75E-03	5,71E-03	3,98E-03	4,37E-02	4,36E-02	8,16E-04	7,23E+00	5,64E+00	5,68E-04
080c1_A_11	4,45E+00	6,82E+00	1,40E-03	n.d.	n.d.	n.d.	1,03E-01	1,17E-01	7,90E-04	7,20E-01	8,70E-01	5,36E-04
080c1_A_12	5,73E+00	3,35E+00	3,58E-03	1,02E-02	8,61E-03	2,72E-03	2,84E-02	4,93E-02	5,81E-04	1,39E+00	1,47E+00	4,55E-04
080c1_A_13	2,13E-01	5,59E-01	3,90E-03	6,53E-03	4,85E-03	1,16E-02	n.d.	n.d.	n.d.	8,07E-02	6,25E-02	5,96E-04
080c1_A_14	n.d.	n.d.	n.d.	5,62E-03	4,14E-03	1,31E-02	3,07E-02	2,89E-02	2,90E-03	1,07E-01	4,39E-02	5,71E-04
080c1_A_15	1,72E+00	2,09E+00	1,34E-03	9,73E-03	1,54E-02	5,44E-03	6,23E-02	6,24E-02	7,14E-04	1,21E-01	6,54E-02	4,92E-04
080c1_A_16	1,21E+02	2,14E+01	6,39E-03	7,18E-02	1,68E-02	2,57E-03	5,89E-01	4,05E-01	1,18E-03	8,36E+00	9,04E-01	7,48E-04
080c1_A_17	1,60E+02	2,32E+01	6,37E-03	9,51E-02	3,32E-02	5,97E-04	2,81E+00	1,60E+00	1,08E-03	1,24E+01	2,40E+00	3,21E-03
080c1_A_18	1,17E+02	5,26E+01	2,50E-03	5,83E-02	1,85E-02	4,46E-03	2,05E+00	1,39E+00	1,59E-03	4,34E+00	2,96E+00	9,53E-04
080c1_A_19	8,79E+01	3,45E+01	3,99E-03	4,15E-02	2,65E-02	5,39E-04	2,95E-02	2,50E-02	7,30E-04	8,10E+00	4,19E+00	5,85E-04
080c1_A_2	9,36E-02	5,73E-01	3,29E-03	7,15E-03	3,24E-03	1,53E-02	n.d.	n.d.	n.d.	2,80E-02	2,04E-02	5,54E-04
080c1_A_21	9,87E-01	8,84E-01	2,40E-03	6,89E-03	4,64E-03	2,78E-02	1,11E-01	8,90E-02	1,47E-03	9,54E-02	7,96E-02	9,45E-04
080c1_A_22	1,11E+00	9,53E-01	2,76E-03	8,91E-03	4,16E-03	6,07E-03	1,86E-02	5,13E-02	1,03E-03	3,24E-02	3,04E-02	9,31E-04
080c1_A_3	n.d.	n.d.	n.d.	8,37E-03	6,31E-03	8,28E-03	8,00E-05	1,31E-02	1,16E-05	3,36E-02	1,97E-02	4,01E-04
080c1_A_4	2,09E+02	4,25E+01	5,24E-03	5,21E-02	2,71E-02	2,64E-03	5,83E+00	6,26E+00	1,58E-03	7,83E+00	9,26E-01	9,44E-04
080c1_A_5	2,36E+01	2,24E+00	5,43E-03	4,51E-03	3,57E-03	4,44E-02	2,41E-01	1,86E-01	1,53E-03	3,74E+00	6,07E-01	9,91E-04
080c1_A_6	1,94E+01	1,09E+01	3,49E-03	1,58E-02	2,30E-02	6,53E-03	1,44E+00	6,99E-01	2,11E-03	7,74E-01	3,74E-01	1,33E-03
080c1_A_7	2,99E+00	4,69E+00	7,97E-03	5,91E-03	5,95E-03	3,18E-02	9,74E-02	1,39E-01	8,90E-04	9,21E-01	1,21E+00	6,08E-04
080c1_A_8	1,00E+01	2,25E+00	4,69E-03	8,04E-03	5,68E-03	6,68E-03	5,38E+00	6,70E+00	1,25E-03	7,76E+00	4,79E+00	7,71E-04
080c1_A_9	2,22E+01	1,05E+01	3,52E-03	1,71E-02	2,11E-02	3,17E-03	2,68E+00	1,84E+00	2,15E-03	8,33E+00	4,87E+00	5,06E-03
080c2_B_1	1,47E+01	4,32E+00	1,36E-02	3,12E-02	2,17E-02	5,13E-03	2,45E-01	2,45E-01	2,26E-03	4,10E-01	2,75E-01	1,40E-03
080c2_B_10	1,50E+01	3,46E+00	3,43E-03	2,23E-02	1,01E-02	4,40E-03	2,99E-01	2,05E-01	2,12E-03	4,20E-01	2,36E-01	1,33E-03
080c2_B_11	1,36E+01	7,18E+00	7,73E-03	8,72E-03	8,99E-03	5,87E-03	1,83E-01	1,63E-01	1,34E-03	3,56E-01	2,44E-01	8,59E-04
080c2_B_12	2,27E+01	6,11E+00	9,55E-03	2,01E-02	9,94E-03	3,93E-03	3,41E-01	1,80E-01	1,95E-03	5,81E-01	2,28E-01	1,22E-03
080c2_B_13	2,32E+01	6,95E+00	4,33E-03	5,90E-02	6,48E-02	4,07E-03	4,43E-01	1,48E-01	2,67E-03	3,66E-01	2,14E-01	8,89E-03
080c2_B_14	1,68E+01	2,91E+00	1,31E-02	1,61E-02	6,74E-03	5,20E-03	2,89E-01	3,83E-02	2,45E-03	2,38E-01	5,42E-02	1,53E-03
080c2_B_15	1,83E+01	7,01E+00	2,65E-03	1,69E-02	1,74E-02	7,42E-03	4,38E-01	1,71E-01	1,62E-03	2,85E-01	8,45E-02	1,01E-03
080c2_B_16	1,56E+01	9,66E+00	9,03E-03	1,52E-02	6,95E-03	6,35E-03	6,62E-01	9,46E-01	2,43E-03	3,14E-01	9,16E-02	1,47E-03
080c2_B_17	2,07E+01	6,83E+00	1,10E-02	2,42E-02	1,24E-02	5,35E-03	3,51E-01	3,46E-02	3,06E-03	4,40E-01	1,46E-01	1,92E-03
080c2_B_18	1,47E+01	1,72E+00	8,99E-03	2,81E-02	8,40E-03	9,92E-03	4,33E-01	1,27E-01	5,48E-03	3,46E-01	2,12E-01	3,41E-03
080c2_B_19	3,13E+01	8,25E+00	1,00E-02	3,45E-02	1,37E-02	6,37E-03	3,90E-01	1,68E-01	3,20E-03	4,57E-01	1,11E-01	1,99E-03
080c2_B_2	2,44E+01	1,72E+01	1,44E-02	4,21E-02	3,83E-02	7,21E-03	5,00E-01	4,11E-01	3,11E-03	6,56E-01	6,83E-01	1,94E-03
080c2_B_20	1,06E+01	1,76E+00	4,92E-03	1,17E-02	4,66E-03	7,08E-03	1,59E-01	1,08E-01	2,93E-03	1,83E-01	2,58E-02	1,85E-03
080c2_B_21	2,60E+01	4,48E+00	1,06E-02	9,31E-02	2,00E-02	3,02E-03	3,56E-01	8,05E-02	2,26E-03	2,91E-01	1,05E-01	1,41E-03
080c2_B_22	1,77E+01	3,41E+00	4,82E-03	1,11E-02	9,54E-03	6,25E-03	3,32E-01	9,51E-02	2,92E-03	2,70E-01	4,72E-02	1,82E-03
080c2_B_23	1,79E+01	5,10E+00	3,29E-03	5,29E-02	4,16E-02	1,33E-03	3,72E-01	1,67E-01	2,02E-03	2,14E-01	1,48E-01	1,24E-03
080c2_B_24	9,69E+01	2,46E+01	9,91E-03	2,07E-02	9,09E-03	6,24E-03	3,10E-01	1,83E-01	2,43E-03	1,80E-01	8,79E-02	1,51E-03
080c2_B_25	4,16E+01	9,24E+00	7,61E-03	1,52E-01	7,77E-02	6,53E-03	2,11E-01	7,70E-02	2,16E-03	1,57E-01	8,15E-02	1,34E-03
080c2_B_4	1,62E+01	5,76E+00	1,20E-02	3,84E-02	2,05E-02	5,66E-03	3,06E-01	1,23E-01	2,26E-03	2,73E-01	1,47E-01	1,40E-03

Sample	Analysis	Li7_mean	Li7_2SD	Li7_LOD	Be9_mean	Be9_2SD	Be9_LOD	Na23_mean	Na23_2SD	Na23_LOD	Mg25_mean	Mg25_2SD	Mg25_LOD	Al27_mean
		(ppm)	(ppm)	(ppm)	(ppm)	(ppm)	(ppm)	(ppm)	(ppm)	(ppm)	(ppm)	(ppm)	(ppm)	(ppm)
NA007-080c2	080c2_B_7	5,89E+00	9,01E-01	1,30E-01	1,89E-01	8,12E-02	3,17E-02	1,13E+03	1,31E+03	2,20E+00	1,70E+04	2,56E+03	3,06E+00	2,25E+04
NA007-080c2	080c2_B_8	8,66E+00	1,92E+00	1,35E-01	2,83E-01	1,57E-01	6,18E-02	1,33E+03	3,89E+02	2,11E+00	2,06E+04	4,22E+03	2,82E+00	2,55E+04
NA007-080c2	080c2_B_9	7,04E+00	2,57E+00	1,24E-01	2,36E-01	3,33E-01	2,86E-02	1,05E+03	2,18E+02	2,09E+00	1,79E+04	2,78E+03	2,83E+00	2,19E+04
NA007-080c3	080c3_A_1	1,85E+00	6,09E-01	1,19E-01	4,50E-02	1,13E-01	1,88E-02	3,53E+02	2,81E+03	5,08E-01	1,09E+04	3,14E+03	3,31E+00	1,60E+04
NA007-080c3	080c3_A_10	2,78E+00	9,72E-01	9,94E-02	1,93E-02	5,91E-02	9,74E-03	n.d.	n.d.	n.d.	1,83E+04	3,85E+03	2,60E+00	2,11E+04
NA007-080c3	080c3_A_11	3,58E+00	1,31E+00	1,06E-01	1,80E-01	2,48E-01	5,10E-02	6,79E+02	5,82E+02	9,18E-01	2,01E+04	2,69E+03	2,83E+00	2,74E+04
NA007-080c3	080c3_A_12	2,00E+00	5,70E-01	1,28E-01	n.d.	n.d.	n.d.	n.d.	n.d.	n.d.	1,81E+04	5,06E+03	2,87E+00	2,20E+04
NA007-080c3	080c3_A_13	2,76E+00	1,17E+00	1,28E-01	2,79E-02	7,93E-02	1,34E-02	n.d.	n.d.	n.d.	1,92E+04	3,37E+03	3,11E+00	2,39E+04
NA007-080c3	080c3_A_14	3,75E+00	1,18E+00	1,24E-01	1,10E-01	5,37E-02	6,86E-02	4,28E+02	4,41E+02	8,05E-01	1,99E+04	5,48E+03	3,22E+00	2,44E+04
NA007-080c3	080c3_A_15	3,19E+00	8,40E-01	1,45E-01	2,04E-02	8,94E-02	4,64E-02	n.d.	n.d.	n.d.	2,57E+04	9,07E+03	3,45E+00	2,57E+04
NA007-080c3	080c3_A_16	4,33E+00	9,44E-01	1,34E-01	3,75E-02	1,25E-01	4,61E-02	n.d.	n.d.	n.d.	2,77E+04	8,45E+03	3,36E+00	2,66E+04
NA007-080c3	080c3_A_17	6,24E+00	4,29E+00	1,52E-01	2,98E-03	4,80E-02	9,11E-03	n.d.	n.d.	n.d.	1,76E+04	1,74E+03	3,94E+00	2,58E+04
NA007-080c3	080c3_A_18	2,08E+00	1,00E+00	1,24E-01	1,52E-02	6,31E-02	5,48E-02	n.d.	n.d.	n.d.	1,79E+04	8,63E+03	3,13E+00	2,18E+04
NA007-080c3	080c3_A_19	2,29E+00	9,29E-01	1,21E-01	n.d.	n.d.	n.d.	n.d.	n.d.	n.d.	1,51E+04	4,23E+02	3,11E+00	2,15E+04
NA007-080c3	080c3_A_2	1,48E+00	1,54E+00	1,10E-01	2,92E-02	6,26E-02	3,55E-02	n.d.	n.d.	n.d.	1,01E+04	8,31E+03	3,06E+00	1,63E+04
NA007-080c3	080c3_A_20	2,73E+00	9,91E-01	1,16E-01	5,65E-02	1,34E-01	1,61E-02	n.d.	n.d.	n.d.	1,61E+04	3,84E+03	3,23E+00	2,14E+04
NA007-080c3	080c3_A_21	2,22E+00	1,67E+00	1,37E-01	3,64E-02	8,43E-02	2,25E-02	n.d.	n.d.	n.d.	1,90E+04	5,05E+03	3,58E+00	2,30E+04
NA007-080c3	080c3_A_22	7,28E+00	1,67E+00	1,12E-01	1,67E-01	2,90E-01	1,89E-02	5,52E+02	1,17E+03	1,00E+00	4,50E+04	8,19E+03	3,15E+00	3,40E+04
NA007-080c3	080c3_A_23	2,26E+00	6,69E-01	1,27E-01	2,76E-02	7,90E-02	4,20E-02	n.d.	n.d.	n.d.	1,88E+04	4,40E+03	3,20E+00	2,35E+04
NA007-080c3	080c3_A_24	2,77E+00	1,23E+00	1,84E-01	3,90E-02	8,26E-02	2,73E-02	n.d.	n.d.	n.d.	2,19E+04	5,33E+03	4,10E+00	2,58E+04
NA007-080c3	080c3_A_25	1,07E+00	3,53E-01	1,45E-01	3,10E-02	8,79E-02	8,32E-02	n.d.	n.d.	n.d.	1,04E+04	4,93E+02	3,90E+00	1,46E+04
NA007-080c3	080c3_A_26	1,24E+00	5,06E-01	1,33E-01	5,17E-02	9,81E-02	2,30E-02	n.d.	n.d.	n.d.	1,02E+04	2,80E+03	3,61E+00	1,50E+04
NA007-080c3	080c3_A_27	1,33E+00	3,26E-01	1,14E-01	1,80E-02	6,84E-02	3,69E-02	n.d.	n.d.	n.d.	1,16E+04	7,77E+02	3,26E+00	1,46E+04
NA007-080c3	080c3_A_28	1,30E+00	5,48E-01	1,23E-01	3,64E-02	9,05E-02	6,46E-02	n.d.	n.d.	n.d.	1,23E+04	5,17E+03	3,39E+00	1,73E+04
NA007-080c3	080c3_A_29	1,81E+00	7,03E-01	1,37E-01	4,31E-02	1,06E-01	3,61E-02	n.d.	n.d.	n.d.	1,30E+04	3,40E+03	3,72E+00	1,70E+04
NA007-080c3	080c3_A_3	1,22E+00	6,53E-01	1,24E-01	1,69E-02	5,64E-02	1,78E-02	n.d.	n.d.	n.d.	1,08E+04	3,21E+03	3,10E+00	1,75E+04
NA007-080c3	080c3_A_30	1,41E+00	5,76E-01	1,24E-01	2,19E-02	5,60E-02	7,80E-02	n.d.	n.d.	n.d.	1,17E+04	2,05E+03	3,38E+00	1,87E+04
NA007-080c3	080c3_A_31	1,61E+00	6,48E-01	1,34E-01	3,15E-02	1,27E-01	3,34E-02	1,86E+02	3,05E+03	7,42E-01	1,24E+04	2,65E+03	3,48E+00	1,33E+04
NA007-080c3	080c3_A_32	2,42E+00	1,34E+00	1,27E-01	8,19E-02	1,02E-01	1,99E-02	7,26E+02	2,15E+03	1,34E+00	1,19E+04	2,97E+03	3,20E+00	1,49E+04
NA007-080c3	080c3_A_33	2,32E+00	8,82E-01	1,12E-01	6,26E-02	1,47E-01	6,75E-02	n.d.	n.d.	n.d.	2,17E+04	2,78E+03	3,06E+00	2,25E+04
NA007-080c3	080c3_A_34	3,22E+00	8,59E-01	1,39E-01	7,01E-02	1,36E-01	3,12E-02	n.d.	n.d.	n.d.	2,26E+04	3,15E+03	3,59E+00	2,36E+04
NA007-080c3	080c3_A_35	2,94E+00	1,91E+00	1,26E-01	1,42E-01	1,71E-01	2,04E-02	8,54E+02	1,38E+03	1,49E+00	1,26E+04	3,92E+03	3,14E+00	1,51E+04
NA007-080c3	080c3_A_36	1,58E+00	7,00E-01	1,15E-01	5,50E-02	9,77E-02	6,96E-02	n.d.	n.d.	n.d.	1,42E+04	3,24E+03	3,23E+00	2,17E+04
NA007-080c3	080c3_A_37	2,32E+00	7,80E-01	1,10E-01	4,46E-02	6,14E-02	2,63E-02	5,05E+02	1,12E+03	1,21E+00	1,50E+04	3,03E+03	3,24E+00	3,00E+04
NA007-080c3	080c3_A_38	2,25E+00	9,56E-01	1,19E-01	2,26E-02	4,71E-02	4,59E-02	n.d.	n.d.	n.d.	1,55E+04	1,79E+03	3,14E+00	2,25E+04
NA007-080c3	080c3_A_39	2,41E+00	3,31E-01	1,48E-01	n.d.	n.d.	n.d.	n.d.	n.d.	n.d.	1,58E+04	1,72E+03	3,53E+00	2,27E+04
NA007-080c3	080c3_A_4	1,26E+00	5,23E-01	1,12E-01	5,75E-03	8,66E-02	7,35E-03	n.d.	n.d.	n.d.	1,19E+04	1,23E+03	3,00E+00	1,98E+04
NA007-080c3	080c3_A_40	1,55E+00	7,20E-01	1,16E-01	2,46E-02	4,35E-02	9,30E-02	n.d.	n.d.	n.d.	1,42E+04	4,28E+03	2,84E+00	2,04E+04
NA007-080c3	080c3_A_41	2,22E+00	1,04E+00	1,37E-01	9,23E-02	1,06E-01	3,23E-02	1,25E+03	3,63E+03	2,25E+00	1,34E+04	3,12E+03	3,63E+00	1,93E+04
NA007-080c3	080c3_A_42	1,70E+00	1,09E+00	1,70E-01	2,84E-02	6,85E-03	7,91E+00	4,35E+02	2,42E+03	1,81E+00	1,38E+04	2,94E+03	3,92E+00	1,80E+04
NA007-080c3	080c3_A_43	2,64E+00	1,63E+00	1,52E-01	2,08E-01	3,37E-01	8,63E-02	5,58E+03	9,25E+03	2,69E+00	1,71E+04	3,58E+03	3,83E+00	3,18E+04
NA007-080c3	080c3_A_44	2,47E+00	3,37E-01	1,50E-01	1,18E-01	1,11E-01	9,81E-02	1,07E+03	5,48E+02	2,19E+00	1,77E+04	4,45E+03	3,69E+00	1,76E+04
NA007-080c3	080c3_A_45	2,64E+00	1,19E+00	1,98E-01	5,79E-02	1,16E-01	1,09E-01	1,87E+03	6,40E+03	3,14E+00	2,21E+04	1,19E+04	4,57E+00	2,39E+04
NA007-080c3	080c3_A_5	1,62E+00	5,90E-01	1,48E-01	1,78E-03	5,74E-02	3,60E-03	n.d.	n.d.	n.d.	1,26E+04	2,86E+03	3,44E+00	2,10E+04
NA007-080c3	080c3_A_6	1,56E+00	3,40E-01	1,36E-01	1,56E-03	6,36E-02	7,58E-03	n.d.	n.d.	n.d.	1,09E+04	2,19E+03	3,77E+00	1,87E+04
NA007-080c3	080c3_A_7	3,03E+00	7,93E-01	1,15E-01	n.d.	n.d.	n.d.	n.d.	n.d.	n.d.	1,52E+04	2,97E+03	3,14E+00	2,19E+04
NA007-080c3	080c3_A_8	2,33E+00	3,79E-01	1,01E-01	2,90E-02	8,07E-02	4,39E-02	n.d.	n.d.	n.d.	1,83E+04	4,68E+03	2,64E+00	2,04E+04
NA007-080c3	080c3_A_9	2,25E+00	1,49E+00	1,15E-01	3,41E-03	5,00E-02	4,64E-03	n.d.	n.d.	n.d.	1,82E+04	5,74E+03	2,75E+00	2,08E+04
NA007-092c	092c_A_1	5,40E+00	2,96E+00	3,82E-01	6,98E-01	7,18E-01	8,53E-02	n.d.	n.d.	n.d.	1,04E+04	6,12E+03	3,63E+01	2,64E+04
NA007-092c	092c_A_10	1,38E+00	4,45E-01	1,10E-01	6,07E-02	8,38E-02	6,79E-02	n.d.	n.d.	n.d.	3,93E+03	7,42E+02	8,36E+00	9,29E+03
NA007-092c	092c_A_11	3,91E+00	2,70E+00	1,67E-01	4,61E-01	4,80E-01	7,95E-02	n.d.	n.d.	n.d.	4,83E+03	8,75E+02	7,91E+00	1,21E+04
NA007-092c	092c_A_12	3,82E+00	2,29E+00	1,59E-01	2,83E-01	1,51E-01	7,90E-02	n.d.	n.d.	n.d.	5,28E+03	3,98E+02	8,33E+00	1,17E+04
NA007-092c	092c_A_13	2,97E+00	2,28E+00	1,40E-01	2,71E-01	3,53E-01	1,88E-02	7,60E+02	8,33E+03	5,37E-01	4,96E+03	1,25E+03	6,86E+00	1,07E+04
NA007-092c	092c_A_2	2,77E+00	3,46E+00	2,93E-01	7,27E-01	1,42E+00	1,76E-01	2,49E+03	7,87E+03	1,67E+00	8,13E+03	7,66E+03	3,89E+01	2,95E+04
NA007-092c	092c_A_4	6,52E+00	9,98E+00	8,62E-01	2,40E+00	3,23E+00	2,41E-01	1,04E+04	2,23E+04	7,29E+00	1,38E+04	1,55E+04	1,14E+02	6,36E+04
NA007-092c	092c_A_5	1,03E+01	1,24E+01	1,15E+00	3,10E+00	4,91E+00	2,88E-01	1,87E+04	3,27E+04	1,05E+01	1,87E+04	2,06E+04	1,21E+02	9,46E+04
NA007-092c	092c_A_6	5,93E+00	3,41E+00	4,17E-01	5,35E-01	4,87E-01	8,47E-02	n.d.	n.d.	n.d.	3,03E+04	5,35E+04	1,77E+01	1,91E+04
NA007-092c	092c_A_9	1,77E+00	8,99E-01	1,47E-01	1,13E-01	1,53E-01	1,97E-02	n.d.	n.d.	n.d.	4,27E+03	1,15E+03	1,03E+01	1,13E+04
NA007-100b (matrix)	100bA_matrix_1	5,14E+00	1,14E+00	1,20E-01	2,11E-02	3,06E-02	4,93E-02	n.d.	n.d.	n.d.	3,79E+03	5,38E+02	6,88E+00	7,94E+03
NA007-100b (matrix)	100bA_matrix_10	4,14E+00	1,80E+00	1,33E-01	1,12E-01	2,07E-01	2,50E-02	n.d.	n.d.	n.d.	6,22E+03	1,80E+03	5,74E+00	8,38E+03
NA007-100b (matrix)	100bA_matrix_2	3,55E+00	5,04E-01	1,26E-01	3,39E-02	8,40E-02	2,35E-02	n.d.	n.d.	n.d.	4,09E+03	6,65E+02	7,23E+00	8,56E+03
NA007-100b (matrix)	100bA_matrix_3	4,08E+00	1,05E+00	1,22E-01	2,20E-02	4,14E-02	4,43E-02	n.d.	n.d.	n.d.	3,43E+03	3,78E+02	7,89E+00	7,85E+03
NA007-100b (matrix)	100bA_matrix_4	4,25E+00	8,59E-01	1,30E-01	3,38E-02	6,20E-02	1,06E-01	n.d.	n.d.	n.d.	3,84E+03	3,10E+02	7,36E+00	8,18E+03
NA007-100b (matrix)	100bA_matrix_5	4,86E+00	2,11E+00	1,70E-01	3,21E-02	8,74E-02	1,57E-01	n.d.	n.d.	n.d.	5,34E+03	8,03E+02	7,55E+00	7,78E+03
NA007-100b (matrix)	100bA_matrix_6	4,58E+00	1,10E+00	1,16E-01	2,42E-02	7,87E-02	1,22E-01	n.d.	n.d.	n.d.	5,71E+03	1,11E+03	5,62E+00	8,36E+03
NA007-100b (matrix)	100bA_matrix_7	3,10E+00	8,52E-01	1,16E-01	3,84E-02	1,42E-01	9,37E-02	n.d.	n.d.	n.d.	5,62E+03	3,41E+02	5,29E+00	8,49E+03
NA007-100b (matrix)	100bA_matrix_8	2,75E+00	4,64E-01	1,26E-01	5,34E-02	1,58E-01	8,19E-02	n.d.	n.d.	n.d.	5,10E+03	1,16E+03	5,47E+00	7,86E+03
NA007-100b (matrix)	100bA_matrix_9	3,60E+00	1,45E+00	1,32E-01	3,74E-02	7,46E-02	6,99E-02	n.d.	n.d.	n.d.	5,64E+03	1,26E+03	6,19E+00	8,29E+03

Analysis	Al27_2SD	Al27_LOD	Si29_mean	Si29_2SD	Si29_LOD	P31_mean	P31_2SD	P31_LOD	K39_mean	K39_2SD	K39_LOD	Ca43_mean	Ca43_2SD	Ca43_LOD
	(ppm)	(ppm)	(ppm)	(ppm)	(ppm)	(ppm)	(ppm)	(ppm)	(ppm)	(ppm)	(ppm)	(ppm)	(ppm)	(ppm)
080c2_B_7	4,83E+03	7,83E-01	n.d.	n.d.	n.d.	5,40E+01	1,90E+02	6,18E+00	3,38E+02	2,99E+02	1,18E+00	n.d.	n.d.	n.d.
080c2_B_8	2,33E+03	7,15E-01	n.d.	n.d.	n.d.	2,96E+02	2,48E+02	1,30E+01	6,16E+02	1,60E+02	1,05E+00	n.d.	n.d.	n.d.
080c2_B_9	3,46E+03	7,30E-01	n.d.	n.d.	n.d.	1,60E+02	1,56E+02	1,07E+01	3,67E+02	1,24E+02	1,07E+00	n.d.	n.d.	n.d.
080c3_A_1	3,63E+03	6,28E-01	n.d.	n.d.	n.d.	n.d.	n.d.	n.d.	3,17E+02	1,18E+02	7,72E-01	1,10E+03	1,62E+03	7,66E+01
080c3_A_10	4,77E+03	5,92E-01	n.d.	n.d.	n.d.	n.d.	n.d.	n.d.	2,01E+02	2,74E+02	6,98E-01	n.d.	n.d.	n.d.
080c3_A_11	4,32E+03	6,14E-01	n.d.	n.d.	n.d.	n.d.	n.d.	n.d.	6,13E+02	4,33E+02	8,01E-01	3,37E+03	4,55E+02	8,74E+01
080c3_A_12	7,12E+03	6,48E-01	n.d.	n.d.	n.d.	< Det. Lim	1,15E+02	1,22E+02	1,08E+02	2,73E+02	8,86E-01	n.d.	n.d.	n.d.
080c3_A_13	4,95E+03	7,09E-01	n.d.	n.d.	n.d.	n.d.	n.d.	n.d.	4,63E+01	5,61E+01	9,12E-01	n.d.	n.d.	n.d.
080c3_A_14	6,75E+03	7,08E-01	n.d.	n.d.	n.d.	n.d.	n.d.	n.d.	9,68E+02	7,71E+02	9,02E-01	5,23E+02	1,59E+03	4,97E+01
080c3_A_15	6,95E+03	7,73E-01	n.d.	n.d.	n.d.	n.d.	n.d.	n.d.	4,02E+01	3,58E+01	9,98E-01	n.d.	n.d.	n.d.
080c3_A_16	2,21E+03	7,63E-01	n.d.	n.d.	n.d.	n.d.	n.d.	n.d.	3,28E+02	5,03E+02	9,58E-01	n.d.	n.d.	n.d.
080c3_A_17	2,98E+03	8,78E-01	n.d.	n.d.	n.d.	< Det. Lim	1,17E+02	1,80E+02	5,74E+02	6,66E+02	1,15E+00	n.d.	n.d.	n.d.
080c3_A_18	4,69E+03	6,71E-01	n.d.	n.d.	n.d.	n.d.	n.d.	n.d.	6,91E+01	1,18E+02	9,76E-01	n.d.	n.d.	n.d.
080c3_A_19	3,65E+03	6,67E-01	n.d.	n.d.	n.d.	n.d.	n.d.	n.d.	9,63E+01	4,05E+01	9,22E-01	n.d.	n.d.	n.d.
080c3_A_2	1,16E+04	5,80E-01	n.d.	n.d.	n.d.	n.d.	n.d.	n.d.	1,63E+01	1,32E+02	4,94E-01	n.d.	n.d.	n.d.
080c3_A_20	3,58E+03	7,05E-01	n.d.	n.d.	n.d.	n.d.	n.d.	n.d.	2,67E+02	3,24E+02	9,43E-01	n.d.	n.d.	n.d.
080c3_A_21	8,75E+03	8,05E-01	n.d.	n.d.	n.d.	n.d.	n.d.	n.d.	2,15E+01	3,12E+01	1,27E+00	n.d.	n.d.	n.d.
080c3_A_22	3,64E+03	6,85E-01	n.d.	n.d.	n.d.	n.d.	n.d.	n.d.	5,77E+02	7,14E+02	9,28E-01	9,69E+03	9,52E+03	9,79E+01
080c3_A_23	7,72E+03	7,02E-01	n.d.	n.d.	n.d.	n.d.	n.d.	n.d.	9,62E+01	8,65E+01	1,01E+00	n.d.	n.d.	n.d.
080c3_A_24	7,14E+03	8,81E-01	n.d.	n.d.	n.d.	< Det. Lim	1,28E+02	2,21E+02	6,33E+01	5,83E+01	1,34E+00	n.d.	n.d.	n.d.
080c3_A_25	1,28E+03	8,51E-01	n.d.	n.d.	n.d.	n.d.	n.d.	n.d.	3,41E+01	3,90E+01	1,50E+00	n.d.	n.d.	n.d.
080c3_A_26	4,18E+03	9,86E-01	n.d.	n.d.	n.d.	n.d.	n.d.	n.d.	3,18E+02	2,58E+02	1,06E+00	n.d.	n.d.	n.d.
080c3_A_27	1,29E+03	7,17E-01	n.d.	n.d.	n.d.	< Det. Lim	1,27E+02	1,17E+02	1,86E+01	4,33E+01	1,47E+00	n.d.	n.d.	n.d.
080c3_A_28	5,39E+03	7,15E-01	n.d.	n.d.	n.d.	< Det. Lim	7,56E+01	1,26E+02	1,86E+02	1,68E+02	1,06E+00	n.d.	n.d.	n.d.
080c3_A_29	3,03E+03	7,89E-01	n.d.	n.d.	n.d.	n.d.	n.d.	n.d.	2,37E+02	2,60E+02	1,17E+00	n.d.	n.d.	n.d.
080c3_A_3	6,14E+03	5,86E-01	n.d.	n.d.	n.d.	n.d.	n.d.	n.d.	3,59E+00	4,76E+01	2,30E-01	n.d.	n.d.	n.d.
080c3_A_30	3,41E+03	6,96E-01	n.d.	n.d.	n.d.	n.d.	n.d.	n.d.	4,91E+01	5,41E+01	1,30E+00	n.d.	n.d.	n.d.
080c3_A_31	2,45E+03	7,49E-01	n.d.	n.d.	n.d.	< Det. Lim	8,87E+01	1,85E+02	2,60E+02	3,25E+02	1,14E+00	n.d.	n.d.	n.d.
080c3_A_32	6,98E+03	6,76E-01	n.d.	n.d.	n.d.	< Det. Lim	1,22E+02	1,19E+02	4,19E+02	4,96E+02	9,78E-01	n.d.	n.d.	n.d.
080c3_A_33	3,23E+03	6,57E-01	n.d.	n.d.	n.d.	n.d.	n.d.	n.d.	3,01E+01	2,00E+01	1,58E+00	n.d.	n.d.	n.d.
080c3_A_34	5,21E+03	7,48E-01	n.d.	n.d.	n.d.	n.d.	n.d.	n.d.	1,09E+02	6,33E+01	1,32E+00	n.d.	n.d.	n.d.
080c3_A_35	5,74E+03	6,47E-01	n.d.	n.d.	n.d.	n.d.	n.d.	n.d.	9,16E+02	9,89E+02	9,03E-01	n.d.	n.d.	n.d.
080c3_A_36	5,33E+03	6,49E-01	n.d.	n.d.	n.d.	n.d.	n.d.	n.d.	1,55E+02	1,52E+02	1,01E+00	n.d.	n.d.	n.d.
080c3_A_37	7,50E+03	6,46E-01	n.d.	n.d.	n.d.	n.d.	n.d.	n.d.	1,78E+02	1,48E+02	1,01E+00	1,88E+03	5,54E+03	4,42E+01
080c3_A_38	3,25E+03	6,53E-01	n.d.	n.d.	n.d.	n.d.	n.d.	n.d.	2,49E+02	1,58E+02	1,05E+00	n.d.	n.d.	n.d.
080c3_A_39	1,75E+03	7,34E-01	n.d.	n.d.	n.d.	n.d.	n.d.	n.d.	3,48E+02	4,79E+02	1,19E+00	n.d.	n.d.	n.d.
080c3_A_4	3,06E+03	6,68E-01	n.d.	n.d.	n.d.	7,23E+01	4,48E+02	6,19E+00	n.d.	n.d.	n.d.	3,70E+02	4,03E+02	1,18E+02
080c3_A_40	5,90E+03	5,82E-01	n.d.	n.d.	n.d.	n.d.	n.d.	n.d.	3,04E+01	2,72E+01	1,88E+00	n.d.	n.d.	n.d.
080c3_A_41	5,51E+03	8,34E-01	n.d.	n.d.	n.d.	n.d.	n.d.	n.d.	3,12E+02	2,70E+02	1,30E+00	n.d.	n.d.	n.d.
080c3_A_42	6,83E+03	9,00E-01	n.d.	n.d.	n.d.	< Det. Lim	2,29E+02	5,22E+02	2,05E+02	4,86E+02	1,55E+00	n.d.	n.d.	n.d.
080c3_A_43	1,90E+04	1,04E+00	n.d.	n.d.	n.d.	n.d.	n.d.	n.d.	1,06E+03	2,20E+03	1,30E+00	2,96E+03	1,05E+04	6,19E+01
080c3_A_44	3,37E+03	8,54E-01	n.d.	n.d.	n.d.	n.d.	n.d.	n.d.	4,78E+02	2,65E+02	1,34E+00	1,82E+03	3,15E+03	4,84E+01
080c3_A_45	7,58E+03	1,05E+00	n.d.	n.d.	n.d.	n.d.	n.d.	n.d.	4,26E+02	2,12E+02	1,63E+00	9,60E+03	2,20E+04	1,30E+02
080c3_A_5	3,12E+03	7,73E-01	n.d.	n.d.	n.d.	n.d.	n.d.	n.d.	1,56E+01	5,90E+01	7,40E-01	8,97E+01	2,16E+02	1,27E+02
080c3_A_6	2,75E+03	8,49E-01	n.d.	n.d.	n.d.	n.d.	n.d.	n.d.	1,19E+02	8,06E+01	9,61E-01	1,09E+02	3,63E+02	6,58E+01
080c3_A_7	4,83E+03	7,12E-01	n.d.	n.d.	n.d.	n.d.	n.d.	n.d.	2,53E+01	1,73E+01	7,38E-01	n.d.	n.d.	n.d.
080c3_A_8	2,50E+03	6,01E-01	n.d.	n.d.	n.d.	n.d.	n.d.	n.d.	4,86E+01	6,29E+01	7,09E-01	n.d.	n.d.	n.d.
080c3_A_9	6,97E+03	6,37E-01	n.d.	n.d.	n.d.	n.d.	n.d.	n.d.	7,22E+01	1,86E+02	7,40E-01	n.d.	n.d.	n.d.
092c_A_1	2,67E+04	4,06E+00	n.d.	n.d.	n.d.	< Det. Lim	1,26E+03	2,82E+02	5,25E+03	8,48E+03	4,56E+00	n.d.	n.d.	n.d.
092c_A_10	2,08E+03	8,85E-01	< Det. Lim	2,37E+04	6,44E+04	4,42E+03	9,07E+03	3,41E+01	4,69E+01	9,67E+01	8,58E-01	2,58E+03	1,10E+04	4,92E+01
092c_A_11	2,78E+03	9,36E-01	n.d.	n.d.	n.d.	< Det. Lim	3,40E+02	1,01E+02	9,34E+02	8,55E+02	1,30E+00	n.d.	n.d.	n.d.
092c_A_12	2,13E+03	1,03E+00	n.d.	n.d.	n.d.	< Det. Lim	2,77E+02	8,22E+01	7,23E+02	5,43E+02	1,31E+00	n.d.	n.d.	n.d.
092c_A_13	9,17E+02	8,50E-01	n.d.	n.d.	n.d.	< Det. Lim	3,30E+02	6,33E+01	4,18E+02	4,37E+02	1,09E+00	n.d.	n.d.	n.d.
092c_A_2	3,37E+04	2,49E+00	n.d.	n.d.	n.d.	< Det. Lim	9,35E+02	2,70E+02	6,22E+03	8,51E+03	3,11E+00	n.d.	n.d.	n.d.
092c_A_4	8,39E+04	5,94E+00	n.d.	n.d.	n.d.	< Det. Lim	1,84E+03	3,82E+02	2,12E+04	2,89E+04	8,03E+00	n.d.	n.d.	n.d.
092c_A_5	1,21E+05	7,25E+00	n.d.	n.d.	n.d.	< Det. Lim	4,97E+03	6,52E+02	3,66E+04	5,23E+04	1,09E+01	n.d.	n.d.	n.d.
092c_A_6	5,75E+03	3,27E+00	n.d.	n.d.	n.d.	7,99E+03	1,82E+04	1,19E+02	8,96E+02	6,85E+02	3,26E+00	4,65E+03	2,12E+04	1,46E+02
092c_A_9	3,03E+03	1,00E+00	n.d.	n.d.	n.d.	< Det. Lim	6,10E+02	9,37E+01	1,07E+03	5,68E+02	1,24E+00	n.d.	n.d.	n.d.
100bA_matrix_1	1,49E+03	7,97E-01	< Det. Lim	1,98E+04	5,42E+04	< Det. Lim	5,67E+02	1,74E+02	n.d.	n.d.	n.d.	n.d.	n.d.	n.d.
100bA_matrix_10	1,14E+03	8,13E-01	n.d.	n.d.	n.d.	< Det. Lim	5,26E+02	7,91E+01	1,21E+02	1,25E+02	1,07E+00	n.d.	n.d.	n.d.
100bA_matrix_2	1,71E+03	8,18E-01	n.d.	n.d.	n.d.	< Det. Lim	4,31E+02	7,50E+01	n.d.	n.d.	n.d.	n.d.	n.d.	n.d.
100bA_matrix_3	8,72E+02	7,73E-01	< Det. Lim	1,21E+04	3,38E+04	n.d.	n.d.	n.d.	n.d.	n.d.	n.d.	n.d.	n.d.	n.d.
100bA_matrix_4	1,11E+03	8,12E-01	n.d.	n.d.	n.d.	< Det. Lim	3,29E+02	6,50E+01	2,25E+02	5,07E+02	9,91E-01	n.d.	n.d.	n.d.
100bA_matrix_5	1,49E+03	1,08E+00	< Det. Lim	1,71E+04	4,07E+04	< Det. Lim	5,03E+02	1,32E+02	3,07E+00	1,24E+01	3,16E-01	n.d.	n.d.	n.d.
100bA_matrix_6	2,22E+03	7,98E-01	n.d.	n.d.	n.d.	n.d.	n.d.	n.d.	5,92E+01	1,03E+02	9,51E-01	n.d.	n.d.	n.d.
100bA_matrix_7	8,39E+02	7,43E-01	n.d.	n.d.	n.d.	< Det. Lim	3,83E+02	2,18E+02	5,32E+01	1,01E+02	8,44E-01	n.d.	n.d.	n.d.
100bA_matrix_8	2,01E+03	7,46E-01	n.d.	n.d.	n.d.	n.d.	n.d.	n.d.	9,48E+00	2,32E+01	5,38E-01	n.d.	n.d.	n.d.
100bA_matrix_9	1,95E+03	8,28E-01	< Det. Lim	2,83E+04	2,06E+04	8,20E+03	5,88E+03	3,61E+01	5,11E+01	9,11E+01	9,94E-01	5,85E+03	7,40E+03	6,73E+01

Analysis	Ca44_mean (ppm)	Ca44_2SD (ppm)	Ca44_LOD (ppm)	Sc45_mean (ppm)	Sc45_2SD (ppm)	Sc45_LOD (ppm)	Ti47_mean (ppm)	Ti47_2SD (ppm)	Ti47_LOD (ppm)	V51_mean (ppm)	V51_2SD (ppm)	V51_LOD (ppm)	Cr53_mean (ppm)	Cr53_2SD (ppm)
080c2_B_7	n.d.	n.d.	n.d.	2,42E+01	5,37E+00	6,51E-02	6,93E+04	1,62E+04	8,44E-01	5,59E+03	3,21E+02	8,97E-02	4,40E+02	5,46E+01
080c2_B_8	n.d.	n.d.	n.d.	2,59E+01	3,31E+00	5,54E-02	8,25E+04	5,62E+03	7,97E-01	6,08E+03	3,52E+02	8,35E-02	4,51E+02	4,92E+01
080c2_B_9	n.d.	n.d.	n.d.	2,63E+01	3,74E+00	5,81E-02	7,36E+04	5,01E+03	8,25E-01	5,86E+03	2,62E+02	8,28E-02	3,19E+02	7,29E+01
080c3_A_1	4,21E+02	1,87E+03	1,67E+00	2,40E+01	6,47E+00	4,87E-02	5,35E+04	8,99E+03	1,01E+00	4,04E+03	8,57E+02	7,43E-02	6,31E+01	1,27E+01
080c3_A_10	n.d.	n.d.	n.d.	2,36E+01	4,51E+00	4,65E-02	4,94E+04	9,70E+03	7,10E-01	3,69E+03	9,03E+02	6,55E-02	1,11E+01	5,17E+00
080c3_A_11	3,09E+03	7,55E+02	4,94E+00	2,51E+01	2,46E+00	5,28E-02	4,83E+04	7,15E+03	7,81E-01	3,56E+03	7,93E+02	7,50E-02	9,54E+00	1,35E+00
080c3_A_12	n.d.	n.d.	n.d.	1,76E+01	6,03E+00	5,68E-02	4,59E+04	8,17E+03	7,86E-01	3,54E+03	7,60E+02	7,31E-02	9,78E+00	4,19E+00
080c3_A_13	n.d.	n.d.	n.d.	2,23E+01	4,03E+00	5,75E-02	4,55E+04	8,59E+03	8,19E-01	3,40E+03	1,06E+03	8,15E-02	1,21E+01	8,49E+00
080c3_A_14	n.d.	n.d.	n.d.	2,44E+01	1,12E+01	6,24E-02	4,96E+04	1,36E+04	8,67E-01	3,71E+03	7,75E+02	8,42E-02	1,25E+01	3,58E+00
080c3_A_15	n.d.	n.d.	n.d.	2,72E+01	8,28E+00	6,43E-02	4,69E+04	1,50E+04	9,72E-01	3,77E+03	9,73E+02	9,00E-02	1,31E+01	5,69E+00
080c3_A_16	n.d.	n.d.	n.d.	2,68E+01	4,87E+00	6,11E-02	5,02E+04	9,44E+03	9,18E-01	3,74E+03	6,56E+02	8,97E-02	1,05E+01	3,09E+00
080c3_A_17	n.d.	n.d.	n.d.	2,05E+01	1,79E+00	7,78E-02	4,81E+04	6,18E+03	1,02E+00	3,63E+03	9,69E+02	1,02E-01	1,33E+01	4,02E+00
080c3_A_18	n.d.	n.d.	n.d.	1,95E+01	2,69E+00	5,84E-02	4,90E+04	6,66E+03	7,83E-01	3,54E+03	5,51E+02	7,56E-02	9,98E+00	2,85E+00
080c3_A_19	n.d.	n.d.	n.d.	1,85E+01	1,95E+00	5,81E-02	4,88E+04	4,04E+03	7,83E-01	3,40E+03	4,11E+02	8,00E-02	9,68E+00	2,64E+00
080c3_A_2	n.d.	n.d.	n.d.	1,50E+01	7,20E+00	4,96E-02	3,69E+04	1,54E+04	9,32E-01	3,04E+03	1,19E+03	7,06E-02	2,44E+02	8,16E+01
080c3_A_20	n.d.	n.d.	n.d.	2,01E+01	3,17E+00	6,02E-02	5,33E+04	6,39E+03	7,99E-01	4,07E+03	7,13E+02	8,09E-02	1,24E+01	4,80E+00
080c3_A_21	n.d.	n.d.	n.d.	2,19E+01	8,04E+00	6,88E-02	4,70E+04	1,88E+04	9,39E-01	3,48E+03	1,59E+03	9,56E-02	1,11E+01	7,14E+00
080c3_A_22	1,04E+04	1,10E+04	6,49E+00	4,44E+01	1,20E+01	5,80E-02	5,27E+04	8,36E+03	8,33E-01	3,14E+03	4,06E+02	8,62E-02	1,15E+01	6,34E+00
080c3_A_23	n.d.	n.d.	n.d.	2,35E+01	7,95E+00	6,10E-02	5,31E+04	9,74E+03	8,44E-01	3,78E+03	6,12E+02	8,28E-02	1,39E+01	1,83E+01
080c3_A_24	n.d.	n.d.	n.d.	2,21E+01	2,94E+00	8,27E-02	5,21E+04	9,01E+03	1,08E+00	5,07E+03	7,25E+02	1,09E-01	1,08E+02	2,55E+01
080c3_A_25	n.d.	n.d.	n.d.	2,71E+01	3,79E+00	7,06E-02	5,79E+04	5,21E+03	9,74E-01	3,60E+03	5,07E+02	9,30E-02	2,32E+01	1,13E+01
080c3_A_26	n.d.	n.d.	n.d.	1,93E+01	5,53E+00	6,67E-02	4,64E+04	1,37E+04	8,64E-01	3,10E+03	8,58E+02	8,93E-02	1,43E+01	4,77E+00
080c3_A_27	n.d.	n.d.	n.d.	2,24E+01	3,40E+00	6,37E-02	5,10E+04	2,55E+03	8,35E-01	3,40E+03	5,23E+02	8,28E-02	1,17E+01	2,12E+00
080c3_A_28	n.d.	n.d.	n.d.	2,30E+01	5,42E+00	6,32E-02	5,14E+04	1,32E+04	8,44E-01	3,32E+03	5,43E+02	8,58E-02	1,44E+01	1,67E+01
080c3_A_29	n.d.	n.d.	n.d.	2,51E+01	4,95E+00	7,31E-02	5,92E+04	1,39E+04	9,54E-01	3,64E+03	9,39E+02	9,46E-02	1,27E+01	3,55E+00
080c3_A_3	n.d.	n.d.	n.d.	1,49E+01	4,72E+00	5,40E-02	3,89E+04	9,80E+03	9,25E-01	3,38E+03	7,98E+02	7,47E-02	2,74E+02	5,94E+01
080c3_A_30	n.d.	n.d.	n.d.	2,45E+01	5,63E+00	6,18E-02	5,38E+04	1,08E+04	8,23E-01	3,86E+03	8,27E+02	8,67E-02	2,98E+02	9,08E+01
080c3_A_31	n.d.	n.d.	n.d.	3,84E+01	6,25E+00	6,28E-02	7,29E+04	1,54E+04	8,79E-01	4,32E+03	8,36E+02	9,25E-02	2,40E+01	1,19E+01
080c3_A_32	n.d.	n.d.	n.d.	4,24E+01	4,70E+00	6,01E-02	9,23E+04	1,06E+04	8,43E-01	4,81E+03	6,78E+02	8,28E-02	1,53E+01	4,07E+00
080c3_A_33	n.d.	n.d.	n.d.	2,85E+01	5,92E+00	5,88E-02	5,94E+04	1,12E+04	8,09E-01	3,91E+03	6,94E+02	8,36E-02	1,12E+01	5,74E+00
080c3_A_34	n.d.	n.d.	n.d.	2,78E+01	4,45E+00	7,19E-02	5,81E+04	7,87E+03	9,36E-01	3,87E+03	7,89E+02	9,56E-02	1,22E+01	1,01E+01
080c3_A_35	n.d.	n.d.	n.d.	3,73E+01	7,51E+00	6,07E-02	7,18E+04	2,17E+04	8,02E-01	4,19E+03	1,29E+03	8,21E-02	2,14E+01	2,05E+01
080c3_A_36	n.d.	n.d.	n.d.	2,46E+01	3,42E+00	6,43E-02	5,81E+04	8,33E+03	8,23E-01	4,06E+03	3,03E+02	8,07E-02	1,17E+01	7,53E+00
080c3_A_37	1,96E+03	6,27E+03	2,90E+00	2,38E+01	2,97E+00	6,52E-02	5,73E+04	8,20E+03	8,38E-01	4,00E+03	5,15E+02	8,50E-02	9,08E+00	3,68E+00
080c3_A_38	n.d.	n.d.	n.d.	2,36E+01	1,47E+00	6,06E-02	5,57E+04	4,38E+03	8,15E-01	3,96E+03	9,57E+02	8,49E-02	1,28E+01	2,98E+00
080c3_A_39	n.d.	n.d.	n.d.	2,53E+01	2,34E+00	7,22E-02	5,84E+04	9,33E+03	9,23E-01	4,09E+03	8,47E+02	9,79E-02	2,39E+01	8,07E+00
080c3_A_4	n.d.	n.d.	n.d.	1,72E+01	1,15E+00	5,42E-02	4,35E+04	4,11E+03	7,68E-01	3,63E+03	4,23E+02	7,20E-02	2,89E+02	6,09E+01
080c3_A_40	n.d.	n.d.	n.d.	2,37E+01	4,50E+00	5,47E-02	5,99E+04	1,35E+04	7,29E-01	4,20E+03	1,20E+03	7,73E-02	8,88E+00	2,82E+00
080c3_A_41	n.d.	n.d.	n.d.	3,74E+01	3,26E+00	7,71E-02	7,08E+04	6,93E+03	9,01E-01	4,42E+03	3,27E+02	9,74E-02	3,29E+01	1,20E+01
080c3_A_42	n.d.	n.d.	n.d.	3,78E+01	4,61E+00	7,73E-02	7,25E+04	6,73E+03	1,01E+00	4,62E+03	5,95E+02	1,07E-01	2,61E+01	3,19E+00
080c3_A_43	3,35E+03	1,19E+04	4,72E+00	4,04E+01	4,54E+00	7,85E-02	7,30E+04	1,07E+04	1,01E+00	4,58E+03	9,00E+02	1,04E-01	3,58E+01	1,39E+01
080c3_A_44	2,64E+03	4,05E+03	4,23E+00	4,05E+01	5,52E+00	8,10E-02	7,53E+04	9,11E+03	1,01E+00	4,91E+03	1,71E+03	1,03E-01	1,51E+01	5,46E+00
080c3_A_45	1,14E+04	2,39E+04	9,95E+00	4,54E+01	2,51E+01	9,58E-02	6,48E+04	8,71E+03	1,17E+00	4,25E+03	1,38E+02	1,24E-01	2,99E+01	7,23E+00
080c3_A_5	n.d.	n.d.	n.d.	1,79E+01	1,73E+00	6,50E-02	4,41E+04	6,53E+03	8,75E-01	3,92E+03	6,98E+02	8,47E-02	2,62E+02	1,27E+02
080c3_A_6	n.d.	n.d.	n.d.	2,11E+01	4,11E+00	6,48E-02	4,51E+04	9,86E+03	9,14E-01	3,36E+03	8,26E+02	8,87E-02	2,95E+01	6,99E+00
080c3_A_7	n.d.	n.d.	n.d.	1,63E+01	2,59E+00	5,82E-02	4,37E+04	5,57E+03	7,96E-01	3,49E+03	1,52E+03	7,94E-02	9,44E+00	1,57E+00
080c3_A_8	n.d.	n.d.	n.d.	2,13E+01	3,63E+00	4,96E-02	4,81E+04	8,65E+03	7,19E-01	3,42E+03	4,85E+02	6,59E-02	1,09E+01	5,65E+00
080c3_A_9	n.d.	n.d.	n.d.	2,02E+01	5,70E+00	5,10E-02	4,43E+04	1,26E+04	7,60E-01	3,18E+03	9,72E+02	7,07E-02	2,24E+01	3,71E+01
092c_A_1	n.d.	n.d.	n.d.	2,96E+00	1,21E+00	1,21E-01	6,26E+04	1,69E+04	3,59E+00	4,75E+02	1,58E+02	1,98E-01	8,80E+01	1,12E+01
092c_A_10	2,78E+03	1,23E+04	4,13E+00	4,01E+00	1,31E+00	5,86E-02	5,73E+04	1,03E+04	1,06E+00	5,03E+02	8,90E+01	7,37E-02	2,47E+01	3,91E+00
092c_A_11	n.d.	n.d.	n.d.	5,00E+00	8,69E-01	7,71E-02	7,00E+04	7,71E+03	1,25E+00	6,31E+02	2,14E+02	9,76E-02	3,61E+01	9,35E+00
092c_A_12	n.d.	n.d.	n.d.	4,94E+00	1,37E+00	7,45E-02	6,86E+04	8,49E+03	1,33E+00	6,05E+02	1,46E+02	9,78E-02	2,62E+01	2,15E+00
092c_A_13	n.d.	n.d.	n.d.	4,81E+00	8,52E-01	6,16E-02	6,41E+04	2,56E+03	1,11E+00	5,83E+02	1,29E+02	8,18E-02	2,00E+01	3,38E+00
092c_A_2	n.d.	n.d.	n.d.	2,74E+00	3,23E+00	9,07E-02	5,83E+04	1,14E+04	2,70E+00	3,99E+02	2,06E+02	1,48E-01	4,87E+01	3,10E+01
092c_A_4	n.d.	n.d.	n.d.	2,25E+00	2,32E+00	1,36E-01	7,65E+04	3,57E+04	6,67E+00	3,80E+02	7,05E+01	2,95E-01	5,81E+01	4,84E+01
092c_A_5	n.d.	n.d.	n.d.	2,34E+00	4,74E+00	1,25E-01	8,95E+04	4,46E+04	7,15E+00	4,16E+02	2,53E+02	2,81E-01	7,72E+01	6,97E+01
092c_A_6	5,59E+03	2,49E+04	1,27E+01	8,84E+00	1,07E+01	1,87E-01	6,37E+04	1,43E+04	3,09E+00	4,14E+02	2,21E+02	1,80E-01	5,15E+01	7,46E+00
092c_A_9	n.d.	n.d.	n.d.	3,41E+00	1,49E+00	6,27E-02	5,89E+04	1,71E+04	1,17E+00	5,04E+02	1,65E+02	8,66E-02	2,67E+01	7,16E+00
100bA_matrix_1	n.d.	n.d.	n.d.	4,06E+00	1,31E+00	5,41E-02	6,37E+04	5,84E+03	9,32E-01	4,45E+02	1,02E+02	6,98E-02	2,54E+01	7,02E+00
100bA_matrix_10	n.d.	n.d.	n.d.	4,83E+00	1,33E+00	5,37E-02	6,30E+04	1,04E+04	1,06E+00	4,61E+02	7,02E+01	8,03E-02	2,34E+01	8,10E+00
100bA_matrix_2	n.d.	n.d.	n.d.	4,62E+00	1,64E+00	5,38E-02	6,69E+04	1,88E+04	1,01E+00	4,85E+02	1,89E+02	7,59E-02	3,16E+01	6,52E+00
100bA_matrix_3	n.d.	n.d.	n.d.	3,56E+00	1,13E+00	4,62E-02	5,92E+04	9,40E+03	8,82E-01	4,18E+02	1,19E+02	6,80E-02	2,72E+01	4,65E+00
100bA_matrix_4	n.d.	n.d.	n.d.	3,89E+00	1,04E+00	5,22E-02	5,74E+04	8,09E+03	1,00E+00	4,53E+02	5,67E+01	7,43E-02	2,73E+01	3,21E+00
100bA_matrix_5	n.d.	n.d.	n.d.	3,77E+00	1,79E+00	6,48E-02	6,14E+04	1,43E+04	1,32E+00	4,14E+02	1,30E+02	9,36E-02	7,65E+00	1,74E+00
100bA_matrix_6	n.d.	n.d.	n.d.	4,23E+00	1,28E+00	5,17E-02	5,84E+04	8,04E+03	9,85E-01	3,79E+02	5,17E+01	7,37E-02	9,06E+00	5,35E+00
100bA_matrix_7	n.d.	n.d.	n.d.	4,72E+00	1,35E+00	4,94E-02	6,79E+04	9,02E+03	9,59E-01	4,62E+02	7,42E+01	7,03E-02	1,54E+01	3,55E+00
100bA_matrix_8	n.d.	n.d.	n.d.	4,67E+00	1,22E+00	4,96E-02	6,17E+04	1,30E+04	9,73E-01	4,39E+02	6,24E+01	7,04E-02	1,52E+01	5,08E+00
100bA_matrix_9	7,81E+03	9,96E+03	5,89E+00	4,61E+00	8,79E-01	5,40E-02	6,59E+04	6,91E+03	1,01E+00	4,09E+02	6,14E+01	7,75E-02	1,71E+01	4,22E+00

Analysis	Cr53_LOD	Mn55_mean	Mn55_2SD	Mn55_LOD	Fe57_mean	Fe57_2SD	Fe57_LOD	Co59_mean	Co59_2SD	Co59_LOD	Ni60_mean	Ni60_2SD	Ni60_LOD	Cu63_mean
	(ppm)	(ppm)	(ppm)	(ppm)	(ppm)	(ppm)	(ppm)	(ppm)	(ppm)	(ppm)	(ppm)	(ppm)	(ppm)	(ppm)
080c2_B_7	1,05E+00	3,56E+03	2,74E+02	1,92E+00	5,99E+05	0,00E+00	4,49E+00	2,75E+02	5,89E+01	6,31E-02	2,36E+02	3,66E+01	1,14E-01	8,17E+01
080c2_B_8	9,62E-01	3,59E+03	3,93E+02	1,80E+00	5,99E+05	0,00E+00	4,18E+00	2,68E+02	2,10E+01	5,89E-02	2,49E+02	1,71E+01	1,05E-01	9,22E+01
080c2_B_9	9,81E-01	3,58E+03	9,36E+02	1,79E+00	5,99E+05	0,00E+00	4,11E+00	2,55E+02	2,72E+01	5,93E-02	2,03E+02	2,07E+01	1,05E-01	9,62E+01
080c3_A_1	8,99E-01	3,68E+03	5,69E+02	1,76E+00	5,93E+05	0,00E+00	4,94E+00	1,28E+02	2,80E+01	5,34E-02	1,17E+01	1,06E+00	1,05E-01	1,82E+01
080c3_A_10	1,46E+00	2,99E+03	5,42E+02	1,54E+00	5,93E+05	0,00E+00	4,00E+00	1,80E+02	6,13E+01	4,81E-02	2,03E+01	1,36E+01	8,49E-02	7,50E+02
080c3_A_11	1,85E+00	2,87E+03	3,46E+02	1,69E+00	5,93E+05	0,00E+00	4,41E+00	1,62E+02	1,17E+01	5,40E-02	1,16E+01	2,60E+00	8,95E-02	1,71E+01
080c3_A_12	1,83E+00	2,92E+03	7,52E+02	1,72E+00	5,93E+05	0,00E+00	4,36E+00	1,50E+02	2,44E+01	5,60E-02	1,10E+01	3,23E+00	9,84E-02	1,25E+01
080c3_A_13	1,91E+00	3,07E+03	1,28E+03	1,85E+00	5,93E+05	0,00E+00	4,72E+00	1,58E+02	3,53E+01	6,07E-02	8,64E+00	3,08E+00	9,01E-02	1,06E+01
080c3_A_14	1,70E+00	3,12E+03	1,07E+03	1,94E+00	5,93E+05	0,00E+00	4,83E+00	1,57E+02	2,51E+01	5,99E-02	1,58E+01	6,88E+00	1,13E-01	3,99E+01
080c3_A_15	1,96E+00	2,61E+03	4,52E+02	2,04E+00	5,93E+05	0,00E+00	5,10E+00	1,58E+02	4,41E+01	6,78E-02	1,48E+01	7,60E+00	1,01E-01	1,47E+01
080c3_A_16	2,60E+00	3,14E+03	7,58E+02	2,05E+00	5,93E+05	0,00E+00	5,13E+00	1,96E+02	7,07E+01	6,79E-02	1,20E+01	2,93E+00	1,12E-01	1,37E+01
080c3_A_17	2,18E+00	3,23E+03	4,21E+02	2,26E+00	5,93E+05	0,00E+00	5,62E+00	1,73E+02	8,01E+00	7,87E-02	1,95E+01	8,30E+00	1,30E-01	1,43E+01
080c3_A_18	1,90E+00	3,50E+03	7,48E+02	1,79E+00	5,93E+05	0,00E+00	4,48E+00	1,57E+02	3,35E+01	5,87E-02	1,41E+01	3,93E+00	8,98E-02	9,11E+00
080c3_A_19	1,82E+00	3,23E+03	2,65E+02	1,81E+00	5,93E+05	0,00E+00	4,42E+00	1,74E+02	4,66E+01	6,18E-02	1,44E+01	2,95E+00	9,35E-02	1,05E+01
080c3_A_2	8,09E-01	2,92E+03	8,06E+02	1,68E+00	5,93E+05	0,00E+00	4,82E+00	1,27E+02	2,80E+01	5,15E-02	1,62E+01	5,06E+00	1,01E-01	1,13E+01
080c3_A_20	1,72E+00	3,39E+03	6,90E+02	1,85E+00	5,93E+05	0,00E+00	4,55E+00	1,69E+02	2,57E+01	6,16E-02	1,43E+01	2,08E+00	1,02E-01	2,00E+01
080c3_A_21	2,44E+00	3,00E+03	1,09E+03	2,15E+00	5,93E+05	0,00E+00	5,00E+00	1,67E+02	3,18E+01	7,00E-02	1,49E+01	8,85E+00	1,08E-01	8,98E+00
080c3_A_22	1,98E+00	3,53E+03	3,41E+02	1,95E+00	5,93E+05	0,00E+00	4,82E+00	1,82E+02	1,56E+01	6,47E-02	2,66E+00	8,67E-01	9,85E-02	2,26E+01
080c3_A_23	1,94E+00	3,24E+03	7,11E+02	1,87E+00	5,93E+05	0,00E+00	4,51E+00	1,81E+02	4,19E+01	6,26E-02	1,46E+01	4,45E+00	9,17E-02	1,22E+01
080c3_A_24	1,33E+00	3,17E+03	4,24E+02	2,47E+00	5,83E+05	0,00E+00	6,03E+00	2,61E+02	1,14E+02	8,50E-02	2,98E+01	5,43E+00	1,37E-01	1,32E+01
080c3_A_25	1,48E+00	3,84E+03	6,88E+02	2,16E+00	5,83E+05	0,00E+00	5,19E+00	1,54E+02	4,16E+01	7,06E-02	1,53E+01	5,21E+00	1,09E-01	1,13E+01
080c3_A_26	1,73E+00	3,47E+03	9,73E+02	2,03E+00	5,83E+05	0,00E+00	4,82E+00	1,43E+02	3,59E+01	7,50E-02	1,39E+01	3,44E+00	1,13E-01	2,05E+01
080c3_A_27	1,61E+00	3,72E+03	5,69E+02	1,89E+00	5,83E+05	0,00E+00	4,49E+00	1,61E+02	6,63E+01	6,35E-02	1,84E+01	2,29E+00	9,26E-02	7,26E+00
080c3_A_28	1,69E+00	3,76E+03	8,52E+02	1,92E+00	5,83E+05	0,00E+00	4,45E+00	1,63E+02	2,77E+01	6,55E-02	1,99E+01	7,80E+00	9,95E-02	1,92E+01
080c3_A_29	1,86E+00	3,98E+03	8,61E+02	2,17E+00	5,83E+05	0,00E+00	5,12E+00	1,77E+02	4,93E+01	7,41E-02	2,00E+01	2,33E+00	1,16E-01	2,59E+01
080c3_A_3	8,18E-01	2,79E+03	3,82E+02	1,71E+00	5,93E+05	0,00E+00	4,92E+00	1,26E+02	2,19E+01	5,17E-02	1,43E+01	2,09E+00	9,90E-02	6,37E+00
080c3_A_30	9,81E-01	4,17E+03	1,64E+03	1,96E+00	5,83E+05	0,00E+00	8,10E+00	1,64E+02	2,35E+01	6,72E-02	9,53E+00	2,43E+00	9,93E-02	1,06E+01
080c3_A_31	1,31E+00	4,50E+03	7,38E+02	2,03E+00	5,83E+05	0,00E+00	4,61E+00	1,40E+02	1,77E+01	6,98E-02	7,14E+00	6,75E+00	1,03E-01	4,19E+01
080c3_A_32	1,41E+00	5,47E+03	9,24E+02	1,87E+00	5,91E+05	0,00E+00	4,22E+00	1,54E+02	2,42E+01	6,24E-02	5,43E+00	1,63E+00	9,65E-02	1,28E+01
080c3_A_33	1,76E+00	3,47E+03	7,44E+02	1,88E+00	5,91E+05	0,00E+00	4,27E+00	1,94E+02	3,32E+01	6,51E-02	1,61E+01	4,33E+00	9,75E-02	1,10E+01
080c3_A_34	2,11E+00	3,38E+03	5,26E+02	2,17E+00	5,91E+05	0,00E+00	4,86E+00	2,14E+02	5,16E+01	7,20E-02	1,74E+01	4,50E+00	1,11E-01	1,27E+01
080c3_A_35	1,30E+00	4,29E+03	1,20E+03	1,83E+00	5,91E+05	0,00E+00	4,04E+00	1,52E+02	2,11E+01	6,30E-02	5,45E+00	1,89E+00	8,47E-02	1,92E+01
080c3_A_36	1,69E+00	3,98E+03	3,73E+02	1,89E+00	6,06E+05	0,00E+00	4,29E+00	1,94E+02	5,43E+01	6,98E-02	1,50E+01	4,29E+00	9,92E-02	1,46E+01
080c3_A_37	2,04E+00	3,97E+03	5,68E+02	1,89E+00	6,06E+05	0,00E+00	4,25E+00	1,90E+02	2,15E+01	6,52E-02	1,59E+01	1,88E+00	9,40E-02	1,51E+01
080c3_A_38	1,43E+00	3,81E+03	3,77E+02	1,88E+00	6,06E+05	0,00E+00	4,23E+00	1,90E+02	2,00E+01	6,77E-02	1,53E+01	2,72E+00	1,00E-01	1,50E+01
080c3_A_39	1,39E+00	4,02E+03	2,44E+02	2,12E+00	6,06E+05	0,00E+00	4,79E+00	1,98E+02	2,58E+01	7,59E-02	1,60E+01	2,73E+00	1,19E-01	1,96E+01
080c3_A_4	8,10E-01	2,93E+03	3,98E+02	1,66E+00	5,93E+05	0,00E+00	4,63E+00	1,38E+02	1,86E+01	5,24E-02	1,50E+01	2,16E+00	9,41E-02	7,24E+00
080c3_A_40	1,48E+00	3,86E+03	6,31E+02	1,65E+00	6,06E+05	0,00E+00	3,68E+00	1,87E+02	3,06E+01	5,75E-02	1,53E+01	5,46E+00	9,03E-02	9,70E+00
080c3_A_41	1,36E+00	4,77E+03	5,01E+02	2,16E+00	6,13E+05	0,00E+00	4,72E+00	1,84E+02	1,17E+01	7,72E-02	9,77E+00	1,53E+00	1,17E-01	1,50E+01
080c3_A_42	1,55E+00	4,81E+03	4,23E+02	2,36E+00	6,18E+05	0,00E+00	5,02E+00	1,80E+02	1,29E+01	8,58E-02	8,13E+00	1,84E+00	1,11E-01	1,16E+01
080c3_A_43	1,49E+00	5,19E+03	4,46E+02	2,35E+00	6,18E+05	0,00E+00	5,08E+00	1,87E+02	1,91E+01	8,33E-02	8,29E+00	2,29E+00	1,07E-01	1,01E+01
080c3_A_44	1,76E+00	5,19E+03	4,81E+02	2,27E+00	6,21E+05	0,00E+00	1,42E+01	1,83E+02	1,38E+01	8,04E-02	6,06E+00	1,07E+00	1,12E-01	1,63E+01
080c3_A_45	1,83E+00	4,84E+03	2,34E+02	2,79E+00	6,21E+05	0,00E+00	6,25E+00	1,73E+02	1,11E+01	1,03E-01	1,03E+01	2,08E+00	1,34E-01	4,71E+01
080c3_A_5	9,89E-01	3,03E+03	5,28E+02	1,94E+00	5,93E+05	0,00E+00	5,20E+00	1,47E+02	2,96E+01	6,24E-02	1,59E+01	3,07E+00	1,13E-01	8,11E+00
080c3_A_6	1,27E+00	3,43E+03	3,37E+02	2,03E+00	5,93E+05	0,00E+00	5,41E+00	1,19E+02	2,47E+01	6,37E-02	1,06E+01	4,81E+00	1,15E-01	1,51E+01
080c3_A_7	2,32E+00	3,29E+03	1,02E+03	1,82E+00	5,93E+05	0,00E+00	4,84E+00	1,40E+02	2,30E+01	5,88E-02	1,32E+01	9,93E+00	1,13E-01	8,22E+01
080c3_A_8	1,54E+00	2,88E+03	3,80E+02	1,56E+00	5,93E+05	0,00E+00	4,08E+00	1,52E+02	4,58E+01	4,97E-02	1,44E+01	3,74E+00	8,97E-02	1,23E+01
080c3_A_9	1,07E+00	2,88E+03	5,87E+02	1,64E+00	5,93E+05	0,00E+00	4,26E+00	1,48E+02	5,66E+01	5,28E-02	1,41E+01	4,37E+00	9,20E-02	1,20E+01
092c_A_1	3,56E+00	9,81E+03	1,75E+03	6,01E+00	6,17E+05	0,00E+00	2,12E+01	4,55E+01	1,57E+01	2,86E-01	8,69E+00	2,02E+00	4,67E-01	2,81E+01
092c_A_10	1,23E+00	9,05E+03	1,57E+03	1,99E+00	6,23E+05	0,00E+00	7,02E+00	2,40E+01	3,16E+00	5,79E-02	4,59E+00	1,23E+00	1,27E-01	4,79E+00
092c_A_11	1,37E+00	1,02E+04	3,17E+03	2,44E+00	6,23E+05	0,00E+00	8,53E+00	3,24E+01	9,04E+00	6,92E-02	6,88E+00	3,17E+00	1,38E-01	2,89E+01
092c_A_12	1,62E+00	9,26E+03	1,51E+03	2,54E+00	6,23E+05	0,00E+00	8,92E+00	3,12E+01	3,70E+00	7,37E-02	6,61E+00	1,46E+00	1,55E-01	4,08E+01
092c_A_13	1,43E+00	9,11E+03	1,01E+03	2,11E+00	6,23E+05	0,00E+00	7,32E+00	2,81E+01	7,16E+00	6,29E-02	5,93E+00	2,60E+00	1,20E-01	1,91E+01
092c_A_2	3,50E+00	1,02E+04	2,09E+03	4,61E+00	6,22E+05	0,00E+00	1,65E+01	3,85E+01	2,62E+01	2,36E-01	5,94E+00	2,83E+00	4,00E-01	1,38E+01
092c_A_4	1,17E+01	1,05E+04	1,25E+03	1,04E+01	6,17E+05	0,00E+00	3,59E+01	5,50E+01	5,38E+01	8,07E-01	7,62E+00	4,21E+00	1,09E+00	4,23E+01
092c_A_5	1,26E+01	1,07E+04	1,57E+03	1,11E+01	6,17E+05	0,00E+00	3,62E+01	7,28E+01	6,47E+01	8,17E-01	1,14E+01	7,75E+00	1,19E+00	6,57E+01
092c_A_6	3,87E+00	1,94E+04	2,18E+04	6,73E+00	6,17E+05	0,00E+00	2,00E+01	4,49E+01	1,55E+01	2,31E-01	8,28E+00	8,51E-01	4,29E-01	2,82E+01
092c_A_9	1,42E+00	9,82E+03	3,29E+03	2,30E+00	6,21E+05	0,00E+00	7,96E+00	2,63E+01	5,99E+00	7,11E-02	4,57E+00	1,13E+00	1,61E-01	5,80E+00
100bA_matrix_1	1,07E+00	1,26E+04	2,23E+03	1,84E+00	6,59E+05	0,00E+00	6,38E+00	2,12E+01	2,73E+00	5,77E-02	2,08E+00	6,28E-01	1,44E-01	4,83E+00
100bA_matrix_10	1,31E+00	1,22E+04	1,88E+03	2,10E+00	6,59E+05	0,00E+00	7,19E+00	4,24E+01	3,41E+00	5,87E-02	7,13E+00	2,75E+00	1,20E-01	2,35E+01
100bA_matrix_2	1,08E+00	1,26E+04	3,37E+03	1,91E+00	6,59E+05	0,00E+00	6,66E+00	2,25E+01	3,68E+00	5,77E-02	2,20E+00	6,66E-01	1,42E-01	4,53E+00
100bA_matrix_3	1,06E+00	1,06E+04	2,28E+03	1,80E+00	6,59E+05	0,00E+00	6,31E+00	2,23E+01	3,59E+00	5,64E-02	2,11E+00	2,96E-01	1,25E-01	4,16E+00
100bA_matrix_4	1,10E+00	1,18E+04	2,37E+03	1,97E+00	6,59E+05	0,00E+00	6,82E+00	2,26E+01	4,93E+00	5,95E-02	2,09E+00	3,12E-01	1,29E-01	4,43E+00
100bA_matrix_5	4,76E+00	1,43E+04	2,94E+03	2,49E+00	6,59E+05	0,00E+00	8,62E+00	3,28E+01	1,08E+01	6,79E-02	2,96E+00	8,49E-01	1,68E-01	7,08E+00
100bA_matrix_6	2,62E+00	1,32E+04	1,96E+03	1,93E+00	6,59E+05	0,00E+00	6,70E+00	3,03E+01	4,67E+00	5,78E-02	4,00E+00	1,95E+00	1,26E-01	1,12E+01
100bA_matrix_7	1,37E+00	1,13E+04	1,59E+03	1,85E+00	6,59E+05	0,00E+00	6,41E+00	4,00E+01	2,81E+00	5,05E-02	3,33E+00	7,60E-01	1,17E-01	1,07E+01
100bA_matrix_8	1,35E+00	1,09E+04	1,02E+03	1,85E+00	6,59E+05	0,00E+00	6,53E+00	3,66E+01	4,55E+00	4,72E-02	3,20E+00	4,80E-01	1,13E-01	4,66E+00
100bA_matrix_9	1,51E+00	1,11E+04	2,60E+03	2,03E+00	6,59E+05	0,00E+00	6,93E+00	3,85E+01	5,58E+00	5,41E-02	3,90E+00	9,75E-01	1,33E-01	1,35E+01

Analysis	Cu63_2SD	Cu63_LOD	Zn66_mean	Zn66_2SD	Zn66_LOD	Ga69_mean	Ga69_2SD	Ga69_LOD	Ge72_mean	Ge72_2SD	Ge72_LOD	Ge73_mean	Ge73_2SD
	(ppm)	(ppm)	(ppm)	(ppm)	(ppm)	(ppm)	(ppm)	(ppm)	(ppm)	(ppm)	(ppm)	(ppm)	(ppm)
080c2_B_7	1,27E+01	6,12E-02	9,51E+02	2,31E+02	3,56E-01	1,64E+01	3,09E+00	6,15E-02	1,73E+00	3,03E-01	2,70E-01	1,28E+00	2,41E-01
080c2_B_8	1,46E+01	6,53E-02	9,43E+02	2,00E+02	3,39E-01	1,60E+01	2,07E+00	4,98E-02	1,82E+00	4,84E-01	2,44E-01	1,28E+00	1,39E-01
080c2_B_9	1,30E+01	6,05E-02	8,98E+02	2,41E+02	3,26E-01	1,54E+01	2,07E+00	5,51E-02	1,51E+00	3,09E-01	2,58E-01	1,19E+00	1,78E-01
080c3_A_1	1,05E+01	8,23E-02	5,56E+02	2,07E+02	3,31E-01	1,24E+01	2,90E+00	7,54E-02	9,05E-01	2,61E-01	3,00E-01	8,46E-01	1,58E-01
080c3_A_10	2,03E+03	4,98E-02	4,88E+02	1,23E+02	2,83E-01	1,28E+01	3,08E+00	7,09E-02	1,10E+00	4,99E-01	2,50E-01	8,61E-01	1,99E-01
080c3_A_11	1,60E+01	6,11E-02	4,36E+02	9,80E+01	3,13E-01	1,32E+01	1,99E+00	6,91E-02	8,46E-01	3,90E-01	3,25E-01	8,98E-01	1,23E-01
080c3_A_12	6,98E+00	6,98E-02	4,72E+02	1,60E+02	3,11E-01	1,30E+01	3,26E+00	8,07E-02	9,18E-01	4,97E-01	3,07E-01	8,56E-01	1,91E-01
080c3_A_13	4,87E+00	7,55E-02	4,77E+02	1,88E+02	3,27E-01	1,52E+01	5,08E+00	9,79E-02	1,22E+00	6,80E-01	3,08E-01	1,00E+00	3,13E-01
080c3_A_14	7,59E+01	6,76E-02	4,78E+02	1,22E+02	3,36E-01	1,41E+01	4,46E+00	8,94E-02	1,21E+00	1,09E+00	3,13E-01	9,68E-01	3,70E-01
080c3_A_15	1,97E+01	7,84E-02	4,21E+02	1,92E+02	3,73E-01	1,56E+01	5,01E+00	1,10E-01	1,33E+00	1,69E+00	3,41E-01	1,05E+00	3,34E-01
080c3_A_16	6,15E+00	7,63E-02	5,09E+02	1,64E+02	3,78E-01	1,63E+01	4,29E+00	1,09E-01	1,38E+00	1,34E+00	3,44E-01	1,08E+00	2,49E-01
080c3_A_17	9,98E+00	9,36E-02	5,45E+02	2,26E+02	4,06E-01	1,72E+01	4,24E+00	1,27E-01	1,20E+00	1,52E+00	4,60E-01	1,15E+00	2,03E-01
080c3_A_18	3,30E+00	7,53E-02	4,28E+02	1,03E+02	3,28E-01	1,43E+01	4,60E+00	1,00E-01	8,92E-01	5,43E-01	3,67E-01	9,51E-01	2,87E-01
080c3_A_19	1,41E+00	7,47E-02	4,59E+02	1,35E+02	3,25E-01	1,34E+01	2,55E+00	8,58E-02	7,93E-01	2,40E-01	3,76E-01	8,85E-01	1,23E-01
080c3_A_2	2,65E+01	9,44E-02	4,62E+02	2,60E+02	3,18E-01	1,25E+01	4,35E+00	8,15E-02	1,23E+00	1,10E+00	2,72E-01	8,16E-01	3,20E-01
080c3_A_20	1,66E+01	6,93E-02	5,36E+02	1,27E+02	3,32E-01	1,53E+01	2,78E+00	9,74E-02	1,09E+00	5,89E-01	3,43E-01	1,02E+00	1,68E-01
080c3_A_21	3,05E+00	9,96E-02	3,92E+02	1,29E+02	3,76E-01	1,66E+01	8,20E+00	1,14E-01	1,15E+00	1,59E+00	4,39E-01	1,09E+00	5,51E-01
080c3_A_22	1,03E+01	6,99E-02	4,45E+02	1,03E+02	3,53E-01	1,57E+01	3,81E+00	1,03E-01	8,82E-01	4,88E-01	4,56E-01	1,11E+00	1,96E-01
080c3_A_23	6,70E+00	7,50E-02	4,87E+02	1,57E+02	3,29E-01	1,63E+01	1,05E+01	1,06E-01	1,24E+00	1,66E+00	3,25E-01	1,07E+00	6,63E-01
080c3_A_24	2,38E+00	9,48E-02	4,76E+02	1,91E+02	4,53E-01	1,87E+01	5,18E+00	1,76E-01	1,16E+00	6,16E-01	5,24E-01	1,23E+00	3,27E-01
080c3_A_25	4,49E+00	8,65E-02	5,82E+02	1,04E+02	3,81E-01	1,66E+01	4,68E+00	1,27E-01	1,32E+00	8,29E-01	3,78E-01	1,16E+00	3,41E-01
080c3_A_26	1,80E+01	7,55E-02	5,62E+02	2,18E+02	3,54E-01	1,66E+01	5,44E+00	1,14E-01	1,12E+00	4,97E-01	3,85E-01	1,13E+00	3,72E-01
080c3_A_27	1,62E+00	8,56E-02	4,78E+02	6,71E+01	3,36E-01	1,48E+01	5,82E+00	1,10E-01	9,23E-01	2,92E-01	3,84E-01	1,03E+00	4,60E-01
080c3_A_28	2,30E+01	7,48E-02	5,20E+02	1,08E+02	3,37E-01	1,65E+01	4,98E+00	1,02E-01	1,17E+00	9,31E-01	3,46E-01	1,12E+00	3,31E-01
080c3_A_29	2,38E+01	7,82E-02	6,12E+02	1,86E+02	3,94E-01	1,62E+01	2,26E+00	1,07E-01	1,18E+00	7,86E-01	3,92E-01	1,13E+00	1,42E-01
080c3_A_3	3,28E+00	8,91E-02	4,42E+02	1,94E+02	3,29E-01	1,10E+01	3,03E+00	8,79E-02	6,47E-01	3,24E-01	3,51E-01	7,22E-01	1,99E-01
080c3_A_30	4,83E+00	7,29E-02	5,61E+02	2,15E+02	3,48E-01	1,58E+01	3,11E+00	1,05E-01	9,59E-01	4,80E-01	4,24E-01	1,07E+00	2,48E-01
080c3_A_31	1,08E+02	8,36E-02	6,75E+02	1,61E+02	3,54E-01	1,67E+01	5,78E+00	1,15E-01	1,20E+00	5,53E-01	3,77E-01	1,15E+00	3,68E-01
080c3_A_32	2,94E+00	7,93E-02	7,91E+02	3,86E+02	3,22E-01	1,58E+01	2,23E+00	1,04E-01	1,20E+00	4,40E-01	3,22E-01	1,12E+00	1,79E-01
080c3_A_33	3,15E+00	7,49E-02	4,49E+02	1,00E+02	3,35E-01	1,67E+01	6,33E+00	1,06E-01	1,09E+00	4,80E-01	3,64E-01	1,13E+00	4,51E-01
080c3_A_34	3,85E+00	8,99E-02	5,06E+02	2,39E+02	3,88E-01	1,75E+01	6,31E+00	1,24E-01	1,10E+00	4,35E-01	4,49E-01	1,17E+00	3,90E-01
080c3_A_35	8,52E+00	6,51E-02	6,13E+02	2,95E+02	3,23E-01	1,55E+01	5,38E+00	9,24E-02	1,02E+00	5,09E-01	3,63E-01	1,07E+00	3,55E-01
080c3_A_36	5,01E+00	7,05E-02	4,96E+02	1,67E+02	3,30E-01	1,62E+01	6,05E+00	1,03E-01	9,59E-01	2,70E-01	4,12E-01	1,08E+00	4,10E-01
080c3_A_37	6,60E+00	7,49E-02	4,71E+02	3,09E+01	3,43E-01	1,55E+01	3,78E+00	9,57E-02	1,05E+00	4,81E-01	3,74E-01	1,03E+00	2,32E-01
080c3_A_38	5,02E+00	7,40E-02	4,78E+02	5,95E+01	3,29E-01	1,49E+01	2,94E+00	9,13E-02	8,95E-01	1,61E-01	3,96E-01	9,94E-01	1,94E-01
080c3_A_39	1,40E+01	8,54E-02	5,63E+02	1,27E+02	3,72E-01	1,67E+01	3,25E+00	1,06E-01	1,34E+00	1,05E+00	3,57E-01	1,14E+00	2,66E-01
080c3_A_4	4,58E+00	7,45E-02	4,51E+02	9,89E+01	3,00E-01	1,24E+01	2,47E+00	8,28E-02	8,58E-01	1,98E-01	2,97E-01	8,30E-01	1,82E-01
080c3_A_40	2,25E+00	6,65E-02	4,37E+02	1,15E+02	3,00E-01	1,43E+01	4,16E+00	8,19E-02	1,04E+00	5,93E-01	3,04E-01	9,72E-01	3,25E-01
080c3_A_41	8,13E+00	7,61E-02	7,52E+02	1,07E+02	3,80E-01	1,87E+01	5,93E+00	1,11E-01	1,29E+00	7,22E-01	4,27E-01	1,30E+00	3,99E-01
080c3_A_42	7,33E+00	9,30E-02	6,70E+02	2,03E+02	4,01E-01	1,92E+01	4,29E+00	1,27E-01	1,39E+00	6,11E-01	4,20E-01	1,33E+00	2,92E-01
080c3_A_43	3,57E+00	9,79E-02	5,82E+02	1,29E+02	4,21E-01	1,95E+01	3,35E+00	9,52E-02	1,31E+00	1,15E+00	4,72E-01	1,29E+00	3,12E-01
080c3_A_44	8,87E+00	9,06E-02	7,02E+02	6,27E+01	3,95E-01	1,80E+01	4,84E+00	1,09E-01	1,35E+00	2,78E-01	3,85E-01	1,24E+00	3,84E-01
080c3_A_45	8,60E+01	9,80E-02	6,74E+02	1,95E+02	4,99E-01	2,00E+01	2,76E+00	1,47E-01	1,38E+00	3,22E-01	5,37E-01	1,36E+00	2,57E-01
080c3_A_5	2,93E+00	8,79E-02	4,68E+02	1,33E+02	3,57E-01	1,36E+01	3,44E+00	8,71E-02	8,84E-01	3,42E-01	3,57E-01	8,90E-01	2,16E-01
080c3_A_6	1,46E+01	8,45E-02	5,20E+02	2,31E+02	3,63E-01	1,45E+01	3,33E+00	9,90E-02	9,90E-01	4,43E-01	3,68E-01	9,73E-01	2,01E-01
080c3_A_7	2,37E+02	6,84E-02	4,62E+02	1,40E+02	3,27E-01	1,37E+01	2,62E+00	9,05E-02	1,06E+00	8,13E-01	3,10E-01	9,22E-01	2,17E-01
080c3_A_8	4,03E+00	5,91E-02	4,37E+02	1,29E+02	2,79E-01	1,27E+01	2,37E+00	7,79E-02	9,03E-01	2,17E-01	2,77E-01	8,36E-01	1,02E-01
080c3_A_9	4,54E+00	6,39E-02	4,14E+02	1,18E+02	3,03E-01	1,30E+01	1,89E+00	7,26E-02	7,44E-01	2,17E-01	3,35E-01	8,64E-01	1,37E-01
092c_A_1	3,50E+00	3,67E-01	3,57E+03	1,77E+03	1,14E+00	4,97E+01	4,12E+01	5,04E-01	7,59E+00	1,72E+00	6,40E-01	5,36E+00	1,28E+00
092c_A_10	6,14E-01	1,89E-01	9,07E+02	1,87E+02	3,83E-01	1,62E+01	3,38E+00	9,93E-02	2,56E+00	2,21E+00	2,24E-01	2,51E+00	2,56E+00
092c_A_11	1,97E+01	1,05E-01	4,46E+03	1,74E+03	4,55E-01	1,74E+01	2,21E+00	6,58E-02	6,63E+00	2,95E+00	2,15E-01	3,87E+00	1,83E+00
092c_A_12	2,82E+01	1,02E-01	3,83E+03	8,14E+02	4,69E-01	1,94E+01	5,51E+00	7,08E-02	5,98E+00	2,26E+00	2,26E-01	3,54E+00	1,08E+00
092c_A_13	2,52E+01	9,32E-02	2,64E+03	1,57E+03	3,95E-01	1,72E+01	1,42E+00	7,09E-02	4,08E+00	3,11E+00	2,04E-01	2,52E+00	1,64E+00
092c_A_2	1,97E+01	6,39E-01	7,92E+02	2,89E+02	9,96E-01	4,31E+01	4,87E+01	3,93E-01	2,87E+00	2,47E+00	1,09E+00	2,99E+00	3,16E+00
092c_A_4	2,42E+01	7,12E-01	1,35E+03	4,48E+02	2,27E+00	7,87E+01	9,78E+01	8,66E-01	5,82E+00	6,11E+00	2,37E+00	5,81E+00	7,04E+00
092c_A_5	3,79E+01	7,01E-01	2,32E+03	6,79E+02	2,09E+00	1,09E+02	1,39E+02	9,83E-01	9,75E+00	6,22E+00	1,76E+00	8,90E+00	8,88E+00
092c_A_6	6,12E+00	3,30E-01	4,00E+03	9,14E+02	1,13E+00	4,23E+01	2,72E+01	4,08E-01	9,80E+00	1,36E+00	5,58E-01	6,84E+00	2,41E+00
092c_A_9	1,69E+00	1,99E-01	8,84E+02	2,45E+02	4,25E-01	1,85E+01	5,02E+00	1,13E-01	1,64E+00	6,20E-01	3,52E-01	1,45E+00	3,86E-01
100bA_matrix_1	1,16E+00	1,46E-01	1,12E+03	2,77E+02	3,49E-01	1,46E+01	2,70E+00	8,30E-02	1,66E+00	3,05E-01	2,35E-01	1,24E+00	2,75E-01
100bA_matrix_10	2,45E+01	9,18E-02	1,25E+03	2,03E+02	3,82E-01	1,45E+01	2,34E+00	1,04E-01	1,59E+00	2,91E-01	2,79E-01	1,31E+00	2,41E-01
100bA_matrix_2	1,06E+00	1,83E-01	1,06E+03	3,10E+02	3,54E-01	1,57E+01	2,42E+00	8,97E-02	1,64E+00	3,77E-01	2,64E-01	1,31E+00	2,61E-01
100bA_matrix_3	5,89E-01	1,69E-01	1,02E+03	2,52E+02	3,25E-01	1,48E+01	1,52E+00	8,05E-02	1,72E+00	5,69E-01	2,30E-01	1,26E+00	1,70E-01
100bA_matrix_4	7,08E-01	1,68E-01	1,10E+03	1,63E+02	3,74E-01	1,45E+01	2,01E+00	9,31E-02	1,64E+00	5,29E-01	2,50E-01	1,26E+00	1,18E-01
100bA_matrix_5	2,84E+00	1,53E-01	1,35E+03	3,38E+02	4,86E-01	1,59E+01	3,41E+00	1,11E-01	1,87E+00	1,54E-01	3,07E-01	1,36E+00	3,09E-01
100bA_matrix_6	1,02E+01	9,66E-02	1,33E+03	3,17E+02	3,57E-01	1,53E+01	4,02E+00	9,96E-02	1,76E+00	3,60E-01	2,48E-01	1,31E+00	2,81E-01
100bA_matrix_7	1,10E+01	8,67E-02	1,19E+03	2,19E+02	3,45E-01	1,52E+01	2,53E+00	7,36E-02	1,59E+00	3,48E-01	2,52E-01	1,27E+00	1,57E-01
100bA_matrix_8	7,23E-01	1,32E-01	1,14E+03	1,79E+02	3,50E-01	1,39E+01	3,63E+00	8,89E-02	1,55E+00	2,66E-01	2,41E-01	1,22E+00	3,42E-01
100bA_matrix_9	1,71E+01	1,06E-01	1,21E+03	2,19E+02	3,93E-01	1,59E+01	3,42E+00	9,82E-02	2,78E+00	1,18E+00	2,17E-01	2,57E+00	1,44E+00

Analysis	Ge73_LOD (ppm)	Ge74_mean (ppm)	Ge74_2SD (ppm)	Ge74_LOD (ppm)	As75_mean (ppm)	As75_2SD (ppm)	As75_LOD (ppm)	Rb85_mean (ppm)	Rb85_2SD (ppm)	Rb85_LOD (ppm)	Sr88_mean (ppm)	Sr88_2SD (ppm)	Sr88_LOD (ppm)	Y89_mean (ppm)
080c2_B_7	6,62E-02	5,46E+00	1,83E+00	2,38E-01	6,77E+00	3,03E+00	3,29E-01	5,48E-01	3,58E-01	3,12E-02	2,02E+01	2,27E+01	1,37E-02	1,16E+00
080c2_B_8	6,11E-02	7,12E+00	1,55E+00	2,38E-01	3,71E+00	1,23E+00	3,03E-01	1,83E+00	1,04E+00	2,24E-02	1,62E+01	2,41E+00	1,05E-02	2,11E+00
080c2_B_9	6,26E-02	5,27E+00	1,74E+00	2,19E-01	7,04E+00	3,59E+00	2,99E-01	9,81E-01	3,84E-01	2,05E-02	1,80E+01	1,84E+00	1,15E-02	2,16E+00
080c3_A_1	1,12E-01	6,12E-01	6,97E-01	8,12E-02	1,82E+00	1,46E+00	2,82E-01	8,80E-01	4,42E-01	1,56E-02	1,02E+01	7,32E+00	8,43E-03	3,62E-02
080c3_A_10	1,13E-01	3,85E-01	3,89E-01	5,02E-02	2,00E+00	1,39E+00	2,47E-01	5,21E-01	6,15E-01	1,75E-02	3,58E+00	7,75E+00	4,83E-03	1,26E-01
080c3_A_11	1,12E-01	2,06E-01	2,36E-01	3,30E-02	2,80E+00	3,55E+00	2,77E-01	1,13E+00	1,13E+00	1,57E-02	4,67E+01	1,34E+01	1,21E-02	1,63E+00
080c3_A_12	1,45E-01	1,40E-01	5,41E-01	2,35E-02	1,80E+00	1,04E+00	2,68E-01	3,41E-01	2,68E-01	2,87E-02	2,37E-01	1,09E+00	7,93E-04	n.d.
080c3_A_13	1,66E-01	n.d.	n.d.	n.d.	2,59E+00	2,17E+00	3,02E-01	2,57E-01	1,25E-01	4,92E-02	n.d.	n.d.	n.d.	n.d.
080c3_A_14	1,35E-01	3,02E-01	5,16E-01	4,92E-02	2,44E+00	2,56E+00	3,06E-01	2,12E+00	1,16E+00	1,90E-02	1,60E+01	1,90E+01	1,16E-02	2,65E+00
080c3_A_15	1,65E-01	n.d.	n.d.	n.d.	5,52E+00	1,51E+01	3,10E-01	2,93E-01	1,97E-01	4,54E-02	7,75E-01	2,43E+00	2,35E-03	n.d.
080c3_A_16	1,82E-01	n.d.	n.d.	n.d.	2,06E+00	1,03E+00	3,25E-01	7,73E-01	6,98E-01	2,31E-02	3,46E+00	7,61E+00	6,76E-03	1,36E-01
080c3_A_17	2,26E-01	n.d.	n.d.	n.d.	2,64E+00	1,97E+00	3,62E-01	1,17E+00	7,94E-01	2,79E-02	1,51E+00	5,88E+00	3,99E-03	n.d.
080c3_A_18	1,60E-01	n.d.	n.d.	n.d.	1,46E+00	1,45E+00	2,79E-01	2,53E-01	1,14E-01	4,15E-02	8,83E-01	1,55E+00	2,73E-03	n.d.
080c3_A_19	1,44E-01	n.d.	n.d.	n.d.	1,91E+00	2,91E+00	2,94E-01	3,93E-01	1,87E-01	2,61E-02	2,43E+00	3,13E+00	4,95E-03	n.d.
080c3_A_2	1,44E-01	n.d.	n.d.	n.d.	2,16E+00	3,45E+00	2,84E-01	1,84E-01	1,08E-01	5,00E-02	n.d.	n.d.	n.d.	n.d.
080c3_A_20	1,56E-01	1,23E-01	1,06E+00	1,84E-02	1,91E+00	1,20E+00	2,96E-01	7,88E-01	4,98E-01	2,21E-02	2,26E+00	3,08E+00	5,30E-03	n.d.
080c3_A_21	2,16E-01	n.d.	n.d.	n.d.	1,43E+00	7,76E-01	3,48E-01	2,16E-01	7,53E-02	1,54E-01	1,75E+00	3,69E+00	4,82E-03	n.d.
080c3_A_22	1,30E-01	2,22E-01	7,87E-01	3,21E-02	6,20E+00	1,62E+01	3,29E-01	1,45E+00	1,21E+00	1,84E-02	1,65E+01	1,78E+01	1,25E-02	6,96E+00
080c3_A_23	1,83E-01	n.d.	n.d.	n.d.	2,07E+00	1,79E+00	3,28E-01	4,04E-01	2,90E-01	2,77E-02	2,10E+00	1,12E+00	5,79E-03	n.d.
080c3_A_24	3,14E-01	n.d.	n.d.	n.d.	2,22E+00	2,44E+00	3,92E-01	4,29E-01	2,76E-01	3,79E-02	1,37E+01	3,30E+01	1,26E-02	n.d.
080c3_A_25	1,56E-01	4,44E-01	1,05E+00	6,08E-02	2,57E+00	2,81E+00	3,69E-01	2,63E-01	1,54E-01	7,85E-02	2,64E+00	7,24E-01	6,75E-03	n.d.
080c3_A_26	1,61E-01	8,10E-02	1,32E+00	1,24E-02	1,68E+00	9,42E-01	3,27E-01	9,25E-01	4,47E-01	2,24E-02	3,41E+00	2,28E+00	8,30E-03	n.d.
080c3_A_27	1,41E-01	4,77E-01	8,21E-01	6,05E-02	1,75E+00	7,16E-01	3,09E-01	2,27E-01	1,15E-01	6,39E-02	2,58E+00	1,02E+00	7,52E-03	n.d.
080c3_A_28	1,51E-01	2,32E-01	8,43E-01	3,09E-02	2,50E+00	2,71E+00	3,13E-01	8,11E-01	6,84E-01	2,30E-02	2,99E+00	1,34E+00	8,24E-03	n.d.
080c3_A_29	1,51E-01	6,52E-01	6,93E-01	8,47E-02	3,31E+00	1,99E+00	3,62E-01	7,39E-01	5,43E-01	2,52E-02	4,24E+00	1,47E+00	9,20E-03	n.d.
080c3_A_3	1,52E-01	3,84E-02	5,85E-01	8,69E-03	1,74E+00	1,96E+00	2,81E-01	2,95E-01	6,87E-01	2,76E-02	n.d.	n.d.	n.d.	n.d.
080c3_A_30	1,67E-01	n.d.	n.d.	n.d.	1,63E+00	6,02E-01	3,19E-01	2,95E-01	1,94E-01	4,05E-02	3,02E+00	1,41E+00	8,71E-03	n.d.
080c3_A_31	1,53E-01	3,50E-01	8,44E-01	4,49E-02	3,99E+00	5,58E+00	3,58E-01	8,01E-01	8,71E-01	2,33E-02	5,97E+00	3,20E+00	1,45E-02	5,05E-01
080c3_A_32	1,13E-01	9,25E-01	1,00E+00	9,54E-02	2,12E+00	9,07E-01	3,11E-01	1,01E+00	1,13E+00	2,12E-02	2,74E+01	3,34E+01	1,09E-02	3,95E-01
080c3_A_33	1,39E-01	n.d.	n.d.	n.d.	1,97E+00	2,84E+00	3,07E-01	2,80E-01	1,57E-01	5,49E-02	3,83E+00	9,78E-01	1,25E-02	n.d.
080c3_A_34	2,08E-01	n.d.	n.d.	n.d.	2,09E+00	2,29E+00	3,69E-01	4,71E-01	2,47E-01	3,59E-02	4,40E+00	8,46E-01	1,12E-02	1,13E-02
080c3_A_35	1,32E-01	3,80E-01	1,36E+00	4,84E-02	2,46E+00	3,94E+00	3,34E-01	1,94E+00	1,87E+00	1,62E-02	1,94E+01	2,16E+01	1,28E-02	1,69E+00
080c3_A_36	1,66E-01	n.d.	n.d.	n.d.	3,36E+00	7,42E+00	3,10E-01	1,05E+00	2,47E+00	1,95E-02	6,84E+00	6,76E+00	1,23E-02	2,00E-01
080c3_A_37	1,67E-01	n.d.	n.d.	n.d.	1,50E+00	5,44E-01	3,06E-01	5,95E-01	3,77E-01	3,04E-02	5,92E+01	4,97E+01	1,55E-02	2,55E-01
080c3_A_38	1,56E-01	1,46E-01	7,78E-01	2,23E-02	2,00E+00	1,08E+00	3,15E-01	8,40E-01	4,49E-01	2,29E-02	8,13E+00	6,31E+00	1,24E-02	3,60E-01
080c3_A_39	1,63E-01	8,47E-02	4,88E-01	1,36E-02	2,14E+00	1,06E+00	3,44E-01	1,12E+00	1,10E+00	2,12E-02	6,13E+00	9,35E-01	1,49E-02	2,14E-01
080c3_A_4	1,19E-01	n.d.	n.d.	n.d.	1,75E+00	3,87E-01	2,57E-01	1,76E-01	6,30E-02	8,45E-02	n.d.	n.d.	n.d.	n.d.
080c3_A_40	1,28E-01	n.d.	n.d.	n.d.	2,47E+00	5,48E+00	2,88E-01	2,15E-01	1,09E-01	6,13E-02	6,88E+00	4,43E+00	1,33E-02	2,36E-01
080c3_A_41	1,53E-01	4,42E-01	2,04E+00	5,36E-02	2,53E+00	1,55E+00	3,59E-01	6,96E-01	4,68E-01	3,31E-02	5,97E+01	1,88E+02	2,02E-02	6,72E-01
080c3_A_42	1,80E-01	4,76E-01	1,29E+00	6,16E-02	2,78E+00	2,36E+00	4,02E-01	5,87E-01	8,16E-01	3,51E-02	3,20E+01	7,42E+01	1,84E-02	9,49E-01
080c3_A_43	1,55E-01	4,96E-01	1,21E+00	6,56E-02	2,05E+00	1,60E+00	4,03E-01	1,81E+00	4,11E+00	2,65E-02	1,26E+02	1,74E+02	1,55E-02	2,85E+00
080c3_A_44	1,42E-01	7,91E-01	1,18E+00	9,36E-02	2,26E+00	1,46E+00	3,70E-01	1,23E+00	7,69E-01	3,01E-02	2,73E+01	1,03E+01	1,71E-02	2,08E+00
080c3_A_45	2,35E-01	5,34E-01	1,44E+00	7,94E-02	4,51E+00	2,56E+00	4,70E-01	1,67E+00	2,06E+00	3,20E-02	3,60E+01	4,61E+01	2,33E-02	4,71E+00
080c3_A_5	1,51E-01	n.d.	n.d.	n.d.	2,39E+00	3,11E+00	3,03E-01	1,98E-01	1,17E-01	8,07E-02	n.d.	n.d.	n.d.	n.d.
080c3_A_6	1,41E-01	1,99E-01	4,20E-01	3,52E-02	2,64E+00	1,63E+00	3,20E-01	5,49E-01	2,53E-01	3,14E-02	n.d.	n.d.	n.d.	n.d.
080c3_A_7	1,36E-01	n.d.	n.d.	n.d.	1,82E+00	1,37E+00	2,78E-01	2,50E-01	4,35E-02	3,96E-02	n.d.	n.d.	n.d.	n.d.
080c3_A_8	1,30E-01	2,97E-01	3,76E-01	4,08E-02	1,73E+00	5,00E-01	2,46E-01	2,99E-01	2,28E-01	2,86E-02	n.d.	n.d.	n.d.	n.d.
080c3_A_9	1,24E-01	n.d.	n.d.	n.d.	1,42E+00	6,77E-01	2,53E-01	2,70E-01	1,98E-01	3,10E-02	4,17E-01	5,90E+00	9,43E-04	n.d.
092c_A_1	1,86E-01	3,08E+01	2,30E+01	6,62E-01	1,16E+02	5,71E+01	1,18E+00	1,43E+01	2,22E+01	7,84E-02	8,00E+00	7,68E+00	1,72E-02	1,38E+01
092c_A_10	5,42E-02	3,88E+00	2,09E+00	1,86E-01	1,40E+00	1,56E+00	1,73E-01	2,14E-01	2,63E-01	2,26E-02	6,59E+00	8,75E+00	9,99E-03	5,99E+01
092c_A_11	4,94E-02	4,03E+01	2,37E+01	2,99E-01	6,68E+01	4,44E+01	4,95E-01	1,47E+00	1,04E+00	2,13E-02	2,13E+01	8,82E+00	1,66E-02	2,12E+01
092c_A_12	5,31E-02	3,23E+01	1,66E+01	2,95E-01	4,89E+01	3,36E+01	4,86E-01	1,21E+00	1,31E+00	2,37E-02	2,06E+01	1,50E+01	1,48E-02	1,59E+01
092c_A_13	4,84E-02	1,96E+01	2,19E+01	2,37E-01	3,02E+01	4,37E+01	3,83E-01	1,10E+00	1,28E+00	2,10E-02	1,43E+01	1,76E+01	1,30E-02	1,15E+01
092c_A_2	5,15E-01	5,41E-01	5,38E+00	6,84E-02	1,85E-01	6,77E+00	3,38E-02	2,29E+01	3,21E+01	4,89E-02	1,01E+01	1,61E+01	2,44E-02	5,31E+00
092c_A_4	1,03E+00	6,45E+00	8,89E+00	6,63E-01	9,79E+01	5,64E+00	2,19E+00	8,99E+01	1,22E+02	1,43E-01	2,89E+01	2,66E+01	6,64E-02	2,50E+01
092c_A_5	6,37E-01	2,41E+01	1,61E+01	9,98E-01	1,78E+02	7,43E+01	2,06E+00	1,33E+02	1,93E+02	1,72E-01	6,24E+01	7,12E+01	8,77E-02	4,67E+01
092c_A_6	1,47E-01	4,49E+01	3,01E+01	6,50E-01	2,34E+02	1,45E+02	1,12E+00	1,94E+00	2,22E+00	6,16E-02	2,11E+01	1,05E+01	2,73E-02	7,26E+01
092c_A_9	1,26E-01	2,64E+00	1,19E+00	1,83E-01	9,23E-01	1,61E+00	1,39E-01	3,53E+00	1,49E+00	2,08E-02	2,13E+00	1,23E+00	5,49E-03	1,15E+00
100bA_matrix_1	8,91E-02	3,81E+00	1,46E+00	1,70E-01	1,09E+00	8,26E-01	1,53E-01	9,28E-02	4,51E-02	4,67E-02	2,55E+00	8,88E-01	6,30E-03	6,81E-01
100bA_matrix_10	9,34E-02	4,27E+00	1,13E+00	1,97E-01	2,23E+00	1,83E+00	2,56E-01	3,35E-01	2,79E-01	1,96E-02	2,90E+00	1,64E+00	9,11E-03	9,55E-01
100bA_matrix_2	1,03E-01	4,02E+00	1,29E+00	1,74E-01	3,52E-01	8,52E-01	6,65E-02	8,89E-02	3,13E-02	5,20E-02	2,69E+00	9,01E-01	6,91E-03	7,32E-01
100bA_matrix_3	8,33E-02	4,05E+00	8,51E-01	1,69E-01	5,29E-01	8,36E-01	9,11E-02	8,50E-02	3,85E-02	5,06E-02	2,51E+00	1,23E+00	6,64E-03	1,82E+00
100bA_matrix_4	9,49E-02	3,59E+00	9,58E-01	1,77E-01	1,29E+00	9,33E-01	1,80E-01	1,06E+00	2,15E+00	1,88E-02	2,57E+00	9,55E-01	8,46E-03	2,14E+00
100bA_matrix_5	1,23E-01	4,31E+00	1,23E+00	2,33E-01	1,66E+00	9,11E-01	2,54E-01	1,06E-01	4,40E-02	4,91E-02	3,11E+00	1,28E+00	9,48E-03	6,91E-01
100bA_matrix_6	9,62E-02	4,32E+00	9,30E-01	1,77E-01	1,92E+00	1,61E+00	2,14E-01	2,07E-01	2,08E-01	2,31E-02	2,43E+00	1,24E+00	7,09E-03	7,24E-01
100bA_matrix_7	8,82E-02	4,28E+00	1,24E+00	1,71E-01	2,45E+00	2,17E+00	2,35E-01	1,96E-01	2,39E-01	2,05E-02	3,21E+00	1,51E+00	8,31E-03	8,32E-01
100bA_matrix_8	9,17E-02	4,29E+00	9,68E-01	1,73E-01	1,83E+00	3,55E-01	2,11E-01	1,21E-01	4,37E-02	3,03E-02	2,87E+00	7,70E-01	6,69E-03	7,29E-01
100bA_matrix_9	5,43E-02	5,29E+00	1,92E+00	1,92E-01	3,01E+00	2,62E+00	2,66E-01	1,87E-01	1,63E-01	2,56E-02	9,66E+00	6,91E+00	1,28E-02	6,15E+01

Analysis	Y89_2SD	Y89_LOD	Zr90_mean	Zr90_2SD	Zr90_LOD	Nb93_mean	Nb93_2SD	Nb93_LOD	Mo95_mean	Mo95_2SD	Mo95_LOD	Ag107_mean	Ag107_2SD	Ag107_LOD
	(ppm)	(ppm)	(ppm)	(ppm)	(ppm)	(ppm)	(ppm)	(ppm)	(ppm)	(ppm)	(ppm)	(ppm)	(ppm)	(ppm)
080c2_B_7	4,02E-01	4,45E-03	4,97E+01	9,02E+00	3,88E-03	7,72E+00	1,11E+00	6,38E-03	2,68E+00	8,84E-01	5,37E-02	3,76E-02	1,18E-01	1,35E-02
080c2_B_8	1,05E+00	3,90E-03	5,76E+01	7,09E+00	1,76E-02	7,97E+00	9,87E-01	9,68E-03	3,51E+00	5,46E-01	8,57E-02	4,61E-02	1,62E-01	1,28E-02
080c2_B_9	8,95E-01	6,16E-03	5,48E+01	5,59E+00	1,92E-02	8,30E+00	1,30E+00	5,70E-03	3,01E+00	6,85E-01	6,50E-02	1,94E-02	5,41E-02	9,22E-03
080c3_A_1	3,25E-01	3,40E-04	8,36E+01	1,49E+01	1,33E-02	1,40E+01	2,30E+00	4,18E-03	2,76E+00	3,49E-01	4,85E-02	n.d.	n.d.	n.d.
080c3_A_10	1,03E+00	9,44E-04	3,93E+01	7,37E+00	1,27E-02	5,99E+00	9,06E-01	7,19E-03	1,60E+00	8,64E-01	4,05E-02	9,11E-02	1,89E-01	1,15E-02
080c3_A_11	3,28E+00	9,88E-04	4,36E+01	8,44E+00	1,30E-02	7,21E+00	5,53E-01	5,13E-03	9,47E-01	2,55E-01	4,02E-02	1,86E-02	5,43E-02	7,13E-03
080c3_A_12	n.d.	n.d.	2,49E+01	5,91E+00	1,08E-02	4,22E+00	1,10E+00	5,42E-03	1,18E+00	6,42E-01	4,27E-02	6,57E-03	7,89E-02	3,74E-03
080c3_A_13	n.d.	n.d.	2,39E+01	6,34E+00	1,37E-02	4,78E+00	2,09E+00	3,64E-03	6,89E-01	3,44E-01	3,34E-02	2,55E-03	5,66E-02	1,23E-03
080c3_A_14	3,54E+00	1,57E-03	4,69E+01	1,57E+01	1,47E-02	8,35E+00	3,06E+00	7,76E-03	8,27E-01	3,78E-01	4,06E-02	9,00E-03	2,62E-02	3,97E-03
080c3_A_15	n.d.	n.d.	2,80E+01	8,38E+00	1,87E-02	7,89E+00	2,50E+00	6,81E-03	7,62E-01	2,51E-01	3,87E-02	1,41E-03	2,66E-02	1,01E-03
080c3_A_16	1,61E+00	5,52E-04	3,07E+01	4,93E+00	3,00E-03	6,50E+00	1,73E+00	1,05E-02	8,96E-01	5,56E-01	2,89E-02	1,38E-03	4,79E-02	8,74E-04
080c3_A_17	n.d.	n.d.	3,09E+01	5,80E+00	1,77E-02	3,64E+00	5,65E-01	7,75E-03	9,11E-01	6,34E-01	4,86E-02	4,90E-02	1,17E-01	1,22E-02
080c3_A_18	n.d.	n.d.	3,76E+01	6,59E+00	1,07E-02	6,03E+00	1,14E+00	6,45E-03	1,13E+00	6,30E-01	4,34E-02	6,45E-03	6,46E-02	3,04E-03
080c3_A_19	n.d.	n.d.	3,35E+01	5,20E+00	1,35E-02	5,74E+00	1,77E+00	4,55E-03	1,09E+00	6,26E-01	4,44E-02	1,18E-02	6,19E-02	6,14E-03
080c3_A_2	n.d.	n.d.	3,23E+01	1,25E+01	1,40E-02	4,87E+00	1,50E+00	5,44E-03	1,05E+00	7,62E-01	3,73E-02	n.d.	n.d.	n.d.
080c3_A_20	n.d.	n.d.	4,27E+01	7,44E+00	1,14E-02	7,07E+00	1,00E+00	4,85E-02	1,53E+00	7,42E-01	5,40E-02	1,26E-02	5,08E-02	6,33E-03
080c3_A_21	n.d.	n.d.	3,73E+01	1,49E+01	1,62E-02	6,08E+00	2,77E+00	8,56E-03	9,11E-01	1,59E+00	4,83E-02	6,14E-03	5,30E-02	5,32E-03
080c3_A_22	7,12E+00	4,83E-03	3,21E+01	1,59E+01	1,35E-02	7,73E+00	3,74E+00	6,18E-03	9,37E-01	9,17E-01	4,34E-02	6,53E-02	2,91E-01	1,49E-02
080c3_A_23	n.d.	n.d.	4,30E+01	9,09E+00	1,52E-02	7,16E+00	1,61E+00	4,65E-03	1,06E+00	8,49E-01	3,39E-02	7,34E-03	2,38E-02	5,54E-03
080c3_A_24	n.d.	n.d.	1,53E+01	3,62E+00	1,91E-02	2,26E+00	9,04E-01	2,26E-03	9,00E-01	8,76E-01	5,18E-02	5,56E-03	3,53E-02	4,44E-03
080c3_A_25	n.d.	n.d.	7,42E+01	2,12E+01	1,78E-02	1,72E+01	6,05E+00	9,40E-03	3,27E+00	2,02E+00	7,56E-02	2,28E-02	6,26E-02	1,35E-02
080c3_A_26	n.d.	n.d.	6,21E+01	1,80E+01	1,48E-02	1,03E+01	3,18E+00	1,75E-02	2,06E+00	8,10E-01	6,93E-02	6,72E-03	2,29E-02	3,97E-03
080c3_A_27	n.d.	n.d.	5,96E+01	7,35E+00	1,57E-02	1,08E+01	9,17E-01	5,36E-03	2,72E+00	9,59E-01	6,80E-02	1,61E-02	4,44E-02	5,71E-03
080c3_A_28	n.d.	n.d.	5,78E+01	9,93E+00	1,17E-02	9,10E+00	2,36E+00	9,42E-03	1,82E+00	9,19E-01	5,93E-02	1,10E-03	3,49E-02	9,51E-04
080c3_A_29	n.d.	n.d.	6,40E+01	3,85E+00	9,86E-03	1,09E+01	1,45E+00	2,29E-03	2,81E+00	1,35E+00	4,86E-02	9,06E-03	1,79E-02	8,77E-03
080c3_A_3	n.d.	n.d.	3,43E+01	9,74E+00	1,51E-02	5,14E+00	1,16E+00	6,93E-03	9,24E-01	5,13E-01	4,09E-02	n.d.	n.d.	n.d.
080c3_A_30	n.d.	n.d.	6,25E+01	1,24E+01	1,13E-02	9,86E+00	1,89E+00	4,47E-03	1,74E+00	6,59E-01	4,43E-02	1,80E-02	3,39E-02	9,62E-03
080c3_A_31	1,41E+00	8,27E-04	7,73E+01	3,10E+01	1,42E-02	1,89E+01	8,52E+00	6,83E-03	3,16E+00	2,01E+00	6,60E-02	2,15E-02	3,42E-02	1,07E-02
080c3_A_32	3,36E-01	2,09E-03	9,03E+01	1,86E+01	1,34E-02	2,55E+01	6,31E+00	4,80E-03	4,83E+00	1,91E+00	7,47E-02	3,03E-02	4,50E-02	1,10E-02
080c3_A_33	n.d.	n.d.	4,27E+01	1,97E+01	7,41E-03	8,66E+00	4,43E+00	6,25E-03	1,32E+00	7,61E-01	5,27E-02	3,37E-02	9,98E-02	1,38E-02
080c3_A_34	3,26E-01	3,64E-05	4,68E+01	9,57E+00	1,50E-02	8,39E+00	1,49E+00	1,71E-03	1,21E+00	4,73E-01	4,48E-02	2,20E-02	3,06E-02	1,74E-02
080c3_A_35	2,31E+00	3,80E-03	8,87E+01	4,72E+01	1,27E-02	1,77E+01	9,68E+00	9,15E-03	2,81E+00	2,02E+00	6,11E-02	3,20E-02	5,96E-02	1,39E-02
080c3_A_36	6,15E-01	4,90E-04	5,09E+01	2,62E+01	1,19E-02	7,73E+00	4,11E+00	6,88E-03	1,45E+00	1,58E+00	4,64E-02	6,45E-02	2,10E-01	1,46E-02
080c3_A_37	2,04E-01	5,99E-04	5,25E+01	7,63E+00	1,31E-02	8,40E+00	1,75E+00	5,50E-03	1,31E+00	3,84E-01	4,53E-02	1,84E-02	2,74E-02	1,08E-02
080c3_A_38	4,62E-01	2,80E-03	5,13E+01	4,57E+00	1,41E-02	6,68E+00	1,05E+00	1,72E-03	1,48E+00	4,30E-01	5,51E-02	2,72E-02	3,63E-02	1,30E-02
080c3_A_39	9,98E-02	6,95E-04	5,21E+01	6,20E+00	3,54E-03	7,21E+00	1,03E+00	5,32E-03	1,72E+00	9,03E-01	6,00E-02	3,44E-02	6,23E-02	1,25E-02
080c3_A_4	n.d.	n.d.	3,85E+01	4,57E+00	8,17E-03	5,79E+00	7,95E-01	6,93E-03	1,36E+00	3,98E-01	5,27E-02	n.d.	n.d.	n.d.
080c3_A_40	3,04E-01	2,22E-03	4,92E+01	2,59E+01	6,43E-03	7,87E+00	4,27E+00	5,31E-03	1,60E+00	1,28E+00	5,42E-02	2,05E-02	3,42E-02	1,66E-02
080c3_A_41	7,16E-01	1,27E-03	9,41E+01	1,40E+01	1,27E-02	1,70E+01	3,73E+00	1,02E-02	3,12E+00	2,34E+00	6,59E-02	4,59E-02	4,53E-02	1,57E-02
080c3_A_42	1,44E+00	6,92E-03	9,64E+01	2,01E+01	9,67E-03	1,82E+01	5,56E+00	5,81E-03	3,02E+00	1,03E+00	6,04E-02	5,80E-02	1,14E-01	1,86E-02
080c3_A_43	4,30E+00	5,04E-03	1,01E+02	1,82E+01	1,09E-02	1,85E+01	2,24E+00	6,89E-03	2,56E+00	7,73E-01	7,61E-02	4,04E-02	6,19E-02	1,35E-02
080c3_A_44	7,39E-01	7,98E-03	1,13E+02	1,55E+01	1,28E-02	2,37E+01	3,14E+00	9,49E-03	4,06E+00	1,08E+00	9,14E-02	2,45E-02	5,28E-02	1,79E-02
080c3_A_45	6,66E+00	9,51E-03	9,74E+01	2,59E+01	2,19E-02	1,42E+01	1,99E+00	1,25E-02	1,97E+00	1,32E+00	7,93E-02	1,46E-02	3,56E-02	2,12E-02
080c3_A_5	n.d.	n.d.	3,84E+01	8,46E+00	1,32E-02	5,43E+00	1,75E+00	4,49E-03	1,12E+00	9,54E-01	4,98E-02	n.d.	n.d.	n.d.
080c3_A_6	n.d.	n.d.	5,65E+01	9,84E+00	1,63E-02	8,73E+00	1,71E+00	8,58E-03	1,53E+00	7,26E-01	5,13E-02	n.d.	n.d.	n.d.
080c3_A_7	n.d.	n.d.	2,90E+01	5,25E+00	1,19E-02	5,41E+00	1,42E+00	6,27E-03	7,68E-01	6,51E-01	2,75E-02	3,83E-03	5,91E-02	1,79E-03
080c3_A_8	n.d.	n.d.	3,77E+01	3,93E+00	8,20E-03	6,12E+00	7,35E-01	5,11E-03	1,40E+00	6,23E-01	3,66E-02	n.d.	n.d.	n.d.
080c3_A_9	n.d.	n.d.	3,46E+01	1,15E+01	7,51E-03	5,45E+00	1,84E+00	1,32E-03	7,60E-01	6,11E-01	3,51E-02	1,26E-02	7,11E-02	4,84E-03
092c_A_1	3,81E+00	1,87E-02	7,06E+01	1,72E+01	2,62E-02	9,50E+01	1,44E+01	1,60E-02	3,49E+01	1,51E+01	1,48E-01	6,44E-02	2,36E-01	2,63E-02
092c_A_10	1,11E+02	3,83E-03	2,23E+01	5,85E+00	1,19E-02	8,32E+01	1,97E+01	4,23E-03	3,04E+01	6,38E+00	3,95E-02	4,18E-02	7,06E-02	1,21E-02
092c_A_11	1,05E+01	6,77E-03	1,04E+02	4,65E+01	1,76E-02	1,19E+02	2,54E+01	6,25E-03	3,57E+01	1,46E+01	9,28E-02	3,03E-01	7,02E-01	2,87E-02
092c_A_12	9,82E+00	2,28E-03	8,65E+01	5,00E+01	1,35E-02	1,12E+02	3,21E+01	2,39E-03	3,73E+01	1,89E+01	6,76E-02	1,57E-01	9,10E-02	2,50E-02
092c_A_13	1,37E+01	4,06E-03	6,77E+01	4,10E+01	1,12E-02	1,09E+02	3,42E+01	4,75E-03	3,31E+01	1,37E+01	5,95E-02	1,04E-01	1,14E-01	1,76E-02
092c_A_2	6,70E+00	3,27E-03	4,85E+01	4,43E+01	2,20E-02	7,90E+01	1,34E+01	1,75E-02	2,96E+01	6,69E+00	1,48E-01	1,24E-02	1,04E-01	4,30E-03
092c_A_4	2,74E+01	3,70E-02	1,43E+02	1,85E+02	1,15E-01	1,16E+02	7,12E+01	4,11E-02	3,31E+01	1,18E+01	4,57E-01	8,16E-02	4,35E-02	5,90E-02
092c_A_5	5,44E+01	6,95E-02	2,23E+02	2,73E+02	9,76E-02	1,42E+02	1,16E+02	3,74E-02	3,64E+01	1,01E+01	3,50E-01	7,55E-02	2,81E-01	4,66E-02
092c_A_6	1,04E+02	1,86E-02	1,02E+02	2,90E+01	3,40E-02	9,08E+01	2,45E+01	1,83E-02	3,41E+01	1,10E+01	1,30E-01	4,59E-01	8,60E-01	5,94E-02
092c_A_9	3,65E-01	1,11E-02	2,31E+01	6,23E+00	1,70E-02	8,45E+01	1,48E+01	4,64E-03	3,37E+01	1,17E+01	6,38E-02	4,57E-02	5,34E-02	1,17E-02
100bA_matrix_1	1,47E-01	9,26E-03	1,72E+01	4,25E+00	1,29E-02	1,33E+02	4,28E+01	4,39E-03	5,93E+01	1,12E+01	5,97E-02	7,07E-02	5,46E-02	1,21E-02
100bA_matrix_10	5,89E-01	1,17E-02	1,72E+01	5,42E+00	1,22E-02	9,72E+01	2,62E+01	1,69E-03	5,56E+01	8,50E+00	6,79E-02	3,66E-02	5,09E-02	1,35E-02
100bA_matrix_2	1,70E-01	1,22E-02	1,99E+01	3,64E+00	1,44E-02	1,41E+02	3,91E+01	5,83E-03	6,25E+01	2,06E+01	4,89E-02	6,35E-02	7,04E-02	1,20E-02
100bA_matrix_3	2,45E+00	6,34E-03	1,47E+01	2,24E+00	8,86E-03	1,16E+02	2,99E+01	1,01E-01	5,78E+01	1,22E+01	5,38E-02	6,56E-02	3,70E-02	1,30E-02
100bA_matrix_4	1,09E+00	4,64E-03	1,39E+01	3,06E+00	1,48E-02	1,06E+02	2,78E+01	7,06E-03	5,54E+01	1,56E+01	5,26E-02	2,11E-02	5,53E-02	1,02E-02
100bA_matrix_5	1,35E-01	1,29E-02	1,40E+01	1,56E+00	2,10E-02	1,12E+02	2,01E+01	7,85E-03	6,51E+01	1,45E+01	9,06E-02	5,66E-02	5,90E-02	1,81E-02
100bA_matrix_6	2,54E-01	1,09E-02	1,59E+01	5,34E+00	9,32E-03	1,05E+02	2,47E+01	4,19E-03	5,81E+01	1,22E+01	5,13E-02	4,75E-02	5,09E-02	1,17E-02
100bA_matrix_7	1,36E-01	7,02E-03	1,87E+01	2,79E+00	1,50E-02	1,25E+02	1,36E+01	5,03E-03	5,79E+01	1,31E+01	5,56E-02	6,04E-02	7,85E-02	1,08E-02
100bA_matrix_8	2,46E-01	7,67E-03	1,61E+01	5,07E+00	1,25E-02	1,08E+02	2,70E+01	6,04E-03	5,68E+01	1,50E+01	5,71E-02	6,20E-02	9,44E-02	1,39E-02
100bA_matrix_9	6,66E+01	1,54E-03	1,83E+01	6,12E+00	1,33E-02	1,27E+02	3,01E+01	6,42E-03	5,92E+01	1,33E+01	6,34E-02	8,30E-02	7,22E-02	1,69E-02

Analysis	Cd111_mean (ppm)	Cd111_2SD (ppm)	Cd111_LOD (ppm)	In113_mean (ppm)	In113_2SD (ppm)	In113_LOD (ppm)	In115_mean (ppm)	In115_2SD (ppm)	In115_LOD (ppm)	Sn118_mean (ppm)	Sn118_2SD (ppm)	Sn118_LOD (ppm)	Sb121_mean (ppm)
080c2_B_7	1,58E-01	2,06E-01	3,26E-02	1,74E-01	1,32E-01	2,26E-02	3,65E-01	5,56E-02	5,52E-03	4,47E+00	8,16E-01	6,52E-02	1,18E+00
080c2_B_8	2,03E-01	3,88E-02	4,58E-02	1,96E-01	1,65E-01	1,81E-02	3,65E-01	8,20E-02	5,35E-03	5,37E+00	1,41E+00	5,62E-02	1,55E+00
080c2_B_9	1,23E-01	1,38E-01	5,71E-02	1,75E-01	3,87E-02	6,44E-03	3,79E-01	6,65E-02	4,49E-03	4,35E+00	4,96E-01	5,36E-02	1,22E+00
080c3_A_1	1,12E-01	2,61E-01	3,74E-02	7,71E-02	6,80E-02	2,56E-02	2,04E-01	7,62E-02	4,04E-03	2,29E+00	3,79E-01	6,61E-02	9,94E-02
080c3_A_10	1,61E-01	2,67E-01	3,95E-02	1,13E-01	9,80E-02	1,71E-02	2,42E-01	3,49E-01	2,63E-03	1,07E+01	4,52E+01	3,53E-02	1,75E-01
080c3_A_11	2,65E-02	8,41E-02	2,99E-02	1,01E-01	6,15E-02	1,75E-02	1,93E-01	7,49E-02	3,15E-03	3,03E+00	2,78E+00	5,99E-02	4,56E-01
080c3_A_12	7,98E-02	6,93E-02	1,01E-02	9,00E-02	5,57E-02	5,89E-03	1,74E-01	7,41E-02	3,31E-03	3,18E+00	3,97E+00	6,83E-02	1,93E-01
080c3_A_13	5,95E-02	9,01E-02	4,70E-02	7,95E-02	2,71E-02	1,99E-02	1,80E-01	5,41E-02	3,69E-03	2,52E+00	6,72E-01	1,20E-01	2,32E-01
080c3_A_14	1,12E-01	9,94E-02	5,23E-02	1,19E-01	4,97E-02	2,54E-02	1,88E-01	8,80E-02	3,84E-03	2,39E+00	7,25E-01	1,29E-01	4,70E-01
080c3_A_15	3,25E-02	1,18E-01	4,86E-02	1,03E-01	5,78E-02	1,84E-02	1,85E-01	7,75E-02	4,61E-03	2,85E+00	7,51E-01	1,57E-01	1,26E-01
080c3_A_16	8,05E-02	7,79E-02	1,11E-02	1,05E-01	5,26E-02	2,34E-02	1,62E-01	4,17E-02	6,66E-03	2,74E+00	6,93E-01	1,45E-01	3,82E-01
080c3_A_17	9,89E-02	4,60E-02	1,41E-02	8,60E-02	4,80E-02	3,92E-02	1,74E-01	1,03E-01	5,53E-03	6,21E+00	1,67E+01	7,25E-02	4,09E-01
080c3_A_18	7,21E-02	7,03E-02	1,02E-02	7,89E-02	4,74E-02	2,44E-02	1,81E-01	5,16E-02	3,39E-03	2,49E+00	6,59E-01	1,22E-01	1,17E-01
080c3_A_19	5,65E-02	7,44E-02	3,73E-02	7,26E-02	2,28E-02	2,88E-02	1,46E-01	3,15E-02	6,18E-03	2,31E+00	4,54E-01	1,18E-01	6,77E-01
080c3_A_2	8,12E-02	1,70E-01	2,21E-02	1,05E-01	5,48E-02	1,59E-02	1,68E-01	6,00E-02	4,22E-03	2,15E+00	7,37E-01	1,00E-01	1,22E-01
080c3_A_20	1,16E-01	1,27E-01	3,61E-02	9,47E-02	8,46E-02	2,43E-02	4,53E-01	1,07E+00	3,92E-03	4,41E+01	1,74E+02	4,27E-02	2,89E-01
080c3_A_21	6,96E-02	8,47E-02	1,66E-02	1,02E-01	1,18E-01	3,51E-02	1,82E-01	7,23E-02	4,81E-03	2,79E+00	1,07E+00	1,56E-01	4,36E-02
080c3_A_22	8,31E-02	1,26E-01	5,88E-02	1,08E-01	3,97E-02	2,37E-02	3,17E-01	6,16E-01	4,85E-03	2,33E+01	1,02E+02	5,79E-02	1,32E+00
080c3_A_23	1,01E-01	1,18E-01	1,07E-02	1,19E-01	8,13E-02	5,07E-03	3,15E-01	5,54E-01	5,19E-03	1,98E+01	7,63E+01	7,21E-02	6,26E-01
080c3_A_24	9,08E-02	9,15E-02	7,91E-02	9,03E-02	6,93E-02	4,79E-02	1,71E-01	1,30E-01	6,62E-03	8,31E+00	2,62E+01	7,65E-02	1,15E-01
080c3_A_25	9,28E-02	1,09E-01	4,32E-02	1,11E-01	6,86E-02	2,08E-02	2,48E-01	9,12E-02	6,35E-03	3,60E+00	1,77E+00	1,24E-01	5,45E-02
080c3_A_26	1,18E-01	1,74E-01	6,17E-02	1,20E-01	6,63E-02	3,02E-02	5,86E-01	1,47E+00	4,15E-03	5,70E+01	2,23E+02	4,91E-02	8,32E-02
080c3_A_27	1,12E-01	1,58E-01	1,30E-02	1,22E-01	6,12E-02	2,54E-02	4,16E-01	8,36E-01	4,73E-03	3,61E+01	1,44E+02	4,37E-02	n.d.
080c3_A_28	9,68E-02	6,97E-02	5,10E-02	1,26E-01	5,02E-02	5,07E-03	4,47E-01	8,75E-01	4,59E-03	4,01E+01	1,58E+02	5,94E-02	4,78E-02
080c3_A_29	1,09E-01	5,14E-02	6,27E-02	1,15E-01	7,20E-02	2,13E-02	2,87E-01	8,76E-02	6,83E-03	3,41E+00	9,34E-01	1,26E-01	2,76E-01
080c3_A_3	2,27E-02	1,32E-01	1,53E-02	7,22E-02	5,83E-02	2,28E-02	1,41E-01	3,90E-02	3,94E-03	1,94E+00	5,52E-01	9,28E-02	3,44E-02
080c3_A_30	9,96E-02	7,11E-02	3,83E-02	1,05E-01	4,41E-02	2,91E-02	2,26E-01	7,09E-02	4,78E-03	2,78E+00	5,67E-01	1,45E-01	1,88E-02
080c3_A_31	1,13E-01	8,93E-02	4,67E-02	1,20E-01	4,26E-02	5,75E-03	5,13E-01	9,91E-01	3,58E-03	5,37E+01	1,79E+02	5,05E-02	2,04E-01
080c3_A_32	1,50E-01	1,14E-01	4,58E-02	1,46E-01	9,85E-02	1,81E-02	2,59E-01	8,60E-02	4,78E-03	3,11E+00	1,09E+00	1,13E-01	1,48E-02
080c3_A_33	1,01E-01	1,09E-01	6,19E-02	1,02E-01	7,95E-02	2,34E-02	1,82E-01	6,30E-02	4,54E-03	2,78E+00	9,81E-01	1,49E-01	1,64E-01
080c3_A_34	1,21E-01	9,31E-02	1,38E-02	1,19E-01	7,20E-02	2,93E-02	2,56E-01	1,93E-01	7,14E-03	9,61E+00	3,09E+01	7,49E-02	7,71E-01
080c3_A_35	1,24E-01	1,08E-01	3,52E-02	1,13E-01	6,04E-02	2,34E-02	7,04E-01	2,42E+00	4,06E-03	7,69E+01	3,86E+02	5,79E-02	9,96E-02
080c3_A_36	8,86E-02	6,40E-02	4,61E-02	1,10E-01	4,47E-02	5,75E-03	2,06E-01	5,94E-02	4,38E-03	3,60E+00	4,88E+00	1,05E-01	9,68E-01
080c3_A_37	8,28E-02	4,92E-02	7,62E-02	1,25E-01	9,15E-02	2,41E-02	2,16E-01	6,44E-02	4,66E-03	2,86E+00	1,20E+00	1,26E-01	2,90E-02
080c3_A_38	8,99E-02	8,22E-02	6,81E-02	1,02E-01	4,08E-02	2,46E-02	2,67E-01	3,11E-01	4,18E-03	1,23E+01	4,78E+01	4,83E-02	2,51E-02
080c3_A_39	1,28E-01	1,36E-01	4,56E-02	9,81E-02	5,97E-02	3,57E-02	2,65E-01	2,78E-01	4,86E-03	1,16E+01	3,86E+01	6,22E-02	2,92E-01
080c3_A_4	4,12E-02	1,38E-01	2,53E-02	8,59E-02	3,54E-02	2,11E-02	1,52E-01	2,36E-02	4,16E-03	2,12E+00	4,07E-01	8,80E-02	9,89E-03
080c3_A_40	9,57E-02	6,08E-02	3,74E-02	1,22E-01	8,20E-02	2,03E-02	1,98E-01	6,60E-02	4,26E-03	3,99E+00	2,98E+00	6,68E-02	6,97E-02
080c3_A_41	1,32E-01	8,50E-02	5,62E-02	1,57E-01	7,84E-02	2,24E-02	5,35E-01	1,20E+00	3,79E-03	4,14E+01	1,91E+02	4,99E-02	1,31E-01
080c3_A_42	1,80E-01	9,29E-02	3,95E-02	1,44E-01	6,80E-02	4,05E-02	2,77E-01	5,22E-02	5,75E-03	3,45E+00	8,78E-01	1,41E-01	1,70E-01
080c3_A_43	1,33E-01	1,57E-01	7,97E-02	1,09E-01	4,59E-02	3,16E-02	2,61E-01	1,11E-01	6,31E-03	3,26E+00	4,79E-01	1,62E-01	1,39E-01
080c3_A_44	1,26E-01	8,29E-02	6,31E-02	1,40E-01	8,34E-02	2,17E-02	2,86E-01	8,13E-02	6,89E-03	3,36E+00	9,82E-01	1,29E-01	9,43E-02
080c3_A_45	1,43E-01	8,81E-02	2,84E-02	1,62E-01	6,75E-02	3,50E-02	3,11E-01	9,97E-02	6,89E-03	3,78E+00	4,12E-01	1,71E-01	2,06E-01
080c3_A_5	n.d.	n.d.	n.d.	9,41E-02	3,41E-02	2,54E-02	1,76E-01	8,14E-02	4,30E-03	2,40E+00	8,09E-01	1,03E-01	n.d.
080c3_A_6	7,99E-02	3,64E-01	4,55E-02	1,17E-01	5,96E-02	2,17E-02	2,11E-01	5,94E-02	4,15E-03	2,47E+00	6,61E-01	1,28E-01	3,84E-02
080c3_A_7	8,39E-02	1,86E-01	5,62E-02	8,88E-02	4,84E-02	2,44E-02	1,64E-01	2,74E-02	3,41E-03	2,28E+00	4,70E-01	1,23E-01	1,96E-01
080c3_A_8	4,91E-02	1,43E-01	2,37E-02	8,74E-02	5,66E-02	2,15E-02	1,74E-01	9,93E-02	2,18E-03	2,33E+00	3,35E-01	6,91E-02	2,09E-01
080c3_A_9	2,71E-02	1,61E-01	2,01E-02	8,32E-02	6,57E-02	1,38E-02	1,93E-01	6,35E-02	3,42E-03	2,20E+00	5,30E-01	1,02E-01	2,34E-01
092c_A_1	2,12E-01	4,97E-01	2,40E-01	2,76E-01	2,18E-01	9,01E-02	5,12E-01	1,08E-01	3,03E-03	9,22E+00	5,13E+00	1,59E-01	2,40E+01
092c_A_10	4,55E-02	3,59E-02	6,10E-02	8,76E-02	4,34E-02	1,72E-02	1,74E-01	4,84E-02	5,92E-04	3,69E+00	6,21E-01	2,78E-02	2,04E-01
092c_A_11	4,81E-01	4,45E-01	4,59E-02	2,33E-01	1,49E-01	3,07E-02	3,92E-01	1,69E-01	3,32E-03	4,63E+00	1,24E+00	3,19E-02	4,20E+01
092c_A_12	3,79E-01	2,54E-01	4,45E-02	2,51E-01	4,87E-02	2,41E-02	3,84E-01	1,52E-01	4,47E-03	4,75E+00	1,37E+00	3,36E-02	3,60E+01
092c_A_13	3,06E-01	1,25E-01	5,24E-02	1,66E-01	8,97E-02	2,22E-02	6,72E-01	1,33E+00	2,80E-03	6,77E+01	2,22E+02	2,46E-02	1,92E+01
092c_A_2	1,39E-01	1,84E-01	8,35E-02	1,96E-01	2,48E-01	7,36E-02	2,73E-01	2,00E-01	1,33E-02	7,41E+00	6,53E+00	1,29E-01	1,71E+00
092c_A_4	n.d.	n.d.	n.d.	3,68E-01	3,99E-01	3,62E-01	3,88E-01	3,17E-01	4,69E-02	1,26E+01	1,42E+01	4,38E-01	8,72E+00
092c_A_5	5,40E-01	6,96E-01	1,63E-01	4,69E-01	4,90E-01	2,57E-01	5,59E-01	4,99E-01	1,24E-02	1,62E+01	1,80E+01	4,99E-01	1,90E+01
092c_A_6	6,84E-01	6,65E-01	1,27E-01	3,70E-01	2,94E-01	7,02E-02	4,50E-01	7,14E-02	1,69E-02	7,52E+00	3,04E+00	1,94E-01	3,60E+01
092c_A_9	8,35E-02	1,83E-01	4,23E-02	1,04E-01	8,23E-02	3,08E-02	1,88E-01	6,90E-02	5,04E-03	4,10E+00	9,12E-01	3,11E-02	5,26E-01
100bA_matrix_1	8,84E-02	9,83E-02	8,20E-03	7,63E-02	3,89E-02	2,49E-02	1,63E-01	5,52E-02	1,91E-03	3,53E+00	6,42E-01	2,97E-02	2,15E-02
100bA_matrix_10	8,10E-02	1,30E-01	5,11E-02	1,03E-01	4,14E-02	5,60E-03	1,75E-01	8,57E-02	4,33E-03	3,60E+00	7,84E-01	3,02E-02	2,35E-01
100bA_matrix_2	9,05E-02	5,98E-02	3,93E-02	8,43E-02	4,42E-02	2,96E-02	1,78E-01	4,65E-02	3,80E-03	3,72E+00	7,00E-01	3,11E-02	n.d.
100bA_matrix_3	6,94E-02	7,96E-02	3,83E-02	8,43E-02	4,46E-02	1,92E-02	1,68E-01	3,00E-02	4,64E-03	3,50E+00	4,49E-01	2,51E-02	n.d.
100bA_matrix_4	6,88E-02	6,43E-02	4,11E-02	9,01E-02	6,23E-02	2,31E-02	1,70E-01	5,44E-02	4,86E-03	3,66E+00	3,68E-01	2,52E-02	3,47E-02
100bA_matrix_5	5,70E-02	6,88E-02	6,55E-02	8,42E-02	3,66E-02	1,27E-02	2,01E-01	7,80E-02	6,30E-03	4,25E+00	1,25E+00	3,25E-02	2,01E-01
100bA_matrix_6	9,51E-02	1,53E-01	6,42E-02	9,84E-02	4,82E-02	1,38E-02	2,34E-01	1,67E-01	4,16E-03	1,02E+01	1,88E+01	1,95E-02	7,90E-02
100bA_matrix_7	6,69E-02	1,07E-01	5,13E-02	8,78E-02	6,83E-02	2,43E-02	1,78E-01	5,31E-02	2,06E-03	4,35E+00	4,68E+00	2,38E-02	8,64E-02
100bA_matrix_8	7,52E-02	8,64E-02	6,07E-02	8,11E-02	5,60E-02	2,91E-02	1,69E-01	4,07E-02	3,67E-03	3,55E+00	8,79E-01	2,94E-02	4,32E-02
100bA_matrix_9	7,98E-02	1,63E-01	5,90E-02	1,06E-01	4,66E-02	2,28E-02	1,79E-01	6,97E-02	4,35E-03	3,74E+00	8,45E-01	2,81E-02	1,38E-01

Analysis	Sb121_2SD	Sb121_LOD	Cs133_mean	Cs133_2SD	Cs133_LOD	Ba137_mean	Ba137_2SD	Ba137_LOD	La139_mean	La139_2SD	La139_LOD	Ce140_mean	Ce140_2SD
	(ppm)	(ppm)	(ppm)	(ppm)	(ppm)	(ppm)	(ppm)	(ppm)	(ppm)	(ppm)	(ppm)	(ppm)	(ppm)
080c2_B_7	2,64E-01	2,66E-02	1,31E-01	4,20E-02	8,26E-03	1,28E+01	1,71E+01	6,34E-02	1,09E+00	5,23E-01	7,80E-03	2,25E+00	5,44E-01
080c2_B_8	7,88E-01	3,02E-02	2,48E-01	8,07E-02	7,69E-03	1,08E+01	3,86E+00	2,52E-02	3,30E+00	3,71E+00	5,74E-03	3,95E+00	1,60E+00
080c2_B_9	1,85E-01	2,89E-02	1,95E-01	2,79E-02	7,23E-03	8,80E+00	2,43E+00	2,79E-02	3,58E+00	3,45E+00	1,96E-03	4,28E+00	2,44E+00
080c3_A_1	3,46E-01	1,69E-02	2,04E-02	2,20E-02	6,38E-03	1,77E+01	4,03E+01	5,47E-02	1,80E-01	2,03E-01	5,12E-03	5,10E-01	4,01E-01
080c3_A_10	3,44E-01	2,05E-02	9,94E-03	1,70E-02	6,78E-03	4,94E+00	5,62E+00	8,68E-02	2,03E-01	4,95E-01	2,60E-03	6,82E-01	1,20E+00
080c3_A_11	1,16E+00	2,13E-02	2,35E-02	4,51E-02	6,32E-03	1,54E+01	1,60E+01	3,63E-02	6,30E-01	8,85E-01	3,37E-03	2,51E+00	4,07E+00
080c3_A_12	4,41E-01	2,04E-02	3,11E-03	9,98E-03	7,68E-03	2,69E+00	1,34E+00	3,68E-02	4,34E-02	1,48E-01	3,60E-03	2,87E-01	3,40E-01
080c3_A_13	4,47E-01	2,24E-02	3,99E-04	8,15E-03	7,80E-03	2,81E+00	1,96E+00	2,05E-01	6,05E-03	4,05E-02	2,31E-03	2,05E-01	1,19E-01
080c3_A_14	8,14E-01	1,90E-02	2,93E-02	3,62E-02	8,61E-03	1,50E+01	5,58E+00	7,48E-02	9,67E-01	7,76E-01	7,23E-03	3,82E+00	2,94E+00
080c3_A_15	2,13E-01	2,41E-02	6,21E-03	2,40E-02	9,36E-03	5,86E+00	8,69E+00	9,76E-02	2,88E-02	3,68E-02	3,29E-03	2,66E-01	1,61E-01
080c3_A_16	6,78E-01	2,21E-02	1,57E-02	3,27E-02	5,42E-03	6,37E+00	6,02E+00	8,89E-02	7,54E-02	1,61E-01	4,30E-03	4,21E-01	5,32E-01
080c3_A_17	8,71E-01	2,40E-02	2,41E-02	2,04E-02	8,19E-03	1,24E+01	2,13E+01	7,62E-02	2,08E-02	4,06E-02	5,36E-03	1,98E-01	8,99E-02
080c3_A_18	3,30E-01	1,79E-02	3,01E-04	6,08E-03	8,54E-03	2,77E+00	2,08E+00	2,17E-01	1,86E-02	6,48E-02	5,81E-03	1,66E-01	1,28E-01
080c3_A_19	2,89E+00	2,69E-02	1,08E-02	1,99E-02	6,58E-03	3,89E+00	6,91E+00	1,11E-01	2,77E-02	6,12E-02	6,69E-03	2,14E-01	3,03E-01
080c3_A_2	6,52E-01	1,91E-02	2,24E-03	1,03E-02	5,89E-03	2,74E+00	3,26E+00	9,54E-02	n.d.	n.d.	n.d.	8,68E-02	1,55E-01
080c3_A_20	4,89E-01	2,94E-02	1,93E-02	2,89E-02	5,67E-03	5,36E+00	6,58E+00	1,13E-01	7,46E-02	1,90E-01	9,11E-03	2,82E-01	3,04E-01
080c3_A_21	2,37E-01	1,16E-02	2,02E-03	5,64E-03	8,77E-03	2,95E+00	1,32E+00	2,86E-01	2,25E-02	1,05E-02	1,92E-02	2,01E-01	6,54E-02
080c3_A_22	6,06E+00	3,28E-02	2,55E-02	4,80E-02	5,27E-03	1,82E+01	3,92E+01	9,34E-02	6,00E-01	6,58E-01	7,46E-03	2,58E+00	2,68E+00
080c3_A_23	2,00E+00	3,33E-02	8,52E-03	3,01E-02	1,19E-02	8,58E+00	2,34E+01	7,65E-02	8,73E-02	1,14E-01	7,63E-03	3,48E-01	2,26E-01
080c3_A_24	2,61E-01	2,58E-02	5,98E-04	1,10E-02	7,27E-03	5,70E+00	5,30E+00	2,35E-01	9,35E-02	1,23E-01	3,05E-03	3,97E-01	2,16E-01
080c3_A_25	1,76E-01	2,16E-02	3,72E-03	1,36E-02	8,25E-03	3,90E+00	2,02E+00	5,87E-02	6,52E-02	6,57E-02	1,04E-02	3,43E-01	3,35E-01
080c3_A_26	2,60E-01	2,55E-02	2,81E-02	3,11E-02	7,07E-03	5,53E+00	5,57E+00	8,88E-02	1,25E-01	1,87E-01	5,75E-03	4,28E-01	2,98E-01
080c3_A_27	n.d.	n.d.	3,62E-03	9,62E-03	7,44E-03	3,76E+00	2,36E+00	1,44E-01	5,99E-02	8,09E-02	1,34E-02	2,38E-01	9,40E-02
080c3_A_28	1,33E-01	1,95E-02	1,46E-02	3,93E-02	7,52E-03	5,20E+00	4,19E+00	1,55E-01	1,09E-01	1,82E-01	2,52E-03	3,43E-01	2,47E-01
080c3_A_29	7,44E-01	3,53E-02	1,35E-02	2,15E-02	1,22E-02	9,24E+00	1,03E+01	2,90E-02	1,01E-01	3,63E-02	1,17E-02	3,56E-01	5,36E-02
080c3_A_3	3,10E-01	1,01E-02	5,16E-03	3,11E-02	8,36E-03	3,00E+00	5,54E+00	9,93E-02	2,88E-02	1,96E-01	4,73E-03	1,66E-01	5,33E-01
080c3_A_30	1,54E-01	1,13E-02	4,21E-03	9,58E-03	8,89E-03	3,79E+00	3,32E+00	2,77E-01	7,91E-02	8,76E-02	3,74E-03	2,95E-01	1,72E-01
080c3_A_31	5,91E-01	2,76E-02	2,20E-02	3,05E-02	5,71E-03	9,14E+00	1,88E+01	1,26E-01	3,01E-01	7,08E-01	6,34E-03	9,11E-01	2,37E+00
080c3_A_32	6,48E-02	1,49E-02	1,90E-02	2,30E-02	7,68E-03	1,57E+01	1,79E+01	4,27E-02	3,54E-01	3,86E-01	4,59E-03	7,62E-01	6,75E-01
080c3_A_33	6,38E-01	2,13E-02	4,89E-03	2,88E-02	6,75E-03	4,04E+00	4,26E+00	1,77E-01	8,17E-02	3,65E-02	2,40E-02	3,39E-01	9,74E-02
080c3_A_34	3,83E+00	2,57E-02	5,19E-03	1,31E-02	5,68E-03	6,58E+00	1,39E+01	1,07E-01	1,12E-01	5,86E-02	1,45E-02	4,75E-01	1,99E-01
080c3_A_35	2,40E-01	2,47E-02	4,87E-02	4,96E-02	6,27E-03	1,71E+01	1,39E+01	1,57E-02	1,03E+00	1,03E+00	5,90E-03	2,80E+00	3,56E+00
080c3_A_36	4,86E+00	3,64E-02	1,70E-02	2,20E-02	7,14E-03	6,05E+00	7,09E+00	1,10E-01	1,21E-01	8,01E-02	2,13E-02	3,93E-01	2,06E-01
080c3_A_37	5,15E-02	3,05E-02	1,34E-02	2,01E-02	4,64E-03	5,55E+00	1,16E+00	2,73E-02	1,96E-01	5,97E-02	6,63E-03	5,53E-01	1,07E-01
080c3_A_38	6,85E-02	2,47E-02	2,74E-02	3,13E-02	7,26E-03	5,75E+00	5,47E+00	1,31E-01	2,31E-01	3,43E-01	2,44E-03	6,44E-01	8,23E-01
080c3_A_39	8,72E-01	2,23E-02	4,09E-02	6,11E-02	7,43E-03	9,83E+00	1,65E+01	6,42E-02	1,63E-01	8,35E-02	1,74E-02	5,69E-01	2,15E-01
080c3_A_4	2,61E-01	2,04E-03	n.d.	n.d.	n.d.	2,33E+00	1,72E+00	3,25E-02	1,29E-01	3,82E-01	3,33E-03	5,77E-01	1,24E+00
080c3_A_40	3,22E-01	2,81E-02	3,77E-03	1,43E-02	7,50E-03	4,15E+00	5,34E+00	1,86E-01	1,01E-01	3,70E-02	1,66E-02	3,10E-01	9,20E-02
080c3_A_41	4,24E-01	3,67E-02	2,36E-02	5,56E-02	1,16E-02	1,96E+01	2,49E+01	5,89E-02	5,99E-01	8,31E-01	1,15E-02	1,11E+00	1,32E+00
080c3_A_42	4,76E-01	3,50E-02	1,81E-02	2,46E-02	1,01E-02	1,73E+01	4,26E+01	7,08E-02	4,51E-01	8,36E-01	9,45E-03	9,48E-01	1,46E+00
080c3_A_43	5,15E-01	3,09E-02	5,24E-02	1,49E-01	1,00E-02	6,36E+01	9,47E+01	1,03E-01	2,24E+00	4,83E+00	1,09E-02	8,43E+00	2,89E+01
080c3_A_44	2,15E-01	2,78E-02	3,67E-02	4,45E-02	1,03E-02	1,61E+01	1,21E+01	8,70E-02	5,33E-01	4,99E-01	9,21E-03	1,30E+00	9,76E-01
080c3_A_45	2,65E-01	4,04E-02	4,61E-02	9,54E-02	1,36E-02	1,63E+01	1,39E+01	4,21E-02	7,67E-01	9,11E-01	1,05E-02	2,18E+00	2,25E+00
080c3_A_5	n.d.	n.d.	2,70E-03	9,97E-03	8,51E-03	2,38E+00	1,90E+00	1,30E-01	n.d.	n.d.	n.d.	1,18E-01	1,86E-01
080c3_A_6	1,10E-01	1,19E-02	8,44E-03	5,72E-03	6,37E-03	5,03E+00	7,51E+00	2,94E-02	1,24E-02	5,65E-02	1,06E-03	1,67E-01	9,30E-02
080c3_A_7	4,12E-01	1,85E-02	5,83E-03	1,17E-02	5,46E-03	2,63E+00	1,88E+00	2,12E-01	2,76E-02	1,38E-01	3,13E-03	2,98E-01	8,24E-01
080c3_A_8	3,96E-01	1,74E-02	1,05E-02	1,37E-02	7,73E-03	2,52E+00	1,01E+00	9,51E-02	n.d.	n.d.	n.d.	1,17E-01	6,21E-02
080c3_A_9	7,58E-01	1,95E-02	6,18E-04	5,24E-03	7,04E-03	1,81E+00	6,75E-01	4,01E-01	n.d.	n.d.	n.d.	1,03E-01	2,11E-02
092c_A_1	1,21E+01	6,65E-02	5,98E-01	6,07E-01	2,69E-02	1,12E+02	2,66E+02	2,98E-01	1,63E+01	4,78E+00	1,54E-02	3,14E+01	1,35E+01
092c_A_10	3,05E-01	2,07E-02	6,82E-03	2,17E-02	4,36E-03	8,06E+00	1,86E+01	7,77E-02	5,59E+01	1,02E+02	5,65E-03	1,28E+02	2,27E+02
092c_A_11	2,51E+01	3,09E-02	3,53E-01	9,44E-02	9,98E-03	1,07E+02	1,82E+02	7,25E-02	2,41E+01	1,59E+01	7,39E-03	5,04E+01	4,50E+01
092c_A_12	2,57E+01	3,41E-02	3,37E-01	3,26E-01	1,12E-02	5,02E+01	3,11E+01	1,04E-01	1,94E+01	1,36E+01	8,61E-03	3,99E+01	3,62E+01
092c_A_13	2,36E+01	2,25E-02	1,82E-01	2,57E-01	3,94E-03	2,80E+01	3,32E+01	5,71E-02	1,17E+01	1,47E+01	6,99E-03	2,42E+01	3,53E+01
092c_A_2	4,44E+00	6,79E-02	6,01E-01	8,61E-01	1,39E-02	1,13E+02	1,83E+02	1,18E-01	6,05E+00	9,15E+00	1,13E-02	1,12E+01	1,64E+01
092c_A_4	2,23E+00	1,64E-01	2,56E+00	4,33E+00	7,37E-02	3,88E+02	5,46E+02	5,67E-01	2,93E+01	4,10E+01	3,70E-02	5,24E+01	6,24E+01
092c_A_5	7,17E+00	1,67E-01	3,33E+00	4,84E+00	7,78E-02	5,59E+02	9,16E+02	6,21E-01	4,99E+01	6,47E+01	6,24E-02	8,61E+01	1,07E+02
092c_A_6	1,50E+01	9,76E-02	3,60E-01	1,66E-01	1,85E-02	9,89E+01	1,54E+02	2,16E-01	6,91E+01	8,34E+01	2,87E-02	1,52E+02	1,90E+02
092c_A_9	6,58E-01	2,62E-02	1,12E-01	6,65E-02	8,74E-03	1,81E+01	7,97E+00	1,35E-02	8,19E-01	3,75E-01	8,96E-03	1,55E+00	8,03E-01
100bA_matrix_1	2,33E-02	7,92E-03	1,07E-02	1,15E-02	4,48E-03	2,93E+00	4,94E-01	2,30E-01	1,20E-01	2,22E-02	2,07E-01	1,60E-01	1,19E-01
100bA_matrix_10	2,22E-01	2,50E-02	1,40E-02	1,85E-02	5,53E-03	9,66E+00	1,43E+01	2,02E-02	6,26E-01	1,34E+00	5,91E-03	1,37E+00	2,62E+00
100bA_matrix_2	n.d.	n.d.	1,13E-02	1,95E-02	6,09E-03	3,02E+00	7,50E-01	4,40E-01	1,29E-01	2,25E-02	3,22E-01	1,52E-01	2,91E-02
100bA_matrix_3	n.d.	n.d.	8,35E-03	1,33E-02	3,98E-03	3,28E+00	8,79E-01	1,97E-01	1,64E+00	2,76E+00	7,58E-03	4,40E+00	7,71E+00
100bA_matrix_4	1,15E-01	1,03E-02	3,49E-02	5,92E-02	5,99E-03	4,82E+00	1,40E+00	1,13E-01	1,94E+00	1,84E+00	7,16E-03	5,23E+00	5,34E+00
100bA_matrix_5	4,38E-01	3,07E-02	1,76E-02	1,25E-02	9,49E-03	5,13E+00	4,34E+00	1,18E-01	1,79E-01	5,85E-02	2,67E-02	3,65E-01	5,14E-02
100bA_matrix_6	8,67E-02	1,45E-02	1,05E-02	2,05E-02	5,81E-03	6,08E+00	1,26E+01	1,37E-01	1,83E-01	1,06E-01	4,51E-03	2,65E-01	1,93E-01
100bA_matrix_7	1,32E-01	1,47E-02	1,16E-02	1,38E-02	5,69E-03	4,82E+00	6,40E+00	9,94E-02	3,07E-01	1,69E-01	1,23E-02	7,55E-01	7,60E-01
100bA_matrix_8	6,99E-02	1,40E-02	5,40E-03	1,54E-02	4,26E-03	3,52E+00	9,32E-01	1,86E-01	1,53E-01	9,71E-02	2,24E-02	1,73E-01	8,10E-02
100bA_matrix_9	1,73E-01	2,25E-02	1,29E-02	2,10E-02	9,50E-03	6,17E+00	7,19E+00	7,89E-02	6,27E+01	8,86E+01	8,22E-03	1,47E+02	1,71E+02

Analysis	Ce140_LOD (ppm)	Pr141_mean (ppm)	Pr141_2SD (ppm)	Pr141_LOD (ppm)	Nd146_mean (ppm)	Nd146_2SD (ppm)	Nd146_LOD (ppm)	Sm147_mean (ppm)	Sm147_2SD (ppm)	Sm147_LOD (ppm)	Eu151_mean (ppm)	Eu151_2SD (ppm)	Eu151_LOD (ppm)
080c2_B_7	6,53E-03	3,08E-01	1,89E-01	3,51E-03	8,51E-01	2,54E-01	8,13E-03	2,11E-01	1,47E-01	1,07E-02	5,56E-02	7,63E-02	4,03E-03
080c2_B_8	6,10E-03	3,39E-01	7,89E-02	3,41E-03	1,09E+00	2,41E-01	7,45E-03	2,65E-01	1,76E-01	2,38E-02	5,00E-02	2,66E-02	3,61E-03
080c2_B_9	8,70E-03	4,20E-01	1,48E-01	3,14E-03	1,21E+00	4,72E-01	7,40E-03	2,78E-01	9,73E-02	2,17E-02	5,24E-02	3,55E-02	3,40E-03
080c3_A_1	6,23E-03	4,45E-02	8,40E-02	8,33E-04	1,43E-01	3,12E-01	1,29E-02	1,08E-01	1,35E-01	8,79E-03	2,62E-02	2,58E-02	2,36E-03
080c3_A_10	4,62E-03	7,51E-02	2,05E-01	3,40E-03	2,74E-01	7,72E-01	3,44E-03	1,19E-01	1,94E-01	1,88E-02	1,90E-02	2,64E-02	2,95E-03
080c3_A_11	5,66E-03	3,28E-01	6,13E-01	2,06E-03	1,60E+00	2,94E+00	5,12E-03	3,93E-01	6,15E-01	1,93E-02	1,07E-01	1,08E-01	2,19E-03
080c3_A_12	7,64E-03	6,20E-03	1,25E-02	3,72E-04	4,50E-02	1,98E-01	1,03E-02	5,06E-02	4,32E-02	1,49E-02	1,46E-02	1,24E-02	7,82E-03
080c3_A_13	9,29E-03	3,82E-03	1,57E-02	7,88E-04	1,27E-02	4,69E-02	1,12E-03	5,52E-02	5,12E-02	1,44E-02	1,93E-02	2,15E-02	6,01E-03
080c3_A_14	6,29E-03	4,89E-01	5,03E-01	1,21E-03	2,46E+00	2,43E+00	7,36E-03	6,35E-01	6,77E-01	9,34E-03	1,04E-01	1,47E-01	3,29E-03
080c3_A_15	8,96E-03	6,98E-03	2,81E-02	1,62E-03	5,95E-02	2,42E-01	4,48E-03	5,26E-02	3,04E-02	2,47E-02	2,04E-02	1,11E-02	1,21E-02
080c3_A_16	8,81E-03	4,16E-02	1,06E-01	2,41E-03	2,42E-01	6,29E-01	4,78E-03	1,41E-01	2,22E-01	8,64E-03	4,30E-02	4,98E-02	3,41E-03
080c3_A_17	2,02E-02	n.d.	n.d.	n.d.	2,30E-02	8,52E-02	3,67E-03	6,46E-02	6,29E-02	3,00E-02	2,54E-02	9,98E-03	1,17E-02
080c3_A_18	1,35E-02	9,10E-04	1,95E-02	4,80E-04	4,53E-02	2,12E-01	3,75E-03	6,87E-02	5,10E-02	1,30E-02	3,76E-02	8,46E-02	3,31E-03
080c3_A_19	1,19E-02	5,76E-03	1,34E-02	7,63E-04	2,22E-02	4,46E-02	5,02E-03	5,46E-02	3,16E-02	2,29E-02	1,98E-02	1,09E-02	1,60E-02
080c3_A_2	1,16E-02	n.d.	n.d.	n.d.	n.d.	n.d.	n.d.	n.d.	n.d.	n.d.	5,26E-03	1,58E-02	4,96E-03
080c3_A_20	2,34E-02	2,58E-02	6,53E-02	7,94E-04	1,76E-01	5,04E-01	5,28E-03	6,59E-02	5,38E-02	1,66E-02	2,60E-02	1,59E-02	8,49E-03
080c3_A_21	4,05E-02	2,82E-03	8,94E-03	7,26E-04	4,89E-02	5,46E-02	6,50E-03	4,94E-02	2,02E-02	1,19E-01	2,68E-02	1,37E-02	1,70E-02
080c3_A_22	5,88E-03	4,45E-01	4,53E-01	9,21E-04	2,76E+00	3,23E+00	5,64E-03	1,01E+00	1,07E+00	6,75E-03	3,10E-01	3,09E-01	2,22E-03
080c3_A_23	1,09E-02	2,45E-02	3,40E-02	3,88E-03	1,68E-01	3,81E-01	6,82E-03	7,62E-02	7,25E-02	5,87E-02	2,95E-02	2,84E-02	1,23E-02
080c3_A_24	1,28E-02	2,13E-02	3,66E-02	4,49E-03	1,14E-01	9,83E-02	1,02E-02	8,12E-02	7,32E-02	3,61E-02	3,51E-02	5,99E-03	1,78E-02
080c3_A_25	9,34E-03	1,33E-02	1,68E-02	5,64E-03	8,82E-02	3,59E-02	1,03E-02	7,58E-02	5,98E-02	2,86E-02	3,18E-02	1,19E-02	4,74E-02
080c3_A_26	9,93E-03	2,72E-02	4,63E-02	4,04E-03	1,24E-01	1,26E-01	2,18E-02	1,03E-01	1,30E-01	1,61E-02	3,23E-02	1,67E-02	1,58E-02
080c3_A_27	2,86E-02	1,35E-02	1,26E-02	1,76E-03	6,41E-02	7,41E-02	1,23E-02	6,53E-02	3,27E-02	2,72E-02	2,74E-02	1,78E-02	4,71E-02
080c3_A_28	1,18E-02	2,46E-02	4,50E-02	1,36E-03	1,24E-01	1,55E-01	8,69E-03	8,97E-02	8,24E-02	1,53E-02	3,58E-02	1,96E-02	1,13E-02
080c3_A_29	1,29E-02	2,40E-02	1,65E-02	5,63E-03	1,38E-01	1,32E-01	1,30E-02	7,40E-02	4,32E-02	3,72E-02	3,81E-02	3,05E-02	3,92E-02
080c3_A_3	7,09E-03	5,75E-03	7,62E-02	3,97E-04	3,05E-02	3,77E-01	2,37E-03	4,31E-02	7,12E-02	1,22E-02	9,05E-04	4,73E-03	1,99E-03
080c3_A_30	1,83E-02	1,99E-02	2,42E-02	1,59E-03	8,16E-02	4,92E-02	1,60E-02	6,82E-02	6,17E-02	3,17E-02	3,60E-02	2,02E-02	1,08E-02
080c3_A_31	7,33E-03	6,43E-02	1,28E-01	4,72E-03	2,66E-01	6,36E-01	9,10E-03	8,99E-02	7,52E-02	2,23E-02	4,33E-02	3,21E-02	2,83E-02
080c3_A_32	4,30E-03	6,80E-02	7,02E-02	4,45E-03	2,91E-01	3,29E-01	6,73E-03	1,17E-01	1,49E-01	1,17E-02	7,32E-02	7,13E-02	3,31E-03
080c3_A_33	1,07E-02	2,12E-02	1,13E-02	6,24E-03	1,08E-01	7,29E-02	4,39E-02	9,02E-02	8,04E-02	1,65E-02	3,81E-02	1,51E-02	1,58E-02
080c3_A_34	1,69E-02	2,50E-02	1,54E-02	2,78E-03	1,65E-01	5,85E-02	1,31E-02	8,83E-02	5,38E-02	2,90E-02	4,00E-02	2,47E-02	4,14E-02
080c3_A_35	5,15E-03	3,14E-01	3,58E-01	8,94E-04	1,20E+00	1,44E+00	5,64E-03	2,56E-01	2,57E-01	7,84E-03	7,36E-02	5,66E-02	3,60E-03
080c3_A_36	2,08E-02	3,17E-02	2,12E-02	5,70E-03	1,76E-01	1,14E-01	1,18E-02	7,36E-02	3,38E-02	4,29E-02	3,95E-02	1,99E-02	2,40E-02
080c3_A_37	1,06E-02	4,58E-02	9,96E-03	1,44E-03	2,06E-01	1,32E-01	9,91E-03	1,02E-01	4,64E-02	1,65E-02	7,25E-02	3,21E-02	3,81E-03
080c3_A_38	7,21E-03	6,71E-02	1,06E-01	1,37E-03	3,29E-01	3,90E-01	2,72E-02	1,18E-01	8,39E-02	1,40E-02	4,35E-02	3,29E-02	9,94E-03
080c3_A_39	1,20E-02	4,36E-02	3,36E-02	8,35E-03	2,02E-01	1,29E-01	1,59E-02	9,03E-02	6,18E-02	3,43E-02	4,25E-02	1,03E-02	3,24E-02
080c3_A_4	5,02E-03	3,04E-02	1,00E-01	1,66E-03	2,36E-01	5,91E-01	3,98E-03	1,06E-01	2,16E-01	7,42E-03	1,32E-02	1,39E-02	3,01E-03
080c3_A_40	2,40E-02	2,88E-02	1,12E-02	2,29E-03	1,33E-01	7,22E-02	2,15E-02	6,96E-02	3,04E-02	3,82E-02	4,24E-02	1,61E-02	9,74E-03
080c3_A_41	7,60E-03	1,27E-01	1,71E-01	1,53E-03	7,12E-01	1,67E+00	9,63E-03	1,49E-01	1,44E-01	1,73E-02	9,02E-02	4,72E-02	4,94E-03
080c3_A_42	9,20E-03	1,07E-01	1,91E-01	7,32E-03	4,19E-01	5,10E-01	1,29E-02	1,31E-01	1,25E-01	2,43E-02	1,12E-01	1,85E-01	5,39E-03
080c3_A_43	8,38E-03	1,09E+00	3,99E+00	4,83E-03	2,67E+00	6,54E+00	8,46E-03	1,34E+00	4,85E+00	1,02E-02	3,21E-01	4,41E-01	3,34E-03
080c3_A_44	8,22E-03	1,70E-01	1,25E-01	5,79E-03	8,90E-01	7,91E-01	1,10E-02	2,99E-01	1,41E-01	1,38E-02	1,41E-01	1,29E-01	4,87E-03
080c3_A_45	1,29E-02	3,86E-01	5,33E-01	6,39E-03	1,77E+00	2,54E+00	3,15E-02	6,43E-01	5,85E-01	1,74E-02	2,23E-01	2,67E-01	6,03E-03
080c3_A_5	6,51E-03	n.d.	n.d.	n.d.	n.d.	n.d.	n.d.	5,70E-02	8,22E-02	1,37E-02	1,29E-02	1,53E-02	1,72E-02
080c3_A_6	9,42E-03	n.d.	n.d.	n.d.	n.d.	n.d.	n.d.	4,92E-02	4,16E-02	1,80E-02	1,25E-02	9,61E-03	6,35E-03
080c3_A_7	4,97E-03	1,18E-02	1,00E-01	1,01E-03	5,87E-02	4,80E-01	2,63E-03	6,11E-02	1,61E-01	1,16E-02	1,74E-02	3,43E-02	1,18E-02
080c3_A_8	4,19E-03	n.d.	n.d.	n.d.	n.d.	n.d.	n.d.	4,32E-02	7,46E-02	1,04E-02	1,02E-02	6,71E-03	6,44E-03
080c3_A_9	6,81E-03	n.d.	n.d.	n.d.	n.d.	n.d.	n.d.	4,11E-02	3,90E-02	1,37E-02	1,29E-02	1,57E-02	5,66E-03
092c_A_1	1,29E-02	3,83E+00	1,10E+00	2,92E-03	1,22E+01	1,96E+00	6,87E-02	2,68E+00	1,56E+00	2,12E-02	2,35E-01	1,21E-01	1,87E-02
092c_A_10	5,31E-03	1,76E+01	3,12E+01	6,47E-04	7,84E+01	1,39E+02	3,97E-03	1,53E+01	2,70E+01	4,80E-03	9,02E-01	1,64E+00	1,48E-03
092c_A_11	7,31E-03	6,32E+00	4,69E+00	1,56E-03	2,07E+01	1,39E+01	9,58E-03	3,82E+00	2,71E+00	1,15E-02	3,83E-01	2,80E-01	8,57E-03
092c_A_12	6,88E-03	5,40E+00	4,36E+00	1,36E-03	1,75E+01	1,37E+01	1,94E-02	3,57E+00	2,99E+00	1,01E-02	3,15E-01	2,02E-01	9,47E-03
092c_A_13	4,34E-03	3,06E+00	3,91E+00	3,30E-03	1,03E+01	1,29E+01	4,90E-03	2,16E+00	2,81E+00	5,87E-03	1,72E-01	2,40E-01	1,72E-03
092c_A_2	1,18E-02	1,15E+00	1,65E+00	7,48E-03	3,54E+00	4,68E+00	1,08E-02	7,40E-01	1,70E+00	1,35E-02	6,63E-02	2,47E-01	3,05E-03
092c_A_4	3,70E-02	6,36E+00	8,65E+00	1,14E-02	2,09E+01	2,66E+01	6,79E-02	4,38E+00	6,05E+00	8,03E-02	3,95E-01	6,06E-01	2,23E-02
092c_A_5	4,89E-02	1,05E+01	1,29E+01	2,42E-02	3,44E+01	4,22E+01	6,76E-02	8,22E+00	1,02E+01	8,14E-02	6,34E-01	6,18E-01	5,99E-02
092c_A_6	1,40E-02	1,90E+01	2,45E+01	3,92E-03	7,49E+01	1,03E+02	2,42E-02	1,54E+01	2,20E+01	2,93E-02	1,06E+00	1,37E+00	8,71E-03
092c_A_9	6,71E-03	1,61E-01	9,11E-02	8,43E-04	4,94E-01	3,82E-01	1,53E-02	7,60E-02	9,89E-02	4,42E-03	n.d.	n.d.	n.d.
100bA_matrix_1	3,00E-02	1,40E-02	4,80E-03	1,33E-02	2,31E-02	3,05E-02	1,31E-02	n.d.	n.d.	n.d.	n.d.	n.d.	n.d.
100bA_matrix_10	5,67E-03	1,60E-01	3,57E-01	1,10E-03	5,95E-01	1,77E+00	6,24E-03	1,21E-01	3,91E-01	7,42E-03	n.d.	n.d.	n.d.
100bA_matrix_2	6,54E-02	1,48E-02	7,96E-03	4,28E-03	1,15E-02	2,27E-02	3,49E-03	< Det. Lim	1,21E-02	2,12E+02	n.d.	n.d.	n.d.
100bA_matrix_3	4,83E-03	4,64E-01	7,99E-01	2,39E-03	2,93E+00	5,64E+00	1,30E-02	3,72E-01	6,47E-01	4,67E-03	1,30E-02	4,82E-02	7,63E-04
100bA_matrix_4	2,77E-03	5,82E-01	6,15E-01	1,01E-03	2,48E+00	3,00E+00	1,57E-02	4,91E-01	5,90E-01	7,20E-03	1,27E-02	5,81E-02	3,24E-03
100bA_matrix_5	8,88E-03	2,91E-02	1,84E-02	2,75E-03	7,10E-02	8,62E-02	2,16E-02	1,92E-02	5,50E-02	7,37E-03	< Det. Lim	2,94E-03	3,29E-01
100bA_matrix_6	8,94E-03	2,98E-02	2,51E-02	1,39E-03	3,41E-02	5,83E-02	4,92E-03	1,69E-03	3,86E-02	3,22E-03	n.d.	n.d.	n.d.
100bA_matrix_7	6,67E-03	5,67E-02	5,44E-02	9,29E-04	1,36E-01	1,97E-01	4,47E-03	2,16E-02	4,17E-02	4,06E-03	n.d.	n.d.	n.d.
100bA_matrix_8	2,19E-02	1,61E-02	1,31E-02	3,26E-03	1,91E-02	3,97E-02	5,65E-03	5,51E-04	2,14E-02	5,53E-04	n.d.	n.d.	n.d.
100bA_matrix_9	5,66E-03	2,03E+01	2,75E+01	3,46E-03	9,19E+01	1,29E+02	5,80E-03	1,70E+01	2,48E+01	7,02E-03	8,88E-01	1,55E+00	2,19E-03

Analysis	Gd157_mean (ppm)	Gd157_2SD (ppm)	Gd157_LOD (ppm)	Gd158_mean (ppm)	Gd158_2SD (ppm)	Gd158_LOD (ppm)	Tb159_mean (ppm)	Tb159_2SD (ppm)	Tb159_LOD (ppm)	Dy161_mean (ppm)	Dy161_2SD (ppm)	Dy161_LOD (ppm)	Ho165_mean (ppm)
080c2_B_7	1,39E-01	1,39E-01	4,04E-02	1,97E-01	1,38E-01	2,35E-02	3,31E-02	2,69E-02	4,71E-03	7,56E-02	2,42E-01	7,15E-03	1,52E-02
080c2_B_8	1,63E-01	1,36E-01	2,92E-02	2,21E-01	1,65E-01	2,14E-02	4,79E-02	1,39E-02	5,39E-03	1,26E-01	1,74E-01	3,71E-03	4,29E-02
080c2_B_9	2,11E-01	1,92E-01	8,24E-03	2,58E-01	1,16E-01	2,45E-02	4,68E-02	3,47E-02	1,57E-03	2,35E-01	9,43E-02	5,00E-03	6,27E-02
080c3_A_1	7,85E-02	1,72E-01	2,66E-02	8,00E-02	1,49E-01	4,44E-03	1,09E-02	1,30E-02	2,41E-03	5,27E-03	8,60E-02	1,02E-03	2,95E-02
080c3_A_10	8,25E-02	1,52E-01	2,71E-02	5,51E-02	2,27E-01	7,70E-03	1,73E-02	3,75E-02	2,12E-03	9,23E-03	2,33E-01	3,25E-04	2,72E-02
080c3_A_11	3,06E-01	5,62E-01	2,06E-02	3,32E-01	6,06E-01	1,47E-02	5,29E-02	9,32E-02	1,04E-03	1,99E-01	5,25E-01	3,77E-03	7,90E-02
080c3_A_12	3,35E-02	3,94E-02	2,81E-02	1,43E-03	3,19E-02	8,07E-04	3,17E-03	4,57E-03	1,43E-03	n.d.	n.d.	n.d.	1,19E-02
080c3_A_13	3,08E-02	8,30E-02	4,96E-02	n.d.	n.d.	n.d.	2,68E-03	1,42E-02	1,10E-03	n.d.	n.d.	n.d.	1,61E-02
080c3_A_14	6,81E-01	6,66E-01	1,00E-02	6,67E-01	9,67E-01	6,22E-03	8,74E-02	9,07E-02	4,01E-03	4,94E-01	4,61E-01	1,73E-02	1,21E-01
080c3_A_15	4,80E-02	3,65E-02	5,15E-02	n.d.	n.d.	n.d.	3,14E-03	1,28E-02	6,29E-04	n.d.	n.d.	n.d.	7,95E-04
080c3_A_16	1,35E-01	1,94E-01	2,43E-02	9,60E-02	2,61E-01	1,01E-02	1,39E-02	4,13E-02	2,41E-03	1,02E-02	3,88E-01	3,94E-04	4,37E-02
080c3_A_17	7,29E-02	7,25E-02	2,03E-02	n.d.	n.d.	n.d.	n.d.	n.d.	n.d.	n.d.	n.d.	n.d.	8,47E-03
080c3_A_18	8,41E-02	7,63E-02	6,27E-02	1,51E-02	1,29E-01	6,26E-03	9,24E-04	5,57E-03	2,23E-04	n.d.	n.d.	n.d.	6,24E-03
080c3_A_19	4,79E-02	5,49E-02	1,72E-01	n.d.	n.d.	n.d.	3,20E-03	9,39E-03	2,20E-03	n.d.	n.d.	n.d.	7,19E-03
080c3_A_2	3,15E-03	3,67E-02	6,81E-03	n.d.	n.d.	n.d.	5,85E-04	1,19E-02	4,13E-04	n.d.	n.d.	n.d.	1,19E-02
080c3_A_20	6,85E-02	7,71E-02	1,08E-01	9,80E-03	7,24E-02	4,87E-03	5,32E-03	8,63E-03	2,26E-03	n.d.	n.d.	n.d.	1,24E-02
080c3_A_21	n.d.	n.d.	n.d.	7,65E-03	5,17E-02	3,83E-03	n.d.	n.d.	n.d.	n.d.	n.d.	n.d.	n.d.
080c3_A_22	1,36E+00	1,33E+00	3,32E-02	1,22E+00	1,30E+00	1,28E-02	1,82E-01	1,78E-01	4,24E-03	1,20E+00	1,39E+00	1,55E-02	2,50E-01
080c3_A_23	8,68E-02	6,66E-02	7,64E-02	3,48E-02	4,02E-02	1,02E-02	7,00E-03	1,67E-02	7,50E-04	n.d.	n.d.	n.d.	8,10E-03
080c3_A_24	1,03E-01	8,06E-02	1,41E-01	n.d.	n.d.	n.d.	n.d.	n.d.	n.d.	n.d.	n.d.	n.d.	n.d.
080c3_A_25	9,84E-02	5,72E-02	1,67E-01	1,51E-02	2,50E-02	1,16E-02	2,07E-03	1,23E-02	1,69E-03	n.d.	n.d.	n.d.	1,15E-02
080c3_A_26	1,23E-01	7,08E-02	7,29E-02	1,71E-02	8,15E-02	1,07E-02	5,06E-04	1,25E-02	5,69E-04	n.d.	n.d.	n.d.	2,30E-03
080c3_A_27	1,02E-01	3,90E-02	8,15E-02	9,34E-03	2,95E-02	8,88E-03	8,59E-04	9,66E-03	6,14E-04	n.d.	n.d.	n.d.	7,02E-03
080c3_A_28	1,36E-01	1,04E-01	1,07E-01	3,44E-02	9,79E-02	1,03E-02	4,13E-03	1,07E-02	1,81E-03	n.d.	n.d.	n.d.	6,66E-04
080c3_A_29	1,40E-01	5,73E-02	3,23E-02	1,48E-03	4,11E-02	3,23E-03	1,00E-02	1,00E-02	1,31E-03	n.d.	n.d.	n.d.	1,99E-03
080c3_A_3	8,74E-03	6,61E-02	1,26E-02	5,69E-03	6,35E-02	3,37E-03	7,11E-03	3,69E-02	2,88E-03	n.d.	n.d.	n.d.	1,19E-02
080c3_A_30	1,20E-01	6,40E-02	1,07E-01	1,72E-02	4,44E-02	1,24E-02	2,34E-03	8,35E-03	4,45E-04	n.d.	n.d.	n.d.	n.d.
080c3_A_31	1,88E-01	2,21E-01	8,73E-02	5,57E-02	6,21E-02	1,30E-02	1,21E-02	3,32E-02	3,73E-03	n.d.	n.d.	n.d.	1,42E-02
080c3_A_32	1,77E-01	7,00E-02	5,33E-02	5,35E-02	4,65E-02	4,23E-03	4,19E-03	1,86E-02	6,01E-04	n.d.	n.d.	n.d.	1,25E-02
080c3_A_33	1,31E-01	6,63E-02	3,37E-01	2,66E-02	4,86E-02	1,03E-02	3,47E-03	1,21E-02	3,18E-03	n.d.	n.d.	n.d.	n.d.
080c3_A_34	1,69E-01	1,17E-01	1,19E-01	2,94E-02	3,90E-02	2,91E-02	1,29E-03	9,34E-03	3,70E-04	n.d.	n.d.	n.d.	n.d.
080c3_A_35	4,08E-01	3,66E-01	4,46E-02	2,80E-01	3,64E-01	1,18E-02	4,22E-02	6,44E-02	3,35E-03	2,44E-01	5,92E-01	4,04E-03	5,50E-02
080c3_A_36	1,71E-01	7,07E-02	1,08E-01	3,21E-02	6,78E-02	1,73E-02	4,36E-03	9,43E-03	7,25E-04	n.d.	n.d.	n.d.	1,51E-03
080c3_A_37	1,56E-01	6,49E-02	1,82E-01	4,22E-02	5,84E-02	2,41E-02	6,46E-03	1,16E-02	7,95E-04	n.d.	n.d.	n.d.	1,47E-03
080c3_A_38	2,10E-01	1,99E-01	8,67E-02	9,65E-02	1,86E-01	5,75E-03	1,20E-02	3,01E-02	3,31E-03	1,73E-02	3,47E-01	9,50E-04	2,82E-02
080c3_A_39	1,51E-01	5,65E-02	7,09E-01	5,12E-02	4,67E-02	2,84E-02	4,20E-03	1,50E-02	9,26E-04	n.d.	n.d.	n.d.	n.d.
080c3_A_4	6,75E-02	1,26E-01	2,10E-02	4,54E-02	1,58E-01	8,54E-03	1,82E-02	3,54E-02	9,24E-04	n.d.	n.d.	n.d.	2,88E-02
080c3_A_40	1,33E-01	2,90E-02	3,81E-01	3,71E-02	3,85E-02	1,42E-02	3,30E-03	1,10E-02	1,65E-03	n.d.	n.d.	n.d.	n.d.
080c3_A_41	2,59E-01	1,40E-01	9,03E-02	1,00E-01	1,76E-01	2,73E-02	2,15E-02	6,55E-02	4,02E-03	n.d.	n.d.	n.d.	n.d.
080c3_A_42	2,83E-01	2,19E-01	2,47E-02	1,00E-01	1,50E-01	2,99E-02	2,23E-02	3,84E-02	1,66E-03	n.d.	n.d.	n.d.	n.d.
080c3_A_43	6,31E-01	1,16E+00	1,39E-02	5,16E-01	1,01E+00	1,88E-02	8,47E-02	1,59E-01	1,67E-03	7,42E-01	2,39E+00	7,86E-03	9,16E-02
080c3_A_44	4,25E-01	2,85E-01	6,18E-02	3,54E-01	2,59E-01	2,74E-02	6,09E-02	5,24E-02	5,64E-03	2,92E-01	2,48E-01	1,84E-02	4,44E-02
080c3_A_45	8,71E-01	1,01E+00	4,28E-02	7,58E-01	9,47E-01	2,90E-02	1,23E-01	1,75E-01	7,32E-03	8,61E-01	1,07E+00	2,83E-02	1,83E-01
080c3_A_5	4,12E-02	8,49E-02	1,68E-02	n.d.	n.d.	n.d.	n.d.	n.d.	n.d.	n.d.	n.d.	n.d.	1,43E-02
080c3_A_6	1,92E-02	4,77E-02	1,23E-02	n.d.	n.d.	n.d.	6,57E-04	1,07E-02	6,55E-04	n.d.	n.d.	n.d.	6,58E-03
080c3_A_7	5,37E-02	1,92E-01	6,22E-03	n.d.	n.d.	n.d.	7,57E-03	2,84E-02	2,11E-03	n.d.	n.d.	n.d.	1,39E-02
080c3_A_8	2,68E-02	4,88E-02	1,50E-02	n.d.	n.d.	n.d.	1,73E-03	8,46E-03	9,78E-04	n.d.	n.d.	n.d.	1,02E-02
080c3_A_9	2,65E-02	3,38E-02	1,44E-02	n.d.	n.d.	n.d.	4,32E-03	5,64E-03	5,51E-04	n.d.	n.d.	n.d.	1,30E-02
092c_A_1	2,63E+00	1,01E+00	6,28E-02	2,44E+00	5,31E-01	1,62E-02	4,12E-01	1,42E-01	1,20E-02	2,61E+00	1,00E+00	2,14E-02	6,07E-01
092c_A_10	1,42E+01	2,50E+01	2,92E-02	1,40E+01	2,45E+01	2,13E-02	1,94E+00	3,38E+00	8,40E-04	1,10E+01	1,91E+01	4,54E-03	2,12E+00
092c_A_11	3,51E+00	2,46E+00	3,43E-02	3,68E+00	3,32E+00	1,79E-02	6,48E-01	5,39E-01	2,03E-03	4,55E+00	3,04E+00	1,10E-02	9,72E-01
092c_A_12	2,75E+00	2,17E+00	4,24E-02	2,97E+00	2,48E+00	7,30E-03	6,15E-01	4,69E-01	5,63E-03	4,04E+00	3,49E+00	9,62E-03	8,22E-01
092c_A_13	1,68E+00	1,81E+00	3,17E-02	1,73E+00	2,10E+00	2,11E-02	3,35E-01	3,79E-01	1,06E-03	2,59E+00	2,90E+00	1,72E-02	5,17E-01
092c_A_2	8,60E-01	1,01E+00	1,87E-02	7,02E-01	9,36E-01	6,00E-02	1,30E-01	1,99E-01	1,48E-02	7,69E-01	1,04E+00	1,38E-02	2,06E-01
092c_A_4	3,38E+00	2,39E+00	2,12E-01	4,08E+00	6,31E+00	1,25E-01	8,00E-01	1,07E+00	1,53E-02	5,20E+00	8,93E+00	1,87E-01	1,19E+00
092c_A_5	6,71E+00	9,67E+00	2,99E-01	6,09E+00	6,82E+00	5,80E-02	9,78E-01	8,86E-01	1,30E-02	7,06E+00	8,08E+00	1,89E-01	1,86E+00
092c_A_6	1,36E+01	1,98E+01	1,10E-01	1,43E+01	2,06E+01	4,89E-02	2,04E+00	2,26E+00	4,96E-03	1,37E+01	1,59E+01	2,69E-02	2,57E+00
092c_A_9	1,45E-01	6,92E-02	6,11E-02	9,61E-02	8,33E-02	1,76E-02	2,52E-02	2,77E-02	1,69E-03	1,48E-01	1,01E-01	8,67E-03	5,42E-02
100bA_matrix_1	6,45E-02	3,75E-02	4,10E-01	n.d.	n.d.	n.d.	1,12E-02	6,62E-03	1,24E-02	7,76E-02	6,19E-02	1,87E-02	3,11E-02
100bA_matrix_10	1,53E-01	4,16E-01	7,09E-02	6,77E-02	2,59E-01	1,87E-02	2,96E-02	5,69E-02	2,07E-03	2,11E-01	4,23E-01	1,18E-02	5,53E-02
100bA_matrix_2	8,02E-02	5,93E-02	1,32E-01	n.d.	n.d.	n.d.	1,08E-02	6,39E-03	2,05E-02	8,19E-02	6,02E-02	9,18E-02	3,33E-02
100bA_matrix_3	3,43E-01	5,31E-01	2,16E-02	3,21E-01	5,80E-01	1,46E-02	6,56E-02	1,17E-01	9,73E-04	2,78E-01	3,97E-01	2,53E-02	7,34E-02
100bA_matrix_4	4,02E-01	4,21E-01	3,71E-02	4,35E-01	6,77E-01	2,16E-02	7,92E-02	9,29E-02	7,20E-03	4,42E-01	5,89E-01	2,24E-02	9,70E-02
100bA_matrix_5	9,91E-02	7,07E-02	8,35E-02	< Det. Lim	1,96E-02	1,73E-01	1,55E-02	1,00E-02	5,78E-03	9,21E-02	1,67E-02	1,29E-01	3,88E-02
100bA_matrix_6	8,99E-02	6,33E-02	8,27E-02	< Det. Lim	1,05E-02	5,42E-02	1,29E-02	1,09E-02	4,95E-03	9,58E-02	4,20E-02	2,58E-02	3,33E-02
100bA_matrix_7	1,05E-01	9,01E-02	7,25E-02	1,40E-02	2,58E-02	2,11E-03	1,45E-02	9,52E-03	1,28E-02	1,15E-01	7,50E-02	4,61E-02	3,96E-02
100bA_matrix_8	n.d.	n.d.	n.d.	n.d.	n.d.	n.d.	n.d.	n.d.	n.d.	n.d.	n.d.	n.d.	3,31E-02
100bA_matrix_9	1,50E+01	2,25E+01	2,81E-02	1,45E+01	2,03E+01	1,30E-02	1,97E+00	2,83E+00	1,23E-03	1,16E+01	1,63E+01	6,63E-03	2,36E+00

Analysis	Ho165_2SD	Ho165_LOD	Er167_mean	Er167_2SD	Er167_LOD	Tm169_mean	Tm169_2SD	Tm169_LOD	Yb172_mean	Yb172_2SD	Yb172_LOD	Lu175_mean	Lu175_2SD
	(ppm)	(ppm)	(ppm)	(ppm)	(ppm)	(ppm)	(ppm)	(ppm)	(ppm)	(ppm)	(ppm)	(ppm)	(ppm)
080c2_B_7	8,85E-02	6,00E-04	8,18E-02	9,32E-02	4,83E-03	1,74E-02	1,28E-02	1,30E-03	1,70E-01	1,44E-01	6,76E-03	3,93E-02	2,80E-02
080c2_B_8	2,76E-02	9,86E-04	1,97E-01	8,42E-02	1,55E-02	4,08E-02	1,23E-02	1,49E-03	3,02E-01	1,32E-01	7,17E-03	5,40E-02	3,73E-02
080c2_B_9	5,34E-02	1,12E-03	2,64E-01	2,41E-01	6,34E-03	4,90E-02	2,67E-02	1,53E-03	3,46E-01	1,65E-01	7,34E-03	7,52E-02	1,76E-02
080c3_A_1	2,59E-02	1,53E-03	9,25E-02	2,17E-01	4,66E-03	7,34E-03	9,42E-03	8,94E-04	8,54E-02	1,16E-01	5,00E-03	1,25E-02	3,45E-02
080c3_A_10	4,65E-02	8,78E-04	4,60E-02	1,43E-01	1,85E-03	1,31E-02	3,05E-02	7,36E-04	5,63E-02	1,39E-01	2,73E-03	1,50E-02	2,28E-02
080c3_A_11	1,29E-01	1,14E-03	1,26E-01	2,93E-01	3,68E-03	2,98E-02	5,08E-02	1,11E-03	1,81E-01	3,48E-01	4,92E-03	2,23E-02	3,57E-02
080c3_A_12	1,09E-02	1,11E-03	n.d.	n.d.	n.d.	3,03E-03	5,78E-03	5,99E-04	4,45E-02	2,62E-02	3,33E-03	7,26E-03	1,79E-02
080c3_A_13	1,72E-02	9,70E-04	n.d.	n.d.	n.d.	4,60E-03	1,36E-02	5,87E-04	1,97E-02	9,69E-02	1,62E-03	3,38E-03	1,50E-02
080c3_A_14	1,53E-01	1,59E-03	2,87E-01	3,89E-01	1,58E-02	5,03E-02	6,92E-02	1,66E-03	2,92E-01	1,77E-01	7,30E-03	4,76E-02	1,40E-02
080c3_A_15	7,72E-03	2,56E-04	n.d.	n.d.	n.d.	n.d.	n.d.	n.d.	1,86E-03	6,17E-02	2,70E-04	7,00E-03	1,37E-02
080c3_A_16	7,03E-02	1,14E-03	3,00E-02	1,66E-01	1,55E-03	1,30E-02	2,11E-02	4,56E-03	6,30E-02	1,84E-01	3,48E-03	1,60E-02	2,00E-02
080c3_A_17	1,37E-02	1,03E-03	n.d.	n.d.	n.d.	6,89E-03	1,38E-02	1,35E-03	n.d.	n.d.	n.d.	1,26E-02	2,45E-02
080c3_A_18	1,19E-02	6,97E-04	n.d.	n.d.	n.d.	8,23E-03	1,18E-02	1,05E-03	5,69E-02	1,18E-01	3,25E-03	1,43E-02	1,79E-02
080c3_A_19	1,83E-02	9,01E-04	n.d.	n.d.	n.d.	1,35E-02	1,31E-02	1,49E-03	2,30E-02	2,96E-02	2,67E-03	1,15E-02	1,13E-02
080c3_A_2	1,05E-02	1,54E-03	3,50E-03	7,82E-02	4,14E-04	4,49E-03	1,39E-02	5,99E-04	2,21E-02	8,21E-02	2,07E-03	1,19E-03	1,82E-02
080c3_A_20	1,98E-02	7,30E-04	n.d.	n.d.	n.d.	1,30E-02	2,10E-02	1,11E-03	4,90E-02	9,48E-02	2,79E-03	1,84E-02	1,65E-02
080c3_A_21	n.d.	n.d.	n.d.	n.d.	n.d.	5,91E-03	1,51E-02	1,36E-03	3,63E-02	1,37E-01	8,54E-03	1,46E-02	3,66E-02
080c3_A_22	2,69E-01	1,21E-03	6,12E-01	7,89E-01	5,11E-03	1,06E-01	1,35E-01	1,30E-03	4,62E-01	6,49E-01	5,77E-03	7,17E-02	6,75E-02
080c3_A_23	1,23E-02	5,83E-04	n.d.	n.d.	n.d.	1,32E-02	1,46E-02	1,19E-03	1,17E-02	6,17E-02	1,02E-03	1,17E-02	2,15E-02
080c3_A_24	n.d.	n.d.	n.d.	n.d.	n.d.	2,19E-03	5,19E-03	2,20E-03	n.d.	n.d.	n.d.	7,33E-03	2,83E-02
080c3_A_25	1,85E-02	8,71E-04	n.d.	n.d.	n.d.	1,54E-02	2,17E-02	1,74E-03	5,86E-02	1,49E-01	4,02E-03	1,93E-02	3,26E-02
080c3_A_26	1,75E-02	2,34E-04	n.d.	n.d.	n.d.	1,24E-02	1,45E-02	4,91E-03	4,56E-02	1,14E-01	3,20E-03	2,13E-02	1,96E-02
080c3_A_27	1,15E-02	5,77E-04	n.d.	n.d.	n.d.	1,30E-02	1,31E-02	1,63E-03	6,98E-02	1,06E-01	4,30E-03	2,15E-02	2,76E-02
080c3_A_28	1,09E-02	6,53E-05	n.d.	n.d.	n.d.	1,39E-02	1,64E-02	1,46E-03	3,96E-02	9,69E-02	2,35E-03	2,17E-02	1,44E-02
080c3_A_29	1,32E-02	2,65E-04	n.d.	n.d.	n.d.	1,44E-02	1,37E-02	2,28E-03	8,21E-02	9,50E-02	5,59E-03	1,46E-02	2,09E-02
080c3_A_3	1,89E-02	2,15E-03	n.d.	n.d.	n.d.	3,68E-03	1,70E-03	7,34E-04	5,45E-02	1,19E-01	1,28E-02	8,12E-03	1,27E-02
080c3_A_30	n.d.	n.d.	n.d.	n.d.	n.d.	1,49E-02	1,51E-02	1,47E-03	2,35E-02	5,88E-02	1,72E-03	2,32E-02	3,44E-02
080c3_A_31	5,06E-02	7,32E-04	n.d.	n.d.	n.d.	2,38E-02	3,56E-02	1,72E-03	7,24E-02	2,40E-01	1,10E-02	2,82E-02	4,65E-02
080c3_A_32	1,50E-02	5,63E-04	n.d.	n.d.	n.d.	1,47E-02	1,23E-02	1,55E-03	6,54E-02	1,18E-01	3,20E-03	2,60E-02	2,25E-02
080c3_A_33	n.d.	n.d.	n.d.	n.d.	n.d.	1,20E-02	1,21E-02	1,47E-03	n.d.	n.d.	n.d.	1,70E-02	1,94E-02
080c3_A_34	n.d.	n.d.	n.d.	n.d.	n.d.	1,03E-02	1,12E-02	2,73E-03	2,33E-02	9,97E-02	1,92E-03	1,74E-02	2,35E-02
080c3_A_35	1,02E-01	9,22E-04	1,45E-01	3,07E-01	3,25E-03	4,16E-02	4,99E-02	1,35E-03	1,91E-01	3,51E-01	4,79E-03	5,53E-02	3,38E-02
080c3_A_36	1,79E-02	1,09E-04	n.d.	n.d.	n.d.	1,44E-02	1,10E-02	5,78E-03	3,58E-02	9,51E-02	2,53E-03	2,25E-02	2,24E-02
080c3_A_37	1,60E-02	1,10E-04	n.d.	n.d.	n.d.	1,81E-02	1,48E-02	1,87E-03	6,20E-02	1,28E-01	3,52E-03	2,36E-02	2,13E-02
080c3_A_38	1,25E-01	8,84E-04	3,67E-02	2,77E-01	1,71E-03	2,89E-02	3,78E-02	1,75E-03	1,01E-01	1,87E-01	4,81E-03	4,32E-02	4,92E-02
080c3_A_39	n.d.	n.d.	n.d.	n.d.	n.d.	2,04E-02	1,32E-02	2,33E-03	4,04E-02	8,08E-02	3,38E-03	2,07E-02	1,52E-02
080c3_A_4	2,63E-02	1,25E-03	2,03E-02	1,05E-01	1,54E-03	5,92E-03	2,05E-02	6,29E-04	8,31E-02	1,80E-01	4,22E-03	1,36E-02	1,58E-02
080c3_A_40	n.d.	n.d.	n.d.	n.d.	n.d.	1,57E-02	6,55E-03	4,77E-03	4,97E-02	1,14E-01	2,94E-03	2,19E-02	1,98E-02
080c3_A_41	n.d.	n.d.	n.d.	n.d.	n.d.	3,21E-02	2,56E-02	2,09E-03	8,01E-02	1,52E-01	4,20E-03	3,76E-02	2,06E-02
080c3_A_42	n.d.	n.d.	n.d.	n.d.	n.d.	2,71E-02	2,18E-02	2,46E-03	1,12E-01	6,79E-02	5,75E-03	3,90E-02	2,60E-02
080c3_A_43	2,24E-01	1,39E-03	3,12E-01	6,94E-01	6,02E-03	6,34E-02	9,17E-02	2,05E-03	4,31E-01	4,99E-01	7,97E-03	6,20E-02	7,60E-02
080c3_A_44	2,53E-02	1,33E-03	2,12E-01	2,20E-01	2,16E-02	5,93E-02	2,78E-02	2,29E-03	3,15E-01	3,26E-01	9,03E-03	6,00E-02	2,77E-02
080c3_A_45	3,41E-01	2,62E-03	5,32E-01	7,91E-01	1,13E-02	7,33E-02	1,03E-01	3,27E-03	5,97E-01	6,94E-01	1,36E-02	7,12E-02	7,52E-02
080c3_A_5	2,11E-02	1,67E-03	n.d.	n.d.	n.d.	4,41E-03	7,33E-03	7,11E-04	5,82E-02	8,09E-02	4,69E-03	9,85E-03	6,67E-03
080c3_A_6	1,20E-02	4,33E-03	n.d.	n.d.	n.d.	5,26E-03	8,19E-03	8,23E-04	3,41E-02	5,57E-02	3,77E-03	1,23E-02	1,90E-02
080c3_A_7	2,09E-02	1,33E-03	n.d.	n.d.	n.d.	3,52E-03	9,66E-03	5,47E-04	1,37E-02	7,91E-02	1,65E-03	8,52E-05	1,50E-02
080c3_A_8	2,08E-02	9,01E-04	n.d.	n.d.	n.d.	4,27E-03	1,37E-02	4,55E-04	4,18E-02	9,89E-02	2,36E-03	9,90E-03	1,50E-02
080c3_A_9	1,21E-02	1,03E-03	n.d.	n.d.	n.d.	2,59E-03	1,25E-02	4,04E-04	3,32E-02	5,36E-02	2,46E-03	2,91E-03	1,30E-02
092c_A_1	2,29E-01	4,42E-03	2,23E+00	8,50E-01	2,04E-02	3,38E-01	1,52E-01	4,66E-03	n.d.	n.d.	n.d.	4,80E-01	3,11E-01
092c_A_10	3,71E+00	8,82E-04	5,74E+00	1,03E+01	4,08E-03	6,48E-01	1,15E+00	4,88E-03	n.d.	n.d.	n.d.	4,91E-01	8,26E-01
092c_A_11	7,14E-01	2,16E-03	3,15E+00	2,68E+00	2,41E-02	5,41E-01	3,57E-01	2,23E-03	n.d.	n.d.	n.d.	6,51E-01	5,78E-01
092c_A_12	6,63E-01	1,90E-03	2,62E+00	1,85E+00	8,63E-03	5,19E-01	3,87E-01	1,95E-03	n.d.	n.d.	n.d.	5,89E-01	4,67E-01
092c_A_13	5,55E-01	1,14E-03	1,75E+00	2,05E+00	5,13E-03	3,19E-01	3,78E-01	1,16E-03	n.d.	n.d.	n.d.	3,36E-01	3,77E-01
092c_A_2	2,64E-01	3,58E-03	7,46E-01	1,44E+00	6,34E-02	1,10E-01	1,49E-01	3,25E-03	n.d.	n.d.	n.d.	1,01E-01	2,03E-01
092c_A_4	1,82E+00	1,79E-02	3,54E+00	4,18E+00	7,11E-02	5,07E-01	5,60E-01	1,70E-02	n.d.	n.d.	n.d.	5,71E-01	7,09E-01
092c_A_5	2,69E+00	1,76E-02	6,09E+00	9,62E+00	8,16E-02	9,12E-01	1,07E+00	1,60E-02	n.d.	n.d.	n.d.	9,85E-01	1,02E+00
092c_A_6	2,89E+00	1,20E-02	7,51E+00	7,94E+00	2,38E-02	1,18E+00	1,31E+00	5,42E-03	n.d.	n.d.	n.d.	1,00E+00	1,11E+00
092c_A_9	2,42E-02	8,91E-03	1,06E-01	8,70E-02	7,56E-03	2,27E-02	1,17E-02	2,06E-03	n.d.	n.d.	n.d.	1,52E-02	1,93E-02
100bA_matrix_1	1,41E-02	6,44E-03	5,32E-02	3,77E-02	9,58E-03	1,14E-02	1,58E-02	2,24E-03	n.d.	n.d.	n.d.	4,35E-03	8,47E-03
100bA_matrix_10	9,11E-02	3,05E-03	1,08E-01	2,09E-01	9,36E-03	1,80E-02	3,78E-02	1,89E-03	n.d.	n.d.	n.d.	2,12E-02	1,88E-02
100bA_matrix_2	1,13E-02	6,43E-03	5,09E-02	3,87E-02	1,07E-02	1,08E-02	6,78E-03	2,26E-03	n.d.	n.d.	n.d.	9,97E-03	2,10E-02
100bA_matrix_3	8,16E-02	1,42E-03	1,83E-01	2,69E-01	5,07E-03	2,11E-02	4,06E-02	1,31E-03	n.d.	n.d.	n.d.	8,88E-03	1,42E-02
100bA_matrix_4	8,22E-02	1,87E-03	2,21E-01	2,37E-01	7,17E-03	3,01E-02	2,66E-02	1,73E-03	n.d.	n.d.	n.d.	2,78E-02	4,30E-02
100bA_matrix_5	7,56E-03	9,87E-03	5,27E-02	4,05E-02	2,68E-02	9,85E-03	5,56E-03	1,32E-02	n.d.	n.d.	n.d.	8,05E-03	1,01E-02
100bA_matrix_6	1,42E-02	1,25E-02	5,94E-02	6,73E-02	1,13E-02	8,62E-03	7,69E-03	9,14E-03	n.d.	n.d.	n.d.	1,01E-02	9,82E-03
100bA_matrix_7	1,55E-02	3,76E-03	7,07E-02	5,05E-02	2,31E-02	9,71E-03	7,85E-03	2,07E-03	n.d.	n.d.	n.d.	8,30E-03	1,51E-02
100bA_matrix_8	1,46E-02	8,13E-03	5,20E-02	1,59E-02	1,39E-02	5,54E-03	4,47E-03	6,09E-03	n.d.	n.d.	n.d.	1,04E-02	1,20E-02
100bA_matrix_9	3,33E+00	1,29E-03	6,20E+00	9,34E+00	6,04E-03	6,89E-01	1,03E+00	1,37E-03	n.d.	n.d.	n.d.	5,45E-01	7,93E-01

Analysis	Lu175_LOD (ppm)	Hf177_mean (ppm)	Hf177_2SD (ppm)	Hf177_LOD (ppm)	Ta181_mean (ppm)	Ta181_2SD (ppm)	Ta181_LOD (ppm)	W183_mean (ppm)	W183_2SD (ppm)	W183_LOD (ppm)	Au197_mean (ppm)	Au197_2SD (ppm)	Au197_LOD (ppm)
080c2_B_7	2,21E-03	1,26E+00	2,86E-01	1,13E-02	3,61E-01	9,79E-02	2,59E-03	9,54E-02	1,26E-01	4,97E-02	3,60E-03	1,53E-02	1,29E-02
080c2_B_8	2,08E-03	1,64E+00	6,94E-01	1,06E-02	3,42E-01	1,49E-01	7,80E-03	3,02E-01	1,73E-01	4,68E-02	2,07E-03	9,76E-03	1,10E-02
080c2_B_9	2,03E-03	1,49E+00	1,49E-01	1,06E-02	3,62E-01	6,92E-02	7,78E-03	5,08E-01	6,84E-01	3,80E-02	4,78E-03	1,66E-02	1,05E-02
080c3_A_1	9,26E-04	2,26E+00	2,06E-01	9,29E-03	7,14E-01	2,53E-01	5,66E-03	4,28E-02	3,73E-02	5,01E-02	3,79E-03	9,75E-03	1,43E-02
080c3_A_10	8,27E-04	1,17E+00	4,64E-01	6,05E-03	3,65E-01	1,41E-01	1,35E-03	8,54E-03	3,88E-02	3,25E-02	4,16E-03	1,58E-02	1,17E-02
080c3_A_11	1,21E-03	1,42E+00	2,96E-01	8,16E-03	3,25E-01	1,30E-01	4,56E-03	2,50E-02	3,88E-02	4,03E-02	2,60E-03	1,00E-02	1,78E-02
080c3_A_12	1,01E-03	6,78E-01	3,19E-01	8,38E-03	2,02E-01	6,09E-02	4,63E-03	1,36E-02	3,71E-02	2,31E-02	9,04E-04	9,02E-03	7,63E-02
080c3_A_13	5,44E-04	5,98E-01	2,47E-01	7,42E-03	1,92E-01	5,19E-02	4,61E-03	2,79E-02	7,26E-02	2,95E-02	2,42E-03	6,84E-03	1,76E-02
080c3_A_14	1,81E-03	1,33E+00	8,30E-01	1,09E-02	3,98E-01	2,04E-01	2,46E-03	5,44E-02	1,13E-01	4,78E-02	n.d.	n.d.	n.d.
080c3_A_15	1,15E-03	8,11E-01	4,38E-01	9,99E-03	2,71E-01	7,82E-02	2,26E-03	< Det. Lim	3,08E-02	1,65E-02	1,87E-03	1,34E-02	1,65E-02
080c3_A_16	1,26E-03	1,03E+00	4,90E-01	9,08E-03	3,35E-01	2,01E-01	6,07E-03	9,94E-03	7,65E-02	4,13E-02	8,24E-03	1,86E-02	1,00E-02
080c3_A_17	1,65E-03	7,82E-01	4,90E-01	1,15E-02	1,81E-01	5,60E-02	6,98E-03	< Det. Lim	2,72E-02	2,95E-02	8,70E-03	2,98E-02	1,14E-02
080c3_A_18	1,16E-03	9,02E-01	4,35E-01	7,87E-03	2,24E-01	1,44E-01	4,80E-03	2,47E-03	2,03E-02	1,01E-02	2,02E-03	1,21E-02	9,33E-03
080c3_A_19	1,50E-03	8,08E-01	1,79E-01	2,34E-02	2,04E-01	9,09E-02	2,28E-03	1,92E-02	5,86E-02	2,15E-02	5,42E-03	1,18E-03	1,09E-02
080c3_A_2	1,63E-04	8,30E-01	3,16E-01	8,12E-03	2,25E-01	1,37E-01	1,79E-03	4,64E-02	3,77E-02	3,40E-02	5,98E-03	1,27E-02	1,13E-02
080c3_A_20	1,18E-03	1,13E+00	3,91E-01	7,33E-03	4,10E-01	1,17E-01	1,66E-03	2,36E-03	3,08E-02	4,05E-02	1,53E-03	1,25E-02	1,39E-02
080c3_A_21	1,78E-03	7,92E-01	4,86E-01	1,08E-02	2,32E-01	1,07E-01	7,96E-03	2,37E-02	8,64E-02	4,13E-02	7,09E-03	1,82E-02	1,39E-02
080c3_A_22	1,49E-03	1,00E+00	7,14E-01	8,36E-03	3,25E-01	2,21E-01	1,89E-03	7,43E-03	5,96E-02	3,80E-02	2,98E-03	3,15E-02	1,45E-02
080c3_A_23	3,03E-03	1,13E+00	4,41E-01	7,49E-03	2,48E-01	1,59E-01	1,65E-03	1,68E-02	7,03E-02	3,03E-02	3,84E-03	1,86E-02	1,18E-02
080c3_A_24	1,80E-03	4,79E-01	2,88E-01	1,24E-02	1,52E-01	1,86E-01	2,92E-03	< Det. Lim	4,11E-02	6,11E-02	3,44E-03	2,24E-02	1,08E-02
080c3_A_25	1,69E-03	2,17E+00	1,50E+00	3,09E-02	9,25E-01	4,45E-01	2,38E-03	1,71E-02	4,16E-02	4,45E-02	6,93E-03	4,01E-02	1,23E-02
080c3_A_26	1,51E-03	1,58E+00	7,91E-01	2,67E-02	4,46E-01	2,83E-01	2,07E-03	1,54E-02	6,75E-02	3,84E-02	5,54E-03	3,03E-02	1,03E-02
080c3_A_27	1,75E-03	1,88E+00	7,56E-01	9,50E-03	6,27E-01	2,97E-01	6,71E-03	9,11E-03	6,36E-02	8,39E-02	3,92E-03	1,92E-02	7,02E-03
080c3_A_28	1,36E-03	1,47E+00	5,48E-01	7,62E-03	4,29E-01	2,74E-01	6,14E-03	2,08E-02	5,51E-02	3,73E-02	2,52E-02	7,51E-02	1,01E-02
080c3_A_29	2,21E-03	1,74E+00	4,78E-01	1,23E-02	6,21E-01	1,19E-01	1,02E-02	5,27E-04	4,01E-02	1,20E-02	7,71E-04	1,93E-02	7,18E-03
080c3_A_3	9,74E-04	8,10E-01	2,21E-01	1,09E-02	2,02E-01	8,59E-02	2,41E-03	2,20E-02	3,45E-02	7,18E-02	7,28E-03	1,15E-02	8,71E-03
080c3_A_30	1,35E-03	1,54E+00	7,78E-01	7,54E-03	4,24E-01	2,07E-01	5,28E-03	1,35E-02	4,16E-02	6,29E-03	4,31E-03	1,36E-02	8,36E-03
080c3_A_31	1,71E-03	2,32E+00	1,42E+00	8,95E-03	8,01E-01	5,17E-01	1,99E-03	6,18E-02	1,53E-01	8,66E-03	< Det. Lim	1,41E-02	1,89E-02
080c3_A_32	1,40E-03	2,64E+00	9,01E-01	7,55E-03	1,31E+00	2,37E-01	1,72E-03	4,60E-02	7,27E-02	2,63E-02	< Det. Lim	1,15E-02	2,06E-02
080c3_A_33	1,36E-03	1,10E+00	7,61E-01	6,90E-03	3,71E-01	2,47E-01	4,81E-03	2,98E-03	4,25E-02	2,55E-02	< Det. Lim	1,89E-02	1,45E-02
080c3_A_34	1,94E-03	1,11E+00	5,41E-01	9,15E-03	3,04E-01	1,84E-01	2,10E-03	2,21E-02	6,39E-02	3,54E-02	2,10E-02	9,44E-02	1,44E-02
080c3_A_35	4,50E-03	2,40E+00	1,22E+00	7,96E-03	7,20E-01	4,22E-01	1,82E-03	5,23E-02	7,51E-02	8,15E-03	1,33E-04	1,13E-02	5,52E-04
080c3_A_36	1,62E-03	1,22E+00	1,03E+00	8,25E-03	3,29E-01	2,62E-01	1,90E-03	1,51E-02	4,50E-02	1,83E-02	< Det. Lim	5,32E-03	8,41E-02
080c3_A_37	4,74E-03	1,33E+00	3,89E-01	8,23E-03	3,11E-01	8,76E-02	1,92E-03	1,90E-03	2,86E-02	1,93E-02	n.d.	n.d.	n.d.
080c3_A_38	1,77E-03	1,12E+00	5,22E-01	9,17E-03	2,85E-01	1,01E-01	2,14E-03	1,94E-02	4,42E-02	7,88E-03	< Det. Lim	5,19E-03	2,07E-01
080c3_A_39	6,04E-03	1,29E+00	2,71E-01	1,03E-02	3,69E-01	6,20E-02	6,32E-03	3,57E-02	8,73E-02	2,85E-02	6,56E-03	2,32E-02	9,59E-03
080c3_A_4	1,04E-03	1,02E+00	3,69E-01	8,15E-03	3,13E-01	7,15E-02	1,80E-03	1,84E-02	4,97E-02	3,35E-02	3,45E-03	1,04E-02	1,29E-02
080c3_A_40	1,50E-03	1,39E+00	1,22E+00	7,41E-03	3,36E-01	2,29E-01	1,73E-03	7,38E-03	3,37E-02	2,20E-02	n.d.	n.d.	n.d.
080c3_A_41	2,05E-03	2,36E+00	8,22E-01	9,82E-03	7,32E-01	2,10E-01	6,05E-03	2,61E-02	3,80E-02	2,00E-02	< Det. Lim	1,75E-02	2,39E-02
080c3_A_42	2,48E-03	2,67E+00	2,14E+00	1,19E-02	7,80E-01	6,55E-01	2,73E-03	9,13E-03	6,13E-02	2,61E-02	2,96E-03	2,08E-02	7,55E-03
080c3_A_43	2,34E-03	2,31E+00	8,11E-01	1,16E-02	6,34E-01	3,13E-01	7,00E-03	1,69E-02	5,41E-02	2,98E-02	4,71E-03	1,39E-02	9,77E-03
080c3_A_44	2,63E-03	3,62E+00	1,07E+00	1,34E-02	1,09E+00	3,71E-01	3,07E-03	6,15E-02	5,35E-02	3,58E-02	n.d.	n.d.	n.d.
080c3_A_45	3,78E-03	2,41E+00	4,90E-01	1,87E-02	4,92E-01	1,68E-01	9,15E-03	6,51E-03	7,52E-02	1,89E-02	n.d.	n.d.	n.d.
080c3_A_5	1,21E-03	1,13E+00	8,97E-01	1,06E-02	2,78E-01	1,38E-01	2,33E-03	< Det. Lim	1,80E-03	2,30E-02	7,67E-03	1,44E-02	1,27E-02
080c3_A_6	1,42E-03	1,49E+00	8,11E-01	1,14E-02	3,59E-01	1,68E-01	5,81E-03	3,22E-02	5,70E-02	3,66E-02	7,04E-03	8,39E-03	1,42E-02
080c3_A_7	2,51E-05	7,50E-01	2,24E-01	8,96E-03	1,62E-01	5,91E-02	8,97E-03	1,10E-02	4,17E-02	8,31E-03	2,42E-03	1,64E-02	1,88E-02
080c3_A_8	7,58E-04	1,22E+00	2,70E-01	6,16E-03	3,74E-01	1,07E-01	5,56E-03	3,97E-02	5,77E-02	2,47E-02	< Det. Lim	5,23E-03	5,08E-03
080c3_A_9	5,08E-04	1,04E+00	3,50E-01	7,20E-03	1,87E-01	1,29E-01	1,62E-03	1,30E-02	4,46E-02	4,39E-02	1,50E-03	1,11E-02	7,25E-02
092c_A_1	5,23E-03	n.d.	n.d.	n.d.	3,66E+00	1,45E+00	6,75E-03	6,84E-01	7,69E-01	1,34E-01	3,89E-02	7,89E-02	8,14E-02
092c_A_10	1,10E-03	n.d.	n.d.	n.d.	2,94E+00	8,21E-01	1,25E-03	8,32E-02	1,26E-01	3,00E-02	7,46E-03	1,27E-02	2,63E-02
092c_A_11	2,65E-03	n.d.	n.d.	n.d.	3,22E+00	9,69E-01	3,22E-03	9,92E-01	1,11E+00	5,06E-02	7,89E-03	1,56E-02	2,93E-02
092c_A_12	2,30E-03	n.d.	n.d.	n.d.	3,54E+00	1,37E+00	2,88E-03	8,18E-01	7,10E-01	2,95E-02	9,62E-03	4,66E-03	2,25E-02
092c_A_13	1,36E-03	n.d.	n.d.	n.d.	3,47E+00	1,04E+00	5,05E-03	4,69E-01	6,36E-01	2,88E-02	7,25E-03	1,69E-02	2,45E-02
092c_A_2	2,76E-03	n.d.	n.d.	n.d.	3,25E+00	8,57E-01	2,99E-03	1,14E+00	5,63E+00	1,72E-01	3,10E-02	7,22E-02	6,25E-02
092c_A_4	1,76E-02	n.d.	n.d.	n.d.	4,88E+00	4,71E+00	5,08E-02	1,27E+00	2,81E+00	4,71E-01	8,97E-02	2,18E-01	9,06E-02
092c_A_5	1,61E-02	n.d.	n.d.	n.d.	5,89E+00	7,18E+00	2,23E-02	2,35E+00	4,67E+00	4,88E-01	1,03E-01	2,02E-01	1,92E-01
092c_A_6	6,22E-03	n.d.	n.d.	n.d.	2,69E+00	1,45E+00	6,39E-03	4,99E-01	9,32E-01	9,97E-02	3,57E-02	7,91E-02	7,64E-02
092c_A_9	1,09E-03	n.d.	n.d.	n.d.	2,81E+00	8,32E-01	1,56E-03	1,15E-01	1,11E-01	1,75E-02	1,01E-02	1,25E-02	2,13E-02
100bA_matrix_1	1,01E-03	n.d.	n.d.	n.d.	4,27E+00	7,40E-01	6,60E-03	1,60E-01	1,70E-01	4,14E-02	8,45E-03	1,54E-02	1,65E-02
100bA_matrix_10	1,98E-03	n.d.	n.d.	n.d.	4,12E+00	6,98E-01	2,01E-03	1,35E-01	1,11E-01	2,52E-02	5,05E-03	1,01E-02	3,09E-02
100bA_matrix_2	9,99E-04	n.d.	n.d.	n.d.	4,53E+00	1,34E+00	4,28E-03	1,29E-01	1,77E-01	3,76E-02	7,69E-03	1,27E-02	2,10E-02
100bA_matrix_3	1,19E-03	n.d.	n.d.	n.d.	4,23E+00	9,09E-01	1,36E-03	8,12E-02	1,19E-01	2,78E-02	n.d.	n.d.	n.d.
100bA_matrix_4	1,73E-03	n.d.	n.d.	n.d.	3,85E+00	8,79E-01	5,52E-03	1,45E-01	1,78E-01	3,19E-02	n.d.	n.d.	n.d.
100bA_matrix_5	3,04E-03	n.d.	n.d.	n.d.	3,86E+00	8,74E-01	1,12E-02	1,79E-01	3,15E-01	5,60E-02	1,21E-02	1,70E-02	2,20E-02
100bA_matrix_6	1,60E-03	n.d.	n.d.	n.d.	4,11E+00	1,44E+00	5,49E-03	4,28E+01	2,41E+02	4,21E-02	3,97E-03	1,82E-02	3,27E-02
100bA_matrix_7	1,64E-03	n.d.	n.d.	n.d.	4,49E+00	1,41E+00	1,53E-03	1,51E-01	1,59E-01	3,08E-02	8,30E-03	1,60E-02	1,45E-02
100bA_matrix_8	2,10E-03	n.d.	n.d.	n.d.	4,20E+00	1,44E+00	4,77E-03	1,67E-01	2,30E-01	2,45E-02	8,56E-03	1,11E-02	1,49E-02
100bA_matrix_9	1,62E-03	n.d.	n.d.	n.d.	4,53E+00	1,18E+00	4,98E-03	1,59E-01	1,25E-01	3,68E-02	1,08E-02	2,43E-02	1,54E-02

Analysis	Pb208_mean (ppm)	Pb208_2SD (ppm)	Pb208_LOD (ppm)	Bi209_mean (ppm)	Bi209_2SD (ppm)	Bi209_LOD (ppm)	Th232_mean (ppm)	Th232_2SD (ppm)	Th232_LOD (ppm)	U238_mean (ppm)	U238_2SD (ppm)	U238_LOD (ppm)
080c2_B_7	1,36E+01	4,03E+00	3,53E-03	1,37E-02	1,75E-02	4,97E-03	1,87E-01	5,44E-02	2,12E-03	2,53E-01	8,40E-02	1,33E-03
080c2_B_8	1,94E+01	6,03E+00	7,57E-03	2,12E-02	1,51E-02	4,83E-03	2,91E-01	7,95E-02	2,01E-03	3,74E-01	8,58E-02	1,26E-03
080c2_B_9	1,77E+01	2,74E+00	3,29E-03	2,87E-02	1,83E-02	1,41E-03	2,45E-01	7,01E-02	1,99E-03	3,45E-01	1,26E-01	1,25E-03
080c3_A_1	5,57E+00	2,39E+00	2,94E-03	1,59E-02	1,09E-02	3,72E-03	3,82E-02	4,56E-02	1,38E-03	6,61E-02	6,37E-02	1,06E-03
080c3_A_10	3,97E+00	3,51E+00	5,21E-03	1,10E-02	1,07E-02	4,31E-03	2,43E-01	6,65E-01	1,11E-03	5,19E-02	1,26E-01	6,46E-04
080c3_A_11	8,16E+00	9,67E+00	2,53E-03	3,67E-02	3,57E-02	4,90E-03	4,38E-01	8,65E-01	1,47E-03	1,92E-01	3,65E-01	9,32E-04
080c3_A_12	5,07E+00	7,89E+00	1,40E-02	1,58E-02	1,21E-02	2,89E-03	1,26E-02	3,39E-02	7,98E-04	1,89E-02	1,39E-02	7,27E-04
080c3_A_13	2,08E+00	1,57E+00	7,21E-03	7,99E-03	6,74E-03	7,82E-03	n.d.	n.d.	n.d.	4,92E-03	3,05E-02	3,10E-04
080c3_A_14	1,21E+01	1,84E+01	7,74E-03	2,00E-02	9,83E-03	6,16E-03	6,52E-01	4,12E-01	2,06E-03	2,56E-01	2,32E-01	1,34E-03
080c3_A_15	3,25E+00	1,91E+00	1,20E-02	1,21E-02	1,63E-02	5,24E-03	n.d.	n.d.	n.d.	4,54E-03	1,61E-02	3,83E-04
080c3_A_16	4,57E+00	2,90E+00	9,76E-03	2,45E-01	6,30E-01	5,24E-03	8,07E-03	6,30E-02	5,50E-04	9,86E-03	2,87E-02	5,21E-04
080c3_A_17	3,55E+00	2,23E+00	1,10E-02	1,27E-02	1,22E-02	7,69E-03	n.d.	n.d.	n.d.	1,09E-02	1,59E-02	7,21E-04
080c3_A_18	2,07E+00	7,72E+00	2,29E-03	6,50E-03	8,61E-03	5,35E-03	n.d.	n.d.	n.d.	1,04E-02	1,80E-02	5,30E-04
080c3_A_19	1,54E+00	9,33E-01	7,24E-03	9,37E-03	8,28E-03	5,26E-03	n.d.	n.d.	n.d.	5,16E-03	1,36E-02	4,93E-04
080c3_A_2	9,39E-01	2,49E+00	7,53E-03	5,26E-03	6,94E-03	1,27E-02	n.d.	n.d.	n.d.	5,60E-03	1,18E-02	4,25E-04
080c3_A_20	4,09E+00	3,04E+00	9,60E-03	7,22E-03	5,68E-03	1,55E-03	1,66E-02	7,54E-02	8,09E-04	2,04E-02	3,50E-02	6,44E-04
080c3_A_21	1,27E+00	9,27E-01	1,43E-02	8,82E-03	5,81E-03	7,59E-03	n.d.	n.d.	n.d.	7,25E-03	1,47E-02	5,50E-04
080c3_A_22	3,27E+00	1,34E+00	2,66E-03	1,65E-02	1,80E-02	5,48E-03	1,13E-01	1,77E-01	1,46E-03	4,47E-02	8,39E-02	8,43E-04
080c3_A_23	3,04E+00	3,57E+00	2,51E-03	9,91E-03	1,16E-02	8,67E-03	7,74E-03	5,92E-02	6,72E-04	1,91E-02	3,33E-02	6,63E-04
080c3_A_24	2,18E+00	1,89E+00	3,80E-03	1,07E-02	1,41E-02	9,52E-03	1,06E-02	2,98E-02	8,70E-04	n.d.	n.d.	n.d.
080c3_A_25	2,42E+00	2,37E+00	8,48E-03	1,01E-02	1,28E-02	9,10E-03	n.d.	n.d.	n.d.	2,30E-02	3,59E-02	2,64E-03
080c3_A_26	4,54E+00	4,22E+00	8,69E-03	1,17E-02	1,00E-02	7,03E-03	3,23E-02	7,73E-02	1,22E-03	2,43E-02	3,69E-02	7,86E-04
080c3_A_27	7,42E-01	1,24E+00	8,46E-03	5,85E-03	7,72E-03	1,45E-02	n.d.	n.d.	n.d.	3,06E-02	3,28E-02	9,48E-04
080c3_A_28	2,60E+00	4,56E+00	1,17E-02	7,70E-03	1,42E-02	8,46E-03	6,42E-04	3,50E-02	7,71E-05	2,22E-02	3,81E-02	6,90E-04
080c3_A_29	4,59E+00	4,11E+00	9,08E-03	1,58E-02	1,99E-02	5,04E-03	1,35E-02	2,28E-02	1,25E-03	2,38E-02	4,02E-02	1,12E-03
080c3_A_3	8,26E-01	2,68E+00	7,23E-03	5,59E-03	1,19E-02	8,09E-03	n.d.	n.d.	n.d.	2,25E-02	3,30E-02	1,07E-03
080c3_A_30	1,26E+00	1,03E+00	1,08E-02	5,04E-03	5,39E-03	1,23E-02	n.d.	n.d.	n.d.	1,54E-02	2,25E-02	5,87E-04
080c3_A_31	1,02E+01	1,98E+01	7,90E-03	2,68E-01	9,39E-01	4,81E-03	2,00E-02	6,10E-02	1,23E-03	3,95E-02	3,59E-02	9,18E-04
080c3_A_32	4,17E+00	1,14E+00	2,39E-03	7,85E-03	1,16E-02	7,55E-03	6,48E-02	1,00E-01	1,26E-03	5,76E-02	5,56E-02	8,13E-04
080c3_A_33	1,11E+00	1,28E+00	2,15E-03	5,76E-03	6,42E-03	7,97E-03	n.d.	n.d.	n.d.	9,82E-03	2,49E-02	4,44E-04
080c3_A_34	3,91E+00	2,82E+00	3,01E-03	1,07E-02	1,08E-02	8,26E-03	4,42E-02	9,81E-02	1,42E-03	2,83E-02	5,69E-02	8,20E-04
080c3_A_35	6,36E+00	3,82E+00	2,47E-03	2,47E-01	1,22E+00	6,24E-03	3,80E-01	5,26E-01	1,49E-03	1,39E-01	1,21E-01	9,36E-04
080c3_A_36	2,06E+00	1,38E+00	7,00E-03	6,09E-03	5,79E-03	8,84E-03	7,86E-03	2,56E-02	7,56E-04	2,33E-02	3,06E-02	7,90E-04
080c3_A_37	4,12E+00	2,75E+00	2,55E-03	6,52E-03	3,13E-03	7,80E-03	8,57E-03	1,91E-02	2,85E-03	3,77E-02	1,86E-02	8,38E-04
080c3_A_38	2,58E+00	3,45E+00	2,89E-03	1,03E-02	1,19E-02	6,20E-03	9,01E-02	2,89E-01	1,69E-03	2,94E-02	7,25E-02	9,02E-04
080c3_A_39	6,33E+00	4,34E+00	8,49E-03	1,39E-02	5,66E-03	8,10E-03	4,33E-02	7,84E-02	1,65E-03	3,92E-02	3,59E-02	1,04E-03
080c3_A_4	4,23E-01	7,74E-01	1,93E-03	3,49E-03	6,83E-03	4,33E-02	n.d.	n.d.	n.d.	1,96E-02	6,11E-03	7,16E-04
080c3_A_40	4,85E-01	8,10E-01	9,56E-03	3,40E-03	4,55E-03	9,81E-03	n.d.	n.d.	n.d.	2,18E-02	2,63E-02	1,93E-03
080c3_A_41	6,05E+00	2,78E+00	1,16E-02	1,31E-02	1,06E-02	6,51E-03	9,11E-02	1,62E-01	1,87E-03	9,49E-02	7,38E-02	1,12E-03
080c3_A_42	4,27E+00	6,33E+00	1,08E-02	9,06E-03	1,49E-02	8,03E-03	2,64E-02	5,91E-02	1,76E-03	3,42E-02	2,97E-02	1,15E-03
080c3_A_43	2,95E+00	4,22E+00	1,44E-02	7,74E-03	1,85E-02	7,52E-03	2,58E-01	4,96E-01	2,17E-03	1,15E-01	2,74E-01	1,33E-03
080c3_A_44	1,22E+01	7,89E+00	3,96E-03	2,26E-02	2,00E-02	7,13E-03	1,24E-01	1,22E-01	2,44E-03	2,51E-01	9,29E-02	1,54E-03
080c3_A_45	1,05E+01	7,57E+00	1,25E-02	3,18E-02	3,00E-02	7,26E-03	9,01E-02	1,16E-01	3,37E-03	1,25E-01	8,34E-02	2,12E-03
080c3_A_5	4,01E-01	3,93E-01	8,51E-03	n.d.	n.d.	n.d.	n.d.	n.d.	n.d.	2,08E-02	9,22E-03	3,39E-03
080c3_A_6	4,08E+00	2,23E+00	3,57E-03	1,23E-02	1,24E-02	2,15E-02	1,56E-02	2,58E-02	1,04E-03	1,83E-02	3,02E-02	9,60E-04
080c3_A_7	2,89E+00	2,80E+00	7,45E-03	8,38E-03	1,27E-02	4,79E-03	n.d.	n.d.	n.d.	5,09E-03	8,52E-03	3,98E-04
080c3_A_8	1,62E+00	2,22E+00	9,14E-03	5,96E-03	6,51E-03	5,75E-03	n.d.	n.d.	n.d.	1,35E-02	1,87E-02	4,89E-04
080c3_A_9	3,12E+00	4,30E+00	2,16E-03	9,59E-03	1,18E-02	4,24E-03	n.d.	n.d.	n.d.	6,24E-03	1,51E-02	3,77E-04
092c_A_1	1,40E+03	5,74E+02	1,97E-02	1,37E+00	8,36E-01	9,43E-03	3,33E+00	2,66E+00	6,06E-03	6,70E+00	2,70E+00	3,10E-03
092c_A_10	1,60E+00	1,47E+00	1,59E-03	7,04E-03	6,60E-03	7,78E-03	5,84E+00	1,04E+01	1,12E-03	5,19E-01	9,73E-01	6,76E-04
092c_A_11	1,38E+03	1,09E+03	9,65E-03	4,52E-01	3,40E-01	6,85E-03	4,99E-01	3,45E-01	2,73E-03	6,47E+00	6,48E+00	1,67E-03
092c_A_12	1,22E+03	9,20E+02	3,78E-03	3,38E-01	2,56E-01	1,48E-03	3,01E-01	2,62E-01	2,41E-03	5,75E+00	4,85E+00	1,45E-03
092c_A_13	6,69E+02	8,45E+02	1,38E-02	1,84E-01	2,44E-01	8,78E-04	1,44E-01	1,16E-01	1,49E-03	3,35E+00	5,04E+00	8,53E-04
092c_A_2	2,32E+01	6,61E+01	6,17E-03	3,51E-02	4,12E-02	2,69E-03	2,94E+00	4,94E+00	3,19E-03	7,24E-01	1,15E+00	1,86E-03
092c_A_4	4,39E+02	3,35E+02	2,73E-02	2,62E-01	1,80E-01	3,71E-02	1,33E+01	2,09E+01	2,08E-02	5,79E+00	7,10E+00	1,17E-02
092c_A_5	9,26E+02	4,83E+02	2,11E-02	4,07E-01	4,76E-01	5,95E-02	1,39E+01	2,04E+01	2,00E-02	1,03E+01	9,67E+00	1,01E-02
092c_A_6	1,90E+03	1,23E+03	3,38E-02	1,59E+00	1,41E+00	1,16E-02	2,82E+00	2,48E+00	5,92E-03	8,66E+00	5,84E+00	3,27E-03
092c_A_9	3,39E+00	4,43E+00	1,18E-02	7,72E-03	1,07E-02	1,42E-02	3,83E-01	2,61E-01	1,37E-03	1,01E-01	7,20E-02	7,19E-04
100bA_matrix_1	9,63E-02	2,08E-01	5,28E-03	n.d.	n.d.	n.d.	1,04E-02	7,11E-03	4,07E-03	2,51E-03	1,23E-02	1,27E-04
100bA_matrix_10	4,08E+00	3,45E+00	2,71E-03	7,57E-02	9,94E-02	7,62E-03	2,28E-01	2,17E-01	1,80E-03	1,95E-02	1,96E-02	6,51E-04
100bA_matrix_2	2,36E-01	1,25E+00	1,14E-03	n.d.	n.d.	n.d.	1,04E-02	7,95E-03	5,52E-03	4,58E-03	7,32E-03	1,63E-04
100bA_matrix_3	3,39E-03	1,32E-01	3,08E-04	n.d.	n.d.	n.d.	5,85E-02	9,29E-02	1,31E-03	2,36E-02	4,77E-02	4,61E-04
100bA_matrix_4	3,78E-01	1,93E-01	6,57E-03	6,58E-03	1,43E-02	5,54E-03	1,97E-01	2,07E-01	1,73E-03	7,56E-02	6,61E-02	9,10E-04
100bA_matrix_5	1,65E+00	1,32E+00	9,49E-03	8,78E-03	1,70E-02	1,12E-02	4,66E-02	2,93E-02	3,46E-03	6,21E-03	1,83E-02	5,49E-04
100bA_matrix_6	2,01E+00	4,22E+00	7,07E-03	1,14E-02	1,50E-02	6,38E-03	4,07E-02	4,83E-02	1,84E-03	8,85E-03	1,50E-02	3,51E-04
100bA_matrix_7	2,26E+00	4,01E+00	6,36E-03	5,86E-02	6,02E-02	3,99E-03	1,37E-01	1,32E-01	1,34E-03	2,22E-02	2,34E-02	5,14E-04
100bA_matrix_8	3,30E-01	5,21E-01	7,59E-03	3,43E-03	7,52E-03	3,38E-02	1,28E-02	1,61E-02	4,74E-03	4,33E-03	2,80E-02	2,78E-04
100bA_matrix_9	3,21E+00	2,77E+00	8,42E-03	1,00E-01	1,38E-01	1,12E-03	2,10E+00	3,38E+00	1,67E-03	5,38E-01	7,30E-01	9,96E-04

Standards LA-ICP-MS on magnetite

AVERAGE	Li7	Be9	Na23	Mg25	Al27	Si29	P31	K39	Ca44	Sc45	Ti47	V51	Cr53	Mn55	Fe57	Co59	Ni60	Cu63	Zn66
	(ppm)	(ppm)	(ppm)	(ppm)	(ppm)	(ppm)	(ppm)	(ppm)	(ppm)	(ppm)	(ppm)	(ppm)	(ppm)	(ppm)	(ppm)	(ppm)	(ppm)	(ppm)	(ppm)
BCR-2	8,87E+00	2,32E+00	2,40E+04	2,13E+04	7,02E+04	2,57E+05	1,60E+03	1,47E+04	4,97E+04	3,34E+01	1,36E+04	4,20E+02	2,17E+01	1,56E+03	9,64E+04	3,69E+01	1,18E+01	2,04E+01	1,22E+02
BHVO-2	4,53E+00	1,23E+00	1,75E+04	4,34E+04	7,34E+04	2,33E+05	1,29E+03	4,45E+03	8,37E+04	3,30E+01	1,69E+04	3,15E+02	2,97E+02	1,37E+03	8,78E+04	4,55E+01	1,22E+02	1,29E+02	1,04E+02
BIR-1	3,01E+00	1,54E-01	1,42E+04	5,77E+04	8,31E+04	2,18E+05	1,04E+02	2,13E+02	9,51E+04	4,34E+01	6,37E+03	3,24E+02	3,99E+02	1,43E+03	8,08E+04	5,27E+01	1,78E+02	1,22E+02	8,04E+01
2SD																			
BCR-2	2,17E-01	1,12E-01	4,40E+02	2,73E+02	1,09E+03	2,63E+03	9,21E+01	2,36E+02	9,63E+02	7,31E-01	2,44E+02	5,89E+00	8,68E-01	2,66E+01	0,00E+00	6,92E-01	2,73E-01	3,95E-01	2,25E+00
BHVO-2	1,20E-01	7,51E-02	3,01E+02	5,98E+02	1,25E+03	4,67E+03	1,64E+02	9,41E+01	1,47E+03	8,64E-01	2,82E+02	4,22E+00	4,99E+00	1,99E+01	0,00E+00	8,00E-01	2,24E+00	2,65E+00	2,28E+00
BIR-1	1,66E-01	3,35E-02	3,74E+02	1,51E+03	1,88E+03	4,23E+03	4,11E+01	2,35E+01	1,91E+03	8,28E-01	1,31E+02	5,90E+00	9,39E+00	3,08E+01	3,98E-11	1,50E+00	4,45E+00	3,09E+00	1,36E+00

Precision	Li	Be	Na	Mg	Al	Si	P	K	Ca	Sc	Ti	V	Cr	Mn	Fe	Co	Ni	Cu	Zn
BCR-2	0,98	0,95	0,98	0,99	0,98	0,99	0,94	0,98	0,98	0,98	0,98	0,99	0,96	0,98	1,00	0,98	0,98	0,98	0,98
BHVO-1	0,97	0,94	0,98	0,99	0,98	0,98	0,87	0,98	0,98	0,97	0,98	0,99	0,98	0,99	1,00	0,98	0,98	0,98	0,98
BHVO-2	0,95	0,78	0,97	0,97	0,98	0,98	0,61	0,89	0,98	0,98	0,98	0,98	0,98	0,98	1,00	0,97	0,97	0,97	0,98
ACCURACY	Li	Be	Na	Mg	Al	Si	P	K	Ca	Sc	Ti	V	Cr	Mn	Fe	Co	Ni	Cu	Zn
BCR-2	0,97	1,07	1,04	0,98	0,98	1,02	1,02	1,00	0,98	1,00	1,00	1,01	1,37	1,02	1,00	0,99	0,94	1,04	0,94
BHVO-2	1,01	1,14	1,06	0,99	1,03	1,00	1,10	1,05	1,03	1,04	1,03	0,99	1,03	1,04	1,01	1,01	1,02	1,00	1,00
BIR-1	0,94	1,51	1,04	0,99	1,01	0,97	0,79	0,88	1,00	1,00	1,11	1,01	1,02	1,07	1,01	1,01	1,05	1,01	1,14

STD VALUES	Li	Be	Na	Mg	Al	Si	P	K	Ca	Sc	Ti	V	Cr	Mn	Fe	Co	Ni	Cu	Zn
BCR-2*	9,13E+00	2,17E+00	2,31E+04	2,17E+04	7,13E+04	2,52E+05	1,57E+03	1,47E+04	5,08E+04	3,35E+01	1,36E+04	4,18E+02	1,59E+01	1,52E+03	9,63E+04	3,73E+01	1,26E+01	1,97E+01	1,30E+02
BHVO-2*	4,50E+00	1,08E+00	1,65E+04	4,38E+04	7,11E+04	2,32E+05	1,17E+03	4,26E+03	8,15E+04	3,18E+01	1,64E+04	3,18E+02	2,87E+02	1,31E+03	8,67E+04	4,49E+01	1,20E+02	1,29E+02	1,04E+02
BIR-1*	3,20E+00	1,02E-01	1,36E+04	5,84E+04	8,21E+04	2,23E+05	1,31E+02	2,41E+02	9,50E+04	4,32E+01	5,75E+03	3,21E+02	3,93E+02	1,34E+03	7,97E+04	5,22E+01	1,69E+02	1,21E+02	7,04E+01

AVERAGE	Ga69	Ge74	As75	Rb85	Sr88	Y89	Zr90	Nb93	Mo95	Ag107	Cd111	In115	Sn118	Sb121	Cs133	Ba137	La139	Ce140	Pr141
	(ppm)	(ppm)	(ppm)	(ppm)	(ppm)	(ppm)	(ppm)	(ppm)	(ppm)	(ppm)	(ppm)	(ppm)	(ppm)	(ppm)	(ppm)	(ppm)	(ppm)	(ppm)	(ppm)
BCR-2	2,57E+01	1,53E+00	3,02E+00	4,63E+01	3,35E+02	3,47E+01	1,83E+02	1,23E+01	2,56E+02	1,18E+00	2,09E-01	1,02E-01	2,50E+00	2,95E-01	1,14E+00	6,71E+02	2,44E+01	5,27E+01	6,63E+00
BHVO-2	1,83E+01	1,66E+00	2,78E+00	9,31E+00	4,08E+02	2,63E+01	1,72E+02	1,88E+01	4,08E+00	3,95E-01	1,10E-01	1,10E-01	2,65E+00	1,60E-01	1,06E-01	1,31E+02	1,54E+01	3,82E+01	5,44E+00
BIR-1	1,70E+01	1,04E+00	1,73E+00	3,39E-01	1,10E+02	1,46E+01	1,44E+01	5,06E-01	4,80E-02	1,68E-01	1,14E-01	8,84E-02	2,51E+00	5,86E-01	4,71E-03	9,60E+00	7,11E-01	2,04E+00	3,86E-01
2SD																			
BCR-2	6,14E-01	8,49E-02	2,28E-01	9,60E-01	6,59E+00	6,46E-01	3,91E+00	2,73E-01	1,33E+01	4,04E-02	2,09E-02	4,06E-03	6,09E-02	3,03E-02	3,02E-02	1,29E+01	4,58E-01	1,09E+00	1,17E-01
BHVO-2	3,71E-01	1,70E-01	1,22E-01	2,28E-01	7,06E+00	5,19E-01	3,01E+00	3,70E-01	1,23E-01	2,16E-02	1,78E-02	4,32E-03	6,46E-02	2,50E-02	7,96E-03	2,23E+00	3,51E-01	7,18E-01	1,02E-01
BIR-1	4,84E-01	1,27E-01	2,73E-01	6,95E-02	2,23E+00	3,48E-01	3,55E-01	4,34E-02	4,30E-02	1,27E-02	2,10E-02	4,07E-03	6,87E-02	2,82E-02	2,74E-03	7,74E-01	8,51E-02	8,76E-02	1,44E-02

Precision	Ga	Ge	As	Rb	Sr	Y	Zr	Nb	Mo	Ag	Cd	In	Sn	Sb	Cs	Ba	La	Ce	Pr
BCR-2	0,98	0,94	0,92	0,98	0,98	0,98	0,98	0,98	0,95	0,97	0,90	0,96	0,98	0,90	0,97	0,98	0,98	0,98	0,98
BHVO-1	0,98	0,90	0,96	0,98	0,98	0,98	0,98	0,98	0,97	0,95	0,84	0,96	0,98	0,84	0,92	0,98	0,98	0,98	0,98
BHVO-2	0,97	0,88	0,84	0,79	0,98	0,98	0,98	0,91	0,10	0,92	0,82	0,95	0,97	0,95	0,42	0,92	0,88	0,96	0,96
ACCURACY	Ga	Ge	As	Rb	Sr	Y	Zr	Nb	Mo	Ag	Cd	In	Sn	Sb	Cs	Ba	La	Ce	Pr
BCR-2	1,16	1,04	3,52	1,01	0,99	0,96	0,98	0,99	1,02	13,09	0,30	0,15	1,10	0,98	0,99	0,98	0,97	0,99	0,97
BHVO-2	0,85	1,02	3,98	1,01	1,03	1,01	1,01	1,04	1,00	4,44	0,72	0,94	1,49	1,54	1,06	1,00	1,01	1,02	1,02
BIR-1	1,10	0,71	10,17	1,61	1,01	0,94	0,97	0,91	0,71	4,11	1,48	1,54	3,58	1,27	0,73	1,42	1,13	1,06	1,04

STD VALUES	Ga	Ge	As	Rb	Sr	Y	Zr	Nb	Mo	Ag	Cd	In	Sn	Sb	Cs	Ba	La	Ce	Pr
BCR-2*	2,21E+01	1,46E+00	8,60E-01	4,60E+01	3,37E+02	3,61E+01	1,87E+02	1,24E+01	2,51E+02	9,00E-02	6,90E-01	7,00E-01	2,28E+00	3,02E-01	1,16E+00	6,84E+02	2,51E+01	5,31E+01	6,83E+00
BHVO-2*	2,14E+01	1,62E+00	7,00E-01	9,26E+00	3,94E+02	2,59E+01	1,71E+02	1,81E+01	4,07E+00	8,90E-02	1,52E-01	1,17E-01	1,78E+00	1,03E-01	9,96E-02	1,31E+02	1,52E+01	3,75E+01	5,34E+00
BIR-1*	1,55E+01	1,46E+00	1,70E-01	2,10E-01	1,09E+02	1,56E+01	1,48E+01	5,53E-01	6,80E-02	4,10E-02	7,70E-02	5,76E-02	7,01E-01	4,62E-01	6,46E-03	6,75E+00	6,27E-01	1,92E+00	3,72E-01

AVERAGE	Nd146	Sm147	Eu151	Gd158	Tb159	Dy161	Ho165	Er167	Tm169	Yb172	Lu175	Hf177	Ta181	W183	Au197	Pb208	Bi209	Th232	U238
	(ppm)	(ppm)	(ppm)	(ppm)	(ppm)	(ppm)	(ppm)	(ppm)	(ppm)	(ppm)	(ppm)	(ppm)	(ppm)	(ppm)	(ppm)	(ppm)	(ppm)	(ppm)	(ppm)
BCR-2	2,83E+01	6,44E+00	1,95E+00	6,57E+00	1,01E+00	6,31E+00	1,26E+00	3,64E+00	5,07E-01	3,39E+00	4,97E-01	4,75E+00	7,63E-01	4,94E-01	1,87E-02	1,08E+01	4,98E-02	5,81E+00	1,66E+00
BHVO-2	2,53E+01	6,33E+00	2,12E+00	6,40E+00	9,42E-01	5,51E+00	1,00E+00	2,66E+00	3,39E-01	2,04E+00	2,89E-01	4,53E+00	1,19E+00	2,38E-01	4,74E-01	1,82E+00	1,73E-02	1,26E+00	4,33E-01
BIR-1	2,37E+00	1,10E+00	5,19E-01	1,86E+00	3,55E-01	2,56E+00	5,71E-01	1,71E+00	2,50E-01	1,65E+00	2,49E-01	5,56E-01	3,87E-02	4,15E-02	2,76E-01	3,64E+00	1,19E-02	3,11E-02	8,17E-03
2SD																			
BCR-2	5,90E-01	1,96E-01	4,22E-02	1,54E-01	2,43E-02	1,63E-01	3,60E-02	1,04E-01	1,53E-02	8,23E-02	1,56E-02	1,77E-01	3,04E-02	3,10E-02	5,44E-03	2,65E-01	4,11E-03	1,38E-01	3,11E-02
BHVO-2	4,48E-01	1,05E-01	5,81E-02	1,43E-01	3,12E-02	1,03E-01	2,79E-02	9,99E-02	1,32E-02	7,01E-02	1,20E-02	1,55E-01	4,13E-02	2,16E-02	2,02E-02	8,27E-02	2,55E-03	2,60E-02	1,18E-02
BIR-1	7,17E-02	5,22E-02	1,51E-02	6,57E-02	1,10E-02	1,12E-01	2,70E-02	7,58E-02	1,54E-02	9,64E-02	1,06E-02	3,68E-02	5,53E-03	4,02E-02	1,85E-02	1,32E-01	1,55E-03	1,14E-02	3,85E-03

Precision	Nd	Sm	Eu	Gd	Tb	Dy	Ho	Er	Tm	Yb	Lu	Hf	Ta	W	Au	Pb	Bi	Th	U
BCR-2	0,98	0,97	0,98	0,98	0,98	0,97	0,97	0,97	0,97	0,98	0,97	0,96	0,96	0,94	0,71	0,98	0,92	0,98	0,98
BHVO-1	0,98	0,98	0,97	0,98	0,97	0,98	0,97	0,96	0,96	0,97	0,96	0,97	0,97	0,91	0,96	0,95	0,85	0,98	0,97
BHVO-2	0,97	0,95	0,97	0,96	0,97	0,96	0,95	0,96	0,94	0,94	0,96	0,93	0,86	0,03	0,93	0,96	0,87	0,63	0,53
ACCURACY	Nd	Sm	Eu	Gd	Tb	Dy	Ho	Er	Tm	Yb	Lu	Hf	Ta	W	Au	Pb	Bi	Th	U
BCR-2	1,00	0,98	0,98	0,96	0,94	0,98	0,96	0,99	0,95	1,00	0,98	0,95	0,97	1,06	14,41	1,02	1,00	1,00	0,99
BHVO-2	1,04	1,05	1,04	1,03	1,00	1,04	1,01	1,06	1,01	1,02	1,05	1,01	1,03	0,95	182,28	1,10	1,17	1,03	1,05
BIR-1	0,99	0,98	1,00	1,03	0,98	1,00	1,00	1,02	0,98	1,01	1,00	0,95	0,94	1,54	0,11	1,20	2,34	0,95	0,78

STD VALUES	Nd	Sm	Eu	Gd	Tb	Dy	Ho	Er	Tm	Yb	Lu	Hf	Ta	W	Au	Pb	Bi	Th	U
BCR-2*	2,83E+01	6,55E+00	1,99E+00	6,81E+00	1,08E+00	6,42E+00	1,31E+00	3,67E+00	5,34E-01	3,39E+00	5,05E-01	4,97E+00	7,85E-01	4,65E-01	1,30E-03	1,06E+01	5,00E-02	5,83E+00	1,68E+00
BHVO-2*	2,43E+01	6,02E+00	2,04E+00	6,21E+00	9,39E-01	5,28E+00	9,89E-01	2,51E+00	3,35E-01	1,99E+00	2,75E-01	4,47E+00	1,15E+00	2,51E-01	2,60E-03	1,65E+00	1,48E-02	1,22E+00	4,12E-01
BIR-1*	2,40E+00	1,11E+00	5,20E-01	1,81E+00	3,62E-01	2,54E+00	5,72E-01	1,68E+00	2,56E-01	1,63E+00	2,48E-01	5,82E-01	4,14E-02	2,70E-02	2,50E+00	3,04E+00	5,10E-03	3,28E-02	1,05E-02

*Prefered values : Jochum K.P., Weis U., Schwager B., Stoll B., Wilson S.A., Haug G.H., Andreae M.O, Enzweiler J.; | Geostandards and Geoanalytical Research 40 (3) | [2016] 333-350 Title: Reference values following ISO guidelines for frequently requested rock reference materials doi: 10.1111/j.1751-908X.2015.00392.x

Paper V

-

Transfer of sulfur and chalcophile metals via sulfide-volatile compound drops in the Christiana-Santorini-Kolumbo volcanic field.

Patten CGC, **Hector S**, Kilias S, Ulrich M, Peillod A, Beranoaguirre A, Nomikou, P, Eiche E, Kolb J. (in review) Nature Communications

Transfer of sulfur and chalcophile metals via sulfide-volatile compound drops in the Christiana-Santorini-Kolumbo volcanic field

C.G.C. Patten[1*], S. Hector[2], S. P. Kilias[3], M. Ulrich[4], A. Peillod[2], A. Beranoaguirre[2], P. Nomikou[3], E. Eiche[2,5], J. Kolb[2]

[1]*Institute of Mineralogy and Petrography, University of Innsbruck, Austria*

[2] *Chair for Geochemistry and Economic Geology, Institute of Applied Geosciences (AGW), Karlsruhe Institute of Technology, Germany*

[3]*Department of Geology and Geoenvironment, National and Kapodistrian University of Athens, Greece*

[4]*Institut Terre et Environnement de Strasbourg, Université de Strasbourg, CNRS, France*

[5]*Laboratory of Environment and Raw materials Analysis (LERA), AGW, Karlsruhe Institute of Technology, Germany*

**email: clifford.patten@uibk.ac.at*

Abstract

Efficient transfer of S and chalcophile metals through the Earth's crust in arc systems is paramount for the formation of large magmatic-hydrothermal ore deposits and can strongly affect the Earth's climate. The formation of sulfide-volatile compound drops has been recognized as a potential key mechanism for such transfer but their fate during dynamic arc magmatism remains cryptic. We report evidence of compound drops preserved in the active Christiana-Santorini-Kolumbo volcanic field. The observed compound drops are micrometric sulfide blebs associated with vesicles trapped within silicate phenocrysts. The compound drops accumulate and coalesce at mafic-felsic melt interfaces where larger sulfide ovoids form. These ovoids are subsequently oxidized to magnetite during sulfide-volatile interaction. Comparison of metal concentrations between the sulfide phases and magnetite allows for determination of element mobility during oxidation. The formation and evolution of compound drops is an efficient mechanism for transferring S and chalcophile metals into shallow magmatic-hydrothermal arc systems.

Introduction

Effective fluxes of S and chalcophile metals (e.g. Cu, Ag, Te, Au, Bi) in the Earth's crust at arc settings are key for the formation of large hydrothermal ore deposits (porphyry, epithermal, volcanogenic massive sulfide, skarns[1–3]). These fluxes can also lead to important S and metal emissions into the atmosphere, potentially impacting the Earth's climate[4–7]. The processes controlling such fluxes, however, are complex, with competitive effects during arc magmatic-hydrothermal evolution. Sulfur and chalcophile metals can be trapped in the lower crust via sulfide segregation[8,9] or can be released into the upper crust via magmatic volatile degassing[3,10,11]. The relative timing between such processes is critical in determining the fate of S and chalcophile metals[12–14]. The formation of sulfide-volatile compound drops (i.e., droplets of sulfide melt attached to magmatic volatile phases) during magmatic

evolution appears as an alternative and efficient mechanism for the transport of both S and chalcophile metals to the shallow crust[15]. Although such compound drops have been shown experimentally[15–18] and identified in magmatic ultramafic systems[7,19], their preservation in complex magmatic-hydrothermal arc environments is scarce[20,21]. Magmatism in arc environments is dynamic, involving mixing of variably evolved melts via hybridization or mingling. Injection of fertile mafic melt into differentiated magmatic chambers appears as a key process for transferring S and chalcophile metals to shallower magmatic-hydrothermal systems[5,22]. The evolution of the compound drops in such dynamic environments is, however, poorly known and their role in the formation of arc-related hydrothermal ore deposits, although stipulated[15,20,21], remains cryptic.

In this study, we document the presence of compound drop remnants in the active magmatic-hydrothermal system of the Christiana-Santorini-Kolumbo (CSK) volcanic field within 5 Ma-to-present Hellenic volcanic arc, Greece. Based on detailed petrography, high-resolution X-ray fluorescence mapping and in-situ mineral chemistry analysis we highlight the complex mineral reactions and elemental transfers which occur in compound drops during complex magmatic evolution. The findings have important implications for fluxes of S and chalcophile metals in arc-related shallow magmatic-hydrothermal systems.

Results

Geological setting

The CSK volcanic field is part of the Hellenic Volcanic Arc (HVA) and formed in NE-SW oriented extensional basins within the Santorini-Amorgos tectonic zone[23]. The Santorini volcano, including Kameni, is the largest young volcanic centre in the HVA and records a complex volcanic history. After the Minoan eruption (ca. 3600 years ago) the volcanic islands of Palea Kameni and Nea Kameni formed in the centre of the caldera[24]. The Kameni islands show intermittent volcanic activity since the last 2200 years, producing dacite with little compositional variation[25]. The Kolumbo submarine volcano, located north-east of Santorini in the Anhydros basin, last erupted in 1650 CE[26]. Five distinct volcanic units are identified by seismic imaging (K1 to K5). The composition of the volcanic products ranges from basaltic to rhyolitic lava flows and rhyolitic pumices[27]. Despite the proximity between the Kolumbo volcano and the Santorini and Kameni islands along the same tectonic line, seismic tomography and geochemistry suggest that both volcanic centres have distinct magmatic systems[28] tapping into different mantle sources[27].

Sulfide-volatile compound drop remnants in the CSK volcanic field

The CSK volcanic field is an active and complex magmatic-hydrothermal system[23] showing evidence of magma mixing at both the Nea Kameni and Kolumbo volcanoes. Sulfides associated with volatile phases have been observed in five andesitic enclaves from the 1939-1940, 1940-1941 and 1950 lava

flows of Nea Kameni and within three pumice and lava samples from the K2 and K5 unit of Kolumbo (Supplementary Table 1).

Two sulfide populations related to volatile phases have been observed at Nea Kameni and Kolumbo volcanoes. The first population is defined by micrometric sulfide blebs associated with micrometric vesicles hosted by pyroxene phenocrysts from andesitic enclaves in porous dacite from Nea Kameni (Fig. 1c). The sulfide blebs are mainly spherical and contain pyrrhotite and chalcopyrite with minor magnetite (Fig. 1c), characteristic of magmatic sulfide blebs[29,30]. The vesicle associated with the sulfides varies in size from a few microns up to tens of microns (Fig. 1c). They are either directly in contact with or closely related to the sulfides. The sulfide-vesicle pairs have similar shapes, sizes and mineralogy as those observed at the Merapi volcano[20], analogous to compound drops[15] and, hence, are interpreted as well as compound drop remnants. Locally, where the phenocrysts are fractured, the sulfide blebs are replaced by magnetite, hematite and minor covellite (Supplementary Fig. 1) most likely due to dissolution and oxidation by magmatic volatiles during magmatic decompression[20].

The second sulfide population observed is characterized by variably oxidized sulfide ovoids up to a few millimeters in diameter. They have a spherical to elongated ellipsoidal shape, are related to large millimetric vesicles (Fig. 1a,b,d-i), and occur at the interface between andesitic enclaves and dacitic host rocks at Nea Kameni and Kolumbo (Fig. 1a,b,e,f) except for one ovoid from Kolumbo which is present within a rhyolitic matrix (Fig. 1i). The sulfide ovoids are either embayed in, in contact with or disconnected from the vesicles; the latter range in size range from several hundreds of microns to a few millimeters (Fig. 1a,e,h,i, Supplementary Fig. 2e). The sulfide ovoids are constituted mainly of pyrrhotite and pyrite with minor pentlandite, chalcopyrite and covellite. Pyrrhotite appears as large grains (up to a few millimeters) with discrete exsolution of pentlandite. Pyrite occurs as a replacement of pyrrhotite generally along fractures filled with magnetite; additionally, pyrite proportion increases towards magnetite-rich zones (Fig. 1d). Pyrite shows cleavage-like texture and has relatively low reflectance. Chalcopyrite is scarce and has been observed in partly oxidized areas (Fig. 1d). It is often replaced by covellite associated with pyrite. Sulfides are replaced by fine-grained micrometric subhedral magnetite with discrete sulfide grains preserved in between (Fig. 1a,d,g). Sulfide replacement by magnetite ranges from limited, with discrete magnetite along fractures and at vesicle margins, to extensive, with almost magnetite-pure aggregates with discrete sulfides and porosity between the grains (Fig. 1d,g, Supplementary Fig. 2). Locally, magnetite is associated with hematite and shows a frothy texture (Supplementary Fig. 3). The sulfide ovoids, with their mineralogy and variably oxidized state, are similar to magmatic sulfides observed in different arc volcanoes which have sustained advanced oxidation during sulfide-magmatic volatile interaction[31].

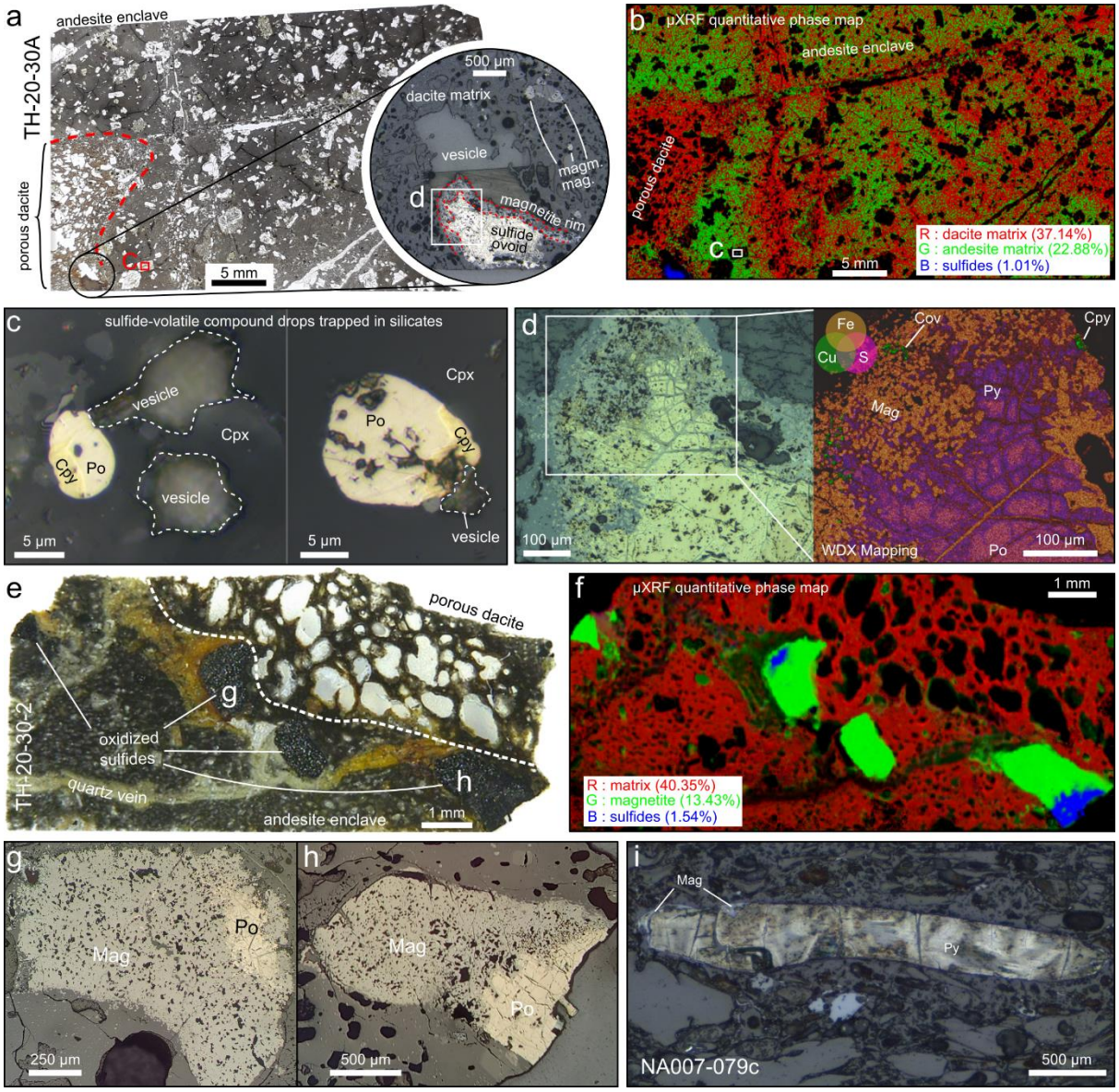

Figure 1: Petrology of sulfide and oxide phases related to sulfide-volatile compound drops at Nea Kameni (a-h) and Kolumbo (i) volcanoes. a) Thin section of an andesite enclave in contact with porous dacite host rock from Kameni volcano. Sulfide ovoid associated with large vesicle at andesite/dacite margin (insert). b) micro-XRF quantitative phase map of a) showing the proportion of dacite matrix, andesitic matrix and sulfide phases (pyrrhotite and chalcopyrite). Mineral proportions are calculated from elemental micro-XRF mapping. The maps show a complex interface between the andesitic enclave and the host dacite where sulfide-volatile compound drops occur. Black zones represent porosity and silicate phenocrysts. c) Sulfide blebs and associated vesicles in pyroxene phenocryst. Sulfide blebs contain pyrrhotite (Po), chalcopyrite (Cpy) and magnetite (Mag). d) Ovoid-shaped, partly oxidized sulfide melt occurring at the dacite/andesite interface in a). The sulfide ovoid is characterized by pyrrhotite (Po) in the core, pyrite (Py), chalcopyrite (Cpy), covellite (Cov) and magnetite (Mag) in the rim. The right part shows WDX scanning electron microscopy elemental mapping of S, Fe and Cu. e) Thin section of an andesite enclave in contact with porous dacite host rock from Kameni also with partly oxidized remnants of sulfide-volatile compound drops. f) micro-XRF quantitative phase map of e) showing the proportion of silicate matrix (both dacitic and andesitic), hydrothermal magnetite and sulfide phases (pyrrhotite and chalcopyrite). Mineral proportions are calculated from elemental micro-XRF mapping. The map shows the relationship between the sulfides and replacing magnetite. g) and h) Details of pyrrhotite partly oxidized to magnetite. i) Sulfide-volatile compound drop from the Kolumbo volcano within a rhyolitic matrix. The sulfide phase is characterized by pyrite with minor magnetite suggesting limited oxidation.

Sulfide and oxide mineral composition

In-situ analysis of sulfide and oxide phases from the sulfide blebs and ovoids allows the characterization of their origin and a better understanding of metal behavior during compound drop evolution (Supplementary Table 2). Fresh sulfide blebs of compound drops in silicate phenocrysts show a distinctive magmatic signature characterized by relatively high chalcophile element concentrations (Co, Ni, Cu, and Ag; Fig. 2a) and an overall similar metal enrichment to compound drops from the Merapi volcano[20], and to sulfide droplets from mid-ocean ridge basalt (MORB)[30,32] and from arc volcanic rocks [33–35]. These similarities imply that the sulfide blebs formed from a sulfide-saturated melt. The sulfide blebs from the CSK volcanic field are more enriched in weakly chalcophile elements (Zn, As, Sb, Pb Fig. 2a) compared to MORB sulfide droplets, which are enriched in strongly chalcophile elements (Co, Ni, Cu, Te, Au), supporting that sulfide saturation occurred in an andesitic melt, slightly more evolved than a MORB.

Pyrrhotite, pyrite and partly oxidized chalcopyrite from the sulfide ovoids show comparable metal enrichment to the sulfide blebs (Fig. 2b; Supplementary Discussion). The partly oxidized chalcopyrite is enriched in As, Ag, Au, Tl, Pb and Bi relative to pyrrhotite and pyrite, while pyrite is enriched in Co, Ni, Mo, Sb and Te (Fig. 2b, Supplementary Table 2). Such metal fractionation is akin to metal distribution during magmatic sulfide crystallization into monosulfide solid solution (MSS) and intermediate solid solution (ISS;[32])suggesting that the sulfide ovoids are well-differentiated magmatic sulfides overprinted by oxidation reactions.

Magnetite present within the sulfide ovoids has low concentrations in Ti, V, Mn, Co, Ni and Zn, which are usually enriched in magmatic magnetite crystallizing from a silicate melt[36] (Fig. 2b, Supplementary Fig. 3) and differ in concentrations from magnetite crystallizing out of a sulfide liquid[37] (Supplementary Fig. 3). Hence, the analyzed magnetite did not form through magmatic process but rather by oxidation and replacement of the magmatic sulfides, as supported by petrographic observations.

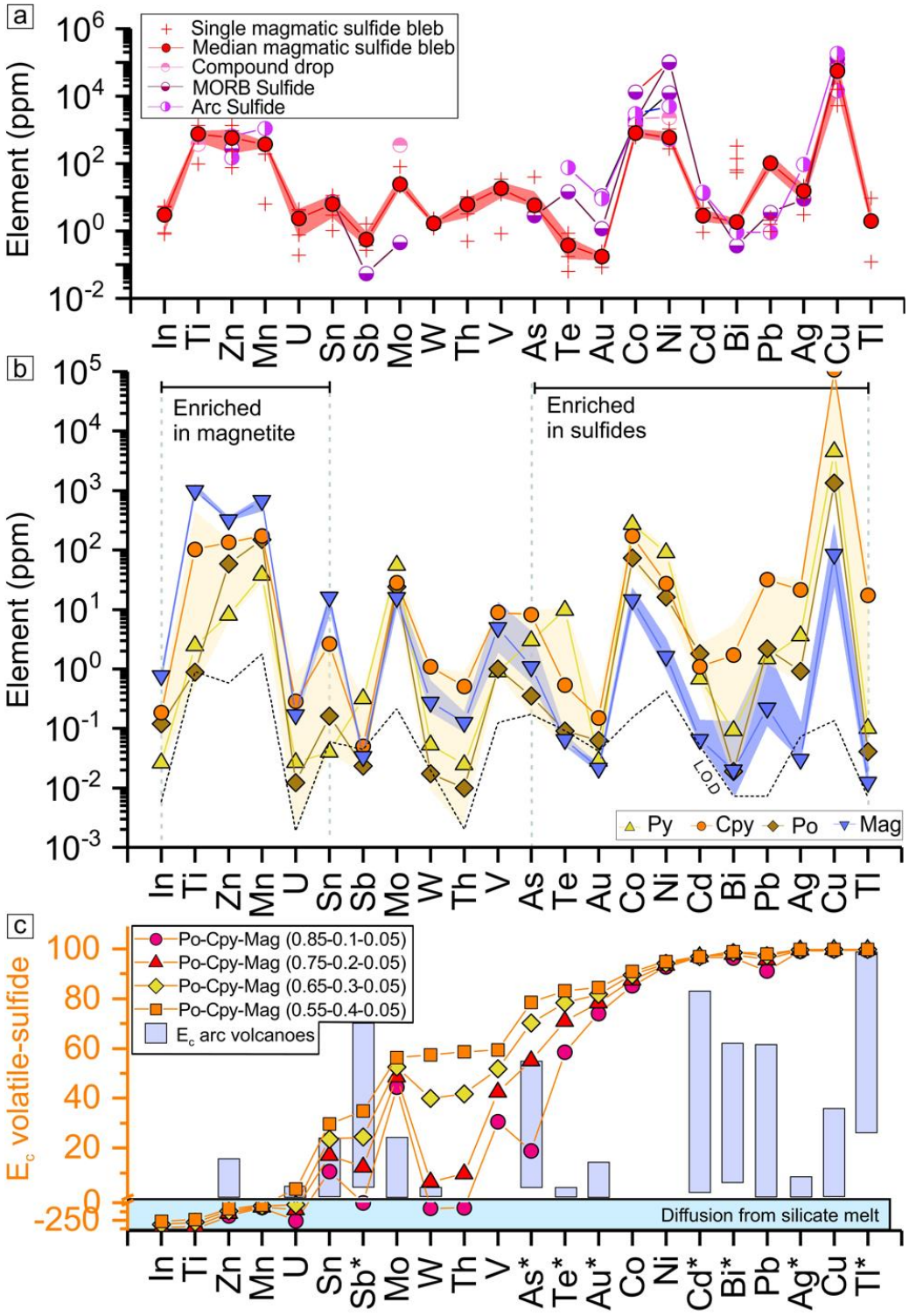

Figure 2: Trace element concentrations in sulfides and magnetite related to compound drops as well as volatile-sulfide emanation and partition coefficients. a) Median trace element concentrations in magmatic sulfide bleb inclusions (n=4). Shaded area corresponds to the upper and lower quartiles. Compound drops data are from Nadeau et al.[20], MORB sulfides from Peach et al.[30] and Patten et al.[32] and arc sulfides from Keith et al.[33], Zelenski et al.[34] and Fulignati et al. [35]. b) Median metal concentrations in pyrrhotite (Po), pyrite (Py), partly replaced chalcopyrite (Cpy) and magnetite formed after sulfide oxidation (Mag). Shaded areas correspond to the upper and lower quartiles. L.O.D = limit of detection. c) Calculated magmatic volatile-sulfide emanation coefficients (E_c). Arc volcano emission coefficients are from Edmonds et al.[6] *Minimum emanation coefficient values calculated due to magnetite concentrations close to or below the limit of detection (see Supplementary discussion).

Discussion

Although the Nea Kameni and Kolumbo volcanoes share distinct magmatic plumbing systems they are both characterized by shallow magmatic chambers (~4 and ~5 km deep, respectively) fed by mafic melts from deeper sources[38–42]. For instance, the 2011-2012 unrest at Santorini was due to the intrusion, into the shallow plumbing system, of new volatile-rich and more primitive mafic andesitic-basaltic magma[43]. The presence of magmatic sulfide blebs within the andesitic enclaves as well as the high S concentrations in andesite-hosted melt inclusions from Nea Kameni (~900-1000 $\mu g \cdot g^{-1}$;[44]) imply that the andesitic melt was sulfide-saturated upon injection into the shallow magmatic chamber. Additionally, the presence of trapped fluid inclusions in olivine and pyroxene in andesitic enclaves at Nea Kameni[43] suggests that magmatic volatile exsolution occurred within a similar timeframe to sulfide saturation; allowing eventual volatile bubble nucleation on magmatic sulfide droplets and formation of sulfide-volatile compound drops (Fig. 3;[17]).

The similar mineralogy and composition, the spatial proximity as well as the close association with vesicles imply a genetic link between the magmatic sulfide blebs and the larger sulfide ovoids (Supplementary Discussion). Unlike small magmatic sulfide blebs (tens of microns), the relatively large size of the sulfide ovoids (>1 mm), does not favor flotation of sulfides through the magmatic crystal mush via compound drops (sulfide phase in compound drops <~0.4 mm;[17]). The formation of the sulfide ovoids is rather likely to have occurred during magma mixing. Repeated injections of volatile-rich mafic (andesitic/basaltic) melts at Nea Kameni and Kolumbo result in their accumulation at the bottom of the magmatic chambers without extensive mixing with the intermediate/felsic (dacitic/rhyolitic) melts[41,43,45]. Continuous volatile exsolution from the mafic melts can lead to the formation of an intermediate hybrid layer between the mafic and felsic magmas[46,47]. The intermediate hybrid layer can eventually be incorporated into the felsic magmas, forming mafic enclaves[47]. The andesitic enclaves observed at Kameni shows diffuse transition with the dacitic host rock, as revealed by μXRF mineral mapping (Fig. 1b) suggesting they are remnants of the intermediate hybrid layer. The mafic enclaves also locally host quartz veins which are cross-cut at the andesite-dacite interface by the dacitic host rocks (Fig. 1e) implying that veins are not related to late hydrothermal processes but are of magmatic origin. Locally these veins crosscut the oxide/sulfide ovoids and show magmatic magnetites aligned at their margins (Fig. 1e), suggesting a sub-solidus process. Similarly to late residual silicate melt which partially fills the volatile fraction of compounds drops at Norilsk'[19], the quartz veins are interpreted as late residual products of the mafic melt differentiation; further supporting that the mafic enclaves are remnants of an intermediate hybrid layer from the underplating mafic melt.

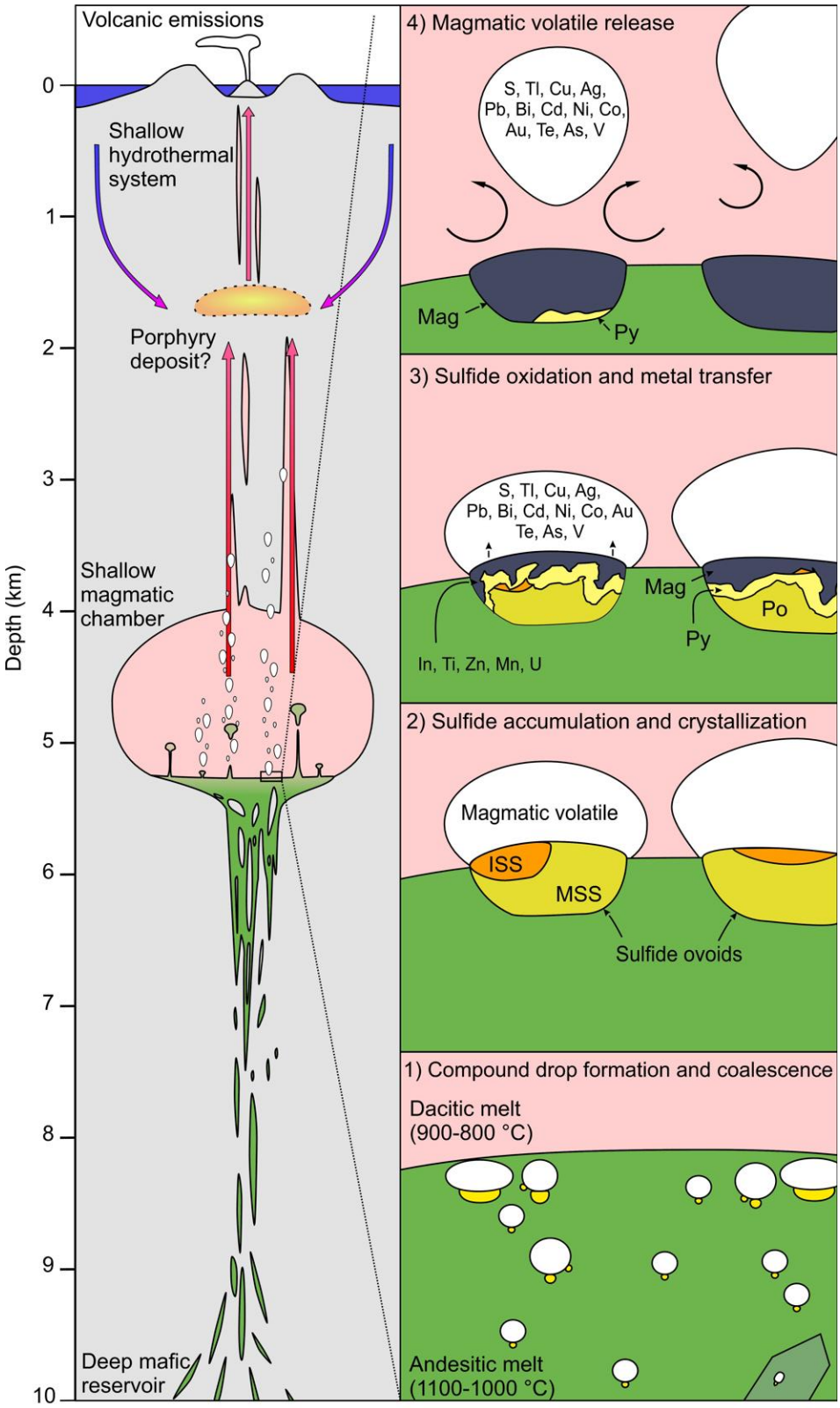

Figure 3: Model for S and chalcophile metal transfer during magmatic mixing. Volcanic architecture and melt composition based on the Nea Kameni volcano. 1) Compound drops formation and coalescence upon andesitic melt injection in the magmatic chamber. 2) Accumulation of compound drops in sulfide ovoids at the andesitic-dacitic melt interface. The sulfide liquid crystalizes into MSS and ISS. 3) Sulfide phases are oxidized into magnetite leading to S and chalcophile metal enrichment in the magmatic volatiles. 4) S and metal-rich magmatic volatiles are then released into shallower hydrothermal system.

The interface between such underplating mafic melt and an overlying felsic melt is often a place where volatile bubbles, which have exsolved from the mafic melt, accumulate[46–48]. Similarly magnetite-volatile aggregates, which also form in mafic magma and which share similar physical properties to sulfide-volatile compound drops, have been shown to gather as well at such interface[49]. Hence, it is inferred that compound drops which formed within the mafic melt rise toward the interface with the felsic melt where they stagnate and accumulate due to differences in physico-chemical conditions. During migration, stagnation and accumulation, the compound drops eventually coalesce[16], resulting in the formation of large sulfide ovoids (Fig. 3). During the coalescence of compound drops into larger sulfide ovoids, the temperature difference between the basaltic/andesitic and dacitic/rhyolitic melts (~1000-1200 °C and 750-900 °C, respectively[38,44,50]) leads the sulfide liquid to crystallize as monosulfide solution (MSS, ~1050-1100 °C) and intermediate solid solution (ISS, ~850 °C[51]) accounting for the differentiated pyrrhotite and chalcopyrite texture preserved in partly oxidized sulfide ovoids (Fig. 1).

The trigger for sulfide oxidation may be related to several processes such as magmatic degassing, change in volatile composition due to magma mixing or late stage hydrothermal alteration. Magmatic differentiation in arc systems generally leads to magnetite crystallization and to increasing reducing conditions[8]. The presence of magmatic magnetites (Supplementary Fig. 3) suggests that the redox is driven towards more reduced conditions during the magmatic differentiation of the Kameni and Kolumbo volcanoes. Hence, it appears unlikely that magma mixing with more evolved melts affects the redox of the magmatic volatile phase towards more oxidizing conditions causing sulfide oxidation. Alternatively arc volcanos are dynamic systems where long lasting hydrothermal fluid circulation occur and late stage hydrothermal fluid circulation can cause sulfide oxidation. Such process, however, would have altered the host rock leading to significant silicate alteration, which is not observed in the samples (Fig. 1e). It is rather inferred that, shortly after sulfide differentiation, sulfide oxidation occurs by reaction with the magmatic volatiles[13], likely through fluid/volatile-induced interface-coupled dissolution–precipitation mechanisms[52], upon magmatic degassing. Replacement of MSS (pyrrhotite) and ISS (chalcopyrite) by pyrite, covellite and magnetite can be described with the following mineral reactions[7,13,20,21] (Fig. 3):

$$4FeS_{(po)} + H_2O_{(fluid)} + 2.5O_{2\,(fluid)} \rightarrow Fe_3O_{4(mag)} + FeS_{2(py)} + H_2S_{(fluid)} + SO_{2\,(fluid)} \quad (1)$$

$$3FeS_{(po)} + 2H_2O_{(fluid)} + 2O_{2\,(fluid)} \rightarrow Fe_3O_{4(mag)} + 2H_2S_{(fluid)} + SO_{2\,(fluid)} \quad (2)$$

$$3CuFeS_{2(cpy)} + 2H_2O_{(fluid)} + 2O_{2\,(fluid)} \rightarrow Fe_3O_{4(mag)} + 3CuS_{(cov)} + 2H_2S_{(fluid)} + SO_{2\,(fluid)} \quad (3)$$

$$3CuFeS_{2(cpy)} + 1.5H_2O_{(fluid)} + 4.25O_{2\,(fluid)} \rightarrow Fe_3O_{4(mag)} + 3CuHS_{(fluid)} + 3SO_{2\,(fluid)} \quad (4)$$

$$3CuFeS_{2(cpy)} + 3HCl_{(fluid)} + 13O_{2\,(fluid)} \rightarrow Fe_3O_{4(mag)} + 3CuCl_{(fluid)} + 1.5H_2S_{(fluid)} + 4.5SO_{2\,(fluid)} \quad (5)$$

The magmatic sulfides partial oxidation into an assemblage of magnetite, pyrite and covellite or complete oxidation to solely magnetite depend on the fO_2, fS_2, fluid composition and temperature[20]. During ISS (chalcopyrite) oxidation, Cu is released into the volatile phase as diverse S- and Cl-complexes[53–55] which equations (4) and (5) are simplified representations.

The variably oxidized ovoids are either embayed into large vesicles (Fig. 1a, Sup. Fig. 2e), partially associated with vesicles (Fig. 1i) or disconnected from vesicle (Fig. 1e, Supplementary Fig. 2d). This diversity of sulfide/oxide ovoid-vesicle textures suggests that the coalesced sulfide-volatile compound drops might eventually become unstable. At the andesitic-dacitic magma interface, changes in surface tension, drop compound size, fluid and melt dynamics likely affect the stability of the compound drops and eventually lead to the separation of the volatile phase from the sulfide/oxide phases[17]. Ultimately, the magmatic volatile phase will rise within the magmatic chambers as plume[46,47] or through volatile pathways[56] and cracks in the magma crystal framework, directly feeding shallower hydrothermal systems[48] (Fig. 3).

Sulfide oxidation by magmatic fluids has been recognized as a key process for mobilizing S and metals to the shallow parts of arc magmatic-hydrothermal systems[6,14,20,31,57]. The efficiency, however, of metal transfer from the magmatic sulfides to the volatiles remains poorly known. The metal concentrations of the sulfide ovoids and replacing magnetite allows to constrain element mobility and calculation of emanation coefficients[6,58]. An emanation coefficient is usually used to determine element behavior upon eruption of lavas and is defined as[6,58]:

$$\varepsilon_x = (C_i - C_f)/C_i \quad (6)$$

With C_i being the concentration of the element *x* in a melt and C_f the concentration of the element in the post-eruptive lava. The emanation coefficients, although developed for lavas, can be applied to the compound drop system as it is based on the initial concentration of a system (here the magmatic sulfides) and the final concentration of the system after "emanation" (here the magnetite). It is however necessary to account for mass variation between the sulfide phases and magnetite during oxidation. Considering that the formation of 1 mole of magnetite requires the oxidation of 3 moles of sulfides (either pyrrhotite or chalcopyrite from equations 2, 3 and 5) the emanation coefficient can be modified to:

$$\varepsilon_{x\ sulf-mag} = \left(C_{X\ sulf} - \frac{M_{mag}}{3*M_{sulf}} * C_{X\ mag}\right)/C_{X\ sulf} \quad (7)$$

with C_{xsulf} and C_{xmag} being the concentration of the element *x* in the primary magmatic sulfides and magnetite, respectively and M_{sulf} and M_{mag} the molar mass of the sulfides and magnetite, respectively (see Supplementary Discussion for details). Numerous elements, such as Ni, Cu, Ag, Cd, Te, Au, Tl, Pb and Bi show high mobility into the volatile phase (ε_x ~80-100 %) while V, As, Mo, Sn, Sb, W and Th show lower mobility (ε_x ~0-80 %, Fig. 2C). Some elements show wide range in emanation

coefficient values (As, Sn, Sb, Te, W and Th) due to the relative proportion of chalcopyrite within the calculated magmatic sulfide composition as they have low concentration in pyrrhotite but higher concentration in chalcopyrite (Supplementary Table 2). Hence the relative proportion of chalcopyrite to pyrrhotite in magmatic sulfide has an impact on certain element mobility during oxidation. Some poorly chalcophile elements, such as Ti, Zn, In, Mn and U, have negative emanation coefficients because the sulfide-volatile compound drops are not closed systems and interact with the surrounding silicate melt. During sulfide oxidation Ti, Zn, In, Mn and U are interpreted to partition from the melt into the newly formed magnetite for which they have moderate to strong affinity[36]. Such partitioning is likely to have little effect on the other more chalcophile elements. The emanation coefficients determined from sulfide oxidation are notably higher than those observed from lavas at arc volcanoes[6], except for Zn and Sb (Fig. 2c). Although sulfide-volatile compound drops have been suggested to play a role in volcanic emissions their specific signature cannot be clearly distinguished from the silicate melt-volatile phase signature[6]. The high emanation coefficients determined from sulfide and magnetite analyses implies that oxidation of the sulfides during sulfide-volatile compound drop evolution is a very efficient mechanisms for releasing moderately to strongly chalcophile elements into the magmatic volatile phase. This process is possibly more efficient than silicate melt-volatile phase interaction and may directly supply metals to ore deposits[15].

The Kolumbo volcano hosts an actively forming hybrid epithermal-seafloor massive sulfide (SMS) mineralization characterized by sulfide-sulfate diffusers enriched in As, Ag, Sb, Au, Tl and Hg[59]. Metal endowment in Kolumbo is noticeably different from the metal enrichment in magmatic sulfides related to sulfide-volatile compound drops (Supplementary Figure 4a). During magmatic volatile migration through the hydrothermal system of Kolumbo several processes such as fluid separation into brine and vapour phases, boiling and sulfide precipitation may occur; strongly impacting the metal load of the fluids and preventing direct comparison of metal content between magmatic sulfides and mineralization. To circumvent eventual metal fractionation processes, element pairs with similar behaviour during hydrothermal fluid evolution and sulfide precipitation are used to test if a genetic link between sulfide-volatile compound drops and Kolumbo's mineralization exists. This approach is similar to that of Nadeau et al.[20] where metal ratios of magmatic sulfide and volcanic gases at Merapedi volcano are compared to establish a genetic link as well as the modelling from Mungall et al.[15] which links compound drop and ore compositions at the Alumbrera Cu-Au deposit. Three element pairs are chosen: 1) As-Pb, representing elements which precipitate at low temperature, 2) Cu-Bi, representing elements which precipitate at high temperature and 3) Au-Ag which are two elements with overall similar behaviour[60–62]. For the three chosen pairs, magmatic sulfides and mineralized samples from the Kolumbo diffusers show good correlation and have similar As/Pb, Bi/Cu and Ag/Au ratios (Fig. 4a-c) despite some natural variability in the diffusers. Although the volatile phase composition of the compound drops is unknown, the high emanation coefficients of the selected elements (over 90% for

Pb, Ag, Cu and Bi and up to ~80 % for Au and As, Supplementary Table 3) suggest little metal fractionation during sulfide oxidation. Hypothetic volatile phase metal ratios, defined as the calculated magmatic sulfide ratio of As/Pb, Bi/Cu and Ag/Au factorized by their respective emanation coefficients, are used to assess metal fractionation during oxidation (Fig. 4). The hypothetic volatile phase ratio ranges show slight differences with the calculated magmatic sulfide ones (Fig. 4), with only the As/Pb showing a wider range as As has the lowest emanation coefficients of the selected elements, implying limited fractionation with Pb. Nevertheless the magmatic sulfide and the hypothetic volatile ratio ranges overlap well with that of the mineralization from Kolumbo (Fig. 4). Hence, the metal ratios of the magmatic sulfides are good proxies for the metal ratios of the volatile phase, allowing comparison with the mineralization (Fig. 4). Other element pairs also show similar distribution (Au/Tl, Tl/Ag, Te/Cu, Supplementary Fig. 4b-c). Comparison of the As/Cu and Pb/Bi ratios (Fig. 4d) allows to compare element pairs with opposite geochemical behaviour and further supports the similar geochemical signature between the magmatic sulfides and mineralization despite the effect of metal fractionation (as well as Cu/Au and Bi/Ag ratios, Supplementary Fig. 4e). Hence, a genetic link likely exists between magmatic sulfides and the mineralization at Kolumbo, supporting that oxidation of sulfide-volatile compound drops can directly supply metals to ore deposits[15]. Finally, Cu, Te and Bi have high emanation coefficients during sulfide oxidation (Fig. 2c) and show similar Cu/Bi and Cu/Te ratios between magmatic sulfides and diffusers, but these elements are poorly enriched in Kolumbo mineralization relative to other metals (Fig. 4 and Supplementary Fig. 4;[59]). Fluids venting at the Kolumbo hydrothermal field have temperature up to 265 °C[63] suggesting that significant Cu, Te and Bi might be enriched below the diffusers at higher temperature, possibly as a Cu-rich stockwork or deeper as a porphyry-style mineralization. The role of compound drops in the CSK volcanic field suggests that in addition to porphyry and magmatic Ni-Cu-PGE deposits compound drops can also be directly involved in the formation of epithermal and VMS deposits.

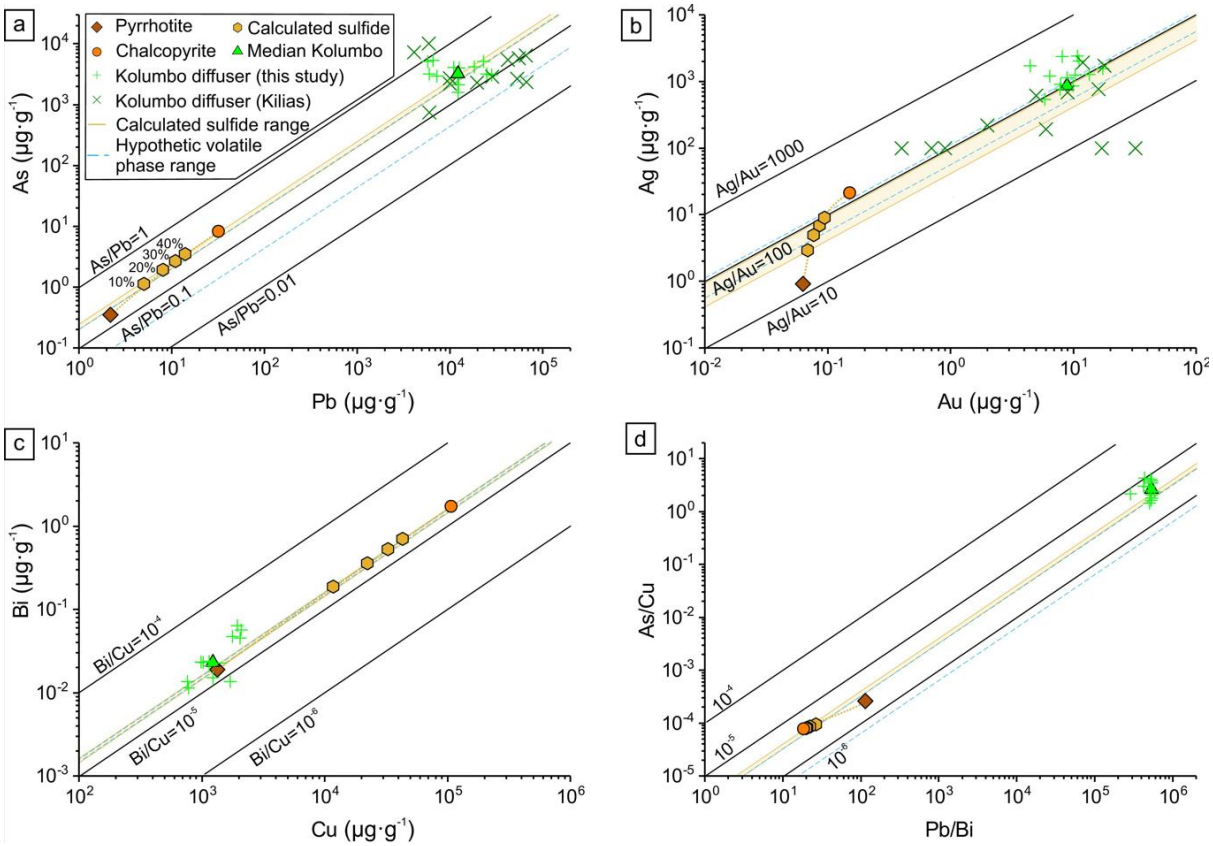

Figure 4: Comparison of metal content in magmatic sulfides and mineralized samples from Kolumbo diffusers. a) Pb vs As, b) Au vs Ag, c) Cu vs Bi and d) Pb/Bi vs As/Cu. The calculated magmatic sulfides are determined with various proportions of pyrrhotite and chalcopyrite (see Supplementary Discussion for details), the percentage represent the chalcopyrite proportion. The calculated sulfide range correspond to the metal ratio of the calculated magmatic sulfides ranging from 10 % to 40 % chalcopyrite in proportion. The hypothetic volatile phase metal ratio range corresponds to the calculated sulfide ratio range factorized by the emanation coefficients of the selected elements (see Supplementary Table 3). The overlap between the magmatic sulfide, hypothetic volatile phase and mineralization metal ratios highlight a genetic link between the compound drops and the mineralization. Kolumbo diffuser data are from Kilias et al.[59] and from this study (see Supplementary Table 6).

Methods

Micro-XRF mapping

Micro-XRF measurements were done on 30 µm-thick polished thin sections using a micro X-Ray fluorescence (µ-XRF) Brucker M4 Tornado at the Institut Terre et Environnement de Strasbourg (France). The instrument is equipped with a Rh anode operating at 400 µA with an accelerating voltage of 50 kV. Polycapillary lenses were used to focus the X-ray beam down to 20 µm full-width-at-half-maximum at the sample surface. Two energy-dispersive silicon drift detectors of 125 eV resolution, and with an active area of 60 mm^2 each were used to measure fluorescence spectra (180 s counting time per spectrum). Measurements were performed in a vacuum chamber at 2 mbar to minimize air absorption and ensure the best signal-to-noise ratio. µ-XRF chemical mappings were acquired with a 30 µm step

specified region of interest (ROI) of the energy range of XRF spectra (Supplementary Fig. 5). Phase maps were calculated using the calculation procedure developed in Ulrich et al.[64].

In-situ mineral analysis

In situ trace element analyses of sulfide and oxide phases were carried out by Electron Micro Probe Analysis (EMPA) and by Laser Ablation-Inductively Coupled Plasma-Mass Spectrometry (LA-ICP-MS). EMPA analyses were carried out at the Institute of Geological Sciences from the University of Bern using a JEOL JXA-8200 Superprobe equipped with five wave-length dispersive crystal spectrometers (WDS) and one energy dispersive spectrometer (EDS). A 15 kV acceleration voltage and a 20 nA probe current were used for analysis. Natural and synthetic oxide, sulfides and silicate minerals were used as standards. LA-ICP-MS analysis were carried out at the Laboratory of Environment and Raw materials Analysis (LERA), Karlsruhe Institute of Technology, using a Teledyne 193 nm Excimer Laser coupled to an ICP-MS (Element XR ThermoFisher). Analyses of pyrrhotite, pyrite, chalcopyrite and magnetite were done with spot size of 35 µm, laser frequency of 10 Hz, fluence of 5 $J.cm^{-2}$ and helium and nitrogen flow of 0.3 $L.min^{-1}$ and 10 $mL.min^{-1}$, respectively. The ^{57}Fe from EMPA analyses were used for internal standard calibration. The following isotopes were measured: ^{29}Si, ^{32}S, ^{49}Ti, ^{51}V, ^{55}Mn, ^{57}Fe, ^{59}Co, ^{60}Ni, ^{63}Cu, ^{66}Zn, ^{75}As, ^{95}Mo, ^{107}Ag, ^{111}Cd, ^{115}In, ^{118}Sn, ^{121}Sb, ^{125}Te, ^{182}W, ^{197}Au, ^{205}Tl, ^{208}Pb, ^{209}Bi, ^{232}Th, ^{238}U. Calibration and data quality checking was done using the sulfide pressed pellets Fe-S1, Fe-S4 and PTC1b from UQAC University for sulfide analyses and basaltic glasses BHVO-2G, BCR-2G and BIR-1G from the USGS for oxide analysis. Although non-matrix matching, calibration of magnetite using Fe-rich basaltic standards is adequate[37]. Data reduction was done using the Iolite software[65] 3DRS plugin in two separate runs for sulfide and oxide analyses. Accuracy and precision for reference materials (<15% for most elements) as well as limits of detections are detailed in Supplementary Table 4.

Diffuser whole rock metal concentration

Thirteen samples from a >1m high diffuser from the Politeia area in the Kolumbo hydrothermal field[59] have been analyzed for metal concentrations. Whole rock analysis was carried out by acid-digest-ICP-MS method using a Thermo X-series 2. Pulverized samples (100 mg) were dissolved in a combined HNO3-HF-HClO4. The powder was heated in a closed Teflon vessel for 16 h at 120°C (DigiPrep, SCP Science) using 40% HF (suprapur), 65% HClO4 (normatom) and 65% HNO3 (subboiled). The final residue was dissolved in 50 mL of ultrapure water. The following isotope were selected for analysis: ^{55}Mn, ^{57}Fe, ^{59}Co, ^{60}Ni, ^{63}Cu, ^{66}Zn, ^{75}As, ^{95}Mo, ^{107}Ag, ^{111}Cd, ^{121}Sb, ^{126}Te, ^{182}W, ^{197}Au, ^{205}Tl, ^{208}Pb, ^{209}Bi and ^{232}Th. Calibration solutions were prepared with the CertiPUR® ICP Multi Element Standard VI (Merck) used as stock solution and different single element standards. To identify and correct measurement drift, 50 µL of an internal standard containing scandium (^{45}Sc), rhodium (^{103}Rh), indium (^{115}In) and thulium (^{169}Tm) added to all samples, including the blanks (1% HNO3). For all measurements the following Ar gas flows were chosen: Nebulizer gas, flow of 0.88 L/min, auxiliary gas flow of 0.68 L/min, and cooling gas flow of 13 L/min. Data quality was assessed by the analysis of the reference materials CH-4 and TUBAF (Supplementary Table 6).

Data availability

Data used in this study are available in the Supplementary Tables and Supplementary Discussion.

References

1. Sun, W. *et al.* Porphyry deposits and oxidized magmas. *Ore Geol. Rev.* **65**, 97–131 (2015).
2. Richards, J. P. The oxidation state, and sulfur and Cu contents of arc magmas: implications for metallogeny. *Lithos* **233**, 27–45 (2015).
3. Richards, J. P. Magmatic to hydrothermal metal fluxes in convergent and collided margins. *Ore Geol. Rev.* **40**, 1–26 (2011).
4. Devine, J. D., Sigurdsson, H., Davis, A. N. & Self, S. Estimates of sulfur and chlorine yield to the atmosphere from volcanic eruptions and potential climatic effects. *J. Geophys. Res. Solid Earth* **89**, 6309–6325 (1984).
5. Wallace, P. J. & Edmonds, M. The sulfur budget in magmas: evidence from melt inclusions, submarine glasses, and volcanic gas emissions. *Rev. Mineral. Geochemistry* **73**, 215–246 (2011).
6. Edmonds, M., Mather, T. A. & Liu, E. J. A distinct metal fingerprint in arc volcanic emissions. *Nat. Geosci.* **11**, 790–794 (2018).
7. Le Vaillant, M., Barnes, S. J., Mungall, J. E. & Mungall, E. L. Role of degassing of the Noril'sk nickel deposits in the Permian–Triassic mass extinction event. *Proc. Natl. Acad. Sci.* **114**, 2485–2490 (2017).
8. Jenner, F. E., O'Neill, H. S. C., Arculus, R. J. & Mavrogenes, J. A. The magnetite crisis in the evolution of arc-related magmas and the initial concentration of Au, Ag and Cu. *J. Petrol.* **51**, 2445–2464 (2010).
9. Jenner, F. E. Cumulate causes for the low contents of sulfide-loving elements in the continental crust. *Nat. Geosci.* **10**, 524 (2017).
10. Yang, K. & Scott, S. D. Possible contribution of a metal-rich magmatic fluid to a sea-floor hydrothermal system. *Nature* **383**, 420–423 (1996).
11. Heinrich, C. A., Günther, D., Audétat, A., Ulrich, T. & Frischknecht, R. Metal fractionation between magmatic brine and vapor, determined by microanalysis of fluid inclusions. *Geology* **27**, 755–758 (1999).
12. Fontboté, L., Kouzmanov, K., Chiaradia, M. & Pokrovski, G. S. Sulfide minerals in hydrothermal deposits. *Elements* **13**, 97–103 (2017).
13. Edmonds, M. & Mather, T. A. Volcanic sulfides and outgassing. *Elements* **13**, 105–110 (2017).
14. Halter, W. E., Pettke, T. & Heinrich, C. A. The origin of Cu/Au ratios in porphyry-type ore deposits. *Science (80-.).* **296**, 1844–1846 (2002).
15. Mungall, J. E., Brenan, J. M., Godel, B., Barnes, S. J. & Gaillard, F. Transport of metals and sulphur in magmas by flotation of sulphide melt on vapour bubbles. *Nat. Geosci.* **8**, 216–219 (2015).
16. Iacono-Marziano, G., Le Vaillant, M., Godel, B. M., Barnes, S. J. & Arbaret, L. The critical role of magma degassing in sulphide melt mobility and metal enrichment. *Nat. Commun.* **13**, 1–10 (2022).

17. Yao, Z. & Mungall, J. E. Flotation mechanism of sulphide melt on vapour bubbles in partially molten magmatic systems. *Earth Planet. Sci. Lett.* **542**, 116298 (2020).

18. Virtanen, V. J. *et al.* Fluids as primary carriers of sulphur and copper in magmatic assimilation. *Nat. Commun.* **12**, 6609 (2021).

19. Barnes, S. J., Le Vaillant, M., Godel, B. & Lesher, C. M. Droplets and bubbles: solidification of sulphide-rich vapour-saturated orthocumulates in the Norilsk-Talnakh Ni–Cu–PGE ore-bearing intrusions. *J. Petrol.* **60**, 269–300 (2019).

20. Nadeau, O., Williams-Jones, A. E. & Stix, J. Sulphide magma as a source of metals in arc-related magmatic hydrothermal ore fluids. *Nat. Geosci.* **3**, 501–505 (2010).

21. Larocque, A. C. L., Stimac, J. A., Keith, J. D. & Huminicki, M. A. E. Evidence for open-system behavior in immiscible Fe–S–O liquids in silicate magmas: implications for contributions of metals and sulfur to ore-forming fluids. *Can. Mineral.* **38**, 1233–1249 (2000).

22. Halter, W. E., Heinrich, C. A. & Pettke, T. Magma evolution and the formation of porphyry Cu–Au ore fluids: evidence from silicate and sulfide melt inclusions. *Miner. Depos.* **39**, 845–863 (2005).

23. Nomikou, P., Hübscher, C. & Carey, S. The Christiana–Santorini–Kolumbo Volcanic Field. *Elem. An Int. Mag. Mineral. Geochemistry, Petrol.* **15**, 171–176 (2019).

24. Druitt, T. H. *et al.* Santorini volcano. *Geol. Soc. Mem.* **19**, (1999).

25. Barton, M. & Huijsmans, J. P. P. Post-caldera dacites from the Santorini volcanic complex, Aegean Sea, Greece: an example of the eruption of lavas of near-constant composition over a 2,200 year period. *Contrib. to Mineral. Petrol.* **94**, 472–495 (1986).

26. Fouqué, F. *Santorin et ses éruptions*. (G. Masson, 1879).

27. Klaver, M. *et al.* A distinct source and differentiation history for Kolumbo submarine volcano, Santorini volcanic field, Aegean arc. *Geochemistry, Geophys. Geosystems* **17**, 3254–3273 (2016).

28. Dimitriadis, I. *et al.* Seismicity and active tectonics at Coloumbo Reef (Aegean Sea, Greece): Monitoring an active volcano at Santorini Volcanic Center using a temporary seismic network. *Tectonophysics* **465**, 136–149 (2009).

29. Patten, C. G. C., Barnes, S.-J. & Mathez, E. A. Textural variations in morb sulfide droplets due to differences in crystallization history. *Can. Mineral.* **50**, 675–692 (2012).

30. Peach, C. L., Mathez, E. A. & Keays, R. R. Sulfide melt-silicate melt distribution coefficients for noble metals and other chalcophile elements as deduced from MORB: Implications for partial melting. *Geochim. Cosmochim. Acta* **54**, 3379–3389 (1990).

31. Stavast, W. J. A. *et al.* The fate of magmatic sulfides during intrusion or eruption, Bingham and Tintic districts, Utah. *Econ. Geol.* **101**, 329–345 (2006).

32. Patten, C. G. C., Barnes, S.-J., Mathez, E. A. & Jenner, F. E. Partition coefficients of chalcophile elements between sulfide and silicate melts and the early crystallization history of sulfide liquid: LA-ICP-MS analysis of MORB sulfide droplets. *Chem. Geol.* **358**, (2013).

33. Keith, M., Haase, K. M., Klemd, R., Schwarz-Schampera, U. & Franke, H. Systematic variations in magmatic sulphide chemistry from mid-ocean ridges, back-arc basins and island arcs. *Chem. Geol.* **451**, 67–77 (2017).

34. Zelenski, M. *et al.* Platinum-group elements and gold in sulfide melts from modern arc basalt (Tolbachik volcano, Kamchatka). *Lithos* **290**, 172–188 (2017).

35. Fulignati, P. *et al.* Magmatic sulfide immiscibility at an active magmatic-hydrothermal system: The case of La Fossa (Vulcano, Italy). *J. Volcanol. Geotherm. Res.* **358**, 45–57 (2018).

36. Dare, S. A. S. *et al.* Trace elements in magnetite as petrogenetic indicators. *Miner. Depos.* **49**, 785–796 (2014).

37. Dare, S. A. S., Barnes, S. J. & Beaudoin, G. Variation in trace element content of magnetite crystallized from a fractionating sulfide liquid, Sudbury, Canada: Implications for provenance discrimination. *Geochim. Cosmochim. Acta* **88**, 27–50 (2012).

38. Cantner, K., Carey, S. & Nomikou, P. Integrated volcanologic and petrologic analysis of the 1650 AD eruption of Kolumbo submarine volcano, Greece. *J. Volcanol. Geotherm. Res.* **269**, 28–43 (2014).

39. Browning, J., Drymoni, K. & Gudmundsson, A. Forecasting magma-chamber rupture at Santorini volcano, Greece. *Sci. Rep.* **5**, 1–8 (2015).

40. Druitt, T. H., Pyle, D. M. & Mather, T. A. Santorini volcano and its plumbing system. *Elem. An Int. Mag. Mineral. Geochemistry, Petrol.* **15**, 177–184 (2019).

41. Martin, V. M., Holness, M. B. & Pyle, D. M. Textural analysis of magmatic enclaves from the Kameni Islands, Santorini, Greece. *J. Volcanol. Geotherm. Res.* **154**, 89–102 (2006).

42. Higgins, M. D., Debecq, A., Vander Auwera, J. & Nomikou, P. Chemical and textural diversity of Kameni (Greece) dacites: role of vesiculation in juvenile and mature basal crystal masses. *Contrib. to Mineral. Petrol.* **176**, 1–20 (2021).

43. Rizzo, A. L. *et al.* New mafic magma refilling a quiescent volcano: Evidence from He-Ne-Ar isotopes during the 2011–2012 unrest at Santorini, Greece. *Geochemistry, Geophys. Geosystems* **16**, 798–814 (2015).

44. Michaud, V., Clocchiatti, R. & Sbrana, S. The Minoan and post-Minoan eruptions , Santorini (Greece), in the light of melt inclusions : chlorine and sulphur behaviour. *J. Volcanol. Geotherm. Res.* **99**, 195–214 (2000).

45. Konstantinou, K. I. Magma chamber evolution during the 1650 AD Kolumbo eruption provides clues about past and future volcanic activity. *Sci. Rep.* **10**, 1–12 (2020).

46. Thomas, N., Tait, S. & Koyaguchi, T. Mixing of stratified liquids by the motion of gas bubbles: application to magma mixing. *Earth Planet. Sci. Lett.* **115**, 161–175 (1993).

47. Plail, M. *et al.* Mafic enclaves record syn-eruptive basalt intrusion and mixing. *Earth Planet. Sci. Lett.* **484**, 30–40 (2018).

48. Edmonds, M. & Woods, A. W. Exsolved volatiles in magma reservoirs. *J. Volcanol. Geotherm. Res.* **368**, 13–30 (2018).

49. Edmonds, M., Brett, A., Herd, R. A., Humphreys, M. C. S. & Woods, A. Magnetite-bubble aggregates at mixing interfaces in andesite magma bodies. *Geol. Soc. London, Spec. Publ.* **410**, 95–121 (2015).

50. Lesher, C. E. & Spera, F. J. Thermodynamic and transport properties of silicate melts and magma. in *The encyclopedia of volcanoes* 113–141 (Elsevier, 2015).

51. Ebel, D. S. & Naldrett, A. J. Crystallization of sulfide liquids and the interpretation of ore

composition. *Can. J. Earth Sci.* **34**, 352–365 (1997).

52. Putnis, A. Fluid–Mineral Interactions: Controlling Coupled Mechanisms of Reaction, Mass Transfer and Deformation. *J. Petrol.* **62**, egab092 (2021).

53. Mountain, B. W. & Seward, T. M. Hydrosulfide/sulfide complexes of copper (I): experimental confirmation of the stoichiometry and stability of Cu (HS) 2− to elevated temperatures. *Geochim. Cosmochim. Acta* **67**, 3005–3014 (2003).

54. Seo, J. H., Guillong, M. & Heinrich, C. A. The role of sulfur in the formation of magmatic–hydrothermal copper–gold deposits. *Earth Planet. Sci. Lett.* **282**, 323–328 (2009).

55. Pokrovski, G. S., Borisova, A. Y. & Harrichoury, J.-C. The effect of sulfur on vapor–liquid fractionation of metals in hydrothermal systems. *Earth Planet. Sci. Lett.* **266**, 345–362 (2008).

56. Polacci, M., Baker, D. R., Bai, L. & Mancini, L. Large vesicles record pathways of degassing at basaltic volcanoes. *Bull. Volcanol.* **70**, 1023–1029 (2008).

57. Keith, J. D. *et al.* The role of magmatic sulfides and mafic alkaline magmas in the Bingham and Tintic mining districts, Utah. *J. Petrol.* **38**, 1679–1690 (1997).

58. Lambert, G., Le Cloarec, M. F., Ardouin, B. & Le Roulley, J. C. Volcanic emission of radionuclides and magma dynamics. *Earth Planet. Sci. Lett.* **76**, 185–192 (1985).

59. Kilias, S. P. *et al.* New insights into hydrothermal vent processes in the unique shallow-submarine arc-volcano, Kolumbo (Santorini), Greece. *Sci. Rep.* **3**, 2421 (2013).

60. André-Mayer, A.-S. *et al.* Boiling and vertical mineralization zoning: a case study from the Apacheta low-sulfidation epithermal gold-silver deposit, southern Peru. *Miner. Depos.* **37**, 452–464 (2002).

61. Williams-Jones, A. E. & Heinrich, C. A. 100th Anniversary special paper: vapor transport of metals and the formation of magmatic-hydrothermal ore deposits. *Econ. Geol.* **100**, 1287–1312 (2005).

62. Grosche, A. *et al.* Sources, transport, and deposition of metal (loid) s recorded by sulfide and rock geochemistry: constraints from a vertical profile through the epithermal Profitis Ilias Au prospect, Milos Island, Greece. *Miner. Depos.* 1–22 (2023).

63. Nomikou, P. *et al.* SANTORY: SANTORini's Seafloor Volcanic ObservatorY. *Front. Mar. Sci.* 421 (2022). doi:https://doi.org/10.3389/fmars.2022.796376

64. Ulrich, M. *et al.* Dissolution–precipitation processes governing the carbonation and silicification of the serpentinite sole of the New Caledonia ophiolite. *Contrib. to Mineral. Petrol.* **167**, 1–19 (2014).

65. Paton, C., Hellstrom, J., Paul, B., Woodhead, J. & Hergt, J. Iolite: Freeware for the visualisation and processing of mass spectrometric data. *J. Anal. At. Spectrom.* **26**, 2508–2518 (2011).

Acknowledgements

This project was funded by the DFG SPP program DOME grant PA 3523/2-1 and the DFG grant INST 121384/213-1 FUGG.

Author contributions

C.G.C.P., S.P.K. and J.K. conceived the project, C.G.C.P., S.H., A.P., S.P.K. and P.N. participated in field sampling, M.U. performed μXRF analyses, A.B. performed LA-ICP-MS analyses, E.E. assisted with laboratory support, C.G.C.P and S.H. wrote the manuscript, all authors participated in manuscript editing.

Competing interests

The authors declare no competing interests.

Correspondence

Correspondence should be addressed to C.G.C. Patten.

Transfer of sulfur and chalcophile metals via sulfide-volatile compound drops in the Christiana-Santorini-Kolumbo volcanic field

Supplementary Discussion

Comparison between sulfide bleb and sulfide ovoid compositions

The magmatic sulfide bleb composition is assumed to be representative of the primary magmatic sulfide liquid while the pyrrhotite and chalcopyrite analyzed in the ovoids are representative of differentiated sulfide phases such as MSS and ISS[1,2]. Direct comparison between the sulfide bleb and the sulfide ovoid composition is not possible and a primary magmatic sulfide composition needs to be calculated:

$$C_{x\,sulf} = C_{x\,Po} * X_{Po} + C_{x\,Cpy} * X_{Cpy} + C_{x\,SMag} * X_{SMag} \quad \text{(S1)}$$

with $C_{x\,Po}$, $C_{x\,Cpy}$ and $C_{x\,SMag}$ the concentration of the element *x* in the pyrrhotite, chalcopyrite and magnetite which have crystallized from the initial magmatic sulfide liquid and X_{Po}, X_{Cpy} and X_{SMag} the fraction of pyrrhotite, chalcopyrite and magnetite which have crystallized from the magmatic sulfide liquid. The pyrrhotite and chalcopyrite concentrations are from the analysis of ovoids (this study) while the magnetite concentrations are from Dare et al.[3] (sample MRC11). Magnetite crystallization from a sulfide liquid is common[1–4] and needs to be taken into account for the calculations. Trace element data of magnetites which crystallized from a sulfide liquid are scarce and the data from Dare et al.[3], although from a radically different magmatic environment, are the closest proxy found for the CSK system. The primary magmatic sulfide liquid is calculated assuming different fractions of pyrrhotite (0.85-0.55), chalcopyrite (0.1-0.4) and magnetite (0.05; Fig. 1).

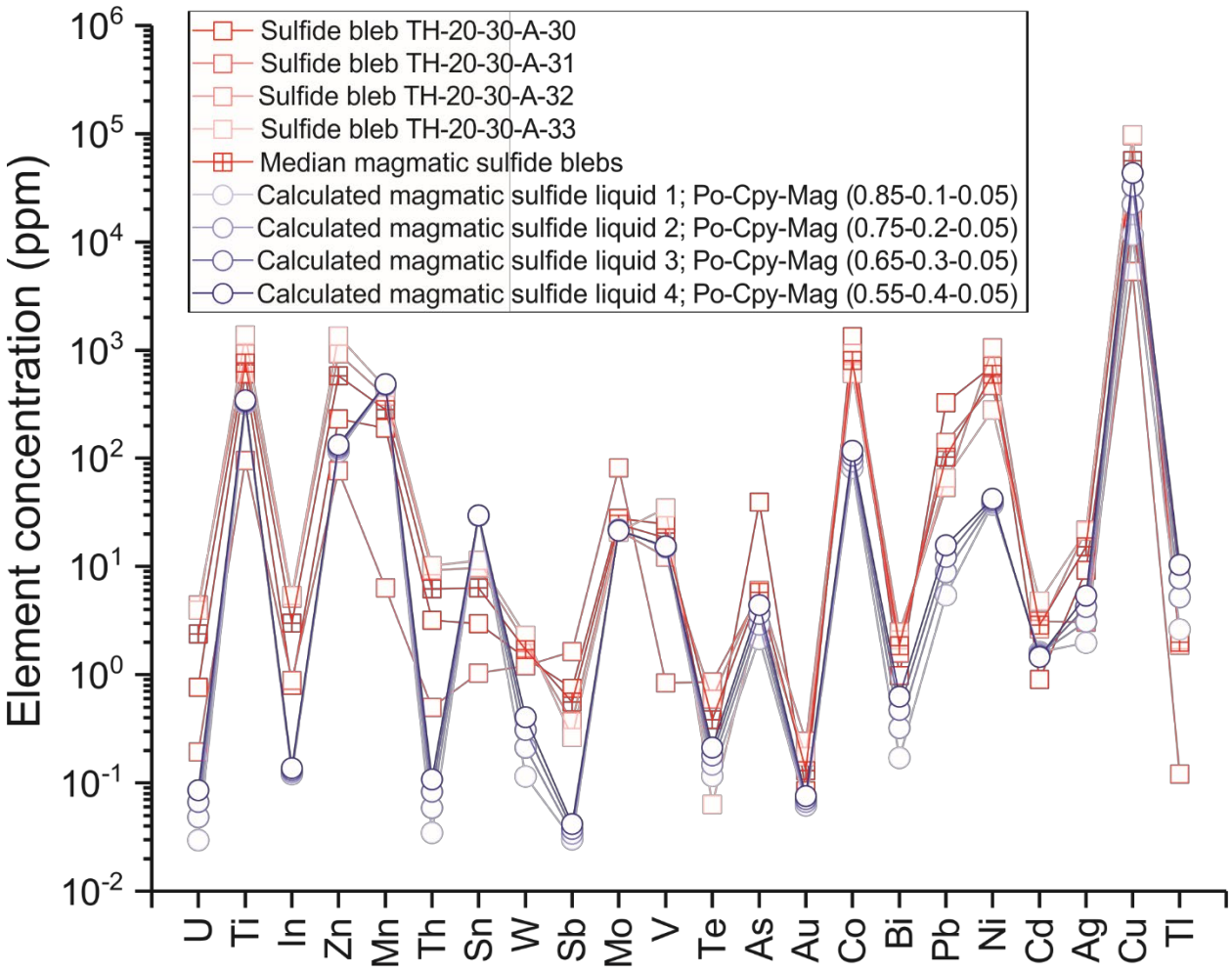

Figure 1.Comparison of trace metal composition of magmatic sulfide blebs and recalculated magmatic sulfide liquid with different proportions of pyrrhotite, chalcopyrite and magnetite.

The calculated primary magmatic compositions and the magmatic blebs have very similar element concentrations and profiles despite some differences for a few elements (U, In, Th and Sb). The overall good correlation between the two groups highlights the genetic link between the magmatic sulfide blebs and the sulfide ovoids.

Calculation of emanation coefficients

The emanation coefficients [5,6], although developed for melts and post-eruptive lavas, can be applied to the compound drop system and are defined as:

$$\varepsilon_{x\,sulf-mag} = (C_{x\,sulf} - \frac{M_{mag}}{3*M_{sulf}} * C_{x\,mag})/C_{x\,sulf} * 100 \quad \text{(S2)}$$

The calculation of the emanation coefficients requires to characterize the concentration of any given element *x* within the whole primary magmatic sulfides as define in the equation (S1). The molar mass of the primary magmatic sulfide is defined as:

$$M_{sulf} = M_{Po} * X_{Po} + M_{Cpy} * X_{Cpy} + M_{SMag} * X_{SMag} \quad \text{(S3)}$$

with M_{Po}, M_{Cpy} and M_{SMag} the density of pyrrhotite, chalcopyrite and magnetite which has crystallized from the sulfide liquid.

The emanation coefficients are then expressed as:

$$\varepsilon_{x\ sulf-mag} = \frac{((C_{x\ Po} * X_{Po} + C_{x\ Cpy} * X_{Cpy} + C_{x\ SMag} * X_{SMag}) - \frac{M_{Mag}}{3*(M_{Po} * X_{Po} + M_{Cpy} * X_{Cpy} + M_{SMag} * X_{SMag})} * C_{x\ Mag})}{(C_{x\ Po} * X_{Po} + C_{x\ Cpy} * X_{Cpy} + C_{x\ SMag} * X_{SMag})} * 100 \quad \text{(S4)}$$

It is important to emphasise that the $C_{x\ Mag}$ and M_{Mag} are the element concentration and the molar mass of the magnetite replacing the magmatic sulfides after oxidation while $C_{x\ SMag}$, M_{SMag} and X_{SMag} are the element concentration, the molar mass and the fraction of the magnetite which crystallizes from the sulfide liquid during sulfide liquid differentiation. Some element analyses in magnetite and pyrrhotite show concentrations below the limit of detection (see Supplementary Table 5). These data are not discarded as they yield important information on element distribution within the sulfide-volatile compound drops. Half the values of the limit of detections are used for the calculations as they are likely more representative of the true concentrations than the limit of detections. The emanation coefficients are calculated for variable fractions of pyrrhotite, chalcopyrite and magnetite in the primary magmatic sulfides and are presented in the Supplementary table 3 and Fig. 2c. Importantly, the emanation coefficients can have negative values, because the compound-drop system is not a closed system and can interact with the silicate melt. Elements compatible in magnetite can partition into the magnetite from the silicate melt during sulfide oxidation; on the other hand, strongly chalcophile and volatile elements are not considered to partition into the magnetite.

Supplementary Figures

Supplementary figure 1

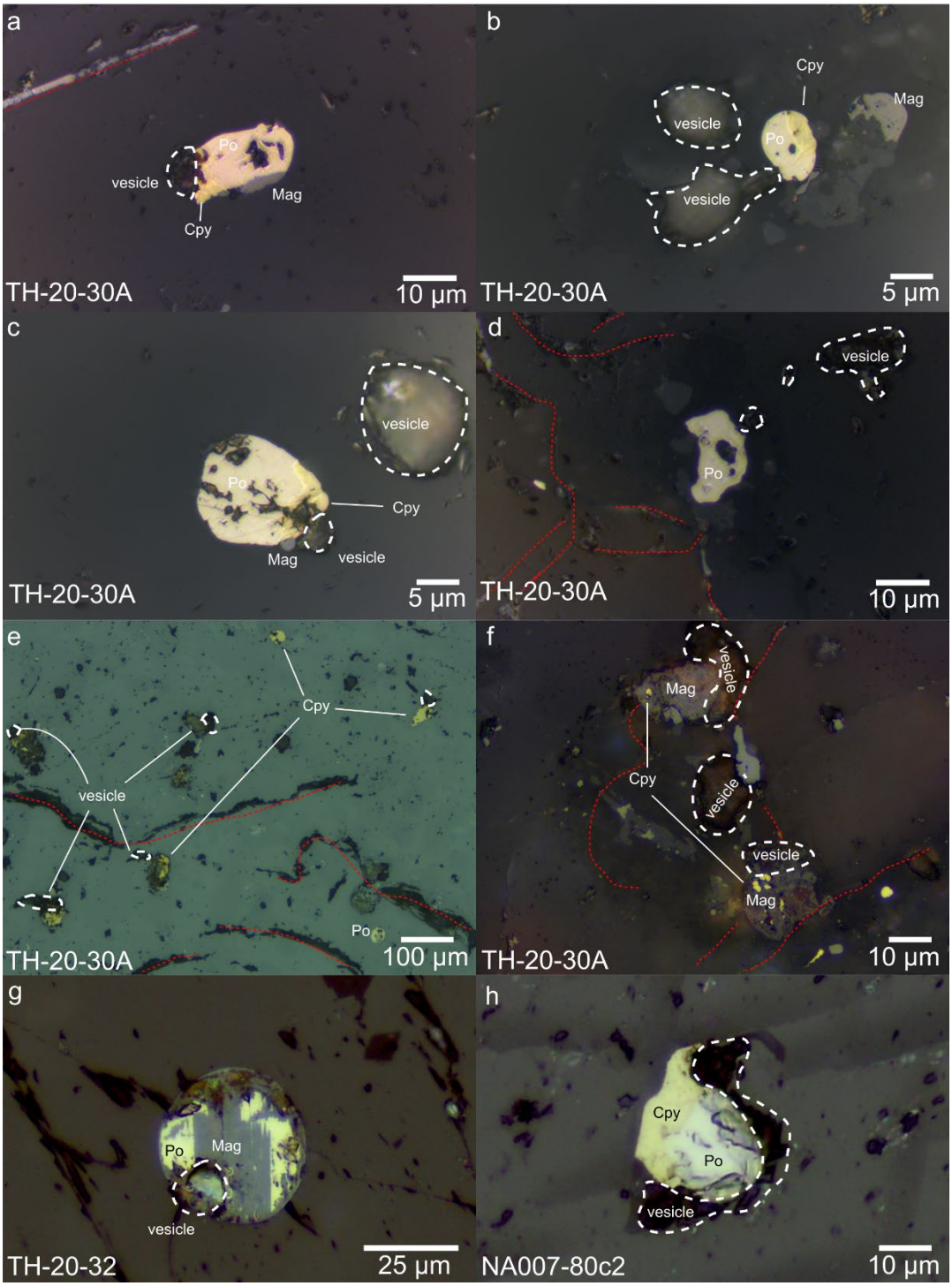

Supplementary figure 1. Magmatic sulfide blebs and associated vesicles in plagioclase phenocrysts within andesitic enclaves. a-b-c-d-h) Fresh magmatic sulfide blebs composed of pyrrhotite (Po), chalcopyrite (Cpy) and minor magnetite (Mag) associated with vesicles. e) Fresh and altered sulfide blebs. f-g) Extensively and partially oxidized magmatic sulfide blebs replaced by magnetite. Vesicles can still be observed. Red dot lines are fractures .

Supplementary figure 2

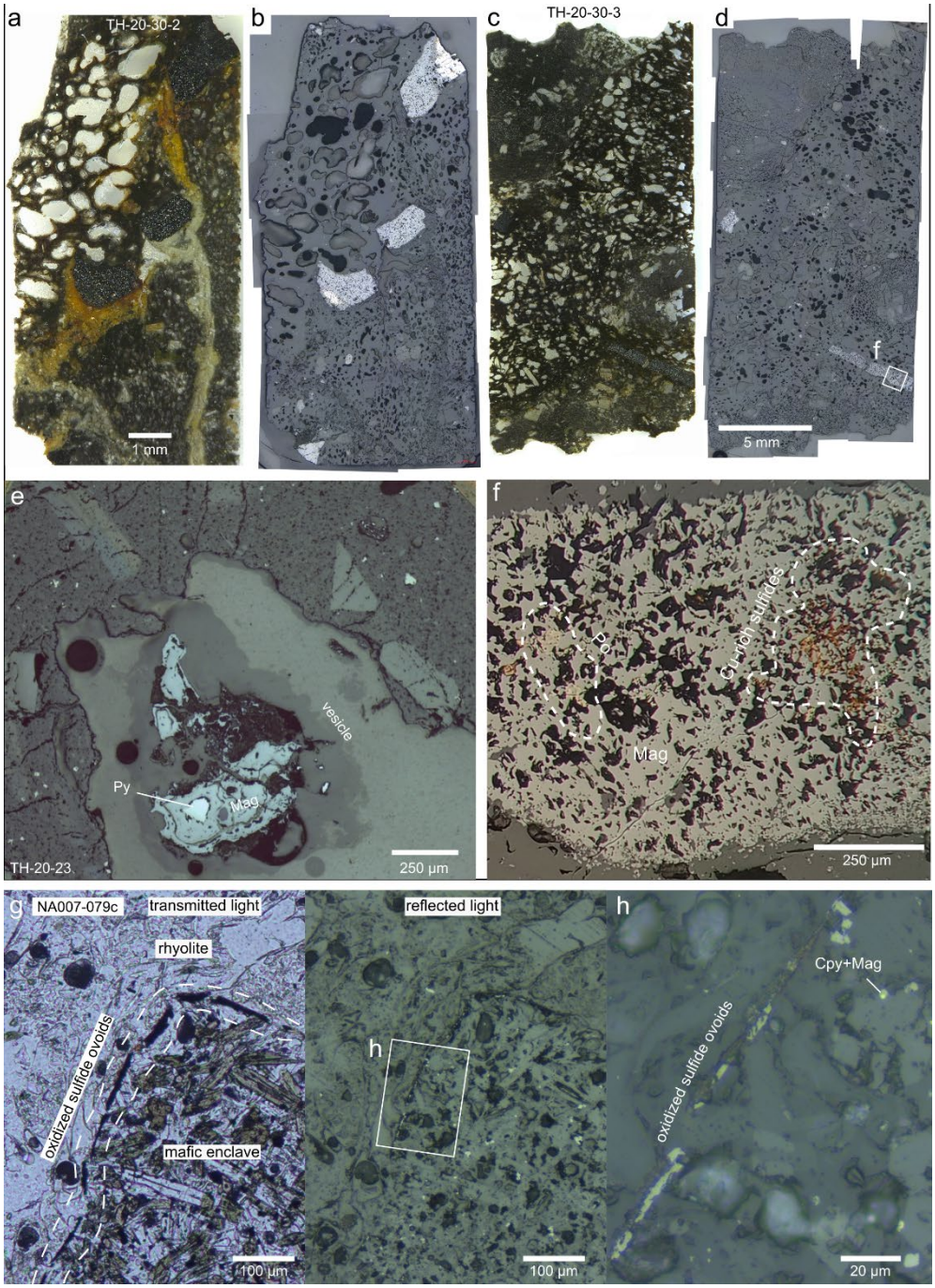

Supplementary figure 2: Overview of variably oxidized sulfide ovoids from Kameni volcanic rocks. a) and c) polished thin section scans showing the andesitic and dacitic melts transition zone. b) and d) reflected light mosaics showing the position of the variably oxidized ovoids. e) Fully oxidized sulfide ovoids within large vesicles. Discrete pyrite is preserved in the core. f) Detail from d) showing preserved interstitial pyrrhotite (Po) and chalcopyrite (Cpy) within porous magnetite (Mag). g) Fine lining of oxidized sulfide ovoid at a mafic-rhyolite interface from the Kameni volcano observed in transmitted and reflected light. h) close up of the oxidized sulfide ovoids at the enclave margin. In the enclave micrometric magmatic sulfides (Po and Cpy) and magnetites are ubiquitous.

Supplementary figure 3

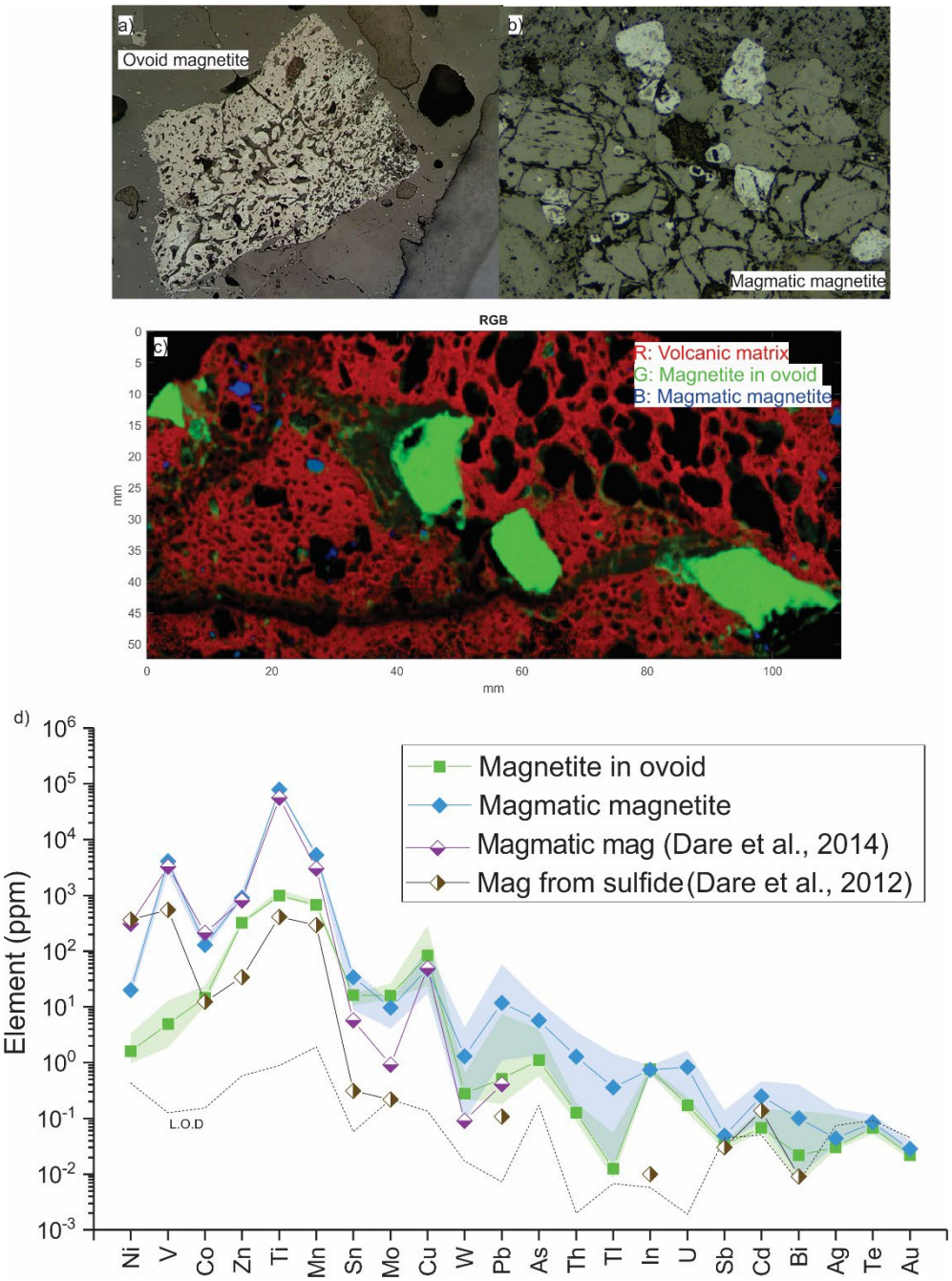

Supplementary figure 3. Different type of magnetites present in the CSK. a) Magnetite related to sulfide ovoid, b) magmatic magnetite found in mafic enclaves, c) micro-XRF map showing spatial relationship between the two magnetite types, magnetites related to the sulfide ovoids (a) are in green and the magmatic magnetite (b) are in blue, and d) Median trace element concentrations of magnetite in ovoids and magmatic magnetites. Shaded areas represent upper and lower quartile. Magmatic magnetite have similar metal concentrations than magmatic magnetite crystallized from a silicate melt[8]. Ovoid magnetite show distinctive metal concentrations from both magmatic magnetite crystallized either from a silicate melt or a sulfide melt.

Supplementary figure 4

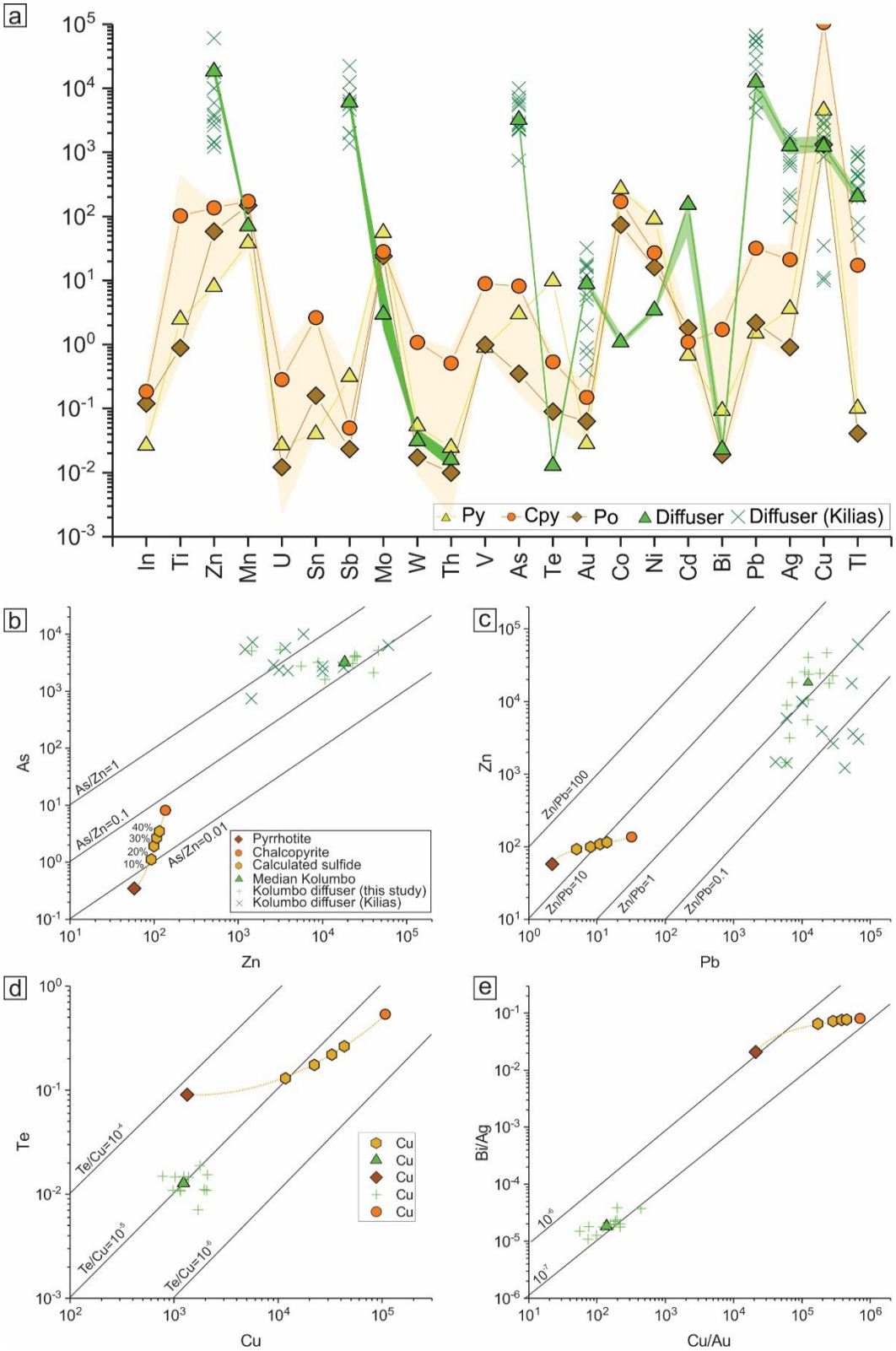

Supplementary figure 4: Comparison of metal content in magmatic sulfides and mineralized samples from Kolumbo diffusers. a) bulk metal content, b) Zn vs As, b) Pb vs Zn, c) Cu vs Te and d) Cu/Au vs Bi/Ag. Despite the different metal endowment between the magmatic sulfides and the diffusers metal pairs of same affinity show similar ratios. Kolumbo diffuser data are from Kilias et al.[59] and from this study (see Supplementary Table 6).

Supplementary figure 5

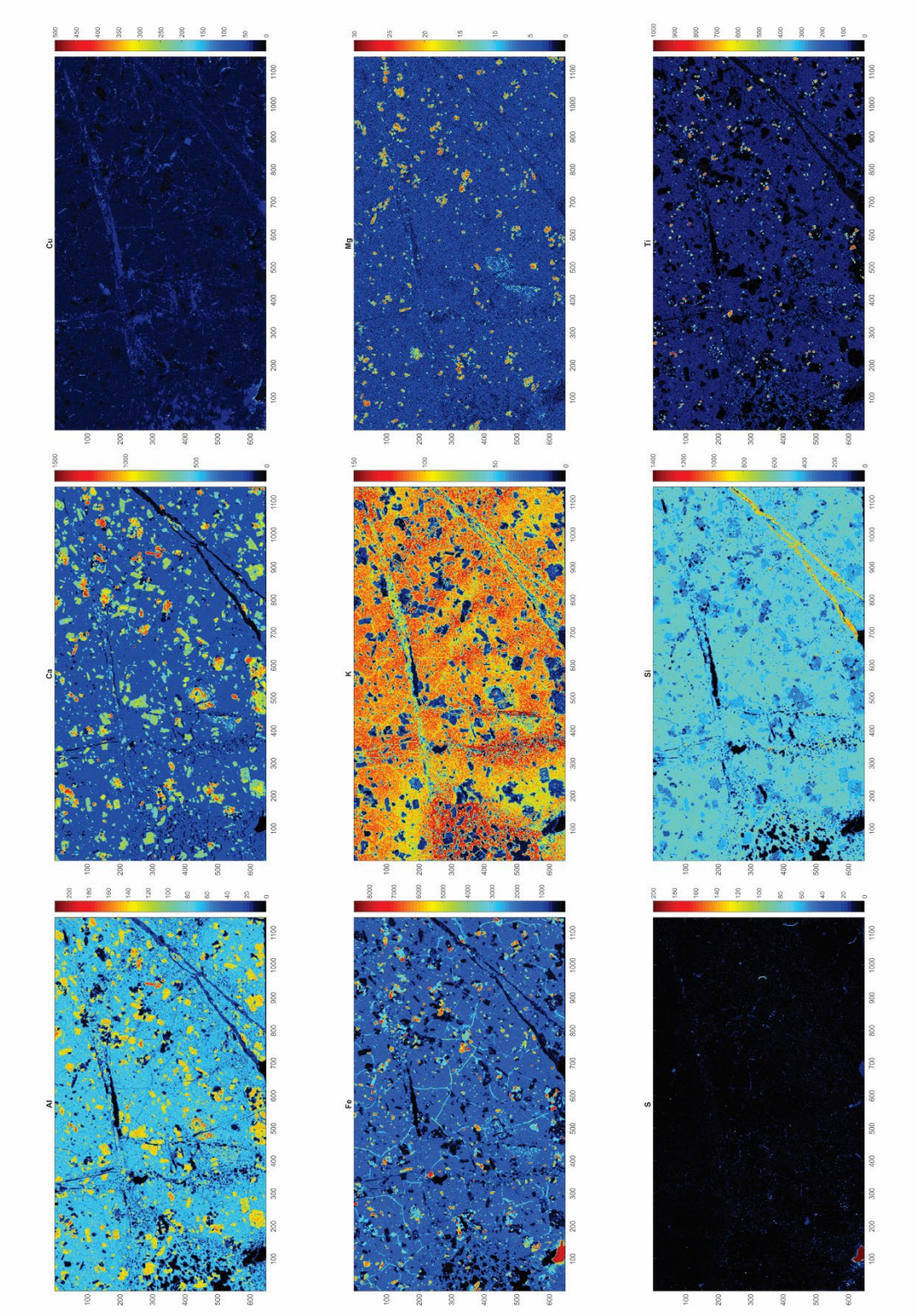

Supplementary figure 5a. Chemical maps of Al, Ca, Cu, Fe, K, Mg, S, Si and Ti from sample TH-20-30-A used for calculation of phase proportions by selecting regions of interests. The scales are absolute counts.

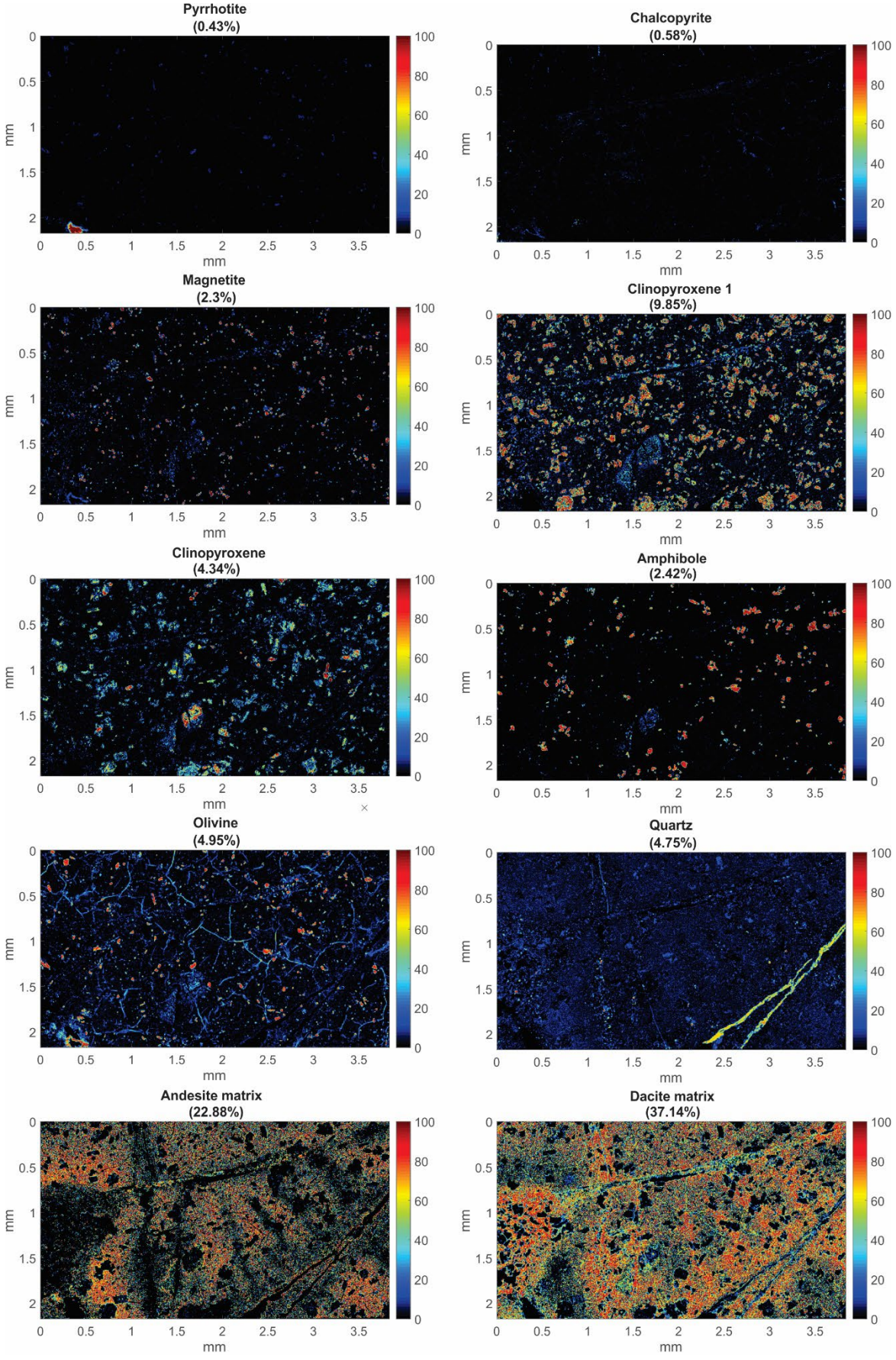
Pyrrhotite
(0.43%)
Chalcopyrite
(0.58%)
Magnetite
(2.3%)
Clinopyroxene 1
(9.85%)
Clinopyroxene
(4.34%)
Amphibole
(2.42%)
Olivine
(4.95%)
Quartz
(4.75%)
Andesite matrix
(22.88%)
Dacite matrix
(37.14%)
mm
0 0.5 1 1.5 2 2.5 3 3.5
0 20 40 60 80 100

92

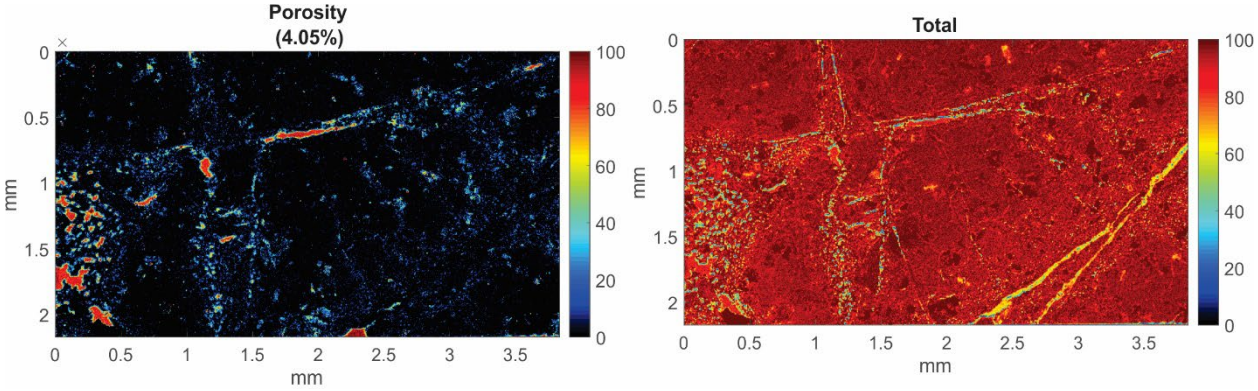

Supplementary figure 5b. Mineral proportion maps calculated from elemental maps for sample TH-20-30-A. Ten phases are recognized in maps plus the porosity. The scale represents the percent of the specific phase at each spot analysis while the percent value below the phase name corresponds to the total phase fraction in the map.

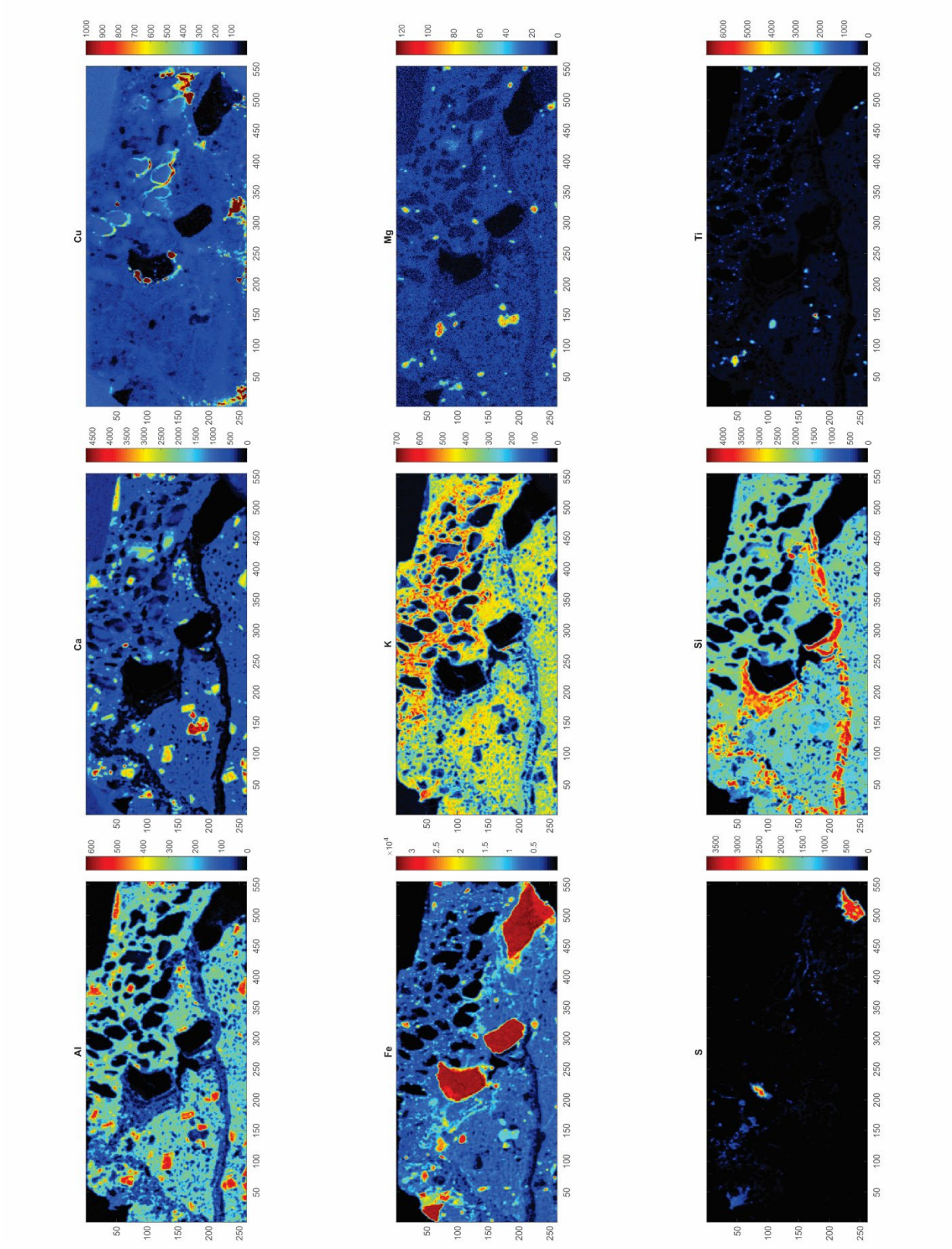

Supplementary figure 5c. Chemical maps of Al, Ca, Cu, Fe, K, Mg, S, Si and Ti from sample TH-20-30-2 used for calculation of phase proportions by selecting regions of interests. The scales are absolute counts.

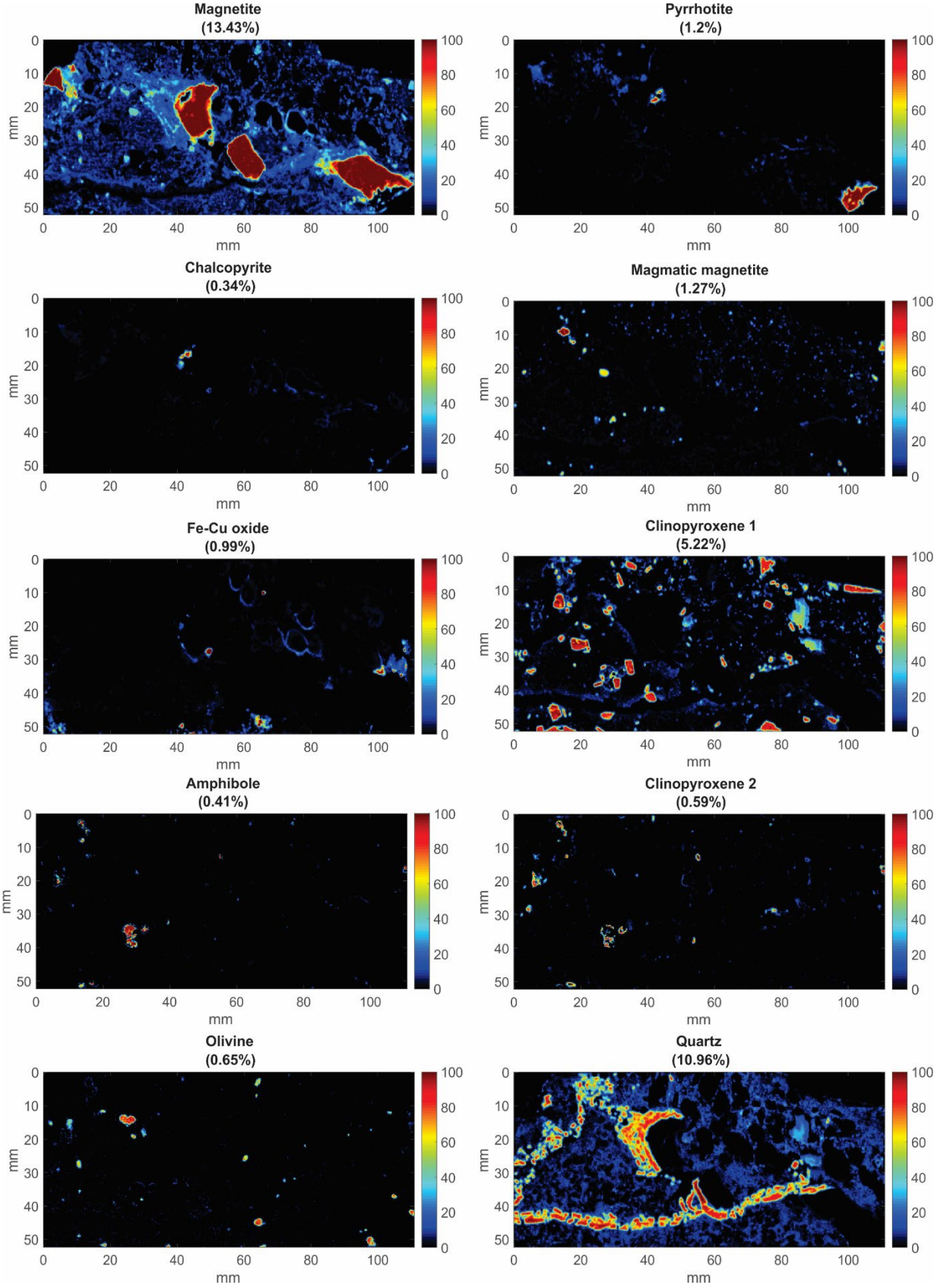
Magnetite
(13.43%)
Pyrrhotite
(1.2%)
Chalcopyrite
(0.34%)
Magmatic magnetite
(1.27%)
Fe-Cu oxide
(0.99%)
Clinopyroxene 1
(5.22%)
Amphibole
(0.41%)
Clinopyroxene 2
(0.59%)
Olivine
(0.65%)
Quartz
(10.96%)
mm
0
10
20
30
40
50
0
20
40
60
80
100
0
20
40
60
80
100

100

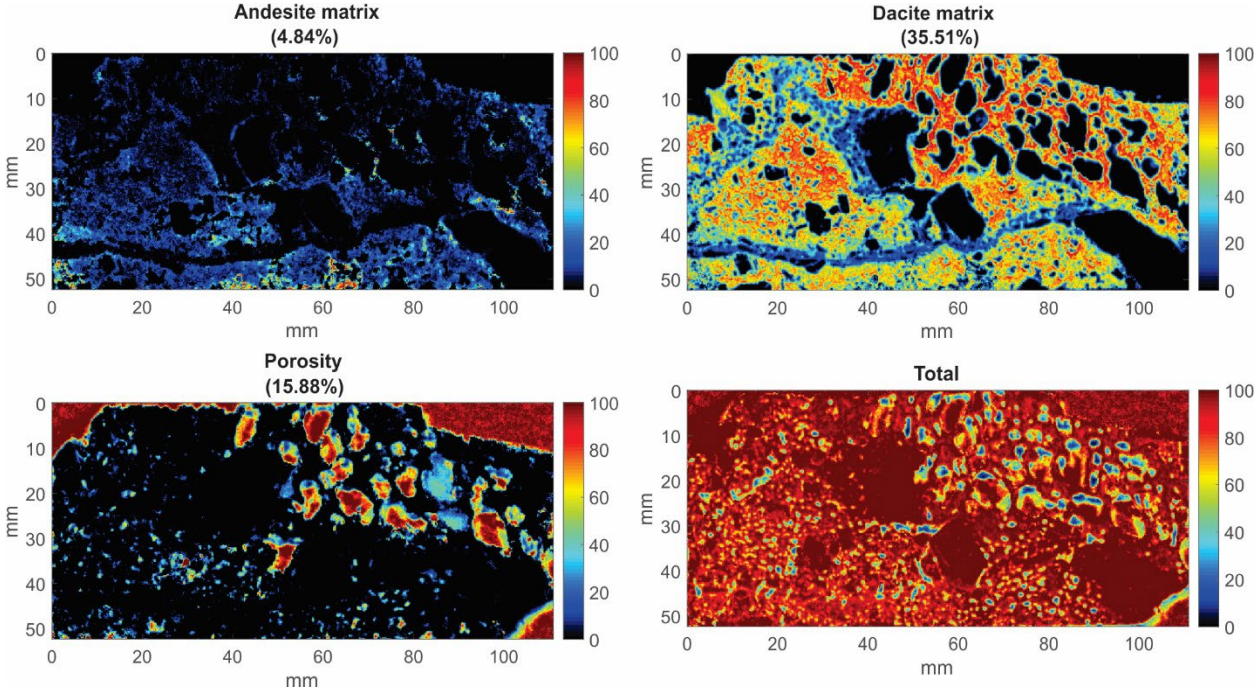

Supplementary figure 5d. Mineral proportion maps calculated from elemental maps for sample TH-20-30-2. Thirteen phases are recognized in maps plus the porosity. The scales represent the percent of the specific phase at each spot analysis while the percent value below the phase corresponds to the total phase fraction in the map.

References

1. Peach, C. L., Mathez, E. A. & Keays, R. R. Sulfide melt-silicate melt distribution coefficients for noble metals and other chalcophile elements as deduced from MORB: Implications for partial melting. *Geochim. Cosmochim. Acta* **54**, 3379–3389 (1990).

2. Patten, C. G. C., Barnes, S.-J. & Mathez, E. A. Textural variations in morb sulfide droplets due to differences in crystallization history. *Can. Mineral.* **50**, 675–692 (2012).

3. Dare, S. A. S., Barnes, S. J. & Beaudoin, G. Variation in trace element content of magnetite crystallized from a fractionating sulfide liquid, Sudbury, Canada: Implications for provenance discrimination. *Geochim. Cosmochim. Acta* **88**, 27–50 (2012).

4. Czamanske, G. K. & Moore, J. G. Composition and phase chemistry of sulfide globules in basalt from the Mid-Atlantic Ridge rift valley near 37 N lat. *Geol. Soc. Am. Bull.* **88**, 587–599 (1977).

5. Edmonds, M., Mather, T. A. & Liu, E. J. A distinct metal fingerprint in arc volcanic emissions. *Nat. Geosci.* **11**, 790–794 (2018).

6. Lambert, G., Le Cloarec, M. F., Ardouin, B. & Le Roulley, J. C. Volcanic emission of radionuclides and magma dynamics. *Earth Planet. Sci. Lett.* **76**, 185–192 (1985).

7. Guo, H. & Audétat, A. Transfer of volatiles and metals from mafic to felsic magmas in composite magma chambers: an experimental study. *Geochim. Cosmochim. Acta* **198**, 360–378 (2017).

8. Dare, S. A. S. *et al.* Trace elements in magnetite as petrogenetic indicators. *Miner. Depos.* **49**, 785–796 (2014).

Supplementary data

Supplementary table 1. Major element concentration of samples hosting sulfides and oxides related to compound drops

Sample	Locality	unit	coordinates	Na2O (%)	MgO (%)	Al2O3 (%)	SiO2 (%)	P2O5 (%)
NA007-079c	Nea Kameni	Pumice (K2)	36.31357N 25.29659E	4,33	0,30	12,46	70,00	0,03
NA007-080c-2	Nea Kameni	Lava (K5)	36.31493N 25.29760E	3,02	3,69	17,72	54,78	0,15
NA007-100b-2A	Nea Kameni	Pumice (K5)	36.31742N 25.28602E	4,31	0,37	12,59	70,24	0,03
TH-20-17	Nea Kameni	1950 lava flow	36.40375N 25.39736E	4,98	1,55	15,48	64,89	0,19
TH-20-23-host rock	Nea Kameni	1940-1941 lava flow	36.40583N 25.39705E	5,05	1,41	15,96	67,00	0,20
TH-20-30-enclave	Nea Kameni	1939-1940 lava flow	36.40647N 25.39771E	4,46	1,77	15,88	62,29	0,17
TH-20-30-host rock	Kolumbo	1939-1940 lava flow	36.40647N 25.39771E	5,00	1,40	15,51	65,18	0,19
TH-20-32	Kolumbo	1939-1940 lava flow	36.40632N 25.39696E	4,95	1,40	15,37	64,40	0,19
TH-20-35	Kolumbo	1939-1940 lava flow	36.40725N 25.39651E	5,01	1,41	15,56	65,02	0,19

Sample	K2O (%)	CaO (%)	TiO2 (%)	MnO (%)	Fe2O3 (%)	BaO(%)	Cr2O3 (%)	LOI (wt%)	SUM
NA007-079c	3,68	1,12	0,11	0,08	1,75	0,03	0,00	5,99	99,89
NA007-080c-2	1,52	8,17	0,79	0,10	6,32	0,03	0,01	2,60	98,97
NA007-100b-2A	3,71	1,22	0,11	0,08	1,70	0,03	0,01	4,83	99,24
TH-20-17	1,86	4,02	0,81	0,15	5,89	0,04	0,00	n.d.	99,87
TH-20-23-host rock	1,90	3,90	0,81	0,15	5,75	0,04	0,00	0,02	102,20
TH-20-30-enclave	1,81	4,74	0,75	0,13	6,99	0,04	0,00	0,16	99,22
TH-20-30-host rock	1,89	3,89	0,80	0,14	5,76	0,04	0,00	0,07	99,90
TH-20-32	1,90	3,90	0,80	0,15	5,68	0,04	0,00	0,08	98,89
TH-20-35	1,89	3,92	0,81	0,15	5,71	0,04	0,00	0,04	99,79

XRF analysis using a WDS Bruker AXS

Supplementary table 2. Sulfide and oxide trace element-revised concentrations

	Ti ppm	V ppm	Mn ppm	Fe* ppm	Co ppm	Ni ppm	Cu ppm	Zn ppm	As ppm	Mo ppm	Ag ppm	Cd ppm	In ppm	Sn ppm	Sb ppm	Te ppm	W ppm	Au ppm	Tl ppm	Pb ppm	Bi ppm	Th ppm	U ppm
Magmatic bleb inclusion																							
Magmatic bleb (n=4)																							
Median	762	18,3	374	434275**	798	595	56082	580,5	5,79	24,6	15,20	2,88	3,00	6,30	0,56	0,38	1,70	0,18	1,99	102	1,85	6,21	2,37
Lower quartile (25%)	474	9,2	282	382142**	650	424	13255	192,3	5,06	21,3	7,68	2,20	0,86	2,43	0,34	0,14	1,37	0,13	1,43	62	1,43	2,52	0,62
Upper quartile (75%)	1036	26,9	411	508250**	1033	801	96532	1034,0	14,41	41,1	21,31	3,54	5,18	10,1	0,96	0,66	2,05	0,21	3,92	186	2,20	9,47	4,09
Sulfide/oxide ovoid																							
Pyrrhotite (n=39)																							
Median	0,88	1,00	150	611000	73,80	16,10	1330	58	0,35	24,10	0,91	1,81	0,12	0,16	0,023	0,09	0,017	0,063	0,041	2,19	0,019	0,010	0,012
Lower quartile (25%)	0,50	0,79	112	601840	53,45	12,70	1187	50	0,17	20,10	0,58	1,56	0,11	0,13	0,018	0,05	0,009	0,043	0,024	1,20	0,013	0,002	0,002
Upper quartile (75%)	1,47	4,18	214	621713	84,15	27,90	1435	98	1,06	26,65	1,17	2,57	0,25	0,25	0,033	0,15	0,095	0,096	0,146	4,81	0,027	0,087	0,091
Pyrite (n=6)																							
Median	2,47	0,90	38	404100	268,50	90,75	4488	8	2,97	55,35	3,61	0,68	0,03	0,04	0,315	9,81	0,053	0,028	0,101	1,50	0,092	0,025	0,027
Lower quartile (25%)	2,00	0,79	28	404100	228,25	71,40	4070	7	2,52	49,38	3,09	0,55	0,02	0,04	0,278	9,30	0,041	0,025	0,091	1,28	0,088	0,020	0,023
Upper quartile (75%)	2,90	1,23	51	404100	332,75	110,78	4759	9	3,33	65,90	4,24	0,76	0,03	0,09	0,398	10,37	0,066	0,033	0,121	1,93	0,103	0,041	0,036
Partly oxidized chalcopyrite* (n=6)**																							
Median	102	8,95	173	543500	170,95	27,20	106448	136	8,23	28,2	21,27	1,10	0,19	2,64	0,05	0,54	1,08	0,15	17,4	31,9	1,73	0,51	0,29
Lower quartile (25%)	70	8,01	150	543500	122,13	25,60	75674	105	5,79	21,3	11,78	0,71	0,17	1,08	0,04	0,37	0,98	0,11	11,5	18,6	1,53	0,21	0,18
Upper quartile (75%)	446	9,1	213	543500	224,95	55,70	116711	163	8,28	34,1	35,61	1,34	0,23	3,57	0,07	0,79	1,30	0,26	30,6	37,0	5,49	0,89	0,82
Magnetite (n=60)																							
Median	990	4,93	680	725450	14,50	1,61	84	324	1,10	15,9	0,03	0,07	0,77	16,2	0,03	0,07	0,28	0,022	0,013	0,22	0,02	0,13	0,17
Lower quartile (25%)	924	1,84	619	718070	10,48	0,97	23	297	0,58	13,8	0,03	0,06	0,63	10,6	0,03	0,05	0,22	0,018	0,008	0,11	0,01	0,09	0,12
Upper quartile (75%)	1263	13,0	794	726310	23,65	3,34	291	353	3,94	26,3	0,15	0,14	0,82	17,5	0,04	0,08	0,64	0,027	0,055	2,57	0,13	0,19	0,24
Magmatic magnetite																							
Magnetite (n=43)																							
Median	78267	4076	5310	599790	128	20,00	48	905	5,74	9,66	0,06	0,24	0,73	34,1	0,05	0,08	1,31	0,03	0,36	11,7	0,10	1,29	0,83
Lower quartile (25%)	72519	2540	4752	582520	99	14,25	17	856	1,35	4,07	0,03	0,08	0,60	8,80	0,04	0,06	0,09	0,02	0,01	1,10	0,01	0,13	0,20
Upper quartile (75%)	83183	4512	6135	627840	168	28,75	115	1263	12,85	12,68	0,15	0,46	0,88	45,9	0,14	0,11	4,26	0,04	1,44	57,7	0,40	3,62	1,62

*Fe57 data from EMPA ** Fe internal standard for magmatic bleb is calculated from modal proportion of pyrrhotite, chalcopyrite and magnetite present in the magmatic sulfide blebs using equation (1) of the supplementary discussion and following Nadeau et al. (2010) approach. ***Partly oxidized chalcopyrite do not have stochiometric concentration and correspond locally to chalcopyrite-pyrite or covellite-pyrite mixture. Data below the limit of detection are not discarded but half of the detection limit value is used instead.

Supplementary table 3. Magmatic volatile-sulfide emanation coefficients

	Emanation coefficients (Ec)						
	U	Ti	In	Zn	Mn	Th	Sn
Po-Cpy-Mag (0.85-0.1-0.05)	-231,0	-345	-377	-165	-57	-60,8	18,5
Po-Cpy-Mag (0.75-0.2-0.05)	-77,4	-283	-313	-123	-42	20,3	26,9
Po-Cpy-Mag (0.65-0.3-0.05)	-15,5	-233	-262	-90	-30	49,7	33,8
Po-Cpy-Mag (0.55-0.4-0.05)	17,3	-193	-219	-64	-19	64,5	39,7

	Emanation coefficients (Ec)						
	W	Sb	Mo	V	Te	As	Au
Po-Cpy-Mag (0.85-0.1-0.05)	-68,6	6,8	49,3	36,8	62,3	26,1	76,4
Po-Cpy-Mag (0.75-0.2-0.05)	17,3	22,6	54,6	49,2	74,4	60,4	80,9
Po-Cpy-Mag (0.65-0.3-0.05)	48,0	34,7	58,9	58,3	81,2	74,2	84,2
Po-Cpy-Mag (0.55-0.4-0.05)	63,5	44,2	62,6	65,1	85,6	81,6	86,7

	Emanation coefficients (Ec)						
	Co	Bi	Pb	Ni	Cd	Ag	Cu
Po-Cpy-Mag (0.85-0.1-0.05)	86,5	92,0	96,7	93,3	97,1	99,2	99,5
Po-Cpy-Mag (0.75-0.2-0.05)	89,0	96,2	98,1	94,3	97,2	99,6	99,7
Po-Cpy-Mag (0.65-0.3-0.05)	90,9	97,6	98,7	95,0	97,3	99,7	99,8
Po-Cpy-Mag (0.55-0.4-0.05)	92,3	98,3	99,1	95,6	97,4	99,8	99,9

	Emanation coefficients (Ec)
	Tl
Po-Cpy-Mag (0.85-0.1-0.05)	99,5
Po-Cpy-Mag (0.75-0.2-0.05)	99,8
Po-Cpy-Mag (0.65-0.3-0.05)	99,8
Po-Cpy-Mag (0.55-0.4-0.05)	99,9

See Supplementary Discussion for emanation coefficient calculations

Supplementary table 4. LA-ICP-MS reference material concentrations

	Ti ppm	V ppm	Mn ppm	Co ppm	Ni ppm	Cu ppm	Zn ppm	As ppm	Mo ppm	Ag ppm	Cd ppm
FeS-1											
Average	310	16	55	610	23551	20691	173	1002	61	162,03	0,95
Standard deviation	65	1	4	17	782	764	43	52	2	8,95	0,28
Working values	*300*	*21*	*56*	*638*	*24956*	*22930*	*257*	*1078*	*65*	*169,00*	*<3*
Accuracy (%)	3	-32	-2	-5	-6	-11	-49	-8	-6	-4,30	
Precision (%)	21	9	8	3	3	4	25	5	3	5,52	29,12
FeS-5											
Average	15	18	870	525	24380	6965	1408	19	42	3,15	2,24
Standard deviation	4	1	254	43	1988	400	317	2	3	0,17	0,64
Working values	*16*	*25*	*992*	*543*	*25361*	*7724*	*1703*	*16*	*37*	*2,80*	*3,30*
Accuracy (%)	-4	-41	-14	-3	-4	-11	-21	12	12	11,17	-47,50
Precision (%)	27	6	29	8	8	6	23	13	6	5,51	28,47
PTC-1b											
Average	619	18	144	2382	82146	66287	1955	286	20	39,96	36,56
Standard deviation	96	3	18	207	5667	10145	389	199	2	3,03	6,07
Working values	*696*	*20*	*193*	*3253*	*112560*	*79700*	*2083*	*222*	*11*	*53,00*	*38,00*
Accuracy (%)	-12	-10	-34	-37	-37	-20	-7	22	45	-32,65	-3,93
Precision (%)	15	16	13	9	7	15	20	69	12	7,57	16,61
BCR-2											
Average	13967	424	1569	41	12	19	123	5,2	250,0	1,26	0,24
Standard deviation	202	9	24	2	0	2	7	0,8	5,3	0,08	0,04
Working values	*14100*	*425*	*1550*	*38*	*13*	*21*	*125*	*3,9*	*270,0*	*1,20*	*0,20*
Accuracy (%)	-1	0	1	8	-13	-12	-2	25,2	-8,0	4,81	16,57
Precision (%)	1	2	2	5	2	9	6	15,5	2,1	6,45	17,82
BHVO-2											
Average	16000	311	1373	49	114	112	96	3,75	4,14	0,25	B.D.L
Standard deviation	1258	16	43	3	6	29	19	0,86	0,40	0,03	0,03
Working values	*16300*	*308*	*1317*	*44*	*116*	*127*	*102*	*3,76*	*3,80*	*0,36*	*0,09*
Accuracy (%)	-2	1	4	10	-1	-13	-7	-0,13	8,15	-44,30	
Precision (%)	8	5	3	7	5	26	20	22,82	9,62	11,38	
BIR-1											
Average	6074	314	1363	57	164	114	76	0,72	0	0,11	0,12
Standard deviation	83	4	23	2	4	3	1	0,70	0	0,03	0,02
Working values	*6233*	*326*	*1471*	*52*	*178*	*119*	*78*	*0,70*	*0*	*0,19*	*0,14*
Accuracy (%)	-3	-4	-8	9	-8	-5	-3	3	-9	-71,40	-17,18
Precision (%)	1	1	2	4	3	2	1	97	40	22,65	18,74
Limit of detection*	0,88	0,13	1,91	0,15	0,43	0,13	0,59	0,17	0,22	0,07	0,05

*Limit of detections calculated from Iolite using the method from Petkke et al. (2012).

Pettke, T., Oberli, F., Audétat, A., Guillong, M., Simon, A. C., Hanley, J. J., & Klemm, L. M. (2012). Recent developments in element concentration and isotope ratio analysis of individual fluid inclusions by laser ablation single and multiple collector ICP-MS. Ore Geology Reviews, 44, 10-38.

Supplementary table 4

	In ppm	Sn ppm	Sb ppm	Te ppm	W ppm	Au ppm	Tl ppm	Pb ppm	Bi ppm	U ppm
FeS-1										
Average	8,76	168	86	142	1814	63,96	0,18	62,31	106,99	2,50
Standard deviation	0,46	14	10	6	248	6,56	0,02	4,91	17,80	0,33
Working values	*9,50*	*185*	*90*	*151*	*1085*	*66,20*	*0,30*	*91,10*	*119,60*	*2,70*
Accuracy (%)	-8,41	-10	-4	-6	40	-3,50	-68,67	-46,21	-11,79	-8,18
Precision (%)	5,30	8	11	4	14	10,25	10,16	7,88	16,63	13,36
FeS-5										
Average	0,77	97	21,00	2,09	9,03	96,69	3,83	12,95	748,34	0,21
Standard deviation	0,06	11	4,49	0,19	1,38	9,78	0,29	2,13	169,23	0,02
Working values	*0,90*	*112*	*18,60*	*2,20*	*9,90*	*91,50*	*4,20*	*23,20*	*807,50*	*0,20*
Accuracy (%)	-17,27	-16	11,44	-5,44	-9,60	5,37	-9,57	-79,17	-7,91	4,45
Precision (%)	7,27	11	21,39	9,24	15,25	10,12	7,65	16,47	22,61	11,81
PTC-1b										
Average	2,43	122	6,99	22,98	1,75	0,73	1,58	729,53	93,72	0,29
Standard deviation	0,19	10	1,55	1,39	0,25	0,15	0,39	101,41	17,44	0,05
Working values	*2,90*	*120*	*6,00*	*30,00*	*2,20*	*1,99*	*1,50*	*795,00*	*97,00*	
Accuracy (%)	-19,46	2	14,12	-30,57	-26,03	-172	4,87	-8,97	-3,51	
Precision (%)	7,70	8	22,24	6,05	14,59	21,09	24,99	13,90	18,61	
BCR-2										
Average	0,11	3,23	0,33	0,034	0,51	B.D.L	0,31	11,08	0,05	1,63
Standard deviation	0,01	0,09	0,04	0,043	0,02		0,01	0,22	0,01	0,06
Working values	*0,11*	*2,60*	*0,35*		*0,50*	*0,02*	*0,30*	*11,00*	*0,05*	*1,69*
Accuracy (%)	3,76	19,53	-4,49		1,09		2,10	0,71	4,37	-3,53
Precision (%)	6,91	2,80	10,46		3,05		4,58	1,97	23,30	3,73
BHVO-2										
Average	0,11	2,71	0,13	B.D.L	0,22	0,46	0,02	1,77	0,02	0,41
Standard deviation	0,01	0,14	0,02		0,03	0,03	0,01	0,11	0,01	0,02
Working values	*0,10*	*2,60*	*0,13*	*0,002*	*0,23*	*0,47*	*0,02*	*1,70*	*0,02*	*0,40*
Accuracy (%)	8,14	4,02	-3,98		-2,30	-2,30	13,58	3,99	1,69	0,64
Precision (%)	5,11	5,31	17,41		11,49	7,18	32,13	6,16	34,22	4,13
BIR-1										
Average	0,07	1,43	0,55	0,04	0,010	0,28	B.D.L	3,43	B.D.L	0,02
Standard deviation	0,00	0,06	0,02	0,03	0,008	0,02		0,09		0,00
Working values	*0,09*	*1,47*	*0,56*			*0,25*	*0,00*	*3,70*	*0,01*	*0,02*
Accuracy (%)	-21,17	-2,93	-2,20			10,45		-7,91		-4,77
Precision (%)	6,70	4,46	4,30			8,29		2,50		10,07
Limit of detection*	0,01	0,058	0,044	0,091	0,017	0,05	0,01	0,0073	0,0071	0,0019

*Limit of detections ca
Pettke, T., Oberli, F., A
in element concentrat
multiple collector ICP-M

Supplementary table 5. Single spot LA-ICP-MS analysis

Sample	Mineral phase	Ti			V			Mn			Fe			Co		
		concentration (ppm)	σ	LOD	concentration (ppm)	σ	LOD	concentration (ppm)	σ	LOD	concentration (ppm)	σ	LOD	concentration (ppm)	σ	LOD
079c-A-1	Pyrite	2,89	1,39	0,41	0,55	0,68	0,06	36,6	3,88	0,69	404100	0,00	6,23	341,00	32,4	0,06
079c-A-2	Pyrite	2,91	2,62	0,48	1,31	2,52	0,07	39,3	8,40	0,74	404100	0,00	6,67	229,00	21,4	0,06
079c-A-3	Pyrite	n.d.	n.d.	n.d.	0,79	1,13	0,08	16,0	32,73	0,42	404100	0,00	6,65	210,00	27,6	0,06
079c-A-4	Pyrite	2,04	1,46	0,38	1,00	0,45	0,05	25,4	7,29	0,55	404100	0,00	5,77	228,00	24,4	0,05
079c-A-5	Pyrite	1,88	1,31	0,44	0,79	1,36	0,07	58,3	6,86	0,83	404100	0,00	6,46	308,00	36,1	0,06
079c-A-6	Pyrite	n.d.	n.d.	n.d.	2,86	4,94	0,05	54,6	22,92	0,74	404100	0,00	5,90	407,00	53,3	0,05
TH-20-30-2-18	Pyrrhotite	3,88	2,63	0,48	2,49	1,82	0,06	175	21	1,10	613800	0,00	6,70	163,90	13,8	0,07
TH-20-30-2-19	Pyrrhotite	6,51	3,53	0,51	4,93	1,70	0,06	194	25	1,24	613800	0,00	7,69	151,90	12,2	0,08
TH-20-30-2-21	Pyrrhotite	22,37	15,71	0,45	7,27	0,98	0,05	169	17	1,11	613800	0,00	6,57	192,40	14,1	0,07
TH-20-30-2-43	Pyrrhotite	4,81	4,94	0,79	8,44	4,11	0,09	266	86	1,90	543500	0,00	12,40	178,90	22,8	0,12
TH-20-30-2-51	Pyrrhotite	n.d.	n.d.	n.d.	n.d.	n.d.	n.d.	n.d.	n.d.	n.d.	601840	0,00	14,25	86,80	8,7	0,13
TH-20-30-2-50	Pyrrhotite	*0,43*	1,15	0,85	*0,06*	0,18	0,12	106	29	1,66	601840	0,00	18,42	77,80	5,6	0,16
TH-20-30-2-42	Pyrrhotite	*0,41*	2,25	0,82	n.d.	n.d.	n.d.	n.d.	n.d.	n.d.	601840	0,00	15,50	84,50	23,6	0,13
TH-20-30-2-47	Pyrrhotite	*0,48*	3,04	0,95	n.d.	n.d.	n.d.	n.d.	n.d.	n.d.	601840	0,00	18,46	77,00	9,6	0,16
TH-20-30-2-48	Pyrrhotite	*0,40*	2,85	0,79	n.d.	n.d.	n.d.	n.d.	n.d.	n.d.	601840	0,00	18,14	78,40	9,3	0,16
TH-20-30-2-41	Pyrrhotite	1,20	0,80	0,80	0,84	0,71	0,11	125	27	1,68	601840	0,00	16,23	74,90	7,9	0,14
TH-20-30-2-44	Pyrrhotite	*0,43*	2,66	0,85	n.d.	n.d.	n.d.	n.d.	n.d.	n.d.	601840	0,00	20,13	72,90	6,3	0,17
TH-20-30-2-45	Pyrrhotite	1,47	0,95	0,76	1,82	1,24	0,09	95	20	1,43	601840	0,00	14,95	80,90	10,5	0,13
TH-20-30-2-49	Pyrrhotite	0,88	2,83	0,86	n.d.	n.d.	n.d.	n.d.	n.d.	n.d.	601840	0,00	17,29	73,80	8,3	0,15
TH-20-30-2-46	Pyrrhotite	n.d.	n.d.	n.d.	n.d.	n.d.	n.d.	n.d.	n.d.	n.d.	601840	0,00	18,18	78,40	8,3	0,16
TH-20-30-3-19	Pyrrhotite	21,80	7	0,91	1,78	0,56	0,16	292	79	2,49	696500	0,00	23,10	94,50	81,3	0,14
TH-20-30-3-20	Pyrrhotite	745,00	154	0,96	24,14	4,09	0,16	421	67	2,79	696500	0,00	28,36	34,80	31,8	0,17
TH-20-30-3-21	Pyrrhotite	1,41	0,89	0,71	6,90	4,59	0,15	257	92	2,17	696500	0,00	16,69	83,80	60,7	0,11
TH-20-30-3-22	Pyrrhotite	0,65	1,24	0,62	3,61	1,05	0,13	329	70	2,31	696500	0,00	19,17	52,10	35,2	0,13
TH-20-30-3-23	Pyrrhotite	1,08	1,12	0,58	0,92	0,57	0,13	230	80	2,05	696500	0,00	16,44	78,80	58,8	0,12
TH-20-30-3-24	Pyrrhotite	2,01	1,17	0,66	0,94	0,44	0,12	171	30	1,73	696500	0,00	15,06	85,00	19,9	0,12
TH-20-30-A-1	Pyrrhotite	*2,03*	3,44	4,06	n.d.	n.d.	n.d.	n.d.	n.d.	n.d.	621713	0,00	22,75	54,90	8,9	0,19
TH-20-30-A-10	Pyrrhotite	*0,73*	3,84	1,46	n.d.	n.d.	n.d.	n.d.	n.d.	n.d.	595500	0,00	25,94	52,10	5,4	0,22
TH-20-30-A-11	Pyrrhotite	*0,50*	1,38	0,99	0,12	0,21	0,10	81	35	1,41	595500	0,00	17,26	70,00	5,2	0,15
TH-20-30-A-12	Pyrrhotite	*1,46*	3,26	2,91	n.d.	n.d.	n.d.	75	46	1,39	595500	0,00	20,27	68,70	12,1	0,17
TH-20-30-A-13	Pyrrhotite	1,46	1,53	1,10	n.d.	n.d.	n.d.	n.d.	n.d.	n.d.	595500	0,00	22,22	53,10	10,7	0,20
TH-20-30-A-15	Pyrrhotite	*0,44*	3,18	0,88	n.d.	n.d.	n.d.	n.d.	n.d.	n.d.	629900	0,00	20,69	55,40	7,0	0,19
TH-20-30-A-16	Pyrrhotite	*0,58*	4,23	1,16	n.d.	n.d.	n.d.	n.d.	n.d.	n.d.	595600	0,00	23,73	51,10	12,7	0,22
TH-20-30-A-17	Pyrrhotite	*0,30*	2,18	0,60	0,77	0,18	0,12	114	41	1,55	617200	0,00	15,51	71,80	8,0	0,14
TH-20-30-A-18	Pyrrhotite	5,02	3,38	0,91	4,37	2,22	0,14	122	43	1,69	647600	0,00	14,63	121,10	20,2	0,13
TH-20-30-A-19	Pyrrhotite	1,02	1,18	0,62	1,02	0,65	0,09	81	30	1,03	595500	0,00	10,05	86,80	9,1	0,09
TH-20-30-A-2	Pyrrhotite	*0,81*	2,62	1,62	*0,10*	0,23	0,19	209	87	2,76	621713	0,00	27,87	53,40	8,6	0,23
TH-20-30-A-20	Pyrrhotite	1,10	0,90	0,55	0,96	0,38	0,09	68	29	0,97	595500	0,00	10,20	82,40	6,3	0,09
TH-20-30-A-3	Pyrrhotite	*0,68*	1,36	1,36	*0,10*	0,20	0,19	152	68	2,33	621713	0,00	26,83	50,90	8,7	0,23
TH-20-30-A-4	Pyrrhotite	*0,50*	3,52	1,00	n.d.	n.d.	n.d.	n.d.	n.d.	n.d.	621713	0,00	26,40	51,80	8,1	0,22
TH-20-30-A-5	Pyrrhotite	*0,73*	3,27	1,46	n.d.	n.d.	n.d.	n.d.	n.d.	n.d.	621713	0,00	26,26	52,70	8,9	0,22
TH-20-30-A-6	Pyrrhotite	*0,64*	1,94	1,27	*0,10*	0,20	0,19	142	63	2,28	621713	0,00	27,13	52,90	8,3	0,23
TH-20-30-A-7	Pyrrhotite	*1,32*	2,15	2,64	0,97	3,80	0,21	147	53	2,33	621713	0,00	27,40	58,70	9,7	0,23
TH-20-30-A-8	Pyrrhotite	*0,50*	2,87	0,99	n.d.	n.d.	n.d.	n.d.	n.d.	n.d.	611000	0,00	24,66	53,50	8,1	0,21
TH-20-30-A-9	Pyrrhotite	*0,58*	1,46	1,16	n.d.	n.d.	n.d.	115	49,17	1,80	611000	0,00	21,40	59,60	6,1	0,18
TH-20-30-2-24	Chalcopyrite	551	119	0,97	15,24	3,10	0,13	295	74	2,49	543500	0,00	20,25	128,20	107,5	0,14
TH-20-30-2-23	Chalcopyrite	73	17	0,92	9,05	2,39	0,12	213	36	2,17	543500	0,00	21,72	67,30	28,5	0,15
TH-20-30-2-17	Chalcopyrite	131	94	1,08	n.d.	n.d.	n.d.	n.d.	n.d.	n.d.	543500	0,00	22,98	213,70	92,4	0,18
TH-20-30-2-22	Chalcopyrite	43	12	2,04	6,04	2,79	0,11	173	50	1,90	543500	0,00	19,39	120,10	28,1	0,15
TH-20-30-2-20	Chalcopyrite	643	326	0,94	8,01	2,40	0,12	150	26	1,77	543500	0,00	18,58	228,70	143,9	0,12
TH-20-30-2-16	Chalcopyrite	69	62	0,93	8,95	3,80	0,11	116	28	1,44	543500	0,00	14,22	247,70	52,8	0,14
TH-20-30-A-30	Magmatic bleb	600	189	1,21	24,58	12,89	0,19	189	75	2,49	484700	0,00	24,10	1332,20	977,9	0,15
TH-20-30-A-31	Magmatic bleb	95	18	1,77	0,84	0,25	0,25	n.d.	n.d.	n.d.	578900	0,00	47,26	663,50	61,6	0,31

Supplementary table 5. Single spot LA-ICP-M

Sample	Mineral phase	Ni			Cu			Zn			As			Nb		
		concentration (ppm)	σ	LOD	concentration (ppm)	σ	LOD	concentration (ppm)	σ	LOD	concentration (ppm)	σ	LOD	concentration (ppm)	σ	LOD
079c-A-1	Pyrite	117,30	14,2	0,18	4449,00	598	0,05	7,90	1,0	0,24	2,73	2,14	0,09	0,08	0,01	0,003
079c-A-2	Pyrite	61,90	4,7	0,19	3863,00	452	0,05	9,80	1,6	0,26	3,37	5,70	0,12	0,04	0,01	0,002
079c-A-3	Pyrite	90,30	83,0	0,23	4836,00	682	0,05	6,20	1,5	0,27	2,33	3,15	0,13	0,03	0,01	0,002
079c-A-4	Pyrite	65,10	4,5	0,16	3944,00	324	0,04	5,80	0,4	0,23	5,25	3,82	0,08	0,02	0,02	0,002
079c-A-5	Pyrite	91,20	15,4	0,17	5486,00	1178	0,05	8,10	2,8	0,27	2,45	3,89	0,11	0,04	0,01	0,003
079c-A-6	Pyrite	162,70	16,6	0,16	4527,00	745	0,04	16,70	20,4	0,25	3,20	2,78	0,08	n.d.	n.d.	n.d.
TH-20-30-2-18	Pyrrhotite	35,40	3,6	0,22	2368	320	0,07	124,90	84,9	0,28	2,16	0,72	0,09	0,02	0,01	0,003
TH-20-30-2-19	Pyrrhotite	34,40	3,9	0,23	2376	295	0,07	86,00	27,2	0,36	3,41	0,98	0,10	0,11	0,06	0,004
TH-20-30-2-21	Pyrrhotite	44,70	3,2	0,21	2594	283	0,08	58,00	5,0	0,30	5,52	1,08	0,08	0,04	0,03	0,003
TH-20-30-2-43	Pyrrhotite	24,60	3,0	0,31	7927	2636	0,10	162,20	55,0	0,47	1,54	0,68	0,14	0,04	0,02	0,006
TH-20-30-2-51	Pyrrhotite	n.d.	n.d.	n.d.	1764	172	0,10	36,10	3,8	0,47	n.d.	n.d.	n.d.	n.d.	n.d.	n.d.
TH-20-30-2-50	Pyrrhotite	16,00	2,0	0,44	1435	195	0,13	114,00	72,8	0,59	*0,05*	0,16	0,10	0,01	0,01	0,006
TH-20-30-2-42	Pyrrhotite	n.d.	n.d.	n.d.	1431	208	0,11	37,60	8,8	0,54	n.d.	n.d.	n.d.	n.d.	n.d.	n.d.
TH-20-30-2-47	Pyrrhotite	n.d.	n.d.	n.d.	1426	162	0,13	39,80	5,5	0,58	n.d.	n.d.	n.d.	n.d.	n.d.	n.d.
TH-20-30-2-48	Pyrrhotite	n.d.	n.d.	n.d.	1415	162	0,13	53,70	9,9	0,58	n.d.	n.d.	n.d.	n.d.	n.d.	n.d.
TH-20-30-2-41	Pyrrhotite	15,00	2,1	0,41	1385	227	0,12	53,60	51,9	0,51	0,35	0,22	0,15	n.d.	n.d.	n.d.
TH-20-30-2-44	Pyrrhotite	n.d.	n.d.	n.d.	1333	139	0,14	52,90	5,9	0,62	n.d.	n.d.	n.d.	n.d.	n.d.	n.d.
TH-20-30-2-45	Pyrrhotite	16,10	2,3	0,38	1330	152	0,28	37,00	2,1	0,48	0,29	0,24	0,14	0,012	0,010	0,005
TH-20-30-2-49	Pyrrhotite	n.d.	n.d.	n.d.	1277	102	0,13	67,70	90,0	0,57	n.d.	n.d.	n.d.	n.d.	n.d.	n.d.
TH-20-30-2-46	Pyrrhotite	n.d.	n.d.	n.d.	1061	299	0,13	31,30	4,8	0,58	n.d.	n.d.	n.d.	n.d.	n.d.	n.d.
TH-20-30-3-19	Pyrrhotite	15,80	13,7	0,40	2540	2333	0,12	161,40	19,6	0,57	*0,06*	0,42	0,12	0,43	0,14	0,007
TH-20-30-3-20	Pyrrhotite	11,80	9,1	0,63	1095	473	0,16	171,20	28,8	0,63	0,44	0,54	0,37	1,33	0,23	0,008
TH-20-30-3-21	Pyrrhotite	21,70	16,0	0,32	1410	899	0,10	120,20	32,4	0,49	0,35	0,43	0,21	0,17	0,10	0,004
TH-20-30-3-22	Pyrrhotite	15,00	10,6	0,38	1291	953	0,11	148,50	19,2	0,52	*0,09*	0,43	0,17	0,33	0,09	0,006
TH-20-30-3-23	Pyrrhotite	18,20	9,8	0,36	1555	1141	0,12	127,80	27,1	0,49	0,35	0,32	0,19	0,13	0,08	0,004
TH-20-30-3-24	Pyrrhotite	21,70	5,5	0,36	2297	1187	0,10	108,20	9,4	0,43	0,33	0,36	0,19	0,07	0,04	0,005
TH-20-30-A-1	Pyrrhotite	n.d.	n.d.	n.d.	1108	202	0,17	53,90	10,9	0,73	n.d.	n.d.	n.d.	n.d.	n.d.	n.d.
TH-20-30-A-10	Pyrrhotite	n.d.	n.d.	n.d.	1179	187	0,19	55,40	11,1	0,89	n.d.	n.d.	n.d.	n.d.	n.d.	n.d.
TH-20-30-A-11	Pyrrhotite	13,60	2,1	0,42	1397	221	0,13	57,70	21,2	0,60	0,21	0,17	0,15	n.d.	n.d.	n.d.
TH-20-30-A-12	Pyrrhotite	n.d.	n.d.	n.d.	1435	186	0,14	45,50	9,8	0,67	n.d.	n.d.	n.d.	n.d.	n.d.	n.d.
TH-20-30-A-13	Pyrrhotite	n.d.	n.d.	n.d.	1194	313	0,16	37,90	8,9	0,76	n.d.	n.d.	n.d.	n.d.	n.d.	n.d.
TH-20-30-A-15	Pyrrhotite	n.d.	n.d.	n.d.	1173	153	0,15	49,80	7,4	0,74	n.d.	n.d.	n.d.	n.d.	n.d.	n.d.
TH-20-30-A-16	Pyrrhotite	n.d.	n.d.	n.d.	1066	199	0,17	47,80	15,3	0,84	n.d.	n.d.	n.d.	n.d.	n.d.	n.d.
TH-20-30-A-17	Pyrrhotite	17,80	2,9	0,39	1267	320	0,12	80,50	27,5	0,59	0,62	0,42	0,13	0,013	0,013	0,003
TH-20-30-A-18	Pyrrhotite	57,00	11,5	0,39	2021	871	0,11	133,50	49,4	0,63	1,55	0,41	0,17	0,120	0,106	0,009
TH-20-30-A-19	Pyrrhotite	31,20	8,0	0,29	1233	307	0,08	59,10	20,1	0,42	1,44	0,79	0,10	0,011	0,015	0,004
TH-20-30-A-2	Pyrrhotite	11,20	3,1	0,69	1152	258	0,20	53,80	8,2	0,84	0,38	0,23	0,27	*0,007*	0,022	0,014
TH-20-30-A-20	Pyrrhotite	37,00	9,1	0,28	1265	371	0,08	66,20	13,1	0,39	0,68	0,31	0,12	0,011	0,010	0,005
TH-20-30-A-3	Pyrrhotite	8,90	1,4	0,65	1096	221	0,20	50,00	7,1	0,83	*0,13*	0,28	0,26	*0,005*	0,019	0,010
TH-20-30-A-4	Pyrrhotite	n.d.	n.d.	n.d.	1029	161	0,19	57,00	16,3	0,84	n.d.	n.d.	n.d.	n.d.	n.d.	n.d.
TH-20-30-A-5	Pyrrhotite	n.d.	n.d.	n.d.	1222	319	0,20	48,30	8,6	0,83	n.d.	n.d.	n.d.	n.d.	n.d.	n.d.
TH-20-30-A-6	Pyrrhotite	11,20	3,4	0,68	1204	287	0,18	67,90	32,7	0,88	*0,13*	0,26	0,26	n.d.	n.d.	n.d.
TH-20-30-A-7	Pyrrhotite	10,90	1,5	0,66	1143	156	0,19	61,40	15,9	0,93	*0,01*	0,22	0,01	*0,006*	0,016	0,012
TH-20-30-A-8	Pyrrhotite	n.d.	n.d.	n.d.	1349	495	0,17	88,60	95,9	0,75	n.d.	n.d.	n.d.	n.d.	n.d.	n.d.
TH-20-30-A-9	Pyrrhotite	11,60	1,7	0,53	1328	274	0,16	68,50	21,6	0,73	0,30	0,27	0,20	n.d.	n.d.	n.d.
TH-20-30-2-24	Chalcopyrite	25,60	23,8	0,40	66642	60700	0,16	207,00	57	0,65	8,33	1,43	0,17	2,02	0,39	0,008
TH-20-30-2-23	Chalcopyrite	14,60	6,6	0,45	47099	20752	0,19	171,00	22	0,69	3,35	0,98	0,18	0,74	0,10	0,006
TH-20-30-2-17	Chalcopyrite	n.d.	n.d.	n.d.	110124	70271	0,21	38,00	12	0,73	n.d.	n.d.	n.d.	0,62	0,20	0,008
TH-20-30-2-22	Chalcopyrite	27,20	6,5	0,44	102771	69199	0,18	138,00	62	0,51	n.d.	n.d.	n.d.	0,56	0,18	0,005
TH-20-30-2-20	Chalcopyrite	55,70	36,4	0,36	118906	95951	0,14	133,00	78	0,65	8,23	3,22	0,17	2,73	1,15	0,005
TH-20-30-2-16	Chalcopyrite	57,40	13,6	0,38	135004	50177	0,16	96,00	87	0,48	n.d.	n.d.	n.d.	0,41	0,21	0,005
TH-20-30-A-30	Magmatic bleb	717,20	547,6	0,44	15902	9196	0,16	231,00	53	0,86	39,53	28,97	0,18	1,64	0,87	0,013
TH-20-30-A-31	Magmatic bleb	472,30	61,4	0,90	5312	3665	0,25	76,00	12	1,38	5,53	1,72	0,35	0,15	0,04	0,013

Supplementary table 5. Single spot LA-ICP-M

Sample	Mineral phase	Mo			Ag			Cd			In			Sn		
		concentration (ppm)	σ	LOD	concentration (ppm)	σ	LOD	concentration (ppm)	σ	LOD	concentration (ppm)	σ	LOD	concentration (ppm)	σ	LOD
079c-A-1	Pyrite	69,10	4,30	0,03	3,07	0,35	0,03	0,78	0,10	0,01	0,03	0,008	0,003	0,13	0,04	0,06
079c-A-2	Pyrite	46,60	4,24	0,04	3,08	0,77	0,03	0,67	0,17	0,01	0,02	0,009	0,003	n.d.	n.d.	n.d.
079c-A-3	Pyrite	56,30	5,37	0,04	4,29	1,21	0,03	0,68	0,23	0,01	0,03	0,012	0,003	*0,04*	0,14	0,08
079c-A-4	Pyrite	47,70	4,15	0,03	3,13	0,39	0,02	0,48	0,11	0,02	0,02	0,007	0,003	*0,04*	0,09	0,07
079c-A-5	Pyrite	54,40	9,21	0,04	4,08	1,13	0,03	0,51	0,17	0,01	0,02	0,005	0,003	n.d.	n.d.	n.d.
079c-A-6	Pyrite	90,90	27,65	0,03	4,97	0,98	0,03	0,86	0,10	0,01	0,05	0,022	0,003	n.d.	n.d.	n.d.
TH-20-30-2-18	Pyrrhotite	18,90	2,09	0,06	1,53	0,45	0,03	4,45	0,69	0,02	0,24	0,04	0,003	0,20	0,05	0,03
TH-20-30-2-19	Pyrrhotite	21,90	2,45	0,07	1,14	0,54	0,03	4,08	0,70	0,02	0,22	0,04	0,003	0,73	0,29	0,03
TH-20-30-2-21	Pyrrhotite	19,70	1,45	0,05	0,92	0,24	0,03	5,59	0,64	0,02	0,23	0,02	0,002	0,27	0,06	0,02
TH-20-30-2-43	Pyrrhotite	18,20	4,06	0,15	1,14	0,51	0,06	2,52	0,49	0,03	0,27	0,08	0,004	22,10	8,58	0,04
TH-20-30-2-51	Pyrrhotite	18,30	1,89	0,18	0,34	0,05	0,05	1,68	0,28	0,04	0,11	0,03	0,005	0,13	0,09	0,04
TH-20-30-2-50	Pyrrhotite	20,10	2,21	0,29	0,68	0,19	0,07	2,62	1,10	0,05	0,19	0,11	0,005	0,09	0,08	0,05
TH-20-30-2-42	Pyrrhotite	19,70	1,86	0,19	0,45	0,19	0,06	1,81	0,61	0,04	0,11	0,02	0,004	0,11	0,05	0,04
TH-20-30-2-47	Pyrrhotite	21,20	2,41	0,27	0,65	0,10	0,08	1,55	0,35	0,06	0,09	0,02	0,006	0,12	0,09	0,05
TH-20-30-2-48	Pyrrhotite	20,20	2,65	0,36	0,63	0,17	0,07	1,91	0,47	0,06	0,12	0,03	0,005	0,13	0,07	0,05
TH-20-30-2-41	Pyrrhotite	19,50	1,49	0,21	0,31	0,17	0,06	1,57	0,35	0,05	0,08	0,02	0,005	0,16	0,09	0,04
TH-20-30-2-44	Pyrrhotite	21,20	2,01	0,34	0,53	0,17	0,08	1,65	0,50	0,05	0,10	0,03	0,007	0,14	0,08	0,05
TH-20-30-2-45	Pyrrhotite	19,70	2,07	0,21	0,16	0,07	0,06	1,72	0,29	0,04	0,10	0,03	0,005	0,09	0,06	0,04
TH-20-30-2-49	Pyrrhotite	20,10	1,54	0,22	0,44	0,13	0,07	1,47	0,98	0,05	0,10	0,05	0,004	0,13	0,06	0,05
TH-20-30-2-46	Pyrrhotite	20,40	2,25	0,29	1,02	0,20	0,07	1,54	0,34	0,06	0,09	0,02	0,006	0,14	0,09	0,05
TH-20-30-3-19	Pyrrhotite	28,80	4,28	0,21	3,11	2,70	0,07	0,29	0,24	0,02	0,25	0,05	0,007	3,46	0,63	0,05
TH-20-30-3-20	Pyrrhotite	31,90	2,62	0,26	1,05	0,68	0,11	0,32	0,24	0,05	0,24	0,05	0,008	3,30	0,61	0,05
TH-20-30-3-21	Pyrrhotite	26,70	4,95	0,21	1,52	0,83	0,06	1,71	1,17	0,03	0,33	0,08	0,005	3,22	1,33	0,04
TH-20-30-3-22	Pyrrhotite	35,60	6,58	0,14	1,47	1,11	0,06	1,31	0,92	0,03	0,36	0,09	0,006	3,98	1,06	0,04
TH-20-30-3-23	Pyrrhotite	24,10	4,54	0,17	2,96	1,69	0,06	1,64	0,74	0,03	0,39	0,10	0,005	3,21	1,40	0,03
TH-20-30-3-24	Pyrrhotite	23,00	4,15	0,15	2,35	0,77	0,06	2,68	0,48	0,03	0,41	0,09	0,004	2,33	0,49	0,03
TH-20-30-A-1	Pyrrhotite	25,80	3,38	0,32	0,23	0,20	0,09	1,88	0,58	0,08	0,13	0,04	0,007	0,11	0,12	0,06
TH-20-30-A-10	Pyrrhotite	27,00	3,14	0,41	1,26	0,22	0,10	1,39	0,40	0,08	0,10	0,03	0,008	0,08	0,08	0,07
TH-20-30-A-11	Pyrrhotite	24,20	4,08	0,20	1,70	0,77	0,07	2,74	1,01	0,05	0,21	0,14	0,004	0,12	0,07	0,05
TH-20-30-A-12	Pyrrhotite	25,50	4,74	0,26	0,99	0,27	0,08	2,21	0,68	0,07	0,13	0,06	0,005	0,18	0,10	0,06
TH-20-30-A-13	Pyrrhotite	24,90	3,65	0,33	0,89	0,24	0,08	1,34	0,35	0,07	0,08	0,04	0,006	*0,05*	0,14	0,09
TH-20-30-A-15	Pyrrhotite	23,30	2,33	0,34	1,25	0,19	0,08	2,01	0,40	0,08	0,11	0,03	0,005	0,11	0,11	0,06
TH-20-30-A-16	Pyrrhotite	25,10	4,32	0,47	0,64	0,21	0,09	1,74	0,58	0,07	0,10	0,05	0,008	0,15	0,12	0,06
TH-20-30-A-17	Pyrrhotite	22,30	4,46	0,20	1,13	0,34	0,06	3,92	0,76	0,06	0,41	0,12	0,005	0,20	0,12	0,04
TH-20-30-A-18	Pyrrhotite	27,10	6,64	0,14	0,89	0,36	0,06	4,13	0,97	0,05	0,94	0,27	0,004	0,99	0,47	0,05
TH-20-30-A-19	Pyrrhotite	19,10	4,08	0,10	0,33	0,08	0,04	4,64	0,49	0,03	0,54	0,28	0,003	0,22	0,14	0,03
TH-20-30-A-2	Pyrrhotite	27,40	3,10	0,51	0,17	0,14	0,10	1,47	0,47	0,08	0,11	0,03	0,009	0,13	0,08	0,07
TH-20-30-A-20	Pyrrhotite	18,40	2,94	0,08	0,66	0,16	0,04	5,25	0,60	0,03	0,52	0,19	0,003	0,23	0,10	0,02
TH-20-30-A-3	Pyrrhotite	26,50	3,41	0,53	0,53	0,18	0,10	1,43	0,38	0,08	0,10	0,03	0,008	0,17	0,15	0,06
TH-20-30-A-4	Pyrrhotite	26,60	2,55	0,43	0,76	0,23	0,10	1,81	0,58	0,08	0,11	0,03	0,006	0,13	0,13	0,07
TH-20-30-A-5	Pyrrhotite	27,40	4,38	0,46	0,86	0,26	0,10	1,67	0,45	0,08	0,11	0,03	0,010	0,16	0,14	0,07
TH-20-30-A-6	Pyrrhotite	27,10	3,22	0,47	0,91	0,26	0,10	2,15	1,02	0,08	0,11	0,04	0,007	0,16	0,13	0,07
TH-20-30-A-7	Pyrrhotite	27,80	3,02	0,51	1,14	0,28	0,10	1,69	0,36	0,10	0,12	0,05	0,009	0,16	0,15	0,08
TH-20-30-A-8	Pyrrhotite	26,50	3,32	0,44	1,08	0,61	0,09	2,12	1,43	0,06	0,13	0,06	0,008	0,12	0,12	0,06
TH-20-30-A-9	Pyrrhotite	24,40	3,32	0,38	1,19	0,25	0,08	2,19	0,63	0,08	0,12	0,04	0,007	0,14	0,09	0,06
TH-20-30-2-24	Chalcopyrite	34,40	4,62	0,13	13,32	6,16	0,07	0,60	0,68	0,04	0,34	0,09	0,007	5,49	1,69	0,11
TH-20-30-2-23	Chalcopyrite	23,40	1,67	0,21	29,21	9,42	0,07	0,49	0,28	0,04	0,24	0,04	0,006	3,49	0,63	0,06
TH-20-30-2-17	Chalcopyrite	20,60	1,86	0,23	37,74	26,90	0,08	1,05	0,30	0,06	0,13	0,04	0,008	0,84	0,33	0,07
TH-20-30-2-22	Chalcopyrite	20,60	1,67	0,19	11,26	4,03	0,07	1,14	0,66	0,04	0,19	0,07	0,007	1,78	0,52	0,05
TH-20-30-2-20	Chalcopyrite	35,80	7,44	0,13	51,72	27,13	0,06	1,40	0,63	0,04	0,17	0,05	0,005	3,60	1,60	0,05
TH-20-30-2-16	Chalcopyrite	33,00	1,81	0,10	4,20	3,53	0,06	1,61	0,45	0,03	0,18	0,05	0,004	0,46	0,15	0,06
TH-20-30-A-30	Magmatic bleb	27,80	3,31	0,21	9,22	5,50	0,07	0,90	0,87	0,06	0,80	0,34	0,008	2,90	0,8	0,06
TH-20-30-A-31	Magmatic bleb	81,10	8,83	0,25	3,04	0,94	0,13	3,12	0,56	0,14	0,88	0,18	0,010	1,00	0,4	0,09

Supplementary table 5. Single spot LA-ICP-M

Sample	Mineral phase	Sb			Te			W			Au			Tl		
		concentration (ppm)	σ	LOD	concentration (ppm)	σ	LOD	concentration (ppm)	σ	LOD	concentration (ppm)	σ	LOD	concentration (ppm)	σ	LOD
079c-A-1	Pyrite	0,300	0,194	0,020	10,14	1,80	0,03	0,028	0,020	0,010	n.d.	n.d.	n.d.	0,11	0,055	0,003
079c-A-2	Pyrite	0,270	0,141	0,022	8,20	1,68	0,03	n.d.	n.d.	n.d.	*0,023*	0,015	0,046	0,10	0,070	0,003
079c-A-3	Pyrite	0,270	0,263	0,022	9,24	2,02	0,04	n.d.	n.d.	n.d.	0,041	0,015	0,021	0,09	0,081	0,003
079c-A-4	Pyrite	0,420	0,133	0,017	9,47	1,61	0,04	0,078	0,077	0,005	0,030	0,018	0,022	0,06	0,028	0,002
079c-A-5	Pyrite	0,330	0,207	0,022	10,73	1,85	0,06	n.d.	n.d.	n.d.	n.d.	n.d.	n.d.	0,13	0,182	0,002
079c-A-6	Pyrite	0,430	0,376	0,018	10,44	1,06	0,03	n.d.	n.d.	n.d.	0,026	0,011	0,025	2,58	1,370	0,002
TH-20-30-2-18	Pyrrhotite	0,010	0,020	0,019	0,16	0,12	0,03	0,476	0,105	0,275	*0,011*	0,020	0,022	0,11	0,103	0,003
TH-20-30-2-19	Pyrrhotite	*0,012*	0,025	0,024	0,17	0,09	0,06	0,567	0,106	0,165	*0,013*	0,025	0,025	2,36	3,477	0,005
TH-20-30-2-21	Pyrrhotite	0,020	0,025	0,017	0,24	0,15	0,04	n.d.	n.d.	n.d.	*0,010*	0,019	0,019	22,08	10,767	0,003
TH-20-30-2-43	Pyrrhotite	0,160	0,081	0,028	0,12	0,20	0,05	0,168	0,116	0,016	0,131	0,054	0,028	2,22	0,591	0,005
TH-20-30-2-51	Pyrrhotite	*0,021*	0,052	0,042	*0,03*	0,14	0,06	*0,007*	0,021	0,013	*0,021*	0,054	0,042	0,01	0,012	0,005
TH-20-30-2-50	Pyrrhotite	*0,024*	0,032	0,047	*0,08*	0,14	0,15	0,021	0,023	0,013	*0,032*	0,060	0,063	0,01	0,010	0,005
TH-20-30-2-42	Pyrrhotite	*0,015*	0,028	0,030	0,11	0,15	0,08	*0,006*	0,022	0,011	0,094	0,311	0,032	0,14	0,168	0,006
TH-20-30-2-47	Pyrrhotite	*0,024*	0,051	0,048	0,19	0,23	0,12	*0,019*	0,025	0,037	0,427	0,661	0,035	0,07	0,133	0,004
TH-20-30-2-48	Pyrrhotite	*0,020*	0,030	0,039	0,12	0,16	0,10	*0,009*	0,023	0,018	0,331	0,650	0,036	0,09	0,145	0,007
TH-20-30-2-41	Pyrrhotite	*0,017*	0,043	0,034	*0,04*	0,18	0,08	*0,011*	0,113	0,022	*0,094*	0,034	0,187	0,03	0,034	0,007
TH-20-30-2-44	Pyrrhotite	*0,021*	0,065	0,041	0,19	0,22	0,11	*0,002*	0,000	0,004	0,101	0,329	0,051	0,02	0,085	0,007
TH-20-30-2-45	Pyrrhotite	*0,011*	0,039	0,022	0,09	0,12	0,08	*0,008*	0,020	0,015	n.d.	n.d.	n.d.	0,01	0,012	0,007
TH-20-30-2-49	Pyrrhotite	n.d.	n.d.	n.d.	*0,05*	0,14	0,09	*0,002*	0,000	0,003	0,088	0,248	0,042	0,04	0,099	0,006
TH-20-30-2-46	Pyrrhotite	*0,017*	0,048	0,033	0,11	0,15	0,06	*0,006*	0,018	0,012	0,095	0,266	0,016	0,01	0,055	0,005
TH-20-30-3-19	Pyrrhotite	n.d.	n.d.	n.d.	n.d.	n.d.	n.d.	0,392	0,232	0,021	*0,059*	0,049	0,117	1,97	1,455	0,008
TH-20-30-3-20	Pyrrhotite	*0,034*	0,064	0,068	*0,07*	0,16	0,13	0,654	0,235	0,004	n.d.	n.d.	n.d.	7,01	4,594	0,010
TH-20-30-3-21	Pyrrhotite	*0,027*	0,076	0,054	0,09	0,16	0,07	0,263	0,147	0,017	*0,066*	0,033	0,131	0,24	0,189	0,006
TH-20-30-3-22	Pyrrhotite	*0,037*	0,062	0,074	0,14	0,10	0,28	0,414	0,201	0,017	*0,202*	0,042	0,403	*0,002*	0,014	0,004
TH-20-30-3-23	Pyrrhotite	n.d.	n.d.	n.d.	0,13	0,19	0,07	0,261	0,186	0,017	*0,053*	0,048	0,106	2,78	2,076	0,007
TH-20-30-3-24	Pyrrhotite	*0,024*	0,066	0,047	0,22	0,17	0,11	0,141	0,102	0,012	0,087	0,040	0,049	0,02	0,020	0,005
TH-20-30-A-1	Pyrrhotite	*0,028*	0,080	0,055	*0,04*	0,14	0,08	*0,013*	0,023	0,025	0,158	0,414	0,023	0,03	0,029	0,009
TH-20-30-A-10	Pyrrhotite	*0,033*	0,060	0,066	*0,03*	0,33	0,05	0,030	0,059	0,029	0,272	0,618	0,050	0,22	0,574	0,009
TH-20-30-A-11	Pyrrhotite	*0,038*	0,077	0,075	*0,04*	0,14	0,07	*0,006*	0,028	0,012	*0,030*	0,040	0,059	0,05	0,031	0,005
TH-20-30-A-12	Pyrrhotite	*0,023*	0,065	0,045	0,19	0,21	0,12	*0,014*	0,026	0,028	*0,034*	0,037	0,067	0,07	0,042	0,008
TH-20-30-A-13	Pyrrhotite	*0,026*	0,075	0,052	n.d.	n.d.	n.d.	*0,010*	0,016	0,019	*0,042*	0,044	0,083	0,04	0,032	0,007
TH-20-30-A-15	Pyrrhotite	*0,022*	0,076	0,043	*0,05*	0,23	0,10	0,018	0,034	0,015	*0,045*	0,051	0,089	0,24	0,856	0,005
TH-20-30-A-16	Pyrrhotite	*0,031*	0,089	0,061	0,26	0,44	0,15	*0,024*	0,058	0,048	0,316	0,724	0,044	0,08	0,249	0,010
TH-20-30-A-17	Pyrrhotite	*0,022*	0,064	0,044	0,09	0,18	0,17	*0,010*	0,045	0,020	0,055	0,040	0,038	0,04	0,032	0,007
TH-20-30-A-18	Pyrrhotite	*0,018*	0,063	0,036	0,11	0,20	0,08	0,117	0,125	0,017	0,063	0,091	0,035	0,15	0,079	0,006
TH-20-30-A-19	Pyrrhotite	*0,013*	0,047	0,026	*0,04*	0,13	0,08	*0,023*	0,043	0,021	0,052	0,059	0,027	0,04	0,019	0,004
TH-20-30-A-2	Pyrrhotite	n.d.	n.d.	n.d.	*0,05*	0,19	0,10	*0,021*	0,022	0,041	*0,045*	0,055	0,089	0,03	0,023	0,010
TH-20-30-A-20	Pyrrhotite	*0,016*	0,029	0,032	*0,03*	0,09	0,05	*0,004*	0,015	0,007	0,056	0,031	0,018	0,02	0,020	0,005
TH-20-30-A-3	Pyrrhotite	*0,035*	0,082	0,070	0,16	0,22	0,15	*0,008*	0,032	0,015	*0,081*	0,049	0,161	0,03	0,021	0,011
TH-20-30-A-4	Pyrrhotite	*0,039*	0,057	0,077	*0,05*	0,16	0,09	*0,017*	0,015	0,033	0,078	0,302	0,046	0,04	0,124	0,005
TH-20-30-A-5	Pyrrhotite	*0,032*	0,084	0,063	0,15	0,23	0,07	*0,014*	0,016	0,028	0,097	0,451	0,082	0,09	0,223	0,010
TH-20-30-A-6	Pyrrhotite	*0,035*	0,076	0,070	*0,07*	0,20	0,14	*0,029*	0,014	0,057	*0,004*	0,049	0,007	0,03	0,020	0,010
TH-20-30-A-7	Pyrrhotite	*0,033*	0,071	0,066	*0,07*	0,21	0,14	*0,011*	0,023	0,021	n.d.	n.d.	n.d.	0,01	0,018	0,008
TH-20-30-A-8	Pyrrhotite	*0,023*	0,049	0,046	0,12	0,20	0,10	*0,021*	0,031	0,041	*0,048*	0,064	0,096	0,02	0,025	0,008
TH-20-30-A-9	Pyrrhotite	n.d.	n.d.	n.d.	*0,08*	0,18	0,15	*0,011*	0,021	0,022	n.d.	n.d.	n.d.	0,04	0,025	0,008
TH-20-30-2-24	Chalcopyrite	0,070	0,074	0,038	0,85	0,38	0,10	1,340	0,23	0,04	0,113	0,100	0,027	19,16	11,490	0,008
TH-20-30-2-23	Chalcopyrite	*0,017*	0,055	0,034	0,33	0,23	0,14	1,170	0,18	0,11	0,188	0,118	0,033	2,44	0,620	0,008
TH-20-30-2-17	Chalcopyrite	0,100	0,113	0,047	0,48	0,19	0,14	0,990	0,09	0,31	0,357	0,626	0,034	15,57	6,150	0,007
TH-20-30-2-22	Chalcopyrite	0,040	0,061	0,035	0,23	0,18	0,09	0,970	0,16	0,25	0,283	0,571	0,029	10,10	4,310	0,008
TH-20-30-2-20	Chalcopyrite	0,040	0,075	0,033	1,36	0,64	0,07	1,360	0,39	0,59	0,105	0,101	0,024	34,46	17,930	0,007
TH-20-30-2-16	Chalcopyrite	0,060	0,054	0,038	0,59	0,52	0,08	0,880	0,24	0,15	0,055	0,060	0,025	61,25	29,110	0,006
TH-20-30-A-30	Magmatic bleb	0,740	0,447	0,050	0,17	0,20	0,13	1,430	0,43	0,07	0,084	0,125	0,026	9,36	11,468	0,005
TH-20-30-A-31	Magmatic bleb	1,630	0,392	0,095	0,85	0,45	0,20	1,200	0,09	0,16	n.d.	n.d.	n.d.	0,12	0,033	0,012

Supplementary table 5. Single spot LA-ICP-M

Sample	Mineral phase	Pb			Bi			Th			U		
		concentration (ppm)	σ	LOD	concentration (ppm)	σ	LOD	concentration (ppm)	σ	LOD	concentration (ppm)	σ	LOD
079c-A-1	Pyrite	1,58	0,27	0,003	0,087	0,02	0,003	0,045	0,015	0,001	n.d.	n.d.	n.d.
079c-A-2	Pyrite	1,23	0,32	0,002	0,084	0,02	0,003	0,021	0,002	0,001	0,027	0,030	0,001
079c-A-3	Pyrite	1,41	0,53	0,003	0,089	0,02	0,003	0,020	0,007	0,001	0,017	0,009	0,001
079c-A-4	Pyrite	0,95	0,14	0,002	0,105	0,03	0,002	0,028	0,014	0,001	0,023	0,007	0,000
079c-A-5	Pyrite	2,04	0,83	0,003	0,095	0,02	0,003	0,012	0,006	0,001	0,036	0,018	0,000
079c-A-6	Pyrite	3,14	0,66	0,006	0,117	0,02	0,003	0,055	0,066	0,0004	0,312	0,547	0,001
TH-20-30-2-18	Pyrrhotite	5,18	3,69	0,003	0,087	0,02	0,003	0,094	0,060	0,001	0,085	0,041	0,001
TH-20-30-2-19	Pyrrhotite	12,18	5,69	0,002	0,112	0,06	0,004	0,195	0,066	0,002	0,111	0,037	0,001
TH-20-30-2-21	Pyrrhotite	38,21	5,19	0,003	0,263	0,14	0,004	0,181	0,056	0,001	0,124	0,024	0,001
TH-20-30-2-43	Pyrrhotite	2,81	0,85	0,006	0,050	0,02	0,005	0,065	0,028	0,000	0,004	0,006	0,002
TH-20-30-2-51	Pyrrhotite	0,42	0,10	0,004	0,009	0,01	0,005	0,008	0,012	0,001	0,004	0,006	0,001
TH-20-30-2-50	Pyrrhotite	0,45	0,08	0,006	0,008	0,01	0,006	0,002	0,005	0,000	0,001	0,003	0,001
TH-20-30-2-42	Pyrrhotite	4,13	5,02	0,006	0,016	0,01	0,007	0,011	0,014	0,001	0,004	0,005	0,001
TH-20-30-2-47	Pyrrhotite	0,60	0,30	0,006	0,009	0,01	0,006	*0,001*	0,003	0,002	0,012	0,013	0,002
TH-20-30-2-48	Pyrrhotite	0,51	0,09	0,009	0,013	0,01	0,006	0,002	0,006	0,001	*0,001*	0,000	0,002
TH-20-30-2-41	Pyrrhotite	1,41	0,96	0,006	0,017	0,00	0,005	0,024	0,021	0,002	0,089	0,034	0,002
TH-20-30-2-44	Pyrrhotite	0,46	0,09	0,012	0,014	0,01	0,008	0,002	0,004	0,000	0,010	0,011	0,002
TH-20-30-2-45	Pyrrhotite	0,57	0,14	0,008	0,012	0,01	0,005	0,018	0,015	0,002	0,002	0,004	0,002
TH-20-30-2-49	Pyrrhotite	0,41	0,10	0,007	0,011	0,01	0,005	0,002	0,003	0,003	0,014	0,014	0,002
TH-20-30-2-46	Pyrrhotite	0,46	0,17	0,007	0,011	0,01	0,007	*0,002*	0,007	0,000	0,002	0,004	0,001
TH-20-30-3-19	Pyrrhotite	6,40	7,89	0,010	1,734	1,17	0,006	0,058	0,024	0,003	0,116	0,037	0,004
TH-20-30-3-20	Pyrrhotite	25,06	14,08	0,012	0,033	0,01	0,008	2,380	1,205	0,000	0,905	0,318	0,001
TH-20-30-3-21	Pyrrhotite	5,58	3,62	0,006	0,022	0,01	0,006	0,104	0,056	0,002	0,110	0,053	0,001
TH-20-30-3-22	Pyrrhotite	3,52	2,09	0,003	0,011	0,01	0,005	0,079	0,035	0,000	0,119	0,048	0,002
TH-20-30-3-23	Pyrrhotite	8,82	5,53	0,003	0,019	0,01	0,006	0,111	0,051	0,002	0,153	0,075	0,001
TH-20-30-3-24	Pyrrhotite	5,81	1,78	0,007	0,025	0,01	0,006	0,125	0,044	0,000	0,130	0,036	0,005
TH-20-30-A-1	Pyrrhotite	1,24	0,43	0,010	0,017	0,01	0,010	*0,010*	0,020	0,002	0,013	0,016	0,003
TH-20-30-A-10	Pyrrhotite	3,29	2,16	0,010	0,016	0,01	0,008	0,002	0,005	0,003	*0,002*	0,002	0,003
TH-20-30-A-11	Pyrrhotite	2,18	0,67	0,006	0,020	0,01	0,006	0,022	0,020	0,002	0,044	0,037	0,002
TH-20-30-A-12	Pyrrhotite	2,19	0,86	0,007	0,027	0,01	0,008	0,031	0,031	0,000	0,031	0,025	0,002
TH-20-30-A-13	Pyrrhotite	1,84	0,79	0,010	*0,004*	0,01	0,008	*0,000*	0,003	0,000	0,002	0,006	0,002
TH-20-30-A-15	Pyrrhotite	5,55	2,99	0,008	0,021	0,01	0,006	0,010	0,020	0,004	0,030	0,024	0,003
TH-20-30-A-16	Pyrrhotite	1,72	0,60	0,013	0,016	0,01	0,010	*0,002*	0,006	0,003	0,002	0,004	0,001
TH-20-30-A-17	Pyrrhotite	2,61	0,77	0,007	0,027	0,01	0,006	0,067	0,025	0,001	0,072	0,042	0,003
TH-20-30-A-18	Pyrrhotite	10,19	2,53	0,006	0,037	0,01	0,007	0,280	0,095	0,003	0,254	0,109	0,004
TH-20-30-A-19	Pyrrhotite	4,44	2,12	0,005	0,020	0,01	0,005	0,124	0,068	0,002	0,092	0,046	0,002
TH-20-30-A-2	Pyrrhotite	1,15	0,52	0,013	*0,005*	0,01	0,009	0,004	0,010	0,002	0,002	0,005	0,001
TH-20-30-A-20	Pyrrhotite	3,00	1,05	0,004	0,026	0,01	0,004	0,131	0,051	0,001	0,083	0,031	0,002
TH-20-30-A-3	Pyrrhotite	2,10	1,18	0,008	0,015	0,01	0,008	0,001	0,004	0,001	*0,002*	0,000	0,003
TH-20-30-A-4	Pyrrhotite	1,05	0,24	0,010	0,014	0,01	0,009	0,002	0,005	0,001	*0,002*	0,000	0,004
TH-20-30-A-5	Pyrrhotite	3,39	1,86	0,013	0,022	0,01	0,011	0,004	0,008	0,003	*0,001*	0,000	0,003
TH-20-30-A-6	Pyrrhotite	1,44	0,50	0,009	*0,009*	0,01	0,017	*0,001*	0,003	0,002	0,000	0,010	0,003
TH-20-30-A-7	Pyrrhotite	1,56	0,48	0,009	0,021	0,02	0,008	*0,002*	0,003	0,003	*0,002*	0,003	0,004
TH-20-30-A-8	Pyrrhotite	3,21	1,34	0,008	0,031	0,02	0,008	0,005	0,005	0,002	0,002	0,007	0,000
TH-20-30-A-9	Pyrrhotite	1,37	0,38	0,007	0,019	0,01	0,005	*0,002*	0,005	0,004	0,003	0,006	0,003
TH-20-30-2-24	Chalcopyrite	28,30	21,94	0,004	6,693	2,27	0,007	0,960	0,315	0,003	0,986	0,300	0,003
TH-20-30-2-23	Chalcopyrite	4,50	1,71	0,007	1,554	0,39	0,009	0,173	0,075	0,002	0,159	0,060	0,002
TH-20-30-2-17	Chalcopyrite	35,40	20,04	0,010	1,897	0,87	0,013	0,682	0,473	0,003	0,334	0,080	0,001
TH-20-30-2-22	Chalcopyrite	15,40	6,54	0,006	1,528	0,47	0,007	0,090	0,044	0,002	0,084	0,030	0,002
TH-20-30-2-20	Chalcopyrite	37,50	25,23	0,005	12,315	5,56	0,008	2,667	1,328	0,000	1,425	0,710	0,002
TH-20-30-2-16	Chalcopyrite	70,90	24,71	0,005	0,954	0,45	0,007	0,335	0,262	0,000	0,236	0,170	0,002
TH-20-30-A-30	Magmatic bleb	326,00	239	0,010	0,978	0,48	0,009	3,189	1,022	0,004	0,763	0,430	0,002
TH-20-30-A-31	Magmatic bleb	139,00	45,69	0,020	1,584	0,69	0,014	0,496	0,226	0,007	0,193	0,080	0,002

Sample	Mineral phase	Ti			V			Mn			Fe			Co		
		concentration (ppm)	σ	LOD	concentration (ppm)	σ	LOD	concentration (ppm)	σ	LOD	concentration (ppm)	σ	LOD	concentration (ppm)	σ	LOD
TH-20-30-A-32	Magmatic bleb	923	379	1,34	12,00	4,25	0,19	374	77	3,21	383850	0,00	44,23	932,60	344,2	0,20
TH-20-30-A-33	Magmatic bleb	1374	519	1,30	34,00	15,41	0,19	448	86	3,42	377020	0,00	45,97	607,90	157,4	0,22
TH-20-30-2-1	Ovoid magnetite	n.d.	n.d.	n.d.	1,16	0,19	0,16	604	73	3,75	730690	0,00	20,39	10,90	1,3	0,18
TH-20-30-2-11	Ovoid magnetite	*652*	93	1304	1,04	0,41	0,17	597	67	3,88	725450	0,00	21,14	15,90	2,7	0,19
TH-20-30-2-12	Ovoid magnetite	*1163*	115	2327	0,30	0,24	0,18	636	57	3,86	725450	0,00	21,43	16,00	3,0	0,19
TH-20-30-2-13	Ovoid magnetite	*1903*	85	3807	2,43	0,59	0,17	615	51	3,77	725450	0,00	20,79	12,50	1,7	0,18
TH-20-30-2-2	Ovoid magnetite	919	103	83	1,50	0,38	0,17	670	59	3,76	730690	0,00	20,37	12,80	4,6	0,18
TH-20-30-2-25	Ovoid magnetite	3312	740	3	130,93	37,75	0,28	845	95	5,76	735740	0,00	31,41	10,60	1,3	0,28
TH-20-30-2-26	Ovoid magnetite	2524	390	2	96,70	12,49	0,19	792	39	4,31	735450	0,00	23,64	10,10	1,0	0,21
TH-20-30-2-27	Ovoid magnetite	*7574*	88	15148	8,92	1,25	0,15	530	29	3,39	721840	0,00	18,85	12,80	3,0	0,17
TH-20-30-2-28	Ovoid magnetite	*463*	109	927	1,34	0,36	0,16	573	44	3,56	721840	0,00	19,76	15,30	5,1	0,18
TH-20-30-2-29	Ovoid magnetite	925	122	45	6,19	1,04	0,16	626	68	3,55	721840	0,00	19,44	15,70	3,2	0,18
TH-20-30-2-3	Ovoid magnetite	998	147	20	8,32	0,83	0,17	691	75	3,93	730690	0,00	21,18	12,50	1,2	0,19
TH-20-30-2-30	Ovoid magnetite	933	112	479	1,94	0,40	0,16	627	44	3,59	721840	0,00	20,43	12,30	1,8	0,18
TH-20-30-2-31	Ovoid magnetite	1043	118	63	9,47	3,39	0,17	650	81	3,98	721840	0,00	22,02	22,90	10,4	0,20
TH-20-30-2-32	Ovoid magnetite	*677*	130	1354	4,27	0,50	0,15	557	35	3,48	721840	0,00	19,22	12,80	1,7	0,18
TH-20-30-2-33	Ovoid magnetite	942	94	24	20,30	2,58	0,16	702	69	3,52	726310	0,00	19,49	17,10	1,6	0,17
TH-20-30-2-34	Ovoid magnetite	965	130	184	3,30	0,37	0,17	634	51	3,78	726310	0,00	20,99	20,00	1,9	0,19
TH-20-30-2-35	Ovoid magnetite	1008	155	213	1,08	0,27	0,17	620	68	3,88	726310	0,00	21,44	22,70	2,2	0,19
TH-20-30-2-36	Ovoid magnetite	930	96	616	1,54	0,26	0,16	760	82	3,60	726310	0,00	20,10	33,80	5,5	0,18
TH-20-30-2-37	Ovoid magnetite	*645*	106	1289	16,46	2,56	0,16	598	51	3,66	726310	0,00	20,19	33,80	3,1	0,18
TH-20-30-2-4	Ovoid magnetite	1247	143	3	16,15	2,51	0,17	811	78	3,75	730690	0,00	20,45	13,80	1,4	0,18
TH-20-30-2-40	Ovoid magnetite	929	93	470	4,89	0,56	0,16	625	49	3,55	726310	0,00	19,67	42,10	3,6	0,18
TH-20-30-2-5	Ovoid magnetite	884	93	42	1,18	0,23	0,16	706	130	3,59	730690	0,00	19,71	14,70	4,3	0,17
TH-20-30-2-52	Ovoid magnetite	963	112	228	2,01	2,50	0,15	815	92	3,51	731890	0,00	19,78	17,50	1,8	0,18
TH-20-30-2-53	Ovoid magnetite	973	115	728	3,83	5,48	0,16	806	63	3,65	731890	0,00	20,13	16,20	2,1	0,19
TH-20-30-2-54	Ovoid magnetite	n.d.	n.d.	n.d.	2,46	1,95	0,17	744	76	3,66	731890	0,00	20,68	14,10	1,3	0,19
TH-20-30-2-55	Ovoid magnetite	1117	199	663	1,95	1,73	0,19	722	105	4,14	731890	0,00	22,56	12,70	2,0	0,21
TH-20-30-2-56	Ovoid magnetite	*658*	273	1316	8,57	8,02	0,20	690	126	4,26	731890	0,00	23,04	14,30	2,1	0,22
TH-20-30-2-57	Ovoid magnetite	1126	256	80	35,36	26,75	0,20	745	98	3,81	731890	0,00	21,88	14,30	1,3	0,20
TH-20-30-2-58	Ovoid magnetite	*1821*	113	3642	3,85	0,57	0,18	802	66	4,06	716860	0,00	22,27	16,20	1,2	0,20
TH-20-30-2-59	Ovoid magnetite	962	105	48	6,91	0,63	0,15	758	87	3,51	716860	0,00	19,13	8,30	0,7	0,18
TH-20-30-2-6	Ovoid magnetite	966	137	12	9,25	1,38	0,16	693	75	3,59	730690	0,00	19,74	13,40	2,4	0,17
TH-20-30-2-60	Ovoid magnetite	*1601*	123	3201	2,09	0,41	0,16	777	67	3,55	716860	0,00	19,58	16,50	1,2	0,17
TH-20-30-2-61	Ovoid magnetite	973	136	873	4,97	0,63	0,16	964	100	3,54	716860	0,00	19,43	32,90	3,4	0,17
TH-20-30-2-62	Ovoid magnetite	1069	156	176	20,50	2,11	0,17	652	57	3,87	716860	0,00	21,05	6,50	2,0	0,20
TH-20-30-2-63	Ovoid magnetite	1174	180	15	13,95	2,12	0,17	820	80	3,91	716860	0,00	21,24	8,00	1,0	0,19
TH-20-30-2-64	Ovoid magnetite	1203	206	8	11,40	1,88	0,17	634	36	3,69	716860	0,00	20,62	6,50	1,3	0,19
TH-20-30-2-65	Ovoid magnetite	1027	110	100	6,47	0,90	0,16	663	78	3,67	716860	0,00	20,17	5,40	1,5	0,18
TH-20-30-2-66	Ovoid magnetite	1231	151	8	14,55	3,04	0,17	731	76	3,91	716860	0,00	21,43	7,40	3,8	0,20
TH-20-30-3-18	Ovoid magnetite	813	101	230	23,43	3,25	0,16	956	224	3,75	719320	0,00	20,60	12,70	2,7	0,17
TH-20-30-3-25	Ovoid magnetite	842	237	301	3,40	1,29	0,17	541	170	3,82	725690	0,00	18,58	83,40	38,9	0,14
TH-20-30-3-26	Ovoid magnetite	1046	566	539	2,39	1,63	0,23	470	229	4,63	725690	0,00	17,99	79,80	74,1	0,09
TH-20-30-3-27	Ovoid magnetite	723	257	454	1,25	0,42	0,14	271	81	3,16	725690	0,00	15,68	93,50	12,5	0,12
TH-20-30-3-28	Ovoid magnetite	818	530	322	2,03	1,67	0,19	388	246	3,75	725690	0,00	13,70	130,90	98,5	0,08
TH-20-30-3-29	Ovoid magnetite	793	100	67	5,60	0,61	0,16	609	44	3,53	725690	0,00	19,58	6,30	0,6	0,16
TH-20-30-3-30	Ovoid magnetite	944	164	23	6,09	0,86	0,18	624	68	4,07	725690	0,00	22,31	7,00	0,9	0,18
TH-20-30-3-31	Ovoid magnetite	1142	100	3	12,93	1,20	0,16	616	76	3,64	725690	0,00	20,09	7,70	0,9	0,17
TH-20-30-3-32	Ovoid magnetite	918	89	20	10,25	1,04	0,17	644	85	3,91	725690	0,00	21,59	7,80	0,6	0,17
TH-20-30-3-36	Ovoid magnetite	*1311*	217	2623	0,77	0,60	0,22	469	171	4,48	723450	0,00	23,64	43,90	32,2	0,22
TH-20-30-3-37	Ovoid magnetite	1579	800	662	0,77	0,84	0,40	726	105	5,37	723450	0,00	30,53	45,00	3,6	0,26
TH-20-30-3-38	Ovoid magnetite	*506*	143	1012	*0,79*	0,24	1,57	674	53	4,17	723450	0,00	23,21	40,50	3,0	0,20
TH-20-30-3-39	Ovoid magnetite	934	144	275	13,06	1,35	0,18	685	78	4,11	723450	0,00	22,11	28,80	3,0	0,19
TH-20-30-3-40	Ovoid magnetite	n.d.	n.d.	n.d.	0,28	0,30	0,15	519	62	4,29	723450	0,00	23,77	25,90	2,2	0,21

Sample	Mineral phase	Ni			Cu			Zn			As			Nb		
		concentration (ppm)	σ	LOD	concentration (ppm)	σ	LOD	concentration (ppm)	σ	LOD	concentration (ppm)	σ	LOD	concentration (ppm)	σ	LOD
TH-20-30-A-32	Magmatic bleb	1052,00	350,2	0,62	96261	38638	0,20	930,00	334	0,96	6,04	2,24	0,26	4,21	1,62	0,008
TH-20-30-A-33	Magmatic bleb	278,10	84,4	0,64	97346	21978	0,22	1346,00	342	1,01	3,63	1,20	0,25	6,06	1,69	0,009
TH-20-30-2-1	Ovoid magnetite	0,97	0,9	0,47	1,50	5,4	0,13	330,00	23	0,77	*0,48*	1,45	0,95	1,43	0,13	0,007
TH-20-30-2-11	Ovoid magnetite	2,19	1,6	0,47	23,70	32,6	0,14	302,00	30	0,81	*0,60*	1,70	1,19	0,81	0,15	0,009
TH-20-30-2-12	Ovoid magnetite	1,53	1,4	0,46	12,50	17,2	0,13	304,00	27	0,80	*0,65*	1,09	1,29	1,49	0,22	0,008
TH-20-30-2-13	Ovoid magnetite	1,59	1,6	0,44	41,10	37,8	0,13	309,00	29	0,80	*0,59*	1,53	1,17	0,48	0,09	0,009
TH-20-30-2-2	Ovoid magnetite	1,63	1,8	0,54	44,30	69,7	0,14	338,00	22	0,79	*0,55*	1,41	1,09	1,80	0,27	0,005
TH-20-30-2-25	Ovoid magnetite	*0,37*	1,1	0,73	450,20	293,5	0,30	336,00	31	1,22	9,09	4,68	1,94	5,91	0,65	0,012
TH-20-30-2-26	Ovoid magnetite	0,82	0,7	0,51	58,00	69,4	0,19	295,00	16	0,91	2,30	3,39	1,46	5,67	0,69	0,009
TH-20-30-2-27	Ovoid magnetite	0,89	1,2	0,41	49,00	81,0	0,14	330,00	23	0,68	*0,49*	1,14	0,97	0,31	0,08	0,007
TH-20-30-2-28	Ovoid magnetite	1,74	1,6	0,45	108,30	142,3	0,16	366,00	28	0,73	*0,58*	1,00	1,16	0,62	0,09	0,009
TH-20-30-2-29	Ovoid magnetite	2,74	1,4	0,43	317,30	410,4	0,14	361,00	38	0,72	*1,14*	1,51	2,28	1,84	0,30	0,009
TH-20-30-2-3	Ovoid magnetite	1,56	0,9	0,54	0,70	1,4	0,12	325,00	21	0,80	*0,64*	1,62	1,27	2,65	0,27	0,007
TH-20-30-2-30	Ovoid magnetite	0,86	0,5	0,44	48,40	66,7	0,15	373,00	35	0,74	*0,48*	1,36	0,96	0,98	0,17	0,009
TH-20-30-2-31	Ovoid magnetite	3,88	2,2	0,46	1491,50	1365,7	0,16	429,00	48	0,80	9,30	5,01	1,18	1,13	0,14	0,010
TH-20-30-2-32	Ovoid magnetite	1,63	1,0	0,42	94,00	104,0	0,14	325,00	30	0,70	*0,56*	1,51	1,12	0,49	0,08	0,005
TH-20-30-2-33	Ovoid magnetite	1,58	0,5	0,42	21,90	26,4	0,13	390,00	33	0,70	4,07	2,25	1,05	3,00	0,29	0,008
TH-20-30-2-34	Ovoid magnetite	1,83	0,6	0,45	31,90	14,5	0,15	397,00	31	0,75	15,42	11,31	1,23	1,45	0,14	0,009
TH-20-30-2-35	Ovoid magnetite	1,58	0,9	0,46	54,00	43,8	0,14	400,00	31	0,77	14,79	6,52	1,17	0,37	0,07	0,010
TH-20-30-2-36	Ovoid magnetite	3,62	2,7	0,45	195,70	345,6	0,15	400,00	42	0,73	1,14	1,90	1,13	1,41	0,20	0,008
TH-20-30-2-37	Ovoid magnetite	2,58	0,8	0,44	2,20	0,9	0,14	378,00	25	0,75	1,47	2,17	1,15	0,36	0,07	0,007
TH-20-30-2-4	Ovoid magnetite	1,36	0,7	0,45	1,90	5,1	0,13	351,00	34	0,79	*0,57*	1,52	1,14	3,90	0,47	0,007
TH-20-30-2-40	Ovoid magnetite	4,26	0,9	0,43	22,60	17,1	0,14	356,00	25	0,73	22,10	15,00	1,13	1,05	0,13	0,007
TH-20-30-2-5	Ovoid magnetite	0,99	0,9	0,44	104,00	140,4	0,12	272,00	21	0,75	*0,51*	1,23	1,01	1,36	0,20	0,007
TH-20-30-2-52	Ovoid magnetite	1,57	0,7	0,43	63,80	9,0	0,13	295,00	18	0,74	3,58	3,52	1,13	0,02	0,02	0,006
TH-20-30-2-53	Ovoid magnetite	1,54	0,5	0,43	75,30	9,4	0,13	297,00	24	0,76	5,69	5,00	1,39	0,02	0,01	0,006
TH-20-30-2-54	Ovoid magnetite	1,24	0,6	0,45	70,60	23,2	0,14	315,00	26	0,76	3,17	2,54	1,27	0,08	0,03	0,009
TH-20-30-2-55	Ovoid magnetite	1,12	0,6	0,50	86,30	46,4	0,17	271,00	25	0,84	3,76	2,68	1,44	0,08	0,03	0,007
TH-20-30-2-56	Ovoid magnetite	2,45	1,4	0,48	147,70	37,3	0,15	308,00	50	0,90	3,94	4,74	1,55	0,01	0,01	0,010
TH-20-30-2-57	Ovoid magnetite	1,78	0,7	0,50	62,90	21,4	0,16	298,00	31	0,81	12,69	13,10	1,57	0,10	0,05	0,008
TH-20-30-2-58	Ovoid magnetite	0,74	0,6	0,48	7,30	13,2	0,14	385,00	28	0,83	*0,44*	1,98	0,88	1,49	0,17	0,009
TH-20-30-2-59	Ovoid magnetite	0,44	0,5	0,39	2,50	3,3	0,13	344,00	23	0,70	1,35	0,85	1,14	1,73	0,22	0,005
TH-20-30-2-6	Ovoid magnetite	1,67	0,8	0,43	30,40	58,2	0,11	340,00	28	0,72	1,66	1,61	1,00	1,69	0,18	0,006
TH-20-30-2-60	Ovoid magnetite	0,65	0,7	0,42	2,60	9,1	0,11	353,00	20	0,71	*0,59*	1,11	1,18	1,03	0,11	0,006
TH-20-30-2-61	Ovoid magnetite	3,35	0,9	0,42	11,10	44,5	0,66	361,00	39	0,71	*0,61*	1,36	1,21	5,74	0,55	0,006
TH-20-30-2-62	Ovoid magnetite	0,67	1,0	0,50	118,20	139,1	0,18	339,00	43	0,77	*0,68*	1,32	1,35	0,06	0,02	0,007
TH-20-30-2-63	Ovoid magnetite	0,79	1,2	0,45	1,30	1,5	0,15	356,00	50	0,79	*1,06*	1,97	2,11	1,64	0,27	0,007
TH-20-30-2-64	Ovoid magnetite	1,10	0,6	0,45	118,60	172,5	0,20	352,00	30	0,75	*0,67*	1,74	1,33	1,25	0,20	0,007
TH-20-30-2-65	Ovoid magnetite	0,70	0,6	0,44	409,50	309,6	0,14	299,00	39	0,75	*0,59*	1,37	1,18	0,65	0,15	0,008
TH-20-30-2-66	Ovoid magnetite	0,52	0,8	0,45	123,90	122,4	0,15	308,00	37	0,80	*0,62*	1,65	1,23	1,35	0,18	0,006
TH-20-30-3-18	Ovoid magnetite	2,65	3,6	0,60	193,00	220,0	0,13	268,00	29	0,81	*0,52*	0,83	1,04	0,37	0,08	0,010
TH-20-30-3-25	Ovoid magnetite	28,47	14,0	0,38	534,70	453,6	0,08	264,00	61	0,78	1,58	1,57	0,80	0,52	0,20	0,010
TH-20-30-3-26	Ovoid magnetite	28,39	29,9	0,24	752,30	726,3	0,07	256,00	110	0,97	1,87	1,87	0,80	0,41	0,33	0,011
TH-20-30-3-27	Ovoid magnetite	32,89	5,2	0,33	1242,00	402,4	0,09	173,00	38	0,67	1,83	0,70	0,74	0,18	0,10	0,007
TH-20-30-3-28	Ovoid magnetite	47,88	36,4	0,21	889,60	729,8	0,06	193,00	102	0,75	7,67	10,39	0,55	0,38	0,35	0,009
TH-20-30-3-29	Ovoid magnetite	*0,21*	0,6	0,41	*0,06*	0,1	0,11	278,00	35	0,74	*0,45*	1,43	0,90	0,80	0,11	0,007
TH-20-30-3-30	Ovoid magnetite	0,86	1,0	0,45	81,70	99,5	0,13	317,00	46	0,86	*0,58*	1,61	1,15	0,89	0,18	0,007
TH-20-30-3-31	Ovoid magnetite	0,95	0,5	0,44	0,40	0,4	0,13	285,00	28	0,77	*0,51*	1,27	1,02	1,41	0,19	0,016
TH-20-30-3-32	Ovoid magnetite	0,89	0,6	0,48	0,90	0,5	0,13	275,00	25	0,81	*0,55*	1,48	1,09	1,03	0,13	0,008
TH-20-30-3-36	Ovoid magnetite	8,22	3,0	0,55	827,40	634,1	0,16	311,00	114	0,96	1,48	1,52	1,18	0,01	0,01	0,007
TH-20-30-3-37	Ovoid magnetite	6,89	1,5	0,69	1310,50	848,8	0,26	391,00	40	1,19	2,08	1,92	1,86	0,04	0,03	0,016
TH-20-30-3-38	Ovoid magnetite	2,95	0,6	0,52	540,30	101,4	0,14	345,00	34	0,88	*0,53*	1,24	1,05	0,01	0,01	0,006
TH-20-30-3-39	Ovoid magnetite	5,21	1,0	0,50	329,20	115,7	0,14	322,00	32	0,85	*0,62*	2,00	1,23	0,62	0,14	0,008
TH-20-30-3-40	Ovoid magnetite	3,33	1,1	0,51	131,00	57,1	0,16	319,00	34	0,92	*0,51*	1,77	1,02	0,01	0,010	0,006

Sample	Mineral phase	Mo			Ag			Cd			In			Sn		
		concentration (ppm)	σ	LOD	concentration (ppm)	σ	LOD	concentration (ppm)	σ	LOD	concentration (ppm)	σ	LOD	concentration (ppm)	σ	LOD
TH-20-30-A-32	Magmatic bleb	21,40	3,90	0,84	21,69	6,21	0,10	2,63	1,28	0,07	5,11	2,05	0,007	9,70	3,1	0,07
TH-20-30-A-33	Magmatic bleb	20,80	2,57	1,01	21,18	10,11	0,09	4,78	1,88	0,07	5,37	1,79	0,010	11,30	2,7	0,07
TH-20-30-2-1	Ovoid magnetite	12,50	1,30	0,09	0,03	0,09	0,05	0,07	0,16	0,13	0,89	0,09	0,010	14,50	2,1	0,33
TH-20-30-2-11	Ovoid magnetite	15,70	1,81	0,10	0,03	0,09	0,05	0,11	0,23	0,11	0,82	0,14	0,012	16,50	3,0	0,17
TH-20-30-2-12	Ovoid magnetite	16,90	2,13	0,10	0,03	0,08	0,05	0,06	0,15	0,11	0,83	0,15	0,010	17,30	2,4	0,16
TH-20-30-2-13	Ovoid magnetite	16,30	2,26	0,10	0,04	0,10	0,07	0,06	0,18	0,11	0,86	0,17	0,010	17,50	2,3	0,16
TH-20-30-2-2	Ovoid magnetite	12,20	1,37	0,10	0,03	0,12	0,05	0,06	0,16	0,12	0,86	0,10	0,010	15,90	1,9	0,28
TH-20-30-2-25	Ovoid magnetite	16,90	2,31	0,14	0,48	0,33	0,09	0,10	0,30	0,20	0,86	0,17	0,021	16,10	2,8	0,19
TH-20-30-2-26	Ovoid magnetite	15,10	2,11	0,10	0,16	0,15	0,06	0,07	0,15	0,13	0,76	0,11	0,010	16,10	1,9	0,14
TH-20-30-2-27	Ovoid magnetite	14,80	1,85	0,09	0,05	0,05	0,05	0,06	0,18	0,11	0,74	0,12	0,009	16,10	2,6	0,10
TH-20-30-2-28	Ovoid magnetite	15,90	1,96	0,09	0,03	0,08	0,05	0,06	0,20	0,11	0,81	0,10	0,010	17,50	1,8	0,11
TH-20-30-2-29	Ovoid magnetite	16,20	1,79	0,08	0,02	0,05	0,04	0,06	0,25	0,12	0,76	0,14	0,010	17,90	3,0	0,12
TH-20-30-2-3	Ovoid magnetite	11,70	1,20	0,09	n.d.	n.d.	n.d.	0,03	0,16	0,05	0,80	0,10	0,010	14,90	1,4	0,26
TH-20-30-2-30	Ovoid magnetite	14,20	1,61	0,09	0,03	0,06	0,06	0,06	0,13	0,12	0,81	0,14	0,010	17,30	1,9	0,11
TH-20-30-2-31	Ovoid magnetite	14,50	2,24	0,10	2,85	2,10	0,05	0,21	0,26	0,12	0,92	0,15	0,009	18,40	2,0	0,12
TH-20-30-2-32	Ovoid magnetite	14,70	1,86	0,09	0,07	0,08	0,05	0,06	0,13	0,11	0,79	0,10	0,010	16,30	1,8	0,10
TH-20-30-2-33	Ovoid magnetite	12,70	1,50	0,09	0,03	0,07	0,06	0,14	0,18	0,10	0,81	0,17	0,010	16,30	2,0	0,11
TH-20-30-2-34	Ovoid magnetite	13,70	1,78	0,09	0,04	0,05	0,08	0,04	0,14	0,08	0,87	0,15	0,008	19,50	2,9	0,11
TH-20-30-2-35	Ovoid magnetite	16,40	1,49	0,10	1,13	0,08	2,26	0,17	0,20	0,10	0,79	0,11	0,012	18,90	2,3	0,11
TH-20-30-2-36	Ovoid magnetite	14,70	1,78	0,09	0,07	0,05	0,04	0,25	0,42	0,10	0,90	0,14	0,011	19,20	1,7	0,12
TH-20-30-2-37	Ovoid magnetite	15,40	1,84	0,09	0,03	0,06	0,05	0,18	0,18	0,10	0,89	0,12	0,010	19,60	3,4	0,11
TH-20-30-2-4	Ovoid magnetite	12,80	1,67	0,09	0,03	0,09	0,05	0,06	0,16	0,11	0,82	0,17	0,014	16,30	2,4	0,23
TH-20-30-2-40	Ovoid magnetite	15,40	1,79	0,08	0,03	0,05	0,05	0,06	0,16	0,12	0,79	0,12	0,010	19,40	2,1	0,10
TH-20-30-2-5	Ovoid magnetite	14,20	1,46	0,09	0,02	0,06	0,04	0,06	0,14	0,11	0,77	0,12	0,013	14,60	1,9	0,20
TH-20-30-2-52	Ovoid magnetite	28,70	2,79	0,08	0,03	0,05	0,05	0,06	0,10	0,12	0,37	0,05	0,010	7,50	0,8	0,11
TH-20-30-2-53	Ovoid magnetite	28,00	4,13	0,10	0,03	0,07	0,05	0,14	0,20	0,12	0,43	0,10	0,010	7,80	1,4	0,10
TH-20-30-2-54	Ovoid magnetite	33,20	4,12	0,10	0,02	0,07	0,04	0,05	0,22	0,10	0,41	0,08	0,011	8,80	1,5	0,10
TH-20-30-2-55	Ovoid magnetite	32,60	3,31	0,09	0,03	0,05	0,05	0,06	0,17	0,12	0,41	0,08	0,010	8,90	1,3	0,12
TH-20-30-2-56	Ovoid magnetite	27,90	4,26	0,10	0,03	0,09	0,05	0,14	0,20	0,13	0,58	0,15	0,012	9,00	1,5	0,12
TH-20-30-2-57	Ovoid magnetite	29,90	3,21	0,10	0,03	0,06	0,05	0,05	0,15	0,09	0,62	0,22	0,012	10,30	1,8	0,11
TH-20-30-2-58	Ovoid magnetite	13,50	2,12	0,09	0,03	0,06	0,05	0,09	0,26	0,18	0,80	0,12	0,011	18,20	2,5	0,11
TH-20-30-2-59	Ovoid magnetite	13,00	2,22	0,09	0,03	0,05	0,05	0,06	0,12	0,11	0,77	0,09	0,009	16,20	1,6	0,10
TH-20-30-2-6	Ovoid magnetite	12,90	1,50	0,09	0,03	0,06	0,05	0,11	0,18	0,09	0,80	0,12	0,011	15,50	1,5	0,19
TH-20-30-2-60	Ovoid magnetite	12,90	1,38	0,08	0,04	0,07	0,07	0,07	0,16	0,13	0,80	0,12	0,010	17,60	2,3	0,10
TH-20-30-2-61	Ovoid magnetite	13,30	1,29	0,09	0,03	0,06	0,05	0,05	0,12	0,10	0,76	0,14	0,012	17,50	2,1	0,10
TH-20-30-2-62	Ovoid magnetite	14,60	1,54	0,10	0,03	0,06	0,05	0,15	0,18	0,12	0,75	0,10	0,011	18,20	2,4	0,10
TH-20-30-2-63	Ovoid magnetite	13,30	2,10	0,10	0,03	0,08	0,05	0,05	0,13	0,09	0,85	0,15	0,010	18,20	3,3	0,11
TH-20-30-2-64	Ovoid magnetite	13,80	1,72	0,09	0,02	0,07	0,04	0,05	0,12	0,09	0,80	0,12	0,011	17,50	2,1	0,10
TH-20-30-2-65	Ovoid magnetite	16,00	1,63	0,09	0,11	0,11	0,05	0,07	0,13	0,13	0,74	0,11	0,011	19,70	2,8	0,11
TH-20-30-2-66	Ovoid magnetite	15,30	2,22	0,10	0,03	0,09	0,06	0,18	0,20	0,11	0,73	0,12	0,009	19,40	3,3	0,11
TH-20-30-3-18	Ovoid magnetite	22,00	2,62	0,10	0,03	0,09	0,05	0,05	0,20	0,10	0,50	0,11	0,013	11,70	2,0	0,09
TH-20-30-3-25	Ovoid magnetite	16,10	2,56	0,08	0,44	0,41	0,03	3,08	2,57	0,06	0,70	0,11	0,011	13,90	4,4	0,09
TH-20-30-3-26	Ovoid magnetite	14,80	4,05	0,09	0,84	0,87	0,03	4,38	4,30	0,05	0,77	0,22	0,008	12,90	8,1	0,14
TH-20-30-3-27	Ovoid magnetite	10,00	1,39	0,07	0,65	0,33	0,03	8,23	1,60	0,08	0,63	0,14	0,008	6,30	1,8	0,07
TH-20-30-3-28	Ovoid magnetite	18,00	2,58	0,06	0,65	0,46	0,02	6,73	4,56	0,05	0,71	0,15	0,103	8,90	6,5	0,09
TH-20-30-3-29	Ovoid magnetite	18,40	2,49	0,10	0,03	0,07	0,05	0,06	0,15	0,12	0,00	0,34	0,008	16,90	2,8	0,09
TH-20-30-3-30	Ovoid magnetite	17,70	2,68	0,09	0,09	0,14	0,05	0,05	0,16	0,09	0,70	0,14	0,013	19,50	2,9	0,10
TH-20-30-3-31	Ovoid magnetite	17,90	1,98	0,08	0,03	0,08	0,05	0,06	0,24	0,12	0,65	0,08	0,008	17,20	1,7	0,09
TH-20-30-3-32	Ovoid magnetite	17,70	1,82	0,11	0,03	0,09	0,06	n.d.	n.d.	n.d.	0,67	0,13	0,012	16,20	2,0	0,08
TH-20-30-3-36	Ovoid magnetite	40,40	5,25	0,10	0,03	0,07	0,06	0,06	0,13	0,12	0,99	0,28	0,013	12,50	2,5	0,09
TH-20-30-3-37	Ovoid magnetite	40,80	7,83	0,13	0,24	0,24	0,15		0,35	0,18	1,52	1,01	0,022	18,00	10,7	0,16
TH-20-30-3-38	Ovoid magnetite	30,10	4,11	0,11	0,03	0,08	0,06	0,08	0,20	0,15	0,40	0,09	0,012	9,20	1,0	0,10
TH-20-30-3-39	Ovoid magnetite	25,90	4,20	0,10	0,04	0,08	0,08	0,08	0,17	0,16	0,64	0,11	0,011	15,80	2,5	0,10
TH-20-30-3-40	Ovoid magnetite	35,70	3,58	0,12	n.d.	n.d.	n.d.	0,05	0,18	0,10	0,53	0,10	0,010	10,70	1,4	0,11

Sample	Mineral phase	Sb			Te			W			Au			Tl		
		concentration (ppm)	σ	LOD	concentration (ppm)	σ	LOD	concentration (ppm)	σ	LOD	concentration (ppm)	σ	LOD	concentration (ppm)	σ	LOD
TH-20-30-A-32	Magmatic bleb	0,370	0,147	0,071	0,59	0,51	0,15	1,970	0,67	0,03	0,243	0,128	0,042	1,87	1,008	0,011
TH-20-30-A-33	Magmatic bleb	0,260	0,092	0,071	*0,06*	0,16	0,12	2,300	0,76	0,05	0,175	0,314	0,038	2,11	0,672	0,009
TH-20-30-2-1	Ovoid magnetite	n.d.	n.d.	n.d.	*0,03*	0,12	0,06	0,230	0,100	0,002	n.d.	n.d.	n.d.	n.d.	n.d.	n.d.
TH-20-30-2-11	Ovoid magnetite	*0,033*	0,067	0,066	*0,06*	0,15	0,11	0,252	0,143	0,016	*0,019*	0,066	0,038	*0,005*	0,020	0,010
TH-20-30-2-12	Ovoid magnetite	*0,029*	0,064	0,058	*0,03*	0,15	0,06	0,210	0,094	0,018	*0,018*	0,053	0,035	*0,008*	0,015	0,015
TH-20-30-2-13	Ovoid magnetite	*0,031*	0,076	0,062	0,20	0,27	0,09	0,208	0,093	0,008	*0,022*	0,061	0,043	0,020	0,035	0,015
TH-20-30-2-2	Ovoid magnetite	*0,027*	0,084	0,053	*0,09*	0,10	0,17	0,212	0,064	0,002	*0,019*	0,075	0,037	*0,008*	0,021	0,016
TH-20-30-2-25	Ovoid magnetite	*0,038*	0,154	0,076	0,31	0,41	0,17	0,522	0,202	0,031	*0,032*	0,098	0,063	0,328	0,262	0,035
TH-20-30-2-26	Ovoid magnetite	*0,037*	0,057	0,073	*0,09*	0,15	0,18	0,369	0,166	0,012	*0,028*	0,048	0,055	0,056	0,060	0,023
TH-20-30-2-27	Ovoid magnetite	*0,008*	0,070	0,015	*0,01*	0,13	0,01	0,159	0,104	0,014	*0,015*	0,059	0,029	*0,008*	0,018	0,016
TH-20-30-2-28	Ovoid magnetite	*0,038*	0,075	0,076	*0,03*	0,11	0,06	0,223	0,112	0,014	*0,023*	0,055	0,045	*0,012*	0,022	0,023
TH-20-30-2-29	Ovoid magnetite	*0,025*	0,052	0,050	*0,06*	0,08	0,11	0,265	0,113	0,012	*0,021*	0,056	0,041	n.d.	n.d.	n.d.
TH-20-30-2-3	Ovoid magnetite	0,050	0,050	0,055	n.d.	n.d.	n.d.	0,284	0,087	0,014	*0,009*	0,039	0,017	*0,009*	0,022	0,018
TH-20-30-2-30	Ovoid magnetite	*0,032*	0,057	0,063	*0,09*	0,09	0,17	0,151	0,084	0,008	*0,021*	0,054	0,041	*0,010*	0,022	0,019
TH-20-30-2-31	Ovoid magnetite	*0,031*	0,067	0,062	*0,07*	0,10	0,13	0,203	0,106	0,012	*0,025*	0,072	0,049	0,428	0,344	0,019
TH-20-30-2-32	Ovoid magnetite	*0,025*	0,067	0,050	*0,06*	0,10	0,11	0,218	0,102	0,008	*0,017*	0,052	0,034	0,045	0,053	0,015
TH-20-30-2-33	Ovoid magnetite	*0,028*	0,040	0,055	*0,07*	0,12	0,14	0,227	0,082	0,002	*0,022*	0,045	0,043	*0,005*	0,019	0,010
TH-20-30-2-34	Ovoid magnetite	*0,029*	0,087	0,058	*0,03*	0,18	0,05	0,232	0,085	0,002	*0,018*	0,055	0,036	*0,007*	0,018	0,013
TH-20-30-2-35	Ovoid magnetite	*0,020*	0,064	0,040	*0,08*	0,13	0,15	0,251	0,110	0,014	*0,023*	0,052	0,046	0,024	0,035	0,019
TH-20-30-2-36	Ovoid magnetite	*0,028*	0,082	0,056	*0,07*	0,12	0,14	0,222	0,092	0,010	0,044	0,082	0,039	*0,008*	0,018	0,015
TH-20-30-2-37	Ovoid magnetite	*0,024*	0,085	0,047	*0,05*	0,28	0,10	0,238	0,066	0,032	*0,018*	0,055	0,035	*0,008*	0,020	0,016
TH-20-30-2-4	Ovoid magnetite	*0,034*	0,071	0,068	*0,03*	0,13	0,05	0,263	0,098	0,014	*0,021*	0,062	0,041	*0,006*	0,016	0,011
TH-20-30-2-40	Ovoid magnetite	*0,027*	0,062	0,054	*0,07*	0,05	0,13	0,230	0,112	0,144	*0,019*	0,065	0,037	*0,008*	0,033	0,015
TH-20-30-2-5	Ovoid magnetite	*0,027*	0,052	0,053	*0,05*	0,16	0,10	0,302	0,162	0,010	*0,020*	0,042	0,039	0,016	0,033	0,014
TH-20-30-2-52	Ovoid magnetite	*0,022*	0,081	0,044	*0,07*	0,19	0,14	0,548	0,130	0,015	*0,025*	0,048	0,049	*0,008*	0,024	0,015
TH-20-30-2-53	Ovoid magnetite	*0,038*	0,075	0,076	*0,14*	0,23	0,27	0,589	0,188	0,008	*0,018*	0,059	0,036	*0,010*	0,031	0,020
TH-20-30-2-54	Ovoid magnetite	*0,039*	0,073	0,077	*0,07*	0,27	0,13	0,701	0,197	0,008	*0,009*	0,064	0,018	*0,008*	0,025	0,016
TH-20-30-2-55	Ovoid magnetite	*0,084*	0,085	0,168	*0,09*	0,14	0,17	0,729	0,200	0,013	*0,024*	0,051	0,047	0,027	0,031	0,018
TH-20-30-2-56	Ovoid magnetite	*0,027*	0,092	0,054	*0,09*	0,22	0,18	0,739	0,249	0,003	*0,029*	0,052	0,058	0,020	0,038	0,015
TH-20-30-2-57	Ovoid magnetite	*0,041*	0,120	0,082	0,18	0,27	0,14	1,031	0,369	0,015	*0,018*	0,039	0,036	0,033	0,035	0,015
TH-20-30-2-58	Ovoid magnetite	*0,034*	0,051	0,067	*0,07*	0,25	0,13	0,253	0,114	0,003	*0,022*	0,056	0,043	*0,008*	0,015	0,015
TH-20-30-2-59	Ovoid magnetite	*0,026*	0,062	0,051	*0,05*	0,16	0,09	0,198	0,095	0,007	*0,021*	0,052	0,041	0,018	0,027	0,015
TH-20-30-2-6	Ovoid magnetite	*0,026*	0,088	0,051	*0,06*	0,07	0,11	0,215	0,083	0,018	*0,020*	0,077	0,039	*0,009*	0,017	0,017
TH-20-30-2-60	Ovoid magnetite	*0,039*	0,067	0,078	*0,09*	0,12	0,18	0,245	0,100	0,007	*0,024*	0,038	0,047	*0,006*	0,022	0,012
TH-20-30-2-61	Ovoid magnetite	*0,026*	0,081	0,052	*0,05*	0,20	0,10	0,221	0,100	0,015	*0,024*	0,036	0,048	*0,007*	0,016	0,013
TH-20-30-2-62	Ovoid magnetite	*0,024*	0,069	0,047	*0,06*	0,15	0,11	0,212	0,083	0,002	*0,012*	0,048	0,024	*0,013*	0,020	0,025
TH-20-30-2-63	Ovoid magnetite	*0,034*	0,088	0,068	*0,08*	0,18	0,16	0,241	0,156	0,009	*0,024*	0,069	0,048	*0,010*	0,023	0,020
TH-20-30-2-64	Ovoid magnetite	*0,035*	0,071	0,069	*0,08*	0,15	0,15	0,211	0,118	0,012	n.d.	n.d.	n.d.	*0,020*	0,021	0,040
TH-20-30-2-65	Ovoid magnetite	*0,032*	0,057	0,063	*0,07*	0,17	0,13	0,274	0,130	0,002	*0,020*	0,073	0,039	0,140	0,116	0,014
TH-20-30-2-66	Ovoid magnetite	*0,028*	0,055	0,055	*0,08*	0,12	0,15	0,240	0,102	0,002	*0,029*	0,056	0,058	*0,002*	0,027	0,003
TH-20-30-3-18	Ovoid magnetite	*0,038*	0,073	0,076	*0,08*	0,14	0,15	0,355	0,134	0,008	n.d.	n.d.	n.d.	*0,008*	0,032	0,016
TH-20-30-3-25	Ovoid magnetite	*0,034*	0,072	0,068	n.d.	n.d.	n.d.	0,298	0,168	0,015	*0,013*	0,059	0,025	3,620	3,127	0,020
TH-20-30-3-26	Ovoid magnetite	*0,014*	0,104	0,027	*0,02*	0,21	0,03	0,278	0,224	0,003	0,026	0,070	0,024	3,556	2,114	0,016
TH-20-30-3-27	Ovoid magnetite	0,050	0,062	0,046	0,18	0,23	0,10	0,110	0,066	0,006	*0,013*	0,045	0,026	0,035	0,026	0,014
TH-20-30-3-28	Ovoid magnetite	0,140	0,152	0,028	0,05	0,19	0,04	0,164	0,122	0,010	0,034	0,068	0,024	3,224	2,363	0,009
TH-20-30-3-29	Ovoid magnetite	*0,035*	0,069	0,070	*0,05*	0,11	0,09	0,326	0,070	0,002	*0,012*	0,070	0,023	*0,009*	0,025	0,017
TH-20-30-3-30	Ovoid magnetite	*0,082*	0,119	0,163	*0,08*	0,06	0,15	0,347	0,148	0,014	*0,012*	0,053	0,024	*0,010*	0,041	0,019
TH-20-30-3-31	Ovoid magnetite	*0,018*	0,070	0,036	*0,05*	0,16	0,10	0,333	0,126	0,013	*0,021*	0,038	0,042	*0,010*	0,020	0,019
TH-20-30-3-32	Ovoid magnetite	*0,034*	0,084	0,068	*0,05*	0,16	0,10	0,399	0,113	0,002	*0,023*	0,039	0,045	0,068	0,061	0,021
TH-20-30-3-36	Ovoid magnetite	0,100	0,119	0,076	*0,05*	0,18	0,09	0,725	0,213	0,011	*0,025*	0,040	0,050	*0,010*	0,053	0,020
TH-20-30-3-37	Ovoid magnetite	0,170	0,210	0,135	*0,02*	0,28	0,03	1,346	0,856	0,016	*0,064*	0,091	0,127	n.d.	n.d.	n.d.
TH-20-30-3-38	Ovoid magnetite	*0,027*	0,097	0,054	*0,07*	0,13	0,14	0,664	0,211	0,003	*0,027*	0,046	0,053	*0,014*	0,022	0,028
TH-20-30-3-39	Ovoid magnetite	*0,031*	0,097	0,062	*0,06*	0,17	0,12	0,689	0,240	0,010	*0,016*	0,052	0,032	*0,010*	0,023	0,019
TH-20-30-3-40	Ovoid magnetite	*0,028*	0,103	0,056	*0,03*	0,19	0,05	0,757	0,211	0,024	*0,021*	0,059	0,041	*0,017*	0,015	0,033

Sample	Mineral phase	Pb			Bi			Th			U		
		concentration (ppm)	σ	LOD	concentration (ppm)	σ	LOD	concentration (ppm)	σ	LOD	concentration (ppm)	σ	LOD
TH-20-30-A-32	Magmatic bleb	53,80	11,80	0,013	2,479	1,40	0,009	9,232	3,188	0,003	4,393	1,890	0,001
TH-20-30-A-33	Magmatic bleb	65,32	6,32	0,013	2,108	1,96	0,012	10,194	2,505	0,006	3,984	1,020	0,005
TH-20-30-2-1	Ovoid magnetite	0,09	0,07	0,014	*0,007*	0,01	0,013	0,136	0,058	0,004	0,211	0,060	0,003
TH-20-30-2-11	Ovoid magnetite	0,19	0,14	0,015	*0,006*	0,01	0,012	0,214	0,061	0,001	0,207	0,050	0,003
TH-20-30-2-12	Ovoid magnetite	*0,01*	0,06	0,014	*0,007*	0,01	0,014	0,274	0,073	0,004	0,245	0,070	0,002
TH-20-30-2-13	Ovoid magnetite	0,16	0,08	0,010	0,054	0,05	0,012	0,170	0,069	0,005	0,193	0,050	0,004
TH-20-30-2-2	Ovoid magnetite	0,14	0,13	0,013	*0,006*	0,01	0,011	0,222	0,060	0,000	0,239	0,040	0,001
TH-20-30-2-25	Ovoid magnetite	3,04	1,40	0,026	1,748	1,27	0,022	3,366	1,606	0,005	1,294	0,510	0,004
TH-20-30-2-26	Ovoid magnetite	1,13	0,95	0,013	0,030	0,07	0,017	2,037	1,739	0,004	0,725	0,510	0,003
TH-20-30-2-27	Ovoid magnetite	*0,01*	0,04	0,016	*0,006*	0,01	0,011	0,000	0,011	0,004	0,117	0,030	0,003
TH-20-30-2-28	Ovoid magnetite	0,15	0,11	0,016	*0,007*	0,01	0,014	0,150	0,057	0,000	0,172	0,040	0,003
TH-20-30-2-29	Ovoid magnetite	0,14	0,08	0,009	0,034	0,02	0,011	0,191	0,103	0,003	0,192	0,060	0,001
TH-20-30-2-3	Ovoid magnetite	0,16	0,10	0,014	*0,007*	0,01	0,013	0,564	0,238	0,000	0,292	0,060	0,002
TH-20-30-2-30	Ovoid magnetite	0,14	0,09	0,010	*0,006*	0,01	0,012	0,080	0,055	0,000	0,151	0,030	0,002
TH-20-30-2-31	Ovoid magnetite	0,49	0,22	0,013	0,504	0,23	0,013	0,206	0,081	0,005	0,250	0,070	0,003
TH-20-30-2-32	Ovoid magnetite	*0,00*	0,07	0,009	0,010	0,02	0,011	0,127	0,074	0,003	0,172	0,040	0,002
TH-20-30-2-33	Ovoid magnetite	*0,01*	0,06	0,013	*0,005*	0,00	0,009	0,109	0,052	0,000	0,144	0,030	0,003
TH-20-30-2-34	Ovoid magnetite	0,41	0,61	0,013	*0,006*	0,01	0,011	0,080	0,047	0,003	0,120	0,050	0,003
TH-20-30-2-35	Ovoid magnetite	3,21	3,93	0,009	*0,008*	0,02	0,016	0,119	0,096	0,003	0,164	0,060	0,002
TH-20-30-2-36	Ovoid magnetite	*0,01*	0,09	0,011	*0,007*	0,02	0,013	0,149	0,075	0,002	0,184	0,030	0,002
TH-20-30-2-37	Ovoid magnetite	*0,01*	0,06	0,013	*0,005*	0,01	0,010	0,063	0,022	0,000	0,148	0,050	0,001
TH-20-30-2-4	Ovoid magnetite	*0,01*	0,03	0,015	*0,006*	0,01	0,012	0,196	0,083	0,003	0,232	0,060	0,001
TH-20-30-2-40	Ovoid magnetite	0,51	0,45	0,009	0,010	0,02	0,012	0,155	0,133	0,001	0,174	0,080	0,003
TH-20-30-2-5	Ovoid magnetite	0,22	0,16	0,008	*0,005*	0,01	0,010	0,177	0,051	0,002	0,292	0,090	0,001
TH-20-30-2-52	Ovoid magnetite	0,32	0,26	0,012	0,030	0,04	0,012	0,050	0,078	0,003	0,091	0,070	0,003
TH-20-30-2-53	Ovoid magnetite	0,59	0,27	0,010	0,110	0,07	0,013	0,043	0,043	0,000	0,097	0,080	0,001
TH-20-30-2-54	Ovoid magnetite	0,41	0,20	0,065	0,040	0,04	0,014	0,049	0,024	0,000	0,083	0,020	0,004
TH-20-30-2-55	Ovoid magnetite	0,31	0,36	0,013	0,040	0,05	0,011	0,090	0,055	0,003	0,151	0,050	0,003
TH-20-30-2-56	Ovoid magnetite	1,60	0,87	0,038	0,183	0,10	0,011	0,062	0,054	0,001	0,161	0,090	0,002
TH-20-30-2-57	Ovoid magnetite	1,42	0,84	0,015	0,174	0,14	0,013	0,235	0,163	0,004	0,358	0,190	0,001
TH-20-30-2-58	Ovoid magnetite	*0,01*	0,10	0,020	*0,007*	0,02	0,014	0,113	0,048	0,005	0,170	0,050	0,003
TH-20-30-2-59	Ovoid magnetite	*0,01*	0,13	0,011	*0,004*	0,01	0,008	0,112	0,056	0,004	0,186	0,060	0,001
TH-20-30-2-6	Ovoid magnetite	0,13	0,05	0,010	*0,005*	0,01	0,009	0,163	0,085	0,002	0,209	0,050	0,001
TH-20-30-2-60	Ovoid magnetite	*0,005*	0,05	0,009	*0,006*	0,01	0,012	0,126	0,090	0,003	0,171	0,060	0,002
TH-20-30-2-61	Ovoid magnetite	*0,01*	0,06	0,013	*0,007*	0,01	0,014	0,083	0,039	0,003	0,158	0,040	0,003
TH-20-30-2-62	Ovoid magnetite	0,22	0,10	0,014	n.d.	n.d.	n.d.	0,156	0,060	0,003	0,162	0,050	0,004
TH-20-30-2-63	Ovoid magnetite	*0,01*	0,05	0,017	*0,007*	0,01	0,013	0,131	0,089	0,001	0,182	0,070	0,001
TH-20-30-2-64	Ovoid magnetite	0,17	0,10	0,013	*0,008*	0,01	0,015	0,088	0,042	0,004	0,123	0,050	0,002
TH-20-30-2-65	Ovoid magnetite	0,26	0,21	0,012	0,183	0,11	0,011	0,110	0,070	0,000	0,120	0,030	0,002
TH-20-30-2-66	Ovoid magnetite	0,18	0,10	0,009	*0,003*	0,01	0,005	0,124	0,057	0,001	0,150	0,040	0,001
TH-20-30-3-18	Ovoid magnetite	0,21	0,16	0,011	0,040	0,07	0,015	0,013	0,016	0,007	0,071	0,020	0,002
TH-20-30-3-25	Ovoid magnetite	34,06	20,02	0,012	0,336	0,25	0,014	0,191	0,098	0,002	0,153	0,060	0,002
TH-20-30-3-26	Ovoid magnetite	14,95	12,85	0,006	0,571	0,43	0,008	0,176	0,071	0,002	0,122	0,050	0,001
TH-20-30-3-27	Ovoid magnetite	8,64	2,34	0,009	0,165	0,08	0,007	0,100	0,072	0,002	0,086	0,040	0,000
TH-20-30-3-28	Ovoid magnetite	34,25	25,27	0,006	0,508	0,29	0,008	0,140	0,077	0,000	0,123	0,040	0,002
TH-20-30-3-29	Ovoid magnetite	*0,01*	0,04	0,015	*0,010*	0,01	0,019	*0,002*	0,008	0,003	0,125	0,030	0,003
TH-20-30-3-30	Ovoid magnetite	0,17	0,10	0,005	0,470	0,69	0,012	0,126	0,068	0,004	0,136	0,030	0,001
TH-20-30-3-31	Ovoid magnetite	0,08	0,06	0,013	*0,005*	0,01	0,010	0,089	0,035	0,003	0,183	0,030	0,001
TH-20-30-3-32	Ovoid magnetite	0,54	0,39	0,012	0,010	0,01	0,009	0,835	0,813	0,003	0,303	0,150	0,001
TH-20-30-3-36	Ovoid magnetite	6,32	2,71	0,019	0,190	0,10	0,015	0,070	0,064	0,003	0,036	0,010	0,001
TH-20-30-3-37	Ovoid magnetite	10,53	8,96	0,030	0,386	0,38	0,031	0,100	0,086	0,006	0,084	0,070	0,002
TH-20-30-3-38	Ovoid magnetite	0,14	0,08	0,016	*0,010*	0,01	0,020	*0,001*	0,003	0,001	0,035	0,010	0,001
TH-20-30-3-39	Ovoid magnetite	2,88	1,98	0,016	0,057	0,04	0,014	0,088	0,039	0,001	0,123	0,050	0,001
TH-20-30-3-40	Ovoid magnetite	2,26	1,56	0,015	0,082	0,03	0,016	0,015	0,018	0,001	0,050	0,020	0,001

Sample	Mineral phase	Ti			V			Mn			Fe			Co		
		concentration (ppm)	σ	LOD	concentration (ppm)	σ	LOD	concentration (ppm)	σ	LOD	concentration (ppm)	σ	LOD	concentration (ppm)	σ	LOD
TH-20-30-3-41	Ovoid magnetite	982	157	171	13,94	8,71	0,18	669	169	4,18	723450	0,00	22,68	54,60	8,7	0,20
TH-20-30-A-21	Ovoid magnetite	3120	893	8	43,25	14,34	0,37	903	115	7,83	718070	0,00	41,50	7,60	5,8	0,43
TH-20-30-A-22	Ovoid magnetite	4046	653	3	102,64	16,69	0,28	901	129	6,16	718070	0,00	32,46	6,80	1,4	0,32
TH-20-30-A-24	Ovoid magnetite	n.d.	n.d.	n.d.	0,82	0,44	0,31	965	112	7,21	718070	0,00	38,46	30,40	6,7	0,38
TH-20-30-A-25	Ovoid magnetite	2149	439	400	35,74	12,93	0,31	952	156	7,39	718070	0,00	38,94	9,90	1,3	0,37
TH-20-30-A-26	Ovoid magnetite	1889	337	1650	2,88	0,89	0,29	811	160	6,61	718070	0,00	34,81	20,80	9,1	0,32
TH-20-30-A-27	Ovoid magnetite	2325	379	42	5,41	2,49	0,36	834	125	7,69	718070	0,00	41,19	9,50	5,3	0,37
TH-20-30-A-28	Ovoid magnetite	1802	268	350	1,38	0,48	0,28	799	145	6,46	718070	0,00	33,23	17,00	2,9	0,32
TH-20-30-2-10	Magmatic magnetite	68664	6787	1,14	3927,0	586,5	0,19	4297	547	4,28	627640	0,00	23,11	173,00	16,2	0,20
TH-20-30-2-38	Magmatic magnetite	11801	1414	1,72	1265,0	85,7	0,28	2009	140	6,32	708410	0,00	34,71	86,00	8,1	0,32
TH-20-30-2-39	Magmatic magnetite	15505	2448	2,36	1282,0	134,5	0,36	2091	266	8,07	708410	0,00	42,17	82,00	8,2	0,39
TH-20-30-2-67	Magmatic magnetite	79943	11128	1,03	4528,0	479,4	0,18	6136	813	4,01	620980	0,00	21,79	99,00	13,2	0,21
TH-20-30-2-68	Magmatic magnetite	78267	7836	1,07	4333,0	321,8	0,18	6093	659	4,01	604260	0,00	21,71	99,00	11,2	0,20
TH-20-30-2-69	Magmatic magnetite	96431	14748	1,18	5247,0	617,8	0,21	6153	867	4,56	597200	0,00	24,89	75,00	7,6	0,23
TH-20-30-2-7	Magmatic magnetite	67162	7641	1,00	3533,0	332,5	0,17	3951	328	3,92	606650	0,00	21,52	166,00	17,7	0,19
TH-20-30-2-70	Magmatic magnetite	86643	10539	1,16	5036,0	698,0	0,21	6163	778	4,62	607680	0,00	25,05	92,00	11,8	0,23
TH-20-30-2-8	Magmatic magnetite	69572	5857	1,06	3596,0	335,6	0,18	4136	418	4,18	628700	0,00	22,82	174,00	22,1	0,20
TH-20-30-2-9	Magmatic magnetite	68636	10107	1,13	3677,0	453,9	0,19	4285	571	4,29	622750	0,00	23,20	165,00	17,4	0,21
TH-20-30-3-10	Magmatic magnetite	83047	7558	1,09	4539,0	418,3	0,21	5066	553	4,73	628040	0,00	25,71	65,00	6,0	0,21
TH-20-30-3-12	Magmatic magnetite	137469	32935	2,25	9086,0	1332,6	0,42	7633	1491	9,80	598570	0,00	47,78	160,00	21,0	0,40
TH-20-30-3-13	Magmatic magnetite	87928	12565	1,19	5666,0	765,1	0,24	5924	681	5,24	565990	0,00	28,55	152,00	17,2	0,24
TH-20-30-3-14	Magmatic magnetite	89344	14209	3,23	4931,0	963,7	0,26	6065	1174	5,80	565990	0,00	30,21	146,00	13,6	0,25
TH-20-30-3-2	Magmatic magnetite	72955	11163	0,81	2299,0	354,6	0,18	6300	588	4,06	599790	0,00	22,70	113,00	13,8	0,18
TH-20-30-3-3	Magmatic magnetite	69858	6959	0,80	2143,0	265,6	0,18	6354	775	4,12	599790	0,00	22,72	111,00	14,5	0,18
TH-20-30-3-34	Magmatic magnetite	100077	10634	2,57	1408,0	157,8	0,49	9848	1120	11,45	663440	0,00	59,66	105,00	9,4	0,51
TH-20-30-3-35	Magmatic magnetite	99212	11978	1,22	1524,0	138,9	0,25	8749	514	5,45	663440	0,00	30,20	103,00	13,3	0,25
TH-20-30-3-4	Magmatic magnetite	73522	8563	0,82	2137,0	264,5	0,17	6181	779	4,01	599790	0,00	22,01	113,00	12,0	0,18
TH-20-30-3-42	Magmatic magnetite	79544	10597	1,44	1172,0	126,2	0,30	8293	1523	7,16	597600	0,00	37,07	100,00	15,4	0,34
TH-20-30-3-43	Magmatic magnetite	74407	6502	0,90	2079,0	281,0	0,19	6386	582	4,26	597600	0,00	23,63	109,00	9,6	0,20
TH-20-30-3-44	Magmatic magnetite	80976	9506	1,39	4241,0	508,9	0,27	4865	571	6,06	582520	0,00	32,11	160,00	18,8	0,28
TH-20-30-3-45	Magmatic magnetite	75530	9916	0,91	4037,0	482,0	0,18	4285	408	3,99	582520	0,00	21,80	169,00	23,6	0,19
TH-20-30-3-46	Magmatic magnetite	77024	6979	1,48	4244,0	452,6	0,21	4854	779	4,76	582520	0,00	25,44	177,00	19,8	0,22
TH-20-30-3-47	Magmatic magnetite	80342	10541	1,13	4482,0	722,9	0,21	4728	569	4,73	582520	0,00	25,50	176,00	26,4	0,22
TH-20-30-3-48	Magmatic magnetite	80586	8754	1,44	4260,0	595,2	0,28	4982	533	5,90	582520	0,00	32,18	168,00	20,6	0,28
TH-20-30-3-49	Magmatic magnetite	77825	9764	1,26	4360,0	600,7	0,23	4770	521	5,10	582520	0,00	27,70	168,00	24,2	0,25
TH-20-30-3-5	Magmatic magnetite	65425	5372	1,21	4933,0	650,6	0,25	5248	788	5,70	637480	0,00	32,01	75,00	10,6	0,25
TH-20-30-3-50	Magmatic magnetite	85644	8112	1,55	4495,0	466,7	0,29	5240	458	6,32	582520	0,00	34,45	175,00	16,4	0,30
TH-20-30-3-51	Magmatic magnetite	70897	9993	1,12	2464,0	395,4	0,20	6098	853	4,52	590550	0,00	24,40	120,00	18,4	0,21
TH-20-30-3-52	Magmatic magnetite	72254	11121	1,20	2547,0	387,2	0,21	5310	683	4,76	569660	0,00	25,84	127,00	18,2	0,22
TH-20-30-3-53	Magmatic magnetite	72783	8490	1,13	2533,0	395,6	0,20	5032	728	4,49	590550	0,00	24,43	128,00	15,4	0,22
TH-20-30-3-54	Magmatic magnetite	74511	8539	1,25	2588,0	367,7	0,21	5834	1149	4,95	569660	0,00	25,97	135,00	15,0	0,27
TH-20-30-3-55	Magmatic magnetite	80176	10652	1,14	3992,0	436,5	0,19	4616	521	4,33	605300	0,00	23,60	172,00	19,7	0,21
TH-20-30-3-56	Magmatic magnetite	80295	9935	1,39	4148,0	494,0	0,23	4854	528	5,26	605300	0,00	28,68	162,00	25,5	0,25
TH-20-30-3-57	Magmatic magnetite	82261	14150	1,35	4076,0	594,2	0,23	4734	750	5,24	605300	0,00	27,77	169,00	23,7	0,25
TH-20-30-3-58	Magmatic magnetite	77604	8142	1,81	4176,0	237,6	0,30	4908	530	6,65	605300	0,00	35,79	169,00	25,0	0,32
TH-20-30-3-6	Magmatic magnetite	62222	7023	0,92	4767,0	577,5	0,20	4587	546	4,67	637480	0,00	25,71	66,00	8,6	0,21
TH-20-30-3-7	Magmatic magnetite	87294	13541	1,06	5139,0	848,1	0,23	6134	821	5,12	637480	0,00	28,08	98,00	13,6	0,23
TH-20-30-3-8	Magmatic magnetite	89998	9482	1,24	5244,0	639,0	0,26	5979	734	5,87	637480	0,00	32,07	63,00	9,0	0,26
TH-20-30-3-9	Magmatic magnetite	80425	12130	1,16	4307,0	579,6	0,25	6009	753	5,28	637480	0,00	28,49	65,00	9,5	0,24
TH-20-30-A-29	Magmatic magnetite	83319	13575	1,78	3485,0	552,0	0,31	5971	960	6,97	568940	0,00	35,58	248,00	43,7	0,35
TH-20-30-A-34	Magmatic magnetite	75613	13272	1,57	3833,0	808,5	0,27	5690	1420	6,13	584280	0,00	31,34	135,00	31,6	0,31

Analyses below the limit of detection are reported in italic as half the value of the limit of detection. Fe data from EMPA are used as internal standard. n.d. not determined.

Sample	Mineral phase	Ni			Cu			Zn			As			Nb		
		concentration (ppm)	σ	LOD	concentration (ppm)	σ	LOD	concentration (ppm)	σ	LOD	concentration (ppm)	σ	LOD	concentration (ppm)	σ	LOD
TH-20-30-3-41	Ovoid magnetite	6,13	2,9	0,53	1110,80	623,7	0,16	351,00	34	0,89	*0,82*	1,94	1,63	0,13	0,07	0,009
TH-20-30-A-21	Ovoid magnetite	2,16	3,9	1,19	231,30	301,5	0,37	354,00	37	1,71	3,95	3,38	2,76	2,06	0,35	0,016
TH-20-30-A-22	Ovoid magnetite	1,15	1,1	0,76	61,50	36,2	0,21	326,00	41	1,34	*1,05*	2,28	2,09	3,36	0,71	0,012
TH-20-30-A-24	Ovoid magnetite	7,25	2,2	0,86	281,60	51,7	0,27	303,00	39	1,56	15,78	9,79	2,42	0,64	0,11	0,016
TH-20-30-A-25	Ovoid magnetite	2,38	1,2	0,84	181,40	433,0	0,28	258,00	46	1,66	10,19	4,92	2,51	8,31	2,43	0,021
TH-20-30-A-26	Ovoid magnetite	3,45	3,0	0,73	244,60	119,8	0,21	316,00	66	1,48	6,30	7,27	2,20	6,74	1,20	0,013
TH-20-30-A-27	Ovoid magnetite	0,98	1,2	0,83	339,80	203,3	0,29	271,00	43	1,74	14,93	13,23	2,49	1,50	0,59	0,020
TH-20-30-A-28	Ovoid magnetite	3,39	1,6	0,73	426,30	216,2	0,23	256,00	25	1,38	35,34	15,07	2,07	1,87	0,35	0,012
TH-20-30-2-10	Magmatic magnetite	23,20	3,1	0,52	8,60	3,8	0,15	737,00	64	0,86	8,22	4,97	1,28	8,10	1,00	0,010
TH-20-30-2-38	Magmatic magnetite	9,60	1,3	0,75	111,10	113,3	0,32	459,00	62	1,34	35,83	36,41	2,49	19,10	2,35	0,012
TH-20-30-2-39	Magmatic magnetite	9,90	1,1	0,94	115,20	98,0	0,44	466,00	81	1,73	37,26	39,48	3,59	17,73	2,50	0,014
TH-20-30-2-67	Magmatic magnetite	20,10	2,8	0,47	27,00	6,8	0,16	1317,00	179	0,75	2,73	2,53	1,36	9,69	1,29	0,010
TH-20-30-2-68	Magmatic magnetite	20,00	2,4	0,47	15,80	3,5	0,16	1334,00	162	0,75	*0,61*	1,73	1,21	9,43	1,13	0,009
TH-20-30-2-69	Magmatic magnetite	16,10	1,7	0,55	131,10	110,7	0,16	1237,00	106	0,87	5,30	2,04	1,54	24,57	4,17	0,008
TH-20-30-2-7	Magmatic magnetite	21,80	3,1	0,49	3,40	0,5	0,14	660,00	68	0,79	*0,23*	1,28	0,45	7,60	0,95	0,008
TH-20-30-2-70	Magmatic magnetite	17,00	2,5	0,55	100,00	41,2	0,18	1286,00	208	0,89	45,33	14,36	1,54	11,33	1,36	0,009
TH-20-30-2-8	Magmatic magnetite	23,60	4,3	0,50	3,90	0,7	0,72	709,00	67	0,81	1,55	1,67	1,17	8,35	0,95	0,008
TH-20-30-2-9	Magmatic magnetite	23,80	4,0	0,52	*0,08*	5,2	0,15	717,00	88	0,86	*0,58*	1,99	1,16	7,82	1,14	0,009
TH-20-30-3-10	Magmatic magnetite	14,10	1,3	0,57	123,50	49,0	0,18	1293,00	149	0,96	16,56	8,27	1,28	7,75	0,94	0,011
TH-20-30-3-12	Magmatic magnetite	14,00	3,2	1,14	90,20	23,1	0,29	1382,00	174	1,86	14,44	6,65	2,88	24,32	10,06	0,035
TH-20-30-3-13	Magmatic magnetite	17,00	2,2	0,66	225,50	53,4	0,18	1432,00	153	1,05	14,00	6,33	1,44	12,29	1,46	0,012
TH-20-30-3-14	Magmatic magnetite	18,00	3,1	0,68	381,80	105,9	0,19	1373,00	138	1,13	34,62	13,84	1,41	14,05	2,78	0,013
TH-20-30-3-2	Magmatic magnetite	15,00	3,3	0,51	7,80	1,4	0,15	903,00	124	0,84	*0,54*	1,09	1,08	10,44	1,48	0,007
TH-20-30-3-3	Magmatic magnetite	14,40	2,1	0,51	8,40	1,3	0,15	897,00	93	0,84	*0,56*	1,58	1,11	10,83	1,12	0,009
TH-20-30-3-34	Magmatic magnetite	8,30	1,5	1,37	21,30	2,5	0,38	1119,00	186	2,31	21,53	8,00	3,21	38,65	6,16	0,023
TH-20-30-3-35	Magmatic magnetite	7,10	1,3	0,67	12,00	1,8	0,20	1109,00	137	1,14	5,36	2,10	1,57	25,51	2,84	0,013
TH-20-30-3-4	Magmatic magnetite	14,40	2,2	0,51	8,30	1,0	0,15	887,00	98	0,80	*0,60*	1,41	1,20	11,55	1,21	0,007
TH-20-30-3-42	Magmatic magnetite	6,10	2,2	0,96	19,60	2,6	0,26	1088,00	217	1,46	5,44	2,72	1,89	23,83	2,78	0,019
TH-20-30-3-43	Magmatic magnetite	8,50	1,3	0,53	16,80	1,7	0,15	1016,00	139	0,86	*0,49*	1,19	0,97	13,34	1,27	0,012
TH-20-30-3-44	Magmatic magnetite	29,70	3,4	0,71	42,90	25,4	0,26	836,00	105	1,24	5,29	4,95	2,24	10,71	1,87	0,014
TH-20-30-3-45	Magmatic magnetite	30,90	5,0	0,49	19,40	4,3	0,14	897,00	112	0,81	1,45	1,61	1,20	9,90	1,29	0,007
TH-20-30-3-46	Magmatic magnetite	33,80	7,6	0,61	114,20	50,6	0,18	904,00	124	0,96	8,04	5,31	1,45	10,50	1,29	0,007
TH-20-30-3-47	Magmatic magnetite	31,30	5,2	0,58	24,30	3,8	0,16	975,00	122	0,95	1,45	1,34	1,29	11,12	1,71	0,011
TH-20-30-3-48	Magmatic magnetite	29,50	3,4	0,70	285,10	64,9	0,22	857,00	144	1,20	10,55	2,78	1,67	10,44	1,47	0,013
TH-20-30-3-49	Magmatic magnetite	29,20	5,0	0,64	167,00	51,6	0,18	899,00	103	1,03	13,59	4,03	1,38	10,89	1,18	0,011
TH-20-30-3-5	Magmatic magnetite	16,20	2,6	0,70	50,60	22,1	0,20	1444,00	176	1,14	12,10	4,23	1,50	10,50	1,00	0,014
TH-20-30-3-50	Magmatic magnetite	30,20	2,7	0,78	159,80	40,5	0,23	887,00	86	1,29	14,33	3,29	1,71	12,31	1,34	0,021
TH-20-30-3-51	Magmatic magnetite	17,90	3,1	0,55	20,00	4,2	0,16	955,00	193	0,95	*0,57*	1,50	1,14	9,22	1,14	0,011
TH-20-30-3-52	Magmatic magnetite	20,70	4,0	0,58	17,50	2,8	0,17	893,00	118	0,96	*0,73*	1,45	1,46	6,22	0,78	0,011
TH-20-30-3-53	Magmatic magnetite	21,40	4,1	0,56	18,10	3,0	0,16	859,00	134	0,91	*0,63*	1,55	1,26	5,78	0,96	0,010
TH-20-30-3-54	Magmatic magnetite	21,50	4,3	0,57	47,60	42,0	0,17	905,00	181	0,96	1,63	1,87	1,28	6,15	0,89	0,009
TH-20-30-3-55	Magmatic magnetite	31,20	5,3	0,53	48,50	17,2	0,15	854,00	146	0,87	1,24	1,79	1,20	12,43	1,95	0,008
TH-20-30-3-56	Magmatic magnetite	31,30	4,4	0,64	115,60	46,3	0,20	915,00	126	1,06	8,14	4,53	1,57	11,94	1,29	0,009
TH-20-30-3-57	Magmatic magnetite	28,30	4,8	0,64	116,00	30,7	0,19	834,00	102	1,03	5,74	2,52	1,47	13,03	1,79	0,012
TH-20-30-3-58	Magmatic magnetite	30,90	4,6	0,78	100,00	23,5	0,23	821,00	115	1,34	8,98	2,89	1,83	12,99	1,37	0,014
TH-20-30-3-6	Magmatic magnetite	16,00	2,5	0,58	16,40	9,1	0,18	1324,00	141	0,94	9,34	6,52	1,35	9,49	1,44	0,011
TH-20-30-3-7	Magmatic magnetite	23,20	3,9	0,65	74,60	37,6	0,21	1267,00	171	1,04	4,24	2,22	1,37	7,88	1,11	0,010
TH-20-30-3-8	Magmatic magnetite	12,50	1,8	0,74	113,60	29,4	0,22	1318,00	152	1,20	10,42	2,31	1,61	17,67	2,59	0,014
TH-20-30-3-9	Magmatic magnetite	12,00	2,2	0,65	109,00	25,9	0,18	1259,00	100	1,04	8,71	5,54	1,44	16,76	2,08	0,013
TH-20-30-A-29	Magmatic magnetite	32,30	4,5	0,79	122,30	28,2	0,24	1122,00	194	1,26	13,90	7,73	2,45	22,63	5,52	0,010
TH-20-30-A-34	Magmatic magnetite	13,20	3,4	0,71	36,70	20,0	0,25	638,00	117	1,20	6,09	3,54	2,18	36,39	8,63	0,012

Analyses below the limit of detection are re

Sample	Mineral phase	Mo			Ag			Cd			In			Sn		
		concentration (ppm)	σ	LOD	concentration (ppm)	σ	LOD	concentration (ppm)	σ	LOD	concentration (ppm)	σ	LOD	concentration (ppm)	σ	LOD
TH-20-30-3-41	Ovoid magnetite	30,40	3,34	0,11	0,09	0,13	0,17	0,24	0,20	0,12	0,40	0,08	0,011	8,70	1,2	0,10
TH-20-30-A-21	Ovoid magnetite	13,20	1,93	0,17	1,14	0,57	0,11	n.d.	n.d.	n.d.	0,64	0,15	0,024	17,30	4,1	0,22
TH-20-30-A-22	Ovoid magnetite	12,70	2,58	0,14	0,04	0,12	0,07	0,09	0,21	0,17	0,62	0,16	0,018	16,80	3,6	0,17
TH-20-30-A-24	Ovoid magnetite	39,70	7,74	0,19	0,27	0,18	0,09	0,16	0,49	0,32	0,49	0,11	0,017	9,20	1,8	0,20
TH-20-30-A-25	Ovoid magnetite	27,60	7,66	0,18	0,21	0,24	0,09	0,10	0,38	0,19	1,83	0,88	0,019	6,20	1,6	0,20
TH-20-30-A-26	Ovoid magnetite	32,40	8,62	0,15	0,56	0,43	0,09	0,31	0,41	0,17	0,37	0,06	0,018	6,60	1,6	0,18
TH-20-30-A-27	Ovoid magnetite	15,80	10,17	0,18	0,44	0,43	0,10	0,34	0,45	0,24	0,92	0,59	0,018	6,40	2,2	0,22
TH-20-30-A-28	Ovoid magnetite	43,50	8,28	0,16	0,34	0,18	0,08	0,09	0,31	0,18	0,54	0,13	0,014	9,10	1,9	0,17
TH-20-30-2-10	Magmatic magnetite	2,74	0,60	0,09	0,06	0,08	0,06	0,07	0,16	0,13	0,57	0,11	0,011	8,20	1,5	0,19
TH-20-30-2-38	Magmatic magnetite	10,89	1,50	0,15	0,02	0,10	0,03	0,28	0,27	0,21	0,66	0,15	0,015	11,50	2,2	0,18
TH-20-30-2-39	Magmatic magnetite	7,69	1,50	0,18	0,08	0,16	0,15	0,08	0,34	0,16	0,74	0,21	0,023	11,30	2,2	0,26
TH-20-30-2-67	Magmatic magnetite	5,62	1,07	0,10	0,03	0,08	0,05	0,24	0,25	0,14	0,74	0,14	0,011	36,80	7,0	0,11
TH-20-30-2-68	Magmatic magnetite	5,70	1,23	0,08	0,03	0,08	0,06	0,06	0,17	0,12	0,71	0,15	0,011	38,40	6,1	0,12
TH-20-30-2-69	Magmatic magnetite	15,55	3,26	0,11	0,14	0,12	0,05	0,68	0,40	0,13	0,57	0,09	0,011	34,10	4,7	0,14
TH-20-30-2-7	Magmatic magnetite	2,20	0,57	0,07	0,03	0,07	0,05	0,19	0,22	0,12	0,49	0,10	0,010	8,00	0,8	0,19
TH-20-30-2-70	Magmatic magnetite	13,90	2,35	0,10	0,11	0,10	0,06	0,43	0,34	0,14	0,70	0,14	0,012	44,90	8,7	0,14
TH-20-30-2-8	Magmatic magnetite	2,45	0,60	0,09	0,04	0,07	0,07	0,07	0,14	0,13	0,59	0,11	0,012	8,50	1,2	0,19
TH-20-30-2-9	Magmatic magnetite	1,86	0,58	0,07	0,03	0,11	0,06	0,06	0,16	0,12	0,57	0,13	0,013	7,80	1,3	0,20
TH-20-30-3-10	Magmatic magnetite	11,20	1,72	0,12	0,14	0,11	0,07	0,45	0,44	0,14	0,89	0,16	0,016	70,30	10,0	0,10
TH-20-30-3-12	Magmatic magnetite	16,72	3,02	0,21	0,12	0,34	0,23	1,62	0,92	0,20	0,48	0,13	0,022	12,90	3,3	0,21
TH-20-30-3-13	Magmatic magnetite	12,85	2,05	0,13	0,16	0,15	0,07	2,37	1,03	0,17	0,70	0,21	0,010	17,50	2,4	0,12
TH-20-30-3-14	Magmatic magnetite	11,95	2,31	0,11	0,15	0,19	0,10	1,00	0,56	0,15	0,71	0,13	0,012	13,90	2,3	0,14
TH-20-30-3-2	Magmatic magnetite	3,46	0,88	0,08	0,03	0,07	0,06	0,18	0,22	0,10	0,72	0,15	0,013	8,70	1,4	0,11
TH-20-30-3-3	Magmatic magnetite	3,67	0,72	0,10	0,03	0,08	0,06	0,18	0,17	0,13	0,73	0,16	0,009	8,90	1,1	0,11
TH-20-30-3-34	Magmatic magnetite	11,04	2,35	0,24	0,27	0,21	0,19	0,35	0,72	0,33	0,83	0,23	0,032	13,30	2,4	0,27
TH-20-30-3-35	Magmatic magnetite	8,87	1,49	0,14	0,73	0,10	1,46	0,26	0,32	0,14	0,67	0,13	0,019	10,30	1,8	0,14
TH-20-30-3-4	Magmatic magnetite	4,31	0,98	0,09	0,03	0,10	0,06	0,21	0,30	0,14	0,72	0,14	0,011	10,70	1,5	0,09
TH-20-30-3-42	Magmatic magnetite	8,13	1,64	0,16	0,08	0,18	0,15	0,19	0,35	0,17	0,58	0,20	0,025	7,90	1,6	0,16
TH-20-30-3-43	Magmatic magnetite	3,82	0,60	0,09	0,03	0,08	0,06	0,08	0,32	0,16	0,58	0,14	0,014	8,00	1,2	0,11
TH-20-30-3-44	Magmatic magnetite	12,15	3,96	0,15	0,08	0,10	0,16	0,16	0,15	0,31	0,82	0,15	0,018	42,20	8,1	0,17
TH-20-30-3-45	Magmatic magnetite	9,66	1,82	0,09	0,04	0,09	0,07	0,09	0,19	0,18	0,84	0,23	0,009	44,70	9,3	0,10
TH-20-30-3-46	Magmatic magnetite	12,51	2,25	0,11	0,04	0,13	0,08	0,02	0,19	0,04	0,82	0,17	0,011	42,00	7,8	0,12
TH-20-30-3-47	Magmatic magnetite	10,49	1,73	0,10	0,04	0,08	0,07	0,06	0,27	0,12	0,86	0,13	0,012	45,50	8,3	0,10
TH-20-30-3-48	Magmatic magnetite	20,70	4,33	0,14	0,28	0,17	0,09	0,72	0,40	0,20	0,89	0,22	0,016	49,20	9,9	0,13
TH-20-30-3-49	Magmatic magnetite	17,53	2,68	0,12	0,18	0,12	0,08	0,63	0,47	0,16	0,85	0,19	0,013	46,30	6,6	0,13
TH-20-30-3-5	Magmatic magnetite	11,62	2,88	0,14	0,04	0,12	0,08	0,59	0,48	0,15	0,85	0,16	0,014	46,90	7,2	0,14
TH-20-30-3-50	Magmatic magnetite	18,51	2,78	0,17	0,23	0,16	0,09	0,47	0,50	0,21	0,92	0,13	0,017	47,40	6,3	0,15
TH-20-30-3-51	Magmatic magnetite	3,28	0,56	0,08	0,02	0,12	0,04	0,09	0,26	0,17	0,65	0,14	0,012	7,00	1,8	0,11
TH-20-30-3-52	Magmatic magnetite	2,69	0,72	0,09	0,04	0,10	0,07	0,06	0,20	0,11	0,46	0,12	0,011	6,00	1,1	0,10
TH-20-30-3-53	Magmatic magnetite	2,55	0,79	0,08	0,03	0,08	0,06	0,08	0,18	0,15	0,47	0,11	0,013	6,10	1,2	0,12
TH-20-30-3-54	Magmatic magnetite	3,03	0,97	0,09	1,75	0,07	3,49	1,40	0,20	2,80	0,60	0,14	0,012	5,80	1,3	0,12
TH-20-30-3-55	Magmatic magnetite	10,58	1,74	0,10	0,07	0,09	0,06	0,05	0,19	0,10	0,91	0,12	0,013	59,00	7,6	0,11
TH-20-30-3-56	Magmatic magnetite	17,20	4,57	0,14	0,14	0,13	0,08	0,35	0,27	0,15	0,96	0,20	0,014	63,90	9,2	0,13
TH-20-30-3-57	Magmatic magnetite	15,41	2,22	0,12	0,03	0,14	0,06	0,23	0,26	0,18	0,91	0,24	0,015	54,90	12,2	0,12
TH-20-30-3-58	Magmatic magnetite	15,08	2,46	0,17	0,04	0,17	0,07	0,26	0,27	0,20	0,93	0,20	0,017	56,70	10,7	0,16
TH-20-30-3-6	Magmatic magnetite	6,83	1,47	0,10	0,04	0,09	0,08	0,27	0,28	0,14	0,77	0,16	0,015	38,90	6,9	0,12
TH-20-30-3-7	Magmatic magnetite	9,43	1,78	0,12	0,09	0,12	0,08	0,40	0,50	0,18	1,02	0,17	0,013	50,80	9,5	0,12
TH-20-30-3-8	Magmatic magnetite	11,62	2,29	0,13	0,25	0,14	0,08	1,67	0,53	0,18	0,94	0,15	0,017	40,70	6,1	0,16
TH-20-30-3-9	Magmatic magnetite	22,66	3,77	0,13	0,15	0,14	0,08	1,41	0,78	0,16	0,90	0,13	0,015	42,70	4,7	0,11
TH-20-30-A-29	Magmatic magnetite	8,27	1,97	0,13	0,17	0,13	0,08	0,22	0,27	0,18	1,28	0,31	0,018	49,40	10,0	0,23
TH-20-30-A-34	Magmatic magnetite	7,42	2,19	0,14	0,04	0,13	0,08	0,32	0,26	0,20	0,44	0,14	0,018	11,50	2,7	0,18

Analyses below the limit of detection are re

Sample	Mineral phase	Sb			Te			W			Au			Tl		
		concentration (ppm)	σ	LOD	concentration (ppm)	σ	LOD	concentration (ppm)	σ	LOD	concentration (ppm)	σ	LOD	concentration (ppm)	σ	LOD
TH-20-30-3-41	Ovoid magnetite	*0,036*	0,105	0,072	*0,05*	0,16	0,10	0,700	0,163	0,011	*0,024*	0,052	0,048	*0,732*	0,019	1,463
TH-20-30-A-21	Ovoid magnetite	*0,090*	0,181	0,180	*0,06*	0,34	0,12	0,690	0,291	0,030	*0,045*	0,098	0,090	2,821	5,076	0,082
TH-20-30-A-22	Ovoid magnetite	*0,050*	0,151	0,100	*0,01*	0,30	0,01	0,362	0,212	0,018	*0,041*	0,100	0,082	*0,016*	0,031	0,031
TH-20-30-A-24	Ovoid magnetite	*0,050*	0,183	0,100	n.d.	n.d.	n.d.	0,638	0,212	0,020	*0,038*	0,091	0,075	0,056	0,075	0,039
TH-20-30-A-25	Ovoid magnetite	*0,055*	0,188	0,110	*0,07*	0,24	0,14	0,969	0,424	0,029	*0,046*	0,069	0,091	0,317	0,254	0,032
TH-20-30-A-26	Ovoid magnetite	*0,048*	0,167	0,096	*0,10*	0,21	0,20	1,286	0,322	0,022	*0,062*	0,117	0,123	0,055	0,054	0,029
TH-20-30-A-27	Ovoid magnetite	0,210	0,181	0,127	*0,22*	0,38	0,43	1,282	0,643	0,024	*0,039*	0,129	0,077	0,278	0,219	0,042
TH-20-30-A-28	Ovoid magnetite	*0,037*	0,146	0,074	*0,15*	0,23	0,29	1,048	0,348	0,023	*0,034*	0,091	0,068	0,226	0,174	0,033
TH-20-30-2-10	Magmatic magnetite	*0,035*	0,102	0,070	*0,05*	0,16	0,10	0,071	0,063	0,017	*0,025*	0,039	0,050	*0,011*	0,030	0,021
TH-20-30-2-38	Magmatic magnetite	0,310	0,446	0,145	*0,26*	0,64	0,51	0,746	0,512	0,037	*0,045*	0,088	0,089	0,459	0,539	0,042
TH-20-30-2-39	Magmatic magnetite	0,150	0,290	0,127	*0,19*	0,43	0,38	0,527	0,307	0,041	*0,009*	0,123	0,018	0,290	0,227	0,055
TH-20-30-2-67	Magmatic magnetite	*0,091*	0,088	0,181	*0,08*	0,06	0,15	0,666	1,091	0,013	*0,021*	0,041	0,041	0,764	0,275	0,018
TH-20-30-2-68	Magmatic magnetite	*0,030*	0,064	0,060	*0,13*	0,14	0,26	0,256	0,150	0,013	*0,024*	0,049	0,048	0,295	0,183	0,015
TH-20-30-2-69	Magmatic magnetite	*0,045*	0,105	0,090	*0,06*	0,12	0,12	5,987	1,933	0,003	*0,022*	0,061	0,044	3,080	1,526	0,021
TH-20-30-2-7	Magmatic magnetite	*0,033*	0,096	0,066	*0,06*	0,19	0,11	0,038	0,054	0,008	*0,023*	0,054	0,045	*0,011*	0,032	0,022
TH-20-30-2-70	Magmatic magnetite	0,160	0,144	0,072	*0,11*	0,14	0,21	3,492	1,388	0,022	*0,022*	0,072	0,044	1,910	0,650	0,020
TH-20-30-2-8	Magmatic magnetite	*0,036*	0,100	0,072	*0,08*	0,07	0,16	0,036	0,038	0,011	*0,024*	0,065	0,048	*0,010*	0,023	0,019
TH-20-30-2-9	Magmatic magnetite	*0,038*	0,073	0,075	*0,03*	0,17	0,06	*0,006*	0,017	0,011	*0,023*	0,056	0,046	*0,007*	0,022	0,014
TH-20-30-3-10	Magmatic magnetite	0,130	0,141	0,078	*0,14*	0,18	0,27	2,725	0,863	0,016	*0,016*	0,062	0,031	2,776	0,868	0,024
TH-20-30-3-12	Magmatic magnetite	*0,074*	0,214	0,147	0,44	0,87	0,33	6,991	2,100	0,036	*0,090*	0,228	0,180	5,110	1,445	0,043
TH-20-30-3-13	Magmatic magnetite	0,180	0,108	0,102	*0,09*	0,10	0,17	5,311	1,908	0,013	*0,024*	0,056	0,048	10,390	4,872	0,023
TH-20-30-3-14	Magmatic magnetite	0,140	0,168	0,064	0,10	0,27	0,06	3,205	1,005	0,004	*0,038*	0,101	0,075	3,688	1,992	0,025
TH-20-30-3-2	Magmatic magnetite	*0,027*	0,079	0,054	*0,06*	0,23	0,12	0,022	0,034	0,013	*0,042*	0,048	0,084	*0,012*	0,033	0,023
TH-20-30-3-3	Magmatic magnetite	*0,040*	0,100	0,079	*0,07*	0,12	0,13	0,047	0,044	0,002	*0,026*	0,063	0,051	*0,009*	0,028	0,018
TH-20-30-3-34	Magmatic magnetite	0,420	0,233	0,216	*0,05*	0,33	0,09	3,193	0,959	0,027	*0,113*	0,230	0,225	0,889	0,359	0,057
TH-20-30-3-35	Magmatic magnetite	*0,050*	0,160	0,099	*0,04*	0,20	0,07	0,374	0,217	0,027	*0,023*	0,099	0,046	0,061	0,068	0,028
TH-20-30-3-4	Magmatic magnetite	*0,038*	0,081	0,075	*0,06*	0,12	0,12	0,067	0,070	0,010	*0,017*	0,067	0,034	*0,009*	0,030	0,017
TH-20-30-3-42	Magmatic magnetite	*0,074*	0,209	0,148	*0,36*	0,20	0,71	1,044	0,332	0,022	n.d.	n.d.	n.d.	0,176	0,101	0,034
TH-20-30-3-43	Magmatic magnetite	*0,010*	0,102	0,020	*0,07*	0,15	0,13	0,061	0,079	0,014	*0,145*	0,069	0,289	*0,018*	0,020	0,036
TH-20-30-3-44	Magmatic magnetite	*0,044*	0,128	0,087	*0,12*	0,15	0,24	4,566	3,681	0,006	*0,038*	0,064	0,076	0,200	0,187	0,051
TH-20-30-3-45	Magmatic magnetite	*0,032*	0,102	0,064	*0,08*	0,22	0,16	0,421	0,343	0,014	*0,037*	0,063	0,074	0,060	0,075	0,022
TH-20-30-3-46	Magmatic magnetite	*0,042*	0,137	0,083	n.d.	n.d.	n.d.	2,976	1,752	0,003	*0,040*	0,070	0,079	0,421	0,275	0,026
TH-20-30-3-47	Magmatic magnetite	*0,047*	0,102	0,093	*0,04*	0,12	0,07	1,568	0,867	0,003	*0,031*	0,061	0,061	*0,013*	0,048	0,025
TH-20-30-3-48	Magmatic magnetite	*0,044*	0,135	0,087	*0,07*	0,15	0,13	10,840	3,565	0,020	n.d.	n.d.	n.d.	1,246	0,571	0,028
TH-20-30-3-49	Magmatic magnetite	0,150	0,122	0,083	*0,05*	0,17	0,10	7,450	2,471	0,011	*0,029*	0,065	0,057	1,258	0,347	0,027
TH-20-30-3-5	Magmatic magnetite	*0,052*	0,136	0,103	*0,09*	0,21	0,18	4,423	1,306	0,026	n.d.	n.d.	n.d.	6,059	1,381	0,029
TH-20-30-3-50	Magmatic magnetite	0,160	0,193	0,098	*0,08*	0,17	0,15	6,854	1,665	0,038	*0,037*	0,104	0,073	0,526	0,203	0,023
TH-20-30-3-51	Magmatic magnetite	*0,034*	0,070	0,068	*0,06*	0,15	0,12	n.d.	n.d.	n.d.	*0,023*	0,088	0,045	*0,014*	0,034	0,027
TH-20-30-3-52	Magmatic magnetite	*0,036*	0,089	0,072	0,15	0,30	0,14	0,014	0,031	0,003	*0,028*	0,060	0,055	*0,014*	0,027	0,028
TH-20-30-3-53	Magmatic magnetite	*0,027*	0,107	0,054	*0,09*	0,17	0,17	*0,010*	0,021	0,020	*0,027*	0,050	0,053	*0,012*	0,020	0,023
TH-20-30-3-54	Magmatic magnetite	*0,026*	0,067	0,051	*0,02*	0,14	0,04	0,062	0,062	0,010	*0,117*	0,069	0,234	*0,009*	0,021	0,017
TH-20-30-3-55	Magmatic magnetite	*0,038*	0,080	0,075	*0,10*	0,20	0,20	0,497	0,479	0,003	*0,027*	0,071	0,053	0,061	0,085	0,022
TH-20-30-3-56	Magmatic magnetite	*0,050*	0,131	0,099	*0,11*	0,15	0,21	5,210	3,534	0,112	*0,028*	0,051	0,055	0,758	0,547	0,032
TH-20-30-3-57	Magmatic magnetite	0,080	0,129	0,074	*0,08*	0,15	0,16	3,774	1,274	0,003	*0,064*	0,096	0,128	0,357	0,243	0,023
TH-20-30-3-58	Magmatic magnetite	0,190	0,143	0,106	*0,11*	0,22	0,22	3,281	0,856	0,023	*0,049*	0,073	0,097	0,403	0,129	0,029
TH-20-30-3-6	Magmatic magnetite	*0,042*	0,066	0,083	*0,07*	0,19	0,14	0,132	0,093	0,017	*0,013*	0,049	0,025	0,907	0,231	0,028
TH-20-30-3-7	Magmatic magnetite	*0,049*	0,091	0,097	*0,10*	0,22	0,19	2,383	0,813	0,015	*0,030*	0,077	0,060	3,909	1,664	0,020
TH-20-30-3-8	Magmatic magnetite	0,120	0,157	0,099	*0,12*	0,13	0,23	2,912	1,238	0,004	*0,038*	0,068	0,076	8,799	2,398	0,029
TH-20-30-3-9	Magmatic magnetite	0,140	0,173	0,101	*0,08*	0,19	0,15	11,703	3,290	0,003	*0,034*	0,072	0,068	9,877	3,438	0,020
TH-20-30-A-29	Magmatic magnetite	0,230	0,274	0,170	*0,14*	0,46	0,28	5,503	1,461	0,029	*0,058*	0,103	0,115	1,631	0,748	0,021
TH-20-30-A-34	Magmatic magnetite	*0,055*	0,114	0,109	*0,12*	0,26	0,24	0,390	0,169	0,015	*0,046*	0,083	0,091	0,124	0,073	0,021

Analyses below the limit of detection are re

Sample	Mineral phase	Pb			Bi			Th			U		
		concentration (ppm)	σ	LOD	concentration (ppm)	σ	LOD	concentration (ppm)	σ	LOD	concentration (ppm)	σ	LOD
TH-20-30-3-41	Ovoid magnetite	1,85	0,91	0,017	0,040	0,04	0,014	0,000	0,012	0,001	0,041	0,030	0,004
TH-20-30-A-21	Ovoid magnetite	12,92	4,13	0,027	0,020	0,05	0,025	5,523	2,518	0,007	1,230	0,440	0,001
TH-20-30-A-22	Ovoid magnetite	12,88	9,26	0,013	0,021	0,02	0,021	0,528	0,243	0,006	0,355	0,110	0,005
TH-20-30-A-24	Ovoid magnetite	47,88	23,42	0,029	0,115	0,07	0,029	0,125	0,056	0,006	0,332	0,100	0,001
TH-20-30-A-25	Ovoid magnetite	24,04	17,28	0,023	0,230	0,11	0,022	0,797	0,298	0,005	1,256	0,360	0,004
TH-20-30-A-26	Ovoid magnetite	34,84	26,59	0,026	0,106	0,07	0,021	0,167	0,095	0,001	0,275	0,080	0,004
TH-20-30-A-27	Ovoid magnetite	n.d.	n.d.	n.d.	0,757	0,60	0,056	0,520	0,433	0,010	0,425	0,220	0,006
TH-20-30-A-28	Ovoid magnetite	81,64	77,05	0,024	0,150	0,29	0,018	0,454	0,133	0,005	0,387	0,090	0,003
TH-20-30-2-10	Magmatic magnetite	0,75	0,33	0,018	*0,008*	0,01	0,016	0,076	0,079	0,004	0,107	0,030	0,001
TH-20-30-2-38	Magmatic magnetite	12,93	10,86	0,025	0,080	0,09	0,024	13,165	9,307	0,007	2,999	2,220	0,004
TH-20-30-2-39	Magmatic magnetite	11,72	6,67	0,038	0,077	0,07	0,028	8,850	3,948	0,008	2,454	1,070	0,006
TH-20-30-2-67	Magmatic magnetite	11,00	5,43	0,037	0,148	0,06	0,014	0,169	0,082	0,001	0,281	0,080	0,004
TH-20-30-2-68	Magmatic magnetite	4,04	2,78	0,013	0,043	0,04	0,013	0,126	0,057	0,004	0,294	0,060	0,003
TH-20-30-2-69	Magmatic magnetite	53,19	27,79	0,021	0,328	0,22	0,013	3,195	2,222	0,004	1,378	0,680	0,004
TH-20-30-2-7	Magmatic magnetite	0,12	0,05	0,012	*0,006*	0,01	0,011	0,127	0,077	0,003	0,136	0,040	0,001
TH-20-30-2-70	Magmatic magnetite	46,48	17,67	0,054	0,250	0,11	0,015	1,285	0,627	0,005	1,065	0,360	0,001
TH-20-30-2-8	Magmatic magnetite	0,57	0,42	0,150	*0,007*	0,01	0,014	0,220	0,370	0,001	0,150	0,060	0,001
TH-20-30-2-9	Magmatic magnetite	*0,01*	0,26	0,014	*0,007*	0,02	0,014	*0,005*	0,003	0,009	0,096	0,020	0,003
TH-20-30-3-10	Magmatic magnetite	57,65	20,79	0,016	0,341	0,17	0,019	0,395	0,270	0,001	0,583	0,190	0,001
TH-20-30-3-12	Magmatic magnetite	90,74	30,87	0,027	0,653	0,43	0,032	10,223	6,095	0,011	4,084	2,370	0,006
TH-20-30-3-13	Magmatic magnetite	164,07	57,07	0,016	1,643	0,56	0,022	2,666	0,910	0,006	1,177	0,290	0,003
TH-20-30-3-14	Magmatic magnetite	102,27	43,67	0,016	0,725	0,42	0,019	4,915	4,084	0,006	1,777	1,240	0,004
TH-20-30-3-2	Magmatic magnetite	0,15	0,11	0,015	*0,006*	0,02	0,011	n.d.	0,000	n.d.	0,084	0,040	0,001
TH-20-30-3-3	Magmatic magnetite	0,09	0,07	0,012	*0,009*	0,02	0,018	*0,001*	0,002	0,001	0,094	0,030	0,001
TH-20-30-3-34	Magmatic magnetite	26,52	8,62	0,042	0,050	0,06	0,039	25,625	5,034	0,015	8,324	1,970	0,006
TH-20-30-3-35	Magmatic magnetite	2,05	0,79	0,030	*0,010*	0,02	0,020	1,572	0,685	0,005	0,667	0,220	0,001
TH-20-30-3-4	Magmatic magnetite	0,08	0,06	0,016	n.d.	n.d.	n.d.	n.d.	0,000	n.d.	0,099	0,040	0,002
TH-20-30-3-42	Magmatic magnetite	5,46	1,79	0,020	*0,011*	0,03	0,022	6,928	2,086	0,007	2,361	0,770	0,001
TH-20-30-3-43	Magmatic magnetite	0,24	0,14	0,018	*0,007*	0,01	0,013	0,140	0,204	0,004	0,158	0,080	0,003
TH-20-30-3-44	Magmatic magnetite	24,95	17,86	0,034	0,198	0,16	0,024	1,880	1,439	0,010	0,727	0,390	0,005
TH-20-30-3-45	Magmatic magnetite	3,98	1,99	0,016	0,019	0,01	0,016	0,116	0,076	0,004	0,291	0,070	0,001
TH-20-30-3-46	Magmatic magnetite	34,48	20,09	0,020	0,405	0,22	0,017	2,590	1,574	0,006	1,108	0,450	0,003
TH-20-30-3-47	Magmatic magnetite	2,57	1,14	0,014	0,156	0,08	0,015	0,110	0,056	0,001	0,280	0,050	0,003
TH-20-30-3-48	Magmatic magnetite	118,95	42,63	0,020	0,386	0,16	0,018	3,041	0,719	0,001	1,554	0,350	0,001
TH-20-30-3-49	Magmatic magnetite	96,37	28,25	0,020	0,070	0,05	0,017	3,911	1,277	0,004	1,673	0,540	0,001
TH-20-30-3-5	Magmatic magnetite	121,91	41,13	0,026	1,259	0,42	0,026	1,152	0,338	0,004	0,825	0,200	0,001
TH-20-30-3-50	Magmatic magnetite	64,74	10,52	0,027	1,219	0,57	0,019	4,724	1,546	0,007	1,566	0,420	0,001
TH-20-30-3-51	Magmatic magnetite	0,15	0,11	0,016	*0,008*	0,02	0,015	0,005	0,015	0,001	0,083	0,030	0,001
TH-20-30-3-52	Magmatic magnetite	0,26	0,19	0,018	*0,008*	0,02	0,016	0,004	0,017	0,001	0,055	0,050	0,003
TH-20-30-3-53	Magmatic magnetite	0,24	0,19	0,018	*0,011*	0,02	0,022	*0,002*	0,007	0,004	0,033	0,010	0,001
TH-20-30-3-54	Magmatic magnetite	1,44	0,99	0,019	0,110	0,12	0,018	0,819	0,684	0,001	0,327	0,250	0,003
TH-20-30-3-55	Magmatic magnetite	4,16	4,89	0,018	*0,009*	0,02	0,018	0,020	0,041	0,006	0,236	0,080	0,003
TH-20-30-3-56	Magmatic magnetite	48,83	27,72	0,023	0,232	0,10	0,016	0,886	0,529	0,007	1,277	0,650	0,001
TH-20-30-3-57	Magmatic magnetite	35,13	10,36	0,019	0,039	0,03	0,016	1,562	0,365	0,004	1,039	0,260	0,003
TH-20-30-3-58	Magmatic magnetite	35,61	7,30	0,027	0,619	0,20	0,024	3,619	0,761	0,005	1,831	0,380	0,003
TH-20-30-3-6	Magmatic magnetite	5,65	1,54	0,023	0,127	0,06	0,021	0,271	0,098	0,001	0,260	0,060	0,003
TH-20-30-3-7	Magmatic magnetite	91,23	32,85	0,025	0,668	0,26	0,020	0,798	0,409	0,004	0,857	0,300	0,003
TH-20-30-3-8	Magmatic magnetite	114,58	36,09	0,089	0,906	0,38	0,019	2,963	0,829	0,005	1,706	0,440	0,003
TH-20-30-3-9	Magmatic magnetite	178,51	61,94	0,020	1,001	0,53	0,019	5,951	1,676	0,001	2,214	0,300	0,003
TH-20-30-A-29	Magmatic magnetite	57,80	18,48	0,027	0,486	0,20	0,023	4,085	2,316	0,007	3,517	1,610	0,004
TH-20-30-A-34	Magmatic magnetite	9,75	3,22	0,023	*0,008*	0,02	0,016	3,473	1,313	0,001	1,245	0,260	0,004

Analyses below the limit of detection are re

Supplementary table 6. ICP-MS analysis of mineralized samples from Kolumbo hydrothermal field

	Mn [mg/kg]	Fe [g/kg]	Co [mg/kg]	Ni [mg/kg]	Cu [mg/kg]	Zn [mg/kg]	As [mg/kg]	Mo [mg/kg]	Ag [mg/kg]	Cd [mg/kg]	Sb [mg/kg]	Te [mg/kg]	Ba [mg/kg]	W [mg/kg]	Au [mg/kg]	Tl [mg/kg]	Pb [mg/kg]	Bi [mg/kg]	Th [mg/kg]
Pr.8b QA-3A	88,8	253	1,16	5,13	1773	17762	3175	5,40	2345	134	7850	0,018	667	b.d.l	9,09	255	25173	0,046	0,019
Pr.9b QA-3B	87,7	287	1,27	7,18	1953	24312	4218	7,75	1706	200	5658	0,011	372	0,05	8,13	355	18453	0,063	0,019
Pr.10b QA-3C	61,2	134	1,64	4,31	1022	40463	2134	2,94	1261	222	11605	0,014	1335	b.d.l	4,45	700	12411	0,022	0,015
Pr.11b QA-3D	62,9	287	0,94	2,51	2047	46615	5154	3,04	2021	407	9305	0,01	331	0,10	13,49	255	23246	0,045	0,011
Pr.12b QA-5A	80,8	318	1,07	2,91	1387	25737	4057	4,04	1134	210	6758	0,014	391	0,03	11,17	188	11049	0,022	0,086
Pr.13b QA-5B	74,1	305	1,21	2,39	1145	23939	3975	3,19	1205	210	5861	0,011	505	b.d.l	8,87	215	12596	0,023	0,031
Pr.14b QA-5C	77,6	303	0,97	3,65	777	8941	3222	4,00	905	53	3576	0,014	1033	b.d.l	6,44	147	5985	0,011	0,019
Pr.15b QA-5D	72,1	243	0,97	3,11	762	18355	2927	2,58	1247	152	5809	b.d.l	489	b.d.l	7,87	234	7229	0,013	0,015
Pr.16b QA-5E	70,6	390	0,66	1,97	1230	3149	5317	1,63	852	39	2647	0,014	143	0,03	10,31	99	6616	0,015	0,009
Pr.17b QA-5F	58,4	386	0,70	2,99	1697	1446	5122	1,56	763	21	2493	0,007	155	0,03	9,99	25	5763	0,013	0,011
Pr.18b QA-5G	70,4	254	0,84	3,49	1152	5612	2744	1,71	541	47	6006	0,01	1514	b.d.l	7,79	142	12108	0,020	0,001
Pr.19b QA-5H	59,0	168	1,19	3,41	981	10648	1600	1,25	1559	82	6861	0,01	2548	b.d.l	5,87	190	12343	0,023	0,003
Pr.20b QA-3C-a	65,9	248	1,94	3,79	2093	22741	3066	2,61	2405	161	24705	0,015	538	b.d.l	17,48	204	28479	0,056	0,020
Method blank in mg/kg	0,72	0,027	0,00	0,11	0,37	4,67	0,6200	0,025	0,15	0,0720	0,36	0,0025	3,31	0,020	0,005	0,0077	4,16	0,0025	0,008
CH4	489,3	54	27,05	55,30	2068	196	n.d.	2,92	2,27	1,10	1,11	0,32	464	3,36	0,84	0,38	12	0,40	2,15
CH-4 working values	*430*	*54*	*26,00*	*51,00*	*2000*	*200*	*8,8*	*3,00*	*2,0*	*1,0*	0,77	n.d.	*425*	*3,00*	*0,88*	*0,40*	*14*	*0,60*	*2,00*
Accuracy (%)	**13,8**	**0,0**	**4,0**	**8,4**	**3,4**	**-2,0**		**-2,7**	**13,5**	**10,0**	**44,2**		**9,2**	**11,8**	**-4,5**	**-5,0**	**-14,3**	**-33,5**	**7,5**
TUBAF	3112,7	277	34,08	8,75	1762	49810	2272	38,29	154	444	82,60	0,13	65	3,18	0,032	1,32	64841	1,449	0,62
TUBAF working value	2910,9	267	30,95	8,92	1646	51700	2172	33,81	147	475	88,56	0,19	44	3,84	0,036	1,45	61400	1,650	0,67
Accuracy (%)	**6,9**	**3,7**	**10,1**	**-1,9**	**7,0**	**-3,7**	**4,6**	**13,3**	**4,8**	**-6,5**	**-6,7**	**-31,6**	**47,7**	**-17,3**	**-11,11**	**-9,0**	**5,6**	**-12,2**	**-7,5**

8 Discussion

8.1 Improving Au detection in samples

Determining the Au concentration in source rocks is crucial to understand the geological processes involved in the formation of Au deposits. However, this is an analytical challenge, as many rocks are usually Au-depleted to sub-ng·g^{-1} content. The method developed in Paper I improves the PPP-LA-ICP-MS limit of detection to values as low as 0.10-0.05 ng g^{-1} Au and routine analysis of reference material shows that Au analysis by PPP-LA-ICP-MS is accurate and precise, making it a suitable method for investigating Au distribution in Au-depleted rocks (thesis aim 1). Even though lower LOD is obtained by other methods (e.g. < 0.01 ng·g^{-1} by solution mode ICP-MS analysis; Pitcairn et al. 2006a), PPP-LA-ICP-MS is sensitive enough to investigate the vast majority of the geological material as samples with Au content < 0.10 ng·g^{-1} are scarce (Patten et al. 2016; Patten et al. 2020b; Pitcairn et al. 2006b; Pitcairn et al. 2015; Pitcairn et al. 2021). Additionally, the production of PPP is cheap, safe and fast, and the pellets may be re-used for trace elements analysis (see Paper IV). The study of the Kolumbo volcano highlights the efficiency of this method. Despite some samples below detection limit, the data is sufficient to identify Au depletion processes during magmatic differentiation (Paper IV). Including additional data on samples of Ios, Anafi, Santorini and Syros, a total of 146 analyses have been carried out on PPP from diverse rock types (i.e. marble, sedimentary rocks, greenschist to eclogitic facies metamorphic rocks and mafic to felsic magmatic rocks) with a detection limit as low as 0.05 ng·g^{-1}. Of the 146 analyses, only 17 are below detection limit, corresponding to very Au poor rocks.

8.2 Orogenic Au deposits

8.2.1 Diversity of metal sources during orogenic Au deposit formation

Orogenic Au deposits in Finland show frequent enrichment in additional metals (i.e. Ag, Cu, Co, Ni, Sb), leading to various metal associations between spatially close deposits. This diversity may be related to varying metal content in the mineralizing fluid. In Paper II, we show that the metals and ligands content in metamorphic fluid released by metamorphic devolatilisation of metavolcano-sedimentary units depend on the dominant lithology. Metavolcanic rocks show strong Au, As and Sn, and locally S depletion, meta-komatiite is slightly depleted in Ni and Co, while metasedimentary rocks show significant depletion in S, C, Cu, As, Se, Mo, Sn, Sb, Te and U. In Paper III, we propose to link the diverse metal association in the studied orogenic Au deposits of the Pohjanmaa Belt with the lithological diversity of the fluid source through time and space. Metamorphic devolatilisation of metavolcanic rocks and ultramafic intrusions of the Evijärvi field likely generated an As-Au (Co, Ni)-rich fluid, while the metasedimentary units of the Evijärvi field subsequently generated a Cu (-Au) rich-fluid during a later event.

8.2.2 Metal transport

Metamorphic fluids forming orogenic Au deposits are usually near-neutral, aqueous-carbonic fluids (pH ≈ 5,5) with salinities between 3 and 7 wt.% NaCl eq. (Garofalo et al. 2014; Ridley and Diamond 2000). Despite their low salinity, they can transport metals (Ag, As, Au, Cu, Mo, Sb, Se, Sn, Te) as chloride or hydrosulfide complexes at pressure-temperature conditions as high as 5 kbar and 560°C, which correspond to the generation of metamorphic fluids at the greenschist-amphibolite facies transition (Pitcairn et al. 2014; Seward 1973; Tomkins 2010; Zhong et al. 2015). In Paper II, we show that metamorphic devolatilisation of

metavolcano-sedimentary rocks releases metals (As, Au, Cu, Mo, Sb, Se, Sn, Te and U) and ligands (C and S). They are transported by the metamorphic fluids as complexes and contribute to the metal diversity observed in orogenic Au deposits.

Orogenic Au deposits with high base metal content (especially Co and Ni) are often proposed to form from saline metamorphic fluids generated when evaporitic rocks are present within the volcano-sedimentary rocks package (Goldfarb et al. 2001; Tapio et al. 2021; Vasilopoulos et al. 2021; Vasyukova and Williams-Jones 2022). In the Pohjanmaa Belt, the Jouhineva deposit (0.18% Co) and in the Kurula deposit (up to 0.20% Co) are enriched in Co despite no evaporite being reported yet in the region (Paper III). However, contribution of a saline metamorphic fluid does not seem critical to base metal enrichment in orogenic Au deposits. Indeed, Co, Cu and Ni can be transported in hydrothermal fluids as chloride complexes at salinities as low as ca. 3 wt.% NaCl eq. at 440°C and acidic to neutral pH, which is within range of metamorphic fluids (Liu et al. 2011; Liu et al. 2012; Williams-Jones and Vasyukova 2022).

Additionally, mineralising conditions during the As-Au (Co, Ni) mineralising event in the Pohjanmaa Belt are average temperatures between 380 and 475°C and pressure < 5 kbar (i.e. host-rock peak metamorphism conditions), which are compatible with transport of Au and base metals in metamorphic fluids (Zhong et al. 2015). Further work to investigate participation of saline metamorphic fluids from meta-evaporite in the mineralising process should focus on fluid inclusions from the different deposits (e.g. Qiu et al. 2021) and composition of tourmaline (e.g. B isotopy in tourmaline; Vasilopoulos et al. 2021).

8.2.3 Ore-forming processes and diversity in metal content

As orogenic Au deposits form by a succession of fault-valve cycles that can spread over tens of millions of years, metamorphic fluids with different metal content may be involved in the mineralisation as different sources are tapped by transcrustal faults over time. Multiple ore-forming events favour more diverse metal association and appears to be a key process to enrich base metals and Au in orogenic Au deposits. In the Central Lapland Greenstone Belt, the deposits are frequently formed by a first Au-only event, and are later overprinted by a second Au-(Cu-Co-Ni) event: e.g. Levijärvi-Loukinen deposit (Kurhila et al. 2017), Iso-Kuotko deposit (Molnár et al. 2018), Saattopora deposit (Molnár et al. 2019). In Paper III, we report successive As-Au (Co, Ni) and Cu(-Au) mineralising events in the deposits of the Pohjanmaa Belt.

Deposits spatially close and affected by the same mineralising events do not necessarily show the same metal association. The case of the Jouhineva and Huhta deposits in the Pohjanmaa Belt (Paper III) illustrates this quite well. Both deposits are located along the same structure, 3 kilometres apart from each other, and form during the successive As-Au (Co, Ni) and Cu(-Au) mineralising events. However, Jouhineva is an Au-Cu-Co-Ag deposit while Huhta is an Au-only deposit. The different metal associations may be explained by the fault-valve process and heterogenous metal content in the mineralising fluids within a single mineralising event. One mineralising event occurs over several millions of years, whereas fault-valve cycles act at the scale of seconds. Depending on the way a fault responds to stress, permeability will not always be generated at the same locus. Thus, deposits distributed along a single structure will not necessarily record the exact same fault-valve cycles. Additionally, considering that the metal content in a metamorphic fluid may change, depending on the nature of the source rock, transient metal content changes in the mineralising fluid may not be recorded in all the deposits.

In the Pohjanmaa Belt, during the As-Au (Co, Ni) mineralising event, the mineralising fluid was sometime locally Ni and Co enriched. These transient enrichments have been recorded in Jouhineva' s mineralisation, while Huhta' s recorded Ni and Co-poor fluid. Similarly, a mineralising event may be more or less expressed in a deposit. The Cu(-Au) mineralising event is well recorded in Jouhineva, leading to further enrichment in Au in addition to Cu, while it is barely recorded in Huhta.

Other critical parameters for Au enrichment in orogenic Au deposits are precipitation conditions, as highlighted in Paper III. In the studied deposits of the Pohjanmaa Belt, the As-Au (Co, Ni) mineralising event is divided into two stages: 1) an arsenide stage, occurring only if the redox and fS_2 conditions are favourable; 2) an ubiquitous arsenopyrite stage at less reduced and higher fS_2 conditions, where arsenopyrite replaces eventual earlier arsenide. The deposits where both stages are represented contain more visible Au (i.e. Laivakangas, Huhta and Kurula) than the others (i.e. Jouhineva). This is the result of the higher compatibility of Au in the crystal lattice of arsenide (up to hundreds of $\mu g \cdot g^{-1}$) than in arsenopyrite (< 10 $\mu g \cdot g^{-1}$) above 300°C (Cathelineau et al. 1989; Neumayr et al. 1993). Early formation of arsenide traps more Au (as invisible Au) than arsenopyrite, increasing the Au budget of a deposit. Replacement of arsenide by arsenopyrite leads to Au exsolution (Tomkins and Mavrogenes 2001), facilitating processing of the ore.

8.2.4 Evaluation of the metamorphic devolatilisation model

The metamorphic devolatilisation model, which is the most accepted model for orogenic Au deposit formation (Goldfarb and Groves 2015), stipulates that Au-rich metamorphic fluids forming orogenic Au deposits are mainly produced during prograde metamorphic devolatilisation of volcano-sedimentary units (Elmer et al. 2006; Phillips and Powell 2010; Pitcairn et al. 2006b). Conversely, the study of orogenic Au deposit formation in the Central

Lapland Greenstone Belt shows that, while most of the deposits start to form close to peak metamorphism or during early retrograde metamorphism, they frequently form in multiple events, spanning over tens of millions of years, long after peak metamorphism (e.g. the Suurikuusikko, Levijärvi-Loukinen and Iso-Kuotko deposits; Molnár et al. 2017; Molnár et al. 2018; Wyche et al. 2015) (Fig.5). However, even in a devolatilised post-peak metamorphism host-rock, orogenic Au formation may occur if deeper fertile source rocks are tapped by transcrustal faults, feeding metamorphic fluid to the deposit. In a complex tectonic setting fertile prograde and retrograde units may be juxtaposed, metamorphic devolatilisation of the former releases metamorphic fluids in the latter (Kolb et al. 2015). Furthermore, rock units that did not experience metamorphic conditions higher than greenschist facies after peak metamorphism are still fertile and may be devolatilised in later metamorphic events, such as crustal heating during orogenic collapse large-scale granitoid magmatism (Gonçalves et al. 2019).

In Paper II, we propose that Au mineralisation in the Central Lapland Greenstone Belt occurred in two events:

1) Metamorphic devolatilisation of metavolcanic rocks related to the early stage of prograde metamorphism reaching peak conditions at ~1.88 – 1.86 Ga promoted the formation of Au-only orogenic Au deposits.
2) The second event is associated with the late-orogenic evolution between ~ 1.83 and 1.76 Ga, leading to formation of orogenic Au deposits with atypical metal association (high Cu and Co). Widespread granitoid magmatism and related high-grade metamorphism likely promoted late metamorphic fluid flow and possibly late metal mobilisation from metasedimentary units, increasing the base metal content in the mineralising fluids.

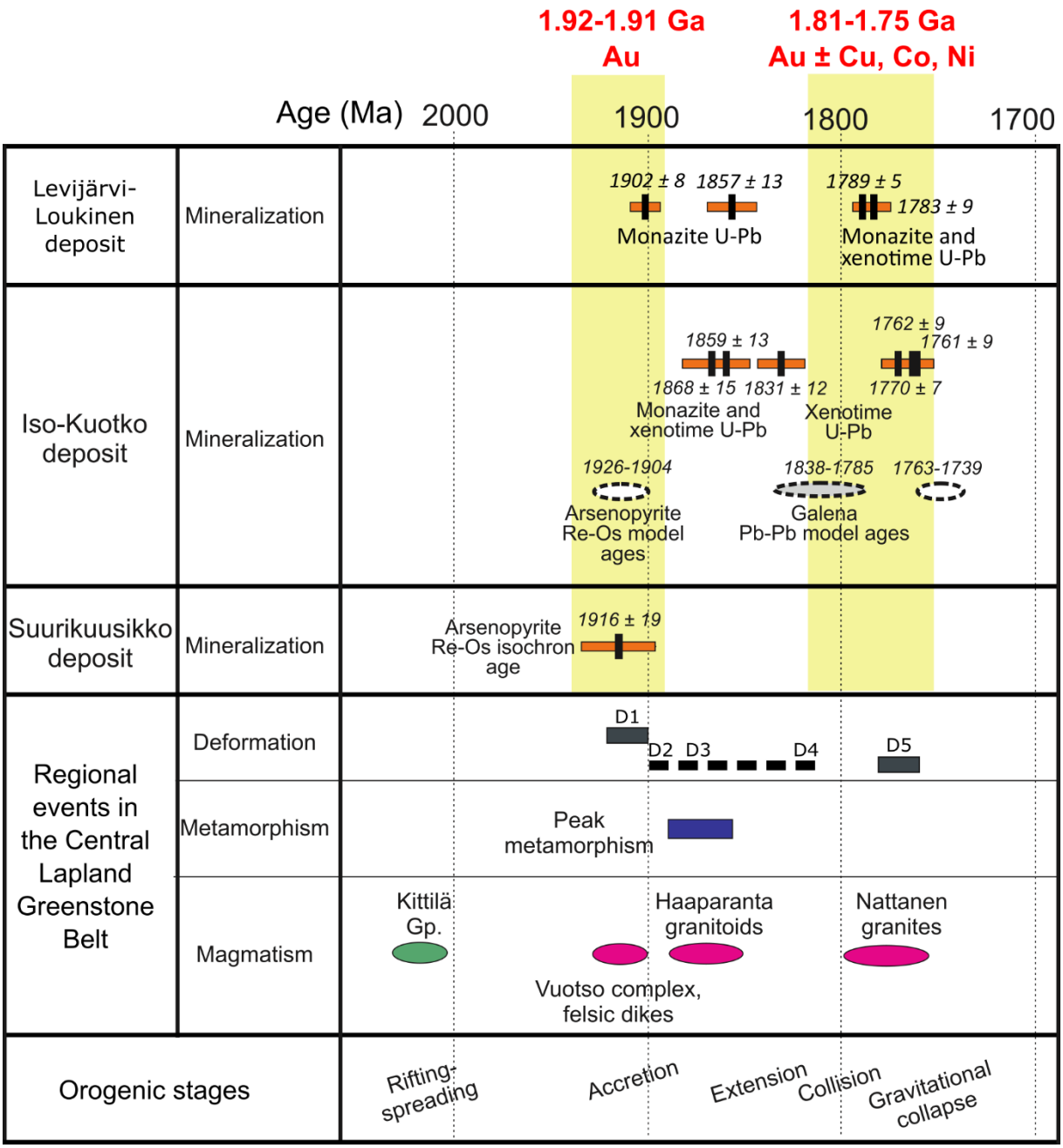

Fig.5: Timing of orogenic Au deposit formation in the Central Lapland Greenstone Belt relative to the regional events and orogenic stages (based on Kurhila et al. 2017; Molnár et al. 2017; Molnár et al. 2018).

The metamorphic devolatilisation model is a plausible mechanism to generate mineralising fluids during both prograde metamorphism and orogenic collapse. In Paper III, we show that the studied orogenic Au deposits of the Pohjanmaa Belt formed in two mineralising events:

1) An As-Au (Co, Ni) event occurs as the deposits are close to peak metamorphic conditions between 1.89 – 1.81 Ga depending on their location. Preliminary U-Pb titanite data from the Jouhineva and Huhta deposits gives a mineralisation age of 1854±15 Ma and 1816±12 Ma, respectively, which is contemporaneous to accretion and buckling during the Fennian stage of the Svecofennian Orogeny (Silva et al. sub.).

2) A Cu (-Au) event on the retrograde path, dated at 1760 ±14 and 1744 ± 30 Ma, based on preliminary U-Pb titanite data from the Jouhineva and Huhta deposits, respectively (Silva et al. sub.). This event is contemporaneous with the orogenic collapse and cooling stages of the Svecofennian Orogeny.

During the first event, the metal association is not identical between the deposits. Local and transient changes in the metal content of the mineralising fluid may be caused by heterogeneities in the source (e.g. Jouhineva and Kurula deposits; Fig.6). The similarities between the deposits of the Central Lapland Greenstone Belt and the Pohjanmaa Belt highlight how orogenic Au deposits formed in successive mineralising events at different stages of the orogenic cycle, each new event increasing the metal content and diversity in the deposit.

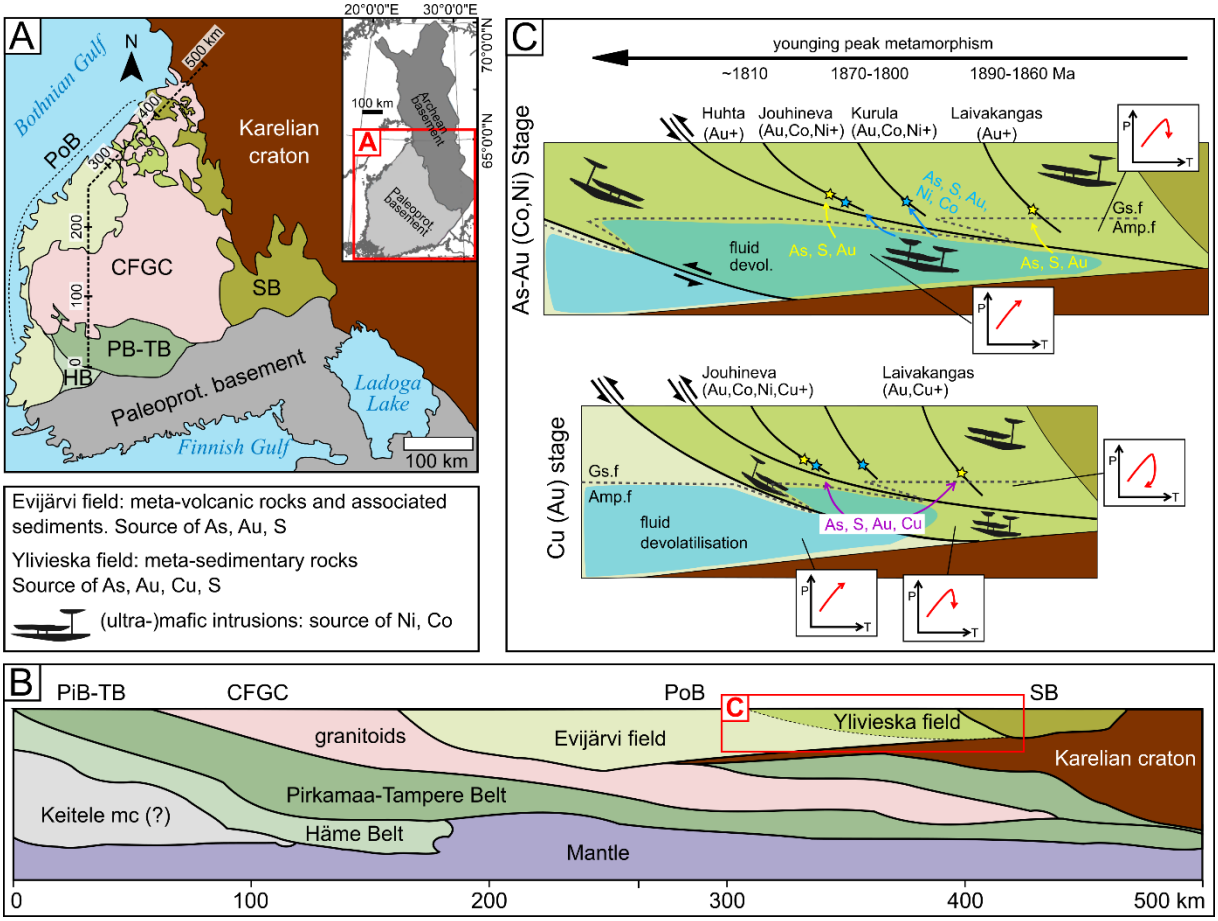

Fig.6: Model of formation for the orogenic Au deposits of the Pohjanmaa Belt. (A) Generalised geological map of the Svecofennian domain. CFGC: Central Finland Granitoid Complex; HB: Häme Belt; PB-TB: Pirkamaa and Tampere belts; PoB: Pohjanmaa Belt; SB: Savo Belt; (B) Interpreted cross-section of the Svecofennian domain showing the structural relationship between the PoB fields and the SB, based on Mints et al. (2020); (C) Genetic model for the studied deposits of the Pohjanmaa Belt. The As-Au (Co, Ni) mineralising event occurs as the host-rock of the deposits is already on the retrograde path and metamorphic fluids are produced by underlying prograde metavolcanic rock units of the Ylivieska field. Devolatilisation of mafic to ultramafic intrusions may cause local Ni, Co enrichment in the fluids leading to formation of orogenic Au deposits enriched in Ni and Co (i.e. Jouhineva, Kurula). The Cu-Au mineralising event involves Cu-rich metamorphic fluids released from the underlying metasedimentary units of the Evijärvi field, leading to Cu and Au enrichment in the Jouhineva prospect and Au (Cu) in the Laivakangas deposit.

8.3 Hybrid SMS-epithermal Au deposits

8.3.1 Source of Au and other metals

Hybrid epithermal-SMS deposits show numerous similarities with typical porphyry-epithermal deposits relative to metal endowment and mineralising processes allowing comparison between the two systems (Alfieris et al. 2013; Keith et al. 2018; Kilias et al. 2013; Naden et al. 2005). In Paper IV, we show the important role of magmatic degassing for the metal budget of the magmatic-hydrothermal system at Kolumbo. Upon degassing, As, Ag, Au, Cu, Hg, Sb, Sn, Pb and Zn become depleted in the magma and likely partition into the volatiles. Most of these metals are highly enriched in Kolumbo Pb-Zn(-Cu) mineralisation which show elevated As, Ag, Au, Hg, Tl and Sb contents (Kilias et al. 2013). The fluids venting from Kolumbo are rich in magmatic gases (>97% CO_2 of mantel origin) and have high Hg concentrations (61 to 1300 $ng \cdot m^{-3}$), indicating a connection between the degassing magmatic chamber and the hydrothermal vents (Rizzo et al. 2019). Several processes impacting the metal load of the fluids may occur during magmatic volatile migration through the hydrothermal system (e.g. fluid separation into brine and vapour phases, boiling and sulfide precipitation), preventing direct comparison of metal content between magmatic sulfides and the mineralisation to establish a genetic link. In Paper V, pairs of elements with similar geochemical behaviour (i.e. As/Pb; Ag/Au; Bi/Cu) are compared between magmatic sulfide and mineralisation of Kolumbo to counteract eventual fractionating processes. The similar ratios indicate that despite different metal endowment, magmatic sulfides are likely a metal source for Kolumbo mineralisation. Additionally, preliminary Pb isotope data from galena of the SMS match the Pb isotopic signature of Kolumbo volcanic rocks (Ahmad 2018; Klaver et al. 2016; Wind et al. 2020). Altogether, these results point toward a genetic link between the metals degassed from the magmatic chamber and the mineralisation. Preliminary work on the sulfide-

sulfate vents of Kolumbo indicates an intermediate sulfidation state during mineralisation (Ahmad 2018). The metal association of the mineralisation and the seemingly dominant magmatic source for the metals enriched in the mineralisation fit well with an intermediate sulfidation Au-Ag-Pb-Zn epithermal ore deposit model (Le Wang et al. 2019; Simmons et al. 2005; Simmons and Graham 2003). The basement rocks of the Kolumbo volcano are an alternative/additional source of metals for the SMS that may be mobilised by hydrothermal fluid circulation and leaching. However, they do not seem to be the main source of metals and their role relative to a magmatic source remains to be determined.

8.3.2 Mobility of Au and other metals

Most of the metals enriched in the Kolumbo SMS are moderately to strongly chalcophile elements, meaning that their mobility from the magmatic source to the sink will be strongly controlled by S-related processes, such as sulfide saturation and magmatic degassing (Wieser and Jenner 2021). Upon sulfide saturation, the chalcophile elements in a silicate melt partition into a sulfide liquid, depleting the melt in metals (Patten et al. 2013). Sulfide phases tend to segregate from the magma and settle at the bottom of the magma chamber because of their high density (Barnes and Lightfoot 2005). Once segregated from the magma, sulfide phases are less likely to be affected by further magmatic metal mobilising processes (e.g. degassing) and metals tend to remain trapped in the magmatic chamber (Jenner 2017). On the other hand, provided that the silicate melt is not metal-depleted, magmatic degassing transfers chalcophile elements to a magmatic-hydrothermal system as sulfide or chloride complexes, as they have good affinity with volatiles (Edmonds and Mather 2017). Constraining the relative timing between these processes during magmatic differentiation is critical for understanding the fate of chalcophile metals and the potential of a magmatic-hydrothermal systems to form ore deposits (Edmonds and Mather 2017; Park et al. 2019; Richards 2011, 2015; Sun et al. 2015).

In Paper IV, we report that, despite early magmatic sulfide saturation, chalcophile element concentrations in the magma do not decrease significantly until water saturation and degassing. The conservation of chalcophile elements in the magma during magmatic differentiation indicates that most of the magmatic sulfides are not physically separated from the silicate melt. Upon degassing, As, Ag, Au, Cu, Hg, Sb, Sn, Pb and Zn become depleted in the silicate magma as they partition into the volatile phase, either from the silicate melt or during interaction with magmatic sulfides which are rich in Cu, Ag, Au, Te, Bi (Patten et al. 2013; Peach et al. 1990). Upon volatile saturation, magmatic sulfides, if present, are preferential nucleation sites leading to the formation of vapour bubbles attached to the sulfides, which then may become buoyant sulfide-volatile compound drops (Mungall et al. 2015; Yao and Mungall 2020). Formation, coalescence, accumulation and oxidation of compound drops during mafic and felsic melt interaction appears as a particularly efficient mechanism for transferring S and chalcophile elements from the magmatic chamber to the shallow hydrothermal system (see Fig.3 - Paper V). The potential of a magmatic system to form sulfide-volatile compound drops may be investigated by modelling numerically the evolution of the silicate melt and identifying if simultaneous volatile and sulfide saturation is achievable during magmatic differentiation (Paper IV). Additional petrography on samples helps to confirm sulfide saturation in the melt and may lead to identification of sulfide-volatile compound drops or remnants of them.

The study presented in Paper V highlights the genetic link between the magmatic processes and the mineralisation of Kolumbo volcano already developed in Paper IV. Furthermore, as magmatic volatile compounds appear to efficiently supply metals to the hydrothermal system associated with the hybrid epithermal-VMS mineralisation, they may also play a role in the formation of deposits within the porphyry-epithermal-hybrid epithermal-SMS continuum (Larocque et al. 2000; Mungall et al. 2015; Nadeau et al. 2010).

From Paper V, the nature and chemical-physical properties of the compound drop volatile phase remain unknown. However, considering the depth (4-5 km) and temperature (~1000°C) prevailing as andesitic enclaves of the Kolumbo volcano formed, the magmatic fluids are likely to be CO_2-H_2O dominated, single phase and with intermediate salinity (Audétat 2019). The magmatic volatile phases in magmatic arc systems are complex and diverse but can be simplified into a fluid exsolving from a melt which eventually separates upon cooling and pressure drop into: 1) a highly saline brine, which promotes formation of porphyry mineralisation and 2) a low salinity vapour phase (Heinrich 2005; Pudack et al. 2009; Sillitoe 2010; Sillitoe and Hedenquist 2003). The latter promotes formation of epithermal mineralisation upon mixing with meteoric water or hybrid epithermal-VMS mineralisation upon mixing with seawater in a marine environment (Alfieris et al. 2013; Müller et al. 2002; Naden et al. 2005), as observed at Kolumbo. However, despite converging hints, there is yet no direct evidence of magmatic contribution to the metals of the Kolumbo SMS, with the exception of Hg (Rizzo et al. 2019) and further work is needed to confirm this (e.g. study of fluids inclusions from Kolumbo sulfide-sulfate chimneys).

8.3.3 Controlling parameters of the metal association

The mineralisation of the Kolumbo volcano occurs as sulfide-sulfate diffusers, typical of SMS deposits (Kilias et al. 2013). This morphology is mostly controlled by precipitation processes, as magmatic-hydrothermal fluid interacts with cold seawater, rather than being related to the source and nature of the hydrothermal fluids (low-salinity vapour phase; Haymon 2005). Conversely, the metal endowment is most likely strongly related to the source of the fluids. Here, the metal association at Kolumbo matches extensively the metals transferred during magmatic degassing except for few elements, notably Cu (Papers IV and V). The strong Cu depletion observed from the melt in Paper IV and the high Cu emanation coefficient from

magmatic sulfides defined in Paper V similar to other metals enriched in the SMS indicates that the mineralising fluid is also enriched in Cu and that the lack of Cu enrichment in the diffusers is likely caused by precipitation processes (Kilias et al. 2013).

Sulfide solubility is temperature-dependant, chalcopyrite precipitating generally between 270 and 360°C, while sphalerite precipitates between 170 and 240°C (Hannington 2014). As magmatic-hydrothermal fluid mixes with cold seawater, temperature drops and leads to strong metal zonation in SMS deposits, with a Cu-rich zone below a Zn-rich zone (Hannington 2014; Large 1992; Lydon 1984). The fluids venting from Kolumbo diffusers have relatively low temperature (< 265°C; Nomikou et al. 2022), indicating that Cu is trapped in the deeper and hotter root zone of the deposit as chalcopyrite forms, explaining the low Cu content in the diffusers. Hence, it is possible that a Cu-rich stockwork exists below the hydrothermal field of the Kolumbo volcano. Additional processes, such as boiling and zone refining can further lead to metal zonation and enrich Au, Ag, As, Sb, Hg, and Tl in the upper part of the mineralised system (Hannington 2014).

Alternatively, significant Cu can be trapped deeper within the hydrothermal system where dense high salinity brines remain after separation from the vapour phase (e.g. Heinrich 2005), promoting porphyry style mineralisation. Seismic evidence for fluids stratigraphically trapped at base of the volcaniclastic sequence of Kolumbo (Hübscher et al. 2015) is an appealing feature for suggesting that the Kolumbo volcano magmatic-hydrothermal system is not only an actively forming hybrid SMS-epithermal deposit but also an actively forming porphyry deposit.

9 Conclusion and future work

This thesis explores the mobility of Au in the continental crust by investigating orogenic Au deposits and hybrid SMS-epithermal Au deposits. It provides new tools to investigate Au in samples. Because of the very low Au content in the mantle and crust, one of the main challenges to track Au mobilisation processes are the detection limit of analytical instruments. By improving the detection limit by PPP-LA-ICP-MS (Paper I), we fulfil the first aim of the thesis. There is now a quick, safe, reliable and relatively inexpensive method to analyse sub-ng·g^{-1} Au content in rocks. This development allows to better study the source-to-sink journey of Au during deposit formation, which corresponds to the second, third and fourth aim of this work.

Gold is able to be transported by various magmatic, metamorphic and hydrothermal fluids within a broad range of temperatures and salinities (e.g. Patten et al. 2016; Pitcairn et al. 2014; Pokrovski et al. 2014; Pudack et al. 2009). The main controlling conditions for the formation of Au deposit in the crust are: 1) Au availability in the source, 2) Au mobilisation by a fluid, 3) efficient Au precipitation mechanisms.

A comparative study of the Central Lapland Greenstone Belt and Pohjanmaa Belt and their orogenic Au deposits highlights how the lithology of the source rocks controls the content in Au, other precious and base metals and ligands in the metamorphic fluid (Paper II). Additionally, we show that orogenic Au deposits frequently form over tens of millions of years (ca.100 m.y for the studied deposits), in a succession of mineralising events. Metamorphic fluids with different metal content and association are generated through time, depending on the nature of the devolatilising source rock. Higher base metal content in the mineralising fluid may lead to Cu-Co-Ni enrichment in the deposits, forming orogenic Au deposits with atypical metal association. Spatially close orogenic Au deposits may have different metal associations

if their structures are not reactivated at the same time and record different mineralising events (Paper III).

The study of the Nea Kameni and Kolumbo volcanoes enable to better constrain the generation of Au-rich magmatic fluids and show how the geological setting controls magmatic-hydrothermal mineralising processes. Despite early sulfide saturation in a magmatic system, Au and other chalcophile elements can still be mobilised later upon magmatic degassing (Paper IV). With the first report of sulfide-volatile compound drop formation in a volcanic arc setting and partition of metals into the volatiles during sulfide oxidation, we show a process generating metal-rich magmatic fluids that is likely involved in porphyry and epithermal deposits formation (Paper V). The study of Kolumbo sulfide-sulfate diffusers highlights how the morphology of hybrid SMS-epithermal deposits is constrained by the precipitation conditions, while the metal association seem mostly controlled by the source (Paper IV).

Several research perspectives emerge from this work, regarding mobility of Au, but also other metals. To this day, the enrichment mechanisms in base metals in orogenic Au deposits is not well understood. Metamorphic fluids can transport base metals to some extent and Cu enrichment is relatively common, but this is not the case for Co and Ni. Fluid inclusions of the Kurula and Jouhineva deposits may give insight into the nature of the mineralising fluid and help understanding the atypical metal enrichment. Additional work is necessary (e.g. fluid inclusions study on sulfide and/or sulfate) to confirm the genetic link between magmatic degassing and the hybrid SMS-epithermal deposit of Kolumbo.

A manuscript is in preparation to address this question, based on the Pb isotopic ratios from the mineralisation, the volcanic rocks and the basement rocks of Kolumbo. This study will allow to estimate which proportion of the mineralisation' s Pb is degassed from the magma or leached from the basement by hydrothermal fluids and extrapolated to other metals.

Altogether, this thesis sets new constrains on the processes mobilising Au in the most Au-rich geodynamic settings (i.e. orogen and volcanic arc; Fig.7) and provides new tools to track

metal mobility during magmatic differentiation. Identifying sulfide-volatile compound drops in volcanic arcs and estimating their role in mobilising metals from the magma is a breakthrough in the understanding of magmatic-related deposit formation (e.g. porphyry Cu-Au and epithermal deposits). Finally, investigating the atypical deposits that are orogenic Au deposits with atypical metal association and hybrid SMS-epithermal deposits reveals metal mobilising processes that may not be observed in deposits fitting the typical text-book descriptions. It highlights that local and transient changes in the source of metals, fluids or mineralising processes may affect the metal association in the deposits and how genetic models must not be too restrictive to account for deposits formation.

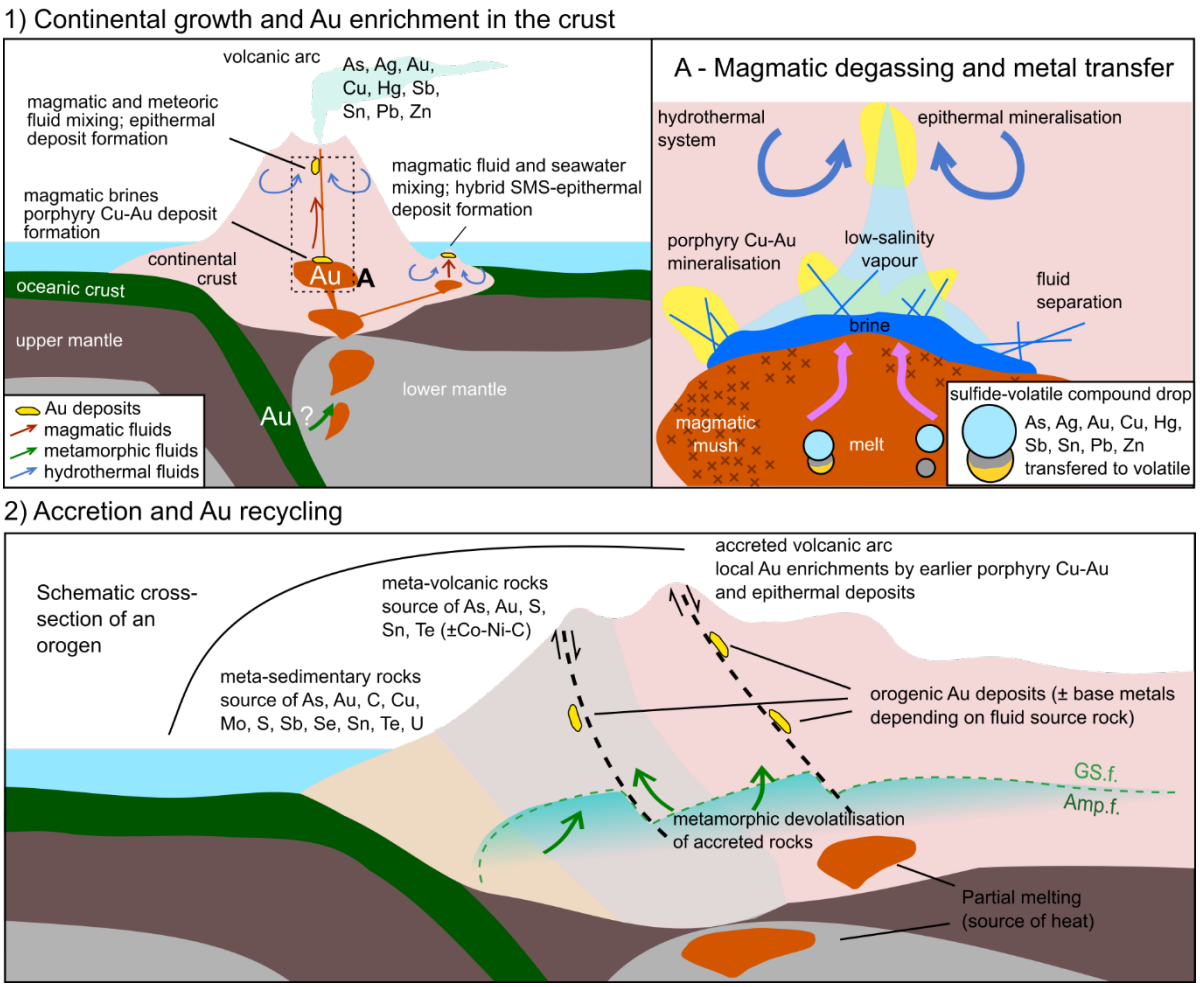

Fig.7: Mobility of Au in the crust, summary of the processes investigated in this work.

10 Acknowledgements

This thesis is the conclusion of almost 5 years within the Institute of Applied Geochemistry at the Karlsruhe Institute of Technology, navigating through the challenges of the 2019-2023 period. First of all, I would like to thank Prof. Dr. Jochen Kolb and Dr. Clifford Patten for their trust, letting me join the research group and giving me a lot of freedom. Their constant support, priceless advices and will to meet the highest standards helped me greatly to improve the quality of my work. I also thank all those who assisted me and made our research possible. For the Finnish part, I thank Otsogold, in particular Timo Aalto and Johanna Alitalo for granting us access to the Laivakangas mine; the Geological Survey of Finland (GTK), in particular Prof. Dr. Ferenc Molnár for granting us access to the Loppi drill core facility, his expertise and fruitful discussions, the German Federal Institute for Geosciences and Natural Resources (BGR), the German Academic Exchange Service (DAAD) and Academy of Finland (grant No. 315188 – project OroTECT) for funding. For the Greek part, I thank the National and Kapodistrian University of Athens, in particular Prof. Dr. Stephanos Kilias and Dr. Paraskevi Nomikou for helping us with the planning of the sampling campaign and providing samples of the Kolumbo volcano and mineralisation, as well as the German Research Foundation (DFG), in particular the DOME Special Priority Project 2238, for funding our research (grant PA 3523/2-1). I thank all the colleagues of the Institute who helped me and supported me in many ways: Dr. Elisabeth Eiche, Dr. Benjamin Walter, Prof. Dr. Kirsten Drüppel, Dr. Aratz Beranoaguirre, Dr. Alexandre Peillod, Dr. Dominik Gudelius; the technical and administrative staff – without which nothing would possible – Andrea Friedrich, Victoria Weist, Laura Neira, Maya Denker, Chantalle Kotschenreuther, Claudia Mößner, Gesine Preuß, Ralf Walter, Janine Wagner, Nadine Hüll, Beate Ötzel, Kristian Nikoloski; my fellow Ph.D. students – who carry the weight together – Magnus Schneider, Klemens Slunitschek, Michèle Jungmann, Rebekka

Reich, Andressa de Araujo Silva, Erke Peng, Michael Eigler and all the other. I do not forget all those who made my time in Karlsruhe what it was, my dear flat mates and my friends in Lorraine and elsewhere. Many thanks to my family, who always supported me in pursuing research, despite the past uncertainties and those to come. Finally, Linda, I cannot thank you enough for always believing in me and making everything better.

« Unde sumus quasi nanus aliquis humeris gigantis superpositus »

Bernard of Chartres, ca.1110 CE

11 References

Ahmad Q (2018) The source of metals in the recent polymetallic seafloor massive sulfide mineralization at the Kolumbo arc-volcano, Greece. M.Sc. thesis, Karlsruhe Institute of Technology

Alfieris D, Voudouris P, Spry PG (2013) Shallow submarine epithermal Pb–Zn–Cu–Au–Ag–Te mineralization on western Milos Island, Aegean Volcanic Arc, Greece: Mineralogical, geological and geochemical constraints. Ore Geology Reviews 53:159–180

Alt JC (1995) Subseafloor Processes in Mid-Ocean Ridge Hydrothennal Systems. In: Humphris SE, Zierenberg RA, Mullineaux LS, Thomson RE (eds) Seafloor Hydrothermal Systems: Physical, Chemical, Biological, and Geological Interactions. American Geophysical Union, Washington, D. C., pp 85–114

Audétat A (2019) The Metal Content of Magmatic-Hydrothermal Fluids and Its Relationship to Mineralization Potential. Economic Geology 114:1033–1056

Barnes S-J, Lightfoot PC (2005) Formation of Magmatic Nickel Sulfide Deposits and Processes Affecting Their Copper and Platinum Group Element Contents. In: Hedenquist J, Thompson JFH, Goldfarb RJ, Richards JP (eds) One Hundredth Anniversary Volume. Society of Economic Geologists

Barrie CT, Hannington M (eds) (1997) Volcanic Associated Massive Sulfide Deposits: Processes and Examples in Modern and Ancient Settings. Society of Economic Geologists

Becker K (1989) Measurements of the Permeability of the Sheeted Dikes in Hole 504B, ODP Leg 111. In: Becker K, Sakai H (eds) Proceedings of the Ocean Drilling Program, 111 Scientific Reports, vol 111. Ocean Drilling Program

Belgrano TM, Milton JA, Teagle DA (2022) Determination of Ultra-Trace Au, Ag, As, Pt and Re Mass Fractions in Volcanic Glasses and Rock Powders by LA-ICP-MS. Geostandards and Geoanalytical Research 46:621–644

Bierlein FP, Pisarevsky S (2008) Plume-related oceanic plateaus as a potential source of gold mineralization. Economic Geology 103:425–430
Boorder H de (2012) Spatial and temporal distribution of the orogenic gold deposits in the Late Palaeozoic Variscides and Southern Tianshan: How orogenic are they? Ore Geology Reviews 46:1–31
Brett-Adams AC, Diamond LW, Weber S, Gilgen SA (2023) Rock-Matrix Porosity and Permeability of the Hydrothermally Altered, Upper Oceanic Crust, Oman Ophiolite. J. Geophys. Res. 128
Carey S, Nomikou P, Bell KC, Lilley M, Lupton JE, Roman C, Stathopoulou E, Bejelou K, Ballard R (2013) CO2 degassing from hydrothermal vents at Kolumbo submarine volcano, Greece, and the accumulation of acidic crater water. Geology 41:1035–1038
Cathelineau M, Boiron M-C, Holliger P, Marion P, Denis M (1989) Gold in Arsenopyrites: Crystal Chemistry, Location and State, Physical and Chemical Conditions of Deposition. In: Keays RR, Ramsay WRH, Groves DI (eds) The Geology of Gold Deposits. Society of Economic Geologists, pp 328–341
Chryssoulis SL, McMullen J (2005) Mineralogical investigation of gold ores. In: Advances in Gold Ore Processing, vol 15. Elsevier, pp 21–71
de Ronde CEJ, Hannington M, Stoffers P, Wright IC, Ditchburn RG, Reyes AG, Baker ET, Massoth GJ, Lupton JE, Walker SL, Greene RR, Soong CWR, Ishibashi J, Lebon GT, Bray CJ, Resing JA (2005) Evolution of a Submarine Magmatic-Hydrothermal System: Brothers Volcano, Southern Kermadec Arc, New Zealand. Economic Geology 100:1097–1133
Dubé B, Gosselin P, Mercier-Langevin P, Hannington M, Galley A (2007) Gold-rich volcanogenic massive sulphide deposits: Mineral deposits of Canada: a synthesis of major deposit-types, district metallogeny, the evolution of geological provinces, and exploration methods. Geol Assoc Can, Mineral Deposits Division Spec Publ 5:75–94
Edmonds M, Mather TA (2017) Volcanic Sulfides and Outgassing. Elements 13:105–110
Eilu P (2015) Overview on Gold Deposits in Finland. In: Mineral Deposits of Finland. Elsevier, pp 377–410
Eilu P, Pankka H (2009) FINGOLD - a public database on gold deposits in Finland: Version 1.0. Geological Survey of Finland, Espoo
Eilu P, Pankka H, Keinänen V, Kortelainen V, Niiranen T, Pulkkinen E (2007) Characteristics of gold mineralisation in the greenstone belts of northern Finland. In: Ojala VJ (ed) Gold in the central Lapland greenstone belt. Geological Survey of Finland, Espoo, pp 57–106
Eilu P, Ahtola T, Äikäs O, Halkoaho T, Heikura P, Hulkki H, Iljina M, Juopperi H, Karinen T, Kärkkäinen N, Konnunaho J, Kontinen A, Kontoniemi O, Korkiakoski E, Korsakova M, Kuivasaari T, Kyläkoski M, Makkonen H, Niiranen T, Nikander J, Nykänen V, Perdahl J-A, Pohjolainen E, Räsänen J, Sorjonen-Ward P, Tiainen M, Tontti M, Torppa A, Västi K (2012) Metallogenic areas in Finland. In: Eilu P (ed) Mineral deposits and metallogeny of Fennoscandia. Geological Survey of Finland, Espoo, pp 207–342
Eisenlohr BN, Groves D, Partington GA (1989) Crustal-scale shear zones and their significance to Archaean gold mineralization in Western Australia. Mineral. Deposita 24

Elmer FL, White DJ, Powell R (2006) Devolatilization of metabasic rocks during greenschist-amphibolite facies metamorphism. Journal of Metamorphic Geology 24:497–513
Fisher AT (1998) Permeability within basaltic oceanic crust. Rev. Geophys. 36:143–182
Fyfe WS, Thompson AB, Price NJ (1978) Fluids in the Earth's crust: Their significance in metamorphic, tectonic, and chemical transport processes. Developments in geochemistry, vol 1. Elsevier Scientific Pub. Co, Amsterdam, New York, New York
Gaál G, Sundblad K (1990) Metallogeny of gold in the Fennoscandian Shield. Mineralium Deposita 25 (Suppl):S 104 - S 114
Gaboury D (2019) Parameters for the formation of orogenic gold deposits. Applied Earth Science 795:1–10
Garbe-Schönberg D, Müller S (2014) Nano-particulate pressed powder tablets for LA-ICP-MS. J. Anal. At. Spectrom. 29:990–1000
Garofalo PS, Fricker MB, Günther D, Bersani D, Paolo Lottici P (2014) Physical-chemical properties and metal budget of Au-transporting hydrothermal fluids in orogenic deposits. Geological Society, London, Special Publications 402:71–102
Gebre-Mariam M, Hagemann S, Groves DI (1995) A classification scheme for epigenetic Archaean lode-gold deposits. Mineralium Deposita:408–410
Goldfarb R, Groves D, Gardoll S (2001) Orogenic gold and geologic time: a global synthesis. Ore Geology Reviews 18:1–75
Goldfarb RJ, Baker T, Dubé B, Groves DI, Hart CJR, Gosselin P (2005) Distribution, Character, and Genesis of Gold Deposits in Metamorphic Terranes. In: Hedenquist JW (ed) Economic geology: One hundredth anniversary volume : 1905-2005. Society of Economic Geologists, Inc, Littleton, CO, pp 407–450
Goldfarb RJ, Groves DI (2015) Orogenic gold: Common or evolving fluid and metal sources through time. Lithos 233:2–26
Goldfarb RJ, Pitcairn I (2023) Orogenic gold: is a genetic association with magmatism realistic? Miner Deposita 58:5–35
Gonçalves GO, Lana C, Buick IS, Alkmim FF, Scholz R, Queiroga G (2019) Twenty million years of post-orogenic fluid production and hydrothermal mineralization across the external Araçuaí orogen and adjacent São Francisco craton, SE Brazil. Lithos 342-343:557–572
Groves D, Goldfarb R, Gebre-Mariam M, Hagemann S, Robert F (1998) Orogenic gold deposits: A proposed classification in the context of their crustal distribution and relationship to other gold deposit types. Ore Geology Reviews 13:7–27
Groves DI, Goldfarb RJ, Robert F, Hart CJR (2003) Gold Deposits in Metamorphic Belts: Overview of Current Understanding,Outstanding Problems, Future Research, and Exploration Significance. Economic Geology 98:1–29
Groves DI, Santosh M, Deng J, Wang Q, Yang L, Zhang L (2020) A holistic model for the origin of orogenic gold deposits and its implications for exploration. Mineral. Deposita 55:275–292
Hagemann S, Cassidy K (2000) Archean Orogenic Lode Gold Deposit. In: Hagemann SG, Brown PE (eds) Gold in 2000. Society of Economic Geologists, [Littleton, Colorado], pp 9–60

Halbach P, Nakamura K, Wahsner M, Lange J, Sakai H, Käselitz L, Hansen R-D, Yamano M, Post J, Prause B, Seifert R, Michaelis W, Teichmann F, Kinoshita M, Märten A, Ishibashi J, Czerwinski S, Blum N (1989) Probable modern analogue of Kuroko-type massive sulphide deposits in the Okinawa Trough back-arc basin. Nature 338:496–499

Hannington M (2014) Volcanogenic Massive Sulfide Deposits. In: Treatise on Geochemistry. Elsevier, pp 463–488

Hannington M, Scott SD (1989) Gold Mineralization in Volcanogenic Massive Sulfides : Implications of Data from Active Hydrothermal Vents on the Modern Sea Floor. In: Keays RR, Ramsay WRH, Groves DI (eds) The Geology of Gold Deposits. Society of Economic Geologists, pp 491–507

Hannington M, Poulsen KH, Thompson JFH, Sillitoe RH (1997) Volcanogenic Gold in the Massive Sulfide Environment. In: Barrie CT, Hannington M (eds) Volcanic Associated Massive Sulfide Deposits: Processes and Examples in Modern and Ancient Settings. Society of Economic Geologists

Hannington M, de Ronde CEJ, Petersen S (2005) Sea-Floor Tectonics and Submarine Hydrothermal Systems. In: Hedenquist J, Thompson JFH, Goldfarb RJ, Richards JP (eds) One Hundredth Anniversary Volume. Society of Economic Geologists

Hanski E, Huhma H (2005) Central Lapland Greenstone Belt. In: Lehtinen M, Nurmi PA, Rämö OT (eds) Precambrian geology of Finland: Key to the evolution of the Fennoscandian shield, 1. ed. Elsevier, Amsterdam, pp 139–194

Haymon RM (2005) TECTONICS | Hydrothermal Vents At Mid-Ocean Ridges. In: Selley RC, Cocks LRM, Plimer IR (eds) Encyclopedia of geology. Elsevier, S.l., pp 388–395

Hedenquist JW, Arribas A, Reynolds TJ (1998) Evolution of an intrusion-centered hydrothermal system; Far Southeast-Lepanto porphyry and epithermal Cu-Au deposits, Philippines. Economic Geology 93:373–404

Heinrich CA (2005) The physical and chemical evolution of low-salinity magmatic fluids at the porphyry to epithermal transition: a thermodynamic study. Miner Deposita 39:864–889

Henley RW (1985) The Geothermal Framework of Epithermal Deposits. In: Berger BR, Bethke PM (eds) Geology and Geochemistry of Epithermal Systems. Society of Economic Geologists, pp 1–24

Hölttä P, Väisänen M, Väänänen J, Manninen T (2007) Paleoproterozoic metamorphism and deformation in Central Lapland, Finland. In: Ojala VJ (ed) Gold in the central Lapland greenstone belt. Geological Survey of Finland, Espoo, pp 7–56

Hölttä P, Heilimo E (2017) Metamorphic map of Finland. In: Nironen M (ed) Bedrock of Finland at the scale 1:1 000 000: Major stratigraphic units, metamorphism and tectonic evolution. Geological Survey of Finland, Espoo, pp 77–128

Hronsky JMA, Groves DI, Loucks RR, Begg GC (2012) A unified model for gold mineralisation in accretionary orogens and implications for regional-scale exploration targeting methods. Miner Deposita 47:339–358

Hübscher C, Ruhnau M, Nomikou P (2015) Volcano-tectonic evolution of the polygenetic Kolumbo submarine volcano/Santorini (Aegean Sea). Journal of Volcanology and Geothermal Research 291:101–111

Jenner FE (2017) Cumulate causes for the low contents of sulfide-loving elements in the continental crust. Nature Geosci 10:524–529
Kähkönen Y (2005) Svecofennian supracrustal rocks. In: Lehtinen M, Nurmi PA, Rämö OT (eds) Precambrian geology of Finland: Key to the evolution of the Fennoscandian shield, 1. ed. Elsevier, Amsterdam, pp 343–406
Keith M, Haase KM, Klemd R, Smith DJ, Schwarz-Schampera U, Bach W (2018) Constraints on the source of Cu in a submarine magmatic-hydrothermal system, Brothers volcano, Kermadec island arc. Contrib Mineral Petrol 173
Kerrick DM, Connolly J (2001) Metamorphic devolatilization of subducted oceanic metabasalts: implications for seismicity, arc magmatism and volatile recycling. Earth and Planetary Science Letters 189:19–29
Kilias SP, Nomikou P, Papanikolaou D, Polymenakou PN, Godelitsas A, Argyraki A, Carey S, Gamaletsos P, Mertzimekis TJ, Stathopoulou E, Goettlicher J, Steininger R, Betzelou K, Livanos I, Christakis C, Bell KC, Scoullos M (2013) New insights into hydrothermal vent processes in the unique shallow-submarine arc-volcano, Kolumbo (Santorini), Greece. Sci Rep 3:2421
Klaver M, Carey S, Nomikou P, Smet I, Godelitsas A, Vroon P (2016) A distinct source and differentiation history for Kolumbo submarine volcano, Santorini volcanic field, Aegean arc. Geochem Geophys Geosyst 17:3254–3273
Koistinen T, Stephens MB, Bogatchev V, Nordgulen Ø, Wennerström M, Korhonen J (2001) Geological Map of the Fennoscandian Shield, Scale 1:2 000 000. Geological surveys of Finland, Norway and Sweden and the North-West Department of Natural Resources of Russia.
Kojonen K, Johanson B (1999) Determination of refractory gold distribution by microanalysis, diagnostic leaching and image analysis. Mineralogy and Petrology 67:1–19
Kolb J, Meyer FM, Kisters AFM (2000) Amphibolite facies gold mineralization at Renco, Zimbabwe: Conditions of ore formation. In: Rammlmair D (ed) Applied mineralogy in research, economy, technology, ecology and culture: Proceedings of the sixth International Congress on Applied Mineralogy / Göttingen, Germany, 17-19 July 2000 / ICAM 2000. A.A. Balkema, Rotterdam, Brookfield, pp 355–357
Kolb J, Hellmann A, Rogers A, Sindern S, Vennemann TW, Böttcher ME, Meyer FM (2004a) The Role of a Transcrustal Shear Zone in Orogenic Gold Mineralization at the Ajjanahalli Mine, Dharwar Craton, South India. Economic Geology 99:743–759
Kolb J (2008) The role of fluids in partitioning brittle deformation and ductile creep in auriferous shear zones between 500 and 700 °C. Tectonophysics 446:1–15
Kolb J, Rogers A, Meyer F, Vennemann TW (2004b) Development of fluid conduits in the auriferous shear zones of the Hutti Gold Mine, India: evidence for spatially and temporally heterogeneous fluid flow. Tectonophysics 378:65–84
Kolb J, Dziggel A, Bagas L (2015) Hypozonal lode gold deposits: A genetic concept based on a review of the New Consort, Renco, Hutti, Hira Buddini, Navachab, Nevoria and The Granites deposits. Precambrian Research 262:20–44

Kurhila M, Molnár F, O`Brien H, Tiljander M, Johanson B, Middleton A (2017) U-Pb dating of hydrothermal monazite and xenotime from the Levijärvi-Loukinen gold deposit, Central Lapland Greenstone Belt, Northern Finland. In: Hölttä P, Nenonen K, Eerola T (eds) Guide 63: Abstract Book, pp 56–57

Large RR (1992) Australian volcanic-hosted massive sulfide deposits; features, styles, and genetic models. Economic Geology 87:471–510

Larocque AC, Stimac JA, Keith JD, Huminicki MA (2000) Evidence for open-system behavior in immiscible Fe-S-O liquids in silicate magmas: Implications for contributions of metals and sulfur to ore-forming fluids. Can Mineral 38:1233–1249

Lawrence DM, Treloar PJ, Rankin AH, Harbidge P, Holliday J (2013) The Geology and Mineralogy of the Loulo Mining District, Mali, West Africa: Evidence for Two Distinct Styles of Orogenic Gold Mineralization. Economic Geology 108:199–227

Le Wang, Qin K-Z, Song G-X, Li G-M (2019) A review of intermediate sulfidation epithermal deposits and subclassification. Ore Geology Reviews 107:434–456

Liu W, Borg SJ, Testemale D, Etschmann B, Hazemann J-L, Brugger J (2011) Speciation and thermodynamic properties for cobalt chloride complexes in hydrothermal fluids at 35–440°C and 600bar: An in-situ XAS study. Geochimica et Cosmochimica Acta 75:1227–1248

Liu W, Migdisov A, Williams-Jones A (2012) The stability of aqueous nickel(II) chloride complexes in hydrothermal solutions: Results of UV–Visible spectroscopic experiments. Geochimica et Cosmochimica Acta 94:276–290

Liu W, Etschmann B, Testemale D, Hazemann J-L, Rempel K, Müller H, Brugger J (2014) Gold transport in hydrothermal fluids: Competition among the Cl−, Br−, HS− and NH3(aq) ligands. Chemical Geology 376:11–19

Liu Y-H, Wan B, Xue D-S (2019) Sample Digestion and Combined Preconcentration Methods for the Determination of Ultra-Low Gold Levels in Rocks. Molecules 24

Lydon J (1984) Ore Deposit Models-8. Volcanogenic massive sulphide deposits part I: A descriptive model. Geoscience Canada Volume 11, Number 4:195–202

Mänttäri I (1995) Lead isotope characteristics of epigenetic gold mineralization in the Palaeoproterozoic Lapland greenstone belt, nothern Finland. Väitöskirja. Bulletin / Geological Survey of Finland, vol 381. Geologian Tutkimuskeskus, Espoo

Martin VM, Holness MB, Pyle DM (2006) Textural analysis of magmatic enclaves from the Kameni Islands, Santorini, Greece. Journal of Volcanology and Geothermal Research 154:89–102

McCuaig TC, Kerrich R (1998) P—T—t—deformation—fluid characteristics of lode gold deposits: evidence from alteration systematics. Ore Geology Reviews 12:381–453

Mercier-Langevin P, Hannington MD, Dubé B, Bécu V (2011) The gold content of volcanogenic massive sulfide deposits. Miner Deposita 46:509–539

Mints MV, Glaznev VN, Muravina OM, Sokolova EY (2020) 3D model of Svecofennian Accretionary Orogen and Karelia Craton based on geology, reflection seismics, magnetotellurics and density modelling: Geodynamic speculations. Geoscience Frontiers 11:999–1023

Molnár F, O'Brien H, Lahaye Y, Kurhila M, Middleton A, Johanson B (2017) Multi-stage hydrothermal processes and diverse metal associations in orogenic gold deposits of the Central Lapland greenstone belt, Finland. In: Mercier-Langevin P. et al. (ed) Mineral Resources to Discover, Québec, Canada, pp 63–66

Molnár F, Middleton A, Stein H, O`Brien H, Lahaye Y, Huhma H, Pakkanen L, Johanson B (2018) Repeated syn- and post-orogenic gold mineralization events between 1.92 and 1.76 Ga along the Kiistala Shear Zone in the Central Lapland Greenstone Belt, northern Finland. Ore Geology Reviews 101:936–959

Molnár F, Lahaye Y, O`Brien H, Matti K, Hulkki H, Demény A, Kirsch N, Richard A (2019) The Saattopora orogenic Au-Cu deposit, Central Lapland Greenstone belt, Finland: fluid sources and timing of hydrothermal processes. Proceedings of the 15th SGA Biennial Meeting, 27-30 August 2019, Glasgow, Scotland:723–726

Müller D, Kaminski K, Uhlig S, Graupner T, Herzig PM, Hunt S (2002) The transition from porphyry- to epithermal-style gold mineralization at Ladolam, Lihir Island, Papua New Guinea: a reconnaissance study. Miner Deposita 37:61–74

Mungall JE, Brenan JM, Godel B, Barnes SJ, Gaillard F (2015) Transport of metals and sulphur in magmas by flotation of sulphide melt on vapour bubbles. Nature Geosci 8:216–219

Nadeau O, Williams-Jones AE, Stix J (2010) Sulphide magma as a source of metals in arc-related magmatic hydrothermal ore fluids. Nature Geosci 3:501–505

Naden J, Kilias SP, Darbyshire DF (2005) Active geothermal systems with entrained seawater as modern analogs for transitional volcanic-hosted massive sulfide and continental magmato-hydrothermal mineralization: The example of Milos Island, Greece. Geology 33:541

Nesbitt BE, St. Louis RM, Muehlenbachs K (1987) Distribution of gold in altered basalts of DSDP hole 504B. Can. J. Earth Sci. 24:201–209

Neumayr P, Cabri L, Groves D, Mikucki E, Jackman J (1993) The mineralogical distribution of gold and relative timing of gold mineralisation in two Archaean settings of high metamorphic grade in Australia. Canadian Mineralogist 31:711–725

Nironen M (2005) Proterozoic orogenic granitoid rocks. In: Lehtinen M, Nurmi PA, Rämö OT (eds) Precambrian geology of Finland: Key to the evolution of the Fennoscandian shield, 1. ed. Elsevier, Amsterdam, pp 443–480

Nironen M (2017) Structural interpretation of the Peräpohja and Kuusamo belts and Central Lapland, and a tectonic model for northern Finland. Report of Investigation

Nomikou P, Polymenakou PN, Rizzo AL, Petersen S, Hannington M, Kilias SP, Papanikolaou D, Escartin J, Karantzalos K, Mertzimekis TJ, Antoniou V, Krokos M, Grammatikopoulos L, Italiano F, Caruso CG, Lazzaro G, Longo M, Sciré Scappuzzo S, D'Alessandro W, Grassa F, Bejelou K, Lampridou D, Katsigera A, Dura A (2022) SANTORY: SANTORini's Seafloor Volcanic ObservatorY. Front. Mar. Sci. 9

Nurmi PA, Lestinen P, Niskavaara H (1991) Geochemical characteristics of mesothermal gold deposits in the Fennoscandian Shield, and a comparison with selected Canadian and Australian deposits. Bulletin / Geological Survey of Finland, vol 351. Geologian Tutkimuskeskus, Espoo, Finland

Park J-W, Campbell IH, Malaviarachchi SPK, Cocker H, Hao H, Kay SM (2019) Chalcophile element fertility and the formation of porphyry Cu ± Au deposits. Miner Deposita 54:657–670

Patison NJ (2007) Structural controls on gold mineralisation in the Central Lapland Greenstone Belt. In: Ojala VJ (ed) Gold in the central Lapland greenstone belt. Geological Survey of Finland, Espoo, pp 105–122

Patten C, Barnes S-J, Mathez EA, Jenner FE (2013) Partition coefficients of chalcophile elements between sulfide and silicate melts and the early crystallization history of sulfide liquid: LA-ICP-MS analysis of MORB sulfide droplets. Chemical Geology 358:170–188

Patten C, Pitcairn IK, Teagle D (2017) Hydrothermal mobilisation of Au and other metals in supra-subduction oceanic crust: Insights from the Troodos ophiolite. Ore Geology Reviews 86:487–508

Patten C, Pitcairn IK, Molnár F, Kolb J, Beaudoin G, Guilmette C, Peillod A (2020a) Gold mobilization during metamorphic devolatilization of Archean and Paleoproterozoic metavolcanic rocks. Geology 48:1110–1114

Patten C, Coltat R, Junge M, Peillod A, Ulrich M, Manatschal G, Kolb J (2022) Ultramafic-hosted volcanogenic massive sulfide deposits: an overlooked sub-class of VMS deposit forming in complex tectonic environments. Earth-Science Reviews 224:103891

Patten CGC, Pitcairn IK, Teagle DAH, Harris M (2016) Mobility of Au and related elements during the hydrothermal alteration of the oceanic crust: implications for the sources of metals in VMS deposits. Miner Deposita 51:179–200

Patten CGC, Pitcairn IK, Alt JC, Zack T, Lahaye Y, Teagle DAH, Markdahl K (2020b) Metal fluxes during magmatic degassing in the oceanic crust: sulfide mineralisation at ODP site 786B, Izu-Bonin forearc. Miner Deposita 55:469–489

Peach C, Mathez E, Keays R (1990) Sulfide melt-silicate melt distribution coefficients for noble metals and other chalcophile elements as deduced from MORB: Implications for partial melting. Geochimica et Cosmochimica Acta 54:3379–3389

Peltonen P (2005) Svecofennian mafic-ultramafic intrusions. In: Lehtinen M, Nurmi PA, Rämö OT (eds) Precambrian geology of Finland: Key to the evolution of the Fennoscandian shield, 1. ed. Elsevier, Amsterdam, pp 407–442

Peters D, Pettke T (2017) Evaluation of Major to Ultra Trace Element Bulk Rock Chemical Analysis of Nanoparticulate Pressed Powder Pellets by LA-ICP-MS. Geostandards and Geoanalytical Research 41:5–28

Phillips GN, Powell R (2010) Formation of gold deposits: a metamorphic devolatilization model. Journal of Metamorphic Geology 28:689–718

Phillips GN, Powell R (2009) Formation of gold deposits: Review and evaluation of the continuum model. Earth-Science Reviews 94:1–21

Phillips GN, Powell R (2015) A practical classification of gold deposits, with a theoretical basis. Ore Geology Reviews 65:568–573

Pitcairn IK, Warwick PE, Milton JA, Teagle DAH (2006a) Method for ultra-low-level analysis of gold in rocks. Anal Chem 78:1290–1295

Pitcairn IK (2011) Background concentrations of gold in different rock types. Applied Earth Science 120:31–38

Pitcairn IK, Teagle DAH, Craw D, Olivo GR, Kerrich R, Brewer TS (2006b) Sources of Metals and Fluids in Orogenic Gold Deposits: Insights from the Otago and Alpine Schists, New Zealand. Economic Geology 101:1525–1546
Pitcairn IK, Craw D, Teagle DA (2014) The gold conveyor belt: Large-scale gold mobility in an active orogen. Ore Geology Reviews 62:129–142
Pitcairn IK, Craw D, Teagle DAH (2015) Metabasalts as sources of metals in orogenic gold deposits. Miner Deposita 50:373–390
Pitcairn IK, Leventis N, Beaudoin G, Faure S, Guilmette C, Dubé B (2021) A metasedimentary source of gold in Archean orogenic gold deposits. Geology 49:862–866
Pokrovski GS, Akinfiev NN, Borisova AY, Zotov AV, Kouzmanov K (2014) Gold speciation and transport in geological fluids: insights from experiments and physical-chemical modelling. Geological Society, London, Special Publications 402:9–70
Pudack C, Halter WE, Heinrich CA, Pettke T (2009) Evolution of Magmatic Vapor to Gold-Rich Epithermal Liquid: The Porphyry to Epithermal Transition at Nevados de Famatina, Northwest Argentina. Economic Geology 104:449–477
Qiu Z-J, Fan H-R, Santosh M, Yang K-F, Li X-C, Lan T-G, Tang Y-W, Pan Y-X (2021) Saline fluids drive Cu mineralization in Precambrian metasediments: Evidence from the Trans-North China Orogen. Ore Geology Reviews 139:104462
Richards JP (2011) Magmatic to hydrothermal metal fluxes in convergent and collided margins. Ore Geology Reviews 40:1–26
Richards JP (2015) The oxidation state, and sulfur and Cu contents of arc magmas: implications for metallogeny. Lithos 233:27–45
Ridley JR, Diamond LW (2000) Fluid chemistry of orogenic lode gold deposits and implications for genetic models. In: Hagemann SG, Brown PE (eds) Gold in 2000. Society of Economic Geologists, [Littleton, Colorado], pp 141–162
Rizzo AL, Caracausi A, Chavagnac V, Nomikou P, Polymenakou PN, Mandalakis M, Kotoulas G, Magoulas A, Castillo A, Lampridou D (2016) Kolumbo submarine volcano (Greece): An active window into the Aegean subduction system. Sci Rep 6:28013
Rizzo AL, Caracausi A, Chavagnac V, Nomikou P, Polymenakou PN, Mandalakis M, Kotoulas G, Magoulas A, Castillo A, Lampridou D, Marusczak N, Sonke JE (2019) Geochemistry of CO2-Rich Gases Venting From Submarine Volcanism: The Case of Kolumbo (Hellenic Volcanic Arc, Greece). Front. Earth Sci. 7
Robert F, Poulsen KH (2001) Vein Formation and Deformation in Greenstone Gold Deposits. In: Richards JP, Tosdal RM (eds) Structural controls on ore genesis. Society of Economic Geologists, Inc, pp 111–155
Rowland JV, Simmons SF (2012) Hydrologic, Magmatic, and Tectonic Controls on Hydrothermal Flow, Taupo Volcanic Zone, New Zealand: Implications for the Formation of Epithermal Vein Deposits. Economic Geology 107:427–457
Rudnick RL, Gao S (2003) Composition of the Continental Crust. In: Treatise on Geochemistry. Elsevier, pp 1–64
Saunders JE, Pearson NJ, O'Reilly SY, Griffin WL (2018) Gold in the mantle: A global assessment of abundance and redistribution processes. Lithos 322:376–391

Sayab M, Molnár F, Aerden D, Niiranen T, Kuva J, Välimaa J (2020) A succession of near-orthogonal horizontal tectonic shortenings in the Paleoproterozoic Central Lapland Greenstone Belt of Fennoscandia: constraints from the world-class Suurikuusikko gold deposit. Mineral. Deposita 55:1605–1624
Seward T (1973) Thio complexes of gold and the transport of gold in hydrothermal ore solutions. Geochimica et Cosmochimica Acta 37:379–399
Seward TM, Williams-Jones AE, Migdisov AA (2014) The Chemistry of Metal Transport and Deposition by Ore-Forming Hydrothermal Fluids. In: Treatise on Geochemistry. Elsevier, pp 29–57
Sibson RH, Robert F, Poulsen KH (1988) High-angle reverse faults, fluid-pressure cycling, and mesothermal gold-quartz deposits. Geology 16:551
Sigurdsson H, Carey S, Alexandri M, Vougioukalakis G, Croff K, Roman C, Sakellariou D, Anagnostou C (2006) Marine investigations of Greece's Santorini volcanic field. Eos, Trans. Am. Geophys. Union 87:337–342
Sillitoe R, Hedenquist J (2003) Linkages between volcanotectonic settings, ore-fluid compositions, and epithermal precious-metal deposits. In: Simmons SF, Graham IJ (eds) Volcanic, geothermal and ore-forming fluids: Rulers and witnesses of processes within the Earth, Special Publication 10, Chapter 18, pp 315–343
Sillitoe RH (1990) Intrusion-related gold deposits. In: Foster RP (ed) Gold metallogeny and exploration, vol 1. Springer US, Boston, MA, pp 165–209
Sillitoe RH, Hannington MD, Thompson JFH (1996) High sulfidation deposits in the volcanogenic massive sulfide environment. Economic Geology 91:204–212
Sillitoe RH (2010) Porphyry Copper Systems. Economic Geology 105:3–41
Silva A, Patten CGC, Kolb J, Hector S, Walter BF, Beranoaguirre A, Eiche E (sub.) Timing of the Orogenic Jouhineva Au-Cu-Co and Huhta Au mineralization: Constraints from titanite U-Pb dating. SGA Abstract 17th SGA Biennial Meeting 2023
Simmons SF, Graham IJ (eds) (2003) Volcanic, geothermal and ore-forming fluids: Rulers and witnesses of processes within the Earth, Special Publication 10
Simmons SF, White NC, John DA (2005) Geological Characteristics of Epithermal Precious and Base Metal Deposits. In: Hedenquist J, Thompson JFH, Goldfarb RJ, Richards JP (eds) One Hundredth Anniversary Volume. Society of Economic Geologists
Stoffers P, Hannington M, Wright I, Herzig P, Ronde C de, Scientific Party S (1999) Elemental mercury at submarine hydrothermal vents in the Bay of Plenty, Taupo volcanic zone, New Zealand. Geology 27:931
Sun W, Huang R, Li H, Hu Y, Zhang C, Sun S, Zhang L, Ding X, Li C, Zartman RE, Ling M (2015) Porphyry deposits and oxidized magmas. Ore Geology Reviews 65:97–131
Tapio J, Ranta J-P, Cook N, Lahaye Y, O'Brien H (2021) Paleoproterozoic Rajapalot Au-Co system associated with evaporites: Chemical composition and boron isotope geochemistry of tourmaline, and sulfur isotopes of sulfates, Peräpohja belt, northern Finland. Precambrian Research 365:106410
Thébaud N, Sugiono D, LaFlamme C, Miller J, Fisher L, Voute F, Tessalina S, Sonntag I, Fiorentini M (2018) Protracted and polyphased gold mineralisation in the Agnew District (Yilgarn Craton, Western Australia). Precambrian Research 310:291–304

Tomkins AG, Mavrogenes JA (2001) Redistribution of Gold within Arsenopyrite and Lollingite during Pro- and Retrograde Metamorphism: Application to Timing of Mineralization. Economic Geology 96:525–534
Tomkins AG (2010) Windows of metamorphic sulfur liberation in the crust: Implications for gold deposit genesis. Geochimica et Cosmochimica Acta 74:3246–3259
Vanhanen E (2001) Geology, mineralogy and geochemistry of the Fe-Co- Au-(U) deposits in the Paleoproterozoic Kuusamo Schist Belt, northeastern Finland. Bulletin, Espoo, Finland
Vasilopoulos M, Molnár F, O'Brien H, Lahaye Y, Lefèbvre M, Richard A, André-Mayer A-S, Ranta J-P, Talikka M (2021) Geochemical signatures of mineralizing events in the Juomasuo Au–Co deposit, Kuusamo belt, northeastern Finland. Mineral. Deposita
Vasyukova OV, Williams-Jones AE (2022) Constraints on the Genesis of Cobalt Deposits: Part II. Applications to Natural Systems. Economic Geology 117:529–544
Ward P, Härkönen I, Nurmi P, Pankka HS (1989) Structural studies in the Lapland greenstone belt, Northern Finland and their application to gold mineralization. In: Autio S (ed) Geological survey of Finland, current research 1988. Geologian Tutkimuskeskus, Espoo, pp 71–77
Weatherley DK, Henley RW (2013) Flash vaporization during earthquakes evidenced by gold deposits. Nature Geosci 6:294–298
Wieser PE, Jenner FE (2021) Chalcophile Elements: Systematics and Relevance. In: Encyclopedia of Geology. Elsevier, pp 67–80
Williams-Jones AE, Vasyukova OV (2022) Constraints on the Genesis of Cobalt Deposits: Part I. Theoretical Considerations. Economic Geology 117:513–528
Wind SC, Schneider DA, Hannington MD, McFarlane CR (2020) Regional similarities in lead isotopes and trace elements in galena of the Cyclades Mineral District, Greece with implications for the underlying basement. Lithos 366-367:105559
Wyche NL, Eilu P, Koppström K, Kortelainen VJ, Niiranen T, Välimaa J (2015) The Suurikuusikko Gold Deposit (Kittilä Mine), Northern Finland. In: Mineral Deposits of Finland. Elsevier, pp 411–433
Yang K, Scott SD (2002) Magmatic Degassing of Volatiles and Ore Metals into a Hydrothermal System on the Modern Sea Floor of the Eastern Manus Back-Arc Basin, Western Pacific. Economic Geology 97:1079–1100
Yao Z, Mungall JE (2020) Flotation mechanism of sulphide melt on vapour bubbles in partially molten magmatic systems. Earth and Planetary Science Letters 542:116298
Zhong R, Brugger J, Tomkins AG, Chen Y, Li W (2015) Fate of gold and base metals during metamorphic devolatilization of a pelite. Geochimica et Cosmochimica Acta 171:338–352